

Handbook of Advanced Electronic and Photonic Materials and Devices

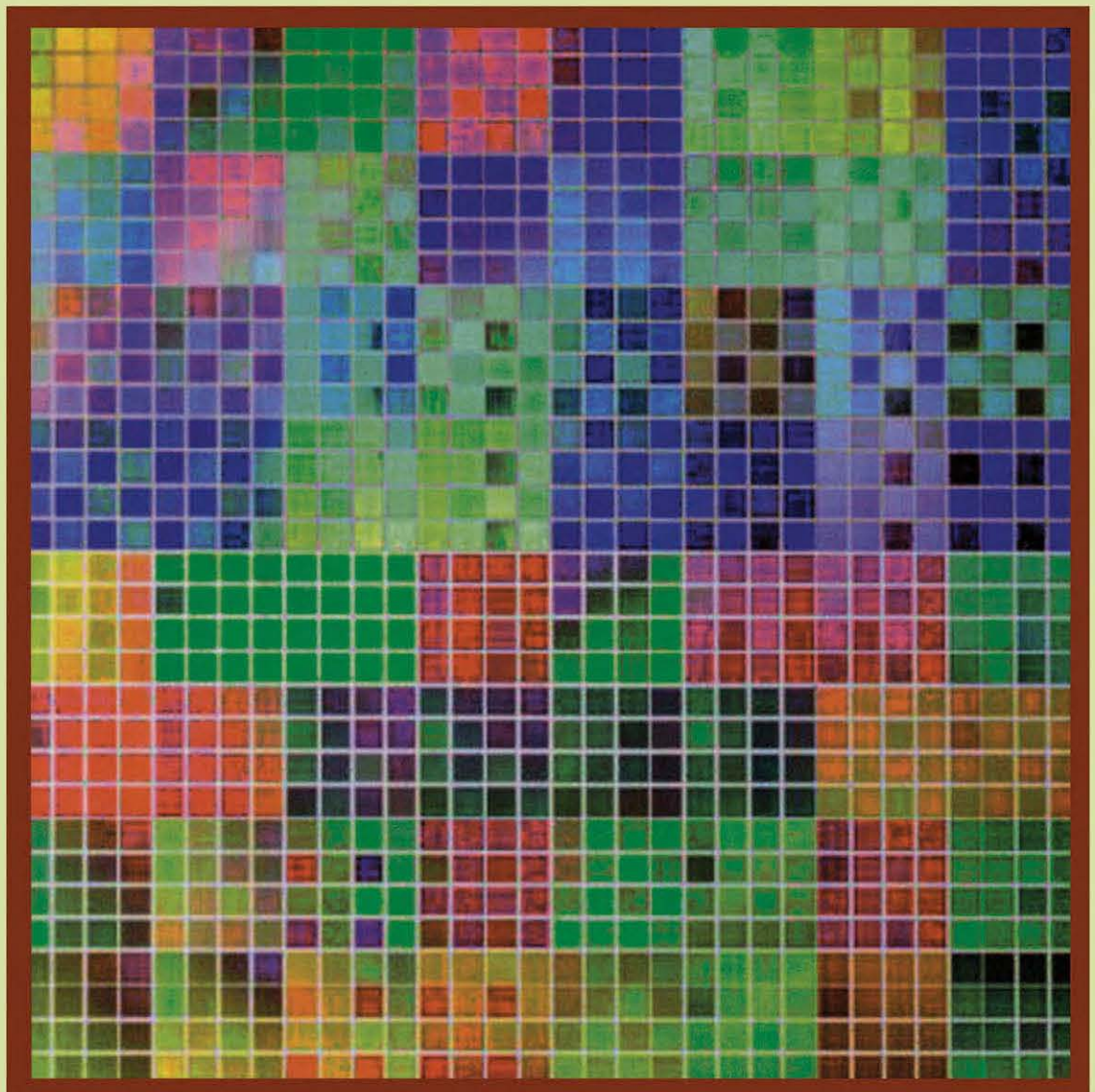
Edited by

Hari Singh Nalwa

Foreword by

Nicolaas Bloembergen, Nobel Laureate

High- T_c Superconductors
and Organic Conductors



ACADEMIC
PRESS

**Handbook of
Advanced Electronic and Photonic
Materials and Devices**

This Page Intentionally Left Blank

Handbook of Advanced Electronic and Photonic Materials and Devices

Volume 8
Conducting Polymers

Edited by

Hari Singh Nalwa, M.Sc., Ph.D.
Stanford Scientific Corporation
Los Angeles, California, USA

Formerly at
Hitachi Research Laboratory
Hitachi Ltd., Ibaraki, Japan



ACADEMIC PRESS

A Harcourt Science and Technology Company

San Diego San Francisco New York Boston
London Sydney Tokyo

The image for the cover of this book was reprinted with permission from Jingsong Wang, Young, Yoo, Chen Gao, Ichiro Takeuchi, Xiaodong Sun, Haiyee Chang, X.-D. Xiang, and Peter G. Schultz, *Science* 279: 1712 (1998). Copyright 1998 American Association for the Advancement of Science.

This book is printed on acid-free paper. ☺

Copyright © 2001 by Academic Press

All rights reserved.

No part of this publication may be reproduced or transmitted in any form or by any means, electronic or mechanical, including photocopy, recording, or any information storage and retrieval system, without permission in writing from the publisher.

The appearance of the code at the bottom of the first page of a chapter in this book indicates the Publisher's consent that copies of the chapter may be made for personal or internal use of specific clients. This consent is given on the condition, however, that the copier pay the stated per-copy fee through the Copyright Clearance Center, Inc. (222 Rosewood Drive, Danvers, Massachusetts 01923), for copying beyond that permitted by Sections 107 or 108 of the U.S. Copyright Law. This consent does not extend to other kinds of copying, such as copying for general distribution, for advertising or promotional purposes, for creating new collective works, or for resale. Copy fees for pre-2001 chapters are as shown on the title pages; if no fee code appears on the title page, the copy fee is the same as for current chapters. 01 \$35.00.

The information provided in this handbook is compiled from reliable sources but the authors, editor, and the publisher cannot assume any responsibility whatsoever for the validity of all statements, illustrations, data, procedures, and other related materials contained herein or for the consequence of their use.

ACADEMIC PRESS

A Harcourt Science and Technology Company

525 B Street, Suite 1900, San Diego, CA 92101-4495, USA

<http://www.academicpress.com>

Academic Press

Harcourt Place, 32 Jamestown Road, London, NW1 7BY, UK

Library of Congress Catalog Number: 00-102887

International Standard Book Number: 0-12-513758-3

Printed in the United States of America

00 01 02 03 IP 9 8 7 6 5 4 3 2 1

To my wife
Dr. Beena Singh Nalwa
(M.A., M.Phil., Ph.D.)

This Page Intentionally Left Blank

Foreword

Since the realization of the first laser 40 years ago, the merging of the fields of quantum electronics and quantum optics has stimulated the development of many new materials and devices. These, in turn, support a flourishing optoelectronics market for optical communications, optical data processing, medical diagnostics, materials processing, display technology, and many other applications.

Therefore, in the year 2000, it is timely to publish *The Handbook of Advanced Electronic and Photonic Materials and Devices*. The editor, Hari Singh Nalwa, is well known for his original work on nonlinear optics of organic molecules and polymers. Together with Seizo Miyata, he edited a comprehensive volume under this title that provides a broad overview of this particular subject. The same authors also edited a volume on organic electroluminescent materials and devices.

The present 10 volume handbook has a much broader scope. It includes semiconductor materials, quantum wells and quantum dots, liquid crystals, conducting polymers, laser materials, photoconductors, electroluminescent and photorefractive materials, nanostructured, supramolecular, and self-assembled materials, ferroelectrics, and superconductors. Applications of these materials in photoconductors, optical fibers, xerography, solar cells, dynamic random access memory, and sensors are described. The Handbook contains contributions by 180 leading experts from 25 different countries. It truly represents the worldwide research efforts and results that support the global market of optoelectronics. All scientific and technical workers in this broad field are indebted to the contributing authors, the editor and Academic Press for publishing this comprehensive handbook for the new millennium. It will support further growth in a field that already has surpassed my wildest expectations of 40 years ago.

Professor Nicolaas Bloembergen
Nobel Laureate in Physics, 1981
Harvard University
Cambridge, MA, USA

This Page Intentionally Left Blank

Preface

Electronic and photonic materials are the key elements of continued scientific growth and technological advances in the new millennium. The electronic and photonic materials discussed in this handbook include semiconductors, superconductors, ferroelectrics, low- and high- κ dielectrics, sol-gel materials, fullerenes and carbon nanotubes, liquid crystals, conducting polymers, organic conductors, nonlinear optical materials, electrochromic materials, laser materials, photoactive chalcogenide glasses, photoconductors, photovoltaic and electroluminescent materials, nanostructured materials, confined systems, supramolecular and self-assemblies, and soft magnetic materials. Compared to electronic materials, photonic materials enable the transport and processing of information at the speed of light. In the communication age of the 21st century, a major technological thrust is to move forward with photonic and optoelectronic technologies as a replacement to the traditional electronic technologies currently utilized to perform various functions such as the acquisition, processing, transmission, storage, and display of information. The present boom in fiber optics technology is an excellent example of how much impact photonic technologies have on the advancement of our society. These materials have already been used and will be the most important components of the next generation of semiconductor devices, the internet, computers, information technology, wireless and telecommunications, satellite communications, integrated circuits, photocopiers, wireless telephones, solar cells, batteries, light-emitting diodes, liquid crystal displays, magneto-optic memories, audio and video systems, recordable compact discs, video cameras, coatings, X-ray technology, advanced lithium batteries, nonvolatile memories, multilayer capacitors, color imaging, printing, flat-panel displays, waveguides, cable televisions, modulators, computer chips, magneto-optic disks, transducers, optoelectronics, lithography, holographic recording, solid-state lasers, and molecular-sized transistors and switches, as well as other emerging cutting edge technologies. Electronic and photonic materials are expected to grow to a trillion-dollar industry in the new millennium and will be the most dominant forces in various fields of science and engineering.

This is the first handbook ever published on electronic and photonic materials, that summarizes the advances made over past the three decades. This handbook is a unique source of in-depth knowledge of molecular design, synthesis, processing, spectroscopy, physical properties and applications of electronic and photonic materials. This handbook contains 73 state-of-the-art review chapters written by more than 180 world leading experts from 25 different countries. With over 25,000 bibliographic citations and thousands of figures, tables, photographs, chemical structures, and equations, this handbook represents the work of the most renowned scientists in the international scientific community. It has been divided into 10 parts based on thematic topics:

- Volume 1: Semiconductors
- Volume 2: Semiconductor Devices
- Volume 3: High T_c Superconductors and Organic Conductors
- Volume 4: Ferroelectrics and Dielectrics
- Volume 5: Chalcogenide Glasses and Sol-Gel Materials
- Volume 6: Nanostructured Materials
- Volume 7: Liquid Crystals, Display, and Laser Materials
- Volume 8: Conducting Polymers
- Volume 9: Nonlinear Optical Materials
- Volume 10: Light-Emitting Diodes, Lithium Batteries, and Polymer Devices

Volume 1 includes topics on the growth and doping of Te-based II–VI layers and quantum structures by molecular beam epitaxy, gallium arsenide heterostructures, photoluminescence in GaN and InGaN and their photonic applications, processing of compound semiconductors, hydrogen in wide bandgap semiconductors, wet etching of semiconductors, combinatorial synthesis and high throughput evaluation of electronic and photonic material chips, and coherent effects in semiconductor heterostructures.

The applications of semiconductor materials are discussed in Volume 2. The various topics on semiconductor devices include Si/GeSi heterostructures for Si-based nanoelectronics, impact ionization in compound semiconductor devices, quantum dot optoelectronic devices, failure mechanisms in compound semiconductors, electron devices, semiconductor quantum materials and their applications in electronics and optoelectronics, and photoelectromotive force effects in semiconductors.

Volume 3 focuses on high T_c superconductors and organic conductors. Topics on superconductors include high T_c superconductors for small scale devices, processing and characterization of Bi-based single crystals and tapes, grain connectivity and vortex pinning in high-temperature superconductors, and yttrium–barium–copper oxide as an infrared sensing materials. The various topics on organic conductors include high magnetic field studies of quasi-two-dimensional organic conductors based on BEDT-TTF, quinonoid π -extended tetrathiafulvalenes, supramolecular aspects of organic conductors, intramolecular electronic transfer phenomena in organic mixed-valence compounds, and organic conducting composites.

Ferroelectric and dielectric materials comprise Volume 4. This volume contains reviews on pyroelectricity: the fundamentals and applications, crystal growth, characterization and domain studies in lithium niobate and lithium tantalate ferroelectrics, bismuth vanadate, the electric field influence on acoustic waves, dielectric ceramics, and low dielectric constant materials for microelectronics interconnects.

Volume 5 includes topics on chalcogenide glasses and sol–gel materials. This volume focuses on conduction and its related phenomena in ion-conducting glasses, photoinduced phenomena in amorphous chalcogenides from phenomenology to nanoscale, photoinduced and electron-beam phenomena in Ag-rich amorphous chalcogenide semiconductors, photoinduced anisotropy in chalcogenide glasses, the nonlinear optical and spectral hole-burning properties of photonic glasses, the structure, chemistry, and applications of sol–gel derived materials, modified sol–gel and metallo-organic deposition techniques for processing oxide films, and sol–gel coatings for optical and dielectric applications.

In Volume 6, various topics related to nanotechnology and nanostructured materials are discussed. The topics include electrochemically self-assembled ordered nanostructured arrays (quantum dots, dashes and wires), mechanical spectroscopy of nanostructured metallic systems, soft amorphous and nanocrystalline magnetic materials, nanoporous materials for microlasers and microresonators, nanoporous materials for optical applications, optical properties and impurity states in nanostructured materials, and confined systems and nanostructured materials.

Volume 7 summarizes new trends on liquid crystals, display, and laser materials. The topics include liquid crystals for electro-optic applications, switchable holographic polymer-dispersed liquid crystals, electrochromism and electrochromic materials for displays, materials for solid-state dye lasers, photophysical properties of laser dyes and correlations with the lasing characteristics, interplay of anisotropy and orientational relaxation processes in luminescence, and lasing of dyes and photosensitive materials for holographic recording.

Electrically conducting polymers are discussed in Volume 8. The coverage in this volume includes the synthesis, and electrical and optical properties of conjugated polymers, conjugated polymer films for molecular and ionic recognition, polyacetylene and its analogs, synthesis, properties, and applications of poly(*p*-phenylenevinylenes), self-organized supramolecular polymer structures to control electrical conductivity, spectroelectrochemistry of conducting polymers, electronic spectra of conjugated polymers and oligomers, and the degradation and stability of electrically conducting polymers.

Nonlinear optical materials and their applications are discussed in Volume 9. The various topics include calculation of dynamic hyperpolarizabilities for small and medium sized molecules, theoretical aspects of the design of organic molecular and polymeric nonlinear optical materials, design and characterization of organic and organometallic molecules for second-order nonlinear optics, crystal growth, processing, and physical properties of photonic crystals, hyper-Rayleigh scattering: molecular, supramolecular, and device characterization by incoherent second-order nonlinear light scattering, nonlinear optical properties of fullerenes and carbon nanotubes, third-order optical nonlinearity in polydiacetylene waveguides at telecommunications wavelengths, organic materials for optical limiting, and Bragg grating in optical fibers.

Volume 10 includes topics on organic and polymer-based light emitting diodes, optical devices based on conducting polymers, intercalation compounds for advanced lithium batteries, polymer electrets for electronics, sensor, and photonic applications, charge transporting polymers and molecular glasses, and electrochemically prepared thin films for solar cells.

I hope these volumes will be very useful for libraries in universities and industrial institutions, governments, and independent institutes, upper-level undergraduate and graduate students, individual research groups, and scientists working in the field of materials science, solid-state physics, chemistry, nanotechnology, electrical and electronics engineering, polymer science, spectroscopy, crystallography, electrochemistry, xerography, superconductivity, optical engineering, device engineering, computational engineering, photophysics, data storage and information technology, and for the technocrats, who are involved in the science and engineering of electronic and photonic materials and devices.

This handbook is the end product of marvelous cooperation of many distinguished experts, who devoted their valuable time and effort to write excellent state-of-the-art review chapters. I am highly thankful to all contributing authors. I highly appreciate all publishers and authors for granting us copyright permissions to use their illustrations for the review chapters in this handbook. I am grateful to my former mentors, Dr. Akio Mukoh and Dr. Shuuichi Oohara at Hitachi Research Laboratory, Hitachi Ltd., for their kind support and encouragement during my stay in Japan. I also extend my special thanks to Krishi Pal Raghuvanshi, Rakesh Misra, Professor Satya Vir Arya, Professor Padma Vasudevan, Jagmer Singh, Ranvir Singh Chaudhary, and other colleagues who supported my efforts to bringing this handbook to fruition. Finally, I greatly appreciate my wife, Dr. Beena Singh Nalwa, for her continuous cooperation and patience for enduring this work at home during weekends and late nights. The moral support of my parents, Sri Kadam Singh and Srimati Sukh Devi, and the love of my children, Surya, Ravina, and Eric during this exciting enterprise are also appreciated.

I express my sincere gratitude to Professor N. Bloembergen for his insightful foreword.

Hari Singh Nalwa
Los Angeles, CA, USA
October 2000

This Page Intentionally Left Blank

Contents

About the Editor	xvii
List of Contributors	xix
Volume Listing	xxi

Chapter 1. SYNTHESIS, ELECTRICAL, AND OPTICAL PROPERTIES OF CONJUGATED POLYMERS

Rafaël Kiebooms, Reghu Menon, Kwanghee Lee

1. Introduction	1
2. Synthesis	5
2.1. Polyacetylenes	6
2.2. Polyaromatics	8
2.3. Poly(<i>p</i> -phenylene vinylene)s	26
2.4. Polyanilines	32
2.5. Chemical Structure and Electronic Properties	33
3. Electrical Properties	47
3.1. Metallic State	49
3.2. Critical and Insulating States	60
4. Optical Properties	62
4.1. Theoretical Considerations	63
4.2. Optical Properties of “Doped” Conducting Polymers	65
4.3. Photophysics of Semiconducting Polymers	78
4.4. Electroluminescence in Conjugated Polymers: Polymer LED	81
4.5. Photoinduced Charge Transfer in Conjugated Polymer/Fullerene Composites	82
5. Concluding Remarks	84
Acknowledgments	86
References	86

Chapter 2. CONJUGATED POLYMER FILMS FOR MOLECULAR AND IONIC RECOGNITION

Bruno Fabre

1. Introduction	103
1.1. Background	103
1.2. Electrochemistry: A Powerful Tool for Recognition	104
1.3. Redox-Active Conjugated Polymer-Based Recognition	104
2. Molecular Recognition	105
2.1. Enzyme-Containing Polymers	105
2.2. Analytes of Biological and Pharmacological Interest	111
2.3. Gases and Vapors	112
2.4. Other Molecules	113
3. Cationic Recognition	114
3.1. Polyether-Functionalized Polymers	114
3.2. Calixarene-Functionalized Polymers	119
3.3. Polyrotaxanes	120
3.4. Polymers Containing Other Functional Groups	121
4. Anionic Recognition	122
5. Conclusions	124
References	124

Chapter 3. POLYACETYLENE AND ITS ANALOGS: SYNTHESIS AND PHYSICAL PROPERTIES

Kristen J. Steenberg Harrell, SonBinh T. Nguyen

1. Introduction	132
2. Polyacetylene	132
2.1. The Discovery of PA	132
2.2. Shirakawa's Method for the Polymerization of Acetylene	132
2.3. Properties of Shirakawa-Type PA	133
2.4. Modifications of the Shirakawa Method	134
2.5. Other Catalysts for the Polymerization of Acetylene	137
2.6. Precursor Routes to PA	138
2.7. Copolymers of PA	141
3. Substituted PA	145
3.1. Synthesis of Substituted PA	145
3.2. Living Systems	148
3.3. Stereospecific Polymerizations	148
3.4. Silicon-Substituted Alkyne Monomers	148
3.5. ROMP of RCOT	149
3.6. α , ω -Diynes	149
3.7. Indirect Routes to Substituted PA	150
3.8. Properties of Substituted PA	150
4. Electronic Properties of PA and Its Analogs	150
4.1. Conductivity and Chemical Doping	150
4.2. Solitons	151
4.3. <i>cis</i> - to <i>trans</i> -Isomerization	154
4.4. Electrochemical Doping	154
4.5. Photochemical Doping	154
5. Applications of PA and Its Analogs	154
5.1. Semiconductor Devices	155
5.2. Rechargeable Batteries	155
5.3. Solar Cells	155
5.4. Environmental Sensing Technology Based on PA	155
5.5. Gas-Liquid Separation Membranes	156
5.6. Other Applications of PA and Its Analogs	157
6. Conclusion	157
Acknowledgments	157
Nomenclature	157
References	158

Chapter 4. SYNTHESIS, PROPERTIES, AND APPLICATIONS OF POLY(*p*-PHENYLENE VINYLENE)S

Jonas Gruber, Rosamaria Wu Chia Li, Ivo Alexandre Hümmelgen

1. Introduction	163
2. Methods of Synthesis	164
2.1. Via the Wittig Reaction	164
2.2. Soluble Precursor Routes	165
2.3. Electrochemical Routes	167
2.4. Other Synthetic Routes	167
3. Spectroscopy	169
3.1. Vibrational Spectra	169
3.2. Ultraviolet-Visible	170
3.3. Nuclear Magnetic Resonance	171
4. Thin-Film Preparation	171
4.1. Methods and Processes	171
5. Physical Properties	172
5.1. Structural, Mechanical, and Thermal Properties	172
5.2. Electrical Properties	173
6. Interfaces with Other Materials	176
6.1. Interfaces with Metals	176

6.2. Interfaces with Oxides	177
6.3. Interfaces with Other Conjugated Polymers and Polymer Blends	178
7. Applications	178
7.1. Light-Emitting Diodes	178
7.2. Photodiodes and Photodetectors	179
7.3. Lasers	180
7.4. Triodes	180
7.5. Light-Emitting Electrochemical Cells	180
7.6. Optocouplers	180
Acknowledgments	180
References	181

Chapter 5. SELF-ORGANIZED SUPRAMOLECULAR POLYMER STRUCTURES TO CONTROL ELECTRICAL CONDUCTIVITY

Olli Ikkala, Gerrit ten Brinke

1. Introduction	185
2. Background on Self-Organization and Supramolecular Concepts	186
2.1. Self-Organization	186
2.2. Supramolecular Assembly	188
2.3. Self-Organized Supramolecular Structures	189
3. Conducting and Semiconducting Polymer Systems Containing Self-Organized Supramolecular Polymers	194
3.1. Ionically Conducting Self-Organized Supramolecular Structures of Polymers Hydrogen-Bonded to Amphiphiles	194
3.2. Self-Organization and Stacking of Dislike Organic Molecules	195
3.3. Self-Organization of Hairy Rods	197
3.4. Self-Organization of Supramolecular Hairy Rods	200
3.5. Externally Controllable Self-Organized Supramolecular Polymer Systems Allowing Electrical Switching	204
4. Concluding Remarks	205
Acknowledgments	205
References	206

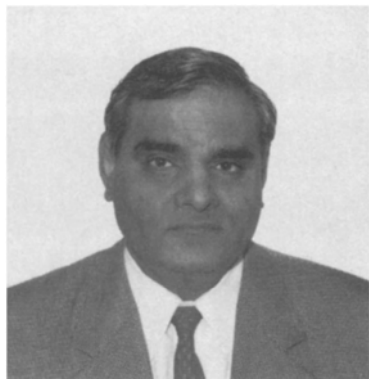
Chapter 6. SPECTROELECTROCHEMISTRY OF CONDUCTING POLYMERS

Rudolf Holze

1. Introduction	209
2. Spectroelectrochemistry: An Introduction	211
2.1. Fundamentals	211
2.2. Spectroscopy at Surfaces	211
2.3. Spectroelectrochemistry	211
3. Polyaniline and Related Polymers	217
3.1. Formation of Polyaniline and Related Polymers	218
3.2. Properties of Polyaniline and Related Polymers and their Electrochemically Induced Changes	227
3.3. Redox Processes of Polyaniline and Polymers of Substituted Anilines	251
3.4. Redox Processes and Electrocatalysis at Polyaniline and Related Polymers	252
3.5. Degradation of Polymers	254
4. Polypyrrole and Related Polymers	256
4.1. Formation of Polypyrrole and Related Polymers	257
4.2. Properties of Polypyrrole and Related Polymers and their Electrochemically Induced Changes	258
4.3. Degradation of Polypyrrole and Related Polymers	265
5. Polythiophene and Related Polymers	266
5.1. Formation of Polythiophene and Related Polymers	267
5.2. Properties of Polythiophene and Related Polymers and their Electrochemically Induced Changes	269
6. Miscellaneous Polymers	283

Appendix	284
Acknowledgments	286
References	286
Chapter 7. ELECTRONIC SPECTRA OF CONJUGATED POLYMERS AND OLIGOMERS	
<i>Yukio Furukawa</i>	
1. Introduction	303
2. Charge Carriers in Conjugated Polymers	304
2.1. Ground-State Structures	304
2.2. Self-Localized Excitations	305
3. Electronic Spectra	305
3.1. Neutral and Charged Oligomers	305
3.2. Neutral and Doped Polymers	313
4. Concluding Remarks	317
Acknowledgments	317
References	318
Chapter 8. STABILITY OF ELECTRICALLY CONDUCTING POLYMERS	
<i>F. Mohammad</i>	
1. Introduction	321
1.1. Electrically Conducting Polymers	321
1.2. Stability of Electrically Conducting Polymers	322
1.3. Stabilization	324
2. Stability of Individual Polymeric Systems	325
2.1. Polyacetylenes	325
2.2. Polyheterocyclics	326
2.3. Polyaromatics	334
2.4. Inorganic and Silicon Polymers	341
2.5. Phthalocyanines	342
2.6. Miscellaneous Systems	343
Acknowledgments	344
References	345
Index	351

About the Editor



Dr. Hari Singh Nalwa is the Managing Director of the Stanford Scientific Corporation in Los Angeles, California. Previously, he was Head of Department and R&D Manager at the Ciba Specialty Chemicals Corporation in Los Angeles (1999–2000) and a staff scientist at the Hitachi Research Laboratory, Hitachi Ltd., Japan (1990–1999). He has authored over 150 scientific articles in journals and books. He has 18 patents, either issued or applied for on electronic and photonic materials and devices based on them.

He has published 11 books, including this 10 volume handbook set: *Ferroelectric Polymers* (Dekker, 1995), *Nonlinear Optics of Organic Molecules and Polymers* (CRC Press, 1997), *Organic Electroluminescent Materials and Devices* (Gordon & Breach, 1997), *Handbook of Organic Conductive Molecules and Polymers*, Vols. 1–4 (Wiley, 1997), *Low and High Dielectric Constant Materials*, Vols. 1 and 2 (Academic Press, 1999), *Handbook of Nanostructured Materials and Nanotechnology*, Vols. 1–5 (Academic Press, 1999), *Advanced Functional Molecules and Polymers*, Vols. 1–4 (Gordon & Breach, 2000), *Photodetectors and Fiber Optics* (Academic Press, 2000), *Silicon-Based Materials and Devices* (Academic Press, 2000), and *Supramolecular Photo-sensitive and Electro-active Materials* (Academic Press, 2000). The *Handbook of Nanostructured Materials and Nanotechnology*, which he edited, received the 1999 Award of Excellence in Engineering Handbooks from the Association of American Publishers.

Dr. Nalwa is the founder and Editor-in-Chief of the *Journal of Porphyrins and Phthalocyanines* published by John Wiley & Sons (1996–) and serves on the editorial boards of *Journal of Macromolecular Science-Physics* (1994–), *Applied Organometallic Chemistry* (1993–1999), *International Journal of Photoenergy* (1998–), and *Photonics Science News* (1995–). He also serves as a referee for many international journals that includes *Journal of American Chemical Society*, *Journal of Physical Chemistry*, *Applied Physics Letters*, *Journal of Applied Physics*, *Chemistry of Materials*, *Journal of Materials Science*, *Coordination Chemistry Reviews*, *Applied Organometallic Chemistry*, *Journal of Porphyrins and Phthalocyanines*, *Journal of Macromolecular Science-Physics*, *Applied Physics*, *Materials Research Bulletin*, and *Optical Communications*.

Dr. Nalwa helped organize the First International Symposium on the Crystal Growth of Organic Materials (Tokyo, 1989) and the Second International Symposium on Phthalocyanines (Edinburgh, 1998) under the auspices of the Royal Society of Chemistry. He also proposed a conference on porphyrins and phthalocyanines to the scientific community that, in part, was intended to promote public awareness of the *Journal of Porphyrins and Phthalocyanines*, which he founded in 1996. As a member of the organizing committee, he helped effectuate the First International Conference on Porphyrins and Phthalocyanines, which was held in Dijon, France, in 2000.

Dr. Nalwa is a member of the American Chemical Society (ACS), the American Physical Society (APS), the Materials Research Society (MRS), the Electrochemical Society (ECS), and the American Association for the Advancement of Science (AAAS). He has been awarded a number of prestigious fellowships, including a National Merit Scholarship, an Indian Space Research Organization (ISRO) Fellowship, a Council of

Scientific and Industrial Research (CSIR) Senior Fellowship, a NEC Fellowship, and a Japanese Government Science & Technology Agency (STA) Fellowship. He was an Honorary Visiting Professor at the Indian Institute of Technology in New Delhi. Dr. Nalwa has been cited in the *Who's Who in Science and Engineering*, *Who's Who in America*, *Who's Who in the World* and the *Dictionary of International Biography*.

Dr. Nalwa received a B.Sc. degree in biosciences from Meerut University in 1974, a M.Sc. degree in organic chemistry from University of Roorkee in 1977, and a Ph.D. degree in polymer science from the Indian Institute of Technology in New Delhi in 1983. His thesis research focused on the electrical properties of macromolecules. Since then, his research activities and professorial career have been devoted to studies of electronic and photonic organic and polymeric materials. His endeavors include molecular design, chemical synthesis, spectroscopic characterization, structure–property relationships, and evaluation of novel high performance materials applied to electronic and photonic applications. He was as a guest scientist at Hahn-Meitner Institute in Berlin, Germany (1983), and a research associate at the University of Southern California in Los Angeles (1984–1987) and the State University of New York at Buffalo (1987–1988). In 1988, he moved to the Tokyo University of Agriculture and Technology as a lecturer (1988–1990), where he taught and conducted research on electronic and photonic materials. His research activities include studies of ferroelectric polymers, nonlinear optical materials for integrated optics, low and high dielectric constant materials for microelectronics packaging, electrically conducting polymers, electroluminescent materials, nanocrystalline and nanostructured materials, photocuring polymers, polymer electrets, organic semiconductors, Langmuir-Blodgett films, high temperature-resistant polymer composites, water-soluble polymers, rapid modeling, and stereolithography.

List of Contributors

Numbers in parenthesis indicate the pages on which the author's contribution begins.

GERRIT TEN BRINKE (185)

Laboratory of Polymer Chemistry and Materials Science Center,
University of Groningen, Groningen, The Netherlands
Helsinki University of Technology, Espoo, Finland

BRUNO FABRE (103)

Laboratoire d'Electrochimie Moléculaire et Macromoléculaire
(Unité Mixte de Recherche no. 6510 associée au CNRS),
Université de Rennes 1, Campus de Beaulieu, Rennes Cedex, France

YUKIO FURUKAWA (303)

Department of Chemistry, School of Science and Engineering, Waseda University,
Shinjuku-ku, Tokyo 169-8555, Japan

JONAS GRUBER (163)

Instituto de Química, Universidade de São Paulo, Caixa Postal 26077,
05513-970 – São Paulo, SP, Brazil

KRISTEN J. STEENBERG HARRELL (131)

Department of Chemistry, Northwestern University, Evanston, Illinois 60208-3113, USA

RUDOLF HOLZE (209)

Technische Universität Chemnitz, Institut für Chemie, D-09107 Chemnitz, Germany

IVO ALEXANDRE HÜMMELGEN (163)

Group of Organic Optoelectronic Devices, Departamento de Física,
Universidade Federal do Paraná, Caixa Postal 19081, 81531-900 – Curitiba, PR, Brazil

OLLI IKKALA (185)

Department of Engineering Physics and Mathematics, Helsinki University of Technology,
Espoo, Finland

RAFAËL KIEBOOMS (1)

Institute for Materials Research, Limburg University, Diepenbeek, Belgium

KWANGHEE LEE (1)

Department of Physics, Pusan National University, Pusan, Korea

ROSAMARIA WU CHIA LI (163)

Instituto de Química, Universidade de São Paulo, Caixa Postal 26077,
05513-970 – São Paulo, SP, Brazil

REGHU MENON (1)

Department of Physics, Indian Institute of Science, Bangalore, India

F. MOHAMMAD (321)

Department of Applied Chemistry, Aligarh Muslim University, Aligarh-202002, India

SONBINH T. NGUYEN (131)

Department of Chemistry, Northwestern University, Evanston, Illinois 60208-3113, USA

This Page Intentionally Left Blank

Handbook of Advanced Electronic and Photonic Materials and Devices

Edited by H.S. Nalwa

Volume 1. SEMICONDUCTORS

- Chapter 1. Growth and Doping of Te-Based II–VI Layers and Quantum Structures by Molecular Beam Epitaxy
K. Saminadayar, S. Tatarenko, K. Kheng, V. Huard, D. Martrou
- Chapter 2. Gallium Arsenide Heterostructures
Eric Donkor
- Chapter 3. Photoluminescence in GaN, InGaN and Their Applications in Photonics
Annamraju Kasi Viswanath
- Chapter 4. Processing of Compound Semiconductors
S. J. Pearton
- Chapter 5. Hydrogen in Wide Bandgap Semiconductors
S. J. Pearton, J. W. Lee
- Chapter 6. Wet Etching of III–V Semiconductors
Walter P. Gomes
- Chapter 7. Combinatorial Synthesis and High Throughput Evaluation of Electronic and Photonic Material Chips
X.-D. Xiang
- Chapter 8. Coherent Effects in Semiconductor Heterostructures
Karl Leo

Volume 2. SEMICONDUCTOR DEVICES

- Chapter 1. Si/SiGe Heterostructures for Si-Based Nanoelectronics
D. Y. C. Lie, K. L. Wang
- Chapter 2. Impact Ionization in Compound Semiconductor Devices
E. Zanoni, G. Meneghesso
- Chapter 3. Recent Advances in Quantum Dot Optoelectronic Devices and Future Trends
S. Kim, M. Razeghi
- Chapter 4. Failure Mechanisms in Compound Semiconductor Electron Devices
F. Fantini, R. Menozzi, M. Borgarino, L. Cattani, D. Dieci
- Chapter 5. Semiconductor Quantum Materials and Their Applications in Electronics and Optoelectronics
Y. Fu, M. Willander
- Chapter 6. Photo-Electromotive-Force Effect in Semiconductors
Serguei Stepanov

Volume 3. HIGH- T_c SUPERCONDUCTORS AND ORGANIC CONDUCTORS

- Chapter 1. High- T_c Superconductors Toward Small Scale Applications
R. Gerbaldo, G. Ghigo, L. Gozzelino, E. Mezzetti
- Chapter 2. Processing and Characterization of Bi-Based Single Crystals and Tapes
Hua kun Liu, Mihail Ionescu, Yuan Chang Guo
- Chapter 3. Grain Connectivity and Vortex Pinning in High-Temperature Superconductors
J. Horvat
- Chapter 4. Yttrium Barium Copper Oxide as an Infrared Radiation Sensing Material
Donald P. Butler, Zeynep Çelik-Butler
- Chapter 5. High-Magnetic-Field Studies of Quasi-Two-Dimensional Organic Conductors Based on BEDT-TTF
J. Singleton
- Chapter 6. Quinonoid π -Extended Tetrathiafulvalenes (TTFs)
Nazario Martin, Enrique Orti
- Chapter 7. Supramolecular Aspects of Organic Conductors
Tomoyuki Akutagawa, Tatsuo Hasegawa, Takayoshi Nakamura
- Chapter 8. Intramolecular Electronic-Transfer Phenomena in Organic Mixed-Valence Compounds
Daniel Ruiz-Molina, Josep Sedó, Concepció Rovira, Jaume Veciana
- Chapter 9. Conducting Organic Composites
Jean-Pierre Farges, André Brau

Volume 4. FERROELECTRICS AND DIELECTRICS

- Chapter 1. Pyroelectricity: Fundamentals and Applications
Sidney B. Lang, Dilip K. Das-Gupta
- Chapter 2. Crystal Growth, Charakterization, and Domain Studies in Lithium Niobate and Lithium Tantalate Ferroelectrics
Venkatraman Gopalan, Norman Sanford, J. A. Aust, K. Kitamura, Y. Furukawa
- Chapter 3. Bismuth Vanadate: A Versatile Ferroelectric Material
K. Shantha, K. B. R. Varma
- Chapter 4. Electric Field Influence on Acoustic Waves
B. D. Zaitsev, I. E. Kuznetsova
- Chapter 5. Dielectric Ceramics
Y. S. Cho, K. H. Yoon
- Chapter 6. Low- k Materials for Microelectronics Interconnects
Patrick G. Chiu, David T. Hsu, Hyung-Kun Kim, Frank G. Shi, Hari Singh Nalwa, Bin Zhao

Volume 5. CHALCOGENIDE GLASSES AND SOL-GEL MATERIALS

- Chapter 1. Conduction and Conduction-Related Phenomena in Ion-Conducting Glasses
Akira Doi
- Chapter 2. Photoinduced Phenomena in Amorphous Chalcogenides: From Phenomenology to Nanoscale
Alexander V. Kolobov, Kazunobu Tanaka
- Chapter 3. Photoinduced and Electron-Beam Phenomena in Ag-Rich Amorphous Chalcogenide Semiconductors
Takeshi Kawaguchi, Keiji Tanaka, Stephen R. Elliott

- Chapter 4. Photoinduced Anisotropy in Chalcogenide Glass
Keiji Tanaka
- Chapter 5. Photonic Glasses: Nonlinear Optical and Spectral Hole Burning Properties
Masayuki Nogami, S. Tamil Selvan, Hongwei Song
- Chapter 6. Structure, Chemistry, and Applications of Sol–Gel Derived Materials
Maryanne M. Collinson
- Chapter 7. Sol–Gel, Modified Sol–Gel, and Mettalo–Organic Decomposition Techniques for Complex Oxide Films: Materials, Processing, and Applications
M. Klee, H. van Hal, W. Keur, W. Brand, R. Kiewitt, U. Mackens, C. Metzmacher
- Chapter 8. Sol–Gel Coatings for Optical and Dielectric Applications
M. R. Böhmer, A. R. Balkenende, T. N. M. Bernards, M. P. J. Peeters, M. J. van Bommel, E. P. Boonekamp, M. A. Verheijen, L. H. M. Krings, Z. A. E. P. Vroon

Volume 6. NANOSTRUCTURED MATERIALS

- Chapter 1. Electrochemically Self-Assembled Ordered Nanostructure Arrays: Quantum Dots, Dashes, and Wires
S. Bandyopadhyay, A. E. Miller
- Chapter 2. Mechanical Spectroscopy of Nanostructured Metallic Systems
Luca Pasquini
- Chapter 3. Soft Amorphous and Nanocrystalline Magnetic Materials
Frédéric Mazaleyrat, Richard Barrué
- Chapter 4. Nanoporous Materials for Microlasers and Microresonators
F. Laeri, J. U. Nöckel
- Chapter 5. Nanoporous Materials for Optical Applications
J. Sauer, F. Marlow, F. Schüth
- Chapter 6. Optical Properties and Impurity States in Nanostructured Materials
Raúl Riera, José L. Marín, Rodrigo A. Rosas
- Chapter 7. Confined Systems and Nanostructured Materials
José L. Marín, Raúl Riera, Rodrigo A. Rosas

Volume 7. LIQUID CRYSTALS, DISPLAY AND LASER MATERIALS

- Chapter 1. Liquid Crystals for Electro-Optic Applications
S. M. Kelly, M. O'Neill
- Chapter 2. Switchable Holographic Polymer-Dispersed Liquid Crystals
Richard L. Sutherland, Lalgudi V. Natarajan, Timothy J. Bunning, Vincent P. Tondiglia
- Chapter 3. Electrochromism and Electrochromic Materials for Displays
P. M. S. Monk
- Chapter 4. Materials for Solid-State Dye Lasers
A. Costela, I. García-Moreno, R. Sastre
- Chapter 5. Photophysical Properties of Laser Dyes: Correlations with the Lasing Characteristics
F. López Arbeloa, T. López Arbeloa, I. López Arbeloa
- Chapter 6. Interplay of an Anisotropy and Orientational Relaxation Processes in Luminescence and Lasing of Dyes
S. V. Sergeyev
- Chapter 7. Photosensitive Materials for Holographic Recording
S. Blaya, L. Carretero, R. F. Madrigal, A. Fimia

Volume 8. CONDUCTING POLYMERS

- Chapter 1. Synthesis, Electrical, and Optical Properties of Conjugated Polymers
Rafaël Kiebooms, Reghu Menon, Kwanghee Lee
- Chapter 2. Conjugated Polymer Films for Molecular and Ionic Recognition
Bruno Fabre
- Chapter 3. Polyacetylene and its Analogs: Synthesis and Physical Properties
Kristen J. Steenberg Harrell, SonBinh T. Nguyen
- Chapter 4. Synthesis, Properties, and Applications of Poly(*p*-Phenylene Vinylene)s
Jonas Gruber, Rosamaria Wu Chia Li, Ivo Alexandre Hümmelgen
- Chapter 5. Self-Organized Supramolecular Polymer Structures to Control Electrical Conductivity
Olli Ikkala, Gerrit ten Brinke
- Chapter 6. Spectroelectrochemistry of Conducting Polymers
Rudolf Holze
- Chapter 7. Electronic Spectra of Conjugated Polymers and Oligomers
Yukio Furukawa
- Chapter 8. Stability of Electrically Conducting Polymers
F. Mohammad

Volume 9. NONLINEAR OPTICAL MATERIALS

- Chapter 1. Calculations of Dynamic Hyperpolarizabilities for Small and Medium-Sized Molecules
David M. Bishop, Patrick Norman
- Chapter 2. Theoretical Approach to the Design of Organic Molecular and Polymeric Nonlinear Optical Materials
Benoît Champagne, Bernard Kirtman
- Chapter 3. Design and Characterization of Organic and Organometallic Molecules for Second-Order Nonlinear Optics
Etienne Goovaerts, Wim E. Wenseleers, M. Helena Garcia, Graham H. Cross
- Chapter 4. Photonic Crystals: Crystal Growth, Processing, and Physical Properties
M. D. Aggarwal, W. S. Wang, K. Bhat
- Chapter 5. Hyper-Rayleigh Scattering: Opportunities for Molecular, Supramolecular, and Device Characterization by Incoherent Second-Order Nonlinear Light Scattering
Koen Clays, André Persoons
- Chapter 6. Nonlinear Optical Properties of Fullerenes and Carbon Nanotubes
Rui Hua Xie
- Chapter 7. Third-Order Optical Nonlinearity in Polydiacetylene Waveguides at Telecommunications Wavelengths
A. Boyle, W. J. Blau
- Chapter 8. Organic Materials for Optical Limiting
Satya Ram Mishra, S. C. Mehendale
- Chapter 9. Bragg Gratings in Optical Fibers
Andreas Othonos, Kyriacos Kalli

Volume 10. LIGHT-EMITTING DIODES, LITHIUM BATTERIES AND POLYMER DEVICES

- Chapter 1. Organic and Polymer-Based Light-Emitting Diodes
Thien-Phap Nguyen, Pierre Destruel, Philippe Molinie

- Chapter 2. Optical Devices Based on Conductive Polymers
W. A. Gazotti, A. F. Nogueira, E. M. Giroto, L. Micaroni, M. Martini, S. das Neves, M.-A. De Paoli
- Chapter 3. Intercalation Compounds for Advanced Lithium Batteries
C. Julien, G. A. Nazri
- Chapter 4. Polymer Electrets for Electronics, Sensors, and Photonics
Simona Bauer-Gogonea, Siegfried Bauer
- Chapter 5. Charge-Transporting Polymers and Molecular Glasses
J. V. Grazulevicius, P. Strohriegl
- Chapter 6. Electrochemically Prepared Thin-Film Solar Cells
Figen Kadirgan

This Page Intentionally Left Blank

Chapter 1

SYNTHESIS, ELECTRICAL, AND OPTICAL PROPERTIES OF CONJUGATED POLYMERS

Rafaël Kiebooms

Institute for Materials Research, Limburg University, Diepenbeek, Belgium

Reghu Menon

Department of Physics, Indian Institute of Science, Bangalore, India

Kwanghee Lee

Department of Physics, Pusan National University, Pusan, Korea

Contents

1. Introduction	1
2. Synthesis	5
2.1. Polyacetylenes	6
2.2. Polyaromatics	8
2.3. Poly(<i>p</i> -phenylene vinylene)s	26
2.4. Polyanilines	32
2.5. Chemical Structure and Electronic Properties	33
3. Electrical Properties	47
3.1. Metallic State	49
3.2. Critical and Insulating States	60
4. Optical Properties	62
4.1. Theoretical Considerations	63
4.2. Optical Properties of "Doped" Conducting Polymers	65
4.3. Photophysics of Semiconducting Polymers	78
4.4. Electroluminescence in Conjugated Polymers: Polymer LED	81
4.5. Photoinduced Charge Transfer in Conjugated Polymer/Fullerene Composites	82
5. Concluding Remarks	84
Acknowledgments	86
References	86

1. INTRODUCTION

Polyconjugated carbon chains consist of alternating single (σ bonds) and double bonds (π bonds). The π electrons are highly delocalized and easily polarizable, features that play important roles in the electrical and optical properties of polyconjugated systems, making them rather different from conventional electronic systems. Moreover, the intrinsic quasi-one-dimensional nature and the extent of both intra- and interchain delocalization of π electrons are important for the structural, electrical, and optical properties of polyconjugated systems. The complex morphology of

polymers plays a crucial role in the physical properties. In general, the conjugation length, the strength of the interchain interaction, and the extent of disorder are some of the significant parameters that govern the physical properties of polyconjugated systems.

The behavior of polyconjugated systems is rather different with respect to conventional polymers. In the case of the latter materials (e.g., polyethylene), the number of monomer units in a chain mount up to several thousands or even millions. In many cases, conventional polymers are soluble in solvents, melt processible, highly tractable, etc. On the other hand, polyconjugated systems have, in general, a few hundreds of monomers in a chain. The

Handbook of Advanced Electronic and Photonic Materials and Devices, edited by H.S. Nalwa
Volume 8: Conducting Polymers

Copyright © 2001 by Academic Press

All rights of reproduction in any form reserved.

alternating single and double bonds make the chains rather stiff with respect to nonconjugated chains. As a consequence, polyconjugated systems are not as soluble and tractable, unless side groups are introduced in the main chain or dopant ions to impart solubility and processibility. These aspects are reflected in the processibility, mechanical, electrical, and optical properties of polyconjugated systems. The combination of the electronic and optical properties of semiconductors with the mechanical properties and processibility of polymers makes conjugated polymers rather unique and potentially useful for a wide array of applications [1–13]. The literature on conducting polymers has exploded during the 1990s to such an extent that providing a comprehensive overview is therefore a very challenging task additionally jeopardized by personal bias. This chapter examines important aspects of the synthesis, electrical, and optical properties of conducting polymers, but makes no claim to be exhaustive.

To develop polymers with specific electronics, it is necessary to have an insight into the available synthetic methods. For further developments in the field of conducting polymers, it is also important to gain a better understanding of the relationships between the chemical structure and the electronic properties (e.g., low bandgap) of these polymers. Despite two decades of research on conjugated polymers, the development of low-bandgap conjugated polymers, especially for electronic applications, still remains an important challenge for synthetic chemists. Gaining an understanding of the structure–property relationships is not only of importance for the development of low-bandgap conjugated polymers, but also for conjugated polymers in general. In this context, in addition to an extensive overview of synthetic principles for conjugated polymers, it seems appropriate to provide an in-depth discussion on the interplay between the chemical structure and the electronic properties of conjugated polymers.

Since the first experiments on polyacetylene, many different conjugated polymers have been synthesized. Section 2 starts with an overview of the major different synthetic methods, which are employed to prepare the most important classes of conducting polymers, still being investigated at present. A classification never pays tribute to all of the contributions that have been made, but nevertheless it should allow the lay scientist to assess the field more easily. Plenty of references have been provided to enable building up a knowledge base, which can be used for further actualization. In most cases, similar synthesis methods have been applied for the development of more exotic species, which have not found wide application but could still have potentially interesting properties. Finally, in Section 2 the discussion of principles concerning the control of electronic properties by means of the chemical structure will be held from two points of view. First, the relationship between structure and properties will be approached on the basis of theoretical concepts used in organic chemistry. Second, the discussion will be held within the framework of the development of low-bandgap conjugated polymers. More specifically, the research on polyisothianaphthene is used as a typical case study to illustrate this discussion. However, it needs to be stressed that these principles can be applied to any other conjugated material for the control of electronic properties.

Conducting polymers are partially crystalline and partially amorphous; hence, they consist of both delocalized and localized states. The delocalization of π electrons depends on the extent of disorder, interchain interactions, etc. The disorder-induced localization plays a dominant role in the metal–insulator (M–I) transition and transport properties of conducting polymers. Moreover,

the structure of the polyconjugated chain, interchain interaction, disorder, and doping level determine the stability of carriers such as solitons, polarons, bipolarons, and free carriers in doped conducting polymers. Hence, due to the coexistence of both delocalized and localized states, as well as the presence of various types of charge carriers, a wide range of behavior, from metallic to insulating regimes, can be observed in the transport properties of doped conducting polymers. The conductivity values of various π -conjugated polymers are summarized in Table I [14–133].

In this chapter, the electrical properties of doped conducting polymers are reviewed in Section 3. The temperature dependence of conductivity, magnetoresistance, thermopower, magnetic susceptibility, and specific heat of various conducting polymers, in the metallic, critical, and insulating regimes, are discussed. The transport properties in the metallic regime can be understood within the framework of the localization–interaction model. The anisotropic magnetoconductance in oriented metallic samples shows the presence of both weak localization and electron–electron interaction contributions in the low-temperature transport, and this can be used as a microscopic probe to estimate the misaligned chains. The Curie contribution to the low-temperature magnetic susceptibility can give a quantitative estimate of the spins trapped in the localized states. The field-induced transitions from the metallic to the critical regime and from the critical to the insulating regime indicate that the Fermi level and mobility edge are situated rather close.

A brief overview of the electrical transport properties of systems from the metallic and insulating regimes, for both oriented and unoriented samples, are also discussed. The suggested models are quite appropriate in understanding the experimental results. Nevertheless, more work is needed to sort out how the structural and morphological features influence the transport properties.

Undoped conjugated polymers have an anisotropic, quasi-one-dimensional electronic structure with a gap of typically 2–3 eV, corresponding to the conventional semiconductor gap size. As a result, undoped conjugated polymers exhibit the electronic and optical properties of semiconductors in combination with the mechanical properties of general polymers, making them potentially useful for a wide array of applications [4, 5]. In contrast with conventional inorganic semiconductors with rigid band, however, upon doping or photoexcitation the carriers are self-localized and form the nonlinear excitations on the polymer chains such as solitons, polarons, or bipolarons. Much of the new physics associated with conjugated polymers is related to the formation and properties of such nonlinear excitations [1–3]. Then, when conjugated polymers are doped to concentrations in excess of a critical concentration, the system undergoes a rapid transition from a nonlinear excitation state to a metallic state.

Although the electrical and optical properties of metallic conducting polymers have been investigated for over a decade, the nature of the metallic states and the corresponding metal–insulator transition are not fully understood. In Section 4, therefore, results are summarized on the optical spectroscopic measurements of the conducting polymers in the metallic regime and in the insulating regime near the metal–insulator transition. Next, since there is controversy over the nature of the primary photoexcitations in undoped conjugated polymers, their photophysical properties are examined through related experimental results. As an active potential application in the use of these materials, a review on the polymer light-emitting device (LED) is given, with an emphasis on the

Table I. Electrical Conductivities of Various π -Conjugated Polymers in Doped State

Polymer	Dopant	Conductivity (S cm ⁻¹)	Reference	
Polypyrrole	HClO ₄	4×10^2	[14]	
	HClSO ₃	2×10^2	[14]	
	FeCl ₃	2×10^4	[15]	
	AsF ₅	3.6×10^3	[16]	
	I ₂	1.7×10^4 – 1.7×10^5	[17–20]	
	K	5×10^3	[21]	
	Na	1.8×10^3	[21]	
	Rb	3×10^3	[21]	
	Catalyst			
	Ti(Obu) ₄ –AlEt ₃		3 – 4×10^4 – 10^5	[22–25]
	Be ²⁺ , Mg ²⁺ , Ca ²⁺ , Sr ²⁺ , Ba ²⁺ , Al ³⁺		0.002–30	[26]
	I ₂		8, 2	[27–29]
	Br ₂		5	[27–29]
	Cl ₂		0.5	[30]
	K ₂ S ₂ O ₈		—	[31]
	DDQ		7×10^{-2}	[32]
	FeOCl		—	[33]
	K ₃ Fe(CN) ₆		—	[34]
	FeCl ₃ · 6H ₂ O		25	[35]
	Fe ₂ (SO ₄) ₃ · 5H ₂ O		1	[35]
	Fe(NO ₃) ₃ · 9H ₂ O		36	[35]
	Fe(ClO ₄) ₃ · 9H ₂ O		33	[35]
	FeBr ₃		44	[35]
	CuCl ₂ · 2H ₂ O		8	[35]
	CuBr ₂		45	[35]
	FeCl ₃		110	[36, 37]
	FeCl ₃		190, 130	[36]
	FeCl ₃		20, 3	[36]
	FeCl ₃		3	[36]
	Fe(BF ₄) ₃		90	[38]
	Na ₃ (PO ₄ 12WO ₃)		1–10	[39]
	FeCl ₃		> 200	[40]
	FeCl ₃		> 100	[41]
FeCl ₃		10^{-2}	[42]	
Poly(octylpyrrole)	Cu(ClO ₄) ₂ , Fe(ClO ₄) ₃	1.6, 1.1	[43]	
Poly(<i>N</i> -methylpyrrole)	Fe(BF ₄) ₃	6×10^{-2}	[44]	
Polypyrrole	PF ₆	240–1500	[45, 46]	
	<i>p</i> -Toluene sulfonate	30	[48]	
	Fe(□) dodecylbenzene sulfonate	80	[49]	
	Sulfonated poly(β -hydroxyether)	3.2–13.4	[50]	
	Sulfonated poly(butadiene)	9.5	[50]	
	Benzene sulfonate	14.8	[50]	
	<i>p</i> -TSA	200–230	[51]	
	Iron(□) salt	2–10	[52]	
	Anionic ferrofluid	2.6×10^{-2} –1.9	[53]	
	ClO ₄ ⁻ , PF ₆ ⁻ · BF ₆ , TSO, HSO ₄	50–200	[54]	
	<i>p</i> -TSA	20	[55]	
	FeCl ₃	1.9–33.5	[56]	
	FeCl ₃	10^{-7} – 10^{-5}	[57]	
	—	10^2	[58]	
	Soluble polypyrrole	DBSA	5	[59]
Poly(3-phenylazopyrrole)	Diazonium salt	10^{-6} – 10^{-5}	[60]	

Table I. Continued.

Polymer	Dopant	Conductivity (S cm ⁻¹)	Reference
Polythiophene	ClO ₄	10–100	[61]
	BF ₄	0.02	[62]
	BF ₄	106	[63]
	AsF ₆	97	[63]
	ClO ₄	10	[64]
	ClO ₄	36	[65]
	ClO ₄	40	[66]
	BF ₄	270	[67]
	PF ₆	370	[68]
	Poly(3-methylthiophene)	PF ₆	1
SO ₃ CF ₃		30–100	[69]
ClO ₄		120	[70]
PF ₆		510	[67]
ClO ₄		750	[71]
ClO ₄		450	[72]
PF ₆		740	[73]
PF ₆		600	[74]
PF ₆		1975	[75]
Polythiophene		AuCl ₃	15
	NOSbF ₆	9 × 10 ⁻⁵	[77]
Poly(bithiophene)	NOSbF ₆	4 × 10 ⁻²	[77]
Thiophene/benzene copolymer	AsF ₅	1.2	[78]
5,5'''-Dimethylquarter thiophene	NOPF ₆	2.1 × 10 ⁻²	[79]
	NOBF ₄	4.4 × 10 ⁻²	[79]
Poly(3-octylthiophene)	NOPF ₆	0.05	[80]
	FeCl ₃	1–180	[80–83]
Poly(3-hexylthiophene)	FeCl ₃	10 ⁻⁸ –10 ⁻⁷	[84]
Polythiophene	I ₂	6–12	[85, 86]
	FeCl ₃	0.5	[87]
5,5'''Dimethylquarterthiophene	I ₂	0.1	[88]
Poly(3-methoxythiophene)	I ₂	1.8	[89]
Poly(3-butoxythiophene)	I ₂	2.1 × 10 ⁻²	[89]
Poly[3-(2-methoxy ethoxy)-thiophene]	I ₂	2.1 × 10 ⁻¹	[89]
Poly(thienylthiophene)	I ₂	315	[90]
Poly(3-phenylthiophene)	ClO ₄	6	[91]
Poly(bithiophene)	ClO ₄	8–10	[92]
Poly(3-decylthiophene)	ClO ₄	0.1	[93]
	FeCl ₃	5	[93]
Poly(2,5-thienylene ethynylene)	FeCl ₃	1 × 10 ⁻³	[94]
Poly(thienylene vinylene)	FeCl ₃	110	[90]
Poly(3,4-dibutoxythienylene vinylene)	FeCl ₃	1	[95, 96]
<i>p</i> -Terphenyl	Benz ⁺ K ⁺ d	4 × 10 ⁻⁵	[97]
	AsF ₅	6.8	[97]
<i>p</i> -Quarterphenyl	Benz ⁺ K ⁺ d	2 × 10 ⁻⁵	[97]
	AsF ₅	5.8	[1, 97]
<i>p</i> -Quinoqnephenyl	AsF ₅	7.4	[1, 97]
<i>p</i> -Sexiphenyl	Benz ⁺ K ⁺ d	0.5	[1, 97]
Poly(<i>p</i> -phenylene)	AsF ₅	500	[1, 98, 99]
	FeCl ₃	0.30	[100]
	MoOCl ₄	20	[1]
	NOBF ₄	70	[1]

Table I. Continued.

Polymer	Dopant	Conductivity (S cm ⁻¹)	Reference
	SbCl ₅	< 10 ⁻³	[101]
	SbF ₅	—	[102]
	I ₂	< 10 ⁴	[103]
	SO ₃	10 ⁻¹ –10 ⁴	[104]
	AlCl ₃	8	[105]
	Naph K ⁺ e	50	[99]
	Naph Li	5	[1]
	AsF ₅	50	[97]
	I ₂	2.2 × 10 ⁻¹⁰	[106]
	Divalent cations	0.1	[107]
Poly(2-butoxy-5-methoxy-4-phenylene vinylene)	FeCl ₃	5.7 × 10 ²	[108]
Poly(phenylene vinylene)	SO ₃	10	[109]
Poly(<i>p</i> -phenylene vinylene co-2,5-thienylene vinylene)	HCl	10 ⁻¹¹ –10 ⁻⁹	[110]
Halogenated poly(phenylene vinylene)	FeCl ₃	10 ⁻¹ –72	[111]
Poly(2-methoxy-1,4-phenylene vinylene)	I ₂	3.2	[112]
Poly(2,5-diheptyl-1,4-phenylene vinylene)	Sulfur trioxide	2.7 × 10 ⁻³	[113]
	Antimony pentafluoride	2.8 × 10 ⁴	[114]
Poly(1,4-phenylene-1,3,5-hexatricnylene)	I ₂	0.50	[115]
Poly(phenylene vinylene)	FeCl ₃	35	[114]
Polyaniline	HCl	210(∥) 23(□)	[115]
	HCl	1 × 10 ²	[116]
Poly(<i>o</i> -toluidine)	HCl/HNO ₃ /H ₂ SO ₄ C/H ₃ COOH/H ₃ PO ₄	2.2 × 10 ⁻¹³ –3.4 × 10 ⁻²	[117]
Sulfonic acid-substituted aniline	Fe(□)	10 ⁻¹ –10 ⁻²	[118]
Poly(dimethylaniline)	HClO ₄	10 ⁻¹ –10 ⁻⁷	[119]
Polyaniline	CSA/ <i>m</i> -cresol	100	[120]
Chlorinated polyaniline	HCl	4.3 × 10 ⁻⁴	[121]
Polyaniline	HCl	3.8 × 10 ⁻⁴ –1.3	[122]
	HCl/CSA/DBSA/MSA	10 ¹ –220	[123]
	H ₃ PO ₄	58	[124]
Poly(<i>N</i> -alkylaniline)	HBF ₄	9 × 10 ⁻⁴ –5.7 × 10 ⁻²	[125]
Cross-linked polyaniline	—	10–10 ²	[126]
Polyaniline	Phosphotungstic acid	0.3	[127]
	CSA/DBSA	100	[128]
	Phosphoric acid	40	[129]
	HCl	350	[130]
	Diphenyl phosphate	65	[131]
Poly(<i>o</i> -methoxyaniline)	TSA/DSA/DBSA	0.1	[132]
Poly(<i>p</i> -bromoaniline)	Pristine polymer	3.0 × 10 ⁻⁷	[133]
	HCl	1.0 × 10 ⁻⁶	[133]
	I ₂	1.1–1.3 × 10 ⁻⁵	[133]

limiting factors for device performance. Finally, the basic photo-physical phenomena of “photoinduced charge transfer” in the conjugated polymer/fullerene composites are reviewed, with a brief introduction into many potential applications of these phenomena.

2. SYNTHESIS

Since the first demonstration of electrical conductivity in polyacetylene upon doping [15–17], several other types of conju-

gated polymers such as polyacetylene, poly(*p*-phenylene), polythiophene, polypyrrole, poly(*p*-phenylene vinylene), and polyaniline (Fig. 1) have been developed. Many applications have emerged among which the development of light-emitting devices (LEDs) is probably the most successful example [134].

The results of the research on these materials have been extensively reviewed in the literature [1–13, 135–138]. One of the advantages of organic materials is the possibility for unlimited chemical modifications. As a consequence, in many cases the reader tends to get lost in elaborate enumerations of the many derivatives and

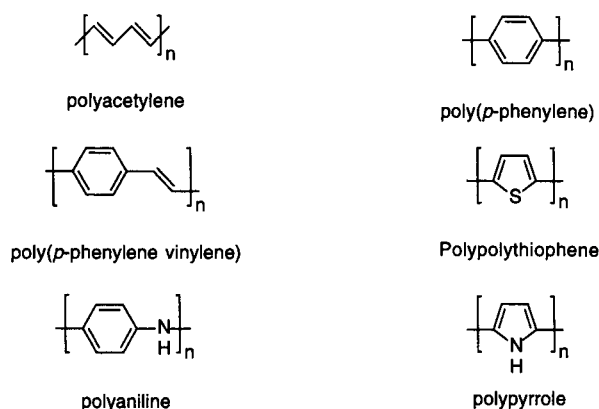


Fig. 1. Basic chemical structures of some of the most common conducting polymers.

their properties. In this section, the focus has been rather on identifying the different synthetic procedures and the application of those procedures to prepare different polymer species. However, references have been provided to enable retrieving information on derivatives of interest.

An important issue for further advancements in the field of plastic electronics is the development of stable polymeric materials with control of their electronic properties. One of those electronic properties is the bandgap (E_g). The reduction of E_g will enhance the thermal population of the conducting band and thus increase the number of intrinsic charge carriers. This would allow one to avoid oxidative or reductive doping in order to obtain intrinsic electrical conductivity. The lower oxidation potential associated with the narrow gap will also result in a stabilization of the corresponding doped state. Furthermore, the redshift of absorption and emission spectra resulting from a decrease in E_g leads to materials becoming transparent in the doped state [137]. To develop such low-bandgap polymers, for example, it is necessary to have a better understanding of the relationships between the chemical structure and the electronic properties of conjugated polymers. Such an understanding is not only of importance for the development of low bandgap conjugated polymers but also for conjugated polymers in general. Despite two decades of research on conjugated polymers, the development of low-bandgap conjugated polymers for electronic applications still remains an important challenge for synthetic chemists. An in-depth discussion on the principles of control of the electronic properties in conjugated materials will be presented from two points of view. First, the relationship between structure and properties will be approached on the basis of theoretical concepts used in organic chemistry. Second, the discussion will be held within the framework of the development of low-bandgap conjugated polymers. More specifically, we shall mainly benefit from the results of the research on poly(isothianaphthene) to illustrate our discussion, although these principles can be applied to any other conjugated material for the control of specific electronic properties.

2.1. Polyacetylenes

Polyacetylene (Fig. 2) is the simplest polyconjugated polymer consisting of repeating $[-(\text{CH}=\text{CH})_n-]$ units. Polyacetylene was first prepared as a linear, high-molecular-weight, polyconjugated polymer of high crystallinity and regular structure by Natta et al. [139],

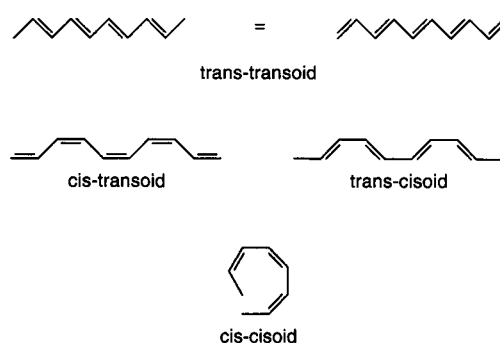


Fig. 2. Possible structures of polyacetylene.

who polymerized acetylene in hexane using $\text{Al}(\text{Et})_3/\text{Ti}(\text{OpPr})_4$ as the initiator system. For a long time, however, polyacetylene was considered of little interest because, irrespective of the method of preparation, it was obtained as an air-sensitive, infusible, and insoluble black powder. It thus remained basically a material subject to academic research by organic chemists [140, 141], polymer chemists [142–146], and theoreticians [147–149], who saw it as an infinitely long conjugated molecule in which one would expect the one-dimensional π electrons to form a half-filled band leading to metallic behavior [150–152].

Interest in polyacetylene increased in the 1970s when the group of Shirakawa developed a simple method for preparing thin-film samples [153], which on treatment with oxidizing agents, such as halogens or AsF_5 , exhibited significant electrical conductivity [154, 155]. These developments can be considered as the birth of the field of conducting polymers with metallic properties. A large amount of the literature on polyacetylene has been summarized in several specialized books and review articles [156–162].

There are a variety of routes toward the synthesis of polyacetylene. These syntheses can be classified into four categories: catalytic polymerization of acetylene, noncatalytic polymerization of acetylene, catalytic polymerization of monomers other than acetylene, and, finally, precursor methods.

2.1.1. Catalytic Polymerization of Acetylene

Ziegler–Natta Catalysts. The polymerization reactions of acetylene that produce not only a polymeric material, cuprene, but also oligomers such as benzene, cyclooctatetraene, and vinyl acetylene have been known for many years [163]. Although a wide variety of catalysts are effective for producing polyacetylene, they are often characterized by the simultaneous formation of cyclic oligomers. Upon selection of a suitable catalyst system, several factors have to be taken into account, such as high selectivity and solubility. Among the available catalysts [161], the preferred one is the combination of $\text{Ti}(\text{O}-n\text{-C}_4\text{H}_9)_4$ and $(\text{C}_2\text{H}_5)_3\text{Al}$ because it is soluble in organic solvents and highly active for acetylene polymerization to produce crystalline polyacetylene in the form of mechanically strong freestanding films. The synthetic process was developed by the group of Shirakawa [153], who employed a very high concentration of the $\text{Ti}(\text{O}-n\text{-C}_4\text{H}_9)_4-(\text{C}_2\text{H}_5)_3\text{Al}$ catalyst and allowed acetylene to polymerize on the free surface of the catalyst solution or on the wall of the reaction flask on which the catalyst solution is coated (Fig. 3). By variation of the reaction conditions, polyacetylene films of different quality can be obtained [164–168].

The aforementioned procedure yields polyacetylene that is mainly *cis*. Baker et al. [169] prepared almost pure *trans* polymer

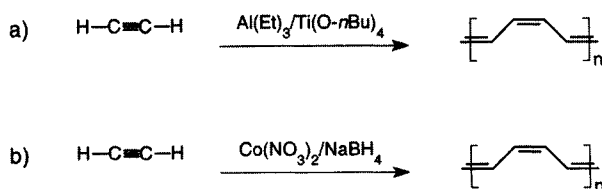


Fig. 3. Catalytic polymerization of acetylene using (a) Ziegler-Natta and (b) Luttinger catalysts, respectively.

by reducing the Al/Ti ratio to unity and omitting the catalyst aging step. Polyacetylene containing an approximately equal proportion of *cis* and *trans* was prepared by the group of Naarmann [170]. They also produced stretchable films with iodine conductivities of 10^5 S cm^{-1} [171]. A further modification by Tsukamoto et al. [172, 173] yielded highly stretchable films with similar high conductivities.

Luttinger Catalysts. Luttinger catalysts consist of a hydridic reducing agent, such as sodium borohydride, plus a salt or complex of a group VIII metal, such as nickel chloride. Reactions carried out with these catalysts yield high-molecular-weight polyacetylene with no indication of the formation of cyclic oligomers [141]. It has been reported that nickel halide-tertiary phosphine complexes are also effective catalysts for the polymerization of acetylene [140]. $\text{Co}(\text{NO}_3)_2$ and binuclear rhenium complexes together with sodium or potassium borohydride also catalyze the polymerization of acetylene [174–177] (Fig. 3). An important aspect to note is that a hydrophilic solvent such as ethanol, tetrahydrofuran (THF), acetonitrile, and even water can be used as a solvent for the Luttinger catalysts, in contrast to the requirement of rigorously dehydrated hydrocarbon solvents for the Ziegler-Natta catalysts and metathesis catalysts. However, the catalytic activity of the Luttinger catalysts is much lower than that of standard Ziegler-Natta catalysts. In general, the *cis*-rich polyacetylenes prepared from Luttinger or Ziegler-Natta catalysts do not differ with regard to overall morphology and other properties. Lieser et al. [178] found, however, a significant difference in chemical reactivity upon exposure to chlorine and bromine.

Metathesis Catalysts. Aldissi et al. [179] demonstrated the formation of uniform films on the quiescent surface of a concentrated solution of a soluble catalyst prepared by mixing equimolar amounts of WCl_6 and $(\text{C}_6\text{H}_5)_4\text{Sn}$ in toluene. A combination of MoCl_5 with $(\text{C}_6\text{H}_5)_4\text{Sn}$ also gave a soluble catalyst, but the catalytic activity was too low to give a uniform film. A more active tungsten catalyst was prepared by Theophilou et al. [180], who used *n*-BuLi as a co-catalyst instead of $(\text{C}_6\text{H}_5)_4\text{Sn}$.

Single-Component Catalysts. There is not always a need for a catalyst and co-catalyst system. Several metal complexes alone, such as tetrabenzyltitanium, are reported to be active for acetylene polymerization. Hsu et al. [181] used a Ti-Ti complex to obtain *cis*-rich or *trans*-rich polyacetylene, depending on the temperature. Alt et al. [182] demonstrated that $\text{Cp}_2\text{Ti}(\text{PMe}_3)_2$ reacts readily with acetylene. Martinez et al. [183] also found that titanium compounds polymerize acetylene to yield *trans*-rich polyacetylene at lower temperatures.

Rh and Re Catalysts. Chlorine-bridged Rh(I) complexes such as $[\text{Rh}(\text{COD})\text{Cl}]_2$ and $[\text{Rh}(\text{NBD})\text{Cl}]_2$, where COD is cycloocta-1,5-

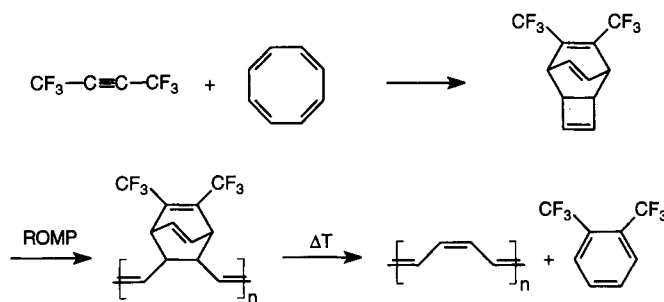


Fig. 4. Durham precursor route to polyacetylene.

diene and NBD is bicyclo[2.2.1]hepta-2,5-diene, in the presence of sodium ethoxide as a co-catalyst can initiate the polymerization of acetylene. The advantage of Rh(I) complexes over the Ziegler-Natta catalysts is that they are stable in air and their catalytic activity is not inhibited by the presence of oxygen and/or moisture [184].

2.1.2. Noncatalytic Polymerization of Acetylene

Electrochemical synthesis has been carried out under different conditions [185]. Acetylene polymerization also occurs on the surface of metal oxides such as TiO_2 and Al_2O_3 to give *trans*-polyacetylene [186–188]. Polyacetylene has been prepared as thin films by exposing acetylene gas to a small amount of AsF_5 [189] or by using AsF_3 [190] as the solvent. Irradiation of acetylene gas with ultraviolet (UV) or ionizing radiation has been shown to produce polyacetylene [191]. Spontaneous polymerization occurs above pressures of 3.5 GPa [192–195].

2.1.3. Catalytic Polymerization of Monomers Other Than Acetylene

Korshak et al. [196] synthesized polyacetylene films by ring-opening polymerization of 1,3,5,7-cyclooctatetraene with a metathesis catalyst, $\text{W}[\text{OCH}(\text{CH}_2\text{Cl})_2]_n\text{Cl}_{6-n}-(\text{C}_2\text{H}_5)_2\text{AlCl}$ ($n = 2$ or 3). Klavetter and Grubbs [197] developed a versatile and convenient route to polyacetylene through condensed phase polymerization of the monomer with well-defined metathesis tungsten-based catalysts.

2.1.4. Precursor Methods

The inherent insolubility and infusibility of polyacetylene coupled with its sensitivity to air imposes a barrier to the processibility of the polymer. As a result, considerable efforts have been directed toward obtaining polyacetylene from workable, easily processible polymers by means of polymer analogous transformations. In particular, the synthesis of polyacetylene from the dehydrohalogenation of poly(vinyl chloride) has attracted a lot of attention but the polymers prepared by this route generally possess relatively short conjugated segments and contain structural defects and cross-links [198, 199].

Another approach involves the use of prepolymers that can be thermally converted to polyacetylene. This approach was first followed by the group of Feast [200–211] (Fig. 4).

The process consists of three steps. The first step is the synthesis of the monomer 7,8-bis(trifluoromethyl)tricyclo[4.2.2.0^{2,5}]deca-3,7,9-triene by a thermal cycloaddition reaction between hexafluoro-

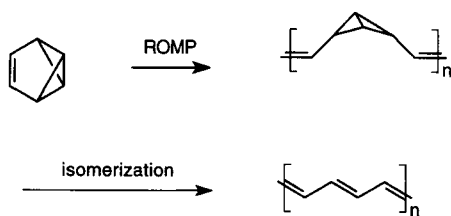


Fig. 5. Synthesis of polyacetylene by isomerization of polybenzvalene.

robust-2-yne and cyclooctatetraene. The second step is the polymerization reaction carried out in the presence of ring opening metathesis polymerization (ROMP) initiators, such as $WCl_6/SnMe_4$, which act only on the strained four-membered ring to form a high-molecular-weight precursor polymer. This precursor polymer is soluble in common organic solvents and can be purified, characterized, and processed by conventional methods. In the last step, the precursor polymer is thermally converted to polyacetylene. This is a rather complex process involving an exothermic symmetry-allowed elimination with the formation of a new *cis* double bond and hexafluoro orthoxylene. The *cis* double bond isomerizes to *trans* and the xylene migrates through the film and evaporates, resulting in a large loss in mass and contraction in volume. By controlling the conversion reaction protocol (temperature, time, pressure, mechanical stress, and presence of solvent), the morphology of the final product can be regulated.

Knoll and Schrock [212] developed a series of well-defined ROMP initiators of the type $M(CH-t-Bu)(NAr)(O-t-Bu)_2$, in which $M = W$ or Mo and $Ar = 2,6-C_6H_3-i-Pr_2$, that allows better control over this polymerization reaction and allows the controlled introduction of end groups [213] to the polymer chain.

Swager et al. [214] demonstrated an alternative precursor route to polyacetylene in which the production of volatile byproducts is avoided. The method involves the ring-opening polymerization of benzvalene and the subsequent catalytic isomerization to polyacetylene of low crystallinity (Fig. 5).

2.1.5. Soluble Polyacetylenes

Irrespective of the method adopted for its synthesis, polyacetylene itself is an insoluble, infusible, and generally intractable material. To obtain soluble polyacetylene analogs, substituted acetylenes have been polymerized to yield polymers with side groups attached to the conjugated backbone replacing the hydrogen atoms. An extensive review on substituted polyacetylene has been provided by Gibson [215]. In most cases, these materials are soluble, but the optical absorption maximum of the resulting polymer is higher in energy than that observed for polyacetylene, indicating a lower effective conjugation length. Furthermore, the electrical conductivity of substituted polyacetylenes is generally lower than that of polyacetylene itself.

2.2. Polyaromatics

2.2.1. Poly(*p*-phenylene)s

Poly(*p*-phenylene) (Fig. 6) continues to receive considerable attention due to its interesting properties, such as thermal stability in the neutral state, resistance to environmental oxidation and irradiation, wide conductivity range upon doping, possibility for *n*

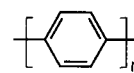


Fig. 6. Structure of poly(*p*-phenylene).

or *p* doping, and blue electroluminescence. Due to its rigid rod-like structure, poly(*p*-phenylene) is rather insoluble in commonly available solvents. Processibility of this material without loss of its properties is therefore a major challenge. It is therefore understandable that direct synthesis routes of poly(*p*-phenylene) do not produce polymers with high molecular weights and long linear chains.

The chemical oxidation of benzene was investigated in the early 1950s, and generally unidentified black products were obtained. Similarly, the electrochemical oxidation of benzene was investigated in the 1960s. The formation of black deposits was observed, but only much later was it realized that benzene was being polymerized, and not until the beginning of the 1980s was electrosynthesis developed with the view of producing poly(*p*-phenylene) films on metallic substrates.

Many chemical reaction schemes have been proposed and they can be classified as follows: direct oxidation of benzene, organometallic coupling, precursor methods, and electrochemical syntheses [135, 158, 216–224].

2.2.1.1. Direct Oxidation of Benzene

This procedure consists of the dehydrocoupling of benzene nuclei by catalyst–oxidant systems, leading to the formation of C–C bonds. The reagent used to carry out the polymerization is either a binary system consisting of a Lewis acid and an oxidant or a single reagent with both Lewis acid and oxidizing properties. The main disadvantages of this method are that polymers with rather low molecular weights are obtained and the materials still contain large amounts of impurities.

Binary Catalyst–Oxidant Systems. $AlCl_3$ as the Lewis acid (catalyst) and $CuCl_2$ as the oxidizing agent was the best catalyst–oxidant combination used by Kovacic et al. [225–227] for the polymerization of benzene (Fig. 7). Polymerization occurs under mild conditions (36–37°C, 15 min) with water as a co-catalyst. The yield of poly(*p*-phenylene) seems to depend on the $AlCl_3$ to $CuCl_2$ ratio. Several catalyst–oxidant systems and the influence of the catalyst–oxidant ratio on the polymerization of benzene have been studied [135]. These various studies indicate that a wide variety of catalyst systems are suitable for the polymerization of benzene to poly(*p*-phenylene). Typically, various oxidizing agents such as MnO_2 , PbO_2 , NO_2 [228], *p*-benzoquinone, chloranil, air, N_2O_3 , or nitrobenzene can be associated with a Lewis acid such as $AlCl_3$. Generally, poly(*p*-phenylene)s obtained under Kovacic's conditions are powdery materials exhibiting a certain crystallinity. A slight modification of the Kovacic procedure was investigated by using $CuCl-AlCl_3$ in the presence of oxygen [229]. Another variation of the Kovacic method was proposed by Kobryanskii and Arnoutov [230], who synthesized poly(*p*-phenylene)s with controlled molecular weights by using an ionic liquid as the solvent. Typically, $AlCl_3$ –butylpyridinium chloride (2:1) constituted an ionic medium in which $CuCl_2$ was dissolved. By controlled addition of benzene at room temperature, poly(*p*-phenylene) derivatives with high molecular weights were obtained.

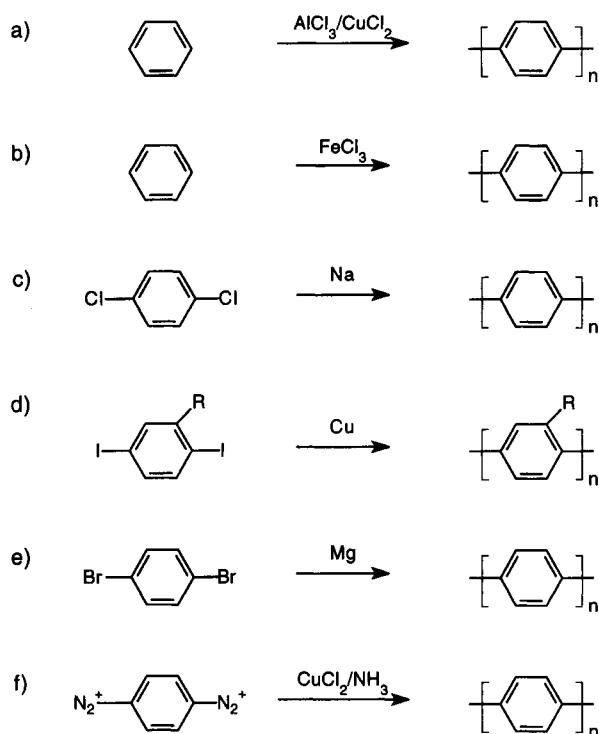


Fig. 7. Direct syntheses of poly(*p*-phenylene): (a) Kovacic's double-catalyst method, (b) single-catalyst method, (c) Wurtz–Fittig method, (d) Ullmann method, (e) Grignard method, and (f) diazonium method.

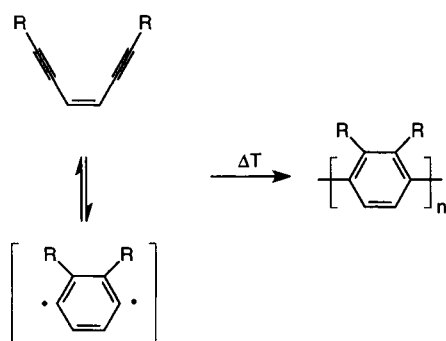


Fig. 8. Bergman cyclization.

1,4-Cycloadditions of bicyclopentadienones with bisacetylenes can yield high-molecular-weight polymers [223, 231, 232]. Low-molecular-weight poly(*p*-phenylene)s containing ethynyl branches were prepared by polycyclotrimerization of diacetylene in the presence of $\text{Al}(i\text{-Bu})_3$ and TiCl_4 . Other substituents can be introduced by using an appropriately substituted acetylene [233–235].

Single-Catalyst Systems. In this case, the reagent used to polymerize benzene has the properties of both a Lewis acid and an oxidizing agent. The most usual catalysts are FeCl_3 , MoCl_5 , AsF_5 , and SbF_5 associated with water as co-catalyst, which appears to determine the polymerization kinetics (Fig. 7) [190, 236–241].

Other Direct Syntheses. One route to substituted poly(*p*-phenylene) derivatives makes use of the Bergman cyclization of enedynes (Fig. 8). Thermal treatment of the enediyne yields poly(*p*-phenylene) derivatives with molecular weights of 1500–2500 [242].

2.2.1.2. Organometallic Coupling Reactions

A large variety of reactions based on the coupling of 1,4-disubstituted aromatic monomers in the presence of various metals have been investigated. The earlier syntheses of poly(*p*-phenylene) using metal-catalyzed coupling reactions have been reviewed by Noren [221]. Progress has been made since then and several new routes have emerged in the literature. Among them, there are two important methods. First, Ni compounds promote the coupling of various 1,4-disubstituted aromatic monomers, extensively investigated by Yamamoto et al. The second method is based on the Suzuki reaction, which consists of coupling aromatic boronic acids with halogenated aromatic compounds in the presence of a Pd(0) catalyst.

Syntheses Using Metal-Catalyzed Coupling Reactions One of the first syntheses of poly(*p*-phenylene) was reported in 1949 by Goldfinger [243], who used a Wurtz–Fittig reaction (Fig. 7).

The Ullmann reaction (Fig. 7) was also attempted for the synthesis of poly(*p*-phenylene), but only low-molecular-weight products with structural irregularities were obtained. The Ullmann reaction, however, was found suitable for the polymerization of substituted phenylenes such as methyl-, nitro-, and perfluorophenylene [244–247].

The Grignard method of polymerization (Fig. 7) was also used in the preparation of polyphenylenes. This reaction usually yields higher molecular weight polymers, but seems to be less efficient [248–252].

Dilithiobenzene and dilithiobiphenyl were coupled using a wide variety of metal halides but produced only low-molecular-weight materials. The polymerization of 1-bromo-4-lithiobenzene upon treatment with hexamethylphosphoramide was also reported [251–255].

Poly(*p*-phenylene) contaminated with small amounts of bridging diazo groups was prepared by heating the bisdiazonium salt of *p*-diaminobenzene in ammoniacal Cu^+ or Fe^{2+} (Fig. 7). In this case, the polymerization mechanism was thought to involve homolytic cleavage of the carbon to diazonium group bonds followed by C–C coupling [256].

Several other reactions have been described, but in general they appeared to be rather unsuccessful [221].

Ni-Catalyzed Coupling Reactions: Yamamoto and Colon Methods.

Yamamoto [257, 258] filled the need for a more efficient and versatile route to poly(*p*-phenylene). Results indicating that transition metals or their complexes catalyze the coupling of Grignard reagents with aryl halides [259–263] were adapted to the coupling of dihalogenoaromatic compounds (Fig. 9). Mild conditions, high selectivity, and quantitative yields were reported to be achieved when transition-metal catalysts were applied to the preparation of various organic aromatic compounds. Indeed, *p*-dibromobenzene was readily dehalogenated and coupled in the presence of Mg and transition-metal compounds, yielding poly(*p*-phenylene) with strictly linear chains. A variety of transition-metal complexes catalyze the reaction but the most efficient catalysts seem to be Ni(II) complexes. In particular, the use of $\text{NiCl}_2(\text{bpy})$, where bpy is 2,2'-bipyridine, leads to high yields under mild conditions. $\text{NiBr}_2(\text{PPh}_3)_2$ and $\text{PbCl}_2(\text{bpy})$ also show high catalytic activities. Of the dialobenzenes, *p*-dibromobenzene proved to be better than *p*-diiodobenzene or *p*-dichlorobenzene. Attempts to use Li instead of Mg as the dehalogenating reagent were unsuccessful [263–271].

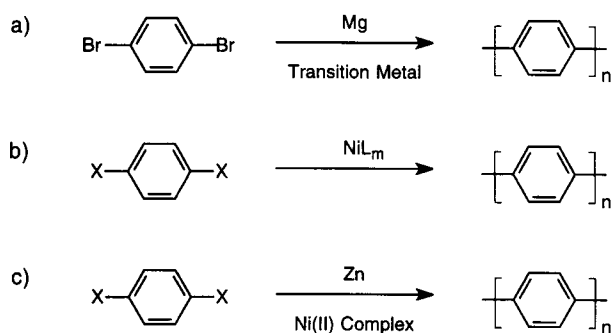


Fig. 9. Ni-catalyzed coupling reactions: (a), (b) Yamamoto, and (c) Colon (X = Cl, Br, I).

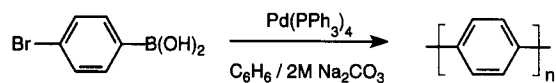


Fig. 10. Pd-catalyzed coupling reactions: Suzuki coupling.

The Yamamoto procedure can also be used to obtain substituted poly(*p*-phenylene). For example, Rehahn et al. [272] investigated the applicability of the Yamamoto procedure to 1,4-dibromobenzenes bearing flexible side chains at carbons 2 and 5.

Yamamoto et al. [273] also presented another route to poly(*p*-phenylene) using Ni(0) as a dehalogenating reagent (Fig. 9). This reaction proceeds under mild conditions and can be applied to a wide range of aromatic compounds, including those with carbonyl and cyano groups. On the basis of this method and the work of Semmelhack and co-worker [274–276], 1,4-dibromo-2,5-bis(4-decyloxybenzoyl)benzene has been polymerized in high yield but with a low degree of polymerization [277]. The keto side groups are not affected by the polymerization process. The procedure, however, suffers from severe limitations: the necessity of stoichiometric amounts of expensive Ni(0) reagents and their air sensitivity.

Several modifications of this reaction have been proposed for the coupling of aryl halides [278–290]. Colon and Kelsey [291] reported that aryl coupling can be realized in high yield using an excess of a reducing metal such as Zn, Mn, or Mg and a catalytic amount of Ni(II) complex (Fig. 9). The advantages of this procedure are that it can rapidly be performed in high yield with chlorides instead of bromides and iodides, all reagents are air stable, and a wide range of substituents are unaffected by the reaction conditions. Direct synthesis of unsubstituted poly(*p*-phenylene) has not been reported, but indirect synthesis has been achieved via a processible substituted poly(*p*-phenylene) [292]. Phillips et al. [293] reported the polymerization of 2,5-dichlorobenzophenone by the Colon procedure. The molecular weight was higher than that of the same product reported in [294, 295].

An interesting alternative to the Colon procedure was presented by Percec and co-workers [296, 297]. They investigated the Colon-type, Ni(0)-catalyzed homocoupling of substituted phenylenebistriflates, which are easily obtained from hydroquinones or bisphenols. They also investigated the effect of alternative leaving groups such as arylsulfonates [298].

Pd-Catalyzed Reactions: Suzuki Coupling. The Suzuki [299] and Miller [300] reactions are based on the use of Pd catalysts to couple various bromobenzene derivatives with benzene boronic acid

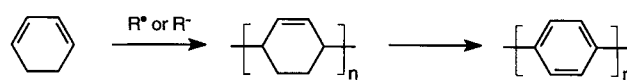


Fig. 11. Marvel's precursor method for poly(*p*-phenylene).

(Fig. 10). This reaction is described as being highly selective and quantitative. The influence of substituents attached to the *ortho* position was reported to be negligible.

Improved synthesis on the basis of this chemistry was achieved in the preparation of poly(*p*-2,5-di-*n*-hexylphenylene). The polymer was obtained with high molecular weight and appeared to be all *para* linked. A large variety of alkyl-chain-substituted poly(*p*-phenylene)s were synthesized according to this method. Copolymerization of substituted and unsubstituted monomers was also investigated [272, 301]. This method has been recognized as a very efficient means of coupling starting materials with a wide variety of *ortho* functional groups. Monomers containing nitro, keto, or ether functions can be condensed without any complication. Relatively high degrees of polymerization can be achieved and keto substituents appear to increase the rate of aryl–aryl coupling considerably.

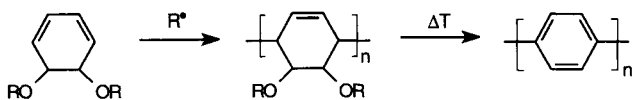
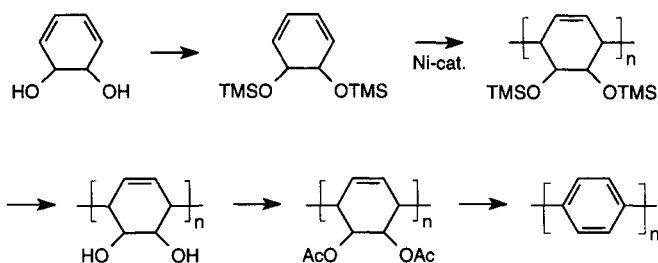
The possibility of obtaining substituted poly(*p*-phenylene)s using water as a solvent has been demonstrated [302, 303]. The synthesis of poly(*p*-phenylene) with $-\text{CH}_2\text{Br}$ substituents opened up the field of new poly(*p*-phenylene)s with polar side groups [304–306]. A poly(*p*-phenylene) decorated with Fréchet-type dendritic fragments of the first and second generation has also been synthesized [307, 308]. The availability of substituted poly(*p*-phenylene) has influenced the research toward ladder-type polymers. The ladder-type frame is obtained in a two-step process consisting of, in a first step, the formation of a suitable functionalized open-chain precursor followed by subsequent ring closure [277, 309–313]. Extensive research efforts have focused on the synthesis of ribbon-type structures consisting of an alternating series of fused six- and five-membered rings. Several of these ladder-type polymers have been synthesized through the general strategy of using substituted poly(*p*-phenylene) precursors [314, 315].

2.2.1.3. Precursor Methods

As a consequence of the insoluble character of conjugated polymers in general, methods in which a well-characterized precursor polymer is transformed in a final step into the fully conjugated target material have attracted increasing research efforts. Three methods have been reported: Marvel's precursor, the ICI route, and the related route proposed by Grubbs.

Marvel's Precursor. Marvel's precursor concept for the synthesis of poly(*p*-phenylene) dates back to the late 1950s (Fig. 11). The route is characterized, however, by several problems such as low molecular weight, poor regiochemical control, lack of stereochemical control, and poor control of the final aromatization process. This strategy nevertheless contains all the important features also found in more modern approaches to precursor polymers for poly(*p*-phenylene): the use of a cyclohexadiene monomer, its chain-growth polymerization to furnish the precursor polymer, and the precursor's subsequent aromatization to poly(*p*-phenylene) [316, 317].

ICI Precursor. Ballard et al. [318] developed a new monomer based on cyclohexadiene. They were looking for a monomer with

Fig. 12. ICI precursor method for poly(*p*-phenylene).Fig. 13. Grubbs precursor method for poly(*p*-phenylene).

functional groups that could not only be carried through the polymerization, but also could allow for clean aromatization to take place. One such approach is to incorporate in the monomer two ester functions that in organic chemistry are known to allow for the generation of unsaturation upon pyrolysis (Fig. 12). Synthesis of such monomers is rather work intensive. This problem was elegantly solved by the ICI chemists through application of biotechnological techniques. A genetically modified microorganism known as *Pseudomonas putida 11767* is able to oxidize benzene without subsequent aromatization. The monomer is polymerized using radical initiators. The use of radical initiators, however, allows limited regio- and stereospecific control during polymerization. It is also difficult to control molecular weight and distribution. Despite these inconveniences, high-molecular-weight polymer was obtained, which could be processed into films and fibers. Aromatization, however, furnished a rather ill-defined, low-molecular-weight phenylenic material as a consequence of the inherent structural defects present in the precursor polymer. The so-obtained polymer was, however, far superior to Marvel's poly(*p*-phenylene) [318–320].

Grubbs Method. As radical initiators did not lead to the desired result, transition-metal complexes were considered as potential initiators. The π -allyl Ni complex bis[η^3 -allyl](trifluoroacetato)nickel(II), which is an excellent catalyst for 1,3-butadiene, however, only led to aromatization of the monomer used in the ICI route. After an intensive search, Gin et al. [321–323] found that silylated dihydroxycyclohexadiene was a monomer compatible with a π -allyl Ni complex (Fig. 13). Two factors seem to be responsible for this. First, the steric effect of the trimethylsilane group prevents the oxygen atoms of the monomer from coordinating to the catalyst and interfering with the polymerization. Second, trimethylsilane ethers are very poor leaving groups compared to esters and carbonates, a feature that inhibits aromatization of the monomer and subsequent catalyst decomposition. All that remained to be done after polymerization was to convert the trimethylsilane ether groups to esters, which are needed for aromatization, by using tetra-*n*-butylammonium fluoride in methanol, followed by treatment with acetic anhydride and catalytic amounts of base. The conversion to poly(*p*-phenylene) is done by heating the precursor to 340°C under vacuum. This seems to lead, however, to significant chain fracture. When acid-catalyzed bulk pyrolysis techniques are used, a polymer with chemically well-defined

structure is obtained and under specific circumstances chain fracture can be avoided. There are indications that using polyphosphoric acid to catalyze the elimination should yield higher quality polymers [321–323].

Other Precursor Methods. The thermal eliminative ring closure of 1,4-diphenyl-3-(*N,N*-dimethylamino)-hex-5-en-1-yne has been shown to give terphenyl [324]. By an analogous method, the poly(*N,N*-dimethylamino)-hex-5-en-1-yne derivative affords phenyl-substituted poly(*p*-phenylene)s on pyrolysis [325].

2.2.1.4. Electrochemical Synthesis

Electrosynthesis is a valuable technique for obtaining conducting poly(*p*-phenylene) films of controlled thickness [326]. Although the technique seems to be quite simple, the structure and the properties of the poly(*p*-phenylene) derivatives will depend significantly on the electrolytic medium and electrolysis conditions.

Anodic Electrochemical Oxidation

Strongly Acidic Media. Shepard and Dannels [327] were able to polymerize benzene in HF. Rubinstein [328, 329] reinvestigated this polymerization using a HF/H₂SO₄ two-phase system. Various other two-phase systems produced poly(*p*-phenylene), such as concentrated sulfuric acid with a Lewis acid (AlCl₃), by using various rotating electrode surfaces such as Pt, Au, Fe, Ti, among others [330]. In the case of a mixture of benzene and concentrated sulfuric acid without Lewis acid catalysts, the two-phase system could be transformed into an emulsion by rapid rotation of the anode (200–400 rpm). Poly(*p*-phenylene) films were deposited on Ni, Nb, Mo, W, and certain alloys such as Ni–Re, Ni–Ru, Ni–W, and Ni–Mo [331, 332]. Polymerization was also performed with the working electrode immersed in the interfacial layer between the benzene and the acid. Methanesulfonic acid (MeSO₃H), sulfuric acid (20%), fuming sulfuric acid, fluorosulfonic acid (FSO₃H), and triflic acid (CF₃SO₃H) were mixed with benzene and it was shown that benzene was only oxidized with the electrode placed in the interfacial layer either at low potential (1 V vs SCE) or at constant current [333, 334]. Homogeneous benzene–acid solutions are achieved by mixing various strong acids and superacids such as the superacid solution of SbF₅ in HF [335]. Another improvement consists of using homogeneous ternary mixtures of benzene either with trifluoroacetic acid (CF₃COOH) + methanesulfonic acid or with trifluoroacetic acid + triflic acid [336, 337]. The two-phase-system benzene-concentrated sulfuric acid can also be transformed into a microemulsion operating as a single phase by the addition of a surfactant, sodium dodecylsulfate [338, 339].

Organic Aprotic Media with Various Electrolytes. Poly(*p*-phenylene) films can be electrosynthesized in organic solvents in the presence of an electrolyte or a composite electrolyte, including, in the latter case, a neutral salt associated with AlCl₃, AlCl₃–CuCl, CuCl₂, H₂SO₄+SO₃, or P₂O₅. As the nucleophilicity of the solvent must be low, the choice of solvent is limited to dichloromethane, nitrobenzene, nitromethane, phenylacetonitrile, acetonitrile, and propylenecarbonate. These solvents can be classified according to their donor number or acceptor number [340–345].

Composite Electrolytes. The electrochemical oxidation of benzene on Pt in nitromethane in the presence of AlCl₃ with small amounts of amine or water led to undoped or lightly doped poly(*p*-phenylene) films [346]. Flexible poly(*p*-phenylene) films

were obtained by anodic polymerization of benzene and biphenyl in phenylacetonitrile or nitrobenzene in the presence of $\text{LiBF}_4 + \text{CuCl}_2$ or $\text{LiAsF}_6 + \text{CuCl}_2$ or CuCl [347–350].

Single Electrolytes. Anodic polymerization of biphenyl was carried out in acetonitrile in the presence of tetrabutyl ammonium tetrafluoroborate [351]. Anodic polymerization of benzene was also studied in several organic solvents using a boron trifluoride ethyl ether complex $\text{BF}_3\text{O}(\text{CH}_2\text{H}_5)_2$ as the electrolyte [352]. A striking difference was observed between fluorinated anions (BF_4^- , PF_6^- , SbF_6^- , or AsF_6^-) and perchlorate anions [340–342]. Extension of the anodic electropolymerization of benzene to disubstituted benzenes with two electron-donating groups was investigated with the view to obtaining soluble poly(*p*-phenylene) films [353–359].

Inorganic Solvents. The electrochemical properties of sulfur dioxide were investigated by Elving et al. [360]. The electropolymerization of benzene and biphenyl on Pt in liquid SO_2 with different salts led to poly(*p*-phenylene) of high electroactivity in the case of fluorinated anions, such as BF_4^- , SbF_6^- or AsF_6^- , and CF_3SO_3^- , but yielded a passivating nonelectroactive film with ClO_4^- as well as with organic solvents. Small amounts of very strong acids such as $\text{CF}_3\text{SO}_3\text{H}$, sulfuric acid, fuming sulfuric acid, or $\text{CH}_3\text{SO}_3\text{H}$ at -75°C were found to favor the electrooxidation of benzene by lowering the oxidation potential of the monomer [239, 361–367].

Melt Salts and Solid-State Polymerization. By using a chloroaluminate melt obtained from a mixture of *N*-acetylpyridinium chloride or *N*-butylpyridinium chloride and AlCl_3 at room temperature, highly conducting poly(*p*-phenylene) films were obtained by electrooxidation of benzene on Pt [368–371].

Solid-state polymerization of phenylene oligomers evaporated under vacuum and deposited on Pt was carried out in dichloromethane +0.1 M tetrabutylammonium – PF_6 [372, 373].

Reductive Electropolymerization. Active catalytic species such as the low-valence metal complexes used in the Yamamoto, Colon, or Suzuki coupling reactions can be generated *in situ* by a reaction with a reducing agent such as Mg or Zn. These conditions can also be reproduced electrochemically, since the active catalytic species can be generated *in situ* by electrochemical reduction instead of using a reducing metal. The adaptation of these electrochemical reactions to the synthesis of poly(*p*-phenylene) has mainly used Ni complexes. Films of variable thickness can be obtained when a working electrode of SnO_2 or indium–tin oxide (ITO) is used. Surprisingly, noble metals do not seem to be suitable [374–379].

2.2.2. Polythiophenes

Thiophene (Fig. 14) is found in tar, gas, and industrial benzene obtained from coal in the 19th century. A large number of thiophene derivatives are described in the literature and their physical properties, nucleophilic substitution, and biological activity are still of current interest [380]. The first polythiophene synthesis was described in 1883 when the purification of thiophene with sulfuric acid yielded a dark, insoluble material [381]. The oxidation of thiophene was reported to be possible through oxidation by, for

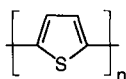


Fig. 14. Structure of polythiophene.

example, orthophosphoric acid or a synthetic silica–alumina catalyst, yielding a series of oligomers [382]. The preparation of electrical conductive polythiophenes, however, only started at the beginning of the 1980s. Since the 1980s, due to the stability of neutral polythiophene, important progress has been made in the chemistry of polythiophene. Not only have many derivatives been made, but also chemical control of the molecular, microscopic, and macroscopic structure of the polymer has become possible. It is not surprising that polythiophene has gradually acquired a prominent position owing to its relatively high conductivity, environmental stability of its neutral state and, to a lesser extent, its doped conductive state, and its structural versatility, allowing the derivatization of the π -conjugated backbone at the price of moderate losses of conjugation and conductivity. The literature on polythiophenes is extensive, with new publications appearing every day. Owing to the tremendous increase in the number of papers devoted to polythiophenes, it is difficult to discuss all of the various topics in great detail. It is not surprising that many detailed reviews have already been published [136, 137, 383–390].

A lot of synthetic effort has been devoted to the synthesis of polymerizable thiophene derivatives, but the principal aim of this review is to focus on the polymerization chemistry. The basic synthesis procedures for polythiophene can be considered in parallel with poly(*p*-phenylene). Indeed, a similar classification can be drawn: direct oxidation of thiophene, organometallic coupling, and electrochemical syntheses. Precursor methods for polythiophene are rather exceptional.

2.2.2.1. Direct Oxidation of Thiophene

Despite its drawbacks, oxidative coupling of thiophene and alkylated thiophenes with FeCl_3 is one of the methods that has been widely used to study the properties of polythiophene (Fig. 15a). This is due mainly to its accessibility to a wide range of scientists. Commercially available 3-alkylthiophenes are used most often because the resulting polymers are soluble in common organic solvents and have a sufficiently high molecular weight to allow them to be cast into films. Sugimoto et al. explored other metal halides as oxidants for the polymerization of 3-hexylthiophene and found that $\text{Fe}(\text{III})$, $\text{Mo}(\text{V})$, and $\text{Ru}(\text{III})$ chlorides were effective. In a typical procedure, FeCl_3 (0.4 mol) was suspended in chloroform under a nitrogen atmosphere. To this solution was added 3-hexylthiophene (0.1 mol) at 30°C under vigorous stirring. The mixture was stirred for 2 hours and poured into a copious amount of methanol. After further workup, films could be obtained showing similar characteristics to those obtained electrochemically [391–395]. Hotta et al. [396, 397] also prepared poly(3-hexylthiophene) via oxidative coupling of 2-halothiophenes. Special care was taken to carry out the polymerization under rigorously deoxidized and water-free experimental conditions. Niemi et al. [398] studied the mechanism of polymerization of 3-alkylthiophene with FeCl_3 . Poly(3-alkylthiophene) derivatives were prepared by several other groups [93, 399, 400] and optimized reaction conditions reported [82, 401, 402]. Alkoxythiophene derivatives were polymerized by oxidative coupling, such as 3-butoxythiophene, 3,4-dibutoxythiophene, 3-methyl-4-octyloxythiophene, and several alkoxybithiophenes [403–405]. A number of researchers have reported the synthesis of different alkoxy-substituted polythiophenes [406–414]. Poly(alkoxythiophene)s were prepared by $\text{Cu}(\text{ClO}_4)_2$ oxidation of bithiophenes [415]. Whereas poly(3-alkylthiophene)

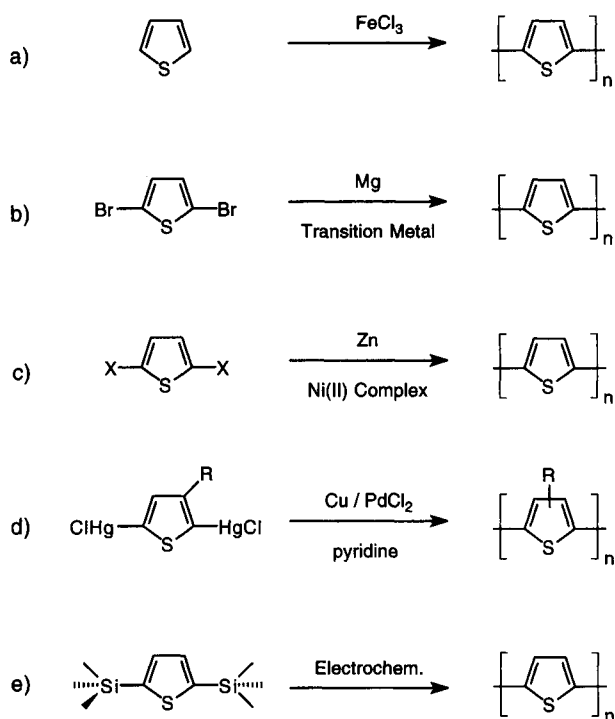


Fig. 15. (a) Oxidative coupling with FeCl_3 , (b) Yamamoto, (c) Colon ($\text{X}=\text{Cl}, \text{Br}, \text{I}$), (d) Curtin, and (e) 2,5-bis(trimethylsilyl)-activated electrochemical polymerization.

can be dedoped by Soxhlet extraction with methanol, the alkoxy-substituted polythiophenes remained in partially doped states. Completely undoped polymers were obtained by reduction with ammonia or hydrazine solutions. Casa et al. [416, 417] prepared several polythiophenes containing ω -hydroxyethyl and hexanoyloxyethyl side-chains by adding the corresponding monomers to a stirred solution of FeCl_3 in nitromethane or chloroform with varying FeCl_3 concentrations. Chen and Tsai [418] prepared a series of 3-ether-substituted polythiophenes and poly(3-alkoxy-4-methylthiophene)s. Some groups [419, 420] reported that, depending on the specific oxidative conditions and a sterically hindered, activating 3-substituent, highly regioregular materials could be prepared as a consequence of the asymmetric reactivity of the oxidized monomers.

One of the major problems of the FeCl_3 method is that it gives variable results [93]. Another disadvantage is that remaining Fe impurities affect application of the so-obtained materials in electronic devices [421, 422].

2.2.2.2. Organometallic Coupling Reactions

As for poly(*p*-phenylene), there are two important methods: the Ni-catalyzed coupling of Yamamoto and Colon, on the one hand, and the Suzuki reaction based on the coupling of aromatic boronic acids with halogenated aromatic compounds in the presence of a Pd(0) catalyst, on the other. Besides these two main methods, a series of other metal-catalyzed couplings have been explored.

Ni-Catalyzed Coupling Reactions

Yamamoto Method. Yamamoto et al. [423] prepared polythiophene by treating 2,5-dibromothiophene with Mg and catalyzing the polymerization by $\text{Ni}(\text{bipyridine})_2\text{Cl}_2$ (Fig. 15). A similar

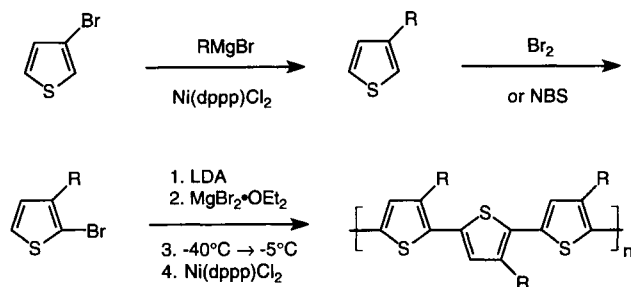


Fig. 16. McCullough method for regiospecific synthesis of poly(3-alkylthiophene)s with 100% head-to-tail couplings.

metal-catalyzed polycondensation reaction was reported by Lin and Dudek [424]. These methods are based on the coupling of Grignard reagents with aryl halides reported by Tamao et al. [263]. Systematic studies of the polymerization of 2,5-dihalothiophene were performed by the group of Yamamoto, as well as by many other groups [259–263]. Varying the amounts of Mg, solvent, type of metal, monomer concentration, type of halogen on the thiophene, temperature, reaction time, and type of catalyst led to some good chemical methods for the synthesis of polythiophene derivatives [85, 87, 273, 425–427]. To be able to process polythiophene, alkyl substituents were introduced to enhance solubility. Poly(3-methylthiophene) was chemically synthesized but was found to be insoluble [426, 429–431]. The first chemical synthesis of environmentally stable and soluble poly(3-alkylthiophene)s based on the Yamamoto method was reported by the group of Elsenbaumer [432–434]. Typically, 2,5-diiodo-3-alkylthiophene was treated with one equivalent of Mg in THF, generating a mixture of Grignard species. A catalytic amount of $\text{Ni}(\text{dppp})\text{Cl}_2$ (dppp = 1,3-diphenylphosphinopropane) was then added, generating the polymer by a dehalogenation coupling reaction. Initially, molecular weights were reported to be rather low, but later reports showed that higher molecular weights were possible [418, 435].

Colon Method. 2,5-Dihalothiophenes were polymerized by a polycondensation dehalogenation reaction where Ni(0) was generated *in situ* by the reduction of NiCl_2 with Zn powder in the presence of triphenylphosphine in dimethylformamide (DMF), also known as the Colon method [428, 436] (Fig. 15). Poly(3-alkylthiophene)s were synthesized according to this method. Diiodothiophenes were found to be more reactive than dibromothiophenes [273].

McCullough Method. Regioregularity in poly(3-alkylthiophene)s has an important influence on the polymer properties and its electronic characteristics [437]. One obvious approach toward the synthesis of regioregular substituted polythiophenes, which has been applied by several groups, is to use common random coupling chemistry to polymerize thiophene derivatives with inherent symmetry [438–449]. An alternative strategy was proposed by McCullough and Lowe [450] in the early 1990s: the utilization of asymmetric coupling of asymmetric monomers in order to achieve regioregular head-to-tail-coupled structures of polythiophene derivatives. This synthetic method [451–461] regiospecifically generates 2-bromo-5-(bromomagnesio)-3-alkylthiophene, which is subsequently polymerized with catalytic amounts of $\text{Ni}(\text{dppp})\text{Cl}_2$ on the basis of the method reported by Tamao et al. [263] (Fig. 16). The method reported by Tamao et al. [263] is also the basis for the Yamamoto procedure [258] mentioned in this chapter. Some key features of the McCul-

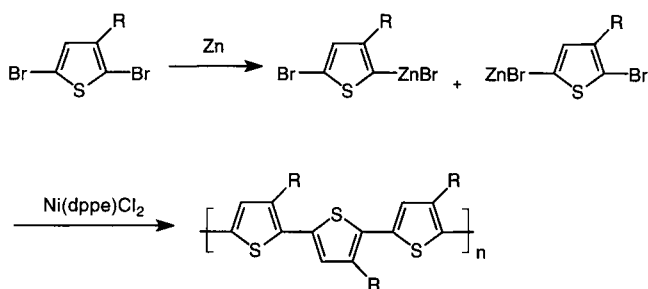


Fig. 17. Rieke method for regiospecific synthesis of poly(3-alkylthiophene)s with 100% head-to-tail couplings.

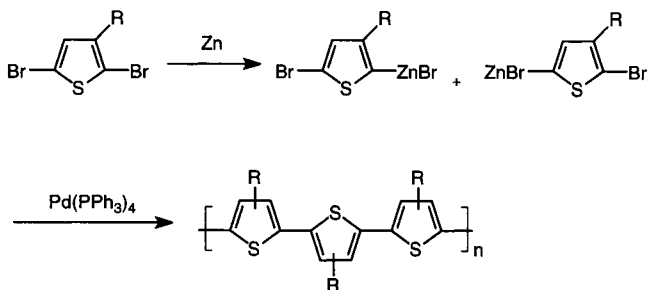


Fig. 18. Rieke method for regiorandom synthesis of poly(3-alkylthiophene)s.

lough method are the selective metallation with lithium diisopropylamide. The intermediate organolithium thiophene compound is stable at -78°C and does not undergo metal-halogen exchange via any process. In addition, thienyl lithium compounds are relatively poor organolithium reagents and therefore unlikely to undergo metal-halogen exchange reactions with 2-bromo-3-alkylthiophenes. The lithium intermediate is then reacted with recrystallized $\text{MgBr}_2\text{-Et}_2\text{O}$ (from Et_2O in a dry box), which results in the formation of 2-bromo-5-(bromomagnesio)-3-alkylthiophene. The latter does not rearrange at higher temperatures. The subsequent polymerization occurs without any scrambling, resulting in all head-to-tail-coupled poly(3-alkylthiophene).

Rieke Method. The second synthetic approach to head-to-tail-coupled poly(3-alkylthiophene)s was described by Chen et al. [462–466]. This coupling method differs primarily in the synthesis of the asymmetric organometallic intermediate. In the Rieke method, a 2,5-dibromo-3-alkylthiophene is added to a solution of highly reactive “Rieke Zn.” This metal reacts quantitatively to form a mixture of isomers, 2-bromo-3-alkyl-5-(bromozincio)thiophene and 2-(bromozincio)-3-alkyl-5-bromothiophene. The ratio between these two is dependent on the reaction temperature and, to a much lesser extent, the steric influence of the alkyl substituent. The addition of a Ni cross-coupling catalyst, $\text{Ni}(\text{dppe})\text{Cl}_2$, leads to the formation of a regioregular poly(3-alkylthiophene) (Fig. 17). An interesting aspect is that, upon addition of a Pd cross-coupling catalyst, $\text{Pd}(\text{PPh}_3)_4$, the reaction results in the formation of a completely regiorandom poly(3-alkylthiophene) (Fig. 18). If 2-bromo-3-alkyl-5-iodothiophene derivatives are reacted with “Rieke Zn,” only 2-bromo-3-alkyl-5-(iodozincio)thiophene is formed. This species, however, will react in an identical fashion to form regioregular or regiorandom poly(3-alkylthiophene), depending on the catalyst used for the polymerization. One advantage of the Rieke method is that highly reactive “Rieke Zn” affords a functional group-tolerant synthesis.

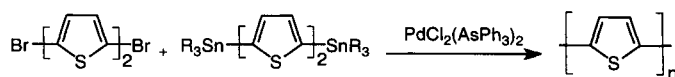


Fig. 19. Stille coupling.

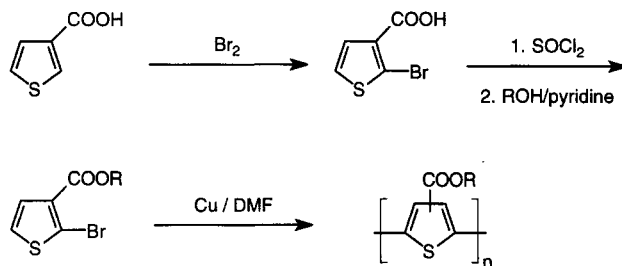


Fig. 20. Ullmann coupling of thiophene ester derivatives.

Pd-Catalyzed Reactions

Curtis Method. McClain et al. [467] report that polymers are generated by PdCl_2 -catalyzed dehalogenation polycondensation of 2,5-bis(chloromercurio)-3-alkylthiophenes with Cu powder in pyridine (Fig. 15). Ester functional groups at the 3-position do not seem to be affected by the polymerization conditions.

Stille Method. 2,5'-dibromobithiophenes have been coupled with 2,5'-bis(trimethylstannyl)bithiophenes using a catalytic amount of $\text{PdCl}_2(\text{AsPh}_3)_2$ [443] (Fig. 19).

Other Syntheses Based on Metal-Catalyzed Coupling Reactions. Polythiophenes have been synthesized by coupling of 5,5'-dilithio-bithiophenes with CuCl_2 [441]. A similar coupling has been reported making use of $\text{Fe}(\text{acac})_3$ (acac = acetylacetonate) in refluxing THF [443]. Ullmann coupling has been used to synthesize 3-ester derivatives of polythiophene [468] (Fig. 20).

2.2.2.3. Electrochemical Synthesis

Good-quality polythiophene can be prepared by electrochemical polymerization of thiophene. The methods used are very similar to those used for poly(*p*-phenylene).

Anodic Electrochemical Oxidation. The anodic electropolymerization of thiophene presents several distinct advantages such as the absence of catalyst, direct grafting of the doped conducting polymer onto the electrode surface (which is of particular interest for electrochemical applications), easy control of the film thickness by deposition charge, and possibility to perform a first *in situ* characterization of the growing process or of the polymer by electrochemical and/or spectroscopic techniques.

The electropolymerization of bithiophene was initially mentioned in 1980 [469], whereas the first report of the electropolymerization of thiophene appeared 2 years later [61]. Following these initial works, a large number of studies have been devoted to the analysis of the electropolymerization reaction and to the optimization of the electrosynthesis conditions [136].

The electropolymerization of five-membered heterocycles involves many experimental variables such as the solvent, concentration of reagents, temperature, cell geometry, nature and shape of the electrodes, and applied electrical conditions. As a consequence of the diversity of these parameters and of the complexity of the electropolymerization pathways, electrosynthesis conditions

determine, to a large extent, the structure and properties of the resulting polymer. Due to the interdependence of many of the experimental variables, however, the analysis of the effects of an individual parameter and hence optimization of the electrosynthesis conditions constitute a complex problem [136].

The solvent of the electrolytic medium exerts a strong effect on the structure and properties of polythiophene films. As a matter of fact, the solvent must simultaneously present a high dielectric constant to ensure ionic conductivity of the electrolyte medium and a good electrochemical resistance against decomposition at the high potentials required to oxidize the thiophene ring (1.4–2.3 V/SCE). Although the electropolymerization of 3-methylthiophene in aqueous medium has been reported, the material obtained has not been characterized in detail [470]. In contrast, several works have shown that the presence of traces of water in the synthesis medium has deleterious consequences for the electropolymerization reaction [471, 472], for the conjugation length, and for the conductivity of the polymer [473]. It has been shown that the presence of water results in the incorporation of carbonyl groups in the polymer [474]. The most conductive polythiophenes have been prepared in rigorously anhydrous aprotic solvents of high dielectric constant and low nucleophilicity such as acetonitrile [61, 62, 69, 469], benzonitrile [63], nitrobenzene [64, 65, 70, 72], and propylene carbonate [475, 476]. These solvents lead to the highest current efficiency of electropolymerization [344].

Polythiophenes are generally electrogenerated in the presence of small anions derived from strong acids such as ClO_4^- , PF_6^- , BF_4^- , and AsF_6^- , associated with lithium or tetraalkylammonium cations [63–65, 70, 72, 75, 430, 475–478]. HSO_4^- and SO_4^{2-} lead to poorly conducting materials [62, 64, 70]. The nature of the anion strongly affects the morphology [479, 480] and electrochemical properties [481] of polythiophenes prepared in acetonitrile. A partial crystallinity has been observed in poly(3-methylthiophene) grown in acetonitrile with CF_3SO_3^- [482, 483]. Unlike polypyrrole, the electropolymerization of thiophene in the presence of electrolytes containing aromatic anions such as halo- or alkylbenzenesulfonates or naphthalenesulfonates yields no or little polymer of low doping level and conductivity [483, 484].

The temperature of electropolymerization has been reported to affect the extent of the conjugated system and hence the optical and electrical properties of the polymer [64, 65, 70, 475, 476, 485].

The anode is of critical consideration since the physicochemical properties of its surface determine the nature and the strength of the bond between the polymer and the electrode, which can affect both the polymerization process and the properties of the resulting polymer. Polythiophenes are generally grown on noble metals such as platinum [61, 62, 72, 477, 478, 486, 487] and gold [488] or on optically transparent electrodes such as tin oxide and ITO-coated glass [63–65, 70, 72, 430, 473, 475–477, 487]. Polythiophenes have also been deposited on other surfaces such as titanium [489] and iron [490]. The most conductive polymers have been obtained on bulk platinum, presumably because thiophene absorbs more efficiently on platinum and also platinum presents a larger number of potentially active sites, thus leading to a high density of initial nucleation sites and to more compact materials [68, 74, 75, 478].

The applied electrical conditions exert considerable effects on the structure and properties of electrogenerated polythiophenes. Polythiophenes have been deposited under potentiostatic [61, 62, 69, 469] or galvanostatic [63, 64, 68, 70–72, 74, 75, 430, 475–479, 485, 487] conditions and by recurrent potential sweeps [491, 492]

or current pulses [68, 74]. Although from a thermodynamic point of view it is likely that the applied potential is the relevant electric parameter, the most homogeneous and conducting films are generally obtained under galvanostatic conditions at potentials approximately 0.5 V more positive than the oxidation potential of the monomer. [63, 64, 68, 70–72, 74, 75, 430, 475–479, 485, 487].

Under constant electrical conditions (2 mA cm^{-2}), high monomer concentrations (0.5–1 M) produce loose, poorly conducting films containing significant amounts of soluble oligomers. The decrease in monomer concentration improves both the cohesion of the films and their conductivity, which reaches values in the range of 500 S cm^{-1} for 0.1 M monomer [72, 477, 493].

The electropolymerization of thiophene oligomers has been investigated by several groups. In general, the conjugated structure of the oligomers results in a decrease of the relative reactivity of the α positions, which has deleterious consequences for the stereoselectivity of the polymerization [73, 442, 477, 493–510]. An alternative strategy to increase the stereoregularity of electrogenerated polythiophenes consists of the activation of the α positions of the thiophene ring in order to increase their relative activity. A first attempt in this direction involved the electropolymerization of 2,5-dilithiothiophene in the presence of CuCl_2 [441]. Another approach consists of the activation of the α - α' positions of the monomer by alkylsilyl groups such as trimethylsilyl (Fig. 15). Although the polymer obtained from 2,5-bis(trimethylsilyl)thiophene is rather similar to that obtained from the unactivated monomer, 2,5'-bis(trimethylsilyl)bithiophene leads to a significant improvement of the electrochemical and electrical properties [510].

Electronic effects drastically affect the electron density of the thiophene ring and hence its reactivity. Thus, monomers substituted by strongly electron-withdrawing groups such as 3-thiophenecarboxylic acid, 3-thiophenecarboxaldehyde, 3-cyanothiophene, and 3-nitrothiophene that have oxidation potentials approximately 0.5–0.7 V higher than thiophene do not electropolymerize. The electropolymerization of monomers with less electron-withdrawing substituents such as 3-thiopheneacetonitrile, or 3-thiopheneacetic acid, proceeds with low-current efficiency and requires highly anodic potentials. Halogen-substituted monomers, i.e., 3-chloro-, 3-bromo-, 3,4-dibromo-, and 3-iodothiophenes, are generally difficult to electropolymerize and lead to poorly conducting polymers with high oxidation potentials. In this latter case, however, the observed effects probably arise from a combination of electronic and steric factors. The impossibility or difficulty of electropolymerizing monomers of high oxidation potentials has been attributed to the high reactivity of the corresponding radicals, which can thus undergo rapid reactions with the solvent or anions to form soluble products rather than to electropolymerize [62, 480, 511–514].

In the other extreme case, the substitution of thiophene by electron-donating groups produces a decrease of oxidation potential and hence a stabilization of the corresponding radicals. These radicals can thus diffuse away from the electrode surface to form soluble oligomers in solution. Thus, attempts to electropolymerize 3-(methylthio)-, 3-(ethylthio)-, and 3,4-bis(ethylthio)thiophenes were unsuccessful or led to the formation of soluble oligomers. Theoretical calculations have shown that the spin density in the corresponding radicals was maximum on the sulfide function and not on the α positions of the thiophene ring, which is a necessary condition for electropolymerization. A similar explanation could

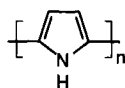


Fig. 21. Structure of polypyrrole.

account for the failure to electropolymerize tetrahydrothieno[3,4-*c*]thiophene, which acts as a radical scavenger capable of inhibiting the electropolymerization of 3-methylthiophene. Although of lesser magnitude, similar effects result from the grafting of alkoxy groups on the thiophene ring. In this case, the electron-donating effect of the oxygen decreases the oxidation potential of the monomer, which stabilizes the resulting radicals and favors the formation of soluble short-chain oligomers [412, 515–519].

Reductive Electropolymerization. Besides the oxidative anodic electropolymerization of the monomer, which is the most convenient and the most widely used method, polythiophene can also be prepared by a cathodic route involving the electroreduction of the complex $\text{Ni}(2\text{-bromo-5-thienyl})(\text{PPh}_3)_4\text{Br}$ in acetonitrile. This method, initially proposed for the synthesis of poly(*p*-phenylene) [374–376], has been extended to polythiophene [520]. The major drawback is that the polymer is produced in its neutral insulating form, which leads rapidly to a passivation of the electrode and limits the attainable film thickness to approximately 100 nm. On the other hand, this technique presents the advantage of being applicable to electrode materials subject to anodic corrosion such as small-bandgap semiconductors [521].

2.2.3. Polypyrroles

Of all of the known conducting polymers, polypyrrole (Fig. 21) is the most frequently used in commercial applications, due to the long-term stability of its conductivity and the possibility of forming homopolymers or composites with improved mechanical properties. The science and application of polypyrrole have already been discussed extensively in some detailed reviews [522, 523].

Polypyrrole was first prepared in 1916 [524, 525] by the oxidation of pyrrole with hydrogen peroxide to give an amorphous powdery product known as “pyrrole black.” Little further interest was shown in this material, however, until it was electrochemically prepared in the form of continuous films. The electrochemical synthesis of polypyrrole dates back to the early work of Dall’Ollio [526], who obtained pyrrole black by electrochemical oxidation of pyrrole in aqueous sulfuric acid on a platinum electrode. In 1979 [527], electrochemical techniques to synthesize polypyrroles became a useful way to obtain highly conductive freestanding materials. Chemical and electrochemical methods of synthesis have been improved in order to optimize the physical and chemical properties of those materials.

2.2.3.1. Chemical Syntheses

Pyrrole was first chemically polymerized in 1916 [524, 525] by the oxidation of pyrrole with hydrogen peroxide to give an amorphous powdery product known as pyrrole black, which was found to be insoluble in organic solvents. In general, pyrrole blacks have been prepared in the presence of various oxidizing reagents, including hydrogen peroxide in acetic acid, lead dioxide, ferric chloride, nitrous acid, quinones, and ozone. Chemical methods of preparation with acid or peroxide initiators have resulted mainly in fairly

oxidative insulating materials with room-temperature conductivity typically on the order of 10^{-10} to 10^{-11} S cm^{-1} [528–532]. Those initially insulating polypyrroles can be doped with halogenic electron acceptors such as bromine and iodine to achieve a stable conductivity on the order of 10^{-5} S cm^{-1} [532].

One of the great advantages of polypyrrole from a synthetic point of view concerns the low oxidation potential of the pyrrole monomer [533]. Pyrrole is one of the most easily oxidized monomers and hence a variety of oxidizing agents are available for preparing polypyrrole. In addition, polypyrrole can be obtained directly in a conducting state, because the polymer oxidation occurs with oxidant salts acting as doping agents. The most often used oxidizing agents for pyrrole polymerization are oxidative transition metal ions, as widely reported in the literature. Several metallic salts have been employed to polymerize pyrrole: FeCl_3 , $\text{Fe}(\text{NO}_3)_3$, $\text{Fe}(\text{ClO}_4)_3$, $\text{Fe}_2(\text{SO}_4)_3$, $\text{K}_3\text{Fe}(\text{CN})_6$, FeBr_3 , CuCl_2 , CuBr_2 , etc. Ferric salts are the most commonly used oxidants for the synthesis of highly conductive polypyrrole complexes [33–36, 38, 534–536]. In general, polymer conductivity is a function of the monomer and oxidant agent concentrations, solvent, time of reaction, and temperature of synthesis. Thus, the optimum reactant $\text{Fe}(\text{III})/\text{monomer}$ ratio for the polymerization of pyrrole by FeCl_3 has been found to be 2.4 [534]. In water/ethanol mixtures, an optimum ratio of 2.25 for the polymerization has been obtained. Conductivities as high as 190 S cm^{-1} have been reported for polypyrrole synthesized in a methanol solution of FeCl_3 [537].

Low temperatures ($0\text{--}5^\circ\text{C}$) are the most appropriate for obtaining the best conductivities in aqueous solutions of ferric salts [538]. Similar behavior for the chemical oxidation of pyrrole in organic solvents has been reported [539]. This seems to suggest that lowering the reaction rate results in an increasing polymer conductivity.

Highly conductive polypyrrole could be obtained if the oxidation potential of the aqueous solution is controlled to the optimum value during chemical polymerization by adding a suitable amount of FeCl_2 . In this way, polypyrrole having a conductivity of more than 200 S cm^{-1} has been prepared [40]. When this procedure is applied to chemical vapor deposition, polypyrrole having a conductivity of more than 100 S cm^{-1} is obtained [41].

Apart from metallic salts, simultaneous chemical synthesis and doping of polypyrrole has been achieved by halogenic electron acceptor, such as bromine or iodine, in several solvents [27, 28, 30, 540, 541]. Pyrrole has also been oxidized by means of halobenzoquinones [28, 542]. Synthesis and doping of polypyrrole has been performed by 2,3-dichloro-5,6-dicyano-*p*-benzoquinone and tetrachloro-*o*-benzoquinone from bulk polymerization [28].

Most of the chemical polymerization procedures described thus far use metal salts, which are consumed stoichiometrically in the reaction. However, effective catalytic processes would be highly favored for mass production, because of the low cost of extensive posttreatment steps. $\text{CuCl}/\text{AlCl}_3/\text{O}_2$ is a typical system applied to synthesize polypyrrole chemically [543, 544]. Bis(acetylacetonato)(oxo)vanadium(IV) has also been used instead of CuCl [42].

Control over 2,5-linked polypyrrole is achieved by means of Stille chemistry. *t*-BOC-protected pyrroles are converted into bromo-trimethyl stannyl monomers and subsequently polymerized using a Pd catalyst. The so-obtained low-molecular-weight material can next be converted to polypyrrole by thermal deprotection [545]. Ullmann coupling has also been used to prepare

polypyrrole of comparable quality to that obtained through Stille chemistry [546].

2.2.3.2. Electrochemical Syntheses

Among all of the methods of synthesis to produce polypyrrole, the electrochemical procedure is one of the most useful procedures to obtain polypyrroles with high conductivities. The general details are similar to other conducting polymers such as poly(*p*-phenylene) or polythiophene. The experimental requirements are not difficult, because it is possible to work in aqueous solution at ambient pressure and temperature. The main problem is related to the difficulty in producing large amounts of polypyrrole due to the limitations imposed by the size of the anode. Second, even the most simple electrochemical process of pyrrole electropolymerization involves different experimental variables in order to optimize polymer properties. These variables can be chemical, such as solvent, monomer concentration, and salt concentration, or physical, such as temperature, nature and shape of the electrodes, cell geometry, or electrical conditions. Commonly, all of these variables are interdependent.

The nature of the electrode is a critical variable for the preparation of polypyrrole films. Since the films are produced by an oxidative process, it is fundamental that the electrode does not oxidize in competence with pyrrole. For this reason, most polypyrrole films have been prepared using inert anodes, such as platinum [547], gold [548], or glassy carbon [549]. From a technological point of view, however, other cheaper materials such as iron or aluminum should be more interesting [550–562]. Apart from metals, polypyrrole films have also been prepared using a variety of semiconducting materials. Generally, polymerization onto metals gives smoother and more adherent films than polymerization on materials such as ITO glass or semiconductors [563, 564], although, in the case of ITO electrodes, interactions between polypyrrole and Sn(II) sites have been proposed [565]. Polypyrrole films have been generated on silicon [566–568], gallium phosphide [569], cadmium sulfide, and cadmium selenide [570]. Photoelectrochemical generation of the polymer has also been performed on semiconductor substrates [571]. It was found that the potential at which the pyrrole polymerizes is lower compared to platinum metal. Protection of *n*-GaAs [571] and *n*-Si photoanodes [572, 573] by photoelectrochemically generated polypyrrole may be a new possibility for the construction of practical electrochemical solar cells.

Solvents have a very strong influence both on the mechanism of electropolymerization and on the polymer properties. In fact, solvents must simultaneously have a high dielectric constant to ensure ionic conductivity of the electrolytic medium and a good electrochemical resistance against decomposition at the potentials required to oxidize the pyrrole ring. A wide variety of solvents have been used for electropolymerization. In most cases, polypyrrole is prepared from electrolyte solutions employing aprotic organic solvents, but since the work of Diaz et al. [527] much work has also been done on the polymerization reaction in aqueous solutions, achieving films with properties similar to those produced from organic solutions [574–577]. An aqueous medium can be used to introduce a wide variety of inorganic anions. The main problem concerning the electrogeneration of polypyrrole in water is associated with the excess of oxygen present in the polymer structure as a consequence of degradation processes taking place during polymerization [574, 578–580]. Among organic solvents, acetonitrile has been the most commonly used. High-quality films were

first reported by Diaz et al. [527, 563] using a tetraethylammonium tetrafluoroborate/acetonitrile solution. Films grown from dry acetonitrile are nonuniform and are poorly adhered to the electrode surface. Increasing the water content of the acetonitrile solutions, better adhesion and conductivity are obtained. In addition to acetonitrile, a wide variety of other aprotic solvents can be used as long as the nucleophilic character of the solvent is poor. Even some nucleophilic aprotic solvents such as dimethylsulfoxide, dimethylformamide, and hexamethylphosphoramide can be used if the nucleophilicity of the solution is reduced by the addition of a protic acid [581]. Good-quality films have been obtained from a dimethylformamide solution [582, 583]. In addition to aprotic solvents, films have been prepared in strong acid media. These preparations are carried out in polyethylene or polypropylene cells, using a platinum, gold, or glassy carbon working electrode and a polymer-coated Ag/AgCl or Pd/H reference electrode [329, 335]. Polypyrrole films have been prepared in AlCl₃/NH₄Cl molten salt mixtures [584, 585].

The main requirements in the choice of the supporting electrolyte are the solubility of the salt, its degree of dissociation, and the reactivity of both the anion and cation, in particular, the nucleophilicity of the anion. On the other hand, since the anion is incorporated into the film during polymerization, modifications of the polymer properties can be made by simply changing the electrolyte salt of the solution. With respect to the cation, most of the salts used to electropolymerize pyrrole contain tetraalkylammonium cations because they are soluble in aprotic solvents and highly dissociated. Lithium salts are also used, although they are highly aggregated. Sodium and potassium salts are less used because they are not very soluble in aprotic solvents. A wide variety of anions have been used to prepare polypyrrole films. Good films are obtained in anions that are not very nucleophilic. Nucleophilic anions such as halides, acetates, alkoxides, and hydroxides do not produce polymers, but react indiscriminately with monomer or monomeric radical cations, giving soluble products that color the solution [581]. Most highly conductive films have been obtained with *p*-toluenesulfonate anions [577]. It is clear that the kind of anion used during the polymerization influences both the structural and the electroactive properties [329, 586].

The polymerization temperature has a substantial influence on the kinetics of polymerization as well as on the conductivity, redox properties, and mechanical characteristics of the films. The rate of polymerization is strongly affected by the temperature of synthesis [587–589]. The generation temperature also affects the conductivity of the resulting polymer. In general, higher conductivities are obtained at lower temperatures, both in aqueous media [577] and in propylene carbonate [590]. Films prepared in a propylene carbonate solution at -20°C are much more conductive than those prepared at 20°C . Mirebeau [591] has studied the effect of temperature and current density on the polymerization of pyrrole on stainless steel from propylene carbonate solutions. On aluminum electrodes, Beck et al. [550, 555] have shown that lower temperatures are also advantageous and that at 0°C smooth and strongly adherent polypyrrole layers are obtained from oxalic acid aqueous solutions.

Polypyrrole can be deposited under potentiostatic or galvanostatic conditions and by potential or current sweep or pulses. In any case, the applied electrical conditions introduce effects on both the structure and the properties of the electrogenerated polypyrrole films and on the rate of polymer production. From electrochemical preliminary studies of the electrode in the absence and

in the presence of monomer, one can choose the potential where monomeric oxidation will take place [522]. Properties of the electrogenerated polypyrrole films can be changed by varying the electrochemical parameters of the synthesis, even while maintaining the same electrolytic conditions. The influence of the electrochemical method on morphology, appearance, and adherence to platinum electrodes has been studied [592]. Smooth and adherent films were obtained at lower current densities [527, 563]. The appearance of higher conductivities was also observed when films were electrogenerated at constant current [593].

2.2.4. Extended Aromatic Ring Systems

The electronic and optical properties of polyconjugated materials are, to a large extent, determined by the characteristics of the conjugated path or the alternation of single and double bonds. Soon after the initial development of poly(*p*-phenylene), polythiophene, and polypyrrole, it was realized that by careful design of the aromatic ring system specific electronic and optical properties could be achieved. One of the major issues that triggered the development of polyaromatics with extended π -electron ring systems was the quest for low-bandgap polymers—a quest that is still continuing because no conjugated polymer meets in a satisfactory way the simultaneous requirements of low bandgap, high charge-carrier mobility, and stability in the conductive state.

2.2.4.1. Fused Ring Systems

Polybenzo[*c*]thiophene (or Polyisothianaphthene). Benzo[*c*]thiophene—in the field of conducting polymers most commonly known as isothianaphthene—is a compound that is very sensitive toward oxidation and whose chemical properties are drastically different from its thiophene analogs [594–598]. As a consequence, the manipulation of isothianaphthene is not straightforward. The preparation of isothianaphthene is well established [596, 599, 600]. Synthesis of a sterically protected isothianaphthene compound has been reported [601].

One of the earliest reports on a polyisothianaphthene-like material describes its accidental discovery when trying to prepare poly(isothianaphthene sulfide) on the basis of the idea that poly(isothianaphthene sulfide) should possess better electronic characteristics and should be more synthetically accessible than poly(sulfur nitride) (SN)_x (Fig. 22). Upon treatment of the 1,3-di(chloromercurio)isothianaphthene with iodine, a blue–black lustrous material was obtained. The material was, however, poorly characterized [602]. It was not until the mid-1980s that polyisothianaphthene (Fig. 23) was synthesized and analyzed in further detail [603].

As could be expected, the electrochemical polymerization of isothianaphthene was initially reported to be rather delicate. Thus, the use of electrolytes such as Bu₄NClO₄ and Bu₄NBF₄ in acetonitrile, conditions commonly employed for electrodeposition of polythiophenes, led to the formation of a white precipitate, which was identified as being poly(1,3-dihydroisothianaphthene). Formation of polyisothianaphthene was achieved by indirect oxidation of isothianaphthene by electrogenerated chlorine or bromine [603–605]. Later it was shown that satisfactory results could be obtained by the application of repetitive potential scans to acetonitrile solutions containing classical electrolytes such as Bu₄NBF₄ and Et₄NBF₄ [606–608].

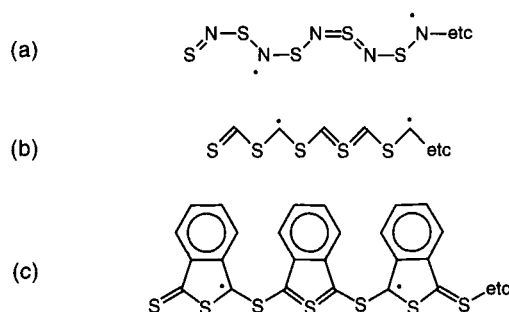


Fig. 22. Poly(sulfur nitride) (SN)_x, (b) replacing the nitrogens by carbons, and (c) stabilizing radicals in an analog carbon–sulfur compound.

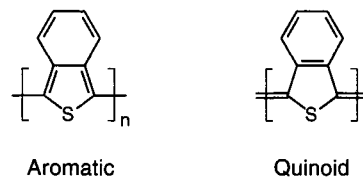


Fig. 23. Two possible structures for polyisothianaphthene: aromatic and quinoid.

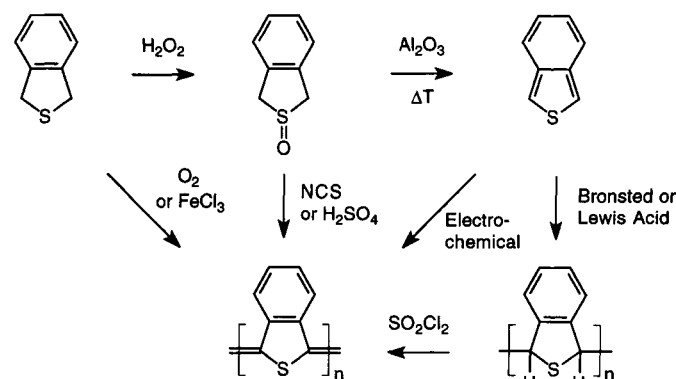


Fig. 24. Syntheses of polyisothianaphthene.

Polyisothianaphthene has also been prepared by means of chemical syntheses (Fig. 24). The oxidation of 1,3-dihydroisothianaphthene with atmospheric oxygen, FeCl₃, SO₂Cl₂, sulfuric acid and *N*-chlorosuccinimide leads directly to the doped conducting polymer [609–611]. Iyoda et al. [612, 613] obtained polyisothianaphthene through photolysis of isothianaphthene in the presence of Bu₄NBr and CCl₄, as well as through photochemical polymerization of 1,3-dihydroisothianaphthene. It has also been reported that polyisothianaphthene can be directly obtained from phthalic anhydride or phthalide by reaction with P₄S₁₀ [614] (Fig. 25). Several substituted polyisothianaphthene derivatives have been prepared in a similar fashion by either chemical syntheses or electrochemical polymerization [615–626]. The bandgap of polyisothianaphthene is typically around 1.0–1.2 eV. Upon doping, the material becomes transparent [603].

Polynaphto[2,3-*c*]thiophene. Naphto[2,3-*c*]thiophene (Fig. 26) can be prepared in a similar way as benzo[*c*]thiophene (isothianaphthene). This compound was electrochemically polymerized in an acetonitrile solution with (PPh₄)Cl as electrolyte. The neutral polymer film was blue and became transparent gray upon dop-

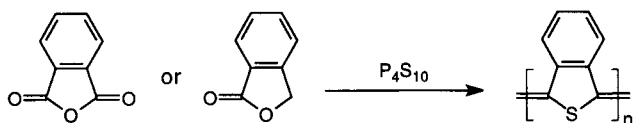


Fig. 25. Synthesis of polyisothianaphthene from phthalic anhydride or phthalide with P_4S_{10} .

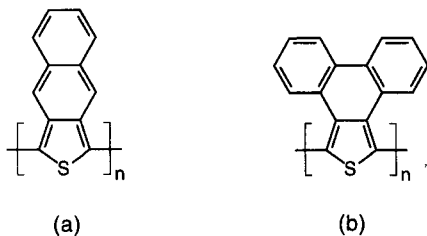


Fig. 26. Structure of (a) polynaphtho[2,3-c]thiophene and (b) polyphenanthro[9,10-c]thiophene.

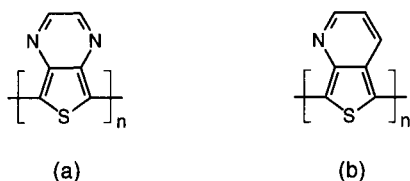


Fig. 27. Structure of (a) polythieno[3,4-b]pyrazine and (b) polythieno[3,4-b]pyridine.

ing. The λ_{\max} is around 575 nm and the edge of the absorption band around 1.5 eV [627–629].

Polyphenanthro[9,10-c]thiophene. Polyphenanthro[9,10-c]thiophene (Fig. 26b) can be prepared by electrochemical polymerization of phenanthro[9,10-c]thiophene in an acetonitrile or nitromethane solution with Bu_4NPF_6 as electrolyte. The material obtained from the polymerization in acetonitrile showed a conductivity as high as 105 S cm^{-1} . The bandgap of this polymer, however, was not determined [630].

Polythieno[3,4-b]pyrazine and Polythieno[3,4-b]pyridine. Polythieno[3,4-b]pyrazine (Fig. 27a) is related to polyisothianaphthene in the sense that the two CH groups adjacent to the thiophene rings have been replaced by sterically less demanding nitrogen atoms. The hexyl derivative of this polymer was chemically polymerized with $FeCl_3$. The absorption spectrum showed a λ_{\max} at 875 nm in chloroform solution and 915 nm for a solution-cast film with a band edge of 0.95 eV. Films cast after doping with $NOBF_4$ in solution exhibited a maximum four-probe conductivity of $3.6 \times 10^{-2} \text{ S cm}^{-1}$ [615, 631]. Other alkylated polythieno[3,4-b]pyrazines have been synthesized [632]. The parent unsubstituted polythieno[3,4-b]pyrazine has also been prepared by reaction of 2,3-pyrazine dicarboxylic anhydride with P_4S_{10} [614].

Polythieno[3,4-b]pyridine (Fig. 27b) has also been prepared by reaction of 2,3-pyridine dicarboxylic anhydride. Conductivities after doping were on the order of $10^{-5} \text{ S cm}^{-1}$ [614].

Polythienothiophenes. Thieno[2,3-b]thiophene [633], thieno[3,2-b]thiophene [634], dithieno[3,2-b:2',3'-d]thiophene [635], and the corresponding electrogenerated polymers have all been investigated [636–639] (Fig. 28). Contrary to theoretical expectations,

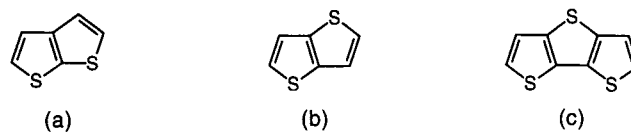


Fig. 28. Structure of (a) thieno[2,3-b]thiophene, (b) thieno[3,2-b]thiophene, and (c) dithieno[3,2-b:2',3'-d]thiophene.

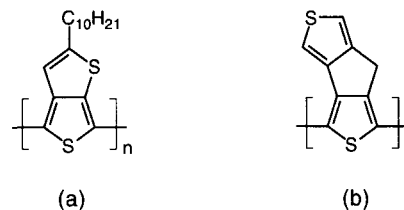


Fig. 29. Structure of (a) poly(4-decylthieno[3,4-b]thiophene) and (b) poly(dithieno[3,4-b:3',4'-d]thiophene).

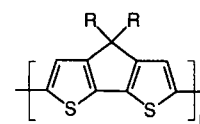


Fig. 30. Cyclopenta[2,1-b:3',4'-b']dithiophene.

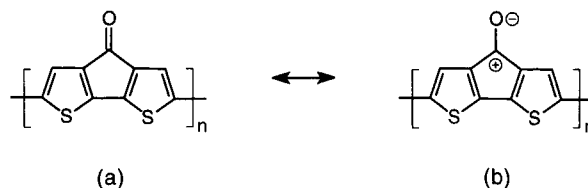


Fig. 31. Poly(cyclopenta[2,1-b:3',4'-b']dithiophen-4-one): (a) aromatic and (b) antiaromatic resonance forms.

these polymers showed bandgaps slightly larger than that of polythiophene [640].

Poly(4-decylthieno[3,4-b]thiophene) (Fig. 29a) has been prepared by Pomerantz et al. [641–643] using $FeCl_3$. The material showed a λ_{\max} at 738 nm. The bandgap obtained from the band edge was around 1.2 eV.

Dithieno[3,4-b:3',4'-d]thiophene [635] (Fig. 29b) can be polymerized electrochemically [640, 644–646] or photochemically [647]. The polymer seems to be transparent in the visible spectral region in its doped form, while the low-energy absorption edge of the undoped neutral state indicates a bandgap of 1.1–1.2 eV [648].

Bridged Bithiophenes. Cyclopenta[2,1-b:3',4'-b']dithiophene [649, 650] (Fig. 30) has been polymerized electrochemically and is characterized by a lower oxidation potential and relatively high conductivity as compared to polythiophene [651–653]. Polymers based on bridged bithiophenes gained a renewed interest when Lambert and Ferraris [654] reported that the electropolymerization of cyclopenta[2,1-b:3',4'-b']dithiophen-4-one led to a polymer with a bandgap of 1.1–1.2 eV. The idea was that the electron-withdrawing effects of the ketone group and the contribution of an antiaromatic resonance form should decrease the aromaticity of the system and hence increase the quinoid character of the polymer (Fig. 31). Encouraged by this result, researchers used cyclopenta[2,1-b:3',4'-b']dithiophen-4-one as the basis for the

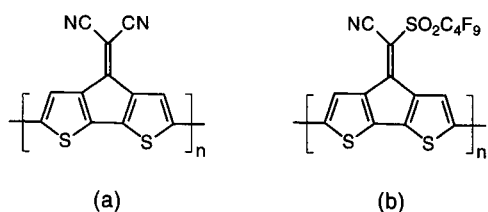


Fig. 32. Structure of (a) poly(4-dicyanomethylene)-4*H*-cyclopenta[2,1-*b*:3',4'-*b'*]dithiophene) and (b) poly(4-[cyano(nonafluorobutyl)sulfonyl]methylidene)cyclopenta[2,1-*b*:3',4'-*b'*]dithiophene).

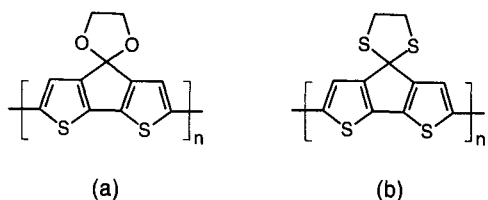


Fig. 33. (a) Dioxolane analog of poly(cyclopenta[2,1-*b*:3',4'-*b'*]dithiophene) and (b) its sulfur derivative.

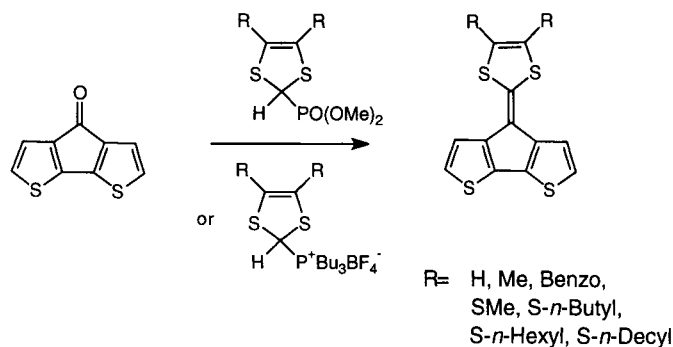


Fig. 34. Wittig-Horner or Wittig olefination of cyclopenta[2,1-*b*:3',4'-*b'*]dithiophen-4-one with appropriate phosphonate esters or phosphonium salts.

synthesis of several derivatives such as 4-dicyanomethylene)-4*H*-cyclopenta[2,1-*b*:3',4'-*b'*]dithiophene [655] and 4-[cyano(nonafluorobutyl)sulfonyl]methylidene)cyclopenta[2,1-*b*:3',4'-*b'*]dithiophene [656] (Fig. 32). The dioxolane analog and its sulfur derivative were polymerized electrochemically (Fig. 33) [657–660]. The compounds of Figure 34 were synthesized by Wittig-Horner or Wittig olefination of cyclopenta[2,1-*b*:3',4'-*b'*]dithiophen-4-one with appropriate phosphonate esters or phosphonium salts [661–663].

2.2.4.2. Ladder-Type Polymers

Polyacenes. Another approach to obtain better organic conductive materials can be found in increasing the dimensionality of low-dimensional π -conjugated polymers through the design of one-dimensional graphite-like ribbons [137]. Polyacene is probably the most famous member of this class of materials. Interest in this material is based on theoretical considerations as well as experimental results obtained for the first members of the oligomer series [664]. Polyacene can be viewed as a combination of two parallel chains of *trans*-(CH)_x fastened together (Fig. 35). Oligomers of the acene series have been synthesized up to heptacene [665]. Examination

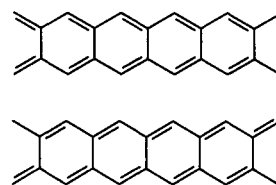


Fig. 35. Polyacene viewed as a combination of two parallel chains of *trans*-(CH)_x fastened together.

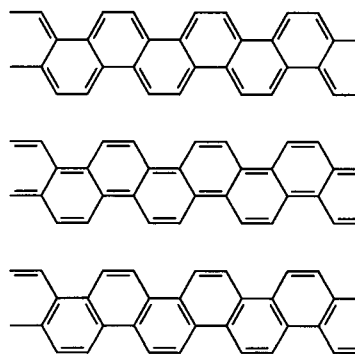


Fig. 36. Polyphenanthrene viewed as the result of various combinations of *cis*-(CH)_x chains.

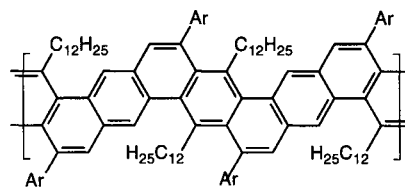


Fig. 37. Polyphenanthrene synthesized by an electrophilic-induced cyclization reaction.

of the redox potential and the highest occupied molecular orbital (HOMO)–lowest unoccupied molecular orbital (LUMO) gap (ΔE) of the first members of the series reveals a sharp decrease of ΔE from naphthalene to heptacene [664, 666]. Several attempts to synthesize polyacene have led to materials of unspecified structure [667–670]. Precursors have been synthesized by means of repetitive Diels–Alder additions [671, 672]. Preparation of polyacene by means of LB methods has also been considered [673]. Oligomers with polyacene-based structures have been prepared by heating diphenyldiacetylene under high pressure [674, 675].

Fastened parallel π -conjugated chains of (CH)_x can be combined in different ways. Thus, polyphenanthrene can be viewed as the result of various combinations of *cis*-(CH)_x chains (Fig. 36). A polymer with a structure close to that of Figure 36 was synthesized by an electrophilic-induced cyclization reaction [277, 309] (Fig. 37). A polyphenanthrene derivative with cyclic imine structures has been synthesized by Tour and Lamba [310, 676] (Fig. 38). The synthesis is based on Suzuki coupling, followed by a ring closure reaction to form the imine structure.

Poly(perinaphthalene). Poly(perinaphthalene) (Fig. 39) can also be viewed as a special kind of combination of (CH)_x chains. Kaplan et al. [677] reported on poly(perinaphthalene)-like material obtained by pyrolysis of 3,4,9,10-perylenetetracarboxylic dianhydride (PTCDA) at 700–900°C in vacuum. Conductivity was measured to be 250 S cm⁻¹. When the pyrolysis was performed in

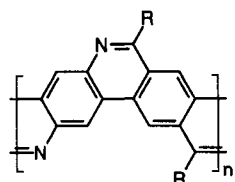


Fig. 38. Polyphenanthrene with cyclic imine structures.

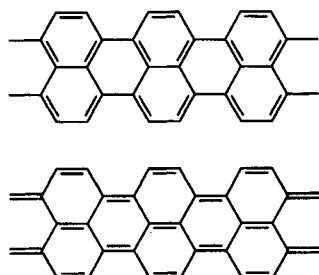


Fig. 39. Poly(perinaphthalene).

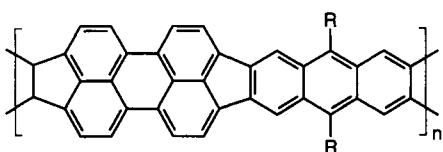


Fig. 40. Ladder polymer consisting of a combination of poly(perinaphthalene) and polyacene.

the presence of niobium, the resulting material appeared to be superconducting with an onset T_c of 12 K [677–679]. Other reports mention different conductivity values, depending on the synthesis parameters [680–682]. Chemical vapor deposition has also been used with PTCDA as the precursor [683]. The difficulties in the synthesis of the polymer triggered the interest in shorter soluble oligomers [684–686]. The synthesis of the soluble oligomers is based on the Pd-catalyzed coupling of alkyl-substituted arylboronic acids with dibromo aromatic compounds (Suzuki coupling).

Another type of ladder polymer consists of a combination of poly(perinaphthalene) and polyacene (Fig. 40). The resulting structure is reminiscent of the open-chain analog of the belt region of C_{60} [687]. More soluble oligomers have also been prepared for these materials [688, 689].

Polyheteroacenes. Polyheteroacenes are polyacenes in which carbon atoms have been replaced by heteroatoms. Polyquinoxalines (Fig. 41a) have initially been developed because of their high tensile strength and excellent thermal stability [690, 691]. Their electronic properties have drawn renewed attention when it was suggested that the rigidification of the structure represented an interesting approach for the improvement of the electronic properties of the polymers with respect to electronic and nonlinear optical applications [692–694]. Polyquinoxalines have been prepared by the condensation of a dihydroxy diketone with aromatic polyamines [690–692].

Other related structures involve rigid oligomers with a heteroacene skeleton such as oligophenothiazines obtained via direct thionation of various aniline derivatives [695]. Polyphenothiazine and polyphenoxazine (Fig. 41b and c) have also been prepared by

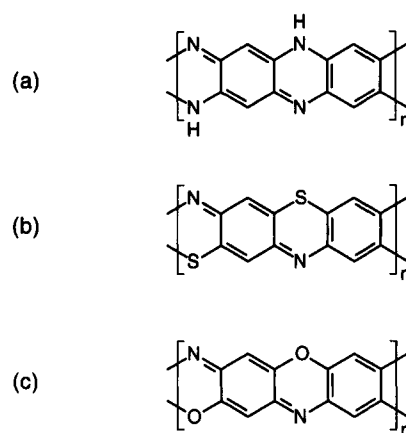


Fig. 41. Polyheteroacenes: (a) polyquinoxaline, (b) polyphenothiazine, and (c) polyphenoxazine.

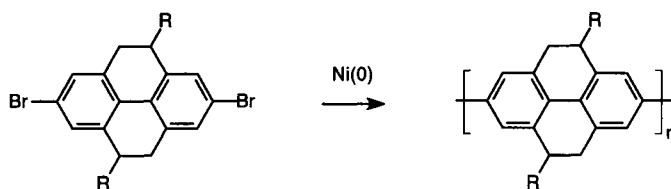


Fig. 42. Synthesis of poly(tetrahydropyrene) from a dibromo precursor.

other groups and their conductivity discussed without reporting data concerning the bandgap [696, 697].

A semiconducting ladder polymer was obtained by polycondensation of 2,3,5,6-tetrachlorobenzoquinone and a 3,7-diaminophenazinium chloride. Depending on the method of preparation, the conductivity ranges between 7.2×10^{-8} and 8×10^{-6} S cm^{-1} . However, conductivity did not increase upon doping [698].

The synthesis of ladder polyanilines was attempted through the electropolymerization of *o*-phenylenediamines or *o*-aminophenols [699–703].

Alkyl-Bridged Poly(*p*-phenylene)s. More conclusive results have been obtained concerning the preparation of rigidified poly(*p*-phenylene)s. One first approach in this direction involved the synthesis of poly(tetrahydropyrene) from a dibromo precursor [277] (Fig. 42).

The synthesis of alkyl-bridged poly(*p*-phenylene)s is based on typical poly(*p*-phenylene) chemistry, followed by a second reaction in which the rigidifying bridge is created. Scherf et al. [314, 315, 704, 705] used Suzuki coupling to create a ketone-substituted poly(*p*-phenylene). In a next step, the ketone functions in this polymer were reduced and, finally, the ladder polymer was obtained by Friedel–Crafts alkylation (Fig. 43).

The so-obtained ladder poly(*p*-phenylene) was converted to poly(arylenemethide) (Fig. 44) by dehydrogenation with DDQ or through lithiation of the benzylic positions followed by oxidation using cadmium chloride [706, 707].

2.2.5. Copolymers of Aromatic Ring Systems

The properties of π -conjugated polymers can be varied over a wide range of conductivity, processibility, and stability, depending on the type and number of substituents, rings, and ring fusions. As is true for other areas of polymer chemistry, the use of copolymers

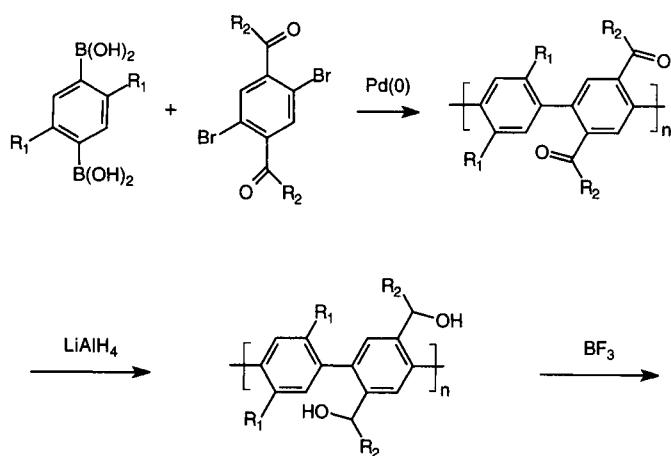


Fig. 43. Synthesis of alkyl-bridged poly(*p*-phenylene)s.

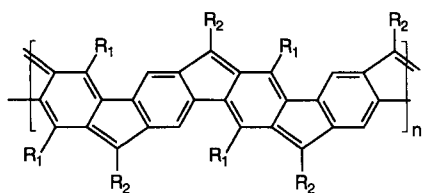


Fig. 44. Dehydrogenation with, e.g., DDQ, yields a ladder-type poly(arylenemethide).

can simultaneously broaden and allow better control over these and other properties. Copolymerization, a process in which two or more monomers are incorporated as integral segments of a polymer, is used to produce copolymers with properties that are different from those of the homopolymers [383]. In general, copolymers possess physical and mechanical properties intermediate between both homopolymers. The magnitude of the numerical values of these properties generally depends on the concentration of the monomer units incorporated into the copolymer. The primary advantage of copolymerization is that it leads to a homogeneous material, the properties of which can be regulated by adjusting the ratio of the concentration of the monomers. By its very nature, copolymerization offers the unique and unlimited capability or opportunity for chemists to design and construct molecules with special optical and electronic properties using established techniques [383].

Due to the various possibilities for copolymerization, every discussion will somehow present only a partial view. The discussion in this section focuses on fully conjugated systems in which aromatic ring systems are being used as monomeric units. This kind of copolymer has already in one way or another been discussed in several reviews [137, 383, 384, 389, 643].

There are four kinds of copolymers: random, alternating, block, and graft. In the case of copolymers in which aromatic ring systems

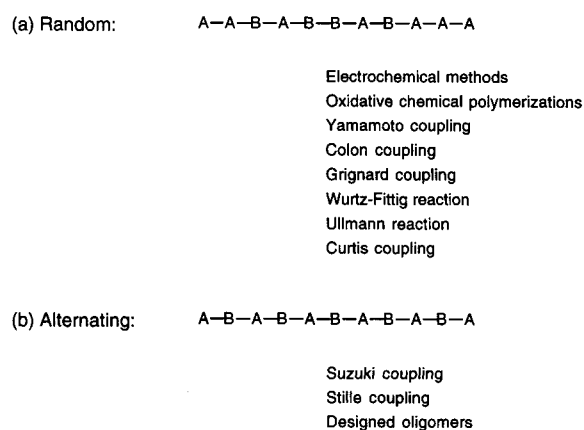


Fig. 45. (a) Random and (b) alternating copolymers.

are being used as monomeric units, one will encounter mainly two types of copolymerizations: random copolymerization, in which the arrangement of monomeric units is in a statistically random placement along the chain, and alternating copolymerization, in which two types of monomeric units alternate regularly in the polymer chain (Fig. 45). The chemistry of copolymerization is, to a large extent, based on the polymerization chemistry presented earlier in this chapter. As a consequence, obtaining random or alternating copolymers depends either on the specificity of the synthetic procedure or on the structure of the monomer used.

Alternating copolymers are obtained either by using procedures in which there is also a chemical differentiation between both monomers at the level of the coupling process (e.g., polycondensation reactions such as Suzuki coupling and Stille coupling) or by using specifically designed oligomeric compounds, which are then polymerized. Random copolymers are obtained by electrochemical methods, oxidative chemical polymerizations, Yamamoto coupling, Colon coupling, Grignard coupling, Wurtz-Fittig reaction, Ullmann reaction, and Curtis coupling (Fig. 45).

In this section, copolymers of the same aromatic systems but with different substituents will be treated first, followed by copolymers of different aromatic systems and the special class of poly(arylene methine)s. Because of its special position in the field of conducting polymers, poly(*p*-phenylene vinylene), which can be considered as an alternating copolymer of poly(*p*-phenylene) and polyacetylene, will be discussed separately.

2.2.5.1. Same Aromatic Ring – Different Substituents

From the previous discussion, it is clear that there are many ways to introduce substituents onto different aromatic ring systems, affording a large number of monomers. These monomers are amenable to oxidative polymerization as substituents, in general, impart little electronic perturbation to a monomer's oxidation potential. When substituents become larger or interact with the aromatic system through conjugation, however, the redox potential of the monomer can be influenced to such an extent as to impede the coupling of the radical cations. Nevertheless, a large number of such copolymers have been prepared as well for thiophene and pyrrole as for phenylene mostly on the basis of their specific chemistry (see previous discussion) (Fig. 46).

Copolymers of Substituted Phenylene. Suzuki polycondensation has been used to copolymerize alternating substituted and non-

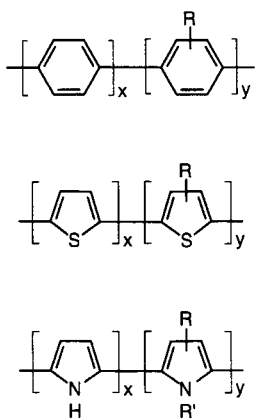


Fig. 46. Copolymers with the same aromatic ring but different substituents.

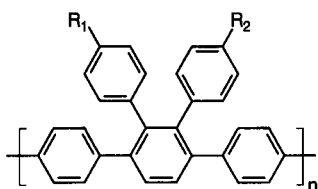


Fig. 47. *P*-phenylene trimer with two aryl substituents at the central phenylene ring.

substituted phenylene moieties [301]. Similar chemistry has been used in the synthesis of the precursors for ladder polymers. These precursors are, in fact, alternating copolymers [224, 309, 310, 314, 315, 676, 704–707] (e.g., Fig. 43). Poly(*p*-phenylene)-based polyelectrolytes have also been prepared by different groups [302, 303, 305, 306, 708]. A *p*-phenylene trimer with two aryl substituents at the central phenylene ring has been polymerized using the Colon method [709] (Fig. 47).

Copolymers of Substituted Thiophenes. Random copolymers of substituted thiophenes have been prepared [71, 93, 396, 433, 434, 512, 710–728]. Several designed bithiophenes and terthiophenes have also been polymerized to produce random but mostly alternating copolymers [503, 652, 729–736]. A copolymer consisting of thiophene and alkoxythiophene units has been obtained by cyclization with Na_2S of an intermediate polymer [737] (Fig. 48).

Copolymers of Substituted Pyrroles. Several groups have copolymerized pyrroles with *N*-substituted pyrroles or pyrroles bearing substituents in the 3- or 4-position [505, 563, 738–765].

2.2.5.2. Different Aromatic Rings

Copolymerization of different aromatic ring systems offers the promise to obtain materials with properties situated in between those of both parent homopolymers. Due to the different chemical reactivities of the various aromatic ring systems, direct oxidative procedures are not always straightforward to carry out. To obtain alternating copolymers, the main strategy relies on the synthesis of suitable oligomeric compounds, which are finally polymerized according to well-known coupling procedures. The major issue in the latter case concerns the sometimes advanced synthetic effort required to obtain the sought-after oligomeric compound.

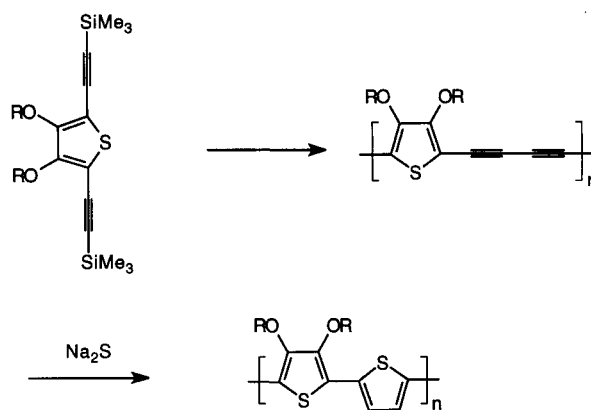


Fig. 48. Substituted thiophene copolymer obtained by cyclization with Na_2S of an intermediate polymer.

Pyrrole–Thiophene. Random copolymers consisting of thiophene and pyrrole units have been prepared on the basis of electrochemistry or direct chemical oxidation. The main problem associated with these processes is the large difference between the electrochemical oxidation potentials of pyrrole (0.6 V vs SCE) and thiophene (1.6 V vs SCE). To overcome this problem, the strategy used to carry out this copolymerization has been to oxidize pyrrole under diffusion-limiting conditions at potentials where thiophene oxidation takes place. Under these conditions, pyrrole is kept at concentrations 100 times lower than thiophene [505, 766–773]. Alternating copolymers have been prepared on the basis of di- or trimeric oligomers, polymerized according to well-established procedures [498, 767, 771, 773–781] (Fig. 49a). A copolymer of alkoxythiophene and pyrrole has been obtained through cyclization of a precursor polymer [737] (Fig. 50).

Pyrrole–furan. 2,2'-furylpyrrole [774] has been synthesized and electrochemically polymerized [778, 782] (Fig. 49b). The low conductivity in some of the derivatives was attributed to overoxidation

Pyrrole–Benzo[*b*]thiophene. A highly conductive polymer has been prepared from the electrochemical polymerization of pyrrole and benzo[*b*]thiophene [783] (Fig. 51).

Thiophene–Furan. A copolymer based on 2-(2'-thienyl)furan has been prepared [652] (Fig. 49c). Most furan-containing polymers, however, have been synthesized from α -linked three-ring systems. The different trimeric systems of Figure 49c have been polymerized [776, 778, 782].

Thiophene–Pyridine. In an effort to combine the electron-donating properties of thiophene with the electron-accepting nature of pyridine, Mitsuhashi et al. [784] electropolymerized 2,5-, 2,6-, and 3,5-[di(2-thienyl)]pyridine derivatives. Others have carried out chemical polymerization of 2-(2-thienyl)pyridine and 2,5-di(2-pyridyl)thiophene by dehalogenative polycondensation of the corresponding dihaloaromatic compounds using a zero-valence nickel complex [785, 786] (Fig. 49d).

Thiophene–Thiazole. Copolymers of thiophene or 3-methoxythiophene with methylthiazole have been electrochemically synthesized from α -linked four-ring monomers. The conductivity and redox potential of this copolymer appear to be comparable to those observed for poly(α -terthiophene) [787] (Fig. 49e).

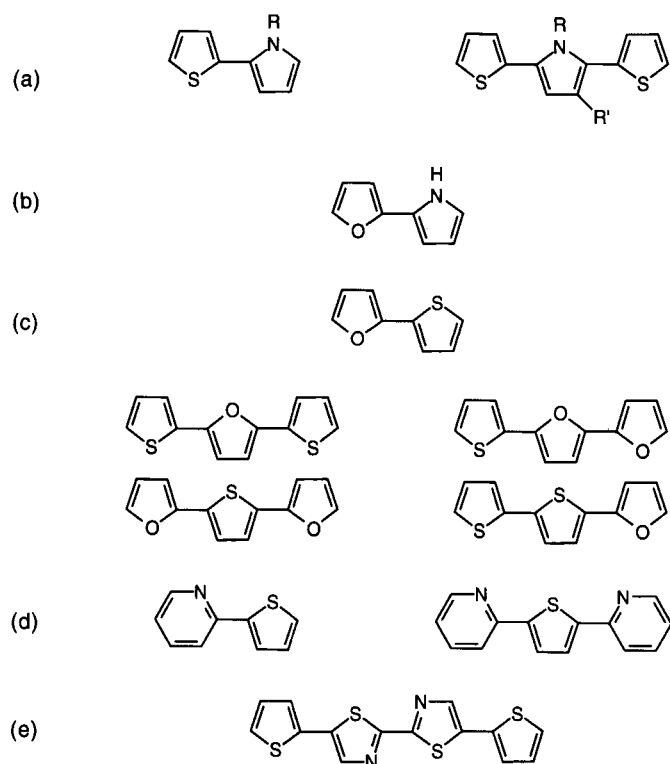


Fig. 49. Various oligomeric compounds used to prepare copolymers with different aromatic ring systems.

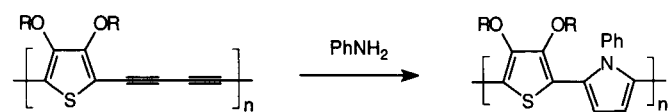


Fig. 50. Copolymer of alkoxythiophene and pyrrole obtained through cyclization of a precursor polymer.

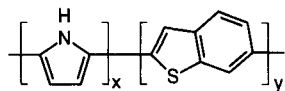


Fig. 51. Highly conductive polymer prepared from the electrochemical polymerization of pyrrole and benzo[*b*]thiophene.

Thiophene–Benzo[*c*]thiophene (or Isothianaphthene). Polymers derived from α -terthiophenes bearing a variety of fused central ring systems have been prepared. These materials were synthesized in the context of small-bandgap polymers. The insertion of a specific ring system into the middle of a trimeric precursor presents several advantages such as the construction of alternate donor and acceptor moieties or the stabilization of rather unstable fused ring systems.

The earliest application of this approach was the development of the three-ring system 1,3-bis(2-thienyl)benzo[*c*]thiophene or 1,3-dithienylisothianaphthene (Fig. 52a). The synthesis of this compound was reported almost simultaneously by four groups [788–792]. The procedure proposed by Kiebooms et al. [790] has been used to prepare several substituted derivatives [793–795]. The electropolymerization of 1,3-dithienylisothianaphthene [788, 791, 792] yielded a material with a bandgap of around 1.7 eV, a value intermediate between those of polythiophene and poly-

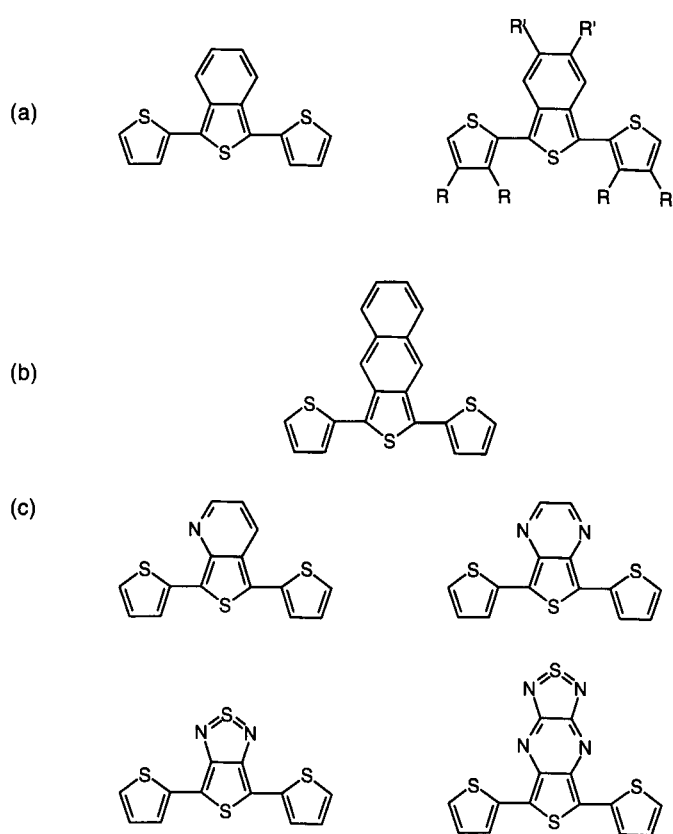


Fig. 52. Thiophene oligomers with fused ring systems on the central unit.

isothianaphthene. The different substituted derivatives possess bandgaps in the range between 1.2 and 1.7 eV [793–795]. Derivatives in which the heteroatom in the central ring was oxygen [788, 791, 792] or N–CH₃ [792] have also been prepared.

Thiophene–Naphto[2,3-*c*]thiophene (or Isonaphthothiophene). A terthienyl containing a central naphto[2,3-*c*]thiophene (or isonaphthothiophene) was prepared using one of the routes also used to obtain 1,3-dithienylisothianaphthene [628] (Fig. 52b). Although a bandgap of 0.65 eV was claimed, this result was not unequivocally confirmed by the optical spectra.

Thiophene–Thieno[3,4-*b*]pyrazine. Interaction between the hydrogens on the 4- and 7-positions of the isothianaphthene rings and the adjacent thiophene rings causes the rings to rotate out of plane. As a consequence, the value of the bandgap becomes larger because of decreased inter-ring conjugation. To reduce steric interactions between the fused benzene ring and the adjacent thiophene rings in 1,3-dithienylisothianaphthene, nitrogens have been introduced at the 4- and 7-positions of the isothianaphthene ring (Fig. 52c). Polymers based on thieno[3,4-*b*]pyrazine [796] and thieno[3,4-*b*]pyridine [797] have been reported. The values of the bandgap are 1.4 and 1.0 eV, respectively. Two other members of

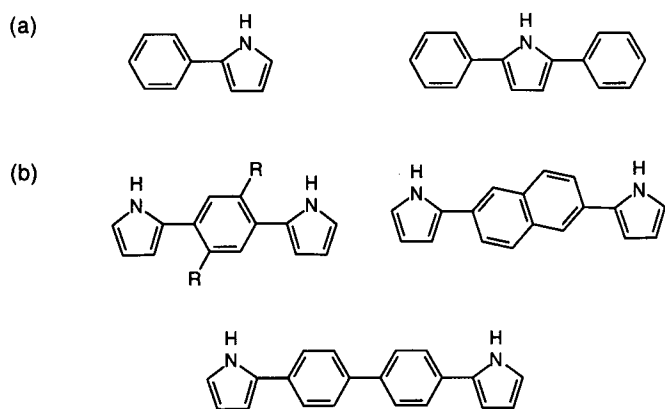


Fig. 53. Different pyrrole-based oligomers used to prepare pyrrole-benzene copolymers.

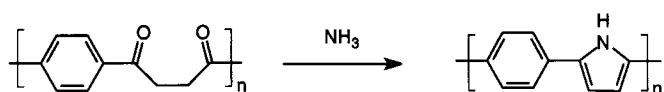


Fig. 54. Pyrrole-benzene copolymers obtained by cyclization of a polyphenylene diketone in the presence of ammonia.

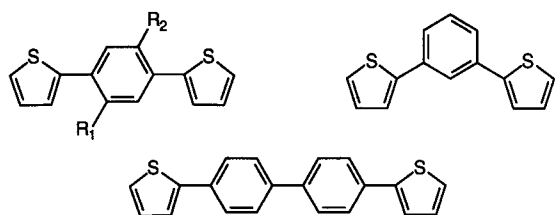


Fig. 55. Different thiophene-based oligomers used to prepare thiophene-benzene copolymers.

this class of compounds are those derived from the monomers incorporating the nonclassical fused thienothiadiazole [798, 799], whose completely planar structure yields a polymer with a bandgap of 0.9 eV, and the extended system [800, 801], which has an estimated gap of 0.3 eV. Benzobis(1,2,5-thiadiazole) has also been prepared [800].

Pyrrole-Benzene. Copolymers of pyrrole and benzene have been synthesized from 2-phenylpyrrole and 1,4-bis(2-pyrrol-yl)phenylene [802] (Fig. 53a). Chemical syntheses of similar copolymers have been carried out by cyclization of a polyphenylene diketone in the presence of ammonia [803] (Fig. 54). Pd(0)-catalyzed coupling of boronic acid derivatives of 1,4-bisdodecylbenzene and 2,5-dibromopyrrole has also been used [804]. A series of 1,4-bis(2-pyrrol-2yl)arylenes have been synthesized and chemically and electrochemically polymerized as well [805] (Fig. 53b).

Thiophene-Benzene. 1,4-bis(2-thienyl)phenylene has been electropolymerized [806, 807]. Electrochemical polymerization of 1,3-bis(2-thienyl)phenylene and 1,4-bis(2-thienyl)biphenylene has also been reported [784, 808] (Fig. 55). Random copolymers have been obtained from the Ni(II) coupling of different molar ratios of 2,5-dibromothiophene and 1,4-dibromobenzene [809, 810]. A series of substituted 1,4-bis(2-thienyl)phenylenes have been polymerized on the basis of a procedure similar to the Rieke method [811, 812]. In addition, the group of Reynolds prepared an exten-

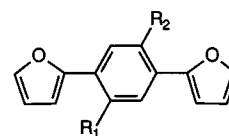


Fig. 56. 1,4-bis(2-furanyl)phenylenes used in copolymerization reactions.

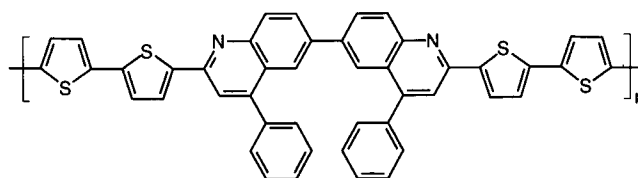
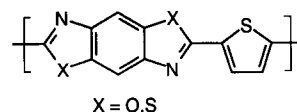
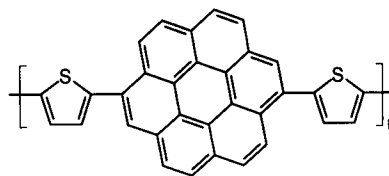


Fig. 57. Copolymers of thiophene and complex arylenes.

sive series of substituted poly(1,4-bis(2-thienyl)phenylene)s [813–817]. Copolymers of thiophene and benzene have also been obtained by means of the Yamamoto method [273, 818]. Copolymers of thiophene- and alkoxy-substituted benzenes have been synthesized by means of the Stille reaction [819, 820].

Furan-Benzene. Pelter et al. [811, 812] have chemically prepared structural isomers of furan-phenylene copolymers by reacting bis-zinc chlorides of 1,4-bis(2-furanyl)phenylenes with 1,3- and 1,4-dibromobenzene. The group of Reynolds has also investigated these copolymers [817, 821] (Fig. 56).

Thiophene-Complex Arylenes. An alternating copolymer of bis-thienyl and corenene has been reported [822]. Numerous other electroactive copolymers containing more complex heterocyclic rings have been prepared [823–829] (Fig. 57).

3,4-Ethylenedioxythiophene-Arylenes. In a series of papers, the Reynolds group reported on a set of monomers that straddle various aryl groups with the 3,4-ethylenedioxythiophene system. These compounds allow wide control over bandgap and redox properties [830–835] (Fig. 58).

Thiophene-Pyrrole-Furan. There are only a few examples in which three different heterocycles have been incorporated into a polymer. One of those is obtained by the chemical polymerization of an α -linked three-ring system containing thiophene, *N*-methylpyrrole, and furan [778, 782] (Fig. 59).

2.2.5.3. Poly(arylene methine)s

Poly(arylene methine)s are a class of conjugated materials based on the association of aromatic and quinoid moieties. These poly-

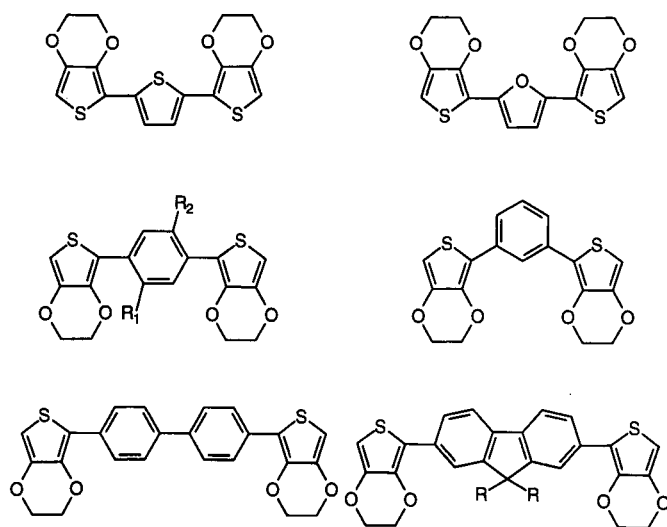


Fig. 58. 3,4-Ethylenedioxythiophene-based oligomers.

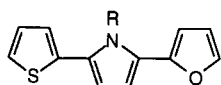


Fig. 59. Triheterocyclic system.

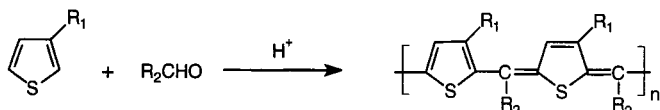


Fig. 60. Synthesis of poly(thiophene methine)s by acid-catalyzed polymerization of thiophene and an aldehyde.

mers were proposed by Jenekhe and co-workers as a new class of low-bandgap polymers. The idea was based on theoretical considerations that led to the conclusion that the quinoid form of polythiophene should possess a significantly smaller bandgap than the aromatic form [836]. By forcing some parts of the π -conjugated system to adopt a quinoid geometry and by mixing the aromatic and quinoid forms in variable proportions, one should, in principle, be able to tune the bandgap between the two limiting values [837]. The synthesis and characterization of poly(thiophene methine)s has been extensively studied by Chen and Jenekhe [838, 839]. The polymers were obtained by acid-catalyzed polymerization of thiophene and an aldehyde (Fig. 60). In the case of oligothiophene, a precursor polymer was obtained, which was in a second step converted to the fully conjugated system by dehydrogenation using DDQ (Fig. 61).

A variation on this method was proposed by Goto et al [840] in which the use of acid was replaced by POCl_3 to synthesize poly(thiophene methine)s bearing liquid crystalline side groups. This method was also applied to prepare poly(isothianaphthene methine) [841] (Fig. 62).

Other groups developed alternative methods toward the synthesis of poly(arylenemethine)s. For example, the condensation of 2-(chloromethyl)-5-formylfuran with pyrrole and thiophene, or the reaction of α,α' -trichloro-*p*-xylene with aromatic compounds in the presence of Friedel-Crafts catalyst [842], was reported. The condensation of 2-lithiothiophene with 2, 5'-dithiophenedicarboxaldehyde or 2,5-dilithiothiophene with 2-formylthiophene gives a

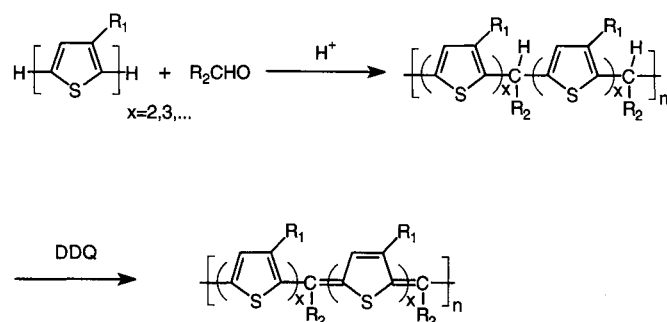
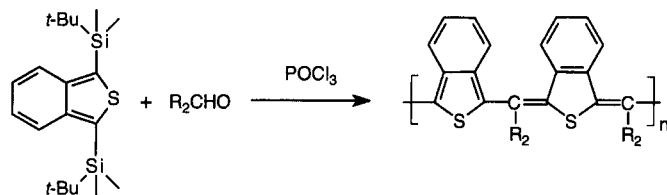
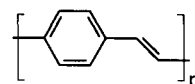


Fig. 61. Synthesis of an oligothiophene by dehydrogenation using DDQ.

Fig. 62. Poly(isothianaphthene methine) obtained by using POCl_3 instead of an acid.Fig. 63. Structure of poly(*p*-phenylene vinylene).

dicarbonyl [843, 844]. The dicarbonyl was believed to polymerize by the addition of protonic or Lewis acids. Both methods, however, yield materials with a considerable number of structural defects.

2.3. Poly(*p*-phenylene vinylene)s

The first reports on poly(*p*-phenylene vinylene) (PPV) (Fig. 63) date back to before the emergence of research on the electronic and photonic properties of polyconjugated materials. PPV can be considered as an alternating copolymer of poly(*p*-phenylene) and polyacetylene. Interest increased during the 1980s because PPV could be prepared by a precursor method discovered by Wessling et al. [845–847]. Further research on PPV was boosted after the use of PPV as an organic electroluminescent layer in light-emitting devices [848]. An increasing number of papers are published, but a lot of questions still remain open. A detailed review on the chemistry and uses of PPV appears in [849].

There are several approaches toward the preparation of PPV, which can be classified as direct and precursor methods. Several of these methods have been applied to synthesize heterocyclic derivatives (e.g., poly(thienylene vinylene) [850–855], alkoxy-substituted poly(thienylene vinylene) [856–859], poly(furylene vinylene) [860]).

2.3.1. Direct Syntheses of PPV

As usual, the recurring problem of the insolubility of polyconjugated systems needed to be overcome in order to obtain a polymer of reasonable quality. In the case of the direct methods, the only way to achieve this goal is by incorporation of solubilizing side chains (e.g., alkyl, alkoxy), which prevent the polymer from precipitating during polymerization. Direct polymerization occurs

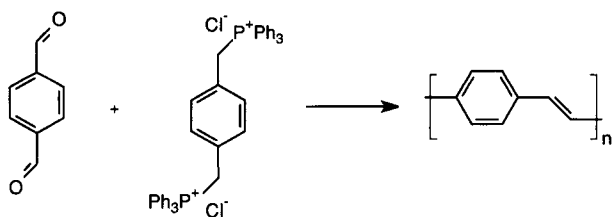


Fig. 64. Wittig reaction.

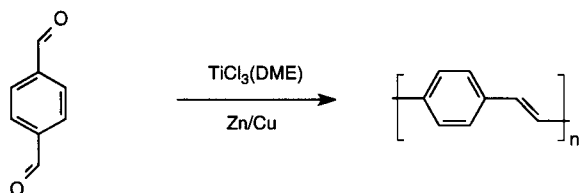


Fig. 65. McMurray reaction.

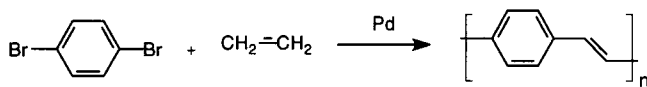


Fig. 66. Heck reaction.

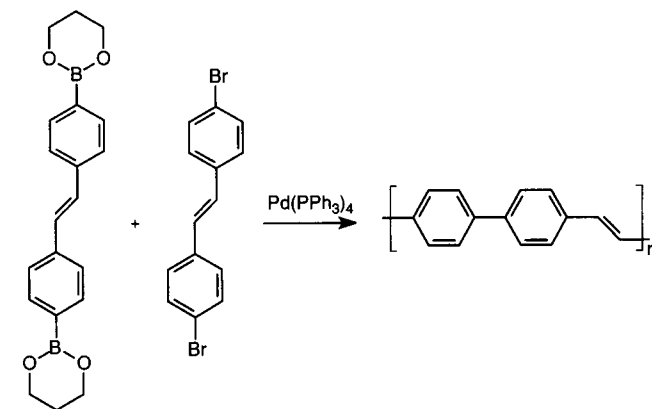


Fig. 67. Suzuki coupling.

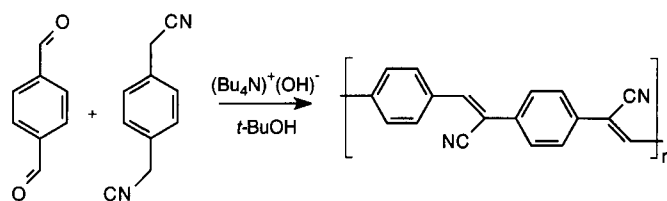


Fig. 68. Knoevenagel condensation.

mostly through polycondensation-like polymerizations based on well-known coupling reactions.

Wittig Coupling. McDonald and Cambell [861] prepared PPV by repetitive Wittig-type couplings between an aromatic bisphosphonium salt and a bisaldehyde (Fig. 64). This reaction was further investigated by Gourley et al. [862]. Since the initial work of McDonald and Cambell, several other PPV derivatives have been synthesized [863–866].

McMurray Coupling. McMurray coupling consists of the deoxygenative coupling of an aromatic dialdehyde (Fig. 65). By improving the reaction conditions for PPV, Rehahn and Schlüter [867] were able to obtain relatively high molecular weight polymers by coupling an alkylated aromatic dialdehyde in the presence of Zn/Cu and TiCl₃(dimethoxyethane)_{1.5}. Other PPV derivatives or related polymers have been synthesized on the basis of this method [851, 868, 869].

Heck Reaction. The Heck reaction [870] allows the double bond to be directly introduced into the polymer chain. A variety of aromatic dibromides have been polymerized with ethylene to produce both PPV and soluble derivatives [871] (Fig. 66). Other dihalogen derivatives can also be used in this reaction [872]. Besides many possible side reactions, another disadvantage of this method is that one of the reactants is gaseous and must be added in precise amounts. Reaction conditions are mild, however, and are tolerant of many functional groups [873–877].

Suzuki Coupling. PPV can also be synthesized by Pd-catalyzed coupling of alkyl-substituted arylboronic acids with dibromo aromatic compounds (Fig. 67). Several derivatives have been synthesized in this way, among which poly(trisphenylene vinylene) [272, 705, 878–880].

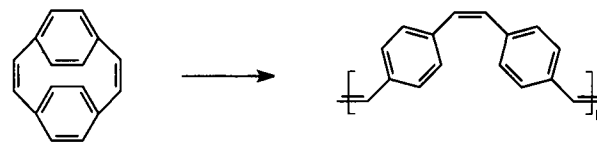


Fig. 69. Synthesis of PPV by metathesis of paracyclophane dienes.

Knoevenagel Condensation. This method can be used to introduce electron-withdrawing groups into conducting polymers by the reaction of an aromatic aldehyde with a benzylic nitrile catalyzed by an amine or amine salt (Fig. 68). Careful optimization of the reaction conditions is needed to reduce unwanted side reactions such as hydrolysis of the nitrile group or Michael addition to the double bond [881–894].

Siegrist Reaction. Double bonds can be synthesized by a variety of base-catalyzed condensations between an active methylene compound and a carbonyl group. Meier et al. [895, 896] used a base-catalyzed self-coupling of the Schiff bases of various *p*-methylbenzaldehydes to prepare PPV.

Metathesis-Catalyzed Reactions. Metathesis catalysts are used to break and recombine double bonds. In this way, unsaturated compounds can be isomerized and rearranged to give new compounds. Kumar and Eichinger [897] oligomerized divinylbenzene with the Schrock catalyst to give low-molecular-weight PPV. This was extended by Thorn-Csányi and co-workers [898, 899] to give a soluble PPV derivative of moderate molecular weight. Due to the sensitivity of the catalysts, the low degrees of polymerization obtained, and the difficulty in synthesizing the appropriate monomers, there seems to be little advantage to this route. PPV is also obtainable by metathesis of paracyclophane dienes [900] (Fig. 69). The synthesis of substituted cyclophanes presents a significant barrier to further exploitation of this idea for other PPV derivatives.

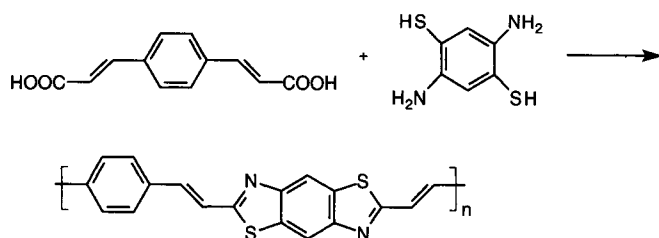


Fig. 70. Benzothiazole condensation.

Coupling of Benzylic Halides. Stilbenes can be produced in high yield by the coupling of benzylic halides in liquid ammonia with sodium amide [901, 902]. This reaction was extended to the preparation of PPV. By using dichloroethylene under the same conditions, researchers produced a yellow solid polymer containing a significant amount of residual chlorine. Similar results were obtained by Hörhold and Opfermann [863] using sodium hydride in DMF. The presence of chloride in the final product was attributed to the presence of incompletely eliminated unsaturated linkages that could be removed by heating to 300°C [862]. A related route was used by Moritani et al. [903] whereupon treatment of tetrabromo-*p*-xylene with two equivalents of methyl lithium gave PPV. The mechanism of this reaction has not yet been fully elucidated [863, 904]. PPV and its derivatives can also be produced by dechlorination condensation of tetrachloroxylenes with Cr(II) acetate [905–907]. Similarly, perchloroethylene can be polymerized with Fe(CO)₅ to give a perchloro-PPV derivative [908].

Benzothiazole Condensation. Osaheni and Jenekhe [909] synthesized a benzobisthiazole PPV derivative by condensation of diacrylic acid with 2,5-diamino-1,4-benzenethiol (Fig. 70).

Electrochemical Polymerization. PPV has also been prepared electrochemically using different types of monomeric compounds [910, 911].

2.3.2. Precursor Routes to PPV

Several different methods have been reported. Those methods that have received less attention will be treated first. The Wessling precursor method has been subject to an enormous amount of research despite its inherent drawbacks. Finally, the Louwet–Vanderzande route provides a new approach for further interesting developments in this field.

Benzoine Condensation. Kaul and Fernandez [912] reported the preparation of functionalized PPV derivatives containing alkyloxy side groups on the vinyl bond. These PPV derivatives were obtained through the formation of a polybenzoine. In the presence of a strong base, the polybenzoine was transformed into a polydi-anion. Reaction of the latter with acetylchloride or dimethylsulfate resulted in the functionalized PPV (Fig. 71).

Ring-Opening Metathesis Polymerization. Conticello et al. [913] reported the coupling of a bicyclooctadiene compound by ring-opening metathesis polymerization to give a high-molecular-weight precursor polymer soluble in organic solvents. The polymer can be converted to PPV by thermal treatment or by using 2,3-dichloro-5,6-dicyanoquinon [914, 915] (Fig. 72).

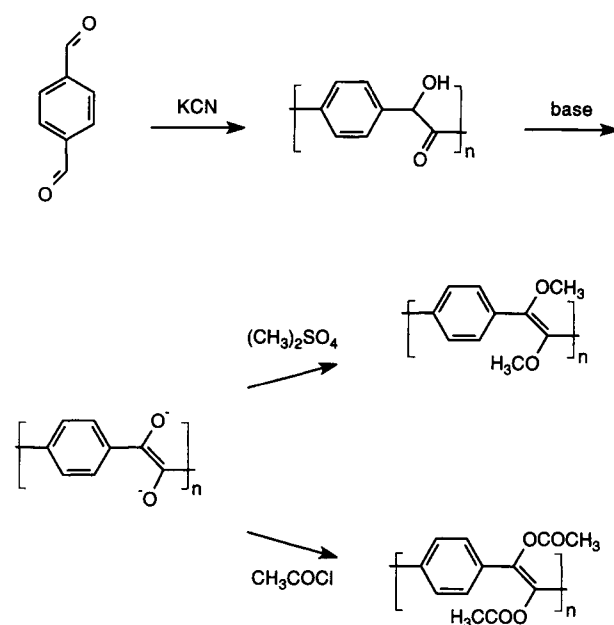


Fig. 71. Benzoine condensation.

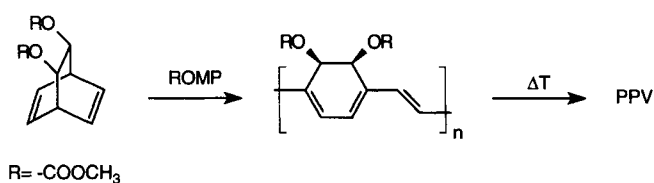


Fig. 72. Ring-opening metathesis polymerization of bicyclooctadienes.

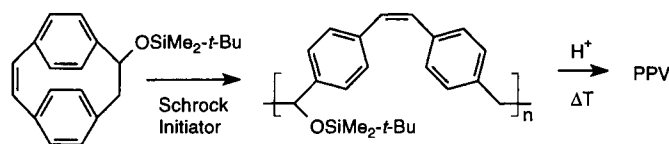


Fig. 73. Modification of the Thorn–Csányi ROMP route to PPV.

A modification of the Thorn–Csányi ROMP route to PPV makes use of a silyl-substituted paracyclophane derivative, which, under ROMP conditions, reacted to give a soluble precursor polymer. Transformation of the PPV could be achieved by treating the precursor polymer with acid or by hydrolysis of the silyl group followed by thermal treatment (Fig. 73). Because the polymerization is “living,” polymers and block copolymers of well-defined molecular weight can be prepared [916].

Chemical Vapor Deposition. In 1947, Szwarc [917] reported the formation *p*-xylylene through gas-phase pyrolysis of 1,4-methylbenzene. By condensation on cold surfaces, the so-obtained compound spontaneously polymerized to PPV. One question that arose was whether these *p*-xylylenes should be described as a diamagnetic *p*-quinodimethane compound or a paramagnetic diradical. Müller et al. [918, 919] showed the diamagnetic character of the compounds of Figure 74, which is an indication of their *p*-quinodimethane structure. Only in cases where a strong steric hindrance prevents planarization are such compounds paramagnetic and thus behave as biradicals (Fig. 75). The polymerization is supposed to be initiated by coupling of two *p*-quinodimethane

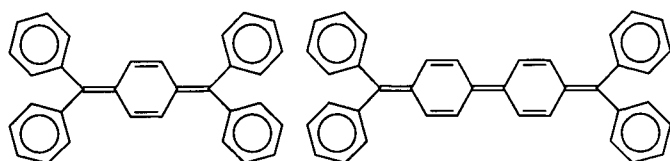
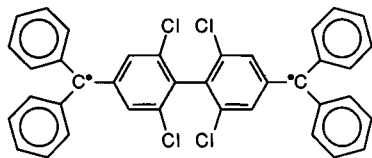
Fig. 74. Diamagnetic *p*-quinodimethane compounds.

Fig. 75. Paramagnetic diradical.

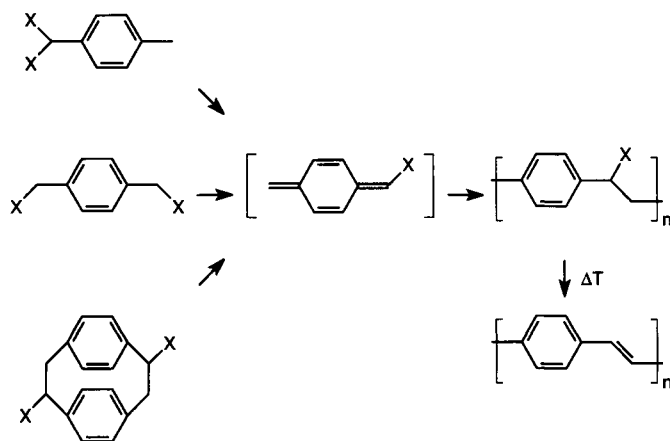


Fig. 76. Synthesis of PPV by chemical vapor deposition.

systems to form a diradical, which then starts growing at both ends through the addition of *p*-xylylene at the radical centers [920]. This method was improved by Gorham [921] using paracyclophane as the starting material for the gas-phase pyrolysis process. Thin films of a chlorinated PPV precursor were produced by gas-phase pyrolysis of 1,9-dichloroparacyclophane [922]. Heating under nitrogen at 300°C results in the conversion to PPV. A similar procedure was applied to 1,4-dihalomethylbenzene and dihalomethyl-4-benzene [923, 924] (Fig. 76).

Sulfonium or Wessling Precursor Route. The best known and most widely used precursor route was discovered by Wessling and Zimmerman [845–847], who were trying to produce conventional polymers via alkylation of *p*-xylylene sulfonium salts. The treatment of the sulfonium salt with a base produced a water-soluble, viscous, yellow–green solution of a polyelectrolyte, which could efficiently be purified by dialysis (Fig. 77). After further work by Hatch [925] and Alfrey [926] concerning the polycondensation of *p*-xylylene bisdialkyl sulfonium salts, Wessling [847] was able to obtain high-molecular-weight polymers. Both open-chain and cyclic sulfides can be used, the latter being preferred because of fewer side reactions upon thermal elimination [891]. Although the Wessling precursor route allows PPV to be produced quickly and cheaply, there are several drawbacks, such as the toxicity, the bad odor of sulfur compounds, the generation of HCl during thermal treatment [927, 928], and the instability of the intermediate polyelectrolytes, leading to side reactions.

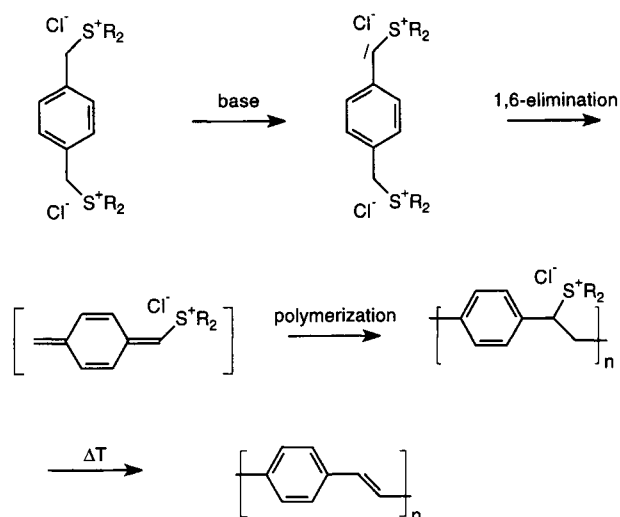


Fig. 77. Sulfonium or Wessling precursor route.

The polymerization mechanism has been studied in some detail, and it is clear that the first steps involve deprotonation and 1,6-elimination of a sulfide group to form a reactive *p*-xylylene derivative. Both steps are reversible and polymerization is inhibited by excess sulfide [929]. If the reaction is carried out in water, then polymer yields can be improved by using either an immiscible organic solvent (e.g., pentane or toluene) to extract the sulfide as it is being formed or a water-insoluble sulfide as the leaving group [930]. It is also possible to use an emulsified dispersion as the polymerization medium [931]. Exchange of the methylene protons occurs even at -50°C , whereas the formation of the *p*-xylylene derivative only occurs at temperatures above -40°C [932]. Generally, the best results are achieved at temperatures around 0°C . If the temperature is too high ($>70^{\circ}\text{C}$), the base tends to attack the polymer instead, resulting in the formation of conjugated insoluble product [847]. The formation of the quinoidal *p*-xylylene intermediate can be monitored by the appearance of a peak in the UV spectrum around 310 nm. This species seems to be the actual monomer required for the polymerization reaction to occur [933]. The quinoidal *p*-xylylene intermediate has been used to optimize reaction conditions for polymerizations involving unreactive sulfonium salts [929]. There has been some controversy over the precise nature of the polymer coupling reaction. The initial assumption was that the polymerization was a radical-promoted process [847]. The presence of radicals was hard to prove and the pendulum swung for a while toward an anionic mechanism [932]. However, careful work by Denton et al. [934] showed that radical trapping reagents did indeed suppress the polymerization. As an example, the addition of TEMPO to the reaction mixture not only dramatically lowered the yields and molecular weights but also caused the disappearance of the spin label. The radical character of the polymerization was further confirmed by Cho et al. [935]. The mechanism of radical initiation is unknown; it may involve spontaneous coupling of two quinoidal *p*-xylylene intermediates to form a biradical.

A wide variety of aromatic polycyclic and heterocyclic sulfonium salts can be used in the polymerization. Formation of the quinoid intermediate is energetically unfavorable due to loss of aromaticity. In practice, if more than two aromatic ring systems have to be forced out of aromaticity when forming the *p*-xylylene

intermediate, then the polymerization is unlikely to succeed [930]. The presence of extra double bonds outside the aromatic ring but within the main chain does not seem to prevent polymerization [936]. Sulfonium salts based on a 1,4-naphthalene system are able to polymerize, as only one ring loses aromaticity during formation of the intermediate quinoid [937]. However, because both aromatic rings would need to lose some conjugation, the 2,6-isomer has been reported not to polymerize [930, 938]. On the other hand, the polymerization is also inhibited if the *p*-xylylene is too stable, as is probably the case for 9,10-substituted anthracene derivatives. *Meta*-substituted phenylene systems also do not polymerize due to the impossibility of forming the necessary quinoid intermediate. The situation regarding *ortho*-phenylene derivatives is not entirely clear. There is no doubt that *o*-xylylenes could be formed; however, these are prone to other reactions such as dimerization or ring closure to form fused cyclobutanes. Successful polymerization of *ortho*-substituted compounds (halide rather than sulfonium leaving groups) via phase-transfer catalysis has been claimed, but the products were not well characterized [939].

A large variety of substituents can be tolerated on the aromatic ring, including aromatic [940–942], alkoxy [112, 943–950], alkyl [845, 846, 943, 951], silyl [952, 953], halogen [954–956], sulfur [957], and amino groups [958]. Electron-poor aromatic systems (e.g., nitro- or cyano-substitute) polymerize with extreme difficulty [929, 934, 959], although polymerization proceeds more smoothly if the electron-withdrawing group is attached to the α -methylene carbon rather than the ring [849]. Mixtures of different sulfonium salts can be used to generate copolymers, which is especially useful if a particular sulfonium salt does not homopolymerize [955, 956, 959–965].

The sulfonium polyelectrolyte is usually soluble in methanol or water, which are the preferred solvents for polymerization. Solubility also depends on the counterion [937, 966, 967]. Solubility in organic solvents can be achieved by substitution of the sulfonium group itself with, e.g., phenylthiolate ions or extended heating in methanol [968–970] (Fig. 78).

There are several complicating factors in the synthesis and pyrolysis of the sulfonium precursor [891, 971]. The intermediate

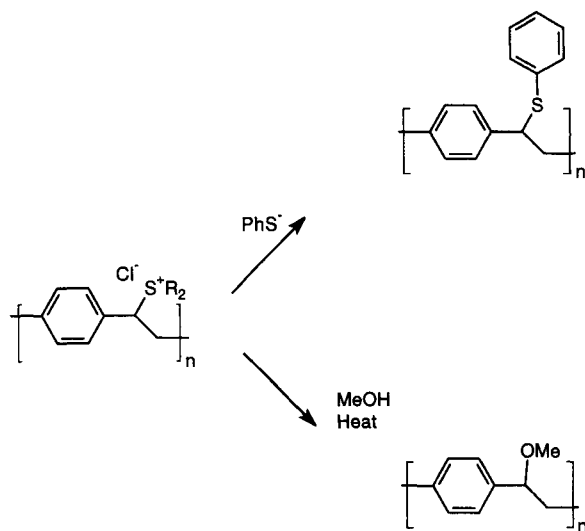


Fig. 78. Solubility of the precursor polymer in organic solvents achieved by substitution of the sulfonium group with, e.g., phenylthiolate ions, or through extended heating in methanol.

precursor is not very stable and partial base-catalyzed elimination can occur as well as hydrolysis, resulting in the presence of alkoxy groups. This complicates the pyrolysis step, leading to the possibility of residual unsaturations in the main chain. Similarly, the sulfonium salt can be substituted by the counterion, although this reaction is more prevalent in the solid state or at higher temperatures in solution [891, 972]. Non-regiospecific coupling of asymmetrically substituted aromatic monomers can also lead to irregularities in the polymer chain, reducing the control on achieved conjugation after pyrolysis. Small levels of carbonyl groups are often noted by infrared (IR) spectroscopy after thermal conversion [973]. This could be the result of oxidation or side reactions involving hydroxy-substituted portions of the chain. Many measurements such as conductivity and fluorescence depend critically on the quality of the precursor polymer and the conversion conditions. Even within the same group, there can sometimes be significant batch-to-batch variation [849].

The sulfonium precursor polymer can be converted to fully conjugated PPV either by treatment with excess base or by heating under vacuum or nitrogen. The temperature needed for full conversion depends on the nature of the counterion. These range from 120°C for bromide, to 200°C for chloride and fluoride, to over 300°C for acetate [966, 967, 974]. Partial elimination starts for all four precursors at the same temperature, but complete conversion is complicated by the presence of side reactions [974]. Elimination of the sulfide group and the counterion is not always synchronous over the entire temperature range of the conversion, suggesting that competing side reactions occur [975] (Fig. 79). Whereas, in practice, most sulfonium precursor polymers are converted to PPV thermally, there has been some interest in other methods. Several groups have reported that exposing films of the sulfonium precursor polymer to light (250–350 nm) causes partial conversion to PPV. This allows any unexposed parts of the film to be washed away. Even longer wavelength light (514 nm) can be used if a sensitizing dye is also present [976]. By exposing the precursor to extended irradiation, the opposite effect is found, wherein the exposed portions become so degraded that they are not converted into PPV upon heating. Thus, photolithography and patterning of PPV becomes an attractive and viable option [977–979]. Other methods that have been used for the conversion of sulfonium precursor polymers to PPV include the use of strong acids [980] and microwave heating [981]. It is also possible to grow films of PPV from the sulfonium precursor electrochemically [847].

Alkoxy Precursor Route. Sulfonium precursor polymers can be readily converted to methoxy-substituted polymers, which are soluble in organic solvents and which are much more stable than the sulfonium precursor. The alkoxy group can be removed by acid catalysis and/or heating to produce fully converted PPV derivatives [950, 968, 970].

Gilch Route. On the basis of the work by Karasch et al. [982], Hoeg et al. [901] reacted 1,4-dichloromethylbenzene with an excess of NaH₂ in NH₃/THF to obtain the insoluble PPV. In a more systematic study, Gilch and Wheelwright [904] developed a procedure to polymerize dichloro-*p*-xylene with potassium *tert*-butoxide in organic solvents (Fig. 80). The reaction mechanism has been investigated and seems to be related to that of the Wessling precursor route [983–987]. The method of Gilch allows easier entry into a large range of substituted organic soluble PPV derivatives [905]. Unlike the sulfonium route, the reaction is usually allowed

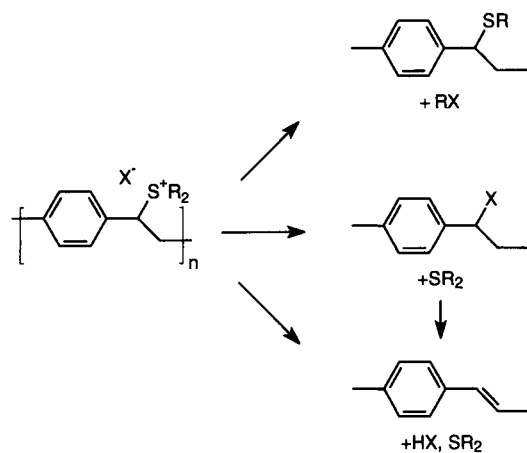


Fig. 79. Competing reactions in the thermal elimination of sulfonium groups.

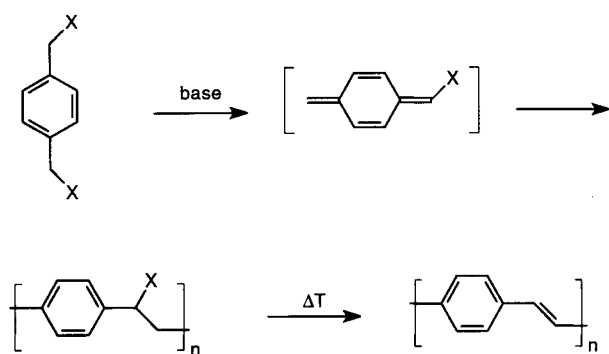


Fig. 80. Gilch precursor route ($X = \text{halide}$).

to proceed to completion by the addition of excess base, solubility being ensured by the use of substituents on the aromatic ring or on the vinylic bond. Both chlorine and bromine leaving groups have been used. An intermediate soluble halide-substituted polymer has been prepared, which can be dehydrohalogenated thermally or partially eliminated in an alcoholic solvent [988–992]. However, the intermediate halogen-containing polymers may not be very stable. Stability is also strongly dependent on storage conditions. Substituents used to give solubility include phenyl, alkoxy, and alkyl groups. The method of Gilch was applied to prepare a series of substituted PPV derivatives. It was observed that branched long-chain alkoxy and alkyl groups of at least six carbons in length are especially good at improving solubility. Asymmetric substitution of the aromatic ring also appears to improve solubility and formation of good-quality films [993].

Xanthate Precursor Route. Son et al. [994] published a modification of the Wessling precursor route. The sulfonium groups were replaced by xanthate groups in order to avoid typical side reactions of the Wessling approach (Fig. 81). The precursor is stable at room temperature and soluble in most common organic solvents. Elimination with formation of the polyconjugated system takes place between 160 and 250°C.

Acetate Precursor Route. The use of acetate groups as elimination functionalities in a PPV precursor polymer have been reported. This precursor polymer is obtained from the sulfonium precursor

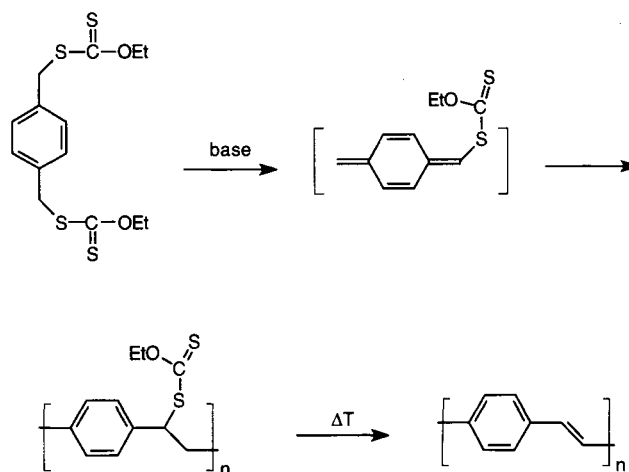


Fig. 81. Xanthate precursor route.

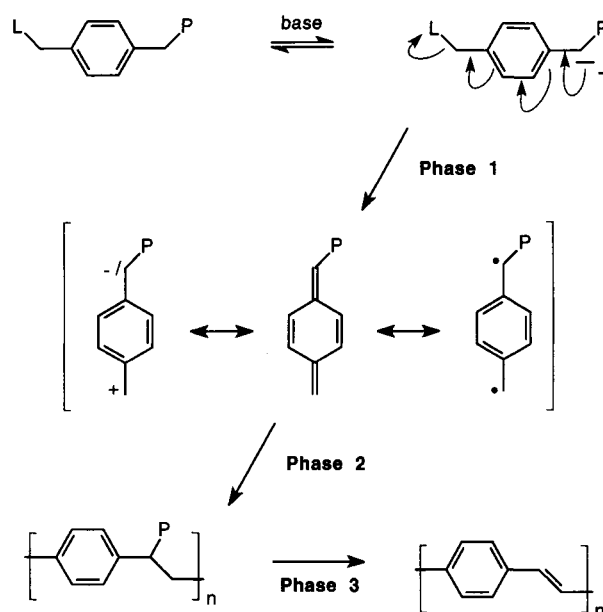


Fig. 82. General scheme for *p*-quinodimethane-based polymerizations as proposed by Louwet and Vanderzande.

polymer by a competitive substitution with methanol and sodium acetate as nucleophiles. The acetate can be eliminated without affecting the methoxy groups, because the acetic acid that is formed is only a mild acid [995].

Sulfinyl or Louwet–Vanderzande Precursor Route. The development of sulfinyl precursor polymers by Louwet et al. [996–998] has overcome many of the drawbacks of the previous precursor routes.

As the Wessling and Gilch precursor routes are characterized by the polymerization behavior of *p*-quinodimethane systems, Louwet et al. [996–998] were aiming to develop a more generalized scheme to study the boundary conditions for such polymerizations. In this more general scheme (Fig. 82), a distinction is made among three phases: first, the *in situ* formation of the *p*-quinodimethane system, which acts as the monomer; second, the polymerization reaction, and, finally, the conversion to the fully conjugated system.

The *p*-quinodimethane system can be formed *in situ* through a base-induced elimination reaction. This is only possible if the α,α' -

functionalized *p*-xylene derivative meets two essential requirements: first, the α -position of the *p*-xylene should bear a polarizer stabilizing the anion formed under the influence of the base, and, second, a suitable leaving group is needed in the α' -position in order to obtain the *p*-quinodimethane intermediate. The polarizer not only allows for the *p*-quinodimethane intermediate to be formed, but also polarizes the system in such a way that regular head-to-tail addition is guaranteed. Finally, the polarizer needs to offer a specific chemistry allowing for the formation of a vinylic double bond in order to obtain the fully conjugated PPV system. In the case of the Wessling and Gilch precursor routes, the polarizer and leaving group are identical, which imposes the same chemistry on the polymerization reaction through the formation of the monomer (*p*-quinodimethane) as on the conversion process toward the conjugated material. Chemical differentiation of the polarizer and leaving group, on the other hand, allows full control over both the polymerization process and the stability of the precursor polymers. On the basis of this idea, Louwet et al. [996–998] chose to use halides as leaving groups because of their good leaving-group characteristics and because halides do not enhance the acidity of the benzylic positions. As the polarizer, they opted for sulfinyl groups for several reasons: first, sulfinyl groups show no leaving-group properties versus nucleophilic reagents; second, the concerted thermal conversion to a vinylic bond is well documented [999]; and, finally, the alkyl or aryl side chain that comes with the sulfinyl group provides the opportunity to control the solubility characteristics of the precursor polymer [1000] (Fig. 83).

The synthesis of the asymmetrically substituted monomer, which used to be a major challenge, is found to be possible with an unexpected high selectivity [1001] (Fig. 84). The effect of the polarizer and leaving group on the polymerization reaction has been studied by Issaris et al. [1002]. Although at first indications were found for a free-radical mechanism in the polymerization process [1003], it seems that, depending on specific parameters, the polymerization process can occur by radical or anionic mechanisms [1004]. Van Der Borght et al. [1005] have shown that it is possible to obtain high-molecular-weight poly(4,4'-bisphenylene vinylene) and poly(2,6-naphthalene vinylene) via this nonionic precursor route.

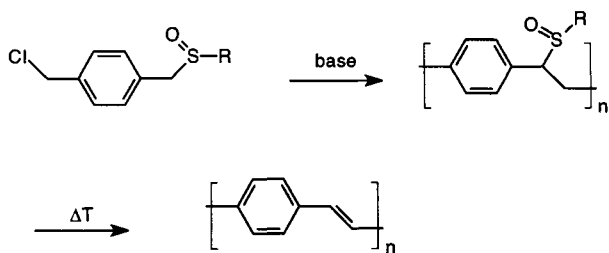


Fig. 83. Sulfinyl or Louwet–Vanderzande precursor route.

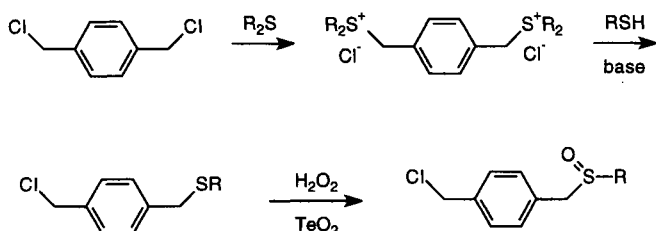


Fig. 84. Synthesis of the asymmetrically substituted monomer for the Louwet–Vanderzande precursor route.

A wide variety of sulfinyl side chains have been used to tune the solubility of the precursor polymers in various organic solvents and water [1000]. The polymerization to obtain sulfinyl precursor polymers has been optimized [1006] and is possible in solvents such as MMF, NMP, dimethyl sulfoxide (DMSO), and alcohols. In branched alcohols such as *s*-butanol, a polymer yield of 88% was achieved. The sulfinyl group also allows for the introduction of well-defined modifications onto the polymer structure by partial oxidation of the sulfinyl groups to obtain sulfonyl groups [1007]. As the sulfonyl groups are stable up to 270°C [996–998], sp^3 defects are introduced into the polyconjugated sp^2 system, resulting in, e.g., an increased photoluminescence efficiency. The thermal conversion process of the sulfinyl precursor polymers toward the fully conjugated system has also been studied in some detail [1008].

2.4. Polyanilines

Polyaniline, known as “aniline black,” was first prepared in 1834 (for a historical review, see [1009]) (Fig. 85). Letheby [1010] developed a procedure based on aniline black for the determination of small quantities of aniline. Scattered publications [1011–1017] appeared in the literature until the advent of the science of conducting polymers triggered by the research on polyacetylene in the 1970s. Thus, oxidative polymerization was reported using mineral acids and oxidants such as persulfate, dichromate, and chlorate. The main reasons for the growth in interest during the 1980s were the low cost, relatively easy production process, stability of the conducting forms, and simple non-redox doping by protonic acids. Some reviews have been published [1018–1020].

Green and Woodhead [1011] describe a number of well-defined oxidation states for polyaniline (Fig. 86). The different states range from fully reduced leucoemeraldine via protoemeraldine, emeraldine, and nigraniline to the fully oxidized pernigraniline. Unlike most other polyconjugated systems, the fully oxidized state in polyaniline is not conducting. Polyaniline only becomes conducting when the moderately oxidized states, in particular the emeraldine base, are protonated and charge carriers generated [1021]. It is this process of “protonic acid doping” that makes polyaniline so unique: no electrons have to be added or removed from the insulating material to make it conducting.

Polyaniline is prepared by either chemical or electrochemical oxidation of aniline under acidic conditions in an aqueous medium. Electrochemical experiments have indicated that oxidative polymerization of aniline occurs at 0.8 V versus SCE. This means that the following oxidants can be used in chemical oxidative polymerization of aniline: $F_2(g)$, $S_2O_8^{2-}$, H_2O_2 , Ce^{4+} , BrO_3^- , Cl_2 , $Cr_2O_7^{2-}$, $O_2(g)$, IO_3^- , Br_2 , and VO_2 [1020]. A second aspect of polyaniline synthesis is the acid dissociation constant (pK_a) of the acid. Because in polyaniline protonation equilibria involves exclusively the quinone diamine segment, having two imine nitrogens with $pK_a = 1.05$ and $pK_a = 2.55$ [1022]. Therefore, any acid whose pK_a value falls within that range would be suitable as a dopant. As the anilinium ion has a pK_a of 4.60 and the ammonium ion a pK_a of 9.24, acids having pK_a values around that of an

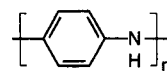


Fig. 85. Structure of polyaniline.

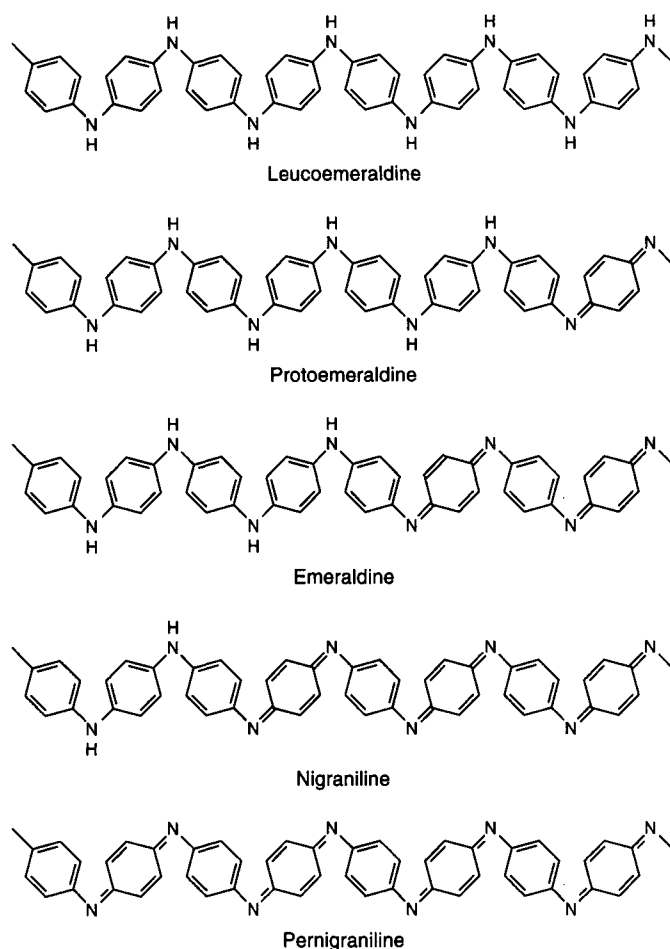


Fig. 86. Different oxidation states in polyaniline.

anilinium ion would be suitable as solvents if they are liquid. They can also be used to prevent overoxidation of polyaniline [1020].

2.4.1. Chemical Synthesis

The most preferred method is to use either hydrochloric or sulfuric acid with ammonium persulfate as oxidant [1021, 1023–1026]. A somewhat smaller quantity than an equimolar concentration is used to avoid degradation through overoxidation. Better quality polymer is obtained at lower temperatures. A variety of oxidants have been used to carry out chemical polymerization of aniline under acid conditions. It seems that there is no relationship between the oxidation potential of the reagent and the polymer yield. Although an oxidizing agent such as ammonium peroxydisulfate appears to yield a polymer of better quality than oxidizing agents containing metal ions such as dichromate, ceric, ferric, manganic, and cobalt salts [1020].

Gebert et al. [1027] have reported a synthesis of polyaniline using Schiff base chemistry. The reactions involve the condensation of *p*-phenylene diamine with *p*-benzoquinone (Fig. 87).

Mattoso et al. [1028] polymerized aniline at -40°C in the presence of LiCl and HCl to yield a high-molecular-weight polyaniline. A similar procedure has been applied to prepare poly(*o*-methoxyaniline) [1029].

Polyaniline can also be obtained by decarboxylation of poly-(anthranilic acid) [1030]. Poly(anthranilic acid) was prepared by

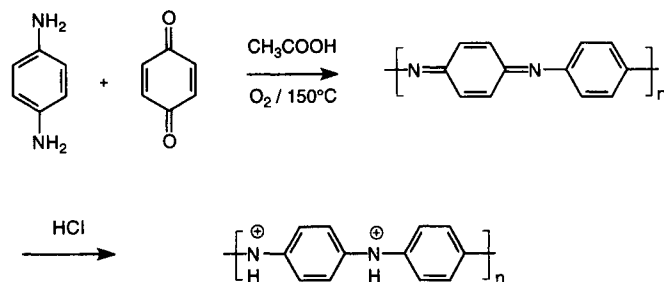


Fig. 87. Synthesis of polyaniline using Schiff base chemistry.

using ammonium peroxydisulfate as an oxidizer [1031]. Decarboxylation is achieved by heat treatment.

2.4.2. Electrochemical Synthesis

The first electrochemical oxidation of aniline to emeraldine salt was reported by Letheby [1010] as a dark-green precipitate under aqueous acidic conditions. This green powdery material soon became known as aniline black. Almost a hundred years later, interest was revived when Mohilner et al. [1013] described the mechanistic aspects of aniline oxidations. However, major interest was only generated after the discovery that aromatic compounds can be anodically polymerized to a conducting film.

Several groups [1032–1034] reported the preparation of polyaniline in an aqueous acid solution using a platinum electrode by cycling the potential between -0.2 and 0.8 V versus SCE. This electrochemically prepared polyaniline is electroactive and switches in aqueous solutions in the potential range -0.2 to 0.65 V versus SCE between two oxidation states. Under these controlled conditions, the process is thermodynamically reversible and the two states of the polymer can be produced repeatedly by cycling the potential. These switching processes with color and conductivity changes under aqueous conditions are important for technological applications [1020]. Bade et al. [1035] investigated the nucleation and growth of polyaniline on gold and platinum microelectrodes in a sulfonic acid medium. Tang et al. [1036, 1037] reported that by using a 1-methyl-3-ethyl imidazolium chloride or an *N*-butyl pyridinium chloride-based AlCl_3 room-temperature melt it was possible to electropolymerize aniline. Alkyl-substituted anilines have been electropolymerized under a wide variety of conditions [1018].

2.5. Chemical Structure and Electronic Properties

2.5.1. Intrinsic Conducting Polymers

2.5.1.1. Poly(sulfur nitride)

One of the most important discoveries [1038] preceding the development of conducting organic polymers is the fact that the inorganic polymer poly(sulfur nitride) $(\text{SN})_x$ possesses a conductivity of 10^4 S cm^{-1} at room temperature, which is almost comparable with the conductivity of copper ($\approx 6 \times 10^5$ S cm^{-1}). Of fundamental importance to attaining the metallic state is the presence of unpaired electrons in the primary molecular units. In the case of poly(sulfur nitride), a single polymer chain can be considered schematically as a collection of covalently bonded monomeric NS free radicals, each of which is the sulfur analog of NO. The NS molecule, like NO, contains an unpaired electron in the lowest occupied π^* -antibonding molecular level. In principle, in a polymer

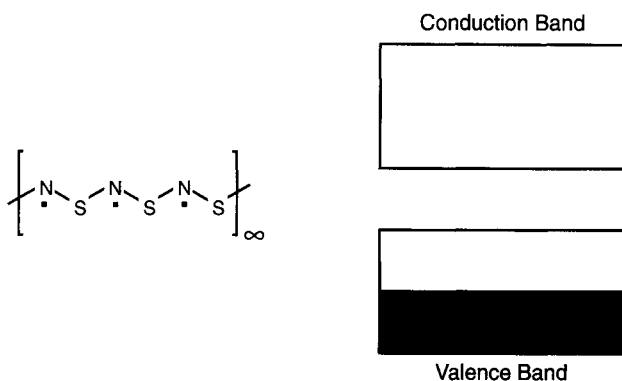


Fig. 88. Poly(sulfur nitride), the first polymer exhibiting metallic conductivity.

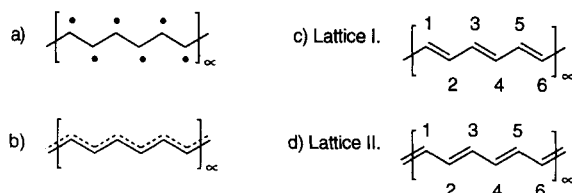


Fig. 89. *Trans*-polyacetylene.

this type of π^* level may form the basis of the metallic conduction band. The “metallic” character of poly(sulfur nitride) appears to be an intrinsic property and is related to the presence of one unpaired electron at every SN unit. As a consequence, the band in the polymer corresponding to the π^* -antibonding molecular level will be half filled. The absence of a forbidden gap makes complete delocalization possible (Fig. 88). Therefore, conductivity in $(\text{SN})_x$ can be considered as similar to the conductivity of metallic conductors [1039, 1040].

In organic conjugated polymers, the presence of unpaired electrons is rather an exception. This implies that the band structure will be characterized by completely filled valence bands. Most of the time, there is a large bandgap, generally larger than 1.5 eV, between the filled valence band and the empty conduction band and therefore intrinsic conductivity will be very low [1041].

2.5.1.2. Peierls Instability

Introduction. The major breakthrough in the area of conducting plastics occurred when it was discovered that polyacetylene, which has an intrinsic conductivity much lower than $10^{-5} \text{ S cm}^{-1}$, could be made highly conducting, 10^3 S cm^{-1} , by exposing it to oxidizing (p-type doping, I_2 , Br_2 , FeCl_3 , ASF_5) or reducing agents (n-type doping, alkali metals) [153]. The most elementary presentation of the structure of polyacetylene is given in Figure 89.

Ideally, polyacetylene can be represented as a long chain of CH groups, each possessing an unpaired electron (Fig. 89a). According to solid-state physics, this structure can be considered as a quasi-one-dimensional metal in which the metal atoms are replaced by CH radicals. Since there is only one unpaired electron per CH group, a half-filled band is obtained as in the case of poly(sulfur nitride). In this situation, metallic conductivity could be possible. In reality, polyacetylene is characterized by an alternating succession of short (double) bonds and long (single) bonds. This behavior is described by the so-called Peierls instability.

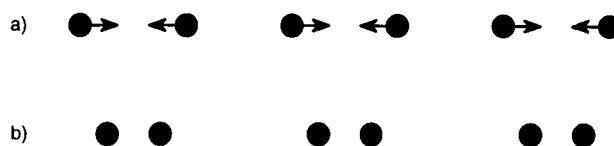


Fig. 90. Antisymmetric vibration of the linear chain (normal vibration) that drives the Peierls distortion.

Peierls instability indicates why a half-filled energy band is split up, resulting in a completely filled valence band and an empty conduction band separated by a forbidden zone, the so-called bandgap. Understanding this mechanism is of fundamental importance because it allows insight into why potential intrinsic conductors appear to be intrinsically insulating in the undoped state.

Linear Chain Model. The transition from a regular linear chain structure to an alternating structure takes place according to a well-defined mechanism. The regular linear chain cannot in any real situation be isolated from its environment but it must always be in contact with some form of a heat bath. This means that the atoms of the chain are vibrating around their equilibrium positions. When the vibrations of a solid are studied, one finds that, as with the electronic energy levels themselves, the vibrational levels are discrete and that a given system will admit a finite number of so-called *normal vibrations* such that they and their harmonics form all possible vibrational states of the system. In each of these normal vibrations, the atoms move in well-determined relationships to one another. An example of such a normal mode is shown at the top of Figure 90. It is clear that when the regular structure starts to vibrate in this particular mode it will go into an alternating form, as shown at the bottom of Figure 90. This will not be the case for other vibrational modes. The chain distortion cannot take place unless there is a normal mode that can drive the structure into the required configuration. Since the alternating form is lower in energy, the system now becomes trapped in this configuration.

The principle of Peierls distortion can be summarized as follows: if a system with a given symmetry has a top occupied electronic orbital that is degenerate, then this function will interact with a vibrational mode that has symmetry lower than that of the original system, causing it to distort from the original configuration and thus splitting the degeneracy, which results in the appearance of a state of lower energy. This principle is also known as the Jahn-Teller effect [1042–1047].

Polyacetylene. Although the Peierls model of the linear chain is important, since it has permitted understanding of the structural instability of linear systems, genuine linear chains are of no serious practical interest, since they rarely occur in nature. If we consider a polyacetylene polymer, a material of considerable technological interest, we can see that it forms a zigzag chain (Fig. 89). Figure 89a shows the regular polyacetylene structure with a π orbital at each atom containing one unpaired electron. It is this electron that can be expected to form a mobile conducting band. For polyacetylene, however, there also exists a structure with alternating double (short) and single (long) bonds (Figs. 89c and 5d) as the result of a Peierls distortion causing the degeneracy at the edge of the Brillouin zone to disappear and thereby lowering the Fermi level. Since there is an energy gap at the Fermi level, however, the material ceases to be a conductor and becomes an insulator.

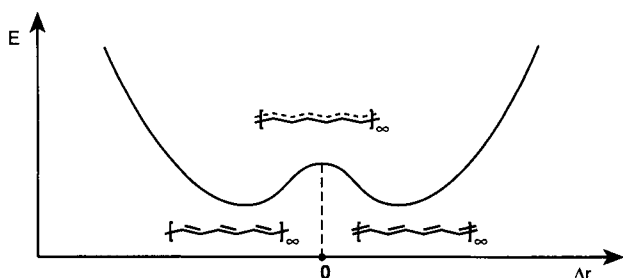
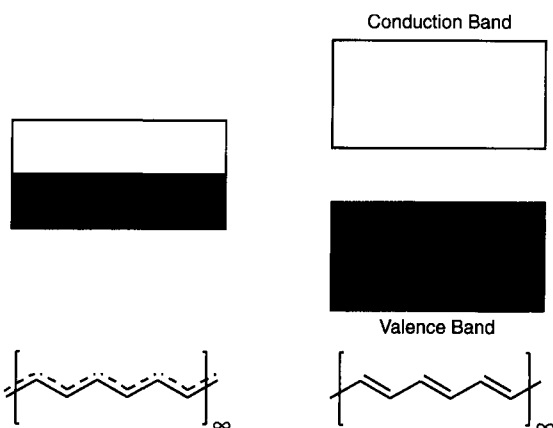
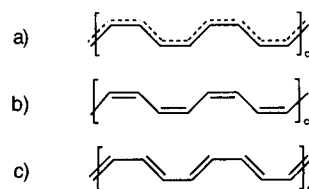
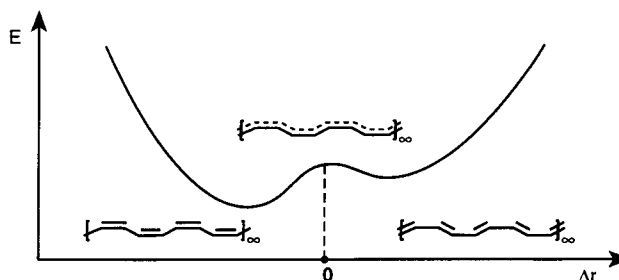
Fig. 91. Potential energy diagram of *trans*-polyacetylene.

Fig. 92. Simplified description of the band structure of polyacetylene.

As a consequence of this Peierls distortion, two minima appear on the potential energy surface characterizing polyacetylene. These two minima correspond to two alternative crystal lattices (Fig. 89c, lattice I, and Fig. 5d, lattice II), which differ from each other by the way the short and long bonds alternate in the crystal lattice. In lattice I, the distance between the lattice points 1-2, 3-4, and 5-6 are shorter as compared to the distance between 2-3 and 4-5. In lattice II, the inverse situation occurs. Particular to polyacetylene is that these two alternative lattices are isoenergetic or degenerate. The lattice with identical distances between the lattice points can be found in the potential energy diagram as a local maximum (Fig. 91).

The preceding picture is a simplified description that can be used as a qualitative model to understand the evolution of valence and conduction bands (Fig. 92). For a complete description of the bandgap evolution, it is necessary to include correlation effects and interactions between polymer chains themselves.

From the analysis of the structure of polyacetylene potential, one-dimensional conductors appear to lose their conducting properties because their lattice structure is driven toward an energetically more favorable configuration. However, some vibrational energy has to be spent for the change to take place. Most of the time, the consumption of vibrational energy is compensated by the gain in electronic energy, although it can be seen that, in general, this is second order with respect to the electronic energy. It is therefore possible that the interactions between the electronic and vibrational states are such that they impede the energy compensation between vibrational energy loss and electronic energy gain. In that specific situation, the Peierls effect will not take place and an intrinsic conductor is obtained [1043].

Fig. 93. Lattice structure of *cis*-polyacetylene.Fig. 94. Potential energy diagram of *cis*-polyacetylene.

Aissing et al. [1048] formulated the conditions that a polymer has to fulfill in order to be a material showing metal-like conductivity. If an *isolated* polymer chain is considered, it will be conducting if the following rules can be applied. First, the polymer chain should possess an almost rigid backbone with a glide plane symmetry and/or a twofold screw axis symmetry because it will then show a double degeneracy at the zone boundary. On the other hand, it should have $4N+2$ electrons per unit cell. Under this condition, the HOMO will be filled exactly up to the zone boundary. If this polymer is then crystallized into a solid and if it can be packed in such a way that the previously mentioned rules still apply, then the resulting system will still be conducting. In that case, three-dimensional packing effects will give rise to such a complex set of vibrational modes that one mode will never be found that can cause the system to distort from the original configuration and the Peierls effect will be avoided.

To evaluate the effect of structural changes on the electronic properties, the concept of bond-length alternation was introduced. The value of the bandgap can be correlated with the bond-length alternation Δr , defined as the length difference between a double and a single bond. In "metallic" polyacetylene (Fig. 89a), all bonds are equal so that Δr is equal to 0 and therefore we have to deal with a conductor. The larger Δr , the more the Peierls effect is active and the larger the bandgap will be [845].

For the sake of completeness and as an example of a system with a lattice of different energy, *cis*-polyacetylene will briefly be discussed. Again, the Peierls distortion will cause the lattice with equal bond lengths (Fig. 93a) to distort to a lattice with pronounced bond-length alternation. For *cis*-polyacetylene, however, the possibility exists to forming two different alternating lattices (Fig. 93b and c). These two lattices differ from each other through the presence of the short or double bonds at different lattice points. In contrast to *trans*-polyacetylene, these two lattices are not isoenergetic. The lattice in Figure 93b has a more efficient conjugation and therefore a lower energy [1049] (Fig. 94).

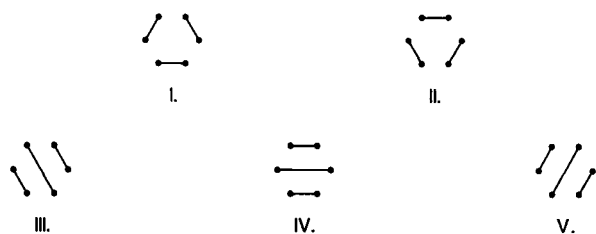


Fig. 95. Pairing schemes for benzene.



Fig. 96. Kékulé resonance structures of benzene.

2.5.2. Polyaromatics and the Valence-Bond Theory

To clarify the discussion further concerning conducting polyaromatics, it is worthwhile to elaborate on some principles described by the valence-bond (VB) theory. The ideas of the (VB) (resonance) theory are found to be of aid to organic chemists for rationalizing in a simple manner the facts of organic structure and reactions. However, quantitative application is much harder for the VB method than for the molecular orbital (MO) method. Indeed, for quantitative calculations, the MO method has overshadowed the VB method. The main advantage of the VB method is that it is based on the familiar chemical ideas of bonding and structure [1050].

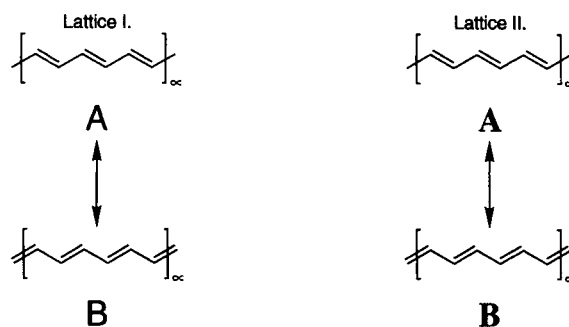
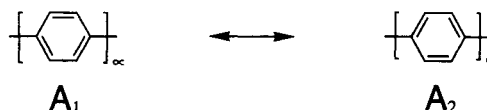
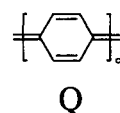
The VB theory is more closely related to the chemist's idea of molecules as consisting of atoms held together by localized bonds and views molecules as composed of atomic cores (nuclei plus inner-shell electrons) and bonding valence electrons. One begins with the atoms that form the molecule and pairs up the unpaired electrons to form chemical bonds. There are generally several ways of pairing up the electrons; each pairing scheme gives a valence-bond "structure" or resonance form.

Consider benzene as an example. When the π -electron approximation, i.e., treating the π electrons separately from the σ electrons, is used, the σ bonds are formed by sp^2 carbon hybrid atomic orbitals (AOs) and 1s hydrogen orbitals; this leaves a p orbital on each carbon to form π bonds. Figure 95 shows the resulting covalent structures for pairing the π orbitals. Structures I and II are the so-called Kékulé structures, commonly represented as in Figure 96.

Each VB resonance "structure" is based on the same internuclear distance but a different electron pairing scheme. The resonance forms depicted in Figure 95 are a linearly independent set of bond eigenfunctions. The molecular wave function is then taken as a linear combination of these bond eigenfunctions for each resonance form and the variation principle is applied. The VB wave function is said to be a resonance hybrid of the various VB structures. Within this resonance hybrid, the contribution of each resonance form is characterized by a certain weight corresponding to the square of its coefficient in the molecular wave function. For benzene, it appears that the Kékulé structures make the greatest contribution ($C_I, C_{II} \gg C_{III}, C_{IV}, C_V$) [1050]:

$$\Psi_{\text{benzene}} = C_I \Psi_I + C_{II} \Psi_{II} + C_{III} \Psi_{III} + C_{IV} \Psi_{IV} + C_V \Psi_V$$

In the discussion of conducting polymers, the main principles of the VB approach can be applied. First, consider *trans*-

Fig. 97. Resonance forms for the different lattices of *trans*-polyacetylene.Fig. 98. Kékulé resonance forms of poly(*p*-phenylene).Fig. 99. Quinoid resonance form of poly(*p*-phenylene).

polyacetylene. For lattices I and II (Fig. 89), the localized resonance pictures can be written as shown in Figure 97.

The wave functions, $\Psi_{\text{lattice I}}$ and $\Psi_{\text{lattice II}}$, of lattices I and II, respectively, can then be written as

$$\begin{aligned} \Psi_{\text{lattice I}} &= C_1 A + C_2 B && \text{with } C_1 > C_2 \\ \Psi_{\text{lattice II}} &= C'_1 A + C'_2 B && \text{with } C'_1 < C'_2 \end{aligned}$$

where A and B are the linear independent bond eigenfunctions obtained by a different pairing scheme of the unpaired electrons and C_1 and C_2 correspond to the weight of the contribution of each resonance form to the lattice wave function. Since both lattices are isoenergetic, it follows that $C_1 = C'_2$. The different contribution of both resonance forms to the final wave function allows us to understand in a qualitative way the notion of bond-length alternation and the existence of a bandgap between valence and conduction band.

Next, we consider the case of poly(*p*-phenylene). As shown in Figure 98, two Kékulé resonance forms can be written for poly(*p*-phenylene). Contrary to the case of benzene, a third resonance form should be considered (Fig. 99).

This quinoid resonance form will make a considerable contribution to the total ground-state π -electron VB wave function. The ground-state wave function of a polymer containing exclusively aromatic units can therefore be considered as a linear combination of aromatic (A) and quinoid (Q) resonance forms.

In the ideal situation where all bond lengths are equal, a conducting material is obtained. However, the Peierls distortion causes a breakdown of symmetry, resulting in an alternation of single and double bonds. Again, in the potential energy diagram, two minima are found (Fig. 100). Since the aromatic resonance forms will make the greatest contribution, the contribution C_A of the aromatic resonance forms will be more important than the contri-

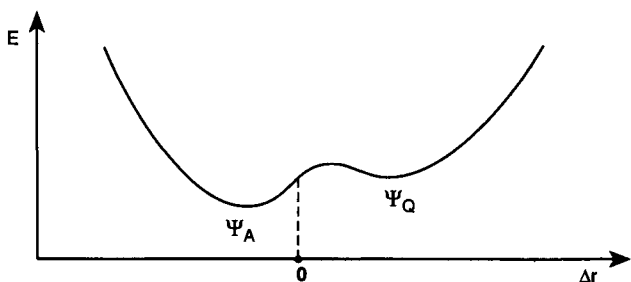


Fig. 100. Potential energy diagram for polymers consisting of aromatic units such as poly(*p*-phenylene).

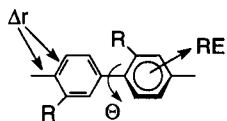


Fig. 101. Different parameters determining the value of E_g : bond-length alternation (Δr), resonance energy (RE), substituents (R), and torsion angle (Θ).

bution C_Q of the quinoid resonance form

$$\Psi_A = C_A A + C_Q B \quad \text{with } C_A > C_Q$$

Although when the contribution C_Q of the quinoid resonance form is more important than the contribution C_A of the aromatic resonance forms, a wave function Ψ_Q describing the quinoid structure is obtained

$$\Psi_Q = C'_A A + C'_Q B \quad \text{with } C'_A < C'_Q$$

It is important to stress that in this way a difference is made between an aromatic structure (Ψ_A) and a quinoid structure (Ψ_Q), on the one hand, and between an aromatic resonance form (A) and a quinoid resonance form (B), on the other hand.

2.5.3. Relationships between Chemical Structure and Bandgap

2.5.3.1. Introduction

Several parameters play an essential role in determining the final intrinsic value of E_g for a specific material. Figure 101 illustrates these different parameters on poly(*p*-phenylene).

The intrinsic bandgap of an isolated conjugated polymer chain can be described by the combination of the contributions of the energy related to the bond-length alternation Δr ($E_{\Delta r}$), the resonance energy stabilization of the aromatic ring system (RE), the inter-ring torsion angle Θ (E_{Θ}), and the inductive or mesomeric effects of substituents R (E_R):

$$E_g = E_{\Delta r} + RE + E_{\Theta} + E_R$$

In the design of low-bandgap conjugated polymers, these parameters have to be considered first. The final goal is then to find the best combination of parameters in order to minimize E_g . In the following discussion, the structural possibilities influencing each of these parameters will be evaluated.

2.5.3.2. Bond-Length Alternation

Polyaromatics. In the case of polyaromatics, the concept of bond-length alternation Δr , as defined for polyacetylene, cannot be used



Fig. 102. Aromatic and quinoid structures of polythiophene.

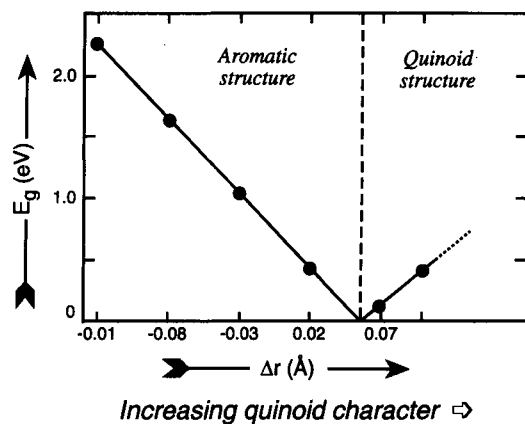


Fig. 103. Evolution of the bandgap E_g (eV) as a function of Δr . Reproduced and adapted by permission of Elsevier Science from J. L. Brédas, *Synth. Meth.* 17, 115 (1987). Copyright © 1987, Elsevier Science.

as such. Brédas et al. [1051] stated that in the case of polyaromatics the notion of bond-length alternation cannot be used as with polyacetylene. The degree of bond-length alternation, Δr , is therefore defined as the maximum difference between the length of a C–C bond inclined relative to the chain axis and a C–C bond parallel to the chain axis.

Brédas et al. [1051] studied the evolution of the bandgap of polythiophene as a function of the bond-length alternation Δr . Their polymer calculations are based on the use of the nonempirical valence-enhanced Hamiltonian (VEH) pseudopotential technique. In the context of conducting polymers, this method has been shown to provide accurate estimates of important electronic parameters such as ionization potentials or π – π^* transitions and bandgaps in a large series of hydrocarbon- or sulfur-containing conjugated systems [1052]. This technique is used in combination with MNDO geometry optimizations to obtain structural data. From these calculations, it appeared that for the normal aromatic ground-state geometry of polythiophene, the Δr value is strongly negative and tends to be more and more positive as quinoid contributions to the geometry increase. As an example, the aromatic and quinoid geometric structures of polythiophene are shown in Figure 102.

Figure 103 illustrates the evolution of the bandgap as quinoid contributions to the aromatic ground state of polythiophene increase. Within the scope of the valence-bond discussion, it can be said that the value of the bandgap is evaluated as a function of a decreasing contribution of the aromatic resonance form, i.e., decreasing value of C_A , or an increasing contribution of the quinoid resonance form, i.e., increasing value of C_Q . As the quinoid contributions to the geometry increase, we observe first that the bandgap decreases linearly. As Δr approaches $+0.06 \text{ \AA}$, the bandgap becomes very small. For $\Delta r > +0.06 \text{ \AA}$, the bandgap increases again. We can thus divide the V-shaped curve into two parts. The left part for $\Delta r < 0.06 \text{ \AA}$ corresponds to an aromatic-type electronic structure ($C_A > C_Q$). The right part for $\Delta r > 0.06 \text{ \AA}$ corresponds to

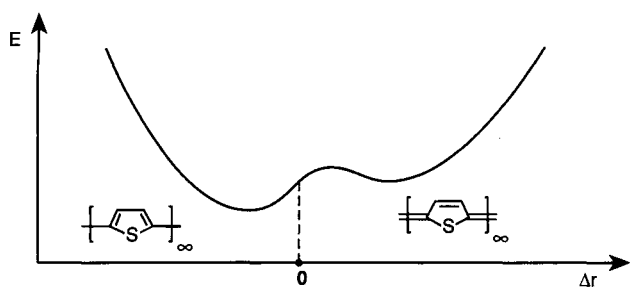


Fig. 104. Potential energy diagram of polythiophene.

a quinoid structure ($C_A < C_Q$). Note, however, that this relationship, established by Brédas [1053], predicts that the corresponding polymeric chains will generally not have a metallic behavior (except as a result of accidental degeneracy) but would constitute semiconductors with possibly very small bandgaps. The potential energy diagram as shown in Figure 104 is similar to that of poly(*p*-phenylene) (Fig. 100).

This relationship can be applied in the search for new polymeric materials with a small bandgap. Indeed, to obtain a small bandgap in the aromatic ground state of a polymer such as, for example, polythiophene, quinoid contributions should be increased. These concepts led to the synthesis by Kobayashi and co-workers [1054, 1055] of polyisothianaphthene. Polyisothianaphthene is a polythiophene derivative in which all thiophene rings are fused to a benzene ring along the β - β' thiophene bond. The presence of a benzene ring stabilizes some quinoid contributions to the ground-state geometry of polyisothianaphthene. As a result, the bandgap is found to decrease from 2.2 eV in polythiophene to 1.0 eV in polyisothianaphthene.

This result appeared from resonant Raman scattering measurements by Poplawski et al. [1056] to be consistent within the framework established by Brédas. Indeed, systematic resonant Raman scattering measurements of polyacetylene and polythiophene have shown a direct correlation between the π -electron gap and the vibrational force constant. This experimental correlation can be explained within the simple Peierls model for degenerate ground-state systems. In this model, larger dimerization amplitudes correspond, on the one hand, to larger bandgaps and, on the other hand, to larger vibrational force constants. The results of their resonant Raman scattering measurements on polyisothianaphthene confirmed the arguments of Brédas that the increased quinoid character of the backbone geometry reduces dimerization and thus the π -electron gap becomes smaller.

Aromatic or Quinoid? The framework established by Brédas et al. [1051, 1053] and the results obtained by Kobayashi et al. [1054] stimulated different theoretical research groups to investigate analogous systems and evaluate the relationship between the bandgap and the aromatic and quinoid structures. The investigated systems each contain an additional fused benzene ring(s) in order to investigate the effect of further stabilizing quinoid contributions to the ground-state geometry. The investigated polymers are polythiophene (PT), polyisothianaphthene (PITN), poly(isonaphthothiophene) (PINT), and poly(isoanthrothiophene) (PIAT) (Fig. 105). The results of the calculations of the involved groups are summarized in Table II. The following will give a comparative overview of these results, concluding with a short sum-

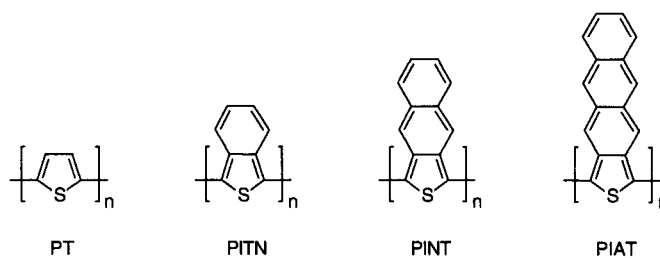


Fig. 105. Chemical structures of polythiophene (PT), polyisothianaphthene (PITN), poly(isonaphthothiophene) (PINT), and poly(isoanthrothiophene) (PIAT).

Table II. Experimental and Calculated Values for the Bandgap E_g (eV) of PT, PITN, PINT, and PIAT

E_g (eV)	PT	PITN	PINT	PIAT
Experimental	2.2	1.0	1.4	—
Brédas et al. [1051, 1053]	1.71	0.54	0.01	—
Hoogmartens et al. [1057]	A(p): 1.59 A(n): 1.68 Q: 0.26	A(p): 0.21 A(n): 0.61 Q: 1.19	—	—
Lee and Kertesz [1058]	A: 1.83 Q: 0.47	0.73 1.16	0.28 1.50	0.08 1.66
Nayak and Marynick [1059]	A(p): 1.76	A(p): 0.68 A(n): 1.64 Q: 0.80	A(p): 0.37 A(n): 1.03 Q: 1.10	—

Abbreviations: A, aromatic; Q, quinoid; p, planar; n, nonplanar.

mary of the scarce experimental data on the structure of polyisothianaphthene.

Since the experimental results on polyisothianaphthene were quite encouraging, Brédas et al. [1051, 1053] calculated the bandgap of polythiophene and polyisothianaphthene to be 1.71 and 0.54 eV, respectively. The difference of 1.17 eV between these values corresponds surprisingly well with the experimentally observed decrease of the bandgap going from polythiophene to polyisothianaphthene by fusing an additional benzene ring onto the thiophene system. Analogous calculations were next performed on the bandgap of PINT and a vanishing small value of 0.01 eV was obtained. This suggested that PINT could be an example of a conducting polymer with a vanishing small bandgap.

In a joint experimental and theoretical publication [1057], the results of nuclear magnetic resonance (NMR) measurements performed on polyisothianaphthene and a series of selected molecular model compounds were combined with quantum-chemical calculations carried out on oligomers within the Austin model 1 (AM1) and valence-effective Hamiltonian (VEH) methodologies in order to study the differences among planar aromatic, nonplanar aromatic, and quinoid polythiophene and polyisothianaphthene.

As expected in the case of polythiophene, the situation is quite clear. The aromatic structure of polythiophene is unequiv-



Fig. 106. Aromatic and quinoid structures of polyisothianaphthene.

ocally more stable than the quinoid one. The energy difference of 8.7 kcal/mol between the two forms is very close to other data in the literature [1059, 1060]. These calculations indicate, however, that aromatic form of polyisothianaphthene is, on average, 2.7 kcal/mol less stable than the quinoid form. This value is very close to the extrapolation of (PRDDO) result to the infinite chain length: $\Delta E = 2.4$ kcal/mol in favor of the quinoid form [1059]. Rotation of the aromatic isothianaphthene units around the interring single bonds to an average optimal dihedral angle of 27° induces a small stabilization of the aromatic isothianaphthene (ITN) oligomers on the order of 0.5 kcal/mol per repeat unit, reducing the energy difference between the two valence-bond isomeric structures to 2.2 kcal/mol.

In the planar aromatic form, polyisothianaphthene shows a very small bandgap (0.21 eV), while the value found for the quinoid polymer is much larger (1.19 eV). In the nonplanar aromatic form, the bandgap increases to 0.6 eV due to partial loss of π conjugation. This value corresponds to that of a single chain "in the gas phase." Most probably, the solid-state packing would somewhat reduce the tilt angle between adjacent isothianaphthene units, thereby leading to a slightly smaller value of the bandgap. On the basis of these results, they predicted aromatic and quinoid polyisothianaphthene (Fig. 106) to present markedly different optical signatures. As the calculated bandgap value of quinoid polyisothianaphthene appeared to be in better agreement with experimental data derived from optical spectroscopy (spectrum onset located at 1.0 eV and λ_{\max} at 1.5–1.6 eV) [1054], it was suggested that polyisothianaphthene should possess a quinoid structure. Moreover, these calculated values correspond quite well with earlier reported data [1058, 1059].

Kertesz and co-workers [1058, 1061, 1062] evaluated polythiophene-based polymers with an increasing number of fused benzene rings. For the geometry optimizations and to obtain the total energy of these polymers, they used an MNDO method based on band theory instead of an MNDO method based on cluster calculations. To obtain the energy bands, an energy-band version of the traditional Hückel theory was used. Apparently, their type of full MNDO geometry optimization for the infinite polymer polyisothianaphthene, regardless of the starting geometry, always converges to a quinoid structure. The opposite was found for the case of poly(*p*-phenylene), where only the aromatic structure is observed.

As noticed in the discussion of the VB theory, the wave function of poly(*p*-phenylene), polythiophene, polypyrrole (PP), and polyfuran is principally determined by the aromatic resonance form ($C_A > C_Q$). In the case of polyisothianaphthene, however, the quinoid resonance form should, according to Kertesz and co-workers, possess a stability such that it has a more important contribution to the ground-state wave function as compared to the aromatic resonance form ($C_A < C_Q$). Thus, a switchover occurs in energetics from the aromatic structure of the quinoid form at the level of polyisothianaphthene in the series of Figure 105.

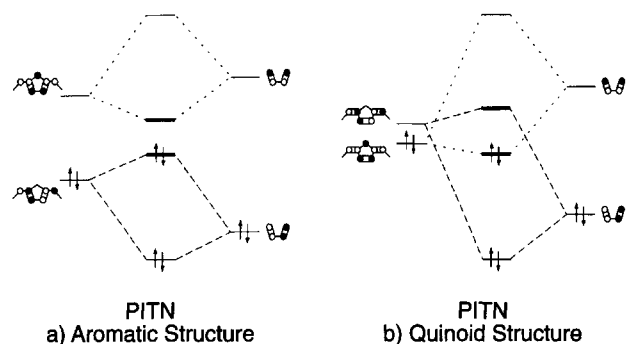


Fig. 107. Perturbation of the frontier orbitals of aromatic and quinoid PT by one butadiene group, resulting in the formation of PITN. Reproduced and adapted by permission of the American Institute of Physics from Y. S. Lee and M. Kertesz, *J. Chem. Phys.* 88, 2609 (1988). Copyright © 1988, American Institute of Physics.

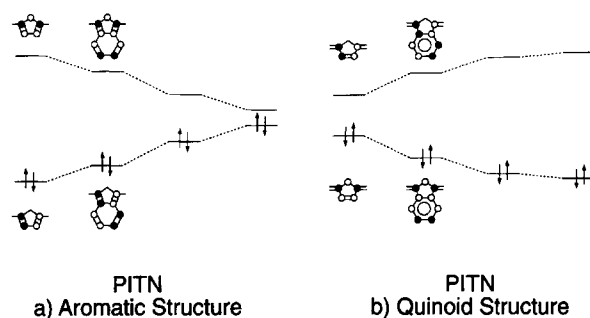


Fig. 108. Perturbation of the frontier orbitals of aromatic and quinoid PT by successive butadiene groups, resulting in the formation of PITN, PINT, and PIAT. Reproduced and adapted by permission of the American Chemical Society from Y. S. Lee, M. Kertesz, and R. L. Elsenbaumer, *Chem. Mater.* 2, 526 (1990). Copyright © 1990, American Chemical Society.

Table II displays the calculated values for the bandgap of each of the polymers in the aromatic ground state as well as in the quinoid ground state. As far as the aromatic ground state is concerned, their results indicate a lowering of the bandgap in the series of Figure 105. This is in accordance with the results of Brédas [1053].

For the quinoid ground state, however, the value of the bandgap will increase. This phenomenon is interpreted in Figures 107 and 108 by treating the butadiene groups as successive perturbations to the frontier orbitals (HOMO and LUMO) of polythiophene.

For the aromatic structure of polythiophene, the successive butadiene groups stabilize the LUMO and destabilize the HOMO, which results in a decrease of the bandgap. For the quinoid structure of polythiophene, the addition of successive butadiene groups stabilizes the HOMO and destabilizes the LUMO. As a result, the bandgap increases steadily with an increase in the number of rings in the system, until a level crossing occurs that tempers the further increase of the gap.

Based on their band structure calculations within the MNDO approximations, Lee and Kertesz [1058] predicted moreover the planar quinoid form of polyisothianaphthene to be the ground-state geometry. They estimated an energy difference of 10.55 kcal/mol per ring between the aromatic and quinoid forms of polyisothianaphthene. They postulated that the delocalization

energy of π electrons over the neighboring rings and the six-membered side rings offsets the repulsion energy arising from the steric interactions between hydrogen and sulfur atoms on adjacent units. Furthermore, they predicted an energy difference of 3.4 kcal/mol per ring between the coplanar and the nonplanar ($\phi = 95^\circ$) forms of the aromatic polymer favoring the latter conformation. This indicates that the energy loss due to the relaxation from the quinoid to the planar aromatic form is much larger than the energy gained from the relaxation from a planar aromatic to a twisted aromatic structure.

Since the semiempirical MNDO method was considered to yield relatively poor estimates for nonbonded repulsions and rotation angles about single bonds in conjugated molecules, Nayak and Marynick [1059] could not consider the results of Lee and Kertesz [1058] as definitive. Nayak and Marynick made use of the PRDDO method to optimize the geometries of their systems and developed a method for extrapolating the *ab initio* and/or PRDDO oligomer energetics to the infinite system. This approach allowed them to perform an assessment of the relative energies of the aromatic and quinoid forms at a highly theoretical level. Application of this method to polyisothianaphthene suggests that the ground state is quinoid, but the relative energies ($\Delta E = 2.4$ kcal/mol per repeat unit for the infinite chain) of the quinoid and aromatic forms are so close that both structures may exist as local minima in the real polymeric system. Steric effects may strongly favor nonplanar geometries, but electronic effects associated with increased conjugation along the backbone are also significant and in some cases may be sufficient to force the polymer into a planar quinoid structure. The calculation of the bandgap of polythiophene, polyisothianaphthene, and PINT, based on the extended Hückel theory, agree well with the results of Lee and Kertesz [1058] and those of Brédas [1053] derived from VEH calculations.

Besides the quantum-chemical calculations, the experimental evidence is inconclusive. Because of the amorphous nature of most conjugated polymers, direct structural information obtained from X-ray or neutron diffraction remains limited. The X-ray photoelectron spectroscopy (XPS) valence spectrum of polyisothianaphthene has been found to be in good agreement with the theoretical curve calculated on the basis of an aromatic backbone [1063]. However, the overall density of valence states, which is probed by XPS, is expected to be very similar for both quinoid and aromatic structures, so that such experimental data cannot provide the clear signature of one of the two structures. From Raman scattering data on neutral and doped polyisothianaphthene, it has been proposed that the ground-state geometric structure of the neutral system is quinoid and becomes aromatic upon doping [1064, 1065]. This hypothesis is based on a comparison between the measured frequencies and the values calculated for the quinoid and aromatic structures from the force constants of thiophene and benzene. However, the experimental Raman frequencies are in agreement with the calculated values for the aromatic structure of polythiophene only after a refinement procedure has been applied. When this procedure is used for polyisothianaphthene, the frequencies obtained for the aromatic and the quinoid structures are so similar to each other that it seems a delicate matter to determine which set of results is closest to the experimental data. It thus appears that the question of the ground-state geometry of polyisothianaphthene is not resolved unequivocally by those results. Comparison of ^{13}C NMR and Fourier transform (FT) Raman data of model compounds and polyisothianaphthene has indicated that the struc-

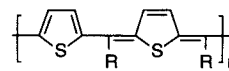


Fig. 109. Conjugated polymers containing mixed aromatic and quinoid moieties.

ture of polyisothianaphthene possesses a high quinoid character [609, 789, 1057, 1066–1071].

These theoretical and experimental results indicate that, to lower the bandgap starting from polyisothianaphthene, one has to stabilize aromatic contributions to the theoretically predicted quinoid ground-state geometry rather than further continue stabilizing quinoid contributions.

Mixed Aromatic and Quinoid Structures. Based on the idea of balancing aromatic and quinoid contributions, Chen and Jenekhe [838, 839, 1072] proposed synthesizing conjugated polymers in which alternating aromatic and quinoid moieties are combined (Fig. 109). Due to the use of appropriate starting materials, it should be possible to mix aromatic and quinoid structures in variable proportions. Such an approach should allow one to tune the bandgap between the value of a fully aromatic and a fully quinoid polymer. Chen and Jenekhe reported values for the bandgap between 1.14 and 1.45 eV.

Kiebooms and Wudl [841], showed that an analogous combination of aromatic and quinoid isothianaphthene structures affords a polymer with a bandgap of 1.2 eV.

2.5.3.3. Resonance Energy

Aromaticity and Bandgap. Since most of the conducting polymers contain aromatic ring systems, it is worthwhile to look closer into a possible correlation among resonance (or π delocalization in terms of the VB theory), aromaticity, and bandgap. The following discussion will be pursued within the framework of the Hückel molecular orbital (HMO) theory [1050, 1073–1082].

More generally speaking, the delocalization stabilization or resonance energy, RE, is defined as the difference between the total π -electron energy, $E_{\pi, \text{HMO}}$, of a certain conjugated molecule obtained from the HMO approach and a corresponding hypothetical reference structure:

$$\text{RE} = E_{\pi, \text{HMO}}(\text{conjugated molecule}) - E_{\pi}(\text{reference structure})$$

The choice of a reference structure is more or less arbitrary. Classically, the RE is defined as

$$\text{CRE} = E_{\pi, \text{HMO}} - n_{=} (2\alpha + 2\beta)$$

where CRE is the classical resonance energy and is the number of isolated carbon-carbon double bonds with the HMO-calculated π -electron energy of ethylene, i.e., $(2\alpha + 2\beta)$. This more traditional method of calculating the Hückel resonance energy of conjugated hydrocarbons by comparing the π -electron energy, $E_{\pi, \text{HMO}}$, with $n_{=} (2\alpha + 2\beta)$ has some serious shortcomings. Indeed, this method predicts a substantial resonance energy for linear polyenes, whereas experiment shows the resonance energy in these molecules to be rather small. Moreover, this method predicts substantial resonance energy for certain cyclic polyenes that experiment reveals to be unstable, with no aromatic character. A cyclic conjugated polyene is said to be *aromatic* when it shows substantially more stability than a hypothetical structure in which the double bonds do not interact with one another and when it undergoes

Table III. Hess-Schaad π -Bonding Energy Values (β) for the Eight Possible Bond Types

Bond type	Calculated π -bonding energy (β)
H ₂ C=CH	2.000
HC=CH	2.0699
H ₂ C=C	2.000
HC=C	2.1083
C=C	2.1716
HC-CH	0.4660
HC-C	0.4362
C-C	0.4358

Source: Reproduced and adapted by permission of the American Chemical Society from B. A. Hess and L. J. Schaad, *J. Amer. Chem. Soc.* 93, 305 (1971). Copyright © 1971, American Chemical Society.

substitution, rather than addition, when treated with electrophilic reagents, thereby maintaining the cyclic conjugated π system.

To produce more reliable predictions of aromaticity, Hess and co-workers proposed a new definition for the resonance energy [1073–1081]. Following a suggestion of Dewar and de Llano [1082], Hess and co-workers calculated the resonance energies of cyclic hydrocarbons by comparing the compounds' Hückel theory $E_{\pi, \text{HMO}}$ with a value, $E_{\pi, \text{loc}}$, calculated for a hypothetical acyclic conjugated polyene with the same number and kinds of bonds as in the localized structure of the cyclic hydrocarbon. Thus,

$$\text{RE} = E_{\pi, \text{HMO}} - E_{\pi, \text{loc}}$$

where $E_{\pi, \text{loc}} \approx \sum n_b E_{\pi, b}$, n_b is the number of bonds of a given type, and $E_{\pi, b}$ is an empirical energy parameter associated with a bond of type b . Hess and Schaad [1073] distinguish eight types of bonds over which the summation should go. Indeed, a conjugated hydrocarbon has three types of carbon-carbon single bonds and five types of double bonds, the types differing in the number of H atoms bonded to the carbons. In the calculations of the resonance energy, the terms involving α always cancel. In Table III, showing the Hess-Schaad values, $E_{\pi, b}$, for the various bond types, the terms involving α will be omitted.

Any acyclic or cyclic polyene can be constructed by various combinations of these eight types of bonds. Using the values of Table III, one is able to calculate the π -electron energy, $E_{\pi, \text{loc}}$, for a localized cyclic polyene in an additive fashion. The resonance energy is then found as the difference between the cyclic polyene's Hückel π -electron energy, $E_{\pi, \text{HMO}}$, and the quantity $E_{\pi, \text{loc}}$. This method gives the resonance stabilization of cyclic polyenes relative to noncyclic polyenes. For comparison of a set of various types of compounds, it is more significant to use the resonance energy per electron (REPE). A compound with a substantially positive REPE value is then predicted to be *aromatic*. A compound with a near-zero REPE is *nonaromatic*. A compound with a substantially negative REPE is predicted to be *antiaromatic*, being less stable than if its double bonds were isolated from one another.

An analogous approach for bond types containing oxygen [1075], nitrogen [1075, 1078], and sulfur [1077] heteroatoms made it possible to evaluate resonance energies in heterocyclic polyenes. Comparison with experiment shows that the Hess-Schaad method is highly successful in predicting aromaticity. Table IV gives the

Table IV. Resonance Energy (RE) and Resonance Energy per Electron (REPE) Values for Various Heterocyclic Polyenes Following the Method of Hess and Schaad Together with the Bandgap Values (E_g) of the Corresponding Polymers

Compound	RE (β)	REPE (β)	E_g (eV)
Benzene	0.390	0.065	3.4
Pyridine	0.348	0.058	—
Pyrazine	0.293	0.049	—
Pyrrrole	0.233	0.039	3.1
Thiophene	0.193	0.032	2.1
Furan	0.044	0.007	2.3
Isobenzofuran	0.018	0.003	—
Isoindole	0.292	0.029	—
Isothianaphthene	0.247	0.025	1.1

Source: Partially reproduced and adapted by permission of Elsevier Science and the American Chemical Society from B. A. Hess, L. J. Schaad, and C. W. Holyoke, *Tetrahedron* 28, 3657 (1972); B. A. Hess and L. J. Schaad, *J. Am. Chem. Soc.* 95, 3907 (1973). Copyright © 1972, 1973, Elsevier Science and the American Chemical Society.

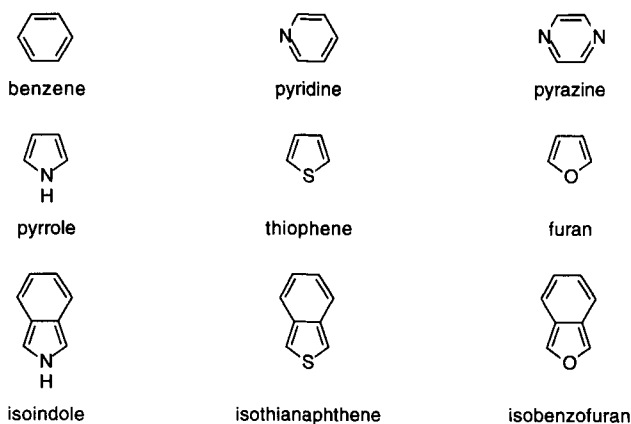


Fig. 110. Various heterocyclic polyenes that can be used for the synthesis of conducting polymers.

RE and the REPE for heterocyclic polyenes (Fig. 110), which can be used in the synthesis of conducting polymers.

To compare the REPE and the value of the bandgap (E_g) of the corresponding polymer, the experimentally available values for the E_g of poly(*p*-phenylene), polypyrrole, polythiophene, polyfuran, and polyisothianaphthene are also given in Table IV. From these data, it appears that the bandgap decreases with decreasing REPE value. This means that the less aromatic the polymer, the lower the bandgap will be. The effect appears to be large enough to result in a decrease of the bandgap from poly(*p*-phenylene) to polyisothianaphthene of about 2.5 eV.

This evolution, however, seems to be limited by the chemical stability of the involved ring systems. Indeed, the reported bandgap of polyfuran appears to be larger than the bandgap reported for polythiophene [1083]. Compared to pyrrole and thiophene, furan is the most chemically unstable as predicted by its REPE value of 0.007 (nonaromatic). The presence of absorptions characteristic of aliphatic and carbonyl moieties in the vibration spectra of polyfuran [1084] are attributed to its chemical instabil-

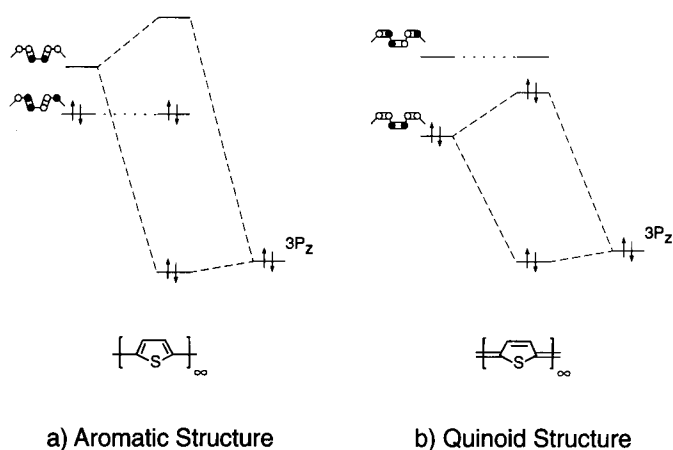


Fig. 111. Interaction of the lone pair of the sulfur heteroatom with the HOMO and LUMO of polyacetylene, resulting in a larger bandgap for the aromatic structure of PT and, on the other hand, in a smaller bandgap for the quinoid structure. Reproduced and adapted by permission of the American Institute of Physics from Y. S. Lee and M. Kertesz, *J. Chem. Phys.* 88, 2609 (1988). Copyright © 1988, American Institute of Physics.

ity, particularly in the oxidized doped state and particularly with respect to ring opening by nucleophilic reagents. Therefore, electrical conductivities and free-carrier mobilities were found to be considerably lower as compared to the other five-membered aromatic heterocycles. In some cases, the ring-opening process during polymerization was so extensive that no conjugated material was obtained.

Resonance Stability of the Aromatic Monomer Unit. The Hess-Schaad method indicates that the resonance stability of the classical aromatic five- and six-membered ring systems is determined, to a large extent, by the presence of heteroatoms. However, the influence of the heteroatom was initially assumed to be an essentially indeterminable effect on the σ bond of the carbon chain. Later, Mintmire et al. [1085] showed that many of the observed properties of heterocyclic ring chain polymers could be understood by incorporating the heteroatom p orbital into the π -band structure and assuming no heteroatom effects on the σ -bond structure, because the latter are theoretically difficult to predict and to understand fully. They suggested that the interaction of the lone pair of the sulfur heteroatom with the HOMO and LUMO of polyacetylene results in a larger bandgap for the aromatic structure of polythiophene and, on the other hand, in a smaller bandgap for the quinoid structure (Fig. 111).

As already appeared from the qualitative aromaticity evaluation by Hess and Schaad, the presence of heteroatoms in aromatic ring systems can thus considerably influence the electronic properties. With the design of low-bandgap conducting polymers in mind, the introduction of heteroatoms into the aromatic ring could be used to stabilize or destabilize aromatic or quinoid contributions to the ground-state geometry of a certain polymer. The effect of such a substitution on the relative stability of aromatic ring systems can be assessed by means of the REPE as defined by Hess and Schaad.

Since the polymer obtained from isothianaphthene possesses a rather small bandgap of 1 eV, we chose to evaluate the relative resonance stabilities of some isothianaphthene derivatives in which additional heteroatoms were introduced. Indeed, it can be

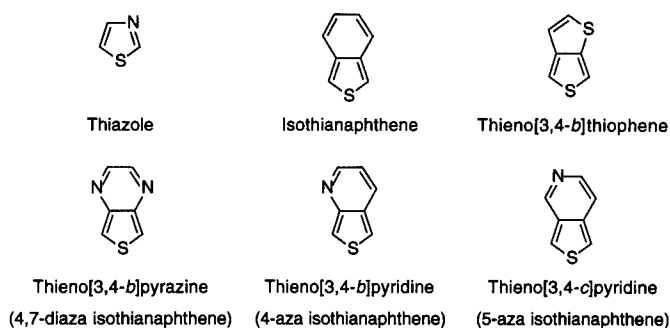


Fig. 112. Introduction of nitrogen and sulfur in the thiophene and isothianaphthene ring systems.

expected that the introduction of nitrogen or sulfur atoms into the additional benzene ring will influence the resonance stabilization to a considerable extent (Fig. 112). If the heteroatom introduction occurs in the fused benzene ring, this will have an important consequence on the resonance stabilization of the aromatic and quinoid structure of the polymer. The resonance stabilization of the quinoid structure will be more importantly influenced than the aromatic structure, since in the aromatic structure the resonance stabilization is mainly governed by the thiophene aromaticity.

Although Hess and Schaad compared the aromaticity of a large number of heterocyclic compounds, only the data on cyclic systems containing one type of heteroatom were reported. To compare the ring systems listed in Figure 112, we needed to calculate the compound's Hückel π -electron energy, $E_{\pi, \text{HMO}}$, and the π -electron energy, $E_{\pi, \text{loc}}$, for the corresponding localized heterocyclic polyene using the different empirical π -bond energies of carbon-carbon and carbon-heteroatom bonds [1073–1081].

The calculation of $E_{\pi, \text{HMO}}$ was performed using a personal computer (PC) program by Vanderzande [1086] and the so-obtained results were checked with the Macintosh program HMO-plus 1.5.1 by Wissner [1087]. Both programs are based on the classical literature of HMO theory [1088–1090]. To use the results of Hess and Schaad for comparison with other heterocycles, the parameter set as published by Hess and Schaad was used to obtain $E_{\pi, \text{HMO}}$. However, the so-obtained value of $E_{\pi, \text{HMO}}$ has to be corrected for the presence of the heteroatom electrons. Indeed, each isolated carbon atom has a π energy α , but that of a heteroatom contributing two electrons to the π system is $2(\alpha + h_x\beta)$, where h_x is a Coulomb integral heteroatomic correcting parameter. This parameter is determined by Hess and Schaad based on semiempirical methods. Therefore, the obtained $E_{\pi, \text{HMO}}$ had to be corrected by subtracting for each heteroatom electron participating in the π system the corresponding Coulomb integral parameter [1075]. Table V gives a list of the final corrected $E_{\pi, \text{HMO}}$, the $E_{\pi, \text{loc}}$ of the localized reference structure, the RE, and the REPE of different aromatic compounds. The calculated values were compared with the available data of Hess and Schaad and appeared to be in excellent agreement with one another. Figure 113 gives a graphic representation of the lowering of the REPE in the different heterocyclic systems.

From a comparison of the REPE values, isobenzofuran appears to be nonaromatic, which corresponds with its reactive nature. Furan also has a very small REPE and behaves much like a polyene as it undergoes Diels-Alder reactions readily, while pyrrole and thiophene do not. Isothianaphthene has a REPE that is considerably lower than that of thiophene. As compared to thio-

Table V. Values for a Series of Aromatic Heterocyclic Systems of the Hückel π Energy, E_{π} , HMO, the $E_{\pi, loc}$ of the Localized Reference Structure as Determined by Hess and Schaad, the RE, and the REPE

Compound	$E_{\pi, HMO}$	$E_{\pi, loc}$	RE (β)	REPE (β)
Benzene	8	7.6080	0.3920	0.0653
Pyridine	7.2493	6.9010	0.3483	0.0581
Pyrazine	6.4881	6.1951	0.2930	0.0488
Pyrrole	5.4351	5.2018	0.2333	0.0389
Thiazole	4.4921	4.286	0.2061	0.0344
Thiophene	5.1855	4.9926	0.1929	0.0322
Isoindole	11.0194	10.7266	0.2928	0.0293
Isothianaphthene	10.7636	10.5174	0.2462	0.0246
4-Aza isothianaphthene	10.0846	9.8395	0.2451	0.0245
5-Aza isothianaphthene	10.0488	9.8111	0.2377	0.0238
4,7-Diaza isothianaphthene	9.3628	9.1616	0.2012	0.0201
Thieno[3,4- <i>b</i>]thiophene	8.1011	7.9552	0.1459	0.0146
Furan	4.5982	4.5540	0.0442	0.0074
Isobenzofuran	10.0960	10.0788	0.0172	0.0017

Source: Partially reproduced and adapted by permission of Elsevier Science and the American Chemical Society from B. A. Hess and L. J. Schaad, *J. Am. Chem. Soc.* 93, 305 (1971); B. A. Hess, L. J. Schaad, and C. W. Holyoke, *Tetrahedron* 28, 3657 (1972); B. A. Hess and L. J. Schaad, *J. Am. Chem. Soc.* 95, 3907 (1973). Copyright © 1971, 1972, 1973, Elsevier Science and the American Chemical Society.

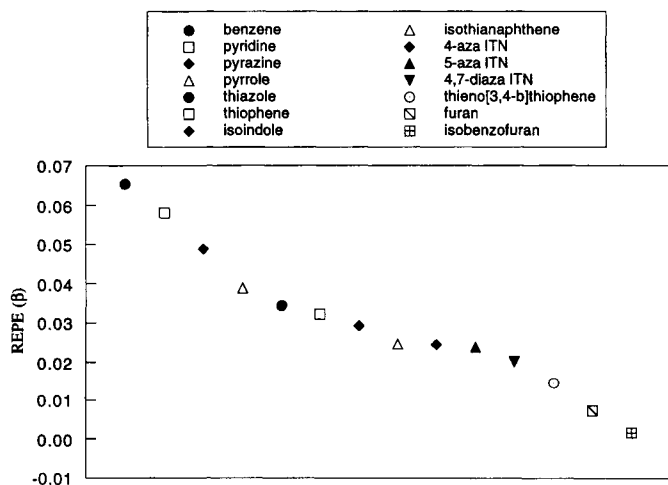
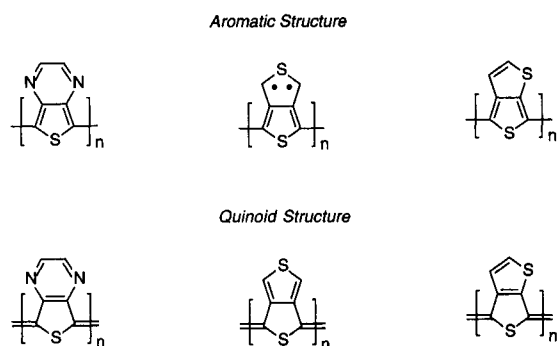


Fig. 113. Comparison of the resonance energy per electron (REPE) values for different aromatic heterocyclic ring systems.

phene, the stability of isothianaphthene is not high due to readily accessible pathways leading to benzene derivatives through, for example, Diels–Alder reactions as demonstrated by Cava and Pollack [596]. The introduction of one nitrogen atom does not lower the REPE substantially, but when a second nitrogen is introduced to obtain the 4,7-diaza derivative of isothianaphthene the REPE drops down further. Finally, thieno[3,4-*b*]thiophene, which can be considered as a thiophene derivative with instead of a β – β' fused benzene ring a β – β' fused thiophene ring, has a REPE that is even lower than that of the 4,7-diaza derivative of isothianaphthene. If there is a link between the REPE and the



Poly(thieno[3,4-*c*]pyrazine) Poly(thieno[3,4-*c*]thiophene) Poly(thieno[3,4-*b*]thiophene)

Fig. 114. Aromatic and quinoid structures of conducting polymers obtained by the introduction of heteroatoms (nitrogen, sulfur) in the isothianaphthene ring system.

bandgap, then the preceding data indicate that poly(thieno[3,4-*c*]pyrazine) and poly(thieno[3,4-*b*]thiophene) could be interesting low-bandgap polymers (Fig. 114).

Indeed, theoretical calculations based on the extended Hückel and PRDDO methods [1059] on poly(thieno[3,4-*c*]pyrazine) indicate that this polymer should possess a bandgap that is about 0.12 eV for the aromatic planar structure and 0.7 eV for the quinoid structure. The same calculations predict that the quinoid structure should be the most stable form. However, the difference between the aromatic and the quinoid structure is about 4.2 kcal/mol per repeat unit. This energy difference is not very large and is comparable with that of polyisothianaphthene (2.4 kcal/mol) within the PRDDO approach. This implies that for poly(thieno[3,4-*c*]pyrazine) the synthesis method can also play an important role in determining the final structure of the polymer. Other theoretical results [1091] based on *ab initio* Hartree–Fock crystal orbital calculations also indicate a lowering of the bandgap as compared to polyisothianaphthene. An additional characteristic of poly(thieno[3,4-*c*]pyrazine) is that, due to the substitution of nitrogen in the 4- and 7-positions, the steric interaction between hydrogen and sulfur has been lost. Therefore, it should be possible in some way to obtain an aromatic planar conformation in this polymer. This configuration should correspond with a good conductivity due to enhanced extended π delocalization.

A publication, where the results of Raman spectroscopy were combined with theoretical calculations, indicates, however, that the ground-state structure should be quinoid as in the case of polyisothianaphthene. The same authors report that their alkylated poly(thieno[3,4-*c*]pyrazine) derivative possesses a bandgap of 0.95 eV [632].

The first calculations evaluating the introduction of additional sulfur atoms into isothianaphthene-like ring systems concerned poly(thieno[3,4-*c*]thiophene). In this polymer, the fused benzene ring of polyisothianaphthene is replaced by a fused thiophene ring. However, the VEH-based calculations [1092] predict a larger bandgap for the aromatic structure of this polymer. Analysis of the HOMO and LUMO band structure showed that the polymer possessed a pronounced quinoid structure. Since the aromatic structure will be characterized by the presence of a diradical, the quinoid structure will be substantially more stable as compared to the aromatic diradical. Calculations by Kertesz and co-workers [1060, 1062] and Hong and Marynick [1093] also indicate that this

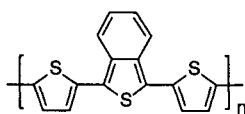


Fig. 115. Copolymer based on thiophene and isothianaphthene.

polymer should possess a quinoid structure and a larger bandgap as compared to polyisothianaphthene.

Hong and Marynick [1093] also studied the electronic properties of poly(thieno[3,4-*b*]thiophene) for which a bandgap of 12 eV was reported by Pomerantz and Gu [642]. In this polymer, however, Hong and Marynick found a very slight energy difference of 0.3 kcal/mol per repeat unit between the aromatic and the quinoid structure, whereas in poly(thieno[3,4-*c*]thiophene) this energy difference is about 30.5 kcal/mole per repeat unit. The bandgap of the aromatic structure was predicted to be somewhat higher as compared to polyisothianaphthene, but the bandgap of the quinoid structure should be lower as compared to the bandgap of quinoid polyisothianaphthene. The small energy difference between the aromatic and the quinoid structure of poly(thieno[3,4-*b*]thiophene) makes it difficult to determine its most stable ground-state structure. However, this implies that its structure can also be controlled by means of appropriate chemical synthetic methods.

Combination of Ring Systems with a Different Aromaticity. When two types of conducting polymers are combined to form a new polymer, the bandgap of the new polymer will be in between those of the corresponding homopolymers. A well-known example is PPV, which can be considered as a copolymer of poly(*p*-phenylene) and polyacetylene and which has a bandgap in between those of the corresponding homopolymers.

Thus, the combination of two different ring systems to form a copolymer allows an important control of the electronic properties. Indeed, if, for example, isothianaphthene units are introduced in a thiophene backbone (Fig. 115), one can expect the bandgap to be lowered significantly as compared to polythiophene itself. A number of calculations [1094–1096] support this idea and several attempts [628, 788, 791, 792, 796, 801] have been made to obtain systems consisting of a combination of thiophene units and isothianaphthene-type ring systems. Although these results mention bandgaps in between those of the homopolymer systems, the presence of important amounts of oligomeric material urges further investigation of the obtained products. Results by Vangeneugden et al. [793, 794] demonstrate that by applying this method a series of polymeric materials can be obtained with bandgaps below 1.5 eV.

2.5.3.4. Substituents

Side Chains. It should be stressed that substituents not only influence the bandgap but also other electronic parameters such as the ionization potential (\approx top of the valence band energy) and the electron affinity (\approx bottom of the conduction band energy). These parameters are of fundamental interest for applications such as the construction of electronic devices (e.g., diodes and transistors) [1097]. Although substituents *in se* have a nonnegligible influence on electronic parameters, in general they are on the order of, as far as the bandgap is concerned, only a few 0.1 eV. Electronic effects originating from the inductive and mesomeric influence of

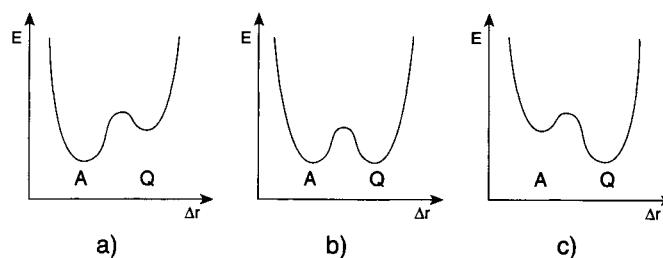


Fig. 116. Potential energy diagrams for three possible ground-state energy situations of a polyaromatic.

substituents can be used to massage the electronic properties in a certain direction. However, the discussion in Sections 4.5 and 5 will show that the effect of substituents through sterical interactions is much more important.

For well-known conducting polymers such as poly(*p*-phenylene), polythiophene, and poly(paraphenylene vinylene) (PPV), the influence of substituents has already been investigated on the experimental and theoretical levels [1097]. In the case of polyisothianaphthene, however, there is a lack of experimental data describing the influence of electron-donating and electron-withdrawing substituents. Therefore, only some earlier theoretical investigations will be discussed.

Only Brédas et al. [1051, 1053] reported the results of calculations on the 5,6-dimethyl-, 5,6-dimethoxy-, and 5,6-dicyano-substituted aromatic polyisothianaphthene derivatives. From these data, it can be concluded that the overall effect of electron-donating and electron-withdrawing substituents is rather small and the reported bandgap values only show a difference of at most 0.05 eV. The results of *ab initio* Hartree–Fock crystal orbital calculations [1091] for dihydroxy- and dicyano-substituted poly(isonaphthothiophene) point in the same direction.

In conclusion, experimental results indicate that the main interest in substituents is not at the level of the search for *intrinsic* low-bandgap conducting polymers. Rather, the main interest should be at the level of fine-tuning of the electronic characteristics for well-defined applications and at the level of processibility.

End Groups. From the previous discussion, it could be concluded that within the class of polyaromatics two ground-state geometries are possible, the aromatic geometry and the quinoid geometry. If one wishes to compare the relative energies of these geometries for a hypothetical polyaromatic, three situations are possible. In the first situation, the ground-state energy of the aromatic structure is significantly lower (Fig. 116a) than the ground-state energy of the quinoid structure (e.g., polythiophene). The potential energy diagram for the inverse situation is shown in Figure 116c (e.g., polynaphthothiophene). Finally, the relative ground-state energies of both the aromatic and the quinoid structure might almost be equal (Fig. 116b).

The question arising at this point is to what extent the geometry of the polymer chain is determined by the energy difference between the aromatic and the quinoid structures. Quantum calculations [1057] have shown that the nature of the end groups and the structure of the chain are directly related. Defect-free systems correspond to the aromatic geometric structure, while the presence of sp^3 defects or sp^2 end groups is related to the quinoid form (Fig. 117). In the case of polythiophene, as the energy difference between the two forms is large (8.7 kcal/mol per repeat unit)



Fig. 117. Different chain end groups corresponding to a quinoid structure.

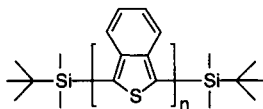


Fig. 118. Aromatic isothianaphthene oligomers ($n = 1-4$) with geometry-orienting silicon end groups.

[1057], quinoid oligomers of increasing length rapidly become less and less stable relative to their aromatic counterparts. For a certain chain length, one thus expects that an alternative structure possessing an aromatic character and two unpaired electrons will be favored over the quinoid form. This has been observed from quantum-chemical calculations on thiophene oligomers [1057]. Therefore, long quinoid oligothiophenes are not expected to exist, a situation that can be considered as typical of systems where the energy difference between the two forms is large.

In contrast, the quinoid and aromatic forms of polyisothianaphthene appear to be almost isoenergetic (2.2 kcal/mol) [1057]. Since this feature is observed with different theoretical methods, this small difference is to be considered an intrinsic characteristic of the polyisothianaphthene system. Consequently, both structures are predicted to be much more stable than the hypothetical diradical intermediate. Therefore, depending on the chemical strategy chosen for the polymerization, one can select the structure that will be obtained, with small probability of crossing over to the other form through the high-energy diradical species. In this situation, the polymerization mechanism and the nature of the monomer and of the end groups can orient the synthesis. Thus, compounds containing from the beginning sp^3 CH_2 sites or carbonyl end groups will most probably result in polyisothianaphthene possessing a quinoid structure. On the other hand, altering on the same basis the synthetic conditions can lead to polyisothianaphthene with an aromatic geometric structure, as demonstrated by Okuda et al. [601], who prepared the aromatic isothianaphthene tetramer using a 1,3-di(*tert*-butyldimethylsilyl) isothianaphthene monomer (Fig. 118).

2.5.3.5. π Delocalization across the Polymer Backbone

Chain-extended π -electron delocalization or resonance across the different ring systems in polyaromatics is, to large extent, dependent on the torsion angle θ between the monomer units (Fig. 119).

On the theoretical level, Brédas et al. [1098] studied the evolution of the bandgap as a function of increasing torsion angle. As could be expected, the bandgap increased going from a coplanar situation (0°) to a perpendicular situation (90°). Up to a torsion angle of about 40° , however, the bandgap showed no important changes. This effect was attributed to the $\cos \theta$ dependence of the π -orbital overlap of neighboring ring systems. Therefore, substituents inducing only a small difference in torsion angle will not have a too important influence on the electronic properties. Analogous results were obtained by Lagerstedt and Wennerström [1099] using HMO calculations. Conformational calculations on

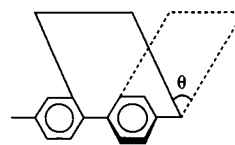


Fig. 119. Torsion angle θ between two aromatic ring systems.



Fig. 120. (a) Steric effect induces an increase in the torsion angle between the ring systems in a fluorinated polyisothianaphthene derivative ($E_g = 2.10$ eV). (b) Introducing nitrogen atoms results in a more planar quinoid system ($E_g = 0.95$ eV).

polythiophene by Cui and Kertesz [1100] also indicated an increase in the bandgap when the torsion angle increases. The value of the bandgap will rise to a maximum value at 90° , corresponding to no π -electron interactions between neighboring ring systems. Further increase of the torsion angle will result in a decrease of the bandgap as π -electron interactions will increase again. The bandgap of 1.7 eV at a torsion angle of 180° (*trans* coplanar) agrees relatively well with the experimental value of 2.1 eV of polythiophene. At a torsion angle of 90° , the bandgap will reach the maximum value of 4.5 eV. This is an increase of about 2.4 eV. Changes in the torsion angle between 180° and 140° only result in an increase of 0.6 eV. Slight deviations from the coplanar situation will therefore result in moderate changes in the bandgap value.

All of these different theoretical calculations are in accordance with one another. Therefore, we can conclude that the difference between a full planar and a perpendicular configuration will be on the order electron-volts of a few. More generally, all of the factors leading to a decrease in π delocalization across the polymer backbone will result in an increasing in the bandgap and *vice versa*.

This effect is nicely illustrated by poly(tetrafluoroisothianaphthene) (Fig. 120a). The steric effect induces an increase of the torsion angle between the ring systems, resulting in a polyisothianaphthene derivative with a large bandgap of 2.10 eV, although analysis of aromatic model compounds also indicates that the polymer possesses an aromatic structure [617, 625, 1101].

The opposite effect is illustrated by the synthesis of an alkylated poly(thieno[3,4-*c*]pyrazine) [631, 632]. This polymer (Fig. 120b) has a quinoid structure and a bandgap of 0.95 eV has been reported. The introduction of nitrogen atoms removes the effects of steric hindrance and favors a more planar inter-ring system.

The effect of the coplanarity of aromatic ring systems was studied in a series of 1,3-dithienylisothianaphthene model compounds (Fig. 121). The synthesis of 1,3-dithienylisothianaphthene (Fig. 121b) was first reported by Hoogmartens et al. [789]. Three other groups reported almost simultaneously on its synthesis in later publications [788, 791, 792]. Finally, the first group reported somewhat later on a very efficient synthesis method for these compounds [790]. The fluorinated 1,3-isothianaphthene derivative was prepared by Kiebooms et al. [790]. The compound in Figure 108c was synthesized by Ferraris et al. [796] and the thieno[3,4-*c*]pyrazine derivative by Kitamura et al. [797]. Figure 121 also lists the λ_{\max} for the different compounds.

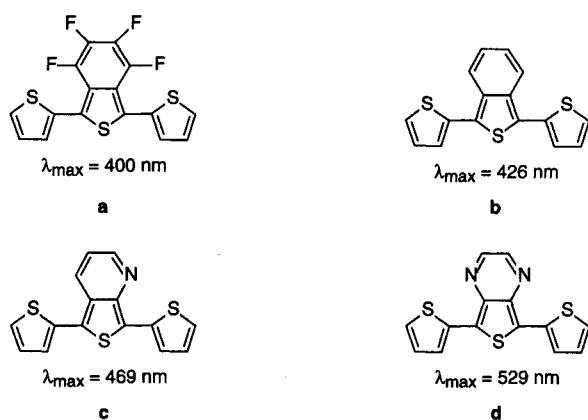


Fig. 121. Considerable redshift is observed with decreasing torsion angle between the aromatic ring systems.



Fig. 122. Significant lowering of the bandgap is achieved in regioregular substituted polythiophenes.

In the series of model compounds given in Figure 121, reducing the torsion angle leads to a considerable redshift of λ_{\max} of about 129 nm. Namely, replacing fluorine by hydrogen results in a redshift of 26 nm. No crystallographic data have been reported on the fluorinated compound. It is clear, however, that this should be the consequence of steric interactions. In the compound in Figure 121c, only one carbon has been replaced by nitrogen. The dihedral angle between thiophene and the central ring system on the nitrogen side is 3.4° , while the dihedral angle on the carbon side is reported to be 38.8° . The so-obtained planarization yields a redshift of λ_{\max} to a value of 469 nm [796]. The dihedral angles in the compound in Figure 121d are 9.5° and 11.6° , indicating that the three ring systems are almost coplanar. This is reflected in a further lowering of the λ_{\max} to 529 nm [797].

The torsion angle between aromatic ring systems is largely determined by steric interactions between those ring systems. The choice of the substituents and their position on the aromatic ring system determine, to a large extent, the value of the torsion angle. In poly(3-alkylthiophene)s, head-to-head coupling leads to polymers with a larger bandgap as compared to poly(3-alkylthiophene)s in which the rings are coupled head to tail [446, 1102, 1103].

McCullough and co-workers [387, 444, 1104] and Rieke and co-workers [462, 465] developed quasi-simultaneously synthetic routes for pure and highly regioregular substituted thiophenes (Fig. 122a). The so-obtained polythiophenes appeared to exhibit surprisingly high conductivities and a bandgap of 1.7 eV, which is about 0.4 eV smaller than those reported for regiorandom poly(alkylthiophene)s.

In the case of alkoxy substituents, it is not only the electron-donating effect of oxygen that plays a role in determining the value of the bandgap. The van der Waals radius of an oxygen atom (0.14 nm) is smaller than that of a methylene core (0.20 nm). As such, alkoxy side chains cause a smaller steric hindrance as



Fig. 123. Rigidification results in an increased effective conjugation length and a lowering of the bandgap.

compared to alkyl side chains. In poly(alkoxythiophene)s therefore more planar systems are achievable as compared to poly(alkylthiophene)s. Poly(3,4-ethylenedioxythiophene) [1105–1108] (Fig. 122b) is an example of an alkoxy-substituted polythiophene with a lower bandgap as compared to regular polythiophene. The two oxygen atoms are bridged together in a six-membered ring system by an ethylene group, thereby lowering the steric influence on neighboring aromatic ring systems. This material shows moreover an improved stability and high conductivity [1109].

Another way of increasing the effective conjugation length by decreasing torsion angles is by planar rigidification. Freezing the inter-ring positions of the thiophenes in a thiophene trimer using CH_2 bridges (Fig. 123a) leads to a considerable increase in the λ_{\max} from 380 to 750 nm [1110]. Similar effects are observed in bridged poly(*p*-phenylene) oligomers (Fig. 123b) [704].

2.5.4. Combining Structural Parameters to Obtain Low E_g

The influence of different chemical structural features on the bandgap of conjugated materials has been discussed previously. For significant lowering of the bandgap, several structural effects should be combined. This has been demonstrated by several groups. Combining several structural effects adds an additional degree of complexity to the understanding of the relationship between those chemical structures and their effect on the bandgap of the compound thus created.

Each structural effect and its influence on the electronic properties has been treated independently. However, these structure-property relationships are not always simply additive. The most obvious example is the synthesis of poly(terfluoroisothianaphthene) [625]. In this polymer, the effect of having an aromatic isothianaphthene structure and electron-withdrawing fluorine substituents is overruled by a very large inter-ring torsion angle. As a consequence, the polymer has a bandgap of 2.1 eV, much higher than that of regular polyisothianaphthene (1.0 eV). Despite this fundamental aspect of complexity, several groups have successfully used a combination of the discussed structural effects to gain control of the bandgap in conjugated polymers. Combining planarization and introducing antiaromaticity, Lambert and Ferraris [654, 655] made some conducting polymers in which some antiaromatic character was introduced by adding a carbonyl group or a dicyano group to the thiophene monomer (cyclopenta[2,1-*b*;3,4-*b'*]dithiophene-4-one and 4-dicyanomethylene-4*H*-cyclopenta[2,1-*b*;3,4-*b'*]dithiophene) (Fig. 124). This results in a monomer with a π system with 12 electrons possessing a lower RE. Incorporation of an empty p orbital is believed to lower the bandgap to an important extent. The bandgap of both polymers is reported to be lower than 1.2 eV.

Vangeneugden et al. [793, 794] combined different ring systems and the effect of substituents to prepare a series of thiophene-

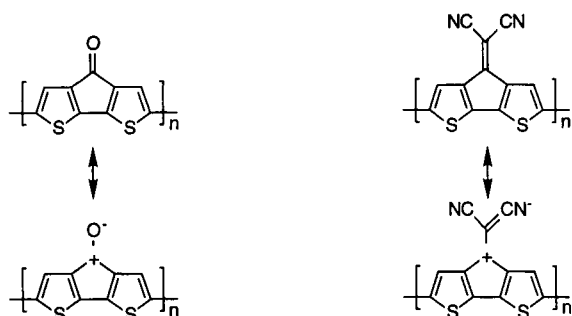


Fig. 124. Two examples of polymers in which some antiaromaticity was introduced: poly(cyclopenta[2,1-*b*;3,4-*b'*]dithiophene-4-one) and poly(4-dicyanomethylene-4*H*-cyclopenta[2,1-*b*;3,4-*b'*]dithiophene).

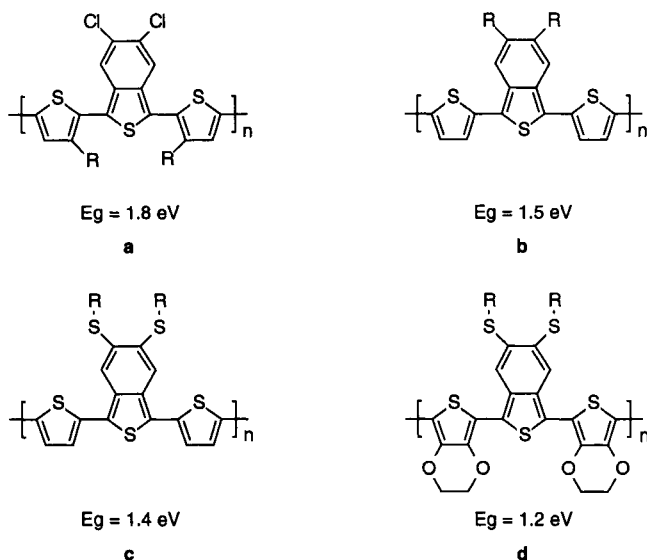


Fig. 125. In substituted poly(1,3-dithienyl isothianaphthene), efficient use of substituents allows control of the bandgap between 1.0 and 1.8 eV.

isothianaphthene copolymers with decreasing values for the bandgap (Fig. 125). By using oligomeric precursors, they showed that it is possible to control more effectively the regiochemistry in the final polymer. Moreover, this approach lowers the presence of inter-chain conjugation defects and improves structural regularity during polymerization.

Another series of examples of the efficient combination of several structural effects is demonstrated by Yamashita and co-workers [797, 799–801]. Figure 126 shows different monomers used to prepare the corresponding polymers. In this case, planarization, sulfur-nitrogen interactions, and a combination of different aromatic ring systems is used to obtain polymeric materials with bandgaps down to 0.5 eV, the lowest values reported so far.

3. ELECTRICAL PROPERTIES

In the past three decades, several types of π -electron systems have shown very interesting features in the electrical transport properties. The charge-transfer complexes [e.g., tetrathiafulvalene-tetracyanoquinodimethane (TTF-TCNQ), etc.], consisting of electron-donating (donors, TTF, etc.) and electron-withdrawing (acceptors, TCNQ, etc.) organic molecules, have a wide range of

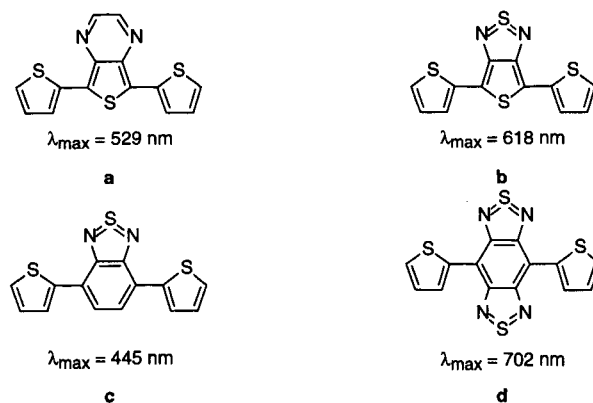


Fig. 126. Efficient combination of chemical structures leads to monomers that can be used to prepare polymers with very low bandgaps.

exciting electronic properties of low-dimensional systems [2, 111]. The typical sp^2 -carbon-rich systems such as intercalated graphite, carbon-60, and carbon nanotubes display a wide range of behavior from metals to insulators [1112]. Usually, the polymeric materials were considered as insulators before the discovery of metallic poly(sulfur nitride) (SN)_x and the enhancement of conductivity in doped polyacetylene (CH)_x by several orders of magnitude [155, 1113]. Among the various π -electron-rich systems, the polymeric materials belong to a special class due to their one-dimensional chain structure, side group-induced variations in electronic, optical, and morphological properties, the coexistence of both crystalline and amorphous regions, etc.

The polyconjugated chains consist of alternating single (σ -bonds) and double bonds (π bonds). The π electrons are highly delocalized and easily polarizable, and these features play important roles in the electrical and optical properties of polyconjugated systems, making them rather different from conventional electronic systems [1, 1049, 1114]. Moreover, the intrinsic quasi-one-dimensional nature and the extent of both intra- and inter-chain delocalization of the π electrons play significant roles in the structural, electrical, and optical properties of polyconjugated systems. Nevertheless, the complex morphology of polymeric systems, which are partially crystalline and partially amorphous in nature, plays a crucial role in the physical properties. In general, the conjugation length, the strength of the interchain interaction, and the extent of disorder are some of the significant parameters that govern the physical properties of polyconjugated systems.

The behaviors of polyconjugated systems are rather different with respect to conventional polymers. In the latter (e.g., polyethylene), the number of monomer units in a chain are several thousands; they are soluble in solvents, melt processible, highly tractable, etc. Polyconjugated systems, on the other hand, have a few hundreds of monomers in a chain, and the alternating single and double bonds make the chains rather stiff with respect to nonconjugated chains. Moreover, polyconjugated systems are not that soluble and tractable, unless side groups are introduced in the main chain or dopant ions to impart solubility and processibility. The addition of side groups onto the polymer chain may induce steric hindrance that reduces the delocalization of π electrons, and hence lower the values of the maximum achievable conductivity. These aspects are reflected in the processibility and mechanical, electrical, and optical properties of polyconjugated systems. Hence, the conventional polymer processing techniques have to be modified in the case of conducting polymers.

The electrical and optical properties of polyacetylene (CH)_x, polyaniline (PANI), polypyrrole (PPy), polythiophene (PT), poly(*p*-phenylene vinylene) (PPV), poly(*p*-phenylene) (PPP), and poly(thienylene vinylene) (PTV) are some of the extensively studied conducting polymers [3, 1049].

In first-generation conducting polymers (1976–1986), the maximum possible values of electrical conductivity were limited due to the presence of structural and morphological disorder, disorder-induced localization, etc. In doped Shirakawa polyacetylene, the room-temperature conductivity was on the order of 10³ S cm⁻¹ [1, 1049]. In the best samples of doped PPy and PT, the values were below 100 S cm⁻¹. Moreover, upon lowering the temperature, the conductivity of previous-generation conducting polymers decreased rapidly and there was no finite value of conductivity at very low temperatures, as in the case of typical insulators. Similarly, in other transport property measurements, the metallic features were rather weak. This was mainly due to the presence of strong structural and morphological disorder, as a result the π electrons were not very well delocalized to facilitate intra- and interchain charge transport [1115].

In the past decade, significant improvement in reducing the structural and morphological disorder has helped to bring forth a new generation of conducting polymers. In iodine-doped Naarmann (CH)_x, conductivities on the order of 10⁴ S cm⁻¹ were observed in 1987 [1116]. Further improvement by Tsukamoto has increased the conductivity by another order of magnitude, which is comparable to those in traditional metals [173]. As the room-temperature conductivity increased, the temperature dependence of conductivity became weaker and a large finite value of conductivity was observed at very low temperatures, as expected in the case of metallic systems.

By the early 1990s, several groups have started making high-quality materials of PPV, PPy, PANI, and polyalkylthiophene (PAT) [3]. In doped oriented PPV samples, room-temperature conductivity values on the order of 10⁴ S cm⁻¹ were observed [1117]. In high-quality PF₆-doped PPy and PT samples, prepared by low-temperature electrochemical polymerization, the conductivity was nearly 500 S cm⁻¹ [1118]. In these samples, for the first time in doped conducting polymers, a positive temperature coefficient of resistivity (TCR) was observed at temperatures below 20 K, demonstrating the real metallic qualities.

Earlier, in protonic acid-doped PANI, the conductivity was only a few tens of siemens per centimeter, and upon lowering the temperature it dropped by several orders of magnitude, typical to that observed in insulating systems. With the development of counterion-induced processibility of PANI by dodecylbenzoyl sulfonic acid (DBSA) and camphor sulfonic acid (CSA) dopants, the conductivity was enhanced to nearly 500 S cm⁻¹, and its temperature dependence showed a significant metallic positive TCR in the range 150–350 K [128, 1119, 1120]. In earlier generation doped regiorandom PATs, the extent of disorder was considerably high; as a result, its conductivity was only a few tens of siemens per centimeter. With the synthesis of regioregular PATs, the conductivity was enhanced to around 10³ S cm⁻¹ [3, 387].

In general, conducting polymers can be considered as a special type of semiconducting material. The conductivity of undoped polyconjugated systems is 10⁻⁶–10⁻¹⁰ S cm⁻¹, hence, it can be considered at the semiconductor–insulator boundary. The bandgaps of known polyconjugated systems vary from 0.8 to 4 eV [3]. The bandwidths, parallel and perpendicular to the chain axis, in a typical polyconjugated system like (CH)_x are nearly 10 and

1 eV, respectively [173]. The charge-carrier density in conducting polymers can be varied by several orders of magnitude (nearly 8 orders) by doping. In fully doped systems, the carrier density could be as high as 10²²/unit volume. The carrier mobility in doped conducting polymers is much lower with respect to that in inorganic semiconductors, and this is largely due to the presence of strong disorder in polymeric systems. Nevertheless, in high-quality conducting polymer systems, the electronic properties are quite similar to those observed in disordered metals, and the transport properties are crucially dependent on the extent of disorder, interchain interactions, etc.

The doping processes in polyconjugated systems and inorganic semiconductors (e.g., silicon) are not identical [2]. In inorganic semiconductors, dopants such as phosphorus and boron are substituted for the host atomic sites, and electrons or holes are generated, depending on the valency of the dopant. In conducting polymers, the dopants are not substitutional but interstitial, and in this case the dopant ions are intercalated in between the chains. The doping mechanism is rather similar to the intercalation process in two-dimensional layered structures such as graphite. The dopant ions can either oxidize (e.g., iodine, ClO₄, PF₆, BF₄, etc.) to create a positive charge or reduce (K, Na, Rb, etc.) to create a negative charge on the chain, depending on the redox process. During the doping process, the dopants randomly diffuse in between the polymer chains, and the doped system can have a commensurate or incommensurate or disordered superlattice structure.

In conducting polymers, the doping process can generate various types of charge carriers such as polarons, bipolarons, solitons, and free carriers, and this, to a large extent, depends on the doping level, structure of polyconjugated chain, interchain interactions, disorder, etc. [1049, 1114]. In degenerate systems such as (CH)_x, solitons are formed, especially at doping levels below 6%, whereas, in nondegenerate systems such as PPy and PT, both polarons and bipolarons are formed, depending on the energetics. Charge carriers such as solitons, polarons, and bipolarons are energetically favored and stabilized by the associated lattice relaxation in one-dimensional polymer chains. However, as the interchain interactions and the carrier density increase and the extent of disorder decreases, these excitations could behave more like free carriers.

In conjugated polymers, transient charge carriers can be generated by photoexcitation [1049, 1114, 1121]. The lifetimes of photodoped carriers vary from femtoseconds to milliseconds, depending on the trapping and recombination processes, whereas in chemical doping the presence of dopant ion stabilizes the charge on the polymer chain. The maximum level of doping in conjugated polymers could be as high as 50%, which corresponds to one dopant per two monomers. The distribution of dopant ions is not uniform due to the complex morphology of the polymer matrix, which consists of both crystalline and amorphous regions. Hence, both the structural and the doping-induced disorder play major roles in the charge transport.

The metal–insulator transition in doped conducting polymers is mainly governed by the extent of disorder, interchain interaction, and doping level [2, 3]. It is well known that disorder potentials can localize the electronic states. If the random component of the disorder potential is large with respect to the bandwidth, then the localization of electronic wave functions can occur. In the presence of strong disorder, the overlap of the wave functions drops off exponentially and the system moves toward the insulating regime.

The main sources of disorder in conducting polymers are the sp³ defects in the chain, chain ends, chain entanglements, voids,

morphological and doping induced defects, etc. [3]. In conducting polymers, both fibrillar and globular morphologies have been observed. In fibrillar morphology, the chains are extended; as a result, it is possible to have delocalized states along the chain length direction. In globular morphology, the chains are coiled up, which tends to localize the electronic states and favors the formation of a granular-type material. In unoriented conducting polymer systems, the chains are randomly dispersed and the physical properties are isotropic. However, by stretch-aligning the chains and fibrills, it is possible to enhance the conductivity along the orienting axis, and anisotropy of conductivity on the order of 100 can be easily achieved. Hence, without macroscopic orientation, the macroscopic properties of conducting polymers are isotropic, even though, on a microscopic level, the electronic structure (intrachain vs interchain) is highly anisotropic. Since conducting polymers are partially crystalline and partially amorphous, the volume fraction of the crystalline regions and the size of the crystalline coherence length play dominant roles in the charge transport.

The electronic wave functions in the crystalline domains are delocalized with respect to that in the amorphous region. If the volume fraction of the crystalline regions exceeds 50% and the wave function of the delocalized states overlaps quite well, then the system sees only an averaged-over disorder potential; moreover, in this case, some metallic features can be observed [2]. On the other hand, when there are large-scale inhomogeneities, as in amorphous regions, granular systems, metallic islands, etc., then the random fluctuations in the disorder potentials are high. As a result, the intrinsic metallic features are suppressed and the system moves toward the insulating regime. In general, the disorder-induced localization plays a dominant role in the metal-insulator (M-I) transition and in the transport properties of conducting polymers.

3.1. Metallic State

The metallic state in doped conducting polymers is inferred from the following: large, finite direct-current (dc) conductivity as $T \rightarrow 0$, temperature-independent Pauli spin susceptibility down to 10 K, linear temperature dependence of the thermopower down to 10 K, linear term in the specific heat at low temperatures, free-carrier absorption, and large metallic reflectance in the infrared, etc. [2, 3]. This evidence shows the presence of a continuous density of states with a well-defined Fermi energy. In some conducting polymers, the typical metallic positive temperature coefficient of resistivity (TCR) was observed from 300 to 150 K, and in some others it was only below 20 K. However, Park et al. [1122] reported a metallic positive TCR in doped $(\text{CH})_x$ from 300 to 1.5 K, which is quite exceptional. Although the typical negative TCR in high-quality conducting polymers is indicative of nonmetallic behavior, its temperature dependence was rather weak so that the logarithmic derivative of conductivity ($W = d \ln \sigma / d \ln T$) has a positive temperature coefficient. This implies a finite value of conductivity and a finite density of states at the Fermi level at very low temperatures, as expected in the case of disordered metallic systems. All this evidence shows that, in spite of the disordered quasi-one-dimensional nature of polymer chains, it is possible to have a metallic state in these systems. In the metallic state, the average size of the delocalized states is considerably larger than that of the structural coherence length; hence, the carrier transport is not hindered very much by the presence of disorder potentials in the amorphous region.

In the strict one-dimensional limit, all wave functions are localized in the presence of any infinitesimal disorder [2]. However, the interchain hopping integral (interchain interaction) suppresses this extreme tendency toward localization in a one-dimensional chain [1123]. For some particular value of disorder potential, the strength of the interchain coupling that is required to suppress the localization depends on the coherence length along the quasi-one-dimensional chains. A charge carrier must be able to hop to an adjacent chain prior to the resonant backscattering, which inevitably leads to localization in one dimension. Thus, although conducting polymers are intrinsically quasi-one-dimensional electronic systems, the interchain coupling can be sufficiently large to enable the formation of three-dimensional metals.

The extent of disorder leads to a qualitatively different charge-transport mechanism in weak and strong disorder limits. In the Anderson model of localization for three-dimensional systems, in which the random fluctuations of the disorder potentials are within the bandwidth of the system, a mobility edge separates the delocalized and localized states in the density-of-states diagram [1124–1126]. In this model, if the Fermi energy lies within the delocalized (localized) states, then the system behaves like a metal (insulator). As the randomness of the disorder potentials increases, the system becomes more like a granular metal. The critical parameter in the M-I transition is the averaged-over value of the correlation/localization length (L_c). If L_c is greater than the averaged-over structural coherence length (which characterizes the size of the crystalline regions), then the disorder can be considered as within the weak limit, which means that the system sees only an average of the random fluctuations of the disorder potentials. Conversely, if L_c is less than the structural coherence length, then the extent of disorder is in the strong limits. The values of L_c and structural coherence length can be determined by transport property measurements and X-ray diffraction, respectively [3].

3.1.1. Conductivity

The electrical conductivity is mainly determined by the carrier density (n), relaxation time (τ), and effective mass (m) of the carrier (electrical conductivity, $\sigma = ne^2\tau/m$). According to the Ioffe-Regel criterion, the interatomic distance is considered as the lower limit to the mean free path (λ) in a metallic system. Hence, for a metallic system, $k_F\lambda > 1$, where $k_F\lambda = [h(3\pi^2)^{2/3}]/(e^2\rho n^{1/3})$, k_F is the Fermi wave vector, and ρ is the electrical resistivity [1125, 1126]. In highly doped conducting polymers, $n \approx 10^{21}$ per unit volume, m is nearly the electron mass, λ is a few tens of angstroms, and $k_F\lambda \approx 1-10$ at room temperature. The mean free path is limited by both the interchain transport and the extent of disorder present in the system. The details about metallic conducting polymers are shown in Table VI [1127].

Pietronero [1128] suggested that in a one-dimensional chain the only possible source of scattering for charge carriers is from $+k_F$ to $-k_F$, involving the high-energy $2k_F$ phonons. Moreover, due to phonon freezing effects, even possible at room temperature, the first-order scattering should induce a strong enhancement in conductivity in one-dimensional chains. The conductivity in the chain direction in a one-dimensional chain is given by

$$\sigma_{\parallel} = (ne^2a/\pi\hbar)v_F\tau = (ne^2a^2/\pi\hbar)/(\lambda/a) \quad (3.1)$$

where a is the carbon-carbon distance, $v_F = (2t_0a/\hbar)$ is the Fermi velocity, t_0 (2–3 eV) is the π -electron hopping matrix element, and τ is the backscattering lifetime. In the limit of elastic scattering for

Table VI. Details of Various Doped Conducting Polymers in the Metallic State

Polymer	Abbreviation	Orientability	Crystallinity ^a	Conductivity ^b
Polyacetylene	(CH) _x	High	80%	10 ⁴ –10 ⁵
Poly(<i>p</i> -phenylene vinylene)	PPV	High	80%	10 ⁴
Polyaniline	PANI	Low	50%	400
Polypyrrole	PPy	Low	40%	300
Poly(3,4-ethylene-dioxythiophene)	PEDOT	Low	40%	300
Poly(3-methylthiophene)	PMT	Low	40%	400

Source: Reproduced and adapted by permission of IOP Publishing from M. Ahlskog and R. Menon, *J. Phys.: Condens. Matter*, 10, 7171 (1998). Copyright © 1998, IOP Publishing.

^a Approximate values for high-quality samples.

^b In S cm⁻¹. The values give approximately the highest observed values. In the cases of (CH)_x and PPV, the conductivity in the highly oriented state along the direction of the chain alignment is given.

a half-filled band system, σ_{\parallel} (300 K) $\approx 10^5$ S cm⁻¹. However, since the main scattering involved in a conducting polymer chain is only the $2k_F$ phonons, and by including the inelastic scattering process below the characteristic temperature ($k_B T \sim \hbar\omega_0/4$ and $T \sim 600$ K), another two orders of magnitude of enhancement in conductivity should be possible, i.e., $\approx 10^7$ S cm⁻¹. Similar estimates of conductivity have been obtained by the Kivelson–Heeger model, too [1129]. In this model, the conductivity is expected to increase exponentially at low temperatures. Hence, the theoretical studies suggest that the intrinsic conductivity in one-dimensional models of conjugated polymers is expected to be even larger than that of conventional metals at room temperature.

In general, the conductivity in disordered systems is determined by the extended and localized states [1125, 1126]. The extent of disorder determines the roles played by localization and electron–electron (e–e) interactions; it also determines the screening length and scattering processes involved in the charge transport. The microscopic length scales involved in the conductivity in disordered systems are the correlation length on the metallic side, localization length on the insulating side, e–e interaction length, thermal diffusion length, and inelastic scattering length, and these length scales determine the scattering and relaxation mechanisms in the charge transport.

The low-temperature conductivity measurement is a simple and sensitive method to get a qualitative level of understanding about the extent of disorder present in the system. Since conductivity is directly related to the mean free path, which is rather sensitive to the presence of any disorder, the variation in low-temperature conductivity is quite dramatic as disorder varies. However, the temperature dependence of conductivity data by itself is not enough to determine whether the system is metallic or insulating.

The characteristic behavior of the temperature dependence of conductivity can be understood in detail by defining the reduced activation energy (W) as the logarithmic derivative of the temperature dependence of conductivity, i.e., $W = d(\ln \sigma)/d(\ln T)$ [3,

1130]. If the system is on the metallic regime with a weak negative TCR, then W shows a positive temperature coefficient at low temperatures. Moreover, this ensures that there is a finite conductivity as $T \rightarrow 0$. The temperature dependence of W is consistent with the resistivity ratio [$\rho_r = \rho(1.4 \text{ K})/\rho(300 \text{ K})$], which is a useful empirical parameter for quantifying the extent of disorder and for classifying the metallic and insulating regimes. In general, as ρ_r increases, the temperature dependence of W gradually moves from a positive (metallic) to a negative (insulating) temperature coefficient at low temperatures. The approximate values of ρ_r for various conducting polymers in the metallic (M), critical (C), and insulating (I) regimes are shown in Table VII [1131].

The conductivity in the disordered metallic regime is expressed by [1126, 1132]

$$\sigma(T) = \sigma(0) + mT^{1/2} + BT^{p/2} \quad (3.2)$$

where $m = \alpha[4/3 - \gamma(F_{\sigma}/2)]$, α is a parameter depending on the diffusion coefficient, γF_{σ} is the interaction parameter, and p is determined by the scattering rate of the dominant dephasing mechanism (for electron–phonon scattering, $p = 3$; for inelastic e–e scattering, $p = 2$ in the clean limit or $3/2$ in the dirty limit). The second term in Eq. (3.2) results from the e–e interactions, and the third term is the correction to $\sigma(0)$ due to localization effects. In disordered metals, e–e interactions play an important role in low-temperature transport. The correction term due to e–e interactions consists of exchange and Hartree contributions, and its sign depends on the screening length, etc. Usually, the sign of m is negative when $\gamma F_{\sigma} > 8/9$, resulting in a change of sign (from negative to positive) in the TCR at low temperatures.

Iodine-doped (CH)_x [I-(CH)_x] is one of the most extensively studied systems among doped conducting polymers [173, 1133]. The maximum room-temperature conductivity parallel to the chain axis in highly oriented I-(CH)_x is nearly 10^5 S cm⁻¹, and the anisotropy of conductivity is 100–200. The stretchability and the maximum obtainable conductivity in I-(CH)_x is very much dependent on the film thickness. The conductivity is higher in thinner films (below 10 μm) in both stretched and unstretched films. The structural and physical properties of I-(CH)_x have been reviewed by Tsukamoto [173]. The average crystalline coherence lengths, parallel and perpendicular to the chain axis, are 150 and 50 \AA , respectively. In highly conducting samples, the carrier density is nearly $10^{22}/\text{cm}^3$ and the mean free path is around 500 \AA . The density of states at the Fermi level is approximately 0.3 state (eV C)⁻¹, which corresponds to 10 emu (mol C)⁻¹.

Park et al. [1122] have observed, for the first time in conducting polymers, a metallic positive TCR, from 300 to 1.5 K, in ClO₄-doped (CH)_x; although in earlier work the positive TCR was observed in FeCl₃-(CH)_x and PANI-CSA down to 180 K. The conductivity of the ClO₄-(CH)_x sample at 300 K is nearly 40,000 S cm⁻¹. Its conductivity increases by a factor of 2 at 1.5 K, as shown in Figure 127. For samples with conductivities in the range 2000–20,000 S cm⁻¹, the positive TCR was observed at temperatures above 150 K. The details about conductivity, ρ_r , etc. for ClO₄-(CH)_x samples are shown in Table VIII [1122]. This indicates that the positive TCR in conducting polymers is quite sensitive to subtle variations in the extent of disorder present in the system.

The room-temperature conductivity of highly oriented I-(CH)_x is nearly a factor of 2 larger than that of ClO₄-(CH)_x and FeCl₃-(CH)_x; yet, it does not show any metallic positive TCR [1122].

Table VII. $\sigma(300\text{ K})$ and $\rho_r \approx [\rho(1.3\text{ K})/\rho(300\text{ K})]$ of Various Conducting Polymers in the Metallic (M), Critical (C), and Insulating (I) Regimes

Polymer	M		C		I	
	ρ_r	$\sigma(300\text{ K})^a$	ρ_r	$\sigma(300\text{ K})$	ρ_r	$\sigma(300\text{ K})$
$(\text{CH})_x\text{-I}_2$	< 10	> 5000	10–20	$3\text{--}5 \times 10^4$	> 20	< 3000
$(\text{CH})_x\text{-I}_2$	< 5	$> 5 \times 10^4$	9.8–165	$2\text{--}5 \times 10^4$	> 400	$< 2 \times 10^4$
$(\text{CH})_x\text{-FeCl}_3$	< 2	$> 2 \times 10^4$	2.6–11.4	$1\text{--}2 \times 10^4$	> 27	$< 10^4$
PPV-AsF ₅ ^b	< 5	300–2400	9.7–34	100–300	> 50	< 100
PPV-H ₂ SO ₄	< 2	$4 \times 10^3\text{--}10^4$	4.7–27	1000–4000	> 60	< 1000
PPy	< 2	300–400	2–10	200–300	> 10	< 200
PANI	< 2	250–350	2–5	200–250	> 10	< 200

Source: Reproduced and adapted by permission of IOP Publishing from M. Ahlskog, M. Reghu, and A. J. Heeger, *J. Phys.: Condens. Matter*, 9, 4145 (1997). Copyright © 1997, IOP Publishing.

^a Conductivity is given in S cm^{-1} .

^b The data come from samples with different degrees of orientation and therefore do not give an entirely consistent picture of the M–I transition in this system.

Table VIII. $\sigma(300\text{ K})$ and $\rho(1.5\text{ K})/\rho(300\text{ K})$ of Various ClO₄-Doped Polyacetylenes

Dopant	$\rho(300\text{ K})$ ($\Omega\text{ cm}$)	$\rho(300\text{ K})$ S cm^{-1}	$\rho(1.5\text{ K})/\sigma(300\text{ K})$	T^* (K)	$\rho(T^*)/\rho(300\text{ K})$
ClO ₄ [−] (Fe)	7.41×10^{-4}	1,350	1.46	227	0.970
	1.30×10^{-4}	7,670	1.07	194	0.894
	1.06×10^{-4}	9,390	1.17	240	0.897
	9.33×10^{-5}	10,720	1.22	220	0.939
	8.84×10^{-5}	11,300	1.07	194	0.894
	8.31×10^{-5}	12,000	1.11	196	0.930
	5.80×10^{-5}	17,200	1.15	195	0.900
	5.01×10^{-5}	19,960	0.98	159	0.916
	4.79×10^{-5}	20,900	0.66		
ClO ₄ [−] (Cu)	2.41×10^{-5}	41,000	0.57		
	1.68×10^{-4}	5,950	1.55	254	0.977
FeCl ₄ [−]	1.11×10^{-4}	8,990	1.38	200	0.905

Source: Reproduced by permission of Elsevier Science from Y. W. Park, E. S. Choi, and D. S. Suh, *Synth. Met.* 96, 81 (1998). Copyright © 1998, Elsevier Science.

The temperature dependence of resistivity of I-(CH)_x samples is shown in Figure 128a [15, 1131]. The metallic samples have a rather weak negative TCR and show a large finite conductivity at $T < 1\text{ K}$. The absence of positive TCR in the case of I-(CH)_x suggests that the doping-induced disorder is higher with respect to that in ClO₄-(CH)_x and FeCl₃-(CH)_x systems. Sample B2 is systematically aged up to B6, so that it continuously moves from the metallic to the insulating regime. The localization of carriers during the aging process not only decreases the room-temperature conductivity but also enhances the negative TCR as the system moves to the insulating side. The W versus T plot of the $\rho(T)$ is shown in Figure 128b. The metallic sample (B2) shows the expected positive temperature coefficient of $W(T)$, and, upon aging, it tends toward the negative temperature coefficient, as expected for insulating systems. Similar variations in the temperature coefficient of $W(T)$ have been observed as the resistivity ratio (ρ_r) increases by lowering the doping levels. For example, in the case of

highly doped samples having $\rho_r < 3$, W shows a positive temperature coefficient; in the case of less doped samples having $\rho_r > 10$, the temperature coefficient of $W(T)$ becomes negative at low temperatures. Similar results have been observed in the case of FeCl₃-(CH)_x.

The $\sigma(T)$'s of I-(CH)_x samples at various stretching ratios are shown in Figure 129 [1131]. The unstretched sample has $\sigma(300\text{ K}) \sim 800\text{ S cm}^{-1}$ and shows a strong negative TCR [2]. Obviously, in stretched samples the conductivity along the stretching direction increases, and in the transverse direction it decreases with respect to that in the unstretched samples. The anisotropy of conductivity increases upon increasing the stretching ratio; however, the $\sigma(T)$ is nearly the same in both the parallel and the perpendicular directions to the chain axis. This indicates that the transport mechanism is nearly identical in both the parallel and the perpendicular directions to the chain axis, and the interchain transport plays an important role in both cases. Moreover, even the maxi-

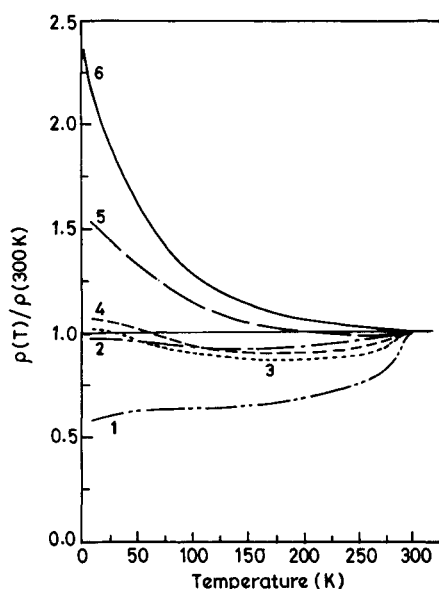


Fig. 127. Normalized resistivity vs temperature for ClO_4 -doped polyacetylene: (1) ClO_4 (Fe) 4-probe, $2.4 \times 10^{-5} \Omega\text{cm}$; (2) ClO_4 (Fe) 4-probe, $5 \times 10^{-5} \Omega\text{cm}$; (3) ClO_4 (Fe) Montgo, $6.58 \times 10^{-5} \Omega\text{cm}$; (4) ClO_4 (Fe) 4-probe, $8.8 \times 10^{-5} \Omega\text{cm}$; (5) FeCl_4 (7.5%) 4-probe, $1.1 \times 10^{-4} \Omega\text{cm}$; and (6) ClO_4 (2.2%) 4-probe, $1.67 \times 10^{-4} \Omega\text{cm}$. Reproduced by permission of Elsevier Science from Y. W. Park, E. S. Choi, and D. S. Suh, *Synth. Met.* 96, 81 (1998). Copyright © 1988, Elsevier Science.

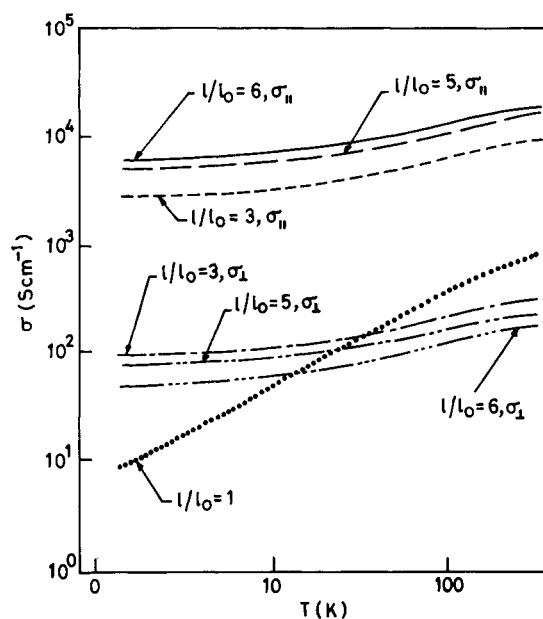


Fig. 129. Conductivity (both parallel and perpendicular) vs temperature for iodine-doped polyacetylene samples at various stretching ratios. Reproduced by permission of John Wiley & Sons Limited from H. S. Nalwa, Ed., "Handbook of Organic Conductive Molecules and Polymers," Vols. 1–4. Wiley, New York (1997). Copyright © 1997, John Wiley & Sons Limited.

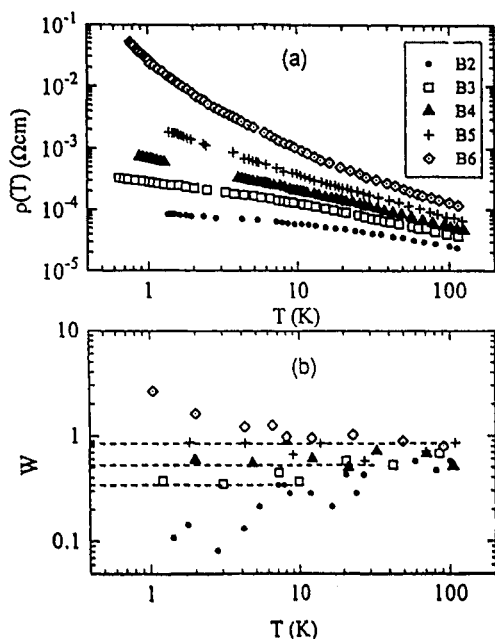


Fig. 128. (a) Resistivity vs temperature for an iodine-doped polyacetylene sample aged from B2 to B6. (b) W vs T for the same data. The dotted lines indicate the power law regime. Reproduced by permission of IOP Publishing from M. Ahlskog, M. Reghu, and A. J. Heeger, *J. Phys.: Condens. Matter.* 9, 4145 (1997). Copyright © 1997, IOP Publishing.

imum stretching ratio of 15:1 is really not enough to achieve significant orientation of all the chains, and the number of misaligned and crisscrossed chains is rather high so that the $\sigma(T)$ is nearly identical in both the parallel and the perpendicular directions to

the chain axis. Hence, further enhancement in the chain orientation ($\sigma_{||}/\sigma_{\perp} > 10^3$) is of considerable importance in order to observe the intrinsic anisotropic features in the charge-transport properties in conducting polymers.

As described in previous works [2, 3], the $\sigma(T)$ below 4.2 K follows a $T^{1/2}$ dependence (see Eq. (3.2)) in both the parallel and the perpendicular directions to the chain axis in oriented $\text{I}-(\text{CH})_x$ samples. The $T^{1/2}$ dependence indicates that the contribution from e-e interactions plays a dominant role at very low temperatures. This is also consistent with the enhanced negative contribution to magnetoconductance (MC), as explained in detail in the next section. For the intermediate temperature range (4–40 K), where $\sigma \propto T^{3/4}$, the inelastic electron-phonon scattering ($p = 3/2$) is the dominant scattering mechanism, for the parallel and the perpendicular directions to the chain axis [1131, 1133]. This is also consistent with the enhanced positive contribution to MC at temperatures above 4 K. This suggests that both interaction and localization play dominant roles in $\sigma(T)$ at low temperatures in metallic $(\text{CH})_x$ samples.

The temperature dependence of the resistivity of a sulfuric acid-doped PPV ($\text{PPV}-\text{H}_2\text{SO}_4$) sample is shown in Figure 130a [1134, 1135]. Freestanding films of PPV (thickness 4–8 μs) were stretch-aligned to a ratio of 10:1 ratio [1117]. The optical anisotropy is nearly 50, as obtained from the dichroic ratio measurement at 1520 cm^{-1} . This indicates that the PPV chains are quite well oriented after tensile drawing. The values of conductivity, ρ_r , etc. of a $\text{PPV}-\text{H}_2\text{SO}_4$ sample (A) as it gradually aged to sample L are shown in Table IX [1134, 1135]. The W versus T plot of the same data is shown in Figure 130b. The metallic samples follow a positive temperature coefficient of W at low temperatures; as ρ_r increases, W gradually moves toward the critical and insulating regimes, similar to that observed in the case of $\text{I}-(\text{CH})_x$.

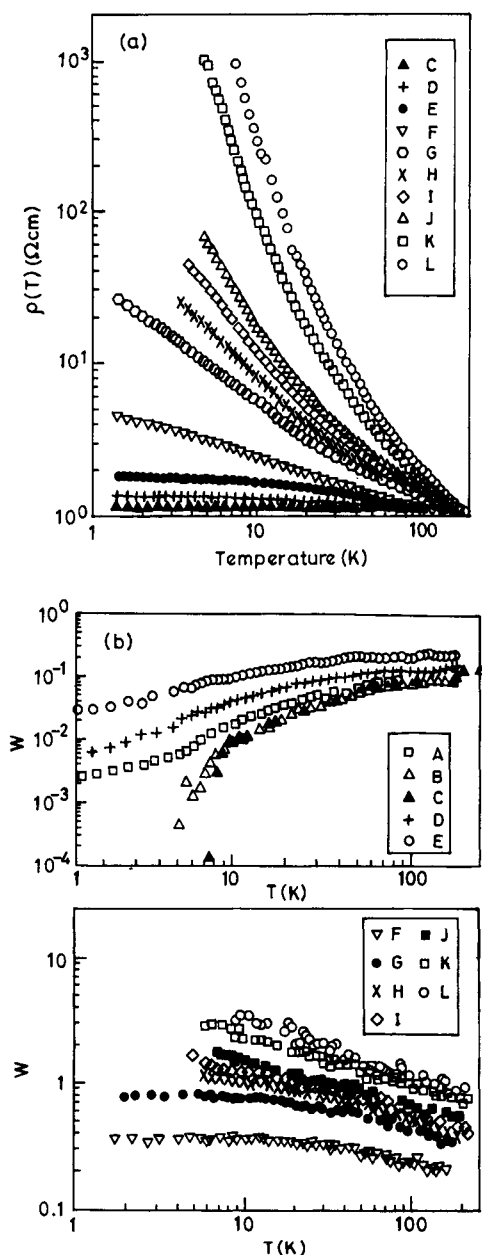


Fig. 130. (a) Resistivity vs temperature for a PPV-H₂SO₄ sample aged from C to L. (b) W vs T for the same data (A-E, on the metallic side; G-L, on the insulating side). Reproduced by permission of the American Physical Society from M. Ahlskog, M. Reghu, A. J. Heeger, T. Noguchi, and T. Ohnishi, *Phys. Rev. B* 55, 6777 (1997). Copyright © 1997, American Physical Society.

In PPV-H₂SO₄ samples, too, the low-temperature conductivity of metallic samples, in both the parallel and the perpendicular directions to the chain axis, can be fitted to Eq. (3.2) [1134, 1135]. At temperatures below 4 K, however, the $T^{1/2}$ fit is rather good, even in the presence of a magnetic field, as shown in earlier works. Hence, in metallic PPV samples, the localization-interaction model is valid at low temperatures, as observed in the case of metallic (CH)_x samples. Moreover, the MC data in both systems are consistent with the localization-interaction model, as explained later. Although the anisotropy of conductivity in metallic/oriented (CH)_x and PPV samples is nearly 100, the $\sigma(T)$ is

Table IX. σ_0 , $\sigma(200\text{ K})$, and $\rho_r \approx [\rho(1.3\text{ K})/\rho(200\text{ K})]$ of a PPV-H₂SO₄ Sample Aged from A to L

Sample	σ_0 S cm ⁻¹	$\sigma(200\text{ K})$ S cm ⁻¹	ρ_r	m^*
A	7330	8670	1.18	29
B	7170	8490	1.19	-20
C	6720	7650	1.16	-120
D	4510	6340	1.39	45
E	2020	3980	1.87	96
				β
F	0	2440	4.7	0.34
G	0	930	27	0.78
				x
H	0	510	100	0.20
I	0	280	390	0.28
J	0	82	750	0.35
K	0	12	3×10^5	0.41
L	0	1.5	4×10^7	0.49

Source: Adapted by permission of the American Physical Society from M. Ahlskog, M. Reghu, A. J. Heeger, T. Noguchi, and T. Ohnishi, *Phys. Rev. B* 55, 6777 (1997). Copyright © 1997, American Physical Society.

rather similar in both the parallel and the perpendicular directions to the chain axis, indicating that an anisotropic three-dimensional model is appropriate in these systems.

The temperature dependence of the conductivity of PPy doped with PF₆ (PPy-PF₆) is shown in Figure 131a [1136]. The details of room-temperature conductivity, etc. are shown in Table X. The W versus T plot of the same data is shown in Figure 131b. Sample M1 shows a positive TCR below 12 K, and the sign of m (in Eq. (3.2)) is negative. The behavior of $W(T)$ is consistent with that observed in metallic (CH)_x and PPV samples. The temperature and field dependence of the resistivity of metallic PPy-PF₆ samples at $T < 1\text{ K}$ show the presence of a large finite conductivity ($\sim 150\text{ S cm}^{-1}$) at 75 mK and 8 T [1137]. This suggests that the three-dimensional transport is quite robust and the intrinsic one-dimensional nature of disordered polymer chains is not causing any severe localization, although the conductivity at temperatures in the millikelvin range is nearly around the Mott minimum metallic conductivity in these systems. This result is quite contrary to the expected localization of all of the electronic states due to the presence of any infinitesimal disorder in one-dimensional polymer chains. Hence, in spite of the disorder, the interchain interactions are sufficiently large enough to prevent any severe localization in the polymer chains and also to make it more like anisotropic three-dimensional systems. Furthermore, PPy-PF₆ samples can be stretched by a factor of 2, and their conductivity increased up to 3000 S cm^{-1} [1118]. This is one of the best values of conductivity in a doped conjugated polymer that has a long-term stability at ambient conditions.

The $\sigma(T)$'s of PANI-CSA and PANI-AMPSA (2-acrylamido-2-methyl-1-propanesulfonic acid) samples are shown in Figure 132a and b, respectively [1138]. The details of the conductivity, resistivity ratio, etc. of the samples are shown in Table XI. Both systems show a positive TCR at temperatures above 80 K. Although the $\sigma(300\text{ K})$ of PANI-AMPSA samples is slightly lower with respect to PANI-CSA, its positive TCR is observed down to much

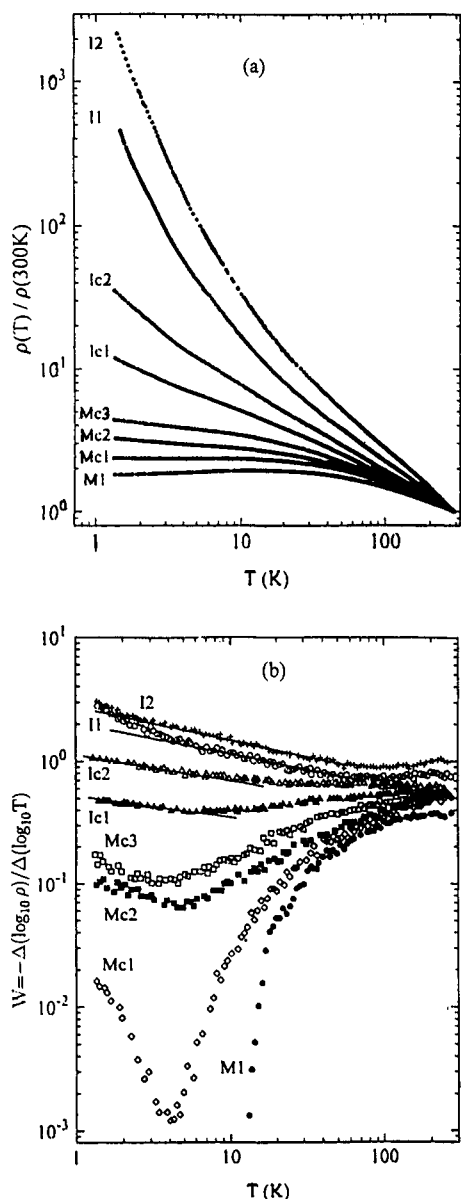


Fig. 131. (a) Normalized resistivity vs temperature for various PPy-PF₆ samples. (M→ for metallic, I→ for insulating, and c for critical). (b) W vs T for the same data. Reproduced by permission of the American Physical Society from C. O. Yoon, M. Reghu, D. Moses, and A. J. Heeger, *Phys. Rev. B* 49, 10851 (1994). Copyright © 1994, American Physical Society.

lower temperatures, as shown in Table XI. The wet-spun PANI-AMPSA fibers have shown an impressive room-temperature conductivity of nearly 2000 S cm⁻¹ [1139]. The difference between CSA- and AMPSA-doped PANI samples in $\sigma(300\text{ K})$ and $\sigma(T)$ is possibly due to the variations in microstructure and its contribution to disorder-induced localization. This shows that the charge transport in doped conducting polymers is rather sensitive to slight variations in the morphological features. Metallic PANI-CSA samples have a finite conductivity at very low temperatures (nearly 50 S cm⁻¹ at 75 mK) [1137], suggesting that PANI-CSA is just on the metallic side of the metal-insulator boundary.

The $\sigma(T)$'s of doped poly(3,4-ethylenedioxythiophene) (PEDOT) samples are shown in Figure 133 [1109, 1140]. The de-

Table X. $\sigma(300\text{ K})$, $\rho_r \approx [\rho(1.4\text{ K})/\rho(300\text{ K})]$, Magnetoresistance ($\Delta\rho/\rho$), and T_m , the Transition Temperature (from Negative to Positive TCR), of Various PPy-PF₆ Samples (M→ for Metallic, I→ for Insulating, and c for Critical)

Sample	Pressure	$\sigma(300\text{ K})$ S cm ⁻¹	ρ_r^a	$\Delta\rho/\rho^b$	T_m (K)
M1	Ambient	338	1.75	0.12	12
M2	Ambient	298	1.97	0.13	7.5
M2	9 kbar	330	1.33	0.05	24
Mc1	Ambient	271	2.40	0.16	
Mc2	Ambient	313	3.22	0.21	
Mc2	4 kbar	358	1.81	0.12	12
Mc2	10 kbar	377	1.54	0.10	19
Mc3	Ambient	192	4.45	0.23	
Ic1	4 kbar	133	2.64	0.18	
Ic1	10 kbar	137	2.08	0.15	

Source: Reproduced and adapted by permission of the American Physical Society from C. O. Yoon, M. Reghu, D. Moses, and A. J. Heeger, *Phys. Rev. B* 49, 10851 (1994). Copyright © 1994, American Physical Society.

^a $\rho_r = \rho(1.4\text{ K})/\rho(300\text{ K})$.

^b Data at $H = 8\text{ T}$ and at $T = 1.4\text{ K}$.

tails of room-temperature conductivity, ρ_r , etc. are shown in Table XII. The room-temperature conductivity of PF₆-doped samples is rather high with respect to other dopants, and the $\sigma(300\text{ K})$ and $\sigma(T)$ can be varied by tuning the extent of disorder present in the sample. In doped PEDOT samples, a positive TCR has been observed at $T < 10\text{ K}$. Similar positive TCR and weak $\sigma(T)$ have been observed in PMeT-PF₆ samples having $\sigma(300\text{ K}) \approx 200\text{ S cm}^{-1}$. In these systems, Fukuhara et al. [1141] have observed a pressure tuning of the M-I transition. However, doped PEDOT samples are somewhat different with respect to other conducting polymers, in the sense that for samples having a rather low room-temperature conductivity (see Table XII) the $\sigma(T)$ can be exceptionally low. For example, even for samples with $\sigma(300\text{ K}) \approx 10\text{ S cm}^{-1}$, which is well below the Mott minimum value, the conductivity at 1 K can be around 4 S cm⁻¹. Probably, the structural disorder in PEDOT samples is considerably less than that in other systems. Since the β -positions in the thiophene rings are blocked by the ethylenedioxy group, the chain extension is possible only through the α -positions. A large finite conductivity ($\sim 150\text{ S cm}^{-1}$) has been observed in metallic PEDOT and PMeT systems; yet, these systems are just on the metallic side of the M-I transition.

In summary, the conductivity and its temperature dependence in doped (CH)_x, PPV, PPy, PANI, and PEDOT samples suggest that, by reducing the role of disorder-induced localization in charge transport, it is possible to observe the intrinsic metallic positive TCR in doped conducting polymers.

3.1.2. Magnetoconductance

It is well known that magnetoconductance (MC) is a sensitive local probe for investigating the microscopic transport parameters (e.g., scattering process, relaxation mechanism, etc.) in metallic and semiconducting systems [2]. The quantitative level of understanding of MC for disordered systems by using the localization-interaction model is rather useful for checking the appropriateness

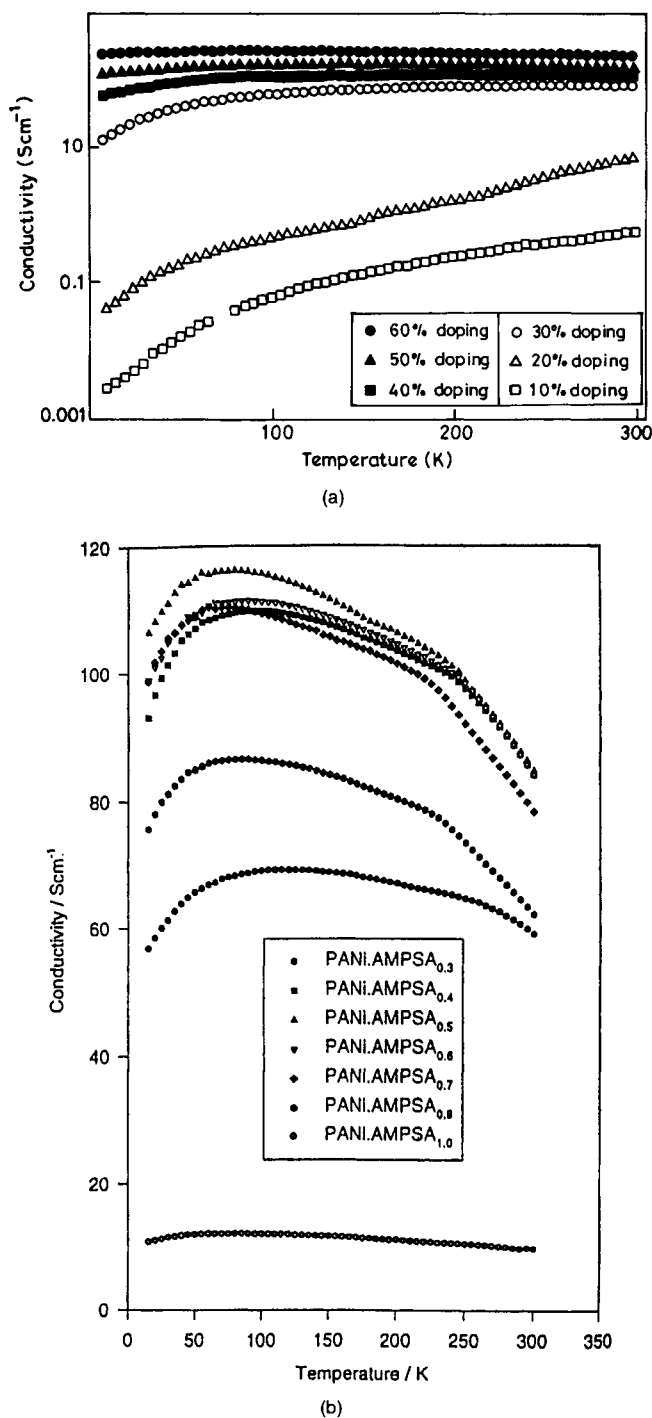


Fig. 132. (a) Conductivity vs temperature for PANI-CSA samples at various doping levels. (b) Conductivity vs temperature for PANI-AMPSA samples at various doping levels. Reproduced by permission from IOP publishing from (a) P. N. Adams, P. Devasagayam, S. J. Pomfret, L. Abell, and A. P. Monkman, *J. Phys.: Condens. Matter.* 10, 8293 (1998). (b) E. R. Holland, S. J. Pomfret, P. N. Adams, and A. P. Monkman, *J. Phys.: Condens. Matter.* 8, 2991 (1996). Copyright © 1996, IOP Publishing.

of this model for metallic conducting polymers. Moreover, the internal consistency of using this model can be verified by comparing the results from the temperature dependence of conductivity and MC measurements.

It is well known that in an ideal one-dimensional conductor the transverse orbital motion is restricted; thus, the carriers cannot make circular motions in the presence of a magnetic field. Hence, one could hardly expect any MC in an ideal one-dimensional conductor. However, in the presence of any finite interchain transfer integral, as in several quasi-one-dimensional conductors, the MC can be used as a powerful tool to investigate the intra-versus interchain transport. Nevertheless, the fine features in anisotropic MC can be easily smeared in the presence of disorder.

In disordered metallic systems, it is well known that the quantum corrections due to weak localization (WL) and e-e interactions contribute to the MC at low temperatures [2, 1133]. Usually, the WL contribution (positive MC) dominates at $T > 4$ K and low fields (below 3 T) and the contribution from e-e interactions (negative MC) dominates at $T < 4$ K and higher fields (above 3 T). As the extent of disorder increases, however, both WL and e-e interaction contributions decrease, and the hopping contribution to MC (large negative MC) increases. Although the theoretical estimate for the upper limit to the quantum corrections to MC in conventional disordered systems is below 3% (i.e., $\Delta\sigma/\sigma < \pm 3\%$), the observed MC in oriented metallic conducting polymers is slightly higher, which is probably associated with the anisotropic diffusion coefficient, anisotropic effective mass, etc.

There are several detailed studies of MC in conducting polymers [2, 15, 1142]. The behavior of MC in oriented and unoriented conducting polymers shows a clear difference. Highly conducting oriented samples (e.g., $(\text{CH})_x$ and PPV) exhibit a positive MC due to the WL contribution (especially when the field is perpendicular to the chain axis) at $T > 2$ K; in unoriented samples (e.g., PPy, PANI, PEDOT, etc.), MC is observed to be negative at all temperatures and fields [1133]. In oriented samples, MC represents an interplay between WL (positive MC at low fields and $T > 2$ K) and e-e interaction (negative MC at high fields and $T < 2$ K) contributions, the sign of MC depending on the angle between the magnetic field and the chain axis. This anisotropic MC in oriented samples is due to the anisotropy in the WL contribution, since the positive MC due to WL is maximized when the field is perpendicular to the chain axis and it is minimized when the field is parallel to the chain axis [1133, 1143, 1144].

The MC's for oriented metallic $\text{I}-(\text{CH})_x$ and $\text{PPV-H}_2\text{SO}_4$ samples are shown in Figure 134a [1133] and b [1134, 1135]. In both systems, the anisotropy of conductivity is nearly 100. As shown in Figure 134, when the field is perpendicular to the chain axis, the sign of MC is positive; whereas, when the field is parallel to the chain axis, the sign of MC is negative. The experimental results in both systems show that the WL contribution is negligible when the field is parallel to the chain axis. However, the positive MC due to the WL contribution vanishes with a slight increase in the extent of disorder by aging a freshly doped $(\text{CH})_x$ or $\text{PPV-H}_2\text{SO}_4$ sample, although the aged sample remains metallic down to 1.4 K. This indicates that even a marginal increase in the extent of disorder in metallic conducting polymers can suppress the quantum transport involved in the WL contribution to positive MC. Hence, the coherent interchain transport in intrinsically quasi-one-dimensional polymer chains can be easily affected by minute variations in the interchain alignments, disorder, etc.

The universal scaling of MC due to the e-e interaction can be used to distinguish the WL and e-e interaction contributions [1133, 1145]. The scaling plot for a metallic/oriented $\text{PPV-H}_2\text{SO}_4$ sample is shown in Figure 135. The expected universal scaling

Table XI. Values of the Conductivity Maxima, Corresponding Temperatures, and $\sigma(10, 15 \text{ K})/\sigma(300 \text{ K})$ for Various PANI-CSA and PANI-AMPSA Samples at Different Doping Levels

Doping level (%)	Peak conductivity, σ (S cm^{-1})		Temperature of peak σ (K)		$\frac{\sigma_{10 \text{ K}}}{\sigma_{300 \text{ K}}}$	$\frac{\sigma_{15 \text{ K}}}{\sigma_{300 \text{ K}}}$
	CSA	AMPSA	CSA	AMPSA		
30	90	69	270	115	0.13	0.96
40	160	110	225	95	0.44	1.10
50	178	116	190	75	0.67	1.26
60	268	111	135	85	0.94	1.18
70	184	110	184	80	0.75	1.26
80	—	87	—	85	—	1.22
90	121	—	185	—	0.71	—
100	—	12	—	85	—	1.11

Source: Reproduced and adapted by permission of IOP Publishing from P. N. Adams, P. Devasagayam, S. J. Pomfret, L. Abell, and A. P. Monkman, *J. Phys.: Condens. Matter* 10, 8293 (1998). Copyright © 1998, IOP Publishing.

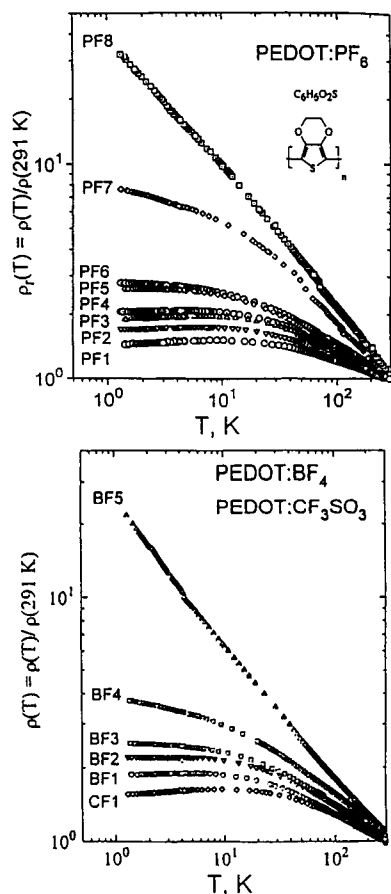


Fig. 133. Normalized resistivity vs temperature for various doped PEDOT samples. Reproduced by permission of Elsevier Science from A. Aleshin, R. Kiebooms, R. Menon, and A. J. Heeger, *Synth. Met.* 90, 61 (1997). Copyright © 1997, Elsevier Science.

behavior in the longitudinal MC, due to the dominant contribution from the e-e interaction, is clearly shown in Figure 135b. However, in the case of transverse MC, the scaling behavior de-

Table XII. Values of σ_0 , $\sigma(291 \text{ K})$, $\rho_r \approx [\rho(1.4 \text{ K})/\rho(300 \text{ K})]$, Magnetoresistance ($\Delta\rho/\rho$), and T_m , the Transition Temperature (from Negative to Positive TCR), for Various PEDOT Samples

Sample	Dopant	$\sigma_{291 \text{ K}}$	ρ_r	σ_0	MR (%) at 8 T	T_m (K)
PF1	PF ₆	131	1.45	93.67	7.65	7.8
PF2		230	1.67	141.53	9.60	5.85
PF3		2.05	1.92	110.24	13.25	7.23
PF4		300	2.06	123.30	8.31	5.4
PF5		100	2.64	29.40	17.73	
PF6		11	2.78	3.76	18.38	
PF7		7	7.53		26.4	
PF8		1.5	20		51	
CF1	CF ₃ SO ₄	48	1.56	29.75	7.62	8.1
BF1	BF ₄	20	1.88	11.11	12.0	5.6
BF2		16	2.19	7.11	14.6	2.6
BF3		31	2.5	11.93	17.6	
BF4		24	3.73	5.54	19.8	
BF5		27	20		60	

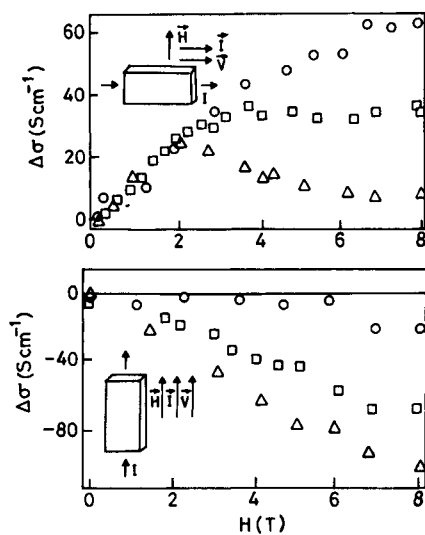
Source: Reproduced by permission of Elsevier Science from A. Aleshin, R. Kiebooms, R. Menon, and A. J. Heeger, *Synth. Met.* 90, 61 (1997). Copyright © 1997, Elsevier Science.

$\rho_r = \rho(1.4 \text{ K})/\rho(291 \text{ K})$.

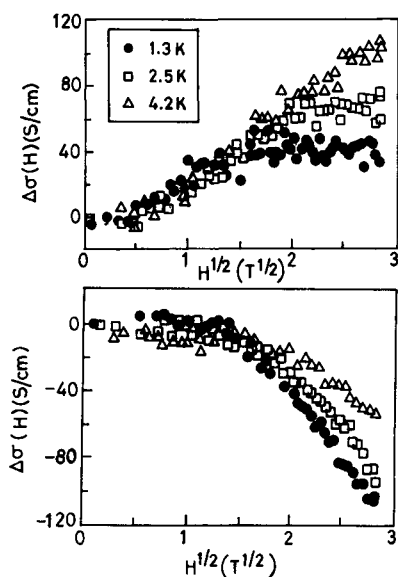
MR: magnetoresistance at $H = 8 \text{ T}$ and $T = 1.4 \text{ K}$.

σ_0 and $\sigma_0(H)$ extrapolated values from square-root dependence of the conductivity at 0 and 8 T, respectively.

viates, as shown in Figure 135a. This clearly shows the importance of the WL contribution to transverse MC. This anisotropic MC can be used to probe the microscopic anisotropy in the molecular length scale, which is usually masked by the morphological features in the bulk conductivity measurements. Hence, modeling the anisotropic MC can provide a quantitative estimate of the number of misaligned chains in oriented samples. In slightly less conducting ($\sim 100 \text{ S cm}^{-1}$) metallic samples of unoriented PEDOT, a uni-



(a)



(b)

Fig. 134. (a) Magnetoconductance vs field for a metallic $I-(CH)_x$ sample at 4.2 K (\circ), 2 K (\square), and 1.2 K (\triangle); upper is transverse and lower is longitudinal. (b) Magnetoconductance vs field for a metallic PPV- H_2SO_4 sample; upper is transverse and lower is longitudinal. Reproduced by permission of the American Physical Society from M. Reghu, K. Vakiparta, Y. Cao, and D. Moses, *Phys. Rev. B* 49, 16162 (1994); M. Ahlskog, M. Reghu, A. J. Heeger, T. Noguchi, and T. Ohnishi, *Phys. Rev. B* 53, 15529 (1996). Copyright © 1994, 1996, American Physical Society.

versal scaling of MC has been observed, as shown in Figure 136 [1109]. In this case, since the chains are not oriented, the scaling behavior is nearly identical in both transverse and longitudinal MC, showing that the e-e interaction is the dominant contribution to MC.

Although the anisotropy of conductivity in metallic oriented $(CH)_x$ or PPV- H_2SO_4 samples is nearly 100, the behavior of MC is identical whether the current is parallel or perpendicular to the chain axis. This suggests that high-quality oriented conducting polymers behave as *anisotropic three-dimensional systems* in which

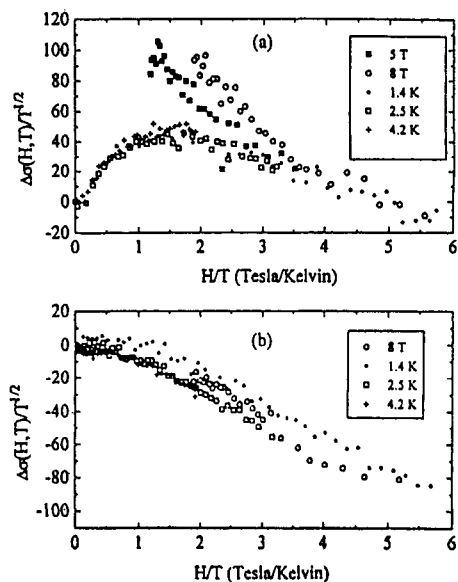


Fig. 135. Universal scaling plot of magnetoconductance for a metallic PPV- H_2SO_4 sample: (a) transverse and (b) longitudinal. Reproduced by permission of the American Physical Society from M. Ahlskog, M. Reghu, A. J. Heeger, T. Noguchi, and T. Ohnishi, *Phys. Rev. B* 53, 15529 (1996). Copyright © 1996, American Physical Society.

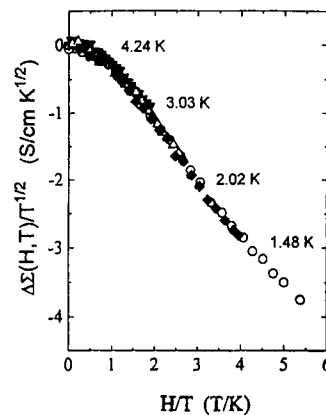


Fig. 136. Universal scaling plot of magnetoconductance for a metallic PEDOT- PF_6 sample. Reproduced by permission of the American Physical Society from A. Aleshin, R. Kiebooms, R. Menon, F. Wudl, and A. J. Heeger, *Phys. Rev. B* 56, 3659 (1997). Copyright © 1997, American Physical Society.

the charge-transport mechanism is nearly identical in both the parallel and the perpendicular directions to the chain axis.

The MC for a metallic PANI-CSA sample, at low and high fields, is shown in Figure 137 [1119, 1120]. The MC shows H^2 and $H^{1/2}$ dependence at low and high fields, respectively. Similar results have been observed for metallic PPy [1136] and PEDOT [1109] samples. This field dependence is consistent with the localization-interaction model. These systems are just on the metallic side of the M-I boundary, and their conductivity values are not high enough to observe any positive MC due to the WL contribution. Hence, in PANI, PPy, and PEDOT systems, the MC remains negative at all temperatures and fields. When the extent of disorder increases and the system moves to the critical and insulating regimes, the negative MC increases dramatically.

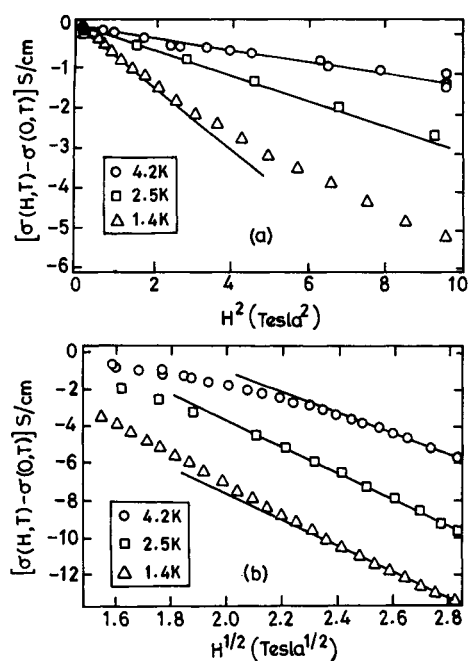


Fig. 137. Magnetoconductance vs field for a metallic PANI-CSA sample: (a) low-field fit and (b) high-field fit. Reproduced by permission of the American Physical Society from M. Reghu, Y. Cao, D. Moses, and A. J. Heeger, *Phys. Rev. B* 47, 1758 (1993); M. Reghu, C. O. Yoon, Y. Cao, D. Moses, and A. J. Heeger, *Phys. Rev. B*, 48, 17685 (1993). Copyright © 1993, American Physical Society.

In summary, MC in metallic conducting polymers is a sensitive probe to investigate the microscopic charge-transport mechanism. In oriented metallic conducting polymers, the anisotropic MC depends on the angle between the chain axis and the field, and this can give qualitative information regarding the molecular-scale anisotropy in these systems. In less conducting and nonoriented systems, the magnitude of the negative MC increases as ρ_r increases, and this can be used to determine the extent of disorder present in the system.

3.1.3. Thermopower

In doped conducting polymers, the thermopower is not as sensitive to disorder as electrical conductivity, since the mean free path involved in the electrical transport is very much affected by the extent of disorder present in the system [2]. Although the metallic positive TCR is rather unusual in highly conducting polymers for a wide range of temperatures, the metallic linear temperature dependence of thermopower [$S(T)$] is quite usual in all conducting polymers for a wide range of temperatures (10–300 K). The quasi-linear temperature dependence of thermopower is observed to persist well into the insulating regime.

The remarkable linearity of $S(T)$ and the negligible nonlinear contribution to thermopower in high-quality metallic $(\text{CH})_x$ indicate that the electron-phonon renormalization of diffusion thermopower, the phonon drag effects, etc. are not playing any significant roles. The $S(T)$ for MoCl_5 -doped $(\text{CH})_x$ is shown in Figure 138 [2]. The $S(T)$ is quite linear even in the case of less conducting insulating samples.

Kaiser [1143] has proposed a heterogeneous model to explain the apparent difference in the behavior of $S(T)$ and $\sigma(T)$. In such a

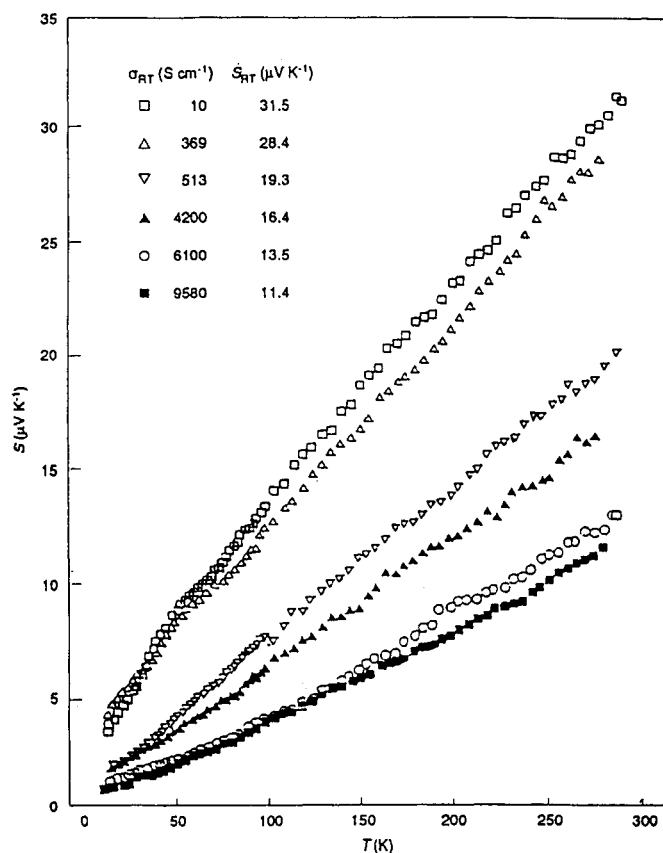


Fig. 138. Thermopower vs temperature for various $\text{MoCl}_5-(\text{CH})_x$ samples: from metallic (\blacksquare) to insulating side (\square). Reproduced by permission of John & Sons Limited from H. S. Nalwa, Ed., "Handbook of Organic Molecules and Polymers," Vols. 1–4. Wiley, New York, 1997. Copyright © 1997, John Wiley & Sons Limited.

model, the less conducting regions that limit the motion of charge carriers determine the bulk transport properties. In thermopower, the geometric factors involved in the electrical conductivity expression are absent. The net thermopower is weighted in favor of the regions where the largest temperature gradient occurs. If the thermal current carried by phonons is impeded less by thin insulating barriers than the electrical current carried by electrons or holes, then the system indeed shows a metallic thermopower. In other words, most of the temperature gradient occurs across the highly conducting regions and most of the electrical potential drop occurs across the thin insulating barriers. A large enhancement of thermopower is expected if the barriers play any significant role in the tunneling contribution to thermopower. However, in conducting polymers, on the metallic and critical regimes of the M–I transition, no such enhancement has been observed, indicating that the barriers contribute little to the thermopower.

The $S(T)$ of various PPy-PF₆ samples on both sides of the M–I transition is shown in Figure 139 [1136]. Similar results have been observed in PANI-CSA samples, too [1144]. In these systems, the quasi-linear thermopower is relatively insensitive to the variations in ρ_r near the disorder-induced M–I transition. The density of states estimated from $S(T)$ is around one state per electron-volt per two rings for PANI-CSA, and nearly one state per electron-volt per four rings for PPy-PF₆, for samples near the M–I transition.

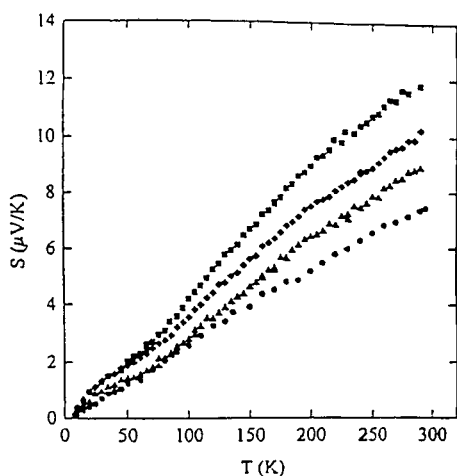


Fig. 139. Thermopower vs temperature for various PPy-PF₆ samples: from metallic side (●) to insulating side (■). Reproduced by permission of the American Physical Society from C. O. Yoon, M. Reghu, D. Moses, and A. J. Heeger, *Phys. Rev. B* 49, 10851 (1994). Copyright © 1994, American Physical Society.

The conventional notion suggests that the sign of the thermopower depends on the sign of the charge carrier. However, Park et al. [21] have observed a positive thermopower for both p- and n-type doped (CH)_x. Since the sign of the thermopower depends on the band structure, etc., it may not be that straightforward in complex systems such as doped conducting polymers. Nevertheless, more work is required to fully understand this anomaly in the sign of thermopower in conducting polymers.

3.1.4. Magnetic Susceptibility and Specific Heat

In metallic systems, the temperature-independent Pauli susceptibility (χ^P) is a characteristic feature for delocalized carriers [2]. χ^P is directly proportional to the density of states at the Fermi level, i.e., $\chi^P = \mu^2/BN(E_F)$. Hence, it is possible to determine the $N(E_F)$ from the temperature-independent χ^P for metallic systems. Usually, in disordered systems, the measured χ is the sum of both Curie and Pauli terms; the Curie term gives an estimate of the localized spins present in the system, and this, in turn, is a measure of the extent of disorder.

A small Curie term has been observed in all metallic conducting polymers at very low temperatures ($T < 20$ K) [2]. This indicates the presence of localized spins due to impurities, defects, etc. The $\chi(T)$ of PANI-CSA samples near the M-I transition is shown in Figure 140 [1146]. The density of states at the Fermi level for metallic PANI-CSA and PPy-PF₆ samples are one state/electron-volt/two rings and three states/electron-volt/four rings, respectively [1147]. These values are rather similar to that obtained from the thermopower measurements. The Curie term at low temperatures is weaker for metallic samples, with respect to that in insulating samples. The magnetic properties and spin dynamics in doped conducting polymers are quite well described in review articles [1147].

The thermal property measurements (e.g., thermal conductivity, specific heat, etc.) are rather few in doped conducting polymers [1148, 1149]. The linear term in specific heat at low temperatures is characteristic evidence of the continuous density of states with a well-defined Fermi energy for any metallic system. The low-temperature specific heat for a metallic PPy-PF₆ sample and for

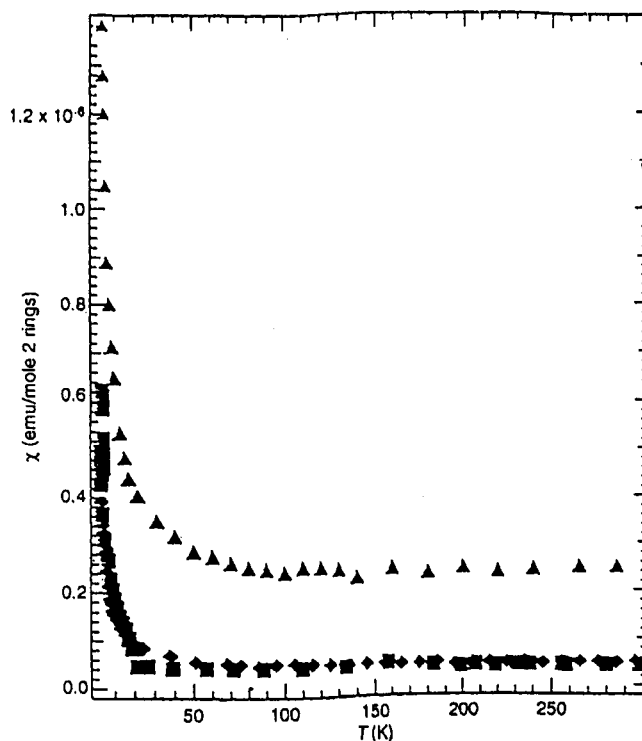


Fig. 140. Magnetic susceptibility vs temperature for PANI-CSA samples: from metallic side (■) to insulating side (▲). Reproduced by permission of the American Physical Society from N. S. Sariciftci, A. J. Heeger, and Y. Cao, *Phys. Rev. B* 49, 5988 (1994). Copyright © 1994, American Physical Society.

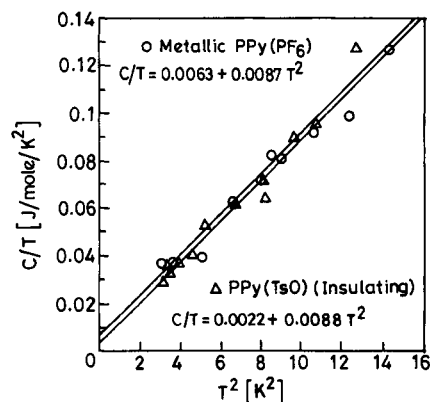


Fig. 141. Heat capacity (C/T) vs temperature for doped PPy samples: metallic PPy-PF₆ (○) and insulating PPy(TSO) (Δ). Reproduced by permission of the Physical Society of Japan from T. H. Gilani and T. Ishiguro, *J. Phys. Soc. Jpn.* 66, 727 (1997). Copyright © 1997, Physical Society of Japan.

an insulating PPy-TSO (*p*-toluenesulfonate) sample is shown in Figure 141 [1150]. The data for both samples are fit to the equation $C/T = \gamma + \beta T^2$, where γ and β are the electronic and lattice contributions, respectively. From the values of β and γ , the calculated density of states for metallic and insulating samples are 3.6 ± 0.12 and 1.2 ± 0.04 states/eV/unit, and the corresponding Debye temperatures are 210 ± 7 and 191 ± 6.3 K, respectively. These values are comparable with respect to that obtained from the spin susceptibility data.

Although the resistivity ratio of an insulating PPy-TSO sample is an order of magnitude larger with respect to the metallic PPy-PF₆ sample, both systems show a linear term in specific heat, and the density of states of an insulating system is only a factor of 3 lower with respect to that in the metallic sample [1150]. Moreover, from the specific heat data, it seems that both systems have a finite density of states at the Fermi level; hence, the insulating system can be considered as slightly less metallic (less density of states due to localization) with respect to the “real” metallic system (i.e., finite conductivity at $T \rightarrow 0$ K). The comparison of specific heat and conductivity data indicates that the latter is more sensitive to determining the extent of disorder and for discerning the metallic and insulating systems near the M-I transition. Furthermore, both systems do not show any anomalies due to glassy behavior, carrier freeze-out in the amorphous regions, one-dimensional localization, etc. Surprisingly, the linear term in the specific heat is strongly present in both metallic and insulating systems down to 2 K, although a Curie term in the spin susceptibility was observed for all conducting polymer samples at low temperatures. This indicates that for conducting polymer samples near the M-I transition, the extent of disorder is not severe enough to induce any drastic localization of charge carriers, contrary to the conventional view that all states are localized in a disordered one-dimensional conductor.

3.2. Critical and Insulating States

The intrinsic metallic state in high-quality doped conducting polymers is suppressed by the disorder-induced localization [2, 3]. As the extent of disorder increases, the effective conjugation length and the interchain transport decrease, and the system gradually moves from the metallic to the insulating state via the critical regime of the M-I transition. From the previous section, it is known that even slight variations in the extent of disorder have dramatic effects on the temperature dependence of conductivity near the M-I transition. In other transport property measurements (e.g., thermopower, specific heat, etc.), the effect of disorder is not that conspicuous near the M-I transition, especially in conducting polymer systems.

The power law behavior of conductivity is universal for systems at the critical regime, and the temperature dependence of conductivity is given by $\sigma(T) \propto T^\beta$, where β is between 0.33 and 1 [3]. In the power law regime [temperature-independent $W(T)$ regime], $W = \beta$. The value of β and the temperature range of the power law regime can be determined from the log-log plots of W versus T . As a typical example, the W versus T plot of various conducting polymer systems near the critical regime is shown in Figure 142 [1151]. Usually, the value of β is lower for systems with a smaller value of ρ_r , and as ρ_r increases the system moves toward the insulating regime in which the $\sigma(T)$ becomes exponential, i.e., $\sigma(T) \propto \exp(-T_0/T)^\gamma$, where $\gamma = 1/(d + 1)$ and d is the dimensionality of the system.

The W versus T plots for various conducting polymers are shown in Figures 128, 130, and 131. In all of these figures, the temperature coefficient of $W(T)$ varies distinctly for metallic (positive), critical (T -independent), and insulating (negative) regimes. Figures 128, 130, and 131 clearly show that the critical regime is rather robust in conducting polymers. Moreover, the critical regime can be easily tuned to the metallic and insulating regimes by pressure and magnetic fields, respectively, as shown in the case of a PPy-PF₆ sample in Figure 143 [1152]. The enhanced interchain transport under pressure is driving the system toward the metallic state.

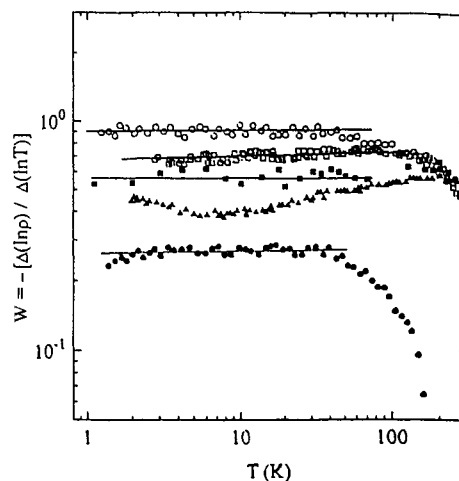


Fig. 142. W vs T plot of various conducting polymers in the critical regime of the M-I transition: unoriented I-(CH)_x (○), oriented I-(CH)_x (□), oriented K-(CH)_x (■), PPy-PF₆ (▲), and PANI-CSA (●). Reproduced by permission of Elsevier Science from M. Reghu, C. O. Yoon, D. Moses, Y. Cao, and A. J. Heeger, *Synth. Met.* 69, 329 (1995). Copyright © 1995, Elsevier Science.

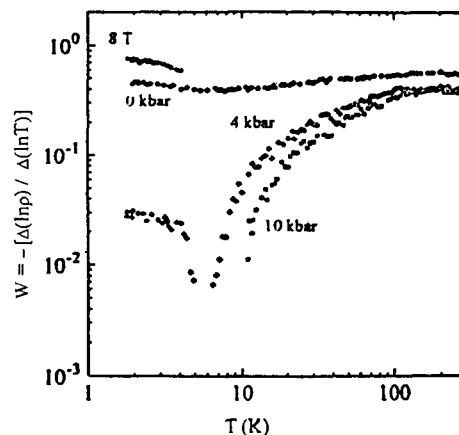


Fig. 143. W vs T for a PPy-PF₆ sample in the critical regime: pressure-induced transition to the metallic side and field-induced transition to the insulating side. Reproduced by permission of Elsevier Science from M. Reghu, C. O. Yoon, D. Moses, Y. Cao, and A. J. Heeger, *Synth. Met.* 69, 329 (1995). Copyright © 1995, Elsevier Science.

The field-induced transition to the critical and insulating regimes occurs when the localization length is comparable to the magnetic length, and the field shrinks the overlap of the wave functions of the delocalized states. The field-induced transition, from the metallic to the critical regime, for a doped PPV sample is shown in Figure 144 [1135]. Although this sample has a large finite conductivity in zero field, it nearly approaches 0 at a field of 8 T. Another typical example of a field-induced transition, from power law to exponential law behavior of conductivity at low temperatures, is shown for a PANI-CSA sample in Figure 145 [1119, 1120]. These field-induced transitions in conducting polymer systems near the M-I transition show that the mobility edge and the Fermi level are situated rather close to each other, and slight variations in the overlap of the wave functions of the delocalized states by magnetic field, disorder, etc. could alter the electronic properties of the system.

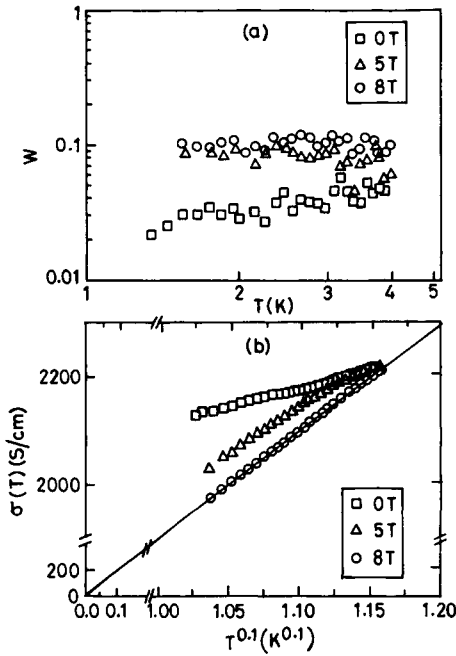


Fig. 144. Field-induced transition from the metallic to the critical regime: (a) W vs T for a metallic PPV- H_2SO_4 sample (E from Fig. 130) at 0, 5, and 8 T. (b) Conductivity vs $T^{0.1}$ for the same data. Reproduced by permission of the American Physical Society from M. Ahlskog, M. Reghu, A. J. Heeger, T. Noguchi, and T. Ohnishi, *Phys. Rev. B* 55, 6777 (1997). Copyright © 1997, American Physical Society.

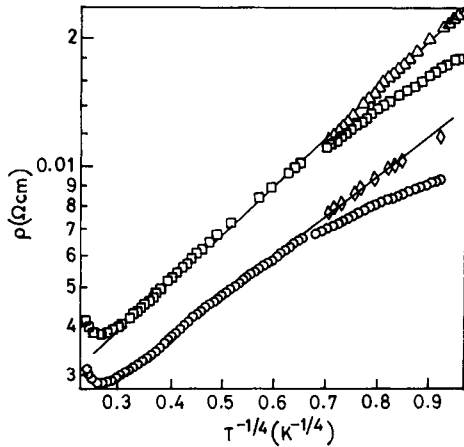


Fig. 145. Field-induced transition from the critical to the insulating regime for PANI-CSA samples: resistivity vs $T^{-1/4}$ plot. $H = 0$ T (\circ) and $H = 10$ T (\diamond) for a sample with $\rho(T) \propto T^{-0.26}$ and $H = 0$ T (\square) and $H = 8$ T (\triangle) for a sample with $\rho(T) \propto T^{-0.36}$. Reproduced by permission of the American Physical Society from M. Reghu, Y. Cao, D. Moses, and A. J. Heeger, *Phys. Rev. B* 47, 1758 (1993); M. Reghu, C. O. Yoon, Y. Cao, D. Moses, and A. J. Heeger, *Phys. Rev. B* 48, 17685 (1993). Copyright © 1993, American Physical Society.

As mentioned previously, the negative magnetoresistance (MR) in metallic $(CH)_x$ and PPV samples is quite sensitive to the extent of disorder [2, 3]. Even in the case of well-oriented metallic samples of $(CH)_x$ and PPV, a marginal increase in disorder can easily suppress the quantum interference process involved in the WL contribution to negative MR [1135]. As disorder increases and the system moves toward the critical and insulating regimes, the posi-

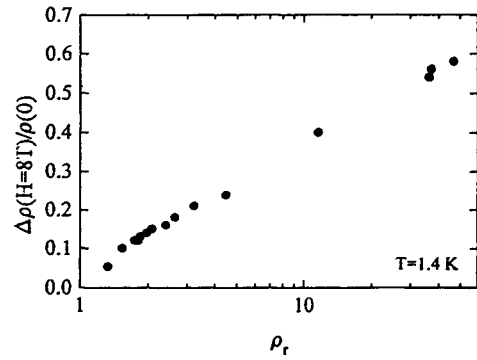


Fig. 146. Magnetoresistance vs resistivity ratio (ρ_r) for various PPy- PF_6 samples from the metallic to the insulating side. Reproduced by permission of the American Physical Society from C. O. Yoon, M. Reghu, D. Moses, and A. J. Heeger, *Phys. Rev. B* 49, 10851 (1994). Copyright © 1994, American Physical Society.

tive MR contribution increases due to the shrinkage of the overlap of the wave function of the localized states. Usually, in conducting polymers, as the chain orientation decreases the contribution to positive MR increases. The MR is positive at all temperatures and fields in PANI, PPy, PMeT, PEDOT, etc., since the chains are less oriented in these systems with respect to $(CH)_x$ and PPV [3]. In these systems, as ρ_r increases the positive MR increases, as shown in the case of PPy- PF_6 samples in Figure 146 [1144]. Hence, the magnitude of the positive MR can be used to get a rough estimate of the extent of disorder present in the system.

Usually, the magnitude of the positive MR at very low temperatures ($T < 4$ K) is as sensitive as the temperature dependence of the conductivity to probe the extent of disorder present in the sample. The typical values of the magnitude of positive MR at 1.4 K and a field of 8 T in the metallic, critical, and insulating regimes are less than 5%, between 5 and 20%, and larger than 20%, respectively [2]. The large positive MR in the variable range hopping (VRH) regime is due to the shrinkage of the overlap of the tails of the wave functions of the localized states, and the hopping transport becomes more difficult at higher fields and lower temperatures. In the VRH regime, the low-field MR follows a H^2 dependence, and this can be used to determine the localization length in the insulating regime. If the localization length is on the order of a few hundreds (few tens) of angstroms, then the extent of disorder is relatively less (large) [1152]. Hence, the MR data are complementary to the low-temperature conductivity data in probing the extent of disorder present in critical and insulating systems.

Although the transport property measurements (e.g., thermopower, specific heat, etc.) are important in the critical and insulating regimes, they are not as sensitive as the low-temperature conductivity and MR. The linear temperature dependence of thermopower and a linear term in the specific heat, which are typical for metallic systems, have been observed in the insulating regime, too. As the system moves well into the insulating side, the hopping contribution to thermopower ($S_{\text{hop}} \propto T^{1/2}$) dominates over the metallic diffusion thermopower ($S_{\text{dif}} \propto T$) [1152]. Usually, the negative hopping contribution can be estimated by subtracting the diffusion contribution, and this gives an estimate of the extent of disorder present at the macroscopic level. The gradual variation of $S(T)$ from the positive linear temperature dependence to the negative U-shaped behavior can be correlated with the microstructure, as the system moves to the highly disordered granular, metallic is-

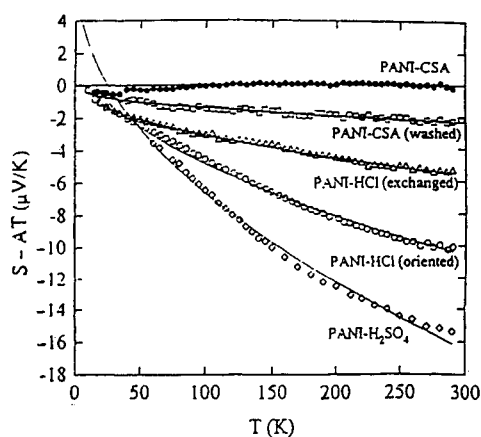


Fig. 147. Hopping contribution to thermopower for various doped PANI samples. Reproduced by permission of Elsevier Science, from C. O. Yoon, M. Reghu, D. Moses, A. J. Heeger, Y. Cao, T. A. Chen, X. Wu, and R. D. Reike, *Synth. Met.* 75, 229 (1995). Copyright © 1995, Elsevier Science.

lands, etc. A typical example of this feature, in the case of doped PANI, is shown in Figure 147 [3, 1152]. These features in $S(T)$ can be used to get a qualitative picture of the macroscopic-scale disorder present in conducting polymers.

The Curie term in $\chi(T)$ is rather dominant, at low temperatures, for systems in the critical and insulating regimes. The temperature-independent Pauli term is usually observed at $T > 100$ K. However, the $\chi(T)$ is not as sensitive as $\alpha(T)$ and MR for identifying the metallic, critical, and insulating regimes near the M-I transition [2].

4. OPTICAL PROPERTIES

Conjugated polymers have attracted considerable interest [1–5, 1049] in applied and fundamental research since the discovery [154] of high conductivity in doped polyacetylene in 1977. Since then, an enormous amount of effort has gone toward the understanding of the electronic and transport properties in conjugated polymers. Subsequently, the family of π -conjugated polymers has been greatly enlarged [1–3] and an elegant theoretical model [1049, 1153] has been developed to describe many novel and fascinating phenomena in these systems.

Conjugated polymers have an anisotropic, quasi-one-dimensional electronic structure with the π electrons coupled to the polymer backbone via electron-phonon interactions. In contrast with conventional inorganic semiconductors with rigid band, upon doping or photoexcitation the carriers are self-localized and form the nonlinear excitations [1, 1049, 1153] on the polymer chains, solitons, polarons, or bipolarons, depending on the ground-state degeneracy. Much of the new physics associated with conjugated polymers is related to the formation and properties of such nonlinear excitations. New subgap optical transitions occur with a corresponding shift of oscillator strength from the π - π^* transitions to the localized gap states associated with these novel quasi-particles. Moreover, these nonlinear excitations are believed to be responsible for the electronic transport in the dilute and intermediate doping level, illustrating a moderate electrical conductivity without significant Pauli susceptibility.

Nevertheless, many conjugated polymers undergo a transition from such a nonlinear excitation state to a metallic state at high

doping level [1154]. The metallic state is verified by measurements of the Pauli spin susceptibility, linear dependence of the thermopower with temperature, and the linear term in heat capacity, i.e., properties that all originate in the appearance of a finite density of states at the Fermi level. In spite of the clear signatures of the metallic state, however, heavily doped conjugated polymers do not exhibit the traditional metallic behaviors in transport and optical properties. Instead, they typically show a negative temperature coefficient of the resistivity ($dp/dT < 0$) with an activating process in dc conductivity [173], and the optical spectra do not follow the Drude-like behavior expected for a typical metal at low frequencies [1155].

These nonmetallic behaviors arise from the disorder of the sample, originating from a combination of molecular-scale disorder and mesoscale inhomogeneity. Such disorder suppresses the intrinsic metallic properties of conducting polymers, complicating their electronic properties. Indeed, it is well known that sufficient disorder causes the localization of the states, thereby inducing the metal-insulator (M-I) transition in spite of the finite density of states at the Fermi level [1125, 1156, 1157]. In such a system, the charge dynamics are expected to be inherently different from those of traditional metals.

Progress in the synthesis and processing of conducting polymers has greatly improved the homogeneity of the material and significantly reduced the degree of structural disorder. These improvements include polyaniline protonated with camphor sulfonic acid (PANI-CSA) [129], the electrochemically synthesized polypyrrole doped with PF_6 (PPy- PF_6) [1158], and poly(3,4-ethylenedioxythiophene) doped with PF_6 (PEDOT- PF_6) [1159]. These structurally improved materials provide opportunities to study the M-I transition and the intrinsic metallic state. Motivated by such features, a series of optical reflectance measurements on these improved materials have been carried out during the last several years [1160–1166], and the major results are summarized in this review. These studies have yielded a wealth of important information on the electronic structure of these materials, both on the metallic and on the insulating side of the M-I transition, and on the role of disorder in the electronic structure. Furthermore, the difference in charge dynamics in the metallic and in the insulating regime has been investigated. Most interestingly, the possibility of new low-lying elementary excitations, which would be screened in the conventional materials due to severe disorder, has been explored in the low-temperature measurements of the structurally improved materials [1166].

As undoped states, conjugated polymers are classified into semiconductors. Conjugated polymers exhibit the electronic and optical properties of semiconductors in combination with the mechanical properties of general polymers, making them potentially useful for a wide array of applications. The electronic structure of such semiconducting conjugated polymers was successfully described by Su et al. [1167] in terms of a quasi-one-dimensional tight binding model in which the π electrons are coupled to distortions in the polymer backbone by the electron-phonon interaction. As in the case of charge-transfer chemical (or electrochemical) doping, extra charges can be injected onto the conduction band of such semiconducting polymers via photoexcitation (i.e., injecting charges onto the polymer backbone by direct optical pumping above the π - π^* energy gap with an intense external light source).

However, although the linear and nonlinear optical properties of conjugated polymers have been investigated for over a decade,

there is still controversy about the nature of the primary photoexcitations [1121, 1168]. Are the lowest energy elementary excitations mobile charge carriers (charged polarons) or bound neutral excitons? Since the answer is of importance not only from the perspective of our basic understanding of the conducting polymers, but also for applications based on these materials, the related experimental results, such as photoexcitation spectroscopy, photoluminescence spectroscopy, and photoconductivity, are examined in this review.

In parallel with these efforts to understand the underlying physics of conducting polymers, there are explosively increased activities in the research for applications of these materials in optoelectronic devices [4, 1169]. In particular, research in the use of these materials as the active electroluminescent media in light-emitting diodes (LEDs) has advanced rapidly after its first report in 1990 [134], and prototype devices now meet realistic specifications for applications. Therefore, we also make an attempt in this review to cover the basic principle of the polymer LED and current issues that determine the limits of device performance.

Finally, we briefly review the photophysics and associated device applications of conjugated polymer/fullerene composites. Upon mixing buckminsterfullerene, C_{60} , into semiconducting polymers, a variety of interesting photophysical phenomena have been discovered [1170]. The photoinduced electron transfer from semiconducting polymers onto C_{60} is reversible, ultrafast (within 300 fs) with a quantum efficiency approaching unity, and metastable. As the first step in artificial photosynthesis, this photoinduced electron transfer leads to a number of potentially interesting applications, including photodetectors, photovoltaic cells, and nonlinear optical devices. In this review, the basic photophysical phenomena are summarized with a brief introduction to many potential applications of these phenomena.

4.1. Theoretical Considerations

4.1.1. Optical Properties of Solids

Since this section is intended to investigate the optical properties of conducting polymers, it is relevant to review some basic optical properties of simple solids. Therefore, this section starts with a rather elementary treatment of the optical constants. The optical constants of solids provide information on their electronic and vibronic structure since the electromagnetic field of the light wave interacts with all fixed and mobile charges [1171, 1172]. For a simple solid (a homogeneous, isotropic, and linear medium that is local in its response), the response of the system to the field is characterized by a complex dielectric function, $\varepsilon(\omega)$, given as

$$\varepsilon(\omega) = \varepsilon_1(\omega) + (4\pi i/\omega)\sigma(\omega) \quad (4.1)$$

where $\varepsilon_1(\omega)$ is the real part of the dielectric function and $\sigma(\omega)$ is the real part of the frequency-dependent conductivity.

As explicitly seen in Eq. (4.1), $\varepsilon_1(\omega)$ and $\sigma(\omega)$ enter into a determination of the optical properties of a solid only in combination [1173]. This fact reflects a genuine ambiguity in the physical definition of $\varepsilon_1(\omega)$ and $\sigma(\omega)$, which describe distinguishable physical processes only in the dc case, where $\sigma(\omega)$ describes the free charges and $\varepsilon_1(\omega)$ describes the bound charges. However, in the case of an alternating-current (ac) field, the distinction blurs, and at sufficiently high frequencies even this distinction disappears. The free charges can have a substantial out-of-phase response (indeed, in metals, $\sigma(\omega)$ is predominantly imaginary at optical frequencies) and the bound charge can have a considerable in-phase

response. In this case, the response of all electrons (core and conduction electrons) is lumped into the single dielectric constant $\varepsilon(\omega)$. This convention enables the optical theories of metals to use the same notation used for insulators.

Introducing a complex refractive index, $N = n + i\kappa$, $\varepsilon(\omega)$ ($= N^2$) is related to the refractive index, n , and the absorption index, κ , by the relations

$$\varepsilon_1(\omega) = n^2 - \kappa^2 = \text{Re}\{\varepsilon(\omega)\} \quad (4.2a)$$

$$\varepsilon_2(\omega) = 2n\kappa = \text{Im}\{\varepsilon(\omega)\} \quad (4.2b)$$

Due to the linear response of simple solids and as a result of causality [1171], $\varepsilon_1(\omega)$ and $\varepsilon_2(\omega)$ are connected by the Kramers–Kronig relation. Thus, if one knows either the real or the imaginary part of the optical constants for all frequencies, one can evaluate the other numerically.

Such optical constants are connected with the experimentally determined absorption coefficient, $\alpha(\omega)$, and reflectivity, $R(\omega)$, through the relations

$$\alpha(\omega) = 2(\omega/c)\kappa(\omega) \quad (4.3)$$

and

$$R(\omega) = [(n-1)^2 + \kappa^2]/[(n+1)^2 + \kappa^2] \quad (4.4)$$

Therefore, having determined both $R(\omega)$ and $\alpha(\omega)$, Eqs. (4.3) and (4.4) serve to obtain the refractive and the absorption indices n and κ , as well as the complex dielectric function. Alternatively, if $R(\omega)$ can be measured over a sufficiently large spectral range, a Kramers–Kronig analysis also allows computations of a series of optical constants. In these circumstances, reflectivity measurements alone suffice in obtaining the dielectric function.

The classical theory of the dielectric response in solids is frequently described by the Drude and Lorentz models. The Drude model is applicable to free-electron metals; its quantum-mechanical analog includes intraband transitions, where intraband transitions are taken to mean all transitions not involving a reciprocal lattice vector. The Lorentz model is applicable to insulators; its quantum-mechanical analog includes all direct interband transitions, i.e., all transitions for which the final state of an electron lies in a different band but with no change in the k vector in the reduced-zone scheme. In the following discussion, both models will be surveyed and evaluated for real metals.

For a single-particle excitation in the conduction band of crystalline materials such as simple metals, charge dynamics are governed by coherent diffusion processes. Electrons drift ballistically and make random collisions with defects or with phonons, resulting in finite resistivity in an ambient temperature. The Drude model [1174] is a classical treatment of such an excitation scheme by free-electron approximation; i.e., this model treats the metallic electron gas in terms of the kinetic theory for a neutral dilute gas in thermal equilibrium with the lattice, suffering collisions that instantaneously change their velocities. In spite of its simple approximation, however, this model has been quite successful in describing the electronic properties of simple metals together with Fermi–Dirac statistics.

The Drude dielectric function is expressed as

$$\varepsilon(\omega) = \varepsilon_\infty - \Omega_p^2/[\omega^2 + i\omega\tau] \quad (4.5)$$

where ε_∞ is the contribution from high-energy interband transition processes and the atomic cores (typically $1 < \varepsilon_\infty < 4$), and

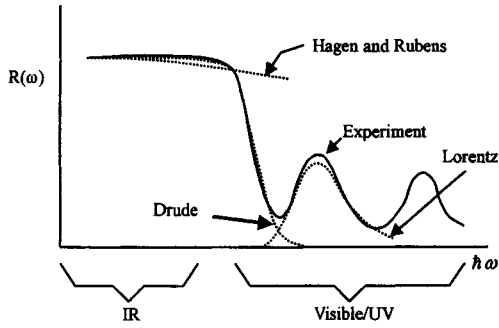


Fig. 148. Schematic frequency dependence of the reflectivity of metals: experimentally (solid line) and according to three models (dotted line).

Ω_p is the plasma frequency given as $\Omega_p^2 = 4\pi n_e e^2 / m^*$ with electron density n_e and effective mass m^* . Therefore, the corresponding $\epsilon_1(\omega)$ and $\sigma(\omega)$ are given as

$$\begin{aligned} \epsilon_1(\omega) &= \epsilon_\infty - \Omega_p^2 / [\omega^2 + 1/\tau^2], \\ \sigma(\omega) &= (\Omega_p^2 \tau / 4\pi) / [1 + \omega^2 \tau^2] \end{aligned} \quad (4.6)$$

For most metals, Ω_p is at a high frequency, typically in the ultraviolet, and at a much higher frequency than $1/\tau$. When $\Omega_p \gg 1/\tau$, $\epsilon_1(\omega)$ is negative for $\omega < \Omega_p / (\epsilon_\infty)^{1/2}$, following the “ $\propto -1/\omega^2$ ” decay. A large, negative $\epsilon_1(\omega)$ causes the high reflectance of a metal below its plasma edge. For an ideal free-electron metal, the reflectivity approaches unity below the plasma frequency. Above the plasma frequency, the metal is transparent and the reflectivity decreases rapidly with increasing frequency. The plasma frequency typically lies in the visible or ultraviolet spectral region ($\omega \geq 10^{15} \text{ s}^{-1}$), and the mean free collision time for electrons in metals is typically $\tau \approx 10^{-14} \text{ s}$.

Even though the Drude model describes well the spectral response of the free carriers in simple metals at low frequencies, the spectral features are more complicated at high frequencies, where the interband transitions start to contribute to the spectral response. In general, interband transitions are characterized by the details of the electronic band structure, thereby allowing transitions from one set of energy eigenstates to a higher lying set of states. Such interband spectra can be represented classically by the Lorentz oscillator model [1175]. Although the details of interband transitions are not well predicted by the Lorentz model, in contrast with the Drude model case, the bound-carrier contribution to the dielectric function is frequently described by this formalism. As a matter of fact, both models are frequently used together to describe the optical response of real metals, as shown in Figure 148.

As with the Drude model, the Lorentzian dielectric function is derived by assuming that motion of the electrons is subject to a viscous damping force. However, in this case, the electrons are bound by a harmonic potential to a site in the solid, so that each atom can be considered as an electric dipole. In this manner, the dielectric response function is given by

$$\epsilon(\omega) = \epsilon_\infty + \Omega_{pe}^2 / [\omega_e^2 - \omega^2 - i\omega\gamma_e] \quad (4.7)$$

where ω_e is the center frequency of the oscillator, γ_e is the linewidth or damping constant, and Ω_{pe} is the oscillator strength or plasma frequency given by $\Omega_{pe} = (4\pi n_o e^2 / m^*)^{1/2}$, where n_o is the number density of oscillators of charge e and effective mass m^* .

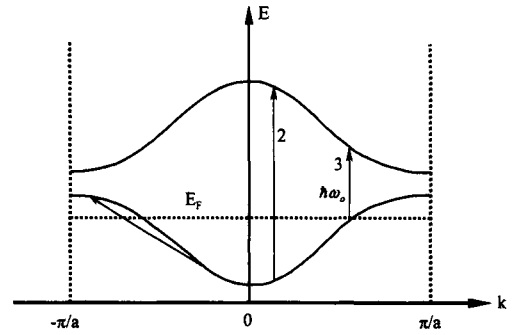


Fig. 149. Schematic band diagram for a metal.

The Lorentz and Drude models can be explained rigorously in relation to electronic band structure. Indeed, both models have quantum-mechanical analogs: intraband transitions for the Drude model and direct interband transitions for the Lorentz model. To see the role of both models in describing real metals, consider the schematic band diagram as shown in Figure 149. Two typical transitions are illustrated in Figure 149. The first of these, called an “intraband transition,” corresponds to the optical excitation of an electron from below the Fermi level (E_F) to another state above the E_F within the same band. There is no threshold energy for such transitions, and they can occur only in metals.

The second transition is a “direct interband transition.” It is the optical excitation of an electron to another band. It is called a direct or vertical transition because it involves only excitations of an electron by a photon. Since the momentum of a photon is very small compared with the range of values of crystal momentum in the Brillouin zone, conservation of total crystal momentum of the electron plus photon means that the value of wave vector k for the electron is essentially unchanged in the reduced-zone scheme. Direct interband transitions have a threshold energy, corresponding to $h\omega_o$ in Figure 149. This threshold energy is analogous to that for the excitation of an electron across the bandgap in an insulator. In general, the optical spectra for metals are dominated by direct interband transitions.

Another type of interband transition is possible, namely the so-called “indirect interband transition,” which involves the absorption of a light quantum with simultaneous participation of a phonon. In general, a phonon can only absorb very small energies, but is able to absorb a large momentum that is comparable to that of an electron. During the indirect interband transition, the excess momentum is transferred to the lattice (or is absorbed from the lattice). Indirect interband transitions may be disregarded for the interpretation of metal spectra because they are generally weaker than direct transitions by two or three orders of magnitude. In the case of semiconductors, however, indirect interband transitions play an important role.

4.1.2. Optical Properties of Disordered Systems

Although heavily doped conducting polymers show clear signatures for a metallic density of states at E_F , their transport properties are not typical of a traditional metal. Instead, the electronic states at E_F are dominated by disorder. In this section, therefore, a brief review is given on the dielectric response of the disordered system in the context of the Anderson transition, both on the metallic and on the insulating side of the M–I transition, derived from the Kubo–Greenwood formalism [1176].

When the mean free path l is on the order of the distance between atoms, the free-electron approximation (i.e., Drude model) breaks down. This occurs particularly in noncrystalline materials and for impurity conduction. In this situation, we make use of the Kubo–Greenwood formula [1176], which has universal validity. This formula uses elementary quantum mechanics to calculate the conductivity of a metal at frequency ω , by listing the transition probabilities from occupied states below E_F to empty states above E_F and then letting ω tend to 0 for dc conductivity [1125, 1156, 1157]. The main steps in the calculation are as follows: we suppose that an electric field $F \cos \omega t$ acts on a specimen of volume Ω . Since the quantity $\sigma(\omega)F^2/2$ is the mean rate of loss of energy per unit volume, the conductivity $\sigma(\omega)$ is given by the product of the following factors:

- (i) the number $N(E_F)$ of electrons that can make the transitions
- (ii) the transition probability given according to the Fermi rule
- (iii) the energy $h\omega$ absorbed in each transition.

Here $\langle E + h\omega|x|E \rangle$ is the matrix element of x , and can be written as

$$\begin{aligned} \langle E + h\omega|x|E \rangle &= h/(m\omega)\langle E + h\omega|\partial/\partial x|E \rangle \\ &= h/(m\omega)D_{E+h\omega, E} \end{aligned} \quad (4.9)$$

Integrating over all energies, we find

$$\sigma(\omega) = (2\pi e^2 h^3 \Omega / m^2) \int |D_{\text{av}}^2 [N(E)N(E+h\omega)/h\omega] dE \quad (4.10)$$

For the dc conductivity, we make ω tend to 0 and obtain

$$\sigma_E(0) = (2\pi e^2 h^3 \Omega / m^2) |D_{E|\text{av}}^2 [N(E)]^2 \quad (4.11)$$

The subscript av represents an average over all states with energies E . Equation (4.10) is called the Kubo–Greenwood formula. For a long mean free path approximation, Eq. (4.10) reduces to the Drude model.

For a Fermi glass, in which the states at E_F are Anderson localized, a photon of frequency ω can activate the hopping near the E_F , resulting in finite $\sigma(\omega)$. In this case, Mott and Kaveh [1125, 1157, 1177] show that $\sigma(\omega)$ can be derived from the Kubo–Greenwood expression given in Eq. (4.10) in the localization regime

$$\sigma(\omega) = 4\pi^2 e^2 h \omega^2 R_\omega^4 N(E_F) \xi \quad (4.12)$$

where

$$R_\omega = \xi \ln(H_0/h\omega) \quad (4.13)$$

and H_0 is the pre-exponential in the transfer integral between two sites a distance r apart, namely, $H_0 \exp(-r/\xi)$. However, Eq. (4.12) is valid only up to a frequency ω_c , such that $h\omega_c$ is the interval between sites in a volume ξ^3 , so that

$$h\omega_c = 1/[\xi^3 N(E_F)] \quad (4.14)$$

For $\omega > \omega_c$, localization does not affect the mobility of the electrons, so that their behavior is essentially metallic. In this case, the conductivity is approximated by [1178]

$$\sigma(\omega) = 0.03e^2/(hL_\omega) \quad (4.15)$$

which is obtained from Mott's "minimum metallic conductivity" in the limit of Ioffe and Regel. Here, $L_\omega = (D/\omega)^{1/2}$ acts as a limiting length scale, corresponding to the distance an electron drifts in the period of the alternating field. Since the diffusion coefficient $D = \sigma/[N(E_F)e^2]$, we find

$$\sigma(\omega) = 0.03(e^2/h)[N(E_F)h\omega]^{1/3} \quad \text{for } \omega > \omega_c \quad (4.16)$$

which gives $\sigma(\omega) \propto \omega^{1/3}$ for $\omega > \omega_c$, in contrast with the $\sigma(\omega) \propto \omega^p$ dependence with $p > 1$ for $\omega < \omega_c$.

4.2. Optical Properties of "Doped" Conducting Polymers

4.2.1. Introduction

At dilute and intermediate doping concentrations, conjugated polymers show a moderate electrical conductivity, characteristic midgap states, but no significant Pauli susceptibility. This combination suggests that significant contribution to the electrical transport is due to mobile charged nonlinear excitations (solitons, polarons, and bipolarons). However, when conjugated polymers are doped to concentrations in excess of a critical concentration (e.g., in *trans*-(CH)_x, $y_c \sim 6\%$), the system undergoes a rapid transition from the nonlinear excitation state to a metallic state in which the metallic Pauli spin susceptibility is evident. This can be observed clearly in *in situ* electron spin resonance (ESR) measurements [1154] of Na-doped polyacetylene during electrochemical doping, demonstrating an abrupt increase of the magnetic susceptibility above a doping concentration of 6 mol%. The large susceptibility above the transition is temperature independent, indicative of the Pauli susceptibility (χ_p) of a metal, in contrast with the weak narrow ESR line below the transition obeying Curie's law ($\chi \sim 1/T$). The metallic state is also characterized by a linear term in the heat capacity and a thermopower that is small and linear in temperature as well as in Pauli spin susceptibility. These properties indicate that the electronic structure of the heavily doped conjugated polymer is that of a metal with a finite density of states at the Fermi level.

In spite of the clear signatures of the metallic state, however, the heavily doped conjugated polymers do not exhibit traditional metallic behavior in transport [173] and optical properties [1155]. Instead, they show a negative temperature coefficient of the resistivity ($d\rho/dT < 0$); the dc conductivity is activated with temperature, so that the dc conductivity decreases by several orders of magnitude as the temperature is lowered. Furthermore, the optical spectra do not show the Drude-like behavior expected for a typical metal in the infrared. Rather, an electronic pseudo-gap of about 0.1–0.2 eV has been observed, below which the optical conductivity is suppressed [1155]. These nonmetallic behaviors arise from the disorder of the sample, originating from a combination of molecular-scale disorder and mesoscale inhomogeneity.

Progress in the synthesis and processing of conducting polymers has greatly improved the homogeneity of the material and significantly reduced the degree of structural disorder. These improvements include polyaniline protonated with camphor sulfonic acid (PANI–CSA) [128], the electrochemically synthesized polypyrrole doped with PF₆ (PPy–PF₆) [1155], and poly(3,4-ethylenedioxythiophene) doped with PF₆ (PEDOT–PF₆) [1159]. Although there have been some previous pioneering works in optical spectroscopic studies, mostly on doped polyacetylene [1179, 1180], such improved materials provide new opportunities to study the M–I transition and the intrinsic metallic state of conducting

polymers with optical spectroscopic measurements. In this section, therefore, results on the optical reflectance measurements on these improved materials are summarized with a brief introduction to optical measurements.

4.2.2. Optical Measurements

The usual way to determine the optical properties of a solid is to shine monochromatic light onto an appropriate sample and then to measure the reflectance or transmittance of the sample as a function of photon energy. Since it is generally not feasible to make thin films of sufficient quality to get meaningful data in metal physics, however, most experiments are measurements of the reflectance. Such reflectance provides information on the electronic structure and on the nature of low-lying elementary excitations over a wide energy range. In particular, measurements in the infrared (IR) range probe the charge dynamics involving intraband excitations, while measurements at higher photon energies probe the interband transitions.

In general, the IR reflectance measurements between 10 and 8000 cm^{-1} (0.001–1 eV) are performed widely in the lab using a suitably modified commercial Fourier transform infrared spectrometer (FTIR). Then, the grating monochromator covers the near-IR, visible (vis), and UV ranges over 8000–50,000 cm^{-1} (1–6 eV). For the absolute values of reflectance, reference mirrors should be used and compared with samples (usually a gold mirror for the IR and an Al mirror for the vis/UV range) with a following correction using the absolute values of the reflectance of the reference as given in the literature.

After measuring the reflectance data, the optical conductivity and the dielectric function can be obtained from a Kramers–Kronig analysis of the reflectance spectra as given in the literature [1171, 1172]. In principle, the Kramers–Kronig transformation requires a knowledge of reflectance over the full spectral range ($0 < h\omega < \infty$). Since data are available from the limited spectral range (typically from 0.001 to 6 eV), reasonable and careful extrapolations of the reflectivity should be made beyond the measurement range. At lower frequencies ($h\omega < 0.0016$ eV), the reflectance spectra of the metallic samples are extrapolated by the Hagen–Rubens relation [1171]. For insulating samples (semiconductors), the reflectance is assumed to be constant for $h\omega < 0.001$ eV. For the high energy range, the energy range is divided into two parts and different approximations are applied to each region; at energies between 6 eV and E_{fg} ($25 \text{ eV} < E_{fg} < 50 \text{ eV}$), the reflectance spectra are extrapolated as ω^{-s} where $1 < s < 4$. Above E_{fg} , the data are extrapolated according to the asymptotic behavior of free electrons (about ω^{-4}). In this procedure, the terminating energy, E_{fg} , and the exponent s should be determined consistently so as to give correct optical spectra over a wide range. Usually, these parameters are determined by comparing the experimentally measured absorption spectra with the Kramers–Kronig calculated absorption spectra, $\alpha(\omega) = 2\omega\kappa(\omega)/c$, where $\kappa(\omega)$ is the imaginary part of the refractive index and c is the velocity of light. When the calculated $\alpha(\omega)$ and measured $\alpha(\omega)$ are consistent, the corresponding E_{fg} and s are assumed to give the correct optical constants. Once the Kramers–Kronig analysis is performed numerically with the reflectance data, including the extrapolation at high and low frequencies as described previously, the optical constants such as optical conductivity and dielectric function can be obtained from the relations given in Section 4.1.

4.2.3. Optical Spectra of Conducting Polymers in the Metallic Regime

4.2.3.1. PANI–CSA

Within the class of conducting polymers, polyaniline (PANI) is unique in that its electronic structure and electrical properties can be reversibly controlled both by charge-transfer doping and by protonation [1181]. Moreover, PANI can be processed in both insulating (emeraldine base) and conducting (emeraldine salt) forms [1182, 1183]. The protonation of the emeraldine base to the conducting emeraldine salt form leads to an electronic structure with one unpaired spin per formula unit, $(-\phi-\text{NH}-\phi-\text{NH}-)^{+\bullet}$, where ϕ denotes a phenyl ring, N and H are nitrogen and hydrogen atoms, respectively, and the dot denotes an unpaired electron delocalized on the repeat unit [1182–1189]. Thus, the electronic structure corresponds to that of a metal with the highest occupied band three-quarters filled [1185].

Although the protonated emeraldine salt is known to exhibit many properties characteristic of the metallic state, polyaniline typically does not exhibit the traditional signatures of metallic transport. The “nonmetallic” temperature dependence of the resistivity and of the thermopower arises from a combination of mesoscale inhomogeneity associated with phase segregation [1186] and molecular-scale disorder [1182, 1183]. Both are introduced during the doping process, and are indicative of the quality of the material. As a result, the conducting form of PANI has been categorized either as a granular metal [1187, 1188] containing “metallic islands” [1186] or as a disordered conductor [1189] in which the electronic states at the Fermi energy are localized.

Functionalized sulfonic acids have been used to protonate PANI and to induce solubility in the conducting form [129, 1189]. Solution processing of corresponding emeraldine salts (with surfactants as counterions) has greatly improved the homogeneity of the material and has resulted in a significant decrease in the extent of molecular-scale disorder [1119, 1120]. The ability to process the conducting form of polyaniline from solution has enabled us to obtain high-quality freestanding films of PANI protonated with camphor sulfonic acid (CSA) appropriate for optical reflectance studies.

Optical Spectra. Figure 150 shows the reflectance spectra (0.006–6.0 eV) of a freestanding PANI–CSA film in the metallic regime as confirmed by complete transport measurements [1160]. At 10 K, the reflectance is greater than 80% in the far-IR ($\omega \leq 100 \text{ cm}^{-1}$) and drops rapidly throughout the mid-IR to a minimum near 1.4 eV. This 1.4-eV minimum is indicative of a free-carrier plasma resonance characteristic of metal-like behavior. The high reflectance in the far-IR and the plasma resonance near 1.4 eV are traditional signatures of metallic behavior [1080]. Above the minimum, the spectrum is featureless to 6 eV, except for the weak structure around 2.8 eV associated with the interband transition (well known in absorption spectra) [1182–1185]. Obvious phonon features appear throughout the IR (500–2000 cm^{-1}).

The implications of the reflectivity spectra become clear when the optical conductivity, $\sigma(\omega)$, is obtained through the Kramers–Kronig transformation. Figure 151 shows $\sigma(\omega)$ over the spectral range below 1.5 eV [1160]. Although the results imply intraband Drude-like excitations centered at $\omega = 0$ (there is no energy gap), the optical conductivity deviates from the normal Drude behavior at low energies; below about 0.2 eV, $\sigma(\omega)$ decreases toward

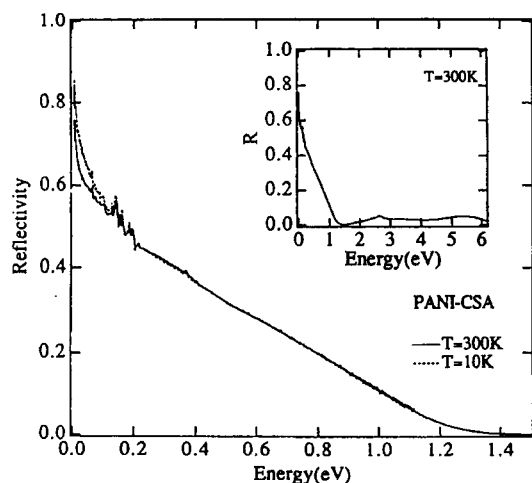


Fig. 150. Reflectance spectra of PANI-CSA freestanding films measured at room temperature (solid curve) and 10 K (dotted curve). The inset shows the spectra as measured up to 4 eV. Reproduced by permission of the American Physical Society from K. Lee, A. J. Heeger, and Y. Cao, *Phys. Rev. B* 48, 14884 (1993). Copyright © 1993, American Physical Society.

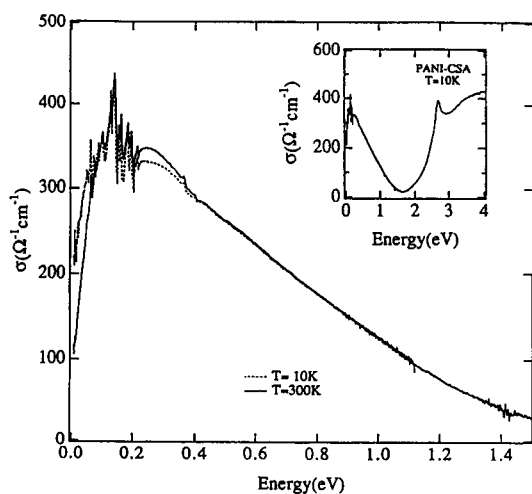


Fig. 151. Optical conductivity, $\sigma(\omega)$, of PANI-CSA obtained from a Kramers-Kronig transformation of the reflectivity data for 10 K (dotted line) and 300 K (solid line). The inset shows $\sigma(\omega)$ over the extended spectral range up to 4 eV, including the low-frequency intraband (metal-like) contribution and the onset of the lowest interband transition near 2.5 eV. Reproduced by permission of the American Physical Society K. Lee, A. J. Heeger, and Y. Cao, *Phys. Rev. B* 48, 14884 (1993). Copyright © 1993, American Physical Society.

the dc value (with phonon features superposed). In fact, the conductivity extrapolated to $\omega = 0$ is in good agreement with that actually measured on this sample ($\sigma_{dc} = 230 \text{ S cm}^{-1}$). This low-frequency behavior arises from molecular-scale disorder, as explicitly explained in the following section.

Above the 1.4-eV minimum, $\sigma(\omega)$ starts to increase again around 2.5 eV, corresponding to the onset of interband transition, and evolves a peak at 2.8 eV. The 2.8-eV peak is consistent with previous spectroscopic results obtained from the emeraldine salt [1182–1185]. For a metal, the onset of interband absorption is associated with transitions from the Fermi surface to the next higher

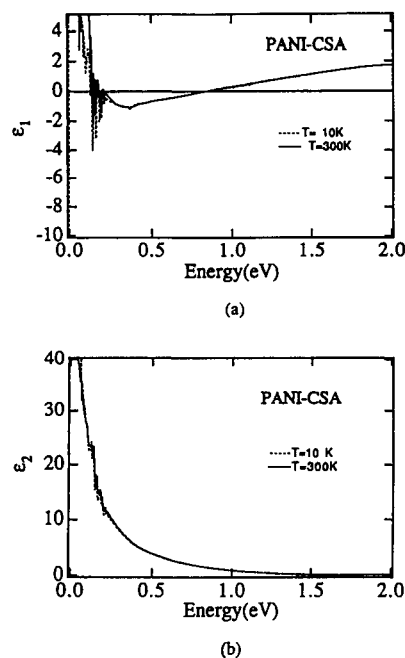


Fig. 152. (a) Real part and (b) imaginary part of the dielectric function, $\epsilon(\omega) = \epsilon_1 + i\epsilon_2$, of PANI-CSA obtained from a Kramers-Kronig transformation of the reflectivity data. Note that the real part of the dielectric function crosses 0 twice, at $\sim 0.8 \text{ eV}$ and again at $\sim 0.2 \text{ eV}$; $\epsilon_1(\omega)$ is positive below 0.2 eV. Reproduced by permission of the American Physical Society from K. Lee, A. J. Heeger, and Y. Cao, *Phys. Rev. B* 48, 14884 (1993). Copyright © 1993, American Physical Society.

empty band or with transitions from a lower lying filled band to the Fermi surface [1180]. Based on the band calculation [1185], the 2.8-eV peak corresponds to the transition from the second highest valence band to the polaron band containing the Fermi surface.

The dielectric function, $\epsilon(\omega) = \epsilon_1 + i\epsilon_2$, and the loss function, $\text{Im}[-1/\epsilon(\omega)]$, can also be obtained by a Kramers-Kronig transformation of the reflectivity spectrum. The real and imaginary parts of the dielectric functions are shown (for energies below 2.0 eV) in Figure 152 [1160]. The real part of the dielectric function crosses 0 at 0.8 eV. Below 0.8 eV, ϵ_1 is negative as expected for a metal, where $\epsilon_1(\omega)$ crosses 0 at the screened plasma frequency [1190], given by $\omega_p = \Omega_p/(\epsilon_\infty)^{1/2}$, where Ω_p is the plasma frequency. However, in contrast to simple Drude behavior, the real part of the dielectric function crosses 0 again at still lower energies, and becomes positive for $\hbar\omega < 0.2 \text{ eV}$. This low-energy zero crossing in $\epsilon_1(\omega)$ occurs near the maximum in $\sigma(\omega)$ (Fig. 151).

The energy loss function, $\text{Im}[-1/\epsilon(\omega)]$ shown in Figure 153 exhibits a well-defined peak with maximum at 1.1 eV [1160]. The maximum in $\text{Im}[-1/\epsilon(\omega)]$ and the reflectivity minimum are indicative of the existence of a damped plasma edge [1191]. In simple metals, the maximum of the loss function occurs near ω_p ; collective plasma oscillations occur at energies where $\text{Im}[-1/\epsilon(\omega)]$ is large and where ϵ_1 and ϵ_2 are both small [1171]. The plasma resonance can be distinguished from an interband transition by the fact that both ϵ_1 and ϵ_2 are small in the vicinity of the maximum in the loss function.

Effective Number of Carriers. The integrated spectral weight, $N_{\text{eff}}(\omega)$, provides information on the free carriers responsible for

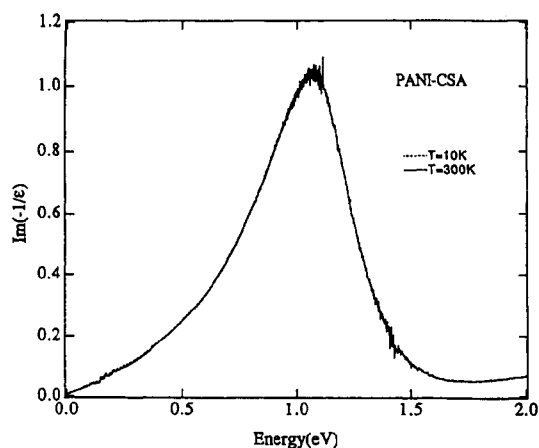


Fig. 153. Energy loss function, $\text{Im}[-1/\epsilon(\omega)]$, of PANI-CSA calculated from the real and imaginary parts of the dielectric function. Reproduced by permission of the American Physical Society from K. Lee, A. J. Heeger, and Y. Cao, *Phys. Rev. B* 48, 14884 (1993). Copyright © 1993, American Physical Society.

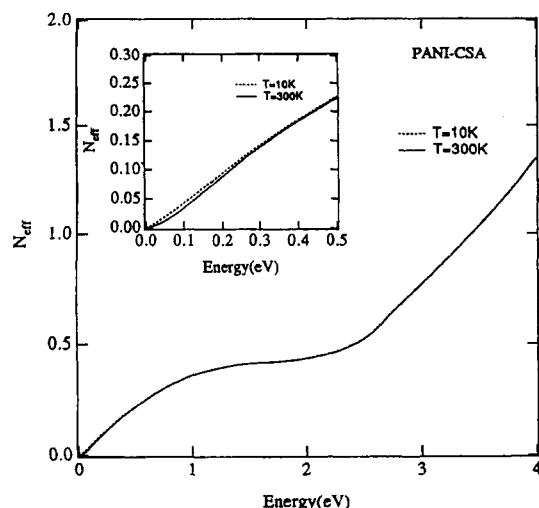


Fig. 154. Effective number of carriers per unit cell, $N_{\text{eff}}(\omega)$, as a function of energy. The effective mass was assumed to be equal to the free-electron mass. The inset shows the low-energy region with an expanded scale. Reproduced by permission of the American Physical Society from K. Lee, A. J. Heeger, and Y. Cao, *Phys. Rev. B* 48, 14884 (1993). Copyright © 1993, American Physical Society.

the Drude-like contribution to $\sigma(\omega)$:

$$N_{\text{eff}}(\omega) = (2m^*V/\pi e^2) \int \sigma(\omega') d\omega' \quad (4.17)$$

where $N_{\text{eff}}(\omega)$ is the effective number of carriers per unit cell contributing to the conductivity at frequencies below ω and V is the unit-cell volume. Figure 154 illustrates the $N_{\text{eff}}(\omega)$ calculated from $\sigma(\omega)$ for $T = 10$ and 300 K [1160]; $N_{\text{eff}}(\omega)$ increases up to 1.2 eV followed by saturation above 1.2 eV. Thus, the free-carrier oscillator strength is almost fully contained on $\sigma(\omega)$ below the plasma frequency, as in a simple metal. Above 1.2 eV, N_{eff} remains constant up to 2.5 eV, above which it increases again due to the onset of the interband transition.

From the saturation value above 1.2 eV, the effective number of carriers per unit cell, involved in the intraband Drude-like con-

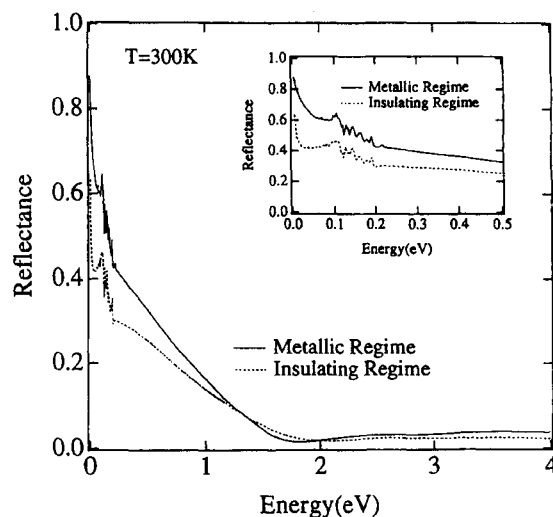


Fig. 155. Reflectance spectra of PPy-PF₆ in the metallic regime (solid line) and in the insulating regime (dotted line) measured at room temperature. The inset shows the low-energy spectra ($h\omega < 0.5$ eV) with expanded scale. Reproduced by permission of the American Physical Society from K. Lee, R. Menon, C. O. Yoon, and A. J. Heeger, *Phys. Rev. B* 52, 4779 (1995). Copyright © 1995, American Physical Society.

tribution to $\sigma(\omega)$, can be estimated; $N_{\text{eff}}(\omega) \approx 0.5$ per unit cell (two rings) when m^* is taken as the free-electron mass m_e [1160, 1161]. Since the chemistry quite clearly indicates one free carrier per unit cell, the optical mass (the effective mass averaged over the occupied states) is approximately $2m_e$. The resulting value for N_{eff} yields a charge-carrier density of $2.4 \times 10^{21} \text{ cm}^{-3}$, in excellent agreement with the $2.3 \times 10^{21} \text{ cm}^{-3}$ obtained from theory based on the calculated band structure [1185] and magnetic susceptibility [1192, 1193].

4.2.3.2. PPy-PF₆

When electrochemically synthesized at low temperatures under rigorous conditions, polypyrrole (PPy) doped with PF₆, hereafter simply denoted as PPy-PF₆, exhibits improved transport properties, achieving a higher dc conductivity at room temperature ($\sigma_{\text{dc}}(300 \text{ K}) \approx 200\text{--}500 \text{ S cm}^{-1}$) and a weaker temperature dependence of σ_{dc} than observed previously in doped polypyrrole [1158, 1194]. Transport studies [46, 1136] on this system have been successful in characterizing the extent of disorder in terms of the temperature dependence of the resistivity, $\rho(T)$, more specifically, the resistivity ratio, $\rho_r \equiv \rho(1.4 \text{ K})/\rho(300 \text{ K})$, and classified the materials into the metallic regime, the critical regime, and the insulating regime as explained previously.

Optical Spectra. Figure 155 shows the reflectance (R) of PPy-PF₆ for samples in the metallic regime and for samples in the insulating regime, measured at room temperature [1162]. Both spectra exhibit a reflectance minimum, around 1.8 eV for the metallic regime and 2 eV for the insulating regime, indicative of a plasma resonance due to free carriers in the conduction band. Below the minimum, R increases monotonically with decreasing frequency, with a rapid rise below 0.2 eV as $\omega \rightarrow 0$. For the metallic regime, R reaches almost 85% in the far-IR ($\omega \leq 100 \text{ cm}^{-1}$). The high reflectance in the far-IR and the free-carrier plasma resonance

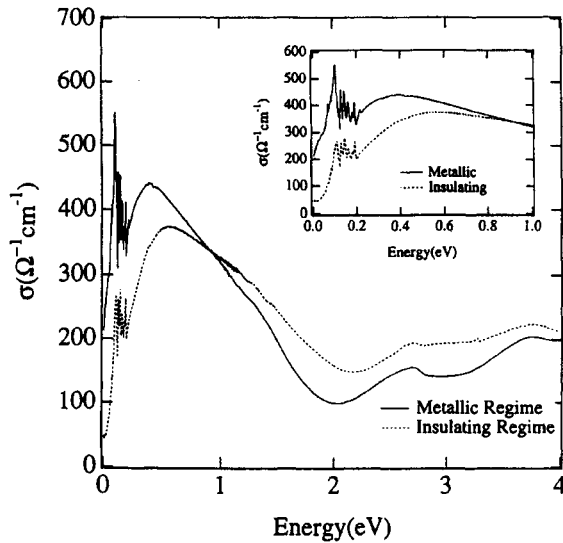


Fig. 156. Optical conductivity, $\sigma(\omega)$, of PPY-PF₆ in the metallic regime (solid line) and in the insulating regime (dotted line), obtained from KK analysis of the reflectivity data. The inset shows the spectra in the IR ($h\omega < 1$ eV) with expanded scale. Reproduced by permission of the American Physical Society from K. Lee, R. Menon, C. O. Yoon, and A. J. Heeger, *Phys. Rev. B* 52, 4779 (1995). Copyright © 1995, American Physical Society.

are traditional signatures of metallic behavior, as demonstrated already in the case of PANI-CSA. For the insulating regime, R also increases with decreasing frequency for $h\omega < 2$ eV, but $R(\omega)$ remains well below that of the metallic regime throughout the IR ($h\omega < 1$ eV).

Figure 156 shows $\sigma(\omega)$ of PPY-PF₆ for $h\omega < 4$ eV [1162]. As expected from the characteristic metallic features in $R(\omega)$ for both regimes, $\sigma(\omega)$ is dominated by intraband excitations (within the conduction band) for $h\omega < 2$ eV; interband transitions are observed at 2.7 and 3.7 eV. The similarity in the spectral features for samples from the two regimes indicates their common electronic band structure.

In spite of the characteristic metallic signatures in the reflectance spectra, however, the corresponding $\sigma(\omega)$ are not typical of a good metal, as with PANI-CSA. Even for the metallic regime, $\sigma(\omega)$ deviates considerably from the normal Drude behavior below 0.4 eV; in contrast to Drude behavior, $\sigma(\omega)$ is suppressed as $\omega \rightarrow 0$. This decrease in $\sigma(\omega)$ also arises from weak localization, as demonstrated in PANI-CSA [1160, 1161]. For the insulating regime, however, $\sigma(\omega)$ is suppressed even more at low frequencies, indicating that the states near E_F in the conduction band are localized. This localization arises from disorder in the context of Anderson localization [1125, 1156, 1157].

Figure 157 shows $\epsilon_1(\omega)$ for both regimes [1162]. Consistent with $\sigma(\omega)$, $\epsilon_1(\omega)$ for the metallic regime does not follow the behavior expected of a pure Drude metal. Instead, $\epsilon_1(\omega)$ remains positive over the entire spectral range below the plasma frequency (ω_p) and increases to larger positive values as $\omega \rightarrow 0$. This non-Drude behavior is again associated with disorder-induced localization, similar to the PANI-CSA case [1160, 1161]. For the insulating regime, $\epsilon_1(\omega)$ exhibits large positive values below 0.8 eV, indicative of localization of the states near E_F .

For a good metal with $\omega_p\tau > 1$ (where τ is the momentum relaxation time), $\epsilon_1(\omega)$ is expected to cross 0 at ω_p . At low frequencies, $\epsilon_1(\omega) \propto -(\omega_p/\omega)^2$ for $\omega > 1/\tau$ and $\epsilon_1(\omega) \approx -(\omega_p\tau)^2$

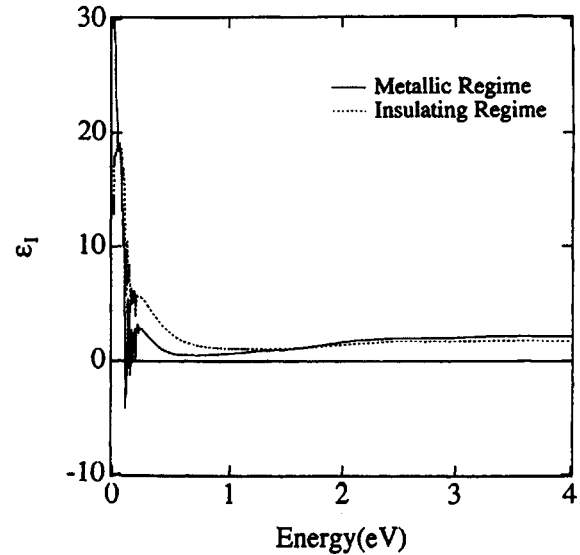


Fig. 157. Real part of the dielectric function, $\epsilon_1(\omega)$, of PPY-PF₆ in the metallic regime (solid line) and in the insulating regime (dotted line). Reproduced by permission of the American Physical Society from K. Lee, R. Menon, C. O. Yoon, and A. J. Heeger, *Phys. Rev. B* 52, 4779 (1995). Copyright © 1995, American Physical Society.

for $\omega < 1/\tau$ [1171, 1190, 1191]. However, in “dirty metals” with $\omega_p\tau \sim 1$, the plasma oscillation is overdamped, preventing even the zero crossing at ω_p . As a result, $\epsilon_1(\omega)$ remains positive at all frequencies. This is the case for PPY-PF₆. The damping of the plasma resonance is evident in the spectral shape of the energy loss function, $\text{Im}[-1/\epsilon(\omega)]$, as shown in Figure 158 [1162]. In the metallic regime, $\text{Im}[-1/\epsilon(\omega)]$ exhibits a well-defined peak with a maximum at 1.4 eV with full width at half-maximum (fwhm) of approximately 1 eV, corresponding to $\omega_p\tau \approx 1$. For the insulating regime, the fwhm is even larger, consistent with an overdamped plasma oscillation.

Effective Number of Carriers. Figure 159 illustrates $N_{\text{eff}}(\omega)$ for both regimes as calculated by Eq. (4.17) [1162]; $N_{\text{eff}}(\omega)$ shows similar behavior for both regimes. The only difference is observed at low energies due to the severe suppression of $\sigma(\omega)$ for the insulating regime. $N_{\text{eff}}(\omega)$ increases smoothly up to $h\omega = 2$ eV, and shows a slight saturation for 2.0 eV $< h\omega < 2.5$ eV, consistent with exhausting the intraband oscillator strength. $N_{\text{eff}}(\omega)$ increases again at higher energies due to the onset of interband transitions. Since the oscillator strength associated with the intraband excitations is fully contained below 2.5 eV, $N_{\text{eff}} \approx 0.6(m^*/m_e)$ at 2.5 eV provides an estimate of the effective number of carriers per unit cell involved in intraband excitations within the conduction band. The X-ray structure analysis [47] indicates one free carrier per unit cell (i.e., one dopant per four pyrrole units), such that $N_{\text{eff}} = 1$ per unit cell. Therefore, the optical mass (the effective mass averaged over the occupied states) is estimated to be $m^* \approx 1.7 m_e$ [1162].

4.2.3.3. PEDOT-PF₆

In an effort to develop better transparent electrode materials, extensive studies have been directed toward new semiconducting polymer systems with low bandgap ($E_g < 1.5$ eV) [1054]. If the

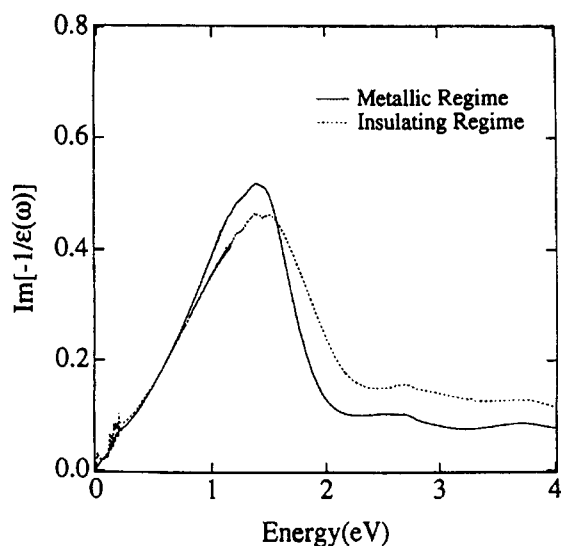


Fig. 158. Energy loss function $\text{Im}[-1/\epsilon(\omega)]$, of PPy-PF₆ in the metallic regime (solid line) and in the insulating regime (dotted line). Reproduced by permission of the American Physical Society from K. Lee, R. Menon, C. O. Yoon, and A. J. Heeger, *Phys. Rev. B* 52, 4779 (1995). Copyright © 1995, American Physical Society.

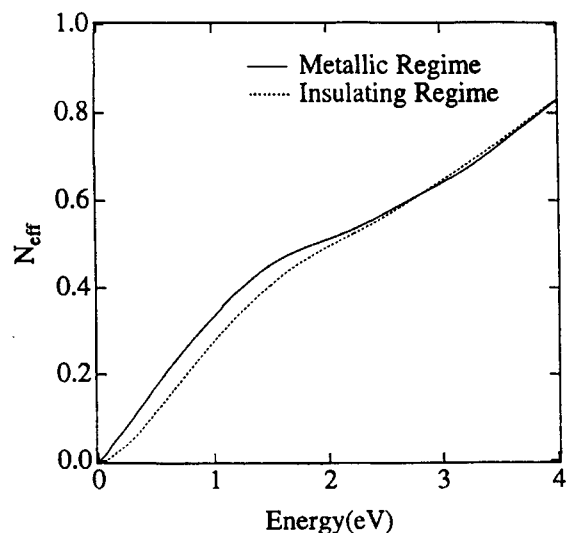


Fig. 159. Effective number of carriers per unit cell, $N_{\text{eff}}(\omega)$, as a function of energy for PPy-PF₆ in the metallic regime (solid line) and in the insulating regime (dotted line). The effective mass was assumed to be that of the free electron. Reproduced by permission of the American Physical Society from K. Lee, R. Menon, C. O. Yoon, and A. J. Heeger, *Phys. Rev. B* 52, 4779 (1995). Copyright © 1995, American Physical Society.

absorption maximum of a low-bandgap semiconducting polymer is in the middle of the near-infrared (IR) range, one can expect the absorption maximum to shift to longer wavelengths (far-IR or mid-IR) after doping. As a result, thin films of the conducting material would become transparent in the visible spectral region.

Poly(3,4-ethylenedioxythiophene) (PEDOT) is such a low-bandgap semiconducting polymer [1106, 1195, 1196]; the bandgap of PEDOT is below 1.5 eV in the undoped state. After doping, this material exhibits reduced absorption in the visible; the oscillator strength shifts from around 1.5 eV (lowest π - π^* transition) to be-

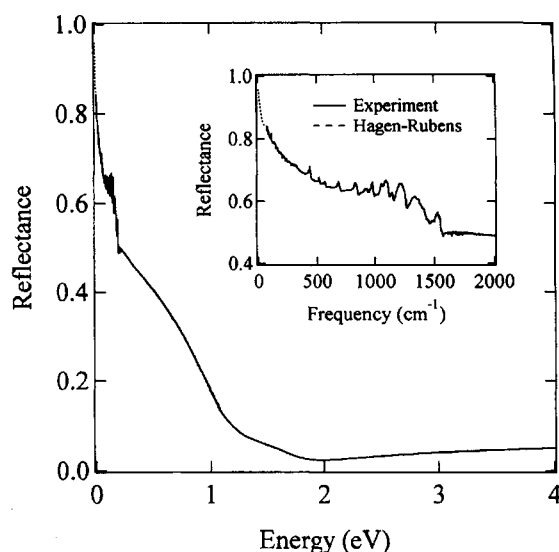


Fig. 160. Reflectance, $R(\omega)$, of freestanding PEDOT-PF₆ films. The inset shows $R(\omega)$ below 2000 cm^{-1} with an expanded scale. The dotted line in the inset below 50 cm^{-1} indicates the extrapolation by the Hagen-Rubens formula. Reproduced by permission of Elsevier Science from Y. Chang, K. Lee, R. Kiebooms, A. Aleshin, and A. J. Heeger, *Synth. Met.* 105, 203 (1999). Copyright © 1999, Elsevier Science.

low 1 eV in the metallic state. Moreover, doped PEDOT has high electrical conductivity and excellent chemical and environmental stability [1106]. These advantages make PEDOT attractive for use in transparent electrodes [1197–1199] and for use in antistatic and electromagnetic shielding materials [1195].

In the synthesis of PEDOT, competing reactions through the 3- and 4-positions (as in polythiophene) are avoided, only the 2,5-couplings of the EDOT monomer are expected. Therefore, polymerization using the EDOT monomer is expected to yield higher quality polymer with fewer defects compared to the thiophene analogs [1159]. In fact, when doped with PF₆ by electrochemical synthesis under rigorous conditions, PEDOT-PF₆ exhibits high electrical conductivity, $\sigma_{\text{dc}}(300 \text{ K}) \approx 200\text{--}300 \text{ S cm}^{-1}$, with a weak temperature (T) dependence [1109, 1140, 1159]. Detailed transport studies have demonstrated that PEDOT-PF₆ can be prepared with properties on the metallic side of the metal-insulator (M-I) transition [1109, 1140].

Reflectance. Figure 160 shows $R(\omega)$ of metallic PEDOT-PF₆ ($\rho_r = 1.67 < 2$ with $\sigma_{\text{dc}} \approx 230 \text{ S cm}^{-1}$ at 300 K) measured at room temperature [1166]. In the far-IR below 100 cm^{-1} , $R(\omega)$ is greater than 80% and drops rapidly throughout the mid-IR. Above 1.2 eV, there is a change in the slope in $R(\omega)$ with a weak shoulder around 1.5 eV and a minimum near 1.8 eV. Above the minimum, the spectrum is featureless to 4 eV. All aspects of the $R(\omega)$ for PEDOT-PF₆ are typical of metallic polymers. There is a free-carrier plasma resonance in the near-IR with $R(\omega)$ increasing toward unity at lower frequencies. In the far-IR below 100 cm^{-1} , the Hagen-Rubens (HR) approximation provides an excellent fit to $R(\omega)$ as indicated in the inset, implying a weak ω -dependence in the corresponding optical conductivity in this frequency range.

Although the spectral features are similar to those of other metallic polymers such as PANI-CSA [295, 296] and PPy-PF₆ [1162–1164], which exhibit transport properties comparable to

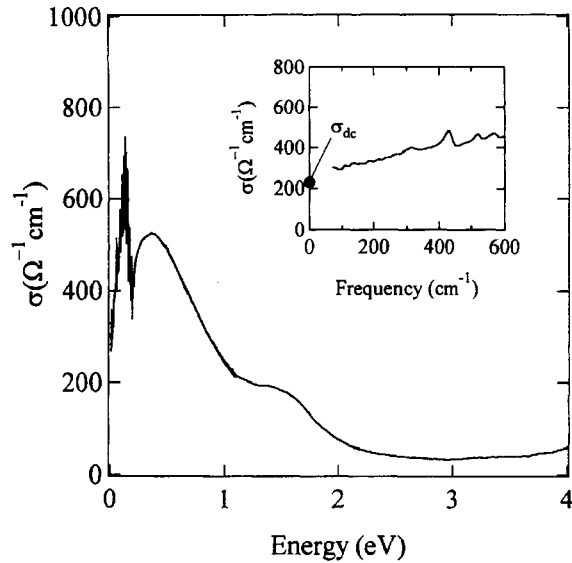


Fig. 161. Optical conductivity, $\sigma(\omega)$, of PEDOT-PF₆, as obtained from Kramers-Kronig analysis of $R(\omega)$. The inset shows the low-energy $\sigma(\omega)$ below 600 cm^{-1} with an expanded scale. Note the 1:1 correspondence between the dc conductivity (σ_{dc}), shown as the symbol at $\omega = 0$, and $\sigma(\omega \rightarrow 0)$. Reproduced by permission of Elsevier Science from Y. Chang, K. Lee, R. Kiebooms, A. Aleshin, and A. J. Heeger, *Synth. Met.* 105, 203 (1999). Copyright © 1999, Elsevier Science.

those of PEDOT-PF₆, the details of $R(\omega)$ above 1 eV show subtle differences. For PPy-PF₆ and PANI-CSA, $R(\omega)$ monotonically decreases to a minimum (1.8 eV for PPy-PF₆ [1162] and 1.4 eV for PANI-CSA [1160]) with increasing frequency. At higher frequencies, both exhibit interband transitions (2.5 eV for PPy-PF₆ [1162] and 2.8 eV for PANI-CSA [1160]). In contrast, for PEDOT-PF₆, a weak shoulder-like feature is observed around 1.5 eV [1166].

Optical Conductivity. Figure 161 displays $\sigma(\omega)$ of PEDOT-PF₆ below 4 eV [1166]. As expected from the characteristic metallic features in $R(\omega)$, $\sigma(\omega)$ is dominated by intraband excitations below 1 eV with a peak around 0.4 eV. However, a weak feature with a peak around 1.5 eV is evident with an oscillator strength that overlaps the tail of the intraband contribution. Above 2 eV, $\sigma(\omega)$ is flat and featureless with a value of $\sigma(\omega) \approx 40 \text{ S cm}^{-1}$ above 2 eV.

The peak in $\sigma(\omega)$ near 1.5 eV is attributed to an interband transition from the Fermi energy to the next higher empty band (or with a transition from a lower lying filled band to the Fermi energy) [1166]. Since this transition lies in the near-IR, at significantly lower energy than for other metallic polymers, PEDOT-PF₆ exhibits low absorption in the visible spectral range: $\sigma(\omega) \approx 40 \text{ S cm}^{-1}$ between 2 and 3 eV. This value is significantly lower than those for other metallic polymers; for PANI-CSA, $\sigma(\omega) \approx 250 \text{ S cm}^{-1}$ at 2.7 eV [1160], and for PPy-PF₆, $\sigma(\omega) \approx 150 \text{ S cm}^{-1}$ at 2.7 eV [1162]. The lower absorption for PEDOT-PF₆ demonstrates why this material has emerged as a promising candidate for use in transparent electrodes.

The low-energy features in $\sigma(\omega)$ below 1 eV are typical of the disordered metallic polymers on the metallic side of the M-I transition; $\sigma(\omega)$ decreases with decreasing ω below 0.4 eV and accurately approaches the measured $\sigma_{\text{dc}}(300 \text{ K})$ value ($\approx 230 \text{ S cm}^{-1}$), consistent with the previous studies of PANI-CSA [295, 296] and

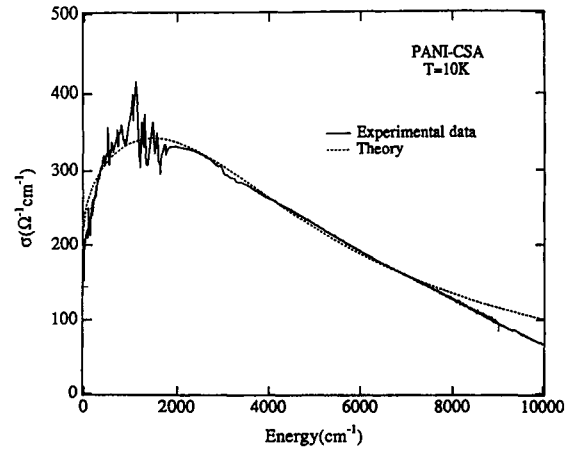


Fig. 162. Optical conductivity, $\sigma(\omega)$ (solid line), of PANI-CSA is compared with that calculated (dashed line) from the localization-modified Drude model, with the following parameters: $\Omega_p = 9970 \text{ cm}^{-1}$ (1.17 eV), $1/\tau = 4340 \text{ cm}^{-1}$ (0.51 eV), and $k_F \Lambda = 1.6$. Reproduced by permission of the American Physical Society from K. Lee, A. J. Heeger, and Y. Cao, *Phys. Rev. B* 48, 14884 (1993). Copyright © 1993, American Physical Society.

PPy-PF₆ [1162–1164]. The suppression of $\sigma(\omega)$ as $\omega \rightarrow 0$ (below 0.4 eV) is attributed to weak localization induced by disorder in the context of the Anderson transition. This is also consistent with the transport studies on this system, confirming that PEDOT-PF₆ is a disordered metal near the border of the M-I transition [1109, 1140].

4.2.4. Localization-Modified Drude Model

Although the overall low-frequency spectral response of all metallic conducting polymers, such as PANI-CSA, PPy-PF₆, and PEDOT-PF₆, can be attributed to free-carrier intraband excitations, their $\sigma(\omega)$ and $\epsilon_1(\omega)$ are not typical of normal Drude-like behavior below 0.2 eV [1160–1165]. The anomalous behavior of $\sigma(\omega)$ and $\epsilon_1(\omega)$ in the low energies (typically below 0.2–0.4 eV) can be attributed to disorder-induced localization, and can be analyzed in terms of the localization-modified Drude (LMD) model [1160–1165]. This LMD model, originally proposed by Mott and co-workers [1125, 1156, 1157], has been modified by Lee et al. [1160] and successfully introduced into the analysis of optical spectra of metallic conducting polymers [1160–1165]. This model is a first-order correction of the Drude model in the regime of weak localization, as given by [1160]

$$\sigma_{\text{LD}}(\omega) = \sigma_{\text{Drude}}(\omega) \{1 - [C/(k_F \Lambda)]^2 [1 - \Lambda/L_\omega]\} \quad (4.18)$$

where Λ is the mean free path ($\Lambda = v_F \tau$ and v_F is the Fermi velocity), k_F is the Fermi wave vector, and L_ω is the distance scale over which an electron diffuses within a period of the incident radiation field. The constant C is not known exactly, but the magnitude of C is of order unity. The value of L_ω is given by the diffusion coefficient, $D = \Lambda^2/3\tau$, and the optical frequency ω using the diffusion equation, $L_\omega = (D/\omega)^{1/2}$.

PANI-CSA. The optical conductivity spectrum of PANI-CSA (Fig. 151) is fitted with the LMD model as shown in Figure 162 [1160], and is in good agreement in the intraband region below 1 eV. The best fit is obtained with the following parameters:

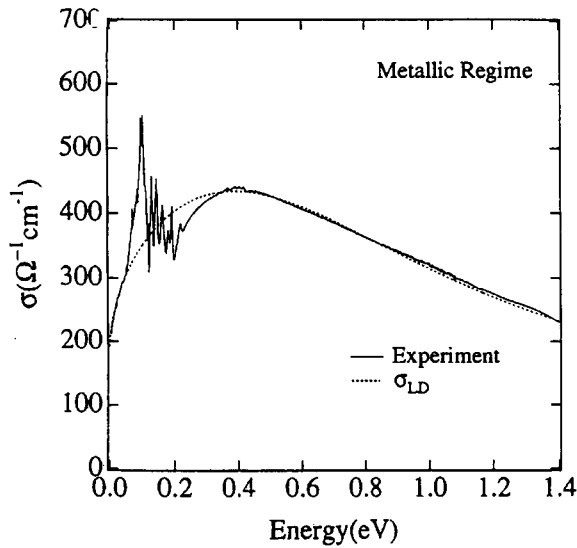


Fig. 163. Comparison of the measured $\sigma(\omega)$ (solid line) of PPy-PF₆ in the metallic regime at 300 K with that calculated (dotted line) from the localization-modified Drude model, with the following parameters: $\Omega_p = 14,200 \text{ cm}^{-1}$ (1.8 eV), $1/\tau = 9600 \text{ cm}^{-1}$ (1.2 eV), and $k_F\Lambda = 1.6$. Reproduced by permission of the American Physical Society from K. Lee, R. Menon, C. O. Yoon, and A. J. Heeger, *Phys. Rev. B* 52, 4779 (1995). Copyright © 1995, American Physical Society.

$\Omega_p = 9970 \text{ cm}^{-1}$ (1.17 eV), $1/\tau = 4340 \text{ cm}^{-1}$ (0.51 eV), and $k_F\Lambda = 1.6$ with an assumption of $C = 1$. These parameters are reasonable. The plasma frequency is close to that obtained from the reflectance minimum ($\approx 1.4 \text{ eV}$) and the peak in the loss function ($\approx 1.1 \text{ eV}$). The value of $k_F\Lambda$ ($= 1.6$) indicates that PANI-CSA is not a good metal [1160]. Instead, this fact supports that PANI-CSA is on the metal-insulator boundary and approaching the Ioffe-Regel limit. Moreover, the deviations from simple Drude behavior in the far-IR are quantitatively consistent with the LMD model [1160, 1161]. As indicated by Eq. (4.18), localization depresses $\sigma(\omega)$ below the Drude curve in the far-IR.

PPy-PF₆. Figure 163 also illustrates the excellent agreement of the LMD model with the data for PPy-PF₆ in the metallic regime with the following parameters: $\Omega_p = 14,200 \text{ cm}^{-1}$ (1.8 eV), $1/\tau = 9600 \text{ cm}^{-1}$ (1.2 eV), and $k_F\Lambda = 1.6$ [1162]. Such analysis by the LMD model provides information on the charge dynamics of the free carriers in the conduction band. The parameters obtained from the curve fitting are reasonable and in good agreement with other experimental results. The screened plasma frequency, $\omega_p = \Omega_p/(\infty)^{1/2} \approx 1.7 \text{ eV}$, is in good agreement with the observed reflectance minimum around 1.8 eV [1162]. As expected from the extremely broad $\sigma(\omega)$, the large scattering rate ($1/\tau = 1.2 \text{ eV}$) leads to $\omega_p\tau \approx 1.5$. Such a small value of $\omega_p\tau$ indicates overdamping of the plasma resonance, resulting in $\varepsilon_1(\omega) > 0$ over the entire intraband energy range. The optical mass is calculated to be $m^* = 1.7m_e$ from the relation $\Omega_p = (4\pi ne^2/m^*)^{1/2}$. This value is in excellent agreement with that obtained from the $N_{\text{eff}}(\omega)$ analysis. Such consistency is expected because of the oscillator strength sum rule existing between the integrated intraband oscillator strength, $N_{\text{eff}}(\omega)$, and Ω_p [1172]. The LMD model yields an estimate of the dc conduc-

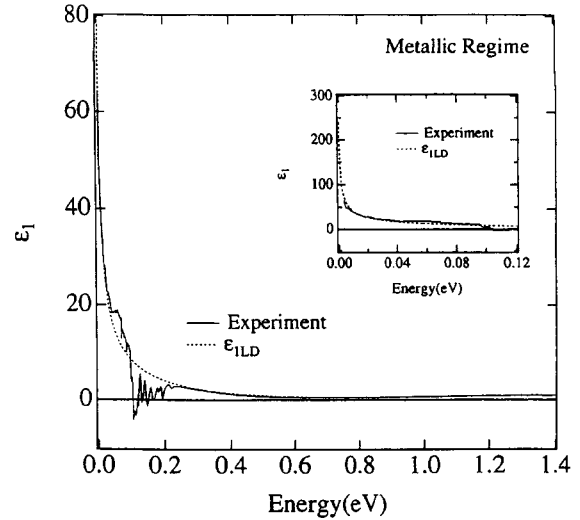


Fig. 164. Comparison of the measured $\varepsilon_1(\omega)$ (solid line) of PPy-PF₆ in the metallic regime with the theoretical prediction of the localization-modified Drude model (dotted line) obtained from the Kramers-Kronig transformation of $\sigma_{LD}(\omega)$. The inset shows the low-energy part on an expanded scale. Reproduced by permission of the American Physical Society from K. Lee, R. Menon, C. O. Yoon, and A. J. Heeger, *Phys. Rev. B* 52, 4779 (1995). Copyright © 1995, American Physical Society.

tivity, given as the $\omega = 0$ limit of Eq. (4.18),

$$\sigma_{LD}(0) = \sigma_{\text{Drude}}(0)[1 - C/(k_F\Lambda)^2] \quad (4.19)$$

with $\sigma_{\text{Drude}}(0) = (1/4\pi)\Omega_p^2\tau$, so that one finds $\sigma_{LD}(0) \approx 200 \text{ S cm}^{-1}$, in good agreement with the experimentally observed $\sigma(\omega \rightarrow 0)$ [1162].

In the studies of localization, $k_F\Lambda$ is an important parameter that characterizes the extent of disorder, often considered as an order parameter for disordered systems [1125, 1126, 1156, 1157, 1200]. One of the advantages for the analysis using the LMD model lies in the direct assessment of $k_F\Lambda$. The $k_F\Lambda \approx 1.6$ obtained from the curve-fitting procedure clearly indicates that PPy-PF₆ is not a good metal. This parameter yields an estimation for the mean free path $\Lambda \approx 10 \text{ \AA}$, comparable to the repeat unit along the polymer chain. Such a short mean free path confirms once again the breakdown of the normal Drude model for describing PPy-PF₆.

The corresponding $\varepsilon_1(\omega)_{LD}$ for the LMD model can be obtained through the Kramers-Kronig transformation of $\varepsilon_2(\omega)_{LD} = 4\pi\sigma_{LD}(\omega)/\omega$ [1172]. Figure 164 shows that the calculated $\varepsilon_1(\omega)_{LD}$ is in excellent agreement with the measured $\varepsilon_1(\omega)$ with $\varepsilon_\infty \approx 1.1$ [1160]. As evident in the calculated $\varepsilon_1(\omega)_{LD}$, the increase of $\varepsilon_1(\omega)$ as $\omega \rightarrow 0$ for $h\omega < 0.2 \text{ eV}$ is associated with the weak localization effect corresponding to the suppression of $\sigma_{LD}(\omega)$ at low frequencies. The calculated $\varepsilon_1(\omega)_{LD}$ predicts a rapid increase in $\varepsilon_1(\omega)$ as $\omega \rightarrow 0$ in the extrapolated region ($\omega < 20 \text{ cm}^{-1}$), implying a divergence in ε_1 as $\omega \rightarrow 0$. This divergence is associated with the "dielectric catastrophe," a signature of the M-I transition [1201-1203].

PEDOT-PF₆. Consistent with metallic PANI-CSA [1160] and PPy-PF₆ [1162], the optical spectra of PEDOT-PF₆ are also dominated by weak localization induced by disorder in the context of the Anderson transition [1165]. Therefore, even for PEDOT-

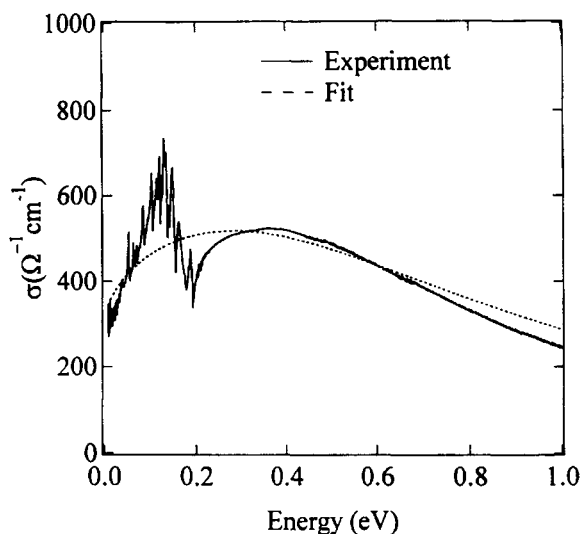


Fig. 165. Comparison of the measured $\sigma(\omega)$ (solid line) of PEDOT-PF₆ with that calculated (dashed line) from the localization-modified Drude model, with the following parameters: $\Omega_p = 9600 \text{ cm}^{-1}$ (1.2 eV), $1/\tau = 6200 \text{ cm}^{-1}$ (0.8 eV), and $k_F\Lambda = 1.6$. Reproduced by permission of Elsevier Science from Y. Chang, K. Lee, R. Kiebooms, A. Aleshin, and A. J. Heeger, *Synth. Met.* 105, 203 (1999). Copyright © 1999, Elsevier Science.

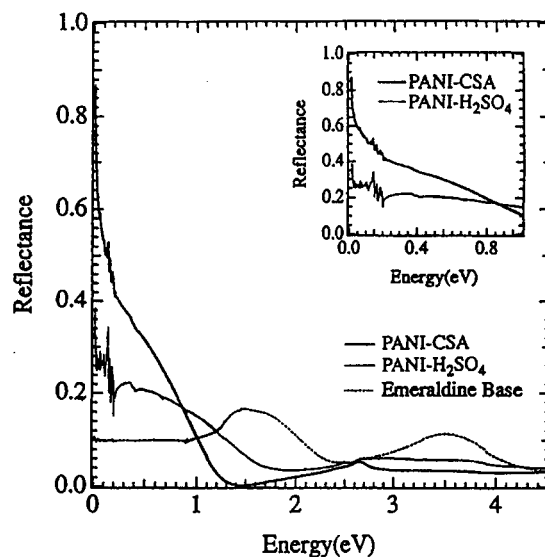


Fig. 166. Reflectance spectra of PANI-CSA (thick solid line), PANI-H₂SO₄ (thin solid line), and the emeraldine base (dotted line) at room temperature. The inset shows the low-energy region for PANI-CSA and PANI-H₂SO₄ with an expanded scale. Reproduced by permission of Elsevier Science from K. Lee, A. J. Heeger, and Y. Cao, *Synth. Met.* 72, 25 (1995). Copyright © 1995, Elsevier Science.

PF₆ the optical constants can be accurately described by the LMD model, as shown in Figure 165 [1165], with the following parameters: $\Omega_p = 9600 \text{ cm}^{-1}$ (1.2 eV), $1/\tau = 6200 \text{ cm}^{-1}$ (0.8 eV), and $k_F\Lambda = 1.6$. These parameters are also reasonable and consistent with the transport measurement results. The plasma frequency, $\Omega_p = 9600 \text{ cm}^{-1}$ (1.2 eV), and scattering time ($\tau \approx 10^{-14}$ – 10^{-15} s) are typical of disordered metals. Although the minimum in $R(\omega)$ is at 1.8 eV in Figure 160, the best fit indicates that the plasma frequency is 1.2 eV. Evidently, the low-energy interband feature with onset below 1.5 eV shifts the minimum in $R(\omega)$. The value of $k_F\Lambda$ (= 1.6) implies that PEDOT-PF₆ is “metallic,” but close to the M–I transition. The excellent success in describing the IR spectral features of PEDOT-PF₆, PPY-PF₆, and PANI-CSA in terms of the LMD model confirms the validity of the LMD model and demonstrates the general applicability of the model to metallic polymers.

4.2.5. Metal–Insulator Transition in Optical Spectra

4.2.5.1. Polyaniline

Polyaniline (PANI) can be converted from the semiconducting emeraldine base form to the conducting emeraldine salt form either by charge-transfer doping or by protonation [1181]. Upon exposure of emeraldine base to protonic acids, the $-N=$ sites are protonated, leading to the formation of doubly charged, spinless bipolarons. These bipolarons are unstable with respect to the formation of two polarons through an internal redox reaction [1183, 1184]. Thus, the polaron lattice model was suggested as a description of the electronic structure of the conducting emeraldine salt [1185]. The internal redox reaction, described as “proton-induced spin unpairing” [1184], leads to one unpaired electron per formula unit, and thereby to the electronic structure of a metal. The temperature-independent Pauli susceptibility of the emeraldine

salt is consistent with the proposed metallic polaron lattice, with a finite density of states at the Fermi level [1192].

Although the protonated emeraldine salt is known to exhibit many properties characteristic of the metallic state [1185, 1192], initial studies yielded transport properties that are not typical of those of a metal [1184–1186]. Instead, the conductivity was found to be activated, and the thermoelectric power showed a complex temperature dependence [1205]. These “nonmetallic” transport properties arise from a combination of a mesoscopic and molecular-scale disorder generated during synthesis and doping of the material.

In this section, the reflectance of metallic PANI-CSA is compared with that of the semiconducting polyaniline (emeraldine base) and the conventional emeraldine salt, PANI protonated with H₂SO₄ (PANI-H₂SO₄), which is classified as a typical insulating-regime material in a doped polyaniline system [1161]. In particular, in order to better understand the role of disorder in the conducting emeraldine salt, the discussion focuses on a comparison of the data obtained from PANI-H₂SO₄ with those obtained from PANI-CSA [1161].

Reflectance. Figure 166 shows the reflectance spectra of PANI-CSA, PANI-H₂SO₄, and the emeraldine base, all obtained with samples at room temperature [1161]. For the emeraldine base, two broad peaks are observed, centered at 1.6 and 3.5 eV, respectively. Upon protonation and conversion to the emeraldine salt, the two spectral features of the emeraldine base disappear as shown in the spectra obtained for PANI-CSA and PANI-H₂SO₄. Two new spectral features develop in both PANI-CSA and PANI-H₂SO₄, a low-frequency reflectance below 1 eV and a higher energy spectral feature around 2.7 eV. For PANI-CSA, the reflectance is greater than 80% in the far-IR and drops rapidly throughout the IR to the minimum near 1.4 eV, as shown in the previous section. This 1.4-eV minimum is indicative of a free-carrier plasma resonance

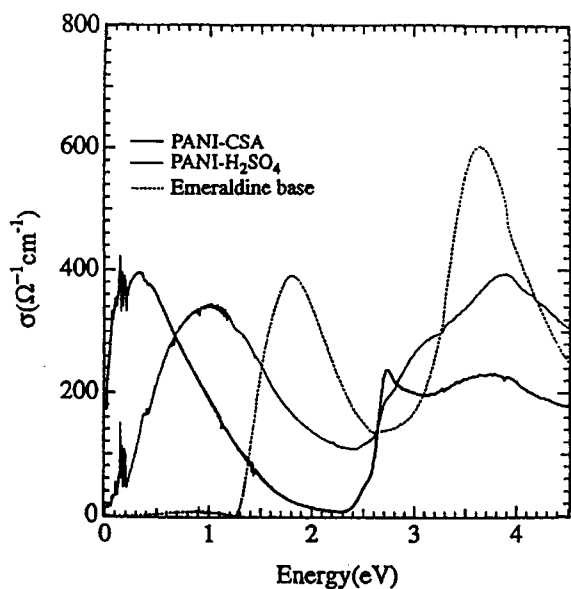


Fig. 167. Optical conductivity of PANI-CSA (thick solid line), PANI-H₂SO₄ (thin solid line), and the emeraldine base (dotted line) obtained from a Kramers–Kronig analysis of the reflectance data. Reproduced by permission of Elsevier Science from K. Lee, A. J. Heeger, and Y. Cao, *Synth. Met.* 72, 25 (1995). Copyright © 1995, Elsevier Science.

[1160]. The plasma resonance and high reflectance in the far-IR are traditional signatures of metallic behavior.

For PANI-H₂SO₄, the reflectance shows a minimum around 1.8 eV and increases substantially with decreasing frequency, but remains well below that of PANI-CSA in the far-IR. The IR reflectance implies that the low-frequency response of PANI-H₂SO₄ also results from intraband excitations associated with the partially filled conduction band, as in PANI-CSA.

Optical Conductivity. The results of the Kramers–Kronig analysis are shown in Figure 167 for PANI-CSA, PANI-H₂SO₄, and the emeraldine base [1161]. For the emeraldine base, $\sigma(\omega)$ shows a spectral response typical of that expected for a semiconductor; there is a clear gap with $\sigma(\omega) \approx 0$ below 1.3 eV. Two distinct peaks associated with interband transitions are observed at 1.8 and 3.7 eV. Previous studies, including both band calculations [1185] and experimental results [1182, 1205], have demonstrated that the 1.8-eV peak is associated with the localized quinoid structure of the emeraldine base, while the 3.7-eV feature corresponds to the π - π^* transition.

Upon protonation and conversion to the emeraldine salt, qualitative changes in the spectra are evident; the 1.8-eV peak disappears and the amplitude of the 3.7-eV peak decreases. Two new features develop for both PANI-CSA and PANI-H₂SO₄. For PANI-CSA, $\sigma(\omega)$ has a sharp peak at 2.7 eV and increases monotonically with decreasing frequency, reaching a maximum in the IR at around 0.2 eV. Although the low-frequency spectral response is attributable to the intraband excitations (free carriers in the conduction band), deviations from the normal Drude behavior are observed at the lowest frequencies, as discussed in the previous section [1160]. Below 0.2 eV, $\sigma(\omega)$ is suppressed toward the dc value from weak localization due to disorder [1160]. In contrast, for PANI-H₂SO₄, $\sigma(\omega)$ has a broad maximum at 1 eV and decreases rapidly with frequency in the IR.

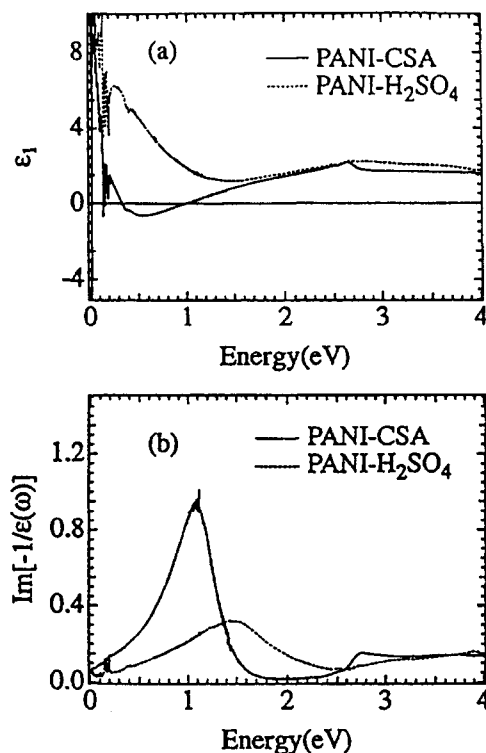


Fig. 168. (a) Real parts of the dielectric function, $\varepsilon(\omega) = \varepsilon_1(\omega) + i\varepsilon_2(\omega)$, and (b) energy loss function, $\text{Im}[-1/\varepsilon(\omega)]$, of PANI-CSA (solid line) and PANI-H₂SO₄ (dotted line). Reproduced by permission of Elsevier Science from K. Lee, A. J. Heeger, and Y. Cao, *Synth. Met.* 72, 25 (1995). Copyright © 1995, Elsevier Science.

Dielectric Function. Figure 168a shows $\varepsilon_1(\omega)$ for PANI-CSA and PANI-H₂SO₄ [1043]. While the $\varepsilon_1(\omega)$ of PANI-H₂SO₄ remains positive over the entire energy range, that of PANI-CSA crosses 0 at 1.0 eV to negative values [1160]. For a metal, ε_1 is expected to cross 0 at the screened plasma frequency, and follows $\varepsilon_1 \propto -(\omega_p/\omega)^2$ at low frequencies. For PANI-CSA, however, ε_1 crosses 0 again at 0.2 eV and becomes positive for $\hbar\omega < 0.2$ eV. This deviation from simple Drude behavior at low frequencies was attributed to weak localization in PANI-CSA [1160]. For PANI-H₂SO₄, however, the disorder completely dominates; the plasma oscillations are damped such that $\omega_p\tau \approx 1$, thus preventing even the zero crossing at the plasma frequency [1161].

The damping of the plasma oscillations is demonstrated more clearly in Figure 168b, which shows the energy loss functions of PANI-CSA and PANI-H₂SO₄ [1161]. For PANI-CSA, $\text{Im}[-1/\varepsilon(\omega)]$ exhibits a well-defined peak with a maximum at 1 eV and a full width at half-maximum (fwhm) of 0.5 eV; i.e., $\omega_p\tau > 1$. For PANI-H₂SO₄, however, $\text{Im}[-1/\varepsilon(\omega)]$ shows a relatively weak, broad peak with a maximum at 1.5 eV and an fwhm approximately 1.5 eV; i.e., $\omega_p\tau < 1$. For PANI-CSA, the maximum of the energy loss function (1 eV) is in good agreement with the zero crossing of ε_1 (at ≈ 1 eV) [1160]; for PANI-H₂SO₄, however, there is no zero crossing [1161].

Role of Disorder in Conducting Polyaniline: Evolution from Fermi Glass to Disordered Metal. Although the IR spectrum of PANI-H₂SO₄ indicates that the low-energy response arises from intraband excitations in the conduction band, the optical spectra are not those of a typical metal. Instead, the charge carriers are local-

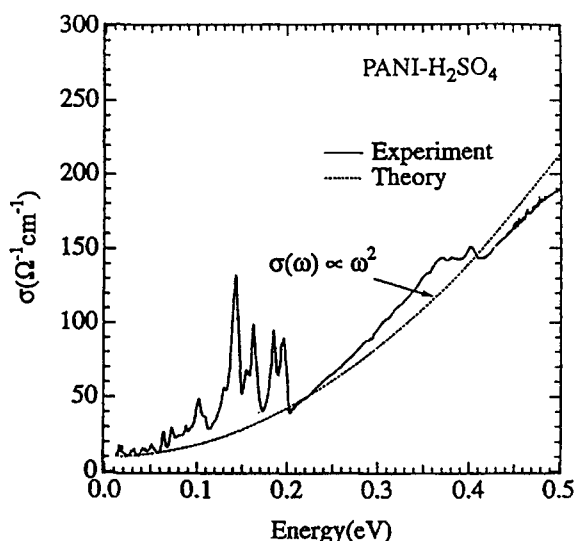


Fig. 169. Comparison of the measured optical conductivity $\sigma(\omega)$ (solid line) of PANI-H₂SO₄ with theoretical prediction (dashed line). Reproduced by permission of Elsevier Science from K. Lee, A. J. Heeger, and Y. Cao, *Synth. Met.* 72, 25 (1995). Copyright © 1995, Elsevier Science.

ized, as demonstrated by the measured $\epsilon_1(\omega)$ and $\sigma(\omega)$. As a consequence, PANI-H₂SO₄ can be categorized as a Fermi glass, in which the electronic states at the Fermi energy (E_F) are localized due to disorder as described by Anderson localization [1125, 1156, 1157, 1177]. In such a system, electronic transport takes place by variable range hopping between exponentially localized states with energies near E_F .

According to the localization theory [1125, 1126, 1156, 1157, 1200], in the Fermi glass insulating regime $\sigma(\omega)$ can be expressed as $\sigma(\omega) = \sigma_{dc} + \beta\omega^s$, where σ_{dc} is the dc conductivity and β and s are constants. According to the theory [1125, 1126, 1156, 1157, 1200], the exponent $s = 2$ at low frequencies. As shown in Figure 169 [1161], the ω^2 dependence is in good agreement with the experimental $\sigma(\omega)$ for PANI-H₂SO₄ below 0.5 eV (except, of course, for the sharp phonon contributions).

While the optical spectra of PANI-CSA exhibit distinct metallic signatures [1160], this is not the case for PANI-H₂SO₄ [1161], as explained previously. The principal difference between PANI-CSA and PANI-H₂SO₄ is the degree of disorder; PANI-CSA is a metal on the border of the metal-insulator transition [1160], while PANI-H₂SO₄ is a Fermi glass in which the electronic wave functions are localized [1161]. The electronic structure of PANI-H₂SO₄ can be understood in terms of the schematic band structure description shown in Figure 170. When the magnitude of the disorder potential is comparable to the bandwidth, the localized and extended states are separated at the mobility edge (E_C) in the conduction band [1125, 1156, 1157]. In such a system, the M-I transition is defined by the position of Fermi energy relative to E_C ; if E_F lies in the region of extended states, the system will be a metal (as is the case for PANI-CSA), whereas if E_F lies in the region of localized states, the system will be a Fermi glass (as is the case for PANI-H₂SO₄).

On the contrary, the optical spectra of PANI-CSA demonstrate the delocalized electronic structure of the wave functions near E_F in the conduction band [1160]. The improved sample quality originates from the counterion-induced processibility of PANI-CSA, where the functional group contained in the counterion induces

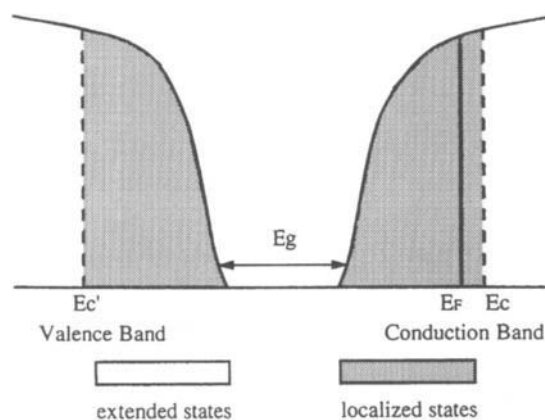


Fig. 170. Schematic description of the band structure for the disordered emeraldine salt of polyaniline. Shaded regions describe states localized by disorder and are separated from extended states by the mobility edge, E_C . The Fermi energy, E_F , lies in the conduction band. Reproduced by permission of Elsevier Science from K. Lee, A. J. Heeger, and Y. Cao, *Synth. Met.* 72, 25 (1995). Copyright © 1995, Elsevier Science.

the solubility in metacresol. Solution processing from metacresol results in a homogeneous material with improved structural order [128].

4.2.5.2. Conducting Polypyrrole

As compared with the optical spectra of PPy-PF₆ in the metallic and insulating regimes [1162], the M-I transition in PPy-PF₆ originates from the degree of disorder in the context of Anderson localization. For the insulating regime, the disorder is sufficiently strong that the electronic states at E_F are localized. Thus, the insulating regime of PPy-PF₆ can be categorized as a Fermi glass. In such a case, similar to with the case of PANI-H₂SO₄, $\sigma(\omega)$ can also be expressed as $\sigma(\omega) = \sigma_{dc} + \beta\omega^s$, where σ_{dc} is the dc conductivity and β and s are constants. For the value of the exponent s , both Mott's localization theory [1125, 1156, 1157] and the scaling theory [1126, 1200] of localization predict $\sigma(\omega) \propto \omega^2$ ($s = 2$) for $\omega < \omega_c$, while $\sigma(\omega) \propto \omega^{1/3}$ ($s = 1/3$) for $\omega > \omega_c$, where ω_c is the crossover frequency, below which the effect of localization is substantial. Above this frequency, localization does not affect the charge-carrier mobility due to photon-assisted hopping between the localized states, so that high-frequency behavior is essentially metallic ($s < 1$) [1201]. Such expected behavior has been proved by the excellent theoretical fits with low-frequency $\sigma(\omega)$ of PPy-PF₆ in the insulating regime, as shown in Figure 171 [1162].

On the contrary, the optical spectra for the metallic regime indicate delocalized electronic states near E_F , as already explained in the previous section. Thus, on the metallic side of the M-I transition, PPy-PF₆ is a disordered metal and can be described well by the LMD model [1162], while, on the insulating side, PPy-PF₆ is characterized as a Fermi glass, which is attributed to disorder in the context of Anderson localization.

4.2.6. Low-Temperature Reflectance in Conducting Polypyrrole

The possibility of collective states arising from many-body effects in conducting polymers has been discussed for many years. The

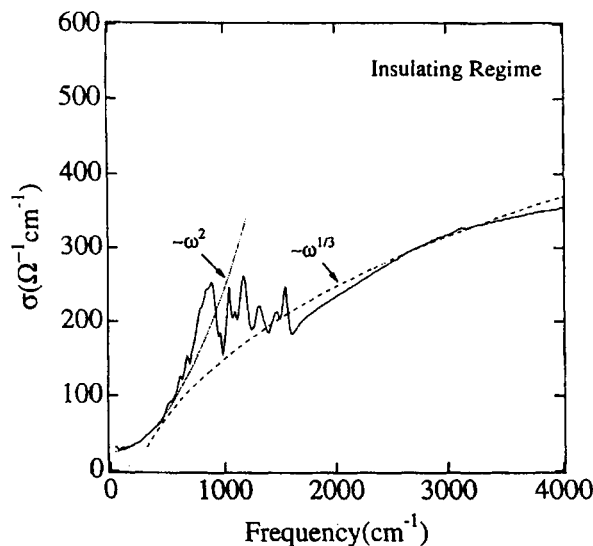


Fig. 171. Comparison of the measured $\sigma(\omega)$ (solid line) of PPy-PF₆ in the insulating regime with the theoretical prediction (dashed line and dotted line). At low frequencies (below 600 cm⁻¹), the data were fit to $\sigma(\omega) \propto \omega^2$, while the high-frequency part (above 600 cm⁻¹) was approximated with $\sigma(\omega) \propto \omega^{1/3}$ dependence. Reproduced by permission of the American Physical Society from K. Lee, R. Menon, C. O. Yoon, and A. J. Heeger, *Phys. Rev. B* 52, 4779 (1995). Copyright © 1995, American Physical Society.

reduced dimensionality and the importance of electron-electron correlations in the metallic state have stimulated predictions of incommensurate charge-density-wave (or spin-density-wave) dynamics and superconductivity in this class of materials [1206, 1207]. Such phenomena have not been realized, in part because the physics of metallic polymers is dominated by severe disorder.

Sample quality, however, has been significantly improved. With these improved materials, one might hope to have an opportunity to observe the onset of density-wave phenomena or superconductivity in conducting polymer systems. PPy-PF₆ is such a case. Furthermore, metallic PPy-PF₆ exhibits an unusual resistivity decrease (vs temperature, T) at low temperatures [1136, 1194]. X-ray structural analysis suggests that PPy-PF₆ is quasi-two-dimensional with good overlap of wave functions both along the polymer chain and in the column direction [1194]. This structure resembles that found in low-dimensional charge-transfer salts, in which charge-density waves (CDWs), spin-density waves (SDWs), and superconductivity (SC) are well known [1208–1211]. In this section, therefore, results on far-IR reflectance measurements [1166] for PPy-PF₆ at low temperatures are reviewed and the results discussed in terms of the formation of a density-wave-like ground state [1166].

Optical Spectra. Figure 172 shows $R(\omega)$ of metallic PPy-PF₆ at various temperatures between 10 and 300 K [1166]. For 300 K, the reflectance spectrum is typical of metallic polymers, as described previously, and can be accurately described by the LMD model [1162]. At 250 K and below, the low-frequency $R(\omega)$ changes dramatically. Between 100 and 800 cm⁻¹, the reflectivity monotonically increases relative to $R(\omega)$ at 300 K. For $\omega < 110$ cm⁻¹, the reflectivity monotonically decreases relative to $R(\omega)$ at 300 K; e.g., at 10 K, $R(\omega)$ remains well below that obtained at 300 K for

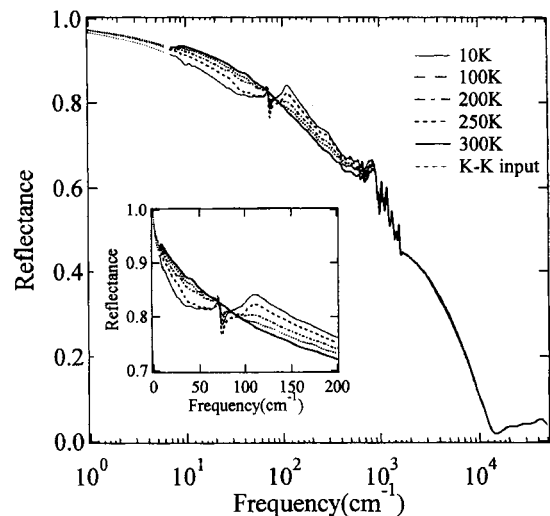


Fig. 172. Reflectance spectra $R(\omega)$ of PPy-PF₆ measured at various temperatures between 10–300 K. The dotted lines below 8 cm⁻¹ indicate the extrapolation by the Hagen-Rubens formula used for the Kramers-Kronig analysis. The inset shows $R(\omega)$ below 200 cm⁻¹ on a linear scale. Reproduced by permission of the American Physical Society from K. Lee, R. Menon, A. J. Heeger, K. H. Kim, Y. H. Kim, A. Schwartz, M. Dressel, and G. Grüner, *Phys. Rev. B*, in press.

$\omega < 80$ cm⁻¹. In the extreme far-IR below 30 cm⁻¹, $R(\omega)$ recovers the “metallic” behavior; the $R(\omega)$ curves for all temperatures approach the 300-K curve and increase toward unity as $\omega \rightarrow 0$. The inset to Figure 172 [1166] shows the long-wavelength data on an expanded scale. At and below 250 K, there are two features: the peak at 110 cm⁻¹ and a Fano-like resonance at 70 cm⁻¹. These two spectral features sharpen and become more well defined (but do not shift) as the temperature is lowered to 10 K. For $\omega > 800$ cm⁻¹, $R(\omega)$ is independent of temperature.

Figure 173 displays $\sigma(\omega)$ at various temperatures [1166]. At 300 K, $\sigma(\omega)$ is typical of a disordered metal; $\sigma(\omega)$ decreases with decreasing ω below 2500 cm⁻¹ and accurately approaches the measured σ_{dc} (300 K) value, consistent with previous reports [1162]. In the far-IR below 300 cm⁻¹, $\sigma(\omega)$ is featureless and frequency independent at 300 K. For lower temperatures, however, $\sigma(\omega)$ develops unusual spectral features in the far-IR. An asymmetric structure that peaked at 110 cm⁻¹ grows at the expense of the oscillator strength below $\omega < 80$ cm⁻¹; thus, $\sigma(\omega)$ decreases for $\omega < 60$ cm⁻¹ as the temperature is lowered. In addition, a sharp Fano-like feature (absent at 300 K) appears at 70 cm⁻¹. The peak positions of these two features are nearly temperature independent below 250 K.

Charge-Density-Wave Dynamics in Conducting Polymers? The peak in $\sigma(\omega)$ and the associated redistribution of oscillator strength are indicative of the formation of a gap in the excitation spectrum similar to that observed in low-dimensional conductors and attributed to the formation of a CDW/SDW ground state [1208–1211]. Below the critical temperature for formation of the broken symmetry state, the periodicity of the CDW or SDW introduces an energy gap in the single-particle excitation spectrum. As a result, $\sigma(\omega)$ is expected to decrease at frequencies within the gap (to 0 in one-dimensional systems), and the corresponding oscillator strength is shifted to frequencies above the gap. In addition, in the

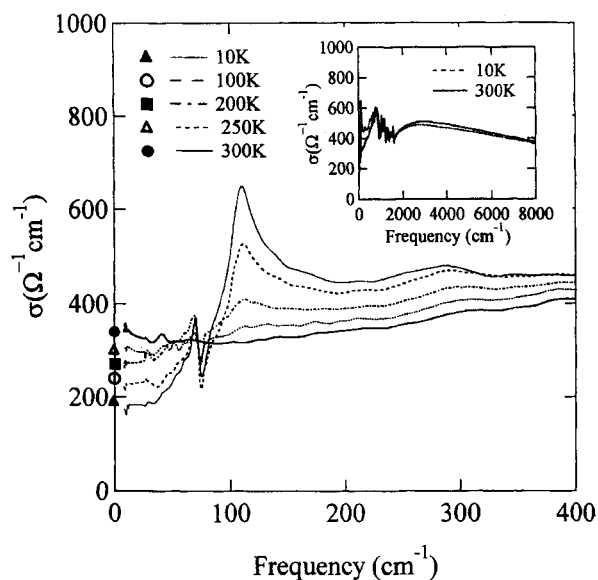


Fig. 173. Optical conductivity $\sigma(\omega)$ of PPy-PF₆ below $\omega = 400 \text{ cm}^{-1}$, as obtained from a Kramers-Kronig analysis of $R(\omega)$. The inset compares $\sigma(\omega)$ for 10 K (dotted line) and 300 K (solid line) in the IR for $\omega \leq 8000 \text{ cm}^{-1}$. Note the 1:1 correspondence between the dc conductivity σ_{dc} , shown as the symbols at $\omega = 0$, and $\sigma(\omega \rightarrow 0)$ at each temperature. Reproduced by permission of the American Physical Society from K. Lee, R. Menon, A. J. Heeger, K. H. Kim, Y. H. Kim, A. Schwartz, M. Dressel, and G. Grüner, *Phys. Rev. B*, in press.

density-wave state there is a collective mode that can be described as a sliding CDW (or SDW) [1208–1211].

The spectral features in the data shown in Figures 172 and 173 resemble those expected for a density-wave state, for example, as in (TMTSF)₂PF₆ where an SDW gap is formed at around 100 cm^{-1} in the direction perpendicular to the chains [1212]. With this interpretation, the resonance at 70 cm^{-1} would be identified with the pinned collective mode. The spectral weight within the 70 cm^{-1} resonance corresponds to a small fraction (approximately 10%) of the oscillator strength, which was redistributed from below 2Δ to above 2Δ . Alternatively, since the gap spans only a part of the Fermi surface, the results reported here can be interpreted in the context of the correlation-induced semimetallic state proposed by Vescoli et al. [1213].

4.2.7. Nature of the Metallic State in Conducting Polymers

The metallic state with finite density of states at the Fermi level does not reconcile with the general concept of a quasi-one-dimensional conjugated polymer, for such a system should be subject to the Peierls instability. Therefore, the existence of the metallic state in conjugated polymers requires the involvement of additional interactions, notably electron–electron interaction, inter-chain coupling, and dopant-mediated interaction. Such additional interactions would result in high dimensionality in the electronic structure of the metallic state, thereby avoiding and stabilizing the Peierls instability.

Another peculiarity of the metallic state is a persistence of the infrared-active vibrational (IRAV) modes into the metallic state with enhanced oscillator strength. In principle, the IRAV modes arise from the localized phonon modes caused by local deviations

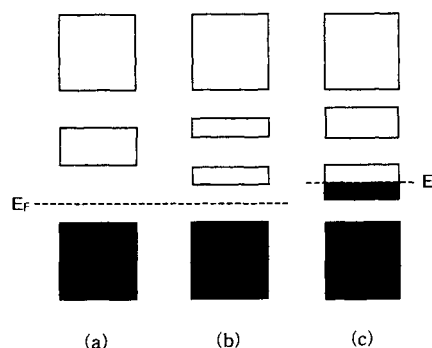


Fig. 174. Schematic representations of the band structures of (a) soliton lattice, (b) bipolaron lattice, and (c) polaron lattice forms.

from the symmetry of the perfectly dimerized pattern in the vicinity of the nonlinear excitations and constitute the characteristics of these quasi-one-dimensional systems [1214]. However, it has been frequently pointed out that the linear dependence of IRAV intensity with doping concentration does not reconcile with the metallic state in which one would expect the Peierls energy gap to close. Therefore, the metallic state is believed to be a dimerized structure with a high density of localized structural distortions rather than a uniform bond-length structure as suggested earlier.

The electronic structure of the metallic state is expected to be fundamentally different from the low doping regime where nonlinear excitations (solitons or bipolarons) are important excitations. Although such nonlinear excitations are self-localized in the dilute doping regime, they start to interact at high concentration. As a result, the wave functions of the adjacent nonlinear excitations overlap sufficiently to form a continuum of energy levels, leading to the suggested soliton lattice band [1215] for degenerate ground-state systems and the bipolaron lattice band [1216] for nondegenerate ground-state systems. However, since such lattice bands are empty, they are not appropriate for the description of the metallic state requiring the finite density of state at the Fermi level. Indeed, in order to make such band models compatible with the metallic state, there was a suggestion that the metallic state could be understood as a merging of soliton (bipolaron) lattice band with a valence band (or a conduction band for n-type doping) to form a partially filled conduction band [1215, 1216].

The polaron lattice model [1217] is an alternative, retaining the doping-induced half-filled polaron band in the π - π^* energy bandgap, consistent with the expectation of a traditional metallic state. Figure 174 describes the schematic diagram for the polaron lattice band together with the soliton and bipolaron lattice band model. In this model, the sharp increase in the Pauli susceptibility of *trans*-(CH)_x could be understood in terms of a first-order phase transition from a soliton lattice to a polaron lattice [1217]. Because the polaron lattice model has a half-filled subband within the π - π^* gap, there is a finite density of states at the Fermi level, and transport occurs by coherent electron motion through this subband. This polaron lattice metal concept can be generalized to most nondegenerate ground-state systems as well as polyacetylene. In this case, the bipolaron state is driven toward polaron lattice conformation with increasing dopant concentration. However, there was a theoretical calculation that predicted weak IRAV modes in the polaron lattice [1218], in contrast with the experimental observations. This result has been used as the main argument against the polaron lattice model together with the fact the polaron lattice is

expected to be unstable toward a Peierls distortion in such a one-dimensional system. In contrast, it is notable that a theoretical consideration [1219] indicates that the polaron lattice provides for significant charge polarization along the polymer chains and can also lead to intensive IRAV modes. In any case, despite a decade of research on the metallic state of conjugated polymers, many of the fundamental issues remain unsolved. In particular, the existence of IRAV modes demonstrates that the heavily doped conjugated polymers are not simple metals.

4.3. Photophysics of Semiconducting Polymers

4.3.1. Introduction

Undoped conjugated polymers have an anisotropic, quasi-one-dimensional electronic structure with the π electrons coupled to the polymer backbone via electron-phonon interactions. The overlapping of π - (also π^* -) electron wave functions forms a valence band (conduction band) with a gap size of typically 2–4 eV, corresponding to the conventional semiconductor gap. As a result, undoped conjugated polymers (hereafter called simply semiconducting polymers) exhibit the electronic and optical properties of semiconductors in combination with the mechanical properties of general polymers, making them potentially useful for a wide array of applications.

The electronic structure of such semiconducting polymers was successfully described by Su et al. [1167] in terms of a quasi-one-dimensional tight binding model. However, in contrast with conventional inorganic semiconductors with rigid band, upon doping or photoexcitation the carriers are self-localized and form the nonlinear excitations [1, 1049, 1153] on the polymer chains—solitons, polarons, or bipolarons, depending on the ground-state degeneracy. In degenerate ground-state polymers such as *trans*-polyacetylene, solitons are the important nonlinear excitations, whereas in nondegenerate ground-state systems, including most of the conjugated polymers such as poly(*p*-phenylene vinylene), polypyrrole, and polythiophene, polarons and bipolarons are the responsible charge-storage excitations [1049].

Much of the new physics associated with conjugated polymers is related to the formation and properties of such nonlinear excitations. New subgap optical transitions occur with corresponding shift of oscillator strength from π - π^* transitions to the localized gap states associated with these novel quasi-particles. Furthermore, these nonlinear electronic excitations couple to the lattice vibrations and allow the symmetrical vibrational modes (Raman active modes) to become infrared active by breaking the local symmetry. Such important information on the nature of the nonlinear excitations in conjugated polymers can be obtained via photoexcitation (i.e., injecting charges onto the polymer backbone by direct optical pumping above the π - π^* energy gap with an intensive external light source).

However, although the linear and nonlinear optical properties of conjugated polymers have been investigated for over a decade, there is still controversy over the nature of the primary photoexcitations [1121, 1168]. Are the lowest energy elementary excitations mobile charge carriers (charged polarons) or bound neutral excitons? The central issue in this argument relates to the strength of the electron-electron interactions relative to the bandwidth and relative to the electron-phonon interaction. Strong electron-electron interactions (electron-hole attraction) lead to the creation of localized and strongly correlated negative and positive

polaron pairs (neutral polaron excitons), whereas well-screened electrons and holes with associated lattice distortions are more appropriately described by charged polarons. Since the answer is of importance not only from the perspective of our basic understanding of the conducting polymers, but also for applications based on these materials, the related experimental results, such as photoexcitation spectroscopy, photoluminescence spectroscopy, and photoconductivity, are briefly examined in this review.

4.3.2. Steady-State and Near-Steady-State Photoexcitation Spectroscopy

Spectroscopy studies of conjugated polymers have been an important source of information on their electronic structure; in particular, photoinduced absorption (excitation spectroscopy) has successfully characterized the gap states associated with the nonlinear excitations (solitons, polarons, and bipolarons) and determined the energies of those states relative to the conduction and valence bands in several conjugated polymers.

Photoinduced absorption (PA) spectroscopy is a measurement of the linear absorption spectrum of the excited state of the system. The measurement is very similar to ground-state linear absorption spectroscopy with the difference that the system is pumped by light of $E > E_{\text{gap}}$ when the measurement is made. To observe the changes in the absorption spectrum between the ground and the excited states, modulation techniques must be used. In principle, however, steady-state photoinduced absorption only sees those species that have long lifetimes, and the changes ($-\Delta T/T$) are typically on the order of 10^{-4} . In near-steady-state PA, most of these excitations have decayed away and a straight absorption spectrum of the photoexcited state would be indistinguishable from that of the ground state. In such a case, in order to measure small change with a large signal, standard phase-sensitive detection techniques are typically used.

A number of steady-state PA spectroscopic measurements have been made since the discovery of conjugated polymers. Blanchet et al. [1220] show the one-to-one correspondence between photoinduced infrared-active vibrational (IRAV) modes and doping-induced IRAV modes in steady-state IR photoexcitation spectroscopy. These results imply that the same charge species are produced in both cases. In nondegenerated ground-state conjugated polymers, Vardeny et al. [1221] reported the photogeneration of confined soliton pairs (bipolarons) in the steady-state photoexcitation spectrum of polythiophene, as shown in Figure 175, and Kim et al. [1222] studied poly(3-methylthiophene) with the same experimental techniques. Wohlgenannt et al. [1223] applied the near-steady-state photoexcitation technique to ladder-type poly(paraphenylene) films for investigating the recombination kinetics of photogenerated neutral and charged excitations such as singlet and triplet excitons and charged polarons in this material.

4.3.3. Sub-Picosecond Photoexcitation Spectroscopy

In sub-picosecond photoexcitation spectroscopy (or time-resolved excited spectroscopy) of the conjugated polymers, one can study the excited-state spectra (absorption, emission, and stimulated emission) and the time decay of the excited-state spectral features. For nonlinear excitations in conjugated polymers, this spectroscopy technique is useful, since their photogeneration processes usually occur in the sub-nanosecond time domain.

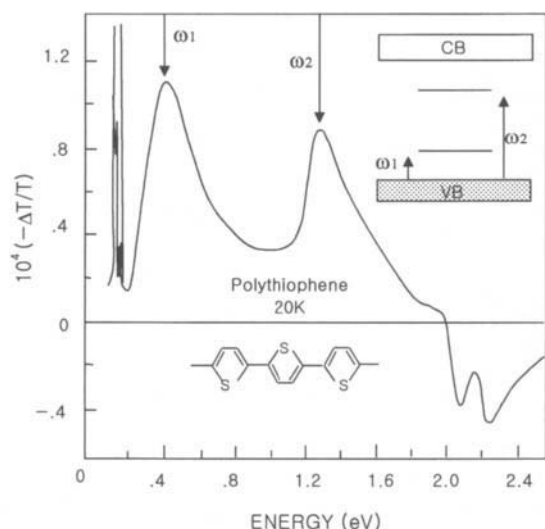


Fig. 175. Photoinduced absorption of polythiophene at 20 K obtained with a sample pumped at 10 mW/cm^2 of a 2.7-eV laser beam. Reproduced by permission of the American Physical Society from Z. Vardeny, E. Ehrenfreund, and O. Brafman, *Phys. Rev. Lett.* 56, 691 (1986). Copyright © 1986, American Physical Society.

Dogariu et al. [1224] studied the magnitudes and decay of the stimulated emission (SE) and the photoinduced absorption (PA) by picosecond PA spectroscopy in a soluble derivative of poly(*p*-phenylene vinylene) (MEH-PPV). They explained the bimolecular decay dynamics results from dipole-dipole interactions between excited species [1224, 1225]. Klimov et al. [1226] reported femtosecond transient-absorption studies of a five-ring oligomer of poly(*p*-phenylene vinylene) prepared in solid-state film and dilute solutions. In this experiment, they showed that the biexciton is stable in a solution state, but unstable in a solid state. Kraabel and Joffe [1227] studied the singlet exciton-relaxation scheme on isolated polydiacetylene (PDA) chains through sub-picosecond pump-probe experiments. They suggested that self-trapping is at best a minor component of exciton relaxation in PDA isolated chains in these experiments [1227]. Femtosecond pump-probe experiments on solutions of MEH-PPV in THF (tetrahydrofuran) have been done by Nguyen et al. [1228]. In this experiment, they reported that with proper choice of excitation wavelength, solvent, and concentration, control over the lifetimes of excitons, and their aggregates, as well as their relative population, is possible [1228].

4.3.4. Photoconductivity

Photoconductivity has also proven to be an important method for providing fundamental information regarding the nature of the photoexcitation in conjugated polymers [1229–1231]. In fact, photoconductivity is a quite complex phenomenon, including optical absorption, electrical transport of carriers, and recombination or trapping of photogenerated carriers. In turn, it offers a valuable tool in the investigation of the fundamental physics underlying this rich complexity of photoelectronic properties of semiconductors. In addition, measurements of photoconductivity by varying the excitation light intensity (photodoping) provides a unique opportunity for investigating the “intrinsic properties” of a material with varying carrier concentrations without changes in chemical composition and/or structural disorder. Furthermore, photoconductivity

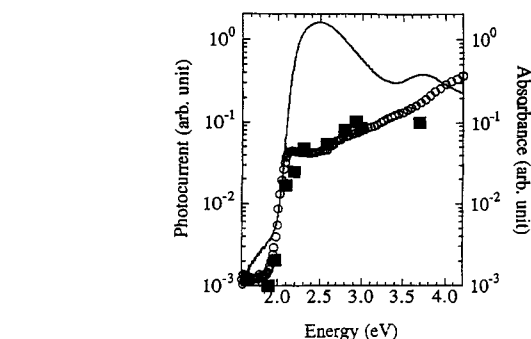


Fig. 176. Spectral response of the magnitude of the peak transient photoconductivity (■) and the steady-state photoconductivity (○) compared with the optical absorption spectrum—for MEH-PPV. Reproduced by permission of Elsevier Science from C. H. Lee, G. Yu, N. S. Sariciftci, A. J. Heeger, and C. Zhang, *Synth. Met.* 75, 127 (1995). Copyright © 1995, Elsevier Science.

effects have been used in broad applications from photodetectors to ultrafast optoelectronics.

The most comprehensive studies on the photoconductivity of conjugated polymers have been made by Lee and co-workers [1229–1231]. In their measurements, mainly on PPV and its derivatives [1229–1231], they compared the spectral response of both steady-state and fast transient photoconductivity with the absorption spectrum in order to investigate whether free carriers (charged polarons) or bound excitons are photogenerated. In particular, their picosecond transient photoconductivity studies offered the possibility of monitoring the generation and transport of charge carriers before charge transport is significantly limited by traps. In their steady-state and transient photoconductivity spectral response on MEH-PPV [1231] as shown in Figure 176, they observed that the onset of photoconductivity coincides with the onset of absorption, consistent with a weak exciton binding energy, less than approximately 0.1 eV. Moreover, from the measurements of transient photoconductivity in the picosecond to nanosecond regime [1231], they observed that there is an initial fast response with decay of about 100 ps followed by a slower component with a decay time of a few hundred picoseconds. This fact, they argued, confirms that carriers are generated by a first-order process that cannot be attributed to interactions between excitations. In sum, since the details of photoconductivity data [1229–1231] are mainly consistent with photoexcitation of charged (positive and negative) polarons, they concluded that a description of the electronic structure of the PPVs in terms of a semiconductor band model is more appropriate than an exciton model.

4.3.5. Photoluminescence Spectroscopy

Time-resolved photoluminescence spectroscopy has emerged as one of the most important tools for studying the properties of solid-state materials suited to optoelectronic applications, including semiconducting polymers. This is due to the relatively direct information about the excitation dynamics, such as recombination and relaxation processes, which is obtained from such experiments. Wong et al. [1232] have reported a luminescence lifetime much smaller than 1 ns in conjugated polymers and have pointed out that nonradiative as well as bimolecular processes might play an important role. Furukawa et al. [1233] have studied time-resolved luminescence in PPV and have explained the re-

sults in terms of self-trapping of the excitation in PPV. Kersting et al. [1234] have studied time-resolved photoluminescence experiments on PPV and explained the results in terms of spectral relaxation associated with the incoherent hopping motion of excitons within a disorder-broadened density of states.

In spite of comprehensive study of the emission dynamics on all time scales, ranging from femtoseconds to nanoseconds, the nature of the primary photoexcitation is controversial. Estimates of the binding energy of the electron and hole in the photoexcited state (the exciton) range from 0.2 eV or less [1235] up to 0.9 eV [1236]. In the case of weak binding, the exciton would be delocalized over many monomers on a given chain and, depending on the strength of the interchain transfer interaction, even over several chains; a large binding energy, on the other hand, would imply localization on a few monomers of a given chain.

A second area of disagreement centers around photoluminescence quenching at high excitation densities in thin films. The formation of nonradiative interchain polarons [1237, 1238] and interchain exciton formation [1239] have been proposed as sources responsible for the quenching mechanism. At moderately high excitation densities, bimolecular decay, resulting from interchain interactions between the excited species, is considered to be responsible for the fast photoluminescence decay [1240–1243]. At high excitation conditions, the formation of biexcitons becomes favored [1244, 1245].

4.3.6. Gain Narrowing in Photoluminescence Spectra: "Lasing" in Conjugated Polymers

There is a new class of laser system, frequently called "mirrorless lasers," for which the gain is so high that they do not need a resonant cavity to emit bright and quasi-coherent beams. To achieve such performance, either of the following processes should be satisfied. First, there is a cooperative process, characterized by the emission of coherent radiation with peak intensity proportional to N^2 , where N is the number of oscillating dipoles, and with the excited-state lifetime proportional to $1/N$. Second, there are collective processes, such as amplified spontaneous emission, where the spontaneous emission coming from a distribution of emitters is linearly amplified by the gain medium.

Gain narrowing refers to the linewidth narrowing of the photoluminescence (PL) emission spectrum above a threshold optical-pump excitation energy. The narrowing is an indication of light amplification by stimulated emission at the gain maximum. Hide et al. [1246] reported an observation of gain narrowing in the PL spectrum of PPV derivatives, as shown in Figure 177. They suggested that achievement of gain narrowing requires that two criteria should be fulfilled. First, the active polymer medium must exhibit stimulated emission under optical or electrical excitation. Second, structures appropriate for amplified spontaneous emission should include planar waveguides [1246]. In fact, they emphasized the role of waveguiding in the achievement of gain narrowing in optically pumped polymer films [1246]. Asymmetric planar waveguides formed from the refractive index mismatch at the polymer/air and polymer/substrate interfaces of a thin film provide a straightforward and relatively simple method for extending the path length of the emitted photons in the gain medium. On the other hand, Tessler et al. [1247] reported an observation of optically pumped lasing from a poly(*p*-phenylene vinylene) (PPV) layer incorporated in an optical microcavity. Although there is

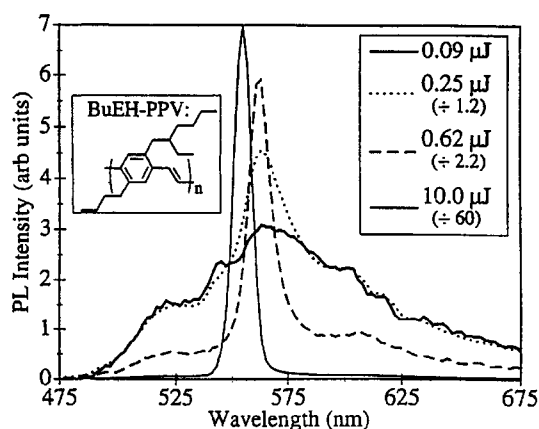


Fig. 177. Photoluminescence spectra at different excitation energies for a 210-nm-thick film of BuEH-PPV pumped at 435 nm. Reproduced by permission of the American Association for the Advancement of Science from F. Hide, M. A. Diaz-Garcia, B. J. Schwarz, M. R. Andersson, Q. Pei, and A. J. Heeger, *Science* 273, 1833 (1996). Copyright © 1996, American Association for the Advancement of Science.

general agreement among the experimental observations of spectral narrowing in conjugated polymers, a detailed picture of the gain mechanism in polymer materials is still lacking. More detailed experiments are required to resolve these issues.

4.3.7. Nature of the Primary Photocarriers in PPV: Neutral Excitons versus Charged Polarons

Although the optical and photoexcitation spectroscopic properties of conjugated polymers have been investigated for over a decade, there is still controversy over the description of the primary photoexcitation species [1121]. The main point is the relative strengths of the electron–electron and the electron–phonon interactions in comparison with the π -electron bandwidth. If the electron–electron (or electron–hole) Coulomb interaction is strong enough, this leads to the creation of localized and strongly correlated polaron pairs (so-called neutral polaron excitons). On the other hand, if electrons (and holes) are well screened with associated lattice distortions, this leads to the formation of charged polarons, which can be more appropriately described using a band picture supplemented by the electron–phonon interaction. In conjugated polymers, both band-based models and exciton-based models have been used to explain aspects of their optical properties [1121].

This issue is also important with regard to applications based on these materials. In particular, the existence of the bound triplet can severely limit the quantum efficiency in electroluminescence devices such as polymer LEDs. If the triplet binding energy and the corresponding cross section for forming a triplet from a pair of injected carriers are large, the singlet–triplet ratio would be determined by the multiplicity of the triplet and singlet states (3:1). In this case, the quantum efficiency for electroluminescence would necessarily be limited to 25% of the corresponding quantum efficiency for photoluminescence [1248]. However, if the dynamics are such that the cross section for triplet formation from a pair of oppositely charged polarons is relatively small, the limiting quantum efficiency for electroluminescence can approach 100% of that of the photoluminescence. Therefore, obviously, these issues are both scientifically interesting and critically important to the assess-

ment of the future potential of light-emitting devices fabricated from semiconducting polymers.

4.4. Electroluminescence in Conjugated Polymers: Polymer LED

Electroluminescence (EL) is the generation of light by electrical excitation, and can be seen in a wide range of semiconductors. However, this phenomenon has also been observed in organic thin-film electroluminescence in the 1980s through the work of Tang and Van Slyke [1249], who demonstrated efficient electroluminescence on two-layer sublimed molecular film devices. Since then, there has been a great deal of activity in the development of these devices with very high levels of performance, including high quantum efficiencies (photons out per charge injected) of several percent [1250].

Electroluminescence from conjugated polymers was first reported in 1990 [134], using PPV as the single semiconductor layer between two electrodes. Devices using soluble PPV, for example, MEH-PPV, were then demonstrated to facilitate easy fabrication and to improve device performance [1251]. After this first stage in the research, development in this field was rapid, and prototype devices now meet realistic specifications for industrial applications. Moreover, such achievements provide opportunities in many aspects, including a better understanding of the fundamental science, design and synthesis of materials, and semiconductor device physics of these polymers. Here we briefly discuss the current understanding of the physics, device properties, and technology of polymer LEDs.

4.4.1. Photoconducting and Semiconducting Physics of Polymer LEDs

The typical structure of a polymer LED, using conjugated polymer as the single semiconductor layer between two electrodes, is illustrated in Figure 178. In this structure, the ITO layer acts as a transparent electrode, allowing the generated light to go through the device, while the top electrode is conveniently formed by thermal evaporation of a metal. Such electrodes are chosen to facilitate charge injection. ITO has a relatively high work function and is therefore suitable for hole-injecting the electrodes, whereas low-work-function metals such as Al, Mg, or Ca are used for the injection of electrons. The band scheme of a polymer LED under forward bias is shown schematically in Figure 179. LED operation is achieved when the device is biased sufficiently to inject positive and negative charge carriers from opposite electrodes into an emissive polymer layer. Then recombination of positive and negative charges occurs within the region of the polymer layer, resulting in photon emission.

Although the general scheme involved in polymer LEDs seems to be relatively simple, the nature of the electronic structure and an appropriate description of polymer LEDs are somewhat controversial. As the underlying physics governing polymer LEDs, both a band-based model [1252] and an exciton-based model [1169] have been proposed to explain measurements. First, according to the band-based model, it is possible to predict the lowest voltage required for tunneling, and hence light emission, to occur. Referring to the schematics shown in Figure 180, tunneling will not take place in reverse or "low" forward bias due to the tilt of the polymer bands. However, once the applied voltage is sufficient to achieve the "flat-band" condition, tunneling can start, and

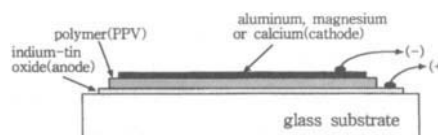


Fig. 178. Device structure of a single-layer polymer electroluminescence diode.

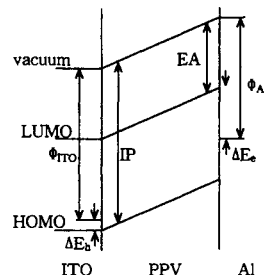


Fig. 179. Schematic energy-level diagram for an ITO/PPV/Al LED under forward bias, showing the ionization potential (I_P) and electron affinity (E_A) of PPV, the work functions of ITO and Al (Φ_{ITO} and Φ_{Al}), and the barriers to injection of electrons and holes (ΔE_e and ΔE_h). There is a small barrier for hole injection from the ITO electrode into the valence band (of highest occupied molecular orbital, HOMO), and with aluminum as cathode, a considerably larger barrier for electron injection into the PPV conduction band states (of lowest unoccupied molecular orbital, LUMO). Reproduced by permission of *Nature* from R. H. Friend, R. W. Gymer, A. B. Holmes, J. H. Burroughes, R. N. Marks, C. Taliani, D. D. C. Bradley, D. A. Dos Santos, J. L. Brédas, M. Lögdlund, and W. R. Salaneck, *Nature* 397, 121 (1999).

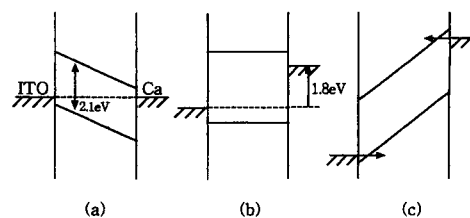


Fig. 180. Schematic band diagrams for the preceding device at various values of forward bias. (a) Zero bias, no tunneling; (b) "flat-band" condition, the onset voltage for tunneling to occur; and (c) forward bias, tunneling of both carriers. Reproduced by permission of the American Physical Society from I. D. Parker, *J. Appl. Phys.* 75, 1656 (1994). Copyright © 1994, American Physical Society.

for higher values of forward bias significant tunnel currents will flow. This turn-on voltage depends only on the energy levels of the polymer and electrodes and should be independent of the polymer thickness. The turn-on voltage is the voltage required to reach the "flat-band" condition and depends only on the bandgap of the polymer and the work function of the electrodes. For an ideal device, the electrodes are matched to the HOMO and LUMO of the polymer, so that the barrier heights are 0. This gives the lowest operating voltage and maximum device efficiency. In this case, the turn-on voltage would be equal to the bandgap of the polymer. In this model, the current-voltage (I - V) characteristics are controlled by the current density of the majority injected carrier (hole), while the device efficiency is controlled by the current density of the minority injected carrier (electron). Manipulating these band offsets can control the operating voltage of the device, as well as its efficiency.

An alternative is the exciton-based model [1169]. In this model, injected electrons and holes capture one another within the polymer film and form neutral bound excited states (so-called excitons). Since such excitons are substantially confined to a single polymer chain, excitons in conjugated polymers are generally considered to be more strongly localized than excitons in three-dimensional inorganic semiconductors. In such a case, the spin wave function of the exciton can be either singlet ($S = 0$) or triplet ($S = 1$). However, because of the confinement of the excitation in this case, it is expected that the energy difference between singlet and triplet may be substantial. Considering only singlet states allows radiative emission (fluorescence), and crossover from triplet to singlet is not expected because of the large energy exchange between the two states. It is generally believed that triplet excitons do not produce light emission, except indirect processes such as triplet-triplet annihilation or phosphorescence. Therefore, in order to achieve efficient luminescence, it is necessary to have good balancing of electron and hole currents, efficient recombination within the emissive layer, strong radiative transitions for singlet excitons, and efficient coupling of these excitons to photon states allowed in the device structure.

4.4.2. Current Status of Polymer LEDs

The most important issues in the performance of polymer LEDs are quantum efficiency and device lifetime [1169]. Although the exciton-based model sets some limits to the efficiency of operation for polymer LEDs (up to 25% of PL efficiency), reported efficiencies are relatively high (above 20 lm/W for green emission), and compare favorably to those reported for sublimed molecular-film devices.

The device lifetime issue (both storage and operational) is more critical. For general applications, operating lifetimes in excess of 10,000 hours are required, together with storage times of 5 years or more. The best results reported for sublimed molecular films, based on the Kodak structure, give more than 10,000 hours to half initial brightness (300 cd m^{-2}) for devices made with quinacridine-doped Alq₃ as the emissive layer and an Al/Li alloy as the cathode [1253]. For the polymer devices, however, there should be more progress in the extension of device lifetime in order to match the requirements of realistic applications. As a consequence, many studies on degradation processes in polymer LEDs are under way [1254]. The main issues in the degradation processes involve deterioration through formation of "black spots," which are commonly attributed to the presence of pinholes in the cathode metal, as well as an ITO electrode quality problem.

The potential for commercialization of these devices is considered to be high. The major advantage lies in the scope of low-cost manufacturing, attributed to solution processibility of film-forming polymers in devices. Moreover, solution processibility of polymers offers new methods for patterning, such as ink-jet printing, which place separated pixels of red-, green-, and blue-emitting polymer onto the prepared substrate [1255, 1256]. The availability of full-color graphics (for computer monitors and video displays) constitutes another attraction of these devices. Such potential advantages make the research of this field quite active, and indeed have led to the new era of "polymer electronics" with abundant scientific results in both fundamentals and applications.

4.5. Photoinduced Charge Transfer in Conjugated Polymer/Fullerene Composites

4.5.1. Photophysics of Conjugated Polymer/Fullerene Composites

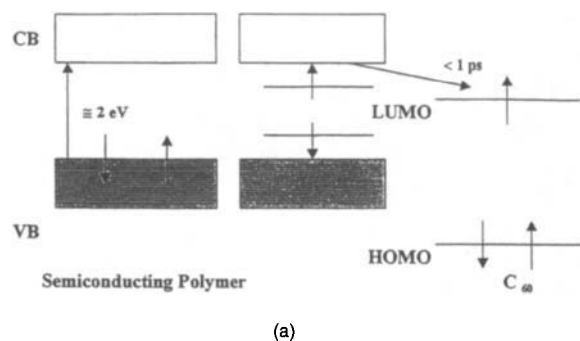
As a new form of carbon, fullerene (C_{60}) is an excellent electron acceptor capable of taking on as many as six electrons. Therefore, fullerene can easily form charge-transfer salts with a variety of alkaline metal donors [1257]. Sariciftci et al. [1170] found photoinduced electron transfer from semiconducting polymers onto fullerene, with interesting and unique photophysical properties in those composites. In such cases, conjugated polymers act as electron donors upon photoexcitation (electrons promoted to the antibonding π^* band), and then fullerene absorbs photoexcited electrons in the LUMO level. As a result, new absorption occurs in the photoexcitation spectrum of those composites, assigning to the allowed HOMO (T_{1g})-LUMO (T_{1u}) transitions of C_{60}^- [1258]. Once the photoexcited electron is transferred to an acceptor unit, the resulting cation-radical (positive polaron) species on the conjugated polymer backbone is known to be highly delocalized and stable as shown in electrochemical and/or chemical oxidative doping studies.

A schematic description of photoinduced electron transfer and metastable charge separation in conjugated polymer/fullerene composites is displayed in Figure 181. The interesting point is the observation that the forward electron transfer from the semiconducting polymer onto C_{60} occurs in less than 1 ps [1259]. Because the charge-transfer rate is more than two orders of magnitude faster than competing radiative and nonradiative recombination processes, the quantum efficiency for charge transfer is close to unity. Subsequently, photoluminescence quenching occurs by ultrafast charge-transfer [1170]. Although the photoinduced charge transfer is reversible, the charge-transfer state is metastable with the back charge-transfer rate many orders of magnitude slower than the forward charge transfer rate. The retarded back electron transfer causes the excited-state absorption to persist to a longer time scale (even on the order of milliseconds) [1260]. Therefore, those unique photophysical properties lead to a number of interesting applications, including sensitization of the photoconductivity [1261], photovoltaic phenomena [1262, 1263], and nonlinear absorption (optical limiting) through excited-state absorption [1264].

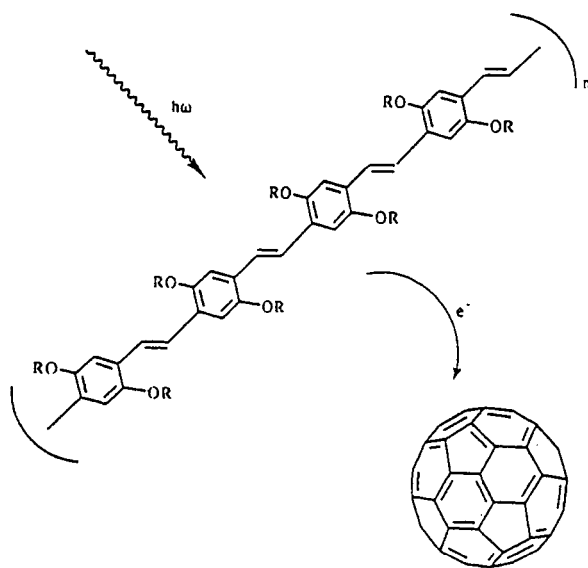
4.5.2. Applications to Optoelectronic Devices

Applications of conjugated polymer/ C_{60} composites to optoelectronic devices such as photodetectors and photovoltaic cells is very interesting. Because of the ultrafast photoinduced electron transfer with long-lived charge separation in the conjugated polymer/ C_{60} composites, this system offers a special opportunity. Using conjugated polymer as donors with different acceptors results in photoinduced charge separation with quantum efficiency near unity and with correspondingly enhanced device performance [1262-1269].

Considering the energy diagram of a conjugated polymer and C_{60} shown in Figure 182, it is clear that the heterojunction, formed at the interface between a semiconducting polymer and a C_{60} film, should function as a diode with a rectifying current-voltage characteristic (analogous to a p-n junction, but with a different mechanism based on molecular redox properties). The inherent polarity of the device results in very low reversed-bias current densities.



(a)



(b)

Fig. 181. (a) Schematic energy band diagram for photoinduced electron transfer between semiconducting, conjugated polymers and buckminsterfullerene, C_{60} . CB, conduction band; VB, valence band; HOMO, highest occupied molecular orbital; LUMO, lowest unoccupied molecular orbital. (b) Schematic illustration of photoinduced electron transfer from the photoexcited conjugated polymer to C_{60} .

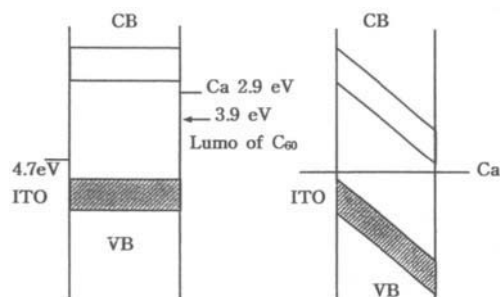


Fig. 182. Flat-band scheme of the Ca/polymer + C_{60} /ITO tunnel diodes under open-circuit and short-circuit conditions.

On the other hand, electron injection into C_{60} and electron removal from the semiconducting polymer is energetically favorable, resulting in relatively high current densities under forward bias.

Sarıçiftci et al. [1262] reported that the rectification ratio is approximately 10^4 in a heterojunction device consisting of successive layers of ITO/MEH-PPV/ C_{60} /Au, as shown in Figure 183. The current-voltage characteristic of this device changes dramati-

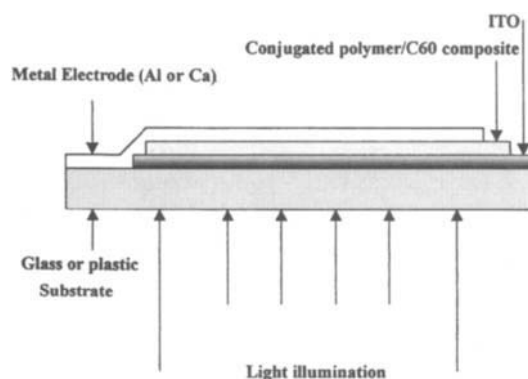


Fig. 183. Schematic diagram of the photovoltaic cell of the conjugated polymer/ C_{60} composites.

cally upon illumination by visible light, that is, increases in both forward- and reverse-bias current. The major increase results from photoinduced charge separation at the heterojunction interface. The strong increase in photocurrent upon illumination at -1 V serves as a relatively sensitive photodiode. Additionally, they report that the generation of photoexcitations, which result in separated charge carriers, occurs only at the heterojunction interface [1262].

As explained previously for polymer LEDs, a semiconducting polymer with asymmetric contacts (a low-work-function metal on one side and a high-work-function metal on the opposite side) functions as a tunneling injection diode [1262]. In forward bias, tunneling injection diodes exhibit relatively high efficiency electroluminescence. In reverse bias, Yu et al. [1265, 1266] reported that the devices exhibit a strong photoresponse with a quantum yield larger than 20% (electron/photon at 10-V reverse bias), which comparable to UV-sensitized Si photodiodes.

In general, there are two ways to approach the organic photovoltaic cell. One is as the successive layers of conjugated polymer/ C_{60} , that is, the bilayer heterojunction device explained previously. The other is as an interpenetrating phase-separated donor/acceptor (D/A) network composite. However, bilayer heterojunction devices have some limitations in conversion efficiency. Because efficient charge separation occurs only at the D/A interface, photoexcitations created far from the D/A junction recombine prior to diffusing to the heterojunction. Moreover, there might be a loss for the separated charges during the carrier-collection process [1262]. In spite of those problems, however, many studies on bilayer heterojunction photovoltaic devices [1267–1269] have been performed with improvement in the performance of the devices.

An alternative is to use the concept of interpenetrating phase-separated D/A network composites. Through control of the morphology of the phase separation into an interpenetrating network, one can achieve a high interfacial area within a bulk material. Since any point in the composite is within a few nanometers of a D/A interface, such a composite is “bulk D/A heterojunction” material. A photovoltaic cell using these materials has been reported by Yu et al. [1263]. They used a C_{60} derivative instead of pure C_{60} as the electron acceptor to form a bicontinuous interpenetrating network in the composites. They reported that the carrier-collection efficiency is about 45% and the energy-conversion efficiency is 3.3% [1263]. Since the “bulk D/A heterojunction” materials exhibit excellent photosensitivity and relatively high energy

conversion efficiencies, it is expected that further optimization of device physics might lead to high device performance in this field.

5. CONCLUDING REMARKS

In this chapter, the synthesis and electrical and optical properties of conjugated polymers have been reviewed. The past several years of work has shown that conjugated polymers are a new type of semiconducting material for electronics, optoelectronics, and photonics applications. In conjugated polymers, the electrical and optical properties can be controlled at the molecular scale. Hence, conjugated polymers are potential materials for the fabrication of single molecular devices. Moreover, the tools in synthetic chemistry are quite sophisticated for molecular-level manipulations to achieve the desired physical properties. Since it is well known that polymeric materials can be easily processed in device fabrication, etc., functionalized conjugated polymers are ideal materials for molecular electronics and photonics. Nevertheless, the fine-tuning of the molecular-level chemistry and the understanding of the details of the molecular structure versus physical property relationships are yet to be fully developed to really make use of these materials for potential and novel applications.

One of the advantages of organic and polymeric materials is the possibility of unlimited structural variation. This also implies the availability of a huge array of synthetic possibilities to obtain those materials. To some extent, there are two main approaches to the synthesis of conducting polymers: the direct approach and the precursor methods.

In the case of the direct approach, the polyconjugated system is obtained at once and often side chains are indispensable for the materials to be soluble. For polyaromatics, besides direct oxidation and oxidative electrochemistry, organometal-catalyzed coupling reactions are frequently used polymerization methods. The McCullough and Rieke organometal-catalyzed coupling reactions allow for the synthesis of head-to-tail-coupled polythiophenes, showing that structural order can, to a large extent, be controlled by the preparation method. In many cases, specific monomeric or oligomeric units are synthesized in order to obtain, after polymerization, conjugated polymers with well-determined properties.

Precursor methods have been developed for polyacetylene and poly(*p*-phenylene). The precursor approach has been intensively stimulated by developments in the field of poly(*p*-phenylene vinylene) and the use of this polymer in light-emitting devices. The Wessling precursor route is one of the most used procedures to prepare this material. The precursor route of Louwet and Vanderzande has overcome many of the limitations inherent in the Wessling precursor route and will most probably allow further interesting developments for the application of poly(*p*-phenylene vinylene) in polymer electronics.

The relationship between chemical structure and bandgap in conjugated polymers is one of the fundamental aspects that needs to be looked into for making progress in this direction. It is well known that the modification of side groups, steric hindrance, π -conjugation length, etc. can vary the HOMO and LUMO levels. This can be used for molecular-scale engineering of the bandgaps. Although polyacetylene $(\text{CH})_x$ is an ideal material to show the intrinsic metallic nature, the effect of Peierls distortion cannot be avoided, thereby increasing the bandgap to 1.5 eV. Hence, undoped $(\text{CH})_x$ is only a semiconducting material. In the case of a wide variety of aromatic conjugated polymers, the stability of the

aromatic versus the quinoid structure comes into play. At present, the bandgap in conjugated polymers varies from 1 to 4 eV. For several potential applications, further reduction in the bandgap is required. The final goal is to synthesize the appropriate chemical structures so that the desired bandgap and other electronic and optical properties can be attained.

Besides providing an overview of the available synthetic procedures, the aim of Section 2 was also to look into the structural tools available for bandgap engineering of conjugated polymers, in particular, the design of low-bandgap materials. Quantum-chemical calculations have shown that the bond-length alternation Δr ($E_{\Delta r}$), the resonance energy stabilization of the aromatic ring system (RE), the inter-ring torsion angle Θ (E_{Θ}), and the inductive or mesomeric effects of substituents R (E_R) are the most significant parameters that play crucial roles in controlling the bandgap (E_g). In this review, the theoretical studies and the experimental results are compared to check the consistency of this approach. As a typical case study, the work on polyisothianaphthene and its derivatives is used to illustrate these principles and to find out whether this methodology can be used to obtain systematic control of the bandgap and other physical properties of conjugated polymers.

From classical Hückel molecular orbital theory and experimental data, it is known that a qualitative correlation exists between the bandgap and the resonance stabilization. Apparently, the lower resonance stabilization of a heterocyclic ring system coincides with the lower bandgap of the corresponding polymer. This qualitative correlation can be used as a rough guideline for the synthesis of low-bandgap polymers. For example, in copolymers, it is possible to combine different types of aromatic ring systems, substantially altering the electronic properties, which are usually situated in between those of the corresponding homopolymers.

The most important tool controlling the electronic properties in conjugated polymers is π delocalization. In general, a fully planar-extended π system favors electron delocalization across the polymer backbone, which leads to a reduction of the bandgap. In addition, the introduction of heteroatoms in the conjugated backbone has an influence on the resonance stability, as well as on the geometric structure by lowering the steric interactions.

It appears that the aromatic-ring resonance stabilization and the reduction of the torsion angle are the most important tools involved in the design of low-bandgap materials. Although the previously mentioned structural and energy parameters have been discussed as being independent of each other, in reality, they interact with each other. The final outcome in terms of the physical properties is often determined by the combined and interactive effects of all of these parameters. Hence, predicting the influence of a particular parameter on the bandgap is not always straightforward. Nevertheless, with the development of better theoretical models, taking into account experimental results, the improvement in quantum-chemical techniques and computational tools has enabled researchers to obtain a quantitative assessment of the combined effect of the molecular structural and energy parameters on the physical properties.

In theoretical modeling, it was assumed that single-polymer chains are not interacting with each other, as in the gas phase. To make the models and calculations more realistic, however, three-dimensional packing effects in solid-state systems should be taken into account, and this can play an important role in the desired properties of conjugated polymers. Usually, the three-dimensional packing effects enhance the interchain interaction, giving rise to a complex set of vibrational modes. This eventually

leads to a suppression of the Peierls distortion in noninteracting one-dimensional chains, thus stabilizing the metallic state in low-bandgap conjugated polymers.

At the next level of modeling, design, and synthesis of low-bandgap materials, intermolecular and interpolymer chain interactions, as well as supramolecular structure formation, etc., should be taken into account. Furthermore, in real systems several other factors, for example, liquid crystallinity, van der Waals interactions, hydrogen bonds, hydrophilic and lipophilic interactions, etc., should be given adequate importance in specific situations.

In the last two decades, the field of conjugated polymers has evolved from one-dimensional linear chains to two-dimensional polymer network structures. Although many research groups are active in the field of supramolecular chemistry and nanotechnology, the ultimate challenge, yet to be resolved, is the secret behind the control of the third supramolecular dimension in π -electron systems.

Section 3 gives a brief overview of the charge-transport properties in doped conducting polymers highlighting the following points:

1. Conducting polymers are rather complex systems, in which the structural and morphological features influence the electrical and optical properties significantly. The charge-transport properties, M–I transition, etc. are strongly governed by both microscopic- and macroscopic-level structural disorder, doping-induced disorder, etc.

2. In general, the effective conjugation length, interchain interactions, and morphology are the most important parameters that influence the physical properties, disorder-induced localization, charge-transport mechanism, etc.

3. In doped conducting polymers, both localized and delocalized states coexist as an interpenetrating network. In oriented materials, the electronic states are delocalized along the chain direction; as a result, the conductivity, carrier mobility, etc. are higher with respect to unoriented systems. In unoriented globular or granular conducting polymer systems, the localized states determine the charge-transport properties.

4. The molecular structure, doping level, interchain interaction, extent of disorder, etc. determine the stability of solitons, polarons, bipolarons, free carriers, etc. in doped conducting polymers.

5. A metallic state has been observed in high-quality samples of doped $(\text{CH})_x$, PPV, PANI, PPy, P3MeT, and PEDOT. The experimental evidence includes the following: finite conductivity at millikelvin temperatures, linear temperature dependence of thermopower, linear term in specific heat, temperature-independent Pauli susceptibility, quantum corrections (weak localization and e–e interaction) to MC, metallic reflectance, and free-carrier absorption in the infrared.

6. A metallic positive TCR has been observed, from 300 to 1.5 K, in ClO_4 -doped $(\text{CH})_x$. In PANI–AMPSA (CSA), the positive TCR is at $T > 70$ (150) K. In several metallic conducting polymer samples, a positive TCR has been observed at $T < 20$ K. These features show the intrinsic metallic nature of doped conducting polymers.

7. The \sqrt{T} dependence of conductivity, at low temperatures, in metallic conducting polymers indicates that the e–e interaction contribution is significant. The universal scaling behavior of magnetoconductance confirms the dominant role of the e–e interaction contribution.

8. In oriented metallic systems, the anisotropic magnetoconductance due to the interplay of WL and e–e interaction contributions [the sign of MC is positive (negative) when the field is perpendicular (parallel) to the chain axis] can be used to probe the misaligned chains.

9. The behavior of $\sigma(T)$ and MC is nearly identical in both the parallel and the perpendicular directions to the chain axis in highly oriented metallic $(\text{CH})_x$ and PPV. This suggests that the charge-transport mechanism is nearly identical in both the parallel and the perpendicular directions to the chain axis, and the system behaves more like an anisotropic three-dimensional system.

10. The metallic, critical, and insulating regimes can be identified from the W versus T plots. The positive, T -independent, and negative temperature coefficients of $W(T)$ correspond to the metallic, critical, and insulating regimes, respectively.

11. In the critical and insulating regimes, the resistivity ratio and positive MR increase as the extent of disorder increases. The field-induced transitions, from the metallic to the critical and from the critical to the insulating regimes, show that the mobility edge and Fermi level are situated rather close. Hence, due to interchain transport and disorder, conducting polymers are at the metal–insulator boundary.

12. From the hopping contribution to the U-shaped behavior in $S(T)$ and the Curie term in $\chi(T)$, a semiquantitative level of information about the extent of disorder can be obtained.

The structurally improved PANI–CSA, PPy–PF₆, and PEDOT–PF₆ samples have provided the opportunity to study the M–I transition and the intrinsic metallic state of conducting polymers by optical spectroscopic measurements. In particular, the optical reflectance spectra of such materials yield a wealth of significant information on the metal physics in the infrared, the electronic structure over a wide energy range, and the nature of the M–I transition in doped conducting polymers. In such a case, a quantitative analysis of the spectra is given in terms of the localization-modified Drude model, leading to the conclusion that doped conducting polymers are “disordered metal” near the M–I transition.

The optical spectra of structurally improved materials are compared with those obtained from conventionally prepared materials. While the structurally improved materials show distinct metallic signatures indicative of delocalized electronic states at the Fermi level, the optical spectra of the conventional samples indicate that the states near the Fermi level are localized due to severe disorder in the context of Anderson localization. Thus, conventional samples can be characterized as a “Fermi glass.” In this case, the two categories of samples show different charge dynamics in the far-infrared consistent with theoretical predictions.

Conjugated polymers, in the undoped state, exhibit the electronic and optical properties of semiconductors in combination with the mechanical properties of general polymers, making them potentially useful for a wide array of applications; particularly in organic optoelectronic devices such as polymer LEDs, photodetectors, photovoltaic cells, etc. Development in the performance of such devices has advanced rapidly, and prototype devices now meet realistic specifications for practical applications. In spite of such successful achievements in the scope of device application, however, there is still controversy over the nature of the electronic structure and the appropriate description of the underlying physics of elementary excitations. Since these issues are both scientifically interesting and critically important to the assessment of the future potential of devices based on conjugated polymers, more detailed

research is required to resolve these issues. Nevertheless, recent research activities on these materials indicate that the rich physics of low-dimensional organic semiconductors can be observed and explored in conjugated polymers.

In conclusion, the past two decades of research in conjugated polymers have grown into an intense interdisciplinary field. The synthesis of conjugated polymers, the processing of these materials within the framework of various studies and applications, the investigation of the electrical and optical properties, the fabrication and performance of conjugated polymer devices all play significant and synergetic roles in the progress that has been achieved so far and in the results that will be obtained in the near future. The status of research and development in this field is quite promising to such an extent that conjugated polymers are probably going to be one of the most important ingredients in the coming generation of molecular electronics and photonics. Moreover, the studies and developments in conjugated polymer electronics can be considered as a bridge and interface between the present-day inorganic semiconductor devices and the electrical and optical devices in organic and even biological systems. It is to be expected that the role of conjugated polymers in biomimetic and biomolecular electronic and photonic devices will also be of considerable importance. The rise of the new and exciting research field of organic conducting materials has been characterized by a holistic approach, which has been imbedded from the very beginning in the scientific approach toward a deeper understanding of material properties and processes. This approach will provide the basis for the fundamental understanding of the intricate and subtle operational mechanisms of electronic and photonic processes not only in purely organic materials and devices, but even at the level of processes and devices interacting with life in its most profound aspects.

Acknowledgments

Raf Kiebooms acknowledges the many fruitful and in-depth discussions with Professor D. Vanderzande and Dr. D. Vangeneugden of the Limburgs Universitair Centrum. Financial support by the National Science Foundation–Flanders is also gratefully acknowledged. Reghu Menon thanks Mr. Ayash K. Mukerjee for his help in preparing this chapter. Kwanghee Lee thanks Heejoo Kim, Yunhee Chang, Jin Young Kim, and Shin-Uk Cho for assistance in preparing the manuscript, and also acknowledges the Korean Science and Engineering Foundation (KOSEF) for financial support under Grant 981-0207-023-2 and also through the Research Center for Dielectric and Advanced Matter Physics at Pusan National University.

REFERENCES

1. T. A. Skotheim, Ed., "Handbook of Conducting Polymers." Vols. 1 and 2. Dekker, New York, 1986.
2. H. S. Nalwa, Ed., "Handbook of Organic Conductive Molecules and Polymers." Vols. 1–4. Wiley, New York, 1997.
3. T. A. Skotheim, R. L. Elsenbaumer, and J. R. Reynolds, Eds., "Handbook of Conducting Polymers." 2nd ed. Dekker, New York, 1998.
4. S. Miyata and H. S. Nalwa, Eds., "Organic Electroluminescent Materials and Devices." Gordon & Breach, Amsterdam, 1997.
5. H. S. Nalwa and S. Miyata, Eds., "Nonlinear Optics of Organic Molecules and Polymers." CRC Press, Boca Raton, FL, 1997.
6. W. R. Salaneck, D. T. Clark, and E. J. Samuelsen, Eds., "Science and Applications of Conducting Polymers." Hilger, New York, 1991.
7. T. A. Skotheim, Ed., "Electroresponsive Molecular and Polymeric Systems." Vols. 1–2. Dekker, New York, 1991.
8. W. R. Salaneck, I. Lundström, and B. Rånby, Eds., "Conjugated Polymers and Related Materials—The Interconnection of Chemical and Electronic Structure." Oxford Univ. Press, Oxford, 1993.
9. M. Aldissi, Ed., "Intrinsically Conducting Polymers: An Emerging Technology." Kluwer Academic, Dordrecht, 1992.
10. R. G. Linford, Ed., "Electrochemical Science and Technology of Polymers." Vol. 2. Elsevier Applied Science, New York, 1990.
11. J. L. Brédas, Ed., "Conjugated Oligomers, Polymers and Dendrimers: From Polyacetylene to DNA." De Boeck Univ., Paris, 1999.
12. J. L. Brédas and R. Silbey, Eds., "Conjugated Polymers." Kluwer Academic, Dordrecht, 1991.
13. M. E. G. Lyons, Ed., "Electroactive Polymer Chemistry." Vols. 1–2. Plenum, New York, 1994.
14. S. Masubuchi, S. Kazama, K. Mizoguchi, F. Shimizu, K. Kume, R. Matsushita, and T. Matsuyama, *Synth. Met.* 69, 71 (1995).
15. H. Kaneko and T. Ishiguro, *Synth. Met.* 65, 141 (1994).
16. W. Tritthart and G. Leising, *Synth. Met.* 57, 4878 (1993).
17. H. Kaneko, Y. Nogami, T. Isohiguro, H. Nishiyama, H. Ishimoto, A. Takahashi, and J. Tsukamoto, *Synth. Met.* 57, 4888 (1993).
18. C. O. Yoon, M. Reghu, A. J. Heeger, E. B. Park, Y. W. Park, K. Akagi, and H. Shirakawa, *Synth. Met.* 69, 79 (1995).
19. Y. Cao, P. Smith, and A. J. Heeger, *Synth. Met.* 41–43, 181 (1991).
20. R. Zuzok, S. Roth, and F. Kremer, *Synth. Met.* 41–43, 193 (1991).
21. E. B. Park, J. S. Yoo, J. Y. Park, Y. W. Park, K. Akagi, and H. Shirakawa, *Synth. Met.* 69, 61 (1995).
22. J. Tsukamoto and A. Takahashi, *Synth. Met.* 41–43, 7 (1991).
23. N. Foxonnet, J. L. Ribet, N. Coustel, and M. Galtier, *Synth. Met.* 41–43, 85 (1991).
24. D. Wang, S. Hasegawa, M. Shimizu, and J. Tanaka, *Synth. Met.* 46, 85 (1992).
25. H. Shirakawa, Y.-K. Zhang, T. Okuda, K. Sakamaki, and K. Akagi, *Synth. Met.* 65, 93 (1991).
26. S. M. Huang and R. B. Kaner, *Synth. Met.* 41–43, 101 (1991).
27. E. T. Kang, T. C. Tan, K. G. Neoh, and Y. K. Ong, *Polymer* 27, 1958 (1986).
28. E. T. Kang, K. G. Neoh, T. C. Tan, and Y. K. Ong, *J. Macromol. Sci., Chem.* A24, 631 (1987).
29. H. S. O. Chan, H. S. Munro, C. Davies, and E. T. Kang, *Synth. Met.* 22, 365 (1988).
30. K. G. Neoh, T. C. Tan, and E. T. Kang, *Polymer* 29, 553 (1988).
31. K. C. Khulbe, R. S. Mann, and C. P. Khulbe, *J. Polym. Sci., Polym. Chem. Ed.* 20, 1089 (1982).
32. E. T. Kang, K. G. Neoh, T. C. Tan, and Y. K. Ong, *J. Polym. Sci., Polym. Chem. Ed.* 25, 2143 (1987).
33. M. G. Kanatzidis, L. M. Tonge, T. K. Marks, H. O. Marcy, and C. R. Kannewurf, *J. Am. Chem. Soc.* 109, 3797 (1987).
34. M. Zagorska and A. Pron, *Synth. Met.* 18, 43 (1987).
35. S. Rapi, V. Bocchi, and G. P. Gardini, *Synth. Met.* 24, 217 (1988).
36. S. Machida, S. Miyata, and A. Techagumpuch, *Synth. Met.* 31, 311 (1989).
37. J. Lei, Z. Cai, and C. R. Martin, *Synth. Met.* 46, 53 (1992).
38. Y. A. Bubitsky, B. A. Zhubanov, and G. G. Maresch, *Synth. Met.* 41–43, 375 (1991).
39. T. Shimidzu, A. Ohtani, M. Aiba, and K. Honda, *J. Chem. Soc., Faraday Trans.* 184, 3941 (1988).
40. S. Machida and S. Miyata, *Polym. Prepr. Jpn.* 36, 1886 (1987).
41. T. Ikegami, S. Machida, S. Miyata, and T. Yoshikawa, *Polym. Prepr. Jpn.* 37, 738 (1988).
42. O. Ithato and N. Toshima, "Proceedings of the 66th Fall Meeting of the Chemical Society Japan, of." No. 2B622, 1993, p. 237.
43. H. Masuda, S. Tanaka, and K. Kaeriyama, *Synth. Met.* 33, 365 (1989).
44. N. M. Castillo-Ortega, M. B. Inoue, and M. Inoue, *Synth. Met.* 28, C65 (1989).

45. M. Yamaura, K. Sato, and T. Hagiwara, *Synth. Met.* 41–43, 439 (1991).
46. M. Reghu, C. O. Yoon, D. Moses, and A. J. Heeger, *Synth. Met.* 64, 53 (1994).
47. Y. Nogami, J. P. Pouget, and T. Ishiguro, *Synth. Met.* 62, 257 (1994).
48. B. Zaid, S. Aeiyaach, and P. C. Lacaze, *Synth. Met.* 65, 27 (1994).
49. M. Satoh, H. Ishikawa, K. Amano, E. Hasegawa, and K. Yoshino, *Synth. Met.* 65, 39 (1994).
50. O. Chauvet, S. Paschen, L. Forro, L. Zuppiroli, P. Bujard, K. Kai, and W. Wernet, *Synth. Met.* 63, 115 (1994).
51. J. H. Lee and I. J. Chung, *Synth. Met.* 53, 245 (1993).
52. N. Toshima and O. Ihata, *Synth. Met.* 79, 165 (1996).
53. O. Jarjayers, P. H. Fries, and G. Bidan, *Synth. Met.* 69, 343 (1995).
54. S. Masubuchi, S. Kazama, R. Matsushita, and R. Matsuyama, *Synth. Met.* 69, 345 (1995).
55. F. L. Dos Santos and C. P. De Melo, *Synth. Met.* 69, 347 (1995).
56. D. Stanke, M. L. Hallenselben, and L. Toppare, *Synth. Met.* 72, 159 (1995).
57. D. Stanke, M. L. Hallenselben, and L. Toppare, *Synth. Met.* 73, 267 (1995).
58. J. Hlavaty, V. Papez, L. Kavan, and P. Krtil, *Synth. Met.* 66, 165 (1994).
59. J. Y. Lee, D. Y. Kim, and C. Y. Kim, *Synth. Met.* 74, 103 (1995).
60. M. Voigt, M. L. Hallenselben, and L. Toppare, *Synth. Met.* 55–57, 1067 (1993).
61. G. Tourillon and F. Garnier, *J. Electroanal. Chem.* 135, 173 (1982).
62. R. J. Waltman, J. Bargon, and A. F. Diaz, *J. Phys. Chem.* 87, 1459 (1983).
63. K. Kaneto, Y. Kohno, K. Yoshino, and Y. Inuishi, *J. Chem. Soc. Chem. Commun.* 382 (1983).
64. S. Hotta, T. Hosaka, and W. Shimotsuma, *Synth. Met.* 6, 69 (1983).
65. S. Tanaka, M. Sato, and K. Kaeriyama, *Makromol. Chem.* 185, 1295 (1984).
66. M. Ito, H. Shioda, and K. Tanaka, *J. Polym. Sci.* 24, 147 (1986).
67. M. Sato, S. Tanaka, and K. Kaeriyama, *J. Chem. Soc., Chem. Commun.* 185 (1984).
68. J. Roncali, A. Yassar, and F. Garnier, *J. Chim. Phys.* 86, 85 (1989).
69. G. Tourillon and F. Garnier, *J. Phys. Chem.* 87, 2289 (1983).
70. S. Hotta, T. Hosaka, and W. Shimotsuma, *Synth. Met.* 6, 317 (1983).
71. S. Hotta, *Synth. Met.* 22, 103 (1988).
72. J. Roncali and F. Garnier, *New J. Chem.* 4–5, 237 (1986).
73. R. M. Eales and A. R. Hillman, *J. Electroanal. Chem.* 250, 219 (1988).
74. J. Roncali, A. Yassar, and F. Garnier, *Synth. Met.* 28, C275 (1989).
75. J. Roncali, A. Yassar, and F. Garnier, *J. Chem. Soc., Chem. Commun.* 581 (1988).
76. M. S. A. Abdou and S. Holdcroft, *Synth. Met.* 60, 93 (1993).
77. G. Kossmehl and G. Chatzitheodorou, *Makromol. Chem., Rapid Commun.* 4, 639 (1983).
78. J. P. Montheard, G. Boiteux, B. Thémans, J. L. Brédas, T. Pascal, and G. Froyer, *Synth. Met.* 36, 195 (1990).
79. K. Waragai and S. Hotta, *Synth. Met.* 41, 519 (1991).
80. G. W. Heffer and D. S. Pearson, *Synth. Met.* 44, 341 (1991).
81. H. Ishikawa, K. Amane, A. Kobayashi, M. Satoh, and E. Hasegawa, *Synth. Met.* 64, 49 (1994).
82. H. Jarvinen, L. Lahtinen, I. Nasman, O. Hormi, and A. L. Tammi, *Synth. Met.* 69, 299 (1995).
83. J. Moulton and P. Smith, *Synth. Met.* 40, 13 (1991).
84. M. Shimomara, M. Kaga, N. Nakayama, and S. Miyauchi, *Synth. Met.* 69, 313 (1995).
85. T. Yamamoto, A. Morita, T. Maruyama, Z. H. Zhou, T. Kanbara, and K. Sanechika, *Polym. J.* 22, 187 (1990).
86. H. S. Nalwa, *Angew. Makromol. Chem.* 188, 105 (1991).
87. T. Yamamoto, T. Maruyama, Z. H. Zhou, Y. Miyazaki, T. Kanbara, and K. Sanechika, *Synth. Met.* 41, 345 (1991).
88. K. Waragai and S. Hotta, *Synth. Met.* 41, 519 (1991).
89. Y. Miyazaki, T. Kanbara, K. Osakada, and T. Yamamoto, *Chem. Lett.* 3, 415 (1993).
90. K. Y. Jen, C. C. Han, and R. L. Elsenbaumer, *Mol. Cryst. Liq. Cryst.* 189, 169 (1990).
91. M. Onoda, H. Nakayama, S. Morita, and K. Yoshino, *J. Appl. Phys.* 73, 2859 (1993).
92. G. Kossmehl and M. Niemitz, *Synth. Met.* 41, 1065 (1991).
93. M. Pomerantz, J. J. Tseng, H. Zhu, S. J. Sproull, J. R. Reynolds, R. Uitz, H. J. Arnott, and M. I. Haider, *Synth. Met.* 41–43, 825 (1991).
94. Y. S. Gai, B. Jung, and S. K. Choi, *J. Appl. Polym. Sci.* 42, 1793 (1991).
95. M. L. Blohm, P. C. van Dort, and J. E. Pickett, *Polym. Mater. Sci. Eng.* 64, 210 (1991).
96. M. L. Blohm, P. C. van Dort, and J. E. Pickett, *CHEMTECH* 22, 105 (1992).
97. L. W. Schacklette, H. Eckhardt, R. R. Chance, G. G. Miller, D. M. Ivory, and R. H. Baughman, *J. Chem. Phys.* 73, 4098 (1980).
98. D. M. Ivory, G. G. Miller, J. M. Sowa, L. W. Schacklette, R. R. Chance, and R. H. Baughman, *J. Chem. Phys.* 71, 1506 (1979).
99. L. Athouel, Y. Pelous, G. Froyer, G. Louarn, and S. Lefrant, *J. Chem. Phys.* 89, 1285 (1992).
100. A. Pron, I. Kusszewicz, D. Billaud, and J. Prylusi, *J. Chem. Soc., Chem. Commun.* 783 (1981).
101. D. R. Rueda, T. A. Ezquerria, M. E. Cagiao, F. J. Balta Calleja, and J. Alonoso-Lopez, *Mol. Cryst. Liq. Cryst.* 118, 263 (1985).
102. M. Peo, S. Roth, K. Dransfeld, B. Ticke, J. Hocker, H. Gross, A. Grupp, and H. Sixl, *Solid State Commun.* 35, 119 (1980).
103. M. Tabata, M. Satoh, K. Kaneto, and K. Yoshino, *J. Phys. Soc. Jpn.* 55, 1305 (1986).
104. M. Tabata, M. Satoh, K. Kaneto, and K. Yoshino, *J. Phys. C: Solid State Phys.* 19, L101 (1986).
105. T. C. Clarke, K. K. Kanazawa, V. Y. Lee, J. R. Rabolt, J. R. Reynolds, and G. B. Street, *J. Polym. Sci., Polym. Phys. Ed.* 20, 117 (1982).
106. K. Miyashita and M. Kaneko, *Synth. Met.* 68, 161 (1995).
107. E. W. Chang, R. J. Kuk, and R. B. Kaner, *Synth. Met.* 55–57, 930 (1993).
108. Y. W. Park, E. B. Park, K. H. Kim, C. K. Park, and J. I. Jin, *Synth. Met.* 41–43, 315 (1991).
109. A. Sakomoto, Y. Furukawa, M. Tasumi, T. Noguchi, and T. Ohnishi, *Synth. Met.* 69, 439 (1995).
110. D. Y. Kim, C. S. Ha, and W. J. Cho, *Synth. Met.* 69, 497 (1995).
111. I. N. Kang, D. H. Hwang, and H. K. Shim, *Synth. Met.* 69, 547 (1995).
112. H. K. Shim, D. H. Hwang, J. I. Lee, and K. S. Lee, *Synth. Met.* 55–57, 908 (1993).
113. Y. Sonoda, Y. Nakao, and K. Kaeriyama, *Synth. Met.* 55–57, 918 (1993).
114. R. Mertens, P. Nagels, R. Callaerts, M. V. Roy, J. Briers, and H. J. Geise, *Synth. Met.* 51, 55 (1992).
115. J. P. Travers, P. Le Guyadec, P. N. Adams, P. J. Laughlin, and A. P. Monkman, *Synth. Met.* 69, 229 (1995).
116. H. Yoon, B. S. Jung, and H. Lee, *Synth. Met.* 41–43, 669 (1991).
117. J. Anand, S. Palaniappan, and D. N. Sathyanarayana, *Synth. Met.* 66, 129 (1994).
118. A. Kitani, K. Satoguchi, H. Q. Tang, S. Ito, and K. Sasaki, *Synth. Met.* 69, 129 (1995).
119. A. Kitani, K. Satoguchi, H. Q. Tang, S. Ito, and K. Sasaki, *Synth. Met.* 69, 131 (1995).
120. J. R. Santos, Jr., J. A. Malmonge, A. J. G. Conceicao Silva, A. J. Motheo, Y. P. Mascarenhas, and L. H. C. Mattoso, *Synth. Met.* 69, 141 (1995).
121. X. H. Wang, L. X. Wang, X. B. Jing, and F. S. Wang, *Synth. Met.* 69, 149 (1995).
122. H. Yan and N. Toshima, *Synth. Met.* 69, 151 (1995).
123. S. K. Jeong, J. S. Suh, E. J. Oh, Y. W. Park, C. Y. Kim, and A. G. MacDiarmid, *Synth. Met.* 69, 171 (1995).

124. G. Boara and M. Sparpaglione, *Synth. Met.* 72, 135 (1995).
125. A. Lian, S. Besner, and L. Dao, *Synth. Met.* 74, 21 (1995).
126. O. Oka, O. Kiyohara, S. Morita, and K. Yoshino, *Synth. Met.* 55–57, 999 (1993).
127. A. Pron, *Synth. Met.* 46, 277 (1992).
128. Y. Cao, P. Smith, and A. J. Heeger, *Synth. Met.* 48, 91 (1992).
129. C. O. Yoon, J. H. Kim, H. K. Sung, J. H. Kim, K. Lee, and H. Lee, *Synth. Met.* 81, 75 (1996).
130. A. P. Monkman and P. Adams, *Synth. Met.* 40, 87 (1991).
131. A. Pron, W. Zuzny, and J. Laska, *Synth. Met.* 80, 191 (1996).
132. W. A. Gazotti, Jr., and M. A. Depaoli, *Synth. Met.* 80, 263 (1996).
133. K. Yoshizawa, A. Ito, K. Tanaka, and T. Yamabe, *Synth. Met.* 48, 271 (1992).
134. J. H. Burroughes, D. D. C. Bradley, A. R. Brown, R. N. Marks, K. Mackay, R. H. Friend, P. L. Burns, and A. B. Holmes, *Nature* 347, 539 (1990).
135. P. Kovacic and M. B. Jones, *Chem. Rev.* 87, 357 (1987).
136. J. Roncali, *Chem. Rev.* 92, 711 (1992).
137. J. Roncali, *Chem. Rev.* 97, 173 (1997).
138. W. J. Feast, J. Tsibouklis, K. L. Pouwer, L. Groenendaal, and E. W. Meijer, *Polymer* 37, 5017 (1996).
139. G. Natta, G. Mazzanti, and P. Corradini, *Atti. Acad. Naz. Lincei Rend. Cl. Sci. Fis. Mat. Natur.* 25, 3 (1958).
140. W. E. Daniels, *J. Org. Chem.* 29, 2936 (1964).
141. L. B. Luttinger, *J. Org. Chem.* 27, 1591 (1962).
142. D. J. Berets and D. S. Smith, *Trans. Faraday Soc.* 64, 823 (1968).
143. M. Hatano, S. Kambara, and S. Okamoto, *J. Polym. Sci.* 51, S26 (1961).
144. H. Shirakawa and S. Ikeda, *Polym. J.* 2, 231 (1971).
145. H. Shirakawa, T. Ito, and S. Ikeda, *Polym. J.* 4, 460 (1973).
146. W. H. Warson, Jr., W. C. McMordie, Jr., and L. G. Lands, *J. Polym. Sci.* 55, 137 (1968).
147. H. C. Longuet-Higgins and L. Salem, *Proc. R. Soc. London, Ser. A* 251, 172 (1959).
148. Y. Ooshika, *J. Phys. Soc. Jpn.* 12, 1238 (1957).
149. A. A. Ovchinnikov, I. I. Ukrainskii, and G. V. Kventsel, *Sov. Phys. Usp.* 15, 575 (1973).
150. N. S. Bayliss, *J. Chem. Phys.* 16, 287 (1948).
151. N. S. Bayliss, *Quart. Rev.* 6, 319 (1952).
152. H. Kuhn, *Helv. Chim. Acta* 31, 1441 (1948).
153. T. Ito, H. Shirakawa, and S. Ikeda, *J. Polym. Sci. Polym. Chem. Ed.* 12, 11 (1974).
154. C. K. Chiang, C. R. Fincher, Y. W. Park, A. J. Heeger, H. Shirakawa, E. J. Lewis, S. C. Gau, and A. G. MacDiarmid, *Phys. Rev. Lett.* 39, 1098 (1977).
155. H. Shirakawa, E. J. Lewis, A. G. MacDiarmid, C. K. Chiang, and A. J. Heeger, *J. Chem. Soc., Chem. Commun.* 578 (1977).
156. J. C. W. Chien, "Polyacetylene: Chemistry, Physics and Materials Science." Academic Press, Orlando, 1984.
157. S. Curran, A. Stark-Hauser, and S. Roth, in "Organic Conductive Molecules and Polymers" (H. S. Nalwa, Ed.), Vol. 2, pp. 2–59. Wiley, New York, 1997.
158. W. J. Feast, J. Tsibouklis, K. L. Pouwer, L. Groenendaal, and E. W. Meijer, *Polymer* 22, 5017 (1996).
159. S. Roth, "One-Dimensional Metals: Physics and Materials Science." VCH, Weinheim, 1995.
160. H. Shirakawa, Y. X. Zhang, and K. Akagi, in "Conjugated Polymers and Related Materials: The Interconnection of Chemical and Electronic Structure" (W. R. Salaneck, I. Lundström, and B. Rånby, Eds.), pp. 65–72. Oxford Univ. Press, Oxford, 1993.
161. H. Shirakawa, in "Handbook of Conducting Polymers" (T. A. Skotheim, R. L. Elsenbaumer, and J. R. Reynolds, Eds.), pp. 197–208. Dekker, New York, 1998.
162. L. Yu, "Solitons and Polarons in Conducting Polymers." World Scientific, Singapore, 1988.
163. J. A. Nieuwand and R. R. Vogt, "The Chemistry of Acetylene." Reinhold, New York, 1945.
164. M. J. M. Abadie and S. M. Bouklie-Hacene, *Eur. Polym. J.* 24, 319 (1988).
165. M. Aldissi, F. Schué, L. Giral, and M. Rolland, *Polymer* 23, 246 (1982).
166. M. Aldissi and F. Schué, *Macromolecules* 17, 1633 (1984).
167. J. A. Shelburne and G. L. Baker, *Macromolecules* 20, 1212 (1987).
168. H. Shirakawa and S. Ikeda, *Synth. Met.* 1, 175 (1980).
169. G. L. Baker, J. A. Shelburne, and F. S. Bates, *J. Am. Chem. Soc.* 108, 7377 (1986).
170. H. Haberkorn, W. Heckman, G. Kohler, H. Naarmann, J. Schlag, P. Simak, N. Theophilou, and R. Voelkel, *Eur. Polym. J.* 24, 497 (1988).
171. H. Naarmann and N. Theophilou, *Synth. Met.* 22, 1 (1987).
172. J. Tsukamoto, A. Takahashi, and K. Kawasaki, *Jpn., J. Appl. Phys.* 29, 125 (1990).
173. J. Tsukamoto, *Adv. Phys.* 41, 509 (1992).
174. V. M. Kobryanskii, *Synth. Met.* 46, 251 (1992).
175. V. M. Kobryanskii, *Synth. Met.* 49, 203 (1992).
176. V. Enkelmann, W. Müller, and G. Wegner, *Synth. Met.* 1 (1980).
177. V. Enkelmann, G. Lieser, W. Müller, and G. Wegner, *Angew. Makromol. Chem.* 94, 105 (1981).
178. G. Lieser, G. Wegner, W. Müller, and V. Enkelmann, *Makromol. Chem., Rapid Commun.* 1, 621 (1980).
179. M. Aldissi, C. Linaya, J. Sledz, F. Schué, L. Giral, J. M. Fabre, and M. Rolland, *Polymer* 23, 243 (1982).
180. N. Theophilou, A. Munardi, T. Aznar, J. Sledz, F. Schué, and H. Naarmann, *Eur. Polym. J.* 23, 15 (1987).
181. S. L. Hsu, A. J. Signorelli, G. P. Pez, and R. H. Baughman, *J. Chem. Phys.* 69, 106 (1978).
182. H. G. Alt, H. E. Engelhardt, M. D. Rausch, and L. B. Kool, *J. Organomet. Chem.* 329, 61 (1987).
183. J. R. Martinez, M. D. Rausch, J. C. W. Chien, and H. G. Alt, *Makromol. Chem.* 190, 1309 (1989).
184. F. Cataldo, *Polym. Commun.* 33, 3073 (1992).
185. S. A. Chen and H. J. Shy, *J. Polym. Sci., Polym. Chem. Ed.* 23, 2441 (1985).
186. J. Heavyside, P. J. Hendra, P. Tsai, and R. P. Coony, *J. Chem. Soc. Faraday Trans. 1* 74, 2542 (1978).
187. N. Kurokawa, M. Tabata, and J. Sohma, *J. Polym. Sci., Polym. Lett. Ed.* 19, 355 (1985).
188. V. Rives-Arnau and N. Sheppard, *J. Chem. Soc., Faraday Trans. 1* 76, 394 (1980).
189. K. Soga, Y. Kobayashi, S. Ikeda, and S. Kawakami, *J. Chem. Soc., Chem. Commun.* 931 (1980).
190. M. Aldissi and R. Liepins, *J. Chem. Soc., Chem. Commun.* 256 (1984).
191. Y. Tabata, B. Saito, H. Shibano, H. Sobue, and K. Oshima, *Makromol. Chem.* 76, 89 (1964).
192. K. Aoki, Y. Kakudate, S. Usuba, M. Yoshida, K. Tanaka, and S. Fujiwara, *Solid State Commun.* 64, 1329 (1987).
193. K. Aoki, Y. Kakudate, S. Usuba, M. Yoshida, K. Tanaka, and S. Fujiwara, *J. Chem. Phys.* 88, 4565 (1988).
194. K. Aoki, S. Usuba, M. Yoshida, Y. Kakudate, K. Tanaka, and S. Fujiwara, *J. Chem. Phys.* 89, 529 (1988).
195. K. Aoki, Y. Kakudate, S. Usuba, M. Yoshida, K. Tanaka, and S. Fujiwara, *Synth. Met.* 28, D91 (1989).
196. Y. V. Korshak, V. V. Korshak, G. Kanischka, and H. Höcker, *Makromol. Chem., Rapid Commun.* 6, 685 (1985).
197. F. L. Klavetter and R. H. Grubbs, *J. Am. Chem. Soc.* 110, 7807 (1988).
198. *Eur. Plas. News* 17 (June 1993).
199. H. J. Bowley, D. L. Gerrard, and W. F. Maddams, *Makromol. Chem.* 186, 715 (1985).
200. D. C. Bott, C. K. Chai, J. H. Edwards, W. J. Feast, R. H. Friend, and M. E. Horton, *J. Phys. Colloq. (Paris)* 44, 143 (1983).

201. D. C. Bott, C. S. Brown, C. K. Chai, N. S. Walker, W. J. Feast, P. J. S. Foot, P. D. Calvert, N. C. Billingham, and R. H. Friend, *Synth. Met.* 14, 245 (1986).
202. D. C. Bott, C. S. Brown, J. N. Winter, and J. Barker, *Polymer* 28, 601 (1987).
203. C. S. Brown, M. E. Vickers, P. J. S. Foot, N. C. Billingham, and P. D. Calvert, *Polymer* 27, 1719 (1986).
204. J. H. Edwards and W. J. Feast, *Polymer* 21, 595 (1980).
205. J. H. Edwards, W. J. Feast, and D. C. Bott, *Polymer* 25, 395 (1984).
206. W. J. Feast and J. N. Winter, *J. Chem. Soc., Chem. Commun.* 202 (1985).
207. W. J. Feast, M. J. Taylor, and J. N. Winter, *Polymer* 28, 601 (1987).
208. P. J. S. Foot, P. D. Calvert, N. C. Billingham, C. S. Brown, N. S. Walker, and D. I. James, *Polymer* 27, 448 (1986).
209. M. M. Sokolowski, E. A. Marseglia, and R. H. Friend, *Polymer* 27, 1714 (1986).
210. J. H. Townsend, C. M. Pereira, D. D. C. Bradley, M. E. Horton, and R. H. Friend, *J. Phys. C: Solid State Phys.* 18, L283 (1985).
211. D. White and D. C. Bott, *Polym. Commun.* 25, 98 (1984).
212. K. Knoll and R. R. Schrock, *J. Am. Chem. Soc.* 111, 7989 (1989).
213. G. Widawski, W. J. Feast, and P. Dounis, *J. Mater. Chem.* 5, 1847 (1995).
214. T. M. Swager, D. A. Dougherty, and R. H. Grubbs, *J. Am. Chem. Soc.* 110, 2973 (1988).
215. H. W. Gibson, in "Handbook of Conducting Polymers" (T. A. Skotheim, Ed.), Vol. 1, pp. 405-439. Dekker, New York, 1986.
216. R. L. Elsenbaumer and L. W. Schacklette, in "Handbook of Conducting Polymers" (T. A. Skotheim, Ed.), Vol. 1, pp. 213-263. Dekker, New York, 1986.
217. M. B. Jones and P. Kovacic, in "Encyclopaedia of Polymer Science and Engineering" (J. I. Kroschwitz, Ed.), Vol. 10, p. 670. Wiley, New York, 1987.
218. M. B. Jones and P. Kovacic, in "Comprehensive Polymer Science" (G. C. Eastmond, A. Ledwith, S. Russo, and P. Sigwalt, Eds.), Vol. 5, p. 465. Pergamon, Oxford, 1989.
219. P. C. Lacaze, S. Aeiya, and J. C. Lacroix, in "Organic Conductive Molecules and Polymers" (H. S. Nalwa, Ed.), Vol. 2, p. 205. Wiley, New York, 1997.
220. H. Naarmann, M. Beaujean, R. Merenyi, and H. G. Viehe, *Polym. Bull.* 2, 683 (1980).
221. G. K. Noren, *J. Polym. Sci., Part D: Macromol. Rev.* 5, 385 (1971).
222. A. D. Schlüter, in "Handbook of Conducting Polymers" (T. A. Skotheim, R. L. Elsenbaumer, and J. R. Reynolds, Eds.), 2nd ed., p. 209. Dekker, New York, 1998.
223. J. G. Speight, P. Kovacic, and F. W. Koch, *J. Macromol. Sci., Rev. Macromol. Chem.* C5, 295 (1971).
224. J. M. Tour, *Adv. Mater.* 6, 190 (1994).
225. P. Kovacic and A. Kyriakis, *J. Am. Chem. Soc.* 85, 454 (1963).
226. P. Kovacic and A. Kyriakis, *J. Org. Chem.* 29, 100 (1963).
227. P. Kovacic and J. Oziomek, *J. Org. Chem.* 29, 100 (1964).
228. P. Kovacic and R. J. Hopper, *J. Polym. Sci. Part A: Polym. Chem.* 4, 1445 (1966).
229. N. Toshima, K. Kanaka, A. Koshirai, and H. Hirai, *Bull. Chem. Soc. Jpn.* 61, 2551 (1988).
230. V. M. Kobryanskii and S. A. Arnoutov, *J. Chem. Soc., Chem. Commun.* 727 (1992).
231. J. K. Stille, F. W. Harris, H. Mukamal, R. O. Rakutis, C. L. Schilling, G. K. Noren, and J. A. Reed, *Adv. Chem. Ser.* 91, 625 (1969).
232. V. F. VanKerckhoven, Y. K. Gilliams, and J. K. Stille, *Macromolecules* 5, 541 (1972).
233. J. N. Braham, T. Hodgins, T. Katto, R. T. Kohl, and J. K. Stille, *Macromolecules* 11, 343 (1978).
234. V. V. Korshak, V. A. Sergeev, and Y. A. Chernomordik, *Vysokomol. Soedin. Ser. B.* 19, 493 (1977).
235. V. V. Korshak, V. A. Sergeev, Y. A. Chernomordik, and S. B. Alaev, *Izv. Akad. Nauk. SSSR, Ser. Khim.* 1645 (1977).
236. P. Kovacic and F. Koch, *J. Org. Chem.* 28, 1836 (1963).
237. P. Kovacic and R. M. Lange, *J. Org. Chem.* 28, 968 (1963).
238. P. Kovacic, F. W. Koch, and C. E. Stephan, *J. Polym. Sci., Polym. Chem. Ed.* 2, 1193 (1964).
239. G. A. Olah, P. Schilling, and I. M. Gross, *J. Am. Chem. Soc.* 96, 876 (1974).
240. J. Simitzis and C. Dimopoulou, *Makromol. Chem.* 185, 2553 (1984).
241. F. Teraoka and T. Takahashi, *J. Macromol. Sci., Phys.* B18, 73 (1980).
242. J. A. John and J. M. Tour, *J. Am. Chem. Soc.* 116, 5011 (1994).
243. G. Goldfinger, *J. Polym. Sci.* 4, 93 (1951).
244. S. Claesson, R. Gehm, and W. Kern, *Makromol. Chem.* 7, 46 (1951).
245. M. Hellmann, A. J. Bilbo, and W. J. Pummer, *J. Am. Chem. Soc.* 77, 3650 (1955).
246. W. Kern and R. Gehm, *Angew. Chem.* 62, 337 (1950).
247. H. O. Wirth, R. Müller, and W. Kern, *Makromol. Chem.* 77, 90 (1964).
248. G. P. Brown, *Chem. Abstr.* 67, 22447 (1967).
249. W. Kern, R. Gehm, and M. Siebel, *Makromol. Chem.* 15, 170 (1955).
250. S. K. Taylor, S. G. Bennett, I. Khoury, and P. Kovacic, *J. Polym. Sci., Polym. Lett. Ed.* 19, 85 (1981).
251. W. Hertz and R. Ullrich, *Makromol. Chem.* 98, 29 (1966).
252. M. Jozefowicz and R. Buvet, *C. R. Acad. Sci. (Paris)* 253, 1801 (1961).
253. M. Jozefowicz, *Bull. Soc. Chim. F.* 2036 (1963).
254. J. M. Tours and E. B. Stephen, *J. Am. Chem. Soc.* 113, 2309 (1991).
255. G. Wittig and F. Bickelhaupt, *Chem. Ber.* 91, 883 (1958).
256. A. A. Berlin, *J. Polym. Sci.* 55, 621 (1961).
257. T. Yamamoto, *Prog. Polym. Sci.* 17, 1153 (1992).
258. T. Yamamoto, in "Organic Conductive Molecules and Polymers" (H. S. Nalwa, Ed.), Vol. 2, pp. 171-204. Wiley, New York, 1997.
259. N. Bumagin and I. P. Beletskaya, *Russ. Chem. Rev. (Engl. Transl.)* 59, 1174 (1990).
260. M. Kumada, *Pure Appl. Chem.* 52, 669 (1980).
261. E. Negishi, *Pure Appl. Chem.* 53, 2333 (1981).
262. J. K. Stille, *Angew. Chem., Int. Ed. Engl.* 25, 508 (1986).
263. K. Tamao, K. Sumitani, and M. Kumada, *J. Am. Chem. Soc.* 94, 4374 (1972).
264. Y. Kiso, M. Zembayashi, A. Fujioka, S. Kodama, I. Nakajima, A. Minato, and M. Kumada, *Bull. Chem. Soc. Jpn.* 49, 1958 (1976).
265. D. G. Morrel and J. K. Kochi, *J. Am. Chem. Soc.* 97, 7262 (1975).
266. A. Sekiya and N. Ishikawa, *J. Organomet. Chem.* 118, 349 (1976).
267. A. Sekiya and N. Ishikawa, *J. Organomet. Chem.* 125, 281 (1977).
268. M. Uchino, A. Yamamoto, and S. Ikeda, *J. Organomet. Chem.* 24, C63 (1970).
269. M. Uchino, K. Asagi, A. Yamamoto, and S. Ikeda, *J. Organomet. Chem.* 84, 93 (1975).
270. T. Yamamoto and A. Yamamoto, *Chem. Lett.* 353 (1977).
271. T. Yamamoto, Y. Hayashi, and A. Yamamoto, *Bull. Chem. Soc. Jpn.* 51, 2091 (1978).
272. M. Rehahn, A. D. Schlüter, G. Wegner, and W. J. Feast, *Polymer* 30, 1054 (1989).
273. T. Yamamoto, A. Morita, Y. Miyazaki, T. Maruyama, H. Wakayama, Z. Zhou, Y. Nakamura, T. Kanbara, S. Sasaki, and K. Kubota, *Macromolecules* 25 (1992).
274. M. F. Semmelhack, P. M. Helquist, and L. D. Jones, *J. Am. Chem. Soc.* 93, 5908 (1971).
275. M. F. Semmelhack and L. S. Ryono, *J. Am. Chem. Soc.* 97, 3874 (1975).
276. M. F. Semmelhack, P. M. Helquist, L. D. Jones, L. Keller, L. Mendelson, L. S. Ryono, J. G. Smith, and R. D. Stauffer, *J. Am. Chem. Soc.* 103, 6460 (1981).
277. K. Chmil and U. Sherf, *Makromol. Chem., Rapid Commun.* 14, 217 (1993).
278. P. Caubere, *Angew. Chem., Int. Ed. Engl.* 22, 599 (1983).
279. C. S. Chao, C. H. Cheng, and C. T. Chang, *J. Org. Chem.* 48, 4904 (1983).
280. P. W. Jennings, D. G. Pillsbury, J. L. Hall, and V. T. Brice, *J. Org. Chem.* 41, 719 (1976).

281. A. S. Kende, L. S. Liebeskind, and D. M. Braitsch, *Tetrahedron Lett.* 3375 (1975).
282. H. Matsumoto, S. I. Inaba, and R. D. Rieke, *J. Org. Chem.* 48, 840 (1983).
283. M. Mori, Y. Hashimoto, and Y. Ban, *Tetrahedron Lett.* 21, 631 (1980).
284. G. Schiavon, G. Bontempelli, and B. Corain, *J. Chem. Soc., Dalton Trans.* 1074 (1981).
285. K. Takagi, N. Hayama, and K. Sasaki, *Bull. Chem. Soc. Jpn.* 57, 1887 (1984).
286. M. Tiecco, L. Testaferri, M. Tingoli, D. Chianelli, and M. Montanucci, *Synthesis* 736 (1984).
287. M. Troupel, Y. Rollin, S. Sibille, J. F. Fauvarque, and J. Perichon, *J. Chem. Res., Synop.* 26 (1980).
288. M. Troupel, Y. Rollin, S. Sibille, J. Perichon, and J. F. Fauvarque, *J. Organomet. Chem.* 202, 435 (1980).
289. R. Vanderesse, J. J. Brunet, and P. Caubere, *J. Organomet. Chem.* 264, 263 (1984).
290. M. Zembayashi, K. Tamao, J. Yoshida, and M. Kumeda, *Tetrahedron Lett.* 4089 (1977).
291. I. Colon and D. Kelsey, *J. Org. Chem.* 51, 14 (1986).
292. V. Chaturvedi, T. Susumu, and K. Kaeriyama, *J. Chem. Soc., Chem. Commun.* 1658 (1992).
293. R. W. Phillips, V. V. Sheares, E. T. Samulski, and J. M. Desimone, *Macromolecules* 27, 2354 (1994).
294. M. L. I. Marrocco, R. R. Gagne, and M. S. Trimmer, *Int. Paten WO* 93/18076.
295. M. L. I. Marrocco, R. R. Gagne, M. S. Trimmer, and L. C. Hsu, *Sampe Proc.* 39, 1063 (1994).
296. V. Percec, S. Okita, and R. Weiss, *Macromolecules* 25, 1816 (1992).
297. V. Percec, C. Pugh, E. Cramer, S. Okita, and R. Weiss, *Makromol. Chem., Macromol. Symp.* 54-55, 113 (1992).
298. V. Percec, J. Bac, M. Zhao, and D. Hill, *Polym. Prepr.* 36, 1 (1995).
299. N. Miyaura, T. Yanagi, and A. Suzuki, *Synth. Commun.* 11, 513 (1981).
300. R. B. Miller and S. Dugar, *Organometallics* 3, 1261 (1984).
301. M. Rehahn, A. D. Schlüter, and G. Wegner, *Makromol. Chem.* 191, 1991 (1990).
302. A. L. Casalnuovo and J. C. Calabrese, *J. Am. Chem. Soc.* 112, 4324 (1990).
303. T. I. Wallow and B. M. Novak, *J. Am. Chem. Soc.* 113, 7411 (1991).
304. I. U. Rau and M. Rehahn, *Makromol. Chem.* 194, 2225 (1993).
305. I. U. Rau and M. Rehahn, *Polymer* 34, 2889 (1993).
306. I. U. Rau and M. Rehahn, *Acta Polym.* 45, 3 (1994).
307. W. Claussen, N. Schulte, and A. D. Schlüter, *Macromol. Rapid Commun.* 16, 89 (1995).
308. A. D. Schlüter, *Polym. Prepr.* 36, 1 (1995).
309. M. B. Goldfinger and T. M. Swager, *J. Am. Chem. Soc.* 116, 7895 (1994).
310. J. J. S. Lamba and J. M. Tour, *J. Am. Chem. Soc.* 116, 11723 (1994).
311. A. Bohnen, K. H. Koch, W. Lütte, and K. Müllen, *Angew. Chem.* 102, 548 (1990).
312. A. Bohnen, K. H. Koch, W. Lütte, and K. Müllen, *Angew. Chem., Int. Ed. Engl.* 29, 525 (1990).
313. K. H. Koch and K. Müllen, *Chem. Ber.* 124, 2091 (1991).
314. U. Scherf and K. Müllen, in "Advances in Polymer Science," pp. 1-40. Springer-Verlag, Berlin, 1995.
315. U. Scherf, in "Handbook of Conducting Polymers" (T. A. Skotheim, R. L. Elsenbaumer, and J. R. Reynolds, Eds.), p. 363. Dekker, New York, 1998.
316. P. E. Cassidy, C. S. Marvel, and S. Ray, *J. Polym. Sci., Part A: Polym. Chem.* 3, 1553 (1965).
317. C. S. Marvel and G. E. Hartzell, *J. Am. Chem. Soc.* 81, 448 (1959).
318. D. G. H. Ballard, A. Courtis, I. M. Shirley, and S. C. Taylor, *J. Chem. Soc., Chem. Commun.* 954 (1983).
319. D. G. H. Ballard, A. Courtis, I. M. Shirley, and S. C. Taylor, *Macromolecules* 21, 294 (1988).
320. D. R. McKean and J. K. Stille, *Macromolecules* 20, 1787 (1987).
321. D. L. Gin, V. P. Conticello, and R. H. Grubbs, *J. Am. Chem. Soc.* 116, 10507 (1994).
322. D. L. Gin, V. P. Conticello, and R. H. Grubbs, *J. Am. Chem. Soc.* 116, 10934 (1994).
323. D. L. Gin, J. K. Avlyanov, and A. G. MacDiarmid, *Synth. Met.* 66, 169 (1994).
324. T. Laird, W. D. Ollis, and I. O. Sutherland, *J. Chem. Soc., Perkin Trans. 1* 1473 (1980).
325. M. Unroe, B. A. Reinhardt, and E. J. Soloski, *Polym. Prepr. (Am. Chem. Soc., Div. Polym. Chem.)* 28, 183 (1987).
326. L. M. Goldenberg and P. C. Lacaze, *Synth. Met.* 58, 271 (1993).
327. A. F. Shepard and B. F. Dannels, *J. Polym. Sci., Part A: Polym. Chem.* 4, 5116 (1966).
328. I. Rubinstein, *J. Polym. Sci., Polym. Chem. Ed.* 21, 3035 (1985).
329. I. Rubinstein, *J. Electrochem. Soc.* 130, 1506 (1983).
330. J. H. Ye, Y. Z. Chen, and Z. W. Tian, *J. Electroanal. Chem.* 229, 215 (1987).
331. M. D. Levi, E. Y. Pisarevskaya, E. B. Molodkina, and I. Danilov, *J. Chem. Soc., Chem. Commun.* 149 (1992).
332. E. Y. Pisarevskaya, S. S. Sedova, A. L. Ignatov, and N. A. Tomilova, *Russ. J. Electro. Chem.* 30, 918 (1994).
333. L. M. Goldenberg, S. Aeiyaich, and P. C. Lacaze, *J. Electroanal. Chem.* 327, 173 (1992).
334. L. M. Goldenberg, S. Aeiyaich, and P. C. Lacaze, *Synth. Met.* 51, 343 (1992).
335. G. Brilmeyer and R. Jasinski, *J. Electrochem. Soc.* 129, 1950 (1982).
336. L. M. Goldenberg, S. Aeiyaich, and P. C. Lacaze, *J. Electroanal. Chem.* 335, 151 (1992).
337. L. M. Goldenberg, S. Aeiyaich, and P. C. Lacaze, *Synth. Met.* 51, 349 (1992).
338. K. L. N. Phani, S. Pitchumain, S. Ravichandron, S. T. Selvan, and S. Bharathay, *J. Chem. Soc., Chem. Commun.* 179 (1993).
339. S. T. Selvan, A. Mani, S. Pitchumain, and K. L. N. Phani, *J. Electroanal. Chem.* 384, 183 (1995).
340. S. Aeiyaich, P. C. Lacaze, and J. E. Dubois, *J. Chem. Soc., Chem. Commun.* 1668 (1986).
341. S. Aeiyaich and P. C. Lacaze, *J. Chem. Phys.* 86, 143 (1989).
342. S. Aeiyaich and P. C. Lacaze, *J. Polym. Sci., Polym. Chem. Ed.* 27, 515 (1989).
343. V. Gutmann and R. Schmied, *Coord. Chem. Rev.* 12, 263 (1974).
344. K. Imanishi, M. Satoh, Y. Yasuda, R. Tsushima, and S. Aoki, *J. Electroanal. Chem.* 242, 203 (1988).
345. K. Kobayashi, T. X. Yang, K. Maruyama, M. Shimomura, and S. Miyauchi, *Synth. Met.* 69, 475 (1995).
346. K. Kaeriyama, M. A. Sato, K. Someno, and S. Tanaka, *J. Chem. Soc., Chem. Commun.* 1199 (1984).
347. G. Froyer, F. Maurice, P. Bernier, and P. McAndrew, *Polymer* 23, 1103 (1982).
348. M. A. Sato, K. Kaeriyama, and K. Someno, *Makromol. Chem.* 184, 2248 (1983).
349. M. Satoh, M. Tabata, K. Kaneto, and K. Yoshino, *J. Electroanal. Chem.* 195, 203 (1985).
350. M. Satoh, M. Tabata, F. Vesugi, K. Kaneto, and K. Yoshino, *Synth. Met.* 17, 595 (1987).
351. J. F. McAleer, K. Ashely, J. J. Smith, S. Bandyopadhyay, J. Ghoroghchian, E. M. Eyring, S. Pons, H. B. Mark, Jr., and G. Dunmore, *J. Mol. Electron.* 2, 183 (1986).
352. T. Oshawa and K. Yoshino, *Synth. Met.* 17, 601 (1987).
353. L. Angely, J. Simonet, and J. P. Morel, *New J. Chem.* 14, 83 (1990).
354. Y. Belabbes, J. J. Aaron, H. Mir Hedayatullah, S. Aeiyaich, and P. C. Lacaze, *J. Lumin.* 48-49, 359 (1992).
355. T. El Moustafid, S. Aeiyaich, J. J. Aaron, H. Mir Hedayatullah, and P. C. Lacaze, *Polymer* 32, 2461 (1991).
356. J. S. Foes, S. M. Erker, and L. M. Rembetsey, *J. Electrochem. Soc.* 133, 836 (1986).

357. V. Le Berre, J. Simonet, and P. Batail, *J. Electroanal. Chem.* 169, 325 (1984).
358. V. Le Berre, L. Angely, J. Simonet, G. Mousset, and M. Bellec, *J. Electrochem. Soc.* 133, 836 (1986).
359. K. Yamamoto, H. Nishida, and E. Tsuchida, *Polym. Bull.* 163 (1987).
360. J. Elving, J. M. Markowitz, and I. Rosenthal, *J. Phys. Chem.* 65, 680 (1961).
361. S. Aeiyaich, P. Soubiran, and P. C. Lacaze, *Polym. Commun.* 29, 130 (1988).
362. S. Aeiyaich, P. Soubiran, P. C. Lacaze, G. Froyer, and Y. Pelois, *Synth. Met.* 32, 103 (1989).
363. S. Aeiyaich, P. Soubiran, P. C. Lacaze, G. Froyer, and Y. Pelois, *Synth. Met.* 68, 213 (1995).
364. M. Delamar, P. C. Lacaze, J. Y. Dumousseau, and J. E. Dubois, *Electrochim. Acta* 27, 61 (1982).
365. S. Hara, S. Aeiyaich, and P. C. Lacaze, *J. Electroanal. Chem.* 364, 223 (1994).
366. S. Hara, S. Aeiyaich, and P. C. Lacaze, *J. Electroanal. Chem.* 370, 197 (1994).
367. P. Soubiran, S. Aeiyaich, J. J. Aaron, M. Delamar, and P. C. Lacaze, *J. Electroanal. Chem.* 251, 89 (1988).
368. R. J. Gale and R. A. Psteryoung, *Inorg. Chem.* 19, 2728 (1978).
369. L. M. Goldenberg, A. E. Pelekh, V. I. Krinichnyi, O. S. Roshchupkina, A. F. Zueva, R. N. Lyubovskaya, and O. N. Efimov, *Synth. Met.* 36, 217 (1990).
370. V. M. Kobryanskii and S. A. Arnoutov, *Makromol. Chem.* 193, 455 (1992).
371. D. C. Trivedi, *J. Chem. Soc., Chem. Commun.* 544 (1989).
372. K. Meerholz and J. Heinze, *Angew. Chem., Int. Ed. Engl.* 29, 692 (1990).
373. K. Meerholz and J. Heinze, *Synth. Met.* 41–43, 2871 (1991).
374. J. F. Fauvarque, M. A. Petit, F. Pfluger, A. Jutand, G. Chevrot, and M. Troupel, *Makromol. Chem.* 4, 455 (1983).
375. J. F. Fauvarque, A. Digua, M. A. Petit, and J. Savard, *Makromol. Chem.* 186, 2415 (1985).
376. J. F. Fauvarque, M. A. Petit, A. Digua, and G. Froyer, *Makromol. Chem.* 188, 1833 (1987).
377. G. Froyer, F. Maurice, J. Y. Goglot, J. F. Fauvarque, M. A. Petit, and A. Digua, *Mol. Cryst. Liq. Cryst.* 118, 267 (1985).
378. G. Schiavon, G. Zotti, and G. Bontempelli, *J. Electroanal. Chem.* 161, 323 (1984).
379. G. Schiavon, G. Zotti, and G. Bontempelli, *J. Electroanal. Chem.* 186, 191 (1985).
380. S. Gronowitz, "Thiophene and Its Derivatives." Wiley, New York, 1991.
381. V. Meyer, *Chem. Ber.* 16, 1465 (1883).
382. S. L. Meisel, G. C. Johnson, and H. D. Hartough, *J. Am. Chem. Soc.* 27, 1910 (1950).
383. J. P. Ferraris and D. J. Guerrero, in "Handbook of Conducting Polymers" (T. A. Skotheim, R. L. Elsembaumer, and J. R. Reynolds, Eds.), p. 259–276. Dekker, New York, 1998.
384. R. W. Gumbs, in "Organic Conductive Molecules and Polymers" (H. S. Nalwa, Ed.), Vol. 2, pp. 469–504. Wiley, New York, 1997.
385. K. Kaeriyama, in "Organic Conductive Molecules and Polymers" (H. S. Nalwa, Ed.), Vol. 2, pp. 271–308. Wiley, New York, 1997.
386. H. Kuzmany, M. Mehring, and S. Roth, "Electronic Properties of Conducting Polymers." Springer-Verlag, Berlin, 1992.
387. R. D. McCullough, *Adv. Mater.* 10, 93 (1998).
388. R. D. McCullough and P. Ewbank, in "Handbook of Conducting Polymers" (T. A. Skotheim, R. L. Elsembaumer, and J. R. Reynolds, Eds.), pp. 225–258. Dekker, New York, 1998.
389. J. Roncali, in "Handbook of Conducting Polymers" (T. A. Skotheim, R. L. Elsembaumer, and J. R. Reynolds, Eds.), pp. 311–341. Dekker, New York, 1998.
390. G. Tourillon, in "Handbook of Conducting Polymers" (T. A. Skotheim, Ed.), Vol. 1, pp. 293–350. Dekker, New York, 1986.
391. H. B. Gu, S. Nakajima, R. Sugimoto, and K. Yoshino, *Jpn. J. Appl. Phys.* 27, 311 (1988).
392. R. Sugimoto, S. Takeda, H. B. Gu, and K. Yoshino, *Chem. Express* 1, 635 (1986).
393. K. Yoshino, S. Nakajima, and R. Sugimoto, *Jpn. J. Appl. Phys.* 26, L1038 (1987).
394. K. Yoshino, S. Nakajima, M. Fujii, and R. Sugimoto, *Polym. Commun.* 28, 309 (1987).
395. K. Yoshino, D. H. Park, B. K. Park, M. Onoda, and R. Sugimoto, *Solid State Commun.* 67, 1119 (1988).
396. S. Hotta, M. Soga, and N. Sonoda, *Synth. Met.* 26, 267 (1988).
397. S. Hotta, M. Soga, and N. Sonoda, *J. Chem. Phys.* 93, 4994 (1989).
398. V. M. Niemi, P. Knuutila, J. E. Österholm, and J. Kolvola, *Polymer* 33, 1559 (1992).
399. I. Kulszewicz-Bajer, A. Pawlicka, J. Plenkiewicz, A. Pron, and S. Lefrant, *Synth. Met.* 30, 335 (1989).
400. M. Leclerc, M. Diaz, and G. Wegner, *Makromol. Chem.* 190, 3105 (1989).
401. J. Laakso, H. Jarvinen, and B. Sagerberg, *Synth. Met.* 55–57, 1204 (1993).
402. T. Taka, P. Nyholm, J. Laakso, M. T. Lopenen, and J. E. Österholm, *Synth. Met.* 41–43, 899 (1991).
403. G. Daoust and M. Leclerc, *Macromolecules* 24, 1991 (1991).
404. K. Faid, R. Cloutier, and M. Leclerc, *Macromolecules* 26, 2501 (1993).
405. L. Robitaille and M. Leclerc, *Macromolecules* 27, 1847 (1994).
406. M. R. Bryce, A. Chissel, P. Kathirgamanthan, D. Parker, and N. R. M. Smith, *J. Chem. Soc., Chem. Commun.* 466 (1987).
407. A. C. Chang, R. L. Blankespoor, and L. L. Miller, *J. Electroanal. Chem.* 236, 239 (1987).
408. G. Daoust and M. Leclerc, *Macromolecules* 24, 455 (1991).
409. M. Feldhues, G. Kampf, H. Litterer, T. Mechlennburg, and P. Wegener, *Synth. Met.* 28, C487 (1989).
410. M. Leclerc and G. Daoust, *J. Chem. Soc., Chem. Commun.* 273 (1990).
411. J. Roncali, P. Marque, R. Garreau, F. Garnier, and M. Lemaire, *Macromolecules* 23, 1347 (1990).
412. S. Tanaka, M. A. Sato, and K. Kaeriyama, *Synth. Met.* 25, 277 (1988).
413. S. Tanaka and K. Kaeriyama, *Bull. Chem. Soc. Jpn.* 62, 1908 (1989).
414. T. Yamamoto, A. Kashiwazaki, and K. Kato, *Makromol. Chem.* 190, 1649 (1989).
415. M. C. Gallazi, L. Castellani, R. A. Marin, and G. Zerbi, *J. Polym. Sci., Polym. Chem. Ed.* 31, 3339 (1993).
416. C. D. Casa, E. Salatelli, F. Andreani, and P. C. Bizzari, *Makromol. Chem., Macromol. Symp.* 59, 233 (1992).
417. C. D. Casa, F. Andreani, P. C. Bizzari, and E. Salatelli, *J. Mater. Chem.* 4, 1035 (1994).
418. S. A. Chen and C. C. Tsai, *Macromolecules* 26, 2234 (1993).
419. M. R. Anderson, D. Selse, M. Berggren, H. Jarvinen, T. Hjertberg, O. Inganäs, O. Wennerström, and J. E. Österholm, *Macromolecules* 27, 6503 (1994).
420. I. Levesque and M. Leclerc, *J. Chem. Soc., Chem. Commun.* 2293 (1995).
421. M. S. A. Abdou, X. Lu, Z. W. Xie, F. Orfino, M. J. Deen, and S. Holdcroft, *Chem. Mater.* 7, 631 (1995).
422. F. Chen, P. G. Mehta, L. Takiff, and R. D. McCullough, *J. Mater. Chem.* 6, 1763 (1996).
423. T. Yamamoto, K. Sanechika, and A. Yamamoto, *J. Polym. Sci., Polym. Lett. Ed.* 18, 9 (1980).
424. J. W. P. Lin and L. P. Dudek, *J. Polym. Sci., Polym. Chem. Ed.* 18, 2869 (1980).
425. C. Z. Hotz, P. Kovacic, and I. A. Khoury, *J. Polym. Sci., Polym. Chem. Ed.* 21, 2617 (1983).
426. T. Yamamoto, K. Sanechika, and A. Yamamoto, *Bull. Chem. Soc. Jpn.* 56, 1497 (1983).
427. T. Yamamoto, K. Osakada, T. Wakabayashi, and A. Yamamoto, *Makromol. Chem., Rapid Commun.* 6, 671 (1985).

428. I. Colon and G. T. Kwiatkowski, *J. Polym. Sci., Polym. Chem. Ed.* 28, 367 (1990).
429. A. Amer, H. Zimmer, K. J. Mulligan, H. B. Mark, S. Pons, and J. F. McAleer, *J. Polym. Sci. Polym. Lett. Ed.* 22, 77 (1984).
430. K. Kaneto, K. Yoshino, and Y. Inuishi, *Solid State Commun.* 46, 389 (1983).
431. T. Yamamoto and K. Sanechika, *Chem. Ind. (London)* 301 (1982).
432. G. G. Miller and R. L. Elsenbaumer, *J. Chem. Soc., Chem. Commun.* 1346 (1986).
433. K. Y. Jen, R. Oboodi, and R. L. Elsenbaumer, *Polym. Mater. Sci. Eng.* 53, 79 (1985).
434. R. L. Elsenbaumer, K. Y. Jen, and R. Oboodi, *Synth. Met.* 15, 169 (1986).
435. H. Mao, B. Xu, and S. Holdcroft, *Macromolecules* 26, 1163 (1993).
436. M. Ueda, Y. Miyaji, T. Itoh, Y. Oba, and T. Sone, *Macromolecules* 24, 2694 (1991).
437. R. L. Elsenbaumer, K. Y. Jen, G. G. Miller, H. Eckhardt, L. W. Shacklette, and R. Jow, in *Springer Series in Solid State Sciences* (H. Kuzmany, M. Mehring, and S. Roth, Eds.), Vol. 76, p. 400. Springer-Verlag, Berlin, 1987.
438. G. Barbarella, A. Bongini, and M. Zambianchi, *Macromolecules* 27, 3039 (1994).
439. G. Barbarella, M. Zambianchi, A. Bongini, and L. Antolini, *Adv. Mater.* 6, 561 (1994).
440. R. H. Baughman and R. R. Chance, *J. Appl. Phys.* 47, 4295 (1976).
441. A. Berlin, G. A. Pagani, and F. Sanniccolo, *J. Chem. Soc., Chem. Commun.* 1663 (1986).
442. B. Krische, J. Hellberg, and C. Lilja, *J. Chem. Soc., Chem. Commun.* 19, 1476 (1987).
443. M. J. Marsella and T. M. Swager, *J. Am. Chem. Soc.* 115, 12214 (1993).
444. R. D. McCullough, R. D. Lowe, M. Jayaraman, and D. L. Anderson, *J. Org. Chem.* 58, 904 (1993).
445. M. Sato and H. Morii, *Polym. Commun.* 32, 42 (1991).
446. M. Sato and H. Morii, *Macromolecules* 24, 1196 (1991).
447. R. M. Souto Maior, K. Hinkelmann, and F. Wudl, *Macromolecules* 23, 1268 (1990).
448. M. Zagorska and B. Krisshe, *Polymer* 31, 1379 (1990).
449. M. Zagorska, I. Kulszewicz-Bajer, A. Pron, L. Firlcj, P. Berier, and M. Galtier, *Synth. Met.* 45, 385 (1991).
450. R. D. McCullough and R. D. Lowe, *J. Chem. Soc., Chem. Commun.* 70 (1992).
451. G. Consiglio, S. Gronowitz, A. B. Hornfeldt, B. Maltesson, R. Noto, and D. Spinelli, *Chem. Scr.* 11, 175 (1977).
452. D. D. Cunningham, L. Laguren-Davidson, H. B. Mark, C. Van Pahn, and H. Zimmer, *J. Chem. Soc., Chem. Commun.* 1021 (1987).
453. S. Kodama, I. Naajima, M. Kumada, A. Minato, and K. Suzuki, *Tetrahedron* 38, 3347 (1982).
454. R. D. McCullough and R. D. Lowe, *Polym. Prepr.* 33, 195 (1992).
455. R. D. McCullough, R. D. Lowe, M. Jayaraman, P. C. Ewbank, D. L. Anderson, and S. Tristam-Nagle, *Synth. Met.* 55, 1198 (1993).
456. R. D. McCullough, S. Tristam-Nagle, S. P. Williams, R. D. Lowe, and M. Jayaraman, *J. Am. Chem. Soc.* 115, 4910 (1993).
457. R. D. McCullough, S. P. Williams, M. Jayaraman, J. Reddinger, S. Miller, and S. Tristam-Nagle, in "Materials Research Society" (L. Dalton and C. Lee, Eds.), Vol. 328, p. 215. Materials Research Society, Pittsburgh, 1994.
458. R. D. McCullough, J. A. Belot, and S. P. Williams, in *NATO Advanced Workshop Series, Series C: Mathematics and Physical Science* (J. Becher and K. Schaumburg, Eds.), Vol. 456, p. 349. Kluwer Academic, Dordrecht, 1995).
459. R. D. McCullough, S. P. Williams, S. Tristam-Nagle, M. Jayaraman, P. C. Ewbank, and L. Miller, *Synth. Met.* 69, 279 (1995).
460. K. Tamao, K. Sumitani, Y. Kiso, M. Zembayashi, A. Fujioka, S. Kodama, I. Nakajima, A. Minato, and M. Kumada, *Bull. Chem. Soc. Jpn.* 49, 1958 (1976).
461. C. Van Pahn, H. B. Mark, and H. Zimmer, *Synth. Commun.* 16, 689 (1986).
462. T. A. Chen and R. D. Rieke, *J. Am. Chem. Soc.* 114, 10087 (1992).
463. T. A. Chen and R. D. Rieke, *Synth. Met.* 60, 175 (1993).
464. T. A. Chen, R. A. O'Brien, and R. D. Rieke, *Macromolecules* 26, 3462 (1993).
465. T. A. Chen, X. Wu, and R. D. Rieke, *J. Am. Chem. Soc.* 117, 233 (1995).
466. X. Wu, T. A. Chen, and R. D. Rieke, *Macromolecules* 28, 2101 (1995).
467. M. D. McClain, D. A. Whittington, D. J. Mitchell, and M. D. Curtis, *J. Am. Chem. Soc.* 117, 3887 (1995).
468. M. Pomerantz, H. Yang, and Y. Cheng, *Macromolecules* 28, 5706 (1995).
469. A. F. Diaz, *Chem. Scr.* 17, 142 (1981).
470. A. Czerwinski, H. Zimmer, C. V. Pham, and H. B. Mark, *J. Electrochem. Soc.* 132, 2669 (1985).
471. A. J. Downward and D. Pletcher, *J. Electroanal. Chem.* 206, 147 (1986).
472. A. R. Hillman and E. Mallen, *J. Electroanal. Chem.* 243, 403 (1988).
473. D. Delabouglise, R. Garreau, M. Lemaire, and J. Roncali, *New J. Chem.* 12, 155 (1988).
474. R. Turcu, O. Pana, I. Bratu, and M. Bogdan, *J. Mol. Electron.* 6, 1 (1990).
475. M. Sato, S. Tanaka, and K. Kaeriyama, *J. Chem. Soc. Chem. Commun.* 713 (1985).
476. M. Sato, S. Tanaka, and K. Kaeriyama, *Synth. Met.* 14, 279 (1986).
477. J. Roncali, F. Garnier, M. Lemaire, and R. Garreau, *Synth. Met.* 15, 323 (1986).
478. A. Yassar, J. Roncali, and F. Garnier, *Macromolecules* 22, 804 (1989).
479. J. R. Reynolds, S. G. Hsu, and H. J. Arnott, *J. Polym. Sci., Part B: Polym. Phys.* 27, 2081 (1989).
480. G. Tourillon and F. Garnier, *J. Polym. Sci., Polym. Phys. Ed.* 22, 33 (1984).
481. P. Marque, J. Roncali, and F. Garnier, *J. Electroanal. Chem.* 218, 107 (1987).
482. F. Garnier, G. Tourillon, J. Y. Barraud, and H. Dexpert, *J. Mater. Sci.* 161, 51 (1984).
483. L. F. Warren, J. A. Walker, D. P. Anderson, and C. G. Rhodes, *J. Electrochem. Soc.* 136, 2286 (1989).
484. J. D. Nilsson and O. Inganäs, *Synth. Met.* 31, 359 (1989).
485. K. Tanaka, T. Shichiri, and T. Yamabe, *Synth. Met.* 16, 207 (1986).
486. P. Lang, F. Chao, M. Costa, and F. Garnier, *Polymer* 28, 668 (1987).
487. J. Roncali and F. Garnier, *J. Chem. Phys.* 92, 833 (1988).
488. A. R. Hillman and E. Mallen, *J. Electroanal. Chem.* 220, 351 (1987).
489. Z. Deng, W. H. Smyrl, and H. S. White, *J. Electrochem. Soc.* 136, 2152 (1989).
490. S. Aciyach, A. Kone, M. Dieng, J. J. Aaron, and P. C. Lacaze, *J. Chem. Soc., Chem. Commun.* 822 (1991).
491. T. F. Otero and E. J. de Larreta-Azelain, *J. Chim. Phys.* 86, 131 (1989).
492. G. Zotti, S. Cattarin, and N. Comisso, *J. Electroanal. Chem.* 235, 259 (1987).
493. J. Roncali, R. Garreau, F. Garnier, and M. Lemaire, *Synth. Met.* 18, 139 (1987).
494. A. F. Diaz, J. Crowley, J. Bargon, G. P. Gardini, and J. B. Torrance, *J. Electroanal. Chem.* 121, 355 (1981).
495. M. A. Druy and R. J. Seymour, *J. Phys. Colloq. (Paris)* 44, 595 (1983).
496. M. A. Druy, R. J. Seymour, and S. K. Tripathy, *Am. Symp. Chem. Soc. Ser., Polym. Electro.* 37, 473 (1984).
497. R. M. Eales and A. R. Hillman, *J. Mater. Sci.* 25, 3806 (1990).
498. J. P. Ferraris and R. T. Hanlon, *Polymer* 30, 1319 (1989).
499. B. L. Funt and S. V. Lowen, *Synth. Met.* 11, 129 (1985).
500. A. Galal, E. T. Lewis, O. Y. Ataman, H. Zimmer, and H. B. Mark, *J. Polym. Sci.* 27, 1891 (1989).

501. G. M. Gamaggi, G. Deluca, and A. Tundo, *J. Chem. Soc., Perkin Trans. 2*, 1594 (1972).
502. M. Gratzl, D. F. Hsu, A. M. Riley, and J. Janata, *J. Phys. Chem.* 94, 5973 (1990).
503. E. E. Havinga and L. W. Van Horssen, *Makromol. Chem., Macromol. Symp.* 24, 67 (1989).
504. J. Heinze, J. Mortensen, and K. Hinkelmann, *Synth. Met.* 21, 209 (1987).
505. O. Inganäs, B. Liedberg, C. R. Wu, and H. Wynberg, *Synth. Met.* 11, 239 (1985).
506. B. Krische and M. Zagorska, *Synth. Met.* 28, C263 (1989).
507. L. Laguren-Davidson, C. V. Pahn, H. Zimmer, and H. B. Mark, *J. Electrochem. Soc.* 135, 1406 (1988).
508. F. Martinez, R. Voelkel, D. Naegle, and H. Naarmann, *Mol. Cryst. Liq. Cryst.* 167, 227 (1989).
509. Y. Yumoto and S. Yoshimura, *Synth. Met.* 13, 185 (1985).
510. G. Zotti and G. Schiavon, *Synth. Met.* 39, 183 (1990).
511. M. Lemaire, W. Büchner, R. Garreau, A. H. Huynh, A. Guy, and J. Roncali, *J. Electroanal. Chem.* 281, 293 (1990).
512. W. J. Albery, L. Fengbin, and A. R. Mount, *J. Electroanal. Chem.* 310, 239 (1991).
513. H. S. Li, J. Roncali, and F. Garnier, *J. Electroanal. Chem.* 263, 155 (1989).
514. R. J. Waltman and J. Bargon, *Can. J. Chem.* 64, 76 (1986).
515. G. Dian, G. Barbey, and B. Decroix, *Synth. Met.* 13, 281 (1986).
516. R. Garreau, J. Roncali, F. Garnier, and M. Lemaire, *J. Chim. Phys.* 86, 93 (1989).
517. J. Roncali, F. Garnier, R. Garreau, and M. Lemaire, *J. Chem. Soc., Chem. Commun.* 1500 (1987).
518. J. P. Ruiz, K. Nayak, D. S. Marynick, and J. R. Reynolds, *Macromolecules* 22, 1231 (1989).
519. E. W. Tsai, S. Basak, J. P. Ruiz, J. R. Reynolds, and K. Rajeshwar, *J. Electrochem. Soc.* 136, 3683 (1989).
520. G. Zotti and G. Schiavon, *J. Electroanal. Chem.* 163, 385 (1984).
521. Z. Xu, G. Horowitz, and F. Garnier, *J. Electroanal. Chem.* 246, 467 (1988).
522. J. Rodriguez, H. J. Grande, and T. F. Otero, in "Organic Conductive Molecules and Polymers" (H. S. Nalwa, Ed.), Vol. 2, pp. 415-468. Wiley, New York, 1997.
523. G. B. Street, in "Handbook of Conducting Polymers" (T. A. Skotheim, Ed.), Vol. 1, pp. 265-291. Dekker, New York, 1986.
524. A. Angeli, *Gazz. Chim. Ital.* 46, 279 (1916).
525. A. Angeli and L. Alessandri, *Gazz. Chim. Ital.* 46, 283 (1916).
526. A. Dall'Ollio, Y. Dascola, V. Varacca, and V. Bocchi, *C. R. Acad. Sci. (Paris)* 267, 433 (1968).
527. A. F. Diaz, K. K. Kanazawa, and G. P. Gardini, *J. Chem. Soc., Chem. Commun.* 635 (1979).
528. G. P. Gardini, *Adv. Heterocycl. Chem.* 15, 67 (1973).
529. H. S. Nalwa, L. R. Dalton, W. F. Schmidt, and J. G. Rabe, *Polym. Commun.* 27, 240 (1985).
530. H. S. Nalwa, J. G. Rabe, W. F. Schmidt, and L. R. Dalton, *Makromol. Chem., Rapid Commun.* 7, 533 (1986).
531. H. S. Nalwa, *J. Mater. Sci.* 27, 210 (1992).
532. M. Salmon, K. K. Kanazawa, A. F. Diaz, and M. Krounbi, *J. Polym. Sci. Polym. Lett. Ed.* 20, 187 (1982).
533. J. W. Loveland and G. R. Dimeler, *Anal. Chem.* 33, 1196 (1961).
534. S. P. Armes, *Synth. Met.* 20, 365 (1987).
535. T. H. Chao and J. March, *J. Polym. Sci., Polym. Chem.* 26, 743 (1988).
536. E. T. Kang, K. G. Neoh, Y. K. Ong, K. L. Tan, and B. T. G. Tan, *Macromolecules* 24, 2822 (1991).
537. A. Pron, Z. Kucharski, C. Budrowski, M. Zagorska, S. Kirchene, J. Suwalski, G. Dehe, and S. Lefrant, *J. Chem. Phys.* 83, 5923 (1985).
538. V. Bocchi and G. P. Gardini, *J. Chem. Soc., Chem. Commun.* 148 (1986).
539. R. E. Myers, *J. Electron. Mater.* 15, 61 (1986).
540. E. T. Kang, K. G. Neoh, and H. C. Ti, *Solid State Commun.* 60, 457 (1986).
541. K. G. Neoh, E. T. Kang, and T. C. Tan, *Polym. Degrad. Stab.* 21, 93 (1988).
542. E. T. Kang and K. G. Neoh, *Mol. Cryst. Liq. Cryst.* 173, 141 (1989).
543. N. Toshima and J. Tayanagi, *Chem. Lett.* 1369 (1990).
544. N. Toshima, *Makromol. Chem., Macromol. Symp.* 59, 123 (1992).
545. S. Martina, V. Enkelmann, G. Wegner, and A. D. Schlüter, *Synth. Met.* 51, 299 (1992).
546. L. Groenendaal, H. W. I. Peerlings, J. L. J. van Dongen, E. E. Havinga, J. A. J. M. Vekemans, and E. W. Meijer, *Macromolecules* 28, 116 (1995).
547. R. A. Bull, F. R. F. Fan, and A. J. Bard, *J. Electrochem. Soc.* 129, 1009 (1982).
548. M. L. Daroux, E. B. Yeager, M. Kalaji, N. H. Cuong, and A. Bewick, *Makromol. Chem., Macromol. Symp.* 8, 127 (1987).
549. B. R. Scharifker, E. Garcia-Pastoriza, and W. Marino, *J. Electroanal. Chem.* 300, 85 (1991).
550. F. Beck and P. Hülser, *J. Electroanal. Chem.* 280, 159 (1990).
551. K. M. Cheung, D. Bloor, and G. C. Stevens, *Polymer* 29, 1709 (1988).
552. R. R. Dogonadze and A. M. Kuznetsov, *Electrochim. Acta* 22, 967 (1977).
553. S. Glenis, G. Tourillon, and F. Garnier, *Thin Solid Films* 139, 221 (1986).
554. K. E. Heusler and K. S. Yun, *Electrochim. Acta* 22, 977 (1977).
555. P. Hülser and F. Beck, *J. Appl. Electrochem.* 20, 596 (1990).
556. T. Jwasita, W. Schmickler, and J. W. Schnetze, *Ber. Bunsen-Ges. Phys. Chem.* 89, 138 (1985).
557. T. Jwasita, W. Schmickler, and J. W. Schnetze, *J. Electroanal. Chem.* 194, 395 (1985).
558. T. F. Otero, E. Angulo, C. Santamaria, and J. Rodriguez, *Synth. Met.* 54, 217 (1993).
559. T. F. Otero, C. Santamaria, E. Angulo, and J. Rodriguez, *Synth. Met.* 57, 1574 (1993).
560. J. Rodriguez, T. F. Otero, H. Grande, J. P. Moliton, A. Moliton, and T. Trigaud, *Synth. Met.* 76, 301 (1996).
561. M. Schirmeisen and F. Beck, *J. Appl. Electrochem.* 19, 401 (1989).
562. M. S. Ynu and C. S. Huh, *Synth. Met.* 28, 715 (1989).
563. K. K. Kanazawa, A. F. Diaz, W. D. Gill, P. M. Grant, G. B. Street, G. P. Gardini, and J. F. Kwak, *Synth. Met.* 1, 329 (1980).
564. J. Prejza, I. Lundström, and T. Skotheim, *J. Electrochem. Soc.* 129, 1685 (1982).
565. I. Rodriguez, M. L. Marcos, and J. Gonzalez-Velasco, *Electrochim. Acta* 32, 1181 (1987).
566. T. Skotheim, *Polym. Prepr.* 23, 136 (1982).
567. T. Skotheim, L. G. Petersson, O. Inganäs, and I. Lundström, *J. Electrochem. Soc.* 129, 1737 (1982).
568. H. Yoneyama, K. Wakamoto, and H. Tamura, *J. Electrochem. Soc.* 132, 2414 (1985).
569. R. Noufi, *J. Electrochem. Soc.* 130, 2126 (1983).
570. K. Jackowska and H. T. Tien, *J. Appl. Electrochem.* 18, 357 (1988).
571. R. Noufi, D. Tench, and L. F. Warren, *J. Electrochem. Soc.* 128, 2596 (1981).
572. R. Noufi, A. J. Frank, and A. J. Nozik, *J. Am. Chem. Soc.* 103, 1849 (1981).
573. T. Skotheim, I. Lundström, and J. Prejza, *J. Electrochem. Soc.* 128, 1625 (1981).
574. S. Asavapiryanont, G. K. Chandler, G. A. Gunawardena, and D. Pletcher, *J. Electroanal. Chem.* 177, 229 (1984).
575. K. Hyodo and A. G. McDiarmid, *Synth. Met.* 11, 167 (1985).
576. A. Murthy, S. Pal, and K. S. Reddy, *J. Mater. Sci. Lett.* 3, 745 (1984).
577. M. Satoh, K. Kaneto, and K. Yoshino, *Synth. Met.* 14, 289 (1986).
578. S. Dong and J. Ding, *Synth. Met.* 20, 119 (1987).
579. R. Qian, J. Qiu, and D. Shen, *Synth. Met.* 18, 13 (1987).
580. W. Wernet and G. Wernert, *Makromol. Chem.* 188, 1465 (1987).
581. A. F. Diaz and J. Bargon, in "Handbook of Conducting Polymers" (T. A. Skotheim, Ed.), Vol. 1, pp. 81-115. Dekker, New York, 1986.
582. T. F. Otero and A. H. Arevalo, *Synth. Met.* 66, 25 (1994).

583. T. F. Otero, C. Santamaria, and R. K. Bunting, *J. Electroanal. Chem.* 380, 291 (1995).
584. P. G. Pickup and R. A. Osteryoung, *J. Am. Chem. Soc.* 106, 2294 (1984).
585. P. G. Pickup and R. A. Osteryoung, *J. Electroanal. Chem.* 195, 271 (1985).
586. K. J. Wynne and G. B. Street, *Macromolecules* 18, 2361 (1985).
587. T. F. Otero, J. Rodriguez, E. Angulo, and C. Santamaria, *Synth. Met.* 43, 2831 (1991).
588. T. F. Otero and E. Angulo, *J. Appl. Electrochem.* 22, 369 (1992).
589. T. F. Otero, *Electrochim. Acta* 39, 245 (1994).
590. M. Ogasawara, K. Funahashi, T. Demura, T. Hagiwara, and K. Iwata, *Synth. Met.* 14, 61 (1986).
591. P. Mirebeau, *J. Phys. Colloq. (Paris)* 44, 579 (1983).
592. T. F. Otero and E. De Larreta-Azelain, *Synth. Met.* 26, 79 (1988).
593. Y. Nakazawa, T. Ebine, M. Kusunoki, H. Nishizawa, J. Hanna, and K. Kokado, *Jpn. J. Appl. Phys.* 27, 1304 (1988).
594. M. P. Cava and A. A. Deana, *J. Am. Chem. Soc.* 81, 4266 (1959).
595. M. P. Cava, M. J. Mitchell, and A. A. Deana, *J. Am. Chem. Soc.* 25, 1481 (1960).
596. M. P. Cava and N. M. Pollack, *J. Am. Chem. Soc.* 88, 4112 (1966).
597. M. P. Cava, N. M. Pollack, O. A. Mamer, and M. J. Mitchell, *J. Org. Chem.* 36, 3932 (1971).
598. R. Meyer, H. Kleinert, S. Richter, and K. Gewald, *J. Prakt. Chem.* 20, 244 (1963).
599. J. Drabowicz and M. Mikolajczyk, *Synth. Commun.* 11, 1025 (1981).
600. J. F. King, A. Hawson, B. L. Huston, L. J. Danks, and J. Komery, *Can. J. Chem.* 49, 943 (1971).
601. Y. Okuda, M. V. Lakshmikantham, and M. P. Cava, *J. Org. Chem.* 56, 6024 (1991).
602. F. Wudl, A. A. Kruger, and G. A. Thomas, *Ann. N.Y. Acad. Sci.* 313, 79 (1978).
603. F. Wudl, M. Kobayashi, and A. J. Heeger, *J. Org. Chem.* 49, 3382 (1984).
604. N. Colaneri, M. Kobayashi, A. J. Heeger, and F. Wudl, *Synth. Met.* 14, 45 (1986).
605. H. Yashima, M. Kobayashi, K. B. Lee, T. C. Chung, A. J. Heeger, and F. Wudl, *J. Electrochem. Soc.* 134, 46 (1987).
606. P. A. Christensen, J. C. Kerr, S. J. Higgins, and A. Hammett, *Faraday Discuss. J. Chem. Soc.* 88, 261 (1989).
607. S. M. Dale, A. Glide, and A. R. Hillman, *J. Mater. Chem.* 2, 99 (1992).
608. M. Onoda, H. Nakayama, S. Morita, T. Kawai, and K. Yoshino, *Synth. Met.* 69, 605 (1995).
609. I. Hoogmartens, D. Vanderzande, H. Martens, and J. Gelan, *Synth. Met.* 47, 367 (1992).
610. K. Y. Jen and R. L. Elsenbaumer, *Synth. Met.* 16, 379 (1986).
611. T. L. Rose and M. C. Liberto, *Synth. Met.* 31, 395 (1989).
612. T. Iyoda, M. Kitano, and T. Shimidzu, *J. Chem. Soc., Chem. Commun.* 1618 (1991).
613. T. Iyoda, M. Kitano, and T. Shimidzu, *Polym. J.* 27, 875 (1995).
614. R. van Asselt, I. Hoogmartens, D. Vanderzande, J. Gelan, P. E. Froehling, M. Aussems, O. Aagaard, and R. Schellekens, *Synth. Met.* 74, 65 (1995).
615. M. Pomerantz, B. Chaloner-Gill, O. Harding, J. J. Tseng, and W. J. Pomerantz, *Synth. Met.* 55, 960 (1993).
616. G. M. Brooke and S. D. Mawson, *J. Chem. Soc., Perkin Trans.* 1919 (1990).
617. G. M. Brooke, C. J. Drury, D. Bloor, and M. J. Swann, *J. Mater. Chem.* 5, 1317 (1995).
618. S. J. Burbridge, H. Page, A. Drury, A. P. Davey, J. Callaghan, and W. Blau, *J. Mod. Opt.* 41, 1217 (1994).
619. E. Funatsu, Jpn. Kokai Tokkyo Koho JP, 1990.
620. E. Funatsu, Jpn. Kokai Tokkyo Koho JP, 1990.
621. Y. Ikenoue, F. Wudl, and A. J. Heeger, *Synth. Met.* 40, 1 (1991).
622. G. King and S. J. Higgins, *J. Chem. Soc., Chem. Commun.* 825 (1994).
623. G. King, S. J. Higgins, S. E. Garner, and A. R. Hillman, *Synth. Met.* 67, 241 (1994).
624. G. King and S. J. Higgins, *J. Mater. Chem.* 5, 447 (1995).
625. M. J. Swann, G. Brooke, and D. Bloor, *Synth. Met.* 55-57, 281 (1993).
626. F. Wudl, A. J. Heeger, Y. Yoshiaki, and M. Kobayashi, Eur. Patent, 0, 273, 643, 1988.
627. Y. Ikenoue, *Synth. Met.* 35, 263 (1990).
628. M. V. Lakshmikantham, D. Lorcy, C. Scordilis-Kelley, X. L. Wu, J. P. Parakka, R. M. Metzger, and M. P. Cava, *Adv. Mater.* 5, 723 (1993).
629. R. M. Metzger, P. Wang, X. L. Wu, G. V. Tormos, D. Lorcy, I. Shcherbakova, M. V. Lakshmikantham, and M. P. Cava, *Synth. Met.* 70, 1435 (1995).
630. P. Kathirgamanathan and M. K. Sheperd, *J. Electroanal. Chem.* 354, 305 (1993).
631. M. Pomerantz, B. Chaloner-Gill, O. Harding, J. J. Tseng, and W. J. Pomerantz, *J. Chem. Soc., Chem. Commun.* 1672 (1992).
632. J. Kastner, H. Kuzmany, D. Vegh, M. Landl, L. Cuff, and M. Kertesz, *Macromolecules* 28, 2922 (1995).
633. S. Gronowitz and B. Persson, *Acta Chem. Scand.* 21, 812 (1967).
634. V. P. Litvinov and Y. L. Goldfarb, *Adv. Heterocycl. Chem.* 19, 123 (1976).
635. F. De Jong and M. J. Janssen, *J. Org. Chem.* 36, 1645 (1971).
636. M. Biserni, A. Marinangeli, and M. Mastragostino, *J. Electrochem. Soc.* 132, 1597 (1985).
637. R. Danieli, C. Taliani, R. Zamboni, G. Giro, M. Biserni, M. Mastragostino, and A. Testoni, *Synth. Met.* 13, 328 (1986).
638. P. Di Marco, M. Mastragostino, and C. Taliani, *Mol. Cryst. Liq. Cryst.* 118, 241 (1985).
639. T. R. Jow, K. Y. Jen, R. Elsenbaumer, and L. W. Schacklette, *Synth. Met.* 14, 53 (1986).
640. C. Taliani, R. Zamboni, R. Danieli, P. Ostoja, W. Porzio, R. Lazzaroni, and J. L. Brédas, *Phys. Scr.* 40, 781 (1989).
641. X. Gu, Thesis, Univ. of Texas at Arlington, 1995.
642. M. Pomerantz and X. Gu, *Synth. Met.* 84, 243 (1997).
643. M. Pomerantz, in "Handbook of Conducting Polymers" (T. A. Skotheim, R. L. Elsenbaumer, and J. R. Reynolds, Eds.), pp. 277-309. Dekker, New York, 1998.
644. A. Bolognesi, M. Catellani, S. Destri, R. Zamboni, and C. Taliani, *J. Chem. Soc., Chem. Commun.* 246 (1988).
645. A. Bolognesi, M. Catellani, S. Destri, C. Taliani, and R. Zamboni, *Synth. Met.* 37, 134 (1990).
646. C. Taliani, G. Ruani, R. Zamboni, A. Bolognesi, M. Catellani, S. Destri, and W. Porzio, *Synth. Met.* 28, C507 (1989).
647. M. Catellani, T. Caronna, and S. J. Valdo Meille, *J. Chem. Soc., Chem. Commun.* 1911 (1994).
648. M. Siekierski and J. Plochanski, *Synth. Met.* 51, 81 (1992).
649. A. T. Jeffries, K. C. Moore, D. M. Ondeyka, A. W. Sringsteen, and D. W. H. MacDowell, *J. Org. Chem.* 46, 2885 (1981).
650. A. Kraak, A. K. Wieserma, P. Jordens, and H. Wynberg, *Tetrahedron* 24, 3381 (1968).
651. A. Berlin, E. Brenna, G. A. Pagani, and F. Sanniccolo, *Synth. Met.* 51, 287 (1992).
652. D. D. Cunningham, A. Galal, C. V. Pham, E. T. Lewis, A. Burkhardt, L. L. Laguren-Davidson, A. N. Nkansah, O. Y. Ataman, H. Zimmer, and H. B. Mark, *J. Electrochem. Soc.* 135, 2750 (1988).
653. G. Zotti, G. Schiavon, A. Berlin, G. Fontana, and G. Pagani, *Macromolecules* 27, 1938 (1994).
654. T. M. Lambert and J. P. Ferraris, *J. Chem. Soc., Chem. Commun.* 752 (1991).
655. J. P. Ferraris and T. M. Lambert, *J. Chem. Soc., Chem. Commun.* 1268 (1991).
656. J. P. Ferraris, C. Henderson, D. Torres, and D. Meeker, *Synth. Met.* 72, 147 (1995).
657. H. Brisset, C. Thobie-Gautier, A. Gorgues, M. Jubault, and J. Roncali, *J. Chem. Soc., Chem. Commun.* 1305 (1994).

658. J. Roncali, R. Garreau, F. Garnier, and M. Lemaire, *J. Chem. Soc., Chem. Commun.* 1500 (1987).
659. J. Roncali, H. S. Li, R. Garreau, F. Garnier, and M. Lemaire, *Synth. Met.* 36, 267 (1990).
660. J. Roncali, H. Brisset, C. Thobie-Gautier, M. Jubault, and A. Gorgues, *J. Chim. Phys.* 92, 771 (1995).
661. M. Kozaki, S. Tanaka, and Y. Yamashita, *J. Chem. Soc., Chem. Commun.* 1500 (1987).
662. M. Kozaki, S. Tanaka, and Y. Yamashita, *Chem. Lett.* 533 (1993).
663. M. Kozaki, S. Tanaka, and Y. Yamashita, *J. Org. Chem.* 59, 442 (1994).
664. H. Meier, "Organic Semiconductors." VCH, Weinheim, 1974.
665. W. J. Bailey and C. W. Liaio, *J. Am. Chem. Soc.* 77, 992 (1955).
666. J. Simon, F. Tournilhac, and J. J. André, *New J. Chem.* 11, 383 (1987).
667. F. Bohlmann and B. Inhoffen, *Chem. Ber.* 89, 1276 (1956).
668. G. A. Edwards and G. J. Goldfinger, *J. Polym. Sci.* 16, 589 (1955).
669. H. A. Pohl and E. H. Engelhart, *J. Phys. Chem.* 66, 2085 (1962).
670. P. Teyssie and A. Korn-Girard, *J. Polym. Sci.* 2, 2849 (1964).
671. P. R. Ashton, J. P. Mathias, and J. F. Stoddart, *Polym. Prepr.* 32, 419 (1991).
672. T. Vogel, K. Blatter, and A. D. Schlüter, *Makromol. Chem., Rapid Commun.* 10, 427 (1989).
673. M. Ozaki, Y. Ikeda, and I. Nagoya, *Synth. Met.* 28, C801 (1989).
674. Y. Kojima, M. Tsuji, T. Matsuoka, and H. Takahashi, *Macromolecules* 27, 3735 (1994).
675. Y. Kojima, T. Matsuoka, N. Sato, and H. Takahashi, *Macromolecules* 28, 2893 (1995).
676. J. M. Tour and J. J. Lamba, *J. Am. Chem. Soc.* 115, 4935 (1993).
677. M. L. Kaplan, P. H. Schmidt, C. H. Chen, and W. M. Walsh, *Appl. Phys. Lett.* 36, 867 (1980).
678. S. R. Forrest, M. L. Kaplan, P. H. Schmidt, T. Venkatesan, and A. J. Lovinger, *Appl. Phys. Lett.* 41, 708 (1982).
679. P. H. Schmidt, C. David, M. L. Kaplan, and W. L. Feldmann, *Appl. Phys. Lett.* 40, 93 (1982).
680. Z. Iqbal, D. M. Ivory, J. Marti, J. L. Brédas, and R. H. Baughman, *Mol. Cryst. Liq. Cryst.* 118, 103 (1985).
681. M. Murakami and S. Yoshimura, *J. Chem. Soc., Chem. Commun.* 1649 (1984).
682. M. Murakami and S. Yoshimura, *Mol. Cryst. Liq. Cryst.* 118, 95 (1985).
683. H. Kamo, M. Yudasaka, S. Kurita, T. Matsui, R. Kikuchi, Y. Ohki, and S. Yoshimura, *Synth. Met.* 68, 61 (1994).
684. A. Bohnen, K. H. Koch, W. Lütte, and K. Müllen, *Angew. Chem., Int. Ed. Engl.* 29, 525 (1990).
685. E. Clar, R. Kelly, and R. M. Laird, *Monatsh. Chem.* 80, 391 (1956).
686. E. Clar and W. Schmidt, *Tetrahedron* 34, 3219 (1978).
687. A. D. Schlüter, M. Löffler, and V. Enkelmann, *Nature* 368, 331 (1994).
688. M. Löffler, A. D. Schlüter, K. Gessler, W. Saenger, J. M. Toussaint, and J. L. Brédas, *Angew. Chem., Int. Ed. Engl.* 33, 2209 (1994).
689. B. Schlicke, H. Schirmer, and A. D. Schlüter, *Adv. Mater.* 7, 544 (1995).
690. F. De Schrijver and C. S. Marvel, *J. Polym. Sci., Part A: Polym. Chem.* 5, 545 (1967).
691. J. K. Stille and E. L. Mainen, *Macromolecules* 1, 36 (1968).
692. X. F. Cao, J. P. Jiang, D. P. Bloch, R. W. Hellwarth, L. P. Yu, and L. Dalton, *J. Appl. Phys.* 65, 5012 (1989).
693. P. J. S. Foot, V. Montgomery, C. J. Rhodes, and P. Spearman, *Mol. Cryst. Liq. Cryst.* 236, 199 (1993).
694. S. A. Jenekhe, *Macromolecules* 24, 1 (1991).
695. C. Della, F. Andreani, P. Costa Bizzari, M. Fiorini, E. Salatelli, L. Grossi, and W. Porzio, *Synth. Met.* 29, E477 (1989).
696. M. D. Pace and O. K. Kim, *Polymer* 25, 333 (1988).
697. L. R. Dalton, J. Thomson, and H. S. Nalwa, *Polymer* 28, 543 (1987).
698. A. J. Bandara, J. Curley, and G. Pritchard, *Synth. Met.* 72, 1 (1995).
699. C. Barbero, J. J. Silber, and L. Sereno, *J. Electroanal. Chem.* 291, 81 (1990).
700. K. Chiba, T. Ohsaka, Y. Ohnuki, and N. Oyama, *J. Electroanal. Chem.* 219, 117 (1987).
701. M. A. Goyette and M. Leclerc, *J. Electroanal. Chem.* 382, 7 (1995).
702. S. Kunimura, T. Ohsaka, and N. Oyama, *Macromolecules* 21, 894 (1988).
703. L. Yu, M. Chen, and L. R. Dalton, *Chem. Mater.* 2, 649 (1990).
704. J. Grimme, M. Kreyenschmidt, F. Uckert, K. Müllen, and U. Scherf, *Adv. Mater.* 7, 292 (1995).
705. U. Scherf and K. Müllen, *Makromol. Chem., Rapid. Commun.* 12, 489 (1991).
706. U. Scherf and K. Müllen, *Polym. Commun.* 33, 2443 (1992).
707. U. Scherf, *Synth. Met.* 55–57, 767 (1993).
708. A. D. Child and J. R. Reynolds, *Macromolecules* 27, 1975 (1994).
709. J. K. Kallitsis and H. Naarmann, *Synth. Met.* 44, 247 (1991).
710. M. R. Anderson, Q. Pei, T. Hjertberg, O. Inganäs, and O. Wennerström, *Synth. Met.* 55–57, 1227 (1993).
711. S. A. Chen and J. M. Ni, *Macromolecules* 26, 3230 (1993).
712. S. A. Chen and J. M. Ni, *Synth. Met.* 55, 576 (1993).
713. S. A. Chen and C. S. Liao, *Synth. Met.* 57, 4950 (1993).
714. R. L. Elsenbaumer, K. Y. Jen, G. G. Miller, and L. W. Shacklette, *Synth. Met.* 18, 277 (1987).
715. H. J. Fell, E. J. Samualson, E. Bakken, and P. H. J. Carlsen, *Synth. Met.* 72, 193 (1995).
716. S. Hotta, T. Hosaka, M. Soga, and W. Shimotsuma, *Synth. Met.* 9, 381 (1984).
717. S. Hotta, *Synth. Met.* 22, 103 (1987).
718. S. Hotta, S. D. D. V. Rughooputh, A. J. Heeger, and F. Wudl, *Macromolecules* 20, 212 (1987).
719. S. Hotta, S. D. D. V. Rughooputh, and A. J. Heeger, *Synth. Met.* 22, 79 (1987).
720. M. Kamath, J. O. Lim, K. G. Chittibabu, R. Sarma, L. A. Samuelson, J. A. Akkara, D. L. Kaplan, J. Kumar, and K. A. Marx, *J. Macromol. Sci., Pure Appl. Chem.* A30, 493 (1993).
721. J. Lowe and S. Holdcroft, *Polym. Prepr.* 35, 297 (1994).
722. M. J. Miyazaki and T. Yamamoto, *Chem. Lett.* 41–44 (1994).
723. Q. Pei and O. Inganäs, *Synth. Met.* 46, 353 (1992).
724. Q. Pei, O. Inganäs, G. Gustafsson, M. Granström, M. Andersson, T. Hjertberg, O. Wennerström, J. E. Osterholm, J. Lakso, and H. Jarvinen, *Synth. Met.* 55–57, 1221 (1993).
725. S. Pouzet and A. Ricard, *Polym. Bull.* 30, 291 (1993).
726. M. Sato, S. Tanaka, K. Kaeriyama, and F. Tomanga, *Polymer* 28, 1071 (1987).
727. S. Tanaka, M. Sato, and K. Kaeriyama, *Polym. Commun.* 26, 303 (1985).
728. X. Xu, H. Ishikawa, M. Satoh, and S. Hasegawa, *Synth. Met.* 57, 4873 (1993).
729. M. Berggren, O. Inganäs, G. Gustafsson, J. Rasmuson, M. R. Anderson, T. Hjertberg, and O. Wennerström, *Nature* 372, 444 (1994).
730. J. P. Ferraris and M. D. Newton, *Polymer* 33, 391 (1992).
731. M. Granström and O. Inganäs, *Synth. Met.* 55–57, 460 (1993).
732. M. J. Marsella and T. M. Swager, *Polym. Prepr.* 35, 271 (1994).
733. J. Roncali, A. Gorgues, and M. Jubault, *Chem. Mater.* 5, 1456 (1993).
734. C. Visy, J. Lukkari, and J. Kankare, *Macromolecules* 27, 3322 (1994).
735. C. Wang, M. E. Benz, E. LeGoff, J. L. Schindler, C. R. Kannewurf, and M. G. Kanatzidis, *Polym. Prepr.* 34, 422 (1993).
736. G. Zotti, M. C. Gallazi, G. Zerbil, and S. V. Meille, *Synth. Met.* 73, 217 (1995).
737. B. R. McKellar and W. A. Feld, *Polym. Prepr.* 34, 380 (1993).
738. C. P. Andrieux, P. Audebert, and C. Salou, *J. Electroanal. Chem.* 318, 235 (1991).
739. G. Bidan, B. Ehui, and M. Lapkowski, *J. Phys. D: Appl. Phys.* 21, 1043 (1988).
740. H. S. O. Chan, E. T. Kang, K. G. Neoh, K. L. Tan, B. T. G. Tan, and Y. K. Lim, *Synth. Met.* 30, 189 (1989).
741. A. F. Diaz and J. I. Castillo, *J. Chem. Soc., Chem. Commun.* 397 (1980).

742. A. F. Diaz, J. I. Castillo, J. A. Logan, and W. Y. Lee, *J. Electroanal. Chem.* 129, 115 (1981).
743. A. J. Downard, N. A. Surridge, T. J. Meyer, S. Cosnier, A. Deronzier, and J. G. Moutet, *J. Electroanal. Chem.* 246, 321 (1988).
744. A. Haimerl and A. Merz, *Angew. Chem., Int. Ed. Engl.* 25, 180 (1986).
745. K. K. Kanazawa, A. F. Diaz, R. H. Geiss, W. D. Gill, J. F. Kwak, J. A. Logan, J. F. Rabolt, and G. B. Street, *J. Chem. Soc., Chem. Commun.* 854 (1979).
746. K. K. Kanazawa, A. F. Diaz, M. F. Diaz, M. T. Kroundi, and G. B. Street, *Synth. Met.* 4, 119 (1981).
747. M. S. Kiani and G. R. Mitchell, *Synth. Met.* 46, 293 (1992).
748. A. Merz, A. Haimerl, and A. J. Owen, *Synth. Met.* 25, 89 (1988).
749. K. G. Neoh, E. T. Kang, T. C. Tan, and K. L. Tan, *J. Appl. Polym. Sci.* 38, 2009 (1989).
750. N. Nishizawa, T. Sawaguchi, T. Matsue, and I. Ochida, *Synth. Met.* 45, 241 (1991).
751. N. Noma, K. Namba, and Y. Shirota, *Synth. Met.* 64, 227 (1994).
752. P. Novak and W. Vielstich, *Mater. Sci. Forum* 62–64, 471 (1990).
753. P. Novak and W. Vielstich, *J. Electroanal. Chem.* 300, 99 (1991).
754. P. Novak, *Chem. Listy* 85, 1005 (1991).
755. A. Paul, D. Sarkar, and T. N. Misra, *Solid State Commun.* 89, 363 (1994).
756. J. R. Reynolds, P. A. Poropatic, and R. L. Toyooka, *Synth. Met.* 18, 95 (1987).
757. J. R. Reynolds, N. S. Sundaresan, M. Pomerantz, S. Basak, and C. K. Baker, *J. Electroanal. Chem.* 250, 355 (1988).
758. J. R. Reynolds, J. P. Ruiz, F. Wang, C. A. Jolly, K. Nayak, and D. S. Marynick, *Synth. Met.* 28, C621 (1989).
759. M. V. Rosenthal, T. A. Skotheim, C. Linkous, and M. I. Florit, *Polym. Prepr.* 25, 258 (1984).
760. D. Stanke, M. L. Hallensleben, and L. Toppare, *Synth. Met.* 72, 167 (1995).
761. B. Tieke and W. Gabriel, *Polymer* 31, 20 (1990).
762. J. P. Travers, P. Audebert, and G. Bidan, *Mol. Cryst. Liq. Cryst.* 118, 149 (1985).
763. M. Velazquez-Rosenthal, T. A. Skotheim, C. Linkous, and M. I. Florit, *Polym. Prepr.* 25, 258 (1984).
764. M. Velazquez-Rosenthal, T. A. Skotheim, A. Melo, M. I. Florit, and M. Salmon, *J. Electroanal. Chem.* 185, 297 (1985).
765. S. J. Vigmond, K. M. R. Kallury, and M. Thompson, *Anal. Chem.* 64, 2763 (1992).
766. M. Fujitsuka, R. Nakahara, T. Iyoda, T. Shimidzu, and H. Tsuchiya, *J. Appl. Phys.* 74, 1283 (1993).
767. B. L. Funt, E. M. Peters, and J. D. Van Dyke, *J. Polym. Sci., Part A: Polym. Chem.* 24, 1529 (1986).
768. P. Kathiramanathan, *J. Electroanal. Chem.* 247, 351 (1988).
769. S. Kuwabata, S. Ito, and H. Yoneyama, *J. Electrochem. Soc.* 135, 1691 (1988).
770. F. R. Mayo and F. M. Lewis, *J. Am. Chem. Soc.* 66, 1594 (1944).
771. S. Naitoh, K. Sanui, and N. Ogata, *J. Chem. Soc., Chem. Commun.* 1348 (1986).
772. E. M. Peters and J. D. Van Dyke, *J. Polym. Sci., Part A: Polym. Chem.* 29, 1379 (1991).
773. W. Torres and M. A. Fox, *Chem. Mater.* 4, 146 (1992).
774. M. Aldissi, *Mol. Cryst. Liq. Cryst.* 160, 121 (1988).
775. A. Berlin, W. Wernet, and G. Wegner, *Makromol. Chem.* 188, 2963 (1987).
776. J. P. Ferraris and G. D. Skiles, *Polymer* 28, 179 (1987).
777. J. P. Ferraris, R. G. Andrus, and D. Hrnir, *J. Chem. Soc., Chem. Commun.* 1318 (1989).
778. M. V. Joshi, C. Hemler, M. P. Cava, J. L. Cain, M. G. Bakker, A. J. McKinley, and R. M. Metzger, *J. Chem. Soc., Perkin Trans.* 2 1081 (1993).
779. G. G. McLeod, M. G. B. Nahboubian-Jones, R. A. Pethrick, S. D. Watson, N. D. Truong, J. C. Galin, and J. Francois, *Polymer* 27, 455 (1986).
780. S. Naitoh, *Synth. Met.* 18, 237 (1988).
781. E. M. Peters and J. D. Van Dyke, *J. Polym. Sci., Part A: Polym. Chem.* 24, 1891 (1992).
782. M. V. Joshi, M. P. Cava, M. G. Bakker, A. J. McKinley, J. L. Cain, and R. M. Metzger, *Synth. Met.* 55–57, 948 (1993).
783. M. Seki, H. An, K. Sato, and R. Yosomiya, *Synth. Met.* 26, 33 (1988).
784. T. Mitsuhashi, S. Tanaka, and K. Kaeriyama, *Makromol. Chem.* 189, 1755 (1988).
785. T. Yamamoto, Z. H. Zhou, T. Maruyama, and T. Kanbara, *Synth. Met.* 55–57, 1209 (1993).
786. Z. H. Zhou, T. Maruyama, T. Kanbara, T. Ikeda, K. Ichimura, T. Yamamoto, and K. Tokuda, *J. Chem. Soc., Chem. Commun.* 1210 (1991).
787. I. H. Jenkins and P. G. Pickup, *Macromolecules* 26, 4450 (1993).
788. P. Bäuerle, G. Götz, P. Emerle, and H. Port, *Adv. Mater.* 4, 564 (1992).
789. I. Hoogmartens, P. Adriaensens, R. Carleer, D. Vanderzande, H. Martens, and J. Gelan, *Synth. Met.* 51, 219 (1992).
790. R. H. L. Kiebooms, P. J. A. Adriaensens, D. J. M. Vanderzande, and J. M. J. V. Gelan, *J. Org. Chem.* 62, 1473 (1997).
791. D. Lorcy and M. P. Cava, *Adv. Mater.* 4, 562 (1992).
792. S. Musmanni and J. P. Ferraris, *J. Chem. Soc., Chem. Commun.* 172 (1993).
793. D. Vangeneugden, R. Kiebooms, P. Adriaensens, D. Vanderzande, J. Gelan, J. Desmet, and G. Huybrechts, *Acta Polym.* 49, 687 (1998).
794. D. Vangeneugden, Ph.D. Thesis, Limburgs Univ. Centrum, Belgium, 1999.
795. D. Vangeneugden, R. Kiebooms, D. Vanderzande, and J. Gelan, *Synth. Met.* 101, 120 (1999).
796. J. P. Ferraris, A. Bravo, W. Kim, and D. C. Kmcir, *J. Chem. Soc., Chem. Commun.* 991 (1994).
797. C. Kitamura, S. Tanaka, and Y. Yamashita, *J. Chem. Soc., Chem. Commun.* 1585 (1994).
798. T. Suzuki, H. Fuji, Y. Yamashita, C. Kabuto, S. Tanaka, H. Hara-sawa, T. Mukai, and T. Miyashi, *J. Am. Chem. Soc.* 114, 3034 (1992).
799. S. Tanaka and Y. Yamashita, *Synth. Met.* 55–57, 1251 (1993).
800. M. Karikomi, C. Kitamura, S. Tanaka, and Y. Yamashita, *J. Am. Chem. Soc.* 117, 6791 (1995).
801. S. Tanaka and Y. Yamashita, *Synth. Met.* 69, 599 (1995).
802. J. R. Reynolds, A. R. Katritzky, J. Soloducho, S. Belyakov, G. A. Sotzing, and M. Pyo, *Macromolecules* 27, 7225 (1994).
803. K. L. Pouwer, T. R. Vries, E. E. Havinga, E. W. Meijer, and H. Wyn-berg, *J. Chem. Soc., Chem. Commun.* 1432 (1988).
804. S. Martina and A. D. Schlüter, *Macromolecules* 25, 3607 (1992).
805. G. A. Sotzing, J. R. Reynolds, A. R. Katritzky, J. Soloducho, S. Belyakov, and R. Musgrave, *Macromolecules* 29, 1679 (1996).
806. R. Danieli, P. Ostojka, M. Tiecco, R. Zamboni, and C. Taliani, *J. Chem. Soc., Chem. Commun.* 1473 (1986).
807. D. M. Haynes, A. R. Hepburn, D. M. Goldie, J. M. Marshall, and A. Pelter, *Synth. Met.* 55–57, 839 (1993).
808. T. Mitsuhashi, K. Kaeriyama, and S. Tanaka, *J. Chem. Soc., Chem. Commun.* 764 (1987).
809. W. Czerwinski, N. Nucker, and J. Fink, *Synth. Met.* 25, 71 (1988).
810. W. Czerwinski, *Synth. Met.* 35, 229 (1990).
811. A. Pelter, M. Rowlands, and I. H. Jenkins, *Tetrahedron Lett.* 28, 5213 (1987).
812. A. Pelter, J. M. Maud, I. Jenkins, C. Sadeka, and G. Coles, *Tetrahe-dron Lett.* 30, 3461 (1989).
813. S. A. Child and J. R. Reynolds, *J. Chem. Soc., Chem. Commun.* 1779 (1991).
814. J. R. Reynolds, J. P. Ruiz, A. D. Child, K. Nayak, and D. S. Marynick, *Macromolecules* 24, 678 (1991).
815. J. P. Ruiz, A. D. Child, K. Nayak, D. S. Marynick, and J. R. Reynolds, *Synth. Met.* 41–43, 783 (1991).
816. J. P. Ruiz, J. R. Dharia, J. R. Reynolds, and L. J. Buckley, *Macro-molecules* 25, 849 (1992).

817. B. Sankaran, A. D. Child, F. Larmat, and J. R. Reynolds, *Polym. Prepr.* 35, 263 (1994).
818. J. Kowalik and L. M. Tolbert, *Polym. Mater. Sci. Eng.* 64, 214 (1991).
819. A. Bao, R. Cai, and L. Yu, *Polym. Prepr.* 34, 749 (1993).
820. L. Yu, Z. Bao, and R. Cai, *Angew. Chem., Int. Ed. Engl.* 32, 1345 (1993).
821. J. R. Reynolds, A. D. Child, J. P. Ruiz, S. Y. Hong, and D. S. Marynick, *Macromolecules* 26, 2095 (1993).
822. M. Thelakkat and H. Naarmann, *Synth. Met.* 68, 153 (1995).
823. A. K. Agrawal and S. A. Jenekhe, *Macromolecules* 24, 6806 (1991).
824. A. K. Agrawal and S. A. Jenekhe, *Polym. Prepr.* 33, 349 (1993).
825. M. O. Bevierre, F. Mercier, L. Ricard, and F. Mathey, *Angew. Chem., Int. Ed. Engl.* 29, 655 (1990).
826. P. A. DePra, J. G. Gaudiello, and T. J. Marks, *Macromolecules* 21, 2297 (1988).
827. M. Dotrong, R. Mehta, G. A. Balchin, R. C. Tomlinson, and M. Sinsky, *J. Polym. Sci., Part A: Polym. Chem.* 31, 723 (1993).
828. J. H. Promislow, J. Preston, and E. T. Samulski, *Macromolecules* 26, 1793 (1993).
829. K. Tamao, S. Yamaguchi, M. Shiozaki, Y. Nakagawa, and Y. Ito, *J. Am. Chem. Soc.* 114, 5867 (1992).
830. D. J. Irvin and J. R. Reynolds, *Polym. Prepr.* 37, 532 (1996).
831. D. J. Irvin and J. R. Reynolds, *Polym. Prepr.* 37, 682 (1996).
832. F. Larmat, J. R. Reynolds, B. Reinhart, and L. L. Brott, *Polym. Prepr.* 37, 799 (1996).
833. J. R. Reynolds, G. A. Sotzing, B. Sankara, S. A. Sapp, D. J. Irvin, and J. L. Kedding, *Polym. Prepr.* 37, 135 (1996).
834. S. A. Sapp, G. A. Sotzing, J. L. Reddinger, and R. Reynolds, *Polym. Prepr.* 37, 797 (1996).
835. G. A. Sotzing, J. L. Reddinger, and J. R. Reynolds, *Polym. Prepr.* 37, 795 (1996).
836. J. L. Brédas, *J. Chem. Phys.* 82, 3808 (1985).
837. S. A. Jenekhe, *Nature* 322, 345 (1986).
838. W. C. Chen and S. A. Jenekhe, *Macromolecules* 28, 454 (1995).
839. W. C. Chen and S. A. Jenekhe, *Macromolecules* 28, 465 (1995).
840. H. Goto, K. Akagi, and H. Shirakawa, *Synth. Met.* 84, 385 (1997).
841. R. Kiebooms and F. Wudl, *Synth. Met.* 101, 40 (1999).
842. R. Jira and H. Braunling, *Synth. Met.* 17, 691 (1987).
843. H. Braunling, G. Blöchl, and R. Becker, *Synth. Met.* 41–43, 487 (1991).
844. H. Braunling, R. Becker, and G. Blöchl, *Synth. Met.* 55–57, 833 (1993).
845. R. A. Wessling and R. G. Zimmerman, U.S. Patent 3,404,132, 1968.
846. R. A. Wessling and R. G. Zimmerman, U.S. Patent 3,532,643, 1970.
847. R. A. Wessling, *J. Polym. Sci., Polym. Symp.* 72, 55 (1985).
848. J. H. Burroughes, D. D. C. Bradley, A. R. Brown, R. N. Marks, K. Mackay, R. H. Friend, P. L. Burns, and A. B. Holmes, *Nature* 347, 539 (1990).
849. S. C. Moratti, in "Handbook of Conducting Polymers" (T. Skotheim, Ed.), pp. 343–361. Dekker, New York, 1998.
850. S. Iwatsuki, M. Kubo, and H. Yamashita, *Chem. Lett.* 729 (1989).
851. S. Iwatsuki, M. Kubo, and Y. Itoh, *Chem. Lett.* 1085 (1993).
852. K. Y. Jen, M. R. Maxfield, L. W. Shacklette, and R. L. Elsenbaumer, *J. Chem. Soc., Chem. Commun.* 309 (1987).
853. I. Murase, T. Ohnishi, T. Noguchi, and M. Hirooka, *Polym. Commun.* 28, 229 (1987).
854. L. Pecters, W. Eevers, M. Van Der Borgh, S. Jacobs, and H. J. Geise, *Polymer* 34, 4589 (1993).
855. S. Yamada, S. Tokito, T. Tsutsui, and S. Saito, *J. Chem. Soc., Chem. Commun.* 1448 (1987).
856. H. Cheng and R. L. Elsenbaumer, *J. Chem. Soc., Chem. Commun.* 1451 (1995).
857. Y. Fu and R. L. Elsenbaumer, *Polym. Mater. Sci. Eng.* 72, 315 (1995).
858. G. A. Sotzing, J. R. Reynolds, A. R. Katritzky, J. Soloducho, and R. Musgrave, *Polym. Mater. Sci. Eng.* 72, 317 (1995).
859. G. A. Sotzing and J. R. Reynolds, *J. Chem. Soc., Chem. Commun.* 703 (1995).
860. K. Y. Jen, T. R. Jow, and R. L. Elsenbaumer, *J. Chem. Soc., Chem. Commun.* 1113 (1987).
861. R. N. McDonald and T. W. Cambell, *J. Am. Chem. Soc.* 82, 4669 (1960).
862. K. D. Gourley, C. P. Lillya, J. R. Reynolds, and J. C. W. Chien, *Macromolecules* 17, 1025 (1984).
863. H. H. Hörhold and J. Opfermann, *Makromol. Chem.* 131, 105 (1970).
864. W. S. Huang, K. Y. Jen, M. Angelopoulos, A. G. McDiarmid, and M. P. Cava, *Mol. Cryst. Liq. Cryst.* 189, 237 (1990).
865. V. G. Kossmehl, M. Härtel, and G. Manecke, *Makromol. Chem.* 131, 37 (1970).
866. V. G. Manecke and D. Zerpner, *Makromol. Chem.* 129, 183 (1969).
867. M. Rehahn and A. D. Schlüter, *Makromol. Chem., Rapid Commun.* 11, 375 (1990).
868. A. W. Cooke and K. B. Wagener, *Macromolecules* 24, 1404 (1991).
869. F. Cataldo, *Polym. Commun.* 32, 354 (1991).
870. R. F. Heck, *Org. React.* 27, 345 (1982).
871. A. Greiner and W. Heitz, *Makromol. Chem., Rapid Commun.* 9, 581 (1988).
872. M. Reetz, G. Lohmer, and R. Schwickardi, *Angew. Chem., Int. Ed. Engl.* 37, 481 (1998).
873. A. Greiner, H. Martelock, A. Noll, N. Siegfried, and W. Heitz, *Polymer* 32, 1857 (1991).
874. H. Martelock, A. Greiner, and W. Heitz, *Macromol. Chem.* 192, 967 (1991).
875. M. Brenda, A. Greiner, and W. Heitz, *Macromol. Chem.* 191, 1083 (1990).
876. W. Heitz, *Makromol. Chem.* 189, 119 (1988).
877. M. Pan, Z. Bao, and L. Yu, *Macromolecules* 28, 5151 (1995).
878. J. Huber, K. Müllen, J. Salbeck, H. Schenk, U. Scherf, T. Stehlin, and R. Stern, *Acta Polym.* 45, 244 (1994).
879. N. Miyama, T. Yano, and A. Suzuki, *Tetrahedron Lett.* 21, 2865 (1980).
880. N. Miyama, T. Ishiyama, H. Sasaki, M. Ishikawa, M. Satoh, and A. Suzuki, *J. Am. Chem. Soc.* 111, 314 (1989).
881. D. R. Baigent, P. J. Hamer, R. H. Friend, S. C. Moratti, and A. B. Holmes, *Synth. Met.* 71, 2175 (1995).
882. D. Debord and J. Golé, *Bull. Soc. Chem.* 4, 1401 (1971).
883. V. W. Funke and E. C. Schütze, *Makromol. Chem.* 74, 71 (1963).
884. N. C. Greenham, S. C. Moratti, D. D. C. Bradley, R. H. Friend, and A. B. Holmes, *Nature* 365, 628 (1993).
885. M. Helbig and H. H. Hörhold, *Makromol. Chem.* 194, 1607 (1993).
886. H. H. Hörhold, D. Gräf, and J. Opfermann, *J. Plaste Kautschuk* 17 (1970).
887. H. H. Hörhold, *Z. Chem.* 12, 41 (1972).
888. H. H. Hörhold, M. Helbig, D. Raabe, J. Opfermann, U. Scherf, R. Stockmann, and D. Weiss, *Z. Chem.* 27, 126 (1987).
889. P. M. Lahti, A. Sarker, R. O. Garay, R. W. Lenz, and F. E. Karasz, *Polymer* 35, 1312 (1994).
890. R. W. Lenz and C. E. Handlovits, *J. Org. Chem.* 25, 813 (1960).
891. R. W. Lenz, C. C. Han, J. Stenger-Smith, and F. E. Karasz, *J. Polym. Sci., Part A: Polym. Chem.* 26, 3241 (1988).
892. S. C. Moratti, D. D. C. Bradley, R. H. Friend, N. C. Greenham, and A. B. Holmes, *Polym. Prepr.* 35, 214 (1994).
893. S. C. Moratti, R. Cervini, A. B. Holmes, D. R. Baigent, R. H. Friend, N. C. Greenham, J. Gruner, and P. J. Hamer, *Synth. Met.* 71, 2117 (1995).
894. E. G. J. Staring, R. C. J. E. Demandt, D. Braun, G. L. J. Rikken, Y. A. R. R. Kessener, A. H. J. Venhuizen, M. M. F. Knippenberg, and M. Bouwmans, *Synth. Met.* 71, 2179 (1995).
895. H. Kretzschmann and H. Meier, *Tetrahedron Lett.* 32, 5059 (1991).
896. H. Meier, H. Kretzschmann, and M. Lang, *J. Prakt. Chem.* 336, 121 (1994).
897. A. Kumar and B. E. Eichinger, *Makromol. Chem., Rapid Commun.* 13, 311 (1992).

898. E. Thorn-Csányi and K. P. Pflug, *Makromol. Chem., Rapid Commun.* 14, 619 (1993).
899. E. Thorn-Csányi and P. Kraxner, *Makromol. Chem., Rapid Commun.* 16, 147 (1995).
900. E. Thorn-Csányi and H. D. Höhnk, *J. Mol. Catal.* 76, 101 (1992).
901. D. F. Hoeg, D. I. Lusk, and E. P. Goldberg, *J. Polym. Sci. Part B: Polym. Phys.* 2, 697 (1964).
902. G. H. Smith, U.S. Patent 3, 110, 687, 1963.
903. I. Moritani, T. Nagai, and Y. Shirota, *Kogyo Kagaku Zasshi* 68, 296 (1965).
904. H. G. Gilch and W. L. Wheelwright, *J. Polym. Sci., Part A: Polym. Chem.* 4, 1337 (1966).
905. H. H. Hörhold, J. Gottschaldt, and J. Opfermann, *J. Prakt. Chem.* 139, 611 (1977).
906. H. H. Hörhold and D. Raabe, *Acta Polym.* 30, 86 (1979).
907. H. H. Hörhold, H. Rätche, M. Helbig, and J. Opfermann, *Makromol. Chem.* 188, 2083 (1987).
908. F. Fors, L. Julia, J. Riera, J. M. Tura, and J. Saulo, *J. Polym. Sci., Part A: Polym. Chem.* 30, 2489 (1992).
909. J. A. Osaheni and S. A. Jenekhe, *Macromolecules* 26, 4726 (1993).
910. W. P. Chang, W. T. Whang, and P. W. Lin, *Polymer* 37, 1513 (1996).
911. H. Nishihara, M. Tateishi, K. Aramaki, T. Ohsawa, and O. Kimura, *Chem. Lett.* 539 (1987).
912. S. N. Kaul and J. E. Fernandez, *Macromolecules* 23, 2875 (1990).
913. V. P. Conticello, D. L. Gin, and R. H. Grubbs, *J. Am. Chem. Soc.* 114, 9708 (1992).
914. L. Pu, M. W. Wagaman, and R. H. Grubbs, *Macromolecules* 29, 1138 (1996).
915. M. W. Wagaman and R. H. Grubbs, *Macromolecules* 30, 2837 (1997).
916. Y. J. Miao and G. C. Bazan, *J. Am. Chem. Soc.* 116, 9379 (1994).
917. M. Szwarc, *Discuss. Faraday Soc.* 2, 46 (1947).
918. X. Müller and Y. Müller-Rodloff, *Annalen* 517, 134 (1935).
919. X. Müller and Y. Tietz, *Chem. Ber.* 74, 807 (1941).
920. L. A. Errede and M. Szwarc, *Quart. Rev.* 12, 301 (1958).
921. W. F. Gorham, *J. Polym. Sci., Part A: Polym. Chem.* 4, 3027 (1966).
922. S. Iwatsuki, M. Kubo, and T. Kumeuchi, *Chem. Lett.* 1071 (1991).
923. O. Schäfer, A. Greiner, J. Pommerehne, W. Guss, H. Vestweber, H. Y. Tak, H. Bässler, C. Schmidt, G. Lüssem, B. Schartel, V. Stümpflen, J. H. Wendorff, S. Spiegel, C. Möller, and H. W. Spiess, *Synth. Met.* 82, 1 (1996).
924. E. G. J. Staring, D. Braun, G. L. J. Rikken, R. C. J. E. Demandt, Y. A. R. R. Kessener, M. Bouwmans, and D. Boer, *Synth. Met.* 67, 71 (1994).
925. M. J. Hatch, *Prog. Org. Coatings* 4, 61 (1976).
926. T. Alfrey, "Biennial Polymer Symposium, Ann Arbor, MI," 1972.
927. W. Brutting, M. Meier, M. Herold, S. Karg, and M. Schwoerer, *Synth. Met.* 163 (1997).
928. M. Herold, J. Gmeiner, C. Drummer, and M. Schwoerer, *J. Mater. Sci.* 32, 5709 (1997).
929. F. R. Denton, A. Sarker, P. M. Lahti, R. O. Garay, and F. E. Karasz, *J. Polym. Sci., Part A: Polym. Chem.* 30, 2233 (1992).
930. R. Garay and R. W. Lenz, *Makromol. Chem. Suppl.* 15, 1 (1989).
931. M. J. Cherry, S. C. Moratti, A. B. Holmes, P. L. Taylor, J. Grüner, and R. H. Friend, *Synth. Met.* 69, 493 (1995).
932. P. M. Lahti, D. A. Modarelli, F. R. Denton, R. W. Lenz, and F. E. Karasz, *J. Am. Chem. Soc.* 110, 7258 (1988).
933. M. Kanbe and M. Okawara, *J. Polym. Sci., Part A: Polym. Chem.* 6, 1058 (1968).
934. F. R. Denton, P. M. Lahti, and F. E. Karasz, *J. Polym. Sci., Part A: Polym. Chem.* 30, 2223 (1992).
935. B. R. Cho, Y. K. Kim, and M. S. Han, *Macromolecules* 31, 2098 (1998).
936. Y. Sonada and Y. Suzuki, *J. Chem. Soc., Perkin Trans. 1*, 317 (1994).
937. J. D. Stenger-Smith, T. Sauer, G. Wegner, and R. W. Lenz, *Polymer* 31, 1632 (1990).
938. J. D. Capistran, D. R. Gagnon, S. Antoun, R. W. Lenz, and F. E. Karasz, *Polym. Prepr.* 282 (1984).
939. L. M. Leung and G. L. Chik, *Polymer* 34, 5174 (1993).
940. R. O. Garay, F. E. Karasz, and R. W. Lenz, *J. Macromol. Sci., Pure Appl. Chem.* 32, 905 (1995).
941. M. Pomerantz, J. Wang, S. Seong, K. P. Starkey, L. Nguyen, and D. S. Marynick, *Macromolecules* 27, 7478 (1994).
942. A. Sarker, P. M. Lahti, and F. E. Karasz, *J. Polym. Sci., Part A: Polym. Chem.* 32, 65 (1994).
943. P. L. Burn, D. D. C. Bradley, R. H. Friend, D. A. Halliday, A. B. Holmes, R. W. Jackson, and A. Kraft, *J. Chem. Soc., Perkin Trans. 1*, 3225 (1992).
944. R. O. Garay, H. Naarmann, and K. Müllen, *Macromolecules* 27, 1922 (1994).
945. M. S. Jang and H. K. Shim, *Polym. Bull.* 35, 49 (1995).
946. K. Y. Jen, L. W. Shacklette, and R. Elsenbaumer, *Synth. Met.* 22, 179 (1987).
947. W. B. Liang, R. W. Lenz, and F. E. Karasz, *J. Polym. Sci., Part A: Polym. Chem.* 28, 2867 (1990).
948. K. J. Moon, K. S. Lee, and H. K. Shim, *Synth. Met.* 71, 1719 (1995).
949. I. Murase, T. Ohnishi, T. Noguchi, and M. Hirooka, *Polym. Commun.* 26, 362 (1985).
950. S. Tokito, T. Momii, H. Murata, T. T., and S. Saito, *Polymer* 31, 1137 (1990).
951. Y. Sonada and K. Kaeriyama, *Bull. Chem. Soc. Jpn.* 65, 853 (1992).
952. S. Höger, J. J. McNamara, S. Schrieter, and F. Wudl, *Chem. Mater.* 6, 171 (1994).
953. D. H. Hwang, H. K. Shim, J. I. Lee, and K. S. Lee, *J. Chem. Soc., Chem. Commun.* 2461 (1994).
954. J. J. Jin, J. C. Kim, and H. K. Shim, *Macromolecules* 25, 5519 (1992).
955. I. N. Kang, G. J. Lee, D. H. Kim, and H. S. Kim, *Polym. Bull.* 33, 89 (1994).
956. R. K. McCoy and F. E. Karasz, *Chem. Mater.* 3, 941 (1991).
957. J. I. Jin, C. K. Park, and H. K. Shim, *J. Polym. Sci., Part A: Polym. Chem.* 29, 93 (1991).
958. J. D. Stenger-Smith, A. P. Chafin, and W. P. Norris, *J. Org. Chem.* 59, 6107 (1994).
959. J. I. Jin, S. H. Yu, and H. K. Shim, *J. Polym. Sci., Part B: Polym. Phys.* 31, 87 (1993).
960. R. M. Gregorius, P. M. Lahti, and F. E. Karasz, *Macromolecules* 25, 6664 (1992).
961. C. C. Han, R. W. Lenz, and F. E. Karasz, *Polym. Commun.* 28, 261 (1987).
962. J. I. Jin, Y. H. Lee, and H. K. Shim, *Macromolecules* 26, 1805 (1993).
963. J. I. Jin, Y. H. Lee, C. K. Park, and B. K. Nam, *Macromolecules* 27, 5239 (1994).
964. J. I. Jin, C. K. Park, and H. K. Shim, *Polymer* 35, 480 (1994).
965. H. K. Shim, R. W. Lenz, and J. I. Jin, *Makromol. Chem.* 28, 261 (1989).
966. R. O. Garay, U. Baier, C. Bubeck, and K. Müllen, *Adv. Mater.* 5, 561 (1993).
967. A. Beerden, D. Vanderzande, and J. Gelan, *Synth. Met.* 52, 387 (1992).
968. P. L. Burn, D. D. C. Bradley, A. R. Brown, R. H. Friend, and A. B. Holmes, *Synth. Met.* 41-43, 261 (1991).
969. J. M. Machado, F. R. Denton, J. B. Schlenoff, F. E. Karasz, and P. M. Lahti, *J. Polym. Sci., Part B: Polym. Phys.* 27, 199 (1989).
970. T. Momii, S. Tokito, T. Tsutsui, and S. Saito, *Chem. Lett.* 1201 (1988).
971. D. R. Gagnon, J. D. Capistran, F. E. Karasz, R. W. Lenz, and S. Antoun, *Polymer* 28, 567 (1987).
972. V. Massardier, J. C. Beziat, and A. Guyot, *Eur. Polym. J.* 31, 291 (1995).
973. F. Papadimitrakopoulos, K. Konstantinidis, T. M. Miller, R. Opila, E. A. Chandross, and M. E. Galvin, *Chem. Mater.* 6, 1563 (1994).
974. J. B. Schlenoff and L. J. Wang, *Macromolecules* 24, 6653 (1991).
975. G. Montaudo, D. Vitalini, and R. W. Lenz, *Polymer* 28, 837 (1987).
976. A. Torres-Filho and R. W. Lenz, *J. Polym. Sci., Part B: Polym. Phys.* 31, 959 (1993).
977. J. Bullot, B. Dulieu, and S. Lefrant, *Synth. Met.* 61, 211 (1993).

978. W. Schmid, R. Dankesreiter, J. Gmeiner, T. Vogtmann, and M. Schwoerer, *Acta Polym.* 44, 208 (1993).
979. S. S. Taguchi and T. Tanaka, U.S. Patent 4, 816, 383, 1989.
980. V. Massardier, A. Guyot, and V. H. Tan, *Polymer* 35, 1561 (1994).
981. A. Torres-Filho and R. W. Lenz, *J. Appl. Polym. Sci.* 52, 377 (1994).
982. M. S. Karasch, W. Nudenberg, and E. K. Fields, *J. Am. Chem. Soc.* 66, 1276 (1944).
983. B. R. Hsieh, W. C. Wan, Y. Yu, Y. Gao, T. E. Goodwin, S. A. Gonzalez, and W. A. Feld, *Macromolecules* 31, 651 (1998).
984. B. R. Hsieh, Y. Yu, G. M. Schaaf, and W. A. Feld, *Polym. Prepr.* 38, 72 (1998).
985. B. R. Hsieh, Y. Yu, G. M. Schaaf, and W. A. Feld, *Polym. Prepr.* 38, 163 (1998).
986. B. R. Hsieh, Y. Yu, E. W. Forsythe, G. M. Schaaf, and W. A. Feld, *J. Am. Chem. Soc.* 120, 231 (1998).
987. B. R. Hsieh, W. C. Wan, Y. Yu, Y. Gao, T. E. Goodwin, S. A. Gonzalez, and W. A. Feld, *Macromolecules* 31, 631 (1998).
988. D. Braun, E. G. J. Staring, R. C. J. E. Demandt, G. L. J. Rikken, Y. A. R. R. Kessener, and A. H. J. Venhuizen, *Synth. Met.* 66, 75 (1994).
989. B. R. Hsieh and W. A. Field, *Polym. Prepr.* 34, 410 (1993).
990. G. J. Sarnecki, P. L. Burn, A. Kraft, R. H. Friend, and A. B. Holmes, *Synth. Met.* 55–57, 914 (1993).
991. G. J. Sarnecki, R. H. Friend, A. B. Holmes, and S. C. Moratti, *Synth. Met.* 69, 545 (1995).
992. W. J. Swatos and B. Gordon, *Polym. Prepr.* 30, 505 (1990).
993. F. Wudl, P. M. Allemand, G. Srdanov, Z. Ni, and D. McBranch (S. R. Marder, J. E. Sohn, and G. D. Stucky, Eds.), p. 683. Am. Chem. Soc., Washington, DC, 1991.
994. S. Son, A. Dodabalapur, A. J. Lovinger, and M. E. Galvin, *Science* 269, 376 (1995).
995. R. Gowri, D. Mandal, B. Shivkumar, and S. Ramakrishnan, *Macromolecules* 31, 1819 (1998).
996. F. Louwet, D. Vanderzande, and J. Gelan, *Synth. Met.* 52, 125 (1992).
997. F. Louwet, D. Vanderzande, J. Gelan, and J. Mullens, *Macromolecules* 28, 1330 (1995).
998. F. Louwet, D. Vanderzande, and J. Gelan, *Synth. Met.* 69, 509 (1995).
999. B. M. Trost, T. N. Salzman, and K. Hiroi, *J. Am. Chem. Soc.* 98, 4887 (1976).
1000. D. J. Vanderzande, A. C. Issaris, M. J. Van Der Borgh, A. J. van Breemen, M. M. de Kok, and J. M. Gelan, *Macromol. Symp.* 125, 189 (1997).
1001. A. J. J. M. van Breemen, D. J. M. Vanderzande, P. J. Adriaensen, and J. M. J. V. Gelan, *J. Org. Chem.* 64, 3106 (1999).
1002. A. Issaris, D. Vanderzande, P. Adriaensen, and J. Gelan, *Macromolecules* 31, 4426 (1998).
1003. A. Issaris, D. Vanderzande, and J. Gelan, *Polymer* 38, 2571 (1997).
1004. L. Hontis, M. Van Der Borgh, D. Vanderzande, and J. Gelan, *Polymer* 40, 6615 (1999).
1005. M. Van Der Borgh, D. Vanderzande, and J. Gelan, *Polymer* 17, 4171 (1998).
1006. A. J. J. M. van Breemen, A. C. J. Issaris, M. M. de Kok, M. J. A. N. Van Der Borgh, P. J. Adriaensen, J. M. J. V. Gelan, and D. J. M. Vanderzande, *Macromolecules* 32, 5728 (1999).
1007. M. M. de Kok, A. J. J. M. van Breemen, P. J. Adriaensen, A. van Dixhoorn, J. M. Gelan, and D. J. Vanderzande, *Acta Polym.* 49, 510 (1998).
1008. M. M. de Kok, A. J. J. M. van Breemen, R. A. A. Carleer, P. J. Adriaensen, J. M. Gelan, and D. J. Vanderzande, *Acta Polym.* 50, 28 (1999).
1009. E. M. Geniès, A. Boyle, M. Lapkowski, and C. Tsintavis, *Synth. Met.* 36, 139 (1990).
1010. H. Letheby, *J. Am. Chem. Soc.* 15, 161 (1862).
1011. A. G. Green and A. E. Woodhead, *J. Chem. Soc.* 97, 2388 (1910).
1012. H. N. McCoy and W. C. Moorer, *J. Am. Chem. Soc.* 33, 273 (1911).
1013. D. M. Mohilner, R. H. Adams, and W. J. Argersinger, *J. Am. Chem. Soc.* 84, 3618 (1962).
1014. R. Surville, M. Josefowicz, L. T. Yu, J. Perichon, and R. Buvet, *Electrochim. Acta* 13, 1451 (1968).
1015. X. Willstater and Y. Moore, *Chem. Ber.* 40, 2665 (1907).
1016. X. Willstater and Y. Dorogi, *Chem. Ber.* 42, 2147 (1909).
1017. X. Willstater and Y. Dorogi, *Chem. Ber.* 42, 4118 (1909).
1018. J. Anand, S. Palaniappan, and D. N. Sathyanarayana, in "Handbook of Organic Conductive Molecules and Polymers" (H. S. Nalwa, Ed.), Vol. 2, pp. 573–624. Wiley, New York, 1997.
1019. A. G. McDiarmid, in "Conjugated Polymers and Related Materials" (W. R. Salaneck, I. Lundström, and B. G. Rånby, Eds.), pp. 73–98. Oxford Univ. Press, Oxford, 1993.
1020. D. C. Trivedi, in "Handbook of Organic Conductive Molecules and Polymers" (H. S. Nalwa, Ed.), Vol. 2, pp. 505–572. Wiley, New York, 1997.
1021. J. C. Chiang and A. G. McDiarmid, *Synth. Met.* 13, 193 (1986).
1022. W. S. Huang, A. G. McDiarmid, and A. J. Epstein, *J. Chem. Soc., Chem. Commun.* 1784 (1987).
1023. S. P. Armes and J. F. Miller, *Synth. Met.* 22, 385 (1988).
1024. G. E. Asturias, A. G. McDiarmid, and A. J. Epstein, *Synth. Met.* 29, E157 (1989).
1025. Y. Cao, A. Andreatta, A. J. Heeger, and P. Smith, *Polymer* 30, 2305 (1989).
1026. A. G. McDiarmid, J. C. Chiang, M. Halpern, W. S. Huang, S. L. Mu, N. L. Somasiri, W. Wu, and S. I. Yaniger, *Mol. Cryst. Liq. Cryst.* 121, 173 (1985).
1027. P. H. Gebert, C. D. Batich, D. B. Tanner, and S. L. Herr, *Synth. Met.* 29, E371 (1989).
1028. L. H. C. Mattoso, R. M. Faria, L. O. S. Bulhoes, and A. G. McDiarmid, *J. Polym. Sci., Part A: Polym. Chem.* 32, 2147 (1994).
1029. L. H. C. Mattoso, S. K. Manokar, A. G. McDiarmid, and A. J. Epstein, *J. Polym. Sci., Part A: Polym. Chem.* 33, 1227 (1995).
1030. N. Toshima, H. Yan, Y. Gotoh, and M. Ishiwatari, *Chem. Lett.* 2229 (1994).
1031. H. S. O. Chan, S. C. Ng, W. S. Sim, K. L. Tan, and B. T. G. Tan, *Macromolecules* 25, 6029 (1992).
1032. A. F. Diaz and J. A. Logan, *J. Electroanal. Chem.* 111, 111 (1980).
1033. E. M. Geniès, A. A. Syed, and C. Tsintavis, *Mol. Cryst. Liq. Cryst.* 121, 181 (1985).
1034. R. Noufi, A. J. Nozik, J. White, and L. Watten, *J. Electrochem. Soc.* 129, 2261 (1982).
1035. K. Bade, V. Tsakova, and J. W. Schultze, *Electrochim. Acta* 37, 2255 (1992).
1036. J. Tang and R. A. Osteryoung, *Synth. Met.* 44, 307 (1991).
1037. J. Tang, R. D. Allendoerfer, and R. A. Osteryoung, *J. Chem. Phys.* 96, 3531 (1992).
1038. V. V. Walatka, M. M. Labes, and J. H. Perlstein, *Phys. Rev. Lett.* 31, 1139 (1973).
1039. C. M. Mikulski, P. J. Russo, M. S. Saran, A. G. MacDiarmid, A. F. Garito, and A. J. Heeger, *J. Am. Chem. Soc.* 97, 6358 (1975).
1040. M. J. Cohen, A. F. Garito, A. J. Heeger, A. G. MacDiarmid, C. M. Mikulski, M. S. Saran, and J. Kleppinger, *J. Am. Chem. Soc.* 98, 3844 (1976).
1041. J. L. Brédas and G. B. Street, *Acc. Chem. Res.* 18, 309 (1985).
1042. S. L. Altmann, "Band Theory of Solids: An Introduction from the Point of View of Symmetry." Clarendon, Oxford, 1991.
1043. S. L. Altmann, "Ions and Symmetries." Clarendon, Oxford, 1992.
1044. B. J. Duke and B. O'Leary, *J. Chem. Educ.* 65, 319 (1988).
1045. B. J. Duke and B. O'Leary, *J. Chem. Educ.* 65, 379 (1988).
1046. B. J. Duke and B. O'Leary, *J. Chem. Educ.* 65, 513 (1988).
1047. R. Hoffmann, *Angew. Chem.* 26, 846 (1987).
1048. G. Aissing, H. J. Monkhorst and C. Hu, *Int. J. Quantum Chem.: Quantum Chem. Symp.* 27, 245 (1993).
1049. A. J. Heeger, S. Kivelson, J. R. Schrieffer, and W. P. Su, *Rev. Mod. Phys.* 60, 781 (1988).
1050. I. N. Levine, "Quantum Chemistry." Allyn & Bacon, Boston, 1983.
1051. J. L. Brédas, A. J. Heeger, and F. Wudl, *J. Chem. Phys.* 85, 4673 (1986).

1052. J. L. Brédas, R. R. Chance, R. H. Baughman, and R. Silbey, *J. Chem. Phys.* 76, 3673 (1982).
1053. J. L. Brédas, *Synth. Met.* 17, 115 (1987).
1054. M. Kobayashi, N. Colaneri, M. Boysel, F. Wudl, and A. J. Heeger, *J. Chem. Phys.* 82, 5717 (1985).
1055. F. Wudl, M. Kobayashi, N. Colaneri, M. Boysel, and A. J. Heeger, *Mol. Cryst. Liq. Cryst.* 118, 199 (1985).
1056. J. Poplawski, E. Ehrenfreund, H. Schaffer, F. Wudl, and A. J. Heeger, *Synth. Met.* 28, 539 (1989).
1057. I. Hoogmartens, P. Adriaensens, D. Vanderzande, J. Gelan, C. Quatrochi, R. Lazzaroni, and J. L. Brédas, *Macromolecules* 25, 7347 (1992).
1058. Y. S. Lee and M. Kertesz, *Int. J. Quantum Chem.: Quantum Chem. Symp.* 21, 163 (1987).
1059. K. Nayak and D. S. Marynick, *Macromolecules* 23, 2237 (1990).
1060. A. Karpfen and M. Kertesz, *J. Phys. Chem.* 95, 7680 (1991).
1061. Y. S. Lee and M. Kertesz, *J. Chem. Phys.* 88, 2609 (1988).
1062. Y. S. Lee, M. Kertesz, and R. L. Elsenbaumer, *Chem. Mater.* 2, 526 (1990).
1063. R. Lazzaroni, J. Riga, J. Verbist, J. L. Brédas, and F. Wudl, *J. Chem. Phys.* 88, 4257 (1988).
1064. W. Wallnöfer, E. Faulques, and H. Kuzmany, *Synth. Met.* 28, 533 (1989).
1065. W. Wallnöfer, H. Kuzmany, and E. Faulques, in "Electronic Properties of Conjugated Polymers III" (H. Kuzmany, M. Mehring, and S. Roth, Eds.) Vol. 91, pp. 119–122. Springer-Verlag, Berlin/Heidelberg, 1989.
1066. I. Hoogmartens, D. Vanderzande, H. Martens, and J. Gelan, *Synth. Met.* 41–43, 513 (1991).
1067. I. Hoogmartens, P. Adriaensens, D. Vanderzande, and J. Gelan, *Anal. Chim. Acta* 283, 1025 (1993).
1068. R. Kiebooms, I. Hoogmartens, P. Adriaensens, D. Vanderzande, and J. Gelan, *Synth. Met.* 52, 395 (1992).
1069. R. Kiebooms, D. Vanderzande, and J. Gelan, *Synth. Met.* 69, 555 (1995).
1070. R. Kiebooms, I. Hoogmartens, P. Adriaensens, D. Vanderzande, and J. Gelan, *Macromolecules* 28, 4961 (1995).
1071. G. Zerbi, M. C. Magnoni, I. Hoogmartens, R. Kiebooms, R. Carleer, D. Vanderzande, and J. Gelan, *Adv. Mater.* 7, 1027 (1995).
1072. S. A. Jenekhe, *Macromolecules* 19, 2663 (1986).
1073. B. A. Hess and L. J. Schaad, *J. Am. Chem. Soc.* 93, 305 (1971).
1074. B. A. Hess and L. J. Schaad, *J. Am. Chem. Soc.* 93, 2413 (1971).
1075. B. A. Hess, L. J. Schaad, and C. W. Holyoke, *Tetrahedron* 28, 3657 (1972).
1076. B. A. Hess, L. J. Schaad, and C. W. Holyoke, *Tetrahedron* 28, 5299 (1972).
1077. B. A. Hess and L. J. Schaad, *J. Am. Chem. Soc.* 95, 3907 (1973).
1078. B. A. Hess, L. J. Schaad, and C. W. Holyoke, *Tetrahedron* 31, 295 (1975).
1079. B. A. Hess and L. J. Schaad, *Pure Appl. Chem.* 52, 1471 (1980).
1080. L. J. Schaad and B. A. Hess, *J. Am. Chem. Soc.* 94, 3068 (1972).
1081. L. J. Schaad and B. A. Hess, *J. Chem. Educ.* 51, 640 (1974).
1082. M. J. S. Dewar and C. de Llano, *J. Am. Chem. Soc.* 91, 789 (1969).
1083. M. G. Kanatzidis, S. Glenis, M. Benz, E. LeGoff, J. L. Schindler, and C. R. Kannewurf, *Polym. Prepr.* 35, 303 (1994).
1084. S. Glenis, M. Benz, E. LeGoff, J. L. Schindler, C. R. Kannewurf, and M. G. Kanatzidis, *J. Am. Chem. Soc.* 115, 12519 (1993).
1085. J. W. Mintmire, C. T. White, and M. L. Elert, *Synth. Met.* 16, 235 (1986).
1086. D. Vanderzande, Personal Communication, 1989.
1087. A. Wissner, *Tetrahedron Comput. Methodol.* 3, 63 (1990).
1088. A. Streitwieser, "Molecular Orbital Theory for Organic Chemists." Wiley, New York, 1961.
1089. C. A. Coulson, B. O. Larny, and R. B. Mallion, "Hückel Theory for Organic Chemists." Academic Press, New York, 1978.
1090. F. A. Van-Catledge, *J. Org. Chem.* 45, 4801 (1980).
1091. P. Otto and J. Ladik, *Synth. Met.* 36, 327 (1990).
1092. J. L. Brédas, B. Thémans, J. M. André, A. J. Heeger, and F. Wudl, *Synth. Met.* 11, 343 (1985).
1093. S. Y. Hong and D. S. Marynick, *Macromolecules* 25, 4652 (1992).
1094. A. K. Bakhshi, C. M. Liegener, and J. Ladik, *Synth. Met.* 30, 79 (1989).
1095. J. Kürti, P. R. Surjan, and M. Kertesz, *J. Am. Chem. Soc.* 113, 9865 (1991).
1096. J. Kürti and P. R. Surján, *Synth. Met.* 49–50, 537 (1992).
1097. J. L. Brédas and A. J. Heeger, *Chem. Phys. Lett.* 217, 507 (1994).
1098. J. L. Brédas, G. B. Street, B. Thémans, and J. M. André, *J. Chem. Phys.* 83, 1323 (1985).
1099. I. C. Lagerstedt and O. Wennerström, *Synth. Met.* 20, 269 (1987).
1100. C. X. Cui and M. Kertesz, *Am. Phys. Soc.* 40, 9661 (1989).
1101. R. Kiebooms, P. Adriaensens, D. Vanderzande, J. Gelan, M. J. Swann, D. Bloor, C. J. Drury, and G. M. Brooke, *Synth. Met.* 84, 189 (1997).
1102. M. Sato, T. Shimizu, and A. Yamauchi, *Macromol. Chem.* 191, 313 (1990).
1103. M. Sato, T. Shimizu, and A. Yamauchi, *Synth. Met.* 41, 551 (1991).
1104. R. D. McCullough, and S. P. Williams, *J. Am. Chem. Soc.* 115, 11608 (1993).
1105. F. Jonas and L. Schrader, *Synth. Met.* 41, 831 (1991).
1106. G. Heywang and F. Jonas, *Adv. Mater.* 4, 116 (1992).
1107. F. Jonas and G. Heywang, *Electrochim. Acta* 39, 1345 (1994).
1108. F. Jonas, W. Krafft, and B. Muys, *Macromol. Symp.* 100, 169 (1995).
1109. A. Aleshin, R. Kiebooms, R. Menon, F. Wudl, and A. J. Heeger, *Phys. Rev. B* 56, 3659 (1997).
1110. J. Roncali and C. Thobie-Gautier, *Adv. Mater.* 6, 846 (1994).
1111. A. Graja, "Low-Dimensional Organic Conductors." World Scientific, Singapore, 1992.
1112. H. Ehrenreich and F. Spaepan, Eds., "Solid State Properties of Fullerene." Academic Press, Boston, 1994.
1113. K. Kaneto, K. Yoshino, and Y. Inushi, in "Electronic Properties of Inorganic Quasi-One-Dimensional Materials" (P. Monceau, Ed.), Vol. 2. Reidel, Dordrecht, 1985.
1114. H. G. Kiess, Ed., "Conjugated Conducting Polymers." Springer Series in Solid State Sciences, Vol. 102, Springer-Verlag, Berlin, 1992.
1115. S. Roth and H. Bleier, *Adv. Phys.* 36, 385 (1987).
1116. N. Basescu, Z. -N. X. Liu, D. Moses, A. J. Heeger, H. Naarmann, and N. Theophilou, *Nature* 327, 403 (1987).
1117. T. Ohnishi, T. Noguchi, T. Nakano, M. Hirooka, and I. Murase, *Synth. Met.* 41–43, 309 (1991).
1118. T. Hagiwara, M. Hirasaka, K. Sato, and M. Yamaura, *Synth. Met.* 36, 241 (1990).
1119. M. Reghu, Y. Cao, D. Moses, and A. J. Heeger, *Phys. Rev. B* 47, 1758 (1993).
1120. M. Reghu, C. O. Yoon, Y. Cao, D. Moses, and A. J. Heeger, *Phys. Rev. B* 48, 17685 (1993).
1121. N. S. Sariciftci, Ed., "Primary Photoexcitations in Conjugated Polymers." World Scientific, Singapore, 1997.
1122. Y. W. Park, E. S. Choi, and D. S. Suh, *Synth. Met.* 96, 81 (1998).
1123. S. Stafstrom, *Phys. Rev. B* 51, 4137 (1995).
1124. P. W. Anderson, *Phys. Rev.* 109, 1492 (1958).
1125. N. F. Mott, "Metal-Insulator Transition" 2nd ed. Taylor & Francis, London, 1990.
1126. P. A. Lee and T. V. Ramakrishnan, *Rev. Mod. Phys.* 57, 287 (1985).
1127. M. Ahlskog and R. Menon, *J. Phys.: Condens. Matter* 10, 7171 (1998).
1128. L. Pietronero, *Synth. Met.* 8, 225 (1983).
1129. S. Kivelson and A. J. Heeger, *Synth. Met.* 22, 371 (1989).
1130. A. G. Zbrodskii and K. N. Zeninova, *Zh. Eksp. Teor. Fiz.* 86, 727 (1984) [*Sov. Phys. JETP* 59, 425 (1984)].
1131. M. Ahlskog, M. Reghu, and A. J. Heeger, *J. Phys.: Condens. Matter* 9, 4145 (1997).
1132. P. Dai, Y. Zhang, and M. P. Sarachik, *Phys. Rev. B* 46, 6724 (1992).
1133. M. Reghu, K. Vakiparta, Y. Cao, and D. Moses, *Phys. Rev. B* 49, 16162 (1994).

1134. M. Ahlskog, M. Reghu, A. J. Heeger, T. Noguchi, and T. Ohnishi, *Phys. Rev. B* 53, 15529 (1996).
1135. M. Ahlskog, M. Reghu, A. J. Heeger, T. Noguchi, and T. Ohnishi, *Phys. Rev. B* 55, 6777 (1997).
1136. C. O. Yoon, M. Reghu, D. Moses, and A. J. Heeger, *Phys. Rev. B* 49, 10851 (1994).
1137. J. C. Clark, G. G. Ihas, A. J. Rafanello, M. W. Meisel, M. Reghu, C. O. Yoon, Y. Cao, and A. J. Heeger, *Synth. Met.* 69, 215 (1995).
1138. (a) P. N. Adams, P. Devasagayam, S. J. Pomfret, L. Abell, and A. P. Monkman, *J. Phys. Condens. Matter* 10, 8293 (1998); (b) E. R. Holland, S. J. Pomfret, P. N. Adams, and A. P. Monkman, *J. Phys. Condens. Matter* 8, 2991 (1996).
1139. S. J. Pomfret, P. N. Adams, N. P. Comfort, and A. P. Monkman, *Adv. Mater.* 10, 1351 (1998).
1140. A. Aleshin, R. Kiebooms, R. Menon, and A. J. Heeger, *Synth. Met.* 90, 61 (1997).
1141. (a) T. Fukuhara, S. Masubuchi, and S. Kazama, *Synth. Met.* 92, 229 (1998); (b) S. Masubuchi, T. Fukuhara, and S. Kazama, *Synth. Met.* 84, 601 (1997).
1142. Y. Nogami, H. Kaneko, H. Ito, T. Ishiguro, T. Sasaki, N. Toyota, A. Takahashi, and J. Tsukamoto, *Phys. Rev. B* 43, 11829 (1991).
1143. A. B. Kaiser, *Phys. Rev. B* 40, 2806 (1989).
1144. C. O. Yoon, M. Reghu, D. Moses, A. J. Heeger, and Y. Cao, *Phys. Rev. B* 48, 14080 (1993).
1145. S. Bogdanovich, P. Dai, M. P. Sarachik, and V. Dobrosavljevic, *Phys. Rev. Lett.* 74, 2543 (1995).
1146. N. S. Sariciftci, A. J. Heeger, and Y. Cao, *Phys. Rev. B* 49, 5988 (1994).
1147. K. Mizoguchi and S. Kuroda, in "Handbook of Organic Conductive Molecules and Polymers" (H. S. Nalwa, Ed.), Vol. 3, Wiley, New York, 1997.
1148. D. Moses, A. Denenstein, A. Pron, A. J. Heeger, and A. G. MacDiarmid, *Solid State Commun.* 36, 219 (1980).
1149. L. Piraux, E. Ducarme, J. P. Issi, D. Begin, and D. Billaud, *Synth. Met.* 41-43, 129 (1991).
1150. T. H. Gilani and T. Ishiguro, *J. Phys. Soc. Jpn.* 66, 727 (1997).
1151. M. Reghu, C. O. Yoon, D. Moses, Y. Cao, and A. J. Heeger, *Synth. Met.* 69, 329 (1995).
1152. C. O. Yoon, M. Reghu, D. Moses, A. J. Heeger, Y. Cao, T. A. Chen, X. Wu, and R. D. Reike, *Synth. Met.* 75, 229 (1995).
1153. Y. Lu, "Solitons and Polarons in Conducting Polymers." World Scientific, Singapore, 1988.
1154. J. Chen, T.-C. Chung, F. Moraes, and A. J. Heeger, *Solid State Commun.* 53, 757 (1985); F. Moraes, J. Chen, T.-C. Chung, and A. J. Heeger, *Synth. Met.* 11, 271 (1985).
1155. X. Q. Yang, D. B. Tanner, M. J. Rice, H. W. Gibson, A. Feldblum, and A. J. Epstein, *Solid State Commun.* 62, 335 (1987); Y. H. Kim and A. J. Heeger, *Phys. Rev. B* 40, 8393 (1989).
1156. N. F. Mott and E. Davis, "Electronic Processes in Non-Crystalline Materials." Clarendon, Oxford, 1979.
1157. N. F. Mott and M. Kaveh, *Adv. Phys.* 34, 329 (1985).
1158. K. Sato, M. Yamaura, T. Hagiwara, K. Murata, and M. Tokumoto, *Synth. Met.* 40, 35 (1991).
1159. R. Kiebooms, A. Aleshin, K. Hutchison, and F. Wudl, *J. Phys. Chem.* 101, 11037 (1997).
1160. K. Lee, A. J. Heeger, and Y. Cao, *Phys. Rev. B* 48, 14884 (1993).
1161. K. Lee, A. J. Heeger, and Y. Cao, *Synth. Met.* 72, 25 (1995).
1162. K. Lee, R. Menon, C. O. Yoon, and A. J. Heeger, *Phys. Rev. B* 52, 4779 (1995).
1163. K. Lee, M. Reghu, E. L. Yuh, N. S. Sariciftci, and A. J. Heeger, *Synth. Met.* 68, 287 (1995).
1164. K. Lee, E. K. Miller, A. N. Aleshin, R. Menon, A. J. Heeger, J. H. Kim, C. O. Yoon, and H. Lee, *Adv. Mater.* 10, 456 (1998).
1165. Y. Chang, K. Lee, R. Kiebooms, A. Aleshin, and A. J. Heeger, *Synth. Met.* 105, 203 (1999).
1166. K. Lee, R. Menon, A. J. Heeger, K. H. Kim, Y. H. Kim, A. Schwartz, M. Dressel, and G. Grüner, *Phys. Rev. B*, in press.
1167. W. P. Su, J. R. Schrieffer, and A. J. Heeger, *Phys. Rev. Lett.* 42, 1698 (1979).
1168. K. Pakbaz, C. H. Lee, A. J. Heeger, T. W. Hagler, and D. McBranch, *Synth. Met.* 64, 295 (1994).
1169. R. H. Friend, R. W. Gymer, A. B. Holmes, J. H. Burroughes, R. N. Marks, C. Taliani, D. D. C. Bradley, D. A. Dos Santos, J. L. Brédas, M. Lögdlund, and W. R. Salaneck, *Nature* 397, 121 (1999).
1170. N. S. Sariciftci, L. Smilowitz, A. J. Heeger, and F. Wudl, *Science* 258, 1474 (1992).
1171. F. Wooten, "Optical Properties of Solids." Academic Press, New York, 1972.
1172. F. Abeles, Ed., "Optical Properties of Solids." North-Holland, London, 1972.
1173. N. W. Ashcroft and N. D. Mermin, "Solid State Physics." Holt, Rinehart & Winston, New York, 1976.
1174. P. Drude, *Ann. Phys.* 1, 566 (1900); P. Drude, *Ann. Phys.* 3, 369 (1900).
1175. H. A. Lorentz, "The Theory of Electron." Dover, New York, 1952.
1176. R. Kubo, *Can. J. Phys.* 34, 1274 (1956); D. A. Greenwood, *Proc. Phys. Soc.* 71, 585 (1958).
1177. N. F. Mott, *Philos. Mag.* 22, 7 (1970).
1178. M. Ortuno and M. Kaveh, *J. Phys. C: Solid State Phys.* 17, L487 (1984).
1179. G. Leising, *Phys. Rev. B* 38, 10313 (1988).
1180. K. Kamiya and J. Tanaka, *Synth. Met.* 25, 59 (1988).
1181. W. R. Salaneck, I. Lundström, W.-S. Huang, and A. G. MacDiarmid, *Synth. Met.* 13, 291 (1986).
1182. Y. Cao, P. Smith, and A. J. Heeger, in "Conjugated Polymeric Materials: Opportunities in Electronics, Optoelectrics and Molecular Electronics," NATO Advanced Study Institute, Series E: Applied Sciences (J. L. Brédas and R. R. Chance, Eds.), Vol. 82. Kluwer Academic, Dordrecht, 1990.
1183. A. G. MacDiarmid and A. J. Epstein, in "Science and Applications of Conducting Polymers" (W. R. Salaneck, D. T. Clark, and E. J. Samuelson, Eds.). Hilger, Bristol, 1991.
1184. F. Wudl, R. O. Angus, F. L. Lu, D. M. Allemand, D. J. Vachon, M. Nowak, Z. X. Liu, and A. J. Heeger, *J. Am. Chem. Soc.* 109, 3677 (1987).
1185. S. Stafström, J. L. Brédas, A. J. Epstein, H. S. Woo, D. B. Tanner, W. S. Huang, and A. G. MacDiarmid, *Phys. Rev. Lett.* 59, 1464 (1987); D. S. Boudreaux, R. R. Chance, J. F. Wolf, L. W. Shacklette, J. L. Brédas, B. Thémans, J. M. André, and R. S. Silbey, *J. Chem. Phys.* 85, 4584 (1986).
1186. H. B. Wang, E. M. Scherr, A. G. MacDiarmid, and A. J. Epstein, *Phys. Rev. B* 45, 4190 (1992).
1187. P. Sheng, B. Abeles, and Y. Arie, *Phys. Rev. Lett.* 31, 44 (1973).
1188. A. L. Efros and B. I. Shklovskii, *J. Phys. C: Solid State Phys.* 8, L49 (1975).
1189. Y. Cao, G. M. Treacy, P. Smith, and A. J. Heeger, *Appl. Phys. Lett.* 60, 1 (1992).
1190. C. Kittel, "Introduction to Solid State Physics." Wiley, New York, 1976.
1191. H. Ehrenreich and H. R. Philipp, *Phys. Rev.* 128, 1622 (1962).
1192. C. Fite, Y. Cao, and A. J. Heeger, *Solid State Commun.* 73, 607 (1990).
1193. Y. Cao and A. J. Heeger, *Synth. Met.* 52, 193 (1992).
1194. T. Ishiguro, H. Kaneko, Y. Nogami, H. Ishimoto, H. Nishiyama, M. Yamaura, T. Hagiwara, and K. Sato, *Phys. Rev. Lett.* 69, 660 (1992).
1195. M. Dietrich, J. Heinze, G. Heywang, and F. Jonas, *J. Electroanal. Chem.* 369, 87 (1994).
1196. Q. Pei, G. Zuccarello, M. Ahlskog, and O. Inganäs, *Polymer* 35, 1347 (1994).
1197. Y. Cao, G. Yu, C. Zhang, R. Menon, and A. J. Heeger, *Synth. Met.* 87, 171 (1997).
1198. M. Granström and O. Inganäs, *Adv. Mater.* 7, 1022 (1995).
1199. M. Granström, M. Berggren, and O. Inganäs, *Science* 267, 1479 (1995).

1200. E. Abrahams, P. W. Anderson, D. C. Liccardello, and T. V. Ramakrishnan, *Phys. Rev. Lett.* 42, 673 (1979).
1201. T. G. Castner, in "Hopping Transport in Solids" (M. Pollak and B. I. Shklovskii, Eds.). Elsevier/North-Holland, Amsterdam, 1990.
1202. T. G. Castner and R. J. Deli, in "Disordered Semiconductors." Plenum, New York, 1987.
1203. E. M. Gershenzon, A. P. Mel'nikov, and R. I. Rabinovich, in "Electron-Electron Interactions in Disordered Systems." North-Holland, Amsterdam, 1985.
1204. A. J. Epstein, J. M. Ginder, F. Zuo, R. W. Bigelow, H. S. Woo, D. B. Tanner, A. F. Richter, W. S. Huang, and A. G. MacDiarmid, *Synth. Met.* 18, 303 (1987); J. M. Ginder, A. F. Richter, A. G. MacDiarmid, and A. J. Epstein, *Solid State Commun.* 63, 97(1987).
1205. A. J. Epstein, R. P. McCall, J. M. Ginder, and A. G. MacDiarmid, in "Spectroscopy of Advanced Material" (R. J. H. Clark and R. E. Hester, Eds.). Wiley, New York, 1991.
1206. J. Voit, *Phys. Rev. Lett.* 64, 323 (1990).
1207. S. A. Kivelson and V. J. Emery, *Synth. Met.* 65, 249 (1994).
1208. A. J. Heeger, in "Highly Conducting One-Dimensional Solids" (J. T. Devereese, R. P. Evrard, and V. E. van Doren, Eds.). Plenum, New York, 1979.
1209. G. Grüner, "Density Waves in Solids." Addison-Wesley, Reading, MA, 1994.
1210. D. Jerome and H. J. Schulz, *Adv. Phys.* 31, 299 (1982).
1211. P. A. Lee, T. M. Rice, and P. W. Anderson, *Solid State Commun.* 14, 703 (1974).
1212. L. Degiorgi, M. Dressel, A. Schwartz, B. Alavi, and G. Grüner, *Phys. Rev. Lett.* 76, 3838 (1996).
1213. V. Vescoli, L. Degiorgi, W. Henderson, G. Grüner, K. P. Starkey, and L. K. Montgomery, *Science* 281, 1181 (1998).
1214. B. Horovitz, *Solid State Commun.* 41, 729 (1982); E. Ehrenfreund, E. Vardeny, O. Brafman, and B. Horovitz, *Phys. Rev. B* 36, 1535 (1987).
1215. E. M. Conwell, H. A. Mizes, and S. Jeyadev, *Phys. Rev. B* 40, 1630 (1989).
1216. E. M. Conwell and H. A. Mizes, *Phys. Rev. B* 44, 937 (1991).
1217. S. Kivelson and A. J. Heeger, *Phys. Rev. Lett.* 55, 308 (1985).
1218. H. Y. Choi and E. J. Mele, *Phys. Rev. B* 34, 8750 (1986).
1219. S. Stafström and J. L. Brédas, *Phys. Rev. B* 38, 4180 (1988).
1220. G. B. Blachet, C. R. Fincher, T. C. Chung, and A. J. Heeger, *Phys. Rev. Lett.* 50, 1938 (1983).
1221. Z. Vardeny, E. Ehrenfreund, and O. Brafman, *Phys. Rev. Lett.* 56, 691 (1986).
1222. Y. H. Kim, S. Hotta, and A. J. Heeger, *Phys. Rev. B* 36, 7486 (1987).
1223. M. Wohlgenannt, W. Graupner, G. Leising, and Z. V. Vardeny, *Phys. Rev. B* 60, 5321 (1999).
1224. A. Dogariu, D. Vacar, and A. J. Heeger, *Phys. Rev. B* 58, 10218 (1998).
1225. A. Dogariu, D. Vacar, A. J. Heeger, and H. Wang, *Synth. Met.* 100, 95 (1999).
1226. V. I. Klimov, D. W. McBranch, N. Barashkov, and J. Ferraris, *Phys. Rev. B* 58, 7654 (1998).
1227. B. Kraabel and M. Joffe, *Phys. Rev. B* 58, 15777 (1998).
1228. T. Nguyen, V. Doan, and B. J. Schwartz, *J. Chem. Phys.* 110, 4068 (1999).
1229. C. H. Lee, G. Yu, and A. J. Heeger, *Phys. Rev. B* 47, 15543 (1993).
1230. C. H. Lee, G. Yu, D. Moses, and A. J. Heeger, *Phys. Rev. B* 49, 2396 (1994).
1231. C. H. Lee, G. Yu, N. S. Sariciftci, A. J. Heeger, and C. Zhang, *Synth. Met.* 75, 127 (1995).
1232. K. S. Wong, D. D. C. Bradley, W. Hayes, J. E. Ryan, R. H. Friend, H. Lindenberger, and S. Roth, *J. Phys. C: Solid State Phys.* 20, L187 (1987).
1233. M. Furukawa, K. Mizuno, A. Matsui, S. D. D. V. Rughooputh, and W. C. Walker, *J. Phys. Soc. Jpn.* 58, 2976 (1989).
1234. R. Kersting, U. Lemmer, R. F. Mahrt, K. Leo, H. Kurz, H. Bässler, and E. O. Göbel, *Phys. Rev. Lett.* 70, 3820 (1993).
1235. I. H. Campbell, T. W. Hagler, D. L. Smith, and J. P. Ferraris, *Phys. Rev. Lett.* 76, 1900 (1996).
1236. M. Chandross and S. Mazumdar, *Phys. Rev. B* 55, 1497 (1997).
1237. M. Yan, L. J. Rothberg, F. Papadimitralopoulos, M. E. Gavin, and T. M. Miller, *Phys. Rev. Lett.* 72, 1104 (1994).
1238. M. Yan, L. J. Rothberg, E. W. Kwock, and T. M. Miller, *Phys. Rev. Lett.* 75, 1992 (1995).
1239. L. J. Rothberg, M. Yan, F. Papadimitrakopoulos, M. E. Galvin, E. W. Kwock, and T. M. Miller, *Synth. Met.* 80, 41 (1996).
1240. N. T. Harrison, G. R. Hayes, R. T. Phillips, and R. H. Friend, *Phys. Rev. Lett.* 77, 1881 (1996).
1241. E. S. Maniloff, V. I. Klimov, and D. W. McBranch, *Phys. Rev. B* 56, 1876 (1997).
1242. R. G. Kepler, V. S. Valencia, S. J. Jacobs, and J. J. McNamara, *Synth. Met.* 78, 227 (1996).
1243. N. Tessler, G. J. Denton, N. T. Harrison, M. A. Stevens, S. E. Burns, and R. H. Friend, *Synth. Met.* 91, 61 (1997).
1244. V. I. Klimov, D. W. McBranch, N. N. Barashkov, and J. P. Ferraris, *Chem. Phys. Lett.* 277, 109 (1997).
1245. G. Kranzelbinder, M. Nisoli, S. Stagira, S. D. Silverstri, G. Lanzani, K. Müllen, U. Scherf, W. Graupner, and G. Leising, *Appl. Phys. Lett.* 71, 2725 (1997).
1246. F. Hide, M. A. Diaz-Garcia, B. J. Schwarz, M. R. Andersson, Q. Pei, and A. J. Heeger, *Science* 273, 1833 (1996).
1247. N. Tessler, G. J. Denton, and R. H. Friend, *Nature* 382, 695 (1996).
1248. D. D. C. Bradley, *Synth. Met.* 54, 401 (1993).
1249. C. W. Tang and S. A. Slyke, *Appl. Phys. Lett.* 51, 913 (1987).
1250. C. Adachi, T. Tsutsui, and S. Saito, *Appl. Phys. Lett.* 55, 1489 (1989).
1251. D. Braun and A. J. Heeger, *Appl. Phys. Lett.* 58, 1982 (1993).
1252. I. D. Parker, *J. Appl. Phys.* 75, 1656 (1994).
1253. M. Nomura, S. Yamamura, H. Matsumoto, H. Nakada, R. Murayama, T. Wakimoto, Y. Yonemoto, J. Funaki, and M. Tsuchida, *Synth. Met.* 91, 15 (1997).
1254. J. R. Sheats, H. Antoniadis, M. Hueschen, W. Leonard, J. Miller, R. Moon, D. Roitman, and A. Stocking, *Science* 273, 884 (1996).
1255. T. R. Heibner, C. C. Wu, D. Marcy, and M. H. Lu, *Appl. Phys. Lett.* 72, 519 (1998).
1256. J. Bharathan and Y. Yang, *Appl. Phys. Lett.* 72, 2660 (1998).
1257. M. M. Allemand, A. Koch, F. Wudl, Y. Rubin, F. Diederich, M. M. Alvarez, S. J. Anz, and R. L. Whettestea, *J. Am. Chem. Soc.* 113, 1050 (1991).
1258. K. Lee, R. A. Janssen, N. S. Sariciftci, and A. J. Heeger, *Phys. Rev. B* 49, 5781 (1994).
1259. B. Kraabel, C. H. Lee, D. McBranch, D. Moses, N. S. Sariciftci, and A. J. Heeger, *Chem. Phys. Lett.* 213, 389 (1993).
1260. N. S. Sariciftci, L. Smilowitz, R. Wu, C. Gettinger, A. J. Heeger, and F. Wudl, *Phys. Rev. B* 47, 13835 (1993).
1261. C. H. Lee, G. Yu, D. Moses, K. Pakbaz, C. Zhang, N. S. Sariciftci, A. J. Heeger, and F. Wudl, *Phys. Rev. B* 48, 15425 (1993).
1262. N. S. Sariciftci, D. Braun, C. Zhang, V. Srdaov, A. J. Heeger, G. Stucky, and F. Wudl, *Appl. Phys. Lett.* 62, 585 (1993).
1263. G. Yu, J. Gao, J. C. Hummelen, F. Wudl, and A. J. Heeger, *Science* 270, 1789 (1995).
1264. M. Cha, N. S. Sariciftci, A. J. Heeger, J. C. Hummelen, and F. Wudl, *Appl. Phys. Lett.* 67, 3850 (1995).
1265. G. Yu, C. Zhang, and A. J. Heeger, *Appl. Phys. Lett.* 64, 1540 (1994).
1266. G. Yu, C. Pakbaz, and A. J. Heeger, *Appl. Phys. Lett.* 64, 3422 (1994).
1267. L. A. A. Pettersson, L. S. Roman, and O. Inganäs, *J. Appl. Phys.* 86, 487 (1999).
1268. M. Granström, K. Petritsch, A. C. Arias, A. Lux, M. R. Andersson, and R. H. Friend, *Nature* 395, 257 (1998).
1269. M. Onoda, K. Tada, A. A. Zakhidov, and K. Yoshino, *Thin Solid Films* 331, 76 (1998).

CONJUGATED POLYMER FILMS FOR MOLECULAR AND IONIC RECOGNITION

Bruno Fabre

Laboratoire d'Electrochimie Moléculaire et Macromoléculaire (Unité Mixte de Recherche no. 6510 associée au CNRS), Université de Rennes 1, Campus de Beaulieu, Rennes Cedex, France

Contents

1. Introduction	103
1.1. Background	103
1.2. Electrochemistry: A Powerful Tool for Recognition	104
1.3. Redox-Active Conjugated Polymer-Based Recognition	104
2. Molecular Recognition	105
2.1. Enzyme-Containing Polymers	105
2.2. Analytes of Biological and Pharmacological Interest	111
2.3. Gases and Vapors	112
2.4. Other Molecules	113
3. Cationic Recognition	114
3.1. Polyether-Functionalized Polymers	114
3.2. Calixarene-Functionalized Polymers	119
3.3. Polyrotaxanes	120
3.4. Polymers Containing Other Functional Groups	121
4. Anionic Recognition	122
5. Conclusions	124
References	124

1. INTRODUCTION

1.1. Background

The *recognition* principle is based on the modification of a measurable signal characteristic of a species (*receptor*), caused by the external interaction (*stimulus*) with another species (*analyte*) [1, 2]. As a matter of fact, changes in signal reflect changes in one or several properties (e.g., electrical, optical) of the receptor. If the signal recorded in the absence of the analyte is identical to that in its presence, the recognition does not take place. This reveals either that the interaction is not sufficiently strong to significantly change the signal or the considered signal is not able to *transduce* the interaction.

Another feature of the recognition is *selectivity*. The interaction has to be specific and the analyte has to be detected among other interfering species. Moreover, changes in signal must make it pos-

sible to quantify the analyte. So a correlation between the signal magnitude and the quantity of analyte, in terms of concentration or mass, is required over a large range. Generally, practical linear or logarithmic relationships are often obtained.

Two other criteria to be fulfilled by recognition are *rapidity* and *sensitivity*. A rapid transduction will allow measurements in real time which are essential for clinical or biological applications. A sensitive system will be able to respond to a low-level stimulus, i.e., a weak receptor-analyte interaction or a low concentration in analyte.

Finally, the development of a sensory device for long-term uses will be possible if the interaction does not irreversibly change the properties of the sensing element, i.e., the original signal is recovered after the recognition event. In the contrary case, the system can function only if a preferentially mild and fast method yields the original signal.

Clearly, there are few systems which are able to fulfill simultaneously all of the conditions described previously: selectivity, sensitivity, rapidity, and chemical reversibility. Consequently, a compromise must often be found, depending on the nature of the foreseen application. For example, the criterion of reversibility is not important for *in vivo* applications, which generally involve one-use sensory devices.

1.2. Electrochemistry: A Powerful Tool for Recognition

When the receptor is redox-active or is bound to a redox-active group, the electrochemical behavior of such a moiety can be affected by the presence of an ion or molecule with which it interacts [3]. In this case, different types of reactions can lead to recognition events: electrochemical catalysis, host-guest complexation, ion pairing, etc. (Table I), and the modified parameters are generally the rate of electron transfer and/or the formal potential of the electroactive system. Then the attachment of such functional groups to electrode surfaces to take advantage of their properties observed in solution is a prerequisite for the technological development of recognition devices. For this purpose, different routes have been used: immobilization in redox-active polymer films (electronically conducting and metallic centers containing polymers) and in electroinactive polymer-based membranes (Nafion and polysiloxane) and functionalization of organized architectures (self-assembled mono- and multilayers, dendrimers). Furthermore, since the electrochemical properties of those materials are usually tied to other characteristic properties, techniques other than electrochemistry can be also used to transduce the recognition event. For example, numerous reports have demonstrated that conformational changes resulting in the host-guest complexation between an alkali cation and a crown ether-functionalized conducting polymer led to a less conjugated and less electroactive polymer. So, binding could be evidenced from the shift of the cyclic voltammetry curve of the polymer toward more anodic potentials, the hypsochromic shift of the π - π^* transition band on its UV-visible spectrum, or the lowering of its electron conductivity.

A large number of application fields can be overlaid by this type of electroactive structure endowed with recognition properties: namely, (i) ionic and molecular detection (biological and chemical sensors, microsensors); (ii) extraction for recuperation and depollution (water and radioactive wastes, environmental protection); (iii) ionic and molecular transport for separation (artificial membranes); (iv) chemical and electrochemical syntheses, e.g., asymmetric synthesis (Fig. 1).

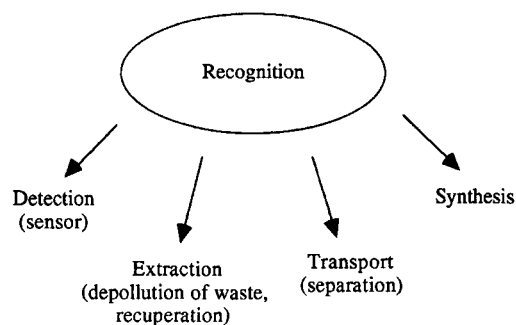


Fig. 1. Principal applications of electroactive film-based recognition.

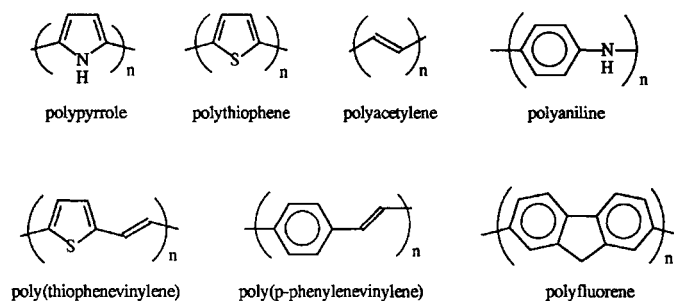


Fig. 2. Classical conjugated polymers.

1.3. Redox-Active Conjugated Polymer-Based Recognition

The electroconducting conjugated polymers (ECPs) are an exciting class of materials with unique electronic, electrochemical, and optical properties [4-7]. The common characteristic of ECPs is a delocalized electronic structure along the conjugated organic backbone which is composed of successive aromatic units (Fig. 2). One of the most interesting aspects of these polymers is that they can be reversibly converted upon electron transfer from an electronically insulating, neutral form to a conducting, oxidized form. This change of redox state is accompanied by the incorporation of electrolyte anion (doping anion) within the polymer structure, ensuring electroneutrality.

The synthesis of ECPs can be electrochemically or chemically achieved. The significance of the electrochemical method is that the polymer is obtained in one step as a film deposited on the electrode surface from the oxidation of the corresponding monomer in solution. The film thickness can be easily controlled from the electric charge consumed during the electropolymerization reaction. So, nanometric-thickness films can be electrodeposited on macroelectrodes but also on ultramicroelectrodes. Moreover, the electrochemical route allows the deposition of uniform films onto

Table I. Different Components of a Recognition Event Based on Electroactive Films

Stimuli	Consequences	Transduction signals
Catalysis	Decrease of the activation barrier	Electrochemistry (amperometry, potentiometry, cyclic voltammetry, impedancemetry)
Host-guest complexation	Conformational changes	Spectroscopy (absorbance, fluorescence)
Electrostatic interaction	Conductivity changes	
Permselectivity	Changes in electron work function	Conductivity
Adsorption	Changes in diffusion and/or migration rates	Gravimetry

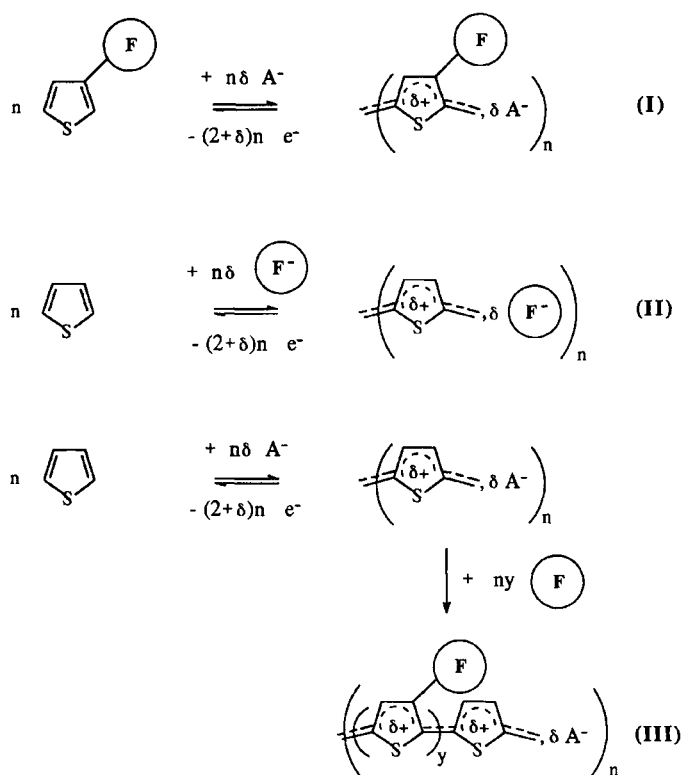


Fig. 3. Functionalization of polythiophene before (I), in the course of (II), and after (III) the electropolymerization step. δ is the doping level of the p-doped polymer (number of positive charges per monomer unit), and F is the functional group.

electrode surfaces of different geometries (sheet, disk, cylinder, drop, or felt).

Thus, the functionalization of ECPs by receptor centers is an approach suitable to the attachment of these specific moieties to electrode surfaces. It can be achieved in three principal ways: (i) before, (ii) in the course of, and (iii) after the electropolymerization step (Fig. 3). The prepolymerization approach consists of binding a covalently specific group to the starting monomer and subsequently oxidizing this assembly electrochemically to obtain the functionalized polymer. This is the most investigated method, and it is possible if the specific group is not degraded when oxidizing potentials are applied. The electrostatic incorporation of specific anions, such as heteropolyanions, in the course of the electrosynthesis of p-doped polymers constitutes the second approach. In this manner, the functionalization will be durable if the doping anion is irreversibly captured in the polymer matrix, but also if the electrostatic bindings between the anion and the positively charged polymer are strong. The first condition is generally fulfilled if the size of the anion is roughly more than 1 nm. Moreover, the environment offered by the polymer structure should not impair the specific properties of the anion. A typical example is the incorporation of biological molecules, such as enzymes. Finally the postpolymerization functionalization consists of modifying an ECP electrochemically after its electrosynthesis. This approach is applied when the electropolymerization of the starting monomer is not possible because of the oxidative degradation of the functional group or the impediment of the electropolymerization process caused by the electron-withdrawing effect or the steric bulkiness of the functional group.

So, from these three methods of functionalization, a large number of conjugated polymers possessing recognition units (redox catalysts, enzymes, host molecules) have been synthesized and characterized [8–17]. Among them, polypyrrole [8–10] and polythiophene [11–15] derivatives have been the most used polymer matrices. So, it seems likely that the interaction between the receptor immobilized within the polymer structure and the target analyte in solution may result in the modification of the electrochemical response of the material. As illustrated in the following, other characteristic properties can also be changed with the interaction.

2. MOLECULAR RECOGNITION

2.1. Enzyme-Containing Polymers

Redox enzyme-based molecular recognition has been the subject of considerable interest, principally because of the exceptional selectivity of this type of catalyst and the large number of commercially available enzymes, which allows the detection of numerous molecules of biological interest [18–21]. Three groups of redox enzymes in particular have been investigated:

- *Nicotinamide adenine dinucleotide (NAD⁺)-dependent dehydrogenases*. In these systems, NAD⁺, which is the termed cofactor (a small molecule essential for enzyme activity), is the redox center and is reducible to NADH.
- *Flavoproteins*. They contain one or more flavin redox groups which are tightly bound to the enzyme. Among them, the most studied system is glucose oxidase (GOD).
- *Cytochromes*. They contain one or more hemes (complex between an ferrous or ferric ion and a porphyrin) as prosthetic groups.

Different strategies have been developed to attach these enzymes to electrode surfaces:

- *Adsorption*. The interactions between the enzyme and the electrode material are van der Waals forces (e.g., adsorption to a conducting polymer) or ionic bonds (e.g., electrostatic complex between glucose oxidase and a polycationic redox polymer).
- *Covalent binding*. For example, GOD can be grafted onto a vitreous carbon electrode from the formation of amide bonds between $-\text{NH}_2$ groups of enzyme and $-\text{COOH}$ groups of the previously oxidized electrode.
- *Cross-linking*. Cross-linking can be made to occur within a polymer or redox polymer network.
- *Entrapment within a polymer film or gel*. Because of the negative surface charge of most enzymes at physiological pH, enzyme can be incorporated into a conducting polymer as a doping agent, provided that the electropolymerization conditions are appropriate.

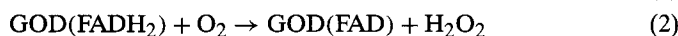
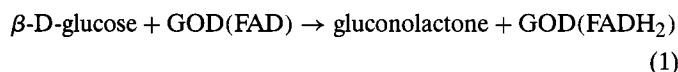
Among the different methods used to detect the catalysis of an analyte by the immobilized enzyme, the electrochemical method has been the most extensively investigated. The analyte can be detected either from the potential measurement between the modified electrode and a reference electrode (potentiometric method) or from the measurement of current crossing the modified electrode when a potential is applied (amperometric method). Based on kinetic considerations, amperometric biosensors are largely

preferred to potentiometric ones [18]. Nevertheless, the fundamental problem for the development of these enzyme electrodes is to establish the electrical contact between the redox center of the enzyme and the electrode. As the redox center is located sufficiently far from the outermost surface, the direct electron transfer to the electrode is not possible. Consequently, enzyme electrodes can efficiently function only if a redox mediator accepting and transferring electrons is included in the device [22]. The mediator is usually a small and low-molecular-mass molecule (O_2 , ferrocene, quinone) that is able to diffuse freely inside the reduced enzyme and to closely approach the active site to oxidize. It can be solubilized in the electrolyte or incorporated within the conducting polymer simultaneously with enzyme, either as doping anion or by binding it covalently to the starting monomer.

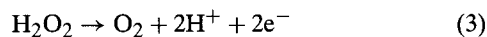
2.1.1. Glucose Oxidase

GOD is a glycoprotein containing two flavine adenine dinucleotide FAD molecules as redox centers. The great interest in this enzyme can be explained by (i) its chemical resistance to acid media and denaturing agents such as urea and sodium dodecylsulfate [23], (ii) its commercial availability at a low price, and (iii) the extent of applications of glucose sensors in clinical analysis (diabetics control) and the food and pharmaceutical industries (fermentation control).

In the cellular medium, GOD catalyzes the oxidation of glucose by O_2 to give gluconolactone and H_2O_2 as indicated below:



GOD(FAD) and GOD(FADH₂) represent the oxidized and reduced forms of the enzyme, respectively. As the two-electron oxidation of GOD(FADH₂) into GOD(FAD) is much too slow [24, 25], the use of a redox mediator is necessary to regenerate GOD(FAD) (Fig. 4). The physiological mediator for oxidases is O_2 . When it is involved, the enzyme regeneration is thus possible from the oxidation of H_2O_2 :



So, the glucose sensors using O_2 as a mediator are based on the measurement of oxidation current of H_2O_2 at potentials of ca. 0.6–0.7 V (vs. SCE). The principle of the glucose detection based on GOD-containing polymer films is schematized in Fig. 4. Provided that the detection potential is sufficiently high and steady-state conditions are used (e.g., rotating disk electrode or magnetic

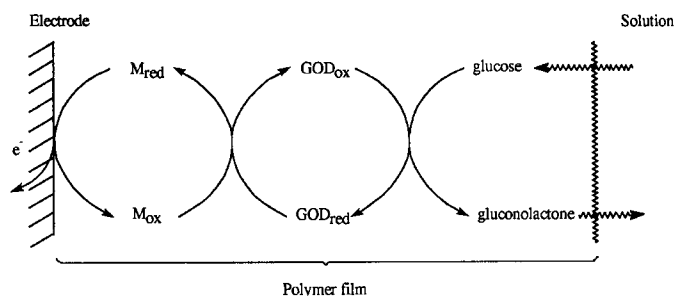


Fig. 4. Principle of an amperometric enzyme electrode for glucose based on a GOD-containing polymer in the presence of a redox mediator M.

stirring), the kinetics of the global process will be essentially controlled by the rate of the enzymatic reaction.

Among the different immobilization methods used, electrostatic entrapment within conjugated polymer films has been the most explored, with particular emphasis on polypyrrole (PPy) and derivatives which can be efficiently electroformed in aqueous media [26–48].

Reports have also focused on polyaniline [49–52], poly(phenylenediamine) [53–59] and other functionalized polyphenylenes [60, 61, 64], polythiophene [39, 62], and other less classical ECPs [63, 65]. Table II gathers the principal results obtained from these GOD-containing ECP films in the presence of glucose.

At the pH usually used for the immobilization procedure (pH 6–7), GOD is negatively charged (isoelectric point of 4.2) and therefore may be included within an oxidized polymer film. After its electrosynthesis, the GOD-entrapping film held at the oxidation potential of H_2O_2 showed a steady-state amperometric response dependent on the amount of glucose in solution. Generally the steady-state currents I_{ss} varied with the bulk concentration in glucose C_G according to the Michaelis–Menten kinetics (Eq. (4)) available in homogeneous phase:

$$I_{ss} = I_{max} \frac{C_G}{K'_m + C_G} \quad (4)$$

Characteristic parameters such as the apparent Michaelis–Menten constant K'_m and the maximum current under saturating substrate conditions I_{max} could be determined from linear Lineweaver–Burk- ($1/I_{ss}$ vs. $1/C_G$; Fig. 5), Eadie–Hofstee- (I_{ss} vs. I_{ss}/C_G), or Hanes- (C_G/I_{ss} vs. C_G) type plots. As an example, Fig. 5 shows the calibration curve for glucose and the corresponding Lineweaver–Burk plot obtained at pH 7 with a GOD-entrapping PPy film.

However, such parameters are very dependent on the experimental conditions, the structure of the polymer film, and the environment of the immobilized enzyme. Sometimes, values of K'_m agreed well with the K_m value of the soluble GOD, indicating that the enzymatic activity was unaffected after the immobilization step.

In addition to the popular entrapment method, the immobilization of GOD inside an ECP film could be also achieved by covalently binding the enzyme to the starting monomer or the polymer. This has been applied to N- [31, 42, 46] and 3-substituted [29, 45] pyrroles, bithiophene [62], aniline [52], and azulene [63] (Fig. 6). Compared to the entrapment procedure, the covalent attachment of GOD led to higher activity and stability and faster glucose detection.

The adsorption of GOD to an ECP, such as PPy [66, 67] or poly(3-methylthiophene) [39], has also been reported to be a simple route to enzyme electrodes that is less denaturing than physical entrapment. Recently, an innovative strategy has been described by Cosnier and Lepellec [48]. It involves initially the deposition of a biotin-substituted PPy film, followed by the successive attachment of avidin and biotin-labeled GOD, driven by the specific avidin–biotin interaction.

Owing to the high potential required to oxidize H_2O_2 enzymatically, the electroactivity of some ECP matrices, such as PPy, was irreversibly lost. Under these conditions, H_2O_2 was oxidized at the electrode surface after diffusion through the polymer film. Moreover, at high potentials, the mechanical behavior of the polymer film can be altered, and numerous organic molecules, such as ascorbic acid and uric acid, can interfere. Thus, the enzymatic electrodes involving O_2 as a mediator showed serious limitations

Table II. Glucose Electrodes Based on GOD-Containing Conjugated Polymer Films

Polymer matrix ^a	Method of immobilization of GOD ^b	Redox mediator ^c	Detection pH	Detection potential (V) ^d	Sensor performances ^e		Comments	Ref.
					K'_m (mM)	j_{max} ($\mu A cm^{-2}$)		
OPPy	E	O ₂	7.0	0.7 V (Ag)	30.7	40		[26]
PPy	E	O ₂	7.0	0.7 V (SCE)	— ^f	— ^f	Linear amperometric response for glucose concentrations lower than 10 mM. Response observed only after the loss of PPy electroactivity	[27]
PPy	E	O ₂	7.0	0.7 V (SCE)	40	30	Effect of film thickness on the amperometric response	[28]
PPy-NH ₂	CB	O ₂	— ^f	— ^f	— ^f	— ^f		[29]
PPy	E	— ^f	— ^f	— ^f	— ^f	— ^f	The amperometric response has not been reported	[30]
PPy-NH ₂	CB	O ₂	7.0	0.7 V (SCE)	17	— ^f	Different coupling methods between the functionalized pyrrole monomer and GOD were investigated. Optimal coupling was achieved with the carbodiimide reaction	[31]
PPy	E	O ₂	5.3	0.6 V (SCE)	30	500 to 1000	Effect of flavin coenzymes added in the electropolymerization solution. Better amperometric response for glucose was obtained with FAD	[32]
PPy	E	H ₂ O ₂ with I ⁻	7.0	0.0 V (Ag)	— ^f	— ^f	Investigation of PPy/GOD electrode surfaces by scanning tunneling microscopy	[33]
PPy	E	H ₂ O ₂ with I ⁻		0.0 V (Ag)	— ^f	— ^f		[34]
PMePy	E	O ₂	7.2	0.95 V (SCE)	— ^f	— ^f	Linear response for glucose in the range 0–0.22 M	[35]
PPy/PSS	E	FeCp ₂ -TMA ⁺	7.0	0.5 V (SCE)	— ^f	25	Coimmobilization of GOD and redox mediator into poly(styrenesulfonate)-doped PPy	[36]
PPy	E	O ₂ , potent.	7.0		— ^f		Linear E -log[$C_{Glucose}$] response in the range 1–10 mM	[37]
PPy	E	HQ-SO ₃ ⁻	7.0	0.35 V (SCE)	9.0	≈5	Redox mediator was incorporated into the polymer film as doping anion	[38]
PPy	E	BQ	6.8	0.35 V (SCE)	68	105	Redox mediator in solution	[39, 40]
PPy	E	FeCp ₂	5.6	0.3 V (Ag)	— ^f	— ^f	Polypyrrole films N-substituted by ferrocene-containing groups	[41]
PPy	CB	FeCp ₂ -COOH	7.0	0.3 V (Ag)	11.9	≈4.5	The covalent binding of GOD was achieved from a carbodiimide-promoted reaction between <i>N</i> -(2-cyanoethyl)pyrrole and the modified enzyme	[42]
PPy	CB	PPy	7.0	0.3 V (Ag)	2.8	— ^f	The GOD-modified pyrrole was obtained by coupling the surface lysyl residues of GOD covalently to 3-carboxymethylpyrrole	[45]
PPy	CB	BQ	7.0	0.35 V (SCE)	340	690	Linear response for glucose in the range 0–80 mM. Redox mediator in solution	[46]
Amp. PPy	EB	O ₂	7.0	0.5 V (SCE)	3.5–25	50–210	The sensitive layer was electroformed from a preadsorbed coating of GOD mixed with <i>N</i> -alkylammonium pyrrole. Low detection limit in glucose (0.1 μM)	[47]
Bio. PPy	C	O ₂	7.0	0.6 V (SCE)	— ^f	— ^f	Biotin-substituted PPy was used for the successive attachment of avidin and biotin-labeled GOD. Sensitivity to glucose: 7.0 ± 0.1 mA cm ⁻² M ⁻¹	[48]
PAni	E	O ₂	5.5	0.6 V (SCE)	12.4–19.6	≈35	Maximum current response at 40°C	[49]
PAni/PPDA	E	TTF ⁺	5.0	0.2 V (SCE)	— ^f	— ^f	Immobilization of GOD within PPDA grown on a preformed PAni layer	[50, 51]
PAni/PAA	CB	O ₂ , spectro.	6.0		80.6		Redox mediator in solution Covalent immobilization of GOD on the copolymer through amide linkage formation	[52]

(continues)

Table II. (continued)

Polymer matrix ^a	Method of immobilization of GOD ^b	Redox mediator ^c	Detection pH	Detection potential (V) ^d	Sensor performances ^e		Comments	Ref.
					K'_m (mM)	j_{max} ($\mu\text{A cm}^{-2}$)		
PPDA	E	O ₂	7.0	0.7 V (SCE)	14.2	181		[53]
PPDA	E	O ₂	7.0	0.7 V (Ag)	— ^f	— ^f	Entrapment of GOD into a composite PPDA/phospholipid layer	[54]
PPDA/PTMOS	E	O ₂	6.0–7.0	0.6 V (Ag)	4.3	170	Glucose sensor based on a composite membrane of GOD-entrapping polysiloxane and PPDA	[55]
PPDA/Nafion	E	O ₂	7.4	0.7 V (Ag)	— ^f	— ^f	Immobilization of GOD between inner PPDA and outer Nafion coatings	[56]
PPy/PPDA	E	O ₂	7.0	0.7 V (Ag)	— ^f	— ^f	Bilayer membrane PPy/PPDA	[57, 58]
PPDA	E	O ₂	7.4	0.65 V (Ag)	— ^f	— ^f	PPDA film electroformed onto GOD-containing carbon paste electrode	[59]
PHQ	E	PHQ	7.0	0.4 V (SCE)	— ^f	— ^f	GOD was mixed with PHQ and graphite powder	[60]
PPhs	E	O ₂	7.0	0.9 V (SCE)	— ^f	— ^f		[61]
PTh	CB	O ₂	7.4	0.6 V (SCE)	— ^f	— ^f	Covalent binding of GOD via its lysine residues to activated ester-substituted PTh	[62]
PMeTh	A	BQ	6.8	0.35 V (Ag)	— ^f	— ^f	Redox mediator in solution	[39]
PAz	CB	O ₂	7.4	0.6 V (SCE)	— ^f	— ^f	Covalent binding of GOD to amino-functionalized PAz	[63]
PDAB	E	O ₂	7.0	0.7 V (SCE)	14.5	— ^f	Linear response to glucose in the range 10^{-6} to 2×10^{-3} M.	[64]
PI	E	PI	7.0	1.6 V (Ag)	27.3	≈ 24		[65]

^aPAni, polyaniline; PAni/PPDA, polyaniline/poly(phenylenediamine) bilayer; PAni/PAA, polyaniline/poly(acrylic acid) copolymer; PAz, polyazulene; PDAB, poly(diaminobenzidine); PHQ, poly(hydroquinone); PI, polyindole; PMeTh, poly(3-methylthiophene); PPDA, poly(phenylenediamine); PPDA/PTMOS, poly(phenylenediamine)/poly(tetramethoxysilane) composite; PPhs, polyphenol and derivatives; PPy, polypyrrole; PPy-NH₂, amino-functionalized polypyrrole; PPy/PSS, polypyrrole/poly(styrenesulfonate); amp. PPy, poly(amphiphilic pyrrole); bio. PPy, biotin-functionalized polypyrrole; PMePy, poly(*N*-methylpyrrole); PTh, polythiophene.

^bA, adsorption; C, complexation; CB, covalent binding; E, entrapment; EB, electrostatic binding.

^cAmperometric reduction of I₂ produced from the Mo(VI)-catalyzed reaction between enzymatically liberated H₂O₂ and I⁻; BQ, *p*-benzoquinone; FeCp₂-COOH, ferrocenemonocarboxylic acid; FeCp₂-TMA⁺, (ferrocenylmethyl) trimethylammonium; HQ-SO₃⁻, hydroquinonesulfonate; Poten., potentiometric response to glucose; Spectro., spectrophotometric response to glucose; TTF⁺, tetrathiafulvalenium ion.

^dAg, vs. Ag/AgCl; SCE, saturated calomel electrode.

^e K'_m , Michaelis–Menten constant; j_{max} , maximum current density (see text).

^fNot indicated.

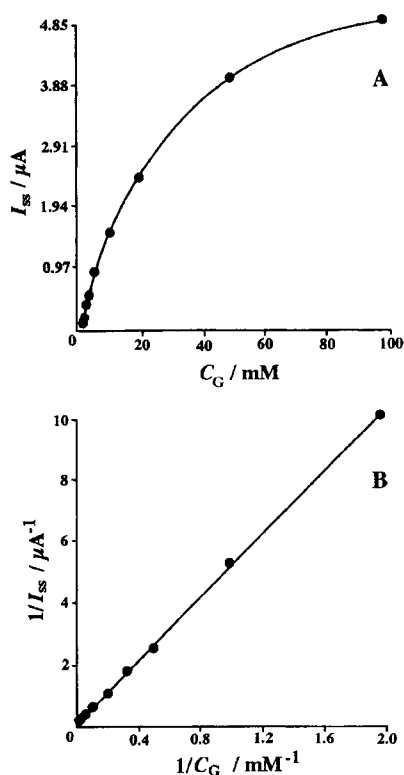


Fig. 5. (A) Steady-state currents I_{ss} obtained at a GOD-entrapping PPy film-coated electrode in the presence of glucose. Potential, 0.7 V (vs. Ag/AgCl). Electrolyte, 0.1 M phosphate buffer, pH 7.0. (B) Corresponding Lineweaver-Burk plot. Reprinted with permission from N. C. Foulds and C. R. Lowe, *J. Chem. Soc., Faraday Trans. 1* 82, 1259. Copyright 1986 by The Royal Society of Chemistry.

for *in vitro* or *in vivo* applications. Different approaches have been proposed to lower the detection potential. One approach involved the use of other electron mediators instead of O_2 , such as ferrocene [36, 41, 42], and quinone [38–40, 46], and derivatives such as tetrathiafulvalene [50, 51]. Other groups have reported an alternative and judicious method that still uses O_2 . This was based on the amperometric reduction of I_2 produced from the Mo(VI)-catalyzed reaction between enzymatically liberated H_2O_2 and I^- added to the electrolytic solution [33, 34]. With a lowered detection potential, the ECP electroactivity could be retained and the oxidation of the mediator could occur inside the polymer film. It has been demonstrated that the retention of the conducting properties of the polymer led to a more sensitive sensor exhibiting a faster amperometric response [43, 44].

The electron mediator could be solubilized or immobilized in the polymer film with GOD. Obviously, the biological application of an enzymatic electrode will require the mediator to be incorporated within the polymer. So, ferrocene carboxylate [68] and hydroquinonesulfonate [38] have been entrapped as doping anions within PPy. Another cationic ferrocene derivative, namely (ferrocenylmethyl) trimethylammonium, was coimmobilized with GOD into a PPy/poly(styrenesulfonate) film [36]. Covalent binding of the mediator has been the route chosen by Foulds and Lowe with a PPy film N-substituted by a ferrocene unit [41]. Nevertheless, such a film associated with GOD exhibited a strong oxygen sensitivity and a weak long-term stability.

2.1.2. Other Enzymes and Bionzymatic Systems

Numerous reports concerned with the immobilization of GOD in ECP films have demonstrated that such polymers could be used in the fabrication of biosensor arrays. Since these reports, this approach has been extended to other enzymes [69–113]. Like GOD, PPy has been the most extensively selected immobilization matrix, essentially because of its stability, processability, and compatibility with physiological conditions. Data gathered in Table III show the large range of target substrates which can be detected from different enzymes immobilized in ECP films.

As the isoelectric point of most enzymes is lower than 7, the entrapment procedure has generally been preferred, particularly when PPy has been involved. However, this method could lead in some cases to a loss of enzyme activity [93, 95]. It has been suggested that such a loss could be avoided by covalent immobilization of the enzyme, as has already been reported for 3-acetic acid-substituted polythiophene [92].

For polyaniline (PAni), enzyme entrapment into the polymer film was not easy since the pH at which enzymes are stable is not optimum for aniline electropolymerization. For some enzymes, such as urease [101], the postelectropolymerization cross-linking procedure was thus preferred. Bartlett et al. have shown that horseradish peroxidase (HRP) could be easily adsorbed to a PAni film [107, 108]. Nevertheless, the resulting modified electrode was reported to be less stable than that obtained from cross-linked HRP. Additionally, it has also been demonstrated that the catalytic efficiency of the enzyme electrodes constructed using HRP immobilized by cross-linking and covalent binding was significantly higher than that of the electrode constructed using HRP immobilized by adsorption [109]. Furthermore, one important limitation for PAni is that the device operated at weakly acidic pH (pH 5), whereas it would be more useful if it were to operate at neu-

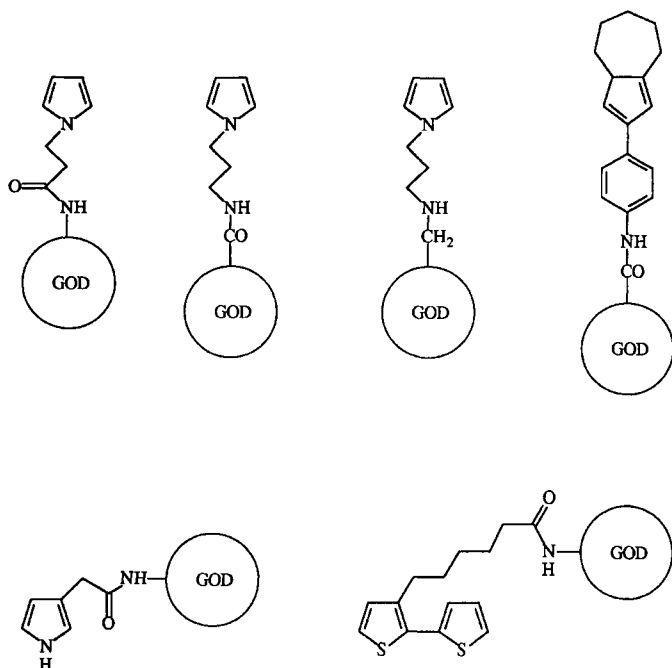


Fig. 6. Electropolymerizable aromatic molecules covalently bound to GOD.

Table III. Amperometric Detection of Different Substrates from Enzyme-Containing ECP Films

Detected substrate	Enzyme	ECP matrix ^a	Ref.
D-alanine	D-amino acid oxidase	PPy	[69]
Atrazine	Tyrosinase	PPy	[70]
Cholesterol	Cholesterol oxidase	PPDA	[71]
	Cholesterol oxidase and cholesterol esterase	PPy	[72–74]
Choline	Choline oxidase	PPy	[75]
Dopamine, catecholamines	Tyrosinase	PPy	[76, 100]
Ethanol	Alcohol dehydrogenase	PPy	[90]
Fructose	Fructose dehydrogenase	PPy	[82]
Glucose	GOD and horseradish peroxidase	PPy	[68, 77, 78]
		PAni	[111]
	GOD and catalase	PPy	[79]
	Glucose dehydrogenase	PPy	[80]
Glutamate	Glutamate dehydrogenase	PPy	[81]
	Glutamate oxidase	PPy	[100]
		PPDA	[104]
Glutamic acid	Glutamate oxidase and horseradish peroxidase	PAni	[111]
Hydrogen peroxide	Horseradish peroxidase	PPy	[83, 84]
		PAni	[108, 109]
		PThn	[110]
		PAni/PPDA	[107, 108]
L-lactate	Flavocytochrome <i>b</i> ₂	PPh	[85]
	Lactate oxidase	PPy	[103]
Lactic acid	Lactate oxidase and horseradish peroxidase	PAni	[111]
NADH	Diaphorase	PPy	[86, 106]
	Alcohol dehydrogenase	PI	[112]
Nitrate	Nitrate reductase	PTh	[92]
		PPy	[93–95, 102]
Nitrite	Nitrite reductase	PPy	[96]
O ₂	Cytochrome <i>c</i>	PPy	[113]
Phenols	Tyrosinase	PPy	[75, 87, 97]
Saccharose	GOD, invertase, and mutarotase	PPy	[91]
Thiourea	Uricase	PPy	[105]
Triglycerides	Lipase	PAni	[98]
Urea	Urease	PPy	[88]
		PAni	[98, 101]
Uric acid	Uricase	PAni	[89]
Peptide synthesis	Serine protease	PPy	[99]

^aPAni, polyaniline; PI, polyindole; PPDA, poly(phenylenediamine); PPh, polyphenol; PPy, polypyrrole; PTh, polythiophene; PThn, polythionine.

tral pH. This problem could be overcome by associating PAni with poly(styrenesulfonate) [114] or poly(vinylsulfonate) [115, 116].

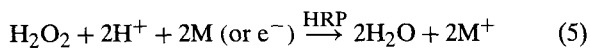
In contrast to GOD, some enzymes such as HRP can undergo direct electron transfer with unusual facility. For this reason, no mediator was required when those enzymes were used [100, 105, 107, 108]. In general, the sensitivity of the detection of a target substrate could be significantly improved by the use of a mediator. For the construction of reagentless biosensors, it is necessary to immobilize the mediator together with an enzyme inside the polymer film. So, ferrocene [74, 104, 109, 111], quinone and related compounds [106], redox dye [97], and mono- [102] and bipyridinium [92–94, 96] have been incorporated into ECP films.

In some cases, the mediator could be the polymer itself [77, 101, 110, 112]. Among the immobilization methods of the mediator, it appears that covalent binding provides some advantages, as shown for poly(anilinomethylferrocene)-modified HRP electrode, which responded rapidly to micromolar concentrations of H₂O₂ [109].

2.1.2.1. Bienzymatic Systems

As detailed in the preceding section, several ideas have been proposed to overcome the problems caused by the high potential of H₂O₂ oxidation. Among them is the concept of bienzyme electrodes. Hydrogen peroxide produced from GOD can be detected at lower potential values by the use of HRP coimmobilized with

GOD in polymer films [68, 77, 78, 111]. As a matter of fact, HRP efficiently catalyzes the reduction of H_2O_2 into H_2O following



where M is an electron mediator. In this case, the amperometric determination of glucose was achieved either from the direct reduction of H_2O_2 or from the reduction of M^+ solubilized or attached to the polymer film. So, a polymer film containing both GOD and HRP could operate as a glucose sensor at 0.15 or -0.05 V (vs. Ag/AgCl) when the polymer (PPy) matrix itself [77] or an attached ferrocene unit [111], respectively, was used as an electron mediator. According to a similar principle, HRP has been coimmobilized with other oxidase enzymes producing H_2O_2 , such as lactate and glutamate oxidases [111].

The deleterious effects of H_2O_2 produced by GOD could be eliminated by incorporating this enzyme with catalase into a PPy film [79]. Such a bienzyme electrode responded to glucose with high sensitivity and specificity.

Immobilization of cholesterol esterase and cholesterol oxidase made it possible to measure the total cholesterol content in blood serum [72–74]. Nevertheless, the long-term stability of the bienzyme system was limited by the degradation of the cholesterol esterase activity. Last, a PPy film containing up to three enzymes, namely GOD, invertase, and mutarotase, has been developed for the determination of saccharose [91].

2.2. Analytes of Biological and Pharmacological Interest

The presence of a functional moiety immobilized within a conjugated polymer film is not a prerequisite for obtaining a system sensitive to biologically interesting molecules. Sensitivity and selectivity of such a system can be based on differences in the permeabilities of target molecules through the polymer film. Factors such as the molecule size, concentration, the nature, the morphology, and the thickness of the polymer film can affect permeability [117]. A significant example is that of PANi and PPy films, investigated in the presence of various amino acids (histidine, methionine, tryptophan, tyrosine, and cysteine), which are potential interferents in the enzyme-based measurements [118]. The goal was the development of a polymer electrode that could respond selectively to H_2O_2 . This selectivity was only obtained for PANi, for which the oxidation of amino acids was not observed. However, the results were not convincing because they were strongly dependent on the electropolymerization conditions and the polymer morphology. Generally, the latter parameter is not easy controlled for classical ECPs. A similar trend has been observed for PPy films doped with different anions and used as amperometric sensors for other amino acids (e.g., L-aspartic acid and L-arginine) [119, 120] and haloacetic acids, which are known as carcinogenic products resulting from the chlorination of drinking water [121]. Different selectivities could be obtained by changing either the electrochemical conditions or the nature of doping anion.

Other examples have focused on the permselective properties of ECP films rendered nonconjugated and electroinactive after the application of high oxidizing potentials. It has been reported that an overoxidized PPy film acted as a permselective, antifouling membrane capable of rejecting interferents [122–126]. The permselective response of this film arose from the introduction of carbonyl groups onto the polymer backbone during the overoxidation step. The overoxidized PPy-coated electrode has been successfully used for the detection of neurotransmitters such as dopamine

[122–124] and epinephrine [122]. However, sensitivity and selectivity were also strongly dependent on the film thickness [122, 124], the overoxidation treatment [125], and the exposure time in solution containing the analyte [124].

Besides the permselective properties, the electrocatalytic properties of ECP films can be also used for the amperometric detection of some target molecules. Accordingly, electrodes modified with PPy, polythiophene (PTh), PANi, and their derivatives were found to catalyze the electrochemical oxidation of ascorbic acid [127–129], NADH [115, 116, 130], dopamine [128], pyrroloquinoline quinone [131] as a coenzyme of some oxidoreductases, and quinone and derivatives [132, 133]. Selectivity exhibited by these materials could be enhanced by the introduction of an appropriate substituent onto the polymer backbone. So, a facilitated electron transfer between cytochrome *c* and carboxylic acid or carboxylate-substituted PPy [134] or polyindole [135] has been observed. As such an effect was not obtained with unsubstituted polymer films, the cytochrome *c*-polymer interaction was explained on the basis of binding between the polymer substituents and the lysine residues on the redox protein.

A classical approach to improving the sensitivity of ECP-based sensors consists of the immobilization of catalytic moieties, such as metallic particles [136–142], Prussian blue [143], ferrocene [144], metalloporphyrins [145–148], and oxometalates [149–152], within ECP films. Compared to polymers without a catalyst, these materials exhibited more pronounced electrocatalytic effects and were suitable for the detection of numerous molecules of biological interest, e.g., carbohydrates [136, 141], catecholamines [144], and NO [145, 150–152].

Moreover, selectivity could be also enhanced if a specific interaction between the immobilized catalyst and the substrate in solution were to occur. A significant example is that of the voltammetric detection of NO in the rat brain from a carbon fiber microelectrode modified with a $[(\text{H}_2\text{O})\text{Fe}^{\text{III}}\text{PW}_{11}\text{O}_{39}]^{4-}$ -containing poly(*N*-methylpyrrole) film and a Nafion outer layer [150]. The good selectivity of this sensor was attributed not only to the Nafion membrane, which constituted an efficient electrostatic barrier against anionic interferents, but also to the formation of a metal-nitrosyl complex between the heteropolyanion and NO. The *in vivo* NO measurements were validated by injecting the rat with an NO-synthase inhibitor, which led gradually to the disappearance of the NO oxidation peak (Fig. 7).

Novel, promising route toward the ECP-based recognition of biologically active species has been proposed. The specific interaction between a biological unit that is included in an ECP film and its complementary target in solution has been used to recognize biological species [153–161], including DNA, peptides, and enzymes. The recognition event was detected either by radioactive labels [153], or by a significant change in the electrochemical [154, 155, 157], spectrochemical [157, 160, 161], or gravimetric [158] response of the ECP.

Because of its permeability and biocompatibility, PPy has been preferentially chosen as a conjugated backbone [153–156, 158, 159]. However, several reports [157, 160, 161] have demonstrated that PTh could also be designed for the recognition of biological species.

Thus, the bioactive dipeptide–proteolytic enzyme [154], oligonucleotide–complementary oligonucleotide [153, 155, 157, 158], antigen–antibody [156, 161], and biotin–avidin [159, 160] interactions have been transduced into changes of a signal characteristic of the functionalized conjugated polymer. As shown in Fig. 8,

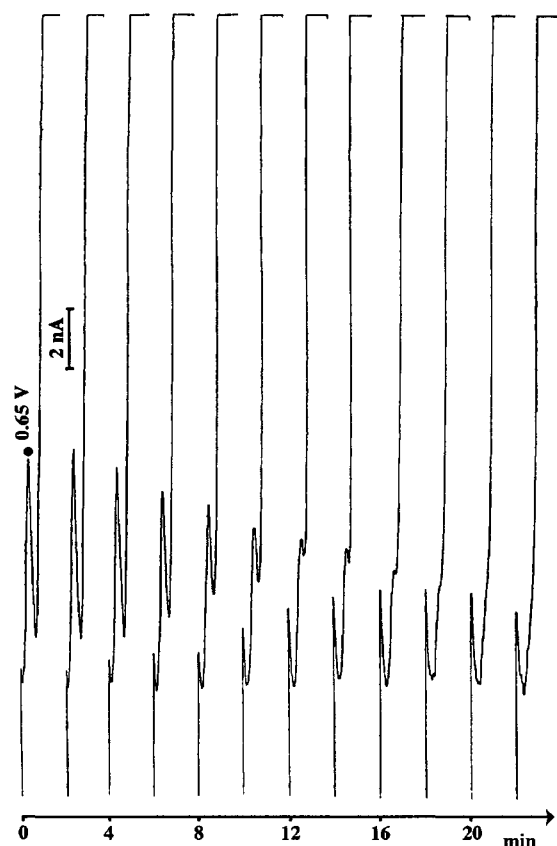


Fig. 7. Effect of an NO-synthase inhibitor (L-arginine *p*-nitroanilide) on the differential normal pulse voltammetry measurements obtained at a carbon fiber/ $[(\text{H}_2\text{O})\text{Fe}^{\text{III}}\text{PW}_{11}\text{O}_{39}]^{4-}$ -doped poly(*N*-methyl pyrrole)/Nafion microelectrode in the rat brain. Electrochemical recording between 0.4 and 1.35 V (vs. Ag/AgCl) at 10 mV s^{-1} with one cycle every 2 min. The indicated potential corresponds to the oxidation peak of NO and the zero time indicates the injection of the inhibitor into the rat. (From [150].)

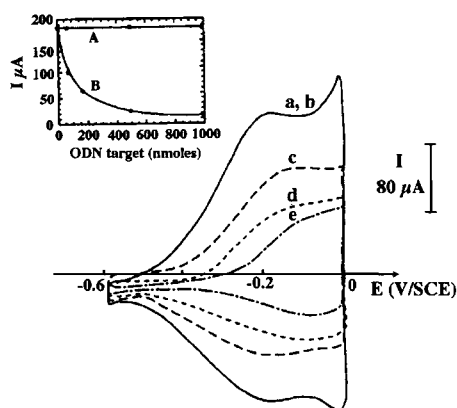


Fig. 8. Cyclic voltammograms of an oligonucleotide-functionalized PPy after incubation in buffered aqueous solutions containing 0.5 M NaCl or poly(ethylene glycol) (a), in noncomplementary oligonucleotide II (b), and in complementary oligonucleotide I in concentrations of 66 nmol (c), 165 nmol (d), and 500 nmol (e). (Inset) Variation of electrode current at $E = -0.2 \text{ V/SCE}$ as a function of the concentration of noncomplementary II (A) and complementary I (B). Reprinted with permission from H. Korri Youssoufi, F. Garnier, P. Srivastava, P. Godillot, and A. Yassar, *J. Am. Chem. Soc.* 119, 7388. Copyright 1997 American Chemical Society.

the specific hybridization of the oligonucleotide unit grafted to the PPy matrix with its complementary oligonucleotide target in solution induced a significant modification in the electrochemical response of PPy, which was attributed to conformational changes along the conjugated backbone.

The specific interaction between a biological unit and another molecule has been also exploited for the synthesis of new processable electroactive polymers [162] and the extraction/delivery of biologically active molecules [154, 163]. An approach to the trapping delivery of neutral drugs has been reported by Bidan and co-workers [163]. The neutral guest *N*-methylphenothiazine was encapsulated in the host sulfonated cyclodextrin previously incorporated as a doping anion in PPy. This drug could be electrochemically released from the polymer by the application of an appropriate potential.

Last, the host-guest complexation between cyclodextrin and bithiophene has allowed the electrosynthesis in water of the corresponding ECP film, with enhanced solubility and processability properties [162].

2.3. Gases and Vapors

The sensing of gases and vapors from conducting polymers was essentially based on reversible changes in either the electrical conductivity of an ECP film electrosynthesized onto an interdigitated metal (e.g., gold) electrode [164–173] or the electron work function [174–178] when ECP-modified field effect transistors were involved. Other sensory devices have used volume changes of the polymer [179] or changes in frequency of a ECP-coated piezoelectric crystal [164, 180–182] as transduction signals. It has frequently been reported that an electron-donating or -accepting gas decreased or increased, respectively, the conductivity of PPy [164–168] and other conducting polymers, including PTh and derivatives [169] and PANi [168, 170]. The sensitivity of ECPs to gases and vapors has been investigated with NO_2 [165–169, 176], SO_2 [166], I_2 [166, 179], and Br_2 [172, 173], PCl_3 [166] as electron-accepting gases; dimethyl methylphosphonate [168, 176] and tetrachloroethene [176] as weak electron donors; and NH_3 [167–170, 179], triethylamine [180, 182], and H_2S [167, 169] as stronger electron-donating gases. However, the mechanism of interaction between an ECP and a gas or vapor is often not clearly elucidated. The observed conductivity changes were commonly attributed to the interaction of electronically active gases (e.g., NH_3 , NO_2) and vapors with either the polymer backbone itself or the doping anion incorporated within the film, thereby modulating the mobility and/or the number of free charge carriers available.

For interactions with neutral molecules, such as water [171, 174, 177, 180, 182], aliphatic alcohols [171, 174, 175, 177, 180, 182], chloroform [177], acetonitrile [171, 180, 182] and other organic vapors [181, 182], the changes in electrical properties of ECP films were thought to be caused by a partial electron transfer from these vapors to the polymer. In some cases, the formation of a charge transfer complex has been proposed when O_2 [183] and HCN [178] have been involved. However, differences in polymer-vapor interactions may also result in a much larger adsorption of some vapors than others [164].

Owing to the diversity of polymer-gas interactions capable of inducing changes in a signal characteristic of the ECP film, the selectivity of ECP-based gas sensors was generally poor. An approach to the improvement of selectivity is to incorporate a functional group within the polymer film which will specifically in-

teract with the analyte. For this purpose, the three functionalization methods schematized in Fig. 3 have been used. As some metallophthalocyanines exhibited high sensitivity to NO_2 (down to 1 ppb in air [167, 184]), these complexes have been immobilized in their tetrasulfonated forms as doping anions in PPy films [176]. The best results in terms of stability and sensitivity to NO_2 were obtained with tetrasulfonated copper phthalocyanine. Conductimetric sensors for Br_2 vapors have been developed with different bromo-substituted polythiophene films [172, 173]. The electrical conductivity of these films was not changed in the presence of other halogenated vapors, N_2 , and CO_2 [173]. The covalent binding of a cyano group to PPy has been used to enhance interactions with some polar species such as nitriles and alcohols [180, 182]. However, compared to the responses obtained with other PPy derivatives in the presence of gases and vapors [182], the interest of such a group was not really demonstrated.

The postelectropolymerization incorporation of metal clusters into the bulk of a PANi film yielded an electroactive material sensitive to HCN at concentrations on the order of ppm [178]. The affinity for this gas was ascribed to the formation of a $\text{M}(\text{CN})_n$ complex between the immobilized metal and HCN.

The enhancement of selectivity and sensitivity of ECP-based gas sensors could also be achieved with the functionalization of ECP films by catalytic species. So, metal particles such as Pt [138, 185] and Pd [139], heteropolyanions [149, 186–190], metalloporphyrins [148, 191], metallophthalocyanines [192], and others [193, 194] have been immobilized in various ECP films. Most of these electroactive materials showed electrocatalytic effects on the oxidation or reduction of dissolved O_2 [139, 148, 187, 188, 190–194], CO [138], CO_2 [193], and H_2 [185], which could be used for the development of electrochemical sensors.

The application of conjugated polymer films as gas separation membranes has also been described [195–197]. The ability of ECPs to separate mixtures of gases was related to differences in permeabilities of gases through the polymer films. Provided that the morphology and the porosity of this class of electroactive polymers were precisely controlled after synthesis, a remarkable gas selectivity could be achieved. For PANi investigated in the presence of different gas pairs, selectivity values of 3590 for H_2/N_2 , 30 for O_2/N_2 , and 336 for CO_2/CH_4 were obtained [195]. It has also been demonstrated that other ECPs such as poly(dimethoxy-*p*-phenylenevinylene) were appropriate for gas separations [197].

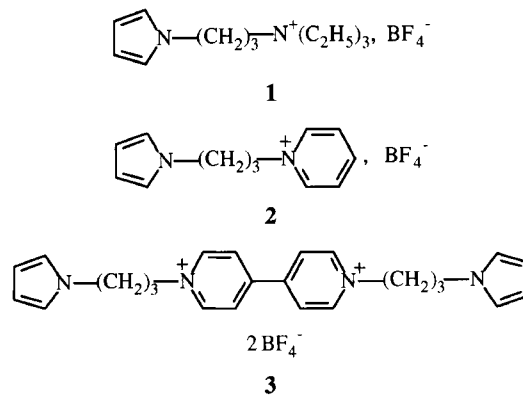
2.4. Other Molecules

The electrocatalytic activity of ECP films containing a dispersed catalyst has been used for the detection or transformation of other target molecular analytes, such as alcohols, unsaturated organic compounds, and others.

Owing to highly corrosive acid conditions, stable catalysts and supports are required for the development of anodes working in direct methanol–air fuel cells. Platinum is the only stable catalyst material that shows a significant amount of activity for methanol oxidation. However, platinum has to be modified with other metals, such as ruthenium and tin, to obtain lower oxidation potentials. So, platinum and tin or ruthenium particles have been electrochemically immobilized in poly(3-methylthiophene) [142] and polyaniline [137] films, respectively. Compared to electrodes modified with platinum alone, the electrocatalytic properties

of the bimetallic electrodes with respect to the oxidation of methanol [137, 142] and other small molecules (e.g., HCOOH , HCHO) [137] were enhanced. Furthermore, a faster and more efficient conversion of methanol into carbon dioxide was observed.

The electrochemical deposition of precious metal microparticles into alkylammonium- (1) and pyridinium- (2 and 3) substituted polypyrrole films has also been achieved by Moutet and co-workers [140, 198, 199]. The electrodes coated with those polymers were successfully used for the electrocatalytic hydrogenation of some unsaturated organic compounds in aqueous media. It was demonstrated that the redox-active viologen groups in poly(3) improved markedly the conductivity and the stability of the catalytic films [198].



In the absence of inserted metal particles, other electrocatalytic reactions such as the reduction of alkyl dibromide from poly(3) could be performed [200]. Nevertheless, inhibition of the catalytic activity caused by a loss of the film permeability was observed.

In the latter example and others involving polypyrrole films electroformed from a complex between a transition metal (Ru(II)) and a bi- or terpyridine-substituted pyrrole [201, 202], the electron self-exchange was ensured by either the viologen or Ru(II) units and not by the polymer. As a matter of fact, the PPy matrix was undoped when poly(3) was used for electrocatalytic reduction experiments or overoxidized when the films containing ruthenium(II)-based complexes were involved in oxidation experiments [201, 202].

The electrochemical immobilization of other metallic complexes like metalloporphyrins in PPy [147, 203, 204] led to materials exhibiting electrocatalytic properties with respect to the oxidation of hydrocarbons [147] and hindered phenols [204] by molecular oxygen.

In view of some technological applications, the synthesis and the design of electroactive polymers capable of enantioselective molecular recognition for chemical or electrochemical synthesis are required. For this purpose, numerous chiral ECPs [205–220] have been developed in which the main-chain chirality was induced by the presence of enantiomerically pure side groups. Generally, these polymers were electrosynthesized anodically from the chiral pyrrole and thiophene monomers, as the resulting films were electrochemically stable and exhibited a good reversibility. Various chiral amino acids (e.g., L-valine) were preferentially used as substituents, but several reports have focused on the properties of ECPs functionalized with other chiral groups (Fig. 9).

The optical activity of chiral monomers and relevant polymers was evaluated by circular dichroism measurements. It has been

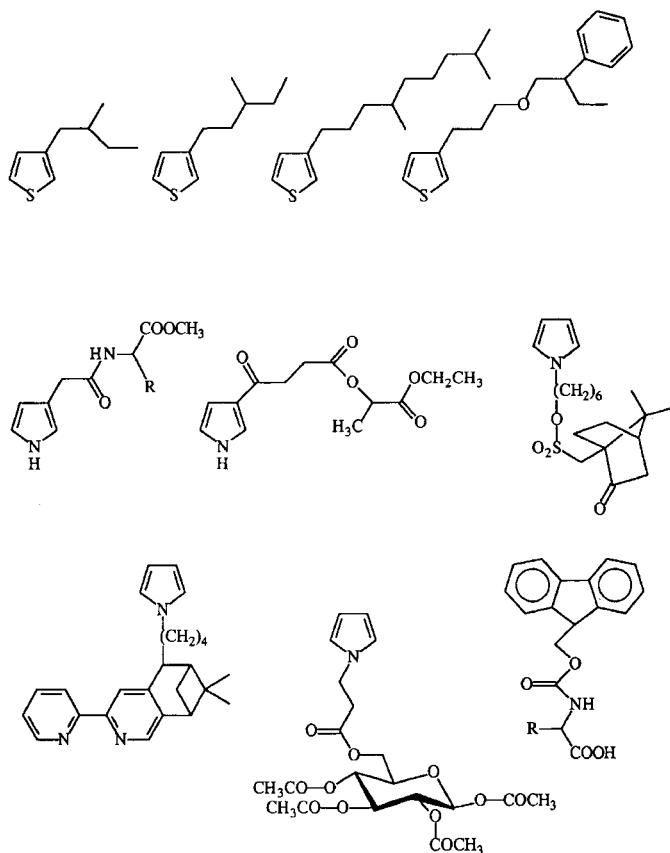


Fig. 9. Examples of electropolymerizable aromatic units substituted by chiral groups.

shown that this factor could be enhanced by introducing regioregularity into this type of polymer [217, 218]. Provided that the optical activity of chiral centers was unaffected after the electropolymerization step [212, 213, 219], the chiral polymers were thus suitable for enantioselective recognition or electrochemical asymmetric induction of prochiral organic molecules. For example, amino acid-substituted polyfluorene has been used for the chiral discrimination between two enantiomeric forms of (\pm)-methylbenzylamine [211]. The enantioselective recognition of this polymer was rather moderate (maximum optical yield of 15%) but roughly equivalent to that observed with chiral PPy or PTh derivatives. The electrochemical stereoselective reduction of 4-methylbenzophenone at a chiral PPy-coated electrode in the presence of a proton donor led to the corresponding *R*-configured alcohol with a 17% maximum optical yield [215].

The incorporation of a transition metal within a chiral ECP film should make it possible to expand the application of chiral electrodes to enantioselective electrocatalytic reactions. Such an approach has been validated by Moutet and co-workers, who have electrosynthesized a functionalized PPy film from a rhodium(III) complex with a pendant chiral bipyridyl ligand bound to a pyrrole unit [219]. The efficiency of this material was demonstrated through the electrocatalytic hydrogenation of prochiral ketones. The *S*-configured corresponding alcohols were produced with current efficiencies of around 60% and with optical yields between 5% and 12%. However, enantioselectivity was found to be strongly dependent on the film thickness and the electropolymerization

conditions. Papillon et al. have proposed a weakly different approach for the asymmetric electrocatalysis in the sense that the bipyridyl ligand was incorporated between two thienyl units replaced by a chiral group [220]. Unfortunately, attempts to electrochemically homo- or copolymerize this compound were unsuccessful.

3. CATIONIC RECOGNITION

3.1. Polyether-Functionalized Polymers

The monocyclic polyethers called crown ethers were discovered in 1967 by Pedersen [221, 222] and can be defined as uncharged macroheterocycles containing the repeating unit $(-O-CH_2-CH_2-)_n$. They are designed as molecular hosts that are able to complex alkali and alkaline earth cations, transition metal cations, and ammonium cations. Since then, other ligands such as the cryptands of Lehn [223, 224] and the spherands and the chiral crown ethers of Cram [225] have been synthesized, and their complexing properties have been extensively studied. In addition to these compounds, acyclic polyethers known as podands can also undergo strong interactions with cations when the number of oxygen atoms is suitable [226].

The cation-polyether complexation phenomenon appears to be a Lewis acid-base phenomenon and is principally a function of the size relationship between the crown diameter and the ionic diameter. Generally, the most stable complexes are formed when the ionic diameter is almost equal to the crown diameter [227, 228].

With the aim of enhancing the power of binding of the ligand to the cation, numerous authors have synthesized ionophoric compounds of the crown ether or polyether type attached to a redox center, such as ferrocene, quinone and derivatives, and nitrobenzene [229–235]. Indeed, the cation binding should be enhanced by electrostatic interaction when the redox center is reduced. In addition, the binding affinity may be accompanied by selective discrimination toward one cation relative to others. Thus these systems can in principle be designed to *recognize electrochemically* the binding of the cations.

In the case where the redox center is either incorporated into or constitutes a block of a solid polymer matrix, it thus becomes possible to modify electrode surfaces with cation-responsive macromolecular assemblies.

If the properties of the functional group are not perturbed after its immobilization on the electrode surface and if it is in close proximity to the redox center, the electrochemical behavior of the redox center is expected to be modified by the complexation effect.

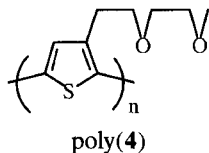
However, the host-guest interaction can also give rise to changes in other characteristic properties of the polymers.

3.1.1. Acyclic Polyether-Substituted ECP Films

The substitution of polythiophene films by linear oligo(oxyethylene) chains has been largely used to obtain materials that are not only endowed complexing properties toward cations, but also soluble, with a highly hydrophilic character [11].

Among the polythiophenes 3-substituted by oligo(oxyethylene) chains of different lengths, the best electroactive and conducting properties were exhibited by poly[3-(3,6-dioxaheptyl)thiophene]

poly(**4**) with conductivity values in the range of 80–250 S cm⁻¹ [236, 237].

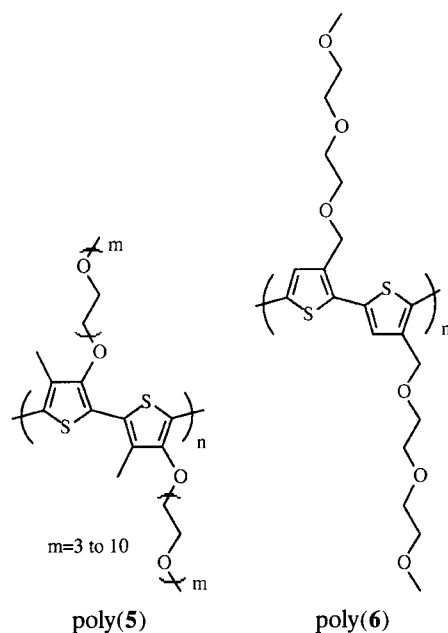


Compared to poly(3-alkylthiophene)s, the presence of the polyether chain in poly(**4**) stabilizes more planar conformations and induces a higher degree of electrochemical reversibility [238]. Moreover, this substitution also induces a strong hydrophilic character [239, 240]. The electroactivity and the electrochemical reversibility of poly(**4**) were almost unmodified in the aqueous medium, in contrast to poly(3-heptylthiophene) and poly[3-(3-oxaheptyl)thiophene]. The effect of factors such as the nature and the concentration of the electrolyte cation on the electrochemical and optical responses of poly(**4**) has been largely examined by Roncali et al. [241–243]. The replacement of NBU₄⁺ by Li⁺ in acetonitrile resulted in the shift toward more negative values of the oxidation potential of poly(**4**), about 100–150 mV for a concentration of 0.1 M [241]. The improvement of the rate and efficiency of the processes of charge and mass transport in the polymer in the presence of Li⁺ could be explained by the complexation of this cation by the oligo(oxyethylene) chains. Indeed, this complexation would contribute to localization of the counteranion of the electrolyte in the vicinity of the conjugated backbone by electrostatic interactions, or to the dissociation of ion pairs present in the polymer structure [241].

However, changes in the structure and the geometry of the polymer chains can also modify the redox behavior of the polymer to the same extent. From UV–visible absorption spectroscopy complementary data, Roncali et al. suggested that the complexation of Li⁺ by the polyether side chains increased simultaneously the coplanarity of the conjugated backbone and the rigidity of the polymer framework [241, 242]. Nevertheless, the ionic effect observed with poly(**4**) in the solid state could be considered to be weak because of the slight bathochromic shift of the absorption maximum of the polymer (about 10 nm).

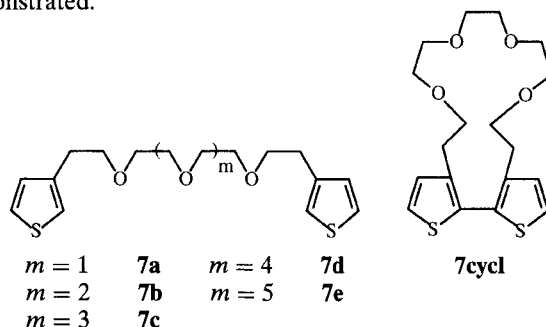
More dramatic effects were observed with regioregular polyether-substituted polythiophenes. As reported by Lévesque and Leclerc, chemically synthesized head-to-tail poly[3-oligo(oxyethylene)-4-methylthiophene] poly(**5**) led to ionochromic effects, with a clear isosbestic point on the UV–visible absorption spectrum, indicating the coexistence of long sequences of nonplanar and planar thiophene units [244, 245]. With the addition of a cation such as K⁺, the main chain became twisted. However, in contrast to poly(**4**), this phenomenon was observed only with the polymer in solution.

In contrast, ionochromic effects were visible with head-to-tail poly[3-(2,5,8-trioxanonyl)thiophene] poly(**6**) both in solution and in the solid state [246–249]. With the addition of cations such as Pb²⁺ and Hg²⁺, the conjugation of this polymer, characterized by an absorption maximum at 439 nm in CHCl₃ and 486 nm in the solid state, was completely eliminated [247]. Thus, the cationic complexation would induce the twisting of the polymer backbone away from planarity. However, although the response was chemoselective (Li⁺ and Zn²⁺ were found not to interfere), the ionochromic effects observed with Pb²⁺ and Hg²⁺ were irreversible, as the conjugation of the polymer was not restored after the complexation.



For all examples reported before, the integrity of the functional group was kept after the chemical or electrochemical polymerization step, and the complexation of cations was ensured with an acyclic ligand.

An original approach developed by some authors consisted of the electroformation of complexing macrocyclic cavities from the oxidation of the thiophene derivatives substituted with acyclic polyether chains. In this context, symmetrical monomers possessing two thiophene units linked together by a polyether subunit have been synthesized [250–253], and their electrochemical behavior has been investigated. Based on electrochemical considerations, Roncali et al. claimed that the oxidation of 1,14-(3-thienyl)-3,6,9,12-tetraoxatetradecane (**7b**) in the presence of Li⁺ yielded a conducting polythiophene containing pseudo-crown ether cavities [250]. As a matter of fact, the complexation of this cation by the polyether chain would promote the cyclization (template effect) and the concomitant polymerization of the terminal thiophene groups. Although the authors justified this mechanism by a significant shift of the electropolymerization potential of **7b** (250–300 mV) relative to that of 3-alkylthiophenes or of other thiophenes 3-substituted by ether groups, such an effect was not really demonstrated.



A recent study from Simonet's laboratory has clearly demonstrated that such an effect could not be involved in the electropolymerization of **7b** [253]. Indeed, no significant shift of the oxidation potential of **7b** was observed when the nature of the electrolyte cation was changed. Moreover, the electrochemical and spectroscopic responses of poly(**7b**) were different from those obtained for poly(**7cycl**).

Table IV. Proportions of Uncomplexed Cations (in %) Remaining after the Reaction for 24 h of 0.3 g of Undoped Poly(7) with an Aqueous Solution Initially Containing 4×10^{-7} M Cation

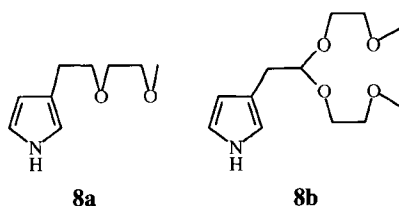
Polymer	Cation			
	Ag ⁺	Mn ²⁺	Co ²⁺	Sb ³⁺
Poly(7a)	48.5	2.4	4.4	77.5
Poly(7b)	51.4	10	1.0	80
Poly(7c)	10	15	4.0	82

The detection was achieved by γ -spectrometry. (From [252].)

The properties of complexation of different undoped poly(7) with respect to inorganic cations (Ag⁺, Mn²⁺, Co²⁺, and Sb³⁺) have been investigated by γ -spectrometry, and the principal results are summarized in Table IV. It can be seen that these polymers exhibited a binding power toward Mn²⁺ and Co²⁺ that was much stronger than that toward Sb³⁺. Furthermore, the same affinity was obtained for Co²⁺ (ionic radius, 0.72 Å [254]) whatever the polymer, whereas Mn²⁺ (0.80 Å) and Ag⁺ (1.26 Å) were more specifically complexed by poly(7a) and poly(7c), respectively. Thus this result is well correlated with the length of the polyether chain.

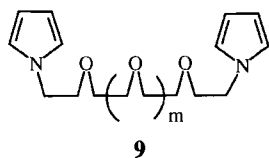
Compared with polythiophenes, the functionalization of polypyrroles by oligo(oxyethylene) ligands has been exploited much less.

The substitution at the 3-position has been preferred by Garnier and co-workers, owing to the excellent conducting properties of the resulting polypyrrole films. Accordingly, they have reported the synthesis and the electrochemical behavior of a new polypyrrole 3-substituted by a polyether chain [255]. 3-(3,6-Dioxaheptyl)pyrrole (**8a**) was potentiostatically electropolymerized, whereas the electrooxidation of **8b** did not give rise to a polymer film because of the steric effect caused by the substituents.



Poly(**8a**) exhibited an enhanced redox reversibility compared with the unsubstituted polypyrrole. This result, which is interesting for battery applications, was explained by a greater mobility of the ionic species inside the polymer caused by the pendant polyether chain.

Using an approach analogous to that developed for polythiophenes, Simonet and co-workers have synthesized monomers consisting of two pyrrolyl units linked together by long-chain polyether spacers (**9**) [256, 257].



In accordance with the electrochemical results obtained for **7** [253], macrocyclic cavities could be potentiostatically generated after the polymerization step of **9**. However, in contrast to **7**, **9** was less efficiently electropolymerized, probably owing to lower

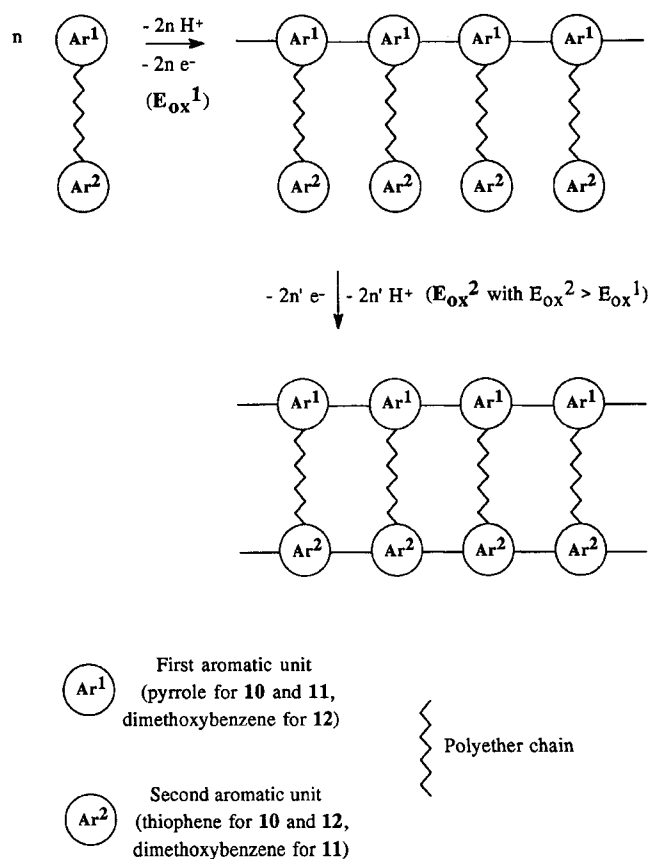
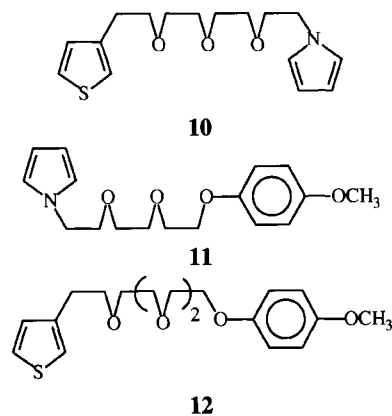


Fig. 10. Electroformation of pseudo-crown ether cavities containing materials according to a two-step anodic route.

conducting and electroactive properties of the corresponding *N*-substituted polypyrroles. The complexing properties of such polymers, exemplified by poly[1,11-di(1-pyrrolyl)-3,6,9-trioxaundecane] (**9**, $m = 1$), have been investigated by γ -spectrometry with the extraction of cations contained in radioactive wastes [256]. A strong affinity for Co²⁺ was obtained, whereas Cs⁺ and K⁺ were complexed much less by this polymer.

A novel strategy for forming controlled-size pseudo-crown ethers from acyclic polyethers has recently been proposed by Fabre et al. [258]. As conceptualized in Fig. 10, it consisted of the electrosynthesis of electroactive copolymers from compounds possessing two different electropolymerizable aromatic groups (pyrrole/thiophene (**10**), pyrrole/dimethoxybenzene (**11**), and thiophene/dimethoxybenzene (**12**)) linked together by a polyether chain.



At a low anodic potential, the oxidation of the first electropolymerizable unit led to an electroactive homopolymer film composed of pendant polyether-substituted aromatic moieties. A subsequent oxidation of the polymer by the application of a more positive potential promoted the electropolymerization of the second aromatic unit. So, complexing macrocyclic cavities were electrogenerated, the sizes of which were thought to be adjustable, depending on the length of the polyether chain of the starting monomer.

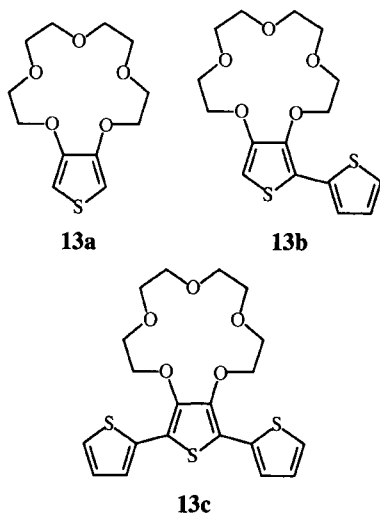
The two aromatic units were chosen so that the electroactivity of the preformed polymer was not degraded through an overoxidation process in the course of the electroformation of the second polymer. Generally this condition was fulfilled when the oxidation potentials of these two units were relatively close. The effect of cations on the electrochemical behavior of the homo- and copolymer resulting from **10** has been investigated in the presence of alkali cations [259].

For the homopolymer, only small redox changes have been observed with K^+ , with an anodic shift of the PPy system of about 40 mV. For the copolymer, the situation is completely different. Large redox changes have been obtained for Li^+ , Na^+ , and K^+ . In the presence of these cations, the reversibility of the doping-undoping process, reflected by the separation between the anodic and cathodic peaks, was found to be decreased.

Such kinetic limitations were thought to be caused by (i) a reduced mobility of the positively charged carriers along the conjugated polymer backbone owing to the presence of complexed cation and (ii) effects of ion pairing between the complexed cation and the doping anion.

3.1.2. Crown Ether-Substituted ECP Films

Large modifications of the characteristic properties of a conducting polymer substituted by a macrocyclic ligand are expected when the binding site is in close proximity to the conjugated backbone. So, the cationic complexation should be efficiently and rapidly recognized. However, in this case, it is predictable that an electrochemical-type recognition based on the shift of the redox potentials of the electroactive polymer will be strongly dependent on environmental events. First, in the course of its oxidation, positive charges are generated along the polymer chain, which results in electrostatic repulsions with the inorganic cation. Second, the short distance between the ligand and the polymer backbone may hinder the migration and transport of the cation into the polymer.



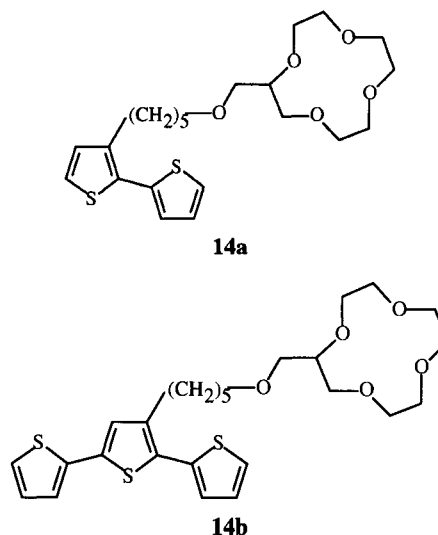
These features have been considered by Bäuerle and Scheib in the study of novel 15-crown-5 substituted (oligo-)thiophenes (**13**) in which the macrocycle is directly grafted to the thiophene moiety [260].

These compounds could be potentiodynamically polymerized, except for **13c**, which did not form adhering films at an electrode surface.

The influence of alkali cations such as Na^+ , Li^+ , and K^+ on the redox behavior of poly(**13a**) and poly(**13b**) has been analyzed from multisweep cyclic voltammetry experiments. The electrochemical response of poly(**13b**) was found to be unaffected by the presence of alkali cations. In contrast, a large shift of the oxidation peak of poly(**13a**) toward more positive potentials was observed in the presence of Na^+ . Upon the cationic complexation, the electron density contributed by the oxygen atoms of the crown ether to the conjugated polymer backbone was decreased, and consequently, the oxidation potential of the polymer was enhanced.

Nevertheless, as the cyclic voltammograms were stabilized only after a very large number of scans, poly(**13a**) was not suitable for the electrochemical recognition of cations in real time.

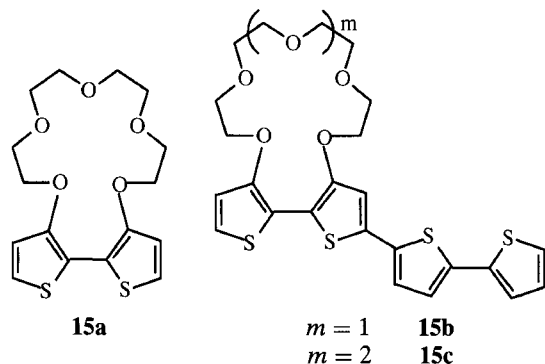
The increase in the distance between the conjugated backbone and the crown ether could contribute not only to the facilitation of the transport of the cation in the polymer, but also to the reduction of the steric constraints of the macrocycle on the polymer. The negative effect is that the interaction between the crown ether and the conjugated system would be lowered, and consequently the electrochemical recognition of cations would be less sensitive. However, when the length of the spacer group separating the macrocycle from the polymer was suitable, sensitive and selective cation-responsive polymers could be obtained. This was the case for 12-crown-4-functionalized poly(alkylthiophene)s (poly(**14**)) in which the crown ether was linked to the thiophene ring via an oxalkyl chain [261].



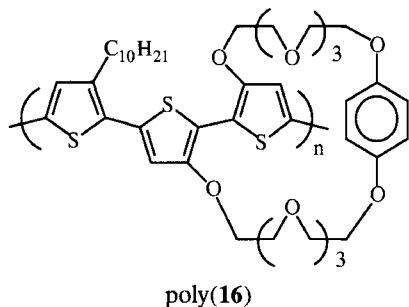
After the addition of alkali cations to the electrolyte solution, the cyclic voltammograms of electrogenerated poly(**14a**) and poly(**14b**) were shifted toward more positive potentials, but in contrast to poly(**13**), their stability was reached after a few scans for a given cation concentration.

The perturbation of the p-doping-undoping process of the conjugated polymer upon the complexation effect may be caused either by electronic effects or by conformational changes in the polymer. Swager and co-workers have demonstrated that conforma-

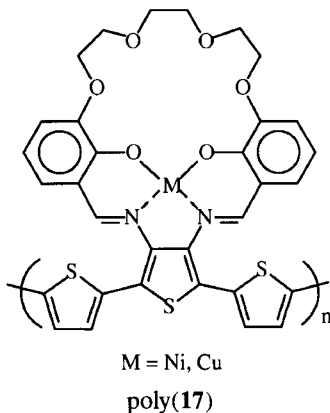
tional changes induced by the complexation lead to a modification of the conjugation length of the polymer backbone, which could be detected from UV-visible measurements [262, 263]. So, large band gap changes have been observed for poly(**15**) in the presence of different alkali metal ions [263]. These results were ascribed to the metal complexation, which forced a rotation of the thiophene rings to accommodate maximum chelation.



Recently, Swager's group has reported a new approach to ion-sensing polymers, illustrated with polythiophene-based pseudopolyrotaxanes, such as poly(**16**), which transduced recognition events into measurable changes in conductivity [264, 265].

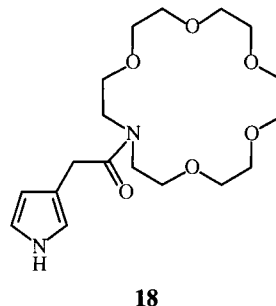


Ditopic systems have been presented by Reddinger and Reynolds, with poly(**17**) capable of detecting not only cationic species but also neutral organic molecules [266]. In addition to the macrocyclic host able to bind cations, σ -donor ligands could coordinate to the oxidized transition-metal ion in the bis(salicylidene) core. Such a polymer could detect pyridine at nanomolar concentrations.



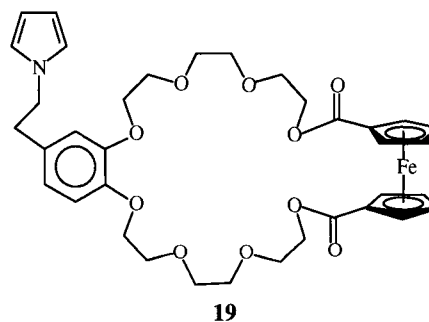
As has been observed for crown ether-substituted polythiophenes [260, 261], the aza crown ether-substituted polymer poly(**18**) exhibited a cation-selective electrochemical response with an an-

odic shift of the PPy system in the presence of Na^+ or K^+ [267, 268].



Such an increase in the oxidation potential of the polymer upon the complexation effect could be interpreted as a consequence of the deviation from coplanarity of the polypyrrole chain. This explanation was supported by the results obtained with polypyrrole N-substituted with a benzo-15-crown-5 unit which did not show any electrochemical recognition property toward alkali cations [269].

As a matter of fact, the N-substitution induced in the polymer backbone a much weaker configurational flexibility than the 3-substitution. To circumvent this problem, Moutet et al. have synthesized polypyrroles N-substituted by ferrocene crown ether [270] and aza crown ether-linked bipyridine ruthenium (II) complexes [271]. Poly(**19**) was found to be Ba^{2+} and Ca^{2+} -responsive [270], whereas the ruthenium(II)-based PPy was more sensitive to alkali metal cations [271]. The recognition of the cation binding was based on the changes in the electrochemical response of the metallic center instead of PPy.

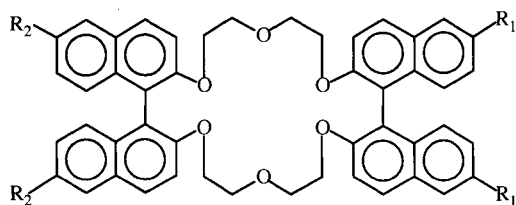


Very recently, the grafting of a crown ether unit to the PPy backbone has been achieved after the polymerization step, with the incorporation of aminomethyl-18-crown-6 by PPy bearing an easily removable leaving group [272].

In addition to PPy and PTh derivatives, numerous reports have focused on the synthesis and the properties of electroactive polymer films electrogenerated from the oxidation of crown ether-substituted benzenes [273–286] and naphthalenes [17, 287–293]. Among them, poly(dibenzo-crown ether)s and, especially, poly(dibenzo-18-crown-6) have been the most extensively studied, owing to their remarkable structural, electrochemical, and complexing properties [278–280]. Furthermore, their affinity for a large variety of cations, including heavy metal and precious metal cations, was greatly improved when they were previously undoped [281–286].

In the 1970s, Cram and co-workers developed an important concept of complexation, based on a new class of crown ethers which had properties of chiral recognition due to their atropoisomerism [225, 294]. Furthermore, the molecules containing crown-6-ether and binaphthalene units showed the ability to distinguish

enantiomers of protonated amine and amino acid [295], as well as to trap spherical cations like alkali metal ions [296]. Systems such as bis-binaphtho-22-crown-6 (**20a**) and its derivatives were extensively studied and used in many applications [297, 298] (e.g., preparative optical resolution by chromatography, chiral recognition in transport).



$R_1 = R_2 = \text{H}$	20a
$R_1 = R_2 = \text{tert-butyl}$	20b
$R_1 = \text{H}, R_2 = \text{Br}$	20c
$R_1 = \text{H}, R_2 = \text{nitrophenyl}$	20d

In the context of modified electrode design and its potential use in cation-sensitive electrodes, Simonet and co-workers have demonstrated that p-doped electroactive polymer films could be electrogenerated from the oxidation of (*S,S*)- or (*R,R*)-**20a** [291, 292]. It must be noted that the enantiomeric form of the monomers did not affect at all the electrochemical response and other characteristic properties of the corresponding polymers. Such a conjugated polymer exhibited the complexation properties of the monomeric unit [291]. However, although the binaphthalene crown ether derivatives could be reversibly reduced at about -2.9 V (vs. $\text{Ag}/10^{-1}$ M Ag^+), the occurrence of a reversible n-doping has not been demonstrated for the corresponding polymers. Contrariwise, a reversibly n- and p-doped material has been obtained from the oxidation of substituted bis-binaphthalene crown ethers **20c** and **20d**. Polymers derived from these compounds in which the 6 and 6' positions on one of the binaphthalenes are free led to conjugated polynaphthalenes, while on the other binaphthalene subunit, the blocking of these positions induced the formation of electroreducible perylenes by intramolecular coupling between the 8 and 8' positions [293]. Such functionalized polymers should be of great interest for an electrochemically switchable cation complexation. Indeed, an enhancement of the cation binding through electrostatic interactions is expected when the polymer is negatively charged. Contrariwise, a lowering of the cation binding is expected when the polymer is in its p-doped state.

3.2. Calixarene-Functionalized Polymers

The functionalization of ECPs by calixarene-type cage molecules [299–301] has recently been achieved. The first examples related to calixarenes modified at their lower rim either by bithiophenes [302, 303] or by N-substituted pyrrole [304] moieties. The copolymerization of the calixarene-based bithiophene receptor with a vinylene [302], disubstituted bithiophene [302], or phenylene [303] produced conjugated polymers which exhibited efficient and specific cation recognition. The sensory properties of these polymers could be evidenced from changes in voltammetric, chromic, fluorescent, and resistive responses upon exposure to a guest cation. Of all of these transduction methods, Swager and co-workers have proved that conductivity was the most sensitive to external perturbations undergone by the conjugated polymer. As an example, Fig. 11 shows changes in the voltammetric and resistive re-

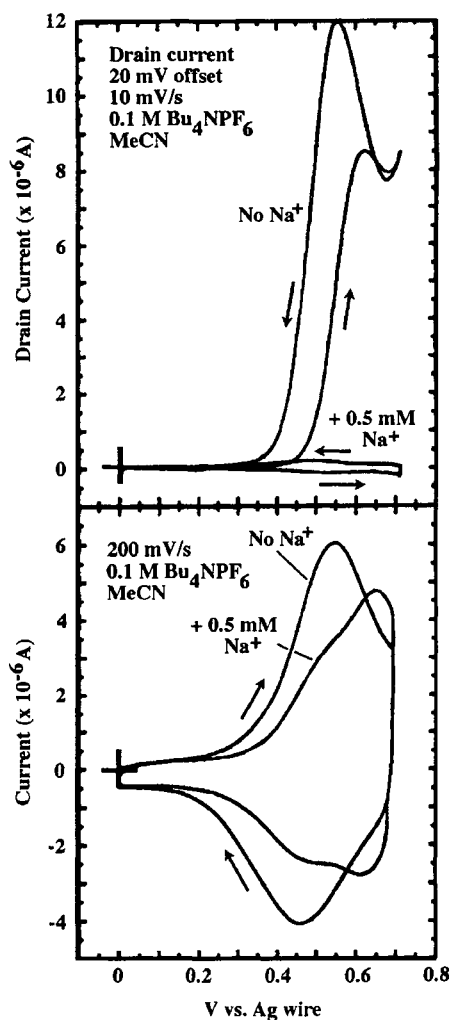
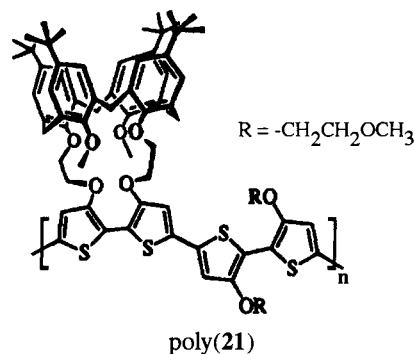


Fig. 11. Cyclic voltammograms and corresponding drain current $I_d - V_g$ curves for poly(**21**) in the absence and presence of Na^+ . Reprinted with permission from M. J. Marsella, R. J. Newland, P. J. Carroll, and T. M. Swager, *J. Am. Chem. Soc.* 117, 9842. Copyright 1995 American Chemical Society.

sponses of a solution casting film of calix[4]arene-substituted polythiophene poly(**21**) on exposure to Na^+ . In the presence of this alkali cation, a very large (>99%) decrease in peak conductivity (as measured by $I_{d(\text{max})}$) was observed.



Concerning the functionalization of PPy by calixarene, the first attempts to electrochemically homopolymerize a calix[4]arene modified at its lower rim by a N-substituted pyrrole moiety

failed [304]. Only a copolymerization with pyrrole could lead to the functionalized polymer. By changing the substitution site on the cage molecule, Bidan and co-workers have shown that calixarenes modified on their upper rim by four N-substituted pyrroles were efficiently homopolymerized under potentiodynamical conditions [305, 306]. Owing to conformational restrictions and steric hindrance, the electropolymerization process was limited when an ethyl spacer between the monomer unit and the functional molecule was used instead of a butyl spacer.

The attachment of a redox center to a calixarene-substituted PPy has been achieved by the anodic oxidation of pyrrole-substituted trisbipyridylruthenium(II)-linked calixarenes [307]. However, only thin films with a low amount of immobilized $[\text{Ru}(\text{bpy})_3]$ ($\text{bpy} = 2, 2'$ -bipyridine) were obtained by homopolymerization. Thicker films could be grown from copolymerization with *N*-methylpyrrole. Even if the sensory properties of these polymers have not been investigated yet, it can be predicted that the electrochemical and/or luminescent responses of the ruthenium complex could be changed upon the complexation of a guest cation by the immobilized host calixarene. It must be pointed out that such a recognition event had been already observed with a polypyrrole film *N*-substituted by an aza crown ether-linked bipyridine ruthenium (II) complex [271].

The one-step immobilization of sulfonated calixarenes as doping anions during the anodic electropolymerization of pyrrole has also been proposed to produce cation-responsive electroactive films [308, 309]. In this way, calix[4]arene-*p*-tetrasulfonate and calix[6]arene-*p*-hexasulfonate were irreversibly incorporated into the PPy structure. The recognition abilities of these molecules were retained after the entrapment step, as shown by the redox changes observed in the presence of trimethyl(ferrocenylmethyl)ammonium [308] and uranyl [309] as guest cations.

3.3. Polyrotaxanes

As depicted in Fig. 12, rotaxanes are composed of a dumbbell-shaped component, in the form of a rod and two bulky stopper groups, around which there are encircling macrocyclic component(s) [310]. The stoppers of the dumbbell prevent the macrocycle(s) from unthreading from the rod.

Such molecules have attracted much attention, in relation to photoinduced electron transfer [311, 312] and electro- or photochemically triggered molecular motions [313–316]. A strategy for forming ECP polymer films possessing interlocked structures has initially been developed by the groups of Sauvage and Bidan, who used transition metals as templating agents [317–319]. This was

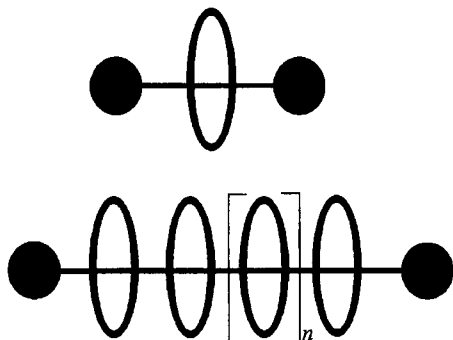
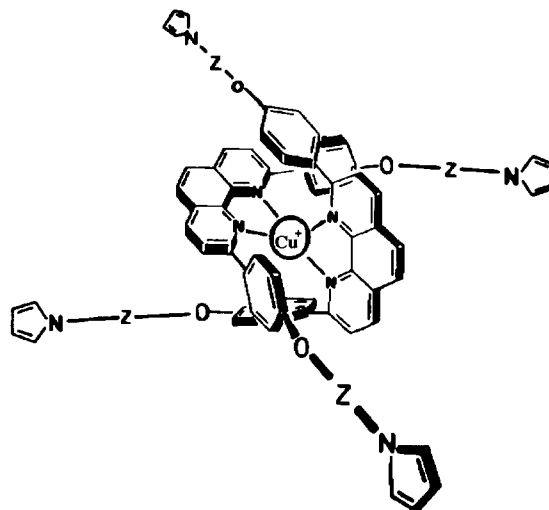


Fig. 12. Rotaxane and corresponding polymeric system.

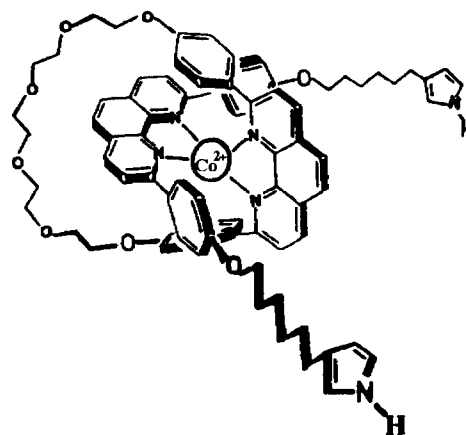
based on the anodic electropolymerization of a preformed assembly (22) between 1,10-phenanthroline moieties linked to pyrrole rings and a transition metal. Generally, Cu(I) was chosen, owing to its ability to gather the two constitutive organic fragments and to force the string to thread through the ring.



22

After electropolymerization, the film could be demetalated (using CN^- or SCN^-) without modification of the geometrical shape of the preformed complexing cavities, and other metals could be incorporated, such as Co(II), Zn(II), Ag(I), and Li(I). Consequently, the possibility of replacing a transition metal with another one appears to be of great interest in the applications in catalysis of homogeneous organic reactions.

The functionalized PPy films deposited on an electrode surface showed the characteristic electrochemical response of both the redox centers and the conjugated polymer. In contrast, any contribution of the incorporated metal to electron conductivity was not observed. With the same strategy, other polyrotaxane-like networks have been electrosynthesized from an intertwined heteroleptic cobalt complex (23) [320]. The spectroscopic and electrochemical properties of this complex were reported to be very similar to those of the homoleptic series 22.

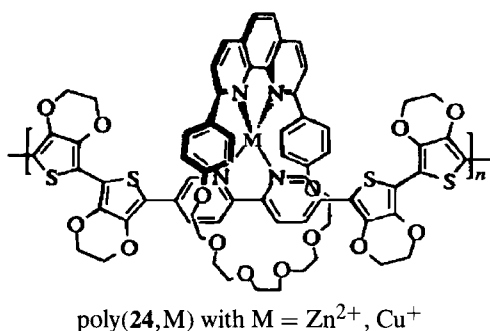


23

When a macrocycle containing two different chelating units, namely 2,9-diphenyl-1,10-phenanthroline and 2,2';6',6''-terpyridine, was used, electrochemically induced molecular motions

could be observed within the relevant polyrotaxane film [321]. The principle was based on the difference in the preferred coordination number for the two different redox states of the coordinated metal: four for Cu(I) and five for Cu(II). So the gyration of the hetero-bis-chelating macrocycle entrapped on a polymer coordinating thread occurred after the reduction of stable five-coordinate divalent complex to an unstable monovalent form. Because of the presence of the PPy matrix, the conformational change that would regenerate the starting complex was too slow to be observed.

Other polyrotaxanes containing a thiophene-based conjugated backbone have been synthesized from the Cu(I)- or Zn(II)-driven assembly between a macrocyclic phenanthroline and a bithiophene-substituted phenanthroline [322] or bipyridine [323, 324]. Swager and co-workers have demonstrated that the contribution of the metal ion to the electronic properties of the polyrotaxane was possible when more electron-rich 3,4-(ethylenedioxy)thiophene groups were used in place of thiophenes in the polymer backbone [324]. So a 10^6 – 10^7 -fold increase in the polymer's conductivity was observed after poly(24) was treated with Cu(II) solution. This result was ascribed to the oxidation of the poly(24) backbone by Cu^{2+} ions to generate poly(24,Cu) with charge carriers in the polymer backbone.

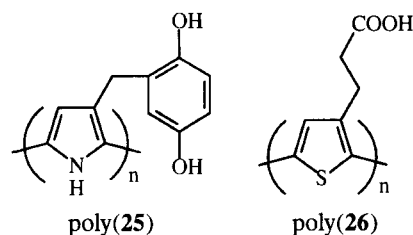


3.4. Polymers Containing Other Functional Groups

The cation sensitivity of some ECP films incorporating poorly mobile, large anions was related to the participation of cations in the doping–undoping process. So, PPy films doped by sulfate [325, 326], naphthalene sulfonate [325], polyanions [327, 328], and sulfonated organic electrocatalysts [203, 329] were reported to be cation sensitive. However, those systems were often poorly selective, and their response was strongly dependent on numerous experimental factors, such as the electrosynthesis conditions and the conditioning and pretreatment of the films. Among them, the composite polymer poly(*N*-methylpyrrole)/poly(styrenesulfonate) exhibited interesting cation-binding properties [328, 330]. Indeed, protonated amines could be incorporated into this composite when the film was cathodically reduced and released when the film was reoxidized. This electrochemically controlled binding and release from the film could also be achieved with other cations like protonated procaine, methyl viologen, and the bipyridine ruthenium complex [328]. A better cation selectivity could be obtained with ECP films doped by complexing ligands such as Alizarin Red S, bathocuproin sulfonate [331, 332], and Pyrocatechol Violet [333]. The electrodes modified by these films were used for the extraction and the voltammetric determination of copper species. A detection limit of about 0.1 μM was estimated for the sys-

tem based on Pyrocatechol Violet [333]. A PPy *N*-substituted by a carbodithioate moiety has also enabled to uptake copper ions from aqueous solutions [334]. Unfortunately, the voltammetric response of the resulting metal complex disappeared rapidly after two or three scans.

The functionalization of the monomer by a specific group has also been the route preferred by numerous groups to electrogenerate pH-sensitive electroactive materials. ECP films derivatized in the 3-position with hydroquinone [335, 336] and alkylcarboxylic acid [337–342] functionalities exhibited an electrochemical behavior depending on the pH of the electrolytic medium. For example, poly(25) showed a sub-Nernstian potentiometric response of 46 mV pH^{-1} at 25°C with a detection limit of 10^{-10} M [336].



As demonstrated by McCullough and co-workers, regioregularity in 3-substituted polythiophenes provided new conjugated polymers with remarkable sensory properties [342]. Both poly(26) and its water-soluble deprotonated derivative underwent protein-like hydrophobic assembly to generate a self-assembled conducting polymer aggregate. For the carboxylate polymer, this state was favored when small cations were used, whereas large cations could completely disrupt the aggregated phase. Figure 13 displays the chemoselective ionochromatic response of regioregular, head-to-tail poly(26) with different added bases. λ_{max} could be varied over a 130-nm range (from purple to yellow) simply by changing the counteranion.

With the objective of preparing fiber optic chemical sensors for pH measurements, Millar et al. have recently synthesized a polythiophene poly(27) derivatized by a pH-sensitive fluorescein unit [343]. As expected, the fluorescence properties of the polymer

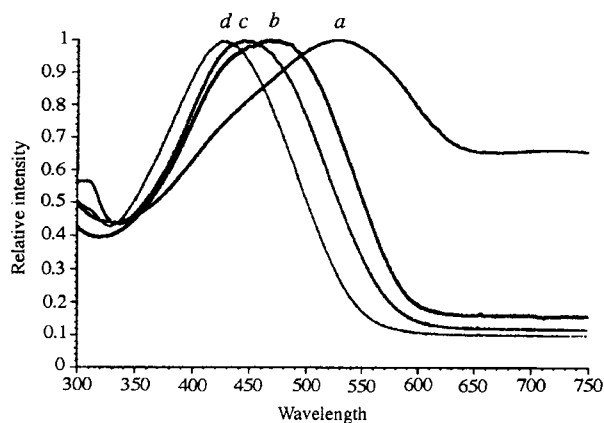
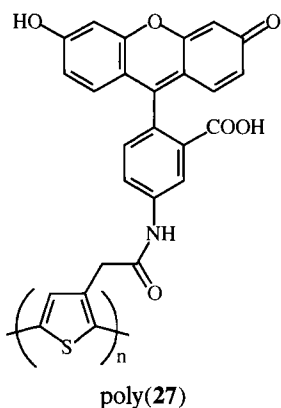


Fig. 13. UV-visible spectra of poly(26) with added base. (a) H_4NOH ; (b) Et_4NOH ; (c) Pr_4NOH ; (d) Bu_4NOH . Reprinted with permission from R. D. McCullough, P. C. Ewbank, and R. S. Loewe, *J. Am. Chem. Soc.* 119, 633. Copyright 1997 American Chemical Society.

were strongly dependent on pH, with a lower sensitivity compared to fluorescein in solution.



Other electroactive materials based on poly(hydroquinone) [344, 345], polyanilines [346–349], and amino-substituted ECPs [350, 351] showed a pH-sensitive voltammetric, potentiometric, or optical response.

The fixation of metallic cations such as Ni(II), Co(II), Cu(II), Zn(II), Mn(III), and Fe(III) in ECP films incorporating suitable ligands has been a strategy greatly used to prepare modified electrodes for electrocatalytic applications. Accordingly, numerous coordination complexes based on bipyridyl [352–358], cyclam [359, 360], porphyrin [203, 361], salicylidene [362–364], and phosphine [365] ligands bound to a conjugated polymer backbone (essentially PPy or PTh) have been synthesized. Generally these functionalized materials were electrogenerated from the anodic oxidation of the coordination complex between the metallic cation and the ligand-bound monomer. Evidence was provided for the similarity of electrochemical and spectrophotometrical behaviors of polymerized coordination complexes and in solution.

Recent reports have focused on the tuning of the optical and electronic properties of polymers via the incorporation of metal centers. The electrochromic properties of salicylidene-substituted polythiophene films (poly(28)) were strongly dependent on the incorporated metal type [362, 363]. So Ni-containing films exhibited an orange-to-green redox transition, while the Cu-containing analog displayed a light green–dark green pair. It must be pointed out that the blocking of the 4-positions of the salicylidene rings was required to prevent polymerization at those sites. As claimed by Kingsborough and Swager [364], the redox activity of the incorporated metal cation could be enhanced if complex 29 were chosen as the starting monomer.

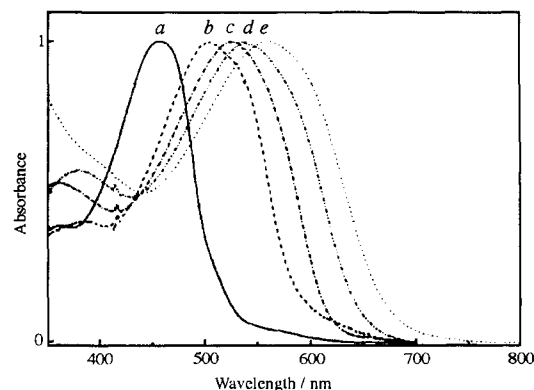
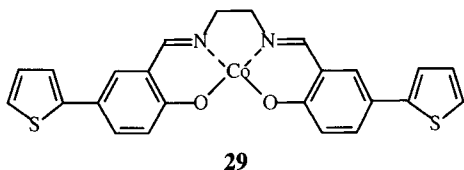
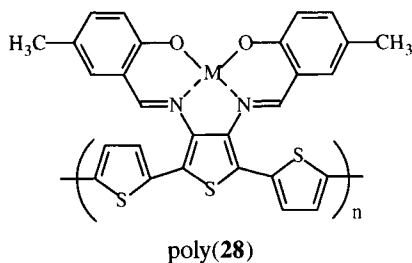
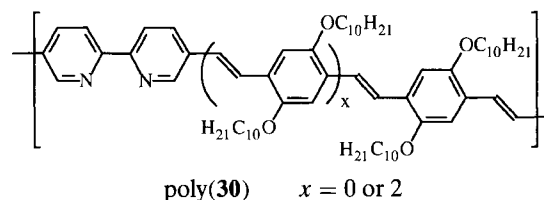
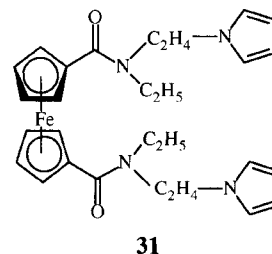


Fig. 14. Visible absorption spectra recorded in CHCl_3 at room temperature for poly(30) ($x = 0$) without (a) and in the presence of AgClO_4 (b), $\text{Cu}(\text{OAc})_2$ (c), $\text{AlK}(\text{SO}_4)_2$ (d), or PdCl_2 (e). The polymer concentration was 1.0×10^{-5} M, corresponding to a 2,2'-bipyridyl unit, and the metal ion concentration was 1.0×10^{-4} M. Reprinted with permission from B. Wang and M. R. Wasielewski, *J. Am. Chem. Soc.* 119, 12. Copyright 1997 American Chemical Society.

Another representative example pertains to the design and synthesis of metal ion-sensitive ligand-containing conjugated polymers. A polymer-like poly(30) underwent conformational changes upon incorporating metal ions, thus converting the polymer from the initial partially conjugated one to a fully or nearly fully conjugated entity [358]. As shown in Fig. 14, large ionochromic effects were visible with a wide variety of transition and main group metal ions.



Finally, the interaction of other cations such as alkali metal cations, the iron–sulfur cluster, and tropylium has been investigated in the presence of PPy films N-substituted with specific groups, namely ferrocene bisamide derivatives 31 [366], cystine [367], and phenothiazine [368]. The charge transfer complex produced between phenothiazine-substituted PPy and the tropylium cation was used in a photoelectrode device [368].



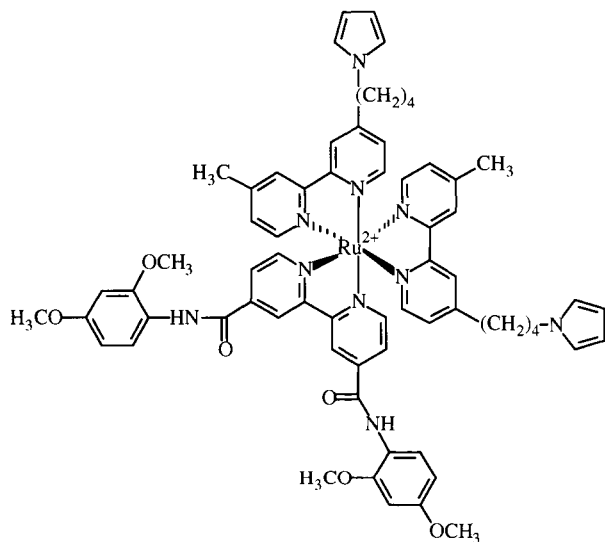
4. ANIONIC RECOGNITION

Compared with a large number of papers devoted to cation-sensitive conjugated polymers, the development of responsive systems for anionic species has been much less reported. This is somewhat surprising in view of the numerous anions playing a key role in biological and chemical processes and the importance of

detecting/extracting anionic pollutants such as phosphate and nitrate. Generally, the synthetic anion receptors are either positively charged or neutral. The positively charged receptors have protonated nitrogen atoms (e.g., polyammonium, polyguanidinium, quaternary ammonium) or metal ions. In these systems, the interactions are mainly of the Coulomb type. The neutral anionic receptors can either bind anions (solely by hydrogen bonding or ion-dipole interactions) or coordinate anions at the Lewis acidic centers of a neutral organometallic ligand [369].

With the aim of developing electroactive systems capable of electrochemically and specifically recognizing anions [370], some anionic receptors have been bound to redox-active groups such as cobaltocenium, ferrocene, and transition-metal bipyridyl moieties [370–373]. Although such compounds were suitable for the electrochemical recognition of some anionic species in solution, their immobilization on an electrode surface to achieve sensitive layers has been investigated with very few examples.

The electrochemical recognition of chloride ions by a functionalized PPy film electrogenerated from a substituted tris-bipyridine ruthenium (II) complex (32) has been reported by Lopez et al. [374]. The first one-electron reduction wave of the electroactive polymer was cathodically shifted (maximum shift of 40 mV) when Cl^- was added to the electrolytic medium. Unexpectedly, the electroactivity of the film was also dramatically changed in the presence of F^- , while I^- and Br^- had no effect.



32

Another example of conjugated polymer films incorporating an anionic receptor has been reported by Nicolas et al. [375]. Such films were electrogenerated from pyrrole and thiophene derivatives substituted by boronic acid or boronate groups. These functional groups were used as sensing elements owing to the strong interaction of the boron atom with hard bases like fluoride, giving rise to specific orbital changes from sp^2 to more stable sp^3 [376–379]. As an example, the redox system corresponding to the p-doping–undoping process of a boronate-substituted PPy film (poly(33)) was shifted to less anodic potentials in the presence of KF (Fig. 15). A similar trend was observed by Shinkai and co-workers with ferroceneboronic acid in solution [379]. The easier oxidation of the F^- -bound polymer could be explained by the stabilization of F^- bound to the boron atom by the positive charges along the oxidized PPy backbone. It must be pointed out that the

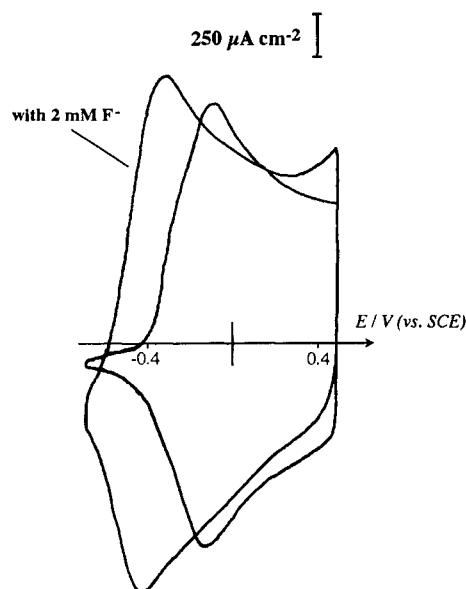
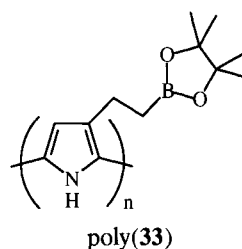


Fig. 15. Cyclic voltammograms at 100 mV s^{-1} of poly(33) (electroformation charge: 70 mC cm^{-2}) in $\text{H}_2\text{O}/\text{CH}_3\text{CN}$ (1/1 v/v) + $5 \times 10^{-1} \text{ M LiClO}_4$ in the absence and presence of 2 mM KF . (From [375].)

electrochemical response of poly(33) was not changed when F^- was replaced by Cl^- or Br^- . Moreover, the interaction with F^- was specific for the boronate-containing polymer, as the voltammetric response of an unfunctionalized PPy film was found to be unmodified in the presence of this halide.



poly(33)

A nitrite-sensitive material has been developed by Fabre et al. with a poly(*N*-methylpyrrole) film incorporating a metal-substituted heteropolyanion $[(\text{H}_2\text{O})\text{Fe}^{\text{III}}\text{XW}_{11}\text{O}_{39}]^{n-}$ ($\text{X} = \text{P}$, $n = 4$, or $\text{X} = \text{Si}$, $n = 5$) as a doping anion [380–382]. Such a film was electrochemically stable and exhibited an efficient electrocatalytic activity vis-à-vis the nitrite reduction. In contrast, poor results were obtained when PPy was used as the immobilization matrix [383, 384]. The key step of this electrocatalytic process was the formation of an iron–nitrosyl complex generated from the replacement of H_2O initially coordinated to the iron center by an NO group, the reduction of which led to the catalytic conversion of NO_2^- into ammonium ions [385, 386]. The measured catalytic currents were linear with the nitrite concentration over the range 1×10^{-4} to $3 \times 10^{-2} \text{ M}$ [382]. Furthermore, anions such as NO_3^- , Cl^- , SO_4^{2-} , PO_4^{3-} , and CO_3^{2-} were found not to interfere. The remarkable selectivity of this electrochemical sensor was explained by the formation of the nitrosyl complex.

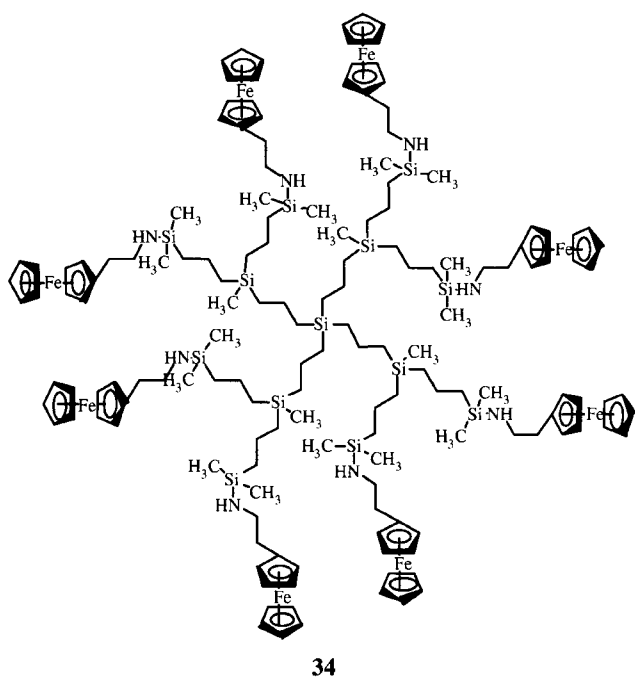
Other ECP films incorporating unsubstituted heteropolyanions have been used for the electrocatalytic reduction of anions such as nitrite, bromate, and chlorate [149]. However, for these systems no adduct was produced in the course of the electrocatalysis, and consequently, a lower selectivity was observed.

5. CONCLUSIONS

The immobilization of functional groups in conjugated polymer films led to redox-active materials capable of recognizing a great variety of substrates. In most cases, these materials were electrochemically generated from the anodic oxidation of an aromatic compound (e.g., pyrrole, thiophene) covalently bound to the functionality. Owing to the environment offered by the polymer framework, the reactivity, the stability, and the accessibility of the immobilized recognition sites could be modified compared with those exhibited in solution. Different parameters such as the film thickness and the nature and the length of the spacer arm between the recognition site and the conjugated backbone could affect these characteristic properties. Moreover, the transduction method has to be judiciously chosen to obtain a sensitive system. From representative examples, it appears that the conductimetric and spectroscopic methods are generally more sensitive to recognition events than are the electrochemical methods like cyclic voltammetry. Furthermore, the introduction of regioregularity in this type of polymer was found to be a way to enhance their sensory properties. Consequently, the structural organization of the immobilization matrix is an essential component of the recognition phenomenon.

With this feature in mind, numerous organized macromolecular architectures have been deposited on electrode surfaces. Accordingly, self-assembled monolayers [387] and Langmuir-Blodgett-type [388] multilayers have been used to attach numerous functional moieties to electrode surfaces, e.g., crown ethers [389–391] and other complexing macrocyclic cavities (calixarene [392], cyclodextrin [393], and cyclophane [394–396]), viologens [397], porphyrins [398, 399], and enzymes [400–402].

The derivatization of electrode surfaces by redox-active dendrimers [403–410] has also been explored to generate electrochemical sensors. So the ferrocenyl dendrimer **34** was reported to be sensitive to some anions such as H_2PO_4^- and HSO_4^- [409].



Thus these macromolecules offer attractive possibilities as supramolecular receptors for molecular recognition because of their precisely defined three-dimensional molecular architectures

and controlled chemical constitution. Compared with functionalized conjugated polymers, the interaction between the recognition sites and the analyte is expected to be stronger, provided that the conformation of the dendrimer is not modified after its immobilization. However, the disadvantages of this type of structures lie in a weaker fixation to the electrode surface as well as a surface coverage (and consequently a film thickness) that is not really variable over a large range of magnitude.

REFERENCES

1. J. P. Desvergne and A. W. Czarnik, *Chemosensors of Ion and Molecule Recognition*, NATO ASI Series, Series C, Vol. 492. Kluwer Academic Publishers, Dordrecht, 1997.
2. M. Gomez-Lopez and J. R. Stoddard, in "Handbook of Nanostructured Materials and Nanotechnology," (H. S. Nalwa, Ed.), Vol. 5. Academic Press, New York, 1999.
3. P. L. Boulas, M. Gomez-Kaifer, and L. Echegoyen, *Angew. Chem. Int. Ed.* 37, 216 (1998).
4. F. Garnier, *Angew. Chem.* 101, 529 (1989).
5. J. Simonet and J. Rault-Berthelot, *Prog. Solid State Chem.* 21, 1 (1991).
6. J. N. Barisci, C. Conn, and G. G. Wallace, *Trans Polym. Sci.* 4, 307 (1996).
7. O. A. Sadik, *Anal. Methods Instrum.* 2, 293 (1995).
8. A. Deronzier and J. C. Moutet, *Acc. Chem. Res.* 22, 249 (1989).
9. D. Curran, J. Grimshaw, and S. D. Perera, *Chem. Soc. Rev.* 20, 391 (1991).
10. M. E. G. Lyons, C. H. Lyons, C. Fitzgerald, and T. Bannon, *Analyst (Cambridge, U.K.)* 118, 361 (1993).
11. J. Roncali, *Chem. Rev.* 92, 711 (1992).
12. H. S. Nalwa, Ed., "Handbook of Organic Conducting Molecules and Polymers," Vols. 1–4. John Wiley & Sons, Chichester, 1997.
13. R. D. McCullough, *Adv. Mater. (Weinheim, Ger.)* 10, 93 (1998).
14. M. Leclerc and K. Faïd, *Adv. Mater. (Weinheim, Ger.)* 9, 1087 (1997).
15. H. Sze on Chan and S. C. Ng, *Prog. Polym. Sci.* 23, 1167 (1998).
16. J. Rault-Berthelot, *Recent Res. Dev. Macromol. Res.* 3, 425 (1998).
17. L. Pu, *Chem. Rev.* 98, 2405 (1998).
18. P. N. Bartlett and R. G. Whitaker, *Biosensors* 3, 359 (1987–88).
19. P. N. Bartlett and J. Cooper, *J. Electroanal. Chem.* 362, 1 (1993).
20. M. Trojanowicz and T. Krawczynski vel Krawczyk, *Mikrochim. Acta* 121, 167 (1995).
21. W. Schuhmann, *Mikrochim. Acta* 121, 1 (1995).
22. A. Heller, *Acc. Chem. Res.* 23, 128 (1990).
23. S. Nakamura, S. Hayashi, and K. Koga, *Biochim. Biophys. Acta* 445, 294 (1976).
24. A. Szucs, G. D. Hitchens, and J. O' M. Bockris, *Bioelectrochem. Bioenerg.* 21, 133 (1989).
25. R. M. Ianniello, T. J. Lindsay, and A. M. Yacynych, *Anal. Chem.* 54, 1098 (1982).
26. N. C. Foulds and C. R. Lowe, *J. Chem. Soc., Faraday Trans. 1* 82, 1259 (1986).
27. D. Bélanger, J. Nadreau, and G. Fortier, *J. Electroanal. Chem.* 274, 143 (1989).
28. D. Bélanger, J. Nadreau, and G. Fortier, *Electroanalysis* 4, 933 (1992).
29. W. Schuhmann, *Synth. Met.* 41–43, 429 (1991).
30. S. I. Yabuki, H. Shinohara, and M. Aizawa, *J. Chem. Soc., Chem. Commun.* 945 (1989).
31. B. F. Y. Yon-Hin, M. Smolander, T. Crompton, and C. R. Lowe, *Anal. Chem.* 65, 2067 (1993).
32. A. Kitani, N. Kasyu, and K. Sasaki, *Electrochim. Acta* 39, 7 (1994).
33. D. R. Yaniv, L. McCormick, J. Wang, and N. Naser, *J. Electroanal. Chem.* 314, 353 (1991).
34. M. Umana and J. Waller, *Anal. Chem.* 58, 2979 (1986).

35. P. N. Bartlett and R. G. Whitaker, *J. Electroanal. Chem.* 224, 37 (1987).
36. P. Caglar and G. E. Wnek, *Pure Appl. Chem.* A32, 349 (1995).
37. M. Trojanowicz and M. L. Hitchman, *Electroanalysis* 8, 263 (1996).
38. Y. Kajiya, H. Sugai, C. Iwakura, and H. Yoneyama, *Anal. Chem.* 63, 49 (1991).
39. E. M. Geniès and M. Marchesiello, *Synth. Met.* 55–57, 3677 (1993).
40. M. Marchesiello and E. M. Geniès, *Electrochim. Acta* 37, 1987 (1992).
41. N. C. Foulds and C. R. Lowe, *Anal. Chem.* 60, 2473 (1988).
42. S. E. Wolowacz, B. F. Y. Yon Hin, and C. R. Lowe, *Anal. Chem.* 64, 1541 (1992).
43. P. N. Bartlett and R. G. Whitaker, *J. Electroanal. Chem.* 224, 27 (1987).
44. M. Marchesiello and E. Geniès, *J. Electroanal. Chem.* 358, 35 (1993).
45. K. Yamada, H. Koizumi, K. Ikeda, and Y. Ohkatsu, *Chem. Lett.* 201 (1997).
46. K. Kojima, T. Yamauchi, M. Shimomura, and S. Miyauchi, *Polymer* 39, 2079 (1998).
47. L. Coche-Guérente, A. Deronzier, P. Mailley, and J. C. Moutet, *Anal. Chim. Acta* 289, 143 (1994).
48. S. Cosnier and A. Lepellec, *Electrochim. Acta* 44, 1833 (1999).
49. M. Shaolin, X. Huaiguo, and Q. Bidong, *J. Electroanal. Chem.* 304, 7 (1991).
50. P. N. Bartlett and P. R. Birkin, *Anal. Chem.* 66, 1552 (1994).
51. P. N. Bartlett and P. R. Birkin, *Anal. Chem.* 65, 1118 (1993).
52. Z. F. Li, E. T. Kang, K. G. Neoh, and K. L. Tan, *Biomaterials* 19, 45 (1998).
53. C. Malitesta, F. Palmisano, L. Torsi, and P. G. Zambonin, *Anal. Chem.* 62, 2735 (1990).
54. J. Wang and H. Wu, *Anal. Chim. Acta* 283, 683 (1993).
55. T. Yao and K. Takashima, *Biosens. Bioelectron.* 13, 67 (1998).
56. F. Moussy, D. J. Harrison, D. W. O'Brien, and R. V. Rajotte, *Anal. Chem.* 65, 2072 (1993).
57. C. G. Zambonin and I. Losito, *Anal. Chem.* 69, 4113 (1997).
58. I. Losito and C. G. Zambonin, *J. Electroanal. Chem.* 410, 181 (1996).
59. J. Wang, L. Chen, and D. B. Luo, *Anal. Commun.* 34, 217 (1997).
60. P. Wang, S. Amarasinghe, J. Leddy, M. Arnold, and J. S. Dordick, *Polymer* 39, 123 (1998).
61. P. N. Bartlett, P. Tebbutt, and C. H. Tyrrell, *Anal. Chem.* 64, 138 (1992).
62. M. Hiller, C. Kranz, J. Huber, P. Bäuerle, and W. Schuhmann, *Adv. Mater. (Weinheim, Ger.)* 8, 219 (1996).
63. W. Schuhmann, J. Huber, A. Mirlach, and J. Daub, *Adv. Mater. (Weinheim, Ger.)* 5, 124 (1993).
64. Z. Zhang, C. Lei, and J. Deng, *Analyst* 121, 971 (1996).
65. P. C. Pandey, *J. Chem. Soc., Faraday Trans.* 1 84, 2259 (1988).
66. E. Tamiya, I. Karube, S. Hattori, M. Suzuki, and K. Yokoyama, *Sens. Actuators* 18, 297 (1989).
67. C. G. J. Koopal, B. DeRuiter, and R. J. M. Nolte, *J. Chem. Soc., Chem. Commun.* 1691 (1991).
68. C. Iwakura, Y. Kajiya, and H. Yoneyama, *J. Chem. Soc., Chem. Commun.* 1019 (1988).
69. P. N. Bartlett and D. J. Caruana, *Analyst (Cambridge, U.K.)* 117, 1287 (1992).
70. F. M. McArdle and K. C. Persaud, *Analyst (Cambridge, U.K.)* 118, 419 (1993).
71. S. Dong, Q. Deng, and G. Cheng, *Anal. Chim. Acta* 279, 235 (1993).
72. B. F. Y. Yon Hin and C. R. Lowe, *Sens. Actuators, B* 7, 339 (1992).
73. W. Trettnak, I. Lioni, and M. Mascini, *Electroanalysis* 5, 753 (1993).
74. Y. Kajiya, R. Tsuda, and H. Yoneyama, *J. Electroanal. Chem.* 301, 155 (1991).
75. L. Coche-Guérente, S. Cosnier, C. Innocent, P. Mailley, J. C. Moutet, R. M. Moréllis, B. Leca, and P. R. Coulet, *Electroanalysis* 5, 647 (1993).
76. M. V. Deshpande and E. A. H. Hall, *Biosens. Bioelectron.* 5, 431 (1990).
77. T. Tatsuma, T. Watanabe, and T. Watanabe, *J. Electroanal. Chem.* 356, 245 (1993).
78. M. G. Garguilo, N. Huynh, A. Proctor, and A. C. Michael, *Anal. Chem.* 65, 523 (1993).
79. J. M. Cooper and D. Bloor, *Electroanalysis* 5, 883 (1993).
80. Y. Kajiya, H. Matsumoto, and H. Yoneyama, *J. Electroanal. Chem.* 319, 185 (1991).
81. S. Yabuki, F. Mizutani, and M. Asai, *Biosens. Bioelectron.* 6, 311 (1991).
82. G. F. Khan, E. Kobatake, H. Shinohara, Y. Ikariyama, and M. Aizawa, *Anal. Chem.* 64, 1254 (1992).
83. T. Tatsuma, M. Gondaira, and T. Watanabe, *Anal. Chem.* 64, 1183 (1992).
84. U. Wollenberger, V. Bogdanovskaya, S. Bobrin, F. Scheller, and M. Tarasevich, *Anal. Lett.* 23, 1795 (1990).
85. P. N. Bartlett and D. J. Caruana, *Analyst (Cambridge, U.K.)* 119, 175 (1994).
86. T. Matsue, N. Kasai, M. Narumi, M. Nishizawa, H. Yamada, and I. Uchida, *J. Electroanal. Chem.* 300, 111 (1991).
87. S. Cosnier and C. Innocent, *J. Electroanal. Chem.* 328, 361 (1992).
88. S. B. Adeloju, S. J. Shaw, and G. G. Wallace, *Anal. Chim. Acta* 281, 611 (1993).
89. S. Mu, J. Kan, and J. Zhou, *J. Electroanal. Chem.* 334, 121 (1992).
90. S. Yabuki, H. Shinohara, Y. Ikariyama, and M. Aizawa, *J. Electroanal. Chem.* 277, 179 (1990).
91. J. M. Slater and E. J. Watt, *Anal. Proc.* 26, 397 (1989).
92. I. Willner, E. Katz, N. Lapidot, and P. Bäuerle, *Bioelectrochem. Bioenerg.* 29, 29 (1992).
93. S. Cosnier, C. Innocent, and Y. Jouanneau, *Anal. Chem.* 66, 3198 (1994).
94. S. Cosnier, B. Galland, and C. Innocent, *J. Electroanal. Chem.* 433, 113 (1997).
95. G. Ramsay and S. M. Wolpert, *Anal. Chem.* 71, 504 (1999).
96. Q. Wu, G. D. Storrier, F. Pariente, Y. Wang, J. P. Shapleigh, and H. D. Abruna, *Anal. Chem.* 69, 4856 (1997).
97. C. Kranz, H. Wohlschläger, H. L. Schmidt, and W. Schuhmann, *Electroanalysis* 10, 546 (1998).
98. H. Sangodkar, S. Sukeerthi, R. S. Srinivasa, R. Lal, and A. Q. Contractor, *Anal. Chem.* 68, 779 (1996).
99. G. Faruque Khan, E. Kobatake, H. Shinohara, Y. Ikariyama, and M. Aizawa, *J. Am. Chem. Soc.* 118, 1824 (1996).
100. S. Cosnier, C. Innocent, L. Allien, S. Poitry, and M. Tsacopoulos, *Anal. Chem.* 69, 968 (1997).
101. W. J. Cho and H. J. Huang, *Anal. Chem.* 70, 3946 (1998).
102. L. M. Moretto, P. Ugo, M. Zanata, P. Guerriero, and C. R. Martin, *Anal. Chem.* 70, 2163 (1998).
103. F. Palmisano, G. E. De Benedetto, and C. G. Zambonin, *Analyst (Cambridge, U.K.)* 122, 365 (1997).
104. L. Qingshan, Z. Siliang, and Y. Juntang, *Anal. Lett.* 28, 2161 (1995).
105. M. Shaolin and C. Shufan, *J. Electroanal. Chem.* 356, 59 (1993).
106. T. Matsue, M. Nishizawa, T. Sawaguchi, and I. Uchida, *J. Chem. Soc., Chem. Commun.* 1029 (1991).
107. P. N. Bartlett, D. Pletcher, and J. Zeng, *J. Electrochem. Soc.* 144, 3705 (1997).
108. P. N. Bartlett, P. R. Birkin, J. H. Wang, F. Palmisano, and G. De Benedetto, *Anal. Chem.* 70, 3685 (1998).
109. A. Mulchandani, C.-L. Wang, and H. H. Weetall, *Anal. Chem.* 67, 94 (1995).
110. R. Yang, C. Ruan, W. Dai, J. Deng, and J. Kong, *Electrochim. Acta* 44, 1585 (1999).
111. A. Mulchandani and C.-L. Wang, *Electroanalysis* 8, 414 (1996).
112. M. Somasundrum and J. V. Bannister, *J. Chem. Soc., Chem. Commun.* 1629 (1993).
113. M. Caselli, M. Della Monica, and M. Portacci, *J. Electroanal. Chem.* 319, 361 (1991).
114. P. N. Bartlett and J. H. Wang, *J. Chem. Soc., Faraday Trans.* 92, 4137 (1996).

115. P. N. Bartlett, P. R. Birkin, and E. N. K. Wallace, *J. Chem. Soc., Faraday Trans.* 93, 1951 (1997).
116. P. N. Bartlett, J. H. Wang, and E. N. K. Wallace, *Chem. Commun.* 359 (1996).
117. P. Burgmayer and R. W. Murray, *J. Am. Chem. Soc.* 104, 6139 (1982).
118. J. C. Cooper, M. Hämmerle, W. Schuhmann, and H.-L. Schmidt, *Biosens. Bioelectron.* 8, 65 (1993).
119. P. Akhtar, C. O. Too, and G. G. Wallace, *Anal. Chim. Acta* 339, 201 (1997).
120. P. Akhtar, C. O. Too, and G. G. Wallace, *Anal. Chim. Acta* 339, 211 (1997).
121. P. Akhtar, C. O. Too, and G. G. Wallace, *Anal. Chim. Acta* 341, 141 (1997).
122. T. F. Kang, G. L. Shen, and R. Q. Yu, *Talanta* 43, 2007 (1996).
123. K. Pihel, Q. D. Walker, and R. M. Wightman, *Anal. Chem.* 68, 2084 (1996).
124. Z. Gao, B. Chen, and M. Zi, *J. Chem. Soc., Chem. Commun.* 675 (1993).
125. Z. Gao, M. Zi, and B. Chen, *J. Electroanal. Chem.* 373, 141 (1994).
126. A. Witkowski, M. S. Freund, and A. Brajter-Toth, *Anal. Chem.* 63, 622 (1991).
127. H. S. O. Chan, S. C. Ng, and S. H. Seow, *Synth. Met.* 66, 177 (1994).
128. R. A. Saraceno, J. G. Pack, and A. G. Ewing, *J. Electroanal. Chem.* 197, 265 (1986).
129. I. G. Casella and M. R. Guascito, *Electroanalysis* 9, 1381 (1997).
130. N. F. Atta, A. Galal, A. E. Karagözler, H. Zimmer, J. F. Rubinson, and H. B. Mark Jr., *J. Chem. Soc., Chem. Commun.* 1347 (1990).
131. H. Shinohara, G. F. Khan, Y. Ikariyama, and M. Aizawa, *J. Electroanal. Chem.* 304, 75 (1991).
132. R. C. M. Jakobs, L. J. J. Janssen, and E. Barendrecht, *Electrochim. Acta* 30, 1313 (1985).
133. A. Haimerl and A. Merz, *J. Electroanal. Chem.* 220, 55 (1987).
134. J. M. Cooper, D. G. Morris, and K. S. Ryder, *J. Chem. Soc., Chem. Commun.* 697 (1995).
135. P. N. Bartlett and J. Farington, *J. Electroanal. Chem.* 261, 471 (1989).
136. I. G. Casella, T. R. I. Cataldi, A. Guerrieri, and E. Desimoni, *Anal. Chim. Acta* 335, 217 (1996).
137. H. Laborde, J. M. Léger, and C. Lamy, *J. Appl. Electrochem.* 24, 1019 (1994).
138. W. T. Napporn, J. M. Léger, and C. Lamy, *J. Electroanal. Chem.* 408, 141 (1996).
139. A. Leone, W. Marino, and B. R. Scharifker, *J. Electrochem. Soc.* 139, 438 (1992).
140. I. M. F. De Oliveira, J. C. Moutet, and S. Hamar-Thibault, *J. Mater. Chem.* 2, 167 (1992).
141. I. Becerik and F. Kadirgan, *J. Electroanal. Chem.* 436, 189 (1997).
142. S. Swathirajan and Y. M. Mikhail, *J. Electrochem. Soc.* 139, 2105 (1992).
143. W. Lu, G. G. Wallace, and A. A. Karayakin, *Electroanalysis* 10, 472 (1998).
144. A. Galal, *J. Solid State Electrochem.* 2, 7 (1998).
145. F. Bedioui, Y. Bouhier, C. Sorel, J. Devynck, L. Coche-Guerente, A. Deronzier, and J. C. Moutet, *Electrochim. Acta* 38, 2485 (1993).
146. F. Bedioui, M. Voisin, J. Devynck, and C. Bied-Charreton, *J. Electroanal. Chem.* 297, 257 (1991).
147. F. Bedioui, S. Gutierrez-Granados, J. Devynck, and C. Bied-Charreton, *New J. Chem.* 15, 939 (1991).
148. S. Gutierrez-Granados, F. Bedioui, and J. Devynck, *Electrochim. Acta* 38, 1747 (1993).
149. M. Sadakane and E. Steckhan, *Chem. Rev.* 98, 219 (1998).
150. B. Fabre, S. Burlet, R. Cespuglio, and G. Bidan, *J. Electroanal. Chem.* 426, 75 (1997).
151. B. Fabre, G. Bidan, R. Cespuglio, and S. Burlet, French Patent CEA/INSERM 94 10290, 1994.
152. B. Keita, A. Belhouari, L. Nadjo, and R. Contant, *J. Electroanal. Chem.* 381, 243 (1995).
153. T. Livache, A. Roget, E. Dejean, C. Barthet, G. Bidan, and R. Téoule, *Nucleic Acids Res.* 22, 2915 (1994).
154. F. Garnier, H. Korri Youssoufi, P. Srivastava, and A. Yassar, *J. Am. Chem. Soc.* 116, 8813 (1994).
155. H. Korri Youssoufi, F. Garnier, P. Srivastava, P. Godillot, and A. Yassar, *J. Am. Chem. Soc.* 119, 7388 (1997).
156. P. Heiduschka, W. Göpel, W. Beck, W. Kraas, S. Kienle, and G. Jung, *Chem. Eur. J.* 2, 667 (1996).
157. P. Bäuerle and A. Emge, *Adv. Mater. (Weinheim, Ger.)* 3, 324 (1998).
158. K. Galasso, T. Livache, A. Roget, and E. Vieil, *J. Chim. Phys.* 95, 1514 (1998).
159. L. M. Torres-Rodriguez, A. Roget, M. Billon, T. Livache, and G. Bidan, *Chem. Commun.* 1993 (1998).
160. K. Faïd and M. Leclerc, *J. Am. Chem. Soc.* 120, 5274 (1998).
161. P. Englebienne and M. Weiland, *Chem. Commun.* 1651 (1996).
162. C. Lagrost, J. C. Lacroix, S. Aeyach, M. Jouini, K. I. Chane-Ching, and P. C. Lacaze, *Chem. Commun.* 489 (1998).
163. G. Bidan, A. Gabelle, R. Téoule, and E. Vieil, *Sens. Mater.* 8, 179 (1996).
164. J. M. Charlesworth, A. C. Partridge, and N. Garrard, *J. Phys. Chem.* 97, 5418 (1993).
165. T. Hanawa, S. Kuwabata, and H. Yoneyama, *J. Chem. Soc., Faraday Trans.* 1 84, 1587 (1988).
166. T. Hanawa and H. Yoneyama, *Synth. Met.* 30, 341 (1989).
167. J. J. Miasik, A. Hooper, and B. C. Tofield, *J. Chem. Soc., Faraday Trans.* 1 82, 1117 (1986).
168. G. E. Collins and L. J. Buckley, *Synth. Met.* 78, 93 (1996).
169. T. Hanawa, S. Kuwabata, H. Hashimoto, and H. Yoneyama, *Synth. Met.* 30, 173 (1989).
170. S. Dogan, U. Akbulut, T. Yalcin, S. Suzer, and L. Toppare, *Synth. Met.* 60, 27 (1993).
171. A. Boyle, E. M. Geniès, and M. Lapkowski, *Synth. Met.* 28, C769 (1989).
172. C. Budrowski and J. Przyluski, *Synth. Met.* 41–43, 597 (1991).
173. J. Przyluski and C. Budrowski, *Synth. Met.* 41–43, 1163 (1991).
174. M. Josowicz, J. Janata, K. Ashley, and S. Pons, *Anal. Chem.* 59, 253 (1987).
175. M. Josowicz and J. Janata, *Anal. Chem.* 58, 514 (1986).
176. R. Cabala, V. Meister, and K. Potje-Kamloth, *J. Chem. Soc., Faraday Trans.* 93, 131 (1997).
177. Y. Ohmori, K. Muro, and K. Yoshino, *Synth. Met.* 55–57, 4111 (1993).
178. J. Langmaier and J. Janata, *Anal. Chem.* 64, 523 (1992).
179. Q. Pei and O. Inganäs, *Synth. Met.* 55–57, 3730 (1993).
180. Z. Deng, D. C. Stone, and M. Thompson, *Can. J. Chem.* 73, 1427 (1995).
181. Z. Deng, D. C. Stone, and M. Thompson, *Analyst (Cambridge, U.K.)* 121, 1341 (1996).
182. Z. Deng, D. C. Stone, and M. Thompson, *Analyst (Cambridge, U.K.)* 122, 1129 (1997).
183. J. Kankare and I. A. Vinokurov, *Anal. Chem.* 69, 2337 (1997).
184. B. Bott and T. A. Jones, *Sens. Actuators* 5, 43 (1984).
185. J. W. Thackeray and M. S. Wrighton, *J. Phys. Chem.* 90, 6674 (1986).
186. B. Fabre, G. Bidan, and D. Fichou, *J. Chim. Phys.* 89, 1053 (1992).
187. G. Bidan, E. M. Geniès, and M. Lapkowski, *Synth. Met.* 31, 327 (1989).
188. G. Bidan, E. M. Geniès, and M. Lapkowski, *J. Chem. Soc., Chem. Commun.* 533 (1988).
189. M. Hasik, A. Pron, J. Pozniczek, A. Bielanski, Z. Piwowska, K. Kruczala, and R. Dziembaj, *J. Chem. Soc., Faraday Trans.* 90, 2099 (1994).
190. P. Wang and Y. Li, *J. Electroanal. Chem.* 408, 77 (1996).
191. S. Dong, Q. Qiu, R. Guillard, and A. Tabard, *J. Electroanal. Chem.* 372, 171 (1994).
192. C. Coutanceau, P. Crouigneau, J. M. Léger, and C. Lamy, *J. Electroanal. Chem.* 379, 389 (1994).
193. J. Losada, I. Del Peso, L. Beyer, J. Hartung, V. Fernandez, and M. Möbius, *J. Electroanal. Chem.* 398, 89 (1995).

194. M. C. Pham and J. E. Dubois, *J. Electroanal. Chem.* 199, 153 (1986).
195. M. R. Anderson, B. R. Mattes, H. Reiss, and R. B. Kaner, *Science (Washington, D.C.)* 252, 1412 (1991).
196. M. R. Anderson, B. R. Mattes, H. Reiss, and R. B. Kaner, *Synth. Met.* 41-43, 1151 (1991).
197. B. R. Mattes, M. R. Anderson, J. A. Conklin, H. Reiss, and R. B. Kaner, *Synth. Met.* 55-57, 3655 (1993).
198. L. Coche and J. C. Moutet, *J. Am. Chem. Soc.* 109, 6887 (1987).
199. L. Coche, B. Ehui, D. Limosin, and J. C. Moutet, *J. Org. Chem.* 55, 5905 (1990).
200. L. Coche, A. Deronzier, and J. C. Moutet, *J. Electroanal. Chem.* 198, 187 (1986).
201. S. Cosnier, A. Deronzier, and J. C. Moutet, *Inorg. Chem.* 27, 2389 (1988).
202. W. F. De Giovanni and A. Deronzier, *J. Electroanal. Chem.* 337, 285 (1992).
203. F. Bedioui, J. Devynck, and C. Bied-Charreton, *Acc. Chem. Res.* 28, 30 (1995).
204. F. Bedioui, C. Bongars, J. Devynck, C. Bied-Charreton, and C. Hinnen, *J. Electroanal. Chem.* 207, 87 (1986).
205. M. Lemaire, D. Delabouglise, R. Garreau, A. Guy, and J. Roncali, *J. Chem. Soc., Chem. Commun.* 658 (1988).
206. D. Delabouglise and F. Garnier, *Synth. Met.* 39, 117 (1990).
207. M. Lemaire, D. Delabouglise, R. Garreau, and J. Roncali, *J. Chim. Phys.* 86, 193 (1989).
208. J. C. Moutet, E. Saint-Aman, F. Tran-Van, P. Angibeaud, and J. P. Utille, *Adv. Mater. (Weinheim, Ger.)* 4, 511 (1992).
209. K. S. Ryder, D. G. Morris, and J. M. Cooper, *J. Chem. Soc., Chem. Commun.* 1471 (1995).
210. E. Schulz, V. Bethmont, K. Fahmi, F. Fache, and M. Lemaire, *J. Chim. Phys.* 92, 783 (1995).
211. J. Rault-Berthelot, E. Raoult, J. Tahri-Hassani, H. Le Deit, and J. Simonet, *Electrochim. Acta* 44, 3409 (1999).
212. M. Salmon and G. Bidan, *J. Electrochem. Soc.* 132, 1897 (1985).
213. M. Salmon, M. Saloma, G. Bidan, and E. M. Genies, *Electrochim. Acta* 34, 117 (1989).
214. T. Komori and T. Nonaka, *J. Am. Chem. Soc.* 106, 2656 (1984).
215. M. Schwientek, S. Pleus, and C. H. Hamann, *J. Electroanal. Chem.* 461, 94 (1999).
216. D. Kotkar, V. Joshi, and P. K. Ghosh, *J. Chem. Soc., Chem. Commun.* 917 (1988).
217. G. Bidan, S. Guillerez, and V. Sorokin, *Adv. Mater. (Weinheim, Ger.)* 8, 157 (1996).
218. M. M. Bouman and E. W. Meijer, *Adv. Mater. (Weinheim, Ger.)* 7, 385 (1995).
219. J. C. Moutet, C. Duboc-Toia, S. Ménage, and S. Tingry, *Adv. Mater. (Weinheim, Ger.)* 10, 665 (1998).
220. J. Papillon, E. Schulz, S. Gélinas, J. Lessard, and M. Lemaire, *Synth. Met.* 96, 155 (1998).
221. C. J. Pedersen, *J. Am. Chem. Soc.* 89, 7017 (1967).
222. C. J. Pedersen, *Angew. Chem., Int. Ed. Engl.* 27, 1021 (1988).
223. J. M. Lehn, "Structure and Bonding," p. 1. Springer-Verlag, Berlin, 1973.
224. J. M. Lehn, *Angew. Chem., Int. Ed. Engl.* 27, 89 (1988).
225. D. J. Cram, *Angew. Chem., Int. Ed. Engl.* 27, 1009 (1988).
226. F. Vögtle and H. Sieger, *Angew. Chem., Int. Ed. Engl.* 16, 396 (1977).
227. C. J. Pedersen and H. K. Frensdorff, *Angew. Chem., Int. Ed. Engl.* 11, 16 (1972).
228. C. J. Pedersen, *J. Am. Chem. Soc.* 92, 386 (1970).
229. P. D. Beer, *Adv. Inorg. Chem.* 39, 79 (1992).
230. P. D. Beer, *Chem. Soc. Rev.* 18, 409 (1989).
231. T. Jorgensen, T. K. Hansen, and J. Becher, *Chem. Soc. Rev.* 23, 41 (1994).
232. R. E. Wolf, Jr., and S. R. Cooper, *J. Am. Chem. Soc.* 106, 4646 (1984).
233. D. A. Gustowski, M. Delgado, V. J. Gatto, L. Echegoyen, and G. W. Gokel, *J. Am. Chem. Soc.* 108, 7553 (1986).
234. A. Kaifer, L. Echegoyen, D. A. Gustowski, D. M. Goli, and G. W. Gokel, *J. Am. Chem. Soc.* 105, 7168 (1983).
235. A. Kaifer, D. A. Gustowski, L. Echegoyen, V. J. Gatto, R. A. Schultz, T. P. Cleary, C. R. Morgan, D. M. Goli, A. M. Rios, and G. W. Gokel, *J. Am. Chem. Soc.* 107, 1958 (1985).
236. M. Lemaire, R. Garreau, J. Roncali, D. Delabouglise, H. Korri-Youssoufi, and F. Garnier, *New J. Chem.* 13, 863 (1989).
237. J. Roncali, R. Garreau, D. Delabouglise, F. Garnier, and M. Lemaire, *J. Chem. Soc., Chem. Commun.* 679 (1989).
238. J. Roncali, P. Marque, R. Garreau, F. Garnier, and M. Lemaire, *Macromolecules* 23, 1347 (1990).
239. J. Roncali, M. Lemaire, F. Garnier, and R. Garreau, *Mol. Cryst. Sci. Technol. Liq. Cryst.* 235, 35 (1993).
240. J. Roncali, L. H. Shi, R. Garreau, F. Garnier, and M. Lemaire, *Synth. Met.* 36, 267 (1990).
241. J. Roncali, L. H. Shi, and F. Garnier, *J. Phys. Chem.* 95, 8983 (1991).
242. L. H. Shi, F. Garnier, and J. Roncali, *Synth. Met.* 41-43, 547 (1991).
243. J. Roncali, R. Garreau, D. Delabouglise, F. Garnier, and M. Lemaire, *Synth. Met.* 28, C341 (1989).
244. I. Lévesque and M. Leclerc, *J. Chem. Soc., Chem. Commun.* 2293 (1995).
245. I. Lévesque and M. Leclerc, *Chem. Mater.* 8, 2843 (1996).
246. R. D. McCullough, S. P. Williams, S. Tristram-Nagle, M. Jayaraman, P. C. Ewbank, and L. Miller, *Synth. Met.* 69, 279 (1995).
247. R. D. McCullough and S. P. Williams, *Chem. Mater.* 7, 2001 (1995).
248. R. D. McCullough and S. P. Williams, *J. Am. Chem. Soc.* 115, 11608 (1993).
249. R. D. McCullough, S. P. Williams, and M. Jayaraman, *Polym. Prepr. (Am. Chem. Soc., Div. Polym. Chem.)* 35, 190 (1994).
250. J. Roncali, R. Garreau, and M. Lemaire, *J. Electroanal. Chem.* 278, 373 (1990).
251. J. M. Barker, J. D. E. Chaffin, J. Halfpenny, P. R. Huddleston, and P. F. Tseki, *J. Chem. Soc., Chem. Commun.* 1733 (1993).
252. P. Marrec, Thesis, University of Rennes 1, France, 1996.
253. P. Marrec, B. Fabre, and J. Simonet, *J. Electroanal. Chem.* 437, 245 (1997).
254. R. A. Robinson and R. H. Stokes, "Electrolyte Solutions," p. 461. Butterworths Scientific Publications, London, 1959.
255. D. Delabouglise and F. Garnier, *Adv. Mater. (Weinheim, Ger.)* 2, 91 (1990).
256. Y. Gache, Thesis, University of Rennes 1, France, 1993.
257. J. Simonet, Y. Gache, and N. Simonet, French Patent EDF 9308789, 1993.
258. B. Fabre, P. Marrec, and J. Simonet, *J. Electrochem. Soc.* 145, 4110 (1998).
259. B. Fabre and J. Simonet, in preparation.
260. P. Bäuerle and S. Scheib, *Acta Polym.* 46, 124 (1995).
261. P. Bäuerle and S. Scheib, *Adv. Mater. (Weinheim, Ger.)* 5, 848 (1993).
262. T. M. Swager, *Acc. Chem. Res.* 31, 201 (1998).
263. M. J. Marsella and T. M. Swager, *J. Am. Chem. Soc.* 115, 12214 (1993).
264. M. J. Marsella, P. J. Carroll, and T. M. Swager, *J. Am. Chem. Soc.* 116, 9347 (1994).
265. M. J. Marsella, P. J. Carroll, and T. M. Swager, *J. Am. Chem. Soc.* 117, 9832 (1995).
266. J. L. Reddinger and J. R. Reynolds, *Chem. Mater.* 10, 3 (1998).
267. H. Korri Youssoufi, M. Hmyene, F. Garnier, and D. Delabouglise, *J. Chem. Soc., Chem. Commun.* 1550 (1993).
268. H. Korri Youssoufi, A. Yassar, S. Baïteche, M. Hmyene, and F. Garnier, *Synth. Met.* 67, 251 (1994).
269. P. N. Bartlett, A. C. Benniston, L. Y. Chung, D. H. Dawson, and P. Moore, *Electrochim. Acta* 36, 1377 (1991).
270. A. Ion, I. Ion, A. Popescu, M. Ungureanu, J. C. Moutet, and E. Saint-Aman, *Adv. Mater. (Weinheim, Ger.)* 9, 711 (1997).
271. J. C. Moutet, A. Popescu, E. Saint-Aman, and L. Tomaszewski, *Electrochim. Acta* 43, 2257 (1998).
272. H. Korri Youssoufi, P. Godillot, P. Srivastava, A. El Kassmi, and F. Garnier, *Synth. Met.* 84, 169 (1997).

273. V. Le Berre, L. Angely, N. Simonet-Gueguen, and J. Simonet, *New J. Chem.* 13, 131 (1989).
274. J. Simonet and J. M. Chapuzet, *J. Electroanal. Chem.* 322, 399 (1992).
275. J. M. Chapuzet, Thesis, University of Rennes 1, France, 1991.
276. B. Fabre and J. Simonet, *Coord. Chem. Rev.* 178–180, 1211 (1998).
277. B. Fabre and J. Simonet, *Curr. Top. Electrochem.*, in press.
278. V. Le Berre, Thesis, University of Rennes 1, France, 1987.
279. V. Le Berre, L. Angely, N. Simonet-Gueguen, and J. Simonet, *New J. Chem.* 9, 419 (1985).
280. V. Le Berre, L. Angely, N. Simonet-Gueguen, and J. Simonet, *J. Electroanal. Chem.* 240, 117 (1988).
281. V. Le Berre, L. Angely, N. Simonet-Gueguen, and J. Simonet, *J. Electroanal. Chem.* 206, 115 (1986).
282. L. Angely, V. Questaigne, and J. Rault-Berthelot, *Synth. Met.* 52, 111 (1992).
283. L. Angely, J. Rault-Berthelot, and G. Peslerbe, *Synth. Met.* 52, 273 (1992).
284. J. Rault-Berthelot and L. Angely, *Synth. Met.* 58, 51 (1993).
285. J. Rault-Berthelot and L. Angely, *Synth. Met.* 65, 55 (1994).
286. A. Morin, F. Bénérière, L. Angely, J. Rault-Berthelot, and J. Simonet, *J. Chem. Soc., Faraday Trans.* 87, 1393 (1991).
287. J. Simonet, H. Patillon, C. Belloncle, N. Simonet-Gueguen, and P. Cauliez, *Synth. Met.* 75, 103 (1995).
288. Y. L. Ma, A. Galal, S. K. Lunsford, H. Zimmer, H. B. Mark, Jr., Z. F. Huang, and P. B. Bishop, *Biosens. Bioelectron.* 10, 705 (1995).
289. Y. L. Ma, A. Galal, H. Zimmer, H. B. Mark, Jr., Z. F. Huang, and P. B. Bishop, *Anal. Chim. Acta* 289, 21 (1994).
290. L. Pu, *Acta Polym.* 48, 116 (1997).
291. C. Belloncle, Thesis, University of Rennes 1, France, 1997.
292. C. Belloncle, B. Fabre, P. Cauliez, and J. Simonet, *Synth. Met.* 93, 115 (1998).
293. C. Belloncle, P. Cauliez, and J. Simonet, *J. Electroanal. Chem.* 444, 101 (1998).
294. D. J. Cram and K. N. Trueblood, *Top. Curr. Chem.* 98, 43 (1981).
295. D. J. Cram, R. C. Helgeson, K. Koga, E. P. Kyba, K. Madan, L. R. Souza, M. G. Siegel, P. Moreau, G. W. Gokel, J. M. Timko, and G. D. Y. Sogah, *J. Org. Chem.* 43, 2758 (1978).
296. R. C. Helgeson, G. R. Weisman, J. L. Toner, T. L. Tarnowski, Y. Chao, J. M. Mayer, and D. J. Cram, *J. Am. Chem. Soc.* 101, 4928 (1979).
297. L. R. Souza, G. D. Y. Sogah, D. H. Hoffman, and D. J. Cram, *J. Am. Chem. Soc.* 100, 4569 (1978).
298. G. D. Y. Sogah and D. J. Cram, *J. Am. Chem. Soc.* 101, 3035 (1979).
299. C. D. Gutsche, *Acc. Chem. Res.* 16, 161 (1983).
300. S. Shinkai, *Tetrahedron* 49, 8933 (1993).
301. F. Arnaud-Neu and M. J. Schwing-Weill, *Synth. Met.* 90, 157 (1997).
302. M. J. Marsella, R. J. Newland, P. J. Carroll, and T. M. Swager, *J. Am. Chem. Soc.* 117, 9842 (1995).
303. K. B. Crawford, M. B. Goldfinger, and T. M. Swager, *J. Am. Chem. Soc.* 120, 5187 (1998).
304. Z. Chen, P. A. Gale, and P. D. Beer, *J. Electroanal. Chem.* 393, 113 (1995).
305. A. Buffenoir, G. Bidan, L. Chalumeau, and I. Soury-Lavergne, *J. Electroanal. Chem.* 451, 261 (1998).
306. A. Buffenoir and G. Bidan, *J. Chim. Phys.* 95, 1547 (1998).
307. H. Cano-Yelo Bettega, M. Hissler, J. C. Moutet, and R. Ziessel, *Chem. Mater.* 9, 3 (1997).
308. G. Bidan and M. A. Niel, *Synth. Met.* 85, 1387 (1997).
309. K. Kaneto and G. Bidan, *Thin Solid Films* 331, 272 (1998).
310. D. B. Amabilino and J. F. Stoddart, *Chem. Rev.* 95, 2725 (1995).
311. A. Harriman, V. Heitz, and J. P. Sauvage, *J. Phys. Chem.* 97, 5940 (1993).
312. J. C. Chambron, A. Harriman, V. Heitz, and J. P. Sauvage, *J. Am. Chem. Soc.* 115, 6109 (1993).
313. E. Cordova, A. E. Kaifer, and J. F. Stoddart, *Nature (London)* 369, 1330 (1994).
314. P. R. Ashton, R. Ballardini, V. Balzani, S. E. Boyd, A. Credi, M. T. Gandolfi, M. Gomez-Lopez, S. Iqbal, D. Philp, J. A. Preece, L. Prodi, H. G. Ricketts, J. F. Stoddart, M. S. Tolley, M. Venturi, A. J. P. White, and D. J. Williams, *Chem. Eur. J.* 3, 152 (1997).
315. J. P. Collin, P. Gavina, and J. P. Sauvage, *New J. Chem.* 21, 525 (1997).
316. J. P. Sauvage, *Acc. Chem. Res.* 31, 611 (1998).
317. G. Bidan, B. Divisia-Blohorn, J. M. Kern, and J. P. Sauvage, *J. Chem. Soc., Chem. Commun.* 723 (1988).
318. G. Bidan, B. Divisia-Blohorn, M. Lapkowski, J. M. Kern, and J. P. Sauvage, *J. Am. Chem. Soc.* 114, 5986 (1992).
319. P. Audebert, P. Hapiot, G. Bidan, B. Divisia-Blohorn, M. Billon, J. M. Kern, and J. P. Sauvage, *Synth. Met.* 63, 247 (1994).
320. J. M. Kern, J. P. Sauvage, G. Bidan, M. Billon, and B. Divisia-Blohorn, *Adv. Mater. (Weinheim, Ger.)* 8, 580 (1996).
321. G. Bidan, M. Billon, B. Divisia-Blohorn, J. M. Kern, L. Raehm, and J. P. Sauvage, *New J. Chem.* 1139 (1998).
322. P. L. Vidal, M. Billon, B. Divisia-Blohorn, G. Bidan, J. M. Kern, and J. P. Sauvage, *Chem. Commun.* 629 (1998).
323. S. S. Zhu, P. J. Carroll, and T. M. Swager, *J. Am. Chem. Soc.* 118, 8713 (1996).
324. S. S. Zhu and T. M. Swager, *J. Am. Chem. Soc.* 119, 12568 (1997).
325. J. Tamm, A. Alumaa, A. Hallik, and V. Sammelselg, *J. Electroanal. Chem.* 448, 25 (1998).
326. J. Tamm, A. Alumaa, A. Hallik, T. Silk, and V. Sammelselg, *J. Electroanal. Chem.* 414, 149 (1996).
327. T. Momma, S. Komaba, T. Osaka, S. Nakamura, and Y. Takemura, *Bull. Chem. Soc. Jpn.* 68, 1297 (1995).
328. Q. X. Zhou, L. L. Miller, and J. R. Valentine, *J. Electroanal. Chem.* 261, 147 (1989).
329. R. A. Bull, F. R. Fan, and A. J. Bard, *J. Electrochem. Soc.* 130, 1636 (1983).
330. L. L. Miller and Q. X. Zhou, *Macromolecules* 20, 1594 (1987).
331. K. K. Shiu, S. K. Pang, and H. K. Cheung, *J. Electroanal. Chem.* 367, 115 (1994).
332. K. K. Shiu, O. Y. Chan, and S. K. Pang, *Anal. Chem.* 67, 2828 (1995).
333. M. R. Nateghi, A. Bagheri, A. Massoumi, and M. H. Kazemeini, *Synth. Met.* 96, 209 (1998).
334. D. M. T. O'Riordan and G. G. Wallace, *Anal. Chem.* 58, 128 (1986).
335. J. S. Foos, S. M. Degnan, D. G. Glennon, and X. Beebe, *J. Electrochem. Soc.* 137, 2530 (1990).
336. C. N. Aquino-Binag, N. Kumar, R. N. Lamb, and P. J. Pigram, *Chem. Mater.* 8, 2579 (1996).
337. H. Korri Youssoufi, F. Garnier, A. Yassar, S. Baïteche, and P. Srivastava, *Adv. Mater. (Weinheim, Ger.)* 6, 755 (1994).
338. D. Delabouglise and F. Garnier, *New J. Chem.* 15, 233 (1991).
339. P. Bäuerle, K. U. Gaudl, F. Würthner, N. S. Sariciffci, H. Neugebauer, M. Mehring, C. Zhong, and K. Doblhofer, *Adv. Mater. (Weinheim, Ger.)* 2, 490 (1990).
340. P. G. Pickup, *J. Electroanal. Chem.* 225, 273 (1987).
341. X. Ren and P. G. Pickup, *J. Electrochem. Soc.* 139, 2097 (1992).
342. R. D. McCullough, P. C. Ewbank, and R. S. Loewe, *J. Am. Chem. Soc.* 119, 633 (1997).
343. D. Millar, M. Uttamlal, R. Henderson, and A. Keeper, *Chem. Commun.* 477 (1998).
344. K. Yamamoto, T. Asada, H. Nishide, and E. Tsuchida, *Bull. Chem. Soc. Jpn.* 63, 1211 (1990).
345. P. Wang, B. D. Martin, S. Parida, D. G. Rethwisch, and J. S. Dordick, *J. Am. Chem. Soc.* 117, 12885 (1995).
346. E. Pringsheim, E. Terpetschnig, and O. S. Wolfbeis, *Anal. Chim. Acta* 357, 247 (1997).
347. D. Orata and D. A. Buttry, *J. Am. Chem. Soc.* 109, 3574 (1987).
348. E. M. Geniès, A. Boyle, M. Lapkowski, and C. Tsintavis, *Synth. Met.* 36, 139 (1990).
349. C. A. Lindino and L. O. S. Bulhões, *Anal. Chim. Acta* 334, 317 (1996).
350. L. Jin, Z. Shi, J. Ye, J. Qian, and Y. Fang, *Anal. Chim. Acta* 244, 165 (1991).

351. J. W. Lee, D. S. Park, Y. B. Shim, and S. M. Park, *J. Electrochem. Soc.* 139, 3507 (1992).
352. F. Daire, F. Bedioui, J. Devynck, and C. Bied-Charreton, *J. Electroanal. Chem.* 205, 309 (1986).
353. G. Bidan, A. Deronzier, and J. C. Moutet, *Nouv. J. Chim.* 8, 501 (1984).
354. S. Cosnier, A. Deronzier, and J. C. Moutet, *J. Electroanal. Chem.* 193, 193 (1985).
355. S. Cosnier, A. Deronzier, and J. C. Moutet, *J. Electroanal. Chem.* 207, 315 (1986).
356. J. G. Eaves, H. S. Munro, and D. Parker, *J. Chem. Soc., Chem. Commun.* (1985) 684.
357. J. G. Eaves, H. S. Munro, and D. Parker, *Inorg. Chem.* 26, 644 (1987).
358. B. Wang and M. R. Wasielewski, *J. Am. Chem. Soc.* 119, 12 (1997).
359. J. P. Collin and J. P. Sauvage, *J. Chem. Soc., Chem. Commun.* 1075 (1987).
360. I. Taniguchi, K. Matsushita, M. Okamoto, J. P. Collin, and J. P. Sauvage, *J. Electroanal. Chem.* 280, 221 (1990).
361. A. Bettelheim, B. A. White, S. A. Raybuck, and R. W. Murray, *Inorg. Chem.* 26, 1009 (1987).
362. J. L. Reddinger and J. R. Reynolds, *Chem. Mater.* 10, 1236 (1998).
363. J. L. Reddinger and J. R. Reynolds, *Macromolecules* 30, 673 (1997).
364. R. P. Kingsborough and T. M. Swager, *Adv. Mater. (Weinheim, Ger.)* 10, 1100 (1998).
365. T. B. Higgins and C. A. Mirkin, *Chem. Mater.* 10, 1589 (1998).
366. J. C. Moutet, E. Saint-Aman, M. Ungureanu, and T. Visan, *J. Electroanal. Chem.* 410, 79 (1996).
367. C. J. Pickett, K. S. Ryder, and J. C. Moutet, *J. Chem. Soc., Chem. Commun.* 694 (1992).
368. A. Deronzier, M. Essakalli, and J. C. Moutet, *J. Chem. Soc., Chem. Commun.* 773 (1987).
369. M. M. G. Antonisse and D. N. Reinhoudt, *Chem. Commun.* 443 (1998).
370. P. D. Beer, *Acc. Chem. Res.* 31, 71 (1998).
371. P. D. Beer, J. Cadman, J. M. Lloris, R. Martinez-Manez, M. E. Padilla, T. Pardo, D. K. Smith, and J. Soto, *J. Chem. Soc., Dalton Trans.* 127 (1999).
372. J. E. Kingston, L. Ashford, P. D. Beer, and M. G. B. Drew, *J. Chem. Soc., Dalton Trans.* 251 (1999).
373. J. M. Lloris, R. Martinez-Manez, M. Padilla-Tosta, T. Pardo, J. Soto, and M. J. L. Tenders, *J. Chem. Soc., Dalton Trans.* 3657 (1998).
374. C. Lopez, J. C. Moutet, and E. Saint-Aman, *J. Chem. Soc., Faraday Trans.* 92, 1527 (1996).
375. M. Nicolas, B. Fabre, and J. Simonet, *Chem. Commun.*, in press.
376. T. D. James, K. R. A. Samankumara Sandanayake, and S. Shinkai, *Angew. Chem. Int. Ed. Engl.* 35, 1910 (1996).
377. C. R. Cooper, N. Spencer, and T. D. James, *Chem. Commun.* 1365 (1998).
378. H. Yamamoto, A. Ori, K. Ueda, C. Dusemund, and S. Shinkai, *Chem. Commun.* 407 (1996).
379. C. Dusemund, K. R. A. Samankumara Sandanayake, and S. Shinkai, *J. Chem. Soc., Chem. Commun.* 333 (1995).
380. B. Fabre, G. Bidan, and M. Lapkowski, *J. Chem. Soc., Chem. Commun.* 1509 (1994).
381. B. Fabre, G. Bidan, and M. Lapkowski, French Patent CEA 93 03588, 1993.
382. B. Fabre and G. Bidan, *J. Chem. Soc., Faraday Trans.* 93, 591 (1997).
383. B. Fabre and G. Bidan, *Electrochim. Acta* 42, 2587 (1997).
384. K. K. Shiu and F. C. Anson, *J. Electroanal. Chem.* 309, 115 (1991).
385. J. E. Toth and F. C. Anson, *J. Am. Chem. Soc.* 111, 2444 (1989).
386. B. Fabre, *Synth. Met.* 89, 125 (1997).
387. R. M. Crooks and A. J. Ricco, *Acc. Chem. Res.* 31, 219 (1998).
388. I. K. Lednev and M. C. Petty, *Adv. Mater. (Weinheim, Ger.)* 8, 615 (1996).
389. Y. Q. Wang, H. Z. Yu, T. Mu, Y. Luo, C. X. Zhao, and Z. F. Liu, *J. Electroanal. Chem.* 438, 127 (1997).
390. S. Flink, B. A. Boukamp, A. Van den Berg, F. C. Van Veggel, and D. N. Reinhoudt, *J. Am. Chem. Soc.* 120, 4652 (1998).
391. F. Arias, L. A. Godinez, S. R. Wilson, A. E. Kaifer, and L. Echegoyen, *J. Am. Chem. Soc.* 118, 6086 (1996).
392. A. R. Bernardo, T. Lu, E. Cordova, L. Zhang, G. W. Gokel, and A. E. Kaifer, *J. Chem. Soc., Chem. Commun.* 529 (1994).
393. M. T. Rojas, R. Königer, J. F. Stoddart, and A. E. Kaifer, *J. Am. Chem. Soc.* 117, 336 (1995).
394. A. E. Kaifer, *Acc. Chem. Res.* 32, 62 (1999).
395. T. Lu, L. Zhang, G. W. Gokel, and A. E. Kaifer, *J. Am. Chem. Soc.* 115, 2542 (1993).
396. M. T. Rojas and A. E. Kaifer, *J. Am. Chem. Soc.* 117, 5883 (1995).
397. J. Stepp and J. B. Schlenoff, *J. Electrochem. Soc.* 144, L155 (1997).
398. T. Lötzbeier, W. Schuhmann, and H.-L. Schmidt, *J. Electroanal. Chem.* 395, 341 (1995).
399. K. Araki, M. J. Wagner, and M. S. Wrighton, *Langmuir* 12, 5393 (1996).
400. I. Willner, N. Lapidot, A. Riklin, R. Kasher, E. Zahavy, and E. Katz, *J. Am. Chem. Soc.* 116, 1428 (1994).
401. I. Willner, M. Lion-Dagan, S. Marx-Tibbon, and E. Katz, *J. Am. Chem. Soc.* 117, 6581 (1995).
402. A. Riklin and I. Willner, *Anal. Chem.* 67, 4118 (1995).
403. G. R. Newkome, C. N. Moorefield, and F. Vögtle, "Dendritic Molecules," VCH, Weinheim, 1996.
404. M. Fischer and F. Vögtle, *Angew. Chem., Int. Ed. Engl.* 38, 884 (1999).
405. J. P. Majoral and A. M. Caminade, *Chem. Rev.* 99, 845 (1999).
406. N. Ardoin and D. Astruc, *Bull. Soc. Chim. Fr.* 132, 875 (1995).
407. J. Losada, I. Cuadrado, M. Moran, C. M. Casado, B. Alonso, and M. Barranco, *Anal. Chim. Acta* 338, 191 (1997).
408. I. Cuadrado, C. M. Casado, B. Alonso, M. Moran, J. Losada, and V. Belsky, *J. Am. Chem. Soc.* 119, 7613 (1997).
409. C. M. Casado, I. Cuadrado, B. Alonso, M. Moran, and J. Losada, *J. Electroanal. Chem.* 463, 87 (1999).
410. B. Alonso, M. Moran, C. M. Casado, F. Lobete, J. Losada, and I. Cuadrado, *Chem. Mater.* 7, 1440 (1995).

This Page Intentionally Left Blank

Chapter 3

POLYACETYLENE AND ITS ANALOGS: SYNTHESIS AND PHYSICAL PROPERTIES

Kristen J. Steenberg Harrell, SonBinh T. Nguyen
Department of Chemistry, Northwestern University, Evanston, Illinois, USA

Contents

1. Introduction	132
2. Polyacetylene	132
2.1. The Discovery of PA	132
2.2. Shirakawa's Method for the Polymerization of Acetylene	132
2.3. Properties of Shirakawa-Type PA	133
2.4. Modifications of the Shirakawa Method	134
2.5. Other Catalysts for the Polymerization of Acetylene	137
2.6. Precursor Routes to PA	138
2.7. Copolymers of PA	141
3. Substituted PA	145
3.1. Synthesis of Substituted PA	145
3.2. Living Systems	148
3.3. Stereospecific Polymerizations	148
3.4. Silicon-Substituted Alkyne Monomers	148
3.5. ROMP of RCOT	149
3.6. α , ω -Diyne	149
3.7. Indirect Routes to Substituted PA	150
3.8. Properties of Substituted PA	150
4. Electronic Properties of PA and Its Analogs	150
4.1. Conductivity and Chemical Doping	150
4.2. Solitons	151
4.3. <i>cis</i> - to <i>trans</i> -Isomerization	154
4.4. Electrochemical Doping	154
4.5. Photochemical Doping	154
5. Applications of PA and Its Analogs	154
5.1. Semiconductor Devices	155
5.2. Rechargeable Batteries	155
5.3. Solar Cells	155
5.4. Environmental Sensing Technology Based on PA	155
5.5. Gas-Liquid Separation Membranes	156
5.6. Other Applications of PA and Its Analogs	157
6. Conclusion	157
Acknowledgments	157
Nomenclature	157
References	158

Handbook of Advanced Electronic and Photonic Materials and Devices, edited by H.S. Nalwa
Volume 8: *Conducting Polymers*

Copyright © 2001 by Academic Press

All rights of reproduction in any form reserved.

1. INTRODUCTION

Polyacetylene (PA), $(\text{CH})_n$, has long been viewed as the prototypical conjugated polymer because of its structural simplicity. It is composed of only carbon and hydrogen, with double bonds alternating down a linear backbone. Despite its elementary structure and long history of over 40 years, PA has remained within the confines of research and development due to limitations in its processability and stability. Because PA has conjugated π electrons, it has a low oxidation potential, allowing for facile oxidation [1]. Additionally, PA has a large electron affinity, so it can be easily reduced. These features give PA and its analogs unique properties, such as electrical conductivity and nonlinear optical behaviors. Researchers have envisioned using these polymers for solar cells, rechargeable batteries, antistatic devices, circuits, and gas and liquid separation membranes. Because of the unsolved processing and stability issues and the potential for commercial use, the chemistry of PA is still a vibrant research area today, with about 300 papers published each year in various journals. The aim of this review is to provide the reader with a general overview of the synthesis, processing, and potential applications of PA. For more in-depth reading on topics in this review, the reader is encouraged to address the reviews and the original references listed at the end of this chapter. Specifically, the synthesis and properties of PA have been reviewed recently by Curran et al. [2]. Leung has written a monograph on the synthesis and modification of electrically conductive PA copolymers [3].

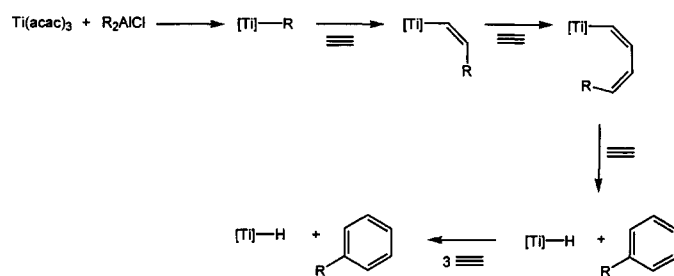
2. POLYACETYLENE

2.1. The Discovery of PA

In 1958, Natta tried to synthesize PA by bubbling acetylene gas through a titanium/trialkyl aluminum catalyst solution while stirring. One of the products in the reaction was a black, semicrystalline powder that was completely insoluble and unstable in the presence of air and water [4]. Although no analyses could be made, Natta assumed that he had made a high-molecular-weight, mostly *trans*, PA. Subsequently, PA was observed as a side product in the attempts to cyclotrimerize and cyclotetramerize acetylene [5].

During the two decades following Natta's report, early transition metal Ziegler–Natta catalysts were heavily explored as potential catalysts for PA synthesis. However, it was not until 1971 that $\text{Ti}(\text{O}i\text{Bu})_4/\text{AlEt}_3$ was found to produce PA exclusively [6], a discovery which led to an explosion of research activity in this field. Another system, $\text{Ti}(\text{acac})_3/\text{Et}_2\text{AlCl}$ (*acac* = acetylacetonato) produced mostly benzene, trace amounts of ethyl benzene, and only a small amount of PA (Scheme I) [7]. The benzene and ethyl benzene are produced because the propagating chain end forms a *cisoid* structure with this particular catalyst. After three or four acetylene insertions, the metal center can easily reductively eliminate the cyclic products.

Because of PA's extended π -system, its chains are rigid rods and are therefore insoluble in organic solvents and intractable. PA is also highly air-sensitive. While exposure to oxygen will initially dope the chain, giving a rise in conductivity (*vide infra*), oxidation is facile and causes the formation of carbonyls and hydroxyls in the PA backbone. PA degrades by simple aging as well, probably because of the presence of residual catalyst or other impurities. The π bonds in the PA backbone are also very susceptible to



Scheme I. A proposed mechanism for the $[\text{Ti}(\text{acac})_3]/\text{R}_2\text{AlCl}$ -catalyzed cyclotrimerization of acetylene.

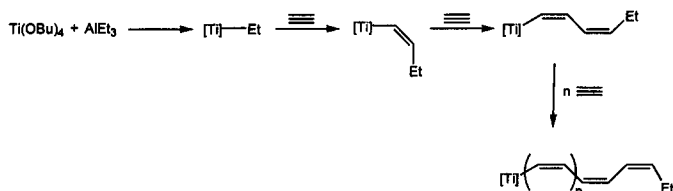
cross-linking reactions. All of this shortens the conjugation length, which ultimately affects the structure and electronic properties of PA. Much of modern research has been aimed at improving the solubility and stability of PA.

2.2. Shirakawa's Method for the Polymerization of Acetylene

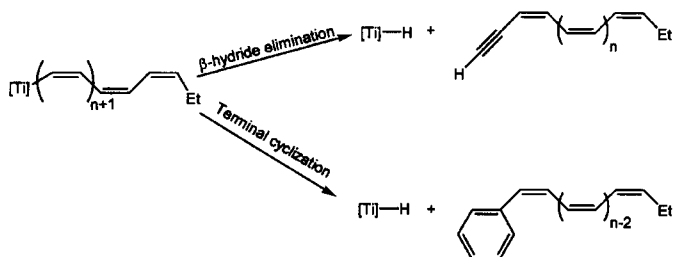
In 1971, Shirakawa revolutionized the fields of PA chemistry and physics with a synthesis of thin PA films that could be manipulated and studied. By 1974, he and his co-workers had fully optimized the method [8]. Shirakawa used high concentrations of catalyst to produce PA films on the metal surface. In a typical experiment, $\text{Ti}(\text{O}i\text{Bu})_4$ was added to a Schlenk flask with 20 ml of toluene followed by the addition of 4 equivalents of the AlEt_3 cocatalyst in an inert atmosphere [9]. The catalyst was aged for 30 min at room temperature. The reaction mixture was degassed at -78°C and then slowly rotated to coat the wall of the flask with catalyst solution. Acetylene gas at 600 torr was introduced at -78°C , and almost immediately the wall of the flask turned a deep red, indicating the formation of a *cis*-PA film. The film turned a coppery color with increasing thickness. When the acetylene pressure dropped to 400–500 torr, the reaction finished. Evacuating the remaining gas terminated the reaction. At first the contents appeared as a homogeneous mixture, but then the PA precipitated out of solution. The PA film was isolated by repeatedly washing it with dry, degassed toluene or hexane until the washings were colorless. It was then removed from the flask and dried under vacuum.

Modifying the acetylene pressure, reaction time, or catalyst concentration can cause variations in the film thickness [9]. The latter effect may be rationalized due to the ability of the monomer to diffuse through the growing film. With a higher concentration of catalyst, the initial polymer film becomes an increasingly denser gel, thus making further monomer diffusion difficult. This diffusion becomes the rate-determining step of the polymerization. The gel permeates the entire reaction solution, forming one mass. This mass is not considered a true gel since it does not swell again after it is dried. It can, however, be pressed into a film that is shiny and smooth. Thus, to obtain a thin PA film a higher concentration of catalyst should be used.

The Shirakawa PA films are shiny, flexible, polycrystalline, and completely insoluble in any solvent. To determine the molecular weight of the polymer, a sample of doped Shirakawa PA was hydrogenated to polyethylene at $175\text{--}260^\circ\text{C}$ for 20 h under a high hydrogen pressure of 30 atm [10–12]. The resulting hydrogenated sample was totally soluble in tetralin. Since linear polyethylene is completely soluble in hot tetralin, it was assumed that Shirakawa's $\text{Ti}(\text{O}i\text{Bu})_4/\text{AlEt}_3$ synthesis produced PA with no



Scheme II. A proposed mechanism for the $[\text{Ti}(\text{OBu})_4]/\text{AlEt}_3$ -catalyzed polymerization of acetylene.



Scheme III. A proposed termination mechanism for Ti-catalyzed polymerization of acetylene.

cross-linking. Molecular weight determinations of the modified polyethylene and back-calculations yield a number-average molecular weight (M_n) between 6000 and 7000 g/mol and a polydispersity index ($\text{PDI} = M_w/M_n$) of ~ 2.4 for the precursor PA. In another instance, it was reported that Shirakawa PA may be chlorinated, but at no point did it become soluble [13]. It was assumed that the polymer must cross-link, either during the synthesis or immediately afterwards, thus making any solubility unrealistic.

A second method for determining the molecular weight of a Shirakawa PA was to terminate the growing chain with radiolabeled methanol [14, 15]. This left tritium on the polymer chain end. The kinetic isotope effect must be taken into account since the rate of reaction of CH_3OH quenching the polymer versus CH_3OT is much faster. After the PA is radioassayed and the kinetic isotope effect is corrected for, the absolute number-average molecular weight can be found. Depending on the reaction conditions, the M_n ranged between 500 and 120,000 g/mol.

The proposed mechanism for acetylene polymerization is shown in Scheme II. It assumes a typical Ziegler-Natta insertion-type mechanism with a *cis* approach of the monomer leading to *cis*-polymer. Two possible modes of termination are assumed: β -hydride elimination and terminal cyclization (Scheme III). The first route produces an acetylenic tail, and the second gives a benzylic end.

2.3. Properties of Shirakawa-Type PA

2.3.1. *cis*- versus *trans*-PA

Four types of *cis* and *trans* structures are possible for PA (Fig. 1). Generally the *trans-transoid* structure is simply termed *trans*, and the *cis-transoid* structure is called *cis*. With the Shirakawa method either *cis*- or *trans*-PA can be synthesized. At a polymerization temperature of -78°C , *cis*-PA is formed exclusively. With increased temperature, a higher percentage of *trans*-PA forms (Table I). *trans*-PA forms exclusively at 150°C . At low temperatures a *cis*-structure arises predominantly from a *cis* insertion of the acetylene into the active site of the catalyst. Fukui and Inagaki suggest that a

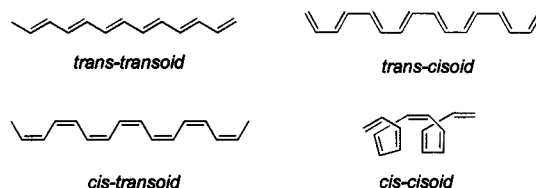


Fig. 1. Four possible stereostructures of PA.

Table I. Percentage *cis*-Structure in PA Prepared by $\text{Ti}(\text{OBu})_4/\text{AlEt}_3$ (1:4) As a Function of Reaction Temperature [9]

Temperature ($^\circ\text{C}$)	% <i>cis</i> -Structure in PA
150	0
100	7
50	32
18	59
0	79
-18	95
-78	98

Table II. Percentage *cis*-Structure in PAs Prepared with Various Catalysts [17]

Catalyst	% <i>cis</i> -Structure in PA
$\text{Ti}(\text{OR})_4/\text{AlEt}_2\text{Cl}$ or AlEtCl_2	0–10
$\text{Ti}(\text{OBu})_4/\text{AlEt}_3$	60
$\text{Ti}(\text{CH}_2\text{Ph})_4$	40
$\text{EuCl}_3/\text{AlEt}_3$	10
$\text{Nd}(\text{Naphthalene})_3/\text{AlEt}_3$	60–70
$\text{WCl}_6/\text{SnPh}_4$	0
$\text{MoCl}_5/\text{SnPh}_4$	0

favorable orbital interaction exists between the active site and the *cis* approach of the monomer [16].

All of the previously mentioned catalysts give a mixture of *cis*- and *trans*-PA (Table II). The specific ratio depends on the nature of the metal, the environment around the active site, and the temperature. In the cases of organoaluminum cocatalysts, changing AlR_3 to AlR_2Cl will increase the amount of *trans*-polymer [17]. *cis*-PA can be isomerized to *trans*-PA simply by heating or doping the sample. *trans*-PA is thermodynamically more stable. The *cis*-to-*trans* isomerization has a barrier of activation, E_{act} , of approximately 11–17 kcal/mol. A large range of values exists, probably because of various degrees of crystallinity in different researchers' samples [18].

2.3.2. Morphology

PA has a highly complex, semicrystalline fibrillar morphology. The diameters of the fibrils vary from 30 Å to 1 μm , as seen by electron microscopy [19–21]. The specific size of the fiber depends on the method of polymerization and, more specifically, the type and

concentration of the catalyst and the solvent. The solvent affects the fibril aggregation, which in turn affects the diameter of the fibrils. For instance, using $\text{Ti}(\text{O}i\text{Bu})_4/\text{AlEt}_3$ in toluene gives PA fibrils with an average diameter of 200 Å, while in benzene the diameter increases to 0.5 μm [17]. Shirakawa and Ikeda also showed that by changing the concentration of the catalyst, the morphology of the PA product varies [22]. With a relatively high concentration of catalyst ($[\text{Ti}] \approx 10^{-1} \text{ M}$) a silvery film of polymer is obtained. A slightly more dilute catalyst solution ($[\text{Ti}] = 10^{-2} \text{ M}$) yields a foam product. With a very dilute catalyst solution ($[\text{Ti}] = 10^{-6} \text{ M}$) a black powder is formed.

Solvent choice will determine the degree of aggregation, but it also plays a role in the catalysis. Coordinating solvents will decrease propagation by hindering access to the active site. On the other hand, coordinating solvents also stabilize the catalyst, so the polymerization may be carried out at an elevated temperature. PA forms fibrous films with polycarbonate, tetrahydrofuran (THF), and dimethylformamide as the reaction solvent [23]. If dioxane is used, no film is formed.

Although stretching the PA film will cause small changes in the morphology, most changes occur during the *cis*-to-*trans* isomerization [24]. To significantly alter the morphology of PA films, synthesis of block and graft copolymers of PA are normally employed.

2.3.3. Optical Properties

Shirakawa PA has a strong $\pi \rightarrow \pi^*$ transition, with $\lambda_{\text{max}} = 594 \text{ nm}$ for all *cis*-PA and $\lambda_{\text{max}} = 700 \text{ nm}$ for all *trans*-PA [9]. *cis*-PA is deep red, but if the film thickness is increased it becomes copper-colored [25]. Likewise, *trans*-PA is deep blue, but with increasing thickness it becomes silvery. For both structures of PA, the extinction coefficient, ϵ_{max} , is about $4 \times 10^5 \text{ l mol}^{-1} \text{ cm}^{-1}$. *cis*-PA is photoluminescent, but the *trans*-form is not [26]. Conversely, *trans*-PA is photoconductive, but *cis*-PA is not. It has been proposed that a photoinduced formation of a soliton-antisoliton (*vide infra*) pair on the PA backbone is responsible for this photoconductivity. In the *trans*-structure the soliton is separated from the antisoliton during the excitation process, which generates photoconductivity. In *trans*-PA these entities never recombine, and hence there is no photoluminescence. On the other hand, in *cis*-PA the soliton and antisoliton migrate and rejoin immediately after photogeneration due to the unfavorable energetics of the separation. This recombination gives rise to photoluminescence.

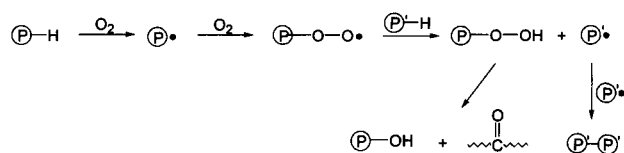
2.3.4. Mechanical Properties

In general, Shirakawa-type PA has low plasticity. The Young's modulus (E) for oriented *cis*-PA and *trans*-PA is 25–30 GPa and 100 GPa, respectively [27, 28]. *cis*-PA is somewhat stretchable, while *trans*-PA is brittle. Any exposure to O_2 will increase the brittleness of both types of films.

2.3.5. Stability

The double bonds in the PA backbone are susceptible to oxidation, leading to degradation of the chain. If PA is to be used commercially, steps must be taken to improve its air stability. Doping PA with oxidizers (p-doping) will stabilize it for longer periods of time. An iodine-doped sample is stable for about 1 week in air [17].

Another method for preventing the air oxidation of PA is to incorporate antioxidizing agents into PA films. The antioxidizing



Scheme IV. A proposed mechanism for the degradation of PA by O_2 .

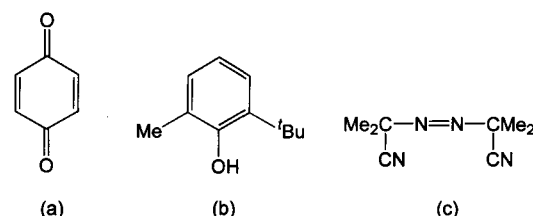


Fig. 2. Antioxidizing agents. (a) Benzoquinone. (b) 2-*t*-Butyl-6-methylphenol. (c) Azo-*bis*(isobutyronitrile).

agents serve as O_2 scavengers and prevent air from attacking the PA chain. Without an oxygen-trapping agent, the backbone quickly cleaves into shorter polymers containing hydroxyls and carbonyls, effectively decreasing the conjugation length (Scheme IV) [29]. Various antioxidizing agents and radical scavengers, including benzoquinone, substituted phenols, and azo-*bis*(isobutyronitrile), have been used (Fig. 2) [17].

2.4. Modifications of the Shirakawa Method

The discovery by Shirakawa and co-workers paved the way for other synthetic PA work and changed the way in which researchers thought about the synthesis and handling of PA. To date, the majority of workers in this area still use Shirakawa's pioneering work as the source for a main method for PA synthesis. Given the ability to make free-standing PA films with high conductivity, other aspects of PA chemistry and physics have been explored and optimized. Table III offers a condensed synopsis of various advances in PA synthesis.

2.4.1. Catalyst Aging

The Shirakawa catalyst was originally aged at room temperature for 30 min [7]. An electron paramagnetic resonance (EPR) spectrum of the aged catalyst shows four distinct Ti(III) signals signifying four active catalysts [30]. Aging the catalyst system at 120°C produces only one active catalyst, as seen by a lone Ti(III) EPR signal.

The catalyst aging temperature affects the density and flexibility of the polymer film [9]. Aging the Ti/Al catalyst mixture at room temperature produces a low-density film ($\sim 0.4 \text{ g/ml}$). Conversely, aging at a higher temperature gives a high-density PA (0.9–1.1 g/ml) that is soft and stretchable.

The catalyst aging time also affects the molecular weight of the PA [15]. If the catalyst is not aged at all, the number-average molecular weight is $\sim 18,000 \text{ g/mol}$. If the catalyst is aged for 1 h at room temperature, M_n doubles to 40,000 g/mol. Aging for longer periods of time does not significantly increase the molecular weight.

Table III. Properties of PA Made by Different Synthetic Routes

Type	Catalyst	Solvent	Morphology	Diameter of fibrils (Å)	Density (g/cm ³)	Draw ratio (l/l_0)	% <i>cis</i>	$\sigma_{25^\circ\text{C}}$ I ₂ -doped (S/cm)	Ref.
Shirakawa	Ti(OBu) ₄ AlEt ₃	Toluene	Fibrillar, shiny, flexible, crystalline	~200	1.23	3	Varies	1000	[7]
Naarmann	Ti(OBu) ₄ AlEt ₃	Silicone oil	Regular, crystalline, compact		1.12	6.5	80	18,000	[31]
Naarmann ARA	Ti(OBu) ₄ AlEt ₃ + <i>n</i> -BuLi	Silicone oil	Fibrillar, stretchy		1.15	5	70	100,000	[31]
Solvent evacuation	Ti(OBu) ₄ AlEt ₃	None	Dull, black, hard, tough	300–500	1–1.15	7–8	80–90	2200	[33]
Intrinsic nonsolvent	Ti(OBu) ₄ AlEt ₃	None	Dull, black, stretchy		1–1.1	6–9	85–95	2200–4300	[34]
Liquid crystal (gravity)	Ti(OBu) ₄ AlEt ₃	Liquid crystal	High local orientation				53–60	6000	[37]
Liquid crystal (magnetic)	Ti(OBu) ₄ AlEt ₃	Liquid crystal	Aligned fibrils	800–1000			50	12,000	[39]
Luttinger	Co(NH ₃) ₂ NaBH ₄	EtOH	Pseudo-fibril, spongy	~200	1.16			12,000	[48]
Ziegler–Natta Metathesis	Ti(CH ₂ Ph) ₄ WCl ₆ SnPh ₄	Toluene	Fibrillar	2000			40	20	[19]
Metathesis	MoCl ₅ SnPh ₄	Toluene	Fibrillar	~300			10		[19]
Durham CF ₃ -TCDD VSO	WCl ₆ SnPh ₄ Anionic Initiation	Cl-Ph THF	Varies Compact				50	10–100	[69, 70]
ROMP COT	W-carbene	None	Smooth				66	>100	[76, 77]
ROMP benzalene	W-carbene	Benzene Toluene	Strong, flexible, mod. Crystalline				40	0.1	[80]

2.4.2. Naarmann's Technique

Naarmann revised the Shirakawa technique by aging the catalyst and cocatalyst in silicone oil instead of toluene to increase the viscosity of the reaction medium [31, 32]. In this method, silicone oil (50 ml) was degassed for 20 min at 0.05 mbar. Under argon, AlEt₃ (31 ml) was added, followed by the dropwise addition of Ti(OBu)₄ (41 ml) over 1 h at 38–42°C. The catalyst was degassed for 1 h at room temperature, stirred for 2 h at 120°C, and finally stirred and degassed for another hour at 0.1 mbar. A homogeneous layer of catalyst was then applied to a stretchy polymer support film such as high-density polyethylene (HDPE) or polypropylene, which was placed in a flat-bottomed carrier. The entire setup was sealed in inside a glove box in a hood equipped with a gas inlet valve. The hood was evacuated, and the acetylene monomer was introduced for 15 min. The acetylene began to polymerize on the catalyst surface, forming a black film. The resulting PA film was very porous and could be removed from the supporting polymer film. The PA was washed successively with toluene, CH₃OH/HCl, and MeOH and dried under vacuum.

The PA made by Naarmann's method was very regular, compact, crystalline, and stretchable. The Naarmann-type PA films were very dense and were made up of thin fibrils that had up

to 80% *cis* content when synthesized at room temperature. The *cis*-form of PA was found to be quite stable and did not isomerize to the *trans*-structure. Upon doping with iodine, conductivities (σ) up to 18,000 S/cm for stretched samples could be measured. Naarmann-type PA films could be stretched by a factor of 6, and ¹³C NMR analysis showed virtually no sp³ carbon defects. This observation may stem from the high *cis* content and high density of the films.

2.4.3. ARA Technique

The addition of a reducing agent (ARA) (e.g., *n*-BuLi) to the Ti/Al catalyst mixture prior to the introduction of acetylene gas increased the conductivity of the resulting PA film significantly. In a typical ARA procedure, the catalyst mixture (10 ml) and *n*-BuLi (1 ml) were combined to form a homogeneous layer of catalyst that was applied to a HDPE film after proper aging. The acetylene was then added. After the polymerization, the resulting composite of the PA film and polymer-support film was stretched. The PA film was then removed and washed with toluene. The conductivity of the PA film made by this method varied proportionally with the amount of reducing agent added. For example, with the addition of 3 ml of *n*-BuLi to the Ti/Al catalyst mixture, a conductivity σ of

more than 100,000 S/cm was found after iodine doping. The conductivity of a stretched PA film made by a nonaged catalyst is only $\sim 1.6 \times 10^4$ S/cm, implying that catalyst aging in the ARA process also plays an important role in the final polymer conductivity.

2.4.4. Akagi's Technique

Akagi and co-workers devised a "solvent evacuation" method [33], where the solvent was removed *in vacuo* after the catalyst was aged and just prior to monomer introduction. By removing the solvent, they increased the activity of the catalyst. In a typical Akagi experiment, $\text{Ti}(\text{O}i\text{Bu})_4$ (0.5 M solution) and AlEt_3 (4 equiv) were mixed in a Schlenk flask. The catalyst was pre-aged for 30–60 min at room temperature and then aged for an additional 1–5 h at a temperature near the boiling point of the solvent (e.g., 110–120°C for use with toluene (boiling point = 110.6°C)) under argon. The Schlenk flask containing the catalyst solution was next connected to a vacuum line, and the solvent was pumped off entirely, leaving a homogeneous layer of catalyst on the walls of the flask. In this manner, the concentration of the catalyst was increased to 2–3 times the initial concentration. At this point, acetylene gas was introduced at -78°C with an initial pressure of 680–750 torr. The gas was allowed to react with the catalyst for 2–26 h. After the polymerization was complete, the film was washed with cold toluene and EtOH at -78°C under argon. The PA films that were obtained were dull black and not shiny at all. They were tough and hard regardless of the thickness. The *cis* content of these films ranged from 80% to 90%. Akagi and co-workers found that their system yields only thin films. They proposed that at later times in the reaction, the acetylene monomer could not easily diffuse through the initially formed polymer film to increase the thickness of the final product. This initially formed film, although thin, is highly dense as the result of a rapid polymerization at the surface of a catalyst that was too concentrated and too active. One study compared the catalyst aging temperature and aging time to the yield of the PA [33]. It was found that the best polymer yields were produced with moderate temperatures and aging time. Aging the catalyst at 110°C for 3 h appeared to maximize the yield.

The PA made by Akagi's solvent evacuation method was highly stretchable. This plasticity was found to also be a function of catalyst aging time and temperature. Both the Young's modulus and tensile strength were measured for Akagi-type *cis*- and *trans*-PA. Akagi-type *trans*-PA could be stretched to 7–8 times the original length and had a Young's modulus of 100 GPa and a tensile strength of 0.9 GPa. A film of Akagi-type *cis*-PA could be stretched to a draw ratio¹ that is the same as that of the *trans*-form and had a Young's modulus of about 25 GPa and tensile strength of 0.6 GPa. In contrast to Shirakawa- and Naermann-type PA, the overall morphology of Akagi-type PA was granular and not fibrillar [33]. However, when Akagi-type PA films were stretched they appeared fibrillar, with a high degree of alignment. The diameter of the fibers ranged from 300 to 500 Å. These fibers are larger than the fibrils made by the conventional Shirakawa method, the diameters of which are only about 200 Å [22].

The stretched Akagi-type PA films were doped with iodine, and their conductivities were measured as a function of catalyst aging

temperature and time. The highest conductivity was $\sigma = 2.2 \times 10^4$ S/cm when the catalyst was aged either in cumene at 150°C for 5 h or in toluene at 110°C for 3 h.

The "intrinsic nonsolvent" (INS) polymerization protocol [34], where solvent is never employed, is a technique that is closely related to the solvent evacuation method. In a typical experiment, neat AlEt_3 was dropped into neat $\text{Ti}(\text{O}i\text{Bu})_4$ in a Schlenk flask at 0°C. The catalyst was aged for 1 h at room temperature and then further aged for another hour at 150°C. The flask was degassed and rotated to coat its walls with the catalyst solution. The system was then cooled to -78°C and acetylene was added. The reaction was allowed to proceed for 30–60 min before quenching. The resulting PA film was washed with toluene at -78°C and dried under vacuum.

The PA film produced in this manner, similar to Akagi-type PA, was black and dull with no metallic luster. It was, however, quite stretchy. As the Al/Ti ratio was increased, the draw ratio of this PA film increased to between 6 and 9. However, when an Al/Ti ratio above 6 was reached, the draw ratio began to decrease.

The conductivity of PA films produced by the INS method was measured as a function of the Al/Ti ratio. No general trend was found, but the highest conductivity was achieved when the Al/Ti ratio was 4. On an iodine-doped stretched sample, the conductivity ranged between 2.2×10^4 and 4.3×10^4 S/cm. These values are twice that found for Akagi-type PA films synthesized by the solvent evacuation method. By comparison, the PA obtained using toluene as the solvent has a maximum conductivity when the Al/Ti ratio is 2 [31, 33, 35]. Researchers proposed that the properties of the INS PA are optimized at an Al/Ti ratio of 4 because the excess AlEt_3 served as a solvent to stabilize the titanium catalyst. (The dielectric constant of AlEt_3 is 2.005, which is similar to that of toluene at 2.237.)

2.4.5. Liquid Crystal Technique

Instead of toluene, liquid crystal solvents can be used in the production of Shirakawa PA [36–39]. An equivolume mixture of 4-(*trans*-4-*n*-propylcyclohexyl)ethoxybenzene and 4-(*trans*-4-*n*-propylcyclohexyl)butoxybenzene proved to be optimal (Fig. 3). Two methods were used to align the PA fibrils. In the first method, the liquid crystalline solvent was first added to a Schlenk flask followed by a dropwise addition of the catalyst ($\text{Ti}(\text{O}i\text{Bu})_4$) and cocatalyst (AlEt_3). The catalyst mixture was aged for 30 min at room temperature and then degassed. The flask was then rotated to coat its walls thoroughly with the catalyst mixture. The flask was then placed upright and acetylene was added. The viscous liquid crystals slowly flowed down the walls of the flask as the acetylene was polymerized. The film was removed, washed with toluene, dried, and analyzed. The resulting PA film had a fibrillar surface with regions of high alignment due to the gravimetric flow of the liquid crystals. The IR spectra of the PA film showed approximately a 53–60% *cis*-structure. Upon iodine doping, a conductivity of 6000 S/cm was measured.

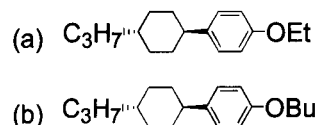


Fig. 3. Liquid-crystal solvents used in the "oriented" polymerization of acetylene.

¹The draw ratio, l/l_0 , is the ratio of the length of the sample after having been stretched to the point of breaking (l) to the length of the original polymer sample (l_0).

To achieve an overall alignment of the fibrils and not just local orientation, an external magnetic field can be employed [36, 39]. The hope was to induce the growth of an oriented film with the PA fibrils aligned along the axis of the magnetic field. The same setup as that used in the gravity method (*vide supra*) was used. The catalyst, cocatalyst, and liquid crystalline solvent mixture were dropped by syringe into a flat-bottomed container inside a Schlenk flask. The flask was connected to a vacuum, degassed, and placed between the poles of a magnet so that the container with the catalyst was kept horizontal. Acetylene gas was then added at an initial pressure of 600–760 torr. The magnetic field strength was kept at 2–14 kGauss, and the temperature was held between 10°C and 15°C to keep the solvent in a nematic phase. The polymerization was allowed to proceed for 4–60 min, after which the PA film was removed, washed with toluene, and dried. The film morphology showed high orientation of the fibers along the direction of the magnetic field. The fibrils were quite large, with an average diameter of 800–1000 Å. These oriented films yielded a conductivity of 1.2×10^4 S/cm upon doping with iodine [39], rivaling that of mercury. The disadvantages of this technique involve the high cost and the handling of a complex solvent.

Recently Akagi et al. have been able to induce the formation of helical PA by using a liquid crystalline solvent containing a chiral dopant [40]. These workers synthesized the chiral dopants (*R*)- and (*S*)-1,1'-binaphthyl-2, 2'-bis{1-[*p*-(*trans*-4-*n*-propylcyclohexyl)phenoxy]hexyl}ether (PCH506-binol), using the Williamson ether synthesis (Fig. 4). Adding 5–14 wt% of (*R*)- or (*S*)-PCH506-binol to an equivolume mixture of 4-(*trans*-4-*n*-propylcyclohexyl)-ethoxybenzene and 4-(*trans*-4-*n*-propylcyclohexyl)-butoxybenzene made the chiral-doped liquid crystalline solvents.² These solvents were then used in the subsequent acetylene polymerization. AlEt₃ and Ti(OBu)₄ in a 4:1 ratio were added to the solvent, and the mixture was allowed to age for 30 min at room temperature. The reaction temperature was kept between 17°C and 18°C to maintain the nematic phase of the solvent, and the acetylene gas was added. After 10–43 min, the polymerization was stopped, and the resulting PA film was removed, washed with toluene, and dried. Scanning electron microscopy (SEM) examina-

tion of the film made in this manner showed PA in the form of helical fibers. The PA film formed using (*R*)-PCH506-binol consists of left-handed helicenes only, and that formed using (*S*)-PCH506-binol consists of right-handed helicenes only. Thus, the helical orientation of the PA fibrils formed is dictated by the enantiomeric nature of the chiral inductor (e.g., (*R*)-PCH506-binol induces the formation of (*R*)-PA fibrils). The individual polymer chains in PA films made in this manner are themselves helical, with several chains gathering together to form the helical fibrils. Control experiments showed that when no chiral inductor was used, the PA film formed consisted of the typical flat fibrils. The helical PA made from this method was found to be 90% *trans* and had a conductivity of about 1500–1800 S/cm at room temperature when doped with iodine.

2.5. Other Catalysts for the Polymerization of Acetylene

Many transition metal catalysts are known to polymerize PA via an insertion mechanism (*vide infra*). Ziegler–Natta catalyst systems can be either heterogeneous or homogeneous. Even alumina by itself will catalyze the formation of PA at high temperature [41, 42]. After γ -alumina is heated to 900 K, acetylene will polymerize on its surface. In addition, many combinations of organoaluminum and transition metal complexes have been documented as being capable of catalyzing the polymerization of acetylene [17]. Nickel-, ruthenium-, and iron-based compounds with alkylaluminum cocatalysts are known acetylene polymerization catalysts [43–46]. Similar combinations with alkylaluminums work for lanthanides as well. For instance, EuCl₃/AlEt₃ and Nd(naphthalene)₃/AlEt₃ are active catalysts [45]. The addition of oxygenated agents, such as acetone, tends to increase the activity of these catalysts. Organometallic complexes, such as Ti(CH₂Ph)₄, can be used alone, but adding AlEt₃ enhances their activity.

2.5.1. Metathesis Catalysts

A class of metathesis catalysts including MoCl₅ or WCl₆ with cocatalysts such as SnPh₄ can polymerize acetylene through a carbene intermediate [19]. The molybdenum and tungsten halides are active when used alone, but a cocatalyst increases their activity. In a typical experiment, the catalyst and cocatalyst were mixed in an equimolar ratio in toluene. The catalyst was then aged for 15 min at 30°C before acetylene was added. The PA films obtained with both the W and Mo catalysts have a 90% *trans*-structure and similar overall morphologies. However, the size of the PA fibrils varied drastically between the two metal catalysts. For films made with the MoCl₅/SnPh₄ catalyst, the average diameter of the fibrils was 300 Å. In comparison, the average diameter of the fibrils made by the WCl₆/SnPh₄ catalyst was 120,000 Å. In general, the following order of catalyst activity is observed [17]: Ti(OBu)₄/AlEt₃ > Ti(CH₂Ph)₄/AlEt₃ > Ti(CH₂Ph)₄ > WCl₆/SnPh₄ > MoCl₅/SnPh₄. Comparing the molecular weights of the polymers made with any of these catalysts is futile since all are insoluble. However, the PA made by the WCl₆/SnPh₄ system is less flexible, implying a higher degree of cross-linking than the polymer made with Ti(OBu)₄/AlEt₃ [17]. The degree of cross-linking may be determined by spectroscopic methods such as IR and ¹³C NMR. In the infrared spectrum, vibrational stretches due to C–C single bonds can be seen, and reso-

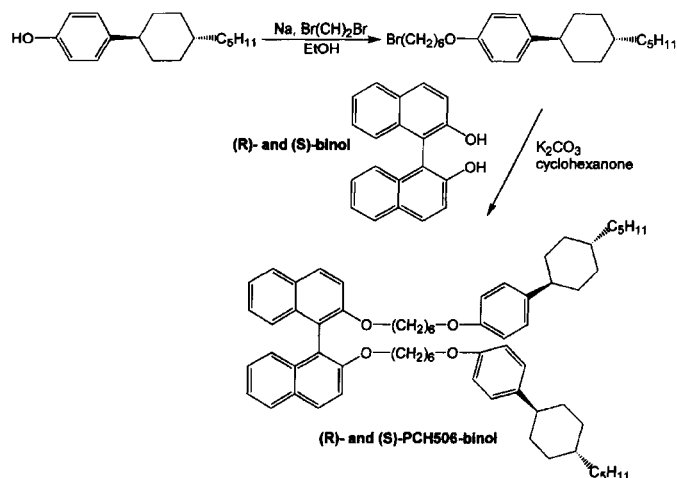


Fig. 4. The synthesis of a chirally enhanced liquid-crystal solvent.

²The phenoxy-cyclohexyl groups enhanced the solubility of the chiral dopants in the liquid crystalline solvent.

nances due to sp^3 carbons can be detected by solid state ^{13}C NMR spectroscopy [18].

2.5.2. Luttinger Catalysts

The combination of a salt or complex of a group VIII metal halide and a hydridic reducing agent is known as a Luttinger catalyst [46, 47]. Almost any group VIII metal complex will polymerize acetylene and monosubstituted alkynes provided that it has labile ligands and good solubility. Luttinger catalysts include complexes of Co, Ni, Ru, Os, Pt, and Pd, while effective reducing agents are the alkali borohydrides, LiAlH_4 , and diborane. The lability of the ancillary ligands around the metal center is quite important in determining the activity of the metal complexes. A hydridic reducing agent, nickel halide (e.g., Br or I), and a tertiary phosphine will polymerize acetylene, but the cobalt- and palladium-phosphine analogs will not. However, linear PA can be synthesized with a cobalt-based Luttinger catalyst in the absence of phosphines. Acetylene gas is first dissolved in EtOH, followed by the addition of $\text{Co}(\text{NO}_3)_2$ (1 wt%) and NaBH_4 (0.1 wt% in EtOH) at -80°C [13, 48]. The catalyst solution is then warmed to -30°C , and eventually *cis*-PA precipitates out of solution as black flakes in quantitative yield. The PA formed in this manner is pseudo-fibrillar and spongy. The advantage of using this and other Luttinger catalysts over Shirakawa's method is their diminished air and moisture sensitivity. The presence of oxygen has little effect on the polymerization. Hydrophilic solvents such as EtOH, THF, CH_3CN , or even water itself may be used, making the cobalt-based Luttinger catalyst much easier to handle than the traditional Ziegler-Natta-type catalysts [9].

PA films made with the Luttinger catalysts exhibit better *cis*-to-*trans* isomerization stability. They can remain in the *cis*-form for several days at room temperature without converting to the *trans*-structure. Luttinger-type polyacetylene can be completely chlorinated at -30°C immediately after polymerization to give soluble poly(1,2-dichloroethylene), the molecular weight of which can be measured. Various literature reports indicate M_n values of about $2\text{--}5 \times 10^4$ g/mol for the chlorinated polymer. From this, a back-calculation gives a molecular weight of 5,000–13,000 g/mol for Luttinger-type PA [13, 48, 49].

2.5.3. Nickel Ylide Catalysts

A number of nickel(II) ylide catalysts (Fig. 5) have been reported to polymerize acetylene effectively [50]. Unlike Ziegler-Natta metal alkyl catalysts, the phosphonium group in the nickel ylide catalyst blocks β -hydride elimination. Using an ylide ligand instead of PPh_3 increases the catalyst activity by a factor of 10. By changing the R group on the bidentate ligand, the degree of polymerization can be controlled. A typical polymerization reaction involves reacting acetylene gas (1 atm) over the nickel catalyst (1 mmol) in toluene (100 ml) for 1 h [51]. Under these conditions and at 60°C the nickel ylide catalyst with $\text{R} = \text{Ph}$ and

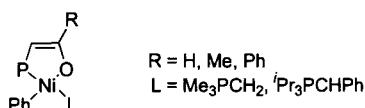


Fig. 5. Nickel(II) ylide catalyst for PA polymerization.

$\text{L} = \text{Me}_3\text{P}=\text{CH}_2$ produces a PA film that is 70% *trans*. The catalyst's activity was 500 mol PA/(mol Ni)·h·atm.

2.5.4. Noncatalytic Methods

Several noncatalytic methods for the synthesis of PA are known, including electrochemically forming a PA film on a platinum cathode [52]. This special electrochemical cell uses a platinum cathode, nickel anode, and NiBr_2 dissolved in acetonitrile as the electrolyte solution. A 4–40-V potential is then applied across the electrodes to commence the polymerization. The PA film forms on the cathode as a thin black layer and becomes thicker with time.

Simply increasing the acetylene pressure to beyond a GPa at room temperature inside a diamond anvil will induce self-polymerization [53–55]. Analysis of the resulting materials by Raman spectroscopy indicates that *trans*-PA is formed predominantly under these conditions, presumably due to steric reasons (*trans*-PA packs better than *cis*-PA).

Finally, Soga and co-workers reported the formation of a thin *cis*-PA film when acetylene gas was exposed to a small amount of AsF_5 in a flask at very low temperature (-78°C to -198°C) [56]. The polymer formed in this manner was doped simultaneously (AsF_5 is a p-dopant (*vide infra*)) and found to have a conductivity $\sigma = 4.8 \times 10^{-2}$ S/cm. Polymerization was not observed with other p-dopants such as SO_3 or I_2 (in place of the AsF_5). Researchers proposed that the AsF_5 and acetylene first reacted to form a charge transfer complex that initiated the polymerization.

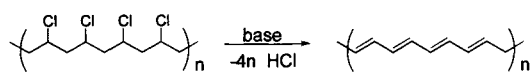
2.6. Precursor Routes to PA

Because of the processing problems associated with the aforementioned methods for synthesizing PA (namely the Shirakawa-type PA (and other PA) films cannot be shaped after synthesis), a new synthetic methodology was developed. The idea was simple: first form soluble polymer precursors that can be processed and cast into the desired shape by spin casting, and then thermally or chemically eliminate a small molecule from each repeating unit, effectively leaving a PA film behind. The final conjugated polymer is still insoluble in all solvents, but with the soluble precursor the processing can be done quite easily. Given the many catalysts and methods available for forming the precursor polymer, the molecular weight of the final PA can also be controlled effectively. The major difficulties of this strategy lie in carrying out a quantitative elimination reaction in the solid state and effectively removing all of the by-products under diffusion control.

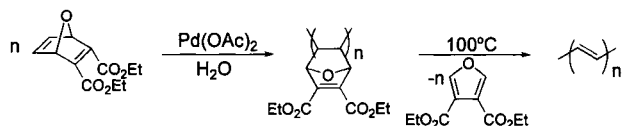
The concept of the precursor method is akin to the process of adding protecting groups in organic synthesis. To be effective, the attachment and removal of the protecting group must proceed in a clean and efficient manner. Ideally the monomers used for the synthesis of the precursor polymers should be inexpensive and readily available. Furthermore, the formation of the precursor polymer should be easy, and its structure, well defined. Finally, the elimination of the small molecule from the precursor polymer should be efficient and quantitative.

2.6.1. PVC Route

An early example of the precursor route to PA was through polyvinylchloride (PVC). A base was used to remove an equivalent of HCl from every repeating unit of the PVC backbone, leaving a conjugated structure (Scheme V) [57–59]. In a typical experiment,



Scheme V. Poly(vinylchloride) precursor method to PA.



Scheme VI. Norbornadiene precursor method to PA.

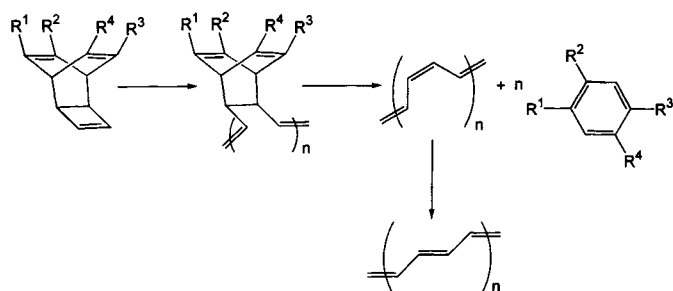
PVC was first added to THF, and the ensuing mixture was refluxed for several hours to ensure complete dissolution of the polymer. In a separate flask, KOH was dissolved in ethanol followed by dilution with THF. This basic solution was added to the solubilized PVC with rapid stirring. The solution goes through a kaleidoscopic change of color, from colorless to pale yellow to yellow to orange to red and finally dark red, implying an increase in the average conjugation length. Adding water at the end of the reaction forms a precipitate, which was isolated, washed with water, and dried. This product was redissolved in THF and filtered to remove any insoluble gels. Dropping the THF solution into methanol precipitated the PA, which was then isolated and dried. Caution must be taken in this synthesis, for excess KOH in the reaction mixture can cause scission of the PVC chains, degrading the polymer. In addition, the problem with this technique was that the elimination of HCl could never be carried out quantitatively.

2.6.2. 7-Oxanorbornadiene Route

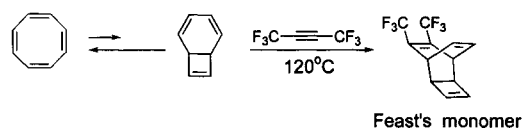
A palladium(II) catalyst has been used to polymerize a 7-oxanorbornadiene derivative which is stable at room temperature [60]. It was discovered that the addition of water to Pd(OAc)₂ led to an increase in the activity of this catalyst and a four- to fivefold increase in polymer yield. With 0.5 mol% catalyst loading, the yield of poly(7-oxanorbornadiene) is 75% with $M_n = 28,000$ g/mol and PDI = 1.8. Upon heating to 100°C, this precursor polymer underwent a *retro*-Diels-Alder reaction and an ester-substituted furan was eliminated to produce PA (Scheme VI). During the elimination step, the solution turns from colorless to deep purple, again indicating an increase in conjugation length. In the analysis of the final PA, it was found that up to 96% elimination from the precursor polymer have occurred.

2.6.3. Durham Route

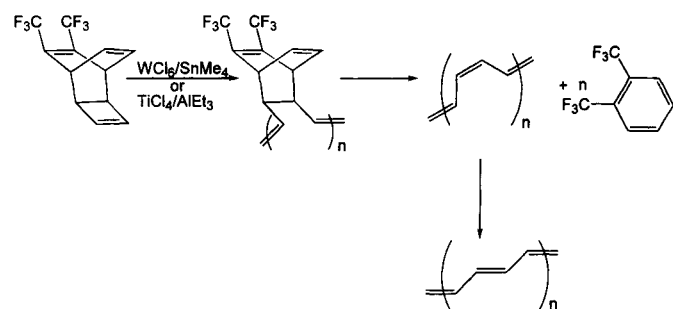
The most elegant and well-studied precursor method is known as the Durham route (Scheme VII). A tricyclic monomer can be made from a thermal reaction between cyclooctatetraene and di-substituted acetylene in 80% yield after one step [61, 62]. The four R groups can be varied easily. With *bis*(trifluoromethylacetylene) and cyclooctatetraene, the product is 7,8-*bis*(trifluoromethyl)tricyclo[4.2.2.0]deca-3,7,9-triene (CF₃-TCDT), which is known as Feast's monomer (R¹ = R² = CF₃, R³ = R⁴ = H), after the principal popularizer of the Durham route (Scheme VIII). This substrate can then be polymerized with a metathesis catalyst, typically WCl₆/SnMe₄, but the traditional Ziegler-Natta catalyst TiCl₄/AlEt₃ will also work (Scheme IX) [63]. The tungsten catalyst produces a 50/50 mixture of *cis*- and *trans*-polymer, while



Scheme VII. Generalized Durham precursor route to PA.



Scheme VIII. Synthesis of Feast's monomer.

Scheme IX. Durham precursor route to PA with R₁ = R₂ = CF₃.

the titanium catalyst yields a mostly *trans*-product. Adding the main-group cocatalysts to the transition metal catalysts in solution generates the active catalysts. Monomer can then be added, either neat or as a solution. Solvent choice is important; an "inert," deactivated solvent like chlorobenzene is needed so as not to deactivate the catalyst [64]. Toluene is a poor choice since it can undergo Friedel-Crafts chemistry. On the other hand, non-aromatic solvents such as THF and ethylacetate disable the propagating chain end. In chlorobenzene the reaction solution quickly becomes viscous and the reaction is then terminated with methanol. The resulting tan polymer is soluble in ketone solvents and chloroform. It can be precipitated out of methanol to remove the catalyst and trace impurities. The polymer decomposes spontaneously in a dark dry box and even faster while in solution. Molecular weights (M_n) of up to 10⁶ g/mol and a PDI as low as 1.8 have been reported for the precursor polymers prepared by this method [64]. The high PDI is a common problem in many metathesis polymerizations: it is possible for the propagating chain end to react with the double bonds in the backbone of the same chain (or another chain). This back-biting mechanism gives rise to an increase in polydispersity and the possibility of cyclic structures in polymers prepared via olefin metathesis [65].

Because the metathesis catalysts used in this process are often nondiscriminating, the precursor polymer is an atactic mixture of *cis*- and *trans*-linkages. According to theoretical calculations, the elimination of the substituted benzene from Feast's precursor polymer is symmetry allowed [66]. At room temperature this precursor polymer spontaneously eliminates hexafluoroxylene, pro-

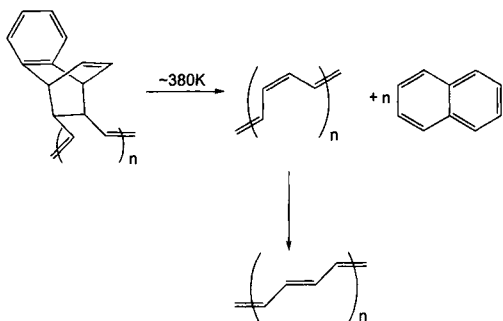
ducing *cis*-PA, which will later isomerize to *trans*-PA. *In situ* monitoring of the polymerization/elimination process by differential scanning calorimetry (DSC) shows an initial exotherm for the ring-opening metathesis polymerization (ROMP) of the cyclobutene monomer [67]. An endotherm quickly follows, indicating the elimination of the hexafluoroxylene to form PA and a final exotherm for the *cis*-to-*trans* isomerization.

The PA films made by the Durham route are of good quality and have a morphology ranging from amorphous to highly oriented, depending on the specific reaction conditions (e.g., temperature, time, and pressure). Less crystalline samples are good for nonlinear optical uses since light scattering off crystalline PA domains can be a problem [68]. To increase the crystallinity of the PA, the sample can be oriented either before or after the removal of the hexafluoroxylene. The diffusion of the small molecule, *cis*-to-*trans* isomerization, and crystallization of the polyacetylene chains also affect morphology [66]. Doping of PA samples made by the Durham route has allowed for reasonably high levels of conductivity [69]. When PA is doped with iodine, $\sigma = 10\text{--}100\text{ S/cm}$, and this conductivity rises to 500–800 S/cm when PA is doped with AsF₅.

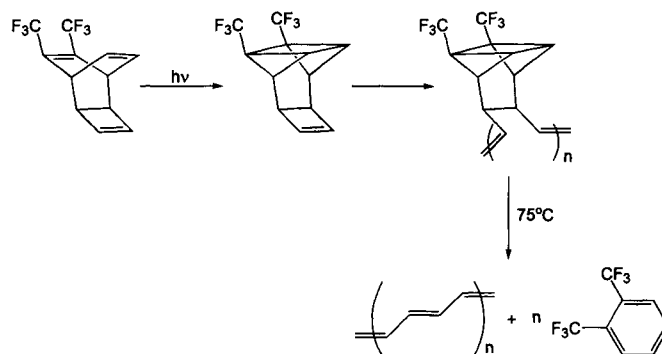
2.6.4. Analogs of Feast's Monomer

The precursor polymer from Feast's monomer is slightly unstable; its half-life is about 20 min at room temperature. Because of this factor, a variation of this monomer was prepared ($R^1\text{--}R^2 = \text{--CH=CH--CH=CH--}$) (Scheme X) [70]. The precursor polymer of this monomer is indefinitely stable at room temperature; however, elevated temperatures (380 K) are required for the *retro*-Diels-Alder reaction to eliminate naphthalene. Naphthalene is much harder to remove because of its slow diffusion in the solid state. A similar analog that eliminates anthracene has been prepared, but its elimination temperature was even higher (550 K).

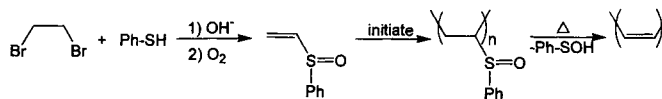
A second improvement on the original Durham route uses light to generate a highly strained cyclic olefin from Feast's monomer (Scheme XI) [71]. This monomer, which contains two three-membered rings, is ring-opened polymerized to the precursor polymer, which is obtained as a stable, white crystalline solid at room temperature. The precursor polymer easily eliminates hexafluoroxylene under mild heating. Precaution should be used whenever this precursor polymer is handled, since the two cyclopropane moieties are highly strained and cause the polymer to be shock-sensitive. An analog of this monomer was made by replacing the two trifluoromethyl groups with methyl esters ($R^1 = R^2 = \text{CO}_2\text{Me}$), but the half-life of the corresponding precursor polymer was only a few minutes [67].



Scheme X. Precursor route to PA with the elimination of naphthalene.



Scheme XI. Alternative route using light to create a stable precursor polymer.



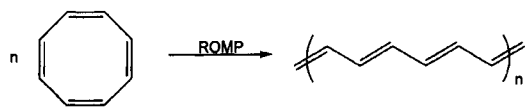
Scheme XII. Poly(VSO) precursor route to PA.

2.6.5. Phenyl Vinyl Sulfoxide Route

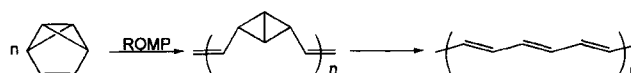
Phenyl vinyl sulfoxide (VSO) is another monomer that has been polymerized to a precursor polymer, which can subsequently be thermalized to produce PA. VSO was made from dibromoethane and thiophenol [72] and was freshly distilled prior to polymerization. Freshly distilled VSO monomer can be anionically polymerized with a carbanion initiator (e.g., sodium naphthalide, MeLi) [73, 74]. The monomer and initiator were added together at -78°C in THF. The polymerization was terminated with methanol, and the polymer was isolated in good yield. The highest molecular weight obtained for poly(VSO) (PVSO) was $M_n = 30,000\text{ g/mol}$, with a PDI < 1.4. The polymerization of VSO was rapid even at -78°C and had a half-life of only 4 s. It was even faster at room temperature, and the resulting PVSO became bimodal, as analyzed by gel-permeation chromatography (GPC). This observation indicated that two initiating or propagating species were present. PVSO was soluble in organic solvents such as CH_2Cl_2 , THF, and toluene. When heated, PVSO eliminated benzenesulfenic acid through a six-electron sigmatropic rearrangement, leaving PA behind (Scheme XII). This elimination can occur at room temperature, but better conversion has been found to take place at elevated temperatures. However, PVSO-derived PA was found to have fewer defects at lower elimination temperatures, while cross-linking occurred at higher temperatures. For PA films made from heating PVSO at 180–200°C for 1.5 h, the conductivity was 3 S/cm after iodine doping [73]. At 150°C the highest degree of benzenesulfenic acid elimination took place (95%), giving PA with $\sigma = 4.4\text{ S/cm}$ after I₂ doping.

2.6.6. ROMP of Cyclooctatetraene

Hocker and co-workers first used a classical tungsten metathesis catalyst to polymerize cyclooctatetraene (COT) via ROMP (Scheme XIII) [75]. Two practical methods were developed for the polymerization. In the first method, $\text{W}[(\text{OCH}(\text{CH}_2\text{Cl}))_n\text{Cl}_{6-n}]$ was first added to a flask, followed by AlEt_2Cl and solvent. After the catalyst mixture aged for 5 min, COT was added all at once. In



Scheme XIII. Synthesis of poly(COT).



Scheme XIV. Benzvalene precursor route to PA.

the second, “intrinsic nonsolvent” procedure, the aluminum cocatalyst was added to a solution of the tungsten complex in a Schlenk flask. The solvent was then evaporated under vacuum while the flask was rotated to form a thin layer of catalyst on the walls. The COT monomer was next condensed onto this catalytic surface over 24 h at such a rate as to form a thin film. The catalyst was removed from the film by washing the latter with a 1:1 mixture of toluene and MeOH. Using a catalyst ratio of Al/W = 2, both oligomers and black polymer were obtained. The polymer was found to be 61% *trans*-PA.

Klavetter and Grubbs used well-defined tungsten-alkylidene catalysts to ROMP cyclooctatetraene [76, 77]. It should be noted that cyclooctatetraene is made by cyclotetramerizing acetylene in the presence of a nickel catalyst [78, 79]. Thus, ROMP of COT is in essence an indirect polymerization of acetylene itself. However, an active catalyst was needed to ring-open it since COT is unstrained. Klavetter and Grubbs employed a variation of the intrinsic nonsolvent procedure used by Akagi and Hocker (*vide supra*). In the Caltech experiment, a pentane solution (1 mol% total catalyst) of the catalyst $((RO)_2W(N(2,6\text{-}^i\text{Pr})_2\text{Ph})CHCMe_3$, where $R = (CF_3)_2CH_3C$ was dropped onto a glass slide. The solvent was allowed to evaporate, leaving a homogeneous thin layer of catalyst. The COT monomer was then dropped onto the catalyst layer and stirred with a glass rod.³ The color of the reaction mixture turned from light yellow (the color of unreacted COT) to orange to red to magenta and finally to silver (PA). At room temperature the reaction mixture solidified within 10–30 s. The film was then removed from the slide and washed with pentane and methanol. The PA formed by this method had a 66% *cis* content. It had a smooth surface and a fibrillar interior. Surface smoothness of the polymer film is a function of how well the polymer chains pack, which itself is related to the local catalyst concentration. Therefore, it was proposed that the nonfibrillar, smooth surface of the Caltech poly(COT) film was a direct consequence of a uniform concentration of catalyst on the slide. In another experiment where the COT monomer was vapor deposited onto the catalyst surface—in imitation of Shirakawa’s technique—the resulting PA was globular, not smooth. This was thought to be the result of a nonuniform interaction between the catalyst and monomer (due to uneven condensation). The well-defined tungsten alkylidene catalysts used in the Caltech experiment are less Lewis acidic than other metathesis catalysts that were used previously to ring-open polymerize COT, therefore fewer saturated carbons (e.g., defects) were found in the backbone [18]. The conductivity of the PA film made in this manner was >100 S/cm after iodine doping. The resulting PA was still insoluble, but the intrinsic nonsolvent method of polymerization allows the ultimate film shape to be fixed before the ring-opening step.

³The catalyst was soluble in hydrocarbon compounds including COT.

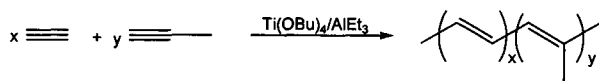
2.6.7. Benzvalene Route

Swager and Grubbs made an all-hydrocarbon precursor polymer that is an isomer to PA [80]. This method avoided the removal of a small molecule in the solid state altogether. They ring-opened commercially available benzvalene to poly(benzvalene) with a well-defined tungsten-based metathesis catalyst (Scheme XIV). The catalyst, $(RO)_2W(N(2,6\text{-}^i\text{Pr})_2\text{Ph})CHCMe_3$ ($R = \text{tBu}$ or $(CF_3)_2CH_3C$), was used at either room temperature ($R = \text{tBu}$) or at -20°C ($R = (CF_3)_2CH_3C$) in either benzene or toluene. The two catalysts produced the same polymeric material. The precursor polymer was 90% *cis*-structure. The polymer was highly strained and easily ring-opened a second time with various organometallic compounds ($HgCl_2$, $HgBr_2$, Ag^+ salts) to produce a silvery PA. The resulting PA film was strong and flexible but had lower crystallinity than PA made by other precursor routes. Despite the high *cis* content in the precursor polymer, IR analysis indicated that the PA film was only 40% *cis*. The ^{13}C NMR spectrum of the PA made by this method shows a fairly high amount of sp^3 carbons present in the PA backbone, probably due to the HgX_2 -induced cross-linking of the bicyclobutane units in the precursor polymer [9]. The PA made by this route exhibited only low conductivity ($\sigma = 10^{-5}$ S/cm for PA worked up with $HgCl_2$). Even when this film was doped with iodine, conductivity rose to only 10^{-1} S/cm [80]. Extreme caution should be exercised when either the benzvalene monomer or polymer (prior to isomerization to PA) is used, due to the shock-sensitive nature of these materials.

2.7. Copolymers of PA

2.7.1. Random Copolymers

Another way to deal with the intractability issue of PA is to copolymerize acetylene with other more substituted monomers. The idea is that such a copolymer may have lower crystallinity compared to pure PA (due to potentially unfavorable packing arrangements) and thus is more soluble. In 1981, Chien and co-workers first attempted the copolymerization of acetylene and methylacetylene (Scheme XV) [81]. Methylacetylene was chosen because its homopolymer was known to be soluble and the methyl substituent was small enough that its incorporation would not significantly change the conjugation length of the resulting copolymer. A third reason for choosing this particular monomer was that it is a gas above -25°C , so a synthetic setup similar to that used for the polymerization of acetylene could be used. The copolymerization was carried out above -25°C so that the comonomer ratio was known precisely. Using Schlenk technique, they added $Ti(OBu)_4$ (2.5 ml) to toluene at 0°C , followed by the dropwise addition of $AlEt_3$ (4 ml). The catalyst was then aged for 30 min at room temperature. The flask was attached to a vacuum line, cooled to -78°C , stirred, and degassed. After 30–60 min, the flask was warmed to room temperature and placed in an ice-salt bath at -10°C . In a separate vessel, both monomers (\equiv and $\equiv\text{-Me}$) were mixed in a predetermined ratio in such a way that the total pressure equaled 720 torr. The catalyst flask was then rotated to coat its wall with the catalyst solution, and the monomer mixture was immediately



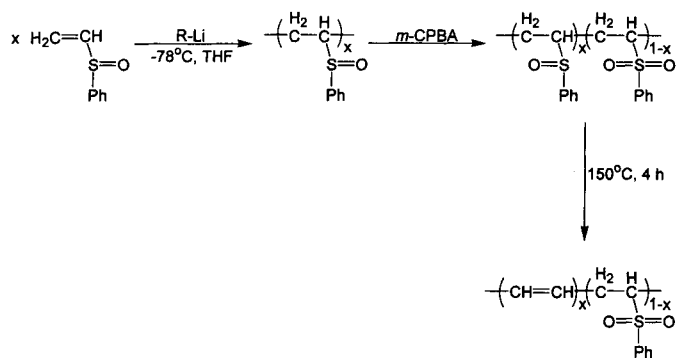
Scheme XV. Acetylene and methylacetylene copolymer.

added all at once. The reaction was allowed to proceed for 20–40 min, after which the catalyst solution was removed. The resulting film was cooled to -78°C and was washed with toluene.

The resulting P(A/MA) copolymer was insoluble in organic solvents when the acetylene content was greater than 15 mol%. Other physical properties of the polymer also varied as a function of the acetylene percentage composition. With 75 mol% PA, the P(A/MA) copolymer was weak and brittle, with a shiny green front side and dull, gray-black back side. The film was shiny green and contained nonfibrillar irregular clumps with 55 mol% PA present. At 33 mol% acetylene content, the film consisted of dull greenish-gold globules that became quite elastic when wetted with solvent ($l/l_0 = 7$). All of these copolymers were much more air- and heat-sensitive than PA itself and had much larger bandgaps. In general, the conductivity of the copolymer was inversely proportional to the amount of methylacetylene present. When doped with I_2 , a conductivity of up to 36 S/cm was achieved for the copolymer with 55 mol% PA content. With 33 mol% PA, the I_2 -doped conductivity fell to 1.5 S/cm. Conductivity could decrease over five to six orders of magnitude with increasing content of methylacetylene, most likely due to the reduction of the planarity of the backbone of the copolymer by the methyl side groups. This sterically imposed twisting conformation decreases π -orbital overlap between the double bond units and leads to a lower conductivity.

Deits and co-workers synthesized an acetylene/phenylacetylene copolymer, P(A/PA), using a partially hydrolyzed $[\text{WCl}_6 \cdot 1/2\text{H}_2\text{O}]$ catalyst [82]. In this method, acetylene was bubbled into a solution of phenylacetylene in toluene at 7°C . The catalyst was prepared by adding the required amount of water (0.5 equiv) to WCl_6 in toluene. After aging for 30 min at 30°C , the catalyst solution was then added to the monomers. After 2 h the polymerization was terminated by stopping the flow of acetylene and bubbling argon through the reaction mixture. The copolymer was then precipitated with the addition of hexane, washed with hexane, and dried. The copolymer made in this way was tough and leathery but could be pressed into shiny metal-like flakes or dissolved in solvent and recast as thin films. The color of these copolymers ranged from the dark red color of poly(phenylacetylene) to the black color of PA. Once again, the properties of the copolymers, both physical and electronic, varied with the monomer ratios. With $>40\%$ phenylacetylene content, the P(A-PA) copolymer was completely soluble in CHCl_3 , DMF, and toluene, but its I_2 -doped conductivity was only 1.4×10^{-4} S/cm. Lowering the content of phenylacetylene to 22% produced an insoluble copolymer, but its conductivity rose to 50 S/cm. None of the acetylene/phenylacetylene copolymers were air stable for long periods of time.

Phenyl vinyl sulfoxide can be polymerized and randomly oxidized to form sections of phenyl vinyl sulfone (VSO₂) before elimination (*vide supra*) to control the conjugation length of the resulting PA (Scheme XVI) [74]. To a flask containing dry and distilled THF was added a few drops of alkyl lithium (1 M solution) to remove any remaining impurities from the solvent. Next, more of the carbanion initiator (0.5 ml of a 1 M solution) was added, and the temperature was lowered to -78°C . The VSO monomer (5 ml) was then added, and the color of the solution turned to

Scheme XVI. Copolymer of PVSO/PVSO₂.

a greenish-yellow, indicating the formation of α -lithiosulfinyl carbanion. The reaction was terminated with methanol after 30 min. The resulting PVSO was precipitated with diethyl ether, dried, and stored at -20°C since it was unstable at room temperature. The M_n of the PVSO polymer ranged from 13,000 to 30,000 g/mol, and its PDI = 1.21–1.37. This precursor polymer was oxidized to a random copolymer of PVSO/PVSO₂, using a 55% solution of *m*-chloroperoxybenzoic acid in methylene chloride. The resulting copolymer was precipitated once in THF and again in diethyl ether. To eliminate the precursor copolymer, it was heated from room temperature to 150°C at a rate of $1^\circ\text{C}/\text{min}$, then held at the maximum temperature for 4 h. Toluene was then used to extract the benzenesulfenic acid side product. The extent of elimination for the copolymer was less than that of the PVSO homopolymer (*vide supra*). The length of the conjugated PA chains was measured and found to have an average conjugation length of two to six double bonds. The lowest observed conductivity was 5.5×10^{-6} S/cm (I_2 doped) for a copolymer with a 24 wt% of PA. The highest conductivity was 1.8×10^{-2} S/cm (I_2 doped) for a copolymer with a 55 wt% PA. As measured by the gravimetric method, this latter copolymer had 14% defects because of the incomplete elimination.

2.7.2. Block Copolymers

Polystyrene (PS) and polyisoprene (PI) form block copolymers with PA in the presence of $\text{Ti}(\text{OBu})_4$ catalysts [83–85]. The two copolymers are prepared similarly. For instance, styrene is first initiated by *n*-BuLi (typically 0.05 M) in an anionic polymerization. A lithiated polystyryl anion can then displace one butoxy group from the titanium center to form a new Ti–C bond, which serves as the active site for the subsequent acetylene polymerization. However, before acetylene was added, this “polymeric” catalyst was often aged for 1 day (PS) or 2 days (PI). The acetylene polymerization was then carried out under dilute conditions so as to minimize side reactions. In this manner, acetylene can be polymerized through the Ti(III) catalyst, forming an AB diblock copolymer. In the case of polystyrene, less than 20 wt% of PA in the copolymer renders the copolymer soluble. Gels that were not soluble could be pressed into thin films for characterization.

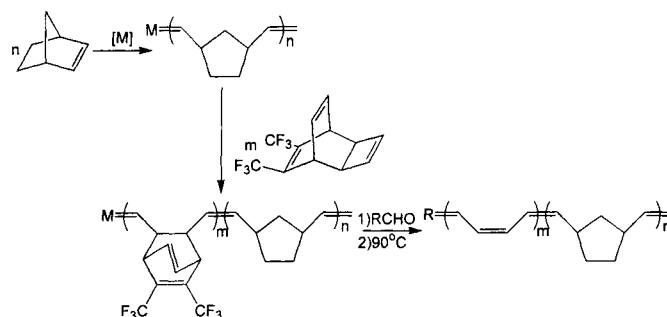
The molecular weights for the soluble copolymers were found by GPC in THF [85, 86]. The molecular weights for the insoluble copolymers were determined by solid-state ^{13}C NMR and IR spectra. As expected, the molecular weight of the PA segments depended on the weight of the carrier polymer. The molecular weight of the PA segment decreased as the molecular weight of the

PS (or PI) segment increased. When the PI segment had $M_w = 7000\text{--}10,000$, the PA segment was only $\sim 1500\text{--}1900$ g/mol [83]. For soluble PA/PI copolymers, the molar fraction of PA varied between 30% and 35%, and the polyisoprene segment had a weight averaged molecular weight $M_w = 8000\text{--}10,000$ g/mol. The soluble PA/PI copolymer had an I_2 -doped conductivity of only 1 S/cm [86]. Through Raman spectroscopy, the conjugation lengths of PA blocks in the soluble copolymers were found to be much shorter than those of the PA blocks in insoluble copolymers.

Chien and co-workers made a block copolymer of norbornene and PA, using $CF_3\text{-TCDDT}$ (*vide supra*) as the PA source [87]. For the copolymerization, $SnMe_4$ (2 mol%) was added to WCl_6 (1 mol%, solution in chlorobenzene), and the resulting catalyst was aged for 5 min. The catalyst was then cooled to $0\text{--}15^\circ\text{C}$ before a mixture of the two monomers was added. The reaction was allowed to proceed and then terminated with methanol. The resulting precursor copolymer solution was redissolved in a mixture of acetone/ $CHCl_3$ and precipitated into MeOH. Thin films of the copolymers with a low PA content were cast from methylene chloride, whereas those from copolymers with a high PA content were cast from acetone. The precursor copolymers were then treated at $80\text{--}90^\circ\text{C}$ for 12–15 h to eliminate hexafluoroxyene. The acetylene content of the resulting copolymer ranged from 45 to 79 mol%. For the copolymer with 79 mol% PA, $\sigma = 2.5 \times 10^{-2}$ S/cm with iodine doping.

Krouse and Schrock also made block copolymers with norbornene and PA, using $CF_3\text{-TCDDT}$ (*vide supra*) as the precursor monomer to polyacetylene (Scheme XVII) [88]. Using $(t\text{-BuO})_2M(N(2,6\text{-}i\text{Pr})_2\text{Ph})(CHR)$ ($M = W, Mo$ and $R = \text{alkyl}$) to ROMP both monomers allowed for the control of the molecular weight and PDI. Controlling the order of monomer addition allowed for the synthesis of di- and triblock copolymers. The polymerization reaction could be terminated with either benzaldehyde or pivaldehyde to cleave the metal catalyst from the propagating polymer chain. Precursor copolymers with norbornene/ $CF_3\text{-TCDDT}$ ratios of 1.7:1 to 5:1 could be made with $M_n = 6,000\text{--}27,000$ g/mol and $PDI = 1.04\text{--}1.23$. The elimination of hexafluoroxyene was then carried out at 90°C for 1 h. The final norbornene/PA copolymer was soluble in organic solvents such as toluene. Typical iodine-doped conductivities for these copolymers are listed in Table IV.

VSO can be used to form block copolymers with PS followed by VSO elimination to form PA-PS block copolymers [73, 89, 90]. Both monomers can be polymerized anionically; the styrene was initiated first and end-capped with 1,1-diphenyl ethylene (DPE). With the addition of a few drops of DPE to the living styryl solution, the styryl carbanions were converted to diphenyl methyl carbanions [91], which were bulky, less reactive, and less nucleophilic than the styryl carbanions, thus minimizing any side reactions. The VSO monomer was then added to the DPE-capped styryl chains to generate a PS/PVSO copolymer. The resulting precursor copolymer had PDIs that were as low as 1.09. To thermally eliminate the benzenesulfenic acid moieties from the PVSO block, the copolymer was heated from room temperature to 80°C at $1^\circ\text{C}/\text{min}$ and then held at 80°C for 1 h [90]. It was then heated to 150°C at $1^\circ\text{C}/\text{min}$ to get the maximum amount of elimination (87–92%). Whereas the PS/PVSO precursor copolymer was soluble in many solvents, the PS/PA copolymer was soluble only when the PA content was less than 50 mol%. With 78 mol% PA content the conductivity of the copolymer was 8×10^{-3} S/cm after iodine doping.



Scheme XVII. Copolymer of norbornene and polyacetylene from a metathesis-based precursor route.

Table IV. Properties of PA Copolymers

Copolymer type	Polyacetylene source	Comonomer	wt% PA	σ , I_2 doping (S/cm)	Ref.
Random	Acetylene	Methylacetylene	15–55 ^a	$2 \times 10^{-2} \sim 36$	[81]
Random	Acetylene	Phenylacetylene	3–90 ^a	$6.8 \times 10^{-6} \sim 5 \times 10^{-1}$	[82]
Random	VSO	VSO ₂	27–81 ^b	$5.5 \times 10^{-6} \sim 4.4$	[74]
AB diblock	Acetylene	Styrene	60–90	$10^{-3} \sim 1 \sim 2 \times 10^2$	[84]
AB diblock	Acetylene	Isoprene	30–35	1	[83, 86]
AB diblock	$CF_3\text{-TCDDT}$	Norbornene	45–79	$7.3 \sim 2.1 \times 10^{-1}$ $1.3 \times 10^{-9} \sim 8 \times 10^{-3}$	[87]
AB diblock	VSO	Styrene	34–79	$9 \times 10^{-7} \sim 8 \times 10^{-3}$	[90]
Comblike	Acetylene	Styrene/butadiene	–6–50	$1.5 \times 10^{-2} \sim 1.2$	[93]
Comblike	Acetylene	Ethylene oxide	50	1	[101]
Blend	Acetylene	LDPE	4–82	1–1200	[108]

^amol%.

^bvol%.

Leung and co-workers formed self-assembled polymer nanoparticles with PA cores in solution, using poly(*p*-methylstyrene)/PVSO precursor copolymers [92]. After the elimination of the benzenesulfenic acid moieties from the PVSO block, the resulting copolymer chains aggregated together in a micelle-like fashion. The insoluble polyacetylene block was the core of the nanoparticle, and the poly(*p*-methylstyrene) (PMS) block became the solvent-swallowable outer shell. In Leung's synthesis, a diblock copolymer of PMS and PVSO, with $M_n \approx 15,000$ g/mol and PDI = 1.12, was first formed anionically. The copolymer was then heated in THF at 30–80°C to eliminate benzenesulfenic acid, leaving behind the PMS/PA copolymer in the form of nanoparticles. The kinetics of the micelle formation could be monitored using laser light scattering spectroscopy when the heating was done slowly at a low temperature. The intensity-weighted hydrodynamic size distribution versus the hydrodynamic radius (R_h) was measured at various reaction times. At $t = 0$, the average R_h for the nanoparticles was 3.67 nm with a narrow size distribution. As the elimination progressed, the color of the solution went from colorless to yellow to dark red, and the initially narrow distribution divided into a bimodal distribution. One group of particles, the self-assembled micelle, had a much larger radius, $R_h = 30$ –60 nm. The other group of particles had a much smaller radius with $R_h = 2$ nm and was rationalized to be single chains of PMS/PA. It was assumed that the poly(*p*-methylstyrene) block wrapped around the PA segment to minimize its contact with solvent. The large nanoparticles were stable in solution up to 55°C.

2.7.3. Graft Copolymers of PA

The first type of graft copolymers of PA is made by first reacting a soluble carrier polymer with an oxidizer to form reactive sites on the chain and then reacting the carrier polymer with acetylene [24]. The resulting graft polymers have comblike structures, with PA chains acting as the teeth of the comb (type A graft copolymer). The structure and electronic properties of the PA side chains remain intact, while the carrier polymer solubilizes and protects the PA from degradation.

Typical carrier polymers were monodisperse PI or PS-polybutadiene (PBD) copolymer with M_n of $\sim 2 \times 10^5$ g/mol. The PI was made anionically at -78°C with an 80% *cis*-1,4–15% *trans*-1,4–5% vinyl structure. In the case of the PS-PBD copolymer, styrene was randomly polymerized with 3% butadiene to provide oxidizable unsaturated sites. The carrier polymers were treated with an oxidizer (e.g., *m*-chloroperoxybenzoic acid) to make random electrophilic epoxide moieties in the backbone. The epoxides were then further oxidized to ketones with BF_3 -etherate in benzene.

Under air-free conditions, $\text{Ti}(\text{O}i\text{Bu})_4$ (0.2 M solution) in toluene was mixed with the ketone-modified carrier polymer and a known amount of acetylene dissolved in toluene. To form the active catalyst, AlEt_3 (4 equiv relative to Ti) in toluene was injected into the mixture. The homogenous reaction mixture was then stirred at room temperature. The PA chains formed with nucleophilic ends (connected to the Ti center), and the polymerization reaction terminated when these chain ends encountered one of the electrophilic ketone sites on the carrier polymer to form the grafted side-chain. The whole reaction was done within minutes. The catalyst was then quenched with dilute acid, which also prevented cross-linking at any unreacted epoxides. By adjusting the ratio between acetylene pressure and the number of graft sites, the

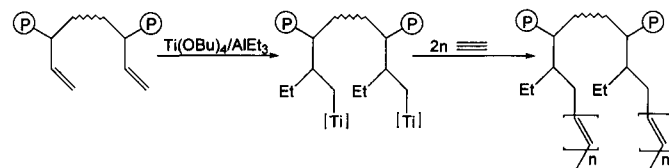
molecular weight of the PA segment could be controlled. Typically, the number of graft sites varied from 15–50 per carrier polymer chain. As the amount of acetylene was increased, there was a shift to lower energy in the UV-Vis spectrum of the polymer, indicative of an increase in conjugation length. Using IR spectroscopy, the molecular weight of the polyacetylene portions was estimated to be between 3 – 6×10^4 g/mol. Typical iodine-doped conductivities for PS-PBD/graft-PA copolymers are listed in Table IV.

A low concentration of PA lends stability to the graft copolymer in solution. If the polyacetylene content is increased beyond a certain value, crystallization takes place, and the copolymer becomes insoluble. With $\geq 50\%$ PA present, the copolymer takes on a fibrillar morphology similar to that of the PA homopolymer (*vide supra*). The most important feature of graft copolymers with polyacetylene is that they contain very few saturated carbon defects (Table V) [24].

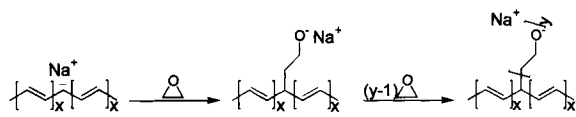
Bolognesi and co-workers synthesized soluble type A graft copolymers of PA and either PBD or PI [93–98]. Two different methods for grafting the acetylene to the carrier polymer were used. In the first method, butadiene was polymerized by $\text{Co}(\text{acac})_2\text{-AlEt}_2\text{Cl}$ in an aromatic solvent. The resulting PBD had a 95% *cis*-1,4–1% *trans*-1,4–4% vinyl structure and a viscosity-average molecular weight (M_v) of 210,000 g/mol. AlEt_3 and $\text{Ti}(\text{O}i\text{Bu})_4$ (4:1 molar ratio) were then added to the polymer solution. The vinyl groups in the PBD inserted into the titanium-alkyl bond, forming new Ti-C bonds that subsequently served as the active sites. The catalyst was aged at room temperature for 1 h, and then acetylene gas was introduced. The reaction was done in a matter of minutes (Scheme XVIII) [93]. Adjusting the concentration ratio between titanium and vinyl groups allowed for the regulation of the number of catalytic sites. The length of the PA side chains in the copolymer was controlled by the quantity of monomer added. The ratio of *cis*- and *trans*-structures in the PA side chains was varied by reaction temperature. At room temperature both *cis*- and *trans*-PA were obtained, and the percentage of *trans*-structure went up as the temperature increased. The conductivity of the graft copolymers varied with the amount of PA present. For I_2 doping, the conductivity $\sigma = 1.5 \times 10^{-2}$ S/cm with 26 wt% PA and could be increased to $\sigma = 1.2$ S/cm with 50 wt% PA. However, the copolymers were only soluble with up to 40 wt% PA.

Table V. Number of Defects in PA As a Function of Structure [24]

Polymer sample	No. of defects/no. of carbons
<i>cis</i> -PA	1/3,000
<i>trans</i> -PA	1/47,000
Graft PA	1/300,000



Scheme XVIII. Graft copolymer (type A) of PA and a soluble matrix.



Scheme XIX. Graft copolymer (type B) of PA and ethylene oxide.

The second method employed *sec*-BuLi and tetramethylethylene diamine (1:1 molar ratio) in cyclohexane at room temperature to deprotonate allylic protons on the PBD backbone [95]. The result was a polymer chain with an allylic carbanion on the backbone. The carbanion reacted with $\text{Ti}(\text{O}i\text{Bu})_4$, displaced one butoxy group, and formed a new Ti–C bond. The resulting titanium(IV) center was reduced to Ti(III) by a second lithiated PBD chain. Acetylene was then polymerized off this Ti(III) metal center. When the Li/Ti ratio was 1, insoluble copolymer precipitated out of solution, but if the proportion of Ti was reduced (Li/Ti > 2), then soluble copolymer was formed. Regardless of the PA content, graft copolymers made in this manner only show low conductivities in the neighborhood of 1.4×10^{-3} S/cm after iodine doping, indicating the presence of PA side chains with only a short conjugation length.

A second type of graft copolymer where PA is the main backbone and the carrier polymer forms the side chains (type B graft copolymer) has also been made. Typical carrier polymers are poly(ethylene oxide) (PEO) and poly(methyl methacrylate) (PMMA) for type B graft copolymers [99–105]. In this method, acetylene is first polymerized by conventional Ziegler–Natta techniques and then lightly doped with sodium naphthalide (1 M solution in THF) so that $\sigma = 5\text{--}50$ S/cm. The doped film is completely dried and then exposed to the carrier polymer monomer (e.g., styrene, methyl methacrylate, ethylene oxide, or isoprene) (Scheme XIX). PA/PEO graft copolymers made in this manner show only low conductivities ($\sigma \approx \sim 1$ S/cm after iodine doping), even with 50% PA content (upper limit). On the other hand, PA/PS graft copolymers obtained by this method do not conduct at all after doping, which is in stark contrast to what is described for PA/PS block copolymers above. It is assumed that the PS side chains form an insulating layer around the PA main chain, so that the dopant molecules cannot diffuse into the conjugated backbone. The insulating outer layer also prevents electronic communication between the chains, thus lowering the overall conductivity of the sample. Another potential explanation for this insulating behavior is that a higher percentage content of PS (versus PA) is needed to keep the graft copolymer soluble. With increasing amounts of PS, the morphology of the graft copolymer becomes less and less fibrillar and less conductive.

Armes and co-workers proposed that the conductivity of graft copolymers of PA is proportional to the level of conductivity of the doped homopolymer of the carrier polymer [106]. They showed that the conductivity of the iodine-doped carrier polymer decreases within the series poly(1,4-isoprene) > poly(3,4-isoprene) > *trans*-PBD > *cis*-poly(butadiene) \sim PS. This trend is then similar for the graft copolymers of these carrier polymers and PA. However, the ultimate conductivity depends on the content ratio of the copolymer and the specific reaction conditions.

2.7.4. Polymer Blends of PA

Acetylene can be polymerized in a low-density polyethylene (LDPE) matrix that is embedded with $\text{Ti}(\text{O}i\text{Bu})_4/\text{AlEt}_3$ catalyst

[18, 107, 108]. In this method, mineral oil was mixed with a high-molecular-weight polyethylene (4×10^6 g/mol) in a flask at room temperature. The viscous mixture was then degassed for an hour at room temperature [108] and then transferred to a machine to spin the LDPE into fibers [109]. In a separate flask, mineral oil was degassed under vacuum. Next, AlEt_3 was added to this mineral oil under argon, followed by the dropwise addition of $\text{Ti}(\text{O}i\text{Bu})_4$ (4:3 v/v equiv to Al) over several minutes. The catalyst mixture was then stirred for 1 h at 120°C and then cooled to room temperature. The spun PE fibers and the catalyst solution were both transferred to a dry box, where the fibers were soaked in the catalyst solution for an hour. The catalyst-imbudded PE fibers were next placed in a tube and degassed, and acetylene (at 510 mmHg) was added. At the end of the reaction, the mineral oil and catalyst were extracted with toluene, and the remaining PE/PA blend was washed with MeOH/HCl and dried. The PE/PA product consisted of fibers that could be split open. The PA was found throughout the PE fiber, not just on the surface. With 4–6 wt% PA content, the conductivity of the blend was 1 S/cm (I_2 doping) [107], but with 82 wt% PA content it rose to 1200 S/cm, indicating a highly oriented PA structure [108].

3. SUBSTITUTED PA

3.1. Synthesis of Substituted PA

Processable analogs of PA can be synthesized from the polymerization of mono- and disubstituted alkynes. Substituted PA typically exhibit greater air stability, better solubility in common organic solvents, lower electrical conductivity, greater range of colors, and higher gas and liquid permeability than normal PA. The enhanced air stability of substituted PA arises from the twisted conformation that the conjugated backbone undergoes to accommodate the substituents (Fig. 6) [110]. In this manner, the conjugated backbone becomes a coiled chain that is protected by the surrounding bulky substituents. Consequently, it is harder for oxygen to react with the backbone and degrade the chain. While twisting of the chain increases the air stability of the polymer, it also disrupts the effective conjugation length of the backbone and decreases the overall conductivity (Table VI).

When substituted alkynes are polymerized, cyclotrimer (substituted benzene) is often formed along with polymer (Scheme XX). The polymers formed are typically low molecular weight ($M_n \approx 10^3$ g/mol). For years, only acetylenes containing electron-withdrawing groups could be polymerized. Recently a group of new catalysts has been developed, so that practically any substituted acetylene monomer can be polymerized [111]. However, the molecular weights of substituted PA still tend to be low. Taking into account all monomers, the average number average M_n of soluble, substituted PA is only about 15,000 g/mol [25]. However, if poly(*t*-butylacetylene) and poly(phenylacetylene) are not included in this calculation, the average M_n falls to only 4000 g/mol.

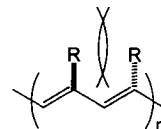
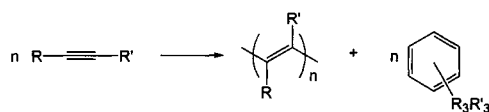


Fig. 6. Steric hindrance between substituents in substituted PA.

Table VI. Conductivities of Various Undoped Substituted Polyacetylene

R	-(RC=CR') _n - R'	σ _{25°C} (S/cm)	Ref.
H	Me	1 × 10 ⁻¹¹	[200]
H	ⁿ Bu	<1 × 10 ⁻¹⁸	[112, 201]
H	^t Bu	<1 × 10 ⁻¹⁸	[116, 202]
H	CH ₂ OH	1 × 10 ⁻⁵	[203]
H	CH(CH ₃)OH	<1 × 10 ⁻¹⁴	[204]
H	CN	1 × 10 ⁻¹⁷	[205, 206]
H	CF ₃	<1 × 10 ⁻¹²	[207]
H	Ph	4 × 10 ⁻¹⁵	[129, 208, 209]
H	<i>o</i> -SiMe ₃ Ph	4 × 10 ⁻¹⁵	[210]
H	<i>o</i> -CF ₃ Ph	2 × 10 ⁻¹⁵	[211, 212]
H	<i>p</i> -MeOPh	1 × 10 ⁻¹⁴	[205]
H	<i>p</i> -ClPh	1 × 10 ⁻¹⁸	[205]
Me	ⁿ Pr	1 × 10 ⁻¹⁸	[213]
Me	ⁿ Pentyl	<1 × 10 ⁻¹⁸	[213]
Me	Ph	1 × 10 ⁻¹⁸	[214]
Me	Si(CH ₃) ₃	1 × 10 ⁻¹⁷	[215, 216]
Et	Et	<1 × 10 ⁻¹⁸	[112]
Et	ⁿ Bu	1 × 10 ⁻¹⁸	[116, 217, 218]
Ph	Ph	1 × 10 ⁻¹⁴	[219, 220]
Ph	Cl	1 × 10 ⁻¹⁸	[221–223]
CN	CN	1 × 10 ⁻⁹	[224]



Scheme XX. Possible products from a polymerization of substituted alkynes.

While it is well known that the Shirakawa Ti(OBu)₄/AlEt₃ catalyst modification will polymerize *un*substituted acetylene, it does not work well for substituted alkynes. In 1981 Chien polymerized propyne (HC≡C-Me) with the Ziegler–Natta catalyst, Ti(OBu)₄/AlEt₃ [81]. Using an air-free technique, Ti(OBu)₄ (1.7 ml) and AlEt₃ (2.7 ml) were mixed together in toluene and aged for 30 min at room temperature. The solution was then cooled to -78°C and degassed for 30–60 min. At this point the flask was warmed to 0°C, and the monomer was added with agitation. The reaction turned a dark brownish red and became viscous. The total reaction time was 60–90 min, and about 300–400 torr of methylacetylene was consumed. The polymer was precipitated with MeOH/HCl, filtered, and redissolved in toluene. This poly(propyne) was an orange, soluble polymer that could be doped to a conductivity of 10⁻³ S/cm with I₂. A UV–visible spectrum of the polymer indicated absorptions at λ_{max} = 220 and 290 nm.

The catalyst Fe(acac)₃/AlEt₃ will polymerize 1° or 2° alkyl-acetylenes (HC≡CR) to soluble high-molecular-weight polymers [112]. However, when the R groups are either 3°-alkyl or aromatic or contain a heteroatom, only oligomers and insoluble polymers are obtained. In general, Ziegler–Natta catalysts are not known to polymerize disubstituted acetylenes (RC≡CR').

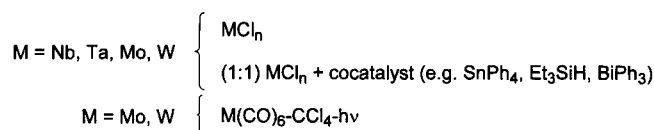


Fig. 7. Group V and VI catalysts for substituted PA synthesis.

On the other hand, metathesis catalysts based on group V and VI metals effectively polymerize mono- and disubstituted alkynes to the corresponding substituted PAs. These catalysts are typically the metal chlorides, used with or without main-group organometallic cocatalysts, or metal carbonyls activated with light (Fig. 7) [110]. The latter type of catalyst is known for Mo and W only. Water can even be used as a cocatalyst with these catalysts for some monomers. For example, WCl₆ · 1/2H₂O polymerizes phenylacetylene to a soluble, powdery poly(phenylacetylene) with M_n = 15,000 g/mol and PDI = 2.06 [113].

In a typical polymerization using metathesis catalysts, the metal salt and the cocatalysts were mixed together in an organic solvent followed by an aging period. If no cocatalyst was used, the catalyst required no aging and was used directly. Subsequently, the substituted acetylene monomer was added, and the extent of conversion was monitored by gas chromatography. The reaction was typically terminated with a mixture of toluene and methanol (5:1 by volume). The reaction mixture was then poured into MeOH to precipitate the polymers.

Molybdenum- and tungsten-based metathesis catalysts tend to be active for monosubstituted and less sterically crowded disubstituted acetylenes. However, MoCl₅ and WCl₆ by themselves will not polymerize disubstituted acetylenes. A cocatalyst is needed to convert Mo(V) and W(VI) to more active forms. Group VI metathesis catalysts will polymerize the monosubstituted acetylenes HC≡CR, but if R contains OH or CO₂H, then the resulting polymers are not soluble. Mo(V) and W(VI) metathesis catalysts will polymerize monosubstituted acetylenes containing 3° alkyl groups, whereas the Ziegler–Natta catalysts will not.

For more bulky disubstituted alkynes (e.g., 1-(trimethylsilyl)-1-propyne), Nb- and Ta-based metathesis catalysts perform better than Mo- and W-based catalysts [114]. For example, TaCl₅ and a main-group organometallic cocatalyst will polymerize diphenylacetylene (PhC≡CPh). With less crowded monomers, the Nb and Ta catalysts tend to give only cyclootrimer product.

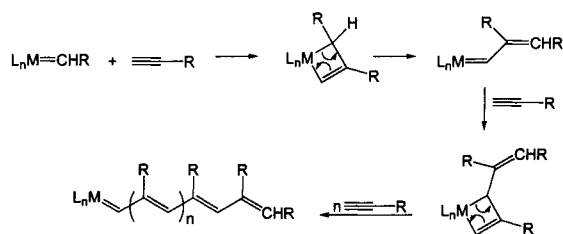
In general, Mo- and W-based metathesis catalysts are very active for the polymerization of pure hydrocarbon alkynes [111]. With alkynes containing electron-donating groups (e.g., HC≡CSiMe₃), only tungsten-based catalysts will work. For alkynes with electron-withdrawing groups (e.g., HC≡CCO₂H, ClC≡CPh), only molybdenum-based catalysts are active. Such trends cannot be outlined for Nb- and Ta-based metathesis catalysts.

Table VII summarizes the products and activities of the various catalysts mentioned versus the types of substrates. With the metathesis mechanism, both polymer and cyclootrimer product are possible for each monomer since the two proposed pathways are very similar [65, 111, 115]. In a metathesis mechanism, after several insertions the propagating chain end can swing around and coordinate to the metal center again instead of inserting another monomer (Scheme XXII). If an intra-molecular olefin metathesis takes place at this point, the product will be cyclic (e.g., cyclootrimer). Due to this possibility of back-biting, sterics play an important role in the production of cyclootrimer. For Mo- and W-

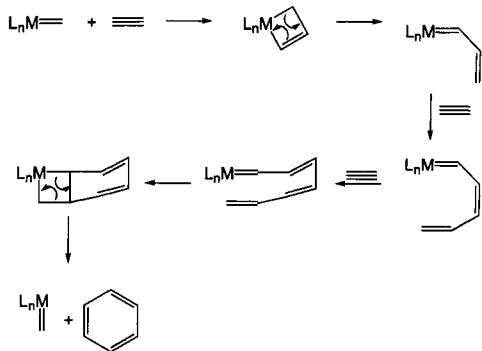
Table VII. General Types of Acetylene Polymerization Products Obtained with Different Catalysts [111]

Catalyst	HC≡CH	Unhindered HC≡CR	Bulky HC≡CR	Unhindered RC≡CR'	Bulky RC≡CR'
Ziegler-Natta	High P	High P	—	—	—
Mo, W	P + C	P + C	High P	High P	—
Nb, Ta	C	C	C	P + C	High P

P, polymer; C, cyclotrimer; —, no activity.



Scheme XXI. A proposed mechanism for the metathesis polymerization of substituted alkynes.



Scheme XXII. A proposed back-biting mechanism for the metathesis polymerization of alkynes. Substituents have been omitted for clarity.

based metathesis catalysts, unhindered alkynes (e.g., 1-hexyne) give a mixture of polymer and cyclotrimer. However, the bulky *t*-butylacetylene monomer produces only polymer. For the Nb- and Ta-based metathesis catalysts, monosubstituted alkynes give cyclotrimer exclusively, while disubstituted monomers yield only polymer. Increasing the rate of polymerization and the molecular weight of the polymer, together with a decrease in the rate of polymer degradation (back-biting), will change the ratio of cyclotrimer to polymer when Nb and Ta catalysts are used [111].

Well-defined tungsten carbene complexes **A** and **B** will polymerize *t*-butylacetylene and phenylacetylene (Fig. 8) [116]. These catalysts are slow but produce good quality polymers in high yield. In a typical experiment, solvent was not used and the reaction was allowed to proceed for 1–2 days. Monomer/initiator ratios ranged from 50 to 100, depending on the acetylene substituent. For poly(phenylacetylene) (PPA) the two catalysts produced similar results. For the phenyl-ethoxy catalyst **A**, the number-average molecular weight of the resulting PPA was 10,400 g/mol, and for the diphenyl catalyst **B**, $M_n = 9000$ g/mol for the resulting PPA.

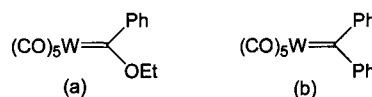


Fig. 8. Tungsten carbenes. (a) Fischer-type carbene **A**. (b) Casey-type carbene **B**.

On the other hand, the polymerization of *t*-butylacetylene gave quite different results. Catalyst **A** yielded poly(*t*-butylacetylene) (P^t BA) with $M_n = 260,000$ g/mol, while catalyst **B** produced P^t BA only in low yield.

The olefin-stabilized carbene **C** shown in Fig. 9 will also catalyze the polymerization of substituted acetylenes since the coordinating olefin is labile and the monomer can easily insert, making it more active [117]. This catalyst is soluble, well defined, and easy to characterize [118]. While the Fischer carbene **A** and the Casey carbene **B** are not very active acetylene polymerization catalysts and need to be at high temperatures to function efficiently, the olefin-stabilized carbene **C** will polymerize substituted acetylenes at room temperature. In a typical experiment, the substituted acetylene (e.g., 1-heptyne, 1-propyne) was added to a solution of catalyst **C** in either hexane or toluene. In the case of 1-heptyne, the red starting catalyst solution progressively turned brown after the addition of the monomer and became more viscous, indicating the formation of a soluble polymer. After 20 h, a 63% yield of the polymer was obtained. The polymer was precipitated out of either hexane or methanol. The M_n of poly(1-heptyne) obtained in this manner is 66,000 g/mol. Gaseous monomers (e.g., acetylene, 1-propyne) form polymers in lower yields than those from liquid monomers. This may be explained by the lower concentration of dissolved gaseous monomer (compared to liquid monomers) in solution at room temperature. Additionally, the reactivity of the alkynes is also a function of the substituent. Monomers containing electron-donating groups (e.g., $R = \text{SiMe}_3$) tend to be more reactive toward carbene-type catalysts than monomers with electron-withdrawing groups.

Since the 1950s, other catalysts have been used to polymerize substituted acetylenes [25]. Free radical initiators (e.g., benzoyl peroxide, di-*t*-butylperoxide) are active catalysts, as are complexes of other transition metals like Ni and Co. Recently, both Rh and Pd cationic complexes have been shown to polymerize monosubstituted acetylenes [119–121]. Thermal polymerizations and γ -

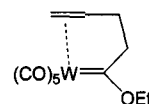


Fig. 9. The olefin-stabilized tungsten carbene **C**.

irradiation of the monomers in both the solid and liquid states also give substituted PA [25]. Both anionic (e.g., *n*-BuLi, NEt₃, NH₂) and cationic (e.g., BF₃) initiators will polymerize substituted alkynes [25]. The products from these last two methods are mostly oligomers.

3.2. Living Systems

With two-component classical metathesis catalysts (e.g., WCl₆/SnPh₄) there is a possibility of unwanted side products from competing reactions like cross-linking or Friedel–Crafts alkylation [18]. The catalyst mixture is made *in situ*, similar to Ziegler–Natta systems, however, only a very small amount of the transition metal centers become the metathesis-active catalyst [65]. Hence, the side products of the acetylene polymerization form partly due to the Lewis-acidic, “left over” metal species. In recent years, a new class of well-defined metathesis catalysts of groups V and VI has emerged as catalysts for the living polymerization of substituted acetylenes [122]. These new complexes are non-Lewis acidic, and every metal center is a metathesis-active catalyst. Thus, there are no side reactions when they are used for acetylene polymerization. For a catalyst system to be considered living, one requirement is that the catalyst initiation rate must be fast relative to the rate of propagation [123, 124]. This ensures that all catalytic centers are activated simultaneously. Furthermore, in a living polymerization there are no termination steps or chain transfers, making the polymer product monodisperse (PDI = 1). Classical catalyst systems such as MoOCl₄-SnBu₄-EtOH (1:1:1) and MoCl₅-SnBu₄-EtOH (1:1:1) are living with certain monomers (e.g., 1-chloro-1-octyne, *o*-(trifluoromethyl)phenylacetylene, and *t*-butylacetylene) [9]. It is important to note that all three components are necessary for the living system. For example, poly(*t*-butylacetylene) synthesized using MoOCl₄ alone had a PDI of 2.29 [125]. Adding a cocatalyst, SnBu₄, to the system lowered the PDI to 1.2. However, when ethanol was added in a 1:1:1 ratio, the system became living, and the resulting poly(*t*-butylacetylene) had a PDI of 1.12 with an $M_n = 149,000$ g/mol.

The same catalyst system, MoOCl₄-SnBu₄-EtOH (1:1:1), is not considered living with poly(phenylacetylene) (PDI > 2.0); however, when there is an *ortho* substituent on the phenyl ring of the acetylene, it is a living system. With *ortho* substituents such as CF₃ and SiMe₃, the polydispersity index of the polymer became as low as 1.06 [126, 127]. The size of the *ortho* substituent also determines the living nature of the polymerization [110]. Phenylacetylene monomers with small *ortho* side groups (e.g., H, F) give polymers with PDI > 2 and are not living. Increasing the steric bulk of the *ortho* group makes the system living. For example, phenylacetylene monomers with medium-sized *ortho* groups (e.g., CH₃, Cl) give polymers with PDI = 1.2–1.3, and those with large, bulky *ortho* substituents (e.g., CF₃, GeMe₃) yield polymers with PDI ≈ 1.1. It is believed that the *ortho* substituents provide the steric protection for the propagating catalyst, effectively blocking any termination reactions. The parent phenylacetylene monomer has no such side group; therefore both chain termination and chain reinitiation are more facile.

3.3. Stereospecific Polymerizations

For poly(*t*-butylacetylene), the catalyst MoOCl₄-SnBu₄-EtOH (1:1:1) is both living and stereospecific [111, 125]. A comparative study between the poly(*t*-butylacetylene) made by MoOCl₄ alone

versus that made by MoOCl₄-SnBu₄-EtOH (1:1:1) has been carried out using ¹³C NMR spectroscopy [128]. For the polymerization made by the MoOCl₄ catalyst only, the ¹³C resonance for the *t*-butyl's methyl signal was split, indicating the presence of both *cis*- and *trans*-*t*-butyl groups, and the polymer was determined to be 57% *cis*. The other ¹³C resonances were broad, denoting an irregular structure. In the ¹³C NMR spectrum of the polymer made by the tricomponent catalyst system (MoOCl₄-SnBu₄-EtOH), there was only one signal for *cis*-*t*-butyl groups, indicating a high selectivity. All other ¹³C signals in the spectrum were also sharp due to the stereoregularity. Temperature played a significant role in the geometry of the polymer. For poly(*t*-butylacetylene) synthesized at 0°C, it had 91% *cis*-content. When the reaction temperature was lowered to -30°C, the percentage of *cis*-structure rose to 97%.

Certain rhodium catalysts are capable of producing stereospecific poly(phenylacetylene) [129–131]. Recently it has been found that stereoregular films of poly(phenylacetylene) can be formed on a water surface in air with Rh(COD)(OTs)(H₂O) catalysts dissolved in the water layer [119]. A 50 μM catalyst solution was made by dissolving the Rh complex in water. The monomer was then dropped onto the water layer as either dilute solution in CHCl₃ or neat. The poly(phenylacetylene) film began to grow within seconds. The film was easily removed from the water surface and found to have $M_n \approx \sim 29,000$ g/mol and PDI = 2.5. The ¹H and ¹³C NMR spectra of this organic-soluble polymer showed very sharp resonances, indicating a regular structure. No *trans*-olefin resonances were detected in the ¹H NMR spectrum of the polymer, so the structure was determined to be 100% *cis*-poly(phenylacetylene). Tang and coworkers believed that a favorable interaction between the phenyl ring and the Rh center must produce the stereoregularity, since other aliphatic monomers did not give similar results.

3.4. Silicon-Substituted Alkyne Monomers

Many silicon-containing acetylene monomers have been successfully polymerized to high molecular weight with metathesis catalysts [111, 132]. It appears that steric effects play an important role in determining the molecular weight. The first class of monomer, **1**, consists of disubstituted acetylenes with one methyl and one silyl substituent. Table VIII shows that high molecular weight polymers were obtained with TaCl₅ and various cocatalysts. It is interesting to note that the analogous Nb-based catalyst does not polymerize the same monomers. The second class of monomer, **2**, is only monosilylated to decrease the steric crowding. Table IX displays various monosilylated alkynes that can be polymerized with WCl₆. When the silyl group was moved away from the triple bond to decrease the steric encumbrance (e.g., HC≡CCH(SiMe₃)R) (**3**), the number average molecular weights did increase up to 320,000 g/mol for R = C₅ and C₇ [132]. A fourth monomer, *o*-(trimethylsilyl)phenylacetylene (**4**), can be polymerized with Mo- and W-based catalysts to quantitative yields with polymer that reaches 1,700,000 g/mol in molecular weight. The bulky silyl group in the *ortho* position plays an important role in increasing the molecular weight since the highest M_n for

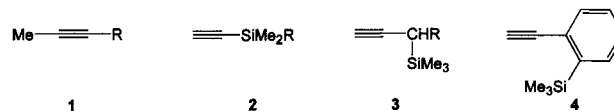


Table VIII. MeC≡CR-Type Monomers that are Polymerizable with TaCl₅ and a Cocatalyst

R	Cocatalyst	% yield	M _n (g/mol)
SiMe ₂ - <i>n</i> -C ₆ H ₁₃	BiPh ₃	70	1,400,000
SiMe ₂ Ph	SnPh ₄	15	460,000
SiEt ₃	SnPh ₄	25	1,200,000
SiMe ₂ CH ₂ SiMe ₃	—	100	1,500,000
SiMe ₂ CH ₂ CH ₂ SiMe ₃	SnPh ₄	58	400,000

Table IX. HC≡CSiMe₂R-Type Monomers that are Polymerizable by WCl₆ in Toluene at Either 30°C or 80°C

R	% yield	M _n (g/mol)
Me	47	*
Ph	44	*
^t Bu	87	*
<i>n</i> -C ₆ H ₁₃	21	9800
CH ₂ CH ₂ CH ₂ Ph	33	9000
CH ₂ CH ₂ Ph	38	7100

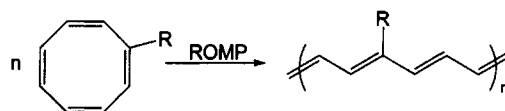
*Partially insoluble.

poly(phenylacetylene) achieved by this method is only around 10,000 g/mol.

3.5. ROMP of RCOT

The ring-opening metathesis polymerization (ROMP) of cyclooctatetraene (COT) with tungsten-based catalysts lead to PA films that are insoluble (*vide supra*). The ROMP of monosubstituted cyclooctatetraene (RCOT) yielded a moderately substituted polyacetylene, containing on average only one side group per eight carbons (Scheme XXIII). This level of substitution allows the polymer to be soluble but with a minimum amount of steric-induced twisting of the backbone. This increased planarity effectively leads to a higher level of conductivity than the polymers derived from mono- and disubstituted acetylenes.

The R group on the monosubstituted cyclooctatetraene dictates the properties of the resulting poly(RCOT) [133]. Monosubstituted COT containing only 1°-alkyl substituents produces soluble *cis*-PAs but upon isomerization to *trans*, the polymers become insoluble. When R is a 2°-alkyl group, the polymer is soluble in both the *cis*- and *trans*-forms and exhibits only modest conductivity with doping. For R = *sec*-Bu, the conductivity is 10 S/cm. RCOT monomers containing tertiary alkyl side groups produce very soluble polymers with very low conductivity. If R is an alkoxy or phenyl group, the polymers are soluble in the *cis*-form but not the *trans*. Obviously the solubility and extent of conductivity are related to the configuration of the backbone. In general, the greater the degree of twisting, the greater the solubility and the lower the conductivity.



Scheme XXIII. The ring-opening metathesis polymerization of RCOT.

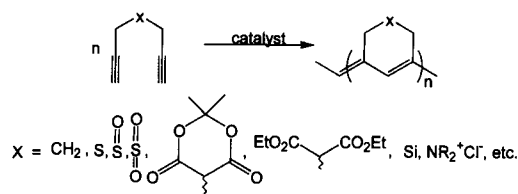
3.6. α, ω -Diyne

A special kind of disubstituted polyacetylene is derivable from the cyclopolymerization of α, ω -diynes (Scheme XXIV). In 1961, Stille and coworkers polymerized 1,6-heptadiyne (X = CH₂) with the classical Ziegler–Natta TiCl₄/Al^{*i*}Bu₃ catalyst to a polymer containing a cyclic conjugated backbone [134]. The polymer was red, soluble, and had a conductivity of 10⁻¹⁰–10⁻¹³ S/cm. Two decades later, Gibson and co-workers improved the conductivity of poly(1,6-heptadiyne) with iodine doping to 10⁻¹ S/cm at room temperature and 1 S/cm at -78°C [135]. The cyclic backbone structure was confirmed by various spectroscopic methods (IR, UV-visible, ¹H and ¹³C NMR). Recently a cationic Pd(II) catalyst has been used to cyclopolymerize α, ω -diynes [136]. These very monodisperse cyclopolymers are freely soluble in a variety of solvents and are of low molecular weight. The polymer structure was determined to contain both a cyclic backbone structure as well as acetylenic side chains.

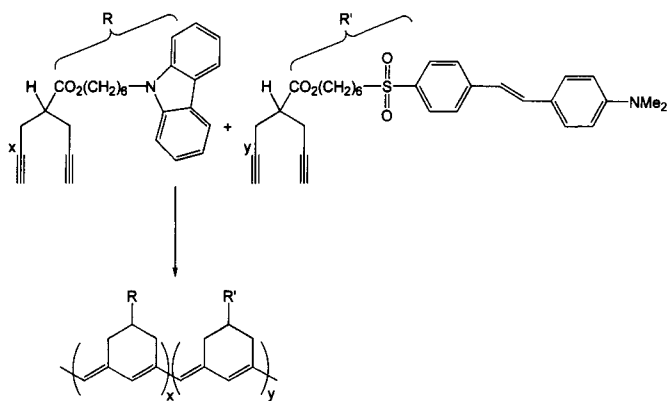
Choi and co-workers explored the cyclopolymerization of α, ω -diynes containing various functionalities with Mo- and W-based metathesis catalysts [137–142]. The number-average molecular weights for these polymers were typically around 10⁵ g/mol. The products were often soluble, and the conductivities were reasonably high, since the double bonds are held closely together by the ring structure. Polymers of this type will probably never conduct as well as the parent PA, since the side ring will hinder interchain contact. These cyclopolymers exhibit λ_{\max} values of up to 480 nm in the UV-visible spectrum and a conductivity of ~10⁻³ S/cm for X = (*n*-C₆H₁₃)₂N⁺ [143].

Recently a photoconductive monomer and a monomer containing a nonlinear optical (NLO) chromophore were cyclopolymerized, using MoCl₅ and WCl₆ catalysts (Scheme XXV) [144]. The resulting copolymer is both photoconductive and photorefractive. (The polymer has two maximum values of photocurrent at 350 nm and 700 nm. Under white light, the photovoltaic response of the polymer is -640 nA. Furthermore, the photo-to-dark conductivity ratio for an undoped polymer is in the range of 30–50.) The number average molecular weight is estimated by GPC to be around 23,000–45,000 g/mol, and the PDI is in the range of ~2.1–3.1. Spectroscopic methods such as IR, UV-visible, and ¹H and ¹³C NMR were used to authenticate the structural assignments.

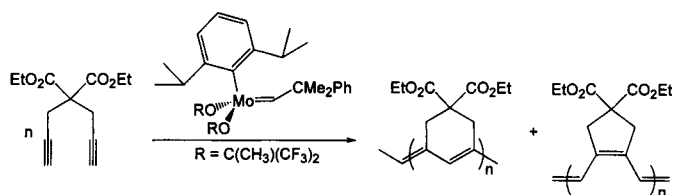
Schrock and co-workers cyclopolymerized diethyl dipropargylmalonate (X = C(CO₂Et)₂) with a well-defined molybdenum alkylidene catalyst [145]. Through ¹³C NMR spectroscopy, equal



Scheme XXIV. The cyclopolymerization of substituted 1,6-heptadiyne.



Scheme XXV. The cyclocopolymerization of substituted 1,6-heptadiynes (R = a photoconductive group and R' = a photorefractive group).

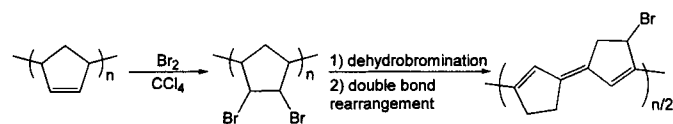


Scheme XXVI. The ring-closing metathesis polymerization of diethyl dipropargylmalonate.

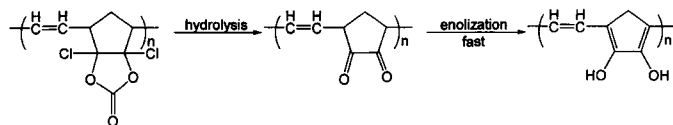
amounts of six-membered rings and five-membered rings were observed (Scheme XXVI). The five-membered rings arose from a tail-to-tail insertion, as opposed to a head-to-tail insertion, to form the six-membered ring.

3.7. Indirect Routes to Substituted PA

A few indirect routes to substituted PAs are known [25]. The first involves bromination of poly(cyclopentadiene) followed by dehydrobromination and a rearrangement of the double bonds (Scheme XXVII) [146]. The resulting polymer is black and has a conductivity of 10^{-6} S/cm. A second method entails a tandem hydrolysis and enolization of a poly(cyclic anhydride) (Scheme XXVIII) [147]. Once again the polymer is black, and its conductivity is fairly low at 10^{-8} S/cm.



Scheme XXVII. An indirect synthesis of substituted PA using the dehydrobromination route.



Scheme XXVIII. An indirect synthesis of substituted PA using the enolate method.

3.8. Properties of Substituted PA

Polymers of substituted acetylenes tend to be highly colored. The colors of these polymers vary throughout the visible spectrum and range from colorless to black. The specific color depends on the degree of steric crowding and whether or not the side group contributes to the conjugation [9]. Alkyl monosubstituted and aromatic disubstituted monomers tend to give lightly colored polymers. Polymers that are derived from alkyl disubstituted monomers, 1-phenyl-1-alkynes, and *t*-butylacetylene are often colorless. *Ortho*-substituted phenylacetylene monomers produce deeply colored polymers. In the UV-visible spectra, λ_{\max} for substituted PAs ranges from 250 to 620 nm. Poly(trimethylsilylacetylene) with an M_n of 50,000 g/mol is yellow with $\lambda_{\max} = 292$ nm in THF [148, 149]. The effective conjugation length of this polymer is only about four double bonds, and it cannot be doped to a conducting state.

Poly(phenylacetylene) has $\lambda_{\max} = 325\text{--}350$ nm [150, 151]. The phenyl side groups can rotate perpendicular to the main chain, minimizing the twisting and increasing the effective conjugation length. Because of this poly(phenylacetylene) is both a semiconductor and a photoconductor. Adding an *ortho*-substituent to the phenyl ring increases the absorption λ_{\max} of the polymer. Poly(*o*-methylphenylacetylene) has a maximum UV-visible absorption at 440 nm; however, the λ_{\max} for poly(*o*-trimethylsilylphenylacetylene) is increased to 520 nm [151]. To accommodate the bulky *ortho* group, the PA chain assumes a *cis*-structure and becomes very planar, raising the effective conjugation length.

Substituted PAs are generally soluble in common organic solvents due to the favorable interactions between the substituents and the solvent [110]. If the volume fraction of the side groups is about equal to or greater than that of the backbone, then the polymer will be soluble [152]. Still, the general solubility trend for conjugated polymers is similar to that for all organic molecules: "like dissolves like." Monomers with alkyl substituents tend to dissolve in nonpolar or slightly polar solvents (e.g., P^tBA is soluble in hexane, toluene, and chloroform). Monomers with aromatic substituents are typically soluble in aromatic solvents.

The degree of conjugation in the backbone of substituted polyacetylenes also plays a role in their solubility in organic solvents. In general, the longer the effective conjugation length, the less soluble a substituted PA will be. For a disubstituted alkyne monomer, if the two substituents are the same (e.g., 3-hexyne, 4-octyne), the corresponding polymer tends not to be soluble since the polymer chains are so densely packed and solvent interaction is minimized. For monosubstituted aromatic acetylenes, the *cis*-polymers are often insoluble. These polymers tend to be too crystalline to dissolve in organic solvent; however, isomerizing the chains to the *trans*-form will aid in solubility. For monosubstituted acetylenes, if the side groups are either too bulky (e.g., $R = 1\text{-adamantyl}$) or too reactive ($R = \text{CH}_2\text{Cl}$) for cross-linking to occur, then the polymers will be insoluble [111].

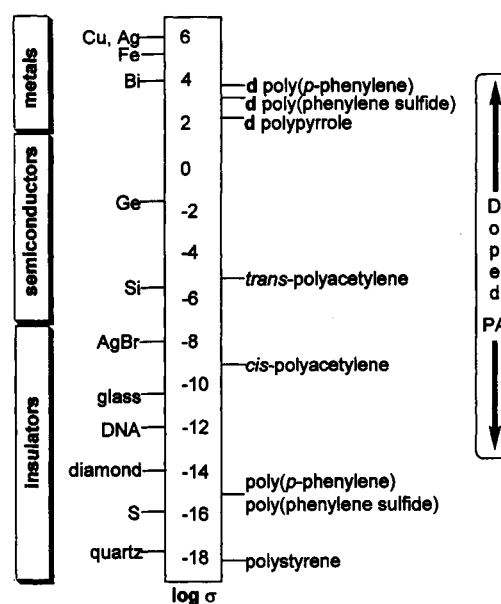
4. ELECTRONIC PROPERTIES OF PA AND ITS ANALOGS

4.1. Conductivity and Chemical Doping

Organic polymers are typically insulators since the valence electrons in sp^3 orbitals are tightly bound to the individual atoms in the backbone and to the σ -based covalent bonds that exist between

the atoms. Because of this structure, little electronic overlap exists between the bonds, and hence the polymers act as insulators. Conjugated polymers, on the other hand, have π bonds and delocalized π electrons extending down the one-dimensional chain axis. The p_z orbitals in a conjugated polymer chain all lie in one direction along the backbone with significant overlap. Theoretically this allows electrons to move freely both down the chain and between chains [153]. When Shirakawa discovered how to make free-standing films of PA, many theoretical models were proposed to predict the conductivity of PA. However, experimental measurements of the conductivity of PA were slow to come due to the inherent instability of PA and the fact that undoped Shirakawa PA is effectively an insulator ($\sigma \approx \sim 10^{-9}$ S/cm). It was not until MacDiarmid and Heeger discovered how to chemically dope crystalline, fibrillar PA [154] and how to measure the resulting significant increase in conductivity that the field really expanded.

It was found that PA could be doped with either electron donors or acceptors, and the conductivity of doped PA could be increased to the metallic state ($\sigma = 1000$ S/cm at room temperature) (Graph 1) (Tables X and XI). With careful control of the extent of doping (e.g., light and heavy doping), the conductivity of PA can be raised to almost any desired level (Fig. 10). Electron acceptors (e.g., I_2 , AsF_5 , ClO_4^-) would oxidize the chain, inducing a hole/positive charge, a process termed p-type doping (Scheme XXIX). Electron donors (e.g., Na, Li, Bu_4N^+) reduce the chain and introduce a negative charge, a reaction called n-type doping (Scheme XXX). Both processes are reversible. n-Doped PA is extremely reactive and moisture sensitive. It does have high thermal stability, however. With electrochemical doping, n-doped PA can be undoped more easily [9]. The specific mechanisms of donor and acceptor doping most likely vary with the particular dopant used and the level of doping [155]. Furthermore, conductivity in conjugated polymers decreases with decreasing tempera-



Graph 1. Comparison of conductivities between inorganic materials and various conjugated polymers (d = doped).

ture, which is the opposite of what is observed for inorganic semiconductors.

4.2. Solitons

The outstanding electronic properties of PA have been attributed to the presence of solitons. It is believed that the soliton is responsible for both the *cis-to-trans* isomerization of PA and the conduc-

Table X. Conductivities of PA with Various Gas-Phase Dopants

Gas-phase Dopant	Equivalents of charge per double bond	$\sigma_{25^\circ C}$ (S/cm)			Ref.
		<i>cis</i>	<i>cis/trans</i>	<i>trans</i>	
-	-	1.7×10^{-9}		4.4×10^{-5}	[225]
I_2	0.50	3.6×10^2			[225, 226]
	0.40			1.6×10^2	[225]
AsF_5	0.28	5.6×10^2			[225]
	0.20			4×10^2	[225]
IBr	0.30	4×10^2			[225]
	0.24			1.2×10^2	[225]
SeF_6	0.17		1.8×10^2		[227]
TeF_6	0.16		2.35×10^2		[227]
ReF_6	0.42		2.3×10^2		[227]
IrF_6	0.04		5×10^1		[227]
MoF_6	0.11		7×10^1		[228]
WF_6	0.087		3.5×10^2		[228]
NbF_5	0.32		2.29×10^2		[229]
TaF_5	0.36		1.47×10^2		[229]
RuF_5	0.02		4.8		[228]
MoF_5	0.19		2.8×10^1		[229]
WF_5	0.04		2.9		[229]

Table XI. Conductivities of PA with Various Solution-Phase Dopants

Solution-phase Dopant	Equivalents of charge per double bond	$\sigma_{25^\circ\text{C}}$ (S/cm)			Ref.
		<i>cis</i>	<i>cis/trans</i>	<i>trans</i>	
MoCl ₅	0.20	2×10^2			[230]
WCl ₆	0.20	2×10^2			[230]
TaCl ₅	0.08	1.05×10^2			[231]
LiFeCl ₄	0.10		5×10^2		[232]
H ₂ PtCl ₄ ·6H ₂ O	0.05	1.2×10^1			[233]
PtCl ₄	0.075	1.34×10^2			[233]
RhCl ₃	0.02	6×10^{-4}			[233]
CuCl ₂	0.08	2×10^{-3}			[233]
InCl ₃	0.11	6×10^2			[234]
TlCl ₃	0.09	5.5×10^2			[234]
NaC ₁₀ H ₈	0.42	2.5×10^1			[225]
	0.56			8×10^1	[225]

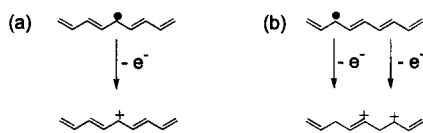
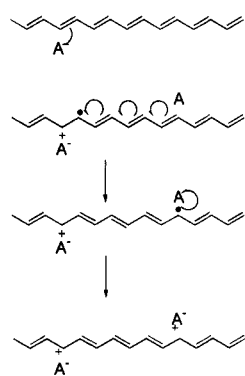
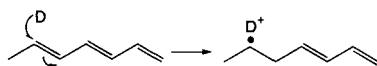


Fig. 10. A schematic representation of a polyacetylene chain with (a) light doping and (b) heavy doping.



Scheme XXIX. The p-type doping mechanism for PA.



Scheme XXX. The n-type doping mechanism for PA.

tivity of doped PA. A soliton is essentially a topological kink in the backbone of the conjugated polymer. It is a defect that can be a radical (single electron), a negative charge (pair of electrons), or a positive charge (zero electrons) (Fig. 11). The soliton's mass is small, thus making the kink mobile. The soliton has a domain wall of about 15 carbons [156]. The presence of solitons has been inferred through various magnetic resonance measurements (e.g., EPR, electron nuclear double resonance spectroscopy) [157].

A soliton may exist naturally as the result of an odd number of carbons in a polymer chain (an odd number of carbons in PA may

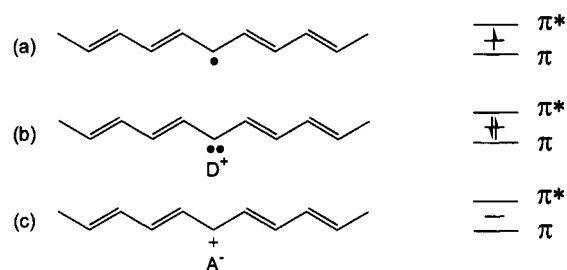


Fig. 11. Schematic representations of (a) neutral soliton, (b) negative soliton, and (c) positive soliton.

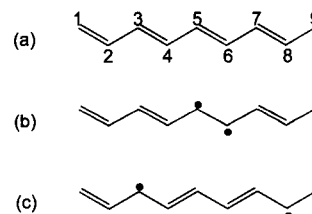


Fig. 12. A schematic representation of a polyacetylene chain (a) at ground state, (b) after the creation of a soliton-antisoliton pair, and (c) after soliton-antisoliton migration.

arise from chain reconstruction, chain oxidation, or chain cleavage); however, solitons are typically generated via chemical means. Solitons created in this way always occurred in pairs of a soliton and an antisoliton. The designation "anti" is a formalism that indicates that the antisoliton "entity" is the one that resides on an even-numbered carbon. By breaking a double bond in the polymer backbone, a neutral soliton-antisoliton pair is formed. The two entities in a soliton-antisoliton pair may migrate away from one another, but the soliton will always remain on odd-numbered carbons, and the antisoliton will always remain on even-numbered carbons (Fig. 12). Charged soliton-antisoliton pairs may also be generated (*vide infra*) (Fig. 13). If a soliton and antisoliton recombine on a chain, they will annihilate one another, but a single soliton (e.g., naturally occurring) will never cease to exist [2].

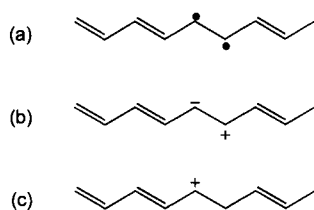


Fig. 13. Schematic representations of (a) a neutral soliton-antisoliton pair, (b) a negative soliton-positive antisoliton pair, and (c) a positive soliton-negative antisoliton pair.

If two neutral solitons travel down the *trans*-PA backbone and meet one another, they will join together to form a double bond. However, if charged solitons approach each other, a different scenario is seen. As seen in Fig. 14, with two acceptor dopant molecules present, two positive solitons are formed on the chain. This doubly charged state is called a bipolaron (spin = 0), and its presence is believed to be responsible for electronic conduction [158]. The two like charges repel one another because of electrostatic forces but attract one another due to interchain interaction. For example, if the interchain geometry is such that the charge on one chain "sees" a like charge on a neighboring chain, they repel each other and move back toward their respective "other half" of the bipolarons. Because of this push-pull relationship, the two charges in a bipolaron pair stay within each other's vicinity. On the other hand, a polaron is a spatially separated combination of a single electron and a positive charge (spin = 1/2). This neutral soliton and positively charged soliton approach each other to form a common defect. Spectroscopic studies of doped PA imply that with light doping the charge in PA is stored in the polaron, and with heavy doping it is stored in the bipolaron [159]. Theoretical calculations show that bipolarons are favored enthalpically, but polarons are preferred entropically.

For the *trans*-structure of PA, a mirror plane exists through the center of the defect. In *cis*-PA, however, there is no such mirror plane and the soliton separates a *cis-transoidal* structure from a *trans-cisoidal* (Fig. 15) [2]. The *trans-cisoidal* structure is higher in energy than the *cis-transoidal*; therefore the soliton will move down the chain through the *trans-cisoidal* domain to isomerize it to the *cis-transoidal* form, thus alleviating the higher energy potential. In *cis*-PA no interchain interaction occurs, but attraction between the soliton and antisoliton still exists because of the energy difference between these two structures.

In *trans*-PA, not all of the bond lengths are equivalent, because two degenerate resonance structures exist (Fig. 16). This physical manifestation is the result of a Peierls distortion [160]. The interactions between bonding electrons dictate the actual spacing of atoms in a one-dimensional solid, and the lowest energy state may not be the one with regular spacing. Not all of the bonds in PA are of equal length; instead they alternate between long and short. This combination of long and short bonds turns out to be more sta-

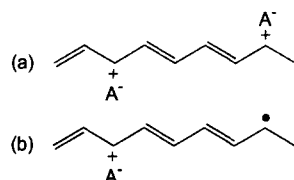


Fig. 14. Schematic representations of (a) a bipolaron and (b) a polaron.

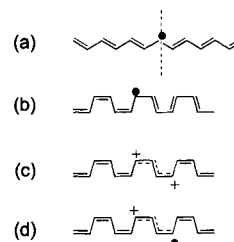


Fig. 15. Schematic representations of (a) a defect in *trans*-PA (a mirror plane can be drawn through the defect itself), (b) a soliton in *cis*-PA, (c) a bipolaron in *cis*-PA, and (d) a polaron in *cis*-PA.

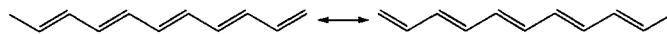


Fig. 16. Resonance structures for *trans*-PA.

ble than the equal bond length scheme. The net effect is the lowering of the total energy and the formation of a bandgap between the valence and conduction bands. It is due to the Peierls distortion that polyacetylene possesses such excellent nonlinear optical properties [161-164].

The rigid band model for PA is similar to that for inorganic semiconductors such as silicon, except that conjugated polymers are treated in the one-dimensional formation. In the structure $-(CH=CH)_n-$ there are $2n$ Hückel-type atomic orbitals divided into n bonding (valence orbitals) and n antibonding (conduction orbitals) [165]. As with small organic molecules, the energy gap between the highest occupied molecular orbital (π) and the lowest unoccupied molecular orbital (π^*) of PA decreases as the number of double bonds and the degree of conjugation increases. For an infinite degree of conjugation, the bandgap is a gap of 1.4 eV for *trans*-PA and 1.8 eV for *cis*-PA [166]. When the PA is excited, whether through photolysis or thermal means, electrons can be promoted from the valence band into the conduction band. Through chain relaxation and a reorganization of bonds, these electrons relax to a mid-gap energy level (Fig. 17). This movement results in a change of bond alteration.

The conductivity of PA increases with an increasing amount of dopant, but a high concentration of dopant is needed to get conductivities up to the metallic state. Polyacetylene is capable of absorbing high levels of dopant, whose concentration is usu-

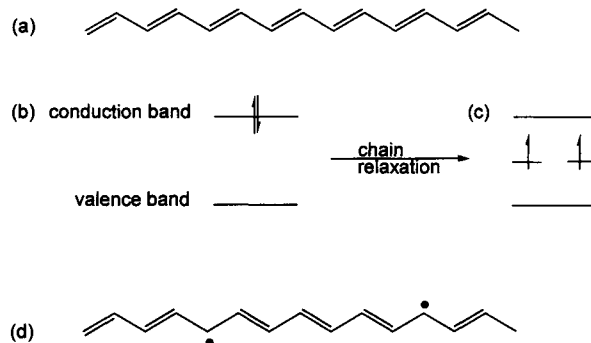
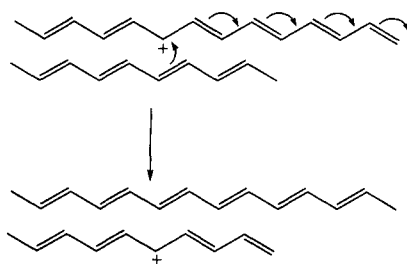


Fig. 17. A schematic representation for the generation of a neutral soliton-antisoliton pair in PA. (a) *trans*-PA. (b) Two electrons were promoted from the valence band to the conduction band via either thermal or photochemical means. (c) Chain relaxation rearranges electrons to the midgap energy level. (d) Rearrangement induces bond alterations between single electrons.



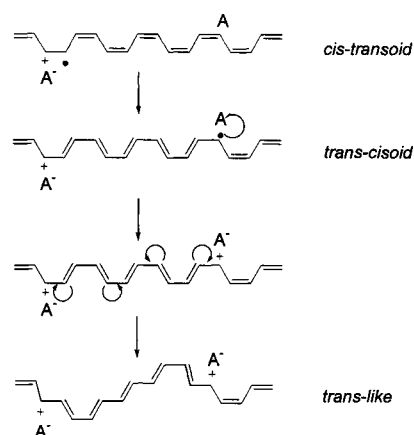
Scheme XXXI. The chain-hopping conduction mechanism in PA.

ally measured with molar fractions—generally 1–20% per carbon atom [66]. With these high dopant concentrations, major structural changes can occur which impede the conductivity at low temperature even though at room temperature the conductivity can reach the metallic regime [66]. With very high levels of doping, so many solitons reside on the chain that they begin to overlap. A soliton is considered a local suppression of the Peierls distortion; when overlapping of solitons occurs the whole chain experiences an overall suppression. At this point the metal-insulator transition is removed and the chain conducts in the metallic regime at room temperature [2].

It is assumed that charge transport occurs down the chain backbone, but PA chains can also fold back onto themselves. There is a probability of charge moving down the backbone, but also it can jump to other sections of the same chain or to a new chain all together (Scheme XXXI). Close contact and the right geometry between chains are the only conditions needed for this chain hopping to occur [13]. The efficiency of charge chain hopping depends on the conjugation length, alignment between chains, and the degree of crystallization. Stretching polyacetylene films often reorients the fibers into better alignment, increasing the conductivity to 10^5 S/cm with iodine doping [18].

4.3. *cis*- to *trans*-Isomerization

The soliton defect can arise naturally from chain reconstruction with an odd number of carbons. The reconstruction may result from chains breaking and forming during the elaborate isomerization process. A mechanism for the isomerization of *cis*- to *trans*-PA via p-type doping has been proposed by Yamabe and co-workers [167]. First, one electron is transferred from the conjugated chain to the dopant, A (Scheme XXXII). This transfer leaves one unpaired electron, but the adjacent electron quickly moves over to create a new double bond. Subsequent electrons move down the chain, forming new double bonds, until a single electron finds a second molecule of the dopant which accepts the unpaired electron. This series of electron jumps changes the direction of bond alteration. In this proposed mechanism, no unpaired electrons are formed in the net reaction, so the spin density remains unchanged, as evidenced by spectroscopy [168]. This latter observation supports the proposed scheme because the total spin density would decrease if the unpaired electron transferred to A were from a natural defect. Furthermore, the defect-based isomerization scenario seems unlikely since the number of natural defects numbers approximately 1/3000 carbons, and typical PA chains contain only 500 carbons. In the third scenario, if the second molecule of A were not to trap the unpaired electron, the electron would continue moving down the chain, effectively increasing the

Scheme XXXII. The *cis*-to-*trans* isomerization of PA induced by doping.

spin density. Again, this is not observed [167]. The Yamabe mechanism is consistent with the observation that while doped *trans*-PA will maintain a *trans*-structure, doped *cis*-PA will shift from a *cis*-structure to *trans-cisoidal* and finally a *trans*-like backbone for the regions between dopant molecules.

4.4. Electrochemical Doping

PA can be electrochemically doped, and the level of doping can be measured with cyclic voltammetry. *cis*-PA can be reversibly oxidized at ~ 3.6 eV versus Li and reduced at ~ 1.4 eV versus Li [169]. The advantage of electrochemical doping is that both n- and p-type doping may be done successively. The degree of doping can be controlled more carefully, and changing the applied charge easily switches the direction (p-type versus n-type). Prolonged electrochemical oxidation often leads to degradation of the chain [170]. The cyclic voltammogram of an electrochemically doped PA film that has been held at an oxidizing potential for a period of time indicates two oxidation peaks: one for the p-doping and another for chain degradation (irreversible). In electrochemical doping, the dopant must diffuse into the PA film to transfer electrons. To facilitate this diffusion process, a film with a high surface area is desirable. Przulski and co-workers have proposed using either a foam or powdered PA electrode to maximize the surface area [171].

4.5. Photochemical Doping

With photoexcitation, it is possible to introduce charge to the PA chain without using chemical dopants. Through optical spectroscopy, the new subgap transitions can be detected and are virtually the same as those found in chemically doped samples [152]. The concentration of long-lived excited states is low, however, and this is not a practical method for maintaining a PA film with stable conductivity.

5. APPLICATIONS OF PA AND ITS ANALOGS

While other conducting polymers such as polypyrrole and polyaniline have found applications in industry, PA has not been employed widely in commercial applications due to its environmental instability. The difficulty in processing and the ease of oxidation, together with the high water/air sensitivity of doped PA, have re-

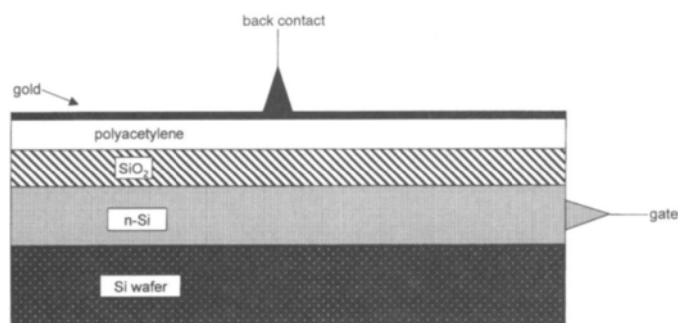


Fig. 18. A schematic drawing of a MISFET device. n-Silicon serves as the metal, SiO_2 is the insulator, and PA is the semiconductor. The top contact layer is made from gold [152].

stricted PA to the confines of laboratory interests. Yet, the potential of PA is enormous because of its exceptional conductivity in comparison to other conducting polymers. As more stable and processable analogs of PA are being developed and as packaging technology becomes more sophisticated in accommodating environmentally sensitive materials, it is hoped that the presence of PA in the modern technological world will increase.

5.1. Semiconductor Devices

In theory, PA would be an excellent material for use in field-effect diodes. For a long time this application was not a realistic endeavor with Shirakawa PA because of its processing problems. PA synthesized by the Durham route would be more ideal, since the polymer layer can be spin-coated to the appropriate shape and thickness. Metal-insulator-semiconductor field effect transistor (MISFET) devices can be fabricated using a solution-processed layer of p-doped PA (instead of the traditional semiconductor layer) on top of a silicon dioxide insulator layer (Fig. 18). Gold would then be evaporated on top to complete the sandwich device. To operate the MISFET device, a negative gate voltage would induce a positive charge that would accumulate on the PA-insulator interface [66, 152]. Spectroscopy indicates the formation of a non-bonding optical absorption at midgap, consistent with the theory for soliton states.

5.2. Rechargeable Batteries

An all-polymer battery that is thin, bendable, lightweight, and very small has been proposed [172]. Conventional batteries can be corrosive, toxic, and harmful to the environment. A plastic battery would eliminate these hazards if it were capable of being continually recharged. The polymer battery technology is becoming increasingly important as electric vehicles and other portable electronic devices become increasingly popular. Among the criteria for portable battery development, a high energy-to-weight ratio is a primary concern. To this end, organic conducting polymers, being lightweight, are potentially excellent materials for active battery electrodes as long as doping levels remain below 10% (per carbon atom). (For heavy dopants (e.g., I_2) higher dopant density will add more weight to the battery.) Furthermore, for a polymer to be used effectively in a battery, it needs to have fast charge transfer kinetics, good reversibility for electrode reactions, high cyclability (e.g., it can be repeatedly charged and recharged many times), and a long shelf life (e.g., low self-discharging activity) [173, 174]. Three

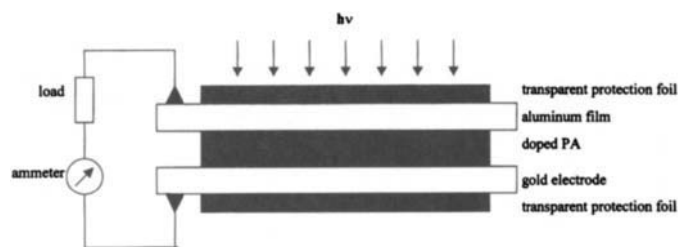


Fig. 19. A schematic drawing of a prototype solar cell containing doped PA.

different configurations of rechargeable batteries are possible: n-doped PA as one electrode, p-doped PA as one electrode, or PA as both electrodes. With PA, although good gravimetric capacity and volumetric capacity can be attained, the issues of low cyclability, difficult processability, high self-discharging activity, and low conducting stability remain [174]. Recently researchers at Johns Hopkins University unveiled a working prototype, all-plastic battery, using fluoro-substituted polythiophenes, a heteroatom analog of PA, for both the anode and cathode [175]. These workers also used gelled polyacrylonitrile as the electrolyte, which facilitated the transportation of the charges between the two terminals. An average potential of ~ 2.75 V per cell could be achieved, and the battery could be recharged repeatedly.

5.3. Solar Cells

Polymers in the semiconducting range can be used in photovoltaic devices (solar cells) when moderately doped [176]. At the heart of a photovoltaic device is a metal-semiconductor junction, which is also a Schottky barrier. When light is shone on this junction, photoinduced excitation and charge separation occur, and electric current can be drawn between the barrier and back contact (Fig. 19). Traditional solid-state solar cells were fabricated using highly pure single crystals of silicon, which is quite costly. To reduce the fabrication cost, moderately doped organic conducting polymers have been employed as the semiconductor part of the Schottky barrier in photovoltaic devices. In achieving the best solar cells using PA, the most notable effort is that by the Caltech group, where soluble poly(RCOT) (*vide supra*) was used as the PA component [177–179]. In the late 1980s and early 1990s, interest in these systems was so high that some researchers envisioned coating the roofs of buildings with conducting polymer films and using the rain gutters as the cell terminals to collect the electricity. At the present time, new generations of solar cells using inexpensive, amorphous silicon is becoming increasingly more economical, so the interest in using conducting polymers for photovoltaic devices has diminished.

5.4. Environmental Sensing Technology Based on PA

The inherent environmental instability of PA turns out to be an advantage in the design of environmental sensors. In these applications, the sensitivity of PA and doped PA toward heat, moisture, impurities, and morphological changes has been utilized in the design of small-scale indicators for radiation, humidity, chemicals, and mechanical abuse [174]. These devices operate on the premise that the electrical conductivity of doped PA will change upon being subjected to environmental changes. Furthermore, PA and doped PA can also be used in gas sensors and biosensors (*vide infra*).

5.4.1. Temperature Limit Detectors

Conducting polymers can be used as indicators for commercial products whose quality can be compromised by temperature changes (e.g., excess heat, freezing, or defrosting) [180]. Such polymers would be useful for inclusion with frozen food, water-based paints, and aqueous medical products. A freeze indicator based on conducting polymers can be fabricated using the inexpensive radio frequency (rf) antitheft target technology that is ubiquitous in retail stores. The rf antitheft target is a small (4 cm in diameter) antenna patch that can be applied to the adhesive side of a label. The antenna itself is a thin strip of aluminum foil in the shape of a square spiral and works at either rf or microwave (μW) frequencies. Upon being excited by a signal from a hand-held transmitter-receiver, the antenna resonates and emits a signal that can be picked up by the detector of the transmitter-receiver. The conducting-polymer-based freeze indicator consists of an rf target that is covered with a layer of undoped conducting polymer (e.g., PA) (Fig. 20). On top of the polymer is a layer of microcapsules containing dopant in solution. In this state the rf target would be ON (e.g., it will emit a signal upon being excited). If the product were to freeze, the mechanical stress induced by the freezing would break the microcapsules and release the dopant solution. The dopant would dope the PA, and the rise in conductivity of the conjugated PA layer would shield the tag from being excited by the radio frequency of the transmitter, effectively turning the detector OFF.

A PA-based defrost indicator works in a similar fashion. First the freezing process ruptures the microcapsules to release the dopant solution. However, a permeable physical barrier exists between the microcapsule layer and the PA film to slow down the diffusion of the dopant solution. This barrier is thick enough that the freezing of the dopant solution (at the freezing temperature) prevents the total penetration of the dopant solution to the conducting polymer. Doping does not begin until the defrost temperature is reached and the dopant solution melts, flowing through the barrier. Once the dopant passes through the barrier, it dopes the polymer. Again the rise in conductivity shields the rf signal, turns the device OFF, and alerts the monitor of a rise in temperature.

The PA-based heat indicator operates on a much simpler level. In this design, the antenna is originally covered with a doped, highly conductive layer of PA, and the device is always in an OFF state. When the tag is exposed to high temperature, thermal degradation sets in and the conductivity of the PA film becomes reduced, which eventually turns the device ON and alerts the receiver of an excess heat situation. Since thermal degradation is a time-dependent process, a constant monitoring of the tag with a variable sensitivity detector over time can reveal the thermal history of the location where the tag is located. Finally, where the temperature fluctuation is small, the monitoring of these heat indicators over time may also be used indirectly in time-indicating applications.

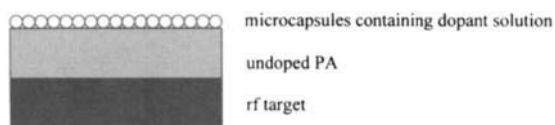


Fig. 20. A schematic drawing of a temperature indicator device. The bottom layer is the rf target. The middle layer is PA. The top layer is made up of microcapsules containing dopant in solution.

5.4.2. Moisture, Radiation, and Mechanical Abuse Detectors

Devices that use PA for the detection of moisture, radiation, and mechanical abuse can also be fabricated using the same rf antitheft tag technology. In the case of moisture detection, the antenna is again covered with a doped, highly conductive layer of PA, and the device is always in an OFF state. When the tag is exposed to moisture, the conductivity is reduced, which eventually turns the device ON. In the cases of radiation and mechanical abuse detection, a similar design can be employed. Again, the external stimuli (radiation or mechanical forces) serve to release the dopant, and the increased in conductivity leads to a lack of rf response by the tag.

The thermally induced solid-state polymerization of diacetylene exhibits a marked change in color as the monomer is polymerized. This behavior has been taken advantage of in the fabrication of a time-temperature indicator [181].

5.4.3. Biosensors

Biosensing is a topic of great interest in modern science. Most conventional tests for biological agents, such as pesticide residues or drugs, require highly trained personnel, sophisticated laboratory instruments, and time measured in days. Traditional approaches utilizing GLC and high-performance liquid chromatography technology often require extensive sample preparation procedures that lead to high costs and long turn around times. Thus it is desirable to develop an inexpensive and quick analytical method for detecting biological compounds, and conducting polymers such as PA allow for the fabrication of such a device. The development of a biosensor using an enzyme-linked immunosorbent assay where either electroconductive PA or polythiophene is used as the solid support has been described [182]. Based on initial studies, these new biosensors are expected to reach sensitivities in the low parts per billion. Sensors that are capable of detecting a range of pesticide residues in food and soil samples as well as in ground water have been proposed.

5.5. Gas-Liquid Separation Membranes

Since polymers of substituted PA have good solubility and good air stability, they make good membranes. Even though substituted PA do not possess very high conductivity, some of them exhibit excellent gas and liquid permeability. These two factors combined imply that substituted polyacetylenes could potentially be used for the oxygen enrichment of air and the separation of ethanol-water mixtures [111].

Among conventional polymers, poly(dimethylsiloxane) (PDMS) has the highest gas permeability known for organic polymers [9]. This permeability can be described by a solution-diffusion mechanism controlled by Henry's law. For substituted polyacetylenes, poly[1-(trimethylsilyl)-1-propyne] (PTMSP) has a gas permeability that is ten times greater than that of PDMS [183-188]. Poly(*t*-butylacetylene) also exhibits high gas permeability. Gases such as N_2 , CH_4 , O_2 , He, H_2 , and CO_2 permeate through both of these substituted polyacetylenes at a rate greater than any previously known polymers (e.g., PDMS, ethyl cellulose, and natural rubber) [185, 189]. In general, bulkier substituents on a substituted PA lead to greater gas permeability. Aromatic or long alkyl substituents on PA give rise to low gas permeability.

Polymer membranes can be used to separate two liquids by pervaporation. One application of this property is in the distilling industry where alcohol or trace organics need to be separated from

water. Cellulose, acetate, poly(phenylene oxide), nylon, polyethylene, and nafion all selectively permeate water over ethanol. However, it is more desirable to select EtOH preferentially [235–237]. Only PDMS and poly[1-(trimethylsilyl)-1-propyne] favor ethanol over water, and they do so equally well [111].

5.6. Other Applications of PA and Its Analogs

A number of novel applications that are specific to other conducting polymers can potentially be extended to PA. Because conducting polymers will change volume depending on their oxidation state, it is possible to convert electrical energy into mechanical works [190]. Thus, electromechanical devices can be made with PA as an integral component. Applications for these include mechanical actuators and artificial muscles [190]. While there are many interesting possibilities in this area there remains a great deal of work to be done.

Electrochromic devices, where a transparent window can be turned opaque at selected regions of the electromagnetic spectrum under a potential, are another area in which PA copolymers and substituted PAs may have potential applications. Promising research opportunities also exist in the fabrication of PA-based controlled-release devices, non-linear optical devices, light-emitting diodes, and radar shielding. The readers are encouraged to consult some older [191–196] and more recent [197–199] review articles on these subjects.

6. CONCLUSION

Polyacetylene has been the subject of intense research activity for many decades. A critical review of its history and evolution reveals that synthetic methods can be used to improve upon the processability of PA, albeit at a cost in the electrical conductivity. Although polyacetylene and its analogs exhibit a wide range of useful properties, none of these polymers are widely used in commercial applications. This observation suggests that the chemistry and physics of PA and PA analogs will continue to be a heavily researched topic for many more years to come.

Acknowledgments

We thank the Dreyfus Foundation, the Beckman Foundation, the Packard Foundation, and the du Pont company for supporting the writing of this manuscript.

NOMENCLATURE

σ	conductivity
acac	acetylacetonato
ARA	addition of reducing agent
bp	boiling point
CF ₃ -TCDT	7,8-bis(trifluoromethyl)tricyclo[4.2.2.0]deca-3,7,9-triene
CH ₃ CN	acetonitrile
CHCl ₃	chloroform
COD	cyclooctadiene
COT	cyclooctatetraene
DMF	dimethylformamide

DPE	1,1-diphenylethylene
DSC	differential scanning calorimetry
E	Young's modulus
ELISA	enzyme-linked immunosorbent assay
ENDOR	electron nuclear double resonance spectroscopy
EPR	electron paramagnetic resonance spectroscopy
EtOH	ethanol
GLC	gas liquid chromatography
GPC	gel permeation chromatography
HDPE	high-density polyethylene
HOMO	highest occupied molecular orbital
HPLC	high pressure liquid chromatography
IR	infrared
LDPE	low-density polyethylene
LUMO	lowest unoccupied molecular orbital
M_n	number-average molecular weight
M_w	weight-average molecular weight
M_v	viscosity-average molecular weight
MeOH	methanol
MISFET	metal-insulator-semiconductor field effect diode
MS	<i>p</i> -methylstyrene
NLO	nonlinear optics
NMR	nuclear magnetic resonance
PA	polyacetylene
P(A/MA)	copolymer of polyacetylene and poly(methylacetylene)
P(A/PA)	copolymer of polyacetylene and poly(phenylacetylene)
P'BA	poly(<i>t</i> -butylacetylene)
PBD	poly(butadiene)
PDI	polydispersity index (M_w/M_n)
PDMS	poly(dimethylsiloxane)
PE	polyethylene
PEO	poly(ethylene oxide)
PI	poly(isoprene)
PTMSP	poly(trimethylsilyl-1-propyne)
PMMA	poly(methylmethacrylate)
PMS	poly(methylstyrene)
PPA	poly(phenylacetylene)
PS	polystyrene
PVC	poly(vinyl chloride)
PVSO	poly(phenyl vinyl sulfoxide)
RCOT	R-substituted cyclooctatetraene
ROMP	ring-opening metathesis polymerization
SEM	scanning electron microscope
THF	tetrahydrofuran
OAc	acetate (O_2CCH_3)
OTs	tosyl ($OSO_2C_6H_4CH_3$)
UV-Vis	ultraviolet-visible spectroscopy
VSO	phenyl vinyl sulfoxide
VSO ₂	phenyl vinyl sulfone

REFERENCES

- W. R. Salaneck, H. R. Thomas, C. B. Duke, A. Paton, E. W. Plummer, A. J. Heeger, and A. G. MacDiarmid, *J. Chem. Phys.* 71, 2044 (1979).
- S. Curran, A. Stark-Hauser, and S. Roth, in "Handbook of Organic Conductive Molecules and Polymers: Conductive Polymers: Synthesis and Electrical Properties" (H. S. Nalwa, Ed.), Vol. 2, p. 1. Wiley, New York, 1997.
- L. M. Leung, in "Handbook of Organic Conductive Molecules and Polymers" (H. S. Nalwa, Ed.), Vol. 2, p. 61. Wiley, New York, 1997.
- G. Natta, G. Mazzanti, and P. Corradini, *Atti. Accad. Naz. Lincei Cl. Sci. Fis. Mat. Natur. Rend. Lincei* 25, 3 (1958).
- R. Fuks and H. G. Viene, in "Chemistry of Acetylenes" (H. G. Viene, Ed.), p. 425. Dekker, New York, 1969.
- H. Shirakawa and S. Ikeda, *Polym. J.* 2, 231 (1971).
- H. Shirakawa and S. Ikeda, *J. Polym. Sci., Polym. Chem. Ed.* 12, 929 (1974).
- T. Ito, H. Shirakawa, and S. Ikeda, *J. Polym. Sci., Polym. Chem. Ed.* 12, 11 (1974).
- H. Shirakawa, T. Masuda, and K. Takeda, in "Chemistry of Triple-Bonded Functional Groups" (S. Patai, Ed.), Vol. 2, p. 945. Wiley, Chichester, UK, 1994.
- K. Soga, S. Kawakami, H. Shirakawa, and S. Ikeda, *Makromol. Chem., Rapid Commun.* 1, 523 (1980).
- K. Soga, S. Kawakami, H. Shirakawa, and S. Ikeda, *Makromol. Chem., Rapid Commun.* 1, 643 (1980).
- H. Shirakawa, A. Hamana, S. Kawakami, M. Sato, S. Koga, and S. Ikeda, *Z. Phys. Chem. (Weisbaden)* 120, 235 (1980).
- V. Enkelman, G. Lieser, W. Muller, and G. Wegner, *Chem. Scr.* 17, 141 (1981).
- J. C. W. Chien, J. D. Capistran, F. E. Karasz, L. C. Dickinson, and M. A. Schem, *J. Polym. Sci., Polym. Lett. Ed.* 21, 93 (1983).
- J. C. W. Chien, "Polyacetylene: Chemistry, Physics, and Materials Science." Academic Press, Orlando, FL, 1984.
- K. Fukui and S. Inagaki, *J. Am. Chem. Soc.* 97, 4445 (1975).
- M. Aldissi, *Synth. Met.* 9, 131 (1984).
- E. J. Ginsburg, C. B. Gorman, and R. H. Grubbs, in "Modern Acetylene Chemistry" (P. Stang and F. Diederich, Eds.), p. 353. VCH, Weinheim, Germany, 1995.
- M. Aldissi, C. Linaya, J. Sledz, F. Schue, L. Giral, J. M. Fabre, and M. Rolland, *Polymer* 23, 243 (1982).
- M. Abadie, S. M. B. Hacene, M. Cadene, and M. Rolland, *Polymer* 27, 2003 (1986).
- M. Rolland, M. Abadie, and M. Cadene, *Rev. Phys. Appl.* 19, 187 (1984).
- H. Shirakawa and S. Ikeda, *Synth. Met.* 1, 175 (1980).
- A. A. Matnishyan and L. S. Grigoryan, *J. Mol. Electron.* 5, 57 (1989).
- G. L. Baker and F. S. Bates, *Mol. Cryst. Liq. Cryst.* 117, 15 (1985).
- H. W. Gibson and J. M. Pochan, in "Encyclopedia of Polymer Science and Engineering" (J. I. Kroschwitz, Ed.), Vol. 1, p. 87. Wiley, New York, 1985.
- L. Lauchlan, S. Etemad, T. C. Chung, A. J. Heeger, and A. G. MacDiarmid, *Phys. Rev. B* 24, 3701 (1981).
- M. A. Druy, C. H. Tsang, N. Brown, A. J. Heeger, and A. G. MacDiarmid, *J. Polym. Sci., Polym. Phys. Ed.* 18, 429 (1980).
- Y. W. Park, M. A. Druy, C. K. Chiang, A. G. MacDiarmid, A. J. Heeger, H. Shirakawa, and S. Ikeda, *J. Polym. Sci., Polym. Lett. Ed.* 17, 195 (1979).
- M. Aldissi, Thesis, "Polymerization of Acetylene with New Catalysts, New Doping Agents, Morphology and Electrical Conductivity of the Doped Polyacetylene Films", Montpellier, 1981.
- A. Pron and I. Kulszewicz-Bajer, *Mater. Sci. Forum* 42, 111 (1989).
- H. Naarmann and N. Theophilou, *Synth. Met.* 22, 1 (1987).
- N. Basescu, Z. X. Liu, D. Moses, A. J. Heeger, H. Naarmann, and N. Theophilou, *Nature (London)* 327, 403 (1987).
- K. Akagi, M. Suezaki, H. Shirakawa, H. Kyotani, M. Shimomura, and Y. Tanabe, *Synth. Met.* 28, D1 (1989).
- K. Akagi, K. Sakamaki, and H. Shirakawa, *Macromolecules* 25, 6725 (1992).
- H. Shirakawa, Y. X. Zhang, K. Mochizuki, K. Akagi, K. Kyotani, and K. Tanabe, *Synth. Met.* 41, 13 (1991).
- H. Shirakawa, K. Akagi, S. Katayama, K. Araya, A. Mukoh, and T. Narahara, *J. Macromol. Sci. Chem.* A25, 643 (1988).
- K. Araya, A. Mukoh, T. Narahara, and H. Shirakawa, *Synth. Met.* 14, 199 (1986).
- K. Akagi, H. Shirakawa, K. Araya, A. Mukoh, and T. Narahara, *Polym. J.* 19, 185 (1987).
- K. Akagi, S. Katayama, H. Shirakawa, K. Araya, A. Mukoh, and T. Narahara, *Synth. Met.* 17, 241 (1987).
- K. Akagi, G. Piao, S. Kanekok, K. Sakamaki, H. Shirakawa, and M. Kyotani, *Science (Washington, D.C.)* 282, 1683 (1998).
- J. Heaviside, P. J. Hendra, P. Tsai, and R. P. Cooney, *J. Chem. Soc., Faraday Trans. 1* 74, 2542 (1978).
- N. Kimokawa, *J. Polym. Sci., Polym. Lett. Ed.* 19, 355 (1981).
- W. E. Daniels, *J. Org. Chem.* 29, 2936 (1964).
- F. D. Kleist and N. R. Byrd, *J. Polym. Sci.* 7, 3419 (1969).
- A. M. Saxman, R. Liepins, and M. Aldissi, *Prog. Polym. Sci.* 11, 57 (1985).
- L. B. Luttinger, *Chem. Ind. (London)* 1135 (1960).
- L. B. Luttinger, *J. Org. Chem.* 27, 1591 (1962).
- G. Lieser, G. Wegner, W. Muller, and V. Enkelman, *Makromol. Chem., Rapid Commun.* 1, 621 (1980).
- V. Enkelman, G. Lieser, M. Monkenbusch, W. Muller, and G. Wegner, *Mol. Cryst. Liq. Cryst.* 77, 111 (1981).
- K. A. O. Starzewski, in "Transition Metal Carbyne Complexes" (F. R. Kreissi, Ed.), p. 67. Kluwer Academic Press, Dordrecht, Netherlands, 1993.
- K. A. O. Starzewski, in "Ziegler Catalysis" (G. Fink and H. H. Brintzinger, Eds.), p. 497. Springer, Berlin, Germany, 1995.
- S. A. Chen and H. J. Shy, *J. Poly. Sci., Poly Chem. Ed.* 23, 2441 (1981).
- K. Aoki, Y. Kakudate, S. Usuba, M. Yoshida, K. Tanaka, and S. Fujiwara, *Solid State Commun.* 64, 1329 (1987).
- K. Aoki, S. Usuba, M. Yoshida, Y. Kakudate, K. Tanaka, and S. Fujiwara, *J. Chem. Phys.* 89, 529 (1988).
- K. Aoki, Y. Kakudate, M. Yoshida, S. Usuba, K. Tanaka, and S. Fujiwara, *Synth. Met.* 28, D91 (1989).
- K. Soga, S. Kobayashi, S. Ikeda, and S. Kawakami, *J. Chem. Soc., Chem. Commun.* 931 (1980).
- H. Kise, *J. Polym. Sci., Polym. Chem. Ed.* 20, 3189 (1982).
- Y. Shindo and T. Hirai, *Makromol. Chem.* 155, 1 (1972).
- A. Baruya, D. L. Gerrard, and W. F. Maddams, *Macromolecules* 16, 578 (1983).
- A. L. Safir and B. M. Novak, *Macromolecules* 26, 4072 (1993).
- R. S. H. Liu and C. G. Krespan, *J. Org. Chem.* 34, 1271 (1969).
- A. R. L. Bursics, E. Bursics-Szekeres, M. Murray, and F. G. A. Stone, *J. Fluorine Chem.* 7, 619 (1976).
- J. H. Edwards and W. J. Feast, *Polymer* 21, 595 (1980).
- P. I. Clemenson, H. Cramail, P. W. Dyer, S. Feast, W. J. Feast, V. C. Gibson, E. Khosravi, D. Parker, and J. N. Winter, "81st Nobel Symposium: Conjugated Polymers and Related Materials," Vol. 1991, 1993, p. 171.
- K. J. Ivin and J. C. Mol, "Olefin Metathesis and Metathesis Polymerization." Academic Press, San Diego, 1997.
- J. W. Feast and R. H. Friend, *J. Mater. Sci.* 25, 3796 (1990).
- W. J. Feast, D. Parker, J. N. Winter, D. C. Bott, and N. S. Walker, in "Electronic Properties of Polymers and Related Compounds" (H. Kuzmany, M. Mehring, and S. Roth, Eds.), p. 45. Springer-Verlag, New York, 1985.
- C. B. Gorman and R. H. Grubbs, in "Conjugated Polymers" (J. L. Bredas and R. Sillbey, Eds.), p. 1. Kluwer, Dordrecht, Netherlands, 1991.
- D. Bott, C. Brown, C. Chai, N. Walker, W. Feast, P. Foot, P. Calvert, N. Billingham, and R. Friend, *Synth. Met.* 14, 245 (1986).
- J. H. Edwards, W. J. Feast, and D. C. Bott, *Polymer* 25, 395 (1984).

71. W. J. Feast and J. N. Winter, *J. Chem. Soc., Chem. Commun.*, 202 (1985).
72. L. A. Paquette and R. V. C. Carr, *Org. Synth.* 64, 157 (1985).
73. R. S. Kanga, T. E. Hogen-Esch, E. Randrianalimanana, A. Soum, and M. Fontanille, *Macromolecules* 23, 4235 (1990).
74. L. M. Leung and K. H. Tan, *Macromolecules* 26, 4426 (1993).
75. Y. V. Korshak, V. V. Korshak, G. Kanischka, and H. Hocker, *Makromol. Chem., Rapid Commun.* 6, 685 (1985).
76. F. L. Klavetter and R. H. Grubbs, *J. Am. Chem. Soc.* 110, 7807 (1988).
77. F. L. Klavetter, "Polyacetylene and Novel Conjugated Derivatives Through The Metathesis Polymerization of 1,3,5,7-Cyclooctatetraenes" Ph.D. Thesis, Division of Chemistry and Chemical Engineering, California Institute of Technology, 1989.
78. W. Reppe, O. Schlichting, K. Klager, and T. Toepel, *Justus Liebigs Ann. Chem.* 560, 1 (1948).
79. R. E. Colborn and K. P. C. Vollhardt, *J. Am. Chem. Soc.* 108, 5470 (1986).
80. T. M. Swager, D. A. Dougherty, and R. H. Grubbs, *J. Am. Chem. Soc.* 110, 2973 (1988).
81. J. C. W. Chien, G. E. Wnek, F. E. Karasz, and J. A. Hirsch, *Macromolecules* 14, 479 (1981).
82. W. Deits, P. Cukor, M. Rubner, and H. Jopson, *Synth. Met.* 4, 199 (1982).
83. M. Aldissi, *Chem. Commun.* 20, 1347 (1984).
84. M. Aldissi and A. R. Bishop, *Polymer* 26, 622 (1985).
85. M. Aldissi, *Synth. Met.* 13, 87 (1986).
86. M. Aldissi, *Synth. Met.* 15, 141 (1986).
87. S. Ramakrishnan, J. A. Hirsch, J. R. Martinez, and J. C. W. Chien, *J. Polym. Sci., Chem. Ed.* 27, 3937 (1989).
88. S. A. Krouse and R. R. Schrock, *Macromolecules* 21, 1888 (1988).
89. J. Allgaier, R. Nuffer, and C. Mathis, *Synth. Met.* 41, 965 (1991).
90. L. M. Leung and K. H. Tan, *Polym. Commun.* 35, 1556 (1994).
91. D. Freyss, P. Rempp, and H. Benoit, *J. Polym. Sci., Polym. Lett.* 2, 217 (1964).
92. C. Wu, A. Niu, L. M. Leung, and T. S. Lem, *J. Am. Chem. Soc.* 121, 1954 (1999).
93. S. Destri, M. Catellani, and A. Bolognesi, *Makromol. Chem., Rapid Commun.* 5, 353 (1984).
94. A. Bolognesi, M. Catellani, and S. Destri, *Mol. Cryst. Liq. Cryst.* 117, 29 (1985).
95. A. Bolognesi, M. Catellani, S. Destri, and W. Porzio, *Polymer* 27, 1128 (1986).
96. W. Porzio, A. Bolognesi, M. Catellani, S. Destri, S. V. Meille, and E. Pedemonte, *Mol. Cryst. Liq. Cryst.* 117, 71 (1985).
97. P. Piaggio, A. Bolognesi, M. Catellani, and S. Destri, *Mol. Cryst. Liq. Cryst.* 117, 311 (1985).
98. C. Cuniberti, P. Piaggio, G. Dellepiane, M. Catellani, L. Piseri, W. Porzio, and R. Tubino, *Makromol. Chem., Rapid Commun.* 7, 471 (1986).
99. G. F. Dandreaux, M. E. Galvin, and G. E. Wnek, *J. Phys. Colloq.* C3, 135 (1983).
100. G. F. Dandreaux, M. E. Galvin, and G. E. Wnek, *Org. Coat. Appl. Polym. Sci. Proc.* 48, 541 (1983).
101. G. F. Dandreaux, M. E. Galvin, and G. E. Wnek, in "Polymers in Electronics" (T. Davidson, Ed.), (ACS Symp. Ser., Vol. 242), p. 507. American Chemical Society, Washington, D.C., 1984.
102. M. E. Galvin and G. E. Wnek, *Polym. Prepr. (Am. Chem. Soc., Div. Polym. Chem.)* 24, 14 (1983).
103. M. E. Galvin and G. E. Wnek, *Polym. Prepr. (Am. Chem. Soc., Div. Polym. Chem.)* 25, 229 (1984).
104. M. E. Galvin and G. E. Wnek, *Mol. Cryst. Liq. Cryst.* 117, 33 (1985).
105. M. E. Galvin and G. E. Wnek, *Polym. Bull.* 13, 109 (1985).
106. S. P. Armes, *Synth. Met.* 44, 95 (1991).
107. M. E. Galvin and G. E. Wnek, *Polym. Commun.* 23, 795 (1982).
108. J. C. Chiang, P. Smith, A. J. Heeger, and F. Wudl, *Polym. Commun.* 29, 161 (1988).
109. P. Smith and P. J. Lemstra, *J. Mater. Sci.* 15, 505 (1980).
110. T. Masuda and H. Tachimori, *J. Macromol. Sci., Pure Appl. Chem.* A31, 1675 (1994).
111. T. Masuda and T. Higashimura, *Adv. Polym. Sci.* 81, 121 (1986).
112. T. Masuda, M. Kawasaki, Y. Okano, and T. Higashimura, *Polym. J.* 14, 371 (1982).
113. T. Masuda, N. Sasaki, and T. Higashimura, *Macromolecules* 8, 717 (1975).
114. T. Masuda, T. Takahashi, and T. Higashimura, *J. Chem. Soc., Chem. Commun.* 1297 (1982).
115. H. Yamazaki and Y. Wakatsuki, *J. Organomet. Chem.* 139, 157 (1977).
116. T. J. Katz and S. J. Lee, *J. Am. Chem. Soc.* 102, 422 (1980).
117. D. J. Liaw, A. Soum, M. Fontanille, A. Parlier, and H. Rudler, *Makromol. Chem., Rapid Commun.* 6, 309 (1985).
118. C. Alvarez, J. Levisalles, M. Rudler, H. Rudler, J. C. Daran, and Y. Jeannin, *J. Organomet. Chem.* 228, C7 (1982).
119. B.-Z. Tang, W. H. Poon, S. M. Leung, W. H. Leung, and H. Peng, *Macromolecules* 30, 2209 (1997).
120. K. J. S. Harrell and S. T. Nguyen, unpublished observations (1999).
121. C. B. Gorman, R. W. Vest, T. U. Palovich, and S. Serron, *Macromolecules* 32, 4157 (1999).
122. J. Feldman and R. R. Schrock, *Prog. Inorg. Chem.* 39, 1 (1991).
123. M. Szwarc, "Carbanions, Living Polymers, and Electron Transfer Processes." Wiley-Interscience, New York, 1968.
124. M. Van Beylen, S. Bywater, G. Smets, M. Szwarc, and D. J. Worsfold, *Adv. Polym. Sci.* 86, 87 (1988).
125. M. Nakano, T. Masuda, and T. Higashimura, *Macromolecules* 27, 1344 (1994).
126. T. Masuda, K. Mishima, J. Fujimori, M. Nishida, H. Muramatsu, and T. Higashimura, *Macromolecules* 25, 1401 (1992).
127. T. Masuda, J. Fujimori, M. Z. A. Rahman, and T. Higashimura, *Polym. J.* 25, 535 (1993).
128. Y. Okano, T. Masuda, and T. Higashimura, *Polym. J.* 14, 477 (1982).
129. A. Furlani, C. Napoletano, M. V. Russo, and W. J. Feast, *Polym. Bull.* 16, 311 (1986).
130. A. Furlani, C. Napoletano, M. V. Russo, A. Camus, and N. Marsich, *J. Polym. Sci., Polym. Chem.* 27, 75 (1989).
131. W. Yang, M. Tabata, S. Kobayashi, K. Yokota, and A. Shimizu, *Polymer* 23, 1135 (1991).
132. T. Masuda and T. Higashimura, in "Silicon-Based Polymer Science," Advances in Chemistry Series, Vol. 224, p. 641. American Chemical Society, Washington, D.C., 1990.
133. R. H. Grubbs, *Polym. Prepr. (Am. Chem. Soc., Div. Polym. Chem.)* 32, 84 (1991).
134. J. K. Stille and D. A. Frey, *J. Am. Chem. Soc.* 83, 1697 (1961).
135. H. W. Gibson, F. C. Bailey, A. J. Epstein, H. Rommelmann, S. Kaplan, J. Harbour, X.-Q. Yang, D. B. Tanner, and J. M. Pochan, *J. Am. Chem. Soc.* 105, 4417 (1983).
136. K. J. S. Harrell and S. T. Nguyen, *Polym. Prepr. (Am. Chem. Soc., Div. Polym. Chem.)* 40, 121 (1999).
137. Y.-S. Gal and S.-K. Choi, *J. Polym. Sci., Polym. Lett. Ed.* 26, 115 (1988).
138. Y.-S. Gal, B. Jung, W.-C. Lee, and S.-K. Choi, *J. Polym. Sci., Polym. Chem.* 30, 2657 (1992).
139. Y.-S. Gal and S.-K. Choi, *J. Polym. Sci., Polym. Chem.* 31, 345 (1993).
140. M.-S. Jang, S.-K. Kwon, and S.-K. Choi, *Macromolecules* 23, 4135 (1990).
141. K. M. Koo, S. H. Han, Y. S. Kang, U. Y. Kim, and S. K. Choi, *Macromolecules* 26, 2485 (1993).
142. M.-S. Ryoo, W.-C. Lee, and S.-K. Choi, *Macromolecules* 23, 3029 (1990).
143. K. L. Kang, S. H. Kim, H. N. Cho, K. Y. Choi, and S. K. Choi, *Macromolecules* 26, 4539 (1993).
144. S.-K. Choi, J.-H. Lee, and H.-K. Kim, *Makromol. Symp.* 118, 67 (1997).
145. H. H. Fox, M. O. Wolf, R. O'Dell, B. L. Lin, R. R. Schrock, and M. S. Wrighton, *J. Am. Chem. Soc.* 116, 2827 (1994).
146. P. E. Blatz, *J. Polym. Sci.* 4, 1335 (1963).

147. A. Alimuniar, J. H. Edwards, J. W. Feast, K. Harper, and I. S. Millichamp, Proceedings of the 28th IUPAC Macromolecular Symposium Preprints, I.U.P.A.C., p. 422. University of Massachusetts, Amherst, MA, 1982.
148. J. M. Ziegler, *Polym. Prepr. (Am. Chem. Soc., Div. Polym. Chem.)* 25, 223 (1984).
149. J. M. Ziegler, U.S. Patent Application, 1986.
150. P. Ehrlich and W. A. Anderson, in "Handbook of Conducting Polymers" (T. A. Skotheim, Ed.), Vol. 1, p. 441. Dekker, New York, 1986.
151. J. Kunzler and V. Percec, *J. Polym. Sci., Polym. Chem. Ed.* 28, 1221 (1990).
152. R. H. Friend, *Synth. Met.* 51, 357 (1992).
153. A. B. Kaiser and S. C. Graham, *Synth. Met.* 36, 367 (1990).
154. C. K. Chiang, C. R. Fincher, Y. W. Park, A. J. Heeger, H. Shirakawa, E. J. Louis, S. C. Gau, and A. G. MacDiarmid, *Phys. Rev. Lett.* 39, 1098 (1977).
155. B. Vincent, *Polym. Adv. Technol.* 6, 356 (1995).
156. A. J. Heeger and A. G. MacDiarmid, *Chem. Scr.* 17, 115 (1981).
157. S. Kuroda, *Int. J. Mod. Phys. B* 9, 221 (1995).
158. M. E. Galvin, *JOM* 49, 52 (1997).
159. A. J. Heeger and P. Smith, in "Conjugated Polymer" (J. L. Bredas and R. J. Silbey, Eds.), p. 141. Kluwer, Dordrecht, the Netherlands, 1991.
160. R. E. Peierls, "Quantum Theory of Solids," p. 108. Clarendon Press, London, 1955.
161. S. Etamad, A. J. Heeger, and A. G. MacDiarmid, *Annu. Rev. Phys. Chem.* 33, 443 (1982).
162. A. J. Heeger and A. G. MacDiarmid, in "The Physics and Chemistry of Low-Dimensional Solids" (L. Alcacer, Ed.), p. 353. Riedel, Dordrecht, the Netherlands, 1980.
163. A. J. Heeger and A. G. MacDiarmid, *Chem. Scr.* 17, 115 (1981).
164. A. J. Heeger and A. G. MacDiarmid, *Mol. Cryst. Liq. Cryst.* 77, 1 (1981).
165. B. E. Kohler, in "Conjugated Polymers" (J. L. Bredas and R. J. Silbey, Eds.), p. 405. Kluwer, Dordrecht, the Netherlands, 1991.
166. S. Lefrant and J. Bullot, *Mater. Sci. Forum* 122, 25 (1993).
167. T. Yamabe, K. Akagi, H. Shirakawa, K. Ohzeki, and K. Fukui, *Chem. Scr.* 17, 157 (1981).
168. Y. Tomkiewicz, T. D. Schultz, H. B. Broom, T. C. Clarke, and G. B. Street, *Phys. Rev. Lett.* 43, 1532 (1979).
169. P. J. Nigrey, A. G. MacDiarmid, and A. J. Heeger, *Mol. Cryst. Liq. Cryst.* 83, 1341 (1982).
170. J. C. W. Chien and J. B. Schlenoff, *Nature (London)* 311, 362 (1984).
171. J. Przyluski and M. Zagorska, *Mater. Sci. Forum* 21, 31 (1987).
172. A. Salzhauer, *Technol. Rev.* 101, 60 (1998).
173. B. Scrosati, S. Panero, P. Prospero, A. Corradini, and M. Mas-tragostino, *J. Power Sources* 19, 27 (1987).
174. A. Techagumpuch, H. S. Nalwa, and S. Miyata, in "Electroresponsive Molecular and Polymeric Systems" (T. A. Skotheim, Ed.), Vol. 2, p. 257. Dekker, New York, 1991.
175. J. G. Killian, Y. Gofer, H. Sarker, T. O. Poehler, and P. C. Searson, *Chem. Mater.* 11, 1075 (1999).
176. S. Roth, W. Graupner, and P. McNeillis, *Acta Phys. Pol. A* 87, 699 (1995).
177. T. H. Jozefiak, M. J. Sailor, E. J. Ginsburg, C. B. Gorman, N. S. Lewis, and R. H. Grubbs, *Proc. SPIE-Int. Soc. Opt. Eng.* 1436, 8 (1991).
178. M. J. Sailor, E. J. Ginsburg, C. B. Gorman, A. Kumar, R. H. Grubbs, and N. S. Lewis, *Science (Washington, D.C.)* 249, 1146 (1990).
179. M. J. Sailor, F. L. Klavetter, R. H. Grubbs, and N. S. Lewis, *Nature (London)* 346, 155 (1990).
180. R. H. Baughman, R. L. Elsenbaumer, Z. Iqbal, G. G. Miller, and H. Eckhardt, *Chim. Ind.* 73, 396 (1991).
181. R. H. Baughman, R. L. Elsenbaumer, Z. Iqbal, G. G. Miller, and H. Eckhardt, in "Electronic Properties of Conjugated Polymers" (H. Kuzmany, M. Mehring, and S. Roth, Eds.), Vol. 87, p. 432. Springer-Verlag, Berlin, 1987.
182. R. G. Sandberg, L. J. Vanhouten, J. L. Schwartz, R. P. Bigliano, S. M. Dallas, J. C. Silvia, M. A. Cabelli, and V. Narayanswamy, in "Biosensor Design and Application" (P. R. Mathewson and J. W. Finley, Eds.), (ACS Symposium Ser., Vol. 511), p. 81. American Chemical Society, Washington, D.C., 1992.
183. T. Masuda, E. Isobe, T. Higashimura, and K. Takada, *J. Am. Chem. Soc.* 105, 7473 (1983).
184. T. Masuda, Y. Iguchi, B.-Z. Tang, and T. Higashimura, *Polymer* 29, 2041 (1988).
185. K. Takada, H. Matsuya, T. Masuda, and T. Higashimura, *J. Appl. Polym. Sci.* 30, 1605 (1985).
186. Y. Ichiraku, S. A. Stern, and T. Nakagawa, *J. Membr. Sci.* 34, 5 (1987).
187. L. C. Witchey-Lakshmanan, H. B. Hopfenberg, and R. T. Chern, *J. Membr. Sci.* 48, 321 (1990).
188. N. A. Plate, A. K. Bokarev, N. E. Kalieuzhnyi, E. G. Litvinova, V. S. Khotimskii, V. V. Volkov, and Y. P. Yampolskii, *J. Membr. Sci.* 60, 13 (1991).
189. H. Yasuda and V. Stannett, in "Polymer Handbook" (J. Brandrup and E. H. Immergut, Eds.), 2nd ed., p. 229. Wiley-Interscience, New York, 1975.
190. R. H. Baughman, *Synth. Met.* 78, 339 (1996).
191. H. Stubb, E. Punkka, and J. Paloheimo, *Mater. Sci. Eng. R-Rep.* 10, 85 (1993).
192. A. K. Bakhshi, *Indian J. Chem., Sect. A* 31, 291 (1992).
193. A. Bhattacharya and A. De, *J. Macromol. Sci., Rev. Macromol. Chem. Phys.* C39, 17 (1999).
194. S. Maiti, *Indian J. Chem., Sect. A* 33, 524 (1994).
195. A. A. Pud, *Synth. Met.* 66, 1 (1994).
196. J. Tsukamoto, *Adv. Phys.* 41, 509 (1992).
197. K. Gurunathan, A. V. Murugan, R. Marimuthu, U. P. Mulik, and D. P. Amalnerkar, *Mater. Chem. Phys.* 61, 173 (1999).
198. J. D. Stenger-Smith, *Prog. Polym. Sci.* 23, 57 (1998).
199. D. Kumar and R. C. Sharma, *Eur. Polym. J.* 34, 1053 (1998).
200. H. A. Pohl and R. P. Chartoff, *J. Polym. Sci., Part A: Polym. Chem.* 2, 2787 (1964).
201. Y. Nakayama, K. Mashima, and A. Nakamura, *Macromolecules* 26, 6267 (1993).
202. T. Masuda, Y. Okano, Y. Kuwane, and T. Higashimura, *Polym. J.* 12, 907 (1980).
203. I. A. Akopyan, S. G. Grigoryan, G. A. Zhamkochyan, and S. G. Matsoyan, *Vysokomol. Soedin.* A17, 2517 (1975).
204. I. A. Akopyan, S. G. Grigoryan, G. A. Zhamkochyan, and S. G. Matsoyan, *Polym. Sci. U.S.S.R.* A17, 2896 (1975).
205. A. G. Hankin and A. M. North, *Trans. Faraday Soc.* 63, 1525 (1967).
206. C. Carlini and J. C. W. Chien, *J. Polym. Sci., Polym. Chem. Ed.* 22, 2749 (1984).
207. W. Deits, P. Cukor, M. Rubner, and H. Jopson, *Ind. Eng. Chem. Prod. Res. Dev.* 20, 696 (1981).
208. T. Masuda, K. Q. Thieu, N. Sasaki, and T. Higashimura, *Macromolecules* 9, 661 (1976).
209. T. Masuda, K. Yamamoto, and T. Higashimura, *Polymer* 23, 1663 (1982).
210. T. Masuda, T. Hamano, K. Tsuchihara, and T. Higashimura, *Macromolecules* 23, 1374 (1990).
211. H. Muramatsu, T. Ueda, and K. Ito, *Macromolecules* 18, 1634 (1985).
212. T. Masuda, T. Hamano, T. Higashimura, T. Ueda, and H. Muramatsu, *Macromolecules* 21, 281 (1988).
213. T. Higashimura, Y. X. Deng, and T. Masuda, *Macromolecules* 15, 234 (1982).
214. T. Masuda, A. Niki, E. Isobe, and T. Higashimura, *Macromolecules* 18, 841 (1985).
215. T. Masuda, E. Isobe, and T. Higashimura, *Macromolecules* 18, 841 (1985).
216. T. Masuda, E. Isobe, T. Hamano, and T. Higashimura, *Macromolecules* 19, 2448 (1986).

217. T. Masuda, T. Takahasi, and T. Higashimura, *J. Chem. Soc., Chem. Commun.* 1297 (1982).
218. T. C. Clarke, C. S. Yannoni, and T. J. Katz, *J. Am. Chem. Soc.* 105, 7787 (1983).
219. T. Masuda, H. Kawai, T. Ohtori, and T. Higashimura, *Polym. J.* 11, 813 (1979).
220. A. Niki, T. Masuda, and T. Higashimura, *J. Polym. Sci., Part A: Polym. Chem.* 25, 1553 (1987).
221. T. Masuda, Y. Kuwane, and T. Higashimura, *J. Polym. Sci., Polym. Chem. Ed.* 20, 1043 (1982).
222. T. Masuda, E. Isobe, and T. Higashimura, *J. Am. Chem. Soc.* 105, 7473 (1983).
223. T. Masuda, M. Yamagata, and T. Higashimura, *Macromolecules* 17, 126 (1984).
224. M. Benes, J. Peska, and O. Wichterlee, *J. Polym. Sci., Polym. Chem. Ed.* 20, 1043 (1982).
225. A. G. MacDiarmid and A. J. Heeger, *Synth. Met.* 1, 101 (1980).
226. J. Kanicki, E. V. Donckt, and S. Boue, *J. Chem. Soc., Faraday Trans. 2* 77, 2157 (1981).
227. H. Selig, J. H. Holloway, and A. Pron, *J. Chem. Soc., Chem. Commun.* 729 (1982).
228. H. Selig, J. H. Holloway, A. Pron, and D. Billaud, *J. Phys. (Paris)* C3, 179 (1983).
229. H. Selig, J. H. Holloway, A. Pron, and D. Billaud, *J. Chem. Soc., Chem. Commun.* 109 (1983).
230. M. Rolland, M. Aldissi, and F. Schue, *Polymer* 23, 834 (1982).
231. H. Shirakawa and T. Kobayashi, *J. Phys. (Paris)* C3, 3 (1983).
232. J. Przulski, M. Zagorska, K. Condor, and A. Pron, *Polymer* 23, 1872 (1982).
233. Y. Cao, K. Guo, M. Wau, P. Wang, R. Qian, F. Wang, and X. Zhao, *Polym. Commun.* 24, 300 (1983).
234. M. Zagorska, A. Pron, J. Przulski, B. Krische, and G. Ahlgren, *J. Chem. Soc., Chem. Commun.* 1125 (1983).
235. T. Masuda, B.-Z. Tang, and T. Higashimura, *Polym. J.* 18, 565 (1986).
236. K. Ishihara, Y. Nagase, and K. Matsui, *Makromol. Chem. Rapid Commun.* 7, 43 (1986).
237. Y. Fusaoka, E. Imazu, and N. Kawabe, *Abstract, 51st Autumnal meeting of Chem. Soc. Jpn., Kanazawa*, 501 (1985).

This Page Intentionally Left Blank

Chapter 4

SYNTHESIS, PROPERTIES, AND APPLICATIONS OF POLY(*p*-PHENYLENE VINYLENE)S

Jonas Gruber, Rosamaria Wu Chia Li

Instituto de Química, Universidade de São Paulo, Caixa Postal 26077, 05513-970 – São Paulo, SP, Brazil

Ivo Alexandre Hümmelgen

Group of Organic Optoelectronic Devices, Departamento de Física, Universidade Federal do Paraná, Caixa Postal 19081, 81531-900 – Curitiba, PR, Brazil

Contents

1. Introduction	163
2. Methods of Synthesis	164
2.1. Via the Wittig Reaction	164
2.2. Soluble Precursor Routes	165
2.3. Electrochemical Routes	167
2.4. Other Synthetic Routes	167
3. Spectroscopy	169
3.1. Vibrational Spectra	169
3.2. Ultraviolet–Visible	170
3.3. Nuclear Magnetic Resonance	171
4. Thin-Film Preparation	171
4.1. Methods and Processes	171
5. Physical Properties	172
5.1. Structural, Mechanical, and Thermal Properties	172
5.2. Electrical Properties	173
6. Interfaces with Other Materials	176
6.1. Interfaces with Metals	176
6.2. Interfaces with Oxides	177
6.3. Interfaces with Other Conjugated Polymers and Polymer Blends	178
7. Applications	178
7.1. Light-Emitting Diodes	178
7.2. Photodiodes and Photodetectors	179
7.3. Lasers	180
7.4. Triodes	180
7.5. Light-Emitting Electrochemical Cells	180
7.6. Optocouplers	180
Acknowledgments	180
References	181

1. INTRODUCTION

Poly(*p*-phenylene vinylene), PPV, was used as the electroluminescent material in the first polymer-based light-emitting diode

(LED), reported in 1990. This fact, associated with the potential advantages of electroluminescent polymers for flat-panel display applications, has provided the necessary background for a worldwide rapid increase in the interdisciplinary research activities on

Handbook of Advanced Electronic and Photonic Materials and Devices, edited by H.S. Nalwa
Volume 8: *Conducting Polymers*

Copyright © 2001 by Academic Press

All rights of reproduction in any form reserved.

PPV and its derivatives. In the last decade, scientists have focused their attention on the fundamental aspects of PPV chemistry, physics, and technology, aiming not only toward pure academic research but, especially, to transform these new polymeric materials into useful commercial products.

This progress passes through several key discoveries, results, developments, improvements, and innovations, which we will describe in this chapter. We start with the PPV chemistry and follow through with the physics up to a description of some PPV-based devices. Due to the huge number of papers published dealing with these topics, we had to select subjects we considered to be representative and, even so, we had to restrain our presentation only to short summaries in most cases. Therefore, this chapter is not to be viewed as an exhaustive review. Several other reviews on PPV, or that include topics on this class of polymer, have been published before [1–7]. Finally, we hope our contribution may be helpful for colleagues working in this fascinating field.

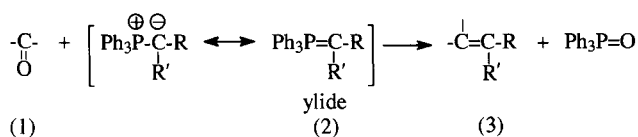
2. METHODS OF SYNTHESIS

2.1. Via the Wittig Reaction

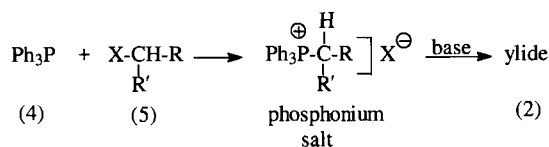
The reaction of a carbonyl compound (1) (aldehyde or ketone) with a phosphorous ylide (2) (also called a phosphorane) to give an olefin (3) is known as the Wittig reaction after the German chemist, Georg F. K. Wittig (1897–1987), who first showed the value of this procedure in the synthesis of alkenes [8] (Scheme 1). The ylide (2) can be prepared in two steps from triphenylphosphine (4) and an alkyl halide (5), as shown in Scheme 2. Reaction conditions are mild and the presence of many different types of functional groups (OH, OR, NR₂, NO₂, etc.) do not interfere. McDonald and Campbell [9], in 1960, applied the Wittig methodology to prepare PPV oligomers (6), starting from an aromatic bisphosphonium salt (7) and terephthalaldehyde (8) (Scheme 3) in a step-growth process.

Although the yield was quite attractive, it was shown later [10] that PPV oligomers produced by this route had a low degree of polymerization of only about 3–9, which implies a high content of end groups, besides the presence of both *cis* and *trans* double-bond configurations. The low degree of polymerization is due to the insolubility of the oligomers as they grow. Thus, they separate from the reaction media and polymerization halts. Lateral substitution of the phenylene rings increases solubility and, therefore, the degree of polymerization [11], as shown in Figure 1.

The presence of both *cis* and *trans* double bonds in the polymer can be explained by looking closely at the mechanism of the Wittig



Scheme 1. The Wittig reaction.

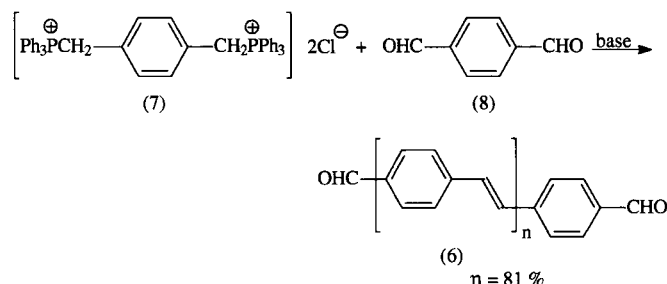


X = Cl, Br

Scheme 2. Phosphonium salt formation.

reaction [12] (Scheme 4). As can be seen, betaine I (9) leads to a *cis* configuration (10) and betaine II (11) to a *trans* one (12). Factors such as the nature of the substituents (R and R'), the solvent used, and the presence of salts can favor a specific path [13]. Electron-withdrawing groups (e.g., CN, –CHO, halogen, aryl) stabilize the carbanion in betaine I and increase its lifetime, permitting it to rearrange in a large extent to the thermodynamically more stable betaine II, which leads to *trans* products. The opposite effect is observed with electron-donating groups such as alkyl and alkoxy.

Isomerization of the polymers to an all-*trans* configuration is possible either by heating to 200–300°C or by heating with iodine in an appropriate solvent.



Scheme 3. Synthesis of PPV via the Wittig reaction.

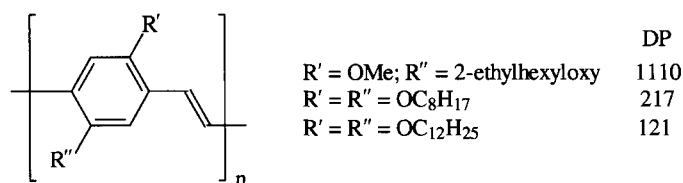
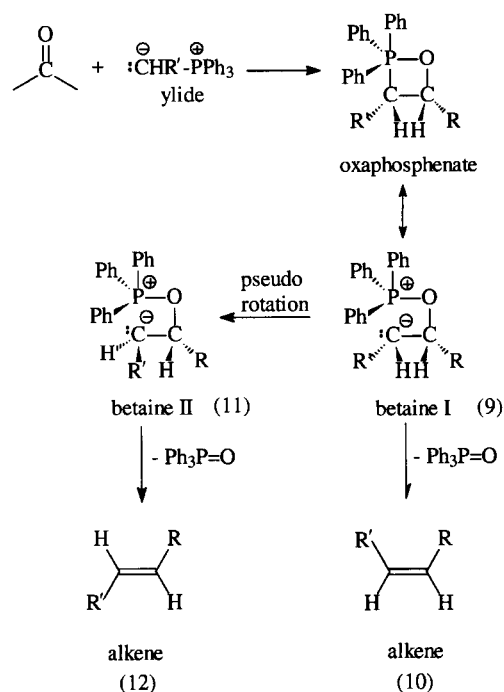
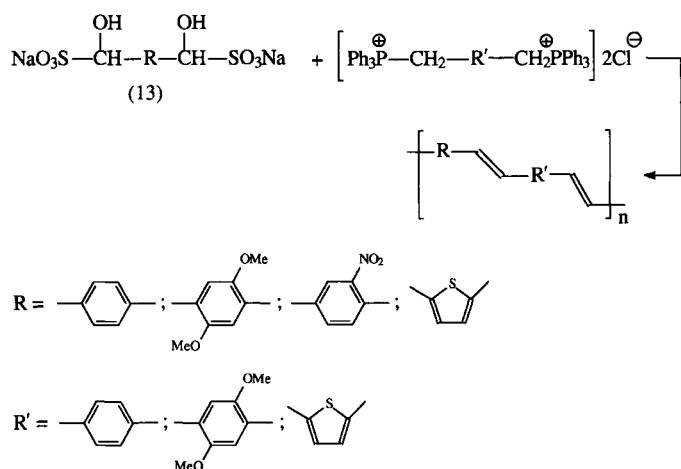


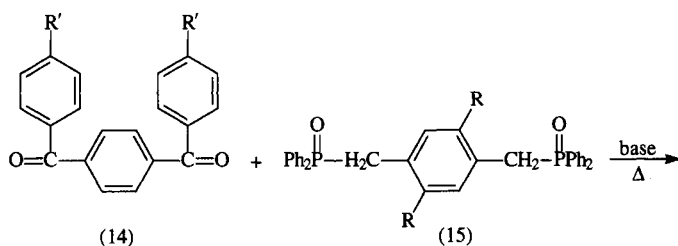
Fig. 1. Degree of polymerization (DP) of some soluble PPVs prepared via the Wittig reaction.



Scheme 4. Mechanism of the Wittig reaction.



Scheme 5. Variation of the Wittig reaction leading exclusively to *trans*-polymers.



Scheme 6. The Wittig-Horner reaction.

A variation of the Wittig reaction was described [14, 15] in which α -hydroxy sulfonates (13) were used, instead of aldehydes, to react with phosphonium salts. Polymers with only *trans*-vinylene units were formed (Scheme 5).

Another variation of this methodology involves the reaction of the carbonyl compound (14) (a diketone) with phosphonates (15) and is called the Wittig-Horner reaction. The advantages of this modification include the higher reactivity of the corresponding ylides, the lower price of starting materials, and the fact that the phosphorous end product is a phosphate ester, soluble in water and easily separable from the polymeric material. An example of a PPV derivative prepared by this method [16] is shown in Scheme 6.

Some illustrative examples of PPV-related polymers obtained by the Wittig route are presented in Figures 2 to 5, [17–20].

The Wittig reaction and other step-growth processes have also been extensively used for the formation of oligomers, because molecular weight can be controlled and end groups incorporated, allowing tailor-made oligomers to be obtained [6].

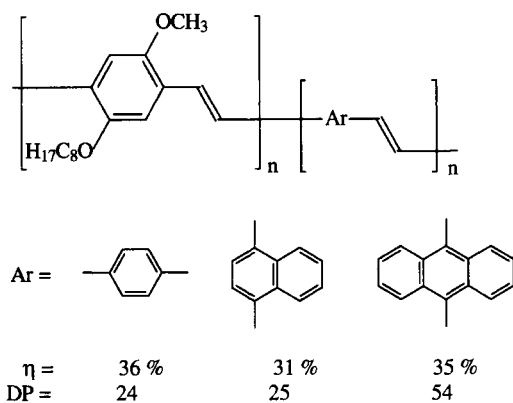


Fig. 2. Recent examples of PPVs obtained via the Wittig reaction. Adapted from N. N. Barashkov, T. S. Novikova, and J. P. Ferraris, *Synth. Met.* 83, 39 (1996).

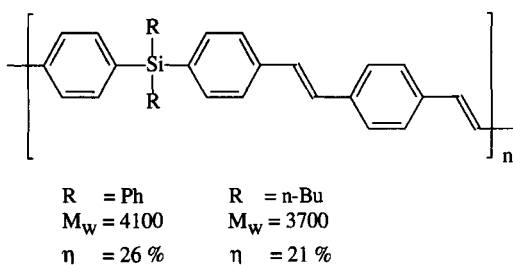


Fig. 3. Recent examples of PPVs obtained via the Wittig reaction. Adapted from H. K. Kim, M.-K. Ryu, and S.-M. Lee, *Macromolecules* 30, 1236 (1997).

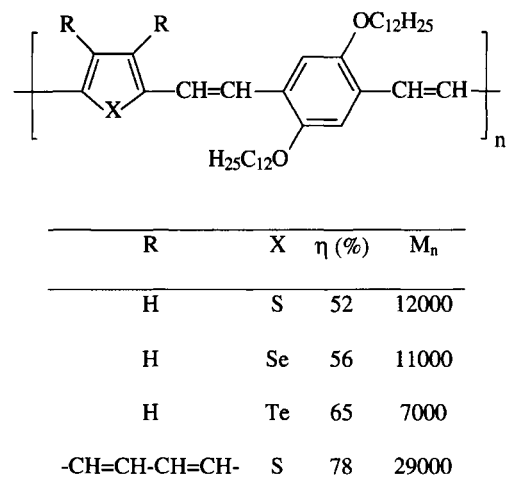
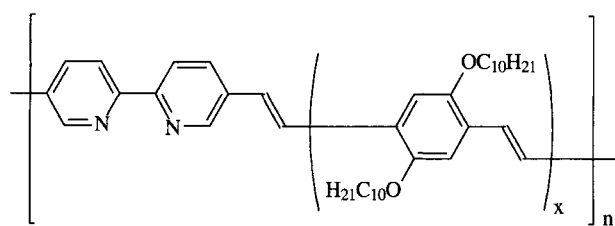


Fig. 4. Recent examples of PPVs obtained via the Wittig reaction. Adapted from H. Saito, S. Ukai, S. Iwatsuki, T. Itoh, and M. Kubo, *Macromolecules* 28, 8363 (1995).

2.2. Soluble Precursor Routes

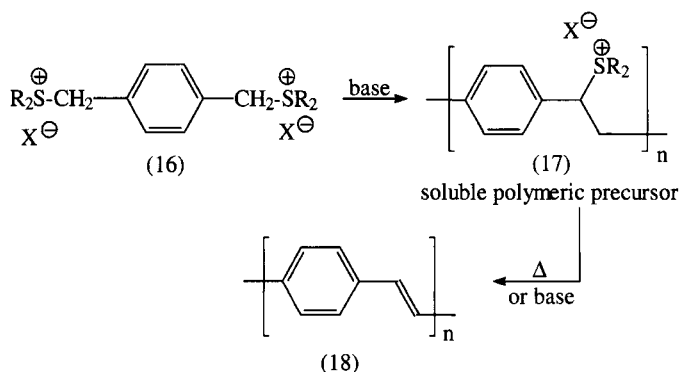
The soluble precursor routes are the most widely used methods to obtain processible, high-quality films of high-molecular-weight (up to over 1,000,000) PPVs and analogous polymers and copolymers.

The basic idea is to prepare first a precursor polymer that can be dissolved in water or in an organic solvent, processed to films by casting or any other physical procedure, and, finally, converted to the fully conjugated polymer via a thermal or chemical elimination step.



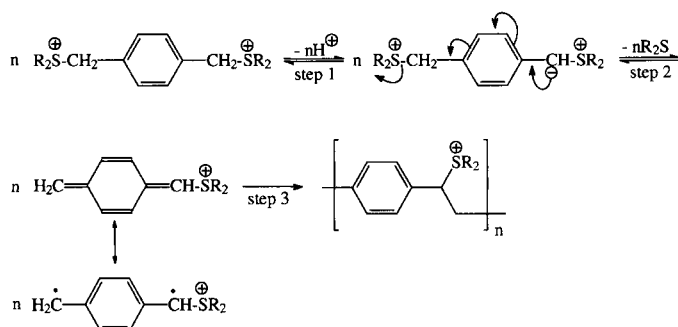
x	η (%)	M_n
1	89	6400
3	92	22000

Fig. 5. Recent examples of PPVs obtained via the Wittig reaction. Adapted from B. Wang and M. R. Wasielewski, *J. Am. Chem. Soc.* 119, 12 (1997).



X^\ominus = counter ion, e.g. Cl^\ominus , Br^\ominus
 $R = Me, Et$ or
 $R_2 = -CH_2(CH_2)_xCH_2-$ $x = 2, 3$

Scheme 7. The Wessling-Zimmerman route to PPV.



Scheme 8. The mechanism of the Wessling-Zimmerman route.

Wessling and Zimmerman [21, 22] discovered over 30 years ago that the treatment of *p*-xylylene sulfonium salts (16) with a base produces a water-soluble polymer (17), which can be purified by dialysis and then converted to PPV (18) either by heating or by treatment with an excess of base (Scheme 7). The mechanism for the conversion of the sulfonium salt to the polymeric precursor involves several steps, as shown in Scheme 8.

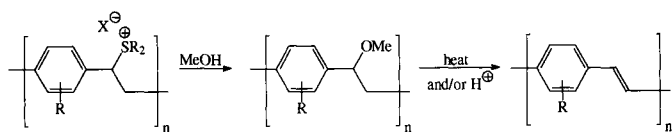
The first two steps are reversible and involve deprotonation by the base, followed by 1,6-elimination of a sulfide group. This equilibrium can be shifted to the right by the use of an organic immiscible solvent, which removes the sulfide from the aqueous phase as it is formed. Whether step 3 is an ionic or a free-radical polymerization process has been under discussion for several years. In 1985, Wessling [21] stated that it had a free-radical character, and, in 1988, Lahti et al. [23] reported a number of experiments from which they concluded that it was ionic. Nevertheless, in a more recent paper [24], some of these authors returned to the free-radical mechanism.

The nature of the groups in the sulfonium salt influences the polymerization yields. Thus, alkyl groups such as Me and Et lead to yields in the range of only 10–20%, due to side reactions involving these groups such as substitution of the sulfonium group by a neutral halogen atom or a SR moiety, leading to defects in the conjugated backbone [2]. Much better yields are achieved when cycloalkylene sulfonium salts are used instead [25] ($R_2 = -CH_2(CH_2)_xCH_2-$; Scheme 7), and the most commonly employed sulfonium salt, *p*-xylylenebis(tetrahydrothiophenium chloride), has been commercially available since 1992 [26].

The aqueous solubility of the polyelectrolyte is influenced by the nature of the counterion (X^\ominus), which can be efficiently exchanged by mixing with or dialyzing against a large excess of sodium salt solutions of anions, as, for instance, I^\ominus , PF_6^\ominus , BF_4^\ominus , and AsF_6^\ominus [27]. Solubility in organic solvents can be achieved by the reaction of the polyelectrolyte with methanol for several hours, replacing the sulfonium moieties by methoxy groups [28]. This procedure is particularly helpful for molar mass determination by gel permeation chromatography (GPC) analyses, since the aqueous polyelectrolyte interacts with the columns and gives irreproducible results [29]. For this purpose, a tetrafluoroborate precursor is also sometimes used, because of its solubility in acetonitrile and *N,N*-dimethyl formamide (DMF).

The stability of the intermediate sulfonium precursor polymers in the solid state is relatively poor due to partial elimination and oxidation reactions, which turn them yellow colored and make them insoluble. Nevertheless, below 0°C, their solutions can be kept for several months. Han and Eisenbaumer [30] described a stabilization method, which consists of the addition of small amounts of a weak base (e.g., pyridine) to the aqueous or non-aqueous precursor solutions. High-quality freestanding films could be cast from pyridine-stabilized aqueous solutions of the polyelectrolyte and, after conversion to PPV and oxidative doping, the films exhibited conductivities 10 times higher than those derived from unstabilized precursors.

The conversion of the precursor to PPV can be accomplished essentially by treatment with excess base [31] or strong acids [32] or by heating under reduced pressure or inert atmosphere. The thermal process is usually preferred since it avoids unwanted oxidation of vinylene moieties of the final PPV to carbonyl or hydroxyl groups, and removes the volatile sulfide formed during the elimination process. The required temperature is dependent on the nature of the substituents and of the counterion, being lower than 200°C for chloride and fluoride and above 350°C for acetate [27]. Thermogravimetry can be very helpful in determining the conversion temperature for each case, as well as, when associated with mass spectrometry, studying the reaction sequence and the formation of byproducts [33].



Scheme 9. Formation of methoxy-substituted precursor polymers and their conversion to PPV.

Higher conjugation lengths can be obtained if freshly prepared and undialyzed precursors are used, and redshifts of 30–50 nm, compared to those obtained from dialyzed samples, were reported [34]. The use of water as a solvent was found to be critical for the attainment of high chain order and to be better than methanol in preserving the chemical and conformational integrity of the polyelectrolyte. This is due to its high ionizing and solvating ability and a lower nucleophilicity compared to methanol.

Other conversion procedures to PPV were also described. Attaching anionic azosulfonic dyes to the positive sites of the polyelectrolyte precursor allows the use of a laser-induced elimination process [35]. Microwave radiation is known to reduce drastically the elimination time to only a few minutes [36]. The inclusion of magnetic species (e.g., Fe) inside the polymer precursor improves the efficiency of this method and offers the possibility of simultaneous elimination and doping.

A large variety of PPVs and analogous conjugated polymers and copolymers have been synthesized by Wessling's route and some key examples are illustrated in Table I.

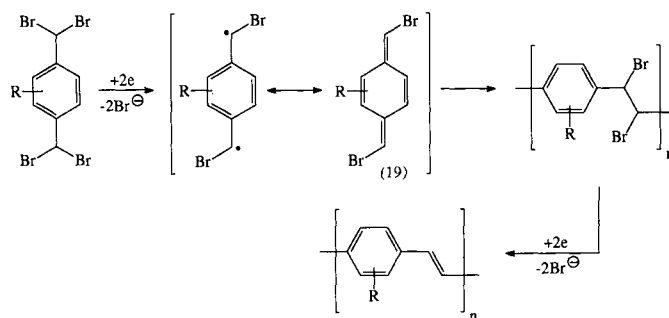
A modification of the Wessling–Zimmerman route consists, as mentioned before, of the conversion of sulfonium polyelectrolytes to methoxy-substituted polymers, which are soluble in organic solvents such as chloroform. These precursor polymers have the advantage of being more stable than the sulfonium ones and can also be further stabilized by weak bases such as pyridine [30]. The conversion to PPV can be carried out by heating, by acid catalysis, or both, as shown in Scheme 9. Some examples of PPVs obtained by this methodology are shown in Table II.

2.3. Electrochemical Routes

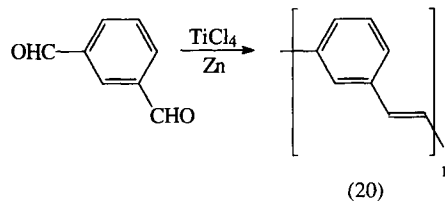
In contrast to the electrochemical route to other important conducting polymers such as polypyrrole and polyaniline, which are obtained anodically and oxidize at the electrode to conducting forms that allow current to be passed continuously, PPV is obtained cathodically and the films formed at solid electrodes are insulating and halt the electrochemical process. Thus, the reduction of $\alpha,\alpha,\alpha',\alpha'$ -tetrabromo-*p*-xylene in aprotic solvents at indium–tin oxide (ITO) or Pt cathodes gives thin PPV films suitable only for optical studies [60, 61]. On the other hand, if the reduction is carried out using a stirred mercury pool cathode [62], the process may be operated at a preparative scale, because any film formed at the electrode is continuously broken up.

The mechanism is shown in Scheme 10 and involves reductive elimination of bromide anions to give quinodimethane intermediates (19) that polymerize. In the case of *o*-quinodimethane, their intermediacy has been proved by trapping via Diels–Alder reaction with a reactive maleic anhydride derivative [63, 64]. The second elimination step is analogous to the cathodic elimination of vicinal dihalides, which is known to give *trans*-alkenes [65].

The main advantage of this route is that it offers the possibility of obtaining organic soluble and insoluble polymers with sub-



Scheme 10. Cathodic route to PPV.



Scheme 11. Synthesis of *meta*-PPV.

stituents that would not survive the pyrolysis or the strongly basic or acidic conditions used in eliminative methods. Besides, *ortho*-PPV, poly(biphenylene vinylene), and copolymers of PPVs can also be prepared. The main disadvantage is the lower degree of polymerization, compared to that achieved by soluble precursor routes, especially in the case of insoluble polymers.

The scope of this electrochemical method can be seen in Table III, which presents some selected examples of PPVs and analogous polymers prepared by this route.

Other electrochemical methods for preparing PPV thin films on solid electrodes have been described, such as the cathodic reductions of *p*-xylylene bis(triphenylphosphonium bromide) [68] and of Wessling's sulfonium precursors [22].

2.4. Other Synthetic Routes

Several other methods for the synthesis of PPVs have been described in the literature. The McMurry reaction, which consists of the deoxygenative coupling of aromatic dialdehydes in the presence of titanium compounds, has been employed to obtain 2,5-dihexyl-PPVs [69], *para*- and *meta*-PPV (20) [70], Scheme 11, the latter very unlikely to be prepared by the Wessling–Zimmerman or electrochemical routes, since there is no possibility of forming the required quinodimethane intermediate. Nevertheless, a drawback of this method is the somewhat tedious workup needed for the isolation of insoluble PPVs from the elementary metal powder (Ti and/or Zn), which is also produced.

Chemical vapor deposition (CVD) is a solvent-free process and is discussed in Section 4.1.

The arylation of olefins by the treatment with an arylpalladium reagent (known as the Heck reaction [71]), which can be generated *in situ* from palladium acetate and an aryl dihalide, in the presence of a base, has been applied to the synthesis of many PPVs, some of which are shown in Scheme 12 [72–74]. Ethylene is the most reactive olefin, but a variety of functional groups, attached to the double bond, such as CO₂R, OR, and CN can be

Table I. Some Examples of PPVs Prepared by the Wessling-Zimmerman Route

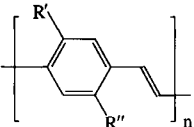
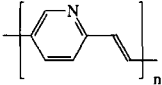
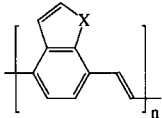
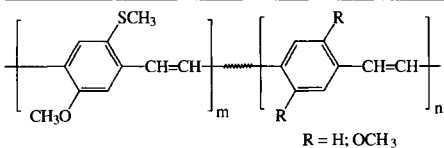
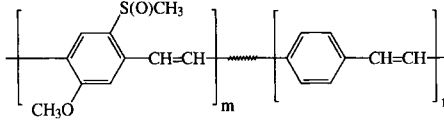
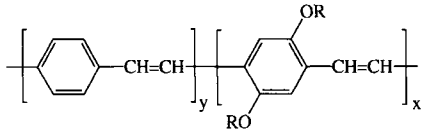
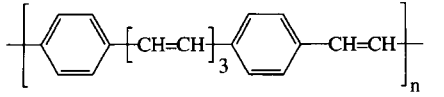
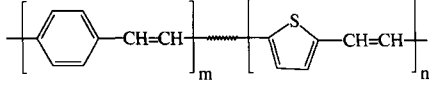
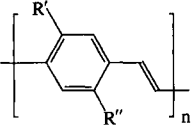
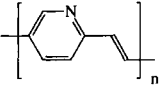
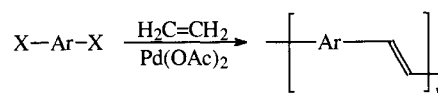
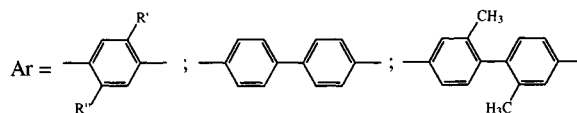
Polymer	R'	R''	Reference
	H	H	[21]
	H	CH ₃	[37]
	H	OCH ₃	[38]
	H	OCH ₃ , OC ₂ H ₅ , OC ₃ H _{7-n} , OC ₄ H _{9-n} , OC ₆ H _{13-n} ,	[39]
	H	N(CH ₃) ₂	[40]
	H	F, Cl, Br, I	[41]
	H	Si(CH ₃) ₃	[42]
	H	HC=CH-C ₆ H ₅	[43]
	H	Phenylanthracene, 9,10-diphenylanthracene	[44]
	CH ₃	CH ₃	[37]
	CH ₃	OCH ₃	[45]
	OCH ₃	OCH ₃	[37]
	OCH ₃	HC=CH-C ₆ H ₅	[43]
	OCH ₃	HC=CH-(<i>p</i> -C ₆ H ₄)-CN	[46]
	OCH ₃	HC=CH-(<i>p</i> -C ₆ H ₄)-NO ₂	[47]
OCH ₃	SCH ₃	[48]	
OCH ₃	S(O)CH ₃	[49]	
OCH ₃	S-CH ₂ -CH(C ₂ H ₅)(<i>n</i> -C ₄ H ₉)	[50]	
C ₇ H ₁₅	C ₇ H ₁₅	[51]	
			[52]
 X = O, S			[53]
Copolymer			Reference
 R = H; OCH ₃			[48]
			[49]
 R = CH ₃ , C ₂ H ₅ , <i>n</i> -C ₄ H ₉			[54]
			[55]
			[56]

Table II. Some Examples of PPVs Prepared via Methoxy-Substituted Precursor Polymers

Polymer	R'	R''	Reference
	OC ₆ H ₁₃	Cl	[57]
	OC ₆ H ₁₃	Br	[57]
	OCH ₂ C≡CH	OCH ₂ C≡CH	[58]
	OCH ₃	OCH ₃	[59]
			[52]



X = Br or I



R'	H	CH ₃	CF ₃	C ₂ H ₅	NO ₂	CH ₃	F
R''	H	H	H	H	H	CH ₃	CH ₃

Scheme 12. Some PPVs obtained via the Heck reaction.

tolerated. A comprehensive study of the influence of several factors, as, for instance, the amount of catalyst, temperature, solvent, halogen, and the nature of the substituent at the halogenated benzene, has been described [73]. The careful control of these factors can greatly reduce the amount of side products and increase the molecular weight up to approximately 10,000. A drawback of this approach is certainly the use of gaseous ethylene, which has to be added in precise amounts.

3. SPECTROSCOPY

3.1. Vibrational Spectra

The infrared (IR) spectrum of unsubstituted PPV has been studied in detail and assignments made to almost all the observed bands [75]. The most relevant ones are listed in Table IV.

The absorptions at approximately 965 ($\delta_{\text{C-H}}$ *trans*-vinylene) and 700 cm^{-1} ($\delta_{\text{C-H}}$ *cis*-vinylene) can be helpful in the characterization of mixtures of *cis*- and *trans*-PPV, normally obtained via Wittig reaction, as well as in monitoring a *cis*-to-*trans* isomerization process. The $\delta_{\text{C-H}}$ out-of-plane bends for substituted ben-

Table III. Some Examples of PPVs Obtained Electrochemically

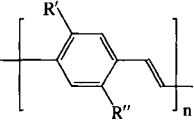
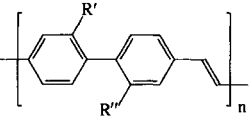
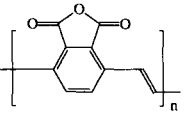
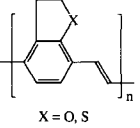
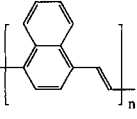
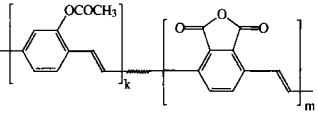
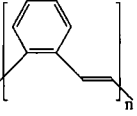
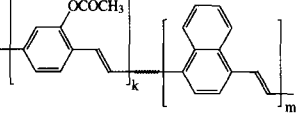
Polymer	R'	R''	Reference
	H	H	[60-62]
	H	OCOCH ₃	[62]
	H	OCH ₃	[62]
	H	CO ₂ CH ₃	[62]
	OCH ₃	OCH ₃	[62]
	H	H	[66]
	OCH ₃	OCH ₃	[66]
	NO ₂	NO ₂	[66]
Polymer	Reference	Polymer	Reference
	[62]		[67]
		X = O, S	
	[62]		[62]
	[62]		[62]

Table IV. Main Absorptions Observed in PPV IR Spectrum

ν (cm^{-1})	Assignment
3076 and 3047	$\nu_{\text{C-H}}$ aromatic (w)
3024	$\nu_{\text{C-H}}$ <i>trans</i> -vinylene (s)
2950, 2920, and 2852	$\nu_{\text{C-H}}$ aliphatic (w)
1519	$\nu_{\text{C=CH}}$ aromatic (vs)
965	$\delta_{\text{C-H}}$ <i>trans</i> -vinylene (oop) (vs)
837	$\delta_{\text{C-H}}$ 1,4-disubstituted phenylene ring (oop) (vs)

w, weak; s, strong; vs, very strong; oop, out of plane.

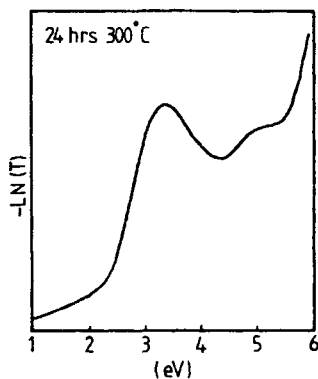


Fig. 6. Optical absorption spectrum of fully converted PPV. Reprinted, by permission of Elsevier Science from D. D. C. Bradley, G. P. Evans, and R. H. Friend, *Synth. Met.* 17, 651 (1987). Copyright © 1987 Elsevier Science.

zene rings are useful not only for discerning *ortho*-, *meta*-, and *para*-PPV, but also for determining if cross-linking occurred during preparation. The undesired oxidation of the vinylene portion to a carbonyl or carboxyl moiety can be checked by examining the spectral region between 1650 and 1770 cm^{-1} [75]. For substituted-PPVs and PPV analogs, besides the basic absorptions cited in Table IV, typical absorption bands of the substituents will be present. Thus, for instance, the IR spectrum of 2,5-dimethoxy-PPV shows strong bands at 1256 and 1036 cm^{-1} due to asymmetric and symmetric stretches of the C–O–C groups [62]. Comprehensive experimental and theoretical studies of the vibrational spectra (IR and Raman) of PPV and other poly(arylene vinylene)s, as well as oligomeric model compounds, have been described in the literature [76–78].

3.2. Ultraviolet-Visible

The ultraviolet-visible (UV-Vis) absorption spectrum of PPV typically consists of a well-defined low-energy maximum at approximately 3.3 eV, a second weaker feature at approximately 5 eV, and a strongly increasing absorption above 5 eV [75, 79] (Fig. 6). The optical absorption coefficient at the low-energy maximum is on the order of $2 \times 10^5 \text{ cm}^{-1}$ [75].

PPV oligomers present optical absorption and luminescence spectra whose peaks are redshifted with increasing chain length (Fig. 7). The principal absorption peak position presents an approximately linear dependence with $1/m$, where m is the number of carbon atoms in the shortest path between the ends of the conjugated chain [80]. The absorption and luminescence spectra of PPV oligomers in solution show a blueshift when compared to those in

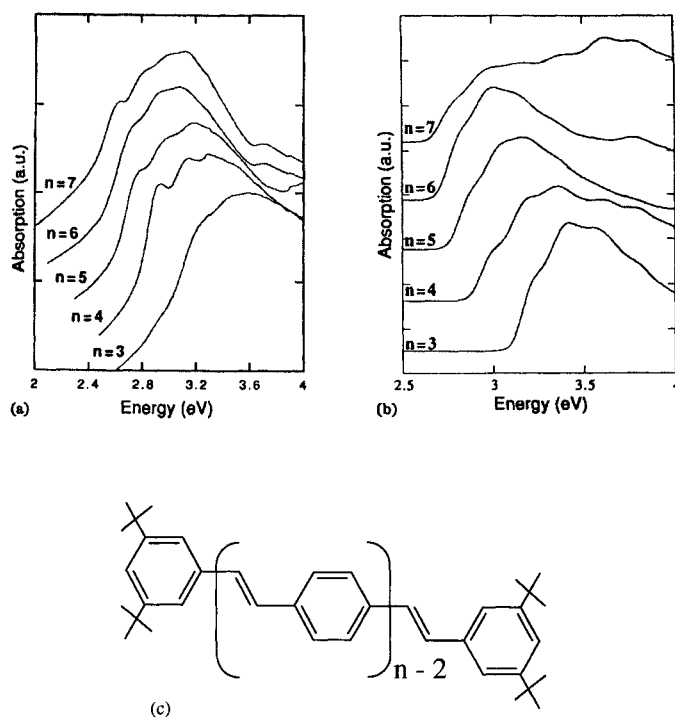


Fig. 7. Room-temperature optical absorption spectra of PPV oligomers (a) in KBr pellets and (b) in chloroform solution. The oligomer structure is represented in (c). Reprinted, by permission of Elsevier Science from H. S. Woo, O. Lhost, S. C. Graham, D. D. C. Bradley, R. H. Friend, C. Quattrocchi, J. L. Brédas, R. Schenk, and K. Müllen, *Synth. Met.* 59, 13 (1993). Copyright © 1993 Elsevier Science.

the solid state [80] (Fig. 7). This phenomenon is attributed to a greater degree of ring torsion in the oligomers in solution.

The peak position of the lowest energy absorption depends on the casting and conversion conditions. Its shape and position are determined by the distribution of conjugated lengths in the polymer sample [75]. A sharp, well-defined absorption band indicates the presence of a narrow distribution of conjugation lengths [75]. As a consequence, the absorption edge position of PPV films prepared by thermal conversion from the polyelectrolyte precursor depends on the elimination temperature [81], on the conversion time [82], and is strongly influenced by order. With increasing intrachain order, a spectral redshift, as well as a spectral line sharpening, has been observed in PPV [83] and MEH-PPV [84]. PPV films obtained from *p*-xylylenebis(triphenylphosphonium bromide) in acetonitrile solution by electropolymerization on ITO electrodes show a blueshift in the absorption when compared to PPV prepared by the precursor route [85].

The absorption spectrum of PPV is also changed when prepared from freshly synthesized and undialyzed polysulfonium chloride, compared to that obtained from dialyzed prepolymer [34]. The water content in the prepolymer solution also plays an important role in determining the optical properties of the converted PPV [34]. The position of the absorption edge, which is directly dependent on the polymer bandgap, can be intentionally modified via substitution by various donor and acceptor groups onto the phenyl rings and/or the vinylene units of PPV [5, 41, 86–89]. These substitutions also produce modifications in the electroaffinity and ionization potential of the polymer and, for this reason,

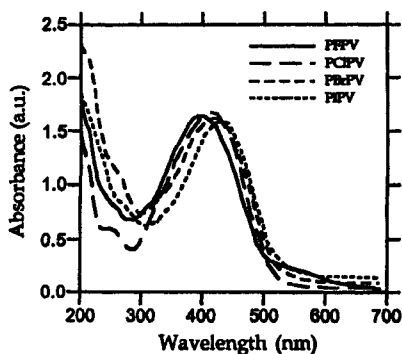


Fig. 8. UV-visible spectra of halogen-substituted PPVs. Reprinted by permission of Elsevier Science from I.-N. Kang, D.-H. Hwang, and H.-K. Shim, *Synth. Met.* 69, 547 (1995). Copyright © 1995 Elsevier Science.

constitute an important tool in the development of polymers for specific device applications. Halogen-substituted PPV derivatives, for example, show a systematic shift of the absorption edge in the ultraviolet-visible spectrum to longer wavelengths when the substituent is changed in the sequence F-Cl-Br-I [41] (Fig. 8).

A defined conjugation length is interesting because a sharper emission peak and a more defined absorption edge are observed. One strategy that permits emission range control in a similar way to that observed by reduction of the oligomer molar mass, but without loss of the useful mechanical properties of polymers, is the use of block copolymers with alternation of conjugated and non-conjugated segments. The emission color control is, in this case, achieved by the control of the length of the conjugated segment [90-93].

The conjugation length of PPV can also be controlled using PPV-PVA blends [94]. It has been demonstrated that the luminescence characteristics of the PPV-PVA-based polymers are dependent on their composition and treating conditions. The emitted light of PPV-PVA-based LEDs shifts from yellow-green (550 nm) to blue (485 nm) as the concentration of PVA increases. Infrared absorption spectra show that possibly some part of the PPV precursor may react with PVA to form C-O-C linkages that interrupt, and hence decrease, the conjugation length in the converted PPV, as observed in ultraviolet-visible absorption spectra [94].

3.3. Nuclear Magnetic Resonance

Nuclear magnetic resonance (NMR) spectroscopy (^1H , ^{13}C , and other nuclei) is an extremely powerful analytical technique capable of providing unequivocal proof of a compound structure, but is usually applied to soluble materials. An interesting example in which this method provided the molecular structure, as well as information about conformations and molecular dynamics, for over 20 soluble *n*-alkoxy-substituted phenylene vinylene oligomers has been described [95].

Solid-state ^{13}C cross-polarization magic-angle spinning (CPMAS) NMR spectra have been obtained for both insoluble and soluble PPVs [62, 96, 97]. This technique can provide some information about the crystallinity and morphology of polymer films. The line shapes depend on the conditions employed for film processing and can be used to monitor its quality. It seems that the spectrum resolution is related to rotational disorder about the phenylene vinylene single bonds. Spectra of PPVs obtained electrochemically [62] or via Wittig reaction [97] present only two

peaks, at δ 136.3 (sharp, quaternary carbons) and 128.3 (broad, all other carbons), while PPVs prepared via sulfonium precursor polymers [96] show four sharp lines at δ 136, 131, 128, and 124.

4. THIN-FILM PREPARATION

PPV and its derivatives are conventionally used in the form of thin films operating as active layers in LEDs, photodetectors, and other optoelectronic devices. An important characteristic of devices constructed with PPV is that they operate with the polymer layer submitted to high electric field strengths. To permit device operation at low voltages, on the order of a few volts, the polymer film thickness is reduced to around 10^2 nm. The production of high-quality polymer thin films constitutes, for these reasons, an important step in the device construction process.

4.1. Methods and Processes

The method used for the preparation of thin films of PPV or its derivatives depends on the specific polymer. For those that present high solubility in common organic solvents, very simple procedures, such as casting, doctor-blade technique [98], or spin-coating of the polymer solution with further solvent evaporation can be used. In the case of spin-coating, the film morphology is sensitive to the solvent evaporation rate, density, viscosity, polarity, and solubility during the process [99].

For insoluble polymers, such as PPV, an elaborate strategy for film production must be used. The most common is the preparation of the film using the soluble precursor sulfonium polyelectrolyte, with further conversion to PPV. This strategy has the advantage that it permits the use of the casting, doctor-blade, or spin-coating techniques for film deposition, but needs a conversion step, which in most of the cases is based on thermal annealing of the film in a vacuum or inert atmosphere, at temperatures up to 300°C [75] (see also Section 2.2).

The elimination conditions influence the resulting PPV, which shows electroluminescence if converted at a minimum temperature of 130°C . Herold et al. [81] observed that the broad low-energy absorption band (300-520 nm) of the π -conjugated system shows no further redshift at elimination temperatures between 160 and 180°C . An exception occurs at 300°C , where a redshift is attributed to crystalline regions grown favorably in this temperature range [75, 100-104]. The photoluminescence, as well as the electroluminescence spectra of PPV present a redshift of approximately 10 nm when the elimination temperature is increased from 120 to 300°C . It is known that the high temperatures are necessary to remove the hydrogen chloride formed from the PPV films [81].

These results are in apparent disagreement with those reported by Murase et al. [105] and Bradley [75], who found that with temperatures in the range $\sim 120^\circ\text{C} \leq T \leq 250^\circ\text{C}$ only intermediate levels of conversion are achieved. The most adequate temperature for elimination of side products depends on the nature of the halogenide in the polysulfonium precursor. PPV films converted from polysulfonium solution containing bromide ion show traces of bromide even when they are converted at high temperature [106].

As seen before, an inert atmosphere is a necessary condition during the conversion process in order to avoid the formation of carbonyl moieties through oxidation of the vinylene carbons [75, 105]. The exposition of the precursor to oxygen-rich atmosphere leads to the appearance of an IR absorption band in the region $1652\text{-}1772\text{ cm}^{-1}$, indicating the presence of the ketone group

(C=O) [107]. It was also observed that the action of light accelerates degradation and leads to the formation of aggregates [107].

Carbonyl and hydroxyl groups are easily formed at the vinyl linkages on the polymer backbone during the thermal conversion process. These undesirable reactions reduce the conjugation length of the polymer, effectively creating oligomeric conjugated sections with unconjugated defects along the length of the polymer chain with a resulting decrease in the after-doping electrical conductivity [105, 108]. For photooxidized PPV, the photoluminescence decay with increasing carbonyl concentration shows the same trend as in thermally oxidized films, suggesting that carbonyl groups act as efficient photoquenchers, and most excitons within 5 nm of the carbonyl moiety will decay nonradiatively. This observation stresses the importance of minimizing carbonyl group in films prepared for electroluminescent applications [108–110].

Investigations performed using XPS (X-ray photoelectron spectroscopy) and UPS (ultraviolet photoelectron spectroscopy) coupled with the results of quantum-chemical calculations demonstrate that the exposition of PPV films to air under UV light leads to the appearance of strong photooxidation products on the film surface. In addition to the formation of carbonyl species, at least two other final products are present on the surface of photooxidized PPV: a higher oxidation product of the carbonyl-containing segments and another, which is likely to be associated with a different type of interaction between oxygen and a phenylene ring. The mechanism leading to this latter product is found to dominate the photooxidation process on the surface of thin films of PPV [111].

Depending on the substrate, the conversion step can introduce additional defects in the polymer layer that reduce the efficiency of devices [112]. Special attention must be given to the preparation of PPV films onto ITO (indium–tin oxide) substrates, considering that this was the anode material used in the first reported PPV LED [113] and continues to be used in a large number of devices. In PPV LEDs prepared by the tetrahydrothiophene precursor route, it has been observed that the leaving group HCl interacts with ITO [112]. Even indium chloride crystals with lateral dimensions up to 40 μm are created during the thermal conversion. InCl_3 is electrically conductive and may promote an inhomogeneous electric field distribution in devices prepared with these films. As a consequence, inhomogeneous current flow and localized heat production are expected, contributing to device failure.

Another material for LED-anode application is gold due to its high-work-function value. Precipitates were observed in PPV films converted at 250°C onto glass substrate previously covered with a gold layer. This observation was interpreted as evidence that gold may diffuse through the PPV film during the conversion process [114].

The conversion can also be promoted by other methods than thermal annealing, such as immersion of the sample in a solution of $\text{H}_2\text{SO}_4 + 20\% \text{SO}_3$, but this process presents the disadvantage of long conversion times and the more pronounced presence of carbonyl groups in the final film [107]. Other conversion procedures based on the use of other acids [32], ion implantation (Na^+ or He^+) [107], or microwave-induced elimination [36] were also reported. In spite of the good results obtained with solution processing, several potential problems exist [115]: (i) substituent groups introduced to improve the solubility may adversely affect the mechanical properties and may contribute to a reduction in the photochemical stability; (ii) pinhole-free films are difficult to produce over large areas; (iii) the construction of multilayered devices is difficult to engineer due to solvent restrictions that may

produce poor-quality interfaces; and (iv) contaminants are difficult to remove from solutions during synthesis and processing.

Chemical vapor deposition (CVD) is an alternative that excludes most of the problems cited, previously providing that a solvent-free technique can be performed in a clean environment at low temperatures with the additional advantage of being suitable for sequential depositions [116–118]. CVD is compatible with traditional inorganic semiconductor technology [115, 119] and allows a uniform coating of irregular substrates and surfaces [120]. Furthermore, the CVD process allows the mixture of monomeric units in the gas phase, offering the possibility of deposition of copolymer thin films with a gradient composition.

The synthesis of PPV via CVD can be achieved by vapor-phase pyrolysis of dihalogenated *p*-xylenes, yielding halogeno functionalized poly(*p*-xylylene), PPX, as films, directly upon condensation on a substrate in a CVD apparatus [121]. The quality of PPV prepared by CVD depends on the reaction parameters for the preparation of the PPV precursor, as well as on the conversion characteristics [121]. An important characteristic of CVD-prepared PPV films is that pinholes were not found within the limits of detection by scanning electron microscopy (SEM) [121]. Pinholes are common in films cast from solutions and cause device failure due to electrical breakdown. PPV prepared via CVD turned out to be amorphous regardless of the starting material used, the substrate on which the vapor deposition occurred, and the temperature of conversion, as long as it was kept below 200°C [121].

Staring et al. [119] obtained, using ITO/PPV/Ca devices with a 550-nm-thick CVD-produced PPV film, an electroluminescent efficiency of 0.002% at 35 V, lower than the value reported for precursor-route-processed films [113]. Later, it was demonstrated that the ITO layer is destroyed by HBr vapor liberated during the CVD process [121]. Using a protected ITO layer or replacing the ITO electrode by an inert anode such as Au, Schäfer et al. [121] were able to obtain an electroluminescence spectrum characteristic of PPV as well as a threshold field of 10^6 V cm^{-1} , typical of ordinary PPV. Analyzing the photoluminescence spectrum, they were also able to estimate the effective conjugation length as being around five to six repeated units and to conclude that the degree of disorder introduced into a PPV film prepared by CVD exceeds that of PPV prepared by the sulfonium precursor route. PPV film deposition by the Langmuir–Blodgett technique onto ITO [122, 123], mica [124], MoS_2 [125], Si [126], and highly oriented pyrolytic graphite [125] substrates has also been reported.

5. PHYSICAL PROPERTIES

5.1. Structural, Mechanical, and Thermal Properties

Earlier X-ray diffraction studies on unoriented PPV reported an amorphous structure [127], but later investigations on fully converted PPV samples indicated an isotropic distribution of crystallites [75]. Electron diffraction and X-ray diffraction investigations performed on oriented PPV samples revealed that crystallization occurs with a monoclinic unit cell [75, 100] (Fig. 9), with $a = 7.90 \pm 0.05 \text{ \AA}$, $b = 6.05 \pm 0.05 \text{ \AA}$, $c = 6.58 \text{ \AA}$, and $\alpha = 123^\circ$ [128]. The value of α is only approximate due to axial fluctuations. The angle between the *a*-axis and the *c*-axis could not be determined due to the lack of registry along the [110] direction and has been arbitrarily set at 90° [128]. Granier et al. [100] have determined that the setting angle ϕ_s (the angular position of the

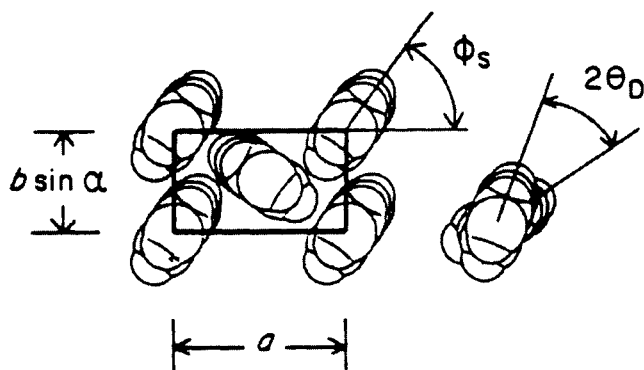


Fig. 9. PPV unit cell structure. Reprinted by permission of Butterworth-Heinemann from D. Chen, M. J. Winokur, M. A. Masse, and F. E. Karasz, *Polymer* 33, 3117 (1992). Copyright © 1992 Butterworth-Heinemann.

projected molecular major axis with respect to the a -axis direction) lies somewhere between 56° and 68° . Later, ϕ_s was found to be 52° [129] or even closer to 50° [130]. It was also found that PPV adopts a nonplanar conformation with the dihedral angle, θ_D (formed by the plane of the phenyl ring and that of the vinyl segment), exceeding 10° [130].

In stretched PPV films, a preferential distribution of crystallites respective to the film surface has been observed. It has been found that two sets of planes, $\{200\}$ and $\{110\}$, are preferentially oriented parallel to the film surface. A convolution of a distribution of crystallites with the planes $[110]$ ($\sim 25\%$), $[200]$ ($\sim 50\%$), and $[\bar{1}10]$ ($\sim 25\%$) parallel to the film surface resulted in calculated peak profiles similar to the experimental data [130].

The thermal conversion of the poly(xylilidene tetrahydrothiophenium chloride) into PPV has been investigated *in situ* using real-time X-ray diffraction [103]. At temperatures above 75°C , changes in the wide-angle X-ray scattering pattern were observed, suggesting that the elimination reaction begins at this temperature. Near 130°C , the characteristic features of an imperfect PPV are already present. At higher temperatures, the elimination process and improvement of crystalline domains follow, leading to better chain packing and crystalline domain growth. At around 300°C , the well-defined crystalline maxima, characteristic of PPV, suggest the almost complete transformation of the precursor into the final polymer.

The crystallite size values for PPV depend on the drawn ratio, and different results were obtained for the lateral crystallite dimensions [75, 102, 131].

In PPV films deposited onto silver substrate, parallel chainlike features were reported, with larger separation (typically 1.8 nm) than expected from the interchain unit cell [132]. This was observed independently of polymer film thickness and material used as substrate and was tentatively attributed to some surface reconstruction, possibly due to adsorption of oxygen. Polarization-dependent photoabsorption measurements made in PPV monolayers prepared by the Langmuir–Blodgett precursor technique onto MoS_2 substrate showed that the phenylene and vinylene moieties are nearly parallel to the surface [125].

Side groups also play an important role on structure and ordering. Investigations performed with poly(2,5-dimethoxy-*p*-phenylene vinylene) demonstrated that the introduction of methoxy substituents onto the phenylene rings results in a saw-tooth molecular unit that allows adjacent chains to interlock and pack

together in a more ordered fashion to form a three-dimensional structure [133]. Poly(2-methoxy-*p*-phenylene vinylene) prepared from the precursor polyelectrolyte was found to be crystalline, with significant amounts of disorder, which includes chain lateral irregularities and axial translational disorder [38]. In the case of diethoxy substitution, an interlocked ordered material is formed and the ethoxy moieties are too short to form a regular arrangement by themselves; i.e., no side chain crystallization is observed [133]. For methyl substituents, a strong repulsive steric interaction with the backbone occurs, distorting the planar geometry [133].

Temperature-dependent small-angle X-ray scattering (SAXS) investigations were used to search for glass transition in PPV [121]. Using PPV films produced by CVD, it was observed that the temperature dependence of the small-angle X-ray intensity, which is directly related to thermal density fluctuations, shows a break at about 220°C . The interpretation of this observation is that structure formation processes start to occur at this temperature, i.e., that PPV displays a glassy transition in this temperature range. This is consistent with dynamical mechanical thermal analysis (DMTA) investigations [121]. The glassy transition temperature has also been determined for α -cyano-substituted poly(2,5-dialkoxy-*p*-phenylene vinylene)s [134]. In these polymers, the glass transition temperature (T_g) is significantly reduced when compared to the value reported for CVD-prepared PPV. $10^\circ\text{C} \leq T_g \leq 70^\circ\text{C}$ was found, depending on the side group.

5.2. Electrical Properties

The electrical conductivity of conjugated polymers is strongly influenced by the presence of doping agents and can be varied several orders of magnitude by changing the dopant concentration [135]. Further, the electrical conductivity also depends on the specific dopant. For these reasons, the discussion of the electrical properties is divided into two parts. The first part corresponds to intrinsic conduction (pristine form) and the second is devoted to doped polymers.

5.2.1. PPV in the Pristine Form

In conjugated polymers, the electron–ion interaction induces static lattice deformations that result in a new potential of different periodicity. At low enough temperature, the elastic energy necessary to produce the deformation can be overcome by the gain in energy for the electrons (Peierls effect [136]), and the material behaves like a Peierls insulator [137]. Considering the magnitude of the highest occupied molecular orbital (HOMO)–lowest unoccupied molecular orbital (LUMO) transition (E_{gap}) in PPV and its derivatives ($E_{\text{gap}} \sim 2.4 \text{ eV}$), a negligible free-carrier density is expected, even at room temperature when semiconductor statistics is applied [138]. For this reason, PPV and its derivatives in the pristine form (intrinsic) are expected to present very low values of electrical conductivity. The conductivity can be increased under illumination (generation of free-carrier pairs) or doping agents.

To discuss the electrical conductivity, σ , it is convenient to use the well-known expression

$$\sigma = \sum_i n_i q_i \mu_i \quad (1)$$

where n is the free-carrier density, q is the charge of the free charge carriers, and μ is its mobility. The summation must be made over all charge carrier types present, which can present different

values of n , μ , and if ionic conductivity is considered, even different values of q .

Apart from ionic conduction, the charge carrier species that must be considered in PPV are electrons, holes, and positive and negative polaronic *quasi*-particles. Different measurement techniques available for thin-film investigation permit one to determine n and μ and to discriminate between positive and negative charge carriers. Due to the high electrical resistance of pristine PPV films, the four-point probe technique [139] presents too many difficulties to be applicable. Electrical measurements are commonly made in thin PPV films using a two-terminal apparatus. In this type of technique, it is not trivial to distinguish between bulk limited and injection limited current; i.e., the current crossing the polymer film depends on the polymer itself (bulk properties) and on the polymer–electrode interface [140].

Under thermodynamical equilibrium conditions, n is negligible in an intrinsic semiconductor with $E_{\text{gap}} \sim 2.4$ eV, so that the free charge carriers must be created via illumination with energy larger than E_{gap} or via injection through the polymer/neighborhood interface, which are external factors. The most important intrinsic characteristic of the polymer is, in this case, μ .

The time-of-flight (TOF) technique (see, e.g., [141]) is the most direct way of measuring mobility. In this method, the charge carriers are injected by one contact or by illuminating one side of the sample and the mobility is obtained by measuring the time the electrical pulse takes to cross the sample up to the other contact. The field dependence of the mobility can be directly determined from data obtained at different electric fields. Time-of-flight measurements may present difficulties when the transport is dispersive and, for this reason, the number of reports applying this technique to determine the mobility of charge carriers in PPV is relatively small.

The mobility of the charge carriers can also be extracted from current versus voltage curves from polymer films sandwiched between two conducting electrodes when the current is limited due to space-charge accumulation. In this case, the current density is expressed by

$$j = \frac{9}{8} \varepsilon \mu \frac{V^2}{d^3} \quad (2)$$

where ε is the permittivity of the polymer and d is the polymer film thickness. If traps (single discrete energy level) are present in the polymer layer, this expression must be modified to [142]

$$j = \frac{9}{8} \varepsilon \theta \mu \frac{V^2}{d^3} \quad (3)$$

where

$$\theta = \frac{n}{n + n_t} \quad \text{or} \quad \theta = \frac{p}{p + p_t} \quad (4)$$

for electrons and holes, respectively (n is the density of free electrons, n_t is the density of trapped electrons, p is the density of free holes, and p_t is the density of trapped holes). In this case, $\theta \mu \equiv \mu_{\text{eff}}$ is the effective charge carrier mobility. To distinguish between μ and μ_{eff} , a more detailed investigation, including, for example, the temperature dependence of the mobility and the dependence on the electrode work function, must be performed [143, 144].

In amorphous materials, a single discrete energy level may no longer be a reasonable approximation. In this case, the trap (localized state) density is expected to be in the form of an exponential

distribution at energies E within the forbidden energy gap, such that

$$h(E) = \frac{N_t}{E_c} \exp\left(-\frac{E}{E_c}\right) \quad (5)$$

where N_t is the trap center density and E_c is the characteristic energy of the distribution. The $j(V, d)$ dependence, in this case, is of the form [145]

$$j \propto \frac{V^{m+1}}{d^{2m+1}} \quad (6)$$

where $m \equiv T_c/T$, $E_c \equiv kT_c$ (k is the Boltzmann constant and T is the absolute temperature).

The low μ values for positive charge carriers reported by different groups [146–155] indicate that the charge-transport-dominating mechanism is phonon-assisted quantum-mechanical tunneling, normally known as hopping [152]. The reported μ values spread over a few orders of magnitude [152] (Table V). This is not surprising since PPV has a predominantly amorphous character and mobility is highly sensitive to structural order and chemical purity. Furthermore, space-charge limited current (SCLC) measurements performed by Karg et al. [150] and Blom et al. [155] identified a field-dependent μ value expressed by $\ln \mu \propto E^{1/2}$. This $\ln \mu \propto E^{1/2}$ dependence, as well as the $\mu(T)$ dependence, is explained by Abkowitz et al. [163] in terms of hopping among a spatially regular array of sites made energetically inequivalent by disorder, even excluding influences of positional disorder (off-diagonal) and site relaxation (polaron formation). This model can simultaneously account for both the Poole–Frenkel-like field dependence of the drift mobility and the transit pulse widths (always in excess of that predicted by simple diffusion) observed in TOF experiments.

For negative charge carrier mobility, only a few estimates of mobility are available in the literature (Table VI). Electron mobility has been estimated to be two orders of magnitude smaller than hole mobility due to trapping [152]. Koehler et al. [140] estimated the electron mobility in PPV as being approximately 10^{-9} cm²/V·s. In an alternating block copolymer with green electroluminescent emission, poly(1,8-octanedioxy-2,6-dimethoxy-1,4-phenylene-1,2-ethenylene-1,4-phenylene-1,2-ethenylene-3,5-dimethoxy-1,4-phenylene), the electron mobility was estimated to be 5×10^{-10} cm²/V·s [144]. A quite low electron mobility was also estimated for PPP, approximately 10^{-11} cm²/V·s, from the analysis of the emission region in PPP-based LEDs [164].

Bozano et al. [162] described the electron mobility in MEH-PPV using a field-dependent mobility expression $\mu = \mu_0 \exp(\gamma \times \sqrt{E})$. They observed a zero-field mobility (μ_0) for electrons lower than that for holes, but a higher γ . Due to the stronger field dependence of the electron mobility, they observed comparable electron and hole mobilities at working voltages applicable to thin films of MEH-PPV. Both electron and hole mobilities are temperature dependent. γ is an electric field coefficient to the mobility due to the interaction between charge carriers and randomly distributed permanent dipoles in the semiconducting polymers [162, 165].

The electrical properties of PPV in its pristine form are determined by several factors, most of them structure dependent. The choice of the precursor polymer and the conditions at which the conversion to PPV is performed have a strong effect on the mobility. It has been found that a higher degree of conversion obtained by elevated temperature also increases μ [146]. A long reaction time, however, tends to reduce μ , in spite of the increased converted fraction [149]. This reduction is attributed to a wider con-

Table V. Positive Charge Carrier Mobility in PPV and Its Derivatives

μ (cm ² ·V ⁻¹ ·s ⁻¹)	Technique, material, comment	Reference
$10^{-4} < \mu < 10^{-3}$	TOF, PPV, mobility independent of E in the range $10^4 < E < 2 \times 10^5$ V·cm ⁻¹	[146]
$10^{-4} < \mu < 10^{-3}$	TOF, PPV, $E = 10^4$ V·cm ⁻¹	[147]
5×10^{-5}	TOF, PPV, $E = 3.3 \times 10^5$ V·cm ⁻¹	[156, 157]
3×10^{-3}	TOF, PPV, $E = 1.5 \times 10^3$ V·cm ⁻¹	[148]
$5 \times 10^{-6} < \mu < 5 \times 10^{-5}$	TOF, PPV, $E = 4.5 \times 10^4$ V·cm ⁻¹	[149]
$10^{-7} < \mu < 3 \times 10^{-6}$	TOF, PPV, $10^5 < E < 10^6$ V·cm ⁻¹ ; E dependence: $\ln \mu \propto E^{1/2}$	[150]
10^{-6}	TOF, PPV, $E = 2 \times 10^4$ V·cm ⁻¹	[151]
2×10^{-4}	TOF, DPOP-PPV, $E = 5 \times 10^5$ V·cm ⁻¹	[157, 158]
5×10^{-5}	SCLC, dialkoxy-PPV, $E < 3 \times 10^5$ V·cm ⁻¹	[153]
2×10^{-6}	SCLC, PPV, $E < 2 \times 10^6$ V·cm ⁻¹	[154]
$\mu(E=0) = 5 \times 10^{-7}$	SCLC, dialkoxy-PPV, $E < 3 \times 10^5$ V·cm ⁻¹ ; E dependence: $\ln \mu \propto E^{1/2}$	[155]
$5 \times 10^{-8} < \mu < 10^{-6}$	SCLC, PPV	[159]
2.1×10^{-7}	TOF, MEH-PPV, $\mu = \mu_0 \sqrt{E/E_0}$	[160]
1.4×10^{-5}	TOF, PPV, $E = 6 \times 10^4$ V·cm ⁻¹	[157, 161]
$3 \times 10^{-11} < \mu_0 < 2 \times 10^{-7}$	SCLC, MEH-PPV, $\mu = \mu_0 \exp(\gamma \sqrt{E})$, $\gamma = (4.8 \pm 0.3) \times 10^{-4}$ (m·V ⁻¹) ^{1/2}	[162]
10^{-7}	SCLC, block copolymer (blue emitting)	[143]
10^{-6}	SCLC, block copolymer (green emitting)	[143]
$5 \times 10^{-7} < \mu < 2.7 \times 10^{-6}$	TOF, MEH-PPV, $\mu = \mu_0 \sqrt{E/E_0}$; $\mu_0 = 2.1 \times 10^{-7}$ cm ² ·V ⁻¹ ·s ⁻¹ , $E_0 = 8.7 \times 10^4$ V·cm ⁻¹	[160]

TOF, mobility obtained from time-of-flight measurements; SCLC, mobility obtained from application of space-charge limited current models to $I(V)$ data; E , electric field strength.

Table VI. Negative Charge Carrier Mobility in PPP, PPV, and Its Derivatives

μ (cm ² ·V ⁻¹ ·s ⁻¹)	Technique, material, comment	Reference
$\sim 10^{-11}$	Analysis of the region with maximum of radiative recombination in an LED, PPP	[164]
$\sim 10^{-9}$	SCTC, PPV	[140]
5×10^{-10}	SCLC, block copolymer (blue emitting)	[144]
$3 \times 10^{-12} < \mu_0 < 2 \times 10^{-9}$	SCLC, MEH-PPV, $\mu = \mu_0 \exp(\gamma \sqrt{E})$, $\gamma = (7.8 \pm 0.5) \times 10^{-4}$ (m·V ⁻¹) ^{1/2}	[162]

TOF, mobility obtained from time-of-flight measurements; SCLC, mobility obtained from application of space-charge limited current models to $I(V)$ data; SCLTI, mobility obtained from application of space-charge limited tunneling injection models to $I(V)$ data; E , electric field strength.

jugation length distribution achieved when longer heating times are employed. As the degree of conversion increases, higher PPV oligomers are formed, but the distribution of their lengths grows wider [152].

Based on TOF measurements, Gailberger and Bäessler [156] observed that the hole mobilities decrease with increasing electric field, carrying a temperature dependence characteristic of hopping within a Gaussian density of states 90 mV in width. They suggested that the $\mu(E)$ dependence is evidence of the importance of off-diagonal disorder. The Gaussian distribution of site energies is justified by the fact that the polarization energy contribution to the site energy is determined by a large number of internal coordinates that vary randomly [152, 166]. Considerable data establishing a relationship between the carrier mobilities and group dipole moments of molecular constituents support this view of charge-dipole interactions as the source of energetic disorder in these systems [165].

Although the standard Gaussian disorder model satisfactorily explains many experimental features, it displays a field dependence of the type $\ln \mu \propto \sqrt{E}$ only in a relatively narrow range and only at large fields ($E > 10^5$ V/cm) [165]. In experiments,

by contrast, the linear dependence of $\ln \mu$ on \sqrt{E} often persists down to the lowest fields probed [167]. This difficulty was eliminated by an analytical confirmation of the idea that correlations arising from charge-dipole interactions should cause a significant field dependence of the mobility at lower fields, resulting in a mobility in quantitative agreement with that observed in experiments [165].

Using a model polymer composed of randomly oriented conjugated segments of length L_C and considering a polymeric layer sandwiched between two metal electrodes, Bussac and Zuppiroli [168] calculated the space-charge current in organic devices. The major factor in preventing the current flow in these systems is assumed [168] to be the space charge created by the injected polarons. The drift mobility of the polarons in the polymer is obtained by applying the Holstein adiabatic model [169]. The polaron transport from one site to another is achieved upon the occurrence of a coincidence between two adjacent segments. A coincidence is a deformation of the segment that allows the tunneling of the carrier. It has been found that when the polaron width is smaller than the average conjugation length, the polaron drift mobility presents a strong field dependence. The current depends exponentially on

the average electric field, presenting a mathematical expression similar to the Fowler–Nordheim tunneling theory. The model is in agreement, considering the order of magnitude and the electric field dependence, with the experimental observations of Parker [170]. The findings of Bussac and Zuppiroli suggest that no real tunnel injection is observed in metal/polymer/metal devices, but, rather, a special case of space-charge limited current determined by the peculiarities of the charge conduction in organic materials. This model does not explain, however, the observed relation between the work function of a series of metals used as electrodes and the barrier height measured with the help of the tunneling theory at metal/polymer interfaces [170–175]. Furthermore, the model poorly reproduces the temperature dependence of the current taken at a constant applied voltage [140].

A complete description of the current dependence on the applied voltage for conjugated polymers sandwiched between electrodes is difficult because it involves both injection through the interface and charge transport through the polymer bulk, which may be interdependent mechanisms [140].

In some cases of space-charge limited current observation, the $j(V, d)$ dependence follows that of Eq. (6), indicating the existence of an exponential distribution of traps. Different values of E_C were reported: $E_C = 0.15$ eV [176] and $E_C = 0.13$ eV [177] in PPV; $E_C = 0.06$ eV and $E_C = 0.05$ eV for a blue-emitting and a green-emitting alternating block copolymer, respectively [143]. Considering that the magnitude of E_C is an indication of the order of the polymer, the reduced E_C values observed in the block copolymers indicate that those are less susceptible to the factors that introduce energetic disorder.

There are some techniques, such as admittance spectroscopy and deep-level transient spectroscopy (DLTS), that are quite powerful in the characterization of deep levels in semiconductors [139]. These techniques have also begun to be used for the characterization of conjugated polymers such as PPV [178] and MEH-PPV [179]. These techniques may permit the determination of several trap parameters such as activation energy, concentration, charge carrier capture cross section, defect donor/acceptor character that can contribute to the chemical identification of the traps.

5.2.2. Doped PPV

The intrinsic electrical conductivity of PPV, at room temperature and on exposure to air, is on the order of 10^{-12} S·cm⁻¹ [75]. After doping, conductivity can increase to values ranging from approximately 10^{-6} to 10^3 S·cm⁻¹, depending on several factors such as the nature and concentration of the dopant, the nature and size of the group(s) attached to the polymer backbone, whether the polymer has been aligned (by stretching) or not, and the effective conjugation length. Generally, the stronger the dopant oxidizing power, the higher the final conductivity. Thus, for instance, PPV pressed disks doped with I₂, BF₃, and SO₃, by exposure to their vapors, exhibited conductivities of 5×10^{-6} , 7×10^{-3} , and 2×10^{-2} S·cm⁻¹, respectively [62]. AsF₅ doping gives much higher values but its toxicity is a serious drawback.

Electron-donating groups such as alkoxy increase the conductivities of PPVs doped with weak Lewis acids (e.g., I₂, BF₃), while electron-withdrawing substituents, such as NO₂, do the opposite [66]. Plots of log(conductivities) versus Hammett σ values have shown a distinct dependence between conductivity and polar substituent effect [62]. With stronger dopants, such as FeCl₃, H₂SO₄,

and AsF₅, this effect is negligible. Alkyl or phenyl groups as well as long side chains lower the conductivity, probably by hindering interchain hopping of charge carriers [2].

Stretched films of doped PPV exhibit much higher conductivities. For instance, I₂ doped 2,5-dimethoxy-PPV presents a 60-fold increase in conductivity after stretching (draw ratio 8) [180].

Studies with PPV model compounds [62, 181] have shown that seven to nine conjugated double bonds are generally sufficient to ensure conductivity values close to those of the corresponding polymers. The soluble oligomers were blended with polystyrene and iodine to give black electrically conducting films ($0.1\text{--}1$ S·cm⁻¹) that were stable over a period of 100 days at room temperature in air [181]. The stability is due to the fact that the doped species are encapsulated in the polystyrene matrix, which strongly retards the uptake of atmospheric moisture and the evaporation of iodine.

6. INTERFACES WITH OTHER MATERIALS

PPV-based devices are commonly constructed in a multilayer structure in which the polymer film is sandwiched between charge injection electrodes. For this reason, the polymer/electrode interface plays an important role on the performance of the devices and will be discussed for different classes of materials in the next sections.

6.1. Interfaces with Metals

Low-work-function metals such as Ca, Mg, and Al are commonly used as electron injection electrodes in organic LEDs, and thin Au films can be used for hole injection electrodes. The interfaces of these and other metals with PPV and its derivatives were investigated by several research groups using different techniques such as X-ray photoelectron spectroscopy (XPS), UV photoelectron spectroscopy (UPS), transmission electron microscopy (TEM), quantum-chemical calculations, and electrical measurements. Some results are summarized in the following paragraphs for different metals.

Aluminum. Theoretical results indicate that aluminum deposited onto PPV tends to form covalent bonds with carbon atoms [182]. The most stable structures are (i) two aluminum atoms interacting with a vinylene group and (ii) two aluminum atoms interacting with a phenylene ring. The most stable configuration for the Al₂/PPV complex is when the two aluminum atoms are bonded to a single vinylene group [183]. Aluminum atoms also preferentially react with the vinylene linkages in poly(2,5-dimethoxy-*p*-phenylene vinylene), but when carbonyl groups appear on the side of the chains, as in poly(2,5-dialdehyde-*p*-phenylene vinylene), new reactive sites are induced. This leads to structures with stabilities comparable to those in the most stable configurations involving a single vinylene group [183]. In the three systems, the interaction with aluminum induces major modifications of the polymer chains with interruptions of the conjugated π -system caused by the formation of sp³-like defects [183]. The consequences of the tendency of Al to form covalent bonds along the conjugated backbone are the following: (i) those carbon sites become sp³ hybridized, (ii) the planarity of the polymer chain is lost in most of the cases, and (iii) the π -electron conjugation can be severely reduced [184].

Konstadinidis et al. [185] observed that during the formation of the Al/PPV interface, no band bending is observed for Al coverage up to 20 Å. The polymer surface is depleted of vinylene groups due to substitution of the double bonds by oxygen-containing groups during conversion. These groups (primarily carbonyls near the surface) are the primary reactive sites for the deposited metal atoms, resulting in the formation of Al–O–C linkages with the surface. The high reactivity of the oxygen-modified PPV surface results in the immobilization of the deposited metal atoms, preventing surface and bulk diffusion and promoting cluster growth of the metal overlayer. These observations are in agreement with cross-sectional TEM investigations, which indicate a sharp frontier at the Al/PPV interface [114]. Nguyen and Mansot [186] observed samples presenting a different interface condition with an intermediate sublayer (~50 nm thick) formed between the polycrystalline Al layer and the PPV bulk. They concluded that this sublayer is strongly affected by the deposition process, although no diffusion of metallic atoms was detected in the polymer. They suggested that the irradiation of the surface by the metal vapor could partially break the conjugation and favor the reticulation of carbon in the polymer network. In this case, the true interface between PPV and Al is formed of mixtures of aluminum oxide and an undetermined complex involving possibly Al–C and Al–O–C bonds.

Electrical measurements performed by Nguyen et al. [187] indicate that the aluminum/PPV interface shows a rectifying behavior when aluminum is deposited as a top electrode, as well as a bottom electrode, after polymer conversion and before polymer conversion, respectively. XPS analyses indicate chemical reactions between the polymer and the metal in the presence of oxygen to form metal–carbon complexes [187].

Calcium. The interaction of Ca with the surface of conjugated polymers appears to be fundamentally different from that of Al. The nature of the interaction between Ca atoms and the conjugated polymer is ionic [184]. The charge transfer from the metal to the polymer is very similar to the classical n-doping of conjugated systems, which leads to the appearance of new occupied electronic states within the former bandgap of the neutral species. In principle, Ca deposition should lead to increased conductivity in the region near the interface, favoring charge transport across the modified polymeric layer [184]. This phenomenon has been observed in poly(diheptylphenylene vinylene) (PDHPV), where, when Ca is deposited, a new band located within the bandgap of pristine PDHPV can be observed in the UPS spectra [184] and in poly(2,3-diphenylphenylene vinylene) (DP-PPV). Near-edge X-ray absorption spectroscopy (NEXAFS) studies performed on DP-PPV indicate that the deposition of Ca results in the formation of new unoccupied states both within the leading edge of the conduction band and at higher energies [188].

When calcium is deposited by vapor deposition upon clean surfaces under ultrahigh vacuum conditions, calcium diffuses into the near surface region, donates electrons to the π -system, and forms Ca^{2+} ions. The interfacial region between the Ca-metal contact and the polymer has an approximate scale in the range of 20 to 30 Å [189].

Chromium. Chromium deposited as a top electrode onto PPV involves rectifying behavior, while Cr deposited as a bottom electrode involves a blocking one. In the latter case, clustering of Cr in the polymer matrix has also been observed [187]. X-ray photoelectron spectra of 4,4'-bis(4 styryl-styryl) benzene oligomer films

metallized with Cr indicate carbide formation, whereas no apparent reaction was observed in the interfacial layer when depositing the oligomer film on the chromium layer [190].

Gold. XPS observations indicate the possible formation of a Au–C interaction on PPV in the initial stages of the Au deposition, but this interaction appears to break down with an increase of Au deposition [191]. When the PPV precursor is deposited on a gold-covered glass substrate and is further converted to PPV at 250°C, during 2 hours, small clusters are observed in the film [114]. Considering that these clusters were observed only when PPV was converted onto gold, their origin was attributed to gold diffusion and precipitation inside the polymer layer.

Magnesium. Quantum-chemical calculations performed on stilbene model molecules indicate that the introduction of Mg disrupts the geometry of the model molecules less than Al does, and the HOMO and LUMO move into the initial energy gap for Mg-doped systems, resulting in the formation of a gap state [192].

Silver. Polycrystalline Ag has a work function value similar to that of Al but, when deposited onto PPV, presents a preferential orientation of {111} planes parallel to the Ag/PPV interface [193]. The work function of Ag{111} surfaces is higher than that of polycrystalline material and, as a consequence, electron injection from Ag into PPV is less probable. Ag electrodes deposited onto PPV present adhesion problems when negatively polarized with respect to the other contact [193].

6.2. Interfaces with Oxides

ITO. ITO is the most widely used transparent conductive material in optoelectronic devices based on PPV derivatives due to its transparency in the visible region of the spectrum. In LEDs, ITO is used as an anode, owing the similarity of its work function with the electroaffinity of PPV and several of its derivatives. The ITO work function depends on the preparative method and is also sensitive to chemical cleaning procedures [194–197], so that it can be matched with the polymer HOMO level. It is observed that the In/Sn ratio can be modified, depending on the substrate cleaning procedure [194, 195].

There are, however, indications that PPV films converted onto ITO substrates present contamination. Indium concentrations up to $5 \times 10^{19} \text{ cm}^{-3}$ [198] were detected in the polymer layer of LEDs, even before their operation. The HCl released as an elimination product during the conversion process reacts with the ITO coating. Many small clusters containing a large amount of indium and chlorine, and in the case of thicker PPV films, even InCl_3 crystals with lateral dimensions up to 40 μm , have been found [112]. Photoluminescence measurements reveal that the fluorescence efficiency is quenched by a factor of 2 to 23 in the case of ITO compared with PPV converted onto usual glass [112, 199]. Brütting et al. [199] found that in devices prepared on ITO substrates doping with InCl_3 leads to acceptor states with a depth of about 0.15 eV. These carriers are mobile and form a depletion layer when a metal with low work function is used as a cathode. This doping is responsible for the observed Schottky diode behavior in PPV devices prepared on ITO.

Photoelectron spectroscopy investigations of ITO-on-PPV interfaces (ITO deposited by argon plasma deposition onto PPV) indicate that this interface layer contains three types of altered

carbon species, corresponding to carbon–oxygen single bonds, carbon–oxygen double bonds, and carbon bonded to two oxygen atoms, as in carboxyl groups [200]. The interfacial species are similar to those found in photooxidation studies of PPV surfaces, strongly suggesting that the interface region in ITO on PPV corresponds to highly oxidized PPV [200].

Tin Oxide. Nominally undoped tin oxide (TO), n-type (10^{19} cm^{-3} attributed to oxygen deficiency), has been investigated as a substitute for ITO as an anode [201, 202] and also as a cathode [202] material in PPV-based LEDs. The electrical and optical properties of TO films are sensitive to the preparation procedures [203] and this fact can be used to improve the charge injection conditions [201]. Contrary to ITO, the work function of nominally undoped TO is not significantly affected by cleaning operations [204].

The photoluminescence quenching observed in PPV converted onto TO is approximately 50% when compared to PPV converted onto quartz [204], which is less than that reported for PPV converted onto ITO [112], revealing that the chemical interaction between the TO substrate and PPV is weaker than that observed between ITO and PPV.

Fluorine-doped TO (FTO) has also been studied as a potential alternative to ITO [205]. Several advantages of using FTO instead of ITO were reported: (i) it is less expensive than ITO, (ii) it is less sensitive to chemical cleaning procedures, and (iii) more light is produced at a given voltage [205].

6.3. Interfaces with Other Conjugated Polymers and Polymer Blends

Polyaniline. Polyaniline (PANI) has been investigated as a hole injection contact into PPV and its derivatives. PANI in its metallic emeraldine salt form, doped with camphor sulfonic acid (CSA), presents high electronic conductivity and low ionic conductivity, reducing metal–electrode interface degradation effects. Further, the barrier height for hole injection at the PANI/MEH–PPV interface is estimated to be approximately 0.08–0.12 eV [206], making this material suitable as an anode in MEH–PPV-based LEDs. Devices made using PANI/ITO as an anode present increased quantum efficiency and reduced operating voltage, when compared to devices constructed with a bare ITO anode [206, 207]. Further, the improvement in degradation is attributed to reduced oxidation as the PANI layer provides a barrier for the passage of oxygen out of the oxide [207]. In addition, the shortening behavior is eliminated due to planarization of the anode interface by the PANI film [207].

Devices constructed using multilayered structures of PPV derivatives and emeraldine base polyaniline layers were also reported [208].

Polyaniline Blends. Polyaniline doped with camphor sulfonic acid, PANI–CSA, in the form of a blend with poly(methyl methacrylate), PMMA, is also used as hole injection material in PPV-based LEDs owing to the low barrier for hole injection [209, 210] and the match of the PPV electroluminescent emission with the transmittance window of the PANI–CSA/PMMA blend (Fig. 10). Blends of polyester resin (PES) with PANI–CSA were also used for this purpose [209]. The barrier height for hole injection at the PANI–CSA–PES/MEH–PPV blend was found to be dependent on the PANI–CSA concentration, ranging from about 0.02 eV at a concentration of 5% w/w to about 0.1 eV for pure PANI [209]. In the case of PANI–CSA–PMMA/PPV interfaces, the barrier height for hole

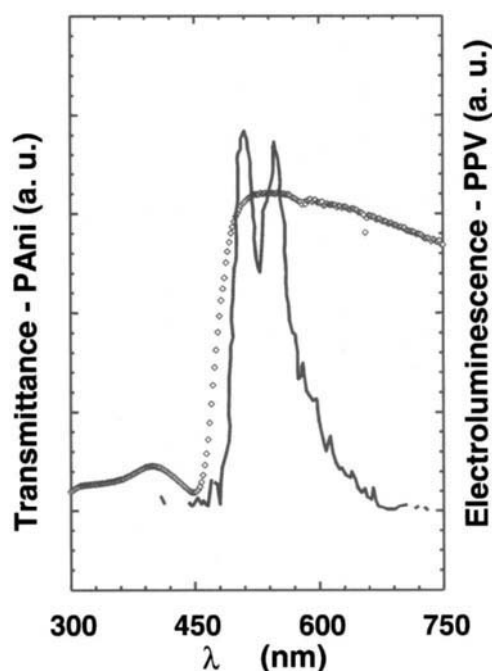


Fig. 10. Optical transmittance of the PANI–CSA/PMMA blend (10% PANI–CSA in PMMA w/w) (\circ) and electroluminescence spectrum of PPV (—).

injection has been found to be approximately 0.1 eV, independent of the concentration in the range 5–25% PANI–CSA [210]. For a concentration lower than 5%, an increase in the barrier height was observed.

Polyaniline also presents an additional potential advantage because uniaxially oriented blends of polyaniline doped with dodecylbenzenesulfonic acid or CSA and common bulk polymers such as polyacrylonitrile, polyethylene, and poly(vinyl alcohol) display a polarizing efficiency over the range from 400 to 4000 cm^{-1} that matches, or surpasses, that of commercial wire grid polarizers [211]. These characteristics permit the use of polyaniline simultaneously as a polarizer and as an anode.

7. APPLICATIONS

7.1. Light-Emitting Diodes

The interest of the scientific community in PPV and its derivatives has strongly increased in the last few years, especially after the report of PPV electroluminescence by the Cambridge group in 1990 [113]. Polymers present attractive mechanical properties such as flexibility and a relatively simple processing technology. Associated with this, different polymers can be produced with electroluminescent emission in different spectral regions, which is a necessary condition for several practical uses of LEDs.

The first generation of PPV-based electroluminescent devices was constructed using a thin PPV layer sandwiched between an indium–tin oxide (ITO) as a hole injection contact (anode) and a low-work-function metal operating as an electron injection contact (cathode) [113], as schematically represented in Figure 11. The bottom electrode and the substrate are, in this case, transparent to permit light to escape. The basic device geometry, the sandwich

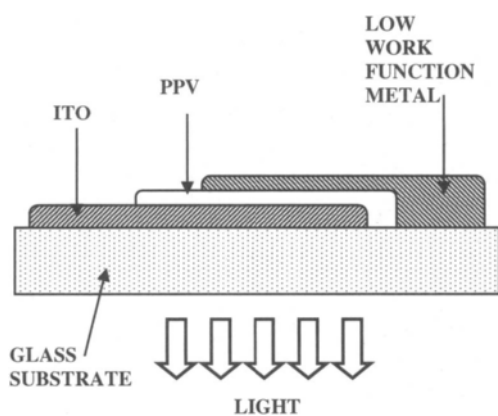


Fig. 11. Schematic representation of a PPV-based LED. A low-work-function metal is used as a cathode, whereas ITO operates as an anode. The bottom contact material (ITO) and the substrate are transparent to permit the light to escape.

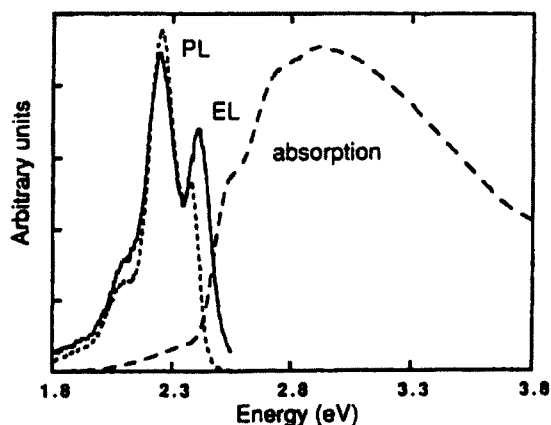


Fig. 12. Optical absorption, photoluminescence (PL), and electroluminescence (EL) emission spectra for PPV. Reprinted by permission of Elsevier Science from D. R. Baigent, N. C. Greenham, J. Grüner, R. N. Marks, R. H. Friend, S. C. Moratti, and A. B. Holmes, *Synth. Met.* 67, 3 (1994). Copyright © 1994 Elsevier Science.

structure, remains the same, in spite of several improvements concerning electrode materials, electroluminescent polymers, and the adoption of multilayered structures [212–215]. PPV-based LEDs were also demonstrated with a planar metal/polymer/metal structure, but this LED geometry presents the disadvantages of high operating voltage and asymmetry in the emissive zone [216].

In organic LEDs, the electroluminescence spectrum is quite similar to the photoluminescence spectrum of the polymer used in the device (Fig. 12), so that the light emission is attributed to the singlet exciton decay. The excitons are formed by electrons and holes injected into the polymer by the cathode and anode, respectively. The injection current density depends on several parameters such as the potential barriers for charge injection at the polymer–electrode interfaces, the mobility of the charge carriers in the polymer layer, the polymer layer thickness, and the applied voltage. The efficiency of these devices is intrinsically limited by the balance between injected electrons and holes and by the fraction of excitons that decay radiatively. Further efficiency limits are imposed by reflections that occur in the interfaces between the materials that compose the device, including the interface formed

between substrate and air, which normally imposes the major efficiency limitation.

Several different materials can be used as transparent electrodes, most of them as anode material: ITO [113, 194, 195, 200], polyaniline and polyaniline blends [206, 207, 209, 210], TO [201, 202, 204], and F-doped TO [112, 205]. The use of transparent material as a cathode has also been reported [202]. In the case of PPV and several of its derivatives, the effective mobility of the electrons is lower than that of the holes, implying a reduction in the extent of the recombination zone in the electroluminescent polymer layer, as observed in PPP LEDs [164]. Further, the values of polymer electroaffinity and ionization potential make the injection and transport of holes easier than that of electrons in single-polymer-layer devices. The injection dynamics also depends on the injected carrier that remains in the polymer (space charge), modifying the electric field distribution in the device [217]. For these reasons, different materials are tested as cathode and anode and, in several cases, intermediate layers are also introduced in order to improve the injection of a specific charge carrier type or to block its transport through the device [212, 213, 218–220].

The charge carrier balance problem has been minimized by the introduction of multilayered polymeric structures that produce potential barriers at the internal interfaces. These potential barriers impose restrictions to charge carrier transport through the device and enhance the recombination probability and, consequently, the device efficiency. One example of such a structure is the ITO/PPV/CN-PPV/metal LED. CN-PPV presents a higher electroaffinity and ionization potential than PPV, so that there is a potential barrier for electron transport from the CN-PPV to the PPV and a potential barrier for holes in the opposite direction [218]. Several other conjugated polymers and molecules are also used in combination with PPV in heterolayer LEDs [213].

7.2. Photodiodes and Photodetectors

PPV and its derivatives are also used as active materials in optoelectronic transducers, which produce an electrical output dependent on the light input. The electrical conductivity of PPV is modulated by its interaction with the incident light, characterizing photoconductivity. Due to the optical absorption, free charge carriers are generated in the polymer and can be collected if an external electric field is applied to the device. This phenomenon permits the use of PPV in light detection devices, such as photodiodes, whose characteristic is a current versus voltage response, which is strongly dependent on illumination conditions.

The photodiode device geometry is similar to that of an LED. The photoconductive polymer layer is sandwiched between two electrodes, one of them transparent to permit light to achieve the polymer. The term “diode” is used due to the rectification characteristics of devices made with materials of different work functions. These devices present rectification in the dark as well as under illumination, owing to the role of the interface in the charge injection process.

The use of materials with different work functions as electrodes in a sandwich structure introduces a “built-in” electric field in the polymeric layer that can be used in photoconductive systems to produce photovoltaic devices [221]. In these devices, the incident light generates free charge carriers that are transported under the influence of the built-in electric field and may produce an electric current in an external circuit. Earlier PPV-based devices constructed on an ITO/PPV/X structure (X: Al, Mg, Ca; PPV film

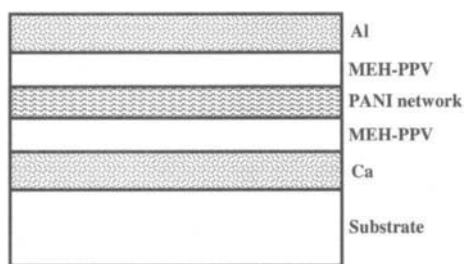


Fig. 13. Schematic representation of the triode structure.

thickness between 0.1 and 1 μm) achieved, taking reflection losses into account, a power conversion efficiency on the order of 0.1% [221].

To increase the charge transfer from the polymer to the electrodes, some improvements were made in the device structure. Additional polymer layers were introduced between the PPV layer and electrode [222, 223], MEH-PPV was sensitized with C_{60} [224], and interpenetrating polymer networks of different PPV derivatives (e.g., MEH-PPV and CN-PPV) [225, 226] or PPV derivatives with other conjugated polymers [227] were used.

7.3. Lasers

The first gain narrowing in a conjugated polymer was accomplished using freestanding films of a blend consisting of MEH-PPV, polystyrene, and TiO_2 nanoparticles [228, 229]. In the sequence, band narrowing through stimulated emission was observed for simple spin-coated films that were deposited onto glass substrates [230–232] and a resonator was incorporated into the device structure [233].

Gain narrowing has been reported for PPV and several PPV derivatives [229]: PPV [234]; poly(2-butyl-5-(2'-ethylhexyl)-1-4-phenylene vinylene) [230]; PPV microcavity [233]; PPV with OC_8H_{17} side groups in the 2,5 positions [232]; copolymer of phenylene vinylene [235]; poly(dimethylsilane-*p*-phenylene vinylene)-(2,5-di-*n*-octyl-*p*-phenylene vinylene) [236].

7.4. Triodes

In 1994, a polymer-based transistor [237] constructed in a geometry closely related to that of a vacuum tube triode was demonstrated [237]. The structure consists of a thin MEH-PPV polymer film sandwiched between two electrodes, with a third electrode (PANI network) [209, 238–241] embedded within the MEH-PPV film (Fig. 13). This third electrode plays a role similar to that of the grid in a vacuum tube, controlling the current between the two outermost electrodes. Using a generalized analysis based on field-assisted carrier injection by tunneling, the carrier injection and transport in the polymer grid triode could be modeled [242].

This Al/MEH-PPV/PANI-network/MEH-PPV/Ca geometry [237] eliminates the relatively long pathways involved in field effect transistors, which constitute a problem considering the low charge carrier mobilities observed in organic materials. As a consequence, a relatively fast response is observed in these device structures.

7.5. Light-Emitting Electrochemical Cells

In 1995, a new device, whose structure was similar to that of a conventional LED, but whose active layer was composed of a

blend of MEH-PPV, poly(ethylene oxide), and $\text{Li}_3\text{CF}_3\text{SO}_3$ salt, was reported by Pei et al. [243]. The device was constructed on an ITO/blend/Al (blend thickness, ~ 250 nm) sandwich structure. Further, PPV with poly(ethylene oxide)/salt was also used in light-emitting electrochemical cells (LECs) [244].

These LECs have some unique properties [245]: the current-voltage characteristics were antisymmetric about the origin, even though electrodes with different work functions had been used; light emission was observed for both positive and negative applied voltage; the onset voltage (independent of polarity) for appreciable current and visible light detection was almost identical to the bandgap of the polymer; and the onset voltage was almost independent of layer thickness.

In the LEC, under the influence of the field created by the applied voltage, the positive charge carriers move from the anode toward the cathode, and the negative charge carriers move from the cathode toward the anode. Between the two regions, these electrons and holes meet in a region that defines an electrochemically induced p-n junction. Within this region, the electrons and holes combine to form neutral pairs, which radiatively decay to the ground state [243].

In spite of the similarity with a conventional inorganic p-n junction, in the LECs, particularly for large-bandgap materials, mobile charges are almost exclusively injected from the electrodes (electrochemical doping). In the conventional inorganic p-n junction, mobile charges are already present in the bulk, prior to contact with the electrodes [245].

Using a bilayer polymer structure composed of PPV and MEH-PPV, two-color LECs were demonstrated [246]. When these devices are biased in one polarity, the voltage induced p-n junction is completely inside the PPV layer and the device emits green light characteristic of PPV. When biased at the opposite polarity, the p-n junction is completely inside the MEH-PPV layer and the LEC emits orange light characteristic of MEH-PPV.

7.6. Optocouplers

Optocouplers are a class of devices with input and output circuits coupled optically while isolated electrically. Such devices were fabricated using Ca/MEH-PPV/ITO diodes, which emit red-orange light, as the input unit and Au/P3OT/ITO as the output unit [247]. The input unit presented approximately 1% photons/electron external quantum efficiency and the output unit a quantum yield of about 35% electrons/photon at 590 nm. This device reached a current transfer ratio of 2×10^{-3} under -10 V reverse bias, comparable to that of commercially inorganic optocouplers. Using the improved devices (optimized LEDs made from MEH-PPV and photodiodes made from P3OT sensitized with C_{60}), a current transfer ratio of 10^{-3} can be achieved even at low bias (0 to -2 V) [248].

Acknowledgments

The authors express their gratitude to PADCT, CNPq, and FAPESP for their financial support during the preparation of this text. The collaboration of Mrs. K. V. D de Souza and of the staff of the Biblioteca do Setor de Ciências Exatas e Tecnologia from Universidade Federal do Paraná is also acknowledged.

REFERENCES

1. R. H. Friend, R. W. Gymer, A. B. Holmes, J. H. Burroughes, R. N. Marks, C. Taliani, D. D. C. Bradley, D. A. Dos Santos, J. L. Brédas, M. Lögdlund, and W. R. Salaneck, *Nature* 397, 121 (1999).
2. S. C. Moratti, in "Handbook of Conducting Polymers" (T. A. Skotheim, R. L. Elsenbaumer, and J. R. Reynolds, Eds.), Chap. 13. Dekker, New York, 1998.
3. R. H. Friend and N. C. Greenham, in "Handbook of Conducting Polymers" (T. A. Skotheim, R. L. Elsenbaumer, and J. R. Reynolds, Eds.), Chap. 29. Dekker, New York, 1998.
4. A. Greiner, *Polym. Adv. Technol.* 9, 371 (1998).
5. A. Kraft, A. C. Grimsdale, and A. B. Holmes, *Angew. Chem., Int. Ed. Engl.* 37, 403 (1998).
6. K. Müllen and G. Wegner, "Electronic Materials: The Oligomeric Approach." Wiley-VCH, Weinheim 1998.
7. W. J. Feast, J. Tsibouklis, K. L. Pouwer, L. Groenendaal, and E. W. Meijer, *Polymer* 37, 5017 (1996).
8. A. Maercker, *Org. React.* 14, 270 (1965).
9. R. N. McDonald and T. W. Campbell, *J. Am. Chem. Soc.* 82, 4669 (1960).
10. K. D. Gourley, C. P. Lillya, J. R. Reynolds, and J. C. W. Chien, *Macromolecules* 17, 1025 (1984).
11. N. N. Barashkov, D. J. Guerrero, H. J. Olivos, and J. P. Ferraris, *Synth. Met.* 75, 153 (1995).
12. M. Schlosser, *Top. Stereochem.* 5, 1 (1970).
13. H. J. Bestman and O. Vostrowsky, *Top. Curr. Chem.* 109, 85 (1983).
14. G. Koszmehl and B. Bohn, *Angew. Chem., Int. Ed. Engl.* 12, 237 (1973).
15. G. Koszmehl, *Ber. Bunsen-ges. Phys. Chem.* 83, 417 (1979).
16. H.-H. Hörhold and M. Helbig, *Makromol. Chem., Macromol. Symp.* 12, 229 (1987).
17. N. N. Barashkov, T. S. Novikova, and J. P. Ferraris, *Synth. Met.* 83, 39 (1996).
18. H. K. Kim, M.-K. Ryu, and S.-M. Lee, *Macromolecules* 30, 1236 (1997).
19. H. Saito, S. Ukai, S. Iwatsuki, T. Itoh, and M. Kubo, *Macromolecules* 28, 8363 (1995).
20. B. Wang and M. R. Wasielewski, *J. Am. Chem. Soc.* 119, 12 (1997).
21. R. A. Wessling, *J. Polym. Sci., Polym. Symp.* 72, 55 (1985).
22. R. A. Wessling and R. G. Zimmerman, U.S. Patents 3,401,152, 1968; 3,404,132, 1968; 3,532,643, 1970; 3,706,677, 1972.
23. P. M. Lahti, D. A. Modarelli, F. R. Denton III, R. W. Lenz, and F. E. Karasz, *J. Am. Chem. Soc.* 110, 7258 (1988).
24. F. R. Denton III, P. M. Lahti, and F. E. Karasz, *J. Polym. Sci., Part A: Polym. Chem.* 30, 2223 (1992).
25. R. W. Lenz, C.-C. Han, J. Stenger-Smith, and F. E. Karasz, *J. Polym. Sci., Part A: Polym. Chem.* 26, 3241 (1988).
26. *Aldrichchimica Acta* 25, 38 (1992).
27. A. Beerden, D. Vanderzande, and J. Gelan, *Synth. Met.* 52, 387 (1992).
28. P. L. Burn, D. D. C. Bradley, A. R. Brown, R. H. Friend, and A. B. Holmes, *Synth. Met.* 41-43, 261 (1991).
29. J. M. Machado, F. R. Denton III, J. B. Schlenoff, F. E. Karasz, and P. M. Lahti, *J. Polym. Sci., Part B: Polym. Phys.* 27, 199 (1989).
30. C. C. Han and R. L. Elsenbaumer, *Synth. Met.* 41-43, 849 (1991).
31. M. Kanbe and M. Okawara, *J. Polym. Sci., Part A: Polym. Chem.* 6, 1058 (1968).
32. V. H. Tran, V. Massardier, and A. Guyot, *Polymer* 35, 1561 (1994).
33. H. V. Shah, A. R. McGhie, and G. A. Arbuckle, *Thermochim. Acta* 287, 319 (1996).
34. M. Woodruff, *Synth. Met.* 80, 257 (1996).
35. A. Torres-Filho and R. W. Lenz, *J. Polym. Sci., Part B: Polym. Phys.* 31, 959 (1993).
36. A. Torres-Filho and R. W. Lenz, *J. Appl. Polym. Sci.* 52, 377 (1994).
37. S. Antoun, F. E. Karasz, and R. W. Lenz, *J. Polym. Sci., Part A: Polym. Chem.* 26, 1809 (1988).
38. W. B. Liang, M. A. Masse, and F. E. Karasz, *Polymer* 33, 3101 (1992).
39. A. Delmotte, M. Biesemans, M. Gielen, J. Gu, and B. V. Mele, *Polymer* 37, 5395 (1996).
40. J. D. Stenger-Smith, A. P. Chafin, and W. P. Norris, *J. Org. Chem.* 59, 6107 (1994).
41. I.-N. Kang, D.-H. Hwang, and H.-K. Shim, *Synth. Met.* 69, 547 (1995).
42. D.-H. Hwang, H.-K. Shim, J.-I. Lee, and K.-S. Lee, *J. Chem. Soc., Chem. Commun.* 21, 2461 (1994).
43. J.-I. Jin, Y.-H. Lee, C.-K. Park, and B.-K. Nam, *Macromolecules* 27, 5239 (1994).
44. S.-J. Chung, J.-I. Jin, and K.-K. Kim, *Adv. Mater.* 9, 551 (1997).
45. J.-I. Lee, H.-K. Shim, G. J. Lee, and D. Kim, *Macromolecules* 28, 4675 (1995).
46. D.-H. Hwang, J.-I. Lee, H.-K. Shim, W.-Y. Hwang, J.-J. Kim, and J.-I. Jin, *Macromolecules* 27, 6000 (1994).
47. J.-I. Jin, Y.-H. Lee, and B.-K. Nam, *Polymer* 36, 193 (1995).
48. J.-I. Jin, C.-K. Park, and H.-K. Shim, *J. Polym. Sci., Part A: Polym. Chem.* 29, 93 (1991).
49. C.-B. Yoon and H.-K. Shim, *Macromol. Chem. Phys.* 197, 3689 (1996).
50. C.-B. Yoon, I.-N. Kang, and H.-K. Shim, *J. Polym. Sci., Part A: Polym. Chem.* 35, 2253 (1997).
51. Y. Sonoda, Y. Nakao, and K. Kaeriyama, *Synth. Met.* 55-57, 918 (1993).
52. X.-C. Li, F. Cacialli, R. Cervini, A. B. Holmes, S. C. Moratti, A. C. Grimsdale, and R. H. Friend, *Synth. Met.* 84, 159 (1997).
53. A. Sarker, P. M. Lahti, and F. E. Karasz, *J. Polym. Sci., Part A: Polym. Chem.* 32, 65 (1994).
54. R. W. Lenz, C. C. Han, and M. Lux, *Polymer* 30, 1041 (1989).
55. J.-I. Jin, Y.-H. Lee, K.-S. Lee, S.-K. Kim, and Y.-W. Park, *Synth. Met.* 29, E47 (1989).
56. J.-I. Jin, H.-K. Shim, and R. W. Lenz, *Synth. Met.* 29, E53 (1989).
57. R. M. Gurge, A. Sarker, P. M. Lathi, B. Hu, and F. E. Karasz, *Macromolecules* 29, 4287 (1996).
58. H.-K. Shim, D.-H. Hwang, and C.-B. Yoon, *Macromol. Chem. Phys.* 197, 2393 (1996).
59. R. Gowri, D. Mandal, B. Shivkumar, and S. Ramakrishnan, *Macromolecules* 31, 1819 (1998).
60. H. Nishihara, M. Tateishi, K. Aramaki, T. Ohsawa, and O. Kimura, *Chem. Lett.* 1987, 539; O. Kimura, T. Ohsawa, and H. Nishihara, Jpn. Patent, JP 63125520, 1988.
61. P. Damlin, C. Kvarnström, and A. Ivaska, *Electrochim. Acta* 44, 1919 (1999).
62. J. H. P. Utley, Y. Gao, J. Gruber, Y. Zhang, and A. Munoz-Escalona, *J. Mater. Chem.* 5, 1837 (1995).
63. Y. Gao, A. Hussain, M. Motevall, J. H. P. Utley, and P. B. Wyatt, *J. Org. Chem.* 58, 3578 (1993).
64. E. Eru, G. E. Hawkes, J. H. P. Utley, and P. B. Wyatt, *Tetrahedron* 51, 3033 (1995).
65. T. Lund, S. U. Pedersen, H. Lund, K. M. Cheung, and J. H. P. Utley, *Acta Chem. Scand. Sect. B* 41, 285 (1987).
66. J. Gruber and R. W. C. Li, *J. Mater. Chem.* 9, 1461 (1999).
67. J. Gruber and R. W. C. Li, *Synth. Met.* 88, 201 (1997).
68. W.-P. Chang, W.-T. Whang, and P.-W. Lin, *Polymer* 37, 1513 (1996).
69. M. Rehahn and A.-D. Schlüter, *Makromol. Chem., Rapid Commun.* 11, 375 (1990).
70. F. Cataldo, *Polym. Commun.* 32, 354 (1991).
71. R. H. Heck, *Org. React.* 27, 345 (1981).
72. A. Greiner and W. Heitz, *Macromol. Chem., Rapid Commun.* 9, 581 (1988).
73. M. Brenda, A. Greiner, and W. Heitz, *Makromol. Chem.* 191, 1083 (1990).
74. H. Martelock, A. Greiner, and W. Heitz, *Makromol. Chem.* 192, 967 (1991).
75. D. D. C. Bradley, *J. Phys. D: Appl. Phys.* 20, 1389 (1987).
76. B. Tian, G. Zerbi, R. Schenk, and K. Müllen, *J. Chem. Phys.* 95, 3191 (1991).
77. B. Tian, G. Zerbi, and K. Müllen, *J. Chem. Phys.* 95, 3198 (1991).

78. J. P. Buisson, S. Lefraut, G. Louarn, J. Y. Mévellec, I. Orion, and H. Eckhardt, *Synth. Met.* 49–50, 305 (1992).
79. D. D. C. Bradley, G. P. Evans, and R. H. Friend, *Synth. Met.* 17, 651 (1987).
80. H. S. Woo, O. Lhost, S. C. Graham, D. D. C. Bradley, R. H. Friend, C. Quattrocchi, J. L. Brédas, R. Schenk, and K. Müllen, *Synth. Met.* 59, 13 (1993).
81. M. Herold, J. Gmeiner, and M. Schwoerer, *Acta Polym.* 47, 436 (1996).
82. M. Esteghamatian and G. Xu, *Appl. Phys. Lett.* 65, 1877 (1994).
83. K. Pichler, D. A. Halliday, D. D. C. Bradley, P. L. Burn, R. H. Friend, and A. B. Holmes, *J. Phys.: Condens. Matter* 5, 7155 (1993).
84. K. Pakbaz, C. H. Lee, A. J. Heeger, T. W. Hagler, and D. McBranch, *Synth. Met.* 64, 295 (1994).
85. W.-P. Chang, W.-T. Whang, and P.-W. Lin, *Polymer* 9, 1513 (1996).
86. H. Eckhardt, L. W. Shacklette, K. Y. Jen, and R. L. Elsenbaumer, *J. Chem. Phys.* 91, 1303 (1989).
87. J. L. Brédas and A. J. Heeger, *Chem. Phys. Lett.* 217, 507 (1994).
88. J. Cornil, D. A. Dos Santos, D. Beljonne, and J. L. Brédas, *J. Phys. Chem.* 99, 5604 (1995).
89. J. L. Brédas, *Adv. Mater.* 7, 263 (1995).
90. Z. Yang, I. Sokolik, and F. E. Karasz, *Macromolecules* 26, 1188, (1993).
91. Z. Yang, B. Hu, and F. Karasz, *Macromolecules* 18, 6151 (1995).
92. R. M. Gurge, M. Hickl, G. Krause, P. M. Lathi, B. Hu, Z. Yang, and F. E. Karasz, *Polym. Adv. Technol.* 9, 504 (1998).
93. B. Hu, F. E. Karasz, D. C. Morton, I. Sokolik, and Z. Yang, *J. Lumin.* 60–61, 919 (1994).
94. W.-P. Chang and W.-T. Whang, *Polymer* 37, 3493 (1996).
95. H. Ndayikengurukiye, S. Jacobs, W. Tachelet, J. V. D. Looy, A. Polaris, H. J. Geise, M. Claeys, J. M. Kauffmann, and S. Janietz, *Tetrahedron* 53, 13811 (1997).
96. J. H. Simpson, N. Egger, M. A. Masse, D. M. Rice, and F. E. Karasz, *J. Polym. Sci., Part B: Polym. Phys.* 28, 1859 (1990).
97. J. Nouwen, D. Vanderzande, H. Martens, J. Gelan, Z. Yang, and H. Geise, *Synth. Met.* 46, 23 (1992).
98. M. Herold, J. Gmeiner, and M. Schwoerer, *Acta Polym.* 45, 392 (1994).
99. J. R. Rasmusson, P. Bröms, J. Birgersson, R. Erlandsson, and W. R. Salaneck, *Synth. Met.* 79, 75 (1996).
100. T. Granier, E. L. Thomas, D. R. Gagnon, F. E. Karasz, and R. W. Lenz, *J. Polym. Sci., Part B: Polym. Phys.* 24, 2793 (1986).
101. T. Granier, E. L. Thomas, and F. E. Karasz, *J. Polym. Sci., Part B: Polym. Phys.* 27, 469 (1989).
102. M. A. Masse, D. C. Martin, E. L. Thomas, F. E. Karasz, and J. H. Petermann, *J. Mater. Sci.* 25, 311 (1990).
103. T. A. Ezquerra, E. Lopez-Cabarcos, F. J. Balt-Calleja, J. D. Stenger-Smith, and R. W. Lenz, *Polymer* 32, 781 (1991).
104. J. H. Simpson, W. Liang, D. M. Rice, and F. E. Karasz, *Macromolecules* 25, 3068 (1992).
105. I. Murase, T. Ohnishi, T. Noguchi, and M. Hirooka, *Polym. Commun.* 25, 327 (1984).
106. T. P. Nguyen, P. Le Rendu, V. H. Tran, and P. Molinié, *Polym. Adv. Technol.* 9, 101 (1998).
107. V. H. Tran, V. Massardier, T. P. Nguyen, and J. Davenas, *Polymer* 37, 2061 (1996).
108. B. H. Cumpston and K. F. Jensen, *Trends Polym. Sci.* 4, 151 (1996).
109. F. Papadimitrakopoulos, M. Yan, L. J. Rothberg, H. E. Katz, E. A. Chandross, and M. E. Galvin, *Mol. Cryst. Liq. Cryst.* 256, 663 (1994).
110. L. J. Rothberg, M. Yan, F. Papadimitrakopoulos, M. E. Galvin, E. W. Kwock, and T. M. Miller, *Synth. Met.* 80, 41 (1996).
111. K. Z. Xing, N. Johansson, G. Beanson, D. T. Clark, J. L. Brédas, and W. R. Salaneck, *Adv. Mater.* 9, 1027 (1997).
112. M. Herold, J. Gmeiner, C. Drummer, and M. Schwoerer, *J. Mater. Sci.* 32, 5709 (1997).
113. J. H. Burroughes, D. D. C. Bradley, A. R. Brown, Q. N. Marks, K. Mackay, R. H. Friend, P. L. Burns, and A. B. Holmes, *Nature* 347, 539 (1990).
114. R. Berton, Dissertation, Curitiba, Brazil, 1998.
115. M. S. Weaver and D. D. C. Bradley, *Synth. Met.* 83, 61 (1996).
116. S. Iwatsuki, M. Kubo, and T. Kumeuchi, *Chem. Lett.* 1071 (1991).
117. K. M. Vaeth and K. F. Jensen, *Adv. Mater.* 9, 490 (1997).
118. K. M. Vaeth and K. F. Jensen, *Appl. Phys. Lett.* 71, 2091 (1997).
119. E. G. J. Staring, D. Braun, G. L. J. A. Rikken, R. J. C. E. Demandt, Y. A. R. R. Kessener, M. Bouwmans, and D. Broer, *Synth. Met.* 67, 71 (1994).
120. A. Greiner, *Trends Polym. Sci.* 5, 12 (1997).
121. O. Schäfer, A. Greiner, J. Pommerehne, W. Guss, H. Vestweber, H. Y. Tak, H. Bässler, C. Schmidt, G. Lüssem, B. Shartel, V. Stümpfen, J. H. Wendorff, S. Spiegel, C. Möller, and H. W. Spiess, *Synth. Met.* 82, 1 (1996).
122. A. Wu, T. Fujiwara, M.-A. Kakimoto, Y. Imai, T. Kubota, and M. Iwamoto, *React. Funct. Polym.* 30, 361 (1996).
123. A. Wu, T. Fujiwara, M. Jikei, M.-A. Kakimoto, Y. Imai, T. Kubota, and M. Iwamoto, *Thin Solid Films* 284–285, 901 (1996).
124. Y. K. Kim, K. S. Kim, W. H. Kang, and S. S. Yang, *Thin Solid Films* 312, 291 (1998).
125. A. Rajagopal, M. Keil, H. Sotobayashi, A. M. Bradshaw, M.-A. Kakimoto, and Y. Imai, *Langmuir* 13, 5914 (1997).
126. M. Keil, A. Rajagopal, S. Yokoyama, H. Sotobayashi, A. M. Bradshaw, M.-A. Kakimoto, and Y. Imai, *Z. Phys. Chem.* 202, 87 (1997).
127. D. R. Gagnon, J. D. Capistran, F. E. Karasz, and R. W. Lenz, *Polym. Bull.* 12, 293 (1986).
128. P. F. van Hutten and G. Hadziioannou, in “Handbook of Organic Conductive Molecules and Polymers” (H. S. Nalwa, Ed.), Vol. 3. Wiley, New York, 1997.
129. D. Chen, M. J. Winokur, M. Masse, and F. E. Karasz, *Phys. Rev. B* 41, 6759 (1990).
130. D. Chen, M. J. Winokur, M. A. Masse, and F. E. Karasz, *Polymer* 33, 3116 (1992).
131. D. R. Gagnon, F. E. Karasz, E. L. Thomas, and R. W. Lenz, *Synth. Met.* 20, 85 (1987).
132. S. F. Bond, A. Howie, and R. H. Friend, *Surf. Sci.* 331, 196 (1995).
133. J. H. F. Martens, E. A. Marseglia, D. D. C. Bradley, R. H. Friend, P. L. Burn, and A. B. Holmes, *Synth. Met.* 55–57, 449 (1993).
134. S.-N. Chen and E.-C. Chang, *Macromolecules* 31, 4899 (1998).
135. R. S. Sethi and M. T. Goosey, in “Special Polymers for Electronics and Optoelectronics” (J. A. Chilton and M. T. Goosey, Eds.). Chapman & Hall, London/New York, 1995.
136. R. E. Peierls, “Quantum-Theory of Solids.” Clarendon, Oxford, 1955.
137. F. Gebhard, “The Mott Metal–Insulator Transition—Models and Methods.” Springer-Verlag, Berlin/New York, 1997.
138. S. M. Sze, “Physics of Semiconductor Devices.” Wiley, New York, 1981.
139. P. Blood and J. W. Orton, “The Electrical Characterization of Semiconductors: Majority Carriers and Electron States.” Academic Press, San Diego, 1992.
140. M. Koehler, J. R. de Lima, M. G. E. da Luz, and I. A. Hümmelgen, *Phys. Status Solidi A* 173, 29 (1999).
141. M. A. Abkowitz, H. Antoniadis, J. S. Facci, B. R. Hsieh, and M. Stolka, *Synth. Met.* 67, 187 (1994).
142. M. A. Lampert, *Phys. Rev.* 103, 1648 (1956).
143. D. Ma, I. A. Hümmelgen, B. Hu, and F. E. Karasz, *J. Appl. Phys.*, 86, 3181 (1999).
144. D. Ma, I. A. Hümmelgen, B. Hu, F. E. Karasz, X. Jing, L. Wang, and F. Wang, *Solid State Commun.* 112, 251 (1999).
145. P. Mark and W. Helfrich, *J. Appl. Phys.* 33, 205 (1962).
146. T. Takiguchi, D. H. Park, H. Ueno, and K. Yoshino, *Synth. Met.* 17, 657 (1987).
147. J. Obrzut, M. J. Obrzut, and F. E. Karasz, *Synth. Met.* 29, E103 (1989).
148. P. Strohiegel and D. Haarer, *Makromol. Chem., Macromol. Symp.* 44, 85 (1991).

149. B. R. Hsieh, H. Antoniadis, M. A. Abkowitz, and M. Stolka, *Polym. Prepr.* 33, 414 (1992).
150. S. Karg, V. Dyakonov, M. Meier, W. Riess, and G. Paasch, *Synth. Met.* 67, 165 (1994).
151. H. Antoniadis, B. R. Hsieh, M. A. Abkowitz, S. A. Jenecke, and M. Stolka, *Mol. Cryst. Liq. Cryst.* 256, 381 (1994).
152. E. M. Conwell, in "Handbook of Organic Conductive Molecules and Polymers" (H. S. Nalwa, Ed.), Vol. 4, Chap. 1. Wiley, New York, 1997.
153. P. W. M. Blom, M. J. de Jong, and J. J. M. Vlegaar, *Appl. Phys. Lett.* 68, 3308 (1996).
154. V. N. Savvate'ev, M. Tarabia, H. Chayet, E. Z. Farragi, G. B. Cohen, S. Kirstein, D. Davidov, Y. Avny, and R. Neumann, *Synth. Met.* 85, 1269 (1997).
155. P. W. M. Blom, M. J. de Jong, and M. G. van Munster, *Phys. Rev. B* 55, R656 (1997).
156. M. Gailberger and H. Bässler, *Phys. Rev. B* 44, 8643 (1991).
157. M. Redecker, D. D. C. Bradley, M. Inbasekaran, and E. P. Woo, *Appl. Phys. Lett.* 73, 1565 (1998).
158. H. Meyer, D. Haarer, H. Naarmann, and H.-H. Hörnhold, *Phys. Rev. B* 52, 2587 (1995).
159. A. J. Campbell, D. D. C. Bradley, and D. G. Lidzey, *J. Appl. Phys.* 82, 6326 (1997).
160. I. H. Campbell, D. L. Smith, C. J. Neef, and J. P. Ferraris, *Appl. Phys. Lett.* 74, 2809 (1999).
161. W. Brütting, E. Lebedev, S. Karg, T. Dittrich, V. Petrova-Koch, and M. Schwoerer, *Proc. SPIE* 3281, 257 (1998).
162. L. Bozano, S. A. Carter, J. C. Scott, G. G. Malliaras, and P. J. Brock, *Appl. Phys. Lett.* 74, 1132 (1999).
163. M. Abkowitz, H. Bässler, and M. Stolka, *Philos. Mag. B* 63, 210 (1991).
164. J. Grüner, M. Remmers, and D. Neher, *Adv. Mater.* 9, 964 (1997).
165. D. H. Dunlap, P. E. Parris, and V. E. Kenkre, *Phys. Ver. Lett.* 77, 542 (1996).
166. H. Bässler, *Phys. Status Solidi B* 175, 15 (1993).
167. L. B. Schein, A. Peled, and D. Glatz, *J. Appl. Phys.* 66, 686 (1996).
168. M. N. Bussac and L. Zuppiroli, *Phys. Rev. B* 55, 15587 (1997).
169. T. Holstein, *Ann. Phys. (N.Y.)* 8, 343 (1958).
170. I. D. Parker, *J. Appl. Phys.* 75, 1656 (1994).
171. I. A. Hümmelgen, L. S. Roman, F. C. Nart, L. O. Péres, and E. L. de Sá, *Appl. Phys. Lett.* 68, 3194 (1996).
172. L. S. Roman, I. A. Hümmelgen, F. C. Nart, L. O. Péres, and E. L. de Sá, *J. Chem. Phys.* 105, 10614 (1996).
173. F. C. Nart, L. O. Péres, E. L. de Sá, L. S. Roman, I. A. Hümmelgen, J. Gruber, and R. W. C. Li, *Synth. Met.* 90, 147 (1997).
174. X. Wei, M. Raikh, Z. V. Vardeny, Y. Yang, and D. Moses, *Phys. Rev. B* 49, 17480 (1994).
175. R. Berton, I. A. Hümmelgen, J. Gruber, R. W. C. Li, and L. O. Péres, *Adv. Mater. Opt. Electron.* 8, 181 (1998).
176. A. J. Campbell, D. D. C. Bradley, and D. G. Lidzey, *J. Appl. Phys.* 82, 6326 (1997).
177. P. W. M. Blom, M. J. M. de Jong, and C. T. H. F. Liedebaum, *Polym. Adv. Technol.* 9, 390 (1998).
178. J. Scherbel, P. H. Nguyen, G. Paasch, W. Brütting, and M. Schwoerer, *J. Appl. Phys.* 83, 5045 (1998).
179. H. L. Gomes, P. Stallinga, H. Rost, A. B. Holmes, M. G. Harrison, and R. H. Friend, *Appl. Phys. Lett.* 74, 1144 (1999).
180. S. Tokito, P. Smith, and A. J. Heeger, *Polymer* 32, 464 (1991).
181. Z. Yang and H. J. Geise, *Synth. Met.* 47, 95 (1992).
182. M. Lögdlund and J. L. Brédas, *J. Chem. Phys.* 101, 4357 (1994).
183. M. Lögdlund and J. L. Brédas, *Int. J. Quantum Chem., Quantum Chem. Symp.* 28, 481 (1994).
184. R. Lazzaroni, M. Lögdlund, A. Calderone, and J. L. Brédas, *Synth. Met.* 71, 2159 (1995).
185. K. Konstadinidis, F. Papadimitrakopoulos, M. Galvin, and R. L. Opila, *J. Appl. Phys.* 77, 5642 (1995).
186. T. P. Nguyen and J. L. Mansot, *Thin Solid Films* 283, 135 (1996).
187. T. P. Nguyen, V. Massardier, V. H. Tran, and A. Guyot, *Synth. Met.* 55-57, 235 (1993).
188. E. Ettetdgui, H. Razafitrimo, Y. Gao, B. R. Hsieh, W. A. Feld, and M. W. Ruckmean, *Phys. Rev. Lett.* 76, 299 (1996).
189. W. Salaneck and J. L. Brédas, *Adv. Mater.* 8, 48 (1996).
190. T. P. Nguyen, S. de Vos, and V. H. Tran, *J. Appl. Phys.* 81, 6815 (1997).
191. T. P. Nguyen and S. de Vos, *Vacuum* 47, 1153 (1996).
192. V.-E. Choong, Y. Park, B. R. Hsieh, and Y. Gao, *J. Phys. D: Appl. Phys.* 30, 1421 (1997).
193. L. S. Roman, I. Denicoló, F. C. Nart, and I. A. Hümmelgen, *J. Mater. Sci. Lett.* 15, 1307 (1996).
194. Th. Kugler, Å. Johansson, I. Dalsegg, U. Gelius, and W. R. Salaneck, *Synth. Met.* 91, 143 (1997).
195. J. S. Kim, M. Granström, R. H. Friend, N. Johansson, W. R. Salaneck, R. Daik, W. J. Feast, and F. Cacialli, *J. Appl. Phys.* 84, 6859 (1998).
196. H. Kim, A. Piqué, J. S. Horowitz, H. Mattoussi, H. Murata, Z. Kadafi, and D. B. Chrisey, *Appl. Phys. Lett.* 74, 3444 (1999).
197. J. S. Kim, F. Cacialli, A. Cola, G. Gigli, and R. Cingolani, *Appl. Phys. Lett.* 75, 19 (1999).
198. A. R. Schlatmann, D. W. Floet, A. Hilberer, F. Garten, P. J. M. Smulders, T. M. Klapwijk, and G. Hadziioannou, *Appl. Phys. Lett.* 69, 1764 (1996).
199. W. Brütting, M. Meier, M. Herold, S. Karg, and M. Schwoerer, *Synth. Met.* 91, 163 (1997).
200. N. Johansson, F. Cacialli, K. Z. Xing, G. Beamson, D. T. Clark, R. H. Friend, and W. R. Salaneck, *Synth. Met.* 92, 207 (1998).
201. I. A. Hümmelgen, Y. P. Yadava, L. S. Roman, A. C. Arias, M. R. Fernandes, and F. C. Nart, *Bull. Mater. Sci.* 19, 423 (1996).
202. A. C. Arias, J. R. de Lima, and I. A. Hümmelgen, *Adv. Mater.* 10, 392 (1998).
203. Y. P. Yadava, G. Denicoló, A. C. Arias, L. S. Roman, and I. A. Hümmelgen, *Mater. Chem. Phys.* 48, 263 (1997).
204. A. C. Arias, L. S. Roman, Th. Kugler, R. Toniolo, M. S. Merúvia, and I. A. Hümmelgen, *Thin Solid Films* 371, 201 (2000).
205. A. Andersson, N. Johansson, P. Bröms, N. Yu, D. Lupo, and W. R. Salaneck, *Adv. Mater.* 10, 859 (1998).
206. Y. Yang and A. J. Heeger, *Appl. Phys. Lett.* 64, 1245 (1994).
207. S. Karg, J. C. Scott, J. R. Salem, and M. Angelopoulos, *Synth. Met.* 80, 111 (1996).
208. H. L. Wang, A. G. McDiarmid, Y. Z. Wang, D. D. Gebler, and A. J. Epstein, *Synth. Met.* 78, 33 (1996).
209. Y. Yang, E. Westerweele, C. Zhang, P. Smith, and A. J. Heeger, *J. Appl. Phys.* 77, 694 (1995).
210. J. R. de Lima, C. Schreiner, I. A. Hümmelgen, C. C. M. Fornari, Jr., C. A. Ferreira, and F. C. Nart, *J. Appl. Phys.* 84, 1445 (1998).
211. Y. Cao, N. Colaneri, A. J. Heeger, and P. Smith, *Appl. Phys. Lett.* 65, 2001 (1994).
212. A. R. Brown, D. D. C. Bradley, J. H. Burroughes, R. H. Friend, N. C. Greenham, P. L. Burn, A. B. Holmes, and A. Kraft, *Appl. Phys. Lett.* 61, 2793 (1992).
213. (a) W. Riess, *Polym. Adv. Technol.* 8, 381 (1997); (b) W. Riess, "Organic Electroluminescent Materials and Devices" (S. Miyata and H. S. Nalwa, Eds.), Chap. 2, p. 73. Gordon & Breach, Amsterdam, 1996.
214. A. C. Fou, O. Onitsuka, M. Ferreira, M. Rubner, and B. R. Hsieh, *J. Appl. Phys.* 79, 7501 (1996).
215. O. Onitsuka, A. C. Fou, M. Ferreira, B. R. Hsieh, and M. F. Rubner, *J. Appl. Phys.* 80, 4067 (1996).
216. U. Lemmer, D. Vacar, D. Moses, A. J. Heeger, T. Onishi, and T. Noguchi, *Appl. Phys. Lett.* 68, 3007 (1996).
217. S. Berleb, W. Brütting, M. Schwoerer, R. Wehrmann, and A. Eischner, *J. Appl. Phys.* 83, 4403 (1998).
218. D. R. Baigent, N. C. Grenham, J. Grüner, R. N. Marks, R. H. Friend, S. C. Moratti, and A. B. Holmes, *Synth. Met.* 67, 3 (1994).
219. D. V. Khramtchenkov, H. Bässler, and V. I. Arkhipov, *J. Appl. Phys.* 79, 9283 (1996).
220. D. V. Khramtchenkov, V. I. Arkhipov, and H. Bässler, *J. Appl. Phys.* 81, 6954 (1997).

221. S. Karg, W. Riess, W. Dyakonov, and M. Schwoerer, *Synth. Met.* 54, 427 (1993).
222. H. Antoniadis, B. R. Hsieh, M. A. Abkowitz, and M. Stolka, *Appl. Phys. Lett.* 62, 3167 (1993).
223. J. J. Halls, K. Pichler, R. H. Friend, S. C. Moratti, and A. B. Holmes, *Appl. Phys. Lett.* 68, 3120 (1996).
224. G. Yu, K. Pakbaz, and A. J. Heeger, *Appl. Phys. Lett.* 64, 3422 (1994).
225. J. J. M. Halls, C. A. Walsh, N. C. Greenham, E. A. Marseglia, R. H. Friend, S. C. Moratti, and A. B. Holmes, *Nature* 376, 498 (1995).
226. G. Yu and A. J. Heeger, *J. Appl. Phys.* 78, 4510 (1995).
227. M. Granström, K. Petrisch, A. C. Arias, A. Lux, M. R. Andersson, and R. H. Friend, *Nature* 395, 257 (1998).
228. F. Hide, B. J. Schwartz, M. A. Diaz-Gracia, and A. J. Heeger, *Chem. Phys. Lett.* 256, 424 (1996).
229. U. Lemmer, *Polym. Adv. Technol.* 9, 476 (1998).
230. F. Hide, M. A. Diaz-Gracia, B. J. Schwartz, M. R. Andersson, P. Qibing, and A. J. Heeger, *Science* 273, 1833 (1996).
231. S. V. Frolov, M. Ozaki, W. Gellermann, Z. V. Vardeny, and K. Yoshino, *Jpn. J. Appl. Phys.* 35, L1371 (1996).
232. S. V. Frolov, W. Gellermann, M. Ozaki, K. Yoshino, and Z. V. Vardeny, *Phys. Ver. Lett.* 78, 729 (1997).
233. N. Tessler, G. J. Denton, and R. H. Friend, *Nature* 382, 695 (1996).
234. G. J. Denton, N. Tessler, M. A. Stevens, and R. H. Friend, *Adv. Mater.* 9, 547 (1997).
235. G. H. Gelinck, J. M. Warman, M. Remmers, and D. Neher, *Chem. Phys. Lett.* 265, 320 (1997).
236. H. J. Brouwer, V. V. Krasnikov, A. Hilberer, and G. Hadziioannou, *Adv. Mater.* 8, 935 (1996).
237. Y. Yang and A. J. Heeger, *Nature* 372, 344 (1994).
238. M. Reghu, C. O. Yoon, C. Y. Yang, D. Moses, and A. J. Heeger, *Macromolecules* 26, 7245 (1993).
239. C. Y. Yang, Y. Cao, P. Smith, and A. J. Heeger, *Synth. Met.* 53, 293 (1993).
240. C. Y. Yang, M. Reghu, A. J. Heeger, and Y. Cao, *Synth. Met.* 79, 27 (1996).
241. C. D. G. Minto and A. S. Vaughan, *Synth. Met.* 81, 81 (1996).
242. J. McElvain and A. J. Heeger, *J. Appl. Phys.* 80, 4755 (1996).
243. Q. Pei, G. Yu, C. Zhang, and A. J. Heeger, *Science* 269, 1086 (1995).
244. Q. Pei, Y. Yang, G. Yu, C. Zhang, and A. J. Heeger, *J. Am. Chem. Soc.* 118, 3922 (1996).
245. D. Neher, J. Grüner, V. Cimrová, W. Schmidt, R. Rulkens, and U. Lauter, *Polym. Adv. Technol.* 9, 461 (1998).
246. Y. Yang and Q. Pei, *Appl. Phys. Lett.* 68, 2708 (1996).
247. G. Yu, K. Pakbaz, and A. J. Heeger, *J. Electron. Mater.* 23, 925 (1994).
248. G. Yu, *Synth. Met.* 80, 143 (1996).

SELF-ORGANIZED SUPRAMOLECULAR POLYMER STRUCTURES TO CONTROL ELECTRICAL CONDUCTIVITY

Olli Ikkala

Department of Engineering Physics and Mathematics, Helsinki University of Technology, Espoo, Finland

Gerrit ten Brinke

Laboratory of Polymer Chemistry and Materials Science Center, University of Groningen, Groningen, The Netherlands; Helsinki University of Technology, Espoo, Finland

Contents

1. Introduction	185
2. Background on Self-Organization and Supramolecular Concepts	186
2.1. Self-Organization	186
2.2. Supramolecular Assembly	188
2.3. Self-Organized Supramolecular Structures	189
3. Conducting and Semiconducting Polymer Systems Containing Self-Organized Supramolecular Polymers	194
3.1. Ionically Conducting Self-Organized Supramolecular Structures of Polymers Hydrogen-Bonded to Amphiphiles	194
3.2. Self-Organization and Stacking of Dislike Organic Molecules	195
3.3. Self-Organization of Hairy Rods	197
3.4. Self-Organization of Supramolecular Hairy Rods	200
3.5. Externally Controllable Self-Organized Supramolecular Polymer Systems Allowing Electrical Switching	204
4. Concluding Remarks	205
Acknowledgments	205
References	206

1. INTRODUCTION

In micro- and nanotechnology, pattern formation is typically achieved using lithography, stamping, or related techniques. There is a constant push to smaller patterns, such as preparation of single-electron transistors, ultrasmall tunnel junctions, and optics components like nanoscale gratings. However, there is an increasing technological demand for preparation of even smaller structures than allowed by the wavelength of the radiation used in today's optical lithography and etching techniques. So far, in nanotechnology mostly metals and inorganic semiconductors are used due to their stability and suitability for processing. However, organic compounds and polymers could offer new options for eco-

nommic processing, for smaller structures, or even for flexible circuit boards [1, 2].

In organic materials, self-organization [3] allows materials manipulation down to smaller structures, generally down to a molecular level. Self-organization is a concept whereby competing attractive and repulsive interactions [4] within a molecule yield nanoscale structures with highly nontrivial phase behavior. In the case of oligomers, surfactants in aqueous solution self-organize to form liquid-crystalline micellar, cylindrical, lamellar, or more complicated phases due to the hydrophilic and hydrophobic moieties [5]. Block copolymers [6] can be regarded as polymeric surfactants, also containing mutually repulsive blocks, leading to analogous structures in organic solvents, in aqueous solvents, and, most important, in the bulk. The use of these techniques in applications of

nanotechnology has not been widespread. Such concepts imitate structure formation in biological materials [7], albeit at a considerably simpler level. The structures are relatively easy to construct and provide an option to construct simple nanostructures in bulk [8] and in films [6, 9]. Therefore, self-organized organic materials consisting of conducting organic components could be interesting materials as such. Metal-organic self-organized nanostructures working as a Coulomb blockade system at room temperature have been demonstrated [10, 11]. There is also another option to use the self-organized organic materials as spontaneously ordered resists in lithography, instead of the conventionally used disordered ones such as poly(methyl methacrylate). Block copolymers have been used as lithographic templates to transfer patterns to inorganic semiconductor substrates [9]. Langmuir–Blodgett techniques have also been used to achieve ordered layers of resists [12].

Self-organization is an example of how nanoscale structures can be formed if different repulsive chemical groups are chemically connected to the same molecules. By contrast, in supramolecular chemistry the functional groups are mutually connected using molecularly matching physical interactions, such as hydrogen bonding, π -stacking, charge transfer, steric match, and interpenetrating ringlike structures [13, 14]. Molecular recognition allows one to build highly specific complexes called supermolecules, which, in turn, are able to form a hierarchy of structures. One of the hallmarks that separates supramolecular chemistry from just any complex formation is the fact that structure formation is accompanied by “functionality” [13]. Self-organization and supramolecular concepts can naturally be combined to allow structuring [15–18]. This review deals with structure formation due to self-organization of supermolecules in electroactive polymers, i.e., conjugated electronically conducting polymers [19] or ionically conducting polymers [20]. Externally controllable conductivity can thus be obtained, allowing “functional” electroactive materials [18].

A variety of other options for achieving functional material on the basis of electroactive polymers have been reported. For instance, self-assembled microactuators, “micromachines” [21], multilayers by consecutive adsorption of conducting polymers yielding surface assemblies [22, 23], and sensors are created by the molecular recognition properties of electroactive polymers [24, 25].

This review limits its scope to the mechanisms of structure formation of self-organizing polymers, general supramolecular concepts, their possibilities and limitations for achieving self-organization of electroactive polymers, and what has so far been achieved concerning functional materials with externally controllable conductivity using such concepts. We do not review optical properties and mention only briefly selected trends if they are particularly closely related to supermolecule formation and self-organization. We also point out that there is a quickly developing field on supramolecular structures based on ringlike oligomers, such as rotaxanes, for achieving functional materials, such as switching electroactive materials [26–28]. Such structures will not be discussed within this review.

2. BACKGROUND ON SELF-ORGANIZATION AND SUPRAMOLECULAR CONCEPTS

2.1. Self-Organization

Molecules of regular shape may crystallize to form three-dimensionally ordered structures at sufficiently low temperatures. If disorder is added, for example, due to less regular molecular structure or due to additional solvent, the crystallization may be inhibited but the material can still undergo spontaneous aggregation, in this case to less ordered nanoscale domains, however. The first example is given by surfactants [3, 5, 29–32], such as dodecyl sulfonic acid [33], which can be crystalline in bulk but which in aqueous solutions form lamellar, cylindrical, or spherical micellar phases (for a typical phase behavior scheme, see Fig. 1). These are examples of self-organized phases of surfactants in solution and emerge due to the competition between the hydrophobic and the hydrophilic interactions of the amphiphilic molecules [3]. The typical length scale of such domains is 20–40 Å, as manifested in small-angle X-ray scattering (SAXS) patterns. A simple criterion has been presented to understand the geometry of the domains, based on a surfactant packing parameter involving the relative volumes of the polar head and nonpolar tail groups, which cause different interface curvatures of the ordered domains [3]. This allows one to systematically control the phases and phase behavior by tailoring the architecture of the alkyl tails, i.e., the length and the number of chains, as well as by selecting small or bulky organic or polar head groups or even combining two or more head groups within the same molecules [34]. Note that the self-organization of surfactants has also been called surfactant self-assembly, lyotropic liquid crystallinity (which in a strict sense might be misleading because there are generally no rigid rodlike mesogenic groups included in the surfactants), or mesomorphism.

Other typical forms of self-organization are self-assembled monolayers (SAMs) or Langmuir–Blodgett films formed on sur-

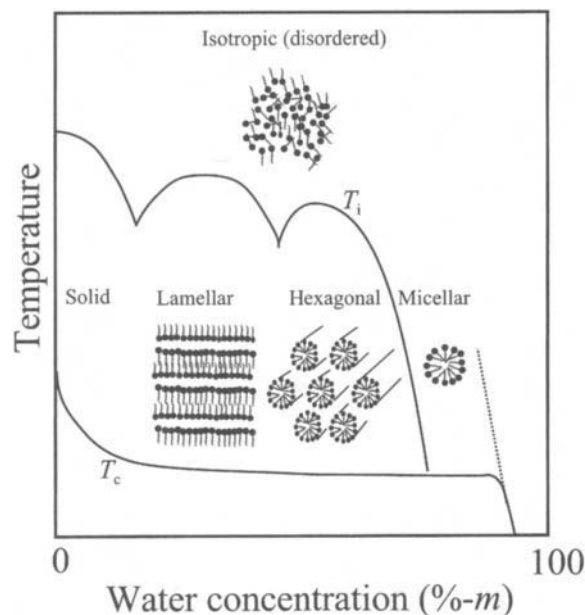


Fig. 1. Schematics for a typical phase diagram of aqueous surfactant solutions, showing the characteristic self-organized structures. Adapted from M. Daoud and C. E. Williams, “Soft Matter Physics.” Berlin, 1999.

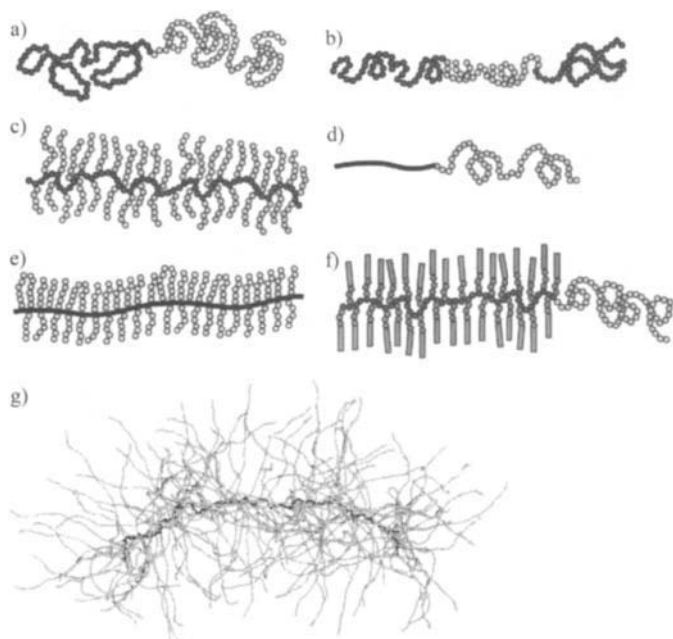


Fig. 2. Selected architectures of block copolymers: (a) diblock; (b) triblock; (c) comb copolymer consisting of flexible chains; (d) rod-coil diblock copolymer consisting of a rodlike block and a coil-like block; (e) hairy rods, i.e., comb-block copolymers consisting of rodlike backbone and coil-like side chains; and (f) LC coil with a side-chain liquid crystalline (LC) block and a flexible block. Many other variations have been introduced, such as multiblock copolymers, block copolymers consisting of several rodlike blocks, or star-shaped block copolymers. Comb-coil block copolymers with dense packing of side chains are also denoted as molecular bottle brushes, as is illustrated in (g) by a simulated structure of an isolated molecule dissolved in a solvent. (Courtesy of Mika Saario.)

faces based on amphiphilic molecules [35, 36] and, of course, the ordered structures formed by block copolymers [6, 8, 37]. The latter materials are important within the context of this review. They are polymeric counterparts of oligomeric surfactants and contain long blocks of mutually repulsive polymer chains, which are covalently connected. Several types of architectures are available, as illustrated in Figure 2 [38]. They form self-organized structures (or microphase separated structures, as they are most often denoted in the block copolymer literature) in bulk as well as in many solutions due to a competition between attraction and repulsion. The repulsion between chemically different molecules is a characteristic property of the most common interactions and, combined with the small entropy of mixing, is the reason that most polymer mixtures tend to phase-separate [39, 40]. This tendency is also present between the polymeric blocks of block copolymers. However, macroscopic phase separation is prohibited by the covalent bond between the blocks, and phase separation, called microphase separation, occurs at a local scale. Since the covalent bond(s) between the blocks acts as an attraction, a somewhat stronger repulsion between the blocks is actually required to induce phase separation [41].

The self-organization of block copolymers gives rise to a characteristic series of structures, which can best be illustrated by taking the most simple example of a melt, i.e., without an added solvent, of diblock copolymers *A*-block-*B* (Fig. 2a). Denote by N the overall degree of polymerization, by f_A the volume fraction of

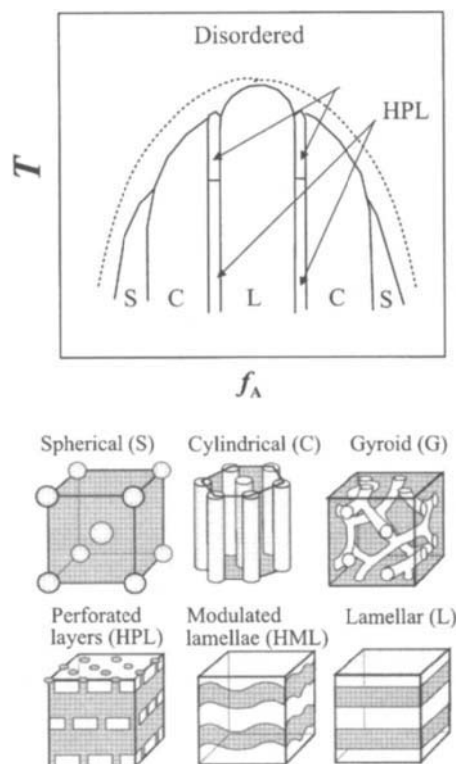


Fig. 3. Schematic phase diagram and characteristic self-organized morphologies of diblock copolymers. Adapted from G. H. Fredrickson and F. S. Bates, *Annu. Rev. Mater. Sci.* 26, 501 (1996).

block A, and by $\chi \propto 1/T$ the interaction parameter between A and B describing the strength of the enthalpic interaction [39]. Figure 3 presents typical examples of the self-organized phases of a diblock copolymer, such as polystyrene-*block*-polyisoprene, and the schematic phase diagram. If f_A is small, a disordered morphology is obtained where the minority block A dissolves in the majority block B. A spherical morphology is obtained upon increasing f_A past a characteristic value, in analogy to the critical micelle concentration (CMC) in the case of oligomeric surfactants. Further increase of f_A yields a cylindrical phase and finally a lamellar phase near $f_A = 0.5$. In a narrow composition window between the cylindrical and lamellar phases, additional phases can be observed for selected materials if the chemical nature of the blocks is sufficiently similar, i.e., have sufficiently small χ ; see Figure 3. Such additional phases consist of the bicontinuous gyroid phase (1a3d), as well as perforated layers (HPLs) and modulated lamellae (HMLs), where the latter are considered to be metastable [42, 43]. Important within the present review is that between the ordered phases there are order-order transitions (OOT) and that upon heating, i.e., for small χ , the system eventually becomes disordered, as illustrated in Figure 3. The latter transition is denoted as an order-disorder transition (ODT). However, ODT transition temperatures in diblock copolymers are in most cases very high, unless the repulsive energy between the blocks is carefully matched, as in poly(ethylene ethylene)-*block*-poly(ethylene propylene) [44], or the molecular weights of the blocks are sufficiently small [45].

As in oligomeric surfactants, the phase behavior of block copolymers can be modified by tailoring the architecture where the polymeric nature obviously allows more possibilities. Examples

include triblock, multiblock, miktoarm (star-shaped with different arms) [46], comb-shaped, molecular bottlebrushes (or cylindrical comb copolymer brushes, i.e., a special case of comb-shaped block copolymers with a dense array of relatively long side chains; see Fig. 2g) [47, 48], and chains with dendritic side chains [49, 50].

The phase behavior can additionally be manipulated by adding block-selective solvents (low-molecular-weight solvents or polymers) [51]. A particularly important example is poly(ethylene oxide)-*block*-poly(propylene oxide)-*block*-poly(ethylene oxide) triblock copolymers in aqueous solvents (selective with respect to polyethylene oxide) [52]. Along a similar line, bicontinuous microemulsions can be achieved in symmetric ternary blends consisting of diblock copolymers mixed with the two corresponding homopolymers [53].

The possibilities are not restricted to flexible polymers. One of the blocks can be rigid rodlike, in which case a “rod-coil” block copolymer [54–57] is formed if the architecture is of the diblock type (see Section 2.3.1 for another example [15]). Other interesting cases comprise diblock copolymers where one of the blocks is a side-chain liquid-crystalline polymer [4, 58–62]. Finally, we mention the important class of “hairy rods” obtained for a comb copolymer architecture consisting of a rigid backbone and flexible side chains [4, 58–61, 63–66], to be discussed in more depth later in this review.

For architectures consisting of more than two flexible blocks, but still involving only two kinds of chemically different blocks (e.g., selected comb copolymers, multiblock copolymers, star copolymers, etc.), the phase behavior will be similar, albeit different in detail. For the more complex architectures involving either rigid blocks (hairy rods, rod-coils [54]) or more than two chemically different blocks (triblock copolymers [67–69]), the situation becomes much more complex.

The characteristic length scale of the self-organized nanostructures in block copolymers is typically 200–1000 Å due to the length of the polymeric blocks, reaching down to 20–50 Å for the comb copolymer architectures.

A final comment on the nomenclature selected for this work is in order. Within the denotation of this review, block copolymers and surfactants are in the general case self-organized systems without supramolecular construction because the organizing structural elements are due to chemical bonds.

2.2. Supramolecular Assembly

In “classical” chemistry, the molecular building blocks are held together by permanent (chemical) bonds and they form, in turn, different structures, such as crystals, amorphous materials, liquid crystals, or self-organized nanostructures. By contrast, in supramolecular chemistry [13, 14, 70, 71], the structural units are supermolecules, which can be considered as molecular complexes held together by molecularly matching physical interactions between their subunits.

Three examples of supermolecules are shown. Figure 4a shows how an individual ringlike crown ether molecule consisting of (–CH₂–CH₂–O–)-groups, so-called [18]-Crown-6, can bind a metal cation K⁺ in aqueous solution [14]. This crown ether binds substantially less other cations, such as Na⁺, and therefore the bonding is selective. On the other hand, Na⁺ can be bonded if the size of the crown ether is reduced to consist of 5 ethylene oxide moieties, [15]-Crown-5. The interaction in crown ether/metal cation complexes is based on steric and charge match. Crown

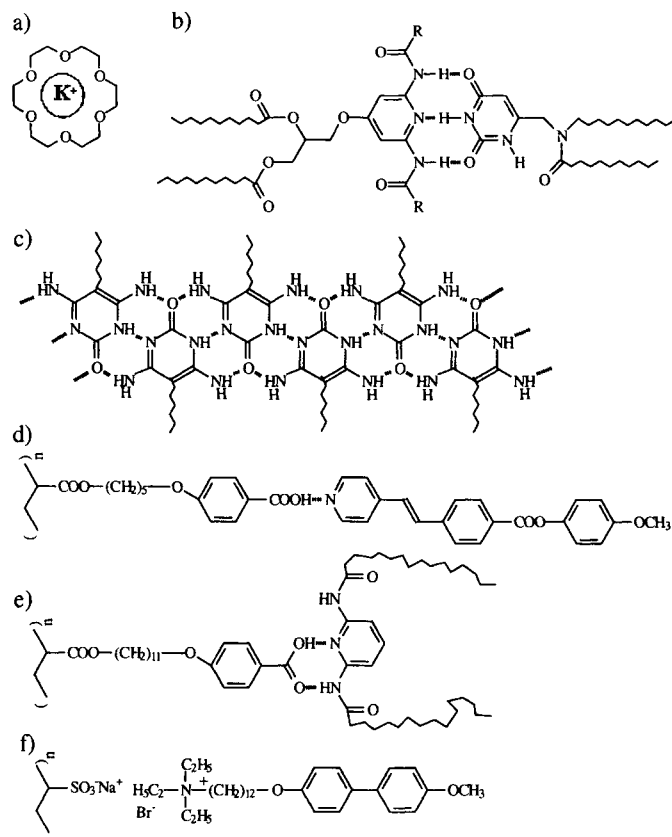


Fig. 4. Examples of organic molecules that are able to “recognize” each other to form supermolecules: (a) individual crown ether molecules coordinated with selected metal cations [14]; (b) supramolecular assembly to form oligomeric liquid crystals based on three hydrogen bonds [74]; (c) supramolecular assembly to form a polymer-like chain (according to Lehn et al. [80]); supramolecular assembly to form side-chain liquid-crystalline polymers using (d) one hydrogen bond (according to Kato and Fréchet [76]); (e) two hydrogen bonds (according to Kato et al. [77]); and (f) ionic complexation (according to Bazuin and Tork [78]).

ethers are examples of ringlike molecules and a wide variety of ringlike molecules, such as rotaxanes, catenanes, and cryptands, play a central role in supramolecular chemistry [13, 14, 72] because they can selectively form complexes with other molecules and can be used to prepare functional molecules, such as molecular shuttles, as elaborated by Stoddart and co-workers [27, 28, 70, 73].

Figure 4b shows another archetype of matching bondings, this time to construct an oligomeric supramolecular liquid crystal [74]. The matching set of three hydrogen bonds facilitates formation of a sufficiently strong bond to form a shape-persistent mesogenic moiety. The concept can be elaborated further to construct supramolecular “polymers” or “ribbons” where the “repeat units” are bonded using a matching set of three hydrogen bonds [13] (see Fig. 4c) or even four hydrogen bonds [75]. The hydrogen bonds thus suffice for individual molecules to assemble in polymer-like chains but now due to hydrogen bonds instead of chemical bonds. The ribbons are often formed in the solid state. However, that hydrogen bonded chains can really behave as polymers, having polymer-like viscoelastic properties, has been explicitly shown by Sijbesma et al. [75]. Further examples of hydrogen bonds used to construct polymeric supermolecules can be given from the field of side-chain liquid-crystalline polymers. Figure 4d shows how even

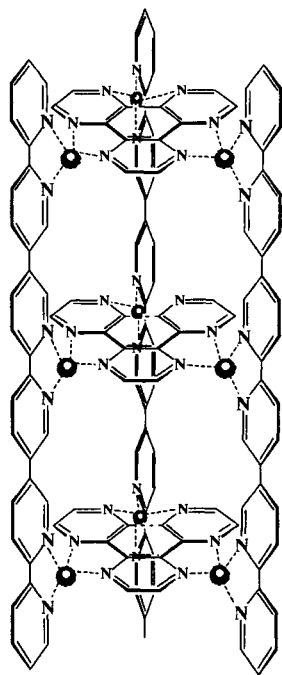


Fig. 5. Supramolecular assembly to form ordered structures due to coordination between pyridine-containing chains and silver cations. Adapted from J.-M. Lehn, "Supramolecular Chemistry." VCH, Weinheim, 1995.

one properly selected hydrogen bond can be strong enough to allow stable complexation of a mesogenic side group to a polymer backbone [76]. In this case, the supermolecules form smectic liquid-crystalline structures. Naturally, the use of several simultaneous hydrogen bonds can make the bond even stronger; see Figure 4e [77]. These examples suffice to show that properly selected hydrogen bonds are very versatile for constructing complicated supramolecular assemblies. Figure 4f shows a related supermolecule in which the side-chain mesogens are complexed to the polymer backbone using ionic interactions [78, 79].

The specific physical interactions required to build the supermolecules illustrated in Figure 4 are simple examples of molecular recognition. In some cases, a single properly selected hydrogen bond suffices for the assembly but frequently more complicated combinations are required. Molecular recognition plays a particularly important role in biological systems where specific binding and selectivity are required, for example, in the formation of the double-stranded structure of DNA [7] and for the binding of enzymes [81]. Molecular recognition is characterized by the simultaneous stability of the supermolecule and the selectivity in its formation. The supermolecules thus formed are interesting either as individual entities, such as the crown ether/metal cations in solutions (Fig 4a), which can form disordered overall structures such as hydrogen-bonded chains, or as complex ordered structures. The latter property will be illustrated using still another specific interaction, which is central in supramolecular science, i.e., coordination based on metal cations and typically nitrogen-containing organic moieties. Figure 5 shows how tetravalent silver cations cause formation of gridlike structures of pyridine-containing chains [13].

The existing biological supramolecular assemblies inspire to build hierarchical supramolecular assemblies based on synthetic materials; see Figure 6 [70]. In this example, the elementary building blocks are rings consisting of two viologens (a) and aromatic

molecules (b), which allow layered structures (c) due to π - π stackings. Such supramolecular dimers (c), in turn, form arrays (d) due to cyclic hydrogen bonding between the two terminal carboxylic acids of molecule (a). These arrays, in turn, form ordered structures (e) due to π - π stackings. In conceptual analogy with proteins, there is a hierarchy of structures [70].

The latter example leads us to still another characteristic feature of supramolecular concepts; i.e., their hierarchical assemblies allow "functional" materials. "Functionality" is regarded as one of the hallmarks of supramolecular science [13] as even in "classical" chemistry and self-organization, complexes, salts, etc. are formed due to chemical "matching." One can point out that the borderline between "classical" chemistry and supramolecular chemistry is not strict. For example, in general block copolymers dissolved in block-selective solvents might not be regarded as supramolecular chemistry, whereas some of the more specific further developments [18, 82] clearly allow supramolecular functional materials, as will be shown in Section 3.

2.3. Self-Organized Supramolecular Structures

In this section representative examples are introduced, which combine self-organization (as defined in Section 1) and supramolecular structure formation. The specific features in designing electrical properties will be discussed in the next section.

2.3.1. Low-Molecular-Weight Rod-Coil Block Copolymers

Stupp et al. have studied extensively low-molecular-weight rod-coil block copolymers [15, 83-85]. Typically, one block contains an aromatic rigid-rod block having an extended conformation, such as aromatic polyester or conjugated phenylene vinylene; see Figure 2d. The other end consists of a coil-like chain, typically polystyrene (PS), which is nonpolar. In between such blocks, there may be an additional flexible spacer, such as oligomeric polybutadiene. Rigid high-molecular-weight polymers do not generally melt and dissolve poorly in common solvents [86]. Also, in the present case, the rigid chains, even though they are short, tend to aggregate to form tight packing. However, the coil-like polystyrene blocks consume substantially more lateral space, which leads to frustration in packing. This limits the number of aggregated molecules (typically 100) and a mushroom-like aggregate is formed; see Figure 7. Such aggregates resemble diphilic surfactant molecules having at one end the collection of the polystyrene coils of all aggregated chains and at the other end all the rigid, possibly polar, chains. Therefore, it can be regarded as a "supramolecular surfactant." Such supramolecular building blocks, in turn, self-organize to form three-dimensional ordered structures [15]. Note also that the rigid-rod block can be conjugated, which offers feasible electrooptical and other properties.

2.3.2. Self-Organized Supramolecular Structures of Polymer-Amphiphile Complexes

In the following sections, we will review the various different ways in which comb copolymer-like architectures (supramolecular comb copolymers) might be obtained using noncovalent physical interactions, e.g., ionic, coordination complexation, or hydrogen bonding; see Figure 8.

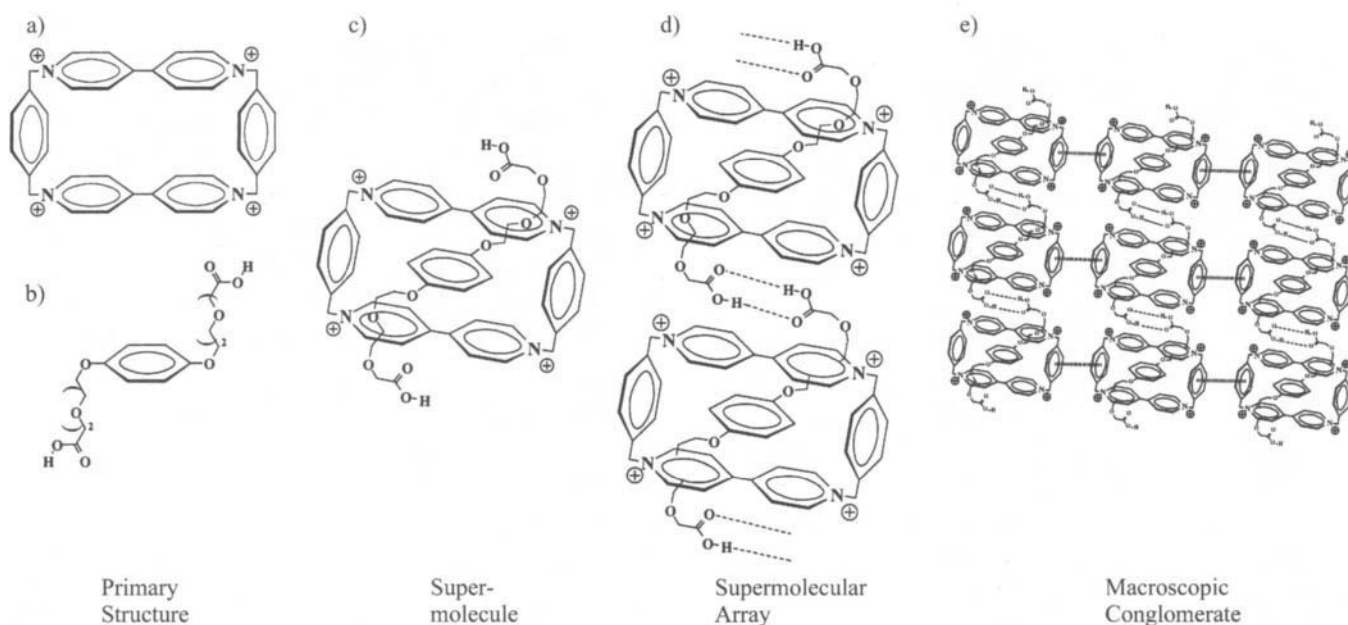


Fig. 6. Example of a complex supramolecular hierarchy. The primary structures (a) and (b) are formed due to covalent bonds. When the dicarboxylic acid threads through the macrocyclic cavity of π -deficient tetracationic cyclophane 2^{4+} , the second level, "supermolecule," is obtained (c). The next level, supramolecular array (d), is created as a result of noncovalent dimerization of the $[1 \cdot 2^{4+}]$ supermolecule's carboxyl groups. Then the highest level, macroscopic conglomerate (e), is formed due to π - π stacking. Adapted from M. C. T. Fyfe and J. F. Stoddart, *Acc. Chem. Res.* 30, 393 (1997).

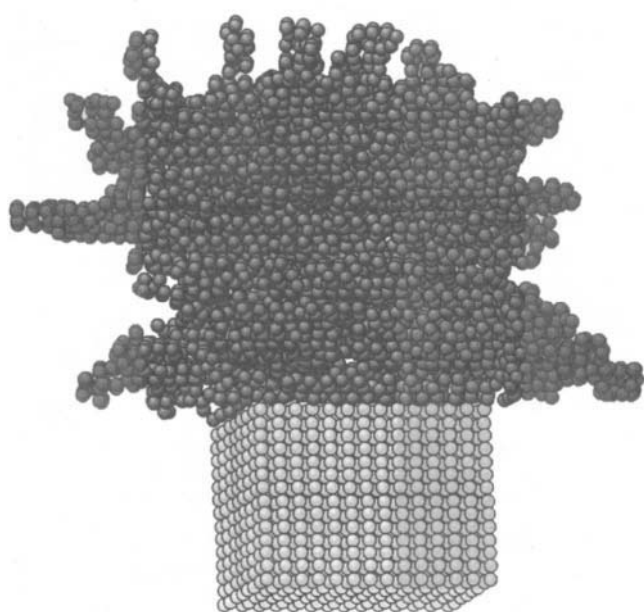
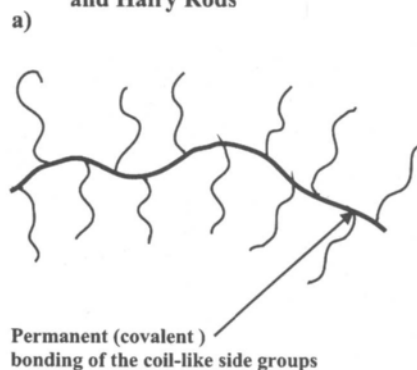


Fig. 7. Scheme of "mushroom-like" supermolecule formed by oligomeric rod-coil triblock copolymers. Adapted from S. I. Stupp, G. N. Tew, and C. M. Whitaker, in "Hyperstructured Molecules I: Chemistry, Physics and Applications" (H. Sasabe, Ed.). Gordon & Breach, Amsterdam, 1999.

Self-Organized Supramolecular Structures of Polyelectrolyte/Surfactant Complexes. Self-organized nanoscale ordered structures are obtained by complexing polyelectrolytes with oppositely charged surfactants, as first shown by Antonietti et al. and confirmed by others using many systems; see Figure 9 [16, 87–99]. For example, using a stoichiometric composition, i.e., 1 mol sodium polystyrene

Comb-block copolymers and Hairy Rods



Supramolecular comb-block copolymers and Hairy Rods

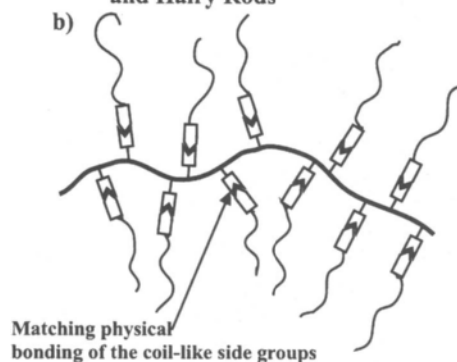


Fig. 8. (a) Scheme for comb copolymer and (b) supramolecular analogy for comb copolymer. The scheme also applies to corresponding hairy rods.

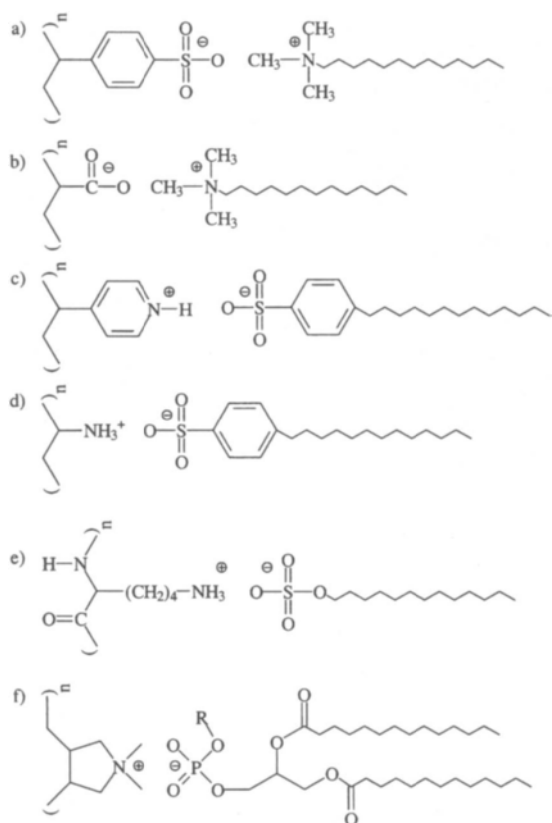


Fig. 9. Typical polyelectrolyte/surfactant pairs that yield self-organized nanostructures.

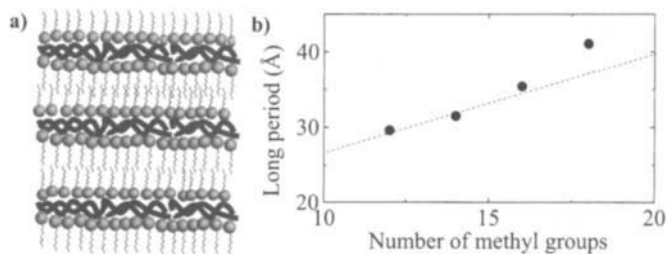


Fig. 10. (a) Scheme of lamellar self-organized phase typically achieved when a polyelectrolyte and an oppositely charged surfactant are complexed. (b) Long period as a function of alkyl chain length in the lamellar phase for sodium polystyrene sulfonate complexed with alkyltrimethylammonium bromide. Adapted from M. Antonietti, J. Conrad, and A. Thünnemann, *Macromolecules* 27, 6007 (1994).

sulfonate repeat units vs 1 mol cetyl trimethyl ammonium chloride (see Fig. 9a), a lamellar structure (Fig. 10a) is obtained with a long period of 35.2 Å [87]. The long period can be increased by selecting a longer alkyl tail, as illustrated in Figure 10b. In this case, the overall structure remains lamellar even for alkyl chain lengths of 12–18 methyl units, although for the longest chains an ordered surface structure (rippling) in the lamellae develops, due to induced curvature of the interfaces. More complicated phases have also been reported for other systems. For example, the small-angle X-ray scattering patterns of polyacrylic acid stoichiometrically complexed with dodecyl alkyltrimethylammonium chloride can be explained by a structure in which the polyelectrolyte chains form cylindrical domains embedded in the background of alkyl

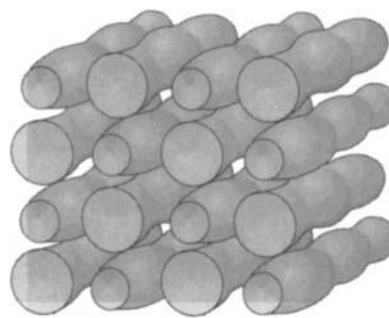


Fig. 11. Cylindrical self-organized phase with fcc undulations in the structure, as suggested for the polyacrylic acid/dodecyl trimethylammonium complex. Adapted from M. Antonietti, C. Burger, J. Conrad, and A. Kaul, *Macromol. Symp.* 106, 1 (1996).

tails, where additionally the polyelectrolyte cylinders have periodic thickness fluctuations yielding an fcc type of structure; see Figure 11 [16, 93].

Self-organized structures in the melt can be realized using many different matching pairs of polyelectrolytes and surfactants (see Fig. 9), in addition to the ones already mentioned, such as poly(4-vinyl pyridine)/dodecyl benzene sulfonic acid [89], polyacrylic acid or polymethacrylic acid with different alkylamines [90, 96] and with fluoroalkyltrialkylammonium [98], poly(diallyldimethylammonium chloride)/soybean lecithine [92], protein/surfactant [95], and branched polyethylene imine/dodecyl benzene sulfonic acid [97]. The concept has also been demonstrated for nitrogen-containing conjugated polymers: polyaniline/sulfonic acid [100], polypyrrole/alkyl sulfonic acid [101, 102], polyquinoline/dodecyl benzene sulfonic acid [103], as will be discussed in more depth later in Section 3.3. As there is a strong polarity difference between the charged backbone and the nonpolar alkyl tails, the repulsion is so strong that typically no transition to the disordered phase upon heating occurs.

The synthesis of most polyelectrolyte/surfactant complexes is extremely simple, with the notable exception of conjugated polymers, which suffer from very poor solubility in common organic solvents and which will be discussed in some detail in Section 3. In general, the product precipitates from solution and can be easily isolated [16]. Among the possible applications we mention the ultralow surface energies obtained when using fluorinated surfactants [98, 104]. Reviews of self-organized polyelectrolyte/surfactant complexes illustrating the various aspects of the complex formation have been published [16, 99].

A final comment should be given. The self-organizing polyelectrolyte/surfactant complexes are supermolecules because the basic structural unit consists of two subunits “recognizing” each other by the opposite charges, the concept aims for functionality, and requires molecular tailoring. However, the attraction based on opposite charges is not highly specific and the concept strongly resembles the polyelectrolyte/surfactant/water phases where the aqueous solvent has been omitted [105]. Therefore, self-organized polyelectrolyte/surfactant complexes in bulk may be regarded to be at the “borderline” between “classical” self-organization and supramolecular self-organization.

There is still another closely related supramolecular concept, whereby a polyelectrolyte is nominally stoichiometrically complexed with oppositely charged oligomers containing a mesogenic (rigid) unit [78, 106, 107], such as shown in Figure 4f. In general,

these complexes lead to “side-chain liquid-crystalline-like” complexes and smectic liquid crystallinity. Note that the structure formation in this case is most likely due to excluded volume effects between the mesogens, thus leading to liquid crystallinity.

Self-Organized Supramolecular Structures of Polymers Coordinated to Amphiphiles. Closely related to the previous examples is a concept demonstrated by Ikkala and ten Brinke et al., whereby a coil-like polymer poly(4-vinyl pyridine), P4VP, is stoichiometrically complexed with a surfactant zinc dodecyl benzene sulfonate, $(C_{12}H_{25}-C_6H_4-SO_3^-)Zn^{2+}$ or $Zn(DBS)_2$ [108]. In this case, the lone electron pair of the pyridine nitrogen of P4VP allows coordination with the Zn^{2+} cation. There is a strong repulsion between the two dodecyl tails of $Zn(DBS)_2$ and the polar polymer complex, thus leading to self-organization into a lamellar phase with a periodicity of 28 Å in bulk. The lamellar structure (as in Fig. 10a) is thermally very stable, even at high temperatures, and no phase transitions are observed upon heating. Many details still remain open. The phase behavior of $Zn(DBS)_2$ is only partly known. Pure $Zn(DBS)_2$ is crystalline [109]. However, it is hygroscopic and readily binds six molecules of water in the zinc sulfonate moiety, in analogy with the well-documented zinc toluene sulfonate [110, 111]. Importantly, the water molecules seem to plasticize the molecule so that “wet” $Zn(DBS)_2$ becomes liquid crystalline. In $Zn(DBS)_2$, there is a strong tendency of Zn^{2+} to coordinate to four ligands, which determines its behavior. In the polymeric complexes of $Zn(DBS)_2$, the actual architecture of bonding is unknown; i.e., how does Zn realize the fourth coordinate site in addition to coordination to the two sulfonates and one pyridine amine?

$Zn(DBS)_2$ also yields self-organized complexes with selected other nitrogen-containing polymers. For example, complexing polyamide 6 stoichiometrically with $Zn(DBS)_2$ yields self-organized lamellar structure with a long period of 28 Å [112] as well as it forms complexes with polyaniline [113], as will be discussed later.

Self-Organized Supramolecular Structures of Polymers Hydrogen-Bonded to Amphiphiles. One can progress further along these lines using hydrogen bonding to connect the amphiphilic side chains to the polymeric backbone to achieve supramolecular self-organized structures as first shown by ten Brinke and Ikkala et al. [17, 114–117] and subsequently by others as well [118]. Several points are noteworthy. Because the attraction is not based on strong Coulombic interactions but on weaker hydrogen bonding, the matching interactions have to be designed much more carefully, i.e., different forms of molecular recognition. Due to lacking charges and water insolubility, it becomes useful to refer to these complexes as polymer/amphiphile, rather than polymer/surfactant, complexes because the physically bonded side chains can no longer be denoted as surfactants. As before, the architecture is comb copolymer-like or, in the case of a rigid backbone, hairy-rod-like, as in Figure 8b.

As for any block copolymer, the self-organized structure formation in comb copolymers is based on the competition between the covalent attraction and the repulsion between the side chains and the backbone. The examples employing ionic attraction and coordination complexation demonstrate that the attractive interaction has to be sufficiently strong. In the case of hydrogen bonding, this is a much more delicate matter and the strength required to self-organize the supramolecular comb copolymers will be determined by a fine balance between attraction and repulsion.

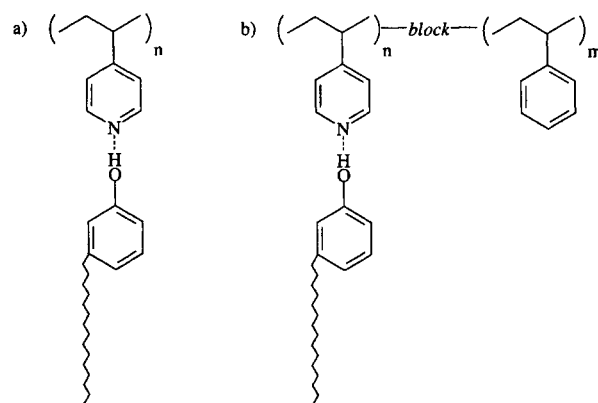


Fig. 12. Supramolecular comb-block architectures achieved by hydrogen-bonding alkylphenols with poly(4-vinyl pyridine)s [116].

Let us start from the most simple example. The pyridine amines of poly(4-vinyl pyridine), P4VP, and poly(2-vinyl pyridine), P2VP (see Fig. 12), are hydrogen-bonding acceptors that have been used to make miscible polymer blends with polymers containing hydrogen-bonding donors, such as poly(hydroxy methacrylate)s [119], or to make supramolecular side-chain liquid-crystalline polymers [76, 77, 79, 120, 121]. Therefore, it is no surprise that P4VP is soluble in, for example, 3-methyl-1-phenol and 3-dodecyl-1-phenol due to hydrogen bond formation. However, if one increases the alkyl chain length up to 15 methyl units, i.e., 3-pentadecyl-1-phenol, PDP, the thus obtained sufficiently high repulsion combined with sufficiently strong hydrogen bonding results in self-organization in the form of a lamellar phase (Figs. 10a and 12a) with, in the case of a stoichiometric composition, a periodicity of 36 Å [114, 116, 117, 122]. That near room temperature the hydrogen bonding takes place nearly stoichiometrically is indicated by Fourier transform infrared (FTIR) measurements [117, 122]. FTIR as a function of temperature further shows that the hydrogen bonding is reduced gradually upon heating and that near ca. 150°C a substantial part of the bonds are broken. The SAXS data recorded upon heating (Fig. 13) show a characteristic scattering peak at the magnitude of the scattering vector $q \cong 0.13 \text{ \AA}^{-1}$. (Note the definition of the scattering vector $q = (4\pi/\lambda) \sin \theta$, where 2θ is the scattering angle and λ is the wavelength.) However, the most interesting observation is the dramatic change in intensity and width of the scattering peak at ca. 65°C.

These data imply that an order–disorder transition (ODT) takes place at 65°C, where the nanoscale lamellar order is lost and the material becomes a disordered fluid. The residual scattering peak is due to the correlation hole effect [123, 124]. Its presence demonstrates that the system contains a large fraction of comb copolymer-like molecules [124, 125]. Hence, the ODT is not due to breaking of the hydrogen bonds, but due to the fact that the polarity difference between the noncharged backbone and the alkyl tails is sufficiently small. In this context, it is also interesting to refer to an analogous system involving P4VP with an aliphatic alcohol, dodecanol [115]. Here, the amphiphile and the polymer turn out to be miscible; however, the number of hydrogen bonds formed is too small to even give rise to a scattering peak due to the correlation hole effect. In the P4VP(PDP)_{1.0} example, the amount of nonpolar material (the alkyl tails) is comparable to the amount of polar material and the layered structure inferred from the SAXS data comes as no surprise. For the slightly longer nonadecylphe-

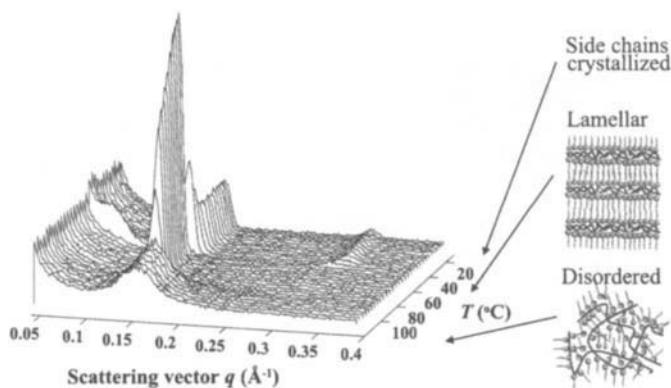


Fig. 13. SAXS patterns as a function of temperature for stoichiometric supermolecules consisting of poly(4-vinyl pyridine) stoichiometrically hydrogen-bonded to pentadecylphenol. Adapted from J. Ruokolainen, M. Torkkeli, R. Serimaa, E. B. Komanshek, G. ten Brinke, and O. Ikkala, *Macromolecules* 30, 2002 (1997).

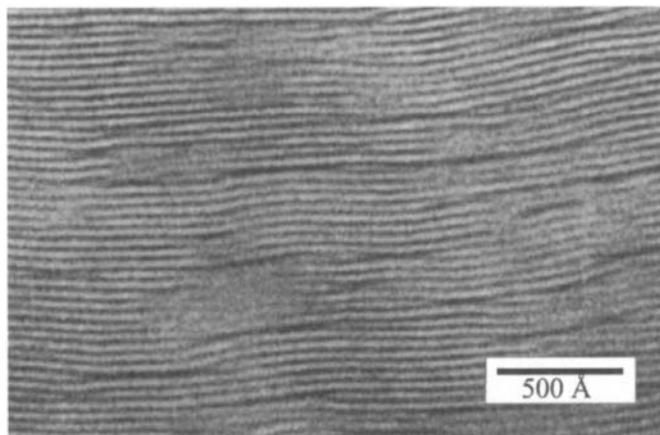


Fig. 14. Transmission electron micrograph of the self-organized lamellar phase of poly(4-vinyl pyridine) stoichiometrically hydrogen-bonded to 4-nonadecylphenol. Adapted from J. Ruokolainen, J. Tanner, O. Ikkala, G. ten Brinke, and E. L. Thomas, *Macromolecules* 31, 3532 (1998).

mol, this has actually been confirmed by transmission electron microscopy (Fig. 14) [117].

The SAXS data presented in Figure 13 show still another transition around room temperature due to the crystallization inside the alkyl layers. After crystallization, the second-order peak, due to symmetry not visible before crystallization, also appears. For the stoichiometric composition considered, the alkyl tails form an interdigitated hexagonally packed crystalline layer [126].

The phase diagram of supramolecular comb copolymers obtained by hydrogen bonding has also been discussed theoretically [127, 128]. Due to the reversibility of the hydrogen bonding, it is in several respects much more complex than for the corresponding “covalent” comb copolymers [129, 130]. However, the general trend in the sequence of structures as a function of composition, as discussed before (Fig. 3), remains valid. Experimentally, it is not a trivial issue to obtain cylindrical or spherical structures along the simple lines discussed previously. On the one hand, decreasing the length of the alkyl tail reduces the repulsion beyond a point where self-organization no longer occurs. On the other hand, the alternative of using much longer alkyl chains will almost certainly lead to

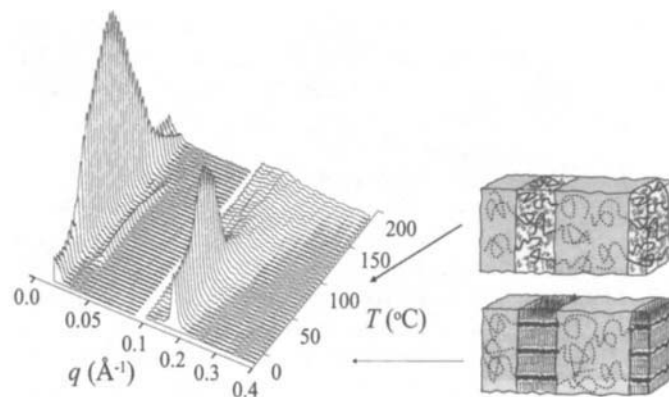


Fig. 15. Temperature-dependent SAXS data for PS-*b*-P4VP(PDP)_{1.0} recorded during heating at 2°C/min; weight fraction polystyrene $f_{PS} = 0.65$. Adapted from J. Ruokolainen, M. Saariaho, O. Ikkala, G. ten Brinke, E. L. Thomas, M. Torkkeli, and R. Serimaa, *Macromolecules* 32, 1152 (1999).

macrophase separation between the amphiphile and the polymer due to insufficient strength of the single hydrogen bond. However, this problem may be overcome in a by now familiar manner, using the concept of matching hydrogen bonds (i.e., more than one) between polymer and amphiphile; see Section 3.3.

A final comment concerns the possibility of using networks instead of linear polymers. In the case of networks synthesized using 4-vinylpyridine and divinylbenzene, the phase behavior is not changed in an essential way until the amount of divinylbenzene exceeds 1.0 mol%, where the network structure severely starts to suppress nanostructure formation [131]. As in the case of liquid-crystalline elastomers, using networks has the potential advantage of elasticity and orientability [132] (see also [133]).

Hierarchical Supramolecular Self-Organization in Block Copolymers Hydrogen-Bonded to Amphiphiles. An example of a hierarchical supramolecular assembly was demonstrated in Figure 6. A corresponding hierarchical supramolecular self-organization can be achieved if different self-organization schemes, each showing order at their own characteristic length, are combined. Ikkala and ten Brinke et al. have combined the self-organized nanostructures of block copolymers, with a characteristic periodicity in the range of 200–1000 Å, with those of supramolecular comb copolymers, with an order-of-magnitude shorter periodicity [18, 82, 134]. Figure 12b illustrates this concept.

As a straightforward extension of the previous work, polystyrene-*block*-poly(4-vinyl pyridine) (PS-*b*-P4VP) was selected as a model diblock copolymer system to which a nominally stoichiometric amount of hydrogen-bonded pentadecylphenol (PDP) [18, 134] or nonadecylphenol [82] was added. Figure 15 presents the characteristic temperature-dependent small-angle X-ray scattering data for a specific PS-*block*-P4VP(PDP)_{1.0} sample. The data demonstrate that for not too high a temperature a self-organized lamellar structure, consisting of alternating layers of the hydrogen-bonded supramolecular P4VP(PDP)_{1.0} blocks and the PS blocks, is formed. This comes as no surprise since for this particular sample the weight fraction polystyrene $f_{PS} \cong 0.65$. The periodicity is approximately 320 Å. Within the P4VP(PSP)_{1.0} layers, an additional self-organization into layers with a periodicity of 36 Å has taken place. As in the P4VP(PDP)_{1.0} homopolymer

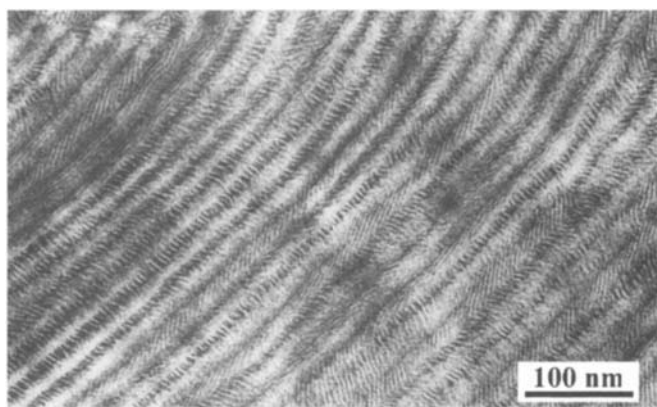


Fig. 16. Transmission electron micrograph of PS-*b*-P4VP(NDP)_{1,0}, where NDP = 4-*n*-nonadecylphenol, showing the lamellar-inside-lamellar structure with a mutually approximately perpendicular orientation. Courtesy of J. Ruokolainen.

case, the latter structure becomes disordered at ca. 65°C and only the diblock copolymer lamellar structure remains above this temperature. A further increase in temperature reduces the number of hydrogen-bonded side chains and part of the alkyl phenol molecules gradually diffuse into the polystyrene phase. This is especially true for temperatures above ca. 135°C, where PDP is miscible with PS [18]. Therefore, at such temperatures, a P4VP-selective solvent PDP becomes an indifferent solvent. As a consequence, the volume fraction of the PS-containing phase increases, which potentially might induce a sequence of lamellar → cylindrical → spherical order-order transitions. The SAXS data presented in Figure 15 are inconclusive in this respect. All these transitions play a major role in the design of controllable ionic conductors, which will be discussed later.

The presence of the room-temperature layer-inside-layer structure has been confirmed by transmission electron microscopy (TEM) [18, 82, 134], which further demonstrates that the two sets of lamellar structures are approximately mutually perpendicular (Fig. 16). By selecting different relative block lengths of P4VP vs PS and stoichiometric amounts of pentadecylphenol, all the classical phases can be obtained combined with the internal short-length-scale lamellar ordering, i.e., lamellae-in-cylinders, lamellae-in-spheres, spheres-in-lamellae, and cylinders-in-lamellae. All these hierarchical structures were also imaged by TEM [82]. One can conclude that supramolecular concepts, hierarchical structures, and self-organization can be combined. This will be discussed in a later section to construct functional, i.e., controllable, ionic conductors [18, 135].

3. CONDUCTING AND SEMICONDUCTING POLYMER SYSTEMS CONTAINING SELF-ORGANIZED SUPRAMOLECULAR POLYMERS

In Section 2, several supramolecular concepts leading to polymer-like molecules were discussed, together with the self-organization thereof. Next, we will concentrate on the conductive properties of selected systems where the possibility of obtaining these or similar systems via self-organization of supramolecular chainlike objects will be the guiding principle.

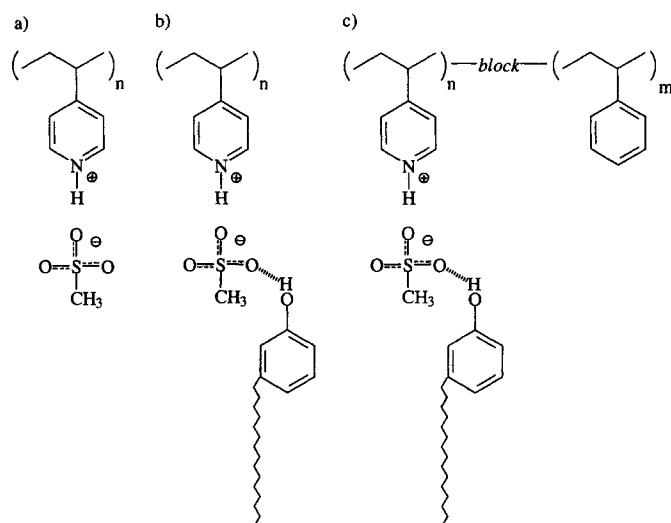


Fig. 17. Schemes for formation of P4VP(MSA)_{1,0}(PDP)_{1,0} and PS-*b*-P4VP(MSA)_{1,0}(PDP)_{1,0}. Adapted from J. Ruokolainen, R. Mäkinen, M. Törkkeli, R. Serimaa, T. Mäkelä, G. ten Brinke, and O. Ikkala, *Science* 280, 557 (1998).

3.1. Ionically Conducting Self-Organized Supramolecular Structures of Polymers Hydrogen-Bonded to Amphiphiles

In Section 2.3.2, the well-ordered self-organized layered structure for a melt of poly(4-vinyl pyridine) (P4VP) hydrogen-bonded to alkylphenol, together with the order-disorder transition to a disordered melt, was discussed in some detail. Conductivity is usually discussed in relation to conjugated polymers where electronic conductivity is achieved. However, in addition to conjugated polymers, which become conductive upon doping, nonconjugated polymers have been discussed in which the conductivity is obtained by the formation of a charge-transfer complex. Well-known examples include poly(2-vinyl pyridine) and poly(4-vinyl pyridine) complexed with iodine [136, 137]. Here we consider the case of a charge-transfer complex of P4VP and one of the simplest strong acids, methane sulfonic acid (MSA), leading to polyelectrolytes that are ionically conducting. The resulting polysalt (Fig. 17a), denoted as P4VP(MSA)_{1,0} for stoichiometric complexation (1 mol MSA vs 1 mol P4VP repeat units), shows a classical thermally activated ion conductivity (Fig. 18a) on the order of 10⁻⁴–10⁻⁵ S/cm. Next, the polysalt was mixed with pentadecyl phenol (cf. Section 2.3.2), which forms hydrogen bonds to the sulfonate group, to obtain the desired comb copolymer-like structure. Nominally, one PDP molecule per sulfonate group was used to obtain P4VP(MSA)_{1,0}(PDP)_{1,0} (Fig. 17b). However, the actual number of PDP molecules that are hydrogen-bonded remains uncertain because the large absorption bandwidth of the sulfonate does not allow an easy assessment by FTIR measurements. Optical microscopy (Fig. 19) indicates a complex phase behavior as a function of temperature, a behavior corroborated by the SAXS data presented in Figure 20. Below ca. 100°C, the supramolecular comb copolymers (as in Fig. 8b) form a self-organized lamellar morphology (see Fig. 10a) with a long period of approximately 48 Å. Upon heating, an order-disorder transition to a disordered melt occurs at approximately 100°C, usually accompanied by a strong decrease in intensity and a strong increase in width of the first-order scattering peak (near $q \cong 0.13 \text{ \AA}^{-1}$ in Fig. 20). Further

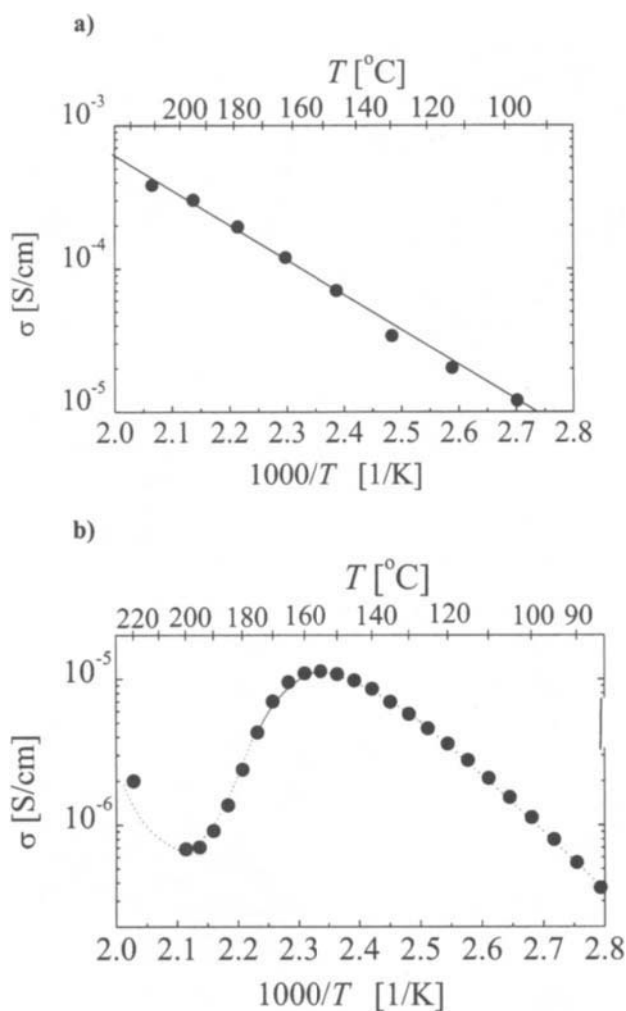


Fig. 18. Electrical conductivity (σ) during heating at 5°C/min, on the basis of ac impedance measurements extrapolated to zero frequency. (a) $P4VP(MSA)_{1.0}$ and (b) $P4VP(MSA)_{1.0}(PDP)_{1.0}$. Adapted from J. Ruokolainen, R. Mäkinen, M. Torkkeli, R. Serimaa, T. Mäkelä, G. ten Brinke, and O. Ikkala, *Science* 280, 557 (1998).

increase in temperature leads to a further decrease in intensity of this correlation hole peak and a shift toward zero scattering angle. This behavior demonstrates that the comb copolymer nature of the system gradually disappears due to breaking of the hydrogen bonds [124, 125]. Still further heating results in macroscopic phase separation between the PDP molecules and the polysalt and the subsequent reappearance of the homogeneous phase at ca. 200°C, a well-known phenomenon in mixtures of hydrogen-bonded molecules [138]. Finally, the system phase separates once more around ca. 220°C, which corresponds to the familiar lower critical solution temperature (LCST) behavior induced by a considerable difference in thermal expansivities of the components [139]. The low-temperature lamellar state consists of alternating polar and nonpolar layers, where the latter consist of insulating alkyl material. Hence, the order–disorder transition corresponds to a transition from locally two-dimensional ionically conductive layers to a three-dimensional ionically conductive system. Despite this dimensionality transition, the order–disorder transition is not reflected in the conductivity (Fig. 18). Note, however, that the or-

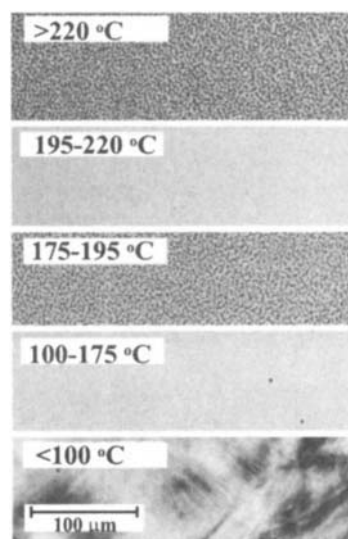


Fig. 19. Optical micrographs illustrating the phase behavior of $P4VP(MSA)_{1.0}(PDP)_{1.0}$. Adapted from J. Ruokolainen, R. Mäkinen, M. Torkkeli, R. Serimaa, T. Mäkelä, G. ten Brinke, and O. Ikkala, *Science* 280, 557 (1998).

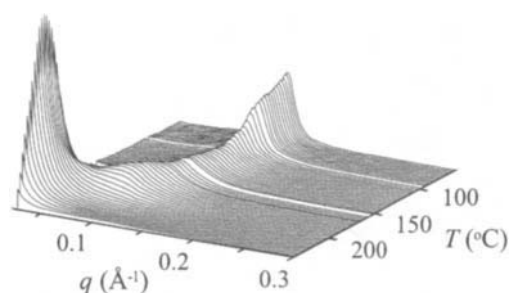


Fig. 20. SAXS intensity curves of $P4VP(MSA)_{1.0}(PDP)_{1.0}$ recorded during heating at 2°C/min. Courtesy of M. Torkkeli and R. Serimaa.

dered system has a macroscopically isotropic grain boundary domain structure [6, 37]. On the other hand, the macrophase separation at ca. 170°C is accompanied by a strong drop in conductivity, because apparently “isolated” domains of $P4VP(MSA)_{1.0}$ are formed (cf. Fig. 19). The complex phase behavior observed in this system will be exploited further on (Section 3.3) to construct externally controllable self-organized structures allowing electric switching.

3.2. Self-Organization and Stacking of Dislike Organic Molecules

Dislike organic molecules consisting of flat-shaped aromatic macrocycles tend to form columnar stacks in the crystalline state as well as in a liquid-crystalline solution [140–148]. As such, phthalocyanines, which behave as molecular semiconductors in the solid state, have been investigated in considerable detail [140, 141]. The basic structural unit consists of four connected pyrrole rings (see Fig. 21a), and the flat-shaped form allows a π -electron cloud delocalized over an array of 18 carbon and nitrogen atoms. Metallophthalocyanines can be prepared by coordinating metals, such as Fe, Ru, Co, Pd, Pt, Pb, Ni, Cu, Zn, Mn, and Cr, in the core; see Figure 21b [141]. In addition, the perimeter can be substituted

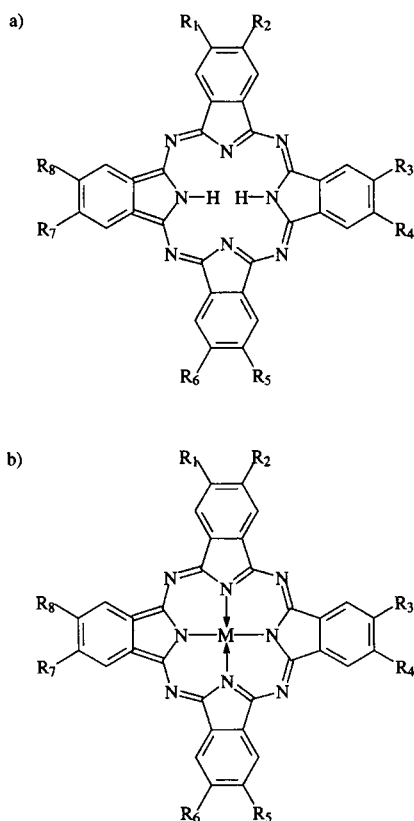


Fig. 21. Schematics of (a) phthalocyanine and (b) metallophthalocyanine. $R_1, \dots, R_8 = \text{H}$ in the unsubstituted case.

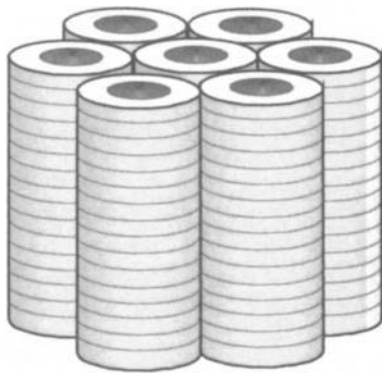


Fig. 22. Schematics of the hexagonally self-organized columns.

using various groups R_1, \dots, R_8 ; notably alkyl, alkoxy, and even crown ether substitutions have been used. Therefore, more than 70 different modifications are known.

The unsubstituted phthalocyanines have a strong π -stacking tendency, which results in insolubility in practically all common solvents. In the solid state, they crystallize in a stacked columnar fashion, where, however, in most cases the rings are inclined rather than perpendicular to the direction of the columns [141]. The peripheral substitutions offer a way of controlling the solubility and the columnar stacking in the solid state [141, 143–145]. For example, alkyl substitutions yield solubility in low polar solvents. If the substitutions are sufficiently irregular, e.g., four octyl chains randomly distributed over the eight possible peripheral sites, the crystallinity can be suppressed. In this case, discotic liquid-crystalline

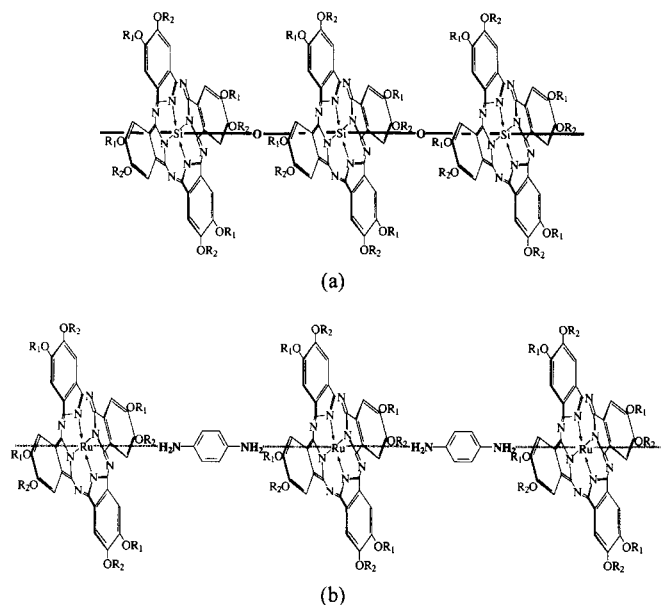


Fig. 23. Examples of connected phthalocyanines to form polymers: (a) phthalocyaninatopolysiloxane and (b) supramolecular polymer chain. Adapted from G. Wegner, *Thin Solid Films* 216, 105 (1992).

phases are obtained. Depending on the conditions, the nature of the side chains, and the possibility of metals in the core, discotic liquid-crystalline phases are observed for alkyl-substituted phthalocyanines with side chains longer than C_4 or C_6 . These self-organized mesophases contain typically hexagonally arranged ordered columns consisting of phthalocyanine molecules closely packed with their planes perpendicular to the column axis due to π -stacking; see Figure 22. The phase transitions can be tailored by changing the substituents. The phthalocyanines equipped with linear chains exhibit often, but not always, phase transitions from the crystalline to the mesophase at lower temperatures than phthalocyanines substituted with branched chains and therefore have a smaller crystallization tendency. Transition temperature can also be lowered by substitution by thiophene, whereas metallation typically raises it [146].

For the present review, the most important observation is the possibility of obtaining similar compounds as polymers. A first variant is realized if the “core” consists of, e.g., Si atoms that are covalently connected by ether linkages to form a phthalocyaninatopolysiloxane polymer; see Figure 23a. If the phthalocyanines are substituted using alkyl or alkoxy side chains, a supramolecular polymer is formed resembling a hairy-rod polymer with a rigid-rod conformation. Other metallophthalocyanines can also be used to form corresponding poly(phthalocyaninatometalloxanes), such as for Ge and Sn [141].

Another possibility, for obtaining the corresponding supramolecular polymers, is by bridging phthalocyanines with transition-metal cores with ligands; see Figure 23b. These are *coordination* polymers compared to backbones of covalently bound polysiloxanes (Fig. 23a) and related compounds. The bridging ligands can be either π -electron-containing molecules, like pyrazine, or negatively charged ligands, such as CN^- or SCN^- , if the oxidation state of the central metal is +III, as in Co^{3+} or Fe^{3+} [141].

Phthalocyanines are π -stacked molecular organic semiconductors. Their electronic properties differ strongly not only from the

inorganic semiconductors [141], but also from the conjugated conducting polymers. The reason is the small orbital overlap along the conducting columns as compared with the overlap between the atoms in inorganic materials. Oxidation using strong electron acceptors leads to a room-temperature conductivity of polycrystalline metallophthalocyanines of up to 1 S/cm. The electrical properties of phthalocyanines and metallophthalocyanines are naturally highly dependent on their macrocyclic morphology. The conductivity of single-crystalline metallophthalocyanines is obviously higher in the stacking direction, being as high as 10^4 S/cm. The charge transport occurs through the π -system of the stacks but if the central atom is oxidized, it can take place through the metal core [141].

The substituents can also be crown ethers, in which case substituted phthalocyanines generally create supramolecular structures with metal cations in solutions [144, 147]. As usual, the conducting properties are dependent on the ions due to the formation of different supramolecular architectures. Rb^+ ions create extended stacks with relatively high and Ba^{2+} ions networks with low alternating-current (ac) conductivity. A specific example demonstrating molecular wires consisting of an electronically conducting core and an ionically conducting mantle is discussed in [144].

Another variety, hexa-*peri*-benzocoronene, has been introduced consisting of 42 carbon atoms bound together by C_6 -membered rings forming a planar disc-shaped aromatic molecule (Fig. 24) [148]. The very extensive π -system makes transport along the hexabenzocoronene stacks particularly rapid and the one-dimensional intracolumnar charge mobility in the liquid-crystalline phase of hexakis-tetradecyl hexabenzocoronene was the largest determined for any discotic liquid-crystalline material to date. Interestingly, the phase transition manifests itself in the charge-transfer mobility; see Figure 24b [148].

3.3. Self-Organization of Hairy Rods

The bridged phthalocyaninatometal complexes considered previously (Fig. 23) consist of extended (supra)polymer backbones with a dense system of side chains, which classifies these structures as hairy rods, i.e., comb copolymers with a rigid backbone. As with other block copolymers (cf. Section 2.1), they tend to self-organize, forming nanoscale structures in bulk and in solutions. In the context of electrical conductivity, it becomes important to consider such architectures, taking into account that the backbone consists of a conjugated rigid polymer. However, before discussing conjugated backbones, we first discuss briefly general "hairy rod" polymers, consisting of a rigid rodlike backbone with different kinds of side chains; see Figure 2e.

Besides block copolymeric self-organization, there is an even more important reason why hairy rods have attracted so much interest. In general, rigid rodlike polymers do not melt and dissolve only poorly, if at all, in common solvents due to a strong aggregation tendency and a small gain of conformational entropy upon dissolution or melting. By covalent connection of substituent groups (notably flexible alkyl chains) to the backbone, a system is achieved whereby the rigid polymer can be regarded as dissolving in the background of the side chains, due to the (infinite) attractive interaction between the solvent molecules and the backbone. This causes melting-point depression [149, 150] without loss of rigidity of the backbone [64]. In this way, fusibility can be achieved and higher solubility in an "additional" solvent, to allow melt and solution processibility. The nature and length of the covalently bonded

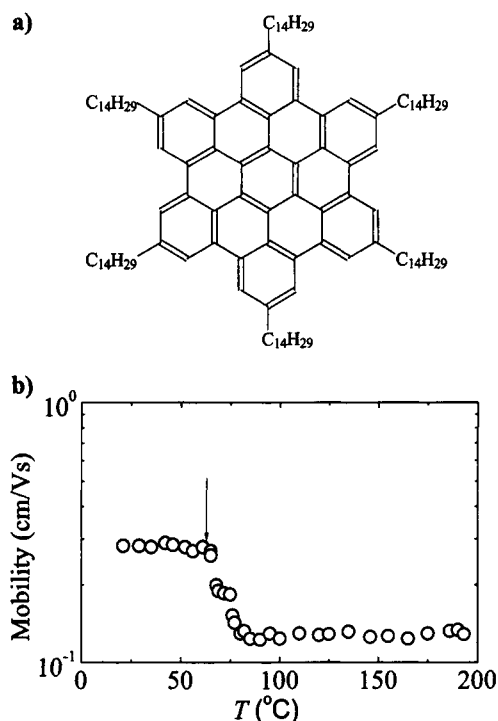


Fig. 24. (a) Tetradecyl-modified hexabenzocoronenes to allow columnar self-organized structure. (b) The mobility as a function of temperature, showing the effect of the phase transition from the crystalline solid to the hexagonally packed columnar liquid crystal at 65°C. Adapted from A. M. van de Craats, J. M. Warman, K. Müllen, Y. Geerts, and J. D. Brand, *Adv. Mater.* 10, 36 (1998).

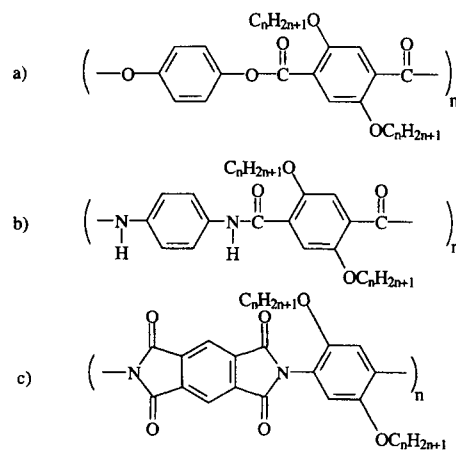


Fig. 25. Examples of hairy-rod polymers consisting of nonconjugated rigid polymers with covalently bonded flexible side chains [63, 152].

side chains have a large effect on the phase behavior. A wide variety of different modifications exist, depending on the selection of the backbone and side chains (see the reviews by Ballauff [64] and Menzel [151]). Figure 25 shows some hairy-rod polymers consisting of nonconjugated rigid rodlike polymers with flexible aliphatic side chains.

Unsubstituted rigid rod polymers typically have a high melting temperature (e.g., ca. 600°C for the polyester of Fig. 25a with a side-chain length $n = 0$). However, even a short alkyl tail of length $0 < n \leq 6$ reduces substantially the melting temperature; i.e., a

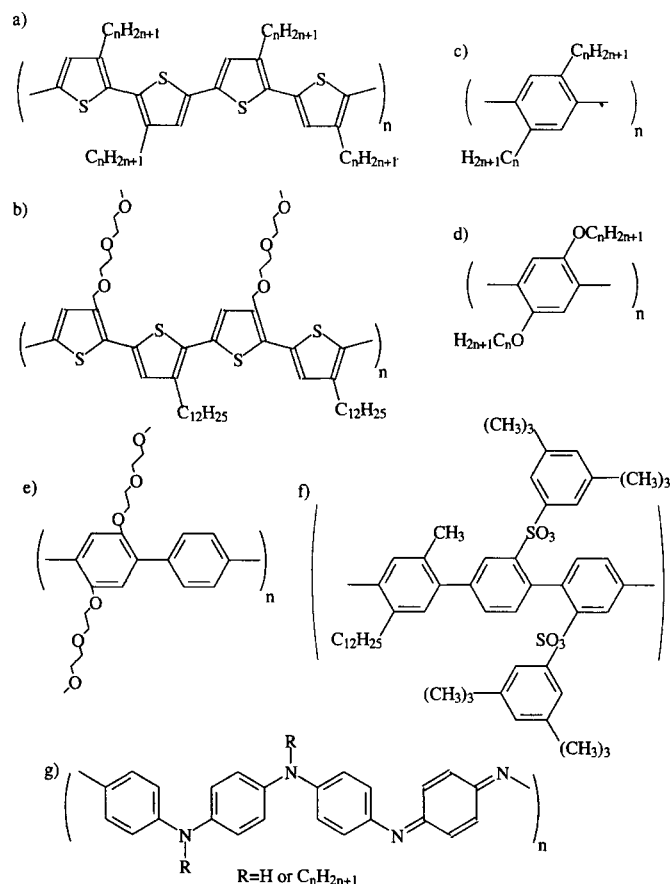


Fig. 26. Examples of alkyl-substituted hairy rods based on conjugated polymers.

transition from a crystalline to a nematic phase is reported [63, 64]. For longer side chains, the melting point is reduced further; e.g., for $n = 12$ it is 150°C . However, as the nonpolar side chain becomes longer, i.e., $n \geq 8$, the repulsion with the backbone becomes correspondingly larger. Therefore, one enters into the regime of self-organization, where the alkyl tails and the backbone microphase separate into typically lamellar self-organized domains; see Figure 10a [63–65, 153]. The evidence for the structure formation is based on SAXS, which typically shows a sharp first-order scattering peak at a specific wave vector q^* , as well as second- and third-order peaks at $2q^*$ and $3q^*$, characteristic of lamellar phases. The long period (i.e., $2\pi/q^*$) of the structure shown in Figure 25a is 23 \AA for $n = 12$ [153].

We now turn our attention to hairy rods consisting of a conjugated polymer backbone, in which case the hairy-rod concept offers possibilities to achieve processible, i.e., soluble or fusible, electroactive materials. It allows one to control the chain conformation in solution [154] and to obtain improved charge transport in the self-organized bulk phase [155]. Here the discussion will still be limited to covalently bonded side chains. In the next section, the extension to *supramolecular* hairy rods will be considered.

Alkyl-substituted polythiophenes (see Fig. 26a) have increased solubility in common solvents [156–158] and show thermo- and solvatochromism; see the reviews by Inganäs [159] and Gustafsson et al. [160]. The self-organized structures in bulk have been systematically studied by Prosa et al. [161] and Chen and Ni [162], demonstrating the formation of self-organized lamellar phases for

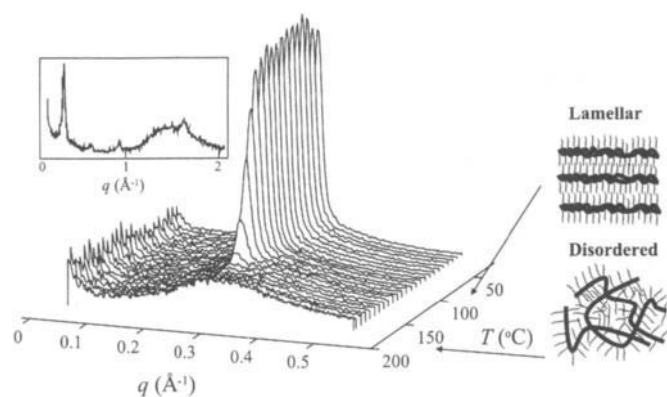


Fig. 27. SAXS intensity patterns of poly(3-octyl thiophene) as a function of temperature during heating at a rate of $2^\circ\text{C}/\text{min}$ [164]. The inset (adapted from S.-A. Chen and J.-M. Ni, *Macromolecules* 25, 6081 (1992)) shows the X-ray pattern at room temperature over a wider scattering vector q regime, where the second- and third-order peaks become resolvable.

$n \geq 4$. As a particular example, we will discuss poly(3-octyl thiophene), which contains octyl side chains covalently connected to the thiophene groups in the 3-positions to produce random head-to-tail and head-to-head mixtures. X-ray scattering curves [161, 163] show a sharp first-order intensity maximum corresponding to a long period of 21.7 \AA , as well as higher order peaks, indicating a lamellar self-organization at room temperature; see Figure 27. Information on the structure formation can be obtained by following the first-order scattering peak as a function of temperature [164]. For $T < 150^\circ\text{C}$, the peak is narrow and indicates a relatively high order. At ca. 150°C , an order–disorder transition (ODT) takes place in which the lamellar order is lost and a disordered structure appears, as manifested by a stepwise increased hwhm (half-width at half-maximum) and a strongly reduced scattering peak height. The remaining peak is due to the correlation hole effect [38]. The transition is reversible upon cooling/heating cycles. Furthermore, the ODT is clearly visible at 149.9°C in calorimetry [162, 165] as an endothermic peak upon heating.

Hence, undoped, i.e., neutral, poly(3-alkyl thiophene)s have a self-organized structure and a phase behavior that is analogous to block copolymers (as pointed out by Qian et al. [166]) where a lamellar melt state is observed below the ODT and above the ODT an isotropic fluid is formed. Implicitly, the materials are melt-processible due to the fluid state at $T > T_{\text{ODT}}$ and therefore the ODT is more commonly denoted as “melting,” although there is no crystallinity if the side chains are relatively short as in the case of poly(3-octyl thiophene). Another type of self-organized hairy-rod polythiophene has been demonstrated by Bjoernholm et al. [167]; see Figure 26b. These consist of regioregular head-to-tail polymers containing two types of side chains, hydrophilic polyoxyethylene and hydrophobic alkyl chains. They allow the construction of self-organized monolayers on surfaces, using Langmuir–Blodgett techniques.

Poly(3-alkyl thiophene) allows drastically modified properties, e.g., solubility in common solvents and fusibility, if the side-chain length exceeds butyl [156–158, 168]. Poly(3-octyl thiophene) yields a thermoreversible gel, i.e., percolating network structure, upon mixing with ultrahigh-molecular-weight polyethylene and decalin [169]. This network can subsequently be doped using iodine vapor for conductivity. At room temperature, the material shows a significant ac conductivity down to fractions of 1% by weight,

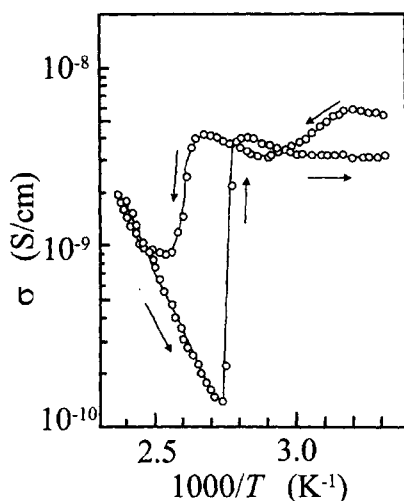


Fig. 28. Conductivity of undoped poly(3-dodecyl thiophene) as a function of temperature. Adapted from K. Yoshino, S. Nakajima, M. Onoda and R. Sugimoto, *Synth. Met.* 28, C349 (1989).

thus indicating the absence of an abrupt percolation threshold and the possibility of tailoring the conductivity to intermediate levels. This shows the feasibility of “tuning” the electrical conductivity by mixing with commodity polymers, which is of great practical importance for applications where antistatic properties are required. In polymer mixtures, blends of poly(3-octyl thiophene) with poly(ethylene-*rand*-vinyl acetate), i.e., EVA, have been shown to be the most interesting [170]. There the relative fraction of polar vinyl acetate units vs ethylene repeat units allows one to tailor the polarity and to tune the solubility of poly(alkyl thiophene)s. Solubility of poly(3-octyl thiophene) is obtained, as long as the weight fraction of the vinyl acetate fraction is small enough, such as 20 mol% [170]. Network structures can also be obtained by spinodal decomposition [170]. Conductive blends are obtained by post-treating the samples with iodine vapor. Semi-interpenetrating networks have been constructed by Wang and Rubner in crosslinked matrices with improved stability [171].

Finally, we will comment on the conductivity of poly(alkyl thiophene) hairy rods. Yoshino et al. studied the electrical conductivity of undoped poly(3-dodecyl thiophene) as a function of temperature [172]. They observed a stepwise small drop in the conductivity upon heating as the order–disorder transition is passed and the easily flowing disordered phase is entered at ca. 100°C; see Figure 28. The transition is reversible upon cooling, although hysteresis is obtained. Doping of the poly(3-octyl thiophene)s of the type shown in Figure 26a using a redox reaction yields a conductivity 1–10 S/cm at room temperature. However, at elevated temperature around 110°C (i.e., below the ODT), the conductivity drops several orders of magnitude within one hour, indicating “thermal undoping” (see the reviews in [159, 173]). This problem was solved by incorporation of the alkyl side chains at every second or third rather than every thiophene ring, thus reducing the “crowding” near the site of the dopant anions [159, 174].

As a further example, unsubstituted poly(*p*-phenylene) (PPP), which is an insoluble and infusible conjugated polymer will be considered. Based on this polymer, Wegner and co-workers prepared several different types of hairy rods (see Fig. 26c–f) [66, 175, 176]. Poly(2,5-di-*n*-dodecyl-1,4-phenylene) contains two flexible alkyl tails at each aromatic ring (see Fig. 26c) [175]. Such

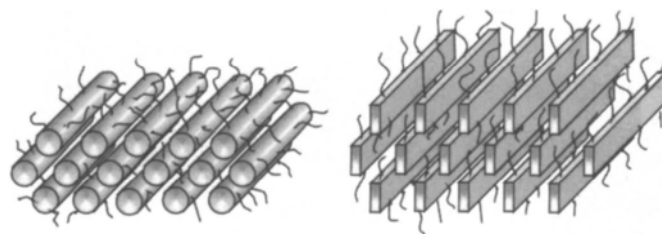


Fig. 29. Cylindrical and lamellar self-organized structures of substituted poly(*p*-phenylenes) according to Wegner and co-workers. Adapted from U. Lauter, W. H. Meyer, and G. Wegner, *Macromolecules* 30, 2092 (1997).

hairy rods have increased solubility in low polar solvents, such as dichlorobenzene, allowing the preparation of solvent-cast films. In the solid state, a self-organized lamellar phase is obtained with a long period of ca. 35 Å at room temperature, based on X-ray scattering patterns showing a sharp first-order peak and distinct third- and fifth-order peaks. Upon heating, the long period slightly decreases until at ca. 190°C an ODT to a disordered state occurs. As before, the sharp scattering peak is replaced by a shallow correlation hole peak [38]. Thus, the behavior is analogous to the poly(alkyl thiophene)s just discussed (see Fig. 27). A modification is reported where the alkyl side chains have been replaced by alkoxy chains [176]. For octyloxy and dodecyloxy side chains (i.e., $n = 8, 12$ in Fig. 26d), lamellar self-organized structures are obtained, whereas for shorter butoxy or pentoxy tails ($n = 4, 5$), cylindrical self-organized phases are observed; see Figure 29.

The side chains can also be oligo(ethylene oxide) (EO) chains, typically having two to six repeat units (see Fig. 26e) [66]. By using a statistical copolymer PPP(EO) x/y involving two different side-chain lengths of x resp. y EO units, self-organized materials have been introduced in which the tendency for side-chain crystallization is suppressed. Additionally, it is well known that poly(oxyethylene) in the uncrystallized state is able to conduct Li^+ ions to allow solid-state ionically conducting membranes. In this respect, the resulting self-organized structures are challenging because the oligo(oxyethylene) side chains support high Li^+ conduction and molecular-level reinforcement due to the rigid polymer chains is achieved at the same time [66]. For longer side chains, consisting of, e.g., $x = 5$ and $y = 6$ EO repeat units, the materials exhibit an ODT (in the range of 90–160°C) to a disordered isotropic state upon heating. The thermally activated ionic conductivity, though only reported for temperatures up to ca. 110°C, shows no effect of this phase transition; see Figure 30. If the side chains are shorter, i.e., $x = 4$ and $y = 2$, the lamellar structure prevails up to 240°C. In this case, however, a transition to another lamellar phase with a slightly different long period takes place upon heating at 190°C.

Hairy-rod architectures involving polyaniline (PANI) with covalently bonded side chains will be considered briefly. Supramolecular hairy-rod architectures of polyaniline will be discussed in considerable detail in the next section. The emeraldine-base (EB) form of polyaniline consists of alternating amine and imine repeat units (see Fig. 32). Side chains have been introduced by covalent connection of short alkyl (methyl or ethyl) chains to the aromatic rings [177] or by a series of different long alkyl chains ranging from butyl to octadecyl to the aminic nitrogens [178] (Fig. 26g).

Zheng et al. [179] prepared *N*-alkylated polyaniline (Fig. 26g) starting from leucoemeraldine, the completely reduced form of polyaniline. For most samples studied, the alkylation was in the

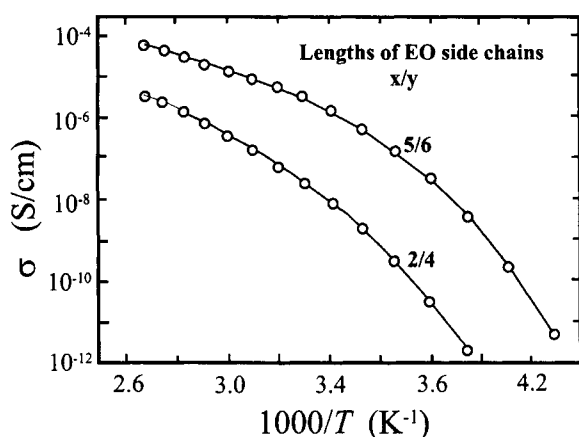


Fig. 30. Li^+ conductivity within the self-organized material consisting of poly(*p*-phenylene) with oligo(ethylene oxide) side chains $\text{PPP}(\text{EO})_{x/y}$, where x and y are the number of EO units per side chain of the statistical copolymer. Adapted from U. Lauter, W. H. Meyer, and G. Wegner, *Macromolecules* 30, 2092 (1997).

range of 50–80%. Products with octyl or longer side chains showed strongly improved solubility in common organic solvents such as chloroform and toluene. Similar to the other systems discussed, self-organized layered structures in the bulk state are formed with a long period linearly increasing from ca. 20 to 32 Å as a function of the side-chain length [179]. Order–disorder transitions to a disordered state were not observed.

The final example discusses hairy rods in which the side chains are covalently connected but where specific physical interactions become crucial. In conjugated polymers, it is, in general, very important to control the conjugation length. However, in aromatic and heterocyclic conjugated polymers, there is a tendency for the consecutive rings to be in out-of-plane conformations, which cause a reduced conjugation length. In ladder polymers, consisting of fused rings, this tendency is strongly reduced [180]. Another possibility for achieving planarity in hairy rods, more related to the present review, is to use matching physical interactions. Delnoye et al. [181] and Moroni et al. [182] showed how to use additional hydrogen bonds to planarize the chains (Fig. 31). The concept is, of course, strongly related to the method in which a ladder structure is formed completely based on matching hydrogen bonds; see Figure 4c [13].

3.4. Self-Organization of Supramolecular Hairy Rods

The results presented in the previous section demonstrate the general possibilities of obtaining self-organized lamellae using the hairy-rod concept. In the case of conjugated polymers, this opens up the possibility of achieving high charge carrier mobilities via two-dimensional transport [155]. Additionally, hairy rods offer opportunities to obtain ionically conducting films with high dimensional stability due to the reinforcing effect of the rigid backbone [66]. In general, rigid and flexible polymers are incompatible [183, 184]; however, the presence of flexible side chains represents one way of overcoming this limitation and creating true “molecular or nano composites” [185, 186].

The possibility of obtaining comb copolymer structures via the supramolecular route, using physical matching interactions, such as ionic, coordination, or hydrogen bonding, was discussed in some

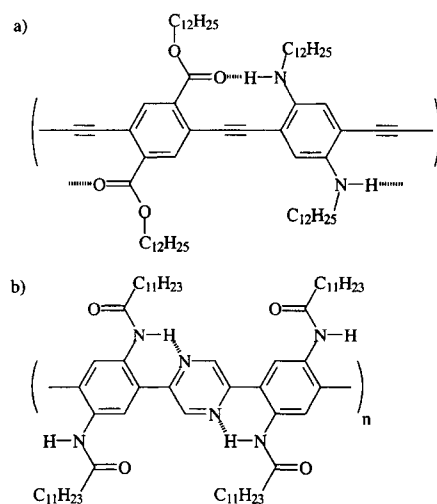


Fig. 31. Concepts to increase the planarity of hairy-rod polymers to be “ladder like” upon formation of hydrogen bonds. Adapted from D. A. P. Delnoye, R. P. Sijbesma, J. A. J. M. Vekemans, and E. W. Meijer, *J. Am. Chem. Soc.* 118, 8717 (1996); M. Moroni, J. Le Moigne, T. A. Pham, and J.-Y. Bigot, *Macromolecules* 30, 1964 (1997).

detail in Section 2. There the emphasis was on supramolecular comb copolymers with flexible polymer backbones. Since the synthesis is so simple, i.e., common precipitation in water for polyelectrolyte/surfactant complexes or solvent casting from a common solvent in the case of hydrogen bonding, the question naturally arises whether hairy rods can be prepared via a similar supramolecular route; i.e., can hairy-rod molecules be synthesized by simply connecting the side chains by “recognizing” physical bonds? However, in the case of rigid rod polymers, the drastically reduced solubility is a most complicating factor. It therefore presents a real and exciting challenge to develop supramolecular routes for hairy-rod polymers.

Working with polyaniline, a concept was introduced by Cao and co-workers [187, 188] for electrically conducting supramolecular hairy-rod polymers to allow increased solubility in low polar solvents and network formation in polymer blends [188–190]. The stable undoped state of polyaniline consists of benzene diamine and quinone diimine moieties, the emeraldine base thus being a copolymer (Fig. 32). It can be doped by redox reactions by electron transfer but, importantly, its salts with strong acids are electronically conducting due to protonation of the iminic nitrogen and a subsequent redox reaction along the chain, as found by MacDiarmid and co-workers [191, 192]. Note, however, that even before their findings conducting polyaniline sulfate had been used [193]. Cao and co-workers took a sulfonic acid, able to protonate for conductivity, which also has a low polar part, such as a flexible dodecyl alkyl tail in the case of dodecyl benzene sulfonic acid (DBSA) shown in Figure 32, two nonyl tails in the case of dinonyl naphthalene sulphonic acid, or an aliphatic ring in the case of camphor sulfonic acid (CSA) [187, 188]. Note that in the latter case there is a characteristic carbonyl group, which can play an important role in the supramolecular structure formation due to its ability to form hydrogen bonds with solvent molecules [194] or to twist the chains to be chiral in solutions [195]. Here the main emphasis will be on the alkyl-modified dopants due to the analogy with hairy rods.

The scheme of protonation of the emeraldine-base form of PANI by DBSA and the subsequent doping are also illustrated

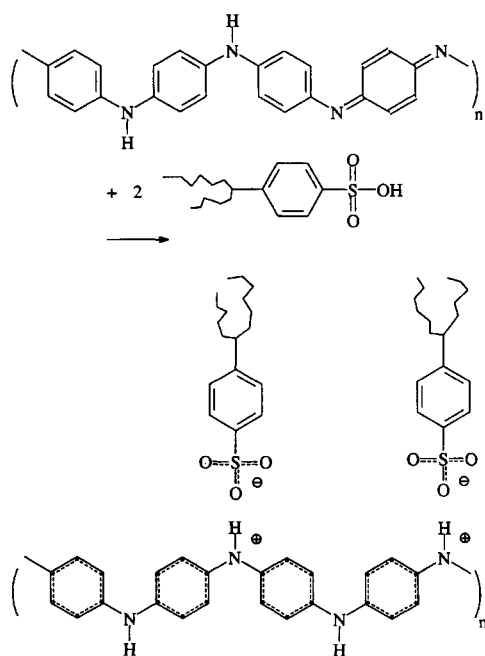


Fig. 32. Emeraldine-base form of polyaniline and the protonation of its iminic nitrogen using DBSA and the subsequent intrachain redox reaction to form a conducting polyelectrolyte/surfactant complex of supramolecular hairy-rod architecture.

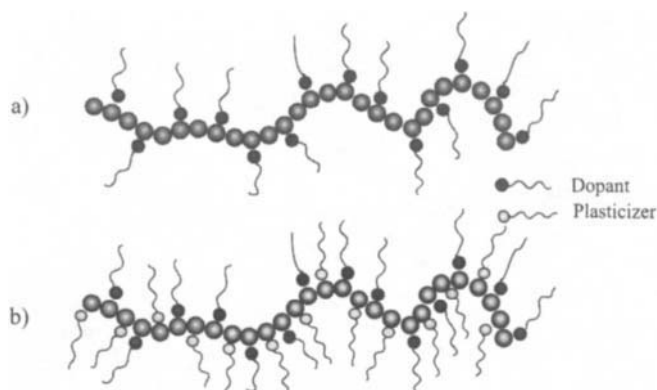


Fig. 33. Schemes of supermolecules consisting of the emeraldine-base form of PANI complexed by (a) a protonating amphiphilic acid, such as DBSA; and (b) a protonating amphiphilic acid and plasticizing amphiphiles, which are strongly bound to the backbone due to hydrogen bonds [100, 188] or coordination bonds [113].

in Figure 32. The DBSA molecules typically consist of branched dodecyl tails, thus effectively suppressing the tendency for crystallization of the side chains. The structure is denoted by the nominal composition $\text{PANI}(\text{DBSA})_{0.5}$. The hairy-rod-like supermolecule consisting of a protonated PANI backbone and DBSA anion substituents is illustrated schematically in Figure 33a. The bonding is due to ionic interaction, thus the material can also be classified as a polyelectrolyte/surfactant complex; see Section 2. The structure was studied by electron diffraction [196] using emulsion-polymerized samples that allow fibers. The structure is solid crystalline, and was determined using electron diffraction to be orthorhombic with lattice parameters $a = 11.78 \text{ \AA}$, $b = 17.91 \text{ \AA}$, and $c = 7.16 \text{ \AA}$. At this point, it is im-

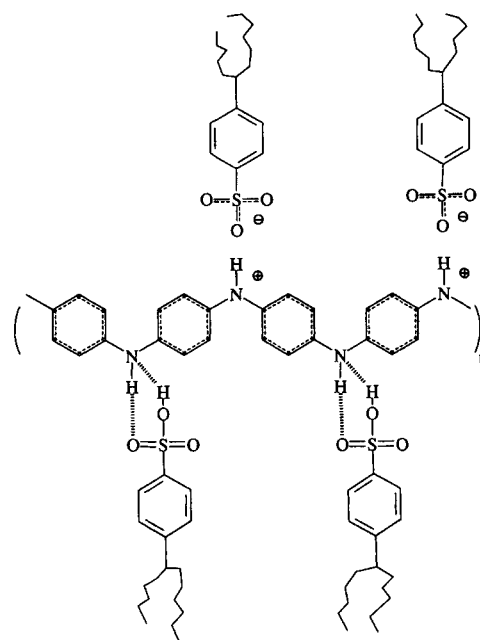


Fig. 34. Polyaniline emeraldine base whose iminic nitrogens have been protonated using DBSA and aminic nitrogens hydrogen-bonded to DBSA to form a supramolecular hairy-rod chain.

portant to compare $\text{PANI}(\text{DBSA})_{0.5}$ with stoichiometric polyelectrolyte/surfactant complexes of flexible nitrogen-containing polymers poly(4-vinyl pyridine) and poly(ethylene imine), i.e., $\text{P4VP}(\text{DBSA})_{1.0}$ [89] and $\text{PEI}(\text{DBSA})_{1.0}$ [97]. In the latter two cases, *fluid-like* self-organized lamellar materials are obtained (see Fig. 10a), with long periods of ca. 27 \AA . By contrast, stoichiometrically protonated $\text{PANI}(\text{DBSA})_{0.5}$ [196] is an infusible crystalline material, as are also previously electrochemically synthesized conducting polymer/surfactant systems showing self-organized lamellar phases [101, 197]. In addition, $\text{PANI}(\text{DBSA})_{0.5}$ is still poorly soluble in low polar organic solvents (such as toluene), which indicates that the volume fraction of the alkyl chains is still insufficient to achieve proper surface activity with respect to such solvents [188]. In the case of hairy rods, the side chains act as plasticizers and lead to melting-point depression, as discussed in Section 2 [64]. For $\text{PANI}(\text{DBSA})_{0.5}$, one of the obvious sources for the crystallinity and the high melting point is the formation of internal hydrogen bonds due to the amines of the PANI chains. This suggests “protecting” the amines by additional plasticizing compounds acting as spacer groups. However, as was pointed out before, most solvent molecules tend to phase-separate from rigid chains, and thus a particularly strong interaction is required. As hydrogen-bonding is an acid/base interaction, the strength can be increased by taking a larger acidity difference between the hydrogen bonding donors and acceptors. Therefore, it is a natural option to hydrogen-bond strongly acidic additional DBSA also to the amines, where protonation probably does not take place. The suggested supermolecule would then be the one shown in Figures 33b and 34. The second motivation for using DBSA for plasticization is to “complete” the hairy rod with similar side chains as used for the protonation sites.

Such $\text{PANI}(\text{DBSA})_x$ with $x \geq \text{ca. } 1.0$ has indeed drastically modified properties in solution and in bulk. Figure 35 demonstrates the improved solubility in low polar solvents, such as xylene

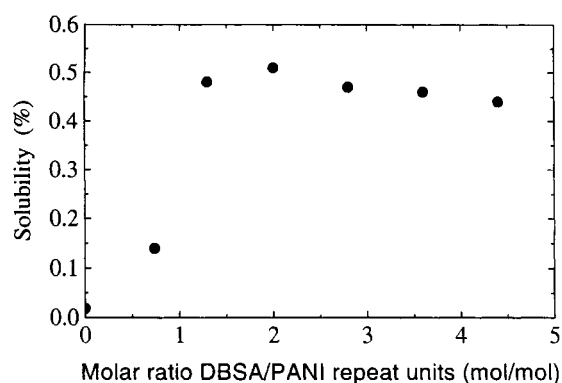


Fig. 35. Effect of added DBSA to promote solubility in xylene due to the surface-active nonpolar alkyl tails of DBSA. Adapted from Y. Cao, P. Smith, and A. J. Heeger, U.S. Patent 5,232,631, 1993.

or toluene [188], which can be achieved by complexing, in addition to the 0.5 mol of DBSA required for the protonation, still another ca. 0.5 mol of DBSA. This concept allows preparation of solid films based on common solvents with conductivities as high as ca. 200–400 S/cm [187, 188]. The solubility and conductivity are strongly dependent on the length and structure of the nonpolar surfactant tail, as was discussed before in this section in the case of poly(alkyl thiophene)s. For example, using octyl sulfonic acid, i.e., an alkyl tail of length $n = 8$ methyl units, the solubility in low polar solvents is reduced in comparison to the $n = 12$ for DBSA [187]. However, the conductivity simultaneously increases for shorter side chains, obviously due to a larger hopping conductivity between the chains [198]. For longer alkyl tails, such as in dinonyl naphthalene sulfonic acid with $n = 18$, the complexes become highly soluble even in, e.g., butoxyethanol, methylethylketone, in addition to xylene, but the conductivity is strongly reduced [199]. Another feasible type of a “diphilic” sulfonic acid is camphor sulfonic acid, which, probably due to its polar hydrogen-bonding carbonyl group, allows high solubility in more polar solvents, such as *m*-cresol or hexafluoroisopropanol [187, 194, 200, 201].

The solubility in common solvents allows preparation of polymer blends based on solvent casting. Figure 36 shows the conductivity of PANI(DBSA)_{1.0} solution blended with ultrahigh-molecular-weight polyethylene (UHMWPE) at different concentrations after evaporation of the xylene solvent [187, 188]. A low percolation limit can thus be obtained in solution processing of commodity polymers. Corresponding results are also obtained in blends with other polymers, such as polystyrene and polyamide 12.

Interestingly, complexing PANI with excessive amounts of DBSA also allows melt processibility. A particularly simple, albeit crude method is to dissolve the emeraldine-base form of polyaniline in DBSA in a mole ratio of ca. 1.0/1.0 mol/mol using an extruder at a temperature of ca. 150°C or higher without auxiliary solvents [202]. This results in a waxy solid material that flows at elevated temperatures. The X-ray analysis indicates a lamellar self-organized fluid-like structure with a long period of 27 Å in bulk [100] (see Fig. 10a) and as also observed in P4VP(DBSA)_{1.0} [89] and PEI(DBSA)_{1.0} [97]. Such fusible complexes allow melt blending using extruders with commodity polymers, such as polyethylene, polystyrene, polypropylene, and poly(vinyl chloride) [203]. The conductivity level is typically 10⁻²–1 S/cm and the percolation takes place at <<10mol% PANI. However, optical microscopy suggests that in such compositions, nom-

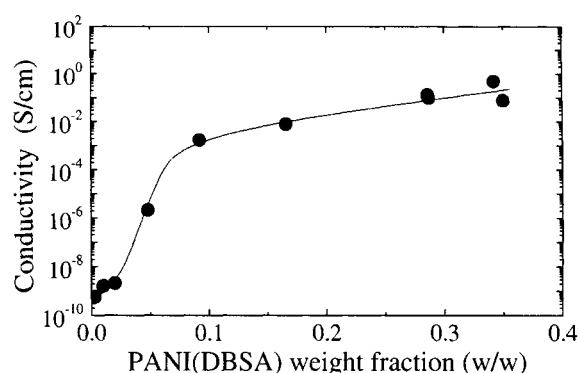


Fig. 36. Electrical conductivity of PANI(DBSA)_{1.0} solution blended in decanol with ultrahigh-molecular-weight polyethylene. Adapted from Y. Cao, P. Smith, and A. J. Heeger, U.S. Patent 5,232,631, 1993.

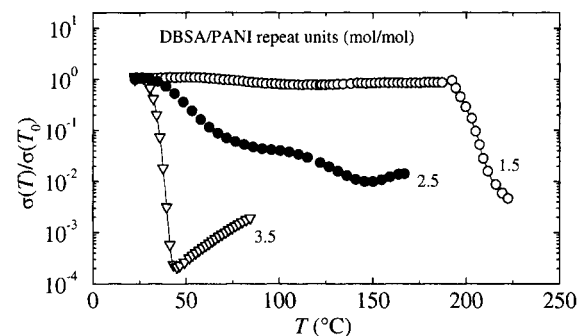


Fig. 37. Temperature-responsive conductivity of reversible PANI gels. Adapted from T. Vikki, J. Ruokolainen, O. T. Ikkala, P. Passiniemi, H. Isotalo, M. Torrkeli, and R. Serimaa, *Macromolecules* 30, 4046 (1997).

inally denoted as PANI(DBSA)_{1.0}, the emeraldine-base form of polyaniline may not dissolve completely in DBSA, as minor insoluble particles can be observed. This observation is not surprising as the emeraldine base is prone to crosslinking at the elevated temperatures required for the dissolution without an additional solvent medium. Therefore, the complexation should ideally be performed in solution. Finding a solvent medium is not straightforward because both the emeraldine base and the dopant acid should be soluble. Moreover, strong acids, such as sulfuric acid and methane sulfonic acid, are excluded because they compete with the protonation reaction by the actual dopant selected. On the other hand, basic solvents cause complexation between the dopant and the basic solvent. Hexafluoroisopropanol has been observed to be a feasible solvent for preparing the complexes in solution [204–206]. Formic acid has also been used as a medium in which the complex between the emeraldine-base form of polyaniline and the dopant acid is formed [207]. The latter concept allows reversible gels, i.e., fusible networks in solvents, taking into account that considerable excess of DBSA is selected [207]. An example of the latter case is that, after evaporation of the formic acid, PANI(DBSA)_{2.0} is a rubber-like elastic solid, indicating the network structure of PANI(DBSA)_{1.0} in additional DBSA, which has a conductivity of 0.01 S/cm. Heating to ca. 200°C causes the material to behave as a viscous fluid and the conductivity drops a few orders of magnitude (see Fig. 37). A phenomenon like this allows external (temperature) control of the conductivity to construct responsive materials. The elastic PANI(DBSA)_x gels can

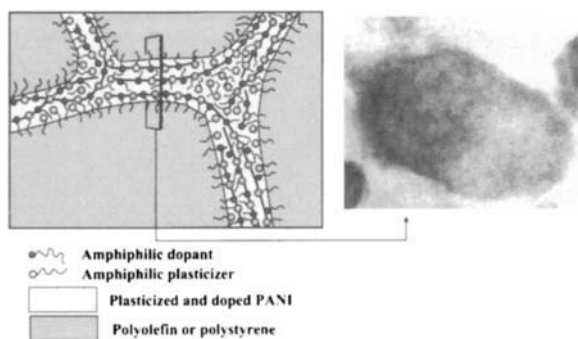


Fig. 38. Scheme of percolative network structures of PANI formed in a polymer blend based on supramolecular hairy rods. TEM illustrates a cross section of PANI hairy rods in polypropylene mixtures, showing areas of lamellar self-organization of the PANI/amphiphiles with a long period of ca. 30 Å [214].

further be blended with thermoplastic elastomers, to render elastic conducting composites that conduct even at high elongation [208].

The previous examples describe concepts in which the supramolecular hairy rods consist of protonating amphiphile dopants that are complexed due to charge transfer to the iminic sites of PANI and plasticizing amphiphiles that are complexed to the aminic sites due to the strong hydrogen bond caused by the highly acidic DBSA. Efforts to use less acidic amphiphilic plasticizers easily lead to macroscopic phase separation due to insufficient bonding. Two possible alternatives for increasing the attraction are either to use coordination bonds [113] or to use multiple hydrogen bonds and π -stacking [209, 210]. The first concept can be illustrated by the amphiphiles zinc(II) dodecyl benzene sulfonate and copper(II) dodecyl benzene sulfonate, i.e., $\text{Zn}(\text{DBS})_2$ and $\text{Cu}(\text{DBS})_2$. The supramolecular hairy-rod architectures are again as illustrated in Figure 33b, but this time the bonding to the aminic nitrogen of DBSA-doped PANI takes place through coordination. The latter concept, using multiple hydrogen bonding, is described later in some detail in the context of polypyridine (see Fig. 40) [211]. Both concepts result in fusible supramolecular self-organized hairy-rod materials that allow melt processing. Such supramolecular hairy rods consisting of PANI complexed with protonating amphiphiles and plasticizing amphiphiles allow network structures in polymer blends with low polar commodity polymers, such as polypropylene, polyethylene, and polystyrene [113, 209, 212, 213]. The network is schematically illustrated in Figure 38 and manifests itself in the achievement of conductivity at low polyaniline weight fractions (see Fig. 39).

Ikkala and ten Brinke et al. [211] introduced a supramolecular route to obtain a supramolecular hairy rod from one of the simplest π -conjugated polymers, poly(2,5-pyridine diyl) or poly(*p*-pyridine) (PPY), involving a combination of ionic and hydrogen bonding (see Fig. 40) [211]. The procedure is reminiscent of the supramolecular $\text{P4VP}(\text{MSA})_{1.0}(\text{PDP})_{1.0}$ structures, considered in Section 3.1. PPY and a stoichiometric amount of MSA (1 mol PPY repeat unit vs 1 mol MSA) were dissolved in formic acid to form poly(2,5-pyridine diyl) methane sulfonate, $\text{PPY}(\text{MSA})_{1.0}$. The polymeric salt obtained after evaporation of formic acid is infusible and wide-angle X-ray scattering (WAXS) data show that a co-crystallized structure has been formed (Fig. 41). $\text{PPY}(\text{MSA})_{1.0}$ was observed to be miscible in *m*-cresol, due to hydrogen bonding between its aromatic hydroxyl group and the sulfonate group

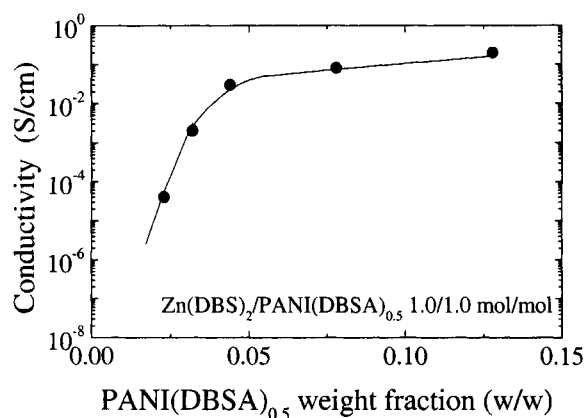


Fig. 39. Conductivity as a function of the weight fraction of supramolecular hairy rods $\text{PANI}(\text{DBSA})_{0.5}/\text{Zn}(\text{DBS})_2$ of molar ratio 1.0/1.0 mol/mol in melt-blended low-density polyethylene blends. Adapted from T. Kärnä, J. Laakso, T. Niemi, H. Ruohonen, E. Savolainen, H. Lindström, E. Virtanen, O. Ikkala, and A. Andreatta, U.S. Patent 5,340,499, 1994.

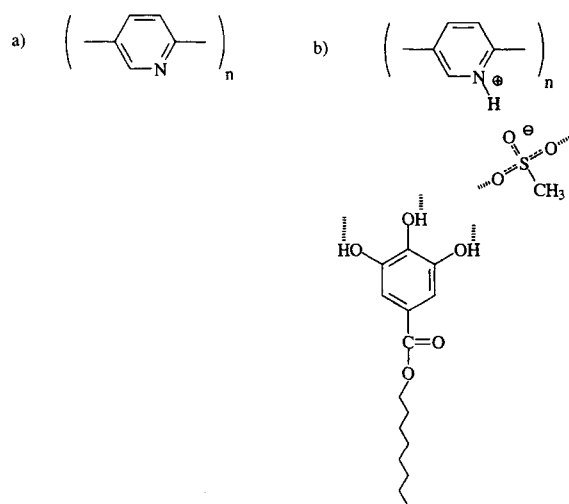


Fig. 40. (a) Poly(*p*-pyridine), i.e., PPY; and (b) polypyridinium methane sulfonate, $\text{PPY}(\text{MSA})_{1.0}$, and octyl gallate (OG). OG is a hydrogen-bonding donor and able to perform simultaneously several hydrogen bonds with the sulfonate groups, which are hydrogen-bonding acceptors. The detailed scheme is unknown. Adapted from O. Ikkala, M. Knaapila, J. Ruokolainen, M. Torkkeli, R. Serimaa, K. Jokela, L. Horsburgh, A. P. Monkman, and G. ten Brinke, *Adv. Mater.* 11, 1206 (1999).

of the polysalt. To yield self-organizing “hairy rods,” however, longer side chains, i.e., stronger repulsion, is required. Due to the rodlike character, the situation is more delicate than in the case of $\text{P4VP}(\text{MSA})_{1.0}$ and, consequently, this can no longer be achieved by simply using alkyl phenols, such as PDP [211] in which case the hydrogen-bonding strength turns out to be too small and macrophase separation occurs. As it turned out, amphiphiles work that allow several hydrogen bonds at the same time, such as octyl gallate (octyl 3,4,5-trihydroxybenzoate, OG); see Figure 40.

Mixtures of $\text{PPY}(\text{MSA})_{1.0}$ and OG were prepared in different molar ratios 1.0:0.5, 1.0:1.0, and 1.0:2.0 between MSA and OG. Here we will restrict our discussion to the last composition. The optical microscopy study of the supramolecular “hairy rod” $\text{PPY}(\text{MSA})_{1.0}(\text{OG})_{2.0}$ showed that the material is an optically isotropic fluid above ca. 180°C, forms an optically anisotropic self-

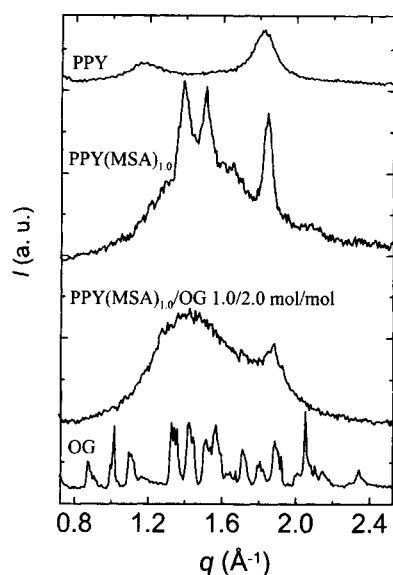


Fig. 41. WAXS patterns of PPY, PPY(MSA)_{1.0}, OG, and PPY(MSA)_{1.0}/OG in the mole ratio 1.0/2.0 mol/mol. Adapted from O. Ikkala, M. Knaapila, J. Ruokolainen, M. Torkkeli, R. Serimaa, K. Jokela, L. Horsburgh, A. P. Monkman, and G. ten Brinke, *Adv. Mater.* 11, 1206 (1999).

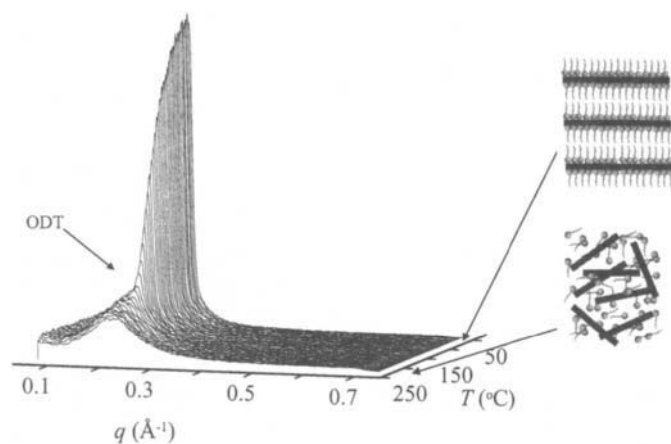


Fig. 42. SAXS intensity data of PPY(MSA)_{1.0}/OG in the ratio 1.0/2.0 mol/mol. Adapted from O. Ikkala, M. Knaapila, J. Ruokolainen, M. Torkkeli, R. Serimaa, K. Jokela, L. Horsburgh, A. P. Monkman, and G. ten Brinke, *Adv. Mater.* 11, 1206 (1999).

organized fluid in the temperature interval 110–180°C, and becomes a brittle co-crystallized solid below 110°C [211]. The SAXS data corroborate these findings (Fig. 42) by showing a distinct order–disorder transition at ca. 180°C. Above the ODT, a shallow correlation hole peak [38] is present, which turns into a sharp peak of much higher intensity on entering the ordered state. The melting of the co-crystallized low-temperature structure at ca. 110°C is clearly visible in the wide-angle X-ray scattering data [211].

Since the pyridyl rings of PPY are deficient of π -electrons, only n-doping yields moderate conductivity of approximately 0.1 S/cm, whereas p-doping, based on electron withdrawal, is ineffective [215, 216], which is also expected for protonation with strong acids. The main purpose of this scheme is therefore not the construction of electronically conducting self-organized supramolecular mate-

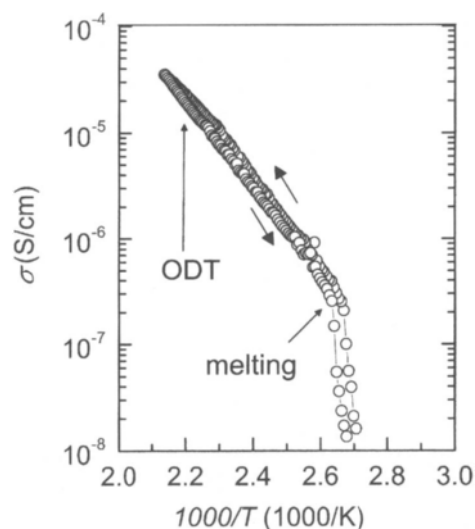


Fig. 43. Electrical conductivity of PPY(MSA)_{1.0}/OG in the mole ratio 1.0/2.0 mol/mol. Adapted from O. Ikkala, M. Knaapila, J. Ruokolainen, M. Torkkeli, R. Serimaa, K. Jokela, L. Horsburgh, A. P. Monkman, and G. ten Brinke, *Adv. Mater.* 11, 1206 (1999).

rials, but rather the presentation of a model system to demonstrate the feasibility of such an endeavor. Still, PPY(MSA)_{1.0}/OG in the 1.0/2.0 mol/mol systems shows moderate conductivities (Fig. 43) [211]. The results presented demonstrate the absence of conductivity in the low-temperature co-crystallized state and the concurrent increase in conductivity with the melting transition. Additionally, as in all previously discussed examples the conductivity is not influenced by the order–disorder transition from the self-organized ordered state consisting of alternating polar (PPY(MSA)_{1.0} and aromatic parts of OG) and nonpolar (the octyl tails) layers.

3.5. Externally Controllable Self-Organized Supramolecular Polymer Systems Allowing Electrical Switching

As a function of temperature, many self-organized supramolecular polymer systems exhibit a series of phase transitions between different ordered structures (i.e., OOT) and from ordered structures to a disordered structure (ODT) as exemplified by the example of PS-*b*-P4VP(PDP) introduced in Section 2.3.2 dealing with hierarchical supramolecular self-organization [134]. To exploit these transitions for, e.g., electroactive materials, a correlation between the functional properties and the transitions has to exist. However, as demonstrated in Section 3.3, the ODT in a characteristic, ionically conducting, supramolecular comb copolymer system, i.e., P4VP(MSA)_{1.0}(PDP)_{1.0}, from two-dimensional conductive layers to a three-dimensional disordered conductive system is not reflected in the conductivity of the material [18]. Similar observations were made with respect to the conductivity of Li⁺ ions in self-organized oligo(ethylene oxide)–substituted poly(*p*-phenylene) [66] and with respect to the ionically conducting supramolecular hairy-rod system obtained from poly(*p*-pyridine), i.e., PPY(MSA)_{1.0}/OG in the ratio 1.0/2.0 mol/mol [211]. All these examples involve transitions from two-dimensional conductive layers in a macroscopically isotropic grain boundary structure to a three-dimensional disordered system. Of course, if the systems

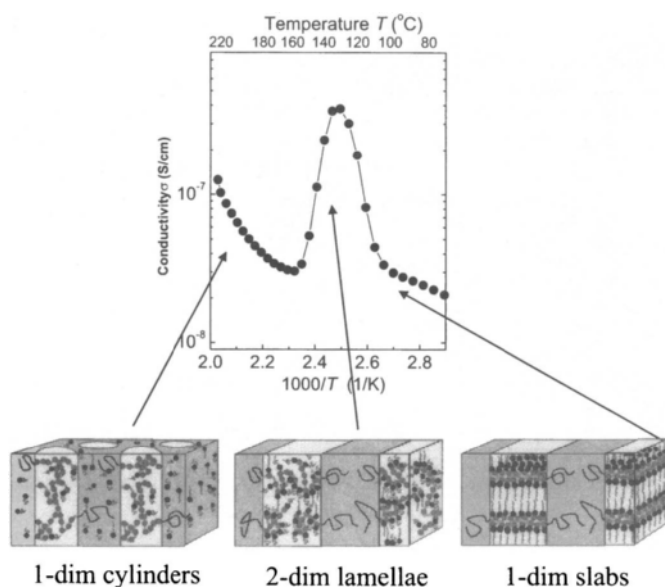


Fig. 44. Schematic illustration of the self-organized structures in PS-*b*-P4VP(MSA)_{1.0}(PDP)_{1.0} supramolecular comb-coil diblock copolymers and their effect on the overall conductivity. A. Alternating layers of PS and layers consisting of one-dimensional slabs of P4VP(MSA) and PDP for $T < \text{ca. } 100^\circ\text{C}$. B. Alternating layers of PS, which may actually contain already a small fraction of the PDP molecules, and disordered P4VP(MSA)(PDP) layers for $T < \text{ca. } 150^\circ\text{C}$. C. Cylinders of P4VP(MSA)_{1.0} inside a matrix consisting of a homogeneous mixture of PS and PDP. Note that for $T > \text{ca. } 175^\circ\text{C}$, part of the PDP will diffuse back in the P4VP(MSA)_{1.0} cylinders due to the phenomenon of reappearing phases (cf. Fig. 19). In principle, this may give rise to a reappearing lamellar structure, for which some indications are present. Electrical conductivity (σ) of PS-*b*-P4VP(MSA)_{1.0}(PDP)_{1.0} is indicated during heating with $5^\circ\text{C}/\text{min}$, on the basis of ac impedance measurements extrapolated to zero frequency. Similar data are observed during cooling. Note that the order-disorder transition in the P4VP(MSA)(PDP) layers at ca. 100°C and the order-order transition at ca. 150°C are distinctively present in the conductivity.

were ordered macroscopically, as in many cases can be achieved by applying an oscillatory shear field [37], the ODT is expected to be reflected in the conductivity, which would then be anisotropic.

A different situation arises when order-order transitions (OOTs) occur. For one specific system, Ikkala and ten Brinke et al. demonstrated a strong correlation between the conductivity and the nature of the ordered state [18]. This was accomplished by “confining” the P4VP(MSA)_{1.0}(PDP)_{1.0} system, discussed in Section 3.1, between polystyrene layers. Diblock copolymers of polystyrene and poly(4-vinyl pyridine) (PS-*b*-P4VP) were combined with MSA and PDP to give rise to supramolecular comb-coil diblock copolymer molecules PS-*b*-P4VP(MSA)_{1.0}(PDP)_{1.0}; see Figure 17c. This system has a lamellar-inside-lamellar morphology of alternating PS layers and layers consisting of alternating one-dimensional slabs of the polysalt P4VP(MSA)_{1.0} and PDP at temperatures up to ca. 100°C (Fig. 44) [18]. The corresponding long periods are ca. 350 \AA and ca. 48 \AA . At around 100°C , an order-disorder transition takes place, where the short-length-scale order vanishes and disordered P4VP(MSA)(PDP) layers appear. The corresponding “unconfined” homopolymer system P4VP(MSA)_{1.0}(PDP)_{1.0}, discussed in Section 3.1, macrophase-separates at ca. 170°C (Fig. 19) due to the fact that most hydrogen bonds are broken. In the present case, the P4VP(MSA)(PDP)

layers are confined in between PS layers and, because PDP happens to be miscible with PS for $T > \text{ca. } 135^\circ\text{C}$, the expulsion of PDP from the P4VP(MSA)_{1.0} phase “pushes” the PDP molecules into the PS phase. As a consequence, the volume fraction of the PS phase increases considerably and an order-order transition to a cylindrical structure consisting of P4VP(MSA)_{1.0} cylinders inside a homogeneous PS/PDP matrix takes place at ca. 150°C ; see Figure 44 [18].

This series of transitions implies that the conductive domains, where the conductive species consists of the polysalt P4VP(MSA)_{1.0}, undergo a sequence of dimensionality transitions: one-dimensional slabs ($T < \text{ca. } 100^\circ\text{C}$) → two-dimensional layers ($T < \text{ca. } 150^\circ\text{C}$) → one-dimensional cylinders. The conductive domains are insulated from each other by insulating PS and/or PDP material. This implies that, as a function of temperature, locally the conductivity first occurs in one direction only, then in two directions, and, finally, again in one direction. Since no effort was taken to macroscopically orient these samples, the macroscopically isotropic grain boundary domain structure makes it impossible to observe the local anisotropy in conductivity. Nevertheless, as shown in Figure 44, the dimensionality transitions are manifestly present in the macroscopic conductivity, the two-dimensional conducting layers giving rise to a higher conductivity than either of the two one-dimensional conducting domain structures. This example shows that control of the microstructure allows a means to control the conductivity.

4. CONCLUDING REMARKS

The examples discussed in this review demonstrate that a combination of self-organization and supramolecular assembly is one of the most fruitful ways to achieve nanostructured materials with potentially externally controllable functionalities, notably electroactivity. Supramolecular comb copolymer-like structures are frequently involved, the simplest ones having been obtained by complexing (block co-) polymers with amphiphiles. In the case of semiflexible conjugated polymers, such as polyaniline or poly(*p*-pyridine), the “side chains” induce the necessary processibility. For both flexible and semiflexible polymers alike, the comb copolymer nature gives rise to self-organized nanostructures with the functional domains being spherical, cylindrical, lamellar, or continuous. However, the anisotropy of the structures can only be fully exploited once the system, e.g., a thin film, is macroscopically oriented. Here several options are available such as imposing an oscillatory shear flow or an electric field. For thin films, the latter seems most promising and we expect to see many new applications in the near future.

Such systems generally exhibit complex phase behavior involving order-order and order-disorder transitions. With respect to the functional domains, these transitions frequently correspond to dimensionality transitions, which, if induced by external means, lead to externally controllable functional (electroactive) materials. In this review, this principle was illustrated using a complex ionically conducting supramolecular comb-coil diblock copolymer with temperature being the external control parameter.

Acknowledgments

The authors gratefully acknowledge collaboration and discussions with Janne Ruokolainen, Matti Knaapila, Mika Saariaho, Riikka

Mäkinen, Mika Torkkeli, Kaija Jokela, Ritva Serimaa, Cor Luyten, Tapio Mäkelä, Heikki Isotalo, Gerd Alberda, Henk Angerman, June Huh, Elena Dormidontova, Karen de Moel, Ernie Komanschek, Edwin Thomas, Andy Monkman, Lochart Horsburgh, Matti Jussila, Jan-Erik Österholm, Toivo Kärnä, Jukka Laakso, Pauli Kirmanen, Juha Hartikainen, and Hannele Eerikäinen. The work was supported by the Technology Development Centre of Finland, Academy of Finland, and the Organization of Scientific Research of the Netherlands (NWO).

REFERENCES

- C. J. Drury, C. M. J. Mutsaers, C. M. Hart, M. Matters, and D. M. de Leeuw, *Appl. Phys. Lett.* 73, 108 (1998).
- K. Ziemelis, *Nature* 393, 619 (1998).
- J. N. Israelachvili, "Intermolecular and Surface Forces." Academic Press, London, 1985.
- M. Muthukumar, C. K. Ober, and E. L. Thomas, *Science* 277, 1225 (1997).
- R. G. Laughlin, "The Aqueous Phase Behavior of Surfactants." Academic Press, San Diego, 1994.
- I. W. Hamley, "The Physics of Block Copolymers." Oxford Univ. Press, Oxford, 1998.
- G. Zubay, "Biochemistry." Brown, Dubuque, IA, 1993.
- F. S. Bates and G. H. Fredrickson, *Annu. Rev. Phys. Chem.* 41, 525 (1990).
- M. Park, C. Harrison, P. M. Chaikin, R. A. Register, and D. H. Adamson, *Science* 276, 1401 (1997).
- R. P. Andres, T. Bein, M. Dorogi, S. Feng, J. I. Henderson, C. P. Kubiak, W. Mahoney, R. G. Osifchin, and R. Reifengerger, *Science* 272, 1323 (1996).
- L. Y. Gorelik, A. Isacson, M. V. Voinova, B. Kasemo, R. I. Shekhter, and M. Jonson, *Phys. Rev. Lett.* 80, 4526 (1998).
- A. Aoki, M. Nakaya, and T. Miyashita, *Macromolecules* 31, 7321 (1998).
- J.-M. Lehn, "Supramolecular Chemistry." VCH, Weinheim, 1995.
- F. Vögtle, "Supramolecular Chemistry." Wiley, Chichester, 1993.
- S. I. Stupp, V. LeBonheur, K. Walker, L. S. Li, K. E. Huggins, M. Keser, and A. Amstutz, *Science* 276, 384 (1997).
- M. Antonietti, C. Burger, and A. Thünemann, *Trends Polym. Sci.* 5, 262 (1997).
- G. ten Brinke and O. Ikkala, *Trends Polym. Sci.* 5, 213 (1997).
- J. Ruokolainen, R. Mäkinen, M. Torkkeli, R. Serimaa, T. Mäkelä, G. ten Brinke, and O. Ikkala, *Science* 280, 557 (1998).
- T. A. Skotheim, R. L. Elsenbaumer, and J. R. Reynolds, Eds., "Handbook of Conducting Polymers." Dekker, New York, 1998.
- F. M. Gray, "Polymer Electrolytes." Royal Soc. Chem., Cambridge, UK, 1997.
- E. Smela, O. Inganäs, and I. Lundström, *Science* 268, 1735 (1995).
- M. Ferreira and M. F. Rubner, *Macromolecules* 28, 7107 (1995).
- A. C. Fou and M. F. Rubner, *Macromolecules* 28, 7115 (1995).
- J. N. Barisci, C. Conn, and G. G. Wallace, *Trends Polym. Sci.* 4, 307 (1996).
- G. G. Wallace, G. M. Spinks, and P. R. Teasdale, "Conductive Electroactive Polymers: Intelligent Materials Systems." Technomic, Lancaster, 1997.
- D. B. Amabilino, O. Diedrich-Buchecker, A. Livoreil, L. Pérez-García, J.-P. Sauvage, and J. F. Stoddart, *J. Am. Chem. Soc.* 118, 3905 (1994).
- P. R. Ashton et al., *J. Am. Chem. Soc.* 120, 11932 (1998).
- C. P. Collier, E. W. Wong, M. Belohradský, F. M. Raymo, J. F. Stoddart, P. J. Kuekes, R. S. Williams, and J. R. Heath, *Science* 285, 391 (1999).
- E. D. Goddard, *Colloids Surf.* 19, 301 (1986).
- E. D. Goddard, *Colloids Surf.* 19, 255 (1986).
- K. Tsujii, "Surface Activity: Principles, Phenomena, and Applications." Academic Press, San Diego, 1998.
- M. Daoud and C. E. Williams, "Soft Matter Physics." Berlin, 1999.
- M. J. Vold, *J. Am. Chem. Soc.* 63, 1427 (1941).
- I. D. Robb, "Specialist Surfactants." London, 1997.
- G. M. Whitesides, *Sci. Am.* 273, 146 (1995).
- A. Ulman, "An Introduction to Ultrathin Organic Films from Langmuir-Blodgett to Self-Assembly." Academic Press, San Diego, 1991.
- G. H. Fredrickson and F. S. Bates, *Annu. Rev. Mater. Sci.* 26, 501 (1996).
- M. Saariaho, A. Subbotin, O. Ikkala, and G. ten Brinke, *Makromol. Chem., Rapid Commun.*, in press.
- P.-G. de Gennes, "Scaling Concepts in Polymer Physics." Cornell Univ. Press, Ithaca, NY, 1979.
- P. J. Flory, "Principles of Polymer Chemistry." Cornell Univ. Press, Ithaca, NY, 1971.
- L. Leibler, *Macromolecules* 13, 1602 (1980).
- D. A. Hajduk, H. Takenouchi, M. A. Hillmyer, F. S. Bates, M. E. Viggild, and K. Almdal, *Macromolecules* 30, 3788 (1997).
- S. Qi and Z.-G. Wang, *Phys. Rev. E* 55, 1682 (1997).
- K. Almdal, K. A. Koppi, F. S. Bates, and K. Mortensen, *Macromolecules* 25, 1743 (1992).
- A. K. Khandpur, S. Förster, F. S. Bates, I. W. Hamley, W. Bras, K. Almdal, and K. Mortensen, *Macromolecules* 28, 8796 (1995).
- S. Sioula, Y. Tselikas, and N. Hadjichristidis, *Macromol. Symp.* 167 (1997).
- J. E. L. Roovers, *Polymer* 16, 827 (1975).
- M. Wintermantel, K. Fischer, M. Gerle, R. Ries, M. Schmidt, K. Kajiwara, H. Urakawa, and I. Wataoka, *Angew. Chem., Int. Ed. Engl.* 34, 1472 (1995).
- V. Percec, C.-H. Ahn, G. Ungar, D. J. P. Yearley, M. Möller, and S. Sheiko, *Nature* 391, 161 (1998).
- S. Förster, I. Neubert, A. D. Schlüter, and P. Lindner, *Macromolecules* 32, 4043 (1999).
- H. Hashimoto, M. Fujimara, T. Hashimoto, and H. Kawai, *Macromolecules* 14, 844 (1981).
- B. Chu and C. Wu, in "Polymer Materials Encyclopedia" (J. C. Salamone, Ed.), p. 8141. CRC Press, Boca Raton, FL, 1996.
- G. H. Fredrickson and F. S. Bates, *J. Polym. Sci., Polym. Phys. Ed.* 35, 2775 (1997).
- J. T. Chen, E. L. Thomas, C. K. Ober, and G.-P. Mao, *Science* 273, 343 (1996).
- H. Fischer and S. Poser, *Acta Polym.* 47, 413 (1996).
- S. Jenekhe and X. L. Chen, *Science* 283, 372 (1999).
- V. Francke, H. J. Räder, Y. Geerts, and K. Müllen, *Makromol. Chem., Rapid Commun.* 19, 275 (1998).
- J. Adams and W. Gronski, *Makromol. Chem., Rapid Commun.* 10, 553 (1989).
- H. Fischer, S. Poser, and M. Arnold, *Macromolecules* 28, 6957 (1995).
- G. Mao and C. K. Ober, *Acta Polym.* 48, 405 (1997).
- G. Galli, *Macromol. Symp.* 109 (1997).
- R. Zentel, G. Galli, and C. K. Ober, "NATO Advanced Research Workshop: Manipulation in Polymers Using Tandem Molecular Interactions, 1997."
- M. Ballauff, *Makromol. Chem., Rapid Commun.* 7, 407 (1986).
- M. Ballauff, *Angew. Chem., Int. Ed. Engl.* 28, 253 (1989).
- G. Wegner, *Thin Solid Films* 216, 105 (1992).
- U. Lauter, W. H. Meyer, and G. Wegner, *Macromolecules* 30, 2092 (1997).
- R. Stadler, C. Auschra, J. Beckmann, U. Krappe, I. Voight-Martin, and L. Leibler, *Macromolecules* 28, 3080 (1995).
- F. S. Bates and G. H. Fredrickson, *Phys. Today* 52, 32 (1999).
- U. Breiner, U. Krappe, E. L. Thomas, and R. Stadler, *Macromolecules* 31, 135 (1998).
- M. C. T. Fyfe and J. F. Stoddart, *Acc. Chem. Res.* 30, 393 (1997).

71. J.-H. Fuhrhop and J. Köning, "Membranes and Molecular Assemblies." Royal Soc. Chem., Cambridge, UK, 1994.
72. D. B. Amabilino, I. W. Parsons, and J. F. Stoddart, *Trends Polym. Sci.* 1994, 146 (1994).
73. P. R. Ashton, V. Balzani, J. Becher, A. Credi, M. C. T. Fyfe, G. Matternsteig, S. Menzer, M. B. Nielsen, F. M. Raymo, J. F. Stoddart, M. Venturi, and D. J. Williams, *J. Am. Chem. Soc.* (1999).
74. M.-J. Brienne, J. Gabard, J.-M. Lehn, and I. Stibor, *J. Chem. Soc., Chem. Commun.* 24, 1868 (1989).
75. R. P. Sijbesma, F. H. Beijer, L. Brunsveld, B. J. B. Folmer, J. H. K. K. Hirschberg, R. F. M. Lange, J. K. L. Lowe, and E. W. Meijer, *Science* 278, 1601 (1997).
76. T. Kato and J. M. J. Fréchet, *Macromolecules* 22, 3818 (1989).
77. T. Kato, M. Nakano, T. Moteki, T. Uryu, and S. Ujiie, *Macromolecules* 28, 8875 (1995).
78. C. G. Bazuin and A. Tork, *Macromolecules* 28, 8877 (1995).
79. D. Navarro-Rodriguez, D. Guillon, and A. Skoulios, *Makromol. Chem.* 193, 3117 (1992).
80. J.-M. Lehn, M. Mascal, A. DeCian, and J. Fischer, *J. Chem. Soc., Chem. Commun.* 479 (1990).
81. J. Rebek, *Top. Curr. Chem.* 149, 189 (1988).
82. J. Ruokolainen, G. ten Brinke, and O. T. Ikkala, *Adv. Mater.* 11, 777 (1999).
83. S. I. Stupp, M. Keser, and G. N. Tew, *Polymer* 39, 4505 (1998).
84. E. R. Zubarev, M. U. Pralle, L. Li, and S. I. Stupp, *Science* 283, 523 (1999).
85. S. I. Stupp, G. N. Tew, and C. M. Whitaker, in "Hyperstructured Molecules I: Chemistry, Physics and Applications" (H. Sasabe, Ed.), p. 9. Gordon & Breach, Amsterdam, 1999.
86. J. I. Kroschwitz, in "High Performance Polymers and Composites." New York, 1991.
87. M. Antonietti, J. Conrad, and A. Thünemann, *Macromolecules* 27, 6007 (1994).
88. M. Antonietti, C. Burger, and J. Effing, *Adv. Mater.* 7, 751 (1995).
89. O. Ikkala, J. Ruokolainen, G. ten Brinke, M. Torkkeli, and R. Serimaa, *Macromolecules* 28, 7088 (1995).
90. R. V. Tal'roze, S. A. Kuptsov, T. I. Sycheva, V. S. Bezborodov, and N. A. Platé, *Macromolecules* 28, 8689 (1995).
91. R. V. Tal'roze, S. A. Kuptsov, T. I. Sycheva, G. Shandryuk, and N. A. Platé, *Polym. Mater. Sci. Eng.* 72, 431 (1995).
92. M. Antonietti, A. Wenzel, and A. Thünemann, *Langmuir* 12, 2111 (1996).
93. M. Antonietti, C. Burger, J. Conrad, and A. Kaul, *Macromol. Symp.* 106, 1 (1996).
94. D. Tsiourvas, M. Arkas, C. M. Paleos, and A. Skoulios, *Polym. Prepr.* 38, 233 (1997).
95. E. A. Ponomarenko, D. A. Tirrel, and W. J. MacKnight, *Macromolecules* 31, 1584 (1998).
96. R. V. Tal'roze and N. A. Platé, *Polym. Sci.* 36, 1479 (1994).
97. H.-L. Chen and M.-S. Hsiao, *Macromolecules* 32, 2967 (1999).
98. M. Antonietti, S. Henke, and A. Thünemann, *Adv. Mater.* 8, 41 (1996).
99. C. K. Ober and G. Wegner, *Adv. Mater.* 9, 17 (1997).
100. W.-Y. Zheng, R.-H. Wang, K. Levon, Z. Y. Rong, T. Taka, and W. Pan, *Macromol. Chem. Phys.* 196, 2443 (1995).
101. W. Wernet, M. Monkenbusch, and G. Wegner, *Makromol. Chem., Rapid Commun.* 1, 151 (1984).
102. G. Wegner and J. Rühle, *Faraday Discuss. Chem. Soc.* 88, 333 (1989).
103. M. C. M. van der Sanden, C. Y. Yang, P. Smith, and A. J. Heeger, *Synth. Met.* 78, 47 (1996).
104. A. F. Thunemann and K. H. Lochhaas, *Langmuir* 14, 4898 (1998).
105. L. Piculell, B. Lindman, and G. Karlström, in "Polymer Surfactant Systems" (J. T. C. Kwak, Ed.), p. 65. Dekker, New York/Basel/Hong Kong, 1998.
106. C. G. Bazuin and F. A. Brandys, *Chem. Mater.* 4, 970 (1992).
107. U. Kumar, T. Kato, and J. M. J. Fréchet, *J. Am. Chem. Soc.* 114, 6630 (1992).
108. J. Ruokolainen, J. Tanner, G. ten Brinke, O. Ikkala, M. Torkkeli, and R. Serimaa, *Macromolecules* 28, 7779 (1995).
109. F. Motamedi, *Liq. Cryst.* 22, 749 (1997).
110. A. Hargreaves, *Acta Cryst.* 10, 191 (1957).
111. J. M. Broomhead and A. D. I. Nicol, *Acta Cryst.* 1, 88 (1947).
112. O. Ikkala, J. Ruokolainen, M. Torkkeli, R. Serimaa, and G. ten Brinke, *Makromol. Chem., Macromol. Symp.* 112, 191 (1996).
113. T. Kärnä, J. Laakso, T. Niemi, H. Ruohonen, E. Savolainen, H. Lindström, E. Virtanen, O. Ikkala, and A. Andreatta, U.S. Patent 5,340,499, 1994.
114. J. Ruokolainen, M. Torkkeli, R. Serimaa, E. Komanschek, O. Ikkala, and G. ten Brinke, *Phys. Rev. E* 54, 6646 (1996).
115. J. Ruokolainen, M. Torkkeli, R. Serimaa, S. Vahvaselkä, M. Saariaho, G. ten Brinke, and O. Ikkala, *Macromolecules* 29, 6621 (1996).
116. J. Ruokolainen, M. Torkkeli, R. Serimaa, E. B. Komanschek, G. ten Brinke, and O. Ikkala, *Macromolecules* 30, 2002 (1997).
117. J. Ruokolainen, J. Tanner, O. Ikkala, G. ten Brinke, and E. L. Thomas, *Macromolecules* 31, 3532 (1998).
118. I. Akiba and S. Akiyama, *Macromolecules* 32, 3741 (1999).
119. L. C. Cesteros, E. Meaurio, and I. Katime, *Macromolecules* 26, 2323 (1993).
120. F. A. Brandys and C. G. Bazuin, *Chem. Mater.* 8, 83 (1996).
121. T. Kato, H. Kihara, T. Uryu, A. Fujishima, and J. M. J. Fréchet, *Macromolecules* 25, 6836 (1992).
122. J. Ruokolainen, G. ten Brinke, O. Ikkala, M. Torkkeli, and R. Serimaa, *Macromolecules* 29, 3409 (1996).
123. P.-G. de Gennes, "Scaling Concepts in Polymer Physics." Cornell Univ. Press, Ithaca, NY, 1979.
124. J. Huh, O. Ikkala, and G. ten Brinke, *Macromolecules* 30, 1828 (1997).
125. J. Huh, O. Ikkala, and G. ten Brinke, *Macromol. Symp.* 121, 123 (1997).
126. M. C. Luyten, G. O. R. Alberda van Ekenstein, G. ten Brinke, J. Ruokolainen, O. Ikkala, M. Torkkeli, and R. Serimaa, *Macromolecules*, to appear.
127. E. Dormidontova and G. ten Brinke, *Macromolecules* 31, 2649 (1998).
128. F. Tanaka and M. Ishida, *Macromolecules* 30, 1836 (1997).
129. H. Benoit and G. Hadziioannou, *Macromolecules* 21, 1449 (1988).
130. A. V. Dobrynin and I. Y. Erukhimovich, *Macromolecules* 276 (1993).
131. M. C. Luyten, G. O. R. Alberda van Ekenstein, J. Wildeman, G. ten Brinke, J. Ruokolainen, O. Ikkala, M. Torkkeli, and R. Serimaa, *Macromolecules* 31, 9160 (1998).
132. R. Zentel and M. Benalia, *Makromol. Chem.* 188, 665 (1987).
133. X. Wang, *J. Polym. Sci., Polym. Phys. Ed.* 37, 667 (1999).
134. J. Ruokolainen, M. Saariaho, O. Ikkala, G. ten Brinke, E. L. Thomas, M. Torkkeli, and R. Serimaa, *Macromolecules* 32, 1152 (1999).
135. O. Ikkala, J. Ruokolainen, R. Mäkinen, M. Torkkeli, R. Serimaa, T. Mäkelä, and G. ten Brinke, *Synth. Met.* 102, 1498 (1999).
136. J. H. Lupinsky, K. Kopple, and J. J. Hertz, *J. Polym. Sci., Symp. Ed.* 16, 1561 (1967).
137. M. Audenaert, G. Gusman, M. Mehbod, R. Deltour, B. Noirhomme, and E. Vander Donckt, *Solid State Commun.* 30, 797 (1979).
138. J. S. Walker and C. A. Vause, *Sci. Am.* 256, 90 (1987).
139. I. C. Sanchez, *Macromolecules* 24, 908 (1991).
140. C. C. Leznoff, in "Phtalocyanines: Properties and Applications." New York, 1989-1993.
141. M. Hanack and M. Lang, *Adv. Mater.* 6, 819 (1994).
142. F. Fernández-Lázaro, T. Torres, B. Hauschel, and M. Hanack, *Chem. Rev.* 98, 563 (1998).
143. C. F. van Nostrum and R. J. M. Nolte, *Makromol. Chem., Macromol. Symp.* 77, 267 (1994).
144. C. F. van Nostrum, S. J. Picken, S. A.-J., and R. J. M. Nolte, *J. Am. Chem. Soc.* 117, 9957 (1995).
145. H. Eichhorn, D. W. Bruce, and D. Wöhrle, *Adv. Mater.* 10, 419 (1998).
146. D. M. Knawby and T. M. Swager, *Chem. Mater.* 9, 535 (1997).
147. O. E. Sielcken, L. A. van de Kuil, W. Drenth, J. Schoonman, and R. J. M. Nolte, *J. Am. Chem. Soc.* 112, 3086 (1990).

148. A. M. van de Craats, J. M. Warman, K. Müllen, Y. Geerts, and J. D. Brand, *Adv. Mater.* 10, 36 (1998).
149. J. Majnusz, J. M. Catala, and R. W. Lenz, *Eur. Polym. J.* 19, 1043 (1983).
150. W. R. Krigbaum, H. Hakemi, and R. Kotek, *Macromolecules* 18, 965 (1985).
151. H. Menzel, in "Polymer Materials Encyclopedia" (J. C. Salamone, Ed.), p. 2916. CRC Press, Boca Raton, FL, 1996.
152. M. Wenzel, M. Ballauff, and G. Wegner, *Makromol. Chem.* 188, 2865 (1987).
153. M. Ballauff and G. F. Schmidt, *Makromol. Chem., Rapid Commun.* 8, 93 (1987).
154. S. D. D. V. Rughooputh, S. Hotta, A. J. Heeger, and F. Wudl, *J. Polym. Sci., Polym. Phys. Ed.* 25, 1071 (1987).
155. H. P. Siringhaus, J. Brown, R. H. Friend, M. M. Nielsen, K. Bechgaard, B. M. W. Langeveld-Voss, A. J. H. Spiering, R. A. J. Janssen, E. W. Meijer, P. Herwig, and D. M. de Leeuw, *Nature* 401, 685 (1999).
156. K. Y. Jen, G. G. Miller, and R. L. Elsenbaumer, *J. Chem. Soc., Chem. Commun.* 1346 (1986).
157. S. Hotta, S. D. D. V. Rughooputh, and A. J. Heeger, *Synth. Met.* 22, 79 (1987).
158. K. Yoshino, S. Nakajima, and R.-I. Sugimoto, *Jpn. J. Appl. Phys.* 6, L2046 (1987).
159. O. Inganäs, *Trends Polym. Sci.* 2, 189 (1994).
160. G. Gustafsson, O. Inganäs, W. R. Salaneck, J. Laakso, M. Lopenen, T. Taka, J.-E. Österholm, H. Stubb, and T. Hjertberg, in "Conjugated Polymers" (J. L. Brédas and R. Silbey, Eds.), p. 315. Kluwer Academic, Dordrecht, 1991.
161. T. J. Prosa, M. J. Winokur, J. Moulton, P. Smith, and A. J. Heeger, *Macromolecules* 25, 4364 (1992).
162. S.-A. Chen and J.-M. Ni, *Macromolecules* 25, 6081 (1992).
163. X. Chen and O. Inganäs, *Synth. Met.* 74, 159 (1995).
164. J. Ruokolainen, M. Törkkeli, K. Levon, R. Serimaa, G. ten Brinke, and O. Ikkala, unpublished manuscript.
165. K. C. Park and K. Levon, *Macromolecules* 30, 3175 (1997).
166. R. Qian, S. Chen, W. Song, and X. Bi, *Makromol. Chem., Rapid Commun.* 15, 1 (1994).
167. T. Bjoernholm, D. R. Greve, N. Reitzel, T. Hassenkam, K. Kjaer, P. B. Howes, N. B. Larsen, J. Boegelund, M. Jayaraman, P. C. Ewbank, and R. D. McCullough, *J. Am. Chem. Soc.* 120, 7643 (1998).
168. M. Sato, S. Tanaka, and K. Kaeriyama, *J. Chem. Soc., Chem. Commun.* 873 (1986).
169. A. Fizazi, J. Moulton, K. Pakbaz, S. D. D. V. Rughooputh, P. Smith, and A. J. Heeger, *Phys. Rev. Lett.* 64, 2180 (1990).
170. K. Levon, E. Chu, K.-S. Ho, T. K. Kwei, J. Mao, W.-Y. Zheng, and J. Laakso, *J. Polym. Sci., Polym. Phys. Ed.* 33, 537 (1995).
171. Y. Wang and M. F. Rubner, *Macromolecules* 25, 3284 (1992).
172. K. Yoshino, S. Nakajima, M. Onoda, and R. Sugimoto, *Synth. Met.* 28, C349 (1989).
173. J. L. Brédas and R. Silbey, Eds., "Conjugated Polymers." Kluwer Academic, Dordrecht, 1991.
174. M. Andersson, Q. Pei, T. Hjertberg, O. Inganäs, O. Wennerström, and J.-E. Österholm, *Synth. Met.* 55, 1227 (1993).
175. T. F. McCarthy, H. Witteler, T. Pakula, and G. Wegner, *Macromolecules* 28, 8350 (1995).
176. T. Vahlenkamp and G. Wegner, *Macromol. Chem. Phys.* 195, 1933 (1994).
177. Y. Wei, W. W. Focke, G. E. Wnek, A. Ray, and A. G. MacDiarmid, *J. Phys. Chem.* 93, 495 (1989).
178. W.-Y. Zheng, K. Levon, T. Taka, J. Laakso, and J.-E. Österholm, *J. Polym. Sci., Polym. Phys. Ed.* 33, 1289 (1994).
179. W.-Y. Zheng, K. Levon, J. Laakso, and J.-E. Österholm, *Macromolecules* 27, 7754 (1994).
180. B. Hauschel, P. Stihler, and M. Hanack, *Trends Polym. Sci.* 4, 348 (1996).
181. D. A. P. Delnoye, R. P. Sijbesma, J. A. J. M. Vekemans, and E. W. Meijer, *J. Am. Chem. Soc.* 118, 8717 (1996).
182. M. Moroni, J. Le Moigne, T. A. Pham, and J.-Y. Bigot, *Macromolecules* 30, 1964 (1997).
183. P. J. Flory, *Adv. Polym. Sci.* 59, 1 (1984).
184. M. Ballauff, *J. Polym. Sci., Part B: Polym. Phys.* 25, 739 (1987).
185. S. J. Krause, T. B. Haddock, G. E. Price, and W. W. Adams, *Polymer* 29, 195 (1988).
186. A. Ciferri, *Polym. Eng. Sci.* 34, 377 (1994).
187. Y. Cao, P. Smith, and A. J. Heeger, *Synth. Met.* 48, 91 (1992).
188. Y. Cao, P. Smith, and A. J. Heeger, U.S. Patent 5,232,631, 1993.
189. A. J. Heeger, *Trends Polym. Sci.* 3, 39 (1995).
190. C. Y. Yang, Y. Cao, P. Smith, and A. J. Heeger, *Synth. Met.* 53, 293 (1993).
191. J.-C. Chiang and A. G. MacDiarmid, *Synth. Met.* 13, 193 (1986).
192. W. R. Salaneck, I. Lundström, W.-S. Huang, and A. G. MacDiarmid, *Synth. Met.* 13, 291 (1986).
193. M. Doriomedoff, F. Hautiere-Cristofini, R. D. Surville, M. Jozefowicz, L.-T. Yu, and R. Buvet, *J. Chim. Phys.-Chim. Biol.* 68, 1055 (1971).
194. O. T. Ikkala, L.-O. Pietilä, L. Ahjopalo, H. Österholm, and P. J. Passiniemi, *J. Chem. Phys.* 103, 9855 (1995).
195. M. R. Majidi, L. A. P. Kane-Maguire, and G. G. Wallace, *Polymer* 35, 3113 (1994).
196. C. Y. Yang, P. Smith, A. J. Heeger, Y. Cao, and J.-E. Österholm, *Polymer* 35, 1142 (1994).
197. G. Wegner, *Makromol. Chem., Macromol. Symp.* 1, 151 (1986).
198. A. Kobayashi, X. Xu, H. Ishikawa, M. Satoh, and E. Hasegawa, *J. Appl. Phys.* 72, 5702 (1992).
199. P. J. Kinlen, J. Liu, Y. Ding, C. R. Graham, and E. E. Remsen, *Macromolecules* 31, 1755 (1998).
200. Y. Cao, J. Qiu, and P. Smith, *Synth. Met.* 69, 187 (1995).
201. A. G. MacDiarmid and A. J. Epstein, *Synth. Met.* 65, 103 (1994).
202. K. Levon, K.-H. Ho, W.-Y. Zheng, J. Laakso, T. Kärnä, T. Taka, and J.-E. Österholm, *Polymer* 36, 2733 (1995).
203. T. Kärnä, J. Laakso, K. Levon, and E. Savolainen, U.S. Patent 5,928,565, 1999.
204. A. R. Hopkins, P. G. Rasmussen, and R. A. Basheer, *Macromolecules* 29, 7838 (1996).
205. A. R. Hopkins, P. G. Rasmussen, R. A. Basheer, B. K. Annis, G. D. Wignall, and W. A. Hamilton, *Synth. Met.* 97, 47 (1996).
206. I. Kulszewicz-Bajer, I. Wielgus, A. Pron, and P. Rannou, *Macromolecules* 30, 7091 (1997).
207. T. Vikki, J. Ruokolainen, O. T. Ikkala, P. Passiniemi, H. Isotalo, M. Törkkeli, and R. Serimaa, *Macromolecules* 30, 4046 (1997).
208. O. Ikkala, M. Tiitu, J. Tanner, and J. Ruokolainen, *Synth. Met.* 102, 1248 (1999).
209. O. Ikkala, L.-O. Pietilä, Y. Cao, and A. Andreatta, U.S. Patent 5,783,111, 1998.
210. O. Ikkala and P. J. Passiniemi, U.S. Patent 5,520,852, 1996.
211. O. Ikkala, M. Knaapila, J. Ruokolainen, M. Törkkeli, R. Serimaa, K. Jokela, L. Horsburgh, A. P. Monkman, and G. ten Brinke, *Adv. Mater.* 11, 1206 (1999).
212. O. T. Ikkala, L.-O. Pietilä, P. J. Passiniemi, T. Vikki, H. Österholm, L. Ahjopalo, and J.-E. Österholm, *Synth. Met.* 84, 55 (1997).
213. O. T. Ikkala, J. Laakso, K. Väkiparta, E. Virtanen, H. Ruohonen, H. Järvinen, T. Taka, P. Passiniemi, J.-E. Österholm, Y. Cao, A. Andreatta, P. Smith, and A. J. Heeger, *Synth. Met.* 69, 97 (1995).
214. P. Passiniemi, J. Laakso, H. Österholm, and M. Pohl, *Synth. Met.* 84, 775 (1997).
215. T. Yamamoto, T. Maruyama, Z.-H. Zhou, T. Ito, T. Kanbara, M. Hishinuma, and K. Kubota, *Synth. Met.* 41-43, 1587 (1991).
216. T. Yamamoto, T. Maruyama, Z.-H. Zhou, T. Ito, T. Fukuda, Y. Yoneda, F. Begum, T. Ikeda, S. Sasaki, H. Takezoe, A. Fukuda, and K. Kubota, *J. Am. Chem. Soc.* 116, 4832 (1994).

SPECTROELECTROCHEMISTRY OF CONDUCTING POLYMERS

Rudolf Holze

Technische Universität Chemnitz, Institut für Chemie, D-09107 Chemnitz, Germany

Contents

1. Introduction	209
2. Spectroelectrochemistry: An Introduction	211
2.1. Fundamentals	211
2.2. Spectroscopy at Surfaces	211
2.3. Spectroelectrochemistry	211
3. Polyaniline and Related Polymers	217
3.1. Formation of Polyaniline and Related Polymers	218
3.2. Properties of Polyaniline and Related Polymers and their Electrochemically Induced Changes	227
3.3. Redox Processes of Polyaniline and Polymers of Substituted Anilines	251
3.4. Redox Processes and Electrocatalysis at Polyaniline and Related Polymers	252
3.5. Degradation of Polymers	254
4. Polypyrrole and Related Polymers	256
4.1. Formation of Polypyrrole and Related Polymers	257
4.2. Properties of Polypyrrole and Related Polymers and their Electrochemically Induced Changes	258
4.3. Degradation of Polypyrrole and Related Polymers	265
5. Polythiophene and Related Polymers	266
5.1. Formation of Polythiophene and Related Polymers	267
5.2. Properties of Polythiophene and Related Polymers and their Electrochemically Induced Changes	269
6. Miscellaneous Polymers	283
Appendix	284
Acknowledgments	286
References	286

1. INTRODUCTION

Intrinsically conducting polymers (ICP) are macromolecular substances with structural features that permit the transport of electrical charge, that is, that show electronic conductivity. The moving electronic charges (i.e., electrons or holes) set these polymers apart from ionic conductors (i.e., ion exchange polymers) and from so-called filled polymers. The latter substances are basically polymers with added conducting materials like graphite powder, carbon fibers, or finely dispersed metal particles. These materials show electronic conductivity values that range from poorly conductive substances to almost metallike conductivities. Typical values of the electrical resistance (the reciprocal of the conductivity)

are displayed in Figure 1. The broad range of values encompassed by the conducting polymers and the possibility to change these values within this range by chemical or electrochemical manipulations are particularly noteworthy. In addition to these materials and the already well established filled resins (polymers), there are numerous crystalline organic conductors composed of mostly large organic ions that are arranged in the solid state in a way that enables electric charges to move along (charge transfer salts) (for a recent review, see [1]). In inorganic chemistry, only $(\text{SN})_x$ is known to exhibit metallike conductivity [2, 3]. These latter substances are not covered in this review.

The observed conductivities have suggested the use of the term “synthetic metals” as a general designation. Of course the actual

materials property	electrical conductivity $\Omega^{-1}\text{cm}^{-1}$		insulating
	electrostatically shielding	electrostatically conducting	
metals			
intr. cond. polymers			
metal-polym. blends			
acetylene bl. polym. blends			
other polym.-cond. blends			
resins			
spec. resistance Ωcm	10^{-4} 10^{-2} 10^0 10^2	10^4 10^6 10^8 10^{10}	10^{12} 10^{14}

Fig. 1. Typical values of electrical conductivities of materials and possible areas of application.

conductivity has some influence on the possible application as also indicated in Figure 1. Beyond the obvious use of these materials instead of traditional ones for electrostatic shielding [4, 5] or as a replacement for all sorts of wiring, ICPs have been suggested for a large number of other applications ranging from active components in batteries (see, e.g., [6]), fuel cells, or supercapacitors [7–12] to coatings in solar energy conversion systems to sensors [13, 14], as corrosion protection [15–19], molecular transistors, and nonlinear polymer devices [20, 21]. These applications have been turned into successful reality sometimes; in many cases, developments and investigations are still under way. Numerous reviews that focus either on selected classes of monomers (anilines, thiophenes, pyrroles, etc.) or on selected fields of application have been published [22–37].

ICPs can be prepared from a large number of organic monomers by chemical or electrochemical methods. Both approaches involve the oxidation of the educt by using either appropriate oxidants or the anode in an electrochemical cell. Except for polyacetylene, all monomers and their respective polymeric oxidation products contain heteroatoms like oxygen, nitrogen, and sulfur. Those monomers, which can be electropolymerized, always contain heteroatoms. A selection of parent compounds is depicted in Figure 2.

This review covers investigations of ICPs either prepared electrochemically or modified/investigated with electrochemical methods. With a few exceptions, most polymers prepared by electropolymerization are also studied with electrochemical methods. This is most likely due to the fact that electropolymerization results preferably in films that adhere to the electrode surface used as a substrate during polymerization. These samples—essentially polymer-coated modified electrodes—lend themselves to further investigations with said methods. On the contrary, chemical oxidation results preferably in powdery samples that are less suitable for electrochemical investigations. The experimental studies of these polymers make use of almost all kinds of electrochemical methods currently available. Unfortunately—and this has been known to electrochemists for a few decades—purely electrochemical methods provide only a rather general or macroscopic picture of the interface between electrolyte solutions and electrodes or of the species (films, adsorbates, etc.) present on the electrode sur-

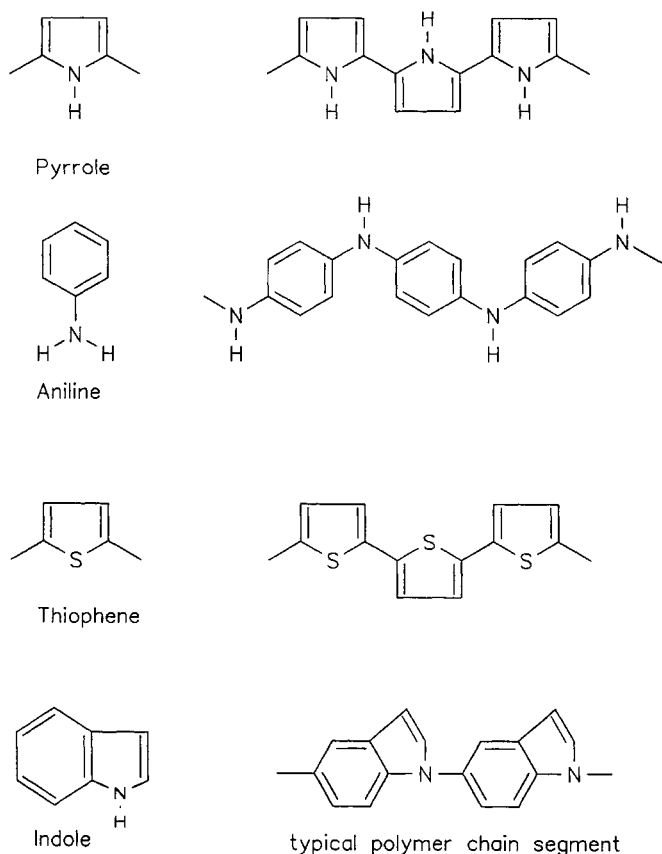


Fig. 2. Heteroatom that contains monomers of organic molecules that can be converted electrochemically into intrinsically conducting polymers.

face. Any information about the microscopic structure—the type and mode of interaction between the species on the electrode and the electrode itself—is difficult or impossible to obtain with these purely electrochemical (sometimes called classical) methods. The use of a number of spectroscopic and surface analytical methods in electrochemical investigations, in particular, when applied under *in situ* conditions, has greatly improved our knowledge and understanding of electrochemical interfaces and interphases. Although a small number of books contain reviews that cover various spectroscopic and surface analytical methods as applied to electrochemical problems [38, 39], the reader may not be familiar with all methods as applied to the investigation of ICPs. Consequently, this review starts with a brief introduction to these methods. Sometimes the family that includes these methods is called *spectroelectrochemistry*. The report given here does not attempt to provide a comprehensive evaluation of all published reports devoted to the almost innumerable aspects of these methods and fascinating materials. It is, instead, focussed on the results of experimental investigations obtained with a family of methods commonly designated “spectroelectrochemical methods.”

Following this overview of methods, the polymers grouped according to their parent compound are treated. This approach does not stress the importance of a single method; instead, the polymer under consideration is the focus of interest. Nevertheless, in the treatment of all polymers, the attempt is made to indicate the synergistic effects of spectroelectrochemical methods, in particular, when the use of more than one technique has resulted in com-

plementary results, which, in addition, support and confirm each other.

2. SPECTROELECTROCHEMISTRY: AN INTRODUCTION

The adaption of a large number of spectroscopic and surface scientific methods to electrochemical systems has resulted in an overwhelming wealth of experimental results that have helped to extend considerably our knowledge of structures and the dynamics of electrochemical interfaces and interphases. Whereas the former term refers to the immediate two-dimensional phase boundary, the latter term stresses the fact that in both adjacent phases, layers in close proximity to the actual phase boundary may be considerably different from the bulk of both phases. Consequently, a new term to describe this third phase in between the two bulk phases had to be coined. In the case of ICP, this aspect gains additional importance. Generally, electrochemical deposition of ICPs as treated in detail herein proceeds on the surface of an electron-conducting material (in rare exceptions, the substrate may be a hole-conducting p-doped semiconductor). This material (the electrode) provides the sink for the electrons released during oxidation of the monomer: it provides a support for the deposition of the polymer. Any other property of the electrode is, in most cases, of no interest. The interest of the investigator (and perhaps the user later on) is focussed on the polymer layer, which forms a new phase at the interface. Because of the strong interaction between the film and the electrolyte solution (in most cases the formed films are polymeric and contain considerable amounts of electrolyte solution) and the less intense interaction with the supporting electrode, this interphase has to be considered and studied while always keeping in mind the presence of the other adjacent phases and their respective properties.

A number of reviews that cover selected methods, families of related methods, or studies of usually narrowly defined subjects have been published [40–43]. Unfortunately, a timely overview to serve as a guide for a researcher looking for a method or a combination of methods particularly suitable for a given problem is lacking: only a cursory review is available [44]. The purpose of this section is to narrow this gap.¹ Starting with a short look at spectroscopies at surfaces and surface sensitive analytical methods, a comprehensive overview of available spectroelectrochemical methods is given. Grouped according to the interfacial property of interest, the methods are characterized briefly. Several examples from various areas of current electrochemical research are briefly discussed to illustrate the use of combined spectroelectrochemical and surface sensitive methods as a way to obtain a more complete picture of electrochemical interfaces and interphases.

2.1. Fundamentals

At any given interface between two phases, the properties of both phases close to the interface, in particular those of the topmost

¹Because of the extremely large number of original reports still appearing in growing numbers, this introduction is far from being a complete overview of the literature. Consequently, the quoted references do not represent an attempt to provide lists of the most recent or the most important publications: they are, instead, selected with respect to the relevance for the topic of the current review or because of their value as introduction to a given method.

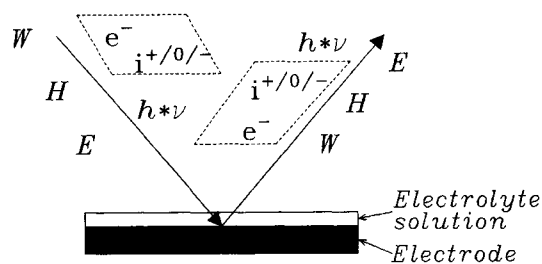


Fig. 3. Probes and signals in surface spectroscopy. Those that are applicable *ex situ* only are printed in italic type: *W*, heat, thermal radiation; *H*, magnetic field; *E*, electric field; *e⁻*, electrons; *i^{+0/-}*, ions or neutral atoms; *h*ν*, electromagnetic radiation.

layers, are different from those in the bulk. To separate this special portion of a system from the bulk, the term *interphase* has been used to denote this quasi-phase in between the bulk phases. This term considerably expands the two-dimensional view of the phase boundary as a simple interface between two completely homogeneous phases. The particular properties of these interphases are of pivotal importance for their behavior in many areas of science and technology. In applied sciences, an improvement of these properties is possible only with as broad as possible a knowledge of them. In electrochemistry, the interphase properties are further complicated by the involvement of charged particles and extremely high electric fields.

Properties of interphases relevant for an understanding of the structures and dynamics present therein can be grouped into atomic (microscopic) and macroscopic. Classical electrochemical methods in most cases have provided only data pertaining to the latter. Nevertheless, the close relationships between both types of properties have allowed conclusions with respect to atomic models to be inferred from macroscopic information. Many spectroscopic methods applied to electrochemical problems in recent years have provided direct information on the atomic level.

2.2. Spectroscopy at Surfaces

The application of spectroscopic methods to surface studies always involves a probe used to stimulate or perturb the interphase in a well defined way. This causes a signal to be emitted from the interphase. In many cases, the signal is simply the modulated or somehow modified probe. Special care has to be exercised to obtain information exclusively from parts of the interface as close as possible to the actual phase boundary. Many techniques are essentially surface sensitive. In some cases, methods or sample systems have to be modified to achieve this surface sensitivity.

Various probes and signals available for surface studies are depicted in Figure 3. Electromagnetic radiation (*h*ν*), neutral atom beams (*i⁰*), ion beams (*i[±]*), magnetic (*H*) or electric (*E*) fields, and thermal excitation (*W*) can be used as probes or quasi-probes. Because of the numerous different types of interactions and resulting signals, the possible combinations of probes and signals are myriad [45–47]. A list of acronyms and abbreviations is provided in the Appendix.

2.3. Spectroelectrochemistry

Obviously some probes and signals can be utilized only under ultra high vacuum conditions. Whereas spectroscopic studies of electro-

chemical systems preferably should be done *in situ* [i.e., in the presence of the electrolyte solution (or electrolyte melt in some cases)], electrons, ions, and neutral particle beams cannot be used without a sample transfer. Even the remaining combinations are manifold. Nevertheless, some answers can be obtained only by using *ex situ* techniques. The methods developed by adopting methods of various origins to electrochemical requirements, in particular for their use under *in situ* conditions, are commonly summarized as spectroelectrochemical methods.

A brief overview of available methods can be obtained easily by looking at the various interphase properties and grouping the methods with respect to their ability to provide information relevant to a particular property. In electrochemical systems, where an electrode is in contact with an electrolyte and possibly has been modified by an adsorbed species or a surface layer, these properties can be outlined as follows:

Macroscopic properties

- Optical absorptivity (color)
- Optical reflectivity
- Electrical conductivity
- Crystallographic structure of the interphase
- Concentration of adsorbed species (see also microscopic properties)

Microscopic properties

- Chemical identity of atoms and molecules in the interface, state of oxidation, coordination with further ligands, their distance from interacting atoms in the electrode surface
- Type, strength and orientation of interaction between these particles and the electrode and their environment

These various properties are collected together with a selection of methods suitable for their investigation in Figure 4. The acronyms are defined in the Appendix. For further information, see also [48, 49]. Methods applicable under *in situ* conditions are emphasized because any conceivable influence of a sample transfer from the electrochemical cell into an ultrahigh vacuum (UHV) analysis system accompanied by drying of the sample or exposure to the atmosphere may result in artifacts. This is most impressively demonstrated in studies of corrosion layers on iron electrodes. Repeatedly, *ex situ* methods have yielded erroneous results, for example, because of dehydration of the corrosion products [50, 51].

2.3.1. Macroscopic Properties

In many cases macroscopic properties of molecular as well as thick adsorbate layers or electrode coatings (e.g., ICPs) are closely related to their chemical composition, thickness, and several application-related parameters like, for example, color, conductivity, and state of passivity.

The optical absorption in the UV-vis region of the electromagnetic spectrum can be measured as a function of electrode potential and wavelength in external reflection or in transmission. In the latter case, the use of optically transparent electrodes (OTE) made, for example, of glass coated with indium-tin oxide or sputtered with gold or platinum are required. To minimize absorption, especially of colored electrolyte solutions, thin layer cells with short optical path lengths are preferred. Nevertheless, in many cases simple cells made of standard cuvettes, working electrodes cut from coated glass, metal wires serving as counterelectrodes, and small sized reference electrodes mounted without protruding into

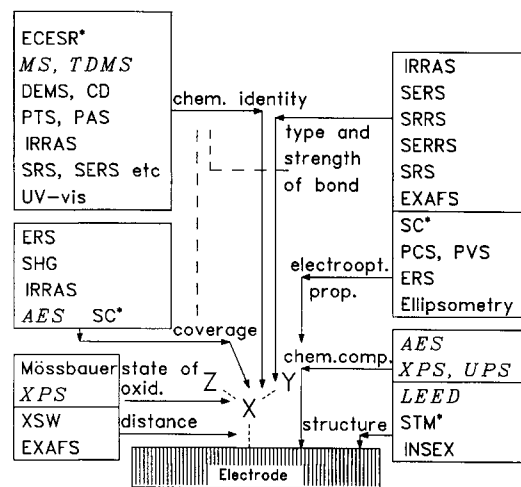


Fig. 4. Selected spectroelectrochemical methods. The acronyms are defined in the text on the Appendix. Methods that are printed in *italic* type are *ex situ* methods; some nonspectroscopic methods are marked with $a_n \equiv$ asterisk (*); dashed lines indicate related properties of investigated species or systems.

the optical beam can be manufactured easily [52, 53]. Experiments can be performed in standard double beam spectrometers (for a typical cell setup, see Fig. 28). In the reference beam, a complete cell is placed with a working electrode without the electrochemically active species present in the other cell. Any absorption of the electrolyte solution or the OTE itself is cancelled out by the nulling procedure of the spectrometer. Typical UV-vis spectra of ITO-coated² and gold sputtered glass electrodes are shown in Figure 5. With this arrangement, electronic transitions in the UV-vis region of surface films of, for example, conducting polymers deposited on the OTE have been investigated. As an example, in Figure 6 UV-vis absorption spectra of a film of poly(2-propylaniline) on an ITO electrode are shown. Various electronic transitions caused by excitation of electrons from $\pi \rightarrow \pi^*$ and from binding to antibinding polaron³ and bipolaron⁴ states that change as a function of electrode potential can be seen. The extension of the electromagnetic spectrum into the near infrared region (NIR) has so far received only scant attention by spectroelectrochemists. This is most likely due to the fact that light absorption in this region tends to be rather unspecific. Mostly absorption by highly conjugated systems and overtone and combination bands of modes with a fairly high absorption cross section are observed. This has suggested the use of NIR spectroscopy for process and quality control. Only recently has NIR spectroscopy attracted some attention because optoelectronic properties of ICPs tend to cause absorption in this particular wavelength region. The observed fairly broad bands are of interest especially in the interpretation of the behavior of mobile charge carriers. Unfortunately no review of this application is currently available.

²ITO is the acronym for Indium-doped tin oxide, which is a transparent and electrically conducting coating.

³In solid state physics, "polarons" are electrostatically induced local lattice distortions caused, for example, by an electron in an ion crystal. In conducting polymers, radical cations (unpaired electrons corresponding to positively charged holes) have a similar effect.

⁴Recombination of two polarons (similar to recombination of two electrons resulting in Cooper pairs) leads to spinless bipolarons with a formal charge of 2+. For a detailed discussion, see the subsequent sections.

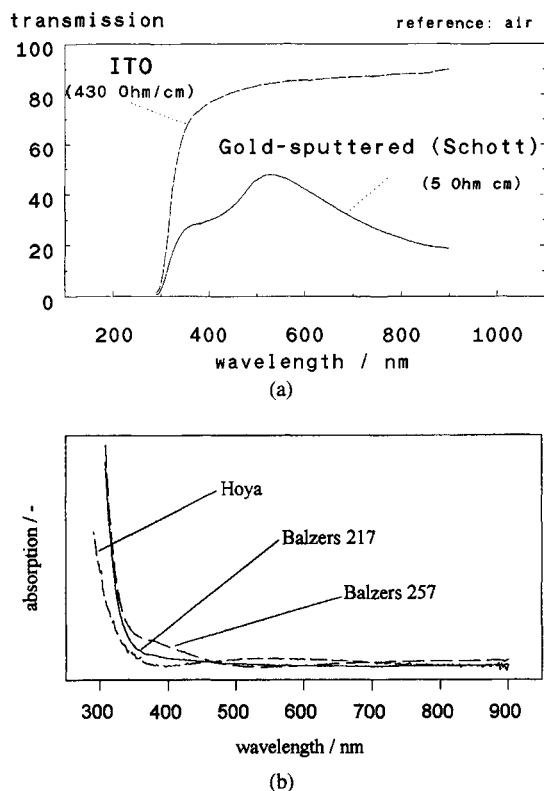


Fig. 5. UV-vis absorption spectra of various optically transparent electrodes.

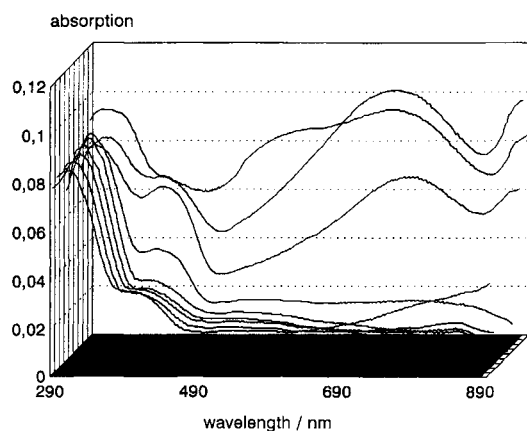


Fig. 6. UV-vis spectra of a conducting polymer layer of poly(2-propylaniline) deposited on a gold-sputtered glass slide electrode, $E_{SCE} = -300$ to $+600$ mV (first to last trace). For details, see [73].

In the case of dissolved reaction intermediates or products, the use of a transmission arrangement and OTE results in the detection of these species in the electrolyte solution. This method is, of course, not surface sensitive: it has been used frequently for the investigation of organic electrochemical reactions that involve various species of distinctly different UV-vis absorption [54, 55]. In the case of optically active disymmetric organic species, circular dichroism (CD) may be observed. Using a spectrometer with linear polarized light, the enhanced stereoselectivity of heterogeneous electron transfer processes can be demonstrated [56].

In the case of interphases on top of opaque or thick supporting electrodes, external reflection of the probe light beam that

arrives at the electrode surface under investigation after passage through the adjoining electrolyte film provides the needed signal. Because no reference such as that necessary in conventional two-beam spectrometers is available, some other parameter has to be modulated to get a spectrum that can be related to the defined states of the interface. Generally the electrode potential is modulated. Consequently, the method is called electroreflectance spectroscopy (ERS). Whereas the interaction of species in the interphase with the light depends on the plane of polarization of the incoming light, spectra obtained with p-polarized and s-polarized light are different in many cases, and these differences between corresponding spectra can be used in the interpretation.⁵ Molecular adsorbates [57] and their orientation [58] as well as electronic transitions within the electrode material itself, which depend on the crystallographic orientation of the electrode, have been studied [59]. Infrequently, measurements with internal reflectance have been reported [60], where the electrode is deposited on a transparent crystal and the probe light is guided into the crystal under an angle, resulting in attenuated total reflectance (ATR) at the electrode-coated surface. Light absorption can be attributed to properties of species on top of the electrode. Unfortunately, self-absorption of the crystal complicates the measured spectra.

In addition to different absorption of s- and p-polarized light by adsorbates or surface layers on electrodes, the phase shift between both is influenced during the passage. Simultaneous measurement of these interfacial properties is done with ellipsometry. The experimental development of automatic ellipsometers has greatly simplified the experimental procedure, but the interpretation of results is difficult. Passive layers [61], underpotential metal deposits [62], organic adsorbates [63], and surface modifying films [64] have been investigated. The range of accessible wavelengths has been extended from the UV-vis into the infrared region [65]; hence, experiments that cover a wide range of wavelengths within one set of measurements have become possible.

The overall reflectance of an electrode surface measured without respect to the wavelength of the incoming light is of low experimental importance. Light of high intensity in a narrow energy interval or at a single wavelength may induce nonlinear effects at the surface. Generation of light at the second (SHG) or the third harmonic frequency (THG) is a possible result. In the presence of molecular adsorbates, sum frequency generation (SFG), which combines the frequency of the incoming light and of molecular vibrations in the light emitted from the electrode surface, is applicable. The former techniques were used in studies of electrode coverage with simple adsorbates and of surface crystallographic structure [66, 67]; the latter technique is suitable for investigations of organic adsorbates [68].

In the previous discussion, only reflection and absorption of light were considered. In many cases, the interaction of light with species in the interphase may cause further processes, for example, by exciting electrons into upper states and forming electron-hole pairs. Photovoltages measured directly (PVS) or photocurrents detected by applying a potential difference across the interphase (PCS) as a function of exciting wavelength can be used, for example, to investigate optoelectronic properties of semiconductors [69].

⁵Despite the fact that measurement of spectra with both types of light and subsequent ratioing should be simple, so far no report of measurements done with polarization modulation has appeared. This is a common technique in infrared spectroscopy at surfaces (see subsequent text).

Although the presence of electronic conductivity of an interphase on an electrode can be related to various optoelectronic properties that also are measurable with spectroscopic techniques, the direct measurement of surface conductivities may provide direct access to data. The technique itself is obviously no spectroelectrochemical method. It is, nevertheless, a surface sensitive method that provides results closely related to those of other methods discussed herein. Data on the electrosorption of alcohols on gold electrodes [70] have been reported. The electrode potential-dependent conductivity of intrinsically conducting polymers deposited on a two band electrode embedded into an inert resin has been obtained with *in situ* measurements [71, 72]. Figure 7a shows the electrical resistance of a polyaniline film measured *in situ* under experimental conditions that suppress any influence of solution phase conduction with an applied small dc voltage (top curve). The influence of the electrode potential on the resistance is obvious. A detailed discussion of this relationship has been presented elsewhere [73]. Instead of a simple setup with only two active electrodes, arrays of several electrodes [74] and comb-shaped arrays have been suggested [75]. A method with a similar sample electrode, but a different electronic setup wherein an ac voltage is applied was described by Kankare and Kupila [76]. Results obtained with an ac voltage are prone to distortion by the solution phase resistance, which is particularly disturbing with poorly conducting polymer layers (see lower part of Fig. 7a). Results reported refer to the presence of polymers in the highly conducting, doped state. The influence of the degree of doping has not been investigated. Instead of the fairly simple setup used in the investigations mentioned before, three other approaches have been used. Frequently, impedance measurements of the solution-polymer-metal electrode interphase are made. From rather complex equivalent circuits or transfer functions, the polymer resistance is extracted as one of several quantities. In a method reviewed elsewhere [77], a constant dc current instead of a constant potential is applied. Especially in the poorly conducting reduced state of many polymers, this may result in considerable potential drops across the polymer (several tens of millivolts) with concomitant inhomogeneities within the polymer layer. Application of an ac voltage across the bandgap electrode as reported by Kankare and Kupila [78] results in the measurement of both the polymer resistance present between the two terminals as well as the solution resistance. Whereas the investigated ICPs are mostly very porous, especially in the reduced state the electrolyte solution, resistance dominates the picture. As shown in Figure 7a, the use of an ac voltage instead of a dc voltage in the simple setup described by Holze and Lippe shows a much smaller range of changing conductivities, which is even more evident when the axis is scaled for both types of applied voltages in the same way (Figure 7b). An experimental approach that involves polymer samples grown laterally between fairly widely spaced electrodes was described by Morvant and Reynolds [79]. Lankinen et al. developed a similar experimental approach termed contact electric resistance [80, 81] that was based on work reported by Charny et al. [82]. With this method, the investigated polymer film is deposited on a flat electrode surface. By means of an inert probe electrode that is brought into contact and an applied direct current, the measured voltage drop is converted into the polymer film resistance. The obvious drawback caused by the constant current instead of a constant voltage (see preceding text) has not been addressed. Another problem not mentioned is the influence of the polymer film compression on the actually measured

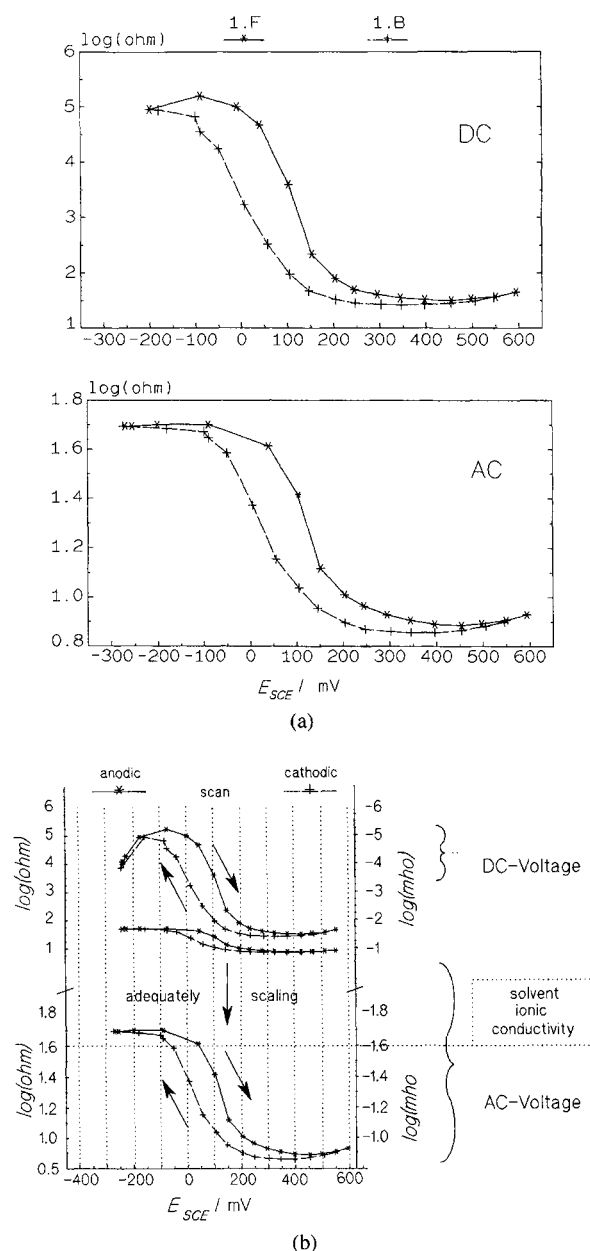


Fig. 7. Electrical conductivity of a film of polyaniline deposited on a double-band electrode measured as a function of electrode potential *in situ* in a solution of 1-N H_2SO_4 with a dc voltage (top) and an ac voltage (bottom) applied. Data for (a) from [72]; data for (b) are from [73].

conductance. An approach that is different in terms of applied signal was developed by John and co-workers [83, 84]. Based on a device developed originally by Deutscher et al. [85] and termed a resistometer, the conductivity of a polymer sample is measured by applying a galvanostatic pulse of short duration. By repeating this during a slow electrode potential scan on line data related to the kinetics, changes of the polymer induced by the electrode potential were supposedly monitored. Based on the reported data, the results closely resemble those obtained by applying an ac voltage.

The crystallographic structure of interphases with at least a minimum of periodicity (i.e. crystallinity) can be investigated with various methods. *In situ* the application of X-ray diffraction (IN-SEX) is possible. Because of the depth of penetration of X-ray

beams, both in the transmission and the external reflection arrangement, the sample has to be made very thin to minimize unwanted contributions from the bulk of the electrode. Crystalline products of corrosion processes [86, 87], surface films [88], surface reconstruction [89], and catalyst systems [90] have been investigated.

Dynamic diffraction of an X-ray beam at lattice planes close to the surface of a perfect single crystal can result in standing X-ray waves (XSW). Measurements of the geometry of the standing wave or of photoelectrons released by the XSW can yield information on the position of atoms relative to the diffracting lattice plane in the interphase [91–93].

The surface morphology of both crystalline and amorphous electrode surfaces or interphase layers can be studied *in situ* with various scanning probe methods. The most popular method seems to be scanning tunnelling microscopy⁶ (STM). This method is based on the very pronounced dependency of the tunnelling current on the distance between a sharp tip and a conducting surface. By scanning a surface with such a tip at a constant mechanical distance, changes in the local distance between surface and tip as a result of atomic morphological features on a microscopic scale result in dramatic changes of the tunnel current. This in turn can be used to map the microscopic morphology of the surface. Numerous studies that pertain to processes that involve metal deposition, dissolution, corrosion, and reconstruction have been reported [94]. The investigation of organic adsorbates has been hampered so far by considerable difficulties during interpretation of the obtained tunnelling current versus surface topography data. The envisioned use of the STM arrangement in tunnelling spectroscopy [95] may provide additional information on vibrational properties of organic adsorbates and thus ease the interpretation of STM data. Experiments with intrinsically conducting polymers have been described [96].

With a small tip scanning the electrode surface mechanically with a very low contact pressure, the morphology including features of adsorbates can be determined. Because van der Waals force interactions basically are probed, this method is termed atomic force microscopy (AFM) [97]. Initial applications in metal deposition studies have been reported [98].

Macroscopic properties of adsorbates and interphases that are not sensitive toward a transfer of the sample from the electrochemical cell into an analysis system (in most cases aUHV chamber) can be studied *ex situ* with additional techniques. Crystallographic data can be derived from low-energy electron diffraction (LEED), which is possible only if the sample has a minimum degree of ordering.

Surface concentrations of adsorbed or deposited species can be derived from a number of methods discussed previously. In the case of absorption spectroscopies, the extinction of the probing light corresponds more or less directly to the degree of coverage; an independent means to perform calibrations is generally necessary. The intensity of SHG signals also corresponds to the coverage. Further details have been reviewed elsewhere [99].

The concentration gradient of species moving either toward the electrode or into the solution can be measured with the probe beam deflection (PBD; also called the “Mirage” effect) technique [100–104]. A light beam (in practically all reported cases,

a laser beam) passes the solution phase close to the solution-electrode interface. Depending on the presence of a concentration gradient in the solution, which in turn causes a density gradient that also affects the optical density, the light beam is deflected. This can be used to monitor the flux of species to and from the electrode surface.

2.3.2. Microscopic Properties

In most electrochemical experiments that involve complex adsorption and/or reaction steps, the identification of adsorbates, intermediates, and reaction products, and their relationship to the electrochemical environment are of central importance. As was pointed out in the previous section, some information about the chemical identity of species involved in the reaction can be gleaned indirectly from the macroscopic properties of the interphase. Unambiguous identification is, nevertheless, possible almost exclusively only with additional spectroscopic techniques.

As already visible in Figure 4, a broad array of methods is available for this task. Direct identification of volatile molecular species present on or near an electrode surface is possible with differential electrochemical mass spectrometry (DEMS) [105–107]. For this method, the electrode has to be porous and gas permeable. It is mounted on the inlet port of a mass spectrometer. Because of the pressure gradient between the vacuum and the electrochemical cell with its porous electrode and adjacent electrolyte solution at ambient pressure, volatile species are sucked into the mass spectrometer and analyzed therein.

Sometimes reactive intermediates, particularly, in electroorganic reactions, have unpaired electrons and, consequently, show typical properties of a radical. Although the free spin of the electron is generally quenched when strong adsorptive interaction with a metallic surface occurs and is, consequently, not detectable, sometimes the electrochemical reaction sequence allows detection of these radicals by electrochemical electron spin resonance spectroscopy (ECESR). This observation is possible when the radical desorbs and is present in the electrolyte solution phase in a concentration sufficiently high for detection by ESR or when the radical is separated from the metal by a suitable spacer (i.e., incorporated in an insulating interphase on the surface). A variety of electrochemically generated radical intermediates have been studied *in situ* with various electrochemical cells [108–110]. The ECESR spectra of the chemically and electrochemically generated radical of nitropropane are displayed in Figure 8. By comparison with calculated spectra and assuming a charge distribution as depicted in the insert, the most likely structure of the radical cation is derived [111]. Radical cations formed during electrooxidation of electrochemically active polymers can also be studied with ECESR [112, 113]. As an example, ECESR spectra of polyindole are displayed as a function of the electrode potential in Figure 9. With an increase of the electrode potential toward anodic values, the polymer is oxidized (p-doped). The unpaired electron causes a radical-cation-like behavior. The high degree of delocalization results in a single line spectrum is discussed in detail subsequently (for further discussion, see [114]).

The chemical identity of molecular adsorbates on electrode surfaces can be derived from their vibrational behavior. *In situ* infrared and Raman spectroscopy are possible. Because of the strong IR absorption of most electrolyte solvents, modulation techniques are necessary. Such methods as electrode potential and polarization modulation have been employed [115, 116]. Modulation is not

⁶This method is obviously not spectroelectrochemical. It is, nevertheless, often mentioned and discussed in the context of spectroscopic techniques.

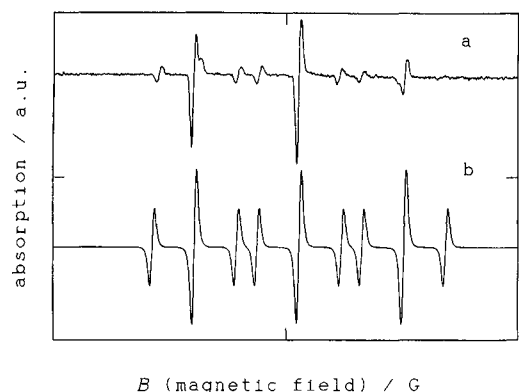


Fig. 8. Electron spin resonance spectrum of the electrochemically formed nitropropane radical anion. (b) Calculated spectrum: coupling constants $a_N = 2.48$ mT, $a_H = 0.998$ mT. Most likely charge distribution in the radical cation. For further details, see [111].

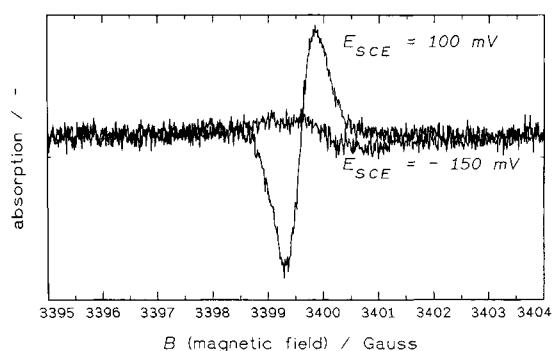


Fig. 9. ECESR spectra of a film of polyindoline in 1-N H₂SO₄ at $E_{SCE} = -10$ and -110 mV.

necessary with Raman spectroscopy in the case of aqueous electrolyte solutions, because water is a very poor scatterer. The low efficiency of the Raman process makes simple surface Raman spectroscopy (SRS) rather insensitive. Giant enhancement of the scattered signal intensity has been observed after various surface treatments, in particular, of coinage metal surfaces (Cu, Ag, and Au). The resulting microstructure of the sample surface and additional surface specific enhancement effects result in a 10^6 -fold increase of the scattered signal intensity. The effect and numerous applications have been reviewed extensively [117]. The extension of the method toward other metals is of considerable interest; overviews have been provided elsewhere [113, 118]. In addition to identification of the adsorbate, these methods also provide information about the orientation of the adsorbate and its interaction with the environment. A combined use of both methods sometimes provide complementary information that yields a more complete model of the adsorbate structure. This can be demonstrated with results of a study on the adsorption of 2-butene-1,4-diol on a polycrystalline gold electrode. Previous electroadsorption studies with classical electrochemical methods have indicated a rather strong physisorption of the alcohol from a neutral aqueous solution [119]. With respect to the orientation of the molecule on the surface and the influence of the electric field in the double layer upon the intramolecular binding, no information could be derived from these electrochemical measurements. Using both vibrational spectroscopies, various vibrational modes were detected (see Figs. 10 and 11). Interpretation of the spectra based on a comparison with vibrational spectra

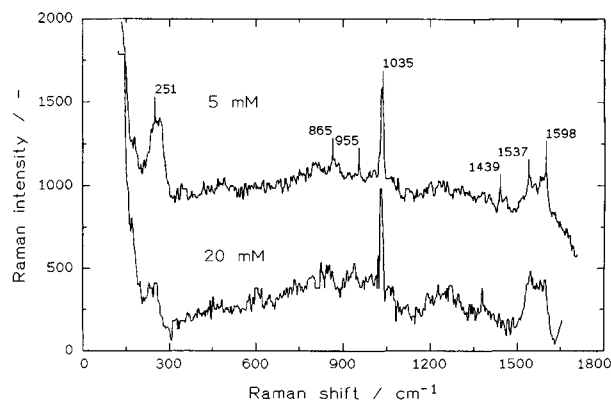


Fig. 10. SER spectra of a polycrystalline gold electrode in a solution of 0.1-M KClO₄ in water. The concentrations of 2-buten-1,4-diol are indicated in the figure. $E_{SCE} = 0$ V (upper trace); 0.245 V (lower trace); resolution 7 cm⁻¹.

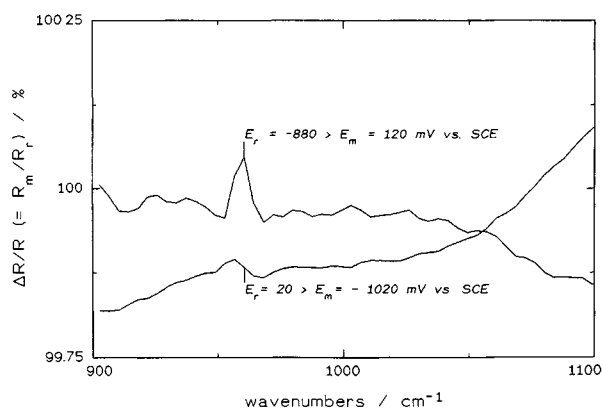


Fig. 11. Potential dependent IR spectra of a gold electrode in an aqueous solution of 2-mM 2-buten-1,4-diol and 0.1-M KClO₄ in water. Electrode potentials are as indicated, 256 or 512 scans at each electrode potential; resolution 8 cm⁻¹.

of the alcohol in bulk form and dissolved in the neutral electrolyte solution resulted in an adsorbate structure with a π -bond system of unsaturated alcohol interacting strongly with the electrode side-on (vibrational mode of the C=C bond around 1598 cm⁻¹) and with the C—OH bond (vibrational mode of the C—OH bond around 1030 cm⁻¹) orientated tilted or perpendicular with respect to the electrode surface toward the electrolyte solution. This information is helpful for understanding the mechanism of electrooxidation of this alcohol [120–122].

Whereas the acquisition of spectra usually takes some time in the second range (or longer), most spectroscopic methods, in particular, vibrational spectroscopies, are less suitable for studies of reaction kinetics and investigation of transient intermediate species with short lifetimes. More recently, in particular, with Fourier transform infrared (FTIR) spectrometers, these studies have become possible, although very fast reactions and unstable species are still beyond reach [123–136]. Similar developments have been made in Raman spectroscopy [137].

These techniques are applicable basically to solid electrodes with a smooth or, in the case of IR spectroscopy, carefully polished surface. For technologically important rough or porous samples, which are sometimes of interest, vibrational spectroscopy at their surface is possible with photoacoustic (PAS) and photothermal spectroscopy (PTS) [138].

After identification of an adsorbate, additional information may be obtained from an intermediate or a reaction product by one of the methods discussed or based on further information about the electrochemical process.

Of course, vibrational spectroscopy generally yields data suitable not only for identification of the adsorbate, but also indicative of intramolecular changes affected by interaction with the electrode surface or interactions within the interphase. These data may even contain information that pertains to the type and strength of interaction with the electrode surface.

In the case of metallic adsorbates (metal deposits, upd layers, catalytically active metal deposits), the type of coordination to surface sites (one-, two-, or threefold, etc.) and the distance to these sites may be of interest. Conversely, the same type of data may be of importance in the case of adsorbed ions on metal electrodes or the atomic environment of a given atom or ion in an interphase. Analysis of the fine structure of X-ray absorption (EXAFS, XANES) close to the X-ray absorption edge of the species (atom) of interest yields these data provided the sample can be prepared in a very thin layer to exclude unwanted bulk interference. Otherwise, the experiment can be done in reflection (SEXAFS). Information about the distance between the atom of interest and the first and sometimes even second shell of the surrounding species can be derived from the spectra [139]. Availability of a suitable light source, generally a synchrotron, is an experimental prerequisite. This method has been applied in studies of passive and corrosion layers on various metals [140] and of molecular and ionic adsorbates on single crystal surfaces [141].

Very similar information can be obtained with the experimentally less demanding Mössbauer spectroscopy. The resonant absorption of γ radiation by certain atomic nuclei (^{57}Fe and ^{119}Sn ; several other isotopes of technical interest, e.g., ^{57}Co , can also be studied in the emission mode) yields information about the close environment of this atom. By comparison with standard samples, the chemical environment of a given atom, the specific type of chemical compound in which it is incorporated, and further morphological information can be derived from the Mössbauer spectra [142].

Local electron densities that typify a chemical environment can be studied with *in situ* positron annihilation spectroscopy (PASCA) [143].

Ex situ identification and investigation of adsorbed species is possible provided the interaction between adsorbate and electrode is strong enough to keep the interface unchanged even after moving the electrode into an UHV chamber. Elemental identification is possible with various electron spectroscopies. Auger electron spectroscopy (AES) is particularly popular and can be used for quantitative measurements (degree of coverage) too [144]. The state of oxidation can be studied with photoelectron spectroscopy [electron spectroscopy for chemical analysis (ESCA) or X-ray photoelectron spectroscopy (XPS)].

Various mass spectroscopies are applicable *ex situ* to obtain molecular information. Secondary ion mass spectroscopy (SIMS) can be used [145]. Thermal desorption mass spectroscopy, a less intrusive and more surface sensitive tool, is a viable alternative [146]. So far, the latter method has been preferred for application to adsorbed hydrogen and carbon monoxide formed in the electrochemical reaction of organic CHO compounds.

3. POLYANILINE AND RELATED POLYMERS

Polyaniline (PANI) is an outstanding member of the family of intrinsically conducting polymers. This family represents a fairly new class of materials that combine typical properties of metals and synthetic polymers. They do this in a way that is so fascinating that they are called synthetic metals sometimes. Essentially these materials are synthetic polymers that contain mostly carbon, hydrogen, and, to a much lesser extent, atoms such as sulfur or nitrogen that are kind called heteroatoms in organic chemistry. Their electronic conductivity is called intrinsic because it is caused by the presence of particular molecular structure elements that enable electric charges to move around without the need of added metallic or metallike materials that are used in filled resins like graphite-containing rubber. Consequently, these new materials combine typical properties of organic polymers like low density and specific forms of polymer processing with properties of metals like conductivity, color, and so forth.

Polyaniline as a chemical substance has been known for quite some time. A black product obtained by treating aniline with oxidizing compounds, it was discovered by Runge in 1834. Its first more precise description as an oxidation product of aniline was reported by Fritzsche [147]. It was obtained later as a product of electrooxidation of aniline by Letheby [148]. A slightly more precise characterization of this material as an oligomer of aniline was provided by Goppelsroeder [149]. The first fairly detailed description of this product as a chain of aniline molecules coupled head-to-tail with the para position of the aromatic ring involved was provided by Green and Woodhead [150] and by Willstätter and Dorogi [151], whereas Yasui [152] described the polymerization product as a "black substance." The electric conductivity and other special properties such, as electrochemical redox activity, reversible doping/dedoping, and electrochromism, are rather recent discoveries [153]. Together with comparable results obtained with other synthetic polymers like polypyrrole or polythiophene (see subsequent text), polyaniline has caused an explosive growth of experimental investigations aimed at identification of the mechanism and kinetics of the formation of these materials, their molecular structure, their electrooptical and solid state properties, and their possible applications.

Polyaniline has attracted extraordinary attention, presumably for at least two reasons: (1) It can be prepared easily by both chemical and electrochemical oxidation processes under fairly convenient experimental conditions (aqueous solutions, many electrode materials are suitable) and (2) it shows a particular sensitivity to the proton activity of its environment because of the nitrogen atom, which is not part of the aromatic ring system. This interest has resulted in an overwhelming number of original reports and a considerable collection of reviews [25, 154–160]. Consequently, there is no need to treat all these aspects in detail. Instead, the following overview aims at a critical discussion of some aspects that are currently the subject of ongoing debate and it incorporates a critical reevaluation of our own contributions in this field. The discussion is organized into sections that deal with the formation, the materials properties, the possibilities to influence and apply these properties, and the degradation. Particular attention is paid to properties of polymers derived from substituted anilines and from molecules related to aniline and considered as suitable replacements for aniline in certain applications. An overview of the molecules investigated within this work is provided in Figure 12.

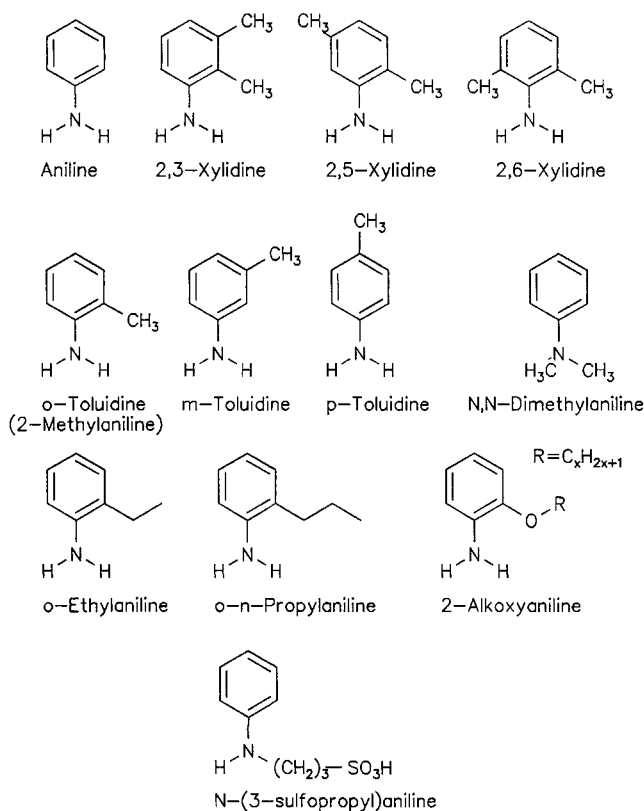


Fig. 12. Structural formulas of aniline and substituted anilines investigated in the work reviewed herein.

The following sections cover the preferred electrochemical aspects of the formation and the materials properties of the investigated monomers and their relatives as revealed with spectroscopic and surface sensitive methods. Results obtained with other methods (scanning probe microscopies and, especially, traditional electrochemical techniques) are quoted only in passing when deemed necessary for a better understanding of the spectroelectrochemical results. Because of the numerous reviews that cover a very broad range of conceivable and potential applications, no attention is paid to this aspect.

3.1. Formation of Polyaniline and Related Polymers

PANI and the polymers of substituted anilines can be formed by chemical oxidation or electrooxidation. Although the former process is more suitable for the production of large volumes of polymers, it results predominantly in powders that are difficult to process. Despite the striking similarity between the polymers discussed here and numerous thermoplastic polymers used in manufacturing, the processability of PANI and its relatives is still poorly developed. Various reported attempts to improve processability are based on suitably substituted monomers (in particular, alkyl-substituted anilines), the use of special counterions that are present in the conducting form of the polymer because of the need for charge compensation (see subsequent text), copolymerization, or blending (for a selection of reports, see [161–182]; approaches to soluble PANI also have been reported [183]). For many projected applications, the deposition of the polymer as a thin film (on a substrate or free standing) or as a more or less thick coating

is desirable. With electrochemical polymerization the products are practically always deposited directly on the electrode.⁷

The mechanism and the kinetics of PANI formation have been the subject of numerous investigations devoted to identification of the steps of the electrooxidation and electropolymerization process and any intermediates. This knowledge gains additional importance when relationships between the mechanism of polymerization and possible reaction pathways and properties of the polymeric product are sought. Figure 13 depicts a very general pathway of aniline oxidation and the formation of first oligomers. The initial step in all cases seems to be the adsorption of the monomer from the electrolyte solution on the electrode surface. This is a necessary prerequisite for the consequent charge transfer during the electrooxidation step. Investigations of the adsorption of aniline or related compounds are scanty. Nevertheless, a detailed understanding of this initial step is desirable. Measurements of the thermodynamics of adsorption have been done with tensammetry [184, 185] and the radiotracer method [186]. Results indicate a strong adsorptive interaction (chemisorption) with a free enthalpy of adsorption of about $\Delta G_{\text{ad}} = -40 \text{ kJ mol}^{-1}$. Information about the geometry of adsorption, which better suits understanding of the geometry of the substrate–electrode interaction, has been obtained with surface enhanced Raman spectroscopy (SERS) [187]. With a neutral electrolyte solutions, an interaction with the gold electrode via the lone electron pair of the nitrogen atom led to the conclusion of a more or less perpendicular orientation. The results of measurements with acidic solutions imply a side-on orientation of the anilinium cation. Similar results obtained with *in situ* infrared spectroscopy were reported by Bockris and Jeng [188, 189]. At first glance, the latter result cannot be brought into close matching agreement with the simple reaction model proposed in Figure 13. According to Dunsch [190], the anilinium cation is deprotonated on the electrode surface before undergoing the oxidation step. This conclusion was based on electrochemical measurements with a rotating-disk electrode. Direct evidence from spectroscopic measurements of this process is lacking so far. Note that results of spectroscopic measurements used in support of a proposed reaction pathway should be considered with care. Practically all spectroscopic methods yield results that primarily support the species that can be detected most easily or that is most stable. Unfortunately this reaction intermediate is not necessarily the reaction intermediate in the main reaction pathway; in the worst case, it is actually a byproduct formed at the end of a dead end reaction [113].

In most reports that deal with electropolymerization of aniline and its derivatives, the formation of a cation radical or another intermediate in the initial stage of the process is assumed [191]. A basic reaction mechanism of the anodic oxidation of anilines

⁷For experimental details of the electrochemical as well as spectroscopic investigations, the reader is generally referred to the original reports quoted in this review. Introductory information with respect to most spectroscopic methods was provided in the preceding sections. Only in a few cases are experimental details that are deemed necessary for the understanding of the figures or are of vital importance included. Some general information: E_{BHE} indicates electrode potentials measured with respect to a hydrogen reference electrode filled with the electrolyte solution used in the experiment; E_{SCE} indicates electrode potentials measured with respect to a saturated calomel electrode ($E_{\text{NHE}} = 241 \text{ mV}$); E_{SSCE} indicates electrode potentials measured with respect to a saturated calomel electrode prepared with a sodium chloride solution ($E_{\text{NHE}} = 236 \text{ mV}$).

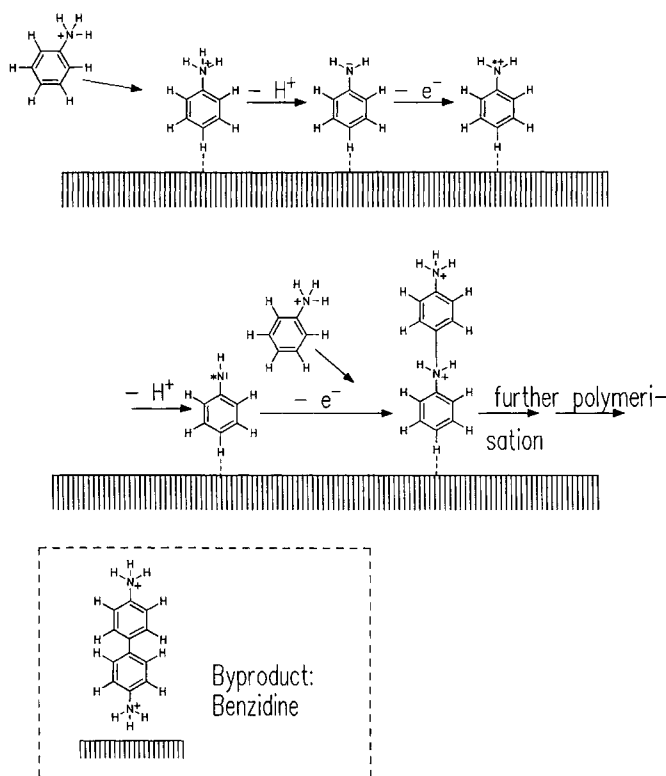


Fig. 13. General reaction mechanism for polyaniline formation.

that leads to head-to-tail, head-to-head, and tail-to-tail dimers as well as to polymer products, with the participation of electrogenerated cation radicals, was proposed in early works [192–196]. Radical–radical coupling as well as radicalic substitution reactions are conceivable pathways. Because the formed oligomers (dimers and higher oligomers) can be oxidized themselves (and in most cases, more easily because of the more extended organic molecule available for charge distribution, i.e., a lower HOMO⁸), they participate in the polymerization reaction as Heinze et al. [197] pointed out for various polymers.

Direct proof of the radicalic nature of the reaction intermediate proposed in the reaction scheme can be expected from *in situ* measurements with ECESR. Experimental attempts with aniline in aqueous solution, using a previously described electrochemical cell [198, 199] (for details see subsequent text) and based on a design by Allendoerfer et al. [200] (reported elsewhere in detail [201]), all have failed. A single line spectrum always has been observed. This indicates the presence of highly delocalized spins attributed to radical cations formed on the polymer chain (see following text). Initial assignments of this line as a Dyson-type line caused by free electrons have turned out to be inappropriate. An investigation of the change of the electron spin resonance (ESR) signal amplitude during electropolymerization revealed interactions between the cations formed on the polymer and the monomer present in solution [202]. The latter detail is the main difference from the numerous ESR studies reviewed in detail subsequently. The major result is the observation that after stopping electrolysis at a highly positive electrode potential, the ESR in-

tensity rapidly increases again. This increase is caused by the conversion of spinless systems in the film into spin-carrying radical cations. Whereas this was observed only in the presence of aniline in the solution phase, participation (perhaps by chemical oxidation of solution phase monomers via the positive charges on the film) seems to be effective. This result fits with observations reported by Pekmez et al. [203], who stated the importance of protonated sites on the polyaniline, in particular, in its pernigraniline form (which essentially does not contain free spins) with aniline monomer units that result in their oxidation with a concomitant loss of pernigraniline sites.

The absence of an ESR signal caused by a monomeric radical cation can be explained readily when considering the reactivity of the aniline radical cation. According to Neugebauer et al. [204], this radical is highly reactive, but ESR spectrum could be recorded only in a flow apparatus under fairly extreme conditions. The failure to observe an ESR spectrum with the hyperfine splitting indicative of a molecular (not an oligomeric) unit with an unpaired electron can be explained with various arguments, which are all related to the high reactivity. The detection limit of ESR spectroscopy is very low. Consequently, the absence of the ESR spectrum implies an extremely low stationary radical concentration (if any). This argument has to be considered with care, because the use of the ECESR cell drastically raises the detection limit. Upon substitution of the aniline molecule, the situation changes considerably. With *N,N*-dimethylaniline, the ESR spectrum displayed in Figure 14 could be recorded [205]. Results similar with respect to the stabilizing influence of *N*-substitution at the nitrogen atom of aniline were obtained during chemical oxidation of various *N*-substituted anilines by Yatsimirskii et al. [206]. Further substitution was used by Male and Allendoerfer [207], who observed a complete ECESR spectrum of *p*-aminodiphenylamine. A highly substituted aniline (2,6-di-*tert*-butylaniline) was investigated by Speiser et al. [208], whose results again imply a radical cation as the oxidation product. No polymerization was observed. Very similar results were observed with 2,4,6-tri-*tert*-butylaniline as the monomer by Cauquis et al. [209, 210]. Yang et al. [211] investigated the ESR and UV-vis absorption of diphenyl-*para*-phenylenediamine and tetraanilinobenzene in the electrode potential range between the first and the second oxidation current wave. The fairly broad, yet extremely poorly resolved, ESR spectra seem to indicate the presence of some hyperfine splitting, which may be taken as an indication of the presence of radicalic species. Optical absorptions observed for both monomers as a function of electrode potential were taken as support for this conclusion. In an electrolyte solution of acidified dimethyl sulfoxide, polymerization of aniline after its initial electrooxidation does not occur. In this solution Dunsch and Petr [212] found the indamine radical cation with ECESR. Its presence can be seen as proof of the aniline radical cation intermediate proposed by the preceding researchers if this indamine radical cation is considered to be part of a reaction sequence that assumes the occurrence of the aniline radical cation as a precondition. Indole and its substituted derivatives (see Fig. 12) can also be considered to be a substituted aniline. With this molecule, ESR spectra of the radical cation of 1,2-dimethylindole could be recorded after both chemical and electrochemical oxidation (Fig. 15) [213, 214]. The spectrum calculated assuming the radical cation structure and charge distribution shown in the inset shows in Figure 15 good agreement with the measured spectra.

Hambitzer and co-workers [215–218] reported the detection of soluble products of aniline electrooxidation by using electrochemi-

⁸HOMO is the acronym for highest occupied molecular orbital. An electron is drawn from this molecular orbital during electrooxidation.

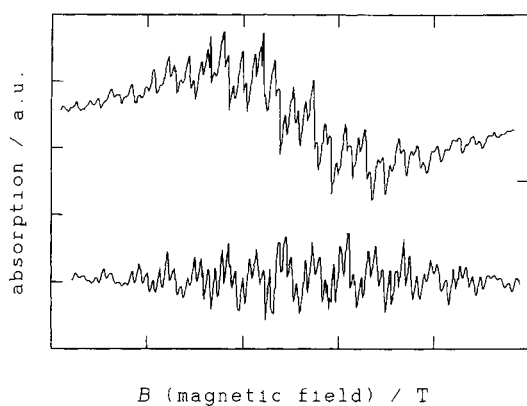


Fig. 14. Top: Electron spin resonance spectrum of the chemically formed *N,N*-dimethylaniline radical cation in concentrated nitric acid: 9.41 GHz, 79 mW, modulation 0.065 mT, sweep 2 min, $T = 10^\circ\text{C}$. Bottom: Calculated spectrum: coupling constants $a_N = 0.775$ mT, $a_{\text{CH}_3} = 0.854$ mT, $a_{\text{H, ortho}} = 0.371$ mT, $a_{\text{H, meta}} = 0.095$ mT, $a_{\text{H, para}} = 0.69$ mT. For further details, see [205].

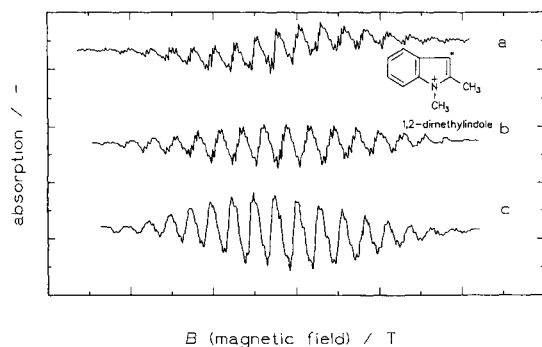


Fig. 15. Electron spin resonance spectra of (a) electrochemically formed 1,2-dimethylindole radical cation in acetonitrile + 0.25-M LiClO_4 and (c) chemically formed radical cation in concentrated nitric acid: 9.41 GHz, 79 mW, modulation 0.65 G, sweep 2 min, $T = 10^\circ\text{C}$. (b) Calculated spectrum: coupling constants $a_N = 5.16$ G, $a_{\text{H}} = 3.8$ G, $a_{\text{H}} = 1.98$ G, $a_{\text{H}} = 1.86$ G, $a_{\text{H}} = 1.55$ G, $a_{\text{H}} = 1.35$ G, $a_{\text{H}} = 1.64$ G, $a_{\text{H}} = 1.39$ G, $a_{\text{CH}_3} = 1.64$ G, $a_{\text{CH}_3} = 1.39$ G. Inset: Most likely charge distribution in the radical cation. For further details, see [205].

cal thermospray mass spectrometry. Certain features of their mass spectra were used as arguments in favor of the presence of a radical species. Less direct evidence of a reaction intermediate and its radicalic nature can be obtained with *in situ* UV-vis spectroscopy. Radicals of aromatic molecules and their derivatives are generally colored, because electronic transitions that are not possible in the educt molecule cause optical absorption. Unfortunately other conceivable reaction intermediates (see below) also show coloration. So far, attempts to record UV-vis spectra of aniline with the aim of observing the monomeric radical cation under conditions where aniline oxidation takes place have failed. Kemp et al. [219] used a fast scan UV-vis spectrometer in an attempt to detect intermediates in the oxidation of various *N*-substituted anilines without success. Radicals of substituted alkyl anilines were identified, whereas unsubstituted aniline did not yield a signal attributable to a radical intermediate. With a combination of *in situ* UV-vis and infrared spectroscopy, Zimmermann et al. [220] studied the initially formed product in an acidic electrolyte solution containing aniline on an electrode deposited on an ATR element for in-

frared spectroscopy and a platinum grid electrode for *in situ* UV-vis spectroscopy in the transmission mode. The obtained spectra did not imply a monomeric reaction intermediate. Instead, it was concluded that *N*-phenyl-quinonediimine is formed in its fully oxidized state. It was only suggested that this dimer must have been formed from two monomers by way of a radical-monomer substitution reaction. This species is reduced during a subsequent electrode potential scan in a two-electron reduction. In a comproportionation reaction with its fully oxidized form, radical dimers are formed that ultimately form a tetramer. UV-vis data obtained with this system as well as data obtained with *p*-aminodiphenylamine support this conclusion. Leger et al. [221] presented a detailed study of *o*-toluidine electropolymerization by fast scan UV-vis differential reflectance spectroelectrochemistry on a gold electrode. These authors obtained UV-vis spectra in the first potential scan that differ from those of the resulting polymer itself, indicating intermediate species as a precursor of the polymer. Genies et al. [222, 223] used fast scan visible spectroscopy during electrolysis of aniline and found a short-lived intermediate created before the formation of polyaniline in a eutectic of $\text{NH}_4\text{F} \cdot 2.3\text{HF}$. They proposed this intermediate to be the nitrenium cation (Ph-NH^+). This electrolyte system was also assumed to be less prone to degradation by overoxidation of the polymer during its formation [224]. Somewhat later, Genies et al. [225] claimed that the formation of the nitrenium cation proceeded during electropolymerization of azobenzene in the same medium, as studied by fast scan UV-vis spectroelectrochemistry Shim et al. [226] observed a transient absorbance band at $\lambda = 430$ nm during electrooxidation of aniline and ascribed it to an intermediate species, probably the nitrenium cation reported by Genies et al. Once formed, the nitrenium cation leads to all three possible dimers, that is, head-to-tail, tail-to-tail, and head-to-head coupling products, which are capable of growing into polyaniline in the presence of aniline. Later, Johnson and Park [227] again observed a spectral band at $\lambda = 440$ nm that is prominent in the early stages of aniline electrooxidation. They believed the nascent products to be the cation radical of aniline or a product formed before the radical undergoes a dimerization reaction. Details of the reaction sequence, including various intermediates, are collected in Figure 16. de Santana et al. [228] used *in situ* resonance Raman spectroscopy to investigate oxidation products of diphenylamine. Various diphenylbenzidine species, including radicalic ones, but no polymer or oligomer were found. A fairly general review on the role of radicals in the chemistry and electrochemistry of synthetic metals including intrinsically conducting polymers was published by Baumgarten and Müllen [229]. It does not contain additional information pertinent to the mechanistic and kinetic aspects of polymer formation discussed here. Based exclusively on electrochemical evidence obtained with cyclic voltammetry of substituted monomers (β -carotenoids, α , ω -diphenylpolyenes, and phenylenevinylens), Heinze et al. [230] concluded that initial radical formation is followed by rapid reversible dimerization.

The effect of the substitution on the reactivity of the monomer was studied in more detail recently [231]. The electrooxidation of a selection of *N*-alkyl-substituted (*N*-ethyl- and *N,N*-dimethyl-) and ring-substituted (*o*-, *m*-, *p*-methyl-, *o*-ethyl-) aniline derivatives at ITO glass electrodes was investigated using UV-vis spectroscopy *in situ* (further details follow). With *N*-ethylaniline, well defined absorbance peaks of an intermediate and an end product were observed after an anodic potential step (Fig. 17). Conversion of the electrogenerated intermediate into an end product

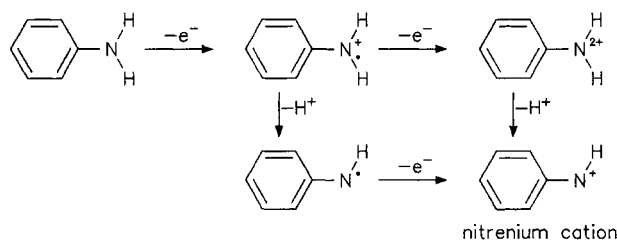


Fig. 16. Pathways for the initial steps of aniline oxidation and deprotonation.

was demonstrated. With *N,N*-dimethylaniline, the formation of an electrogenerated intermediate as well as its consumption after interruption of electrolysis were observed. However, no end product was detected. This is interpreted in terms of a C–C (tail-to-tail) coupling, leading to a benzidine-type end product, which is not detectable in the investigated spectral range. Absorbance transients were detected at $\lambda = 450$ nm for ring-alkyl-substituted anilines, showing the typical time-dependent behavior of an intermediate species. Absorbance transients at $\lambda = 750$ nm were identified as being caused by end products of the electrooxidation of ring-substituted anilines.

The introduction of ionogenic groups in the aniline molecule has an even more stabilizing effect. These groups (e.g., sulfonic acid groups) may act as proton sources for doping of the nitrogen atoms. Consequently, these polymers are called self-doping or self-acid-doping [232–236]. Direct UV–vis spectroelectrochemical observation of an intermediate during anodic oxidation is possible in the case of *N*-(3-sulfopropyl)aniline (NSPA), an aniline derivative that contains a sulfoalkyl group at the nitrogen atom [237]. The relatively high stability of the intermediate enables the time-dependent spectral observation of the intermediate on a multisecond time scale. Figure 18 shows a set of UV–vis spectra recorded with solutions of various concentrations of NSPA (for details, see [238]). The absorption band found at low wavelengths was assigned to a reaction intermediate; the band at high wavelengths was attributed to the polymeric reaction product. The time-dependent absorption of both bands as displayed in Figure 19 shows the typical shape indicative of a reaction intermediate observed with the band around $\lambda = 445$ nm. A subsequent chemical reaction of this intermediate, leading to a soluble oligomer or polymer product, was concluded. These spectroscopic data do not prove the radicalic nature of the species that causes this absorption. Help may be expected from theoretical considerations; in particular, from calculations of the UV–vis spectra of the radical and the nitrenium cation. Comparison of experimental data and modelling should enable the assignment of the electronic spectroscopy data to one of the possible intermediates. The values of λ_{max} of the absorption band assigned to the intermediate reported so far indicate at least a relationship between the type and degree of substitution and the energy of the electronic transition. Values observed are $\lambda = 450$ nm for *N*-ethylaniline, $\lambda = 443$ nm for *N*-methylaniline, $\lambda = 465$ nm for *N,N*-dimethylaniline, $\lambda = 490$ – 520 nm for *p*-toluidine, and 460 nm for *N*-benzylaniline.

As already indicated the stability with respect to the reactivity of the reaction intermediate(s) and the reactivity of the monomer are closely related. In a comparative study, the influence of various substituents on the reactivity of substituted anilines was investigated [239–241]. Slow film formation enabled the detection of two oxidation steps in cyclic voltammograms before the redox pro-

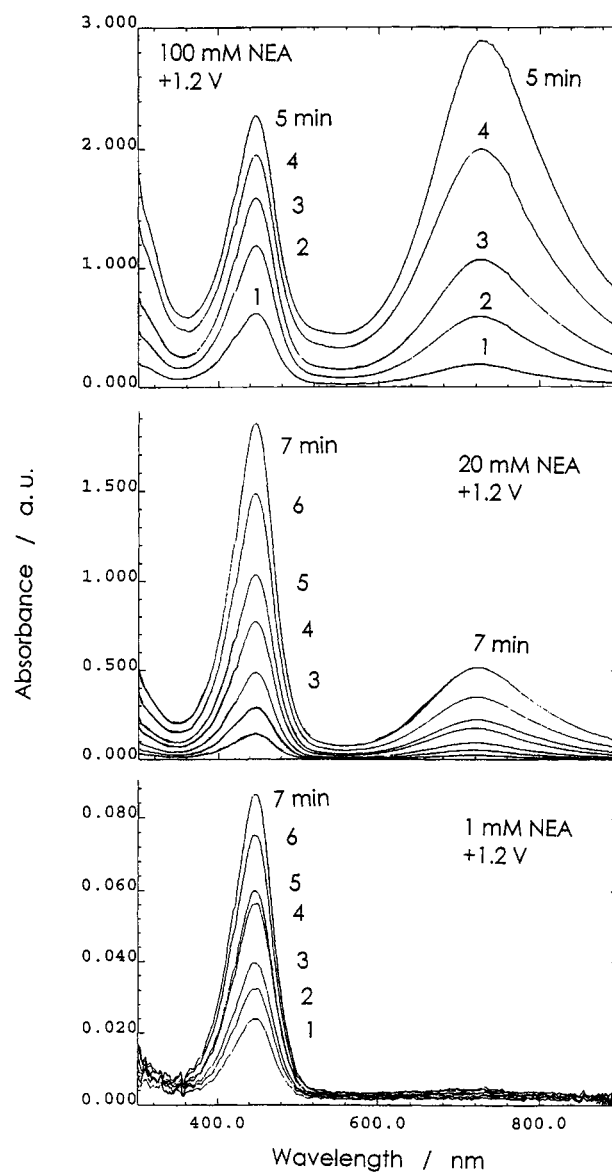


Fig. 17. UV–vis spectra obtained after different time intervals (as indicated in minutes) after a potential step to $E_{\text{RHE}} = +1.2$ V in solutions that contained 100 (top), 20 (middle), and 1 (bottom) of *N*-ethylaniline. For further experimental details, see [231].

cesses of the polymer film became the major cause of the Faradaic currents. Electrode potentials are listed in Table I.

Introduction of two ring substituents reduces the energy needed for the initial oxidation step by about 120 mV as compared to the parent compound. A single alkyl substituent reduces the energy by about 60 mV. This reduction has been attributed to a positive inductive effect of the alkyl substituents [242–244], that elsewhere has been called the electron-donating effect [241]. This effect causes an increase of the electron density on the aromatic ring system by inductive displacement of the bonding electrons. The positively charged intermediate is stabilized and an analogue can be seen in the σ complex in electrophilic substitution of aromatic compounds (Fig. 20). Because formation of this intermediate is the rate-determining step (otherwise detection of the radical with ECESR should pose no problem), this accelerates the overall reaction. The second oxidation takes place at electrode potentials

Table I. Oxidation Potentials E_1 and E_2 of Aniline, Xylidines, and Substituted Anilines in Solutions of 1-M HClO₄ + 10-mM Monomer in Water^a

Monomer	Acronym	E_1 , RHE (mV)	E_2 , RHE (mV)	E_{ox} , SCE (V) [241]
Aniline	PANI	1134	—	1.03
2,3-Xylidine	P23X	1031	1168	—
2,5-Xylidine	P25X	1021	1202	0.81
2,6-Xylidine	P26X	1043	1187	—
<i>o</i> -Toluidine	PoTI	1080	—	0.88
<i>m</i> -Toluidine	PmTI	1085	—	—
<i>o</i> -Ethylaniline	PEtA	1081	—	—
<i>o-n</i> -Propylaniline	PPrA	1055	—	—
<i>N</i> -Methylaniline	PNMA	1170	—	—
<i>N</i> -Ethylaniline	PNEA	1085	—	—
2-Methoxyaniline ^b	MOA	—	—	0.75
2-Aminobenzylalcohol	ABA	—	—	1.01
2-Methoxy-5-methylaniline	MOMA	—	—	0.75
2-Methyl-5-methoxyaniline	MMOA	—	—	0.87
2,5-Dimethoxyaniline	DMOA	—	—	0.67

^aData taken from cyclic voltammograms with a scan rate of $dE/dt = 10 \text{ mV s}^{-1}$ [239, 240] or as in [241].

^b*o*-Anisidine.

about 160 mV more positive; the position of the substituents is only of minor importance. The potential window thus given may correspond to the range wherein the initial oxidation product, perhaps the primary radical cation, exists. Specific kinetic and mechanistic investigations of the initial reaction step of these compounds with spectroscopic methods as outlined have not been reported.

At sufficiently high positive electrode potentials, all investigated aniline derivatives undergo electrooxidation, yielding intermediates. In the following chemical step, intermediates react with solution phase molecules of the substrate. The fastest chemical reaction proceeds with unsubstituted aniline, whereas ring-alkyl-substituted derivatives react somewhat slower. The slowest chemical reaction proceeds with *N*-alkyl-substituted aniline derivatives. This conclusion is again in agreement with the implications of ECESR measurements.

The first reaction intermediate—still a monomeric unit—undergoes further reaction. As indicated in Figure 13, this may be further oxidation or reaction with a solution phase constituent (e.g., radical cation–parent molecule coupling). In addition, reactions between the initial reaction intermediates are conceivable (e.g., radical cation–radical cation coupling). This step has various aspects: the mechanism of the reaction (as indicated in the examples), the kinetics (which in turn may be related closely to the mechanism), and the identity of the next reaction product. A dimer (*p*-aminodiphenylamine) was deduced by Yang and Bard [245] as a first reaction intermediate from electrochemical measurements with fast scan cyclic voltammetry at glassy carbon electrodes. Benzidine was found as a minor intermediate. Based on comparisons with digital simulations, the formation of both species, which are both dimers with respect to the monomer molecule, occurs via a coupling of two radical cations. The rate constant of the chemical radical coupling reaction is estimated to be about $10^8 \text{ mol}^{-1} \text{ s}^{-1}$. A similar study employing cyclic voltammograms (CV) with ultramicrodis electrodes and using diphenylamine as the monomer was

reported by Yang and Bard [246]. At high sweep rates, the CV implies the occurrence of a radical intermediate. Comisso et al. [247] observed formation of polydiphenylamine with only a low degree of polymerization during chemical oxidation of diphenylamine. Benzidine itself may also undergo further polymerization that results in a polymer [248]. Very similar results, in particular, with respect to the radicalic nature of the initial reaction intermediate, were found by Yang et al. with *N,N*-dimethylaniline oxidized in a nonaqueous electrolyte solution [249]. Based on results obtained with surface enhanced Raman spectroscopy (SERS), Gao et al. suggested that aniline adsorbed on the surface of a gold electrode is transformed into a radical cation and should end up in a tail-to-tail coupling reaction product (i.e., benzidine) exclusively [250]. Formation of the head-to-tail coupling product can be understood by assuming a reaction mechanism wherein a radical cation couples with a monomer molecule. Their conclusion was based solely on the occurrence of vibrational bands that were assigned to the adsorbed monomer and the mentioned dimeric reaction products. Basically, these conclusions agree with earlier data that also indicate the formation of a head-to-tail para-coupled substituted aniline with evidence of traces of benzidine [251].

Based on kinetic data of the investigated aniline oxidation reaction as obtained with a variety of methods, including spectroelectrochemical ones, numerous researchers [252–270] have proposed an autocatalytic mechanism of oxidation and growth. In this scheme, polymer growth occurs without further electrooxidation of aniline monomers. The polymer film in its oxidized form contains oxidized aniline units, most likely also at the ends of polymer chains. These units react basically like monomeric radical cations with further monomer molecules from solution (radical cation–parent molecule coupling). Subsequently, the chain has to be re-oxidized, that is, one electron has to be transferred per monomer unit. An alternative proposal is that pernigraniline sites act as oxidants for monomer units [271]. The characterization of this pro-

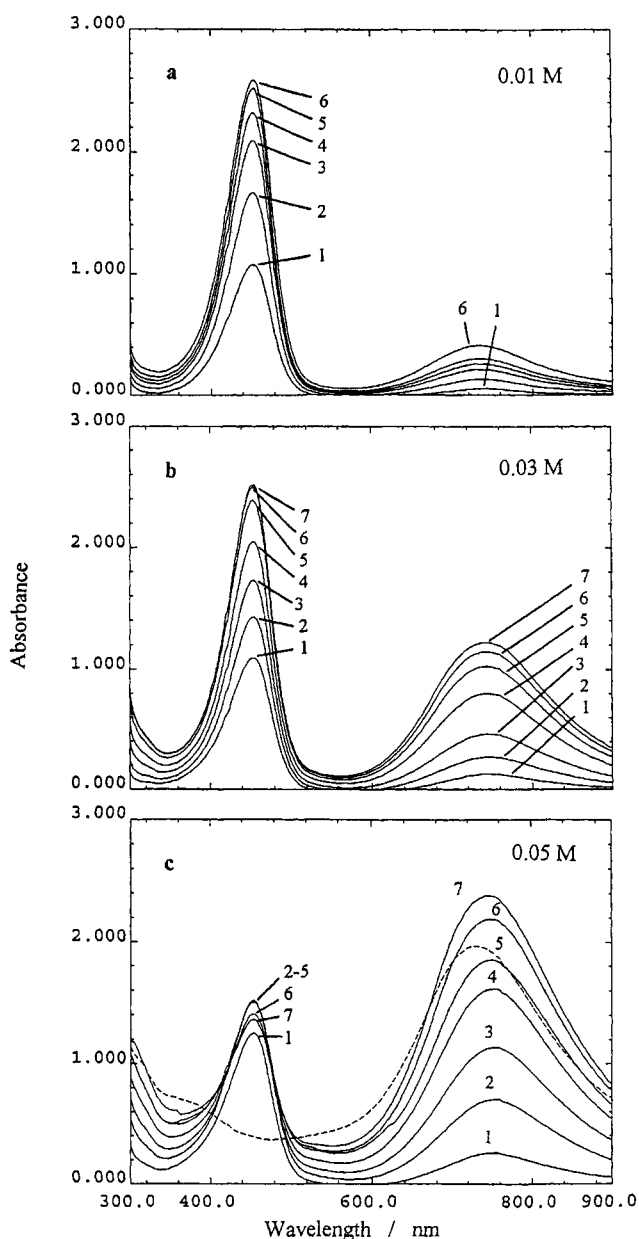


Fig. 18. UV-vis spectra obtained at different time intervals (as indicated in minutes) after applying an electrode potential of $E_{RHE} = +1.1$ V in solutions that contained NSPA in various concentrations (0.01, 0.03, and 0.05 M, as indicated). The dashed line in (c) shows a spectrum obtained 3 min after interruption of an electrolysis performed for 7 min. For further details, see [238].

cess as "autocatalytic" is based on the fact that electrooxidation of the oligomer occurs at lower, less positive electrode potentials than electrooxidation of the aniline monomer. An already mentioned peculiarity of aniline and its polymer—the possibility of protonation and deprotonation at the nitrogen atom—seems to be of importance in the autocatalysis. This effect was observed only in aqueous solutions of considerable acidity. This may be related to the fact that the highest conductivities of polyaniline are obtained in strongly acidic environments. Whereas the polymer is in its conducting (i.e., oxidized) state, this pH effect becomes operative [272]. Unfortunately, exact calculations of the amount of charge used to produce a certain amount of polymer are some-

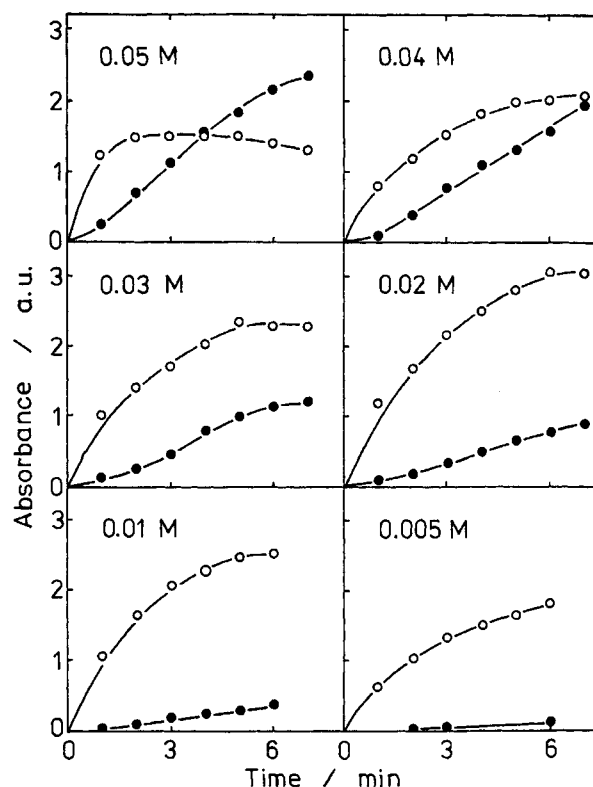


Fig. 19. Time dependence of the absorbance at $\lambda = 453$ (hollow circles) and 745 nm (full circles) after stepping the electrode potential to $E_{RHE} = +1.1$ V in solutions that contained NSPA in a concentration range from 0.005 to 0.05 M (as indicated). For further details, see [238].

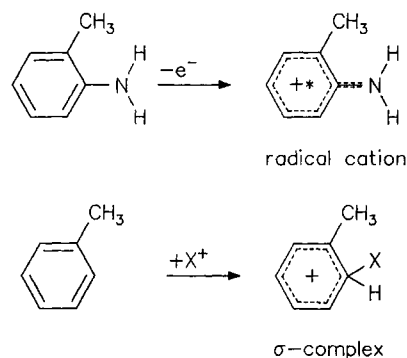


Fig. 20. Comparison of electronic structure and charge distribution in a radical cation and a σ complex formed during electrophilic substitution.

what difficult to perform. In addition to the electric charge consumed simply for charging the electrochemical double layer (which may be rather extensive in the case of porous and highly structured polymer films), the charge recorded in a positive direction electrode potential scan is consumed only in part for polymer formation. Part of the charge is just used to form radical cations on the polymer chain that may not participate completely in polymerization reactions. During a negative direction potential scan, these radical cations are reduced again. An obvious idea is to calculate the difference in charge used for polymer oxidation and for polymer reduction, and to attribute the difference to the polymerization reaction. Because of the very large charges consumed in the film oxidation and the very small differences between the anodic

and the cathodic charge, and because of the obvious difficulty in defining the limits for the integration of the current needed to determine the charge, this approach has not resulted in reasonable results so far [273]. This problem is further enhanced by the fact that an exact determination of the amount of polymer being formed on the electrode is extremely difficult; most likely, it is practically impossible. If only the electrochemically active polymer is considered [the part of the polymer that can be oxidized (doped) and reduced (dedoped)], the charge needed for film oxidation as taken from cyclic voltammograms should provide the requested information. In addition, the fact that charging occurs into a poorly conducting film and is most likely incomplete or at least hardly completely reproducible and the onset of overoxidation and other undesired side reactions influences the obtained results. Consequently, precise determination of yield of electropolymerization is very difficult.

Zotti et al. [274] investigated the influence of the anion in the polymerization mechanism and its kinetics. Using only anions of several strong acids, two distinctly different classes of anions were identified. One (class 1: BF_4^- , ClO_4^- , CF_3COO^-) favors a more compact film structure and morphology, whereas the other (class 2: SO_4^{2-} , NO_3^- , Cl^-) favors formation of an open morphology. With the former ions, the deposition charge shows a linear dependence on the number of potential cycles, whereas ions of the latter class show a quadratic dependence (see subsequent discussion for substituted anilines). From the potential dependence of the deposition currents, it was concluded that PANI growth occurs via adsorption of anilinium–anion couples on fully oxidized pernigraniline sites of PANI. Results pertaining to the morphology of PANI films reported by Huang et al. [275] fit only in part into this picture. With BF_4^- anions (class 1) in the polymerization solution, a smooth film was obtained; with ClO_4^- anions (also class 1), a fibrillar structure was observed. A fibrous PANI was also obtained by electrochemical polymerization from aqueous solution by Kanamura et al. [276]. The radius of the fibers was found to depend on the applied current density. *o*-anisidine (*o*-methoxyaniline) was electropolymerized by Bedekar et al. [277]. Fibrillar deposits were obtained, and the influence of monomer concentration and substrate electrode conductivity was studied in detail. The electropolymerization of aniline at constant electrode potential in aqueous acidic solutions was studied by Yano et al. [278]. With perchlorate as the anion in the polymerization solution, the reaction of an aniline molecule with a perchlorate anion was found to be the rate-determining step; with chloride ions, the rate-determining step was the reaction between two aniline molecules and a chloride ion. The morphology of PANI films can also be controlled by first depositing a self-assembled monolayer of *p*-aminothiophenol on a gold electrode that is subsequently coated with PANI. Based on results obtained with *in situ* ellipsometry, a higher optical density of the formed polymer film was found [279]. Whereas no similar results could be obtained with other self-assembled monolayers, the chemical similarity between aniline and *p*-aminothiophenol was invoked as a reason for this behavior.

So far, no attention has been paid to the way the electrode potential necessary to transform the educt into the first electrooxidation intermediate is applied. The simplest way is the use of a two electrode arrangement, where the electrode upon which the polymer is deposited acts as the anode. A constant current is passed through both electrodes (galvanostatic mode). Obviously, the voltage across the electrodes and, correspondingly, the electrode po-

tential of the anode will settle at a value positive enough to enable the desired anode reaction to proceed. Of course, no electrode potential control is exercised. Consequently, fairly positive electrode potentials and undesired side reactions (such as degradation: see following text) are not reliably excluded. Nevertheless, this method is notably simple and attractive for technical applications. A much better control of the deposition process is maintained in a three electrode arrangement wherein the anode potential is controlled by means of an electronic regulation circuit. The electrode potential basically can be set to every desired value: in practice, a value where polymerization proceeds at sufficient rates without too many side reactions is selected (potentiostatic mode). As repeatedly reported, polymers of high quality (in terms of charge storage capacity, conductivity, or other polymer properties) can be obtained by applying an electrode potential that continuously changes between a positive (anodic) and a negative (cathodic) limit (potentiodynamic method). Finally, a method was reported by Tsakova et al. [280–282], wherein the electrode potential is stepped between a sufficiently high electrode potential, where monomer oxidation as well as polymer oxidation and doping occur, and a negative potential, where the film is reduced. This program yields large amounts of polymer in a short time.

A fairly coarse picture of electropolymerization kinetics emerges simply when the anodic current in the first peak is plotted as a function of the number of electrode potential cycles performed during a potentiodynamic electropolymerization. Of course this simple evaluation takes into account only the part of the polymer involved in the electrochemical redox process of the film, and the oxidation of the monomer, if any, is taking place at the electrode potential where the current values were recorded. Figure 21 shows a plot of the peak current versus the number of cycles for a selection of anilines investigated so far [283]. All experimental parameters (electrode potential during potentiostatic deposition, monomer concentration, pH of deposition solution, etc.) are the same for all monomers. The polymer formed from *N*-methylaniline shows the fastest growth. With increasing thickness of the film, the rate decreases. Whereas the oxidation of the monomer has to occur at the polymer solution interface, the electron transfer has to take place across the polymer film. A highly conducting film will support this step; a poorly conducting film will slow it down.

Accordingly, the film of poly(*N*-methylaniline) is of lower conductivity than other monomers. Aniline shows the next highest rate of deposition and a linear dependence of the current on the cycle number. The plot for *o*-toluidine is initially slightly steeper: after 150 cycles, the rate is lower than the value for aniline. The rate of formation of poly(*m*-toluidine) is even lower. Methyl substitution of aniline slows down the polymer formation. Double substitution as in the case of the xylydines decreases the rate even further. The rapidly dropping slope in case of poly(2,3-xylydine) indicates, in addition, a poorly conducting film. Other substituents in the ortho position (ethyl and *n*-propyl) slow down the polymerization even further. In both cases, the poor conductivity of the films results in very low rates or even stagnation. Rather surprising is the observation that the extremely high rate of polymerization of *N*-methylaniline is in no way matched by the rate of *N*-ethylaniline. This polymer shows an extremely slow growth. Taking the current in the 500 cycle, the influence of the size of an alkyl substituent is most obvious. The rate of the corresponding currents is 6.25:2.23:1 for *o*-toluidine, *o*-ethylaniline, and *o*-propylaniline, respectively.

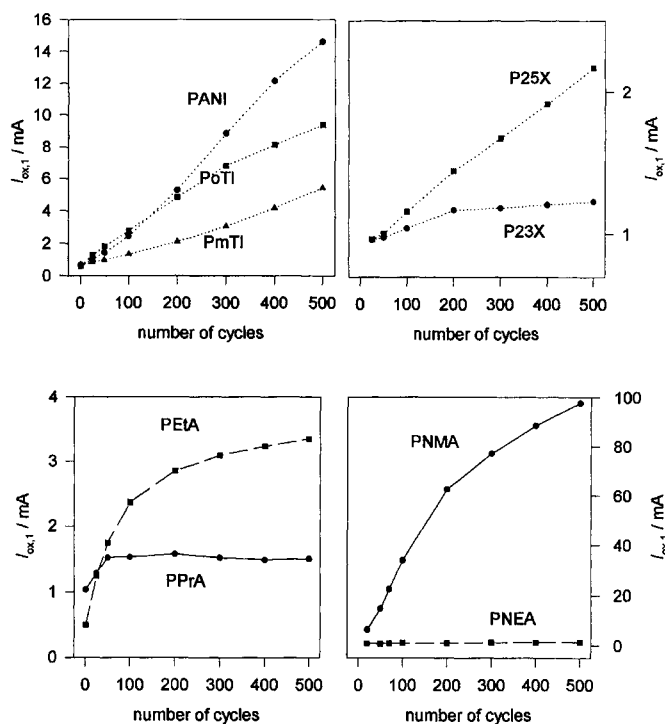


Fig. 21. Anodic peak current of first oxidation peaks of polymers recorded during deposition of various polymers (acronyms are defined in the text and Table I) in aqueous solution with pH = 0 and $E_{\text{anodic limit}}$, RHE = 1000 mV.

Without specific conductivities of these polymers and without kinetic data for the initial oxidation step, further quantitative analysis is highly speculative. Nevertheless, it seems safe to state that the reactivity of the monomer, which is higher for all substituted anilines, is no indicator of the polymer rate of formation. This reactivity is discussed in more detail in relation to the properties of the initial reaction intermediate. So far, only Fujita et al. [284] have reported a similar relationship for *o*-toluidine and *m*-toluidine.

This very straightforward approach also enables the identification of the effect of other experimental parameters on the rate of deposition, which may be of both fundamental as well as practical interest. Figure 22 shows a plot of the peak current versus the cycle number for the deposition of poly(*n*-propylaniline) in two different electrolyte solutions. Although the initial rate of formation in perchloric acid was higher, the value stagnates after about 60 cycles. On the contrary, the initially slower polymerization from a solution of sulfuric acid continues to proceed at an almost constant rate, even after 500 cycles.

Investigations of the polymerization kinetics of aniline and its relatives (as opposed to the oxidation kinetics observed in the initial electrooxidation step) are few. Most studies reported so far are devoted to morphological aspects, nucleation [285–288], nucleation dimensionality, and related features. Preferably, electrochemical (i.e., traditional) methods of investigation were employed. The first application of proton resonance spectroscopy to the investigation of polymerization kinetics of PANI has been reported [289]. Only chemical oxidation (precipitation and dispersion polymerization) was employed; the spectroscopy was used just to monitor the concentration of the monomer in the solution phase. Various oxidizing compounds of different effectiveness were studied. An investigation of the chemical oxidation with

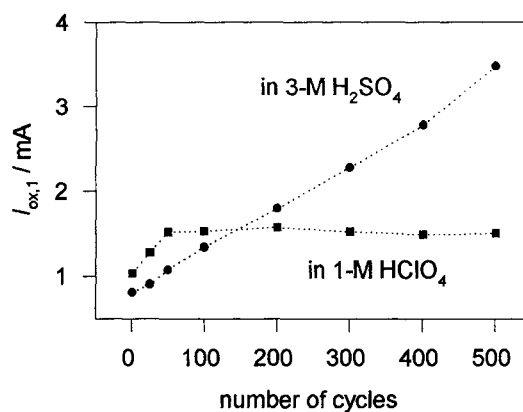


Fig. 22. Anodic peak current of first oxidation peaks of PPrA recorded during deposition in aqueous solution with different supporting electrolytes and $E_{\text{anodic limit}}$, RHE = 1000 mV.

calorimetry was reported by Fu and Eisenbaumer [290]. The reaction was found to be highly exothermic. With an excess of chemical oxidant, typical overoxidation products, hydrolysis products, and chlorination were found. The influence of experimental parameters like type of applied electrode potential versus time program [291] has been studied. The influence of the latter parameter together with a broad array of other parameters (monomer concentration in polymerization solution, pH of this solution, etc.) was reviewed comprehensively and some interesting correlations between preparation parameters and polymer properties were shown [292].

The influence of the employed electrolyte solution, in particular, the identity of the anion present in the supporting electrolyte, was the subject of investigations with respect to the polymerization process and the possible influence of the anion on the obtained polymer [293]. Conclusive evidence obtained with spectroelectrochemical methods is not available.

Ellipsometry was employed *in situ* by Kim et al. [294] during formation and electrochemical conversion of PANI. Results indicate both expansion and contraction during oxidative doping. Similar results that imply close correlations between ellipsometric parameters and the growth of the film during deposition as well as electrochemically induced changes during doping/dedoping were reported by Greef et al. [295]. Nianbing et al. [296] observed a strong correlation between the electrochemical oxidation current and the increment of the ellipsometric parameter Δ , with positive and negative signs corresponding to anodic and cathodic processes. Consequently, they suggested using ellipsometry as a tool for kinetic studies. Grodzicka et al. [297] used *in situ* ellipsometry during the early stages of polymerization of PANI. With films thinner than 20 nm, a one-layer model was employed successfully to fit the obtained data. For layers up to a thickness of 150 nm, a multilayer model was employed. Results were transformed into a two-layer model, combining a rather compact first layer covered with a fibrous top layer.

After polymerization by any electrochemical method, the polymer is present in its oxidized form. This implies the presence of positive charges on the polymer compensated by anions that have moved into the polymer during the oxidation process. This kind of doping has been termed *primary doping* [298] because it refers phenomenologically to the term "doping" as employed in semiconductors. *Secondary doping* has been suggested as a term for a

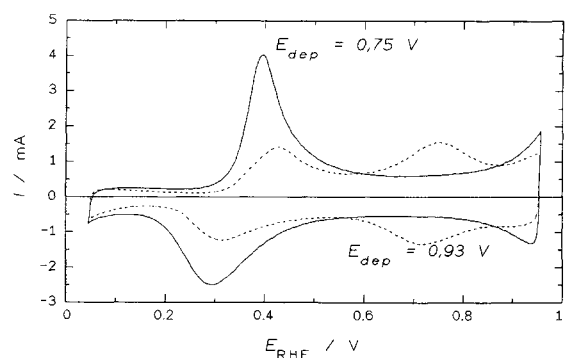


Fig. 23. CVs of polyaniline on a platinum electrode in 1-M HClO₄ prepared potentiostatically at $E_{SCE} = 750$ and 930 mV (from an aqueous solution of 0.1-M aniline + 1-M perchloric acid); scan rate $dE/dt = 100$ mV/s.

process wherein a chemical substance is introduced into the intrinsically conducting polymer and effects further changes, which persist even after complete removal of the second dopant [298, 299]. In the example reported, the changes are primarily a transfer of the “compact coil” form of PANI into an “expanded coil” type with accompanying changes in crystallinity and so forth. Figure 23 depicts typical CVs (for an introduction to this basic electrochemical method, see [300]) of a PANI film exposed to an acidic aqueous solution. Two current waves are seen in the anodic and in the cathodic electrode potential scan. Processes causing both current waves are discussed in the following section. The hysteresis of the corresponding processes was treated by Aoki [301]. The occurrence of a third current peak, located approximately in the middle between the peaks visible in the CV shown here, have been reported repeatedly. Shim et al. [302] assigned this peak to redox processes that involve dimeric species formed during the polymerization reaction. It is noteworthy that a memory effect observed during the first CV at the beginning of a series of CVs has been reported. This term refers to the observation that the initial CV obtained after prolonged exposure of the polymer to negative electrode potentials (i.e., after being held in the reduced state) or the first complete CV after film formation are different in terms of measured currents, observed peak potentials, or number of current peaks from subsequent cycles. Recording UV-vis spectra (for experimental details, see subsequent text) has turned out to be helpful in obtaining information on the time scale of these processes. Results reported so far indicate molecular changes (with a slow dedoping of the polymer) that include changes of the molecular conformation proceeding on a far longer time scale as compared to the electrochemical reactions that initiate these changes as deduced from the position of absorption bands [303, 304]. Investigations with electrochemical *in situ* ECSR have been done [305, 306]. A slow change in the dependence of the exchanged electric charge needed for polymer oxidation and the potential range wherein this process occurs on the electrode potential was found. This was explained by a slow relaxation of the polymer in the reduced state. A possible model of relaxation was related to the evolution of the polaron-bipolaron gap. This, in turn, was expected to show up in changes of the concentration of free spins as measured with ECSR as a function of electrode potential. The reported results do not support this model. Attempts have been made to accelerate this process by enhancing transport of the counterions by using bilayers of various polymers [307, 308].

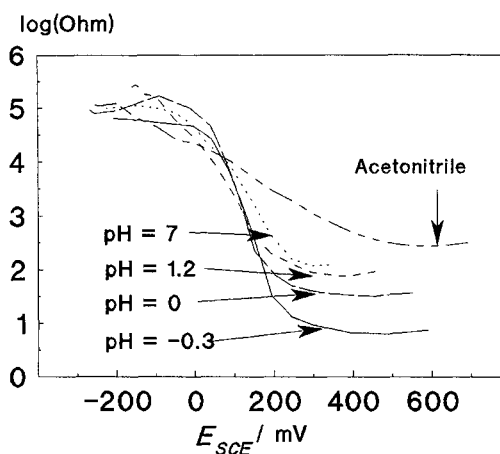


Fig. 24. Change of relative polymer film resistance of PANI deposited potentiostatically as a function of electrode potential (degree of oxidation) and of pH value of the electrolyte solution. For experimental detail, see [72, 309].

The dopng–dedoping process is reversible⁹ if the positive potential limit is kept below a critical value, beyond which polymer degradation becomes dominant. The doping/dedoping of the polymer is accompanied by numerous changes, which also are discussed in more detail in the following section. The most striking change of a polymer property is the change of the electrical conductivity or its reciprocal, the electrical resistance. Figure 24 displays a set of curves that show this change in relative units for PANI as a function of electrode potential (i.e., degree of oxidation or doping) and pH value of the electrolyte solution. Data were recorded *in situ*, that is, in the presence of an electrolyte solution. The experimental setup, which involves the use of a bandgap gold electrode and a specially designed electronic circuit that allows measurements with small dc voltages, has been described previously in detail [72, 309]. The obvious prerequisite for electronic conduction seems to be protonation of the polymer. The particular pH sensitivity of the spectroelectrochemical behavior, which is closely related to electrochemically induced changes of conductivity, has been pointed out repeatedly [310, 311]. The obvious influence of the pH value is only one aspect of the environmental sensitivity of PANI. The behavior of PANI, in particular, the change of conductivity of PANI films, as a function of water or ammonia vapor pressure has been reported [312] and implies applications in sensor technology.

Thermochromism and acidochromism of substituted PANI were reported by Snauwaert et al. [313], who provided no further interpretation beyond the assumption that the positive charge induced by protonation may induce some perturbation on the electron density in the aromatic ring.

So far, some polymers have been polymerized exclusively by more or less complicated chemical routes (as an example, see [314] for acetylene-terminated PANI). Whereas these polymer have not been shown to be electrochemically active and no spectroelectrochemical data have been reported, they are not treated in more detail. The conductivity of samples prepared from oligomers with tightly controlled chain length depends significantly on the number of nitrogen atoms present on the oligomer chain. Oligomers with less than eight atoms are particularly poor conductors [315].

⁹This adjective does not refer to any thermodynamic reversibility. It solely describes the fact that the polymer can be returned to its initial state.

3.2. Properties of Polyaniline and Related Polymers and their Electrochemically Induced Changes

The bulk of spectroelectrochemical studies as well as of other investigations that employ nontraditional methods of investigation devoted to PANI and the related polymers deal with the properties and the behavior of the polymer itself. Because of the very complex nature of these materials that combines central aspects of organic chemistry, polymer chemistry, solid state science, and materials science, and the fact that these materials show interesting and complex responses to a host of environmental influences, the use of only traditional electrochemical methods has resulted in less than satisfying results. Almost from the very beginning, the investigation of PANI and, later, its numerous relatives has employed nontraditional techniques. In many cases, investigations reported by numerous researchers deal with both the properties of the polymer and their changes as a function of various environmental parameters. In some cases, results cannot be assigned to just one of the following sections. This is particularly true in cases where differential methods (modulation techniques) have been used. These methods (e.g., *in situ* Infrared spectroscopy with electrode potential modulation) yield data that represent the change of the investigated property (e.g., vibrational spectrum) as a function of the modulated parameter (in this example, the electrode potential). Consequently, the results contain information both on the polymer itself and on its change as indicated.

From the chemists' point of view, PANI can be treated as a macromolecular polymer. To elucidate its chemical structure, numerous spectroscopies have been employed. Vibrational spectroscopies have turned out to be most helpful. Infrared spectroscopy was initially employed *ex situ* (i.e., with dried samples outside the electrochemical cell); only later were adequate experimental designs developed for *in situ* studies with suitable thin layer electrochemical cells containing polymer-coated metal electrodes for external reflectance measurements. In many cases, IR spectroscopy is just used as a routine tool; only those reports based on more intense applications are considered here [316–340]. A typical set of IR spectra of PANI exposed to an aqueous acidic electrolyte solution recorded *in situ* in the external reflection mode is shown in Figure 25. Interpretation of the spectra and assignment of the observed bands has been done by starting from two completely different points. In the classical approach, the polymer is treated as a collection of monomer units that show molecular connections.

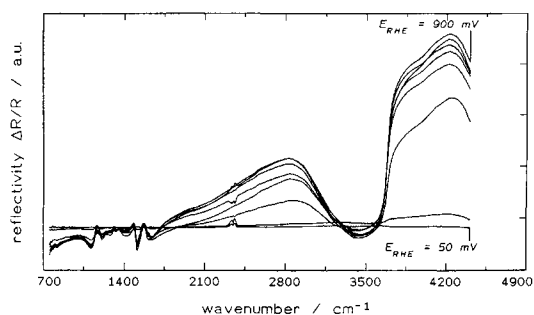


Fig. 25. *In situ* infrared spectrum of a PANI film deposited on a platinum electrode recorded in external reflection mode. Polymer deposited at $E_{RHE} = 992$ mV in an aqueous solution of 0.1-M aniline + 1-M $HClO_4$; reference electrode potential $E_{RHE} = 50$ mV; measurement electrode potentials E_{RHE} as indicated: 50, 150, 400, 500, 600, 700, 800, 900 mV; resolution 4 cm^{-1} , for further details see [273].

Thus the bands are assigned by comparing their position and intensity with those of the parent molecule and with related substituted molecules. This approach is used most often. A second, completely different approach has been proposed by Tian, Zerbi, and other researchers [341–348]. Because of the central importance of changed bond lengths r (shorter single bonds r_{C-C} and longer double bonds $r_{C=C}$ as a function of the state of charge), the concept has come to be connected with the term “effective conjugation coordinate” (ECC). So far, this approach has been applied thoroughly only to polypyrrole and polyacetylene. Because of its central importance and the convincing results obtained so far, this concept is subsequently described briefly. The calculation starts with band positions of IR bands obtained with MNDO calculations, which are compared with experimentally found bands of reduced polypyrrole. Force constants and band assignments were thus obtained. Using the foregoing concept, which describes the changes of the bonding situation in a pyrrole ring when the benzoid reduced state is changed into the quinoid, oxidized state, additional information was obtained. The effective conjugation coordinate is related to a dimerization parameter $d = r_{C=C} - r_{C-C}$. This coordinate describes the movement of atoms of the polymer backbone during the transition from the benzoid to the quinoid state. The movement assigned to this coordinate causes the largest change of polarizability in the reduced state and the largest change of dipole moment in the charged state. Accordingly, bands related to changes of the dipole moment (IR bands), which are connected with the delocalized π electrons, increase in intensity with an increase of electrode potential and accompanying oxidation of the polymer. Because of the changed properties of the involved molecular bonds, their positions change too. Corresponding changes of the Raman spectrum, which are related to the polarizability of molecular bonds, are effective. Application of this successful concept to polyaniline and its relatives is still missing.

In the set of infrared spectra obtained *in situ* up to 4700 cm^{-1} and displayed in Figure 25, the strong absorption around 4250 cm^{-1} ($E = 0.5\text{ eV}$) that frequently is observed when PANI is in its conducting mode is not shown (for comparison, see the infrared spectrum of *o*-toluidine (PoTl) displayed in Figs. 44 and 45). Because of the applied technique, the spectra shown represent differences in absorption of the polymer film as a function of the electrode potential. To obtain these spectra, a single beam spectrum is recorded at a selected electrode potential E_r . In the case displayed here, this electrode potential was set in the region where the polymer is in its reduced state. A second single beam spectrum is recorded at a more positive electrode potential E_m . It is ratioed versus the first spectrum. The resulting differential spectrum is plotted. Further spectra are obtained in the same way, always taking the first spectrum as a “background spectrum.” Unfortunately, the obtained differential bands are considerably more difficult to interpret compared to absolute Raman spectra obtained without the need for any background spectrum or compared to *ex situ* infrared spectra obtained with polymer samples in transmission mode. In many cases, differential (bipolar) bands are obtained that show upward and downward pointing bands indicative of changes of band intensity and position as a function of electrode potential. The precise position of the band at the employed electrode potentials E_r and E_m are difficult to determine. In a few cases, bands that point only in one direction are found. This may be caused by the absence of any IR absorption at one or both potentials. Consequently, the spectral ratioing results in a simple band. Alternatively this may also be caused by the lack of a dependence of the band position

on the electrode potential. Spectral ratioing in this case results in a single-direction band when the intensity of the band is a function of the electrode potential. In the worst case, both intensity and position are unaffected by the changed electrode potential; this yields no band in the differential spectrum at all.

Assignments of the bands observed with a sample of PANI prepared from a solution of 0.1-M aniline in 1-M HClO₄ at an electrode potential of $E_{\text{RHE}} = 992$ mV as based on the work of Sariciftci et al. [324], Lapkowski et al. [349], and Colombari et al. [350] are listed subsequently. Further details are collected elsewhere [273]. Colombari et al. used vibrational spectroscopy to prove the existence of strong hydrogen bridges in the conducting emeraldine form of PANI. The suggested structural model that takes into account this kind of interaction assumes conducting islands in PANI, wherein emeraldine strands are positioned with respect to their neighbors in such a way that quinoid and benzoid rings are juxtaposed. Consequently, protonated amine and nonprotonated imine sites are matched. This results in hydrogen bonds at a degree of protonation of exactly 50%. This network can be two or three dimensional, and it is embedded in a matrix of insulating, nonprotonated PANI. Conduction occurs when hydrogen bonds are switched from amine to imine sites, thus generating mobile charge carriers.

According to the more classical interpretation of Sariciftci et al. [324], the increase of intensity with a more positive electrode potential of those bands at about 1484, 1574, and 1632 cm⁻¹ is indicative of a growing fraction of quinoid aromatic rings. Bands with a decreasing intensity (e.g., around 1512 cm⁻¹) are caused by vibrations of benzoid rings with a decreasing fraction. The bands assigned to the semiquinoid form are not observed in the spectra shown here.

A further increase of the electrode potential results in a higher degree of oxidation (doping) and transformation into the pernigraniline form. Assignments of the bands seen in Figure 25 are listed in Table III.

The fundamental difference in the interpretation is the assignment of the band around 1100 cm⁻¹. In the presence of perchlorate ions in the electrolyte solution, the strongly absorbing symmetric stretching mode of this ion tends to obscure all other spectral features. In *ex situ* measurements with a suitable counterion, Colombari et al. assigned this broad band to the stretching mode of the N-H...N moiety [350]. In comparison, the $\nu_{\text{N-H}}$ is at about 3000 cm⁻¹. Based on a comparison of band positions, Colombari et al. calculated a diminished distance of the nitrogen atoms of about 245 pm. Using perchhenate ions instead of perchlorate ions, Sariciftci et al. were able to remove the disturbing coincidence of the vibrational band of the counterion and of the polymer [351–354]. So far, this step has not resulted in a new interpretation of their spectral data.

According to Colombari et al., within the broad band assigned to the hydrogen-bond mode there are several transmission windows, so-called Evans holes [355, 356]. These holes are caused by the coupling of a narrow band with a very broad band. Principally, this is a phenomenon similar to the Fermi resonance. The interaction of two or more modes results in new modes and bands of different energies with corresponding transmission modes in the infrared spectrum and emissions in the Raman spectrum, which actually have been observed by Colombari et al. [350]. As a consequence, *ex situ* spectra have to be checked for unexpected transmissions. In the spectra recorded *in situ* and shown in Figure 25, band shifts as compared to band positions found in spectra

recorded *ex situ* should be visible. Nevertheless, the interpretation suggested by Colombari et al. seems to be appropriate considering the particular environment and state of aniline units in PANI.

Another difference between the assignments of Sariciftci et al. and Colombari et al. refers to the band at around 1635 cm⁻¹. Sariciftci et al. assign this band to the vibrational mode of a quinoid ring system. Although the differential (bipolar) nature of the band makes exact determination of intensity and position as a function of electrode potential difficult, the spectra in Figure 25 show a significant decrease of absorbance as a function of positively directed electrode potential. This implies a decrease of the fraction of quinoid ring systems. According to Colombari et al., this band is caused by a benzoid mode and corresponds to a C=C stretch mode. The intensity of this mode should indeed decrease with oxidation of the polymer into its pernigraniline form.

A technique that complements infrared spectroscopy is Raman spectroscopy. The strong coloration of PANI, especially in its doped, oxidized form, results with most laser excitation wavelengths in more or less strongly resonantly enhanced Raman spectra. This favorable coincidence has a possible drawback, because of possible photochemical processes caused by the absorption of photons from the laser light. Fukuda et al. [357] reported that illumination of the emeraldine form of PANI by laser light from an argon ion laser at $\lambda_{\text{L}} = 2.41$ eV results in structural transformations of the quinoid rings into benzoid rings. Consequently, only benzoid modes should be visible in Raman spectra. Spectra reported by Brandl [273] as shown in a typical example that follows (see Fig. 26) reveal considerable changes, including an increase of the intensity of bands presumably caused by vibrational modes of quinoid systems after positively directed shifts of the electrode potential. This observation does not support the claims by Fukuda et al. Nevertheless, the change of the Raman spectra, in particular, the decrease of the intensity of bands related to modes of quinoid systems, at even higher potentials, where the emeraldine form is changed into the pernigraniline form, may be due to the reason suggested by Fukuda et al.

An alternative explanation of the obvious decrease of scattered light intensity after an increase of electrode potential to more positive values can be based on the ECC concept described previously. According to this concept, an increasing degree of oxidation reduces the polarizability of all modes relative to the effective coordination coordinate. The agreement between prediction and experimental result is disturbed only at low electrode potentials ($E_{\text{RHE}} = 0$ mV $> E > E_{\text{RHE}} = 400$ mV). In this range, the scattered light intensity decreases with increasing electrode potential. The explanation of this change is simple. At about $E_{\text{RHE}} = 400$ mV, PANI changes under the employed experimental conditions (see Fig. 26) from its leucoemeraldine into its emeraldine form. The corresponding color change from yellow-green to green is visible. The more intense coloration, which can be checked easily in the corresponding UV-vis spectra, results in a stronger resonance enhancement, which in this potential range overcompensates the decrease of intensity as predicted. Bartonek et al. [358] attributed the particular increase in intensity of benzoid ring vibration modes after the first oxidation wave to a resonance enhancement caused by polaronic defect states. These states are generated by oxidation/doping, their concentration as deduced from ECSR measurements bears a striking resemblance to the resonance Raman data.

A typical set of Raman spectra measured *in situ* is displayed in Figure 26. Assignments for bands at selected electrode potentials,

Table II. Assignment of Vibrational Bands for PANI Measured *in situ* in its Emeraldine form at $E_{RHE} = 700$ mV^a

$\bar{\nu}$ (cm ⁻¹)	Assignment						$\bar{\nu}$ (cm ⁻¹)
	Sariciftci [324]			Colomban [350]			
	$\bar{\nu}$ (cm ⁻¹) ^b	Mode ^c	Wilson no.	Mode ^c			
—	$\delta_{C-H}OP$	820*	—	δ_{C-C}	1	B	840
—	—	—	—	γ_{C-H}	10a	B,Q	890
1111	δ_{C-H}	1100	—	$\nu_{N...H...N}$	—	—	1100
1169	$\delta_{C-H}iP$	1141	—	—	—	—	—
1206	—	—	—	δ_{C-H}	9a	B	1195
—	$\nu_{ring-N-ring}$	1248	SQ	—	—	—	—
—	$\nu_{ring-N-ring}$	1301	SQ	—	—	—	—
—	$\nu_{ring-N-ring}$	1375	SQ	ν_{N-ring}	—	B,Q	1360
1484	ν_{ring}	1477*	Q	—	—	—	—
1513	ν_{C-C}	1497	B	ν_{C-C}	19a	B	1514
1571	ν_{C-C}	1560*	Q	—	—	—	—
1635	$\nu_{N=ring}$	1630*	Q	$\nu_{C=C}$	18a	B	1625

^aFor experimental conditions, see Figure 25.

^bThe asterisk (*) indicates bands measured *in situ*.

^cQ designates the quinoid state, B designates the benzoid state, and SQ designates the semiquinoid state.

Table III. Assignment of Vibrational Bands for PANI in its Pernigraniline form at $E_{RHE} = 900$ mV^a

$\bar{\nu}$ (cm ⁻¹)	Assignment according to Sariciftci [324]		Mode ^b
	$\bar{\nu}$ (cm ⁻¹)		
802	—	—	—
821	$\delta_{C-H}Op$	843	—
860	—	—	—
1107	Perchlorate mode		—
1153	$\delta_{C-H}iP$	1148	—
1173	—	—	—
1192	—	—	—
—	$\nu_{ring-N-ring}$	1250	SQ
1325	$\nu_{ring-N-ring}$	1319	SQ
—	$\nu_{ring-N-ring}$	1337	SQ
1377	$\nu_{ring-N-ring}$	1377	SQ
1484	ν_{ring}	1477	Q
1512	ν_{ring}	1502	B
1574	ν_{ring}	1560,1578	Q
1605	—	—	—
1632	$\nu_{ring=N}$	1630	Q

^aFor experimental conditions, see Figure 25.

^bQ designates the quinoid state, B designates the benzoid state, and SQ designates the semiquinoid state.

which correspond to various states of oxidation (leucoemeraldine, emeraldine, and pernigraniline), are collected in Table IV. The molecular structure model, which can be derived from the results

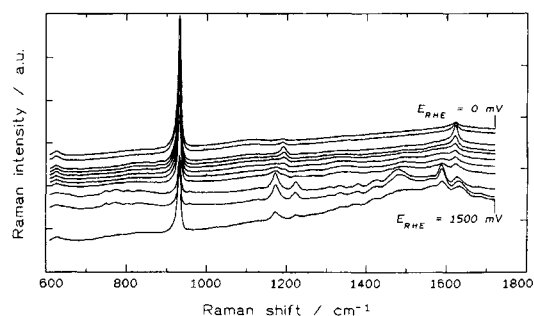


Fig. 26. *In situ* resonance Raman spectra of a PANI-film deposited on a platinum electrode; polymer deposited at $E_{RHE} = 992$ mV in an aqueous solution of 0.1-M aniline +1-M HClO₄, measurement electrode potentials $E_{RHE} = 0, 300, 400, 500, 600, 700, 800, 900, 1000, 1200,$ and 1500 mV as indicated; resolution 2 cm⁻¹. For further details, see [273].

reviewed so far is depicted in a somewhat simplified form in Figure 27 (not all conceivable protonation equilibria and resonance structures are shown; for details, see also [359]). Upon oxidation of PANI by electrochemical processes as well as upon protonation of the polymer, a positively charged macromolecule results. For charge compensation, anions (sometimes called dopant ions or counterions) usually taken from the supporting electrolyte of the solution phase, are incorporated. Their properties may affect the properties of the polymer in various ways as addressed at various points in the following text.

Raman spectra reviewed so far are almost exclusively resonantly enhanced, because the exciting laser light wavelength is more or less close to the optical absorptions of the polymer. As discussed in more detail in the following part, the optical absorption of PANI as well as of its relatives extends into the near infrared region (i.e., beyond $\lambda = 1000$ nm). Excitation of PANI with laser light in this region also has been employed in structural studies of

Table IV. Assignment of Vibrational Bands (in wave numbers per centimeter) for PANI as Measured with *in situ* Raman Spectroscopy

Spectra of Fig. 26			Lapkowski et al. [349]					Colomban [350]			Mode or Wilson number
LE	EM	PG	LE	EM	EM	PG	SQ	EM	EM	PANI modification	
0	700	1000	—	—	—	—	—	—	—	—	Electrode potential E_{RHE}
514,5	514,5	514,5	457,9	457,9	647,1	647,1	1064	477,9	632,8	—	Laser light λ_0
1624	1621	1625	1618	1620	1618	1612	1590	1622	1585	ν_{CC}	8a
—	1560–1600	—	1597	1551	1553	1553	1590	—	—	ν_{CC}	8b
—	1560–1600	1586	—	1590	1586	1579	1590	—	—	ν_{CC}	Q
—	1520	—	—	—	—	—	—	1514	1487	ν_{CC}	19a
—	1495	1480	—	1486	1480	1480	—	—	—	$\nu_{C=N}$	—
—	1420	1427	—	1420	1420	1418	1507	—	—	ν_{CC}	Q
—	1300–1380	1380	—	—	—	—	—	—	—	—	—
—	1300–1380	1333	—	—	—	—	—	1334	1342	ν_{N-ring}	—
—	1300–1380	—	—	—	—	—	≈ 1330	—	—	Protonated structure	—
—	1300–1380	1307	—	—	—	—	—	—	—	—	—
—	1265	1223	1219	1220	1217	1215	1260	—	—	ν_{C-N}	—
1191	1191	—	1181	1186	—	—	1170	1191	1165	δ_{CH}	9a
—	1170	1172	—	1162	1160	1157	—	—	—	δ_{CH}	Q
1120	1100	—	—	—	—	—	—	—	—	—	—
—	—	—	—	—	—	—	—	880	875	γ_{CH}	10a
—	800–860	—	868	880	870	—	—	—	—	δ_{ring}	B
—	800–860	831	—	—	—	—	—	830	810	δ_{CC}	1
—	800–860	—	820	828	826	—	—	—	—	δ_{amine}	—
—	800–860	804	—	—	—	—	—	—	—	—	—
—	800–860	776	—	—	788	788	810	—	—	δ_{ring}	Q
—	720	749	—	720	750	749	714	—	—	δ_{imine}	—
—	720	—	—	—	—	—	—	719	713	γ_{CC}	4
—	—	—	667	668	—	—	—	—	—	δ_{amine}	—
628	627	626	603	—	640	—	—	—	—	—	$\delta_{ring} B$
—	—	—	—	—	—	—	—	606	589	δ_{CC}	6a
—	—	—	—	—	—	—	—	510	522	γ_{CC}	16b
—	—	—	—	—	—	—	—	416	427	γ_{CC}	16a

^aSee Figure 26 for experimental conditions. LE denotes leucoemeraldine, EM denotes emeraldine, PG denotes pernigraniline, and SQ denotes semiquinoid.

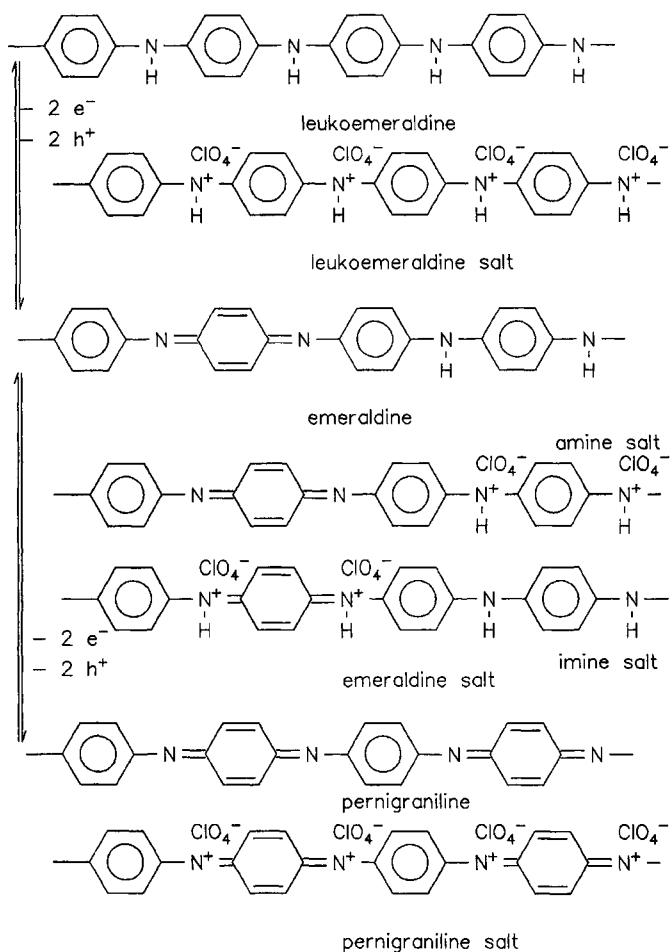


Fig. 27. Simplified molecular structure formulas of PANI in its various states of oxidation and protonation.

PANI by Engert et al. [360]. New spectral features were observed upon excitation with $\lambda = 1047$ nm. Using the resonance Raman spectrum of Michlers ketone in its lowest excited triplet state as a reference, these features were assigned to the dynamic structure of a diimino-1,4-phenylene unit in the PANI chain, which rapidly exchanges a positive charge. As a consequence, a conduction mechanism with a positive charge that migrates from nitrogen site to nitrogen site is proposed and is basically in agreement with the often assumed hopping conduction model.

One of the most striking features of PANI and its relatives already visible in most simple experiments is the more or less pronounced electrochromism, which resulted very early in suggested uses in smart windows [361, 362]. Electrooptical properties of PANI films can be studied most easily with UV-vis spectroscopy. Essential parts of the experimental setup suitable for use in a standard double beam UV-vis spectrometer are depicted in Figure 28. Alternatively, UV-vis spectra can be recorded in the external reflectance mode [363]. In this way, polymers that are difficult to deposit on ITO-coated glass sheets can also be investigated. Whereas the polymers can be deposited directly onto optically transparent electrodes, these measurements are fairly simple. Glass sheets coated with indium-doped tin oxide or sputtered with a thin layer of gold are most commonly used. A measured set of spectra as obtained with electrolyte solutions of different composition (and different pH values accordingly) is shown in

Figure 29. The electrochemically induced change of absorption of major bands is depicted in detail in Figure 30. Assignment of the major spectral bands for the polymer seem to be a settled issue. The absorption band found around $\lambda = 330$ nm has been assigned to a $\pi \rightarrow \pi^*$ transition of the aromatic ring system. Its change both with respect to position and to intensity has been explained by invoking the transition of the aromatic system from a benzenoid into a semiquinoid and, finally, a quinoid state. The electronic absorption at medium wavelength (around $\lambda = 430$ nm; the actual value seems to depend on a large number of experimental parameters) is caused by radical cations (polarons; see following text) introduced into the polymer by electrooxidation. Consequently, this band is almost absent in the reduced state of PANI and grows with oxidation of the film. As will be seen later (cf. Fig. 39), the absorption at this band correlates strongly with the amplitude of the ESR absorption (i.e., the concentration of free spins in the polymer film). Because of the lack of interference with other electronic transitions, this absorption around $\lambda = 430$ nm has been taken as a measure of the polaron concentration [364]. At slightly higher electrode potentials, an additional band at even higher wavelengths rises with positively directed electrode potentials; it is found around $\lambda = 800$ – 900 nm (approx. $E = 1.37$ eV). In many cases, the maximum of the absorption band cannot be observed with standard UV-vis spectrometers, because it is located somewhere in the NIR; sometimes this absorption commences only at about $\lambda = 1000$ nm. This absorption has been designated as a “free-carrier tail” of an absorption in the NIR [365]. The assignment of this band has been the subject of some controversy. As part of the search for the carriers of the electronic conductivity, correlations between the measured conductivity and various spectroscopic and electrooptic PANI properties have been investigated. As shown in Figure 31, the long wavelength absorption correlates fairly well with the electronic resistance of the film. Consequently, it has been proposed that species that cause this electronic absorption are the prevailing carrier of electronic conduction [73]. More recently, this interpretation has come under considerable attack [366]. A starting point to visualize the changes that occur in the UV-vis spectra of a conducting polymer with increasing potential applied is to plot the absorption at selected wavelengths ($\lambda = 310, 410, 880$ nm) as a function of the electrode potential (Fig. 32). The expectation that major changes occur at the two potentials known to mark the transitions from the leucoemeraldine to the emeraldine and, subsequently, to the pernigraniline form of polyaniline ($E_{SCE} = 100$ – 200 mV and 750 – 850 mV) is confirmed. The graph is very similar to diagrams known from kinetic experiments, where the concentration of the reactant and product of a reaction are represented by the absorption at $\lambda = 310$ nm (leucoemeraldine) and $\lambda = 410$ nm (emeraldine). This parallel is not valid for electrode potentials $E_{SCE} > 800$ mV, implying that irreversible reactions take place at the pernigraniline sites. As already seen in Figure 31, the absorption maximum in the low-energy region of the UV-vis spectrum exhibits a remarkable hypsochromic shift upon potential increase. This has been observed before [241, 367], but it either was not discussed or was stated only that this observation could not be reconciled with available band structure calculations as used for the band model frequently employed in discussions of intrinsically conducting polymers. A different approach to the interpretation of UV-vis spectra based on the Alentsev-Fock method [368] was proposed by Nekrasov et al. [369]. Based on an investigation of the spectral changes at selected wavelengths as a function of electrode potential (i.e., degree of

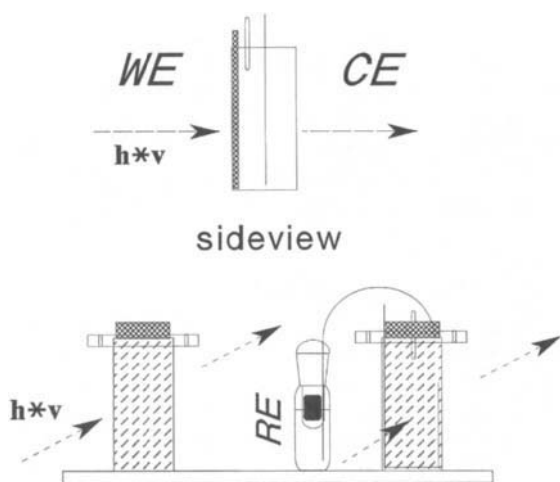


Fig. 28. Experimental setup for *in situ* UV-vis studies with optically transparent electrodes as used with a dual beam spectrometer.

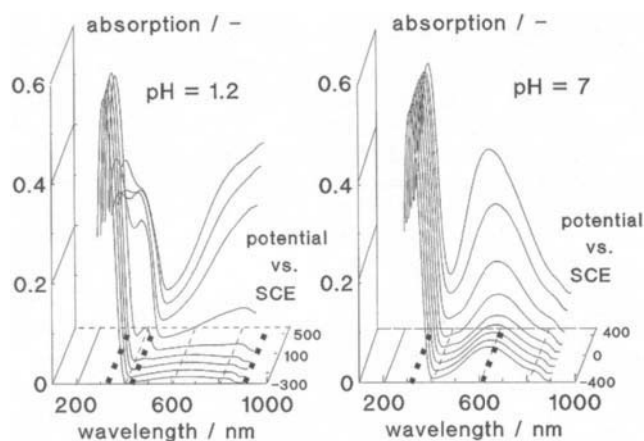


Fig. 29. UV-vis absorption spectra of PANI films recorded with various electrolyte solutions of different pH values.

doping), various bands were identified and assigned: $\lambda = 300$ nm (amine fragments); $\lambda = 357$ and 755 nm (polarons); $\lambda = 665$ nm (quinoid structures); $\lambda = 570$ nm (donor-acceptor interactions between quinoid fragments and counteranions); $\lambda = 895$ nm (electron exchange between polaron-containing areas of the film).

The question of the nature of the charge carriers of an intrinsically conducting polymer will be discussed in detail later on. Some of the results obtained, in particular, with ESR are quoted here to get a more detailed understanding of the changes in the electronic absorption spectra. A closer look at the polaron-bipolaron model is presented subsequently. The question can be reduced to, "What will happen if there are two charges (radical cations, later designated as polarons) on a long conjugated polymer chain?" Will they form a so-called bipolaron (spinless dication)? When the first ESR measurements indicated the absence of spins for the conducting form of some intrinsically conducting polymers, the presence of bipolarons seemed evident. However, Hill et al. [370] found that the ESR signal can be missing for isolated oligothiophene radicals that carry only one charge per molecule. Bipolarons cannot be the explanation for the missing ESR signal when there is only one charge on each oligomer. The group shows that radical cation π dimers cause the loss in ESR activity, and this might also be the

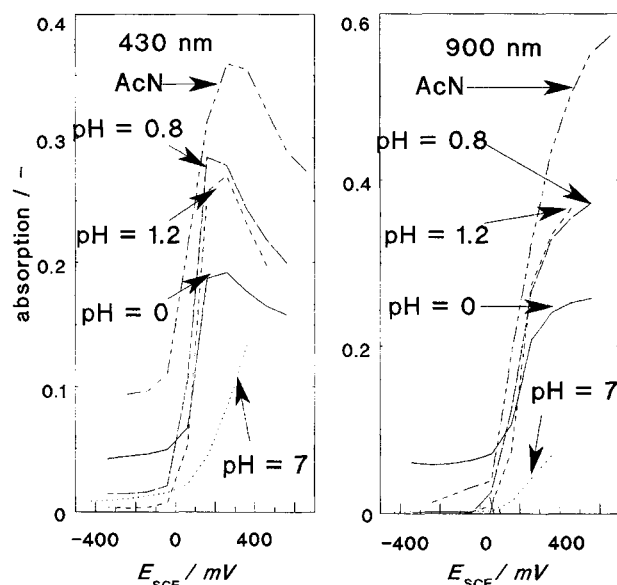


Fig. 30. Change of absorption as a function of electrode potential for PANI films recorded with various electrolyte solutions of different pH values.

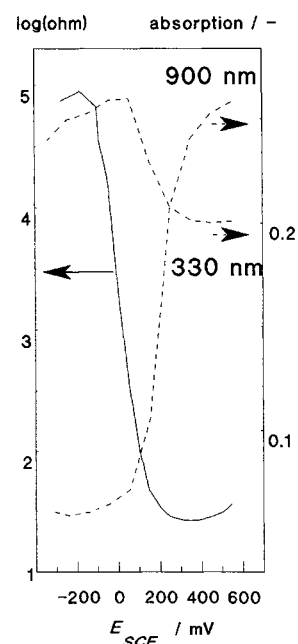


Fig. 31. Correlation of the electronic resistance of PANI with the UV-vis absorption around $\lambda = 800$ nm as recorded in an electrolyte solution of $\text{pH} = 0$ (1-N H_2SO_4 in water).

case for intrinsically conducting polymers (for further details and a general introduction and review, see [371-375]). An interesting parallel is that the UV-vis spectra of the oligothiophene radicals show a peak at $\lambda = 710$ nm.

The shift of the absorption maximum in the low-energy range of the UV-vis spectrum is a key to understanding the behavior of polyaniline at high electrode potential. This shift, calculated from an absorption at ca. $\lambda = 900$ nm at a potential of $E_{\text{SCE}} = -200$ mV, which moved to approximately $\lambda = 620$ nm at $E_{\text{SCE}} = 900$ mV, cannot be the result of two different species

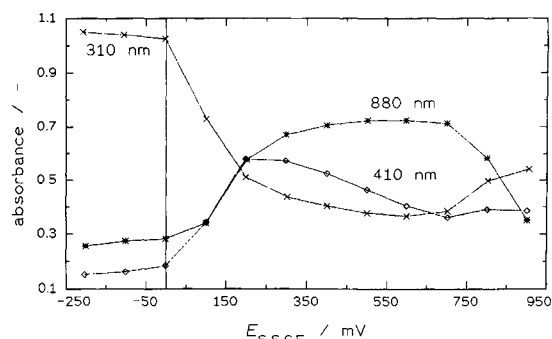


Fig. 32. Changes in absorbance at three specific wavelengths that indicate the presence of aromatic ($\lambda = 310$ nm) and polaron species ($\lambda = 410$ and 880 nm); 1-M HClO₄ in water.

absorbing at $\lambda = 900$ and 620 nm, respectively, even though it is quite tempting to assume that the absorption at $\lambda = 620$ nm results from hydrolysis products of the pernigraniline form of polyaniline. In the latter case, the absorption at $\lambda = 620$ nm should increase with time when polyaniline is exposed to high potentials. More hydrolysis products should be produced, but a decreasing absorption is observed. This shows that another model is necessary to understand such a hypsochromic shift.

Kuhn [376, 377] developed a model to explain the UV-vis behavior of natural dyes that turned out to work exceptionally well for conjugated systems. This model is based on the assumption of an electron gas caught in a potential energy well that corresponds to the size of the conjugated system of the dye molecule and is exposed to the sinusoidal potential energy function resulting from the atoms of the conjugated system. It does not (and never was intended to) fully describe the bonding situation of such a dye molecule, but it can give an astonishingly precise description of its UV-vis behavior. Two main conclusions can be drawn from this model: (1) even for an infinitely extended conjugated system, the absorption energy does not approach zero, but rather a finite value (a consequence of the sinusoidal potential) and (2) the energy of the absorption maximum (approximately) is a linear function of the reciprocal number of monomer units $1/n$ (proportional to $1/\text{length}$) of the conjugated system. Both phenomena were observed experimentally. The latter can be quite useful in estimating conjugation lengths from data derived from oligomers, via UV-vis spectroscopy. The absorption energy of a few oligomers that consist of a known number of monomers is plotted against the reciprocal function of this number of monomers and can be calculated from a linear regression slope and intercept with the y axis (the intercept represents an infinitely extended conjugated system). The linear relationship allows calculation of the number of monomers (effective conjugation length) that correspond to the observed absorption energy of a polymer. This is in agreement with the idea of Min et al. [378], who assigned a band of camphor sulfonic acid-doped polyaniline at $\lambda = 780$ nm to a localized polaron or, in the chemist terms, a cation radical state on a chain of limited conjugation length.

On the basis of this model, an approach to the effects as visualized in Figure 33 is possible. Here, the horizontal axis does not show the reciprocal number of monomers, but the electrode potential applied to the polymer. A linear increase of the absorption energy for potentials exceeding $E_{SCE} = 300$ mV is observed independently of the conditions chosen for the preparation of the

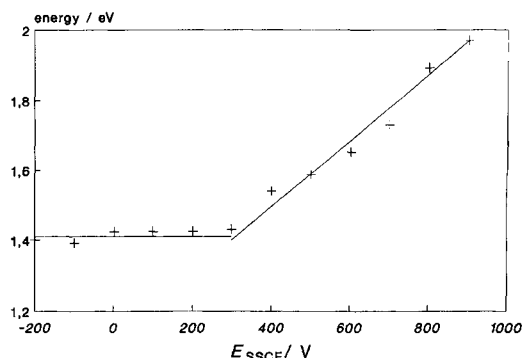


Fig. 33. Energy of the long wavelength maximum in the UV-vis spectrum of polyaniline as a function of the applied potential. A linear relationship with a slope of 1 eV per volt of applied potential is observed. With increasing potential, shorter conjugated segments can be oxidized, and when more polarons are located on shorter segments, a hypsochromic shift (blue shift) results [273].

PANI film. This underlines the fact that a decreasing average conjugation length is responsible for the absorption energy shift. For potentials lower than this limit, no further change in absorption energy is observed; the maximum conjugation length is reached. There is only one charge (polaron) per undisturbed coplanar polymer chain segment and there are charges only on the longest of these segments, because they have the lowest oxidation potential. With increasing electrode potential, more electrons are abstracted from the polymer, and the higher potentials allow the oxidation of shorter coplanar chain segments, with a corresponding increase of the absorption energy. The fact that this shift starts at potentials far below those necessary for the generation of pernigraniline sites indicates that the shift is not a consequence of irreversible oxidation or hydrolysis of the polymer, but a mere consequence of oxidation being extended to shorter coplanar segments.

Table V summarizes the results for slope and y axis intercept of a linear regression of the observed absorption energy-potential shifts for several PANI films prepared under different conditions. For potentials $E_{SCE} < 300$ mV, there is no shift observed, and the average value of the absorption energy at these potentials, which represent the reduced state of PANI, was calculated to find the intercept with the y axis. Typically, a value of just above $E = 1.4$ eV was found. For potentials $E_{SCE} > 300$ mV (emeraldine state), a linear regression allowed calculation of the slope of the absorption energy with increasing potential. Independent of the preparation conditions, a slope of roughly 1 eV/V was found for all films. This implies that there is a direct connection between the availability of a chain segment of given conjugation length for oxidation and its contribution to the absorption signal. This means that the electric and optical properties of polyaniline are connected directly.

In the high potential region, pernigraniline sites are produced and irreversible processes like hydrolysis take place. Such processes cause defects in the polymer backbone and the effective conjugation length is reduced. Whereas the chains with the highest effective conjugation length are oxidized first when the potential is raised, they suffer from defect states first, as well. Because they are responsible for absorption at the longest wavelengths, this wavelength region is where a decrease of absorption is expected to be observed first. The experiment shows that at potentials of $E_{SCE} = 900$ mV or more, an optical absorption at a wavelength of $\lambda = 800$ –900 nm is substantially reduced compared with spectra

Table V. Energy of the Absorption Peak in the Low-Energy Region of the UV-vis Spectrum of PANI Showing a Hypsochromic Shift with Increasing Potential Applied to the Film^a

Polymerization conditions		Aniline conc. (M)	Shift (eV V ⁻¹) ($E_{SCE} > 0.3$ (V))	$E_{abs.}$ (eV) ($E_{SCE} < 0.3$ (V))
Electrolyte	Potential			
1-M HClO ₄	755-mV SSCE	0.1	0.87	1.414
0.5-M H ₂ SO ₄	750-mV SCE	0.1	1.23	1.401
1-M HCl	750-mV SCE	0.1	1.63	1.403
1-M HNO ₃	750-mV SCE	0.1	0.96	1.421
1-M H ₃ PO ₄	750-mV SCE	0.1	0.79	1.427
1-M HAc	750-mV SCE	0.1	—	—
1-M KNO ₃	750-mV SCE	0.1	—	—
1-M KCl	750-mV SCE	0.1	—	—
0.5-M Na ₂ SO ₄	750-mV SCE	0.1	—	—
1-M HClO ₄	680-mV SSCE	0.1	0.84	1.445
1-M HClO ₄	950-mV SSCE	0.1	—	< 1.38
1-M HClO ₄	755-mV SSCE	0.02	1.08	1.400
1-M HClO ₄	755-mV SSCE	0.3	0.92	1.425
0.2-M HClO ₄	755-mV SSCE	0.1	0.81	1.437
5-M HClO ₄	755-mV SSCE	0.1	0.83	1.426

^aListed are the slope resulting from a linear regression of the absorption energy as a function of the potential (for potentials $E > 300$ mV) and the average absorption energy $E_{abs.}$ (for potentials $E < 300$ mV).

taken at $E_{SCE} = 600$ or 700 mV, where formation of pernigraniline is not observed. Films of low conductivity do not show an absorption peak in the low-energy region, which is attributed to the presence of polarons, and, consequently, there are no values listed in the table. It is very difficult to explain such a blue shift on the basis of a band model, because it would imply an increase of the bandgap and a change in the function that describes the density of states. For phenomena of this kind, a model based on a molecular point of view as described previously is preferred.

Monkman [316, 317] reported UV-vis spectra recorded *in situ* that were interpreted by assuming localized oxidatively induced chromophores. This interpretation contradicts the model of mobile polarons. An absorption band found around $E = 0.5$ eV ($\lambda \approx 2478$ nm) was attributed to an internal charge transfer between reduced and oxidized sites on the polymer chain. This agrees with a model of hopping conduction. Geniés and Lapkowski [379] assigned UV-vis spectra recorded *in situ* with a PANI film in eutectic of $NH_4F \cdot 2.3HF$ to two polaron-bipolaron transitions. UV-vis spectra recorded *in situ* in the external reflectance mode were reported by Kessel et al. [185]. Assignment of the band around $\lambda = 330$ nm to the $\pi \rightarrow \pi^*$ transition of the aromatic ring system, of the absorption around $\lambda = 450$ nm to a radical cation, and of the absorption in the region of $\lambda = 700$ – 800 nm to highly conjugated species is basically in agreement with results already reviewed.

UV-vis spectra of electrochemically prepared copolymers of aniline with *o*-toluidine and with *o*-anisidine (MOA), and of PANI for comparison were reported by Ram et al. [380]. In the undoped state, optical absorptions were shown for PANI at 2.17 and 3.8 eV ($\lambda = 570$ and 326 nm), for PANI-PoTl at 2.13 and 3.96 eV ($\lambda = 581$ and 313 nm), and for PANI-MOA at 2.2 and 3.77 eV ($\lambda = 563$ and 328 nm). The transition at higher energies was assigned to the $\pi \rightarrow \pi^*$ interband transition; the transition at lower energies was assigned to the transition of an electron from the nonbonding electron pair at the nitrogen atom into the conduction band.

Compared with spectra reviewed before, the assignment of the former band corresponds to the $\pi \rightarrow \pi^*$ transition of the aromatic ring system; the latter band seems to indicate at least some degree of oxidation (although no electrode potentials or corresponding states of electrooxidation are given). The band may be compared, therefore, with the so-called polaron band. In the band model discussed in more detail in Figure 41, the nonbinding nitrogen electron pair is not represented as a separate band. The difference between the position of the interband transition with PANI and with the copolymers is significant in the undoped state only with PANI-PoTl. In the doped state, optical absorptions were shown for PANI at 1.4, 2.93, and 3.63 eV ($\lambda = 885$, 422, and 341 nm), for PANI-PoTl at 1.33, 2.87, and 3.97 eV ($\lambda = 931$, 431, and 312 nm), and for PANI-MOA at 1.5, 2.84, and 3.6 eV ($\lambda = 826$, 436, and 344 nm). The transition at higher energies is again assigned to the $\pi \rightarrow \pi^*$ interband transition; with PANI, it is shifted to slightly lower energies (red shifted) and with PANI-MOA it is surprisingly shifted in the opposite direction (blue shifted). The remaining absorptions are both assigned to polaron states. With the doped forms the difference in the position of the interband transition again is significantly affected only with PANI-PoTl. The considerable shift to higher energies may imply a decreased extent of conjugation caused by the presence of the alkyl substituent. The effect of doping on the energy of this transition is pronounced with PANI and PANI-MOA; with PANI-PoTl it is negligible. Whereas doping (and oxidation) tends to increase the extent of conjugation and also ultimately change the benzoid nature of the ring system into quinoid, the red shift of the doping is reasonable. Its almost complete absence in the case of PANI-PoTl is also reasonable, because, as already stated, with this copolymer, due to the presence of the alkyl substituent, extension of the conjugation is hindered anyway. This observation is also in good agreement with the very poor electronic

Table VI. Electrode Potentials E_1 for the First Polymer Film Oxidation Step, Redox Potentials of the First Redox Step $E_{\text{redox, RHE}}$, and Electronic Absorption Maxima λ_{max} of the Reduced Form of Aniline and Substituted Anilines in Various Solutions of 1-M HCl [241] and of 1-M HClO₄ [239, 240, 456]

Monomer	Acronym	$E_{1,\text{SCE}}$ (V)	λ_{max} (nm)	$E_{\text{redox, RHE}}$ (V)	λ_{max} (nm)
		1-M HCl	1-M HCl	1-M HClO ₄	1-M HClO ₄
Aniline	PANI	0.12	315	0.31	310
2,3-Xylidine	P23X	—	—	0.445	292
2,5-Xylidine	P25X	0.24	—	0.386	310
<i>o</i> -Toluidine	PoTI	0.20	310	0.354	310
<i>m</i> -Toluidine	PmTI	—	—	0.36	300
<i>o</i> -Ethylaniline	PEtA	—	—	0.365	310
<i>o</i> - <i>n</i> -Propylaniline	PPrA	—	—	0.41	310
<i>N</i> -Methylaniline	PNMA	—	—	0.425	310
<i>N</i> -Ethylaniline	PNEA	—	—	0.52	320
2-Methoxyaniline	MOA	0.08	325	—	—
2-Aminobenzylalcohol	ABA	0.22	308	—	—
2-Methoxy-5-methylaniline	MOMA	0.16	308	—	—
2,5-Dimethoxyaniline	DMOA	0.03	350	—	—

conductivity of PANI-PoTI as compared to PANI itself and PANI-MOA. Electrochromic copolymers of aniline or *o*-toluidine with anthranilic acid, methanilic acid, and 2-aminobenzenesulfonic acid have been described by Krzyczmonik and Blaszczyk [381].

The influence of the counteranion ClO₄⁻ and its concentration on the redox behavior of PANI studied with UV-vis spectroscopy has been stated [382]. No conclusions or explanations were provided.

Photoinduced UV-vis absorption of PANI and related changes in ESR spectra were observed *ex situ* by Coplin et al. [383]. UV-vis spectra of polymers prepared electrochemically from various substituted anilines (2-alkoxyanilines and 2,5-dialkoxyanilines that have alkyl chains with $n = 1, 2, 4, 6$) have been reported by D'Aprano et al. [241, 384]. The absorption maximum around $\lambda = 290$ nm observed for the monomers is not significantly affected by the type, number, or position of the substituent. The position of the corresponding absorption maximum of the polymer assigned to the $\pi \rightarrow \pi^*$ transition of the benzoid system varies considerably with these structural and electronic substituent effects. Data are listed in Table VI. The position of this electronic absorption was correlated to the conjugation length and the electronic conductivity. It is concluded that methyl-substituted anilines result in polymers less planar than do the methoxy-substituted aniline. Steric effects are invoked as the cause. Surprisingly, the electronic conductivity of the polymeric monoalkoxy-substituted anilines is lower compared to the alkyl-substituted polyanilines. The less regular structure of the polyalkoxyanilines is suggested as the reason. The diminished selectivity of head-to-tail coupling which results in less well ordered molecular chains (as determined from CV data) is the cause of the irregularities. With 2,5-disubstituted anilines, more regular materials with higher conjugation length and better electronic conductivity again are obtained. Data compiled by Probst and Holze [239, 240] and collected in Table VI fit nicely into this picture. This finding is also basically in agreement with the previously discussed data reported by Ram et al. [385]. Nevertheless, the considerable influence of the experimental parameters employed during polymer preparation makes a thorough discussion

of this aspect highly speculative [386]. In a comparative study of various ring- and N-substituted polyanilines, Sindhimeshram and Gupta [387] found a hypsochromic shift of the UV-vis spectrum with an increase in the dielectric constant of the solvent and with ring substitution.

As already indicated in the set of structural formulas in Figure 27, the electrochemically induced changes of the polymer effected by oxidation or reduction steps result, in a few cases, in the formation of radical centers on the polymer backbone. Because of the presence of unpaired electrons, this has considerable effects on the UV-vis spectra as already discussed. Even more significant is the change observed with ESR (ECESR when applied *in situ* in electrochemical investigations). Figure 34 shows essential parts of the electrochemical cell as employed in the studies reported by Lippe [73]. Figure 35 shows a series of ECESR spectra obtained with a PANI film in a nonaqueous electrolyte solution at different states of oxidation, that is, different electrode potentials and corresponding degrees of doping. Beginning with a negligible amplitude of the ESR signal observed with the reduced form of PANI (showing a fairly large electrical resistance), the amplitude increases, starting with a single line of Gaussian shape up to a maximum with a line of Lorentzian shape observed at electrode potentials roughly in the middle between the two anodic peaks observed in the CV (cf. Fig. 23). Beyond this point, the shape of the line changes again into the Gaussian type, and the amplitude decreases and almost vanishes. This process is completely reversible as long as the anodic potential limit is below a threshold value beyond which polymer degradation prevails. Only a single line is observed, despite the fact that it is caused by a radical incorporated into a large molecule. This implies strong delocalization of the unpaired electron, causing the complete loss of hyperfine splitting sometimes observed with the molecular radicals studied in the polymerization process. In the case of PANI, the signals are fairly symmetric, whereas in the case of other intrinsically conducting polymers, asymmetric shapes have been observed. The strikingly asymmetric shape of the signal for polyacetylene [388] and for polypyrrole [389, 390] has caused these researchers to con-

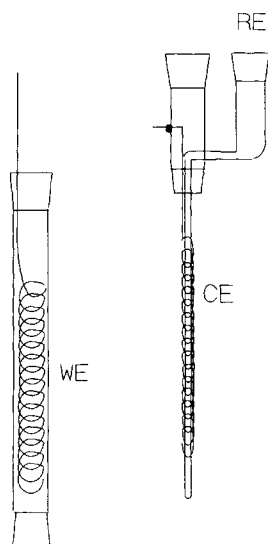


Fig. 34. Electrochemical cell for *in situ* ECSR experiments. The counter-electrode assembly that consists of a metal sheet wrapped around the central tube that connects to the reference electrode compartment is inserted axially into the working electrode coil. This coil is fitted into the cylindrical electrochemical cell made of quartz glass. The cell fits into the microwave cavity of the ESR spectrometer [73].

sider them as Dysonian lines [391, 392]. Whereas the line shape (or width [393]) is related to the mobility of charge carriers in the layers of the polymer sample penetrated by the microwave energy of the ESR spectrometer, the actual morphology and other properties of a polymer sample may influence the actually observed line shape. In the case of PANI and its relatives investigated so far, the line shape is more symmetrical, so the lines are called Dysonian lines only infrequently [394–396]. Even for polypyrrole, a non-Dysonian shape was reported at least once [397]. There is a single report of hyperfine splitting for PANI. With pernigraniline base solutions, Long et al. [398] were able to obtain high resolution ESR spectra [398]. The unpaired electron was found to reside predominantly on the nitrogen atom. The observed spin distribution was found to agree with a model for neutral benzoid–nitrogen solitons as initially suggested by Su and Epstein [399]. Nevertheless, these observations do not seem to bear further importance for understanding the specifics of PANI films as discussed here. The influence of the dielectric constant of the environment on the shape of the ESR absorption line has been discussed elsewhere [400].

The assignment of the ESR signal to radical cations or free spins (from a chemist's point of view) is, nevertheless, straightforward and beyond any doubt (see, e.g., [401, 402]). A closer description of the observed spins in terms of their magnetic and other properties is subject to ongoing debate. Glarum and Marshall [403] recorded the change of spin concentration as a function of electrode potential and injected charge for PANI films of various thicknesses. For thin films, they found a strong correlation between spin concentration and the current registered as a function of electrode potential, whereas for thick films, the ESR absorption correlated strongly with the injected charge, resulting in a ratio of one electron injected per Curie spin. The former result was explained by assuming negligible electron–electron interaction, whereas the latter result implies strong electron–electron interaction. Results were finally fitted into a model with a distribution of energy levels in a one-dimensional band of electronic ener-

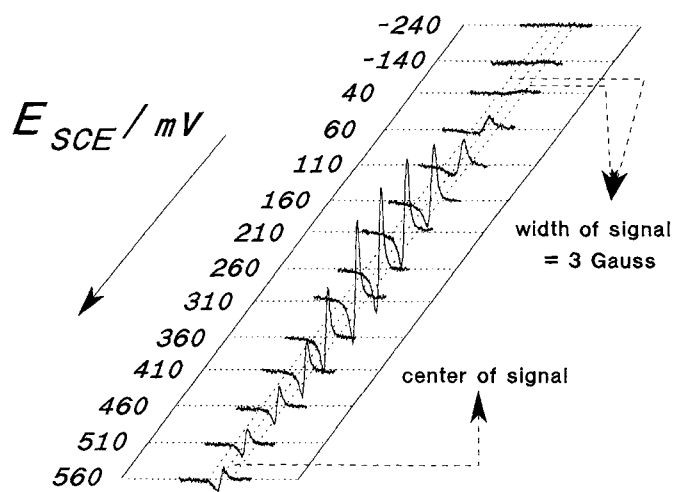


Fig. 35. ECSR spectra of PANI as a function of electrode potential in a solution of 0.1-M LiClO_4 in acetonitrile; 9.41 GHz, 79 mW, 0.2-mT modulation [73].

gies. No explanation for the influence of film thickness on the observed correlations was attempted. The influence of a whole set of experimental conditions, including film thickness, was investigated by Travers et al. [404]. A considerable influence of sample preparation on ECSR results was also found by Genoud et al. [405]. Ohsawa et al. [406] found a single line ESR spectrum upon electrooxidation of PANI in an aprotic electrolyte system. They assigned this spectrum to the formation of polaronic states and supported the assignment with the results of UV–vis spectroscopy. Without providing further evidence, Ohsawa et al. suggested that electronic conduction arises from spinless carriers. Measurements of the g value and of the temperature dependence of the ESR signal line width indicate that the spins are localized at the nitrogen atom. The absence of an ESR signal at low electrode potentials when PANI is in its reduced state was assigned to the lack of π -conjugate systems. In a later study, these authors discussed the influence of the supporting electrolyte anion and the presence of dioxygen and moisture on the already mentioned changes in the ESR spectra as a function of electrode potential. The anion seems to influence the polaron–bipolaron transition. The presence of O_2 and H_2 changes the line width of the ESR signal reversibly. This change is attributed to a relaxation of polaronic spins in the polymer by interaction with paramagnetic dioxygen. Nechtschein and co-workers [407, 408] reported reversible ESR line broadening observed with PANI powders in the presence of air and dioxygen. A possible application of this effect in studies of dioxygen mobility in polymer samples was indicated. It was also proposed that ESR line broadening may provide information on spin carrier mobility and morphology of the polymer. Aasmundtveit et al. [409] investigated dioxygen-induced ESR line broadening with PANI films and powders. Removal of dioxygen resulted in line narrowing. The broadening observed after exposing PANI to dioxygen as a function of time was explained by considering the rate of sorption and diffusion processes. Genoud et al. [410] studied *in situ* the influence of temperature and the degree of doping on the spin susceptibility of PANI. They found that in the conducting emeraldine salt state, the spin susceptibility decreases. The Pauli susceptibility is nil. The results were compatible with a polaron–bipolaron transition model invoked to explain the susceptibility decrease at higher degrees of doping. Further details concerning the line width of

ESR spectra of PANI were reported by Houze et al. [411]. According to their results obtained with chemically prepared and doped PANI, the polymer contains mobile and fixed spins. The former are strongly coupled to the lattice. The induced line broadening is found to be proportional to the spin mobility; this is in contrast to the usual motional narrowing. The line width is proportional to the conductivity. For the reported study, fixed spins were generated by adsorbed dioxygen or by paramagnetic ions like Fe^{3+} . Results that support this point of view were provided by Kahol et al. [412]. Removal of moisture resulted in a decrease of conductivity of PANI samples measured *ex situ* by an order of magnitude. Protonation and the presence of water in PANI were found to be of central importance. The polymer was described as a composite of protonated, highly ordered, and metallike regions separated from unprotonated and amorphous regions by intermediate regions whose thickness depends on the water content. It was concluded that the presence of water increases the size of the metallike islands, resulting in enhanced conductivity. Another influence of the anion was found by Itow et al. [413]. By comparing ESR spectra of PANI protonated with hydrochloric acid and with camphor sulfonic acid, different frequency dependencies of the line width were found. In the case of the latter dopant, a less-metallike electronic state was found. More generally, a weak interchain coupling and a semiconducting diffusion rate of the spin along the polymer chain different from results obtained, for example, with polyacetylene or polypyrrole were observed. Koziel et al. [414] employed *in situ* ECESR spectroscopy with PANI and various electrolyte anions. Only a general statement with reference to the obvious influence of the anions on the formation of positive charges was given. Although observed *ex situ*, it seems noteworthy that elongated doped (conducting) PANI films show an anisotropy of ESR signal that increases with the elongation ratio and the counterion size [415]. As a tentative explanation, a more ordered interchain arrangement parallel to the applied external field was suggested. Whereas an increased electronic conductivity of elongated films stated elsewhere [416] was assigned to an enhanced interchain conduction, this explanation was deemed reasonable. A graphic depiction of the various contributions to the electronic conduction (movement of charges along the molecular chain, between chains, between bundles of chains) is shown in Figure 36. The influence of intrachain movements is clearly visible.

Genies and Lapkowski [379, 417] identified four one-electron transitions and two polaron-bipolaron transitions with PANI in an eutectic melt of $\text{NH}_4\text{F} \cdot 2.3\text{HF}$. The claim for the existence of two slightly different bipolaron states was based on minor differences between the observed ESR signals. Further discussion is facilitated by briefly recalling the underlying models, arguments, and assumptions. Radical cations formed, for example, on a PANI polymer chain, can be treated from a physicist's point of view as polarons. These are quasiparticles in a solid. Localized charges in a potential well within a lattice cause lattice distortions around them because of Coulombic electrostatic interactions (polarization). These self-localizing polarons can move around in the crystal and carry their charge cloud with them. Whereas their effective mass differs from the mass of an electron, they have a different mobility. Although PANI and its relatives form very amorphous solids that are far away from the ideal periodic lattice that is a prerequisite for application of the band model, further discussion invokes exactly this helpful concept. When the number of radical cations (polarons) is increased, the amplitude of the ESR signal grows. This can be seen more clearly when double integration is applied to the original

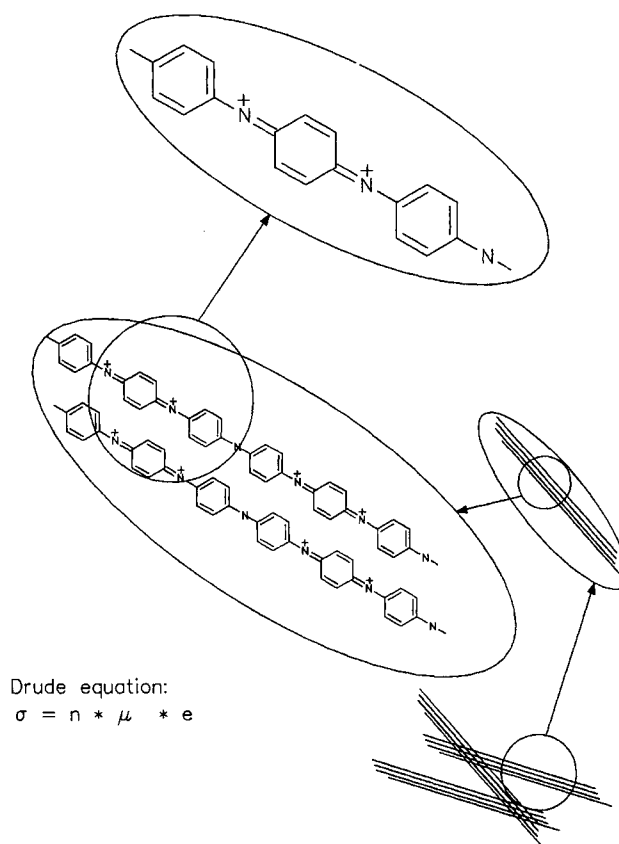


Fig. 36. Schematic that indicates the various contributions of transport types and processes to the electronic conduction in an intrinsically conducting polymer.

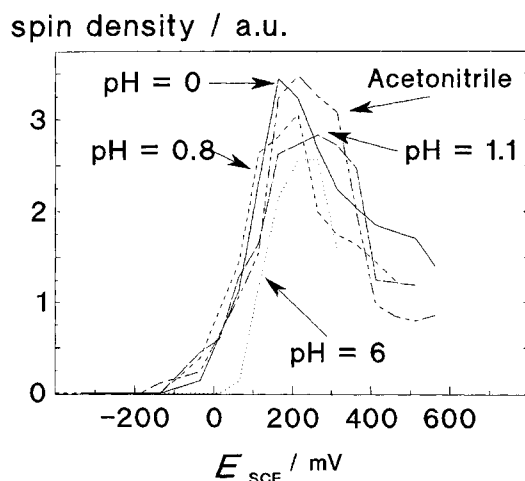


Fig. 37. Integrated intensity of ESR absorption of a PANI film in electrolyte solutions of various compositions and pH values [73].

ESR signal. Results of this procedure are displayed in Figure 37 for a film of PANI exposed to electrolyte solutions with different pH values.

The molecular and electronic information deduced from results obtained with ESR spectroscopy is of fundamental interest. In the discussion of these data, their use in the explanation of the electronic conductivity of these polymers plays a central role. Whereas the electrooxidation of PANI at least initially re-

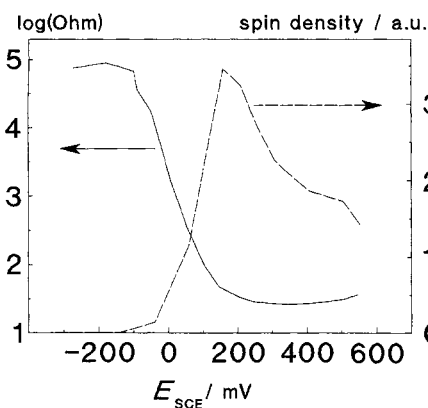


Fig. 38. Comparison of integrated ESR absorption and electronic conductivity of PANI in a solution of 0.5-M H_2SO_4 (pH = 0).

sults in the formation of radical cations (as convincingly demonstrated with ECESR), the onset of electronic conductivity with the increase of ESR absorption readily suggested the identification of the radical cations (polarons) as the carriers of the electronic conduction. Because of their mobility, polarons have been assumed to be the charge carriers responsible for the electronic conductivity of PANI and the other intrinsically conducting polymers. This suggestion is convincingly supported by a plot of the increase of the ESR signal and the decrease of the electric resistance as shown in a typical example in Figure 38. Unfortunately at higher degrees of doping, the resistivity remains low, whereas the amplitude starts to decrease again. This change initially caused a search for a species that is also charged and mobile, but has no unpaired electron and thus does not show up in an ESR spectrum. Again invoking concepts of solid state physics, recombination of polarons into doubly charged bipolarons without unpaired electrons was proposed. Although at first such a recombination seems to be highly unfavorable because of electrostatic repulsion, theoretical calculations for polypyrrole have shown that such recombination is energetically possible [418].

Correlations between the concentration of free spins as deduced from spectroelectrochemical data, especially ECESR and UV-vis absorption data, and the electronic conductivity have been investigated repeatedly. Figure 39 shows a comparison of the integrated ESR absorption and the electronic absorption in the UV-vis spectrum of PANI recorded as a function of electrode potential [73]. The close correlation implies that those species formed during electrooxidation of the polymer film and that cause the absorption band around $\lambda = 430$ nm (see above) are also those that cause the ESR absorption.

Consequently, the electronic absorption can be assigned to the polarons formed during film oxidation. Yoon et al. [419] studied the correlation between electrical conductivity, thermal conductivity, and ESR absorption intensity s . In addition to an obvious influence of solution pH (as already implied in the data displayed in Figure 24, the highest conductivities are observed in strongly acidic solution), a strong correlation between both electronic and thermal conductivity and $\log s$ was found. Yoon et al. concluded that both conductivities involve the same species (i.e., polarons). The fairly large Lorenz number, which was found for PANI with the highest observed conductivity to be an order of magnitude larger than expected for a metal, was taken as support for a model of localized electronic states in PANI as suggested earlier by Focke and

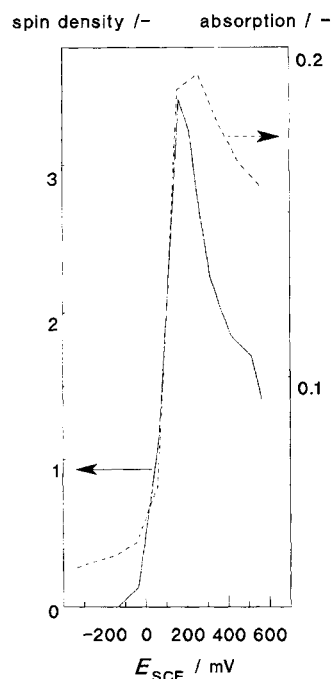


Fig. 39. Comparison of integrated ESR absorption and UV-vis absorption at $\lambda = 430$ nm of PANI in a solution of 0.5-M H_2SO_4 (pH = 0) [73].

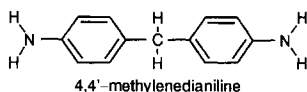
Wnek [420–422]. Accordingly, electronic conduction was assumed to occur via a hopping mechanism (compare also Fig. 36). Hopping conduction was also concluded based on ESR and conductivity data obtained *ex situ* by Choi and Kim [423] with electrochemically prepared PANI-hexafluorophosphate. In the case of self-doping PANI films, differences in the ESR spectra of dissolved sulfonic acid ring-substituted PANI and a free-standing film of this material indicated a higher degree of localization of the spins in the solution system [424]. Microscopic spin and charge dynamics of chemically prepared PANI were studied by Mizoguchi and Kume [425, 426]. Measurements of the diffusion rate of spins along the polymer chain and across the chain indicated a highly anisotropic mobility. Above $T = 150$ K, the mobility along the chain showed a metallike temperature dependence. Accordingly, PANI seems to be a highly one-dimensional electronic system. Further discussion of the temperature dependence of the electronic conductivity of PANI in connection with a simplified band model is provided subsequently.

One of the most striking features of practically all reported ECESR studies (provided that the electrode potentials (i.e., degrees of doping) employed were high enough) is the more or less sudden disappearance of ESR absorption as a function of electrode potential. As already visible in Figure 37, the concentration of free spins (polarons), which is assumed to be proportional to the ESR absorption, passes through a maximum. Two questions have to be asked: What happens to the radical cations certainly still produced by electrooxidation and what is the cause of the electronic conductivity when the concentration of free spins decreases to almost negligible values? Numerous investigations have been devoted to these questions (for an introductory overview, see [427]). Mizoguchi et al. [428] found a single Lorentzian line at low doping levels. At higher doping levels, a double Lorentzian line (a narrow and a broad one) was found, in contrast to the Gaussian shape reported by other researchers [429]. The integrated inten-

sity of the broader line becomes greater than the intensity of the sharp line with more positive electrode potentials. Measurements of the temperature dependence suggested that the sharp line behaves like a Curie spin, whereas the broad line resembles a Pauli spin. (For more details on both types of susceptibility, see [430].) The sharp line is, consequently, assigned to a polaron state created in the electrochemical doping process at low doping levels. The disappearance of the ESR signal upon electrochemical oxidation of the leucoemeraldine form of PANI into its emeraldine form was assigned by MacDiarmid et al. [431] to the change of Curie spins into Pauli spins. The lack of a correlation between the electrical conductivity and the concentration of free spins was stated by Kaya et al. [432]. A simple correlation, that is, an increase of conductivity that occurs simultaneously with an increase in the concentration of free spins, was observed by Genoud et al. [433]; evidence of "spinless conduction" was included. According to Wienk and Janssen [434], the emeraldine salt of PANI is an exception in which polarons are favored over bipolarons. No support of this statement is provided, although it may fit the experimentally observed reality. It is indicated that para-coupled polyaniline is conducting in the emeraldine salt state, whereas meta-para coupling results in a high-spin polymer. Stafström [435] studied geometry, band structure, and electronic transitions in oligomeric aniline tetramers and in polymers based on the tetramer unit using the modified neglect of differential overlap (MNDO) method. The calculated electronic excitation spectrum of the tetramer with a bipolaron conformation was very similar to the experimentally observed spectrum of this species. For the polymer system, the polaron configuration was found to be more stable.

In a more general investigation of PANI, polythiophene (PT), and polypyrrole (PPy) (for the latter polymers, see the following sections), Devreux et al. [436] studied the correlation between injected electric charge per ring and the number of spins per ring. Their results are displayed later in Figure 71. The general shape of the trace corresponds to plots already shown that display the relationship between the electrode potential and the spin concentration. Devreux et al. concluded from a thermodynamic consideration of the results that with PPy and polydithiophene (PdT), polarons and bipolarons are almost degenerate and, consequently, in a thermodynamic equilibrium, whereas for PANI, polaron pairing is hindered by potential barriers that disable the establishment of a thermodynamic equilibrium.

Investigations of chemically prepared oligomers with said type of substitution resulted in ESR spectra with hyperfine structure indicative of polaronic triplet di(cation) radicals. These results bear importance with respect to the development of organic ferromagnetic substances. Ferromagnetic behavior also was found by Mizobuchi et al. [437] with various experimental techniques applied to a copolymer of aniline and 5-amino-2-naphthalene sulfonic acid prepared by electropolymerization



ESR studies of poly(4,4'-methylenedianiline) [438] in its salt form showed evidence of thermally activated and temperature-independent Pauli-type paramagnetism, whereas the corresponding base form showed thermally activated Pauli- and Curie-Weiss-type paramagnetism. Charge transport was proposed to occur via polarons and bipolarons. With UV-vis spectroscopy performed *ex situ* at chemically prepared polymer samples, no evidence of

quinoid structural units was found upon oxidation of the polymer, despite the presence of a significant electronic conductivity [439].

The striking difference between ECESR data and conductivity data has prompted numerous investigations and reports. Lippe et al. [73, 309, 440], extensively investigated the relationship between the concentration of free spins and the electronic conductivity for aniline and a number of substituted anilines as well as related polymers (indole, indoline, pyrrole) with essentially the same results as found with PANI. ECESR has also been employed in studies of the "memory" effect of PANI [441, 442] (see preceding text). A reversible decrease of the conductivity of PANI upon exposure to dioxygen and the reverse process upon evacuation was observed by Kang et al. [443]. Corresponding changes in the ESR spectra as already discussed were seen and explained by assuming a spin-spin interaction between the polarons and the dioxygen molecules. The associated decrease in the mobility of the polarons and a presumed reduction of their concentration was seen as the reason for the only slightly diminished conductivity.

A further complication of the discussion arises when the infrared absorption around 4250 cm^{-1} ($E = 0.5\text{ eV}$) and the electronic resistance are plotted as a function of electrode potential (see, e.g., Fig. 40). The resistance decreases at about the first redox potential (for comparison, see the CV displayed in Fig. 23). At this electrode potential, the said infrared absorption increases. At the second redox potential, the resistance increases again, whereas the IR absorption decreases. The striking correlation is provocative. Contrary to the correlation between the ESR absorption and the resistance, which shows a striking deviation beyond electrode potentials that correspond to the second redox potential, this correlation holds in the entire range of electrode potentials investigated. To assign the IR absorption to polarons already identified as the cause of the optical absorption around $\lambda = 430\text{ nm}$ ($E = 2.8\text{ eV}$) would be in strong disagreement. Nevertheless, it seems safe to associate the species that causes the IR absorption with those mobile carriers that cause electronic conductivity. A satisfactory explanation (not taking into account the arguments presented already that show weak spots of the polaron-bipolaron model) is that the observed absorptions can be visualized using a band model as depicted in Figure 41. Although this model is essentially correct only for perfect periodic crystals, it is fairly often used in an approximation for the explanation of solid state properties of intrinsically conducting polymers. Within this model, the energy levels described as π orbitals from the chemist's point of view are combined into the valence band. The corresponding π^* orbitals are combined into the conduction band. Upon oxidation, radical cations (polarons) are formed. With their increasing number, the discrete levels are combined into a binding (lower) band and an antibinding (higher) band. Because of the electronic occupation of the lower band, transitions between both bands are allowed. In the case of bipolarons, discrete levels again combine into bands, and the different occupation does not allow electronic transitions between these bands. Allowed electronic transitions as derived from electronic symmetry considerations [444] result in the indicated scheme of possible electronic excitations. The transition **w1** corresponds to the $\pi \rightarrow \pi^*$ transition of the benzenoid unit of the polymer as already indicated. The optical absorption around $\lambda = 430\text{ nm}$ is caused by the transition from the lower binding polaron band into the upper one. The optical absorption observed at even higher doping levels (i.e., degrees of oxidation) corresponds to the transition **w2b**. The transition found around $E = 0.5\text{ eV}$ is due most likely to the transition **w1** in the polaron state and **w1b**

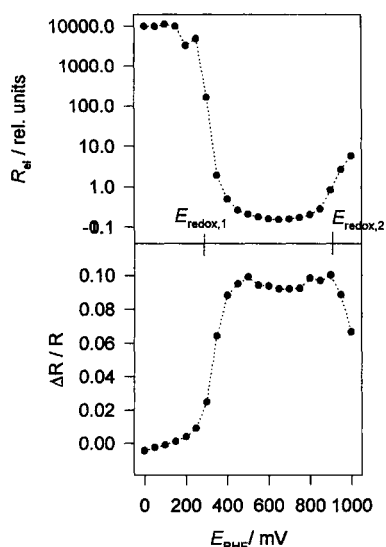


Fig. 40. Comparison of electronic resistance and IR absorption at about 4200 cm^{-1} ($\Delta E = 0.5\text{ eV}$) of a PANI film in an aqueous solution of 1-M HClO_4 as a function of electrode potential [456].

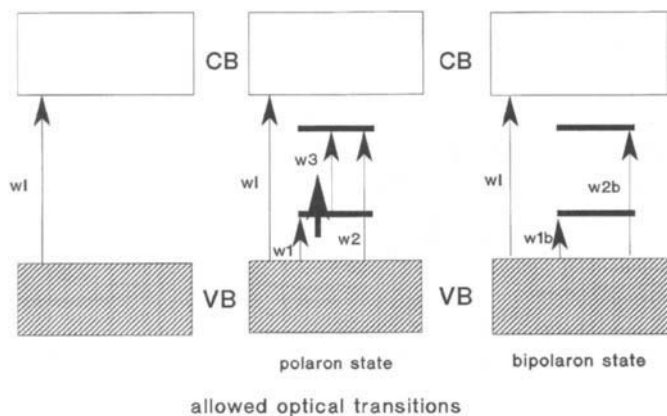


Fig. 41. Simplified band model of PANI in its various states of oxidation.

in the bipolaron state. This explains the presence of this absorption in the whole electrode potential range (between redox potentials $E_{\text{redox},1}$ and $E_{\text{redox},2}$) wherein the polymer maintains its high conductivity. Nevertheless, the change of the position of the absorption band associated with $w1b$ as a function of electrode potential and degree of doping, which would imply an increasing gap between the lower and the higher bipolaron band, remains unexplained. Considering the changes of resistance in the IR spectrum as a function of electrode potential, the intermediate state of oxidation of PANI with semiquinoid units is the best conducting.

A simple way to distinguish between a metallic conductor and a semiconductor is to measure the electronic conductivity of the substance under investigation as a function of temperature. This was attempted with PANI *ex situ*. The first *in situ* measurements were reported by Probst and Holze [445]. PANI was prepared via different electropolymerization routes (i.e., potentiodynamical, potentiostatic, etc.). The conductivities plotted as a function of the temperature are shown in Figure 42. They show an increase of conductivity up to a limiting temperature. The increase implies a semiconductor-like behavior. The appearance of a limiting temperature, beyond which the conductivity dropped, was explained

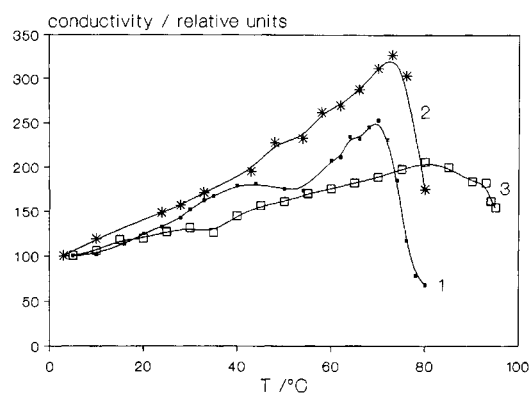


Fig. 42. σ vs temperature plots for PANI in 1-M HClO_4 films deposited by (1) potentiodynamic cycling, (2) potentiostatic deposition, and (3) square wave deposition; nitrogen purged [445].

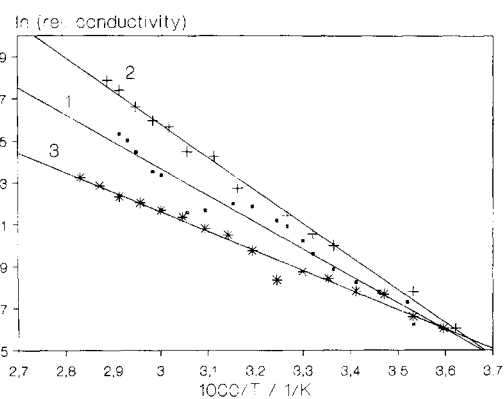


Fig. 43. Plots of $\ln(\sigma)$ vs inverse temperature for PANI in 1-M HClO_4 films deposited by potentiodynamic cycling (1), potentiostatic deposition (2), square wave deposition (3), nitrogen purged [445].

by invoking a glass transition. To identify the dimensionality of the conduction, various plots (for an example, see Fig. 43) as suggested by Heeger and MacDiarmid [446] were tried. The exponent in the equation $\sigma s \approx \exp(-(T_0/T)^{1/(d+1)})$, where d is the dimensionality of the conductivity, was varied to take into account the different possible dimensionalities. Within the investigated range of temperatures, no significant influence of the exponent was found, that is, no conclusion with respect to the dimensionality was possible.

ECESR spectra of polymers prepared electrochemically from substituted anilines (2-alkoxyanilines and 2,5-dialkoxyanilines that have alkyl chains with $n = 1, 2, 4, 6$) were reported by D'Aprano et al. [447]. Two single lines were observed with similar g values during the two oxidation steps generally found during electrooxidation of PANI. The spins were more localized compared to PANI. Correspondingly lower electronic conductivities were found, with particularly low values for longer alkyl chains ($n = 4, 6$). In a comparative study, Yang et al. [448] recorded *in situ* ECESR spectra of PoTl and *o*-ethylaniline (PEtA). The ESR absorption present as a single line without fine structure showed a strong dependence on the electrode potential. In the range between the first and the second electrooxidation wave, the large intensity indicates formation of a radical cation. In comparison, the range of electrode potentials wherein these radical cations were most stable decreases in the order PANI > PoTl > PEtA. The change of absorption inten-

sity correlates well with the optical absorption around $\lambda = 420$ nm. *Ex situ* ESR spectra of PoTI, PEtA, and PPrA prepared by chemical oxidation were reported by Pinto et al. [449, 450]. According to their results, substitution at the ring results in decreased conductivity (in agreement with results already reviewed herein), decreased Pauli susceptibility, and a higher number of Curie spins. Going from PoTI to PPrA, the line shape changes from Lorentzian toward Gaussian form. The results are interpreted in terms of increased electron localization caused by increased interchain disorder.

Although protonation and deprotonation are no electrochemical processes, spectroscopic evidence obtained in investigations of these processes should be considered briefly here because of the central importance of protonation for the occurrence of electronic conductivity in PANI. Wan and Yang [451] studied the protonation (or proton doping because this process induces positively charged sites in the polymer backbone similar to those formed by electrochemical oxidation) of PANI with a variety of spectroscopic methods. Results imply that protonation takes place at the imine site of the emeraldine form of PANI. Results obtained in this investigation with fluorescence spectroscopy support this conclusion. Contributions from chemical and diffusional steps were found, depending on the degree of protonation. At low degrees of protonation, a chemical reaction was rate determining, at medium degrees, diffusion becomes determining. ESR spectra indicate formation of a polaron state (just like with electrooxidation).

Polymers formed from *o*- and *m*-toluidine have been investigated [240, 452–457]. According to Leclerc et al. [458], *p*-toluidine did not yield a polymer upon electrooxidation. PoTI is of particular interest because it has been considered as a material for photolithography [459]. Its soluble base form can be changed into an insoluble form by doping. This, in turn, can be effected by acids that release protons as a consequence of a photochemical reaction. Results reported by Fujita et al. [284] for *o*- and *m*-toluidine obtained with various electrolyte solutions and pH values indicate similarities in UV-vis spectra of PoTI and PANI in solutions of pH = 0, whereas in neutral solutions, considerably different spectra were found. An influence of the counterion was found. In particular, the radical cation (polaron) state of partially oxidized PoTI was unstable in neutral solutions in the presence of large counterions. This was different from PANI. Results obtained with infrared spectroscopy under similarly varied conditions support these conclusions. *m*-toluidine (PmTI) shows strikingly similar spectra that support the suggestion that both polymers are essentially the same. Considering the molecular structure of the monomer and of the most likely polymer connected in the para position, this is no surprise. The infrared spectra reported by Fujita et al. strikingly demonstrate the similarities between PoTI and PmTI; only a few bands were assigned to discrete vibrational modes. Considering the molecular structure of a polymer obtained by para coupling of monomer units, this is reasonable. Indeed the similarity of UV-vis data obtained with both PoTI and PmTI supports this suggestion [460]. Nevertheless, the oxidation of the orthoisomer gave higher polymerization yields and more regular head-to-tail coupled structures [461]. The potential window between the first and the second electrooxidation peak becomes closer upon alkyl substitution. It is also noteworthy that according to Leclerc [462], PoTI is conductive only in its polaronic form, that is, roughly in the range of electrode potentials between the first and the second oxidation peaks. The protonated, fully oxidized form assigned as a bipolaron

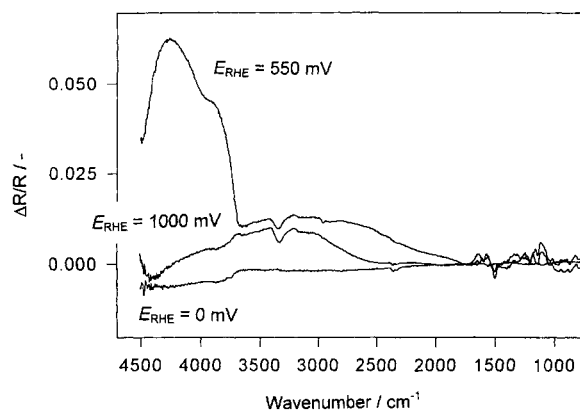


Fig. 44. Electrode potential modulated *in situ* infrared spectra of PoTI in an aqueous solution of 1-M HClO₄ recorded at electrode potentials as indicated; background spectrum recorded at $E_{RHE} = 0$ mV; resolution 4 cm⁻¹ [456].

with strongly acidic electrolyte solutions (pH < -0.5) and identified by means of a UV-vis absorption at $\lambda = 630$ nm was found to be insulating. In a study of PoTI reported by Clark and Yang [463] with *in situ* UV-vis spectroscopy, pronounced electrochromism was observed. From measurements at various pH values, a pH potential phase diagram was constructed. The effect of the methyl substitution seemed to be destabilization of the conductive form (as derived from the intensity of the optical absorption assigned to the polaron transition) of the polymer. An increased steric energy in the molecular conformation of the conductive form was invoked as an explanation. Wei et al. [452] studied PoTI, PmTI, and poly(*o*-ethylaniline). Typical behavior of substituted PANI was found with CV, UV-vis spectroscopy, and conductivity measurements, particularly, after protonation. A comparison with data obtained for PANI implies a reduction in π -conjugation with alkyl substitution caused primarily by steric effects. Wan and Yang [464] measured UV-vis and ESR spectra of PoTI prepared by chemical oxidation. The strongly diminished electronic conductivity was explained based on the blue shift of the peak in the UV-vis spectrum by assuming a decrease in the extent of conjugation as the major cause. Probst [240, 456] reported a more thorough investigation with vibrational spectroscopies of all toluidines. A typical set of *in situ* infrared spectra, obtained by taking a background spectrum at a reference electrode potential $E_r = 0$ mV in the potential region where PoTI is reduced, practically colorless, and only poorly conducting, and further spectra recorded at selected electrode potentials as indicated are shown in Figure 44. The "fingerprint" region recorded at additional electrode potentials is seen in Figure 45. The corresponding set of *in situ* Raman spectra is shown in Figure 46. Tentative assignments of major bands based essentially on known assignments for the monomer as reported in particular by Varsanyi [465] are collected in Tables VII and VIII for poly(*o*-toluidine) and in Tables IX and X for poly(*m*-toluidine).

Resonance Raman spectroscopy has been used as a tool to investigate the mode of corrosion protection by films of PANI on iron [466]. Spectra as displayed in Figure 47 in connection with measurements of the iron electrode potential implied that the emeraldine salt found at positive electrode potentials acts as a corrosion inhibitor of iron in its passive state, whereas the reduced leucoemeraldine salt is indicative of an iron surface at its corrosion potential.

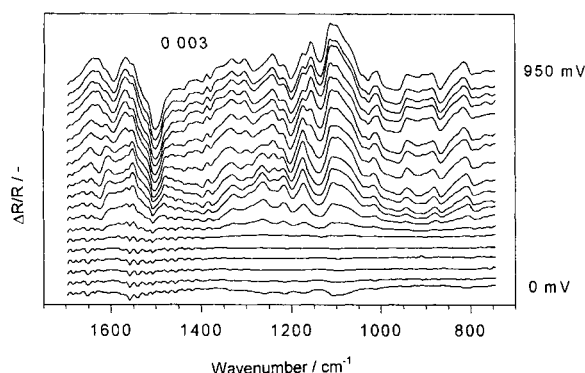


Fig. 45. Electrode potential modulated *in situ* infrared spectra of PoTl in an aqueous solution of 1-M HClO₄ as recorded at electrode potentials indicated ($E_{\text{RHE}} = 0, 50, 100, \dots, 950$ mV); background spectrum recorded at $E_{\text{RHE}} = 0$ mV; resolution 4 cm^{-1} [456].

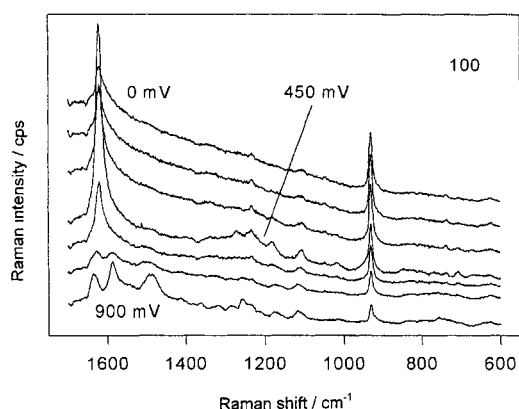


Fig. 46. *In situ* resonance Raman spectra of a film of PoTl in an aqueous solution of 1-M HClO₄ recorded at various electrode potentials $E_{\text{RHE}} = 0, 150, 300, 450, \dots, 900$ mV; resolution 8 cm^{-1} [456].

A correlation of the IR absorption as a function of electrode potential with the electronic resistance of a film of PoTl is shown in Figure 48. Basically the same arguments already presented in the case of PANI have to be discussed, although no ECESR data are available for this polymer. Similar pictures are shown in Figure 49 for PmTl, in Figure 50 for 2,5-xylydin (P25X), and in Figure 51 for *N*-methylaniline (PNMA). The electrooxidation process that occurs around $E_{\text{redox},2}$ results in a disappearance of mobile charge carrier reflected in both types of experimental results. Obviously the change in resistance as a function of electrode potential is considerably less pronounced in case of the substituted polymers as compared to PANI. PoTl is by far closest to PANI. The decrease in resistivity in orders of magnitudes is 5 for PANI, 2.5 for PoTl, 1.5 for PmTl, 1 for P25X and PNMA, and 0.5 for *o*-*n*-propylaniline (PPrA). Although no absolute resistivity data could be obtained with the *in situ* measurement method employed, this trend is basically in agreement with the observation stated elsewhere that substitution of the aniline monomer results in polymers with considerably lower conductivity. It is also noteworthy that the range of low resistance as well as of strong IR absorption becomes narrower with increasing substitution of the monomer. In a not yet understood way, the molecular (most likely the steric) in particular, changes seem to influence the redox potential, which in turn affects the IR absorption.

The particular effect of the state of oxidation of PoTl on the resonance enhancement being the basis of resonantly enhanced Raman spectra was studied in detail by Ouillard et al. [467]. The results showed that certain vibrational modes remain silent in the Raman spectrum because of symmetry considerations.

Henderson et al. [468] studied the behavior of PoTl in an acidic perchloric acid solution with probe beam deflection and electrochemical quartz microbalance (EQMB) [468]. The degree of film hydration affected the relative contributions of protons and anions during the first redox cycle. During further cycles, a proton contribution was observed at electrode potentials around the first redox peak in the CV. During the second redox peak, electroneutrality was established by proton expulsion.

Ex situ ESR data of *o*-toluidine prepared by chemical oxidation were reported by Anand et al. [469, 470]. Using various counteranions, the polymer salts and the corresponding bases were investigated. Highly mobile radical cations (polarons) were found. The salts showed thermally activated paramagnetism, indicating antiferromagnetically coupled polarons, whereas the bases showed only a Pauli-type paramagnetism without any temperature dependence. No correlation between conductivity and spin concentration was found. It was stated that movement of paramagnetic polarons along the polymer chain is not the sole cause of electronic conductivity.

Electropolymerization of 2,3-xylydin (P23X) and 2,5-xylydin was reported by Probst et al. [239, 456]. The obtained thin film of P23X was electrochromic. It showed significant optical absorptions only around $\lambda = 320$ nm ($\pi \rightarrow \pi^*$ transition) and at electrode potentials $E_{\text{RHE}} > 300$ mV, an absorption was detected around $\lambda = 780$ nm (not explicitly assigned; it may be related to polarons or bipolarons). Infrared and Raman spectra recorded *in situ* yielded the bands collected in Tables XI and XII. The absorption around 4400 cm^{-1} did not show a significant dependence on the electrode potential. Whereas no conductivity data could be obtained with the *in situ* method, it can only be assumed that this absorption may be related to charge carriers of only limited mobility. As already mentioned, polymers of 2,5-xylydin also were obtained by electropolymerization [456]. The electrochemically active films were electrochromic and showed an electronic conductivity as a function of pH value of the electrolyte solution and of the electrode potential (compare Fig. 50). The UV-vis spectra recorded *in situ* at pH = 0 showed the tail of an absorption below $\lambda = 350$ nm ($\pi \rightarrow \pi^*$ transition) and a broad absorption feature around $\lambda = 780$ nm at electrode potentials $E_{\text{RHE}} > 400$ mV. A very weak feature around $\lambda = 400$ nm starts to grow with increasing electrode potential from $E_{\text{RHE}} = 0$ mV. The first band moves to higher wavelengths around $\lambda = 310$ nm with increasing pH value (e.g., pH = 1.5). The absorption around $\lambda = 800$ nm already is visible at this pH value at $E_{\text{RHE}} = 0$ mV. At even higher pH values (e.g., pH = 4), electrochromism disappears. *In situ* infrared and Raman spectra yielded the bands collected in Tables XIII and XIV. With both polymers (P23X and P25X), the transition from the benzoid form in the reduced state to the quinoid form in the oxidized state is evident. It is noteworthy that a plot of the IR absorption at various wave numbers as a function of electrode potential yields significant dependencies. The absorption at 1516 cm^{-1} assigned to the benzoid ring stretching mode starts to decrease at $E_{\text{RHE}} = 200$ mV. The band at 1597 cm^{-1} , which is attributed to the same mode of the quinoid form, increases only slightly at the same potential, whereas the mode at 1308 cm^{-1} , which is assigned to the C=N stretching mode of the semiquinoid form, increases

Table VII. Assignment of Vibrational Bands for Poly(*o*-toluidine) from *in situ* Infrared Spectra^a

<i>o</i> -toluidine $\bar{\nu}$ (cm ⁻¹)	PoTl, <i>ex situ</i> $\bar{\nu}$ (cm ⁻¹)	PoTl, red. <i>in situ</i> $\bar{\nu}$ (cm ⁻¹)	PoTl, ox. <i>in situ</i> $\bar{\nu}$ (cm ⁻¹)	Mode	Wilson no.
840	815	866	—	δ_{C-H}	—
—	1107/1119	—	1111	$\delta_{C-H} + \nu_3(\text{ClO}_4^-)$	—
1150	1157	1130	1157	β_{C-H}	9a
1200	1215	1200,1225	—	δ_{C-C}	13
1273	—	1280	—	ν_{C-N}	7a
1303	—	—	—	δ_{ring}	14
—	—	—	1400–1300	$\nu_{C=N}$	—
1380	1380	—	—	δ_{s,CH_3}	—
1499	1496	1500	—	ν_{ring} , benzoid	19b
—	—	—	1568	ν_{ring} , quinoid	—
1622	—	—	—	β_{s,NH_2}	—
—	—	—	—	$\nu_{C=N}$	—

^aSee Figures 44 and 45 for experimental conditions.

Table VIII. Assignment of Vibrational Bands for Poly(*o*-toluidine) from *in situ* Raman Spectra^a

<i>o</i> -Toluidine $\bar{\nu}$ (cm ⁻¹)	PoTl, red. <i>in situ</i> $\bar{\nu}$ (cm ⁻¹)	PoTl, ox. <i>in situ</i> $\bar{\nu}$ (cm ⁻¹)	Mode $\bar{\nu}$ (cm ⁻¹)	Wilson no.
760	—	—	γ_{C-H}	—
—	931	931	$\delta_{C-H} + \nu_3(\text{ClO}_4^-)$	—
1048	—	—	β_{C-H}	18b
—	1109	1118	δ_{C-H}	—
—	1180	1178	δ_{C-C}	—
1215	—	—	ν_{C-H}	13
—	—	1257	?	—
1283	1270; 1232	ν_{C-N}	—	—
1395	—	—	δ_{s,CH_3}	—
—	—	1487	ν_{C-N} , semiquinoid	—
—	—	1586	ν_{ring} , quinoid	—
1599	1622	—	ν_{ring} , benzoid	8a
—	—	1636	$\nu_{C=N}$	—
1623	—	—	β_{s,NH_2}	—

^aSee Figure 46 for experimental conditions.

considerably. The infrared absorption beyond 4000 cm⁻¹, which is considered to be caused by mobile charge carriers, is less pronounced as in the case of PANI. In a further study, Toshima and Yan [471] observed that chemical oxidation of 2,3-xylydine and 2,5-xylydine with ammonium peroxodisulfate did not yield a polymer, whereas Ce(SO₄)₂ resulted in polymer formation. No conductivity was reported.

Electrochemical formation of a polymer by oxidation of *o*-ethylaniline was reported by Probst [472] and the results of kinetic studies were reviewed in the preceding section. An electrochemically active film with considerable electrochromism was obtained. Changes in the UV-vis spectra were most pronounced at pH = 0. The repeatedly mentioned band around $\lambda = 300$ nm,

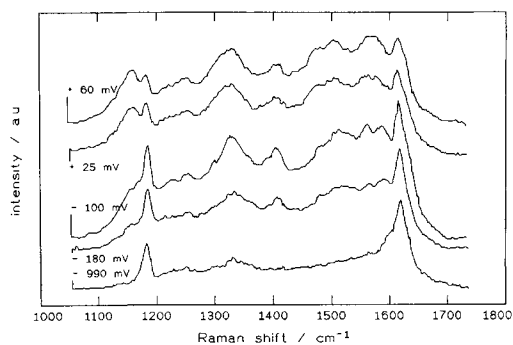
which is assigned to the $\pi \rightarrow \pi^*$ transition, was found. Upon electrooxidation, a band around $\lambda = 400$ nm and a band with a maximum around $\lambda = 900$ nm were seen at fairly low electrode potentials. With further positive shift of the electrode potential, the band around $\lambda = 400$ nm becomes less pronounced, whereas the absorption at longer wavelengths shifts to about $\lambda = 620$ nm at the highest investigated electrode potential of $E_{\text{RHE}} = 900$ mV. No details of an assignment beyond the arguments already presented for the other investigated polymers were given. *In situ* infrared spectra showed a number of vibrational bands that are collected in Table XV. The absorption of the very broad band around 4400 cm⁻¹ passes through a maximum at an electrode potential of about $E_{\text{RHE}} = 600$ mV. In the absence of conductivity data, no

Table IX. Assignment of Vibrational Bands for Poly(*m*-toluidine) as Taken from *in situ* Infrared Spectra [456]

<i>m</i> -Toluidine $\bar{\nu}$ (cm ⁻¹)	PoTl, red. <i>in situ</i> $\bar{\nu}$ (cm ⁻¹)	PoTl, ox. <i>in situ</i> $\bar{\nu}$ (cm ⁻¹)	Mode	Wilson on.
868	871	—	β_{C-H}	—
—	—	1105	$\nu_3(\text{ClO}_4^-)$	—
1168	—	1161	β_{C-H}	9b
1293	1280	—	ν_{C-N}	13
—	—	1400–1300	ν_{C-N} , semiquinoid	—
1495	1505	—	ν_{ring} , benzoid	19a
—	—	1572	ν_{ring}	—
1593	—	—	ν_{ring} , benzoid	8a
1620	—	—	β_{s,NH_2}	—
—	—	1641	$\nu_{C=N}$	—

Table X. Assignment of Vibrational Bands for Poly(*m*-toluidine) as Taken from *in situ* Raman Spectra [456]

<i>m</i> -Toluidine $\bar{\nu}$ (cm ⁻¹)	PoTl, red. <i>in situ</i> $\bar{\nu}$ (cm ⁻¹)	PoTl, ox. <i>in situ</i> $\bar{\nu}$ (cm ⁻¹)	Mode	Wilson no.
739	—	—	γ_{C-H}	11
994	—	—	δ_{ring}	12
—	1115	1125	β_{C-H}	18b
—	—	1258	?	—
1305	1250	—	ν_{C-N}	—
1395	1340	—	δ_{CH_3}	—
—	—	1495	ν_{C-N} , semiquinoid	—
—	—	1590	ν_{ring} , quinoid	—
—	1625	—	ν_{ring} , benzoid	8a
1620	—	—	β_{s,NH_2}	—
—	—	1638	$\nu_{C=N}$	—

Fig. 47. Resonance Raman spectra of a PANI film on an iron electrode at various electrode potentials, $\lambda_0 = 514.5$ nm, based on data from [466].

correlation was attempted. *In situ* Raman spectroscopic data are summarized in Table XVI.

o-*n*-propylaniline can be electrooxidized and deposited on various electrode substrates as reported by Probst [456]. Kinetic data were reviewed in the foregoing text. No films for *in situ* conduc-

tivity measurements could be prepared. The electrochromism of the redox active film is significant. The bands around $\lambda = 300$, 400, and 800 nm appear as functions of electrode potential in the same manner as already reported for other polymers. *In situ* infrared spectra of the very thin films could be measured: the pertinent band positions and their assignments are collected in Table XVII. The transition from the reduced state that shows benzoid units into the oxidized state with quinoid units passes through an intermediate state without bands indicative of C=N bonds. The broad absorption around 4460 cm^{-1} (not included in the table, because no discrete molecular mode is related to this absorption) shows a strong dependence on the electrode potential with a sharp maximum around $E_{\text{RHE}} = 610$ mV. Results of *in situ* Raman spectroscopy are listed in Table XVIII. The influence of the exciting laser light wavelength on the spectral intensity was considerable; no selective enhancement was observed.

Electrochemical oxidation of *N*-methylaniline as described by Probst [456] resulted in polymer films on both ITO-coated glass sheets and metal electrodes. Because of the strong coloration of the electrolyte solution observed during deposition, formation of a considerable amount of soluble oligomers was concluded. UV-vis

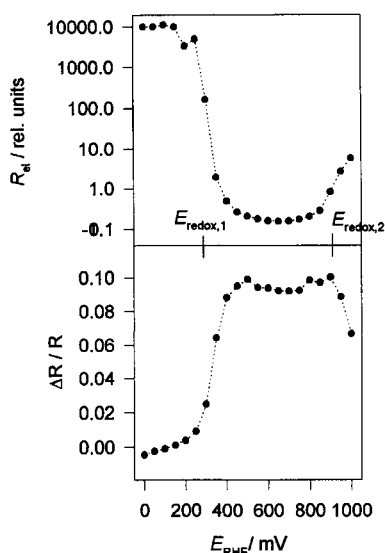


Fig. 48. Comparison of electronic resistance and IR absorption at about 4200 cm^{-1} ($\Delta E = 0.5\text{ eV}$) of a PoTl film in an aqueous solution of 1-M HClO_4 as a function of electrode potential [456].

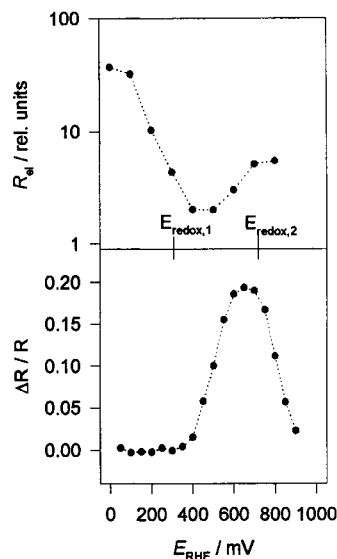


Fig. 50. Comparison of electronic resistance and IR absorption at about 4200 cm^{-1} ($\Delta E = 0.5\text{ eV}$) of a P25X film in an aqueous solution of 1-M HClO_4 as a function of electrode potential [456].

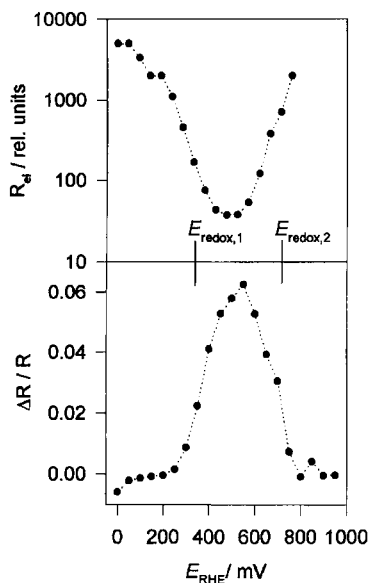


Fig. 49. Comparison of electronic resistance and IR absorption at about 4200 cm^{-1} ($\Delta E = 0.5\text{ eV}$) of a PmTl film in an aqueous solution of 1-M HClO_4 as a function of electrode potential [456].

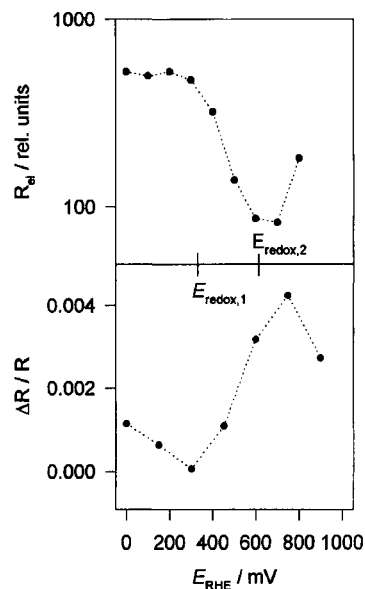


Fig. 51. Comparison of electronic resistance and IR absorption at about 4200 cm^{-1} ($\Delta E = 0.5\text{ eV}$) of a PNM film in an aqueous solution of 1-M HClO_4 as a function of electrode potential [456].

spectra recorded at various electrode potentials showed absorptions at $\lambda = 310\text{ nm}$ and at more positive electrode potentials around $\lambda = 410$ and 800 nm ; the absorption is always fairly low. Data for vibrational bands found in infrared and Raman spectra recorded with these films are collected in Tables XIX and XX. No significant influence of the excitation wavelength on the resonance Raman spectra was found. A strong IR absorption around 4400 cm^{-1} , indicative of mobile charge carriers (not included in Table XIX), is found with the oxidized form of PNMA. This is in agreement with the observed electronic conductivity.

Chemical oxidation of *N*-methylaniline resulted in an electrochemically active electrochromic polymer film as reported by Comisso et al. [473]. Optical absorption bands in the UV-vis spec-

tra observed during *in situ* measurements were found around $\lambda = 330$ and 740 nm (very weak) in the reduced state. Upon oxidation, the band around $\lambda = 330\text{ nm}$ is diminished considerably, whereas a new band at $\lambda = 420\text{ nm}$ and a fairly broad absorption feature around $\lambda = 800\text{ nm}$ as rise. In the fully oxidized form, the latter feature is shifted to about $\lambda = 700\text{ nm}$. No assignments were stated. It seems fair to assume that the observed transitions correspond to those already discussed. A polymer structure with tail-to-tail and head-to-tail coupling was deduced.

A thin, electrochromic film that showed two redox peak pairs in the CV was obtained during electrooxidation of *N*-ethylaniline [456]. UV-vis spectra of this film as deposited on ITO-coated glass electrodes showed an absorption at $\lambda = 320\text{ nm}$ and

Table XI. Assignment of Vibrational Bands for P23X as Taken from *in situ* Infrared Spectra [456]

2,3-Xylidine $\bar{\nu}$ (cm ⁻¹)	P23X, red. <i>in situ</i> $\bar{\nu}$ (cm ⁻¹)	P23X, ox. <i>in situ</i> $\bar{\nu}$ (cm ⁻¹)	Mode	Wilson no.
774	—	—	δ_{C-H}	—
—	—	832	δ_{C-H}	—
—	—	957	δ_{C-H}	—
—	—	1069	δ_{C-H}	—
1091	—	—	δ_{C-H}	—
—	—	—	$\nu_3(\text{ClO}_4^-)$	—
—	—	1157	δ_{C-H}	—
1296	—	1300	ν_{C-N}	20a
—	—	1373; 1324	ν_{C-N} , semiquinoid	—
1385	—	—	β_s, CH_3	—
1475	—	—	?	—
—	1484	—	ν_{ring} , benzoid	19a
—	—	1578	ν_{ring} , quinoid	—
1593	—	—	ν_{ring}	8a
1623	—	—	β_s, NH_2	—
—	—	1638	$\nu_{C=N}$	—

Table XII. Assignment of Vibrational Bands for P23X as Taken from *in situ* Raman Spectra [456]

2,3-Xylidine $\bar{\nu}$ (cm ⁻¹)	P23X, red. <i>in situ</i> $\bar{\nu}$ (cm ⁻¹)	P23X, ox. <i>in situ</i> $\bar{\nu}$ (cm ⁻¹)	Mode	Wilson on.
668	—	—	γ_s, NH_2	—
—	774	772	δ_{C-H}	—
—	934	934	$\nu_3(\text{ClO}_4^-)$	—
—	—	945	δ_{C-H}	—
990	—	—	γ_{C-H}	5
1257	—	—	ν_{C-H}	13
—	—	1292	?	—
1293	1256	1255	ν_{C-N}	—
—	—	1325	?	—
1381	1380	1381	β_s, CH_3	—
1450	—	—	β_{as}, CH_3	—
—	—	1455	$\nu_{C=N}(?)$	—
1478	1494	1488	?	—
—	1560	—	?	—
—	1587	1591	ν_{ring} , quinoid	—
1590	1626	—	ν_{ring} , benzoid	8a
—	—	1637	$\nu_{C=N}$	—
1617	—	—	β_s, NH_2	—

at more positive electrode potentials, around $\lambda = 400$ and 790 nm. Data of vibrational bands found in infrared and Raman spectra recorded with these films are collected in Tables XXI and XXII. A comparison of all wavelengths of major absorption bands in the UV-vis spectra investigated as reported in [456] did not reveal any systematic influence of the type and degree of alkyl substitution on the position of the electronic transitions.

Further exclusively chemically prepared polymers of ring- and N-substituted anilines studied with a variety of *ex situ* methods were studied by Gupta et al. [474]. Both chemical and electrochemical polymerization of a series of *N*-alkyl substituted anilines ranging from methyl to dodecyl substituents were investigated by Chevalier et al. [475]. Primarily electrochemical results, *in situ* UV-vis, and some *ex situ* infrared spectra were reported. The

Table XIII. Assignment of Vibrational Bands for P25X as Taken from *in situ* Infrared Spectra [456]

2,5-Xylidine $\bar{\nu}$ (cm ⁻¹)	P25X, red. <i>in situ</i> $\bar{\nu}$ (cm ⁻¹)	P25X, ox. <i>in situ</i> $\bar{\nu}$ (cm ⁻¹)	Mode	Wilson no.
860	—	—	γ_{CH}	5
—	—	1010	$\delta_{\text{C-H}}$	—
—	—	1100	$\nu_3(\text{ClO}_4^-)$	—
—	1142	—	$\delta_{\text{C-H}}$	18a
—	—	1245	$\gamma_{\text{C-C}}$	—
1297	1260	—	$\nu_{\text{C-N}}$	—
—	—	1300–1400	$\nu_{\text{C-N}}$, semiquinoid	—
—	—	1430	?	—
1460	—	—	β_s , CH ₃	—
1515	1516	—	ν_{ring} , benzoid	19b
—	—	1550	?	—
1578	—	—	ν_{ring} , benzoid	8a
—	—	1597	ν_{ring} , quinoid	—
1629	—	—	β_s , NH ₂	—
—	—	1643	$\nu_{\text{C=N}}$	—

Table XIV. Assignment of Vibrational Bands for P25X as Taken from *in situ* Raman Spectra [456]

2,5-Xylidine $\bar{\nu}$ (cm ⁻¹)	P25X, red. <i>in situ</i> $E_{\text{RHE}} < 450$ mV $\bar{\nu}$ (cm ⁻¹)	P25X, ox. <i>in situ</i> $E_{\text{RHE}} = 600$ mV $\bar{\nu}$ (cm ⁻¹)	P25X, ox. <i>in situ</i> $E_{\text{RHE}} > 600$ mV $\bar{\nu}$ (cm ⁻¹)	Mode	Wilson no.
—	625	630	635	$\delta_{\text{C-H}}$	—
—	—	671	671	$\delta_{\text{C-H}}$	—
778	750	750–780	750	$\beta_{\text{C-C}}$	12
—	—	–863	855	$\delta_{\text{C-H}}$	—
—	—	863	855	$\delta_{\text{C-H}}$	—
—	930	930	930	$\nu_3(\text{ClO}_4^-)$	—
935	—	—	—	$\gamma_{\text{C-H}}$	17b
—	1028	1028	1028	$\delta_{\text{C-H}}$	—
1162	—	1175	1175	$\beta_{\text{C-H}}$	18a
1217	—	1233	—	$\nu_{\text{C-N}}$	13
1284	—	—	—	$\beta_{\text{C-C}}$	14
1297	1250	1250–1273	1250–1325	$\nu_{\text{C-N}}$	—
—	1363	1363	1363	δ_s , CH ₃	—
—	1383	—	1390	?	—
—	—	1417	—	?	—
1440	—	—	—	β_{CH_3}	—
—	—	1509	—	?	—
—	—	1525–1575	1525–1575	$\nu_{\text{C=N}} + \nu_{\text{ring}}$	—
1585	1631	1635	—	ν_{ring} , benzoid	8a
1625	—	—	—	ν_{ring} , benzoid	8b
—	—	—	1642	$\nu_{\text{C=N}}$	—

Table XV. Assignment of Vibrational Bands for PEtA as Taken from *in situ* Infrared Spectra [456]

<i>o</i> -Ethylaniline $\bar{\nu}$ (cm ⁻¹)	PEtA, red. <i>in situ</i> $E_{\text{RHE}} = 0$ mV	PEtA, ox. <i>in situ</i> $E_{\text{RHE}} = 400$ mV	PEtA, ox. <i>in situ</i> $E_{\text{RHE}} = 900$ mV	Mode	Wilson no.
	$\bar{\nu}$ (cm ⁻¹)	$\bar{\nu}$ (cm ⁻¹)	$\bar{\nu}$ (cm ⁻¹)		
752	—	—	—	$\gamma_{\text{C-H}}$	11
—	—	—	826	?	—
—	—	—	1119	?	—
1150	—	—	—	$\beta_{\text{C-H}}$	9a
1276	—	—	—	ν_{CH}	7a
—	—	—	1346	?	—
1455	1456	—	—	ν_{ring}	19a
1497	1505; 1509	—	—	ν_{ring} , benzoid	19b
—	—	1563	1574	ν_{ring} , quinoid	—
1585	—	—	—	ν_{ring} , benzoid	8a
1620	—	—	—	ν_{ring}	8b
—	—	—	1638	$\nu_{\text{C=N}}$	—

Table XVI. Assignment of Vibrational Bands for PEtA as Taken from *in situ* Raman Spectra [456]

<i>o</i> -Ethylaniline $\bar{\nu}$ (cm ⁻¹)	PEtA, red. <i>in situ</i> $E_{\text{RHE}} = 0$ mV	PEtA, ox. <i>in situ</i> $E_{\text{RHE}} = 900$ mV	Mode	Wilson no.
	$\bar{\nu}$ (cm ⁻¹)	$\bar{\nu}$ (cm ⁻¹)		
993	—	—	$\delta_{\text{C-H}}$	5
1029	1031	—	$\beta_{\text{C-H}}$	18b
—	1100–1130	—	$\delta_{\text{C-H}}$	—
1153	—	—	$\beta_{\text{C-H}}$	9a
1180	—	—	ν_{CH}	13
1250	—	—	ν_{CH}	7a
1319	1219	1220–1250	$\nu_{\text{C-N}}(?)$	—
—	—	1415	?	—
1452	—	—	ν_{ring}	19a
—	—	1488	ν_{ring} , semiquinoid	—
—	—	1582	ν_{ring} , quinoid	—
1603	1618	—	ν_{ring} , benzoid	8b
—	—	1632	$\nu_{\text{C=N}}$	—

trends of the three major absorption bands caused by electronic transitions in the UV-vis range are very similar to those already discussed for a variety of substituted polyanilines. All N-alkylated polymers were readily soluble in a host of organic solvents.

As already stated, chemical oxidation of diphenylamine in an aqueous solution resulted in a polymer of low molecular weight [476]. In better solvating, organic systems, slightly higher degrees of polymerization ($n = 10$ – 11 instead of $n = 3$ – 4) were found. UV-vis spectra of the product deposited on optically transparent electrodes showed an absorption at short wavelengths around $\lambda = 400$ nm. At more positive electrode potentials, a shoulder at $\lambda = 450$ nm and a broad absorption between $\lambda = 600$ and 900 nm were found. No assignment was provided.

Electrochemically redox active copolymers of aniline and *o*-

anthranilic acid were obtained by chemical oxidation [477]. From UV-vis and infrared spectra it was concluded that the anthranilic acid group restricts π conjugation along the polymer chain.

Zotti et al. [478] electropolymerized indole and a variety of 5-substituted indoles (5-carboxyindole, 5-cyanoindole) and biindoles. The presence of the NH mode observed with the polymer was taken as proof of coupling in the 2 and 3 positions. The shape and pH dependence of the CV, the electrode potential range wherein electronic conductivity was observed, the disappearance of the NH band during electrooxidation of the polymer, and the pH dependence of the electrochromism were analogous to PANI. This was assumed to indicate regularly alternating 2,2' and 3,3' coupling in the polymer chain. Polyindoles obtained with 2,2'- and 3,3'-biindole differed in chain length.

Table XVII. Assignment of Vibrational Bands for PPrA as Taken from *in situ* Infrared Spectra [456]

<i>o-n</i> -Propylaniline $\bar{\nu}$ (cm ⁻¹)	PPrA, red.	PEtA, ox.	PEtA, ox.	Mode	Wilson no.
	<i>in situ</i> $E_{\text{RHE}} = 0$ mV $\bar{\nu}$ (cm ⁻¹)	<i>in situ</i> $E_{\text{RHE}} = 500$ mV $\bar{\nu}$ (cm ⁻¹)	<i>in situ</i> $E_{\text{RHE}} = 1000$ mV $\bar{\nu}$ (cm ⁻¹)		
750	—	—	—	$\gamma_{\text{C-H}}$	—
—	—	1118	1118	$\delta_{\text{C-H}}$	—
1146	—	—	—	β_{CH}	18a
1311	—	—	—	$\nu_{\text{C-N}}$	—
1377	—	—	—	δ_s, CH_3	—
—	—	1250–1400	1200–1350	$\nu_{\text{CN}}^{\text{a}}$	—
1456	1458	—	—	ν_{ring} , benzoid	19a
—	—	1482	—	(?)	—
1497	1504	—	—	ν_{ring}	19b
1582	—	—	—	ν_{ring}	8a
—	—	1574	1574	ν_{ring}	8b
—	—	—	1656	$\nu_{\text{C=N}}$	—

^aDouble bond with slightly reduced degree of bonding.

Table XVIII. Assignment of Vibrational Bands for PPrA as Taken from *in situ* Raman Spectra [456]

<i>o-n</i> -Propylaniline $\bar{\nu}$ (cm ⁻¹)	PPrA, red.	PPrA, red.	PEtA, ox.	PEtA, ox.	Mode	Wilson no.
	<i>in situ</i> $\lambda_{\text{L}} = 488$ nm $E_{\text{RHE}} = 0$ mV $\bar{\nu}$ (cm ⁻¹)	<i>in situ</i> $\lambda_{\text{L}} = 514.5$ nm $E_{\text{RHE}} = 0$ mV $\bar{\nu}$ (cm ⁻¹)	<i>in situ</i> $\lambda_{\text{L}} = 488$ nm $E_{\text{RHE}} = 900$ mV $\bar{\nu}$ (cm ⁻¹)	<i>in situ</i> $\lambda_{\text{L}} = 514.5$ nm $E_{\text{RHE}} = 900$ mV $\bar{\nu}$ (cm ⁻¹)		
1030	—	—	—	—	$\beta_{\text{C-H}}$	—
—	1121	1150–1110	1123	1120	δ_{CH}	—
1160	—	—	—	—	β_{CH}	9a
—	—	1225	—	1228	?	—
1270	—	—	1253	1252	ν_{CH}	—
1320	—	—	—	—	$\nu_{\text{C-N}}(?)$	—
—	1410	—	1417	1412	?	—
1450	—	—	—	—	ν_{ring}	19a
—	—	—	1480	1480	?	—
—	—	—	1586	1584	ν_{ring} , quinoid	—
1580	1621	1620	—	—	ν_{ring} , benzoid	8a
≈1620	—	—	—	—	ν_{ring}	8b
—	—	—	1630	1629	$\nu_{\text{C=N}}$	—

Electrochemical formation of polyindole perchlorate was reported by Choi et al. [479, 480] and Kong et al. [481]. Only *ex situ* methods were employed to identify the molecular structure of the prepared polymer. A polymerization mechanism that involved the radical cation already observed elsewhere as a reactive intermediate and a polymer structure with 1,3-coupling were postulated. In a further report, Choi et al. [482] described the electropolymerization of polyindole tetrafluoroborate. From electrochemical data, a polymerization mechanism that involves radical cation intermediates was deduced. Further spectroscopic investigations performed *ex situ* resulted in a suggestion for the polymer structure with 1,3 coupling. *Ex situ* measurements of the electric con-

ductivity were compatible with a conduction model based on hopping conduction and polarons. ESR spectra of a dry powder sample showed a single line spectrum that was related by Choi et al. to the observed electric conductivity. Jackowska et al. [483] used *in situ* UV-vis and ECESR spectroscopy to determine the number of electrons transferred during oxidation-reduction of polyindole, films and concluded that ECESR provides more accurate numbers. This was explained by invoking overlapping bands in the fairly weak UV-vis spectra recorded. This conclusion may be questionable, because elsewhere fairly well resolved UV-vis spectra have been recorded *in situ* [440]. Probst and Holze [445] reported on *in situ* measurements of the temperature dependence of the

Table XIX. Assignment of Vibrational Bands for PNMA as Taken from *in situ* Infrared Spectra [456]

<i>N</i> -methylaniline $\bar{\nu}$ (cm ⁻¹)	PNMA, red.	PNMA, ox.	Mode	Wilson no.
	<i>in situ</i> $E_{\text{RHE}} = 0$ mV $\bar{\nu}$ (cm ⁻¹)	<i>in situ</i> $E_{\text{RHE}} = 900$ mV $\bar{\nu}$ (cm ⁻¹)		
—	820	840	$\delta_{\text{C-H}}$	10a
—	—	1090	$\nu_3(\text{ClO}_4^-)$	—
—	—	1180	δ_{CH}	—
1320	1250–1310	—	$\nu_{\text{C-N}}$	—
—	—	1370	ν_{CN}	—
1508	1508	—	ν_{ring} , benzoid	19a
—	—	1585	ν_{ring} , quinoid	—
1604	—	—	ν_{ring}	8a

Table XX. Assignment of Vibrational Bands for PNMA as Taken from *in situ* Raman Spectra [456]

<i>N</i> -methylaniline $\bar{\nu}$ (cm ⁻¹)	PNMA, red.	PNMA, ox.	Mode	Wilson no.
	<i>in situ</i> $E_{\text{RHE}} = 0$ mV $\bar{\nu}$ (cm ⁻¹)	<i>in situ</i> $E_{\text{RHE}} = 900$ mV $\bar{\nu}$ (cm ⁻¹)		
1181	1199	1190; 1204	$\beta_{\text{C-H}}$	9a
1320	1260	—	$\beta_{\text{C-H}}$	14
—	1368	1379	$\nu_{\text{C-N}}$, semiquinoid	—
—	—	1443	$\nu_{\text{C-N}}$, semiquinoid	—
—	1555	1560	ν_{ring} , quinoid	19a
1605	1619	1622	$\beta_{\text{C-H}}$, benzoid	8a
—	1677	1682	$\nu_{\text{C=N}}$	—

Table XXI. Assignment of Vibrational Bands for PNEA as Taken from *in situ* Infrared Spectra [456]

<i>N</i> -Ethylaniline $\bar{\nu}$ (cm ⁻¹)	PNEA, red.	PNEA, ox.	Mode	Wilson no.
	<i>in situ</i> $E_{\text{RHE}} = 0$ mV $\bar{\nu}$ (cm ⁻¹)	<i>in situ</i> $E_{\text{RHE}} = 900$ mV $\bar{\nu}$ (cm ⁻¹)		
868	—	840; 870	$\gamma_{\text{C-H}}$	10a or 17b
—	—	1080	$\nu_3(\text{ClO}_4^-)$	—
1180	—	1180	β_{CH}	9a
1257	1245	—	δ_{CC}	13
1319	1305	—	$\nu_{\text{C-N}}$	—
—	—	1410	ν_{CN} , semiquinoid	—
1506	1510	—	ν_{ring} , benzoid	19a
—	—	1580	ν_{ring} , quinoid	—
1605	—	—	ν_{ring}	8a
—	—	1660	$\nu_{\text{C=N}}$	—

Table XXII. Assignment of Vibrational Bands for PNEA as Taken from *in situ* Raman Spectra [456]

<i>N</i> -Ethylaniline $\bar{\nu}$ (cm ⁻¹)	PNEA, red. <i>in situ</i> $E_{\text{RHE}} = 0$ mV	PNEA, ox. <i>in situ</i> $E_{\text{RHE}} = 900$ mV	Mode	Wilson no.
	$\bar{\nu}$ (cm ⁻¹)	$\bar{\nu}$ (cm ⁻¹)		
1179	1205	1200	$\beta_{\text{C-H}}$	9a
1320	1275	1280	$\nu_{\text{C-N}}$	14
—	—	1375	δ_s, CH_3	—
—	—	1420	$\nu_{\text{C-N}}$, semiquinoid	—
1455	—	—	$\delta_{\text{C-H}}$	19b
—	—	1585	$\nu_{\text{C-N}}$, quinoid	—
1605	1623	1624	ν_{ring} , benzoid	8a
—	—	1683	$\nu_{\text{C=N}}$	—

electronic conductivity of polyindole. The increase of conductivity with increasing temperature implies a semiconductor-like behavior.

Chemical polymerization of *m*-nitroaniline and *p*-nitroaniline has been reported [484]. The poorly conducting polymers obtained were characterized using a variety of *ex situ* techniques. Results were rationalized based on the effects of the nitro group substituent.

During electrooxidation of *o*-methoxyaniline, Widera et al. [485] recorded *in situ* SER spectra. A C–N coupling was observed.

Bilayer structures have been prepared and investigated with various spectroelectrochemical techniques [307, 486]. In the former report, surface resonance Raman spectroscopy showed typical vibrational features of the involved polymers [PANI and poly(*o*-phenylenediamine)] as already discussed were observed. In the latter investigation, involving PANI/poly(5-chlorine,2-methoxyaniline), it was concluded that the topmost layer of the polymerized substituted aniline blocks the electrochemical reduction of the inner layer of PANI. This was first deduced from the diminished height of reduction peaks in the CV. Moreover, this was supported by *in situ* UV–vis spectra that showed typical bands of oxidized PANI even after formal reduction of the film.

3.3. Redox Processes of Polyaniline and Polymers of Substituted Anilines

Redox processes, that is, the removal of electrons from the polymer upon chemical or electrochemical oxidation or the addition of electrons by chemical or electrochemical means during reduction, result in considerable changes of molecular as well as structural, electronic, and optical properties of the polymers prepared from aniline or its relatives. Quite a few of these changes were discussed already in the preceding section, because a clear cut separation of a complete description of the polymer in a given state and the changes of this state is impractical. An additional feature, of PANI and its relatives will further complicate the picture. As already indicated, the nitrogen atom in the monomer as well as in the polymer can be protonated. Of course, the protons can be removed under suitable environmental circumstances. Consequently, in addition to the electrochemical doping mentioned already, protonic acid doping has to be kept in mind. This was already included in Figure 27. Chiang and MacDiarmid [487] reviewed the fairly com-

plicated system with respect to various possible relationships between conductivity, pH value of the solution phase, degree of doping, and $\text{p}K_a$ of the formed emeraldine salt. The numerous redox processes and the corresponding redox states were reviewed based mainly on the results of *ex situ* XPS studies by Kang et al. [488].

The diffusion of anions during doping and dedoping processes at PANI fibers was investigated with *in situ* UV–vis spectroscopy by Kanamura et al. [489]. Using a cylindrical diffusion model, it was found that the estimated diffusion coefficient increases with the radius of the PANI fiber. Data obtained with PANI prepared in nonaqueous solutions showed a similar dependence, and the overall values of the diffusion coefficient were much smaller. Whereas the kinetic measurements were made in the same solution, it was proposed, that the diffusing species were different. No suggestion of their specific identity was made.

The kinetic of redox processes that occur in PANI has been studied with UV–vis spectroscopy by Hugot-Le Goff and Bernard [490]. In addition to more general statements, without particular kinetic data, it was found that the electrochromism of PANI (one of the properties assumed to be of particular interest for practical applications) is more pronounced at slightly elevated pH values (i.e., at pH = 3 it is better than at pH = 0).

Also with UV–vis spectroscopy, the chemical oxidation of leucoemeraldine to emeraldine by oxygen and hydrogen peroxide catalyzed by copper and iron chloride was studied by Moon et al. [491]. The reaction was found to be first order, and the activation energies were determined. Using electrochemical methods, Alpatova et al. [492] performed a similar investigation. Particular attention was paid to the contribution of nucleation of conductive regions in the polymer during oxidation. The term “electrochemical phase transition” was suggested for a description. The kinetics of the doping and dedoping of PANI at low temperatures in the electrolyte system $\text{HClO}_4 \cdot 5.5\text{H}_2\text{O}$ was studied with ultramicroelectrodes by Vuki et al. [493].

The kinetics of doping and dedoping for various copolymers were studied by Ram et al. [494] for PANI, PANI-PoTl, and PANI-MOA. Although PANI-MOA is a poorer electronic conductor, the response to a change of the state of doping and oxidation is much faster as compared to PANI and PANI-PoTl. The response of PANI-PoTl is even slower than the response of PANI alone. The fast response of PANI-MOA is attributed to the presence of the methoxy group in the polymer, which facilitates torsion move-

ments between substituted and unsubstituted rings, thus accelerating the change from the undoped into the doped form. A faster response of a chemically prepared copolymer PANI-PoTI was also observed by Dhawan and Trivedi [495]. The hysteresis of the doping and dedoping process as quantified with *in situ* ECESR spectroscopy was further investigated using the "mirage" effect by Vieil et al. [496]. Data obtained with this method and the quartz crystal microbalance were used to elucidate the movement of various ions involved in the mentioned processes.

Open circuit relaxation of thin PANI films prepared by chemical and electrochemical oxidation from both the oxidized and the reduced state was investigated with UV-vis and infrared spectroscopy by Chinn et al. [497]. In both cases, the emeraldine state is obtained. The process is controlled by disproportionation reaction and semiquinone radical formation.

3.4. Redox Processes and Electrocatalysis at Polyaniline and Related Polymers

Although similar in name, redox processes that take place at electrodes coated with conducting polymers have to be considered separately. As reviewed briefly by Malinauskas and Holze [498–500] and Kazarinov et al. [501], electrodes coated with a variety of conducting polymers (polyaniline, copolymers of aniline, and various aniline derivatives) sometimes have remarkable catalytic activities for a variety of electrochemical redox processes. Malinauskas and Holze used *in situ* UV-vis spectroscopy to monitor the rate of the oxidation process and to determine the reaction zone. Basically, the redox reaction of a solution species (e.g., quinone-hydroquinone, chromate, etc.) can occur at the polymer-solution interface or at the supporting electrode surface, which is at least, to some extent, accessible for the solution phase, because of the extremely porous and three-dimensional structure of most polymers. At first glance, the oxidation is prone to occur at the polymer surface, because the polymer is in its conducting state provided that the oxidation process of the solution species occurs at an electrode potential that is positive to at least the first current peak, where polymer oxidation (doping) occurs. Only in the case of a polymer with a very poor catalytic activity does the process have to take place at the supporting electrode surface. A mechanism that assumes that electron transfer occurs at the outer polymer surface is a multistep process. The species to be oxidized at the polymer surface transfers an electron to the polymer, which is thus reduced. This electron travels to the supporting electrode surface. Upon its transfer into this electrode, the polymer is reoxidized. Depending on the relative rates of both steps, the polymer may be present to a high extent in its reduced state (when the latter process is slow, the first process is fast) or in its oxidized state (when the first step is slow, the last step is fast). In the case of a benzoquinone-hydroquinone couple, it was found that reoxidation of PANI is the faster process, that is, the polymer stays predominantly in its oxidized state. In the opposite case, a considerable fraction of the polymer is still in its conducting state, although basically the redox reaction is a reduction process. Complete reduction of the film, which is a viable option for consideration unless the rates of both steps are known in detail, is unlikely, because the reduced film is a poor medium for electron transfer because of its low conductivity. Results obtained with the redox couple $\text{Fe}^{2+/3+}$ were fairly similar [500]. The interaction of PANI with dioxygen dissolved in the electrolyte solution resulted in the oxidation of the reduced form of PANI [500]. The rate is very low. Because this process

also can be treated as a redox reaction of PANI, where oxygen acts just like an oxidant, corresponding studies with metal halides that act as catalysts with considerably enhancing effects, were previously treated. The chemical oxidation of PANI in its dissolved leucoemeraldine base form with dioxygen and other oxidants into the PANI emeraldine base form was studied by Moon et al. [502]. Reaction orders, reaction rates, and energies of activation as well as UV-vis spectroscopic details have been reported. The use of PANI as a catalyst for dioxygen reduction was investigated by Barsukov et al. [503].

Modification of PANI-coated electrodes with metal tetrasulfonated phthalocyanines (MeTsPc), where the metal is cobalt or iron, resulted in significant changes in the electrocatalysis of the reduction of dioxygen [504]. Obviously, insertion of the MeTsPc into the polymer occurs [505]. This was supported in an investigation by Coutanceau et al. by the results of *in situ* UV-vis spectroscopy. The role of the polymer in the mechanism and the kinetics of dioxygen electroreduction seemed to be somewhat difficult to elucidate. Insertion of CoTsPc resulted in a positive shift of the onset of dioxygen reduction. The two-electron pathway that results in hydrogen peroxide as a reduction product remains.

The reaction of PANI in its oxidized form (both in doped and undoped form) with water, resulting in the formation of superoxide, was studied with ESR spectroscopy by Otsuka et al. [506]. Electrode kinetics of various charge transfer processes at poly(*o*-phenylenediamine), poly(*N*-methylaniline), and poly(*N*-ethylaniline) were investigated by Chiba et al. [507].

The processes reviewed so far involve redox couples with redox potentials in a region of electrode potentials, where PANI is in its conducting (i.e., oxidized) state. This is of importance because of the almost completely absent electronic conductivity in the reduced state and because of possible interactions between positive charges (radical cations, polarons) in the polymer and the redox active species. The reaction of PANI or related polymers in their reduced state with redox species in the solution phase may be considerably different. To elucidate conceivable differences, the reductive interaction between PANI and 1,2-naphthoquinone-4-sulfonate (NQS) was studied with *in situ* UV-vis spectroelectrochemistry [508]. The redox potential of this system lies within the electrode potential range limited by the first and the second oxidation peaks of PANI. A proposed electrocatalytic mechanism of this process includes the cathodic reduction of the PANI film and its subsequent reoxidation by NQS. Accordingly, PANI acts as a redox mediator, cycled between its emeraldine and its leucoemeraldine form. In the equilibrium state, both redox forms of PANI are present in the film. The relative content of both forms was shown to depend on the concentration of NQS in the solution, on the PANI film thickness, and on the applied electrode potential. In addition, the cathodic reduction of sulfopropylviologen (SPV) and benzylviologen (BV) was studied in the potential range where the nonconducting (reduced) leucoemeraldine form of PANI exists. The slowness of the cathodic reduction of both BV and SPV at pH = 0.5 was tentatively attributed to electrostatic repulsion between the positively charged PANI polymer chain and the viologen molecule. At pH = 4.0, the reduction becomes fast, probably due to deprotonation of the leucoemeraldine form of PANI, resulting in the disappearance of the electrostatic repulsion. In the middle pH region (pH = 1.5), a large difference in the rate of the cathodic reduction between BV and SPV was observed. This difference may be attributed to deprotonation of the sulfo groups

of SPV. Deprotonated SPV has no net electric charge, and electrostatic repulsion should not be effective. In contrast, BV has a positive electric charge that is independent of the pH value of the solution.

The interaction of PANI with dichromate is of particular interest because of possible application in waste water treatment systems [499]. Figure 52 (top) shows a UV-vis spectrum of a potassium dichromate solution. The main absorbance band is located at ca. $\lambda = 350$ nm. It does not interfere with the major absorbance band of the oxidized (emeraldine) form of PANI. Figure 52 (bottom) shows spectra obtained at different time intervals after the immersion of the PANI-coated ITO glass electrode into the dichromate solution. Immediately after immersion of the PANI-coated electrode, a shift of the absorbance maximum of PANI film is observed. As compared to the spectrum of PANI obtained at $E_{\text{RHE}} = +0.8$ V [spectrum A in Fig. 52 (bottom)], the absorbance maximum shifts from $\lambda = 750$ nm to ca. $\lambda = 660$ nm. Earlier, a comparable shift of the absorbance maximum after switching the electrode potential from $E_{\text{RHE}} = +0.8$ V to $E_{\text{RHE}} = +1.1$ or $+1.2$ V was found [509]. Consequently, the shift indicates that a redox reaction between dichromate ions and the PANI film proceeds. Because of the high value of E_0 for dichromate ions the PANI film becomes oxidized and shows the corresponding spectral features of the oxidized state found at high electrode potential values.

Immediately, the degradation of PANI film starts to result in a decrease of absorbance in the long wavelength range assigned to PANI in its intact oxidized state as seen in Figure 52 (bottom). The degradation,¹⁰ characterized by $\tau_{1/2}$ of 4–5 min, proceeds at a rate closely similar to that obtained by holding a PANI-modified electrode at $E_{\text{RHE}} = +1.2$ V in a solution without dichromate ions. Thus, both a high electrode potential value and the presence of dichromate ions in solution cause a similar irreversible degradation effect of the PANI film. Simultaneously with PANI degradation, a decrease of dichromate concentration is observed, as expected, and is indicated by a decrease of the absorbance band at $\lambda = 350$ nm [Fig. 52 (bottom)]. Obviously, dichromate is consumed in a chemical reaction with PANI. These observations show that the PANI film is quickly destroyed (i.e., oxidized) under open electric circuit conditions by dichromate, presumably because of the high redox potential value of the latter.

Figure 53 (middle) shows UV-vis spectra obtained when holding the PANI-modified electrode in a dichromate solution at a potential, where the leucoemeraldine (i.e., reduced) form of PANI exists. In the long wavelength range (above $\lambda = 600$ nm), the spectrum obtained is quite similar to that characteristic for the leucoemeraldine form of PANI, that is, like a spectrum obtained at $E_{\text{RHE}} = +0.2$ V in a solution without dichromate [Fig. 53 (top)]. During electrolysis for 1 h, a spectrum in this region does not change remarkably, indicating that PANI is always present in its reduced form under the conditions used. In contrast, the absorbance band of dichromate diminishes in height during electrolysis, obviously indicating the reduction of dichromate [Fig. 53 (middle)].

From the data of Figure 53 (middle), it was calculated that the concentration of dichromate decreases during 1 h of electrolysis from 1 to 0.78 mM. This decrease is approximately two to three times higher than that obtained under open circuit conditions, that is, due to irreversible oxidation of PANI film only [as in

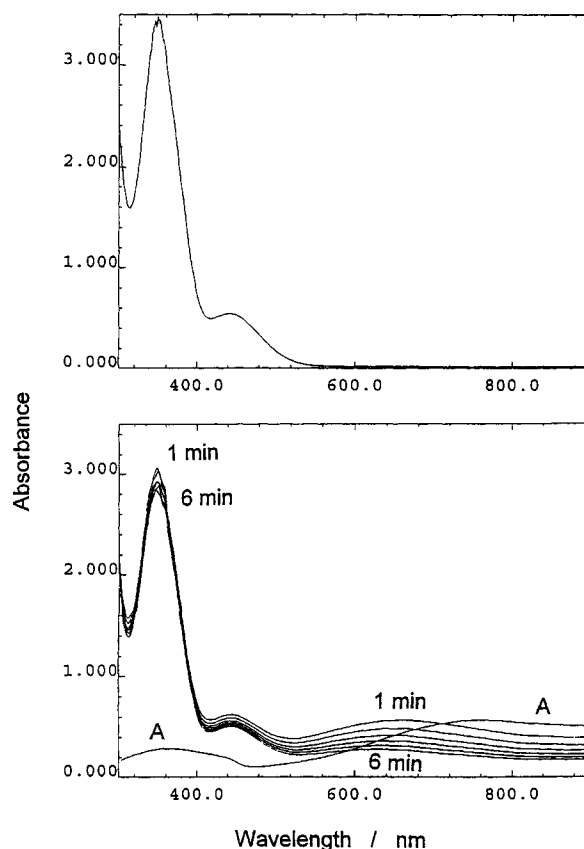


Fig. 52. Top: UV-vis spectrum of a solution of 0.5-M H_2SO_4 that contained 1 mM of potassium dichromate. Bottom: UV-vis spectra, obtained in the same solution recorded at time intervals of 1 min, ranging from 1 to 6 min (as indicated) after immersion of the PANI-coated ITO glass electrode. Spectrum A was obtained for the PANI-coated electrode in 0.5-M H_2SO_4 without potassium dichromate added at a controlled potential of $E_{\text{RHE}} = +0.8$ V.

Fig. 52 (bottom)]. This means that the electrochemical reduction of dichromate proceeds on the electrode covered with PANI. After interruption of electrolysis at $E_{\text{RHE}} = +0.2$ V, the spectrum of the PANI film changes immediately to that which is characteristic for high potential values, and destruction of the polymer film proceeds [Fig. 53 (bottom)]. Simultaneously, the absorbance band of dichromate diminishes in height, indicating its redox interaction with PANI film [Fig. 53 (bottom)]. It is noteworthy that the oxidation of PANI film by dichromate under open circuit conditions proceeds relatively fast, with $\tau_{1/2}$ of 4 or 5 min (cf. bottom parts of Figs. 52 and 53), whereas after applying an electrode potential of $E_{\text{RHE}} = +0.2$ V, the PANI film appears almost unchanged for several hours and no degradation is observed.

It was concluded that the leucoemeraldine form of PANI is oxidized by dichromate ions. By applying an electrode potential of $E_{\text{RHE}} = +0.2$ V, PANI film is reduced to its initial leucoemeraldine form. As a result, a net electroreduction of dichromate takes place at the PANI-modified electrode, wherein the PANI film acts as an electrocatalyst in the reaction sequence presented. Because PANI is present in its reduced form (as seen from spectra of Fig. 53, middle), it was concluded that a chemical redox reaction between dichromate and PANI is the rate-determining step, whereas the cathodic reduction of the PANI film proceeds relatively fast.

¹⁰For a detailed review of spectroelectrochemical investigations of PANI degradation processes, see the following section.

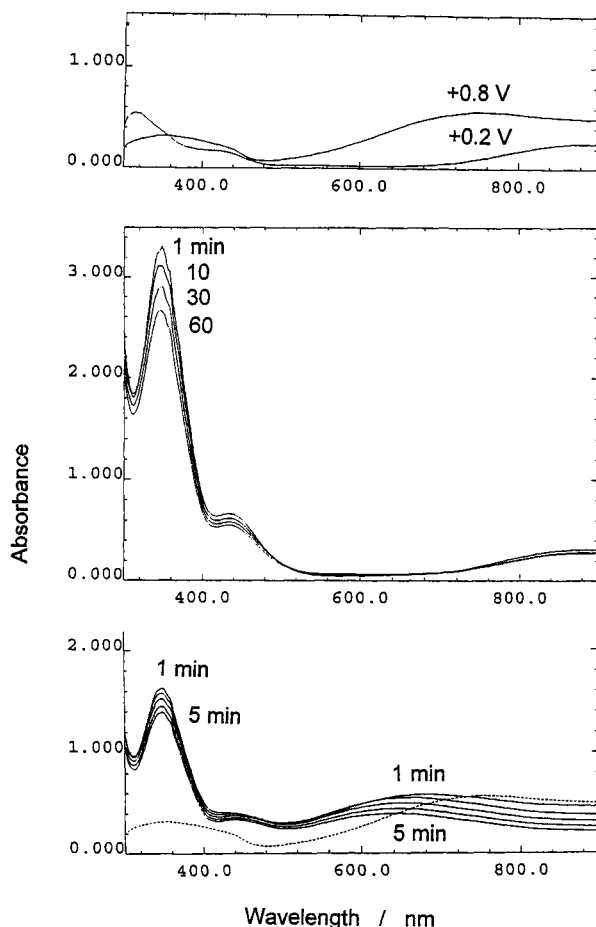


Fig. 53. Top: UV-vis spectra of a PANI-coated electrode at $E_{\text{RHE}} = +0.2$ and $+0.8$ V (as indicated) obtained in an aqueous solution of 0.5-M H_2SO_4 . Middle: UV-vis spectra obtained at different time intervals (as indicated in minutes) with a PANI-coated ITO glass electrode held at $E_{\text{RHE}} = +0.2$ V in a solution of 0.5-M H_2SO_4 that contained 1-mM of potassium dichromate. Bottom: UV-vis spectra obtained in the same solution recorded at time intervals of 1 min (ranging from 1 to 5 min, as indicated) after interruption of electrolysis for 2.5 h at $E_{\text{RHE}} = +0.2$ V with a PANI-coated ITO glass electrode (as in the middle). The dashed trace is the UV-vis spectrum of a PANI-coated ITO glass electrode obtained at an electrode potential of $E_{\text{RHE}} = +0.8$ V in 0.5-M H_2SO_4 solution [499].

Figure 54 (top) shows spectra obtained with a PANI-coated electrode in a solution containing dichromate, after applying an electrode potential of $E_{\text{RHE}} = +0.8$ V. The picture obtained closely resembles that observed for an electrode potential of $E_{\text{RHE}} = +0.2$ V [cf. with Fig. 53 (middle)], with the exception that the spectrum in the high wavelength range shows that PANI is present in its half-oxidized (i.e., emeraldine) form. A decrease of the dichromate absorbance band at $\lambda = 350$ nm proceeds in this case at a rate similar to that obtained at an electrode potential of $E_{\text{RHE}} = +0.2$ V. This indicates, that a cathodic reduction of dichromate proceeds at a PANI-modified electrode at a rate that is independent of its potential within the range studied ($E_{\text{RHE}} = +0.2$ to $+0.8$ V). Because the PANI spectrum in the high wavelength region does not differ markedly from that obtained in the supporting electrolyte without dichromate added [as in Fig. 53 (top)], it can be concluded that even in the present case the cross-reaction between dichromate and the emeraldine form of PANI is the rate-determining step.

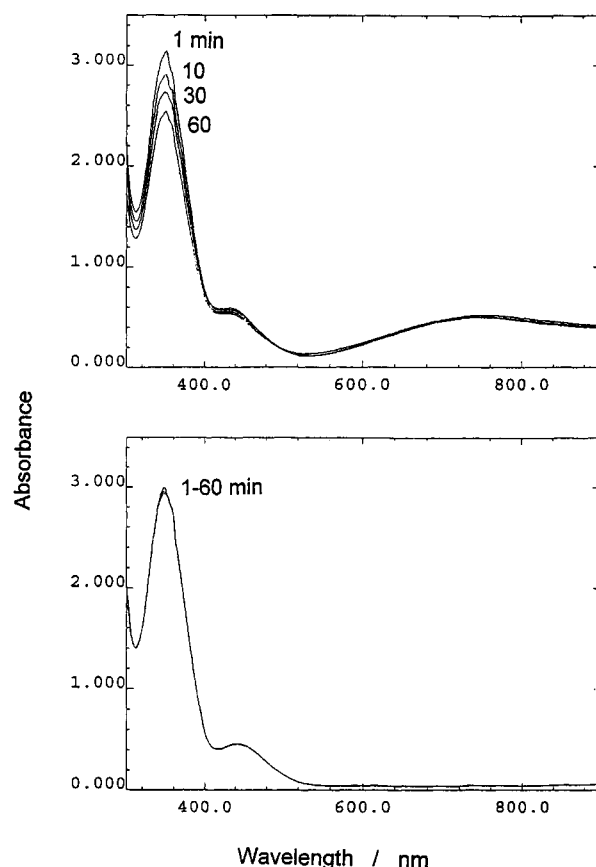


Fig. 54. Top: UV-vis spectra, obtained at different time intervals (as indicated in minutes) with a PANI-coated ITO glass electrode held at $E_{\text{RHE}} = +0.8$ V in an aqueous solution of 0.5-M H_2SO_4 containing 1-mM of potassium dichromate. Bottom: Same the top spectrum, obtained with a bare ITO glass electrode [499].

Figure 54 (bottom) shows four overlapping spectra, obtained on a bare ITO glass electrode after 1, 10, 30, and 60 min [as in Fig. 54 (top)] after a potential step to $E_{\text{RHE}} = +0.2$ V in a solution containing dichromate. Closely similar spectra were obtained also when holding an unmodified ITO glass electrode at $E_{\text{RHE}} = +0.8$ V (not shown). It is seen in Figure 54 (bottom) that almost no electroreduction of dichromate proceeds on a bare ITO glass electrode. This supports the proposed electrocatalytic action of a PANI layer in the electroreduction of dichromate ions.

Direct evidence of redox mediation between sulfonated PANI and dimercaptane combined in an electrode initially investigated for possible use in secondary batteries [510] was observed with *in situ* UV-vis spectroscopy [511].

3.5. Degradation of Polymers

Because of the more practical aspect of polymer stability in the numerous proposed uses of intrinsically conducting polymers, including polyaniline and its relatives, and the more fundamental interest in the chemistry of processes that change the chemical identity and various solid state properties of the polymers, degradation studies are warranted. These studies focussed initially on the mere rate of degradation (which may be of very practical interest). With purely electrochemical measurements, Kobayashi et al. [512, 513] showed that the two peaks in cyclic voltammograms of PANI di-

minish in height during prolonged potential cycling, and a third redox process in the middle potential region becomes evident with increasing intensity. They stated that the diminishing main peaks reflect the degradation of PANI, whereas the newly generated middle peak is associated with degradation products. If the electrode potential is not swept beyond ca. $E_{SCE} = 0.7$ V during potential cycling, no degradation is observed.

The nature of the peak in the middle potential region was the subject of discussion in many works. Based on their voltammetric and spectroscopic studies, Kobayashi et al. [513] presented a reaction scheme for an oxidative degradation. In accordance with this scheme, *p*-benzoquinone was claimed as a product of degradation. Stilwell and Park [514–516] concluded, that the peak in the middle potential region corresponds to redox reactions of degradation products of PANI, including *p*-benzoquinone and quinoneimines. Yang and Bard [517] showed *p*-benzoquinone and *p*-aminophenol to be responsible for the occurrence of the middle peak in the electropolymerization of aniline. *p*-Benzoquinone was also suggested elsewhere as a degradation product [518] formed during the electropolymerization process. It was identified with *in situ* IR spectroscopy by Neugebauer et al. [519]. UV-vis spectra obtained with overoxidized PANI films recorded by Kobayashi et al. showed electronic absorption that was assigned to *p*-benzoquinone.

In contrast, Glarum and Marshall [521] could not confirm formation of *p*-benzoquinone during overoxidation of PANI. Cleavage of polymer chains as well as the linkage of neighboring chains (cross-linking) were suggested as reactions that take place during oxidative degradation of PANI [522–524]. As an alternative, Genies et al. [69, 525] proposed a different phenazin-like structure of PANI that is formed at higher positive electrode potentials as being responsible for the occurrence of the middle peak. In addition to electrochemical degradation of PANI, Pasquali et al. [526] studied degradation processes of PANI and its derivatives in aqueous and organic solutions at open electric circuit and in the dry state. In all cases, different degrees of degradation were observed. Kazarinov et al. [527] observed the release of monomer units from the polymer at very positive electrode potentials using a radio-tracer technique. Finally, parts of the polymer film are stripped off the platinum electrode surface, and the surface becomes available again for adsorption of aniline monomers and other electrolyte solution constituents (e.g., protons). The influence of the anion on the degree of overoxidation (“anion effect”) was studied by Lippe et al. [528, 529]. Results indicate a considerable influence of the anion that is present because of charge compensation in the doped, conducting PANI film upon the stability of the polymer. Although Lippe et al. considered various properties of the anion (charge, charge density, ionic softness, etc.), so far no conclusive evidence has been obtained to explain the striking stability of PANI in a solution of perchloric acid as compared to a number of other acid ions. A detailed review of the degradation of PANI was presented by Pud [530].

Using UV-vis spectroscopy, Malinauskas et al. reported rates of degradation as a function of electrode potential for poly(*N*-benzylaniline) [531] and PANI [532] based on the change of the electronic absorption at about $\lambda = 720$ nm. Degradation of the former compound proceeds faster. In the case of PANI, spectroscopic data indicate structural changes in the polymer as deduced from the relative change of the electronic absorption at different energies. Figure 55 shows the change of the absorption spectrum of a PANI film prepared potentiostatically as a function of electrode potential. In the lower part, the same set of spectra

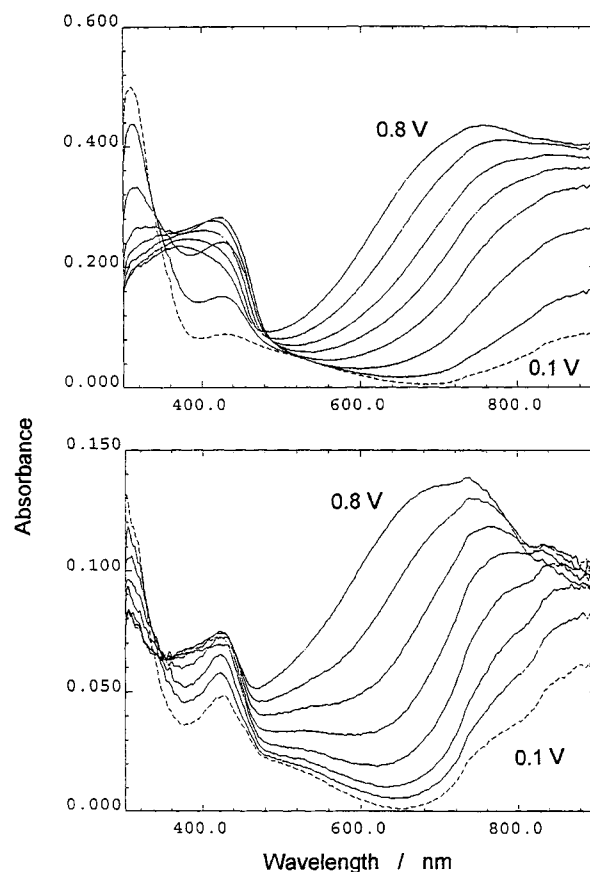


Fig. 55. Top: UV-vis spectra of a PANI-coated ITO glass electrode in 0.5-M H_2SO_4 at different electrode potentials, ranging from $E_{RHE} = 0.0$ to $+0.8$ V, recorded in intervals of 0.1 V. The PANI-coated electrode was prepared by electropolymerization at $E_{RHE} = 1.0$ V in an aqueous solution of 0.5-M H_2SO_4 + 0.05-M aniline. Bottom: spectra of the same electrode obtained after holding at $E_{RHE} = +1.0$ V in 0.5-M H_2SO_4 for 10 min [532].

recorded after exposure of the film to a fairly positive electrode potential, where presumably degradation occurs, is displayed. Obviously, changes of the electrooptic properties of the polymer have occurred. In comparison, the corresponding set of spectra is displayed in Figure 56 for PANI prepared by continuous electrode potential cycling. The absorbance maximum of the oxidized film is shifted toward much longer wavelengths, indicating a higher degree of conjugation (polymerization) and thus a more ordered polymer structure. Whereas degradation most likely will affect the conjugated systems, a change of the absorption maximum to lower wavelengths is expected. With PANI, this is clearly evident. From the change of the absorbance maximum at long wavelengths, rate constants for the degradation were derived. Their dependence upon the electrode potential is shown in Figure 57.

Of course, degradation caused by the exposure of PANI and related polymers in its conducting (doped) state to nucleophilic attack, especially by constituents of aqueous electrolyte solutions, may already be occurring during electropolymerization. Because of the positive electrode potential needed to form the initial reactive intermediate, the polymer will be present in its doped state during electropolymerization. This undesirable situation explains the interest in monomers (e.g., xylidine), that can be oxidized at less positive electrode potentials. Generally, deposition param-

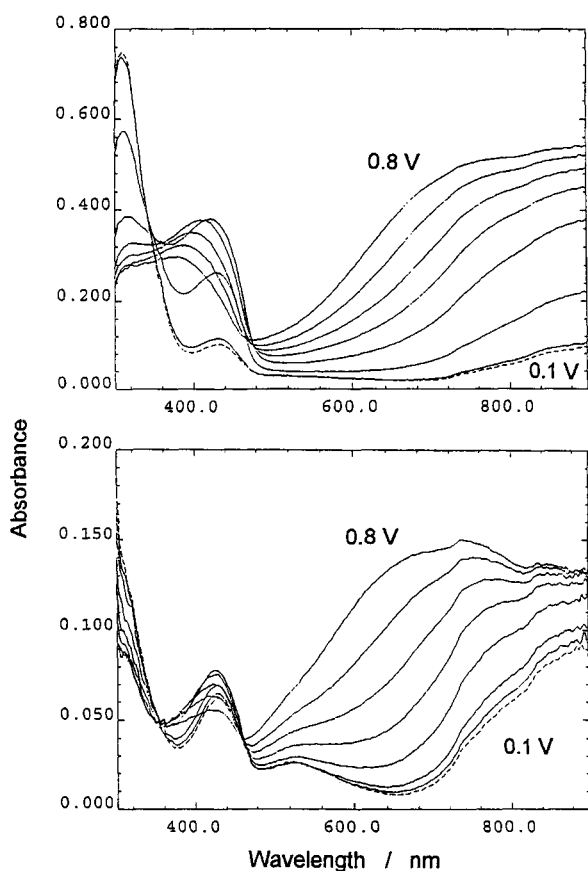


Fig. 56. Same as Figure 55 for a PANI-coated electrode prepared by potential cycling within the limits of $E_{\text{RHE}} = +0.1$ to $+1.2$ V at a scan rate of 50 mV s^{-1} [532].

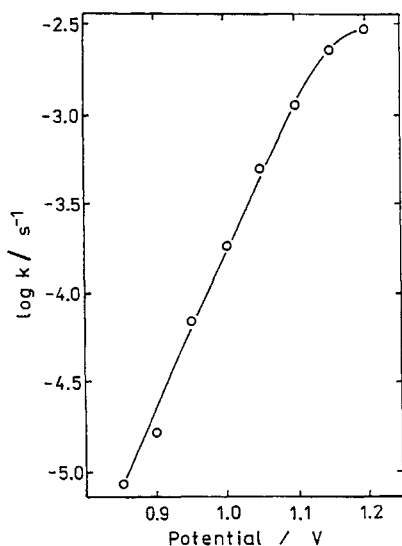


Fig. 57. Dependence of logarithm of the first-order rate constant of electrochemical degradation of a PANI film in an aqueous solution of $0.5\text{-M H}_2\text{SO}_4$ on the electrode potential. The PANI-coated electrode was prepared at $E_{\text{RHE}} = +1.1$ V in $0.5\text{-M H}_2\text{SO}_4 + 0.05\text{-M aniline}$ [532].

ters that expose the electrode to a minimum of positive potentials are favored. In addition to the structural results of overoxidation (e.g., disturbed conjugated systems, cross-linking), hydroly-

ysis products that are formed as a result of nucleophilic attack of solvent constituents either on the polymer already formed or on reactive intermediates may be incorporated into the polymer film with undesirable effects. Cui et al. [533] suggested using the ratio of the current measured in the second peak of the cyclic voltammogram of a polymer-coated electrode versus the current of the first peak as an indicator of the degree of overoxidation. Alternatively, the ratio of the sum of the current at the second and the middle peak versus the current at the first peak was proposed as an indicator [534]. The use of nonaqueous solutions as polymerization media was investigated by Yonezawa et al. [535]. The resulting polymer showed less damage by overoxidation. For practical and economical reasons, these solvents are less attractive.

Although obtained with chemically prepared PANI and measured only with *ex situ* methods, a study of aging reported by Ranou and Nechtschein [536] is noteworthy. The measured conductivity data imply that conductivity on a macroscopic scale decreases rapidly as a function of time, whereas on a microscopic level, the decrease is far less strong. Accordingly, it was proposed that corrosion of the outer surface of good conducting grains impedes conduction. This assumes a model of PANI based on metallike grains embedded in a poorly conducting matrix.

The thermal degradation of conducting copolymer films of PANI and nylon 66 with various dopants exposed to air outside an electrochemical cell, resulting in serious losses of electrical conductivity, was studied by Byun and Im [537]. With increased temperature, thermally enhanced degradation of chemically prepared PANI resulted in a blue shift of the UV-vis absorption band observed at long wavelengths [538, 539]. It was assumed that a decrease in chain length was the cause of this shift. Considering the arguments presented in the preceding text, this implies a decrease in conjugation length. Tsubaki et al. [540] observed a decrease in electric conductivity with temperature that qualitatively agrees with this observation. With UV-vis spectroscopy, it was found that thermal dedoping proceeded without major structural changes. It is noteworthy that, according to Anand et al. [541], poly(4,4'-methylenedianiline) is thermally more stable in the base than in the salt form.

4. POLYPYRROLE AND RELATED POLYMERS

The formation of a polymer film obtained by electrochemical oxidation of pyrrole was first reported by Diaz and Kanazawa [542, 543]. At least initially, electrooxidation of various substituted pyrroles surprisingly resulted in no polymers. A relationship between the oxidation potential and the dipole moment of the pyrroles was found [544]. Nevertheless, redox active films were obtained from *N*-methylpyrrole and *N*-phenylpyrrole [545]. Figure 58 shows the molecular formula of most pyrroles discussed in the following section. An early review of PPy was provided by Street [546].

In addition to the applications of ICPs already mentioned (for a general review of PPy and its applications, see [547]), PPy has been suggested as a matrix for a variety of sensor applications [548, 549, 560–563]. (A special application where a sensor responds to the respective monomer was described by Vinokurov [564].) In a related concept, the size selectivity (“ion sieving”) of PPy membranes is utilized [565]. The influence of the electropolymerization conditions on the size-exclusion selectivity of various ICPs, includ-

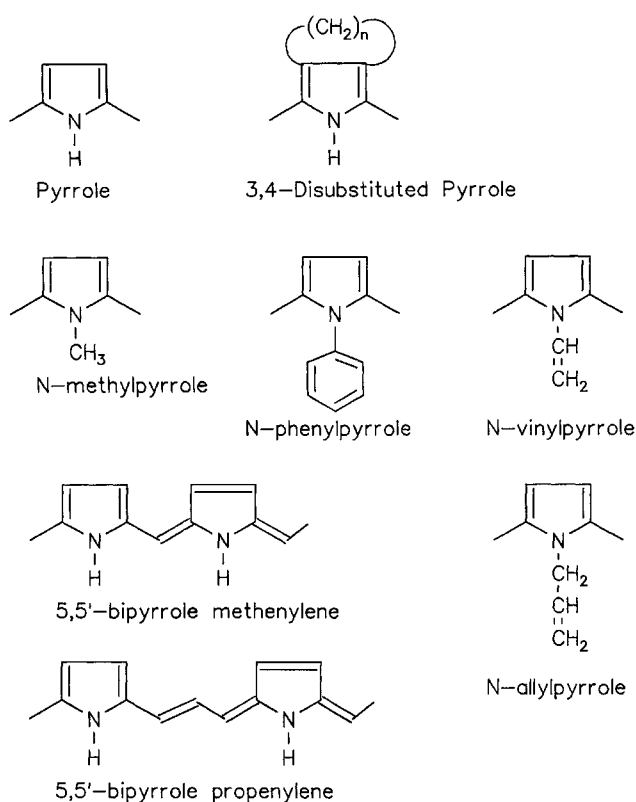


Fig. 58. Structural formulas of pyrrole and substituted pyrroles investigated in the work reviewed in this report.

ing PPy, PANI, and polyphenol, was investigated by Wang et al. [566].

Polypyrrole films have been employed as carriers of catalytically active materials like finely dispersed metal particles [567], whose own catalytic properties in various electrochemical reactions have been studied [568]. These systems sometimes were investigated using spectroelectrochemical techniques. Mostly, measurements were aimed at elucidating catalytic aspects of the embedded catalyst. These reports are beyond the scope of this review.

Similar to the uses suggested for PANI and PT, PPy has been suggested as a conceivable component of electronic equipment including capacitors [569–575], batteries [576–581], and field effect transistors (FET) in combination with polythiophene as a further active component [582], and electrooptic devices [including light emitting diodes (LED)] [583–588]. Coatings of nonnoble metals like steel with corrosion protection properties [589, 590] and of photoelectrochemical devices [591] have been described. PPy as a precoat in the manufacturing of printed circuit boards is now a well established procedure [592, 593]. PPy has been evaluated as an active material in actors [594–598].

Diaz et al. [599] studied the electrooxidation of various aromatic monomers and oligomers, including pyrrole and its oligomers, to identify relationships between the number of repeat units in the substrate molecule and the oxidation potential as well as the UV–vis absorption maximum of the oxidation product (soluble as well as deposited on the electrode). As can be expected based on theoretical calculations already mentioned, the oxidation potential shifts to less positive values with an increasing number of pyrrole units in the educt, whereas the absorption maximum shifts considerably to longer wavelengths.

In a comparative study of various ICPs, Bakhshi et al. predicted, based on theoretical considerations, that PPy is a strong candidate for p-doping. Further properties like the value of the bandgap were found to be in good agreement with experimental results. Attempts from a theoretical point of view to design modified PPy [poly(5,5'-bipyrrole methylene)] with a small bandgap have been reported [600, 601]. Initial experimental data were provided by Pagani et al. [602]. Brocks et al. [603] reported a theoretical study based on the Car–Parrinello *ab initio* molecular dynamics scheme, which very efficiently combines electronic structure calculations with complete geometry optimizations. Equilibrium geometries have been calculated for polypyrrole, polythiophene, polyisothianaphthene, polyparaphenylene, and polyaniline. The obtained bandgaps, calculated with the local density functional, correspond closely with the experimentally observed trend of optical bandgaps.

4.1. Formation of Polypyrrole and Related Polymers

PPy can be synthesized from both aqueous and nonaqueous electrolyte solutions. The influence of the composition of the electropolymerization solution on the properties of the deposited PPy film has been studied with respect to a variety of material properties [604–608].

The kinetics and mechanism of electrochemical PPy formation from aqueous electrolyte solutions have been studied using a quartz crystal microbalance [609]. A dependency on the concentration of pyrrole and perchlorate anions was found. A fairly complicated interfacial reaction mechanism was proposed that takes into account all observed experimental peculiarities. Chung et al. [610] studied the initial stage of growth of PPy with EQMB. The observed influence of the electrolyte cation used was explained by invoking electrostatic interactions between the cations and the radical cations formed during the polymerization reaction. Based on purely electrochemical evidence, Scharifker et al. [611] identified the electrooxidation of pyrrole or its oligomers as the rate-determining step. Rodriguez et al. [612] pointed out the possible involvement of tin species incorporated in the transparent ITO–glass electrode in the electropolymerization of pyrrole.

Genies et al. [613] measured the UV–vis absorption during the oxidation and polymerization of pyrrole as a function of time. The radical coupling step was found to be rate determining. The initial stage of PPy film formation resembles nucleation during metal deposition.

Fermín and Scharifker [614] identified pyrrole oligomers with up to nine pyrrole units during PPy formation with *in situ* UV–vis spectroscopy. The observed influence of solution stirring implied nucleation of PPy deposits by precipitation of oligomeric species. Kim et al. [615] found a high stationary concentration of trimeric and tetrameric species under similar conditions. Raymond and Harrison [616] derived the existence of pyrrole radical species based on results obtained with a rotating ring-disk electrode. In a subsequent study, bipyrrole was identified as an intermediate based on *in situ* UV–vis spectroscopic evidence [617]. With ellipsometry, Hamnett et al. [618, 619] identified three distinctly different stages of PPy growth in nitrate-containing aqueous polymerization solutions in close correlation to previous results of chronocoulometric experiments. In the first step, nucleation occurs, followed by attachment of oligomers to nucleation sites. In the third step, nucleation on top of the already formed PPy film occurs. Kim et al. [620] obtained real-time ellipsometric

data during the potentiostatic deposition of PPy from an aqueous solution containing nitrate anions. An electronic absorption at 3.8 eV ($\lambda = 326$ nm) was assigned to the interband transition. Further absorptions at 1.65 and 2.3 eV ($\lambda = 750$ and 538 nm) were attributed to valence band to defect (bipolaron) transitions. The relative doping level during dedoping was derivable from the real-time measurements. Further analysis of the data revealed a discontinuous structure of the film with a thickness below 15 nm, at about which thickness coalescence occurs. Thicker films show a linear increase of thickness with time and an increasing density of the film. Further theoretical considerations that serve as a basis for the interpretation of ellipsometric data were reported by Stroud and Kazaryan [621].

Abrantes and Correia [622] employed the probe beam deflection technique to investigate the early stages of growth of poly(3-methylthiophene) and PPy. Their results support the assumption (in contrast to the bulk of the reports published so far) that oligomer formation is not determinant for PPy deposition, quite in contrast to the formation of the thiophene-based polymer.

Bacsikai et al. [623] reported an ECSR investigation of the growth of one- and two-dimensional PPy. Measurements were performed at different deposition current densities, resulting in different paramagnetic properties of the PPy film. The observed spin densities do not correlate directly with the consumed oxidation charge. The larger linewidth of PPy deposited at higher current densities is explained by suggesting stronger spin-spin interactions that are compatible with a two-dimensional polymer.

Yurtsever and Yurtsever [624, 625] attempted accurate *ab initio* calculation for pyrrole oligomers bonded through α and β carbons. Assuming a Monte Carlo growth scheme to predict branching as a function of temperature and chain length, it was found that a high degree of branching dominates in PPy.

The influence of the dopant anion on film properties was studied by Kriván and Visy [626]. With sodium dodecylsulfate, an increase of redox capacity and a higher doping level were observed. Results obtained with UV-vis spectroscopy and their interpretation indicate that structural changes that result in a decreased hydrophobicity may be a possible cause.

Using the valence effective Hamiltonian (VEH), Brédas et al. [627] calculated optical as well as electrochemical properties of pyrrole and PPy. Their data agree nicely with reported experimental results.

Lei et al. [628] pointed out the inherent reactivity of PPy with air, which results in difficulties in obtaining spectra of pristine PPy [628]. Using a specially designed spectroelectrochemical setup, spectra of both pristine and doped PPy were obtained. Some additional low wave number bands not reported elsewhere were observed. In the absence of any assignment, they are not included in the data reported herein.

Hlavaty et al. [629] electrooxidized *N*-vinylpyrrole and *N*-allylpyrrole. The former monomer yields only an electroinactive film, because of the products formed via competitive polymerization that involves the vinyl group. The latter monomer yields an electroactive polymer with properties similar to PPy according to *in situ* infrared spectra.

4.2. Properties of Polypyrrole and Related Polymers and their Electrochemically Induced Changes

The influence of the deposition (i.e., electropolymerization) conditions on the properties of the PPy film has been studied in de-

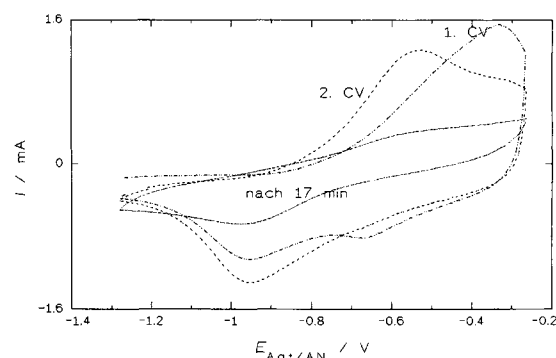


Fig. 59. CVs of PPy deposited galvanostatically at $i = 0.5$ mA onto a platinum sheet from a solution of 0.1-M pyrrole in acetonitrile + 0.1-M LiClO₄ + 0.5% water. The first and second cycles and the cycle measured after 17 min of electrode potential cycling are displayed.

tail before: results have been reported in [273, 630–632]. The first report also contains a critical evaluation of spectroelectrochemical data that pertain to avoid redundancy, in particular, to vibrational and UV-vis spectroscopy. Consequently, the following section contains those contribution from the published literature that are considered to be the most important.

A typical cyclic voltammogram of a film of PPy deposited from a solution of 0.1-M pyrrole in acetonitrile containing 0.1-M LiClO₄ and 0.5% water is shown in Figure 59 as a function of time with respect to cycle number. Bose et al. [633] pointed out the inadequacy of simple chronocoulmetric or voltammetric procedures to determine the doping level of thick (greater than a few hundred nanometers) PPy films, in particular. The separation of Faradaic processes and double-layer charging of PPy-film-coated electrodes as well as electrodes coated with composites of PPy and polystyrenesulfonate was achieved by color impedance spectroscopy (electromodulated optical response, similar to ERS) [634–637]. The propagation of the interface between the conductive zone of PPy and the nonconductive zone assumed to be present during PPy oxidation was demonstrated using addressable microband array electrodes [638]. With a diode array detector, Tezuka et al. [639] measured concentration profiles of conducting species in PPy, in particular during the first potential scan. The difference between the first and the second scan (“first cycle effect”) was related to the occurrence of a moving boundary in the first scan and a uniform interconversion of the nonconducting into the conducting form in the following scans. The significant difference between the first and subsequent electrode potential cycles of PPy was investigated with electrochemical methods, NIR spectroscopy and scanning electron microscopy, by Li [640]. In the NIR spectrum, bands at $\lambda = 520$ and 1700 nm appeared. Upon reduction, the former peak disappeared, and a new peak appeared at $\lambda = 400$ nm; the latter peak shifts to $\lambda = 1100$ nm. After reoxidation, the peak initially observed at $\lambda = 520$ nm did not reappear; only the band around $\lambda = 400$ nm changed in intensity as a function of electrode potential. Consequently, the band at $\lambda = 520$ nm was assigned to a protonated structure of PPy, which did not reappear during the reoxidation.

During the doping and dedoping process, ions have to move in and/or out of the polymer film because of the need for charge compensation. The transport behavior of the anions may be controlled by their own properties (charge, charge density, size, etc.), but also by the film properties. Qiu and Reynolds [641], who used the

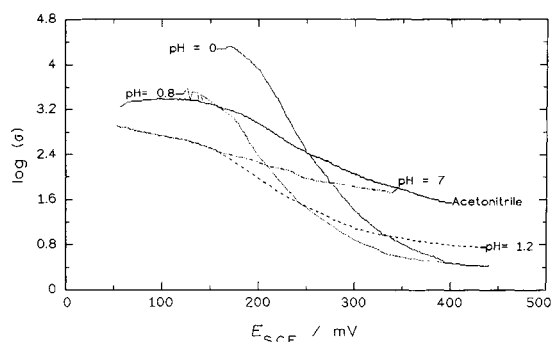


Fig. 60. Dependence of PPy film resistance as a function of electrode potential and electrolyte solution composition (pH = 0, 0.5-M H_2SO_4 ; pH = 0.8, 0.1-M NaHSO_4 ; pH = 1.2, 0.05-M NaHSO_4 ; pH = 7, 0.1-M Na_2SO_4 ; acetonitrile, acetonitrile + 0.1-M LiClO_4 + 1% water). The PPy ups deposited galvanostatically from a solution of 0.1-M pyrrole in acetonitrile + 0.1-M LiClO_4 + 1% water.

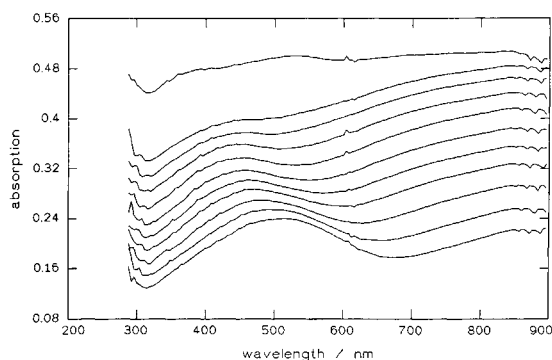


Fig. 61. *In situ* UV-vis spectrum of PPy in a solution of 0.1-M HClO_4 deposited onto an ITO glass electrode, electropolymerized galvanostatically at $i = 0.7$ mA from a solution of 0.1-M pyrrole in acetonitrile that contained 0.5% water and 0.1-M LiClO_4 as a function of electrode potential starting with $E_{\text{Ag}/\text{AgCl}} = -200$ mV at the bottom to $E_{\text{Ag}/\text{AgCl}} = 1000$ mV at the top. For further details, see [273].

electrochemical quartz crystal microbalance, showed that properly selected dopant anions, in turn, can influence the cation transport properties of the PPy film. Using the same method, Schmidt and Heitbaum [642] studied the redox switching of PPy and poly-*N*-methylpyrrole in tosylate-containing electrolyte solutions. During reduction of PPy, cations and water move into the polymer. During oxidation of poly-*N*-methylpyrrole, tosylate and hydroxide ions move into the film. The different transport behavior of both polymers is rationalized by taking into account suggested polymer structures. A first application of the EQMB in investigations of redox cycling of PPy was reported by Kaufman et al. [643], who observed that during reduction, charge compensation is maintained by lithium ion insertion into the film instead of the expected egress of anions. Xie et al. [644] studied the influence of solution pH on the electrochemical properties of PPy with the EQMB. At pH values larger than 3–4, both anions and cations are involved in the ionic movements that accompany charge compensation during redox cycling. At lower pH values, anion movement prevailed. By comparison with the behavior of poly(*N*-methylpyrrole), protonation and deprotonation of the nitrogen atom in PPy was found to be of major importance. Deprotonated PPy allows transient incorporation of hydrated cations during reduction, followed by slow ejection of incorporated cations when electrolytes like KCl or NaClO_4 are used; with NH_4Cl , this behavior was not observed.

The change of the electronic resistance of PPy as a function of electrode potential in solutions of various compositions is shown in Figure 60. Because of the selected electrode potential limits, only a reversible increase/decrease was found; no evidence of overoxidation was observed [73]. With a polymer transistor manufactured with a film of PPy as the active material, Ofer et al. [645] found a limited electrode potential window wherein PPy has a high electronic conductivity.

With ellipsometry applied *in situ* during both deposition and doping–dedoping, Kim et al. [646] indicated a reversible expansion and contraction during the latter process. A similar behavior was observed by Higgins and Hamnett [647]; preliminary results had been reported elsewhere [618]. The optical constants of the PPy films depended critically on the polymerization conditions. An increase of the water content in the polymerization solution resulted in very low values of n ($1.25 < n < 1.3$) as measured at $\lambda = 633$ nm. In a further study with both ellipsometry and infrared spectroscopy, Christensen and Hamnett [619] found that both po-

larons and bipolarons are created with well defined, narrow conjugation lengths. The latter was nine monomer units shorter for bipolarons as compared to polarons. During PPy oxidation, expulsion of solvated protons was found together with a reduction of film thickness. Giacomini et al. [648] studied the influence of electrode potential and electrolyte on PPy films deposited onto platinum electrodes. Results indicate the absence of polarons at highly positive electrode potentials. Film properties and oxidation mechanism change with more acidic electrolyte solution. In all cases, an increase of thickness (in contrast to previous reports already cited) and hydration is observed upon oxidation. Pei and Inganäs [649–651] observed swelling and shrinking of PPy using a bending beam method, wherein the bending of a PPy–polyethylene bilayer is used as an electrode. The extent of both processes is much smaller as reported based on results of the other methods. Lee et al. [652] used ellipsometry during both deposition and redox cycling of PPy. Results obtained during the latter process indicate that redox conversion of the polymer proceeds from the solution toward the supporting electrode controlled by counterion movement. The ion exchange properties of PPy and a copolymer poly[pyrrole-*co*-(4-(pyrrole-1-yl)-butane sulfonate)] were studied by Lopez et al. [653] using the optical beam deflection technique. At electrode potentials positive to the redox potential, PPy exchanges anions with the solution: at potentials below this value, cations are involved. When the copolymer contains negatively charged groups attached to the pyrrole units, exactly the inverse behavior was observed.

UV-vis spectra recorded *in situ* with PPy films deposited from various aqueous as well as nonaqueous electrolyte solutions are displayed in Figures 61–64 to allow detection of conceivable influences of the mode of deposition and of the electrolyte solution composition (pH, concentration, type of anion or cation) on the obtained polymer and its electrooptical properties. The spectra were recorded in solution that was not entirely deaerated [273]. Consequently, the influence of dioxygen dissolved in the electrolyte solution has to be taken into account. Son and Rajeshwar [654] reported an isosbestic point at $\lambda = 480$ nm for the bands at $\lambda = 400$ and 800 nm when using dioxygen-saturated electrolyte solutions of 0.1 M, which was absent in the case of nitrogen-saturated solutions. Instead, an additional band was found at $\lambda = 540$ nm. Because the UV-vis spectra displayed here also show this band, the dioxygen content of the electrolyte solutions used seems

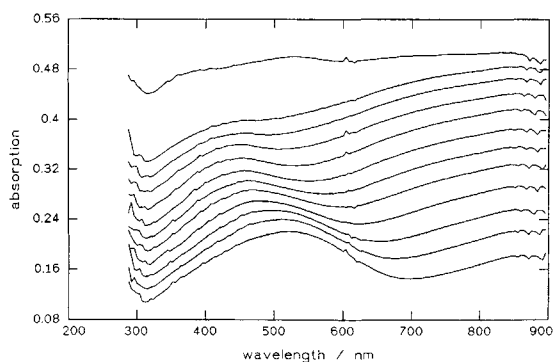


Fig. 62. *In situ* UV-vis spectrum of PPy in a solution of 0.1-M HClO_4 deposited onto an ITO glass electrode, electropolymerized potentiostatically at $E_{\text{Ag}/\text{AgCl}} = 500$ mV from a solution of 0.1-M pyrrole in acetonitrile that contained 0.5% water and 0.1-M LiClO_4 as a function of electrode potential starting with $E_{\text{Ag}/\text{AgCl}} = -200$ mV at the bottom to $E_{\text{Ag}/\text{AgCl}} = 1000$ mV at the top. For further details, see [273].

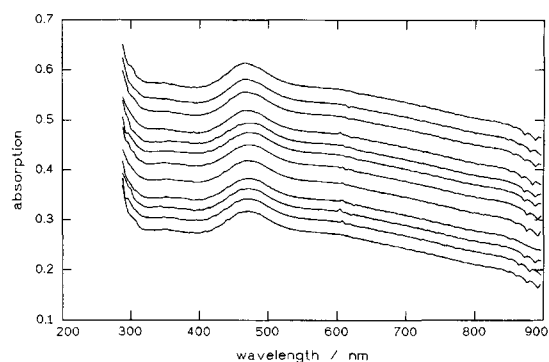


Fig. 63. *In situ* UV-vis spectrum of PPy in a solution of 0.1-M HClO_4 deposited onto an ITO glass electrode, electropolymerized potentiostatically at $E_{\text{SSCE}} = 600$ mV from a solution of 0.1-M pyrrole in an aqueous solution of 1-M acetic acid as a function of electrode potential starting with $E_{\text{Ag}/\text{AgCl}} = -200$ mV at the bottom to $E_{\text{Ag}/\text{AgCl}} = 1000$ mV at the top. For further details, see [273].

to be very low. Independently of the electropolymerization procedure (for details see [273] and the figure captions), bands at $\lambda = 400$ and 540 nm and a NIR absorption with a maximum beyond the accessible range ($\lambda = 900$ nm) were observed. The band at shorter wavelengths were assigned to the $\pi \rightarrow \pi^*$ transition. The band at $\lambda = 540$ nm was attributed by Son and Rajeshwar [655] to a transition from the lower binding polaron state (or band) to the upper antibinding polaron state (or band). Hourch et al. [656] assigned the absorption to an electronic transition from the valence band into the antibinding bipolaron state (or band). The latter authors observed, in addition, bands at $\lambda = 610$ and 710 nm, which have been assigned to the transition between the binding and the antibinding polaron state. Kim et al. [657] found a band at $\lambda = 470$ nm, which they assigned to the transition from the valence band into the antibinding bipolaron band, and a band beyond $\lambda = 600$ nm, which was attributed to the transition from the valence band into the bipolaron band. The band at long wavelengths has been assigned elsewhere to transitions between extended conjugated sections of the polymer [658]. This is in agreement with the reasoning presented by Brandl [273] for PANI (for details, see preceding section) and PPy. This assignment is supported by results of investigations with oligopyrroles reported by van Haare et al. [659], which provided evidence for the formation of π dimers as evidenced by UV-vis spectroscopy. This, in turn, also explains the lack of an ECESR signal at elevated electrode potentials. Deconvolution of *in situ* UV-vis spectra of PPy films recorded during oxidation in solutions that contain various halide anions resulted in four optical absorption bands at $\lambda = 320$, 425 , 542 , and 842 nm [660]. The first and second bands dominate the spectrum of neutral PPy. The second band decreases in intensity upon oxidation. The third and fourth bands appear upon oxidation, where the third band passes through a maximum as a function of electrode potential. Consequently, the third band was assigned to polaronic species and the fourth band to bipolaronic species. With respect to the spectra displayed in Figures 61–64, no significant influence of the mode of deposition (potentiostatic versus galvanostatic) could be identified [273]. Even with an almost neutral solution of 1-M KCl, an electroactive polymer with only slightly different spectral features was obtained. Only deposition from an acetic acid solution resulted in a considerably different polymer. Obviously, no change in the spectrum occurs when the electrode

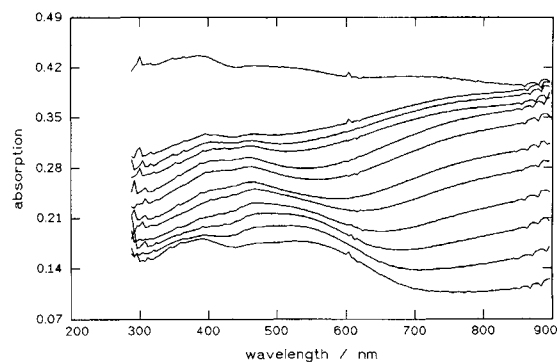


Fig. 64. *In situ* UV-vis spectrum of PPy in a solution of 0.1-M HClO_4 deposited onto an ITO glass electrode, electropolymerized potentiostatically at $E_{\text{SSCE}} = 600$ mV from a solution of 0.1-M pyrrole in an aqueous solution of 1-M KCl as a function of electrode potential starting with $E_{\text{Ag}/\text{AgCl}} = -200$ mV at the bottom to $E_{\text{Ag}/\text{AgCl}} = 1000$ mV at the top. For further details, see [273].

potential is changed. This corresponds to a lack of electrochemical activity. The spectra of the film show features that are typical of the fully oxidized form and the film is slightly conductive [273]. The spectra provided support for the tentative determination of the effective length of conjugation based on a comparison with absorption energies of π dimers of oligopyrrole [661]. The value of the effective length of conjugation was 7.1.

With a combination of quartz microbalance and UV-vis spectroscopy, Kim et al. showed that electrochemically induced mass transport in PPy affects both rheology and electrochromic properties of the polymer film [662].

Skaarup et al. [663] reported on the doping of PPy with LiClO_4 in nonaqueous electrolyte solutions. Highly conjugated, pure sample did not show optical absorptions below 2.5 eV ($\lambda = 495$ nm) in the reduced state and a low energy of 2.88 eV ($\lambda = 430$ nm) for the $\pi \rightarrow \pi^*$ transition. Bipolarons were claimed to be the predominant species in the oxidized form of PPy, with polarons playing only a minor role in systems of lower conjugation length. The conflicting statements in the literature were assigned mainly to differences in polymer preparation and pretreatment.

Zotti and Schiavon [664] determined the concentration of polarons and bipolarons based on *in situ* UV-vis spectroscopic data.

Table XXIII. Assignment of Infrared Bands Observed with PPy in Various States of Oxidation

1-M HClO ₄ [273]		Ref. [676]		Ref. [677]		Ref. [342]	
Red.	Oxid.	Red.	Assignm.	State	Assignm.	State	Assignm.
1225	1242	—	—	—	—	—	—
1276	1277	1280	δ_{C-Hip}	1283	Oligom.	1287	δ_{C-H}
1301	1300	—	—	1316	ν_{C-C}	—	—
1361	1363	1386	Ring breath.	—	—	—	—
1405	1408	—	—	1410	Oligom.	1391	ν_{C-C}
1435	1428	—	—	—	—	1422	ν_{C-C}
—	1445	—	—	1443	Oligom.	—	—
1462	1464	1480	Ring breath.	—	—	1470	$\nu_{C=C}$
1480	—	—	—	1482	Oligom.	—	—
1507	1509	—	—	—	—	—	—
1530	1529	—	—	1524	ν_{N-C}	—	—
1572	1557	1546	$\nu_{C=C}$	1545	$\nu_{C=C}$	1546	$\nu_{C=C}$
1608	1607	—	—	1610	Oligom.	—	—
—	1652	—	—	—	—	—	—
—	1721 ^a	—	—	—	—	—	—
—	1769	—	—	—	—	—	—
—	2340	—	—	—	—	—	—

^aPresumably caused by a carbonyl moiety of a degradation product.

Results were found to be comparable with those of ECESR measurements. Josowicz et al. [665] reported considerable changes of the electronic work function of PPy after incorporation of nitrotoluene as measured with UV-vis spectroscopy.

Genies et al. [666] studied the switching reaction of PPy with chronoabsorptometric UV-vis measurements. An effect of solution composition was found. Ion diffusion in the film was faster during the reduction than during the oxidation. This may be related to the fact that the former process occurs in a fairly good conducting material where the reaction may take place in the whole film. In a subsequent study with the same method, Genies and Pernaut found a Nernstian relationship between the relative state of oxidation and electrode potential for poly(*N*-methylpyrrole). This provides access to formal redox potentials. The change of optical absorption as a function of time was used to calculate the apparent diffusion coefficient for species that limit the rate of conversion.

Tezuka et al. [667] used UV-vis spectroscopy combined with cyclic voltammetry to detect Faradaic and capacitive components during redox processes of PPy films. Results fit a propagation theory for the conversion of the polymer. Curves of band intensity versus electrode potential are sigmoidal, implying the intermediate state of some bands and the species that cause them. It was concluded that the kinetics involve slow conversion of the initially formed radical cation into a dication.

From *ex situ* spectra of PPy-perchlorate, Yakushi et al. concluded that PPy is not a metallike system with Drudelike free carriers. Instead, the mechanism of electronic conduction is hopping between segments of variable conjugation length.

More recently, Otero and Bengoechea [668] reinvestigated *in situ* UV-vis spectra of PPy to complete previous electrochemical measurements [669]. They attributed the considerable shift of the absorption band in the range of $\lambda = 550\text{--}900$ nm to conforma-

tional changes, while still keeping the assignment of the bands found in this range to transitions that involve polaronic and bipolaronic states. So far, this assignment has not been confirmed or supported by further evidence.

A theoretical foundation for the interpretation of vibrational spectra of PPy was provided by Faulques et al. [670, 671]. Their results are taken into consideration in the subsequent interpretation of Raman and infrared spectra, and relevant data are incorporated in the tables herein. The effective conjugation coordinate already introduced and discussed in connection with the interpretation of vibrational spectra of PANI was applied to PPy too [672]. A different approach was employed by Kostic et al. [673]. Based on a single-periodic-chain model and harmonic potential, in-plane and out-of-plane parameters transferred from pyrrole. In addition, infrared absorption intensities were calculated. Results of a comparison with experimental spectra indicate a nonplanar conformation of PPy. In the case of comparison with experimental Raman spectra, electron-phonon coupling was not observed. Kofranek et al. [674] reported the results of a theoretical *ab initio* study of vibrational spectra of pyrrole, oligopyrroles, and PPy based on double zeta quality basis sets. For the monomer, satisfactory agreement between calculated and experimentally observed band positions is concluded. Inspection of data listed in Table XXIII reveals close correspondence between the assignments for PPy as reported by various authors and the assignments and band positions stated by Kofranek et al.

Infrared spectra of PPy measured *in situ* and *ex situ* have been reported by various authors [342, 675–689]. A set of typical infrared spectra measured in the external reflection mode as a function of electrode potential is displayed in Figure 65; the fingerprint region is enlarged in Figure 66. The assignments of the observed bands are collected with data from other reports in Ta-

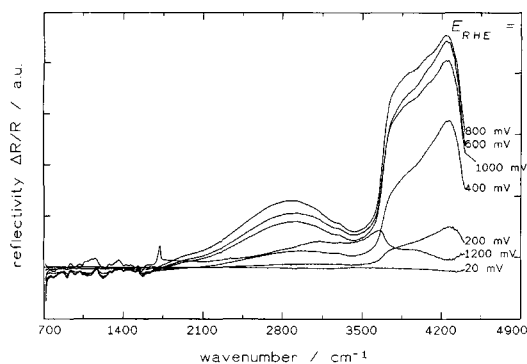


Fig. 65. *In situ* infrared spectrum (PDIRS) of PPy in a solution of 1-M HClO₄ deposited onto an ITO glass electrode, electropolymerized galvanostatically at $i = 2$ mA from a solution 0.1-M pyrrole in acetonitrile that contained 0.5% water and 0.1-M LiClO₄ as a function of electrode potential (see inset); resolution 4 cm⁻¹. For further details, see [273].

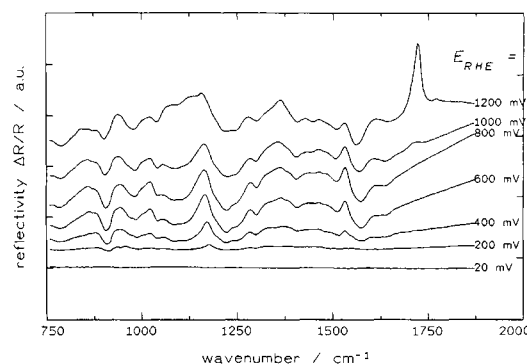


Fig. 66. *In situ* infrared spectrum (PDIRS) of PPy in a solution of 1-M HClO₄ deposited onto an ITO glass electrode, electropolymerized galvanostatically at $i = 2$ mA from a solution 0.1-M pyrrole in acetonitrile that contained 0.5% water and 0.1-M LiClO₄ as a function of electrode potential (see inset); fingerprint region, resolution 4 cm⁻¹. For further details, see [273].

ble XXXIII. Stimulated by inconsistencies between the generally assumed molecular structure of PPy and the determined elemental composition, Lei and Martin [690] proposed that PPy is actually poly(pyrrole-*co*-hydroxypyrrole) based on infrared spectra. Kato et al. [691] combined *in situ* infrared spectroscopy in the external reflection method with *ex situ* measurements at PPy/KBr pellets. Results imply a higher ordering in electropolymerized PPy. Rangamani et al. [642] reported on ATR infrared spectroscopy of PPy deposited onto a silicon rod used as internal reflectance element. Excellent spectra that show electrode potential-induced changes were obtained when both anions and cations were involved in the redox processes. Zhong and Doblhofer demonstrated that an exchange of the anion (e.g., Cl⁻ and ClO₄⁻) does not affect the infrared spectrum except for the appearance of the symmetrical stretching mode of the latter oxoanion.

Rodriguez et al. [693] reported infrared data obtained with the subtractively normalized interfacial Fourier transform infrared spectroscopy (SNIFTIRS) method for PPy films exposed to aqueous solutions containing various anions. In the range between 1000 and 1700 cm⁻¹, reversible changes in the range of electrode potentials below the onset of overoxidation were found. They are consistent with the polaron-bipolaron model. During overoxidation, hydroxyl and carbonyl groups attached to the polymer backbone

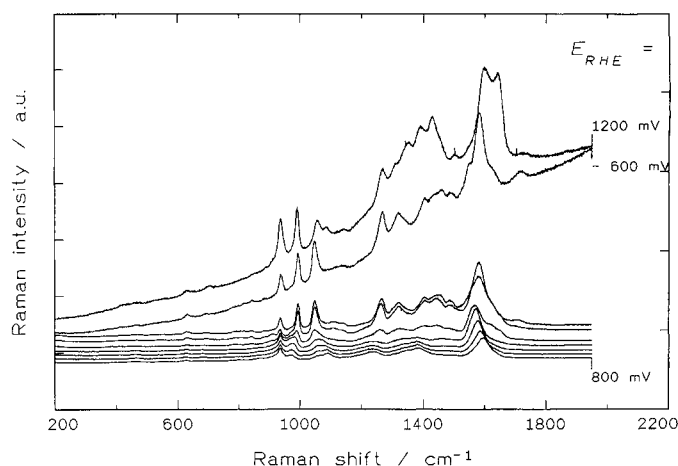


Fig. 67. *In situ* Raman spectrum of PPy in a solution of 1-M HClO₄ deposited onto an ITO glass electrode, electropolymerized galvanostatically at $i = 50$ mA from a solution 0.1-M pyrrole in acetonitrile that contained 0.5% water and 0.1-M LiClO₄ as a function of electrode potential (see inset); resolution 2 cm⁻¹. For further details, see [273].

were found. The influence of the electrolyte anion was weak, implying a small interaction between dopant anion and oxidized polymer matrix. With fluoride anions chemical modifications occur, because in this solution hydroxyl ions presumably act as dopants instead of fluoride anions.

A set of resonantly enhanced Raman spectra of PPy in an aqueous solution of 1-M HClO₄ is shown in Figure 67. Raman spectra measured both *ex situ* as well as *in situ* have been reported frequently [694–703]. Pertinent results and conclusions are incorporated in Table XXIV. The effective conjugation coordinate suggested by Tian and Zerbi [342] also was applied to the interpretation of Raman spectra, and their results are incorporated in the table. Low frequency Raman modes of PPy caused by fractal vibrational modes were reported and discussed by Jin et al. [704]. With laser excitation at $\lambda_0 = 514.5$ nm, bands at 65, 77, and 116 cm⁻¹ were observed; they were explained in terms of a fractal description of localized vibrations.

The π delocalization in oligopyrroles (including protected, i.e., end standing, substituted oligothiophenes) and polypyrroles was studied with *ex situ* off-resonance Raman spectroscopy by Zerbi et al. [705]. The frequency dispersion of the line near 1580 cm⁻¹ was found to be indicative of chain length. Bands of substituents were generally absent in the Raman spectra (contrary to infrared spectra extremely rich in bands). In a subsequent study with conformationally distorted oligo- and polypyrroles, basically the same results were obtained [706].

A typical ECSR spectrum of a PPy sample in a nonaqueous solution is displayed in Figure 68. The significantly asymmetric line was described as Dysonian-like [73]. The spin density as a function of electrode potential in solutions of widely varied composition is shown in Figure 69. A considerable shift of the maximum toward positive electrode potentials with decreasing pH value is noteworthy [73].

Zotti [707] reported *in situ* measurements of conductivity, doping level, and spin concentration of PPy. The observed relationship indicates a threshold value, followed by a linear increase that ends in a plateau value of conductivity as a function of doping level. Both polarons and bipolarons are assumed to be involved in the conduction process, provided the anions do not pin the mobile

Table XXIV. Assignment of Raman Bands Observed with PPy in Various States of Oxidation

1-M HClO ₄ [273] ^a		Furukawa et al. [694]		Assignm.	Calculated [342]
Red.	Oxid.	Red.	Oxid.		
467	464	—	—	—	—
632	627	634	—	β_{1g}	—
—	686	—	—	—	—
937	936	934	—	—	—
—	972	—	979	Polaron mode, δ_{ring}	—
994	—	989	—	δ_{ring}	1000
—	1060	—	1057	Polaron	1051
—	1092	—	1080	Bipolaron	—
—	1237	—	—	—	—
1268	—	1246	—	—	—
1319	—	1316	—	ν_{CC}	1307
—	1350	—	1335	Polaron	—
—	1383	—	—	—	—
1403	—	—	—	—	—
1459	—	—	1443	Polaron	1452
1489	—	1502	—	ν_{NC}	—
1581	—	—	1564	ν_{CC}	1569
—	1595	—	1581	Polaron	—

^aFor the sake of simplicity, some bands observed at even more positive electrode potentials are omitted.

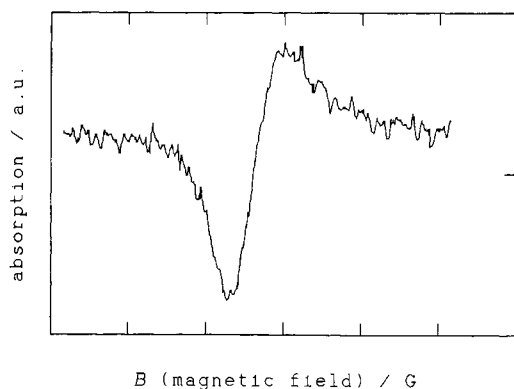


Fig. 68. *In situ* ECSR spectrum of PPy in an aqueous solution of 1-M HClO₄. The PPy was deposited galvanostatically from a solution of 0.1-M pyrrole in acetonitrile + 0.1-M LiClO₄ + 1% water [73].

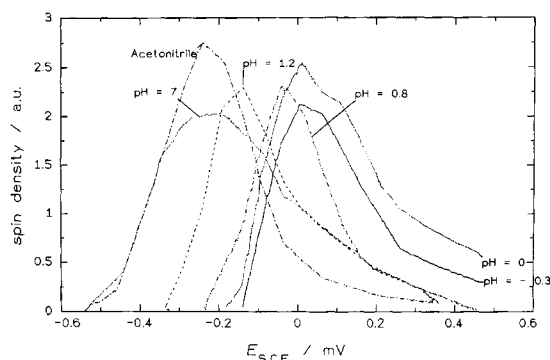


Fig. 69. Spin density of PPy in various electrolyte solutions (pH = -0.3, 1-M H₂SO₄; pH = 0, 0.5-M H₂SO₄; pH = 0.8, 0.1-M NaHSO₄; pH = 1.2, 0.05-M NaHSO₄; pH = 7, 0.1-M Na₂SO₄; acetonitrile + 0.1-M LiClO₄ + 1% water). The PPy was deposited galvanostatically from a solution of 0.1-M pyrrole in acetonitrile + 0.1-M LiClO₄ + 1% water [73].

charges. ESR data again confirmed polarons as stable intermediates. Although CVs of PPy generally show only a single current peak, actually two subsequent processes separated only by about 70 mV of peak potential difference occur. Basically similar results, in particular, concerning the participation of polarons and bipolarons in the conduction process, were reported previously by Zotti and Schiavon [708].

Zhong et al. [709] studied the redox processes of PPy with *in situ* ECSR in combination with Raman spectroscopy. The formation of polarons as well as their interconversion into bipolarons as a function of electrode potential were observed. Both species seem to be involved in the electric conduction. Simultaneous changes in the Raman spectra, in particular, a shift of the band around 1600 cm⁻¹, were observed. This band is commonly assigned to

the C=C stretching mode. Its position shifts from 1568 cm⁻¹ at $E_{SCE} = -0.6$ V to 1623 cm⁻¹ at $E_{SCE} = 0.4$ V. This observation can be explained by assuming an increase of the double bond character of the interring C_α-C_{α'} and intraring C_β-C_α bonds, in agreement with corresponding theoretical considerations. Results reported by Waller and Compton [710] are in partial agreement. Data obtained with ECSR and *in situ* conductivity measurements (using the ac impedance technique) showed a correlation between conductivity and spin concentration at low doping levels. At higher doping levels, this correlation disappears, suggesting the participation of bipolarons in the conduction process. At elevated doping levels, this is in agreement with data previously reported [73] and

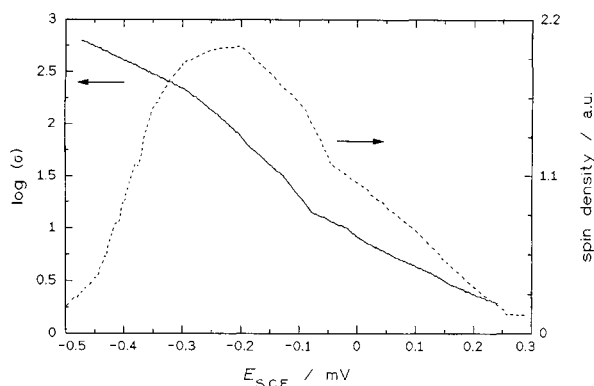


Fig. 70. Correlation of film resistance and spin density for PPy in an aqueous solution of 0.1-M Na_2SO_4 . The PPy was deposited galvanostatically from a solution of 0.1-M pyrrole in acetonitrile + 0.1-M LiClO_4 + 1% water [73].

displayed in Figure 70. Indeed, at higher doping levels (beyond the maximum spin concentration), a strong decrease of film resistance is found together with a decrease of polaron concentration. This resulted in an earlier conclusion that polarons are of only minor importance in the conduction process. The absorption shoulder around $\lambda = 540$ nm observed by Lippe [73] shows a dependence on electrode potential similar to the conductivity. This was only tentatively (because of the inherent difficulties in evaluating an absorption shoulder) taken as an indicator to assign the absorbing species to the charge-carrying species. The subsequent assignment of the electronic absorption at $\lambda = 540$ nm to the transition between the lower and the upper polaron band is only, at first glance, in contrast to the ECESR data, because the disappearance of the ECESR signal implies the absence of polarons, especially at elevated electrode potentials. Based on the reasoning suggested by Brandl [273] for both PANI and PPy, this absorption corresponds to a transition that indeed involves polarons of varying effective conjugation length, whereas the absence of the ECESR signal may be explained reasonably by invoking quenching processes between the free radicals in the polymer. In an *ex situ* investigation of PPy with UV-vis and ESR spectroscopy, Pfluger et al. found supporting evidence of changes in results of both spectroscopies at higher degrees of doping where no further change of conductivity occurs.

Nechtschein et al. [711] reported a similar study with *in situ* measurements of PPy with UV-vis and ESR spectroscopy. Results imply that the energy for creating a bipolaron is the same as the energy needed to create two polarons. These results support earlier theoretical considerations based on *ab initio* studies reported by Brédas et al. [712, 713]. The interconversion of polarons into spinless species (bipolarons) was observed with *in situ* UV-vis and ESR spectroscopy by Kaufman et al. [714]. In an earlier study by Genoud et al. [715], based on ESR data obtained *in situ*, a quasiequilibrium between polarons and bipolarons was concluded; at low doping levels, bipolaron formation is energetically unfavorable as compared with polaron existence.

Singh and Narula [716] investigated *ex situ* correlations between the concentration of free spins and the dc conductivity as a function of temperature for electropolymerized PPy and some substituted PPy's. The obtained parameters support a variable range hopping mechanism of conduction. An almost symmetrical line with Lorentzian shape was observed.

ESR spectra¹¹ of PPy electropolymerized at different current densities were studied with ESR spectroscopy and conductivity measurements by Chaibi et al. [717]. Results show a higher conductivity for samples prepared at higher conductivity: these samples showed no ordering in the ESR spectra. A positive contribution of amorphicity to the conductivity was concluded.

Exclusively with respect to electrode potential and charge transfer Amemiya et al. [718] studied UV-vis spectra of PPy as a function of electrode potential by considering the polaron-bipolaron model and the "monomer unit model." Results favor the latter model.

Oudard et al. [719, 720] recorded ECESR spectra of PPy in a molten salt electrolyte liquid at room temperature. The ESR signal was observed only in a very narrow range of electrode potentials that closely correlate with the electrochemical oxidation current: the line shape was not Dysonian, contrary to the observation reported previously. Evaluation of kinetic data implies slow formation of radical cations (polarons) and fast disappearance, most likely by recombination into spinless dications.

In a more general investigation of PANI, PT, and PPy (for the other polymers, see the preceding and the following sections), Devreux et al. [436] studied the correlation between injected electric charge per ring and the number of spins per ring. Their results are displayed in Figure 71. The general shape of the trace corresponds to plots already shown that display the relationship between the electrode potential and the spin concentration. Devreux et al. concluded from a thermodynamic consideration of the results that with PPy and PdT, polarons and bipolarons are almost degenerate and, consequently, in a thermodynamic equilibrium, whereas for PANI, polaron pairing is hindered by potential barriers that disable the establishment of a thermodynamic equilibrium. Zotti [707] reinvestigated the relationships between electrode potential, injected charge, and *in situ* measured electrical conductivity. As a function of injected charge, with all investigated polypyrroles, three different types of relationships were observed. Up to a certain threshold value (at low charge levels), a slow increase of conductivity was followed by a linear increase that ended in a plateau value. The threshold value cannot be explained by percolation, because only homogeneous polymers were investigated and no evidence of electrochemically induced heterogeneity (formation of conducting islands in an insulating matrix) was found. Instead, charge pinning of both polarons and bipolarons by some (not all) anions was concluded.

Rühe et al. [721] electropolymerized various pyrroles substituted in the 3,4-position with a fused alkyl ring. Using four-probe *ex situ* conductivity measurements as a function of temperature, a decrease in conductivity with an increase in substituent size was found. The temperature dependence implied a variable range hopping conduction mechanism.

Extensive *ex situ* investigations of PPy films with various electron spectroscopies that provide details of the electronic structure were reported by Schmeisser and Göpel [722]. In a related study with the same methods, Schmeisser et al. [723] observed that a two-dimensional structure of PPy can be obtained by applying higher deposition current densities.

Theoretical calculations using the VEH by Brédas et al. [724] resulted in predicted oxidation and reduction potentials for vari-

¹¹The angular dependence of the ESR line width was measured while the sample was rotating in the magnetic field. A correlation between line width and ordering exists.

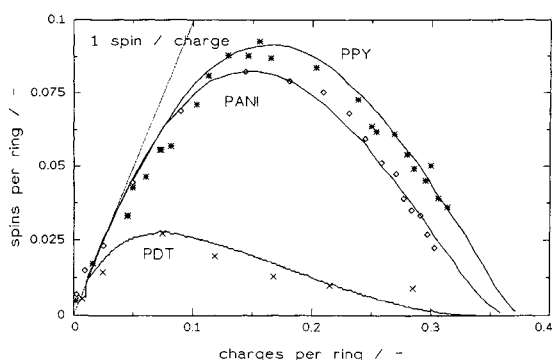


Fig. 71. Spin concentration expressed as spin per ring as a function of charge injected (expressed as charge per ring) for PdT, PANI, and PPy taken from ECESR *in situ* measurements. Data from Devreux et al. [436].

ous intrinsically conducting polymers. With polypyrrole, an oxidation potential of $E_{\text{NHE}} = -0.6$ V was calculated, which compares favorably with the experimental value of $E_{\text{NHE}} = -0.4$ V [725]. Korol [726] reported theoretical considerations of the electronic conductivity of ICPs including PPy. He suggested that an optimum chain length of about 1.5–3 nm exists, which should result in maximum conductivity.

Clarke et al. [727] applied magic angle spinning NMR spectroscopy *ex situ* in a preliminary (and so far not extended) investigation of PPy and some related substituted PPy. Results confirm the linear structure of PPy with α, α' links. Similar results were reported by Street et al. [728].

Copolymers of pyrrole and 2,2'-bithiophene were prepared by electropolymerization using mixed monomer-containing nonaqueous electrolyte solutions by Peters and van Dyke [729]. CVs of the polymer film showed three oxidation peaks. Two could be matched with the corresponding oxidation peaks of the homopolymers; the third (in between) may be caused by a random copolymer. Based on supporting evidence obtained from *in situ* UV-vis spectra, three distinct redox couples could be identified. Two were assigned to short blocks of PPy and poly(2,2'-bithiophene); the third was assigned to the mentioned copolymer. Electric conductivity was lower like for pure PPy.

Elliott et al. [730] studied a composite of PPy and polystyrenesulfonate with various spectroelectrochemical techniques. The films were found to be considerably different from pure PPy. The conductivity is only slightly lower as compared to PPy. The CV is very symmetrical. Otero and Bengoechea [731] measured UV-vis spectra of the same composite and of a PPy-carboxymethyl cellulose composite with particular regard to the switching stability. Polaronic as well as bipolaronic transitions were red shifted because of a stronger interaction between the composite constituents attributed to the more flexible backbone of carboxymethyl cellulose. Polystyrene sulfonate is more rigid and accelerates processes that involve the bipolarons.

A composite of PPy with polytungstate anions was prepared via electropolymerization by Ohtsuka et al. [732]. The PPy sample prepared for comparison showed the usual transition from the reduced to the oxidized state via the polaronic and bipolaronic state as evidenced by UV-vis and Raman spectroscopy. The copolymer does not reach the neutral form even at very low electrode potentials.

Bilayers of PPy with PANI on top or PANI with PPy on top were investigated with confocal Raman microscopy *ex situ* by Sacak

et al. [733]. Depending on deposition conditions, the second polymer is incorporated into the first one or deposited on top in a clearly separated bilayer system. Bi- and multilayer systems of PANI, PPy, and poly(3-methylthiophene) prepared by chemical oxidation were studied with a variety of experimental methods by Nicolau et al. [734]. Results indicate generally lower structural disorder, better crystallinity, a homogeneous space filling, and a closer relationship between degree of polymerization and conjugation length.

Novák et al. [735] identified CO_2 as the oxidation product of propylene carbonate formed at a PPy electrode with infrared spectroscopy [735]. In another study, these authors used *in situ* infrared spectroscopy and differential electrochemical mass spectrometry (DEMS) to observe the simultaneous oxidation of PPy and the solvent propylene carbonate, resulting in its incorporation into the polymer film [736].

4.3. Degradation of Polypyrrole and Related Polymers

Park et al. [737] used various spectroscopic *in situ* and *ex situ* techniques to study the electrochemical degradation of PPy by anodic overoxidation. Results indicate the formation of a soluble mixture of maleimide and succinimide, which implies a reaction mechanism wherein the quinoid bipolaronic form is attacked first by water molecules. A higher rate of formation of these degradation products with increasing electrode potential, sulfuric acid concentration, and thinner films was found [738]. The pH-dependent onset of overoxidation was studied by Lewis et al. [739]. At lower pH values, the corrosion proceeds significantly slower. The rate and mechanism of corrosion of PPy in aqueous solutions was investigated by Beck et al. [740] with electrochemical methods. A two-step mechanism that comprises electrochemical overoxidation followed by a chemical nucleophilic attack at the cationic centers in the polymer was found. Raman spectroscopy was found by Ghosh et al. [741] to be more sensitive for the detection of overoxidation products of PPy as compared to infrared spectroscopy. An increase of the rate of overoxidation (i.e., of polymer degradation) with increasing pH value and electrode potential was observed.

Novák et al. [742] reported inconclusive evidence of overoxidation processes of PPy in various nonaqueous electrolyte systems as obtained with *in situ* infrared spectroscopy. Most likely, OH^- and HCO_3^- ions are the species involved in the nucleophilic attack of the polymer.

Christensen and Hamnett [743] studied overoxidation of PPy with both ellipsometry and infrared spectroscopy. Pyrrolinones with short conjugation lengths and CO_2 were found. Xie et al. [744] investigated the transition of PPy from its electroactive into its inactive state during immersion into alkaline solution by *in situ* infrared spectroscopy. A nucleophilic attack by hydroxyl ions followed by opening of some pentacyclic rings and a significant decrease in electrical conductivity were observed. The corresponding rate constant for the chemical reaction was determined as $5.8 \times 10^{-4} \text{ s}^{-1}$.

The chemical attack of solution phase species generated at both electrodes and by chemical reactions between solution phase species on PPy were studied with various spectroelectrochemical techniques by Chen and Rajeshwar [745].

5. POLYTHIOPHENE AND RELATED POLYMERS

Thiophene and its relatives, including dimeric, trimeric, and even higher oligothiophenes, can be oxidized electrochemically with subsequent formation of a polymer in nonaqueous solutions only. This is basically caused by the fact that electrooxidation of thiophene requires fairly positive electrode potentials. At these potentials, rapid degeneration of the polymer by nucleophilic attack occurs.¹² Taking water and its constituents as a typical example, the passivating action of even small amounts of water in the polymerization solution was shown [746]. Only more recently did Bazaoui et al. [747, 748] show that PT can be prepared successfully from moderately concentrated aqueous perchloric acid solutions on platinum and ITO electrodes. The selected electrolyte solution increases thiophene solubility and decreases the electrode potential necessary for thiophene oxidation from about $E_{SCE} = 1.6$ to about 0.9 V. The properties of the film are reported to be very similar to those of films prepared from nonaqueous solutions. Attempts to modify the polymerization condition further to diminish the required oxidation electrode potential, for example, by substitution of the thiophene ring, the use of oligothiophenes [749], or the use of metal oxide electrodes (CuO) [750], have been reported elsewhere.

An overview of representative thiophenes investigated so far and reviewed here is provided in Figure 72. In particular, because of the considerable environmental stability of some polythiophenes [751, 752] as compared, for example, the stability of PANI, various possible applications have been considered or even been transformed into commercial products [753–758]. Their gas sensitivity, which suggests their use in sensors, was discussed by Hanawa et al. [759]. Beyond this straightforward application, various other uses of PT and PT derivatives in sensing applications have been reported [760–772]. An anion effect termed *ion sieving*, wherein films of poly(3-methylthiophene) show different permeabilities for different anions, was reported by Zhang and Dong [773]. The use of PTs in supercapacitors has been suggested [774–783]. Glenis et al. [784] reported the use of PT and poly(3-methylthiophene) in organic photovoltaic cells (see also [785, 786]). A battery based on PT was described by Kaneto et al. [787]. Further aspects of this possible application have been studied elsewhere [788, 789]. Thermochromism of poly(3-alkylthiophenes) was reviewed by Inganäs et al. [790]; for a general overview, see [791]. Thermochromism as well as the influence of pressure were studied with poly(3-alkylthiophenes) by Iwasaki et al. [792], who explained the observed effects by invoking conformational changes. The wettability of poly(2,2'-bithienyl-5,5'-diyl) films as a function of degree of doping was studied by Kossmehl and Niemitz [793]. The considerable chemical stability and the rich possibility to tune molecular properties was the stimulus for extended investigations with respect to the use of polythiophenes in electrooptical, electroluminescent, and electrochromic devices [794–804], photoswitches [805], and, especially, in LEDs [806–816], lasers [817–822], and macromolecular electronic systems (diodes, transistors, etc.) [823–834]. Suitable substitution that results in a diminished aromaticity was shown to result in a diminished bandgap as needed [835–837]. The influence of alkyl substitution on the value of the bandgap was studied by Chen and Rieke [838]. Similar effects—changes in the size of the bandgap and the value of the oxidation potential as derived from

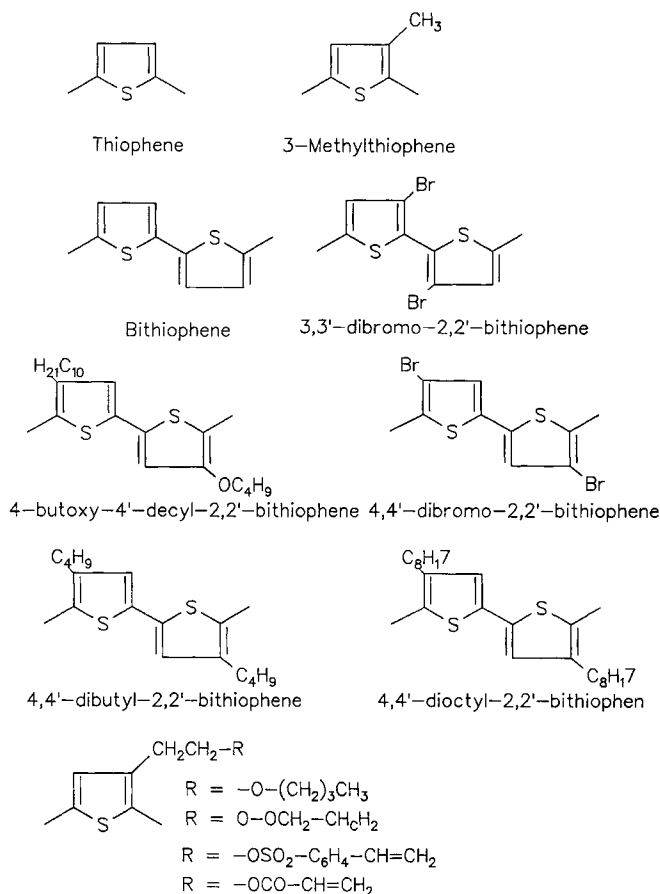


Fig. 72. Structural formulas of thiophene and substituted or otherwise related relatives.

electrochemical measurements—were observed by cyano substitution of oligothiophenes [839]. By making blends with other materials, the array of materials properties that can be tuned is further enlarged. Photodiodes based on a PT-buckminsterfullerene composite material have been described [840–842].

Sulfur–oxygen interactions have been proposed as a possible cause for the considerable stability of polyalkoxythiophenes, based on *ex situ* investigations of a large selection of substituted thiophenes and their polymers [843]. The amplification of chemical and electrical signals has been applied in a microelectrochemical transistor based on poly(3-methylthiophene) [844].

The limited processability of the parent compound polythiophene has stimulated research of substituted polythiophenes as suggested by Faid et al. [845, 846] and others [847–853]. Inclusion of various alkyl and alkoxy substituents as depicted in Figure 72 results in increased solubility, preferably in organic solvents. In addition, substitution results, in most cases, in less positive electrode potentials needed for the electropolymerization. This is a general advantage, because less positive electropolymerization potentials result in diminished damage of the polymer caused by overoxidation of the polymer and the corresponding damage mostly by nucleophilic attack of the polymer [854]. The observation that at very low concentrations of thiophene, no electroactive polymer is formed [855], has also been attributed to overoxidation during polymerization. It has even been suggested that PT is actually a mixture of polymerization and overoxidation products [856]. Results of comparative *in situ* conductivity measurements with poly-

¹²This problem is sometimes designated the polythiophene paradox.

mers of thiophene, bithiophene, and terthiophene have also been explained based on this suggestion [857]. With respect to possible applications of PT in secondary batteries in early investigations, a lower stability during charge–discharge cycling as observed with PPy was reported [858]. Instead of using monomers that already carry the desired substituents, treatment of the polymer is a conceivable method. Nitration, chlorination, and sulfochlorination of PT have been reported [859] without any further information pertaining to molecular properties beyond the molecular structure.

The electropolymerization of thiophene on nonnoble metals like iron, aluminum, and zinc has been studied by Aeyach et al. [860]. With aluminum, excellent adherence of the PT film was found and attributed to the formation of covalent bonds; in all other cases, adherence was not very good. The molecular structure was similar to the structure observed with films deposited on noble metals; in particular, a α - α' coupling was observed with infrared spectroscopy. Generally, the deposition of high-quality films of PT on many metals (including, surprisingly, gold, but also titanium) was found to be impossible because the required electrode potentials exceeded values at which the metal of the supporting electrode is already oxidized [861]. Gratzl et al. [861] found, that high-quality films can be deposited on an interlayer of polypyrrole. They found a cause of the “polythiophene paradox” in the competition between film formation and overoxidation, with the latter being kinetically more hindered. The term “polythiophene paradox” refers to the fact that PT is not stable at electrode potentials where it is formed; consequently, the polymer must be a mixture of real PT and overoxidation products [862]. Zhou et al. [863] could not deposit PT on stainless steel, presumably because of competitive steel corrosion.

Polymer blends and composites of polythiophenes with other nonconducting polymers, which are outside the scope of this review, have been studied elsewhere [864–866]. The formation of copolymeric gels (usually considered to be an inconvenience in polymer formation) has been studied with 3-*n*-octylthiophene, and various substituted benzenes were reported by Pépin-Donat et al. [867].

An interesting bridge between charge transfer salts and conducting polymers was suggested by Miller et al. [868]. They investigated a substituted terthiophene cation radical that forms π stacks, which show electric conductivity without being a true polymer.

General reviews on PT and related derivatives have been provided elsewhere [869–871].

5.1. Formation of Polythiophene and Related Polymers

Diaz et al. [599] have studied the electrooxidation of various aromatic monomers and oligomers including thiophene and its oligomers to identify relationships between the number of repeat units in the substrate molecule and the oxidation potential as well as the UV–vis absorption maximum of the oxidation product (soluble as well as deposited on the electrode). As can be expected based on theoretical calculations already mentioned, the oxidation potential shifts to less positive values with an increasing number of thiophene units in the educt, whereas the absorption maximum shifts considerably to longer wavelengths.

Adsorption studies of thiophene on any of the electrode materials used most often are scant. Although data were obtained under *ex situ* conditions, the conclusion that thiophene is adsorbed flat on the surface of Ag(111) reported by Baumgärtner et al. [872] seems noteworthy because the assumed strong silver–sulfur interaction

suggests otherwise. Bukowska and Jackowska [873] studied the adsorption of thiophene on smooth and electrochemically roughened silver electrodes from aqueous solutions. With the smooth silver electrode, spectra resembling those of liquid thiophene were recorded. No conclusions regarding molecular orientation or any particular adsorbate–interface interaction were drawn. Because the low wave number region was not reported, no conclusion with respect to a specific silver–sulfur interaction is possible. With a roughened electrode, oligomers were found even without applying an electrode potential approaching values considered necessary for electropolymerization to occur. As a possible explanation, photochemically induced decomposition and subsequent chemical oxidation of thiophene by the formed decomposition products were suggested. Fujita et al. [874] provided a study of the adsorption of thiophene on a roughened gold electrode from aqueous solution. Results indicate the formation of thiophene oligomers at electrode potentials $0 < E_{\text{SCE}} < 0.6$ V and of polymers at $0.8 < E_{\text{SCE}} < 1.0$ V. The latter value is considerably lower than electrode potentials taken from cyclic voltammograms recorded during electropolymerization. No evidence was found that corresponded to the photochemical polymerization of thiophene as reported by Bukowska and Jackowska (see preceding text).

Olbrich-Stock et al. [875] obtained UV–vis spectra *in situ* during electrooxidation of thiophene in an acetonitrile-based electrolyte solution using a platinum metal electrode in the transmission mode with light passing through the mesh as well as a long-path cell with a platinum foil electrode with the light beam passing closely in parallel to the platinum electrode. Depending on the electrode, potential absorption bands at $\lambda = 290, 390, 579, 670, 830,$ and 990 nm were observed. Based on a collection of literature data, the bands were assigned tentatively to neutral, cationic, and dicationic forms of thiophene and its oligomers with up to six repeat units. Hillman and Mallen [876] reported a study of PT deposition using *in situ* UV–vis spectroscopy. Within the range of $350 < \lambda < 820$ nm, spectral features were initially observed that indicate the formation of oligomers. Upon further polymerization, a shift to longer wavelengths was found. Finally, typical features of the metallic (doped, i.e., conducting) state were observed.

Hoier and Park [877] studied the electropolymerization of 3-methylthiophene using *in situ* UV–vis spectroscopy as a function of polymerization electrode potential and polymerization time. Results implied that polymerization takes place only when monomer oxidation occurs; this, in turn, seems to suggest a radical–radical coupling reaction as the main pathway. During the polymerization a significant constant concentration of oligomeric intermediates was maintained. In the finally deduced rate equation, the concentration of both monomer and oligomers appear to indicate the participation of the latter in the polymerization reaction. No autocatalytic growth (as observed, e.g., during formation of PANI) was found.

During electropolymerization of PT, infrared spectra in the external reflection mode (SNIFTIRS) were recorded by Rasch et al. [878]. In the fairly poor spectra, bands were assigned to consumption of the solvent and formation of solvent oxidation products. An ingress of perchlorate anions needed for charge compensation in the polymer being formed in its oxidized state was deduced from the occurrence of a band around 1099 cm^{-1} . A barely visible broad absorption feature starting around 1500 cm^{-1} was called the electronic absorption band of the polymer. A similar investigation was reported by Christensen et al. [879]. Spontaneous adsorption of thiophene on the polished platinum electrode resulted only in a

single band assigned to the in-plane ν_{15} mode. This implies a perpendicular orientation. Within the spectral range accessible with the employed equipment, no sulfur-surface mode was observed; consequently, a more specific description of the surface-adsorbate interaction is not possible. After shifting the electrode potential to values where oxidation occurs, massive changes in the differential spectra were seen. They indicated formation of a polymeric product. A broad absorption starting at about 1500 cm^{-1} , indicative of the presence of free charge carrier, was seen together with spectral changes assigned to the formation of quinoid systems and a downshift of the frequency of the ring deformation modes. Differences between "good" (compact) and "bad" (porous) films were found. With the latter films, a considerable amount of the solvent acetonitrile seemed to be present inside the film.

Chao et al. [880] studied electrodeposition of poly(3-methylthiophene) with *in situ* ellipsometry to identify correlations between deposition conditions (parameter employed during both potentiostatic and galvanostatic deposition). No conclusive results were reported. Modulated ellipsometry was employed in a study of deposition of poly(3-methylthiophene) by Tian et al. [881]. Optical constants of the film as a function of time (i.e., of polymer deposited) were reported. Hamnett and Hillman [882] used ellipsometry to study various aspects of PT film formation. Immediately after switching on the positive polymerization potential, formation of solution phase species is observed. In agreement with current-time data, the start of the formation of deposits a short time later was found. Contrary to previous analysis of purely electrochemical data that implied three-dimensional growth, ellipsometric data indicate a somewhat more complicated situation. During film formation at different electrode potentials, different film thicknesses are required to obtain ellipsometric data typical of bulk PT. A particular difference was found between films deposited at electrode potentials below and above $E_{SCE} = 2.0\text{ V}$. The presence of excess water in the polymerization solution again results in a film with significantly different optical properties. Abrantes and Correia [883] employed the probe beam deflection technique to investigate the early stages of growth of poly(3-methylthiophene). Results support the assumption of the initial formation of oligomers preceding their deposition. The more significant role of oligomers in the process as compared the formation of PPy is stressed.

Lukkari et al. [884] studied the electropolymerization of 3-methylthiophene on various substrates with cyclic voltammetry and photocurrent spectroscopy. Results of galvanostatic transient measurements, in particular, imply that polymerization on native ITO-coated glass electrodes starts with the deposition of long oligomeric chains. With surfaces that interact more strongly with the monomer (e.g., platinum or silylated ITO glass), short chains are deposited; the initial step may actually be a reaction that involves surface-bound species. The photocurrent spectra correspond closely to the respective UV-vis absorption spectra. Based on the former data, the lack of a controlled structure of the polymer at the molecular level with varying conjugation lengths is concluded. In a study of electropolymerization of 3-methylthiophene on bare and chemically modified ITO electrodes with STM, Lukkari et al. [885] found that deposition starts with the formation of oligomer islands, whereas bundles of polymer fibers and macroscopic polymer centers appear only later. On the chemically modified surface (treatment with SiCl_4 and bithiophene [886, 887]), a higher rate of nucleation that results in a more ordered growth was seen.

A change from a polymerization process that occurs in the solution phase toward a process that occurs on the surface in the case of weakly adsorbing electrodes like ITO-glass has been concluded from a variety of experimental details obtained by Visy et al. [888] with spectroelectrochemical and surface analytical tools during electropolymerization of thiophene.

Based exclusively on electrochemical evidence as obtained with cyclic voltammetry on substituted thiophene monomers (β , β -disubstituted oligothiophenes), Smie et al. [889] concluded that initial radical formation is followed by rapid dimerization. Only 4,4'-disubstituted monomers are converted into films. The polymerization reaction is suggested to be a sequence of dimerization reactions that involve oligomers with correspondingly increased chain length. This is in agreement with the observation that the electrode potential needed for the oxidation of monomers within a homologous series decreases with increasing chain length. Accordingly, oligomers with longer chain length carry on the polymerization process preferably.

In a study of the metal-polymer interaction at the platinum-poly(3-methylthiophene) interface with near edge X-ray absorption fine structure spectroscopy (NEXAFS) reported by Tourillon et al. [890], the structure of the polymer as well as of the interphase was investigated. The polymer was found to be composed of repeat units identical with the monomer. The appearance of the metallike behavior upon doping was explained by a narrowing of the bandgap. The polymer chains were found to be highly ordered with respect to the metal surface. In the reduced state, strong interactions between the antibonding π^* states of the polymer and the electronic states of the metal were concluded. Upon oxidation, the ordered state of the polymer chains closest to the surface remains unchanged, whereas the more outward lying chains become randomly oriented because of the intercalation of the counterions needed for charge comparison. The extent of the effect as far as visible in the recorded spectra depends on the thickness of the film. With long alkyl substituents, the flat orientation changes toward perpendicular.

The adsorption and subsequent electrochemical coupling of carboxyl-terminated dithiophene and terthiophene molecules at ITO electrodes was studied by Berlin et al. [891]. Two classes of molecules were investigated. In one class, the carboxyalkyl chain was attached sideways to the oligothiophene system; in the other class, the oligothiophene unit was attached at the end of the carboxyalkyl chain. Adsorption of the monomers on the ITO electrode proceeded with both types of molecules. In the nonaqueous electrolyte solution, the adsorbate layers were oxidized. With side-on substituted oligothiophene, electrochemically induced coupling occurred within the adsorbate layer, whereas with the end-on substituted oligothiophenes, coupling was possible only with solution phase molecules. Evaluation of electrochemical data and of UV-vis spectra recorded *in situ* revealed that the films were composed of thiophene hexamers. The adsorbed linear terthiophene seemed to couple with a terthiophene from solution to form an on-end surface-anchored sexithiophene monolayer. In the case of the side-on substituted molecule with no alkyl chain between the thiophene moiety and the carboxyl group, no polymerization or coupling was found. With the alkyl chain in between, coupling between the adsorbed molecules was possible. Further details of the relative orientation of the monomers and oligomers were derived from the UV-vis spectra obtained *in situ*.

ESR spectra of a variety of electrooxidation products of thiophene oligomers, including orthogonally bridged dimers of

α , α -coupled thiophene oligomers and spirofused phenylene-thiophene mixed oligomers, as a function of temperature were reported by Diers et al. [892]. Results imply that the charge remains on the one electron oxidation products and does not hop between two bridged oligomers. The energy for the movement of a paramagnetic center along the oligomer chain was estimated at less than 100 cm^{-1} .

The kinetic of the polymerization of various monomers was investigated with cyclic voltammetry by Tschuncky and Heinze [893]. In the case of alkoxy-substituted monomers, an increase in the rate of polymerization with the size of the substituent was observed. With a variety of terthiophenes, carrying either electron-drawing or electron-pushing substituents, the kinetics and the mechanism of electropolymerization was investigated by Pagels et al. [894]. Radical-radical coupling was concluded. In the case of vinyl-substituted terthiophenes, no involvement of the latter substituent was identified. The kinetics of electrochemical PT formation in nonaqueous electrolyte solutions has been studied using EQMB [895]. A dependency on the concentration of thiophene and perchlorate anions was found. A fairly complicated interfacial reaction mechanism was proposed that takes into account all observed experimental peculiarities.

Kilic et al. [896] performed a complete theoretical study of the electronic structure of thiophene, some of its oligomers, and some of its substituted derivatives. Conclusions with respect to preferred binding sites for coupling during polymerization, planarity, and so forth were reported.

A theoretical treatment of the initial step of electropolymerization (i.e., the electrooxidation reaction) of pyrrole, thiophene, and furan in acetonitrile with molecular orbital methods has resulted in predictions of the oxidation potential: $E_{\text{NHE, pyrrol}} = 0.79 \text{ V}$; $E_{\text{NHE, furan}} = 1.27 \text{ V}$; $E_{\text{NHE, thiophene}} = 1.53 \text{ V}$ [897]. The subsequent step is a coupling reaction of the initially formed radical cations. Whereas the coupling itself is rate-determining for pyrrole and furan, with thiophene, an elimination process with a relatively large activation energy is rate-determining. These results and conclusions are in agreement with the previously cited experimentally observed facts and the often encountered difficulties preparing uniform and thick polythiophene films as compared to polypyrrole films.

Yurtsever and Yurtsever [898] attempted accurate *ab initio* calculation for thiophene oligomers bonded through α and β -carbons. Assuming a Monte Carlo growth scheme to predict branching as a function of temperature and chain length, it was found that linear chains dominate in PT.

Jones et al. [899] combined experimental electrochemical (CV) data, ionization, and attachment energies of thiophene oligomers ($n \leq 5$) with theoretical data (ionization and attachment energies calculated with MINDO/3). Extrapolation to larger values of n provided accurate values as found by *ex situ* (gas phase) PT.

Emphasis on understanding the electrochemical behavior of thiophene (as well as pyrrole) and their substituted relatives is reflected in the observations reported by van Haare et al. [900, 901]. In a study of phenyl end-capped α -oligoheteroaromatic molecules, they found two reversible oxidation waves for molecules with more than two pyrrole units and a decreasing oxidation potential with a growing number of pyrrole units. Monomers with an increasing number of thiophene units end-capped with phenylpyrrolyl units showed an increase of the first and a decrease of the second oxidation wave. The bandgap of both types of molecules showed the expected decrease with increasing conjugation length of the longer

molecules. A theoretical Hückel-type model indicates that with the latter molecules, positive charges tend to localize on the pyrrole units, thus favoring the second oxidation wave.

A cathodic electropolymerization of polythiophene on substrates of gallium arsenide and indium phosphide was reported by Xu et al. [902]. The process involves coupling dihalogenated thiophene monomers with the help of a Ni^{2+} phosphine complex. The complex is transformed by electroreduction of Ni^{2+} , resulting in the corresponding Ni^0 complex and a thiophene coupling product. Strictly speaking, no reduction of the monomer itself is involved. The PT film shows spectral properties in the reduced state that are similar to those of PT prepared by oxidative electropolymerization.

In highly concentrated solutions of phosphoric acid, oligomerization of thiophene has been observed [903]. Starting with an oligomer-containing solution, Dong and Zhang [904] electropolymerized PT. The resulting polymer shows electrical conductivities lower by 2 orders of magnitude compared to PT prepared from nonaqueous solutions. UV-vis spectra of the reduced polymer showed a broad band around $\lambda = 465 \text{ nm}$ assigned to the $\pi \rightarrow \pi^*$ transition. The absorption around $\lambda = 760 \text{ nm}$, found with the polymer in its oxidized form, was related tentatively to a transition involving a bipolaron state.

5.2. Properties of Polythiophene and Related Polymers and their Electrochemically Induced Changes

Because of the electrode potential applied during electrodeposition, the polymer films are always present in the oxidized, doped form. Consequently, the "memory effect" already discussed in detail in the section on PANI has been observed with PT also. Lapkowski et al. [905, 906] investigated this effect with poly(4,4'-dialkyl-2,2'-bithiophenes) and poly(3-alkylthiophenes). Based exclusively on electrochemical measurements, they concluded that the magnitude of the effect is associated with the difficulty of dedoping the oxidized polymer. The frequently observed asymmetry in the CV was investigated by Xu and Horowitz [907] by studying CVs of thiophene oligomers with four, five, and six thiophene units. The polymers obtained behaved like PT. The asymmetry was interpreted based on a polaron-bipolaron model, also taking into account the considerably different electronic conductivity of the polymers in their reduced and oxidized state. From the model it was concluded that the standard oxidation potential of the polymer is given by the reduction peak potential. Extrapolation to infinite chain length resulted in a value of $E_{\text{SCE}} = 0.48 \text{ V}$.

The slow increase of conductivity at open circuit measured directly after with a pristine film of poly(3-methylthiophene) prompted conductivity studies by Visy and Kankare [908] of the non-Faradaic processes in this polymer. Under all investigated circumstances, a slow increase of conductivity was observed after switching off the electrode potential control. Tentatively, charge redistribution within the polymer or a chemical reorganization resulting in an increased conductivity were invoked. In a related study, Visy et al. [909] investigated Faradaic and capacitance processes of a film of poly(3-methylthiophene). In the range of very positive electrode potentials that are accessible because a nitrobenzene-based electrolyte solution was used, a capacitive region was identified wherein no Faradaic processes occurred.

In Figure 73, a typical cyclic voltammogram of a film of poly(3-methylthiophene) deposited from a solution of 3-methylthiophene

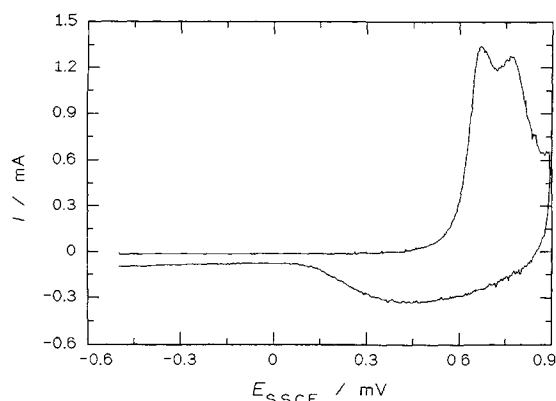


Fig. 73. CV of poly(3-methylthiophene) on a platinum electrode in an aqueous solution of 0.1-M NaClO_4 , $dE/dt = 20 \text{ mV s}^{-1}$, deposited from a solution of 0.3-M 3-methylthiophene in acetonitrile + 0.1-M Et_4NClO_4 .

in acetonitrile is shown. The film was obtained under carefully controlled experimental conditions, which indeed demonstrate the feasibility of preparing films in different laboratories that show—at least in the operant electrochemical methods of characterization—almost identical properties [910]. The asymmetry between the oxidation and the reduction processes already evident from this CV was studied with *in situ* ellipsometry by Chao and Costa [911]. With a polymer film prepared electrochemically from 3-methylthiophene on a platinum electrode, they concluded that oxidation is a homogeneous reaction that proceeds simultaneously in the complete film. Reduction starts at the polymer-solution interface and propagates through the layer. In addition to the asymmetry in terms of different shapes and fairly different peak potentials of characteristic features in the CV, poorly resolved redox peaks are sometimes encountered. As discussed by Faïd and Leclerc [912], this may be caused by the fact that a low degree of localization and consequent stabilization of the intermediately formed polaron result in poorly resolved polaron-bipolaron features. Because it has been suggested that asymmetrically substituted polymers may cause increased localization, Chao and Costa studied poly(4-bromo-4'-(octyloxy)-2,2'-bithiophene). In addition to electrochemical measurements, UV-vis spectra were recorded *in situ*. Absorption bands of the polymer in its slightly oxidized form were found at $\lambda = 750$ and 1350 nm.¹³ With an increase in electrode potential, the latter band stays slightly blue shifted and a new band at $\lambda = 615$ nm appears. Upon complete polymer oxidation, a very broad band around $\lambda = 1000$ nm shows up. Chao and Costa assigned the set of peaks observed first to polaronic species. The band at $\lambda = 615$ nm was assigned to radical cation dimers, whereas the band that finally dominated the spectrum was attributed to bipolaronic species. Surprisingly, the concentration of the dimers seems to be independent of the ratio of polarons-bipolarons, which were found to show a potential-dependent relationship. On the contrary, the concentration of the dimers remains almost constant after reaching a plateau at about 0.2 charges injected per thiophene unit.

¹³Unfortunately, there seems to be a contradiction between the displayed spectra and the quoted numbers. In the spectrum at low electrode potentials, a band appears at $\lambda = 550$ nm a fairly broad absorption appears around $\lambda = 1600$ nm. This is also in agreement with the results obtained with chemical oxidation of the polymer-oligomer in solution.

Plieth et al. [913] used ellipsometry to study the electrooptical properties of poly(2,5-thiophenediyl) (i.e., PT). The refraction index and absorption coefficient of PT were determined as a function of wavelength for $400 < \lambda < 800$ nm. A swelling of the polymer film by about 20% was found after doping. An influence of the monomer concentration (0.4-M thiophene) on film properties was found when the data were compared with those obtained previously with a lower monomer concentration [914].

The use of model compounds (i.e., thiophene oligomers with end groups that prevent polymerization upon application of positive electrode potentials or thiophene monomers substituted in ways that provide controlled changes of electronic and other molecular properties) has resulted in considerable insight with regard to the influence of molecular structure on electrochemical properties of the polymer [915]. These results, in turn, may provide the basis for further development of tailored polymers for specific applications. Theoretical calculations by Brédas et al. [916] using the VEH resulted in predicted oxidation and reduction potentials for various intrinsically conducting polymers. With polythiophene, an oxidation potential of $E_{\text{NHE}} = 0.7$ V was calculated and compares favorably with the value of $E_{\text{NHE}} = 0.6$ V extrapolated from oligomer data by Brédas et al. [917] based on literature data. Alemán and Julià [918] studied 2,2'-bithiophene dications and 2,2',5',2'-terthiophene cations. With an increasing number of thiophene units, the quinoid structure disappears, whereas a benzoid structure gradually develops (for details of these spectroscopic investigations, see subsequent text). Casado et al. [919] studied the doping and undoping of a series of end-capped α , α' -dimethylthiophene oligomers with *ex situ* Fourier transform infrared and Raman spectroscopy. A complete spectroscopic characterization of the positive polaron-type defects was obtained. The effects of ionization on molecular geometries and vibrational spectra was further analyzed using density functional theory quantum-chemical calculations. van der Horst et al. [920] used the “*ab initio* many-body GW method” to calculate the quasiparticle spectrum of polythiophene. In comparison to DFT-LDA calculations, a large increase of the gap was found, which was explained by the absence of long range screening in the one-dimensional model used. Further quantum-mechanical studies have been reported and reviewed elsewhere [921].

Another aspect of the use of model compounds is their application in the study of the electrochemically induced changes of the polymer as evidenced in conductivity measurements, ECESR spectra, and corresponding UV-vis spectra [922]. Using various 3'-substituted 2,2':5',2'-terthiophenes, Visy et al. [922] suggested that the neutral polymer can be described as a mixture of two polymers, wherein one type has an effective conjugation length twice the value of the other. Moraes et al. [923] studied PT *ex situ*. At high doping levels achieved with AsF_5 , a temperature-independent Pauli spin susceptibility indicative of the metallic density of states was found. With less strongly iodine-doped samples, a Curie spin concentration independent of doping level was observed.

In situ UV-vis spectroscopy of PT reported by Onoda et al. [924] revealed the polaron state at 0.4 eV above the valence band and at 0.4 eV below the conduction band with an overall bandgap of 2.1 eV [925]. Interpretation and assignment of UV-vis spectroscopic data can be supported by investigations of model compounds reported by Fichou et al. [926]. Their results obtained with thiophene oligomers strongly support the preceding band

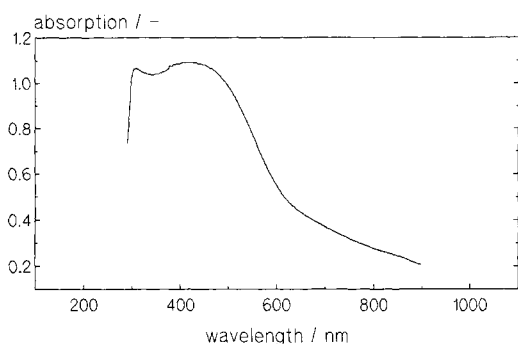


Fig. 74. UV-vis spectrum of a polythiophene film deposited on an ITO glass substrate; 0.1-M Na_2SO_4 electrolyte solution; $E_{\text{SCE}} = 560$ mV. For further details, see [930].

scheme proposed for PANI. Ahonen et al. [927] deposited 3,4-methylenedioxythiophene on ITO and platinum electrodes from various electrolyte solutions with organic solvents. UV-vis data show a bandgap of $\Delta E = 2$ eV similar to PT. This value is higher than the value found for poly(2,3-ethylenedioxythiophene) [928]. This discrepancy was explained by invoking the higher ring strain in the methylene polymer.

In my own early study, UV-vis spectra recorded *in situ* with a film of PT deposited on ITO did not show any significant change in the potential range studied here. The spectrum presented in Figure 74 typifies the spectral behavior; the laser wavelengths used for exciting resonance Raman scattering are in a broad absorption feature that decreases from a maximum around $\lambda_{\text{max}} = 480$ nm (where the preferred laser wavelength for maximum resonance enhancement is situated) to rather low values at $\lambda_{\text{max}} = 900$ nm. Based on the spectra obtained in aqueous solution, an assignment of the observed optical absorptions to various electronic transitions was not considered to be justified, whereas, on the contrary, in nonaqueous solutions, various pronounced bands that change as a function of electrode potential were observed and tentatively assigned [73].

Otero and Angulo [929] used electroreflectance spectroscopy at selected laser wavelengths to measure the population of various species in poly(3-methylthiophene). Although no detailed results were presented, the method was claimed to be equivalent to ECESR with regard to the quantitative measurement of free spins.

Because of the strong coloration of PT, especially in the partly and fully oxidized state, resonance Raman spectroscopy has been employed successfully to elucidate the molecular structure and changes thereof as a function of applied electrode potential and other experimental parameters [930]. Resonance Raman and infrared spectra of polythiophene obtained *ex situ* under various, frequently unsatisfactorily defined experimental conditions have been reported [931–935]. These early results were, in part, inconsistent. In particular, the assignment of bands not found in the thiophene monomer to modes of the newly created polymer was repeatedly contradictory.

In situ Fourier transform infrared spectroscopy with 3-methylthiophene films deposited on a germanium ATR crystal was described by Neugebauer et al. [936–938] as a chain structure with coupling of the monomer units in the α - α' position and the presence of free charge carrier in the conducting form of the polymer. Whereas *in situ* infrared spectroscopy is hampered by the presence of a strongly absorbing electrolyte film in the electrode win-

dow gap, the use of *in situ* Raman spectroscopy should be much easier. Bukowska and Jackowska [939] reported spectra that evidenced polymer formation from pyrrole and thiophene on electrochemically roughened electrodes as commonly used in surface-enhanced Raman spectroscopy—a chemical process that involves surface silver chloride and the respective monomer. Subsequently, Bukowska and Jackowska [940] presented some preliminary Raman spectra of polythiophene with a few assigned bands. A theoretical foundation for the interpretation of vibrational spectra of PT was provided by Faulques et al. [941]. Their results are taken into consideration in the subsequent interpretation of Raman and infrared spectra; relevant data are incorporated in the tables herein. Kofranek et al. [942] reported the results of a theoretical *ab initio* study of vibrational spectra of thiophene, oligothiophenes, and PT based on double zeta quality basis sets. For the monomer, satisfactory agreement between calculated and experimentally observed band positions was concluded. Inspection of data listed in Table XXV reveals close correspondence between the assignments for the polymer reported by various authors and the assignments and band positions stated by Kofranek et al.

SRR spectra were recorded in a wide range of electrode potentials. Typical examples from a range of $E_{\text{SCE}} = -400$ to 1600 mV with both acidic (0.1-M H_2SO_4) and neutral (0.1-M KClO_4 , pH = 4.95) electrolyte solution are shown. Cyclic voltammograms were recorded in this range of electrode potential to establish potentials where PT is present in its reduced or its oxidized form. They were rather featureless, for example, in a sulfate electrolyte solution at approximately $E_{\text{SCE}} = 1000$ mV, an anodic current commences and increases up to the onset of oxygen evolution. A very weak broad shoulder around $E_{\text{SCE}} = 1400$ –1500 mV is presumably caused by an anodic process that involves the PT film (but see, for comparison, Fig. 73, recorded with a different electrolyte). In the reverse cathodic scan, only features known from clean gold electrodes used with this electrolyte solution were observed. A very similar behavior was observed with a solution of 0.1-M KClO_4 used in the experiments by Sunde et al. [943], who explained the absence of a well defined voltammetric peak as attributable to the anodic doping process in sulfate- or perchlorate-containing solutions by various effects, mostly related to the type of anion used, because at least in the initial potential scan, a peak was found with a solution of KNO_3 , which nevertheless deteriorated as rapidly as the features observed here.

SRR spectra obtained with a solution of 0.1-M KClO_4 in the electrode potential range outlined in the preceding text are represented with two typical examples in Figure 75. (Because no significant differences were observed when the exciting wavelength was changed from $\lambda_{\text{L}} = 488$ to 514.5 nm, only spectra obtained with the former wavelength are reported here.) In addition to an increase in the width of the high wave number shoulder of the band around 1455 cm^{-1} with increasingly anodic electrode potentials, no further significant changes in the spectra are observed. The assignments of the bands based on literature data [931–935, 944, 945] are collected in Table XXV. For comparison, the data on liquid thiophene reviewed by Dollish et al. [946] are included in the table.

With an acidic electrolyte solution of 0.1-M H_2SO_4 , a very similar set of spectra was collected (see Fig. 76). Data of the observed bands are also incorporated in Table XXV. At first glance, only a few bands observed with the polymer correspond to monomer modes. From studies that involve isotopic substitution in the thiophene ring and the use of various oligomers [931–933, 935], a fairly

Table XXV. Spectral Assignment of Raman Bands of Polythiophene Based on Literature Data [931–935]; C–C_{interr.} Denotes Interring C–C Mode

Mode	Thiophene liq. [946]	Polythiophene on a gold electrode					Refs. [944], [945] ^a	Ref. [951] ^a	Calc. [957]
		0.1-M KClO ₄		0.1-M H ₂ SO ₄					
		<i>E</i> _{SCE} = 0 mV	<i>E</i> _{SCE} = 1200 mV	<i>E</i> _{SCE} = 0 mV	<i>E</i> _{SCE} = 800 mV	<i>E</i> _{SCE} = 1600 mV			
C–C _{interr.}	—	651	650	655	652	650	—	D ₅	—
γ _{CH}	683	—	—	—	—	—	ν ₁₀	—	—
Sym. ring bend.	—	696	699	700	700	680	—	ν ₇	696
γ _{CH}	714	—	—	—	—	—	ν ₁₉	—	—
δ _{ring}	751	742	—	—	741	—	ν ₁₈	ν ₆	746
δ _{CH, i.p.}	1035	1046	1050	1050	1047	1055	ν ₇	ν ₅	1039
Oligomer mode	—	1175	1175	1180	1180	—	—	D ₂	1197
C–C _{interr.}	—	1222	1222	1221	1218	1219	—	ν ₄	—
δ _{CH}	1257	—	—	—	—	—	ν ₁₅	—	1249
ν _{C=C, sym.}	—	1456	1455	1453	1455	1455	—	ν ₂	1459
ν _{ring}	1502	—	—	—	1504	1525	ν ₁₄	D ₁	1497

^aThe numbers refer to the alternative numbering scheme suggested by Bazzaoui et al.

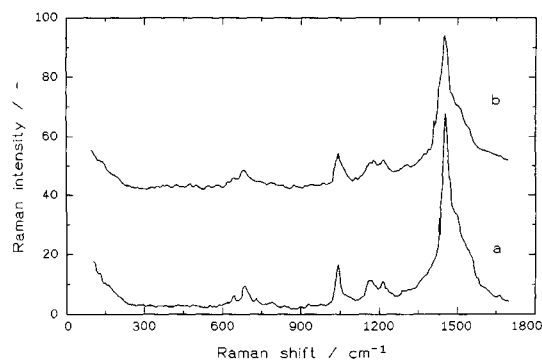


Fig. 75. SRR spectrum of a polythiophene film deposited on a gold electrode from a 0.1-M KClO₄ electrolyte solution at electrode potentials (a) *E*_{SCE} = 0 mV and (b) *E*_{SCE} = 1200 mV; 488-nm laser light; resolution 8 cm⁻¹.

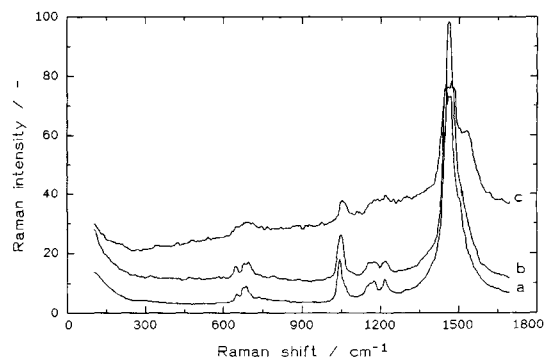


Fig. 76. SRR spectrum of a polythiophene film deposited on a gold electrode from a 0.1-M H₂SO₄ electrolyte solution at electrode potentials (a) *E*_{SCE} = 0 mV, (b) *E*_{SCE} = 800 mV, and (c) *E*_{SCE} = 1600 mV; 488-nm laser light; resolution 8 cm⁻¹.

complete assignment of the bands is deduced. Thus, there are two bands that change only slightly upon polymerization: the in-plane C–H deformation mode (around 1045 cm⁻¹) and the ring deformation found with the monomer at 751 cm⁻¹ and in the polymer at 741 cm⁻¹. The symmetric in-plane ring deformation at 606 cm⁻¹ in the monomer is shifted to around 700 cm⁻¹. The band around 650 cm⁻¹ is related to a C–C_{interring} mode of the polymer chain shifted by structural distortion in the solid polymer. Bands found in the range 1155–1180 cm⁻¹ indicate polymer chains present as cis coplanar isomers in addition to the highly symmetric all-trans conformation [932]. These isomers are found in a solution of terthiophene, indicating the coexistence of rotational isomers, whereas they are absent in the solid state of terthiophene. A satisfactory assignment of this band to a particular molecular mode is possible only when comparing spectra of isotopically marked terthiophene with their unmarked counterparts; this has not been reported so far.

The band observed around 1222 cm⁻¹ corresponds to a band found in the normal Raman spectrum of terthiophene [933]. This band is not observed with bithiophene; thus, its assignment to an interring C–C mode by Akimoto et al. [932] is not quite straightforward. It is nevertheless supported by a strong shift upon isotopic ¹³C substitution and only a small shift after deuteration.

According to Scott [947], the band at 1455 cm⁻¹ is due to a symmetric C=C intraring stretching mode. Akimoto et al. [932] assigned this band to a symmetric C=C stretching mode. Its shoulder at higher wave numbers (“tail”) and weaker bands located therein were assigned to the corresponding antisymmetric C=C stretching mode [933]. The broadness of the tail has been used as an argument for the presence of shorter polymer units, because the position of this band increases in wave numbers with decreasing chain length [933]. Because, based on the molecular structure of polythiophene, the chain length is identical with the conjugation length, the increased tail with an increase in electrode potential (see Fig. 76a and b) seems to indicate at least a small change in the polymer. However, this tail remains even after the potential is switched back to the initial cathodic value of *E*_{SCE} = 0 mV. The degradation of the polymer, that is, a splitting of longer chains into shorter ones with a corresponding higher content of units with the symmetric C=C mode at higher wave numbers, as suggested by Bukowska and Jackowska [948], is a plausible explanation. It is supported by the observation that the anodic current observed at the positive potential limit decreases rapidly in subsequent cycles and is not accompanied by a corresponding cathodic wave. This implies an irreversible change of the polymer film. This degradation by means of a nucleophilic attack of OH⁻ ions at posi-

tively charged centers in the PT chain may lead not only to chain splitting, as deduced from the evidence reported here, it may also result in the formation of oxy- or hydroxy-substituted thiophene units. So far, no direct proof has been found, whereas in the case of polypyrrole, Beck et al. [949] observed pyrrolinones after the irreversible overoxidation. The already discussed "effective conjugation coordinate" approach was applied by Geisselbrecht et al. [950] to the interpretation of Raman spectra of PT and polyisothianaphthene. Results could be used successfully in the interpretation of the line position and dispersion of the major band around 1400–1600 cm^{-1} .

The mentioned lack of observable change in the Raman spectra as a function of degree of doping and state of oxidation was addressed by Bazzaoui et al. [951]. It was explained by the considerably changed resonance conditions. Upon oxidation, the resonance enhancement based on the presence of the broad UV–vis absorption band as seen in Figure 74 was decreased drastically, because, according to the report of Bazzaoui et al., the intensity of this absorption is reduced dramatically. Accordingly, resonance enhancement is found at another wavelength (e.g., $\lambda_L = 1064$ nm). Contrary to the claim of Bazzaoui et al., the expected relationship between degree of oxidation, conceivable resonance enhancement, and observed scattered intensity is, at least, not supported by the reported spectra. Those spectra recorded with short wavelength excitation are always rather poor, whereas the spectra (almost independent of state of oxidation) recorded with $\lambda_L = 1064$ nm always have much better signal to noise ratio. In addition, Bazzaoui et al. provide a different scheme of numbering of observation vibrational modes as collected in Table XXV. The intensity ratio of the bands at 1411 and 1428 cm^{-1} , when measured with $\lambda_L = 1064$ nm, was suggested as a measure of the degree of oxidation. The increase of disorder in polymer films observed with atomic force microscopy was taken as an explanation of the observation that in thick films with a higher degree of disordering the topmost, cauliflower-like layer, which is doped first upon oxidation, ultimately covers undoped parts at the bottom.

Danno et al. [952] obtained *in situ* resonance Raman spectra and UV–vis absorption spectra of poly(3-octylthiophene). Bands indicative of polaron and, at higher electrode potentials, bipolaron formation were observed. The strong decrease of luminescence and of the intensity of major Raman lines is most likely due to the reasons already discussed.

The use of resonant Raman spectroscopy combined with photoluminescence measurements has been suggested by Sauvajol et al. [953, 954] as a tool for determination of the "quality" of PT films expressed in terms of degree of polymerization, degree of conjugation, and percentage of C=O defects. Raman spectra were found to depend only very weakly on the mentioned parameters, whereas photoluminescence showed considerable changes of profile and intensity as a function of film quality.

The use of model compounds in the interpretation of vibrational spectra of PT was been discussed by Poussiguet et al. [955].

Bazzaoui et al. [956] reported *in situ* Raman spectra of films prepared by electropolymerization of bithiophene from a solution of CH_2Cl_2 on a platinum electrode and on a roughened silver electrode. In the case of the latter electrode, surface enhancement was assumed (an overall increase by a factor of 10 was stated). Unfortunately the spectra displayed in the report do not support this claim convincingly. With the platinum electrode, the difference between the spectra of the reduced and the oxidized forms is limited to different overall intensities (as already stated). This

difference was explained by invoking changes in the resonance conditions upon doping and dedoping. Assignment was based on calculated band positions reported by Louarn et al. [957]. Except for minor differences, the observed positions correspond to those listed in Table XXV. The band around 1498 cm^{-1} showed a slight dependency on the conjugation length of the polymer. Its position did not depend on the oxidation state, whereas the band width changes considerably. This broadening was assigned to changes of the conjugation length, which in turn depend on distortions on the polymer brought about by oxidation, resulting in diminished coplanarity of the rings and lower conjugation length. With the silver electrode, additional bands were observed. With respect to the orientation of the polymer on the silver surface, a flat position of the polymer chain with tilted rings of the thiophene moiety was concluded. This also takes care of the considerable silver–sulfur interaction. A contradiction with results obtained with NEXAFS reported by Tourillon et al. [958] is addressed. The latter authors concluded a flat orientation of the reduced poly(3-methylthiophene). The presumed differences are explained by invoking different behavior of substituted and unsubstituted thiophene and by considering the differences in experimental conditions. The possible influence of the very different experimental techniques was not addressed.

Experimentally observed resonance Raman data on poly(3-methylthiophene) and poly(3-octylthiophene) were provided by Laourn et al. together with calculated data based on the concept of a valence force field model listed in Table XXVI [957].

The mentioned silver–sulfur interaction, or, more generally, a metal–sulfur interaction, was not found with aluminum as a substrate metal. From a comparison of theoretical data obtained with *ab initio* Hartree–Fock calculations with experimental data, Boman et al. [959] concluded a α -carbon–aluminum interaction.

To increase the scattered light intensity in Raman spectroscopy, which was thought to be insufficiently low, Bazzaoui et al. [960, 961] prepared polymers of bithiophene in the presence of silver ions in a rather complex electrolyte solution. The silver thus incorporated in the polymer film caused enhancement effects usually observed in SERS. The reported spectroscopic results did not differ markedly from those reported before.

Ex situ resonance Raman spectra of electrochemically prepared polythiophenes deposited under a broad variety of experimental conditions (solvent, temperature, water, and oxygen content in solution) were reported by Sauvajol et al. [962]. From the obtained results (the assignment of bands was based on previously reported results and is in agreement with data collected in Table XXV), they concluded that the structure of the Raman spectra is predominantly driven by the conjugation length. Further parameters of the obtained polymers, like the degree of polymerization and the percentage of C=O defects, were derived from additionally recorded *ex situ* IR spectra.

Wallnöfer et al. [963] investigated various anellated and alkylated polythiophenes [(polyisothianaphthene (PITN), polyisothianaphthoethiophene (PINT), poly(3-octylthiophene) (POT)] prepared by electropolymerization with resonance Raman spectroscopy at various laser wavelengths.¹⁴ The spectrum of POT is dominated by a strong luminescence (which is related to some of the possible applications of this material). The main peak is around 1460 cm^{-1}

¹⁴Results pertaining to PITN and PINT are discussed subsequently. Results pertaining to POT are reviewed subsequently.

Table XXVI. Spectral Assignment of Raman Bands of Poly(3-methylthiophene) and Poly(3-octylthiophene) Based on Data by Louarn et al. [957]

Mode	Poly(3-methylthiophene)		Poly(3-octylthiophene)	
	Exp.	Calc.	Exp.	Calc.
Combin. mode	270	276	—	—
Combin. mode	552	558	—	—
C—C _{alk} stretch.	984	984	1018	1016
Ring deform.	720	716	722	718
Ring deform.	741	733	—	734
Interr. stretch.	—	1208	—	1200
Interr. stretch.	1210	1211	1200	1202
γ_{CH}	1186	1147	1160	1147
C—C stretch.	1360	1367	1375	1374
C=C stretch.	1445	1447	1438	1437
C=C stretch.	1514	1513	1505	1507
C—H stretch.	3060	3060	3060	3060

as found with PT. This band is assigned to the stretching mode of the Peierls distortion. Some small peaks at higher wave numbers indicate the presence of disordered parts. Trznadel et al. [964] reported a study of regioregular poly(3-octylthiophene) investigated with UV-vis NIR and Raman spectroscopy. CVs obtained with this polymer showed two clearly separated oxidation peaks compared to the CV of the nonregioregular polymer, which shows a broad peak only with a very weak shoulder. This observation is considered to be an indicator of an enhanced structural homogeneity of the regioregular polymer that results in more isoenergetic polymer chains with a smaller number of coupling defects and polymer chain segments of different lengths. This observation supports the subsequent interpretation of spectroelectrochemical data. UV-vis spectra of the undoped polymer are dominated by a strong absorption around 2.39 eV ($\lambda = 518$ nm) assigned to the $\pi \rightarrow \pi^*$ transition. This observation confirms previously reported values [965]. Incomplete dedoping is concluded from the observation of very weak peaks around 1.8, 1.3, and 0.7 eV ($\lambda = 688, 953,$ and 1770 nm). Oxidation results in bleaching of this band and a concurrent growth of bands at 0.7 and 1.6 eV ($\lambda = 1770$ and 774 nm). Complete bleaching of the former band was achieved at very positive electrode potentials in excess of the electrode potential of the second oxidation peak in the CV. Assignment of the new peaks was supported by time-dependent measurements of absorption. As a result, subsequent formation of polarons and their recombination into bipolarons is suggested. Raman spectra of the polymer with different excitation wavelengths were obtained. As already discussed for PT, the fairly selective resonance enhancement results in spectra obtained with $\lambda_0 = 514.5$ nm of the undoped segments only (i.e., upon doping, the spectra showed no visible change). With light of $\lambda_0 = 676.4$ nm, monitoring of doping-induced changes was possible. Table XXVII lists the calculated and the experimentally observed band positions. Yuan et al. [966] studied poly(3-methylthiophene) with electroreflectance spectroscopy. An absorption that appears at 1.7 eV ($\lambda = 728$ nm) and is found only at intermediate doping levels was assigned to polaron gap states.

An *in situ* study of doping and dedoping of PT in a nonaqueous electrolyte solution was reported by Ivaska et al. [967]. A broad band at wave numbers higher than about 1500 cm^{-1} that appear

at positive electrode potentials and bands at 1330 and 1020 cm^{-1} were found. They were assigned to two different types of doping, and they disappeared during PT reduction.

With a combination of spectroelectrochemical tools, including, in particular, Raman and infrared spectroscopy (unfortunately *in situ* and *ex situ* measurements were not clearly separated), Louarn et al. [968] studied poly(3-alkylthiophenes) and poly(4,4'-dialkyl-2,2'-bithiophenes) in a comparative investigation. Various monomeric bithiophenes result upon chemical oxidation in "head-to-head" and "tail-to-tail" analogues of the 3-alkylthiophenes. The interband $\pi \rightarrow \pi^*$ transition was found to be blue shifted, indicating a higher torsion angle in the case of the polybithiophenes. Upon oxidation, doping-induced bipolaronic bands were seen in the UV-vis NIR spectra at essentially the same position as found with the corresponding poly(3-alkylthiophenes). This was seen as evidence that the torsion angle of both polymers is getting closer. Bipolaronic bands were also found with infrared spectroscopy. All five bands expected from theoretical calculations already had with the onset of the oxidation peak recorded with cyclic voltammetry.

Agosti et al. [969] reported a number of Raman spectra (no resonance enhancement because of NIR excitation) of a selection of oligo- and polythiophenes, and they searched for structure-property correlations that possibly can be derived from the vibrational data. Some relationships that are particularly useful for chemical diagnosis were proposed.

In a study of the interaction between polymer films and the electrode surface used as a support, Torsi [970] studied electrochemically synthesized films of bithiophene on platinum and p-doped Si(100). From the infrared spectra obtained *ex situ*, he concluded that the polymer chains interact via the π -electrons with the underlying surface.

ESR spectra of PT with a Dysonian-shaped single line (for comparison and further discussion, see the preceding section for ESR measurements with PANI) were observed by Tourillon et al. [971]. ECESR *in situ* investigations of doping and dedoping of PT have been reported frequently. Chen et al. [972] obtained data that imply spinless charged states at low to intermediate doping levels. Consequently, they concluded that bipolarons are energetically lower than polarons. Basically very similar results were reported

Table XXVII. Spectral Assignment of Raman Bands of Regioregular Poly(3-octylthiophene) [964]

Mode	Polythiophene		Regioreg. POT red.		Regioreg. POT oxid. ($\lambda_L = 1064$ nm)	
	Exp.	Calc.	Exp.	Calc.	Exp.	Calc.
Ring deform.	300	304	—	—	—	—
Ring deform.	—	420	—	—	—	—
Ring deform.	—	522	597	586	597	587
C_α -S- C_α deform.	700	696	682	705	682	703
C_α -S- C_α deform.	740	746	728	723	723	724
C_β - C_{alkyl} stretch.	—	—	1016	1016	1006	1011
C_β -H bend.	1045	1040	—	—	—	—
C_α - C_α stretch. + C_β -H bend.	1224	1210	1210	1202	1220	1215
$C_{\beta+}$ -H bend.	—	1249	1182	1143	1185	1149
C_β - C_β stretch.	1365	1359	1378	1376	1375	1377
$C_\alpha=C_\beta$ stretch.	1455	1460	1442	1436	1407	1409
$C_\alpha=C_\beta$ stretch.	1497	1498	1512	1504	1491	1494

by Zotti and Schiavon [973], who observed two consecutive oxidation waves (the CVs displayed in the original report show only shoulders). Consequently, they concluded that PT is oxidized in two steps. The ECESR signal shows only one broad maximum during the current increase of the first oxidation wave (step). No spins are found with the fully oxidized polymer. Obviously spinless species (bipolarons) are energetically favored in the oxidized state. This conclusion is supported by *in situ* UV-vis data. A display of the optical absorption at $\lambda = 700$ and at 900 nm as a function of injected charge shows distinctly different dependencies that confirm the presence of two distinctly different states of oxidation.

In a comparative study of various polythiophenes with *in situ* ECESR, Zotti and Zecchin [974] found considerable differences in the changes of ESR spectra recorded with oxidized polymers after turning the electrode potential to open circuit. With polybithiophene, a decay of the ESR signal following first order kinetics was found. The calculated half-lives decreased with increasing positive oxidation potentials. The latter observation was explained by invoking an electrochemically induced oxidative cross-linking, resulting in a stiffening of the polymer. With alkoxy- and alkyl-substituted polymers, the polaron decay was completely absent and a swelling of the material was observed. The general importance of these structural parameters in the polaron-bipolaron debate was highlighted.

In a critical review based, in particular, on results of ESR, UV-vis, and vibrational spectroscopies, Furukawa [975, 976] reconsidered the polaron-bipolaron discussion. For PT, he concluded that polarons are the dominant species generated by doping. The absence of ESR absorption may be caused by quenching interactions with free spins instead of their true absence (as already discussed).

Genoud et al. [977, 978] measured ECESR spectra of chemically prepared poly(3-butylthiophene) and poly(4,4'-dibutyl-2,2'-bithiophene). Despite the same stoichiometry, the distribution pattern of the butyl substituents is different for the polymers. With the latter, polymer spin creation and annihilation occur within a much smaller range of electrode potentials and at significantly more positive electrode potentials. The latter observation was taken as a sign of a higher stereoregularity.

In a more general investigation of PANI, PT, and PPy (for the other polymers, see the preceding sections), Devreux et al. [436] studied the correlation between injected electric charge per ring and the number of spins per ring. Their results are displayed in Figure 71. The general shape of the trace corresponds to plots already shown that display the relationship between the electrode potential and the spin concentration. Devreux et al. concluded from a thermodynamic consideration of the results that with PPy and PdT, polarons and bipolarons are almost degenerate and, consequently, in a thermodynamic equilibrium, whereas for PANI, polaron pairing is hindered by potential barriers that disable the establishment of a thermodynamic equilibrium. From a different approach, a π -electron tight-binding model was proposed [979] and, subsequently, it was proposed that sulfur-centered functions are important and bipolarons instead of polarons are created in the doped-excited state.

The occurrence of polarons and bipolarons on thiophene oligomers as a function of the degree of doping and their conceivable mutual interconversion were studied with model compounds by Horowitz et al. [980]. Oligomers with 6 and 12 repeat units oxidized by adding $FeCl_3$ ¹⁵ were investigated with *in situ* UV-vis and ESR spectroscopy. With the shorter oligomer, the polaron and the bipolaron are generated successively; with the longer oligomer, only the bipolaron state could be identified. Observed optical transitions were used to estimate bandgap energies. The latter are a direct measure of the chain length. From comparison with further results reported by other authors, it was concluded that short oligomers (with less than 8 repeat units) are more appropriately described with molecular orbital models, whereas longer oligomers (with more than 12 repeat units) are treated better with a one-electron model. The transition point at about 10 repeat units seems to correspond to a chain length sufficient to enable the coexistence of two polarons. In a subse-

¹⁵Strictly speaking, these results are not based on electrochemical investigations. Their importance with respect to the polaron-bipolaron controversy seems to justify their inclusion.

quent study, Nessakh et al. [981] studied the electrooxidation of oligothiophenes with $1 < n < 12$ (number of thiophene rings). Simultaneously UV-vis spectra of the electrolyte solution were recorded. With $4 \leq n \leq 8$, two oxidation waves, indicating the subsequent formation of the radical cation and the dication, were observed. UV-vis data also show two absorption maxima indicative of the presence of a radical cation with two allowed optical transitions that support this assumption in the case of $n = 6$. With $n = 12$ (12T), two oxidation waves, but only one absorption maximum were found. This observation is in agreement with results obtained during chemical oxidation and reviewed already. The formal oxidation potential derived from the UV-vis data corresponds closely to data of the first oxidation wave found with shorter thiophene chains. Nessakh et al. as a result proposed a model wherein two doubly charged 12T species form a π dimer. A study with related compounds [2, 5''-dimethylterthiophene, 2, 5'-(dithiomethyl)-5,2'-bithienyl and 2, 5''-(dithiomethyl)-5, 2', 5',2''-terthienyl] and essentially the same results was reported by Hill et al. [982].

Ex situ measurements with electron diffraction and electron energy loss spectroscopy (EELS) by Fink et al. [983] provided evidence for the presence of bipolarons in doped PT, but polarons cannot be ruled out entirely. Reedijk et al. [984] studied charge transport in PT doped with FeCl_3 .¹⁶ Results imply a change from quasi-one-dimensional variable range hopping at low doping levels to three-dimensional variable range hopping.

The polaron-bipolaron topic has been treated repeatedly from a theoretical point of view. Results may be used to interpret experimental evidence gathered with spectroelectrochemical methods. Aleman [985] studied the spatial extension of bipolaronic defects in various polymers based on five-membered aromatic rings including thiophene: benzoid structure was found for neutral oligomers, whereas a quinoid structure extending over six rings was deduced for dications.

Zotti [986] reinvestigated the relationships between electrode potential, injected charge, and *in situ* measured electrical conductivity. As a function of injected charge, with all investigated polythiophenes, three different types of relationships were observed. Up to a certain threshold value (at low charge levels), a slow increase of conductivity was followed by a linear increase that ended in a plateau value. The threshold value cannot be explained by percolation, because only homogeneous polymers were investigated and no evidence of electrochemically induced heterogeneity (formation of conducting islands in an insulating matrix) was found. Instead, π dimerization of polarons was concluded. Measurements of electrical conductivity often performed with other intrinsically conducting polymers as part of attempts to identify the mobile charge carriers seem to be scant with PT. An *ex situ* study of the conductivity of various 3-alkyl-substituted PTs yielded increasing conductivities with increasing temperatures up to a certain, polymer-typical temperature [987]. Beyond this temperature, the conductivity dropped. These results were correlated with changes in the UV-vis spectra. The absorption found around $\lambda = 500$ nm (2.5 eV) shifted to higher energies with increasing temperature. This change was explained in terms of changing effective conjugation lengths. The decrease of coplanarity of neighboring thiophene

rings with higher temperatures effected by a change in the conformation of the alkyl groups is the likely cause. The occurrence of a glass transition invoked in the case of PANI was considered. Because of the absence of reliable data for the investigated polymers, the transition temperature could be estimated to be between the glass transition temperature and the melting point.

With a combination of *in situ* conductivity and potential-step chronocoulometric measurements, Harima et al. [988] studied the enhancement of carrier mobilities in poly(3-methylthiophene). In addition to the obvious effect of the electrochemically induced increase in the concentration of mobile charge carriers, a drastic mobility enhancement of over 4 orders of magnitude, which implies a change from hopping to metallic transport, was concluded.

The influence of preparation conditions on the conductivity of PT was studied by Kabasakalogu et al. [989], who reported the effects of type and concentration of electrolyte in the electropolymerization solution, deposition time, deposition potential, and deposition current.

Using a somewhat different experimental approach to *in situ* conductivity measurements, Kankare et al. [990] studied the conductivity of poly(3',4'-didodecylterthiophene) and poly(3',3''-didodecylterthiophene) during electropolymerization. With the former polymer, the measured conductance was related to the charge consumed during polymerization (instead of polymerization time); in the latter case, this relationship was not observed. This was explained by taking into account the different reactivities of the radical cation species formed during polymerization, which in turn influence the amount of polymer actually formed in addition to formation of side products. The electrical conductivity of rather thick films of poly(3,4-ethylenedioxythiophene) was reported by Morvant and Reynolds [991]. Maximum conductivity was attained at relatively low electrode potentials; correspondingly, the polymer was rather stable in its conducting state. Lankinen et al. [992] studied poly(3-methylthiophene) with *in situ* conductivity and infrared spectroscopic measurements. With an acetonitrile-based electrolyte solution, higher conductivities were observed with Bu_4NPF_6 than with Bu_4NClO_4 . The onset of overoxidation at $E_{\text{sat.mercurousulfate}} = 1.4$ V was derived from the infrared spectra based on the observed decrease in the absorption assigned to polarons-bipolarons. In aqueous solutions, conductivities lower by about 3 orders of magnitude and with considerably slower doping and dedoping kinetics were found. Infrared results were similar to those found with the nonaqueous solution. The changes in conductivity were generally smaller with aqueous solutions [993]. In a similar study [994] of poly(3-thiophene-3-methanol) with *in situ* conductivity and UV-vis absorption measurements with nonaqueous electrolyte solutions containing various anions, optical absorptions similar to those obtained with PT were observed. Differences between films formed and studied in the presence of Bu_4NPF_6 or Bu_4NClO_4 were found. In a subsequent study with additional spectroelectrochemical *in situ* tools (optical beam deflection and infrared spectroscopy), the redox behavior of these films was investigated further [995]. From CVs, a further covalent coupling in the polymer with the formation of methoxy bridges was inferred. Unfortunately, the infrared spectra did not provide proof of this suggestion. From results of both optical techniques, the exclusive participation of the electrolyte anions in the charge compensation was deduced. *In situ* UV-vis measurements of this polymer revealed an absorption maximum at about $\lambda = 400$ nm (3.05 eV), implying a conjugation length of five to six monomer units [996].

¹⁶Although these results are not based on electrochemical investigations, their importance with respect to the mode of charge propagation seems to justify their inclusion.

Abrantes et al. [997] reported a study of electropolymerization of 3-methylthiophene with probe beam deflection. The observed values of beam deflection as a function of polymerization time were explained by invoking fluxes of various species involved in the process (i.e., monomers, oligomers, protons, anions, and cations).

The photoelectrochemical behavior of films of poly(3-methylthiophene) on platinum electrodes was studied by Semenikhin et al. [998, 999] and Abrantes and Correia [1000]. At negative electrode potentials, a cathodic photocurrent was observed with an acetonitrile electrolyte solution. Upon exposure to light, the current increased. This "photoactivation" behavior was attributed to a photoelectrochemical reduction of the polymer with an accompanying increase in the width of the space-charge region wherein the photocurrent was generated. This region is localized close to the polymer-solution interface. El Rashiedy and Holdcroft [1001] reported an extensive study of the photoelectrochemical properties of poly(3-hexylthiophene). At very negative electrode potentials ($E < E_{SCE} = 0.3$ V) in an aqueous electrolyte solution, a depletion layer at the polymer-solution interface was found. Illumination of the polymer resulted in water splitting. The observed photovoltage correlates linearly with pH (and consequently with the electrode potential of the H_2/H^+ -couple), implying the absence of Fermi-level pinning. Quantum efficiencies as a function of film thickness and incident light wavelength were reported. Photoexcitations in PT were investigated by Moraes et al. [1002]. Hsu et al. [1003] investigated relaxation processes in freshly deposited PT and poly(3-methylthiophene) films with and without electrolyte solution being present. The rather complex processes seem to include reduction of the polymer in the presence of oxidizable species, for example, by water or thiophene monomers. A light illumination effect was observed that was stronger with light of shorter wavelength. No explanation was provided. The a forementioned photoelectrochemical reduction may be the cause. A further study of the relaxation of poly(α,ω -bis(3-thienyl)alkenes) and poly(3-alkylthiophenes) was reported by Mangold and Jüttner [1004], who took into account earlier studies of ICP relaxation phenomena [1005-1007]. A significant influence of the degree of cross-linking and of the length of the alkyl chain used as a substituent was found.

The semiconducting properties of an electrochemically generated film of polybithiophene was studied by Fikus et al. [1008]. The value of the flat band potential for the p-type semiconducting polymer in its reduced state $E_{SCE} = 0.6$ V was confirmed by *in situ* photocurrent measurements.

Photoproduction of both charge- and spin-carrying species was observed with various *ex situ* spectroscopies. Further basically similar results also obtained *ex situ* were reported by Kaneto et al. [1009] and Hattori et al. [1010]. Light-induced phase transitions ("photoswitching") were observed by Hosaka et al. [1011].

The change of PT from its reduced to its conducting oxidized state was studied by Tezuka et al. [1012] with an optical setup capable of detecting the local change in color. With a diode array detector, local changes in optical absorptivity were detected that are indicative of local conductivity. Under potentiostatic control in an acetonitrile-based electrolyte solution, processes in the film itself controlled the rate of conversion, whereas in a propylene-based solution, diffusion control was found. The results were converted into a growth model, in which oxidation starts at the polymer-solution interface and subsequently penetrates into the bulk of the polymer.

Table XXVIII. Absorption Maxima for Dissolved and Solid State Samples

	λ_{max} (nm)	
	Reduced	Oxidized
Dissolved state		
PT8	435	800
PT14	435	800
POMT	420	800
Solid state		
PT8	505	800
PT14	500	800
POMT	545	820

Tourillon and Garnier [1013] reported absorption maxima of the reduced state around $\lambda_{max} = 480$ nm and of the oxidized state around $\lambda_{max} = 650$ nm with the latter band extending into the NIR for poly(3-methylthiophene). Guay et al. [1014] studied a variety of 3-substituted thiophenes. Poly(3-octylthiophene) (PT8), poly(3-tetradecylthiophene) (PT14), and poly[(3-octyloxy)-4-methylthiophene] (POMT) were investigated in solution and as cast films on ITO electrodes using cyclic voltammetry and *in situ* UV-vis spectroscopy. Although these polymers are assumed to have a nonplanar conformation in solution and a coplanar conformation in the solid state, CVs do not show evidence of this conformational difference. It is assumed that the dissolved species adopt a coplanar conformation in the vicinity of the electrode. Further details are provided by the UV-vis data. The respective absorption maxima for dissolved and solid state samples are provided in Table XXVIII.

The differences in the energy of absorption between solid and dissolved state of about 0.4-0.7 eV (70-125 nm) are caused by the conformational changes. The different conformations proposed are supported by experimental evidence obtained with neutron diffraction measurements [1015], light scattering measurements [1016], and X-ray diffraction data [1017]. Assuming symmetrical changes of HOMO and LUMO¹⁷ by the conformational changes, the actual values of the HOMO are changed by about 0.2-0.3 eV. This is not evident from the electrode potential of the first oxidation wave as seen in the CVs. Actually, the oxidation potentials of the dissolved species are lower than those of the solid state samples. Nevertheless, the absorption bands of the oxidized species are very close, implying similar electronic structures. This conclusion is in agreement with the observation reported by Rughooputh et al. [1018] that bipolarons stabilize the coplanar structure of poly(3-alkylthiophenes). Other possible influences may account for the experimentally observed higher oxidation potentials of the solid state samples, for example, film resistance or slow counterion movement.

Li and Aoki [1019] observed a large swelling of poly(3-hexylthiophene) films prepared chemically and subsequently oxidized electrochemically in a nonaqueous solution after transfer into chloroform. More highly oxidized films showed a greater swelling. The shift of the absorbance at $\lambda = 302$ nm, attributed to the

¹⁷LUMO is the acronym for lowest unoccupied molecular orbital. An electron is injected into this orbital upon reduction.

$\pi \rightarrow \pi^*$ transition with higher oxidation potentials applied to the film, indicates an increasing degree of conjugation. The absorption at $\lambda = 765$ nm relative to the presence of mobile charge carriers (i.e., to the presence of electrical conductivity) decreased. The effect of a higher degree of oxidation (attained both by higher electrode potentials and longer times of electrolysis) was explained based on infrared data that indicated the loss of aromaticity caused by structural changes in the 4 position of the thiophene unit.

Christensen et al. [1020] used *in situ* infrared spectroscopy to investigate the relationship between vibrational data and film morphology. Although the preparation of their films was essentially the same, vibrational data varied slightly. This variation was correlated with different films morphologies, which, in turn, may have been caused by minute differences in actual solution composition.

Servagent and Vieil [1021] studied the mass change of a film of poly(3-methylthiophene) using EQMB. Results provided a clear separation of monomer deposition and ionic movement associated with doping. A doping ratio around 0.3 was calculated. A delay of ionic movement that indicates nonequilibrium with respect to charge equilibration in the polymer was observed. The relationship between consumed charge and observed mass increase indicates inclusion of oligomers. Consequently, estimates of film thickness based solely on consumed charge must be treated carefully.

Conformational effects have also been invoked as an explanation for observed effects in *in situ* UV-vis spectra and CVs of poly(*trans*-thiophene-2-yl-2,2':5'2''-terthiophene-5-yl-ethylene) poly[*trans*-TTTE] and of poly(*trans*-2,2'-bithiophene-5-yl-2,2':5'2''-terthiophene-5-yl-ethylene) [poly(*trans*-BTTTE)] [1022]. With both polymers, p doping was observed and the optical transitions were explained based on the polaron-bipolaron model. In the doped state, the interband transition was not seen in the UV-vis spectra. Instead, absorptions that correspond to transitions into lower and upper bipolaron states were found. The red shift of the absorption edge and the smaller bandgaps with both polymers as compared to standard PT are attributed to a larger spacing between neighboring thiophene rings, whereas hindrance effects seem to be smaller. The remaining differences between the two polymers under discussion could not be explained satisfactorily. The assumption of bipolarons only was supported by results from ECESR experiments. In a corresponding report, optical data were treated in more detail [1023]. UV-vis spectra recorded *in situ* with a nonaqueous electrolyte solution showed a band at 2.5 eV ($\lambda = 495$ nm) assigned to the interband transition ($\pi \rightarrow \pi^*$ transition). A small shoulder at 1.3 eV ($\lambda = 953$ nm) was attributed to traces of dopant incorporated during electropolymerization and removed only in part during dedoping. Upon oxidative doping, the band caused by the interband transition disappeared and a band around 1.3 eV ($\lambda = 953$ nm) evolved. At very high oxidation potentials, bands at 1.2 and 1.6 eV ($\lambda = 1032$ and 774 nm) were observed. Spectral changes could be explained within a polaron-bipolaron model. In comparison, the band of undoped poly(*trans*-BTTTE) is larger by about 0.1 eV.

With *in situ* UV-vis spectroscopy, Zagórska and Krische [1024] found evidence to indicate a more regular structure of polymers prepared from 4,4'-dibutyl-2,2'-bithiophene and 4,4'-dioctyl-2,2'-bithiophene and modified electrochemically as compared to polymers prepared from 3-alkylthiophenes. Nevertheless, a shorter conjugation length was found.

Rühe et al. [1025] investigated 3,4-cycloalkylthiophenes. The electric conductivity and the UV-vis spectra recorded *in situ* indicate a decrease of conductivity and conjugation length with in-

creasing ring size. Because the conductivity data fit the predictions of the hopping theory, a considerably larger influence of the chain packing as opposed to the structure of the electronic backbone, on the conductivity is concluded. In a study of chemically prepared polymers from alkyl- and alkoxy-substituted thiophenes, Leclerc and Daoust [1026] found that monosubstituted thiophenes gave soluble and electroactive polymers, whereas processability requires 3,4-disubstitution. Good yields were observed during chemical polymerization of alkoxy-substituted thiophenes [1027]. Good electrical conductivity was found with samples that showed a highly regular substitution pattern with an α, α' -linked backbone and a planar or almost planar conformational structure. As already mentioned, poly(3-alkoxy-4-methylthiophenes) obviously met these requirements particularly well; in addition, they were found to be processable. The observed low oxidation potential of about $E_{SCE} \approx 0.62$ V for the transition of the polymer from its reduced into its oxidized, conducting state implies an enhanced stability of the conducting state. The relationship between conformational preference (in particular, coplanarity) was studied theoretically with 2,2'-bithiophene model compounds by Aléman and Julia [1028].

Zotti et al. [1029] prepared polymers of oligothiophenes ($n = 2-4$) that carry pentoxy groups in position 3 or 4 of both terminal thiophene units by chemical and electrochemical polymerization [1029]. Polymers with the substituent in the 3 position (IT) were almost completely soluble in chloroform, whereas those with the substituent in the 4 position (ET) were only partially soluble; the latter polymer with $n = 2$ was completely insoluble. Osmometric determination of the chain length of the soluble fractions of all polymers gave degrees of polymerization between 3 and 5. UV-vis spectra of films electropolymerized directly onto an ITO electrode were different from those recast from the soluble polymer onto this substrate. Electrodeposited IT with $n = 3$ showed a single strong band at $\lambda = 554$ nm and a weak band at $\lambda = 630$ nm, whereas the chemically polymerized sample showed bands at $\lambda = 478$ and 512 nm. Evaluation of the data under the assumption that they are related to the bandgap energy resulted in a bandgap that corresponded to $\lambda = 650$ nm for infinite polymer chain length. This correlation was suggested as a rough tool for the determination of the degree of polymerization. It also implied, that bandgap energies for these polymers are smaller than those of the corresponding polyalkylthiophenes. A comparison of the results obtained with IT and ET of various values of n shows that with an increase of n , the absorption maximum is blue shifted, implying a lower degree of polymerization. The polymers could be oxidized electrochemically at rather low electrode potentials. Consequently, the doped state was relatively stable. Upon doping the UV-vis spectrum of an electrodeposited film of ET with $n = 3$ at low levels, the band at $\lambda = 554$ nm decreases in intensity, and a broad band around $\lambda = 2200$ nm and a shoulder at $\lambda = 1100$ nm can be seen. In the fully doped state, the band at low wavelengths is practically absent, whereas the band around $\lambda = 2500$ nm dominates the spectrum. These values correspond with those of similar substituted PTs already discussed. Steric effects, which should become evident when comparing data for corresponding ET and IT polymers, were not found.

Roncali et al. [1030] studied a series of 3-substituted polythiophenes [poly(3-methylthiophene) (PMT), poly(3-isoamylthiophene) (PiAT), poly(3-nonylthiophene) (PNT), and poly(3-3,6-dioxyheptylthiophene) (PDHT)]. The symmetry of the current waves increases in the given ranking, implying an enhanced reversibility of

the oxidation–reduction process. The absorption maximum in the UV–vis spectra recorded *in situ* showed a bathochromic shift from PiAT to PDHT. In the doped state, PiAT, PNT, and PDHT show an intense absorption at 1.5 eV at intermediate doping levels that was not seen with PMT. The bandgap is narrower in the highly doped state. These effects are particularly evident with PDHT. They are tentatively explained by assuming an extended effective conjugation length that results from the stabilization of a more planar conformation. The PDHT compound was subjected to further investigations by Roncali et al. [1031]. In particular, the influence of environmental parameters (electrolyte, solvent, etc.) was studied. UV–vis spectra recorded *in situ* showed striking effects of the anion–solvent combination on band positions and on the electrochemical response. The results are discussed in terms of feedback effects of the interactions between the oligo(oxyethylene) substituents and the chemical environment of the polymer on charge and mass transport in the polymer and on the geometry and rigidity of the conjugated poly(thiophene) backbone.

The electropolymerization of α -terthienyl substituted at the β position of the median thiophene unit with methyl, octyl, and dioxahexyl groups was investigated by Roncali et al. [1032]. Surprisingly, the substituents did not significantly affect the oxidation potential, whereas the polymerization process and the polymer properties are influenced to some extent. Although polymers formed from unsubstituted terthienyl monomers are poorly conjugated, the oxidation potential of the polymer investigated here is reduced because of the presence of the substituents. This is supported by a bathochromic shift of the absorption by about 70–80 nm that increases with the size of the substituents. The reported spectra provided evidence of trapped monomers within the polymer film.

Ferraris and Newton [1033] studied a variety of polymers prepared from α -terthienyl and 2,5-di(2-thienyl)pyrrole, *n*-alkylated at the β position of the central ring, to evaluate the effects of the size and position of the substituent and the sequence of substituted and unsubstituted ring units on optical and electrochemical properties of both the monomer and the electrochemically prepared polymer. A superior effective degree of conjugation as compared with the corresponding polymer prepared from the 3-alkylthiophenes was observed. The observed bandgap was slightly smaller than observed with the parent compound.

Shirakawa et al. [1034] prepared chemically as well as electrochemically soluble poly(2,5-thienylene) derivatives [poly(3-(ω -phenylalkyl-2,5-thienylene)]. The UV–vis spectra recorded *in situ* with the polymer in its reduced form showed a band at about $\lambda = 1126$ nm caused by insufficient dedoping of the as-prepared film being formed in its doped state. A strong absorption at $\lambda = 399$ nm is assigned to the $\pi \rightarrow \pi^*$ transition. Upon oxidation, bands at $\lambda = 728$ and 1548 nm appear. Although no assignment is provided, it seems safe to suggest that the former band is caused by polaron states of the slightly doped polymer, whereas the latter band indicates bipolaron states.

Although the investigated polymers of poly(3-octylthiophene) with controlled high molecular weight were prepared chemically [1035], the results of conductivity measurements after elongation are of interest with respect to theories of electrical conduction in ICPs. A higher molecular weight resulted in a higher conductivity, whereas elongation resulted in pronounced anisotropy of conduction. This was explained by assuming a decreased hopping distance caused by the reorientation of the polymer. Dyreklev et al. [1036, 1037] studied the change of conductivity of poly[3-

(4-octylphenyl)-2,2'-bithiophene] after elongation and subsequent doping with iodine. The extent of doping depended on the initial value, the sample orientation, and the amount of elongation. Results were again discussed in terms of variable range hopping.

The already addressed electronic effects of substituents on the oxidation potential, the electronic bandgap, and other properties of the polymer were studied with a particular set of bithiophenes by Demanze et al. [1038, 1039]. They electropolymerized 3,3'-disubstituted-2,2'-bithiophenes with substituents ranging from hydrogen and hexyl groups over methoxy or carboxy functions to cyano substituents. It was found that by merely changing the substituents, the oxidation potential can be changed by as much as 1.12 V. With *in situ* UV–vis spectroscopy of the most intriguing sample (with a cyano and a methoxy substituent), the $\pi \rightarrow \pi^*$ transition was found at $\lambda = 435$ nm. At intermediate oxidation levels, two new bands around $\lambda = 735$ and 1400 nm were observed. Based on comparison with known data, these bands are assigned to polaronic states and a short conjugation length. After further oxidation, a new band around $\lambda = 557$ nm was observed together with a blue shift of the already present lower energy band. This is explained by suggesting the formation of π dimers of the radical cations. Finally, at even more positive electrode potentials, a large band centered around $\lambda = 960$ nm and attributed to the stable bipolaronic state was found. Demanze et al. [1040] reported a further study of these bithienyls (with electron-donating substituents like methoxy or hexyl groups and $-\text{CN}$ as electron-accepting substituents). UV–vis spectra recorded *in situ* with $-\text{O}-\text{Me}$ and $-\text{CN}$ groups showed a band at $\lambda = 435$ nm in the reduced state. This band is attributed to the $\pi \rightarrow \pi^*$ transition. It is close to the corresponding value reported for poly(3-alkylthiophenes). Upon oxidation, the intensity of this band decreases, whereas bands around $\lambda = 735$ and 1400 nm appear. Further oxidation results in a band at $\lambda = 557$ nm and a slight blue shift of the band at $\lambda = 1400$ nm. Finally, a band around $\lambda = 960$ nm dominates the spectrum. These observations are interpreted in terms of three distinct charge storing species successively formed on the polymer. These species are polarons formed in the first oxidation step. Because of the particular properties of the substituents, these polarons are highly localized on the thiophene units that carry the $-\text{O}-\text{Me}$ substituents. In most other PTs and substituted polythiophenes, these polarons are more or less delocalized, resulting in their transformation into bipolarons [1041, 1042]. Descriptions of the subsequently formed species were not provided. Results obtained with the same substituents were reported again by Demanze et al. [1043]. Band positions in all various states of oxidation varied only very slightly. The band found in [1040] at $\lambda = 1400$ nm is not reported correctly at $\lambda = 1141$ nm.

A study of poly(3,3'-dibutoxy-2,2'-bithiophene) with *in situ* Raman spectroscopy was provided by Pron et al. [1044]. Emphasis was placed on selective enhancement as already observed with plain PT. Using laser light $\lambda_L = 458$ and 676 nm, only bands typical of the undoped, reduced form were observed, whereas excitation with $\lambda_L = 1064$ nm resulted in additional bands of the doped form, too. Bands and their assignment together with respective bands of PT and a representative poly(3-decylthiophene) are collected in Table XXIX. UV–vis spectra also recorded *in situ* show typical changes upon oxidation. In the reduced form, a band at $\lambda = 610$ nm assigned to the $\pi \rightarrow \pi^*$ transition dominates the spectrum. Oxidation causes a significant decrease of intensity of this band up to complete bleaching and the occurrence of a very broad feature initially centered around $\lambda = 1000$ nm, which grows

Table XXIX. Spectral Assignment of Raman Bands of PT, Poly(3-decylthiophene), and Poly(3,3'-dibutoxy-2,2'-bithiophene) [1044]

Mode	Polythiophene		Poly(3-decylthiophene)		Poly(3,3'-dibutoxy-2,2'-bithiophene)	
	Exp.	Calc.	Exp.	Calc.	Exp.	Calc.
—	542	558	—	—	—	523
S—C-deform.	741	735	—	562	699	676
—	720	715	725	716	754	757
—	985	984	—	—	—	—
C_{β} — C_{subst} stretch.	—	—	1091	1082	1112	1108
Ring deform.	1014	1010	1018	1015	—	1004
C_{α} — C_{α} stretch.	1186	1147	1160	1148	1170	1163
+ C_{β} —H bend.	1210	1208	1200	1207	1190	1201
—	1370	1367	1375	1373	—	—
C_{β} — C_{β} stretch.	1361	1375	1385	1384	1290	1300
—	—	1435	1438	1436	1415	1401
—	1444	1447	—	—	1451	1456
C_{α} = C_{β} stretch.	1520	1527	1515	1511	1522	1512
—	—	—	2884	—	2874	—
C—H stretch.	—	—	2923	—	2920	—
C—H stretch.						
of alkyl or butoxy group	—	2956	—	2961	—	—
C_{β} —H stretch.	—	—	3055	—	—	—

into a continuously increasing absorption (ranging deep into the NIR range) upon further doping.

Hagiwara et al. [1045] electropolymerized poly(3,4-dimethoxythiophene) on ITO glass electrodes. UV-vis spectra measured *in situ* showed a broad absorption at about $\lambda_{\text{max}} = 1700$ nm with the as-grown (i.e., oxidized) film, which disappeared upon electrochemical reduction and was replaced initially by a band around $\lambda_{\text{max}} = 830$ nm and, finally, by bands around $\lambda_{\text{max}} = 510$, 551, and 598 nm. The proposed assignment was the same as for PT; the multiplicity of bands in the reduced state was attributed to contributions from vibronic levels.

Havinga et al. [1046] prepared polymers of four different thienylene-vinylene monomers that contained the 3,4-alkoxythiophene moiety with various alkoxy groups. The purpose of this investigation was to improve the properties of the polymer prepared from the parent compound 3,4-ethylenedioxythiophene. NIR-vis spectra obtained from films after both chemical and electrochemical doping basically showed changes similar to those observed with other PTs. Contrary to the parent compound, the polymers investigated here change in the energy of absorption bands as a function of doping level. This change attributed to the presence of vinylene spacers. These spacer reduce the bandgap and blue shift the absorption bands by about 0.2–0.3 eV. The electronic conductivity is lower by about 3 orders of magnitude.

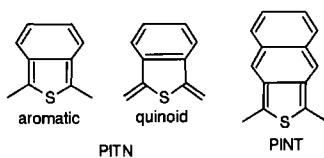
Randazzo et al. [1047] electropolymerized 2-vinylthiophene in a nonaqueous electrolyte solution at a platinum electrode. Two oxidation products were found: a semiconducting dark coating of the electrode and a nonconducting dark precipitate in the anode compartment. The latter product could also be obtained by chemical, benzoyl peroxide-initiated free radical polymerization in a spectroscopically very similar form with a higher molecular

weight. Based on the results of numerous spectroscopic methods employed *ex situ*, a structure is proposed with 25% of the thiophene rings cross-linked at the 5,5'-position. This results in a very short conjugation length of two thiophene units, but the electronic conductivity is comparable with other intrinsically conducting polymers with presumably higher conjugation lengths.

Wallnöfer et al. [1048, 1049] investigated various anellated and alkylated polythiophenes (PITN, PINT, and POT¹⁸) prepared by electropolymerization with resonance Raman spectroscopy at various laser wavelengths. PITN has been the subject of predictions based on theoretical considerations. Brédas [1050] suggested that PITN has an aromatic structure with a bandgap of $\Delta E = 0.5$ eV based on the conclusion that the fused benzene ring on top of the thiophene unit reduces the distance between thiophene units and results in a reduced bandgap. A preliminary synthesis of the polymer reported by Wudl and co-workers [1051–1053] showed a strong optical absorption around 1 eV. In a subsequent report, Lee and Kertesz [1054] concluded that the effect of the benzene ring should be strong enough to make the quinoid state with a bandgap of 1.16 eV the ground state. The spectrum of undoped PITN at long wavelengths was dominated by a band around 1460 cm^{-1} that was assigned to the stretching mode of the polymer backbone. Upon lowering the laser wavelength, the broad band splits into several components that show two different types of resonance enhancement. Resonance Raman spectra of the related compound PINT were very similar. The two types of bands were assigned to different phases of the polymer (benzoid and quinoid). For both

¹⁸Results pertaining to POT were reviewed previously.

PINT and PITN, a quinoid structure of the neutral ground state was postulated:



In a study of PITN with *in situ* and *ex situ* resonance Raman spectroscopy combined with a vibrational analysis, Walln fer et al. [1055] obtained further details of PITN in its various doped and undoped states. A theoretical foundation for the interpretation of vibrational spectra of PITN was provided by Faulques et al. [1056]. Their results were taken into consideration in the previous discussion of Raman and infrared spectra. Zerbi et al. [1057] reinvestigated PITN prepared chemically with Raman spectroscopy *ex situ* because they believed that previous results were inconclusive. Their results, based on the effective conjugation coordinate, imply that PITN in its electronic ground state is present in the quinoid form.

A somewhat different approach toward a modified PT was employed by Huchet et al. [1058]. By using a bithiophene monomer substituted with an oxa-coupled tetrathiafulvalene (TTF) group, they obtained electrochemically active polymers that show electrochromism, too. The fairly complex CVs imply redox processes that involve the substituent. Actually, the oxidation potential of tetrathiafulvalene is at about $E_{\text{SCE}} \approx 0.4 \text{ V}$ [1059], whereas the corresponding value for the oxidation of thiophene is $E_{\text{SCE}} \approx 2.07 \text{ V}$ [871]. Consequently, polymerization of a thiophene-based monomer is accompanied by oxidation of the tetrathiafulvalene. Undoping was found to be extremely slow (on an hour time scale). Huchet et al. took this as a sign of enhanced stability of the oxidized state of this polymer with the tetrathiafulvalene in both its oxidized and its reduced state. Further details of synthetic routes to the respective monomers were described by Bryce et al. [1060]. A similar investigation was reported elsewhere [1061]. In addition to electrochemical evidence of redox processes that involve the polymer backbone and the substituents separately, UV-vis spectra provided information about electrochemically induced changes. Of particular interest was the observation that oxidation of TTF into its radical cation and further into its dication proceeds via a dimeric dicationic TTF_2^{2+} species. The relative oxidation potential for the TTF and the polymer depended on the type of the polymer backbone itself. In the case of a thiophene-like backbone, the TTF was oxidized first, whereas with a hybrid thiophene-ethylenedioxythiophene backbone, the latter was oxidized first.

During overoxidation, the electrochemical redox activity of PT is destroyed. This was found to be accompanied by a loss of UV-vis absorption bands around $\lambda = 480 \text{ nm}$ for neutral and $\lambda = 700 \text{ nm}$ for oxidized PT; the only band observed is around $\lambda = 390 \text{ nm}$ [1062]. In addition to electrochemical overoxidation, which causes degradation of the polymer, chemical degradation by reaction with other substances of the environment has been observed. Studies performed *ex situ* employing UV-vis spectroscopy and infrared spectroscopy led to the conclusion that poly(3-methylthiophene) is stable in its doped state (dopant BF_3 -ethyl ether), whereas PT with the same dopant reacts (most likely with oxygen from the air) as evidenced by a color change [1063]. A study of PT degradation caused by doping-undoping cycles in a nonaqueous solution that contained tetrafluoroborate anions with XPS was reported by

Takenaka et al. [1064]. The observed changes were attributed to chemical reactions that involved fluoride ions released from the electrolyte anions. Wang et al. [1065] investigated PT degradation. The pristine film of PT showed known absorption bands in UV-vis spectra around $\lambda = 488$ and 871 nm . Upon degradation caused by electrode potential excursions to values beyond $E_{\text{SCE}} = 2.2 \text{ V}$, only an absorption around $\lambda = 410 \text{ nm}$ was observed. No absorption indicative of transitions that involve bipolaronic states, which, in turn, are indicative of electrical conductivity, were found. The observed absorption is, instead, suspiciously similar to the value found for quinquethienyl ($\lambda = 416 \text{ nm}$ [1066]). This implies a severely reduced effective conjugation length. Further *ex situ* investigations with infrared spectroscopy provided evidence of the formation of C=O groups (passivation of the film).

Fink et al. [1067] reported results of electron diffraction and electron energy loss spectroscopy measurements of (PT) films performed *ex situ* that yielded data that describe the crystalline structure.

PT and poly(3-methylthiophene) were electropolymerized on iron substrates and characterized *ex situ* with various spectroscopic techniques [1068]. Results imply strong similarities to the corresponding polymers prepared on platinum electrodes. The deposition of these polymers on iron has been suggested as corrosion protection [1069, 1070]. Ochmanska and Pickup [1071] reported data on the conductivity of poly(3-methylthiophene) recorded *in situ* using a somewhat complicated technique described elsewhere in detail [1072]. A linear correlation between electrode potential and conductivity was found. Within an extended range of electrode potentials, Ofer et al. [1073] clearly identified the range of electrode potentials wherein a maximum of conductivity is observed. In slight disagreement with the data of Ochmanska and Pickup, a deviation from the described relationship is observed. As found with most other polymers, a decrease in conductivity is observed in the case of poly(3-methylthiophene) after passing the second oxidation current wave in the CV.

Bazzaoui et al. [1074] investigated PT deposits on oxidizable (zinc, iron, and aluminum) and noble metals (platinum) using resonance Raman spectroscopy and XPS. Data imply better structural organization of the PT films on the former metals with an increase of disorder with increasing film thickness for all metals. With Al, in particular, XPS data suggest specific interactions between the metal and the C_α atoms of the thiophene unit. This may, in part, explain the especially strong adhesion of the film on this metal. Redox reactions at the interface between poly(3-methylthiophene) and aluminum were studied by Uehara et al. [1075]. With the doped polymer used for deposition of aluminum corrosion and undoping with formation of AlClO_4 were observed. With the undoped polymer, no such reaction was found. This redox reaction may play a role in the rectifying and photovoltaic effects shown by this interface.

Hong et al. [1076] prepared polymers of semifluoroalkyl-substituted thiophenes by chemical and electrochemical oxidation. The effect of fluorination as observed in cyclic voltammetry and, in particular, in UV-vis spectroscopy was attributed to intermolecular interactions effected by the end-standing fluor substituents at the alkyl chains. A direct influence of these groups on the polymer backbone was considered unlikely because of the length of the alkyl chain between the thiophene ring and the fluoro substituents.

A copolymer of 3-alkylthiophene and an azo chromophore (2-[*N*-ethyl-*N*-[(4-notrophenyl)azo]phenyl]amino]ethyl-3-thienylacetate) was prepared chemically by Zag rska et al. [1077]. From

a polymer solution in chloroform, films were cast on ITO electrodes for *in situ* UV-vis spectroscopy and cyclic voltammetry. In addition, vibrational spectra were recorded *ex situ*. The azo compound resulted in an additional redox peak pair attributed to the azo chromophore. The UV-vis absorption spectrum with bands caused by the polythiophene and the azo chromophore showed evidence of the mutual influence of the doping state and the absorption energy. The resonance conditions effective in surface resonance Raman spectroscopy with laser excitation at $\lambda_L = 514$ nm were considerably changed as compared to PT. In the oxidized state, the additional absorption caused by the azo chromophore decreased the resonance effect for the polymer backbone considerably, whereas the resonance conditions for the azo chromophore were enhanced. Consequently, in the reduced state, the vibrational spectra were dominated by the polymer, whereas in the oxidized state, the modes of the chromophore were predominant.

A copolymer of 3-methylthiophene with functionalized thiophenes that carry activated ester groups was prepared by electropolymerization by Li et al. [1078]. The conductivity of the film was comparable to values found with unsubstituted PT. The obtained films can be used as substrates for the preparation of further functionalized electrodes. Further details, especially with respect to the polymerization mechanism (preferably radical cation dimerization) and suitable thiophene-substituted thiophene combinations have been reported elsewhere [1079]. With *p*-nitrophenyl substituents and further substituents, the electrochemical features of the polymer backbone and the nitro group were observed [1080]. The electrochemical behavior of the nitro group was more complex than in solution. The presence of the latter group had a dramatic effect on the π system of the polymer chain in terms of electrochemical activity. The redox activity of the polymer was lost rapidly with some of the investigated compounds. An electrochemically formed polymer of 3-thiophene acetic acid was described by Li and Aoki [1081]. In aqueous solutions, oxidation of the film caused a change of the pH value of the solution toward lower, acidic values. This was explained by assuming an activation of the dissociation of the carboxylic acid by means of polymer backbone oxidation. Examination of the polymer in variously doped states *ex situ* with infrared spectroscopy showed a change of the absorbance of the carboxyl group with a state of oxidation corresponding closely with the pK_a value derived from the electrochemical and pH measurements. Bartlett and Dawson [1082] observed rapid passivation of the polymer film in their investigation of the same polymer. This was identified as being specific for this compound with similar esters, no passivation was found. Most likely the activation of the acidic function with the effects observed elsewhere was absent with these compounds.

Latonen et al. [1083] prepared a copolymer of 3-octylthiophene and paraffenylene. The recorded *in situ* infrared spectra showed bands previously found with pure polyparaffenylene (PPP) and POT. A copolymer of 3,4-*b*,3',4'-*d*:dithienothiophene and aniline was studied by Mirzynska et al. [1084] using the rotating ring-disk electrode method.

In an attempt to modify the electrochromic properties of PT, Mudigonda et al. [1085] studied a series of polymerized *N*-substituted 2-(5'-vinyl-2'-thienyl)-5-(2''-thienyl)pyrroles. After chemical oxidation, postprocessing by electrochemically induced cross-linking on platinum and ITO substrates was performed. UV-vis absorption recorded *in situ* in a two electrode arrangement showed a band at $\lambda = 330$ – 380 nm attributed to the $\pi \rightarrow \pi^*$ transition. Upon doping, bands around $\lambda = 450$ – 500 and

850–954 nm were observed. The former band was assigned to the radical cation of the three ring moiety, whereas the latter band was attributed to the radical cation of the six ring moiety. A broad absorption remaining after dedoping–reduction around $\lambda = 400$ – 500 nm was assigned to the neutral sexiaryl monomer. Despite the variation in substituents, the electrochromic properties did not change significantly. Subsequently, copolymers of 5-vinylterthiophene and *N*-phenyl-2-(5'-vinyl-2'-thienyl)-5-(2''-thienyl)pyrrole, of *N*-vinylcarbazole and 5-vinylterthiophene, and *N*-vinylcarbazole and *N*-phenyl-2-(5'-vinyl-2'-thienyl)-5-(2''-thienyl)pyrrole were prepared with different stoichiometries. These polymers showed good cyclability and good color contrast.

Emge and Bäuerle [1086] electropolymerized bithiophenes substituted with diaminopyridine or diaminotriazine. The unprotected amino groups did not interfere with the polymerization reaction. Electrochemically induced doping of the polymer resulted in changes of the UV-vis spectra similar to α , α' -linked PT. The electrochemical properties as evidenced with cyclic voltammetry were considerably changed after the addition of the complementary base uracil. The hydrogen bonding interaction (i.e., basically chemical information) can thus be transformed into an electrical signal.

Poly-benzo(1,2-*b*;3-4*b'*)dithiophene was electropolymerized by Taliani et al. [1087]. Based on *in situ* recorded UV-vis spectra, the low electronic conductivity was explained by the absence of a low-energy doping-induced electronic absorption indicative of mobile charge carriers. This was in agreement with a similar absence in *ex situ* infrared spectra, the low level of doping (one anion per eight monomer units), and the relatively large value of the interband transition energy. The latter argument seems questionable when this value is compared with similar values of other polymers like PPP.

Marrec et al. [1088] electropolymerized polyethers that possess two 3-thienyl units. Results implied that half of the thiophene units are involved in the polymer formation process. The *in situ* measured UV-vis absorption spectra showed the $\pi \rightarrow \pi^*$ transition at about 390–430 nm for the investigated polymers [1089]. No significant influence of the length of the polyether chain was found, contrary to polymers prepared from monomers with a single thiophene unit only [1090]. Upon oxidation, the position of this band is blue shifted and becomes less intense. A new band that corresponds to the formation of bipolarons was observed at $\lambda_{\max} = 770$ nm. At even higher doping levels, this absorption shifted to $\lambda_{\max} = 620$ nm and an additional absorption around $\lambda_{\max} = 1000$ nm, indicating the emergence of metallic behavior. The change of the position of the $\pi \rightarrow \pi^*$ transition was attributed to a distortion of the conjugated backbone caused by further coupling reactions of still available functional groups in the polymer.

The synthesis of *p*- and *n*-dopable 3-*p*-(trimethylammonium-phenyl)bithiophene and its electrochromic properties was described by Loveday et al. [1091]. These materials have been considered as constituents of supercapacitors. The UV-vis spectra recorded *in situ* during *p* doping were reported in passing only. They showed a decrease of a short wavelength absorption, an increase of an intermediate absorption around $\lambda = 800$ nm, and an absorption with a maximum at about $\lambda = 1525$ nm. Although no assignment was provided, the behavior is basically similar to that reported for most other PTs. For investigations of *n* doping of polyalkylterthiophenes, see [1092].

Because of possible ion-selective effects, pseudo-crown ethers were prepared by electropolymerization from suitably substituted thiophenes by Roncali et al. [1093]. The polymer formed from 1,14-(3-thienyl)-3,6,9,12-tetraoxatetradecane showed an absorption maximum at $\lambda = 430$ nm in the undoped state. Compared to the respective value for poly(3-(3,6,9-trioxadecyl)thiophene), a blue shift of about 50 nm, indicating a shorter mean conjugation length, was found. In the oxidized form, this band was considerably reduced in intensity, and a new band at $\lambda = 750$ nm, attributed to a transition into the upper bipolaron band, was seen. The results were found to be inferior to those of polymers prepared from 3-polyether-substituted monomers. A general review of this field was provided by Fabre and Simonet [1094]; for further details, see also [1095].

Results of spectroscopic investigations of transition-metal-substituted oligothiophenes, considered to be suitable for nonlinear optical applications, were reported by Lancellotti et al. [1096].

Electrooptical properties of composites made of TiO_2 coated with PT based on *in situ* UV-vis spectroscopy were reported by Rammelt et al. [1097]. Optical properties of poly(3,4-ethylenedioxythiophene)-sulfated poly(β -hydroxyether) composite films prepared by electrochemical copolymerization were studied with *in situ* UV-vis spectroscopy by Yamato et al. [1098]. In the reduced state, a strong absorption around $\lambda = 600$ nm, assigned to the $\pi \rightarrow \pi^*$ transition, indicating a bandgap of $\Delta E = 1.6$ eV, was found. The actual position of the absorption maximum depended somewhat on the ratio of the components in the composite. The intensity of this band decreased upon oxidation. A fairly broad feature around $\lambda = 900$ – 1000 nm appeared.

6. MISCELLANEOUS POLYMERS

Poly(*o*-aminophenol) was obtained by electropolymerization in an acidic aqueous solution [1099]. The relationship between electrode potential applied to the polymer film, current, conductivity, and concentration of free spins is displayed in Figure 77. The conductivity passes through a fairly narrow maximum, whereas the concentration of free spins (polarons) stays at high levels. Obviously the presence of free spins is not a sufficient precondition of electric conductivity, perhaps because the polarons are trapped between insulating sections of the polymer.

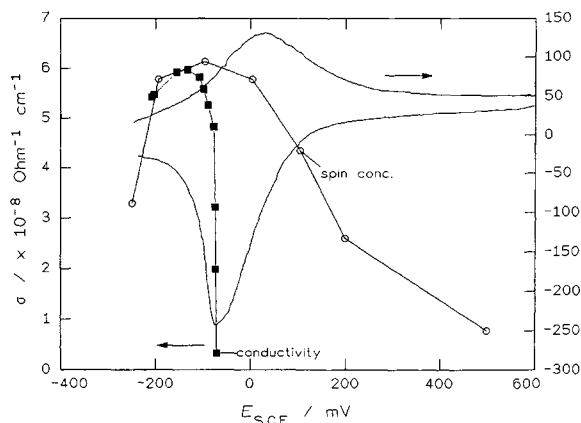


Fig. 77. CV of a film of poly(*o*-aminophenol) in an acidic electrolyte solution with potential-dependent conductivity and concentration of free spins (based on data from [1099]).

Pham et al. [1100] electropolymerized 5-amino-1-naphthol from both aqueous and nonaqueous solutions onto glassy carbon and platinum electrodes. The electrochemically active and conducting films were found to be formed via the amino group based on the infrared spectra recorded *in situ* during the polymerization. With *in situ* Raman spectroscopy, the structure of the film that contained amine and imine links similar to the PANI structure was identified [1101]. Upon oxidation, some amine units are transformed into imine groups.

Agrawal and Jenekhe [1102] reported the electrochemistry and UV-vis spectroscopy of a series of conjugated polyquinolines and polyanthrazolines with systematically varied substituents. The good agreement between the value of the bandgap energy as derived from UV-vis spectroscopy and as derived from electrochemical data (electrode potential of polymer reduction and oxidation) is noteworthy. Despite the fact that such a correlation is logical, experimental support is scant.

Froyer et al. [1103] described a combined chemical-electrochemical routine to obtain PPP on ITO electrodes in a nonaqueous solution. Contrary to all polymerization reactions reviewed herein this reaction proceeds via the reduction of a nickel-dibromophenyl adduct. The film being formed in its neutral, yellowish colored form shows a strong UV-vis absorption around $\lambda = 390$ nm. This is assigned to the interband transition. The position implies a long conjugated structure; this conclusion is supported by infrared data. The polymer could be reduced and oxidized electrochemically. The CVs obtained in a single electrolyte solution showed large redox peaks with prepeaks in both scan directions just before the anodic-cathodic maximum. A thorough interpretation resulted in the conclusion that these prepeaks correspond to the actual onset of reduction-oxidation. Consequently, the potential difference $\Delta E = 2.8$ V corresponds to the energetic difference between the involved molecular orbitals. This value fits nicely with the value of the band gap (interband transition) derived from the UV-vis absorption at 2.8 eV ($\lambda = 390$ nm). Upon oxidation, the intensity of the interband transition diminishes, whereas two bands around 2.65 and 0.9 eV emerge. They are assigned to electronic transitions that involve the presence of bipolarons. No evidence of an optical transition indicative of the existence of polarons was found. During reduction, a strong absorption at about 0.6 eV and a weak absorption around 2.1 eV are observed. Again, the intensity of the interband transition is decreased upon reduction up to the vanishing point. The bands were assigned by taking into account their change as a function of electrode potential to transitions that involve polaron states at intermediate reduction levels and bipolaron states in the fully reduced form of the polymer. A purely electrochemical route via electroreduction of benzene toward PPP was reported by Chang et al. [1104]. Lacaze et al. [1105] prepared PPP electrochemically from a variety of electrolyte solutions under controlled deposition conditions. The structural properties of the obtained films were derived from electrochemical data only. Also via an electrochemical route, Selvan et al. [1106] and Pisarevskaya et al. [1107] prepared PPP. The latter group studied the morphology of the PPP as a function of deposition conditions.

The influence of deposition conditions on the structure of PPP films was studied by Damlin et al. [1108] using *in situ* FTIR spectroscopy. Results indicate that high concentrations of biphenyl (the starting monomer) resulted in PPP with long and cross-linked chains.

Miyashita and Kaneko [1109] studied vapor-deposited films of PPP using cyclic voltammetry and *in situ* UV-vis spectroscopy. In nonaqueous solutions, reversible anion as well as cation doping and dedoping that involve at least two different doping sites with a close correlation between electrochemical and spectroscopical data were found. In an aqueous solution, the electrochemical processes were considerably slower. As an explanation, hindered diffusion of hydrated counterions into the film was proposed. Scanning electron microscopy pictures were considered to support this suggestion. The additional optical absorption bands of the doped PPP film were ascribed to transitions from the valence band into the bipolaron state.

A general treatment of the redox processes of ICPs with special attention to PPP based on considerations of various conceivable processes and species involved therein was provided by Vorotyntsev and Heinze [1110].

Based on theoretical calculations, Brédas et al. [1111] concluded, that bipolarons are energetically favored on PPP as compared to polarons. In a critical review based, in particular, on results of ESR, UV-vis, and vibrational spectroscopies, Furukawa [1112] reconsidered the polaron-bipolaron discussion. For poly(*p*-phenylene) and poly(*p*-phenylene vinylene), Furukawa concluded, that polarons are the dominant species generated by doping. The absence of ESR absorption may be caused by quenching interactions with free spins instead of their absence as already discussed.

Damlin et al. [1113] reported infrared data on poly(paraphenylenevinylene). Various bands associated with atomic movements in the polymer chain were assigned. Upon oxidation, a broad absorption starting at 1700 cm⁻¹ and reaching beyond 5000 cm⁻¹, indicative of mobile charge carriers, was seen. During *n* doping, additional bands were found in the fingerprint region. Bilkiewicz et al. [1114] electrooxidized azulene in a nonaqueous electrolyte solution. CVs and UV-vis spectra recorded *in situ* showed electroactivity of the polyazulene film.

APPENDIX

Acronyms commonly used in surface analysis, surface spectroscopy, and spectroelectrochemistry

AEAPS	Auger electron appearance potential spectroscopy
AES	Auger electron spectroscopy
AFM	Atomic force microscopy
APD	Azimuthal photoelectron diffraction
APS	Appearance potential spectroscopy
ARAES	Angle-resolved Auger electron spectroscopy
ARPEFS	Angle-resolved photoemission extended fine structure
ARUPS	Angle-resolved ultraviolet photoelectron spectroscopy
ATR	Attenuated total reflection spectroscopy
AXAFS	Atomic X-ray absorption fine structure spectroscopy
CD	Circular dichroism
CDAD	Circular dichroism photoelectron angular distribution
CELS	Characteristic energy loss spectroscopy
CL	Chemiluminescence

DAPS	Disappearance potential spectroscopy
DEMS	Differential electrochemical mass spectroscopy
DESERS	De-enhanced surface-enhanced Raman spectroscopy
DRIFT	Diffuse reflection infrared Fourier transform spectroscopy
DS	Desorption spectroscopy
EBMA	Electron beam microanalysis; see EMMA
ECESR	Electrochemical electron spin resonance spectroscopy
ECTDMS	Electrochemical thermal desorption mass spectrometry
EDX	Energy dispersive X-ray (analysis)
EELS	Electron energy loss spectroscopy
EIS	Electron impact spectroscopy
ELEED	Elastic low-energy electron diffraction
ELL	Ellipsometry
ELS	Energy loss spectroscopy
EMIRS	Electrode potential modulated infrared spectroscopy
EM(MA)	Electron microprobe (mass analysis)
EMP	Electron microprobe; see EMMA
EQMB, EQCM	Electrochemical quartz microbalance
ERS	Electroreflectance spectroscopy
ESCA	Electron spectroscopy for chemical analysis
ESD	Electron-stimulated desorption
ESDIAD	Electron-stimulated desorption ion angular distribution
ESR	Electron spin resonance (spectroscopy)
EXAFS	Extended X-ray absorption fine structure (analysis); see also NEXAFS, SEXAFS
EXELFS	Extended electron loss fine structure spectroscopy
FAB	Fast atom bombardment
FD(S)	Flash desorption (spectroscopy)
FES	Field emission spectroscopy
FIM	Field ion microscopy
FIS	Field ion spectroscopy
FMIR	Frustrated multiple internal reflectance (spectroscopy)
FTIR	Fourier transform infrared spectroscopy; see also FTIRRAS, MIRFTIRS, PMFTIRRAS, SNIFTIRS, SPAIRS
FTIRRAS	Fourier transform infrared reflection-absorption spectroscopy
HEED	High-energy electron diffraction
HIID	Heavy-ion-induced desorption
HIXE	Proton-induced X-ray emission spectroscopy
HREELS	High resolution electron energy loss spectroscopy
IES, IETS	Inelastic electron tunneling spectroscopy
ILEED	Inelastic low-energy electron diffraction
IMXA	Ion microprobe X-ray analysis

INS	Ion neutralization spectroscopy	PSD	Photon-stimulated desorption
INSEX	<i>In situ</i> X-ray reflection–transmission diffraction	PTS	Photothermal spectroscopy
IR	Infrared spectroscopy; see also EMIRS, IR-RAS, LPSIRS	PVS	Photovoltage spectroscopy
IRE	Infrared emission spectroscopy	RAIRS	Reflection–absorption infrared spectroscopy
IRRAS	Infrared reflection–absorption spectroscopy; see also PMFTIRRAS	RAS	Raman spectroscopy [also NR(S)]; see also DE-SERS, SERRS, SERS, SRS, SRRS, SUERS
IRS	Internal reflectance spectroscopy	RAS	Reflection anisotropy spectroscopy
IS	Ionization spectroscopy	RBS	Rutherford backscattering
ISS	Ion surface scattering (spectroscopy)	REMPI	Resonance-enhanced multiphoton ionization
IES	Inelastic tunneling spectroscopy	RHEED	Reflected high-energy electron diffraction
ITO	Indium–tin oxide	RRS	Resonance Raman spectroscopy
LD	Laser desorption	SAES	Scanning Auger electron spectroscopy
LEED	Low-energy electron diffraction	SANS	Small-angle neutron scattering
LEEM	Low-energy electron microscopy	SC	Surface conductivity (measurement)
LEIS	Low-energy ion scattering	SHEED	Surface high-energy electron diffraction
LID	Laser-induced fluorescence	SEM	Scanning electron microscope
LIMS	Laser ionization mass spectroscopy	SERS	Surface-enhanced Raman spectroscopy
LIPS	Laser-induced plasma spectroscopy	SERRS	Surface-enhanced resonance Raman spectroscopy
LPSIRS	Linear potential scan infrared spectroscopy	SEXAFS	Surface-extended X-ray absorption fine structure (analysis) spectroscopy
MBRS	Molecular beam relaxation spectroscopy	SFG	Sum frequency generation
MBS	Mossbauer spectroscopy	SHG	Second harmonic generation
MBSS	Molecular beam surface scattering	SI	Surface ionization
MEIS	Medium-energy ion scattering	SIMS	Secondary ion mass spectroscopy
MER(S)	Multiple external reflectance (spectroscopy)	SNIFTIRS	Subtractively normalized interfacial Fourier transform infrared spectroscopy
MIR(S)	Multiple internal reflectance (spectroscopy)	SPAIR(S)	Single potential alteration infrared (spectroscopy)
MIRFTIRS	Multiple internal reflection Fourier transform infrared spectroscopy	SPM	Scanning probe microscopy; see STM, SEM, AFM
MSS	Molecule–surface scattering	SRRS	Surface resonance Raman spectroscopy
NEXAFS	Near edge X-ray absorption fine structure spectroscopy	SRS	Surface Raman spectroscopy; specular reflectance spectroscopy
NR(S)	Normal Raman (spectroscopy)	STM	Scanning tunneling microscope
OSEE	Optically stimulated exoelectron spectroscopy	SUERS	Surface-unenhanced Raman spectroscopy
OTE	Optically transparent electrode	SXAPS	Soft X-ray appearance potential spectroscopy
PAM	Photoacoustic method	SXES	Soft X-ray emission spectroscopy
PAS	Photoacoustic spectroscopy	TDMS, TDS	Thermodesorption mass spectroscopy
PASCA	Positron annihilation spectroscopy for chemical analysis	TEAS	Thermal energy atom scattering
PAX	Photoelectron spectroscopy with adsorbed xenon	THG	Third harmonic generation
PBD	Probe beam deflection	TLC	Thin layer cell
PCS	Photocurrent spectroscopy	TPD	Temperature-programmed desorption
PD	Photodesorption	TPRS	Temperature-programmed reaction spectroscopy
PDIRS	Potential-difference infrared spectroscopy	UPS	Ultraviolet photoelectron spectroscopy
PEEM	Photoelectron emission microscopy	UV–vis	Spectroscopy with ultraviolet and visible light
PES	Photoelectron spectroscopy; see also ESCA, UPS, XPS	XANES	X-ray absorption near edge structure
PhD	Photoelectron diffraction	XES	X-ray emission spectroscopy
PI	Penning ionization	XPD	X-ray photoelectron diffraction
PIXE	Particle-induced X-ray emission spectroscopy	XPS	X-ray photoelectron spectroscopy
PMFTIRRAS	Polarization-modulated Fourier transform infrared reflection absorption spectroscopy	XSW	X-ray standing wave
PMRS	Potential modulated reflectance spectroscopy		

Acknowledgments

Support for this work from the Deutsche Forschungsgemeinschaft, the Fonds der Chemischen Industrie, and the Volkswagen-Stiftung is gratefully appreciated. Various co-workers and colleagues have contributed to this overview. Invaluable contributions by M. Probst, V. Brandl, J. Lippe, and A. Malinauskas are gratefully acknowledged.

REFERENCES

1. A. Bree, *Synth. Met.* 54, 1 (1993).
2. V. V. Walatka, M. M. Labes, and J. H. Peristein, *Phys. Rev. Lett.* 31, 1139 (1973); M. M. Labes, P. Love, and L. F. Nichols, *Chem. Rev.* 79, 1 (1979).
3. A. J. Banister and I. B. Gorrell, *Adv. Mater.* 10, 1415 (1998).
4. N. F. Colaneri and L. W. Shacklette, *IEEE Trans. Instrum. Meas.* 41, 291 (1992).
5. J. Joo and A. J. Epstein, *Appl. Phys. Lett.* 65, 2278 (1994).
6. Y. Gofer, H. Sarker, J. G. Killian, T. O. Poehler, and P. C. Searson, *Appl. Phys. Lett.* 71, 1582 (1997); B. I. Bairachnyi, A. V. Vasilchenko, L. V. Lyashok, T. V. Orekhova, and T. F. Baikova, *Russ. J. Appl. Chem. (Engl. Transl.)* 72, 225 (1999).
7. S. Sarangapani, B. V. Tilak, and C. P. Chen, *J. Electrochem. Soc.* 143, 3791 (1996).
8. O. Haas, D. Häringer, R. Kötz, P. Novák, B. Piro, and M.-C. Pham, "Proceedings of the 50th ISE Meeting," Pavia, Italy, 1999, Abstract 3b-328.
9. Y. L. Kogan, G. V. Gedrovich, M. I. Rudakova, and L. S. Fokeeva, *Russ. J. Electrochem.* 31, 689 (1995); M. Garcia, F. Fusalba, and D. Belanger, "Proceedings of the Electrochemical Society Fall Meeting," San Antonio, 1996, Extended Abstracts 749.
10. H. Yamamoto, M. Oshima, T. Hosaka, and I. Isa, *Synth. Met.* 104, 33 (1999).
11. T. Tatsuma, F. Matsui, E. Shouji, and N. Oyama, *J. Phys. Chem.* 100, 14,016 (1996).
12. S. C. R. Catharino, P. S. de Freitas, C. N. Plo de Fonseca, and M.-A. de Paoli, "Proceedings of the 50th ISE Meeting," Pavia, Italy, 1999, Abstract 1-805.
13. M. Trojanowicz, T. K. Velkrawczyk, and P. W. Alexander, *Chem. Anal.* 42, 199 (1997); G. Bidan, *Sens. Actuators, B* 6, 45 (1992); C. Conn, S. Sestak, A. T. Baker, and J. Unsworth, *Electroanal.* 10, 1137 (1998); G. Cui, J. S. Lee, S. J. Kim, H. Nam, G. S. Cha, and H. D. Kim, *Analyst* 123, 1855 (1998).
14. W. Schuhmann, ACS Symposium Series, Vol. 556, p. 110. American Chemical Society, Washington, DC, 1994.
15. J. L. Camalet, J. C. Lacroix, S. Aeiyaeh, K. Chaneching, and P. C. Lacaze, *J. Electroanal. Chem.* 416, 179 (1996).
16. J. L. Camalet, J. C. Lacroix, S. Aeiyaeh, and P. C. Lacaze, *J. Chim. Phys.-Chim. Biol.* 95, 1494 (1998).
17. J. L. Camalet, J. C. Lacroix, S. Aeiyaeh, K. I. C. Ching, and P. C. Lacaze, *Synth. Met.* 102, 1386 (1999).
18. T. D. Nguyen, J. L. Camalet, J. C. Lacroix, S. Aeiyaeh, M. C. Pham, and P. C. Lacaze, *Synth. Met.* 102, 1388 (1999).
19. P. J. Kinlen, D. C. Silverman, and C. R. Jeffreys, *Synth. Met.* 85, 1327 (1997).
20. G. R. Möhlmann, in "Development and Application of Optically Nonlinear Polymers, III" (H. Kuzmany, M. Mehring, and S. Roth, Eds.) Springer Series in Solid State Science, Vol. 91, p. 232. Springer-Verlag, Berlin, 1989; G. R. Möhlmann, *Synth. Met.* 67, 77 (1994).
21. K. G. Chittibabu, L. Li, M. Kamath, J. Kumar, and S. K. Tripathy, *Chem. Mater.* 6, 475 (1994).
22. A. A. Syed and M. K. Dinesan, *Talanta* 38, 815 (1991).
23. F. Lux, *Polymer* 35, 2915 (1994).
24. S. C. K. Misra and S. Chandra, *Indian J. Chem., Sect. A* 33, 583 (1994).
25. J. Heinze, in "Topics in Current Chemistry," Vol. 152, p. 3. Springer-Verlag, Berlin, 1990.
26. S. Roth and W. Graupner, *Synth. Met.* 55-57, 3623 (1993).
27. E. T. Kang, K. G. Neoh, and K. L. Tan, *Prog. Polym. Sci.* 23, 277 (1998).
28. T. V. Vernitskaya and O. N. Efimov, *Usp. Khim.* 66, 489 (1997).
29. P. Novák, K. Müller, K. S. V. Santhanam, and O. Haas, *Chem. Rev.* 97, 207 (1997).
30. M. D. Imisides, R. John, P. J. Riley, and G. G. Wallace, *Electroanal.* 3, 879 (1991).
31. G. K. Chandler and D. Pletcher, in "Electrochemistry," Vol. 10, p. 117. Royal Chemistry Society, London, 1985.
32. F. Jonas and G. Heywang, *Electrochim. Acta* 39, 1345 (1994).
33. M. C. Bernard, A. Hugot-Le Goff, S. Joiret, N. N. Dinh, and N. N. Toan, *Synth. Met.* 102, 1383 (1999).
34. K. Müllen and G. Wegner, Eds., "Electronic Materials: The Oligomeric Approach." Wiley-VCH, Weinheim, 1998.
35. J. Alper, *Science* 246, 208 (1989).
36. G. Inzelt, *Magy. Kem. Foly.* 105, 293 (1999).
37. A. G. MacDiarmid, *Synth. Met.* 84, 27 (1997); B. Scrosati, "Application of Electroactive Polymers." Chapman & Hall, New York, 1993.
38. A. Wieckowski, Ed., "Interfacial Electrochemistry." Dekker, New York, 1999.
39. R. Holze, "Surface and Interface Analysis: An Electrochemists Toolbox." Springer-Verlag, Heidelberg, in press.
40. J. Lipkowski and P. N. Ross, Eds., "Adsorption of Molecules at Metal Electrodes." VCH, New York, 1992.
41. H. D. Abruna, Ed., "Electrochemical Interfaces." VCH, New York, 1991.
42. R. J. Gale, Ed., "Spectroelectrochemistry." Plenum, New York, 1988.
43. R. Caudano, J.-M. Gilles, and A. A. Lucas, Eds., "Vibrations at Surfaces." Plenum, New York, 1982.
44. R. Holze, *Bull. Electrochem.* 10, 45 (1994).
45. *Spectrosc. Int.* 2(6), 43 (1990).
46. U. Reuter, "Abkürzungen und Akronyme in der Chemie." GIT-Verlag, Darmstadt, 1988.
47. R. Holze, *Bull. Electrochem.* 10, 45 (1994).
48. *Spectrosc. Int.* 2(6), 43 (1990).
49. U. Reuter, "Abkürzungen und Akronyme in der Chemie." GIT-Verlag, Darmstadt, 1988.
50. J. A. Bardwell, G. I. Sproule, and M. J. Graham, *J. Electrochem. Soc.* 140, 50 (1993).
51. J. A. Bardwell, G. I. Sproule, D. F. Mitchell, B. MacDougall, and M. J. Graham, *J. Chem. Soc., Faraday Trans.* 87, 1011 (1991).
52. J. Lippe, Dissertation, Universität Oldenburg, 1991.
53. M. B. G. Pilkington, B. A. Coles, and R. G. Compton, *Anal. Chem.* 61, 1787 (1989).
54. A. J. Bard and L. R. Faulker, "Electrochemical Methods," p. 577ff. Wiley, New York, 1980.
55. B.-S. Kim and S.-M. Park, *J. Electrochem. Soc.* 140, 115 (1993).
56. J. Daub, J. Salbeck, and I. Aurbach, *Angew. Chem.* 100, 278 (1988).
57. J. A. Caram and C. Gutierrez, *J. Electroanal. Chem.* 323, 213 (1992).
58. P. H. Schmidt and W. Plieth, *J. Electroanal. Chem.* 201, 163 (1986).
59. D. M. Kolb, in "Spectroelectrochemistry" (R. J. Gale, Ed.), p. 87. Plenum, New York, 1988.
60. W. N. Hansen, *Adv. Electrochem. Electrochem. Eng.* 9, 1 (1973).
61. B. D. Cahan and R. F. Spaner, *Surf. Sci.* 16, 166 (1969); B. D. Cahan, *Surf. Sci.* 56, 354 (1976); C. T. Chen and B. D. Cahan, *J. Electrochem. Soc.* 129, 17 (1982); R. Parson and W. H. M. Visscher, *J. Electroanal. Chem.* 36, 329 (1972); J. L. Ord and F. C. Ho, *J. Electrochem. Soc.* 118, 46 (1971); J. Horkans, B. D. Cahan, and E. Yeager, *Surf. Sci.* 46, 1 (1974); J. M. M. Droog, P. T. Alderliesten, and G. A. Bootsma, *J. Electroanal. Chem.* 99, 173 (1979); S. Gottesfeld and S. Srinivasan, *J. Electroanal. Chem.* 86, 89 (1978); T. Ohtsuka and K. E. Heiser,

- J. Electroanal. Chem.* 100, 319 (1979); J. L. Ord, *J. Electrochem. Soc.* 129, 335; 767 (1982).
62. R. Adzic, E. Yeager, and B. D. Cahan, *J. Electrochem. Soc.* 121, 474 (1974); R. Adzic, B. D. Cahan, and E. Yeager, *J. Chem. Phys.* 58, 1780 (1973); J. Horkans, B. D. Cahan, and E. Yeager, *J. Electrochem. Soc.* 122, 1585 (1975).
63. L. Tronstad, *Trans. Faraday Soc.* 31, 1151 (1935); M. W. Humphreys and R. H. Parsons, *J. Electroanal. Chem.* 82, 369 (1977); 75, 427 (1977); K. Kunimatsu and R. H. Parsons, *J. Electroanal. Chem.* 100, 335 (1979).
64. M. Zagorska, K. Bruckzewski, and R. Minkowski, *Mater. Sci.* 13, 307 (1987); G. C. Winston and C. M. Carli, *J. Electrochem. Soc.* 135, 789 (1988); S. Gottesfeld, A. Renold, and S. W. Feldberg, *J. Electrochem. Soc.* 134, 271 (1987); C. M. Carlin, L. J. Kepley, and A. J. Bard, *J. Electrochem. Soc.* 132, 353 (1985); F. Chao, M. Costa, E. Museux, and E. Levart, *Elektrokhimiya* 29, 57 (1993).
65. M. J. Dignam, in "Vibrations at Surfaces" (R. Caudano, J.-M. Gilles, and A. A. Lucas, Eds.). Plenum, New York, 1982; R. C. Kainthla and J. O'M. Bockris, *J. Electrochem. Soc.* 135, 134C (1988).
66. R. M. Corn, in "Adsorption of Molecules at Metal Electrodes" (J. Lipkowski and P. N. Ross, Eds.). p. 347 and references therein. VCH, New York, 1992.
67. G. L. Richmond, in "Electroanalytical Chemistry" (A. J. Bard, Ed.), Vol. 17, p. 87. Dekker, New York, 1991.
68. Y. R. Shen, *J. Electrochem. Soc.* 135, 142C (1988); in "Chemistry and Structures at Interfaces" (R. B. Hall and A. B. Ellis, Eds.). VCH, New York, 1986.
69. H. Gerischer and W. Mindt, *Electrochem. Acta* 13, 1329 (1968); R. Memming and G. Schwandt, *Surf. Sci.* 4, 109 (1966); M. Matsumara and S. R. Morrison, *J. Electroanal. Chem.* 144, 113 (1983); 147 (1983) 157; H. Gerischer and M. Liibke, *Ber. Bunsen. Ges. Phys. Chem. NF* 24, 378 (1960); H. Gerischer and F. Beck, *Z. Phys. Chem. NF* 24, 378 (1960); W. P. Gomes, T. Freund, and S. R. Morrison, *J. Electrochem. Soc.* 115, 818 (1968); E. C. Dutoit, F. Cardon, and W. P. Gomes, *Ber. Bunsen. Ges. Phys. Chem.* 80, 1285 (1976); Y. Maeda, A. Fujishima, and K. Honda, *J. Electrochem. Soc.* 128, 1781 (1981); J. F. McAleer and L. M. Peter, *Faraday Discuss. Chem. Soc.* 70, 67 (1980); U. Stimming, *J. Electrochim. Acta* 31, 415 (1986); P. C. Searson, R. M. Latanision, and U. Stimming, *J. Electrochem. Soc.* 135, 1358 (1988); L. M. Peter, *Ber. Bunsen. Ges. Phys. Chem.* 91, 419 (1987); Y. Byun and B. W. Wessels, *J. Electrochem. Soc.* 135, 144C (1988); S. R. Morrison, "Electrochemistry of Semiconductors and Oxidised Metal Electrodes." Plenum, New York, 1980; M. W. Peterson and B. A. Parkinson, *J. Electrochem. Soc.* 135, 1424 (1988).
70. R. I. Tucceri and D. Posadas, *Electrochim. Acta* 32, 27 (1987).
71. G. Schiavon, S. Sitran, and G. Zotti, *Synth. Met.* 32, 209 (1989).
72. R. Holze and J. Lippe, *Synth. Met.* 38, 99 (1990).
73. J. Lippe, Dissertation, Universität Oldenburg, 1991.
74. E. M. Genies and P. Noel, *Synth. Met.* 57, 4192 (1993).
75. E. W. Paul, A. J. Ricco, and M. S. Wrighton, *J. Phys. Chem.* 89, 1441 (1985).
76. J. Kankare and E. L. Kupila, *J. Electroanal. Chem.* 322, 167 (1992)
77. G. Inzelt, "Proceedings of the 50th ISE Meeting," Pavia, Italy, 1999, Abstract 3b-120.
78. J. Kankare and E. L. Kupila, *J. Electroanal. Chem.* 322, 167 (1992).
79. M. C. Morvant and J. R. Reynolds, *Synth. Met.* 92, 57 (1998).
80. E. Lankinen, G. Sundholm, P. Talonen, T. Laitinen, and T. Saario, *J. Electroanal. Chem.* 447, 135 (1998).
81. E. Lankinen, M. Pohjakallio, G. Sundholm, P. Tolonen, T. Laitinen, and T. Saario, *J. Electroanal. Chem.* 447, 167 (1997).
82. L. Charny, T. Saario, and V. A. Marichev, *Surf. Sci.* 312, 422 (1994).
83. R. John, A. Talaie, and G. G. Wallace, *J. Electroanal. Chem.* 319, 365 (1991).
84. A. Talaie and G. G. Wallace, *Solid State Ionics* 70, 692 (1994).
85. R. L. Deutscher, S. Fletcher, and J. A. Hamilton, *Electrochim. Acta* 31, 585 (1986).
86. J. Mcbreen, W. E. O'Grady, D. E. Sayers, and C. Y. Yang, "Proceedings of the ECS Meeting," Philadelphia, 1987, Abstract 523.
87. M. Fleischmann, P. Graves, I. Hill, J. Robinson, and A. Oliver, "Proceedings of the ECS Meeting," Cincinnati, 1984, Abstract 427; *J. Electrochem. Soc.* 135, 144C, 150C (1988).
88. T. Ikashoji and T. Iwasaki, *Inorg. Chem.* 27, 1123 (1988).
89. M. Fleischmann and B. W. Mao, *J. Electroanal. Chem.* 247, 311 (1988).
90. J. MCBreen, "Proceedings of the ECS Meeting," St. Louis, 1992, Abstract 35 and references therein.
91. M. V. Laue, "Röntgenstrahlinterferenzen." Akad. Verlagsgesellschaft, Frankfurt-am-Main, 1960.
92. G. Materlik, J. Zegenhagen, and W. Uelhoff, *Phys. Rev. B* 32, 5502 (1985).
93. J. H. White, in "Electrochemical interfaces" (H. D. Abruna, Ed.), p. 133. VCH, New York, 1991.
94. M. H. Dean, A. Pinkowski, and U. Stimming, *J. Electrochem. Soc.* 135, 143C (1988); C. L. Li, L. D. Bell, C. P. Bankston, and W. J. Kaiser, "Proceedings of the ECS Meeting," Honolulu, 1987, Abstract 1472; O. Lev, F.-R. Fan, and A. J. Bard, *J. Electrochem. Soc.* 135, 783 (1988); F. F. Fan and A. J. Bard, *Anal. Chem.* 60, 751 (1988); D. H. Craston, C. W. Lin, and A. J. Bard, *J. Electrochem. Soc.* 135, 785 (1988); L. D. McCormick, M. H. Dean, U. Stimming, T. Thundat, T. Nagahara, and S. M. Lindsay, *J. Electrochem. Soc.* 135, 144C (1988); R. S. Robinson, *J. Electrochem. Soc.* 135, 143C (1988); L.-L. Ni, L. D. Bell, C. P. Bankston, and W. J. Kaiser, *J. Electrochem. Soc.* 135, 144C (1988); P. Lustenberger, H. Rohrer, R. Christoph, and H. Siegenthaler, *J. Electroanal. Chem.* 243, 225 (1988).
95. P. K. Hansma, in "Vibrational Spectroscopy of Molecules on Surfaces" (J. T. Yates and T. E. Madey, Eds.), p. 135. Plenum, New York, 1987.
96. R. Yang, W. H. Smyrl, and D. F. Evans, *J. Phys. Chem.* 96, 1428 (1992).
97. A. A. Gewirth and K. J. Hanson, *Interface* 2, 37 (1993).
98. R. Mohr Rynders and R. C. Alkire, "Proceedings of the ECS Meeting," St. Louis, 1992, Abstract 475; C.-C. Chen, S. M. Vesecky, and A. A. Gewirth, *J. Am. Chem. Soc.* 114, 451 (1992); B. J. Cruickshank, A. A. Gewirth, R. Mohr Rynders, and R. C. Alkire, *J. Electrochem. Soc.* 139, 2829 (1992); S. Manne, P. K. Hansma, J. Massie, V. B. Elings, and A. A. Gewirth, *Science* 251, 183 (1991).
99. R. Holze, J. Schneider, and C. H. Hamann, *Ber. Bunsen. Ges. Phys. Chem.* 92, 1319 (1988).
100. C. Barbero, M. C. Miras, R. Kötz, and O. Haas, *Solid State Ionics* 60, 167 (1993).
101. R. Kötz, C. Barbero, and O. Haas, *Ber. Bunsen. Ges. Phys. Chem.* 97, 427 (1993).
102. M. A. Vorotyntsev, C. Lopez, and E. Vieil, *J. Electroanal. Chem.* 368, 155 (1994).
103. M. F. Mathias, *J. Electroanal. Chem.* 407, 115 (1996).
104. C. Barbero, M. C. Miras, and R. Kötz, *Electrochim. Acta* 37, 429 (1992).
105. O. Wolter and J. Heitbaum, *Ber. Bunsen. Ges. Phys. Chem.* 88, 6 (1984).
106. B. Bittins-Cattaneo, E. Cattaneo, P. Königshoven, and W. Vielstich, in "Electroanalytical Chemistry" (A. J. Bard, Ed.), Vol. 17, p. 181. Dekker, New York, 1991; S. Wasmus, E. Cattaneo, and W. Vielstich, *Electrochim. Acta* 35, 771 (1990); D. Tegtmeier, A. Heindrichs, and J. Heitbaum, *Ber. Bunsen. Ges. Phys. Chem.* 93, 201 (1989); K. Nishimura, R. Ohnishi, K. Kunimatsu, and M. Enyo, *J. Electroanal. Chem.* 258, 219 (1989); H. Nakajima, H. Kita, K. Kunimatsu, and A. Aramata, *J. Electroanal. Chem.* 201, 175 (1986); Y. Hirata, K. Suga, and M. Fujihira, *Chem. Lett.* 1990, 1155 (1990); M. Fujihira and T. Noguchi, *J. Electroanal. Chem.* 347, 457 (1993).
107. S. Wasmus, S. R. Samms, and R. F. Savinell, *J. Electrochem. Soc.* 142, 1183 (1995).
108. R. Holze, Habilitationsschrift, Universität Oldenburg, 1988.
109. R. G. Compton and A. M. Waller, in "Spectroelectrochemistry" (R. J. Gale, Ed.), p. 87. Plenum, New York, 1988.

110. L. Dunsch and A. Petr, *Ber. Bunsen. Ges. Phys. Chem.* 97, 436 (1993).
111. A. Heinzel, Dissertation, Universität Oldenburg, 1985.
112. R. Holze, *Collect. Czech. Chem. Commun.*, in press.
113. R. Holze, Habilitationsschrift, Universität Oldenburg, 1989.
114. R. Holze and J. Lippe, *Bull. Electrochem.* 8, 516 (1992).
115. R. Holze, "Surface and Interface Analysis: An Electrochemists Toolbox." Springer-Verlag, Heidelberg, in press.
116. P. A. Christensen, A. Hamnett, and P. R. Trevellick, *J. Electroanal. Chem.* 242, 23 (1988).
117. R. Holze, *Electroanalysis* 3, 833 (1991).
118. Z. Q. Tian, B. Ren, Q. J. Huang, J. L. Yao, X. Q. Li, J. S. Gao, W. B. Cai, C. X. She, and Y. Xie, in "Proceedings of the XVI International Conference on Raman Spectroscopy" (A. M. Heyns, Ed.). Wiley, New York, 1998.
119. T. Iuzak, M. Beltowska-Brzezinska, and R. Holze, *Electrochim. Acta* 38, 717 (1993).
120. R. Holze, T. Iuzak, and M. Beltowska-Brzezinska, *Electrochim. Acta* 35, 1345 (1990).
121. T. Iuzak, M. Beltowska-Brzezinska, and R. Holze, *J. Appl. Electrochem.* 27, 999 (1997).
122. M. Bron, Dissertation, Technische Universität Chemnitz, 1998; M. Bron and R. Holze, *Surf. Sci.*, to appear.
123. B. J. Barner, M. J. Green, E. I. Saez, and R. M. Corn, *Anal. Chem.* 63, 55 (1991).
124. Y. Honda, M.-B. Song, and M. Ito, *Chem. Phys. Lett.* 273, 141 (1997).
125. C. Korzeniewski, *Crit. Rev. Anal. Chem.* 27, 81 (1997).
126. L.-W. H. Leung and M. J. Weaver, *J. Electroanal. Chem.* 240, 341 (1988).
127. X. D. Jiang, S. C. Chang, and M. J. Weaver, *J. Chem. Soc. Faraday Trans.* 89, 223 (1993).
128. M. Osawa, K. Yoshii, K. Ataka, and T. Yotsuyanagi, *Langmuir* 10, 640 (1994).
129. S.-C. Chang, Y. Ho, and M. J. Weaver, *J. Am. Chem. Soc.* 113, 9506 (1991).
130. S.-C. Chang, L.-W. H. Leung, and M. J. Weaver, *J. Phys. Chem.* 94, 6013 (1990).
131. J. Daschbach, D. Heisler, and S. Pons, *Appl. Spectrosc.* 40, 489 (1986).
132. P. Gao, S. C. Chang, Z. Zhou, and M. J. Weaver, *J. Electroanal. Chem.* 272, 161 (1989).
133. L.-W. H. Leung and M. J. Weaver, *J. Phys. Chem.* 92, 4019 (1988).
134. L.-W. H. Leung, S.-C. Chang, and M. J. Weaver, *J. Electroanal. Chem.* 266, 317 (1989).
135. L.-W. H. Leung and M. J. Weaver, *J. Electroanal. Chem.* 240, 341 (1988).
136. J. L. J. Daschbach, J. J. Smith, and M. D. Morse, *J. Electroanal. Chem.* 209, 387 (1986).
137. T. Ishioka, T. Uchida, and N. Teramae, *Chem. Lett.* 1998, 771.
138. R. E. Malpas and A. J. Bard, *Anal. Chem.* 52, 109 (1980); G. H. Brilmyer and A. J. Bard, *Anal. Chem.* 52, 685 (1980); S. Yoshihara, M. Ueno, Y. Nagae, and A. Fujishima, *J. Electrochem. Soc.* 243, 475 (1988); C. E. Vallet, S. Berns, J. J. Hendrickson, and C. W. White, *J. Electrochem. Soc.* 135, 387 (1988).
139. M. F. Toney and J. McBeen, *Interface* 2, 22 (1993).
140. H. Baumgärtel, H.-W. Jochims, and B. Brutschy, *Z. Phys. Chem. NF* 154, 1 (1987); A. Michalowicz, J. Huet, and A. Gaudemer, *Nouv. J. Chim.* 1982, 79 (1982); M. S. Co, W. A. Hendrickson, K. O. Hodgson, and S. A. Doniach, *J. Am. Chem. Soc.* 105, 1144 (1983); J. C. Poncet and R. Guilard, *Polyhedron* 2, 417 (1983); W. H. Liu, X. F. Wang, T. Y. Teng, and H. W. Huang, *Rev. Sci. Instrum.* 54, 1653 (1983); J. Goulon, P. Friant, J. L. Poncet, R. Guilard, J. Fischer, and L. Ricard, *Springer Ser. Chem. Phys.* 27, 100 (1983); C. Goulon-Ginet, J. Goulon, J. P. Battoni, D. Mansuy, and J. C. Chottard, *Springer Ser. Chem. Phys.* 27, 349 (1983).
141. L. Blum, A. D. Abruna, J. White, J. G. Gordon, II, G. L. Borges, M. G. Samant, and O. R. Melroy, *J. Chem. Phys.* 85, 6732 (1986).
142. W. E. O' Gardy, *J. Electrochem. Soc.* 127, 555 (1980); C. Fierro, R. E. Carbonio, D. Scherson, and E. B. Yeager, *J. Phys. Chem.* 91, 6579 (1987); D. A. Corrigan, R. S. Conell, C. Fierro, and D. A. Scherson, *J. Chem. Phys.* 86, 5009 (1987); D. A. Scherson, C. Fierro, D. Tryk, S. L. Gupta, E. B. Yeager, J. Elbridge, and R. W. Hoffman, *J. Electroanal. Chem.* 184, 419 (1985); D. A. Scherson, S. B. Yao, E. B. Yeager, J. Elbridge, M. E. Kordesch, and R. W. Hoffman, *J. Electroanal. Chem.* 150, 535 (1983); *Appl. Surf. Sci.* 10, 325 (1982); *J. Phys. Chem.* 87, 932 (1983); H. Leidheiser, *J. Electrochem. Soc.* 135, 5C (1988); M. V. Anath and N. V. Parthasarathy, *J. Sci. Ind. Res.* 47, 28 (1988); D. A. Scherson, S. L. Gupta, C. Fierro, E. B. Yeager, M. E. Kordesch, J. Eldridge, R. W. Hoffman, and J. Blue, *Electrochim. Acta* 28, 1205 (1983).
143. Y. C. Jean and K. C. Cheng, "Proceedings of the ECS Meeting," Toronto, 1985, Abstract 676.
144. A. T. Hubbard, *Eur. Spectrosc.* 78, 28 (1988); J. A. Schoeffel and A. T. Hubbard, *Anal. Chem.* 49, 2370 (1977); A. T. Hubbard, J. L. Stickney, M. P. Soriaga, V. K. F. Chia, S. D. Rosasco, B. C. Schardt, T. Solomun, D. Song, J. H. White, and A. Wieckowski, *J. Electroanal. Chem.* 168, 43 (1984); V. K. F. Chia, J. L. Stickney, M. P. Soriaga, S. B. Rosasco, G. N. Salaita, A. T. Hubbard, J. B. Benzinger, and K. W. P. Pang, *J. Electroanal. Chem.* 163, 407 (1984); A. T. Hubbard, *Acc. Chem. Res.* 13, 177 (1980).
145. H. W. Buschmann, S. Wilhelm, and W. Vielstich, *Electrochim. Acta* 31, 939 (1986).
146. S. Wilhelm, W. Vielstich, H. W. Buschmann, and T. Iwasita, *J. Electroanal. Chem.* 229, 377 (1987); S. Wilhelm, H. W. Buschmann, and W. Vielstich, *DECHEMA Monographie* 112, 113 (1988).
147. J. Fritzsche, *J. Prakt. Chem.* 20, 454 (1840).
148. H. Letheby, *J. Chem. Soc.* 15, 161 (1862).
149. F. Goppelsroeder, *C.R. Acad. Sci.* 82, 331; 1392 (1876).
150. A. G. Green and A. E. Woodhead, *J. Chem. Soc.* 97, 2388 (1910).
151. R. Willstätter and S. Dorogi, *Chem. Ber.* 42, 4118 (1909).
152. T. Yasui, *Bull. Chem. Soc. Jpn.* 10, 306 (1935).
153. A. F. Diaz and J. A. Logan, *J. Electroanal. Chem.* 111, 111 (1980).
154. A. A. Syed and M. K. Dinesan, *Talanta* 38, 815 (1991).
155. F. Lux, *Polymer* 35, 2915 (1994).
156. S. C. K. Misra and S. Chandra, *Indian J. Chem., Sect. A* 33, 583 (1994).
157. S. Roth and W. Graupner, *Synth. Met.* 55-57, 3623 (1993).
158. E. T. Kang, K. G. Neoh, and K. L. Tan, *Prog. Polym. Sci.* 23, 277 (1998).
159. D. Cottevaille, A. Lemehaute, C. Challioui, P. Mirebeau, and J. N. Demay, *Synth. Met.* 101, 703 (1999).
160. A. G. MacDiarmid, Y. Zhou, and J. Feng, *Synth. Met.* 100, 131 (1999).
161. O. Oka, O. Kiyohara, and K. Yoshino, *Jpn. J. Appl. Phys., Part 2* 30, L653 (1991).
162. W. M. Deazevedo and F. B. Diniz, *Synth. Met.* 41, 869 (1991).
163. A. Andreatta, A. J. Heeger, and P. Smith, *Synth. Met.* 41, 1063 (1991).
164. M. Angelopoulos, A. J. Epstein, A. G. MacDiarmid, and A. Ray, *Synth. Met.* 21, 2 (1987).
165. M. Abe, S. Akizuki, M. Ezoe, Y. Noda, A. Ohtani, A. Okuno, H. Higuchi, Y. Umemoto, and K. Nakamoto, *J. Chem. Soc., Chem. Commun.* 1989, 1736 (1989).
166. M. Inoue, M. B. Inoue, and R. E. Navarro, *Synth. Met.* 30, 199 (1989).
167. S. H. Li, Y. Cao, and H. Dong, *Synth. Met.* 29, E329 (1989).
168. E. M. Genies and P. Noel, *J. Electroanal. Chem.* 310, 89 (1991).
169. S. Li, Y. Cao, and Z. Xue, *Synth. Met.* 20, 141 (1987).
170. C. Dearmitt, S. P. Armes, J. Winter, F. A. Uribe, S. Gottesfeld, and Mombourquette, *Polymer* 34, 158 (1993).
171. A. J. Heeger, *Synth. Met.* 57, 3471 (1993).
172. A. Pron, J. E. Osterholm, P. Smith, A. J. Heeger, J. Laska, and M. Zagorska, *Synth. Met.* 57, 3520 (1993).

173. A. Wolter, E. Banka, F. Genoud, A. Pron, and M. Nechtschein, *Synth. Met.* 84, 753 (1997).
174. T. Taka, J. Laakso, and K. Levon, *Solid State Commun.* 92, 393 (1994).
175. O. T. Ikkala, J. Laasko, K. Vakiparta, E. Virtanen, H. Ruohonen, H. Jarvinen, T. Taka, P. Passiniemi, and J. E. Osterholm, *Synth. Met.* 69, 97 (1995).
176. J. Y. Lee, X. H. Su, and C. Q. Cui, *J. Electroanal. Chem.* 367, 71 (1994).
177. J. R. Santos, J. A. Malmonge, A. J. G. C. Silva, A. J. Motheo, Y. P. Mascarenhas, and L. H. C. Mattoso, *Synth. Met.* 69, 141 (1995).
178. M. Angelopoulos, A. J. Epstein, A. G. MacDiarmid, and A. Ray, *Synth. Met.* 21, 21 (1987).
179. A. Andreatta, Y. Cao, J. C. Chiang, P. Smith, and A. J. Heeger, *Adv. ACS Abstracts* 197, 21 (1989).
180. S. J. Pomfret, P. N. Adams, N. P. Comfort, and A. P. Monkman, *Synth. Met.* 101, 724 (1999).
181. S. J. Pomfret, P. N. Adams, N. P. Comfort, and A. P. Monkman, *Adv. Mater.* 10, 1351 (1998).
182. R. Moreno, O. P. Márquez, J. Márquez, and R. Ortiz, "Proceedings of the 50th ISE Meeting," Pavia, Italy, 1999, Abstract 9-807.
183. S. Li, Y. Cao, and Z. Xue, *Synth. Met.* 20, 141 (1987).
184. R. Holze, *J. Electroanal. Chem.* 224, 253 (1987).
185. C. Nguyen van Huong, *J. Electroanal. Chem.* 264, 247 (1989).
186. M. A. Spitsyn, A. V. Shlepakov, and V. N. Andreev, *Sov. Electrochem.* 27, 525 (1991).
187. R. Holze, *J. Electroanal. Chem.* 250, 143 (1988).
188. J. O'M. Bockris and K. T. Jeng, "Proceedings of the ECS Spring Meeting," Los Angeles, 1989, Abstract 542.
189. J. O'M. Bockris and K. T. Jeng, *J. Electroanal. Chem.* 330, 541 (1992).
190. L. Dunsch, *J. Electroanal. Chem.* 61, 61 (1975).
191. G. P. Evans, in "Advances in Electrochemical Science and Engineering" (H. Gerischer and C. W. Tobias, Eds.), Vol. 1, p. 1. VCH, Weinheim, 1990.
192. D. M. Mohilner, R. N. Adams, and W. J. Argersinger, *J. Am. Chem. Soc.* 84, 3618 (1962).
193. A. F. Diaz and J. A. Logan, *J. Electroanal. Chem.* 111, 111 (1980).
194. R. Noufi, A. J. Nozik, J. White, and L. F. Warren, *J. Electrochem. Soc.* 129, 2261 (1982).
195. R. Hand, M. Melicharek, D. I. Scoggin, R. Stotz, A. K. Carpenter, and R. F. Nelson, *Collect. Czech. Chem. Commun.* 36, 842 (1971).
196. R. L. Hand and R. F. Nelson, *J. Am. Chem. Soc.* 96, 850 (1974).
197. J. Heinze, P. Tschuncky, and A. Smie, *J. Solid State Electrochem.* 2, 102 (1998).
198. A. Heinzl, R. Holze, C. H. Hamann, and J. K. Blum, *Electrochim. Acta* 34, 657 (1989).
199. A. Heinzl, R. Holze, C. H. Hamann, and J. K. Blum, *Z. Phys. Chem. NF* 160, 11 (1989).
200. R. D. Allendoerfer, G. A. Martincheck, and S. Bruckenstein, *Anal. Chem.* 47, 890 (1975).
201. R. Holze, *DEHEMA Monographie* 121, 323 (1990).
202. S. L. Mu, J. Q. Kan, J. T. Lu, and Z. Lin, *J. Electroanal. Chem.* 446, 107 (1998).
203. N. Pekmez, K. Pekmez, and A. Yildiz, *J. Electroanal. Chem.* 370, 223 (1994).
204. F. A. Neugebauer, S. Bamberger, and W. R. Groh, *Tetrahedron Lett.* 25, 2247 (1973).
205. R. Holze, F. Köleli, and C. H. Hamann, *DEHEMA Monographie* 117, 315 (1989).
206. K. B. Yatsimirskii, B. G. Zhelyazkova, and N. D. Iordanov, *Dokl. Akad. Nauk SSSR* 233, 646 (1977).
207. R. Male and R. D. Allendoerfer, *J. Phys. Chem.* 92, 6237 (1988).
208. B. Speiser, A. Rieker, and S. Pons, *J. Electroanal. Chem.* 147, 205 (1983).
209. G. Cauquis, G. Fauveleot, and J. Rigaudy, *Bull. Soc. Chim. France* 1968, 4928 (1968).
210. G. Cauquis, G. Fauveleot, and J. Rigaudy, *Bull. Soc. Chim. France* 1968, 1618 (1968).
211. S.-M. Yang, W.-M. Shiah, and J.-J. Lai, *Synth. Met.* 41, 757 (1991).
212. L. Dunsch and A. Petr, *Ber. Bunsen. Ges. Phys. Chem.* 97, 436 (1993).
213. C. H. Hamann, R. Holze, and F. Köleli, *DEHEMA Monographie* 121, 297 (1990).
214. R. Holze and C. H. Hamann, *Tetrahedron* 47, 737 (1991).
215. G. Hambitzer and I. Stassen, *Synth. Met.* 55-57, 1045 (1993).
216. G. Hambitzer, P. P. Heinz, I. Stassen, and J. Heitbaum, *Synth. Met.* 55, 1317 (1993).
217. G. Hambitzer, J. Heitbaum, and I. Stassen, *J. Electroanal. Chem.* 447, 117 (1998).
218. I. Stassen and G. Hambitzer, *J. Electroanal. Chem.* 440, 219 (1997).
219. T. J. Kemp, P. Moore, and G. R. Quick, *J. Chem. Res., Miniprint* 1981, 301 (1981).
220. A. Zimmermann, U. Künzelmann, and L. Dunsch, *Synth. Met.* 93, 17 (1998).
221. J.-M. Leger, B. Beden, C. Lamy, P. Ocon, and C. Sieiro, *Synth. Met.* 62, 9 (1994).
222. E. M. Genies and M. Lapkowski, *J. Electroanal. Chem.* 236, 189 (1987).
223. E. M. Genies, M. Lapkowski, and J. F. Penneau, *J. Electroanal. Chem.* 249, 97 (1988).
224. E. M. Genies, M. Lapkowski, C. Saniter, and E. Vieil, *Synth. Met.* 18, 631 (1987).
225. E. M. Genies, J. F. Penneau, and M. Lapkowski, *J. Electroanal. Chem.* 260, 145 (1989).
226. Y.-B. Shim, M.-S. Won, and S.-M. Park, *J. Electrochem. Soc.* 137, 538 (1990).
227. B. J. Johnson and S.-M. Park, *J. Electrochem. Soc.* 143, 1277 (1996).
228. H. de Santana, M. L. A. Temperini, and J. C. Rubim, *J. Electroanal. Chem.* 356, 145 (1993).
229. M. Baumgarten and K. Müllen, *Top. Curr. Chem.* 169, 1 (1994).
230. J. Heinze, P. Tschuncky, and A. Smie, *J. Solid State Electrochem.* 2, 102 (1998).
231. A. Malinauskas and R. Holze, *Electrochim. Acta* 44, 2613 (1999).
232. J. Yue and A. J. Epstein, *J. Am. Chem. Soc.* 112, 2800 (1990).
233. S. A. Chen and G. W. Hwang, *Macromolecules* 29, 3950 (1996).
234. K. G. Neoh, E. T. Kang, and K. L. Tan, *Synth. Met.* 60, 13 (1993).
235. X. L. Wei, Y. Z. Wang, S. M. Long, C. Bobeczko, and A. J. Epstein, *J. Am. Chem. Soc.* 118, 2545 (1996).
236. A. Kitani, T. Yamashita, H. Tang, and S. Ito, "Proceedings of the 50th ISE Meeting," Pavia, Italy, 1999, Abstract 3b-37.
237. A. Malinauskas and R. Holze, *Electrochim. Acta* 43, 521 (1998).
238. A. Malinauskas and R. Holze, *Electrochim. Acta* 43, 2413 (1998).
239. M. Probst and R. Holze, *Ber. Bunsen. Ges. Phys. Chem.* 100, 1286 (1996).
240. M. Probst and R. Holze, *Macromol. Chem. Phys.* 198, 1499 (1997).
241. G. D'Aprano, M. Leclerc, and G. Zotti, *J. Electroanal. Chem.* 351, 145 (1993).
242. L. H. Dao, M. Leclerc, J. Guay, and J. W. Chevalier, *Synth. Met.* 29, E377 (1989).
243. S. Cattarin, L. Doubova, G. Mengoli, and G. Zotti, *Electrochim. Acta* 33, 1077 (1988).
244. J. Roncali, R. Garreau, A. Yasser, P. Marque, F. Garnier, and M. Lemaire, *J. Phys. Chem.* 91, 6706 (1987).
245. H. Yang and A. J. Bard, *J. Electroanal. Chem.* 339, 423 (1992).
246. H. Yang and A. J. Bard, *J. Electroanal. Chem.* 306, 87 (1991).
247. N. Comisso, S. Daolino, G. Mengoli, R. Samlaso, S. Zecchin, and G. Zotti, *J. Electroanal. Chem.* 255, 97 (1988).
248. P. Chandrasekhar and R. W. Gumbs, *J. Electrochem. Soc.* 138, 1337 (1991).
249. H. J. Yang, D. O. Wipf, and A. J. Bard, *J. Electroanal. Chem.* 331, 913 (1992).
250. P. Gao, D. Gosztola, and M. J. Weaver, *J. Phys. Chem.* 93, 3753 (1989).
251. R. Holze, *J. Electroanal. Chem.* 224, 253 (1987).

252. D. E. Stilwell and S.-M. Park, *J. Electrochem. Soc.* 135, 2254 (1988).
253. D. E. Stilwell and S.-M. Park, *J. Electrochem. Soc.* 135, 2497 (1988).
254. Y. B. Shim and S. M. Park, *Synth. Met.* 29, E169 (1989).
255. Y.-B. Shim, M.-S. Won, and S.-M. Park, *J. Electrochem. Soc.* 137, 538 (1990).
256. G. Zotti, S. Cattarin, and N. Comisso, *J. Electroanal. Chem.* 235, 259 (1987).
257. E. M. Genies and M. Lapkowski, *J. Electroanal. Chem.* 236, 189 (1987).
258. E. M. Genies, M. Lapkowski, and J. F. Penneau, *J. Electroanal. Chem.* 249, 97 (1988).
259. E. M. Genies, J. F. Penneau, M. Lapkowski, and A. Boyle, *J. Electroanal. Chem.* 269, 63 (1989).
260. J.-C. Chiang and A. G. MacDiarmid, *Synth. Met.* 13, 193 (1986).
261. W. S. Huang, B. D. Humphrey, and A. G. MacDiarmid, *J. Chem. Soc., Faraday Trans.* 82, 2385 (1986).
262. A. G. MacDiarmid, J. C. Chiang, A. J. Epstein, and A. F. Richter, *Synth. Met.* 18, 285 (1987).
263. G. E. Wnek, *Synth. Met.* 15, 213 (1986).
264. V. F. Ivanov, O. L. Gribkova, A. A. Nekrasov, and A. V. Vannikov, *Mendeleev Commun.* 1998, 4 (1998).
265. S. L. Mu and J. Q. Kan, *Electrochim. Acta* 41, 1593 (1996).
266. A. A. Nekrasov, V. F. Ivanov, O. L. Gribkova, and A. V. Vannikov, *J. Electroanal. Chem.* 412, 133 (1996).
267. N. Pekmez, K. Pekmez, and A. Yildiz, *J. Electroanal. Chem.* 370, 223 (1994).
268. M. X. Wan and J. Yang, *Synth. Met.* 69, 155 (1995).
269. H. Q. Tang, A. Kitani, S. Maitani, H. Munemura, and M. Shiotani, *Electrochim. Acta* 40, 849 (1995).
270. S. L. Mu and J. Q. Kan, *Synth. Met.* 92, 149 (1998).
271. N. Pekmez, K. Pekmez, and A. Yildiz, *J. Electroanal. Chem.* 370, 223 (1994).
272. P. M. McManus, R. J. Cushman, and S. C. Yang, *J. Phys. Chem.* 91, 744 (1987).
273. V. Brandl, Dissertation, Universität Oldenburg, 1997.
274. G. Zotti, S. Cattarin, and N. Comisso, *J. Electroanal. Chem.* 239, 387 (1988).
275. W. S. Huang, B. D. Humphrey, and A. G. MacDiarmid, *J. Chem. Soc., Faraday Trans.* 82, 2385 (1986).
276. K. Kanamura, Y. Kawai, S. Yonezawa, and Z. Takehara, *J. Phys. Chem.* 98, 13,011 (1994).
277. A. G. Bedekar, S. F. Patil, R. C. Patil, and C. Agashe, *J. Phys. D: Appl. Phys.* 27, 1727 (1994).
278. J. Yano, K. Yashikawa, T. Ohnishi, and A. Kitani, "Proceedings of the 50th ISE Meeting," Pavia, Italy, 1999, Abstract 3b-31.
279. E. Sabatani, Y. Gafni, and I. Rubinstein, *J. Phys. Chem.* 99, 12,305 (1995).
280. V. Tsakova and A. Milchev, *Electrochim. Acta* 36, 1579 (1991).
281. V. Tsakova and A. Milchev, *J. Electroanal. Chem.* 346, 85 (1993).
282. V. Tsakova, A. Milchev, and J. W. Schultze, *J. Electroanal. Chem.* 346, 85 (1993).
283. M. Probst, Dissertation, Technische Universität Chemnitz, 1997.
284. I. Fujita, M. Ishiguchi, H. Shiota, T. Danjo, and K. Kosai, *J. Appl. Polym. Sci.* 44, 987 (1992).
285. K. Bade, V. Tsakova, and J. W. Schultze, *Electrochim. Acta* 37, 2255 (1992).
286. A. Thyssen, A. Hochfeld, and J. W. Schultze, *DEHEMA Monographie* 112, 441 (1988).
287. L. T. Cai, S. B. Yao, and S. M. Zhou, *Acta Chim. Sinica* 53, 1150 (1995).
288. U. König and J. W. Schultze, *J. Electroanal. Chem.* 242, 243 (1988).
289. M. T. Gill, S. E. Chapman, C. L. Dearnitt, F. L. Baines, C. M. Dadswell, J. G. Stamper, G. A. Lawless, N. C. Billingham, and S. P. Armes, *Synth. Met.* 93, 227 (1998).
290. Y. P. Fu and R. L. Elsenbaumer, *Chem. Mater.* 6, 671 (1994).
291. V. Tsakova, A. Milchev, and J. W. Schultze, *J. Electroanal. Chem.* 346, 85 (1993).
292. V. Brandl and R. Holze, *Ber. Bunsen. Ges. Phys. Chem.* 101, 251 (1997).
293. K. Koziel, M. Lapkowski, and S. Lefrant, *Synth. Met.* 69, 217 (1995).
294. D. R. Kim, W. Cha, and W. K. Paik, *Synth. Met.* 84, 759 (1997).
295. R. Greef, M. Kalaji, and L. M. Peter, *Faraday Disc. Chem. Soc.* 88, 277 (1989).
296. L. Nianbing, H. Debing, Z. Shengtao, and D. Peidao, "Proceedings of the ECS Meeting," Seattle, 1999, Abstract 1053.
297. B. Grodzicka, K. Brudzewski, R. Minkowski, J. Plochanski, and J. Przulski, in "Electronic Properties of Conjugated Polymers" (H. Kuzmany, M. Mehring, and S. Roth, Eds.). Springer Series in Solid State Science, Vol. 76, p. 235. Springer-Verlag, Berlin, 1987.
298. A. G. MacDiarmid and A. J. Epstein, *Synth. Met.* 65, 103 (1994).
299. A. G. MacDiarmid and A. J. Epstein, *Macromol. Symp.* 98, 835 (1995).
300. A. J. Bard and L. R. Faulkner, "Electrochemical Methods." Wiley, New York, 1980.
301. K. Aoki, "Proceedings of 50th ISE Meeting," Pavia, Italy, 1999, Abstract 3b-363.
302. Y.-B. Shim, M.-S. Won, and S.-M. Park, *J. Electrochem. Soc.* 137, 538 (1990).
303. K. Koziel, M. Lapkowski, and S. Lefrant, *Synth. Met.* 69, 217 (1995).
304. A. Malinauskas and R. Holze, *Electrochim. Acta* 43, 515 (1998).
305. C. Odin and M. Nechtschein, in "Electronic Properties of Conjugated Polymers III" (H. Kuzmany, M. Mehring, and S. Roth, Eds.) Springer Series in Solid State Science, Vol. 91, p. 172. Springer-Verlag, Berlin, 1989.
306. C. Odin and M. Nechtschein, *Synth. Met.* 41-43, 2943 (1991).
307. A. Malinauskas and R. Holze, *Ber. Bunsen. Ges. Phys. Chem.* 101, 1851 (1997).
308. B. Palys, K. Jackowska, and D. Wojtasiewicz, "Proceedings of the 50th ISE Meeting," Pavia, Italy, 1999, Abstract 3b-272.
309. J. Lippe and R. Holze, *Synth. Met.* 41-43, 2927 (1991).
310. R. J. Cushman, P. M. McManus, and S. C. Yang, *J. Electroanal. Chem.* 219, 335 (1987).
311. S. C. Yang, D. Zhang, and R. J. Cushman, *Synth. Met.* 29, E401 (1989).
312. B. Z. Lubentsov, O. N. Timofeeva, and M. L. Khidekel, *Synth. Met.* 45, 235 (1991).
313. P. Sanuwaert, R. Lazzaroni, J. Riga, and J. J. Verbist, in "Electronic Properties of Conjugated Polymers" (H. Kuzmany, M. Mehring, and S. Roth, Eds.). Springer Series in Solid State Science, Vol. 76, p. 249. Springer-Verlag, Berlin, 1987.
314. J. M. Wilbur, T. C. Sandreczki, I. M. Brown, D. J. Leopold, and S. Mohite, *Synth. Met.* 82, 175 (1996).
315. H. H. S. Javadi, S. P. Treat, J. M. Ginder, J. F. Wolf, and A. J. Epstein, *J. Phys. Chem. Solids* 51, 107 (1990).
316. A. P. Monkman, in "Electronic Properties of Conjugated Polymers III" (H. Kuzmany, M. Mehring, and S. Roth, Eds.). Springer Series in Solid State Science, Vol. 91, p. 310. Springer-Verlag, Berlin, 1989.
317. A. P. Monkman and D. Bloor, in "Electronic Properties of Conjugated Polymers III" (H. Kuzmany, M. Mehring, and S. Roth, Eds.). Springer Series in Solid State Science, Vol. 76, p. 232. Springer-Verlag, Berlin, 1987.
318. W. R. Salaneck, I. Lundström, B. Lieberg, M. A. Hasan, R. Erlands-son, P. Kondradsson, A. G. MacDiarmid, and N. L. D. Somasiri, in "Electronic Properties of Polymers and Related Compounds" (H. Kuzmany, M. Mehring, and S. Roth, Eds.). Springer Series in Solid State Science, Vol. 63, p. 2. Springer-Verlag, Berlin, 1985.
319. M. Ohira, Y. Kobayashi, T. Sakai, M. Takeuchi, and M. Tsuji, *Synth. Met.* 18, 347 (1987).
320. H. Neugebauer, A. Neckel, N. S. Sariciftci, and H. Kuzmany, *Mikrochim. Acta* 1, 265 (1988).
321. M. A. Habib and S. P. Maheswari, *J. Electrochem. Soc.* 135, C380 (1988).
322. H. Neugebauer, A. Neckel, H. Kuzmany, and N. S. Sariciftci, *Synth. Met.* 29, E185 (1989).

323. N. S. Sariciftci, H. Kuzmany, A. Neckel, H. Neugebauer, and M. Bartonek, *Synth. Met.* 29, E193 (1989).
324. N. S. Sariciftci, H. Kuzmany, H. Neugebauer, and A. Neckel, *J. Chem. Phys.* 92, 4530 (1990).
325. S. Quillard, G. Louarn, J. P. Buisson, S. Lefrant, J. Masters, and A. G. MacDiarmid, *Synth. Met.* 55, 475 (1993).
326. P. Herrasti, R. Diaz, and P. Ocon, *New J. Chem.* 17, 279 (1993).
327. L. H. C. Mattoso and L. O. S. Bulhoes, *Synth. Met.* 52, 171 (1992).
328. L. Duic and Z. Mandic, *J. Electroanal. Chem.* 335, 207 (1992).
329. M. X. Wan, M. Li, J. C. Li, and Z. X. Liu, *J. Appl. Polym. Sci.* 53, 131 (1994).
330. A. Gruger, A. Novak, A. Regis, and P. Colomban, *J. Mol. Struct.* 328, 153 (1994).
331. Z. Ping, H. Neugebauer, and A. Neckel, *Synth. Met.* 69, 161 (1995).
332. S. T. Selvan, A. Mani, K. Athinarayanasamy, K. L. N. Phani, and S. Pitchumani, *Mater. Res. Bull.* 30, 699 (1995).
333. K. Meerholz and J. Heinze, *Synth. Met.* 55, 5040 (1993).
334. E. M. Genies and P. Noel, *J. Electroanal. Chem.* 296, 473 (1990).
335. Z. Ping, H. Neugebauer, and A. Neckel, *Electrochim. Acta* 41, 767 (1996).
336. L. H. C. Mattoso and L. O. S. Bulhoes, *Synth. Met.* 52, 171 (1992).
337. M. K. Ram, M. Joshi, R. Mehrotra, S. K. Dhawan, and S. Chandra, *Thin Solid Films* 304, 65 (1997).
338. A. Zimmermann and L. Dunsch, *J. Mol. Struct.* 410, 165 (1997).
339. Z. Ping, G. E. Nauer, H. Neugebauer, J. Theiner, and A. Neckel, *Electrochim. Acta* 42, 1693 (1997).
340. Z. Ping, G. E. Nauer, H. Neugebauer, J. Theiner, and A. Neckel, *J. Chem. Soc., Faraday Trans.* 93, 121 (1997).
341. B. Tian and G. Zerbi, *J. Chem. Phys.* 92, 3886 (1990).
342. B. Tian and G. Zerbi, *J. Chem. Phys.* 92, 3892 (1990).
343. G. Zerbi, C. Castiglioni, and M. Gussoni, *Synth. Met.* 41-43, 3407 (1991).
344. G. Zerbi, C. Castiglioni, B. Tian, and M. Gussoni, in "Electronic Properties of Conjugated Polymers III" (H. Kuzmany, M. Mehring, and S. Roth, Eds.). Springer Series in Solid State Science, Vol. 91, p. 106. Springer-Verlag, Berlin, 1989.
345. G. Zerbi, M. Veronelli, S. Martina, A. D. Schlüter, and G. Wegner, *J. Chem. Phys.* 100, 978 (1994).
346. G. Zerbi, M. Veronelli, S. Martina, A.-D. Schlüter, and G. Wegner, *Adv. Mater.* 6, 385 (1994).
347. G. Zerbi, B. Chierichetti, and O. Ingánas, *J. Chem. Phys.* 94, 4637 (1991).
348. B. Tian and G. Zerbi, in "Electronic Properties of Conjugated Polymers III" (H. Kuzmany, M. Mehring, and S. Roth, Eds.). Springer Series in Solid State Science, Vol. 91, p. 113. Springer-Verlag, Berlin, 1989.
349. M. Lapkowski, K. Berrada, S. Quillard, G. Louarn, S. Lefrant, and A. Pron, *Macromolecules* 28, 1233 (1995).
350. P. Colomban, A. Gruger, A. Novak, and A. Regis, *J. Mol. Struct.* 317, 261 (1994).
351. Z. Ping, H. Neugebauer, and A. Neckel, *Synth. Met.* 69, 161 (1995).
352. Z. Ping, H. Neugebauer, and A. Neckel, *Electrochim. Acta* 41, 767 (1996).
353. Z. Ping, G. E. Nauer, H. Neugebauer, J. Theiner, and A. Neckel, *J. Chem. Soc., Faraday Trans.* 93, 121 (1997).
354. Z. Ping, G. E. Nauer, H. Neugebauer, and J. Theiner, *J. Electroanal. Chem.* 420, 301 (1997).
355. J. C. Evans, *Spectrochim. Acta* 16, 994 (1960).
356. J. C. Evans, *Spectrochim. Acta* 18, 507 (1962).
357. T. Fukuda, H. Takezoe, K. Ishikawa, A. Fukada, H. S. Woo, S. K. Jeong, E. J. Oh, and J. S. Suh, *Synth. Met.* 69, 175 (1995).
358. M. Bartonek, N. S. Sariciftci, and H. Kuzmany, in "Electronic Properties of Conjugated Polymers III" (H. Kuzmany, M. Mehring, and S. Roth, Eds.). Springer Series in Solid State Science, Vol. 91, p. 330. Springer-Verlag, Berlin, 1989.
359. J.-C. Chiang and A. G. MacDiarmid, *Synth. Met.* 13, 193 (1986).
360. C. Engert, S. Umaphathy, W. Kiefer, and H. Hamaguchi, *Chem. Phys. Lett.* 218, 87 (1994).
361. A. Kitani, J. Yano, and K. Sasaki, *J. Electroanal. Chem.* 209, 227 (1986).
362. For a review see: K. Hyodo, *Electrochim. Acta* 39, 265 (1994).
363. R. Kessel, G. Hansen, and J. W. Schultze, *Ber. Bunsen. Ges. Phys. Chem.* 92, 710 (1988).
364. G. Zotti and G. Schiavon, *Synth. Met.* 30, 151 (1989).
365. J. R. Santos, J. A. Malmonge, A. J. G. C. Silva, A. J. Motheo, Y. P. Mascarenhas, and L. H. C. Mattoso, *Synth. Met.* 69, 141 (1995).
366. K. Koziel, M. Lapkowski, and S. Lefrant, *Synth. Met.* 69, 217 (1995).
367. A. P. Monkman, D. Bloor, G. C. Stevens, and J. C. H. Stevens, *J. Phys. D: Appl. Phys.* 20, 1337 (1987).
368. M. V. Fock, in "Luminescence and Nonlinear Optics," Vol. 59, p. 1. Moscow, Nauka, 1972.
369. A. A. Nekrasov, V. F. Ivanov, O. L. Gribkova, and A. V. Vannikov, "Proceedings of the 50th ISE Meeting," Pavia, Italy, 1999, Abstract 3b-484.
370. M. G. Hill, K. R. Mann, L. L. Miller, and J. F. Penneau, *J. Am. Chem. Soc.* 114, 2728 (1992).
371. A. O. Patil, A. J. Heeger, and F. Wudl, *Chem. Rev.* 88, 183 (1988).
372. L. L. Miller and K. R. Mann, *Acc. Chem. Res.* 29, 417 (1996).
373. J. L. Brédas and G. B. Street, *Acc. Chem. Res.* 18, 309 (1985).
374. M. M. Wienk and R. A. J. Janssen, *J. Am. Chem. Soc.* 119, 4492 (1997).
375. M. C. Gupta and D. C. Sindhimeshram, *Indian J. Chem., Sect. A* 33, 558 (1994).
376. H. Kuhn, *Fortschr. Chem. Org. Nat.* 16, 169 (1958).
377. H. Kuhn, *Fortschr. Chem. Org. Nat.* 17, 404 (1959).
378. Y. G. Min, Y. N. Xia, A. G. MacDiarmid, and A. J. Epstein, *Synth. Met.* 69, 159 (1995).
379. E. M. Genniés and M. Lapkowski, in "Electronic Properties of Conjugated Polymers" (H. Kuzmany, M. Mehring, and S. Roth, Eds.). Springer Series in Solid State Science, Vol. 76, p. 223. Springer-Verlag, Berlin, 1987.
380. M. K. Ram, E. Maccioni, and C. Nicolini, *Thin Solid Films* 303, 27 (1997).
381. R. Krzyczmonik and T. Blaszczyk, "Proceedings of the 50th ISE Meeting," Pavia, Italy, 1999, Abstract 3b-138.
382. K. Koziel, M. Lapkowski, and S. Lefrant, *Synth. Met.* 69, 137 (1995).
383. K. A. Coplin, S. Jasty, S. M. Long, S. K. Manohar, Y. Sun, A. G. MacDiarmid, and A. J. Epstein, *Phys. Rev. Lett.* 72, 33,206 (1994).
384. G. D'Aprano, M. Leclerc, G. Zotti, and G. Schiavon, *Chem. Mater.* 7, 33 (1995).
385. M. K. Ram, E. Maccioni, and C. Nicolini, *Thin Solid Films* 303, 27 (1997).
386. V. Brandl and R. Holze, *Ber. Bunsen. Ges. Phys. Chem.* 101, 251 (1997).
387. D. C. Sindhimeshram and M. C. Gupta, *Indian J. Chem., Sect. A* 34, 260 (1995).
388. I. B. Goldberg, H. R. Crowe, P. R. Newman, A. J. Heeger, and A. G. MacDiarmid, *J. Chem. Phys.* 70, 1132 (1979).
389. W. J. Albery and C. C. Jones, *Faraday Discuss. Chem. Soc.* 78, 193 (1984).
390. S. Dong, J. Ding, and R. Zhan, *J. Chem. Soc., Faraday Trans. I* 85, 1599 (1989).
391. F. J. Dyson, *Phys. Rev.* 98, 349 (1955).
392. G. Feher and A. F. Kip, *Phys. Rev.* 98, 337 (1955).
393. E. Houze, M. Nechtschein, and A. Pron, *Synth. Met.* 84, 981 (1997).
394. A. V. Kulikov, Y. L. Kogan, and L. S. Fokeeva, *Synth. Met.* 69, 223 (1995).
395. J. Ding and S. J. Dong, *Acta Chim. Sinica* 54, 193 (1996).
396. S. Dong, J. Ding, and R. Zhan, *J. Chem. Soc., Faraday Trans. I* 85, 1599 (1989).
397. J. F. Oudard, R. D. Allendoerfer, and R. A. Osteryoung, *J. Electroanal. Chem.* 241, 231 (1988).

398. S. M. Long, K. R. Cromack, A. J. Epstein, Y. Sun, and A. G. MacDiarmid, *Synth. Met.* 55, 648 (1993).
399. W. P. Su and A. J. Epstein, *Phys. Rev. Lett.* 70, 1497 (1993).
400. L. Desidera and L. Walmsley, *J. Magn. Reson., Ser. A* 116, 73 (1995).
401. M. Kaya, A. Kitani, and K. Sasaki, *Chem. Lett.* 1986, 147 (1986).
402. L. Dunsch and A. Petr, *Ber. Bunsen. Ges. Phys. Chem.* 97, 436 (1993).
403. S. H. Glarum and J. H. Marshall, *J. Phys. Chem.* 90, 6076 (1986).
404. J. P. Travers, C. Menardo, M. Nechtschein, and B. Villeret, *J. Chim. Phys.* 86, 77 (1989).
405. F. Genoud, J. Kruszka, M. Nechtschein, C. Santier, S. Davied, and Y. Nicolau, *Synth. Met.* 43, 2887 (1991).
406. T. Ohsawa, O. Kimura, M. Onoda, and K. Yoshino, *Synth. Met.* 41, 719 (1991).
407. M. Nechtschein and F. Genoud, *Solid State Commun.* 91, 471 (1994).
408. E. Houze and M. Nechtschein, *Synth. Met.* 84, 947 (1997).
409. K. Aasmundtveit, F. Genoud, E. Houze, and M. Nechtschein, *Synth. Met.* 69, 193 (1995).
410. F. Genoud, M. Nechtschein, and C. Santier, *Synth. Met.* 55, 642 (1993).
411. E. Houze, M. Nechtschein, and A. Pron, *Phys. Rev. B* 56, 12,263 (1997).
412. P. K. Kahol, A. J. Dyakonov, and B. J. McCormick, *Synth. Met.* 89, 17 (1997).
413. M. C. Itow, T. Kawahara, N. Kachi, H. Sakamoto, K. Mizoguchi, Y. Sahara, S. Masubuchi, and S. Kazama, *Synth. Met.* 84, 749 (1997).
414. K. Koziel, M. Lapkowski, and E. Genies, *Synth. Met.* 84, 105 (1997).
415. M. X. Wan and J. Wang, *Synth. Met.* 84, 751 (1997).
416. M. Wan, *Chinese J. Polym. Sci.* 13, 1 (1995).
417. E. M. Genies and M. Lapkowski, *J. Electroanal. Chem.* 236, 199 (1987).
418. J. L. Brédas, B. Thémans, J. G. Fripiat, J. M. André, and R. R. Chance, *Phys. Rev. B* 12, 6761 (1984).
419. H. Yoon, B. S. Jung, and H. Lee, *Synth. Met.* 41, 699 (1991).
420. W. W. Focke and G. E. Wnek, *J. Electroanal. Chem.* 256, 343 (1983).
421. G. E. Wnek, *Synth. Met.* 15, 213 (1986).
422. G. E. Wnek, *J. Electron. Mater.* 15, 321 (1986).
423. K. M. Choi and K. H. Kim, *J. Appl. Polym. Sci.* 44, 751 (1992).
424. S. A. Chen and G. W. Hwang, *Macromolecules* 29, 3950 (1996).
425. K. Mizoguchi and K. Kume, *Solid State Commun.* 89, 971 (1994).
426. K. Mizoguchi and K. Kume, *Synth. Met.* 69, 241 (1995).
427. J. Lippe, Dissertation, Universität Oldenburg, 1991.
428. K. Mizoguchi, T. Obana, S. Ueno, and K. Kume, *Synth. Met.* 55, 601 (1993).
429. A. Raghunathan, T. S. Natarajan, G. Rangarajan, S. K. Dhawan, and D. C. Trivedi, *Phys. Rev. B* 47, 13,189 (1993).
430. K. Mizoguchi, K. Kaneto, K. Kume, K. Misoo, T. Shiraishi, and K. Yoshino, *Synth. Met.* 18, 195 (1987).
431. A. G. MacDiarmid, J. C. Chiang, A. J. Epstein, and A. F. Richter, *Synth. Met.* 18, 285 (1987).
432. M. Kaya, A. Kitani, and K. Sasaki, *Chem. Lett.* 1986, 147 (1986).
433. F. Genoud, J. Kruszka, M. Nechtschein, C. Santier, S. Davied, and Y. Nicolau, *Synth. Met.* 43, 2887 (1991).
434. M. M. Wienk and R. A. J. Janssen, *J. Am. Chem. Soc.* 119, 4492 (1997).
435. S. Stafström, in "Electronic Properties of Conjugated Polymers" (H. Kuzmany, M. Mehring, and S. Roth, Eds.). Springer Series in Solid State Science, Vol. 76, p. 238. Springer-Verlag, Berlin, 1987.
436. F. Devreux, F. Genoud, M. Nechtschein, and B. Villeret, in "Electronic Properties of Conjugated Polymers" (H. Kuzmany, M. Mehring, and S. Roth, Eds.). Springer Series in Solid State Science, Vol. 76, p. 270. Springer-Verlag, Berlin, 1987.
437. H. Mizobuchi, T. Kawai, and K. Yoshino, *Solid State Commun.* 96, 925 (1995).
438. J. Anand, S. Palaniappan, and D. N. Sathyanarayana, *J. Phys. Chem.* 99, 10,324 (1995).
439. J. Anand, S. Palaniappan, and D. N. Sathyanarayana, *Synth. Met.* 83, 97 (1996).
440. R. Holze and J. Lippe, *DECHEMA Monographie* 125, 679 (1992).
441. C. Odin and M. Nechtschein, in "Electronic Properties of Conjugated Polymers III" (H. Kuzmany, M. Mehring, and S. Roth, Eds.). Springer Series in Solid State Science, Vol. 91, p. 172. Springer-Verlag, Berlin, 1989.
442. C. Odin and M. Nechtschein, *Synth. Met.* 41-43, 2943 (1991).
443. Y. S. Kang, H. J. Lee, J. Namgoong, B. Jung, and H. Lee, *Polymer* 40, 2209 (1999).
444. K. Fesser, A. R. Bishop, and D. K. Campbell, *Phys. Rev. B* 27, 4804 (1983).
445. M. Probst and R. Holze, *Electrochim. Acta* 40, 213 (1995).
446. J. Heeger and A. MacDiarmid, *Phys. Rev. Lett.* 39, 1098 (1977).
447. G. D'Aprano, M. Leclerc, G. Zotti, and G. Schiavon, *Chem. Mater.* 7, 33 (1995).
448. S.-M. Yang, J.-H. Chiang, and W.-M. Shiah, *Synth. Met.* 41, 753 (1991).
449. N. J. Pinto, P. K. Kahol, B. J. McCormick, N. S. Dalal, and H. Wan, *Phys. Rev. B: Condens. Matter* 49, 13,983 (1994).
450. P. K. Kahol, N. J. Pinto, and B. J. McCormick, *Solid State Commun.* 91, 21 (1994).
451. M. X. Wan and J. P. Yang, *J. Appl. Polym. Sci.* 55, 399 (1995).
452. Y. Wei, W. W. Focke, G. E. Wnek, A. Ray, and A. G. MacDiarmid, *J. Phys. Chem.* 93, 495 (1989).
453. J. Anand, S. Palaniappan, and D. N. Sathyanarayana, *Synth. Met.* 63, 43 (1994).
454. J. Anand, S. Palaniappan, and D. N. Sathyanarayana, *Synth. Met.* 66, 129 (1994).
455. M. Leclerc, J. Guay, and L. H. Dao, *Macromolecules* 22, 649 (1989).
456. M. Probst, Dissertation, Technische Universität Chemnitz, 1997.
457. K. Barrada, S. Quillard, G. Louarn, and S. Lefrant, *J. Chim. Phys. Phys.-Chim. Biol.* 92, 911 (1995).
458. M. Leclerc, J. Guay, and L. H. Dao, *J. Electroanal. Chem.* 251, 21 (1988).
459. G. Venugopal, X. Quan, G. E. Johnson, F. M. Houlihan, E. Chin, and O. Nalamasu, *Chem. Mater.* 7, 271 (1995).
460. M. Leclerc, J. Guay, and L. H. Dao, *J. Electroanal. Chem.* 251, 21 (1988).
461. M. Leclerc, J. Guay, and L. H. Dao, *Macromolecules* 22, 649 (1989).
462. M. Leclerc, *J. Electroanal. Chem.* 296, 93 (1990).
463. R. L. Clark and S. C. Yang, *Synth. Met.* 29, E337 (1989).
464. M. X. Wan and J. P. Yang, *Synth. Met.* 73, 201 (1995).
465. G. Varsanyi, "Assignments for Vibrational Spectra of 700 Benzene Derivatives." Hilger, London, 1974.
466. M. C. Bernard, A. Hugot-Le Goff, S. Joiret, P. D. Long, and P. V. Phong, "Proceedings of the 50th ISE Meeting," Pavia, Italy, 1999, Abstract 3b-478.
467. S. Quillard, K. Barrada, G. Louarn, S. Lefrant, M. Lapkowski, and A. Pron, *New J. Chem.* 19, 365 (1995).
468. M. J. Henderson, A. R. Hillman, and E. Vieil, *J. Electroanal. Chem.* 454, 1 (1998).
469. J. Anand, S. Palaniappan, and D. N. Sathyanarayana, *Synth. Met.* 63, 43 (1994).
470. J. Anand, S. Palaniappan, and D. N. Sathyanarayana, *Synth. Met.* 66, 129 (1994).
471. N. Tushima and H. Yan, *Bull. Chem. Soc. Jpn.* 68, 1056 (1995).
472. M. Probst, Dissertation, Technische Universität Chemnitz, 1997.
473. N. Comisso, S. Daolino, G. Mengoli, R. Samlaso, S. Zecchin, and G. Zotti, *J. Electroanal. Chem.* 255, 97 (1988).
474. M. C. Gupta, S. S. Umare, M. M. Huque, and S. G. Viswanath, *Indian J. Chem. Soc. B* 36, 703 (1997).
475. J. W. Chevalier, J. Y. Bergeron, and L. H. Dao, *Macromolecules* 25, 3325 (1992).
476. N. Comisso, S. Daolino, G. Mengoli, R. Samlaso, S. Zecchin, and G. Zotti, *J. Electroanal. Chem.* 255, 97 (1988).
477. M. T. Nguyen and A. F. Diaz, *Macromolecules* 28, 3411 (1995).
478. G. Zotti, S. Zecchin, G. Schiavon, R. Seraglia, A. Berlin, and A. Canavesi, *Chem. Mater.* 6, 1742 (1994).

479. K. M. Choi, J. H. Jang, H. W. Rhee, and K. H. Kim, *J. Appl. Polym. Sci.* 46, 1695 (1992).
480. K. M. Choi, J. H. Jang, and K. H. Kim, *Mol. Cryst. Liquid Cryst.* 220, 201 (1992).
481. S. W. Kong, K. M. Choi, and K. H. Kim, *J. Phys. Chem. Solids* 53, 657 (1992).
482. K. M. Choi, C. Y. Kim, and K. H. Kim, *J. Phys. Chem.* 96, 3782 (1992).
483. K. Jackowska, A. Kudelski, and J. Bukowska, *Electrochim. Acta* 39, 1365 (1994).
484. B. C. Roy, M. D. Gupta, and J. K. Ray, *Macromolecules* 28, 1727 (1995).
485. J. Widera, W. Grochala, K. Jackowska, and J. Bukowska, *Synth. Met.* 89, 29 (1997).
486. B. Palys, K. Jackowska, and D. Wojtasiewicz, "Proceedings of the 50th ISE Meeting," Pavia, Italy, 1999, Abstract 3b-272.
487. J.-C. Chiang and A. G. MacDiarmid, *Synth. Met.* 13, 193 (1986).
488. E. T. Kang, K. G. Neoh, and K. L. Tan, *Prog. Polym. Sci.* 23, 277 (1998).
489. K. Kanamura, Y. Kawai, S. Yonezawa, and Z. Takehara, *J. Phys. Chem.* 98, 13,011 (1994).
490. A. Hugot-Le Goff and M. C. Bernard, *Synth. Met.* 60, 115 (1993).
491. D. K. Moon, M. Ezuka, T. Maruyama, K. Osakada, and T. Yamamoto, *Macromolecules* 26, 364 (1993).
492. N. M. Alpatova, E. V. Ovsyannikova, and V. E. Kazarinov, *Russ. J. Electrochem.* 32, 584 (1996).
493. M. Vuki, M. Kalaji, L. Nyholm, and L. M. Peter, *Synth. Met.* 55, 1515 (1993).
494. M. K. Ram, E. Maccioni, and C. Nicolini, *Thin Solid Films* 303, 27 (1997).
495. S. K. Dhawan and D. C. Trivedi, *Synth. Met.* 60, 63 (1993).
496. E. Vieil, T. Matencio, V. Plichon, and S. Servagent, *Synth. Met.* 43, 2837 (1991).
497. D. Chinn, J. Dubow, J. Li, J. Janata, and M. Josowicz, *Chem. Mater.* 7, 1510 (1995).
498. A. Malinauskas and R. Holze, *Ber. Bunsen. Ges. Phys. Chem.* 100, 1740 (1996).
499. A. Malinauskas and R. Holze, *Ber. Bunsen. Ges. Phys. Chem.* 102, 982 (1998).
500. A. Malinauskas and R. Holze, *Electrochim. Acta* 43, 2563 (1998).
501. V. E. Kazarinov, E. Y. Pisarevskaya, E. V. Ovsyannikova, M. D. Levi, and N. M. Alpatova, *Russ. J. Electrochem.* 31, 879 (1995).
502. D. K. Moon, M. Ezuka, T. Maruyama, K. Osakada, and T. Yamamoto, *Macromolecules* 26, 364 (1993).
503. V. Barsukov, S. Chichikov, and V. Khomenko, "Proceedings of the 50th ISE Meeting," Pavia, Italy, 1999, Abstract 3b-387.
504. C. Coutanceau, A. El Hourch, P. Crouigneau, J. M. Leger, and C. Lamy, *Electrochim. Acta* 40, 2739 (1995).
505. A. El Hourch, A. Rakotondrainible, B. Beden, P. Crouigneau, J. M. Leger, C. Lamy, A. A. Tanaka, and E. R. Gonzalez, *Electrochim. Acta* 39, 889 (1994).
506. S. Otsuka, K. Saito, and K. Morita, *Chem. Lett.* 1996, 615 (1996).
507. K. Chiba, T. Ohsaka, and N. Oyama, *J. Electroanal. Chem.* 217, 239 (1987).
508. A. Malinauskas and R. Holze, *J. Electroanal. Chem.* 461, 184 (1999).
509. A. Malinauskas and R. Holze, unpublished results.
510. N. Oyama, T. Tatsuma, T. Sato, and T. Sotomura, *Nature* 373, 598 (1995).
511. D. A. Buttry, S. I. Córdoba de Torresi, and R. M. Torresi, "Proceedings of the 50th ISE Meeting," Pavia, Italy, 1999, Abstract 3b-341.
512. T. Kobayashi, H. Yoneyama, and H. Tamura, *J. Electroanal. Chem.* 161, 419 (1984).
513. T. Kobayashi, H. Tamura, and H. Yoneyama, *J. Electroanal. Chem.* 177, 293 (1984).
514. D. E. Stilwell and S.-M. Park, *J. Electrochem. Soc.* 135, 2491 (1988).
515. D. E. Stilwell and S.-M. Park, *J. Electrochem. Soc.* 135, 2497 (1988).
516. D. E. Stilwell and S.-M. Park, *J. Electrochem. Soc.* 136, 688 (1989).
517. H. Yang and A. J. Bard, *J. Electroanal. Chem.* 339, 423 (1992).
518. Y.-B. Shim, M.-S. Won, and S.-M. Park, *J. Electrochem. Soc.* 137, 538 (1990).
519. H. Neugebauer, N. S. Saricifci, H. Kuzmany, and A. Neckel, in "Electronic Properties of Conjugated Polymers III" (H. Kuzmany, M. Mehring, and S. Roth, Eds.). Springer Series in Solid State Science, Vol. 91, p. 315. Springer-Verlag, Berlin, 1989.
520. T. Kobayashi, H. Yoneyama, and H. Tamura, *J. Electroanal. Chem.* 177, 293 (1984).
521. S. H. Glarum and J. H. Marshall, *J. Electrochem. Soc.* 134, 142 (1987).
522. A. Kabumoto, K. Shinozaki, K. Watanabe, and N. Nishikawa, *Synth. Met.* 26, 349 (1988).
523. C. Q. Cui, X. H. Su, and J. Y. Lee, *Polym. Degrad. Stab.* 41, 69 (1993).
524. A. Hugot-Le Goff and M. C. Bernard, *Synth. Met.* 60, 115 (1993).
525. E. M. Genies and C. Tsintavis, *J. Electroanal. Chem.* 195, 109 (1985).
526. M. Pasquali, G. Pistoia, and R. Rosati, *Synth. Met.* 58, 1 (1993).
527. V. E. Kazarinov, V. N. Andreev, and M. A. Spitsyn, *Electrochim. Acta* 41, 1757 (1996).
528. J. Lippe and R. Holze, *J. Electroanal. Chem.* 339, 411 (1992).
529. J. Lippe and R. Holze, *Mol. Cryst. Liq. Cryst.* 208, 99 (1991).
530. A. A. Pud, *Synth. Met.* 66, 1 (1994).
531. A. Malinauskas and R. Holze, *J. Solid State Electrochem.* 3, 429 (1999).
532. A. Malinauskas and R. Holze, *J. Appl. Polym. Sci.* 73, 287 (1999).
533. C. Q. Cui, L. H. Ong, T. C. Tan, and J. Y. Lee, *Electrochim. Acta* 38, 1395 (1993).
534. A. Q. Zhang, C. Q. Cui, and J. Y. Lee, *Synth. Met.* 72, 217 (1995).
535. S. Yonezawa, K. Kanamura, and Z. Takehara, *J. Electrochem. Soc.* 140, 629 (1993).
536. P. Rannou and M. Nechtschein, *Synth. Met.* 84, 755 (1997).
537. S. W. Byun and S. S. Im, *J. Appl. Polym. Sci.* 56, 425 (1995).
538. H. Tsubakihara, H. Okamura, K. Okada, and A. Sakamoto, *Kobunshi Ronbunshu* 51, 565 (1994).
539. H. Tsubakihara and K. Murakami, *Kobunshi Ronbunshu* 54, 451 (1997).
540. H. Tsubakihara, S. Miyazaki, and S. Fujisawa, *Kobunshi Ronbunshu* 54, 455 (1997).
541. J. Anand, S. Palaniappan, and D. N. Sathyanarayana, *Synth. Met.* 82, 23 (1996).
542. A. F. Diaz and K. K. Kanazawa, *J. Chem. Soc., Chem. Commun.* 1979, 635 (1979).
543. K. K. Kanazawa, A. F. Diaz, G. P. Gardini, W. D. Gill, P. M. Grant, and G. B. Street, *Synth. Met.* 1, 329 (1980).
544. A. F. Diaz, A. Martinez, K. K. Kanazawa, and M. Salmon, *J. Electroanal. Chem.* 130, 181 (1981).
545. A. F. Diaz, J. I. Castillo, J. A. Logan, and W.-Y. Lee, *J. Electroanal. Chem.* 129, 115 (1981).
546. G. B. Street, in "Handbook of Conducting Polymers I" (T. Skotheim, Ed.), p. 265. Dekker, New York, 1980.
547. H. H. Kuhn, A. D. Child, and W. C. Kimbrell, *Synth. Met.* 71, 2139 (1995).
548. S. B. Adeloju, S. J. Shaw, and G. G. Wallace, *Anal. Chim. Acta* 281, 611 (1993).
549. S. B. Adeloju, S. J. Shaw, and G. G. Wallace, *Anal. Chim. Acta* 281, 621 (1993).
550. S. B. Adeloju, S. J. Shaw, and G. G. Wallace, *Electroanalysis* 6, 865 (1994).
551. S. B. Adeloju, S. J. Shaw, and G. G. Wallace, *Anal. Chim. Acta* 323, 107 (1996).
552. D. M. Liu, J. Aguilar-Hernandez, K. Potjekamloth, and H. D. Liess, *Sens. Actuators, B* 41, 203 (1997).
553. G. F. Khan, E. Kobatake, Y. Ikarayama, and M. Aizawa, *Anal. Chim. Acta* 281, 527 (1993).
554. M. Penza, E. Milella, M. B. Alba, A. Quirini, and L. Vasanelli, *Sens. Actuators, B* 40, 205 (1997).

555. C. N. Aquinobinag, N. Kumar, R. N. Lamb, and P. J. Pigram, *Chem. Mater.* 8, 2579 (1996).
556. M. Penza, E. Milella, and V. I. Anisimkin, *Sens. Actuators, B* 47, 218 (1998).
557. H. K. Youssoufi, A. Yassar, S. Baiteche, M. Hmyene, and F. Garnier, *Synth. Met.* 67, 251 (1994).
558. P. N. Bartlett and P. R. Birkin, *Synth. Met.* 61, 15 (1993).
559. L. D. Couves and S. J. Porter, *Synth. Met.* 28, C761 (1989).
560. A. Boyle, E. M. Genies, and M. Lapkowski, *Synth. Met.* 28, C769 (1989).
561. J. Rishpon and S. Gottesfeld, *Biosens. Bioelectron.* 6, 143 (1991).
562. S. Cosnier, A. Senillou, M. Grätzel, P. Comte, N. Vlachopoulos, N. J. Renault, and C. Martelet, *J. Electroanal. Chem.* 469, 176 (1999).
563. V. V. Krasko and A. A. Yakovleva, *Sov. Electrochem.* 25, 1016 (1989).
564. I. A. Vinokurov, *Sens. Actuators, B* 10, 31 (1992).
565. H. Shinohara, M. Aizawa, and H. Shirakawa, *J. Chem. Soc., Chem. Commun.* 1986, 87 (1986).
566. J. Wang, M. S. Lin, and S.-P. Chen, *J. Electroanal. Chem.* 273, 231 (1989).
567. K. Bouzek, K.-M. Mangold, R. H. J. Schmitz, and K. Jüttner, "Proceedings of the 50th ISE Meeting," Pavia, Italy, 1999, Abstract 1-125.
568. D. J. Strike, N. F. Derooij, M. Koudelkahep, M. Ulmann, and J. Augustynski, *J. Appl. Electrochem.* 22, 922 (1992).
569. X. Andrieu, L. Josset, and J. F. Fauvarque, *J. Chim. Phys. Phys.-Chim. Biol.* 92, 879 (1995).
570. F. Larmat, J. R. Reynolds, and Y. J. Qiu, *Synth. Met.* 79, 229 (1996).
571. M. Satoh, H. Ishikawa, K. Amano, E. Hasegawa, and K. Yoshino, *Synth. Met.* 71, 2259 (1995).
572. D. Naegele, in "Electronic Properties of Conjugated Polymers III" (H. Kuzmany, M. Mehring, and S. Roth, Eds.). Springer Series in Solid State Science, Vol. 91, p. 428. Springer-Verlag, Berlin, 1989.
573. M. Satoh and E. Hasegawa, *Macromol. Symp.* 105, 211 (1996).
574. H. Yamamoto, M. Fukuda, I. Isa, and K. Yoshino, *Mol. Cryst. Liq. Cryst.* 227, 255 (1993).
575. M. D. Ingram, A. J. Pappin, F. Delalande, D. Poupard, and G. Terzulli, *Electrochim. Acta* 43, 1601 (1998).
576. F. Trinidad, J. Alonso-Lopez, and M. Nebot, *J. Appl. Electrochem.* 17, 215 (1987).
577. S. Kakuda, T. Momma, T. Osaka, G. B. Appetecchi, and B. Scrosati, *J. Electrochem. Soc.* 142, L1 (1995).
578. M. G. Minnett and J. R. Owen, *Synth. Met.* 28, C211 (1989).
579. H. Münstedt, R. Bitthin, G. Ely, G. Kohler, E. Meissner, H. Möhwald, and D. Naegele, *Synth. Met.* 18, 259 (1987).
580. J. Y. Lee, L. H. Ong, and G. K. Chuah, *J. Appl. Electrochem.* 22, 738 (1992).
581. J. G. Killian, B. M. Coffey, F. Gao, T. O. Poehler, and P. C. Seanson, *J. Electrochem. Soc.* 143, 936 (1996).
582. H. Koezuka, A. Tsumura, H. Fuchigami, and K. Kuramoto, *Appl. Phys. Lett.* 62, 1794 (1993).
583. A. G. MacDiarmid, J. K. Avlyanov, F. Huang, Z. Y. Huang, H. L. Wang, P. C. Wang, and A. J. Epstein, *Macromol. Symp.* 118, 445 (1997).
584. C. Avino, S. Panero, and B. Scrosati, *J. Mater. Chem.* 3, 1259 (1993).
585. J. C. Gustafsson, O. Inganäs, and A. M. Andersson, *Synth. Met.* 62, 17 (1994).
586. N. Leventis and Y. C. Chung, *Chem. Mater.* 4, 1415 (1992).
587. E. M. Giroto and M. A. De Paoli, *Adv. Mater.* 10, 790 (1998).
588. H. T. Chiu, J. S. Lin, and J. N. Shiau, *J. Appl. Electrochem.* 22, 522 (1992).
589. M. Zhou, M. Persin, and J. Sarrazin, *J. Appl. Electrochem.* 26, 711 (1996).
590. M. Schirmeisen and F. Beck, *J. Appl. Electrochem.* 19, 401 (1989).
591. R. Noufi, D. Tench, and L. F. Warren, *J. Electrochem. Soc.* 127, 2310 (1980).
592. S. Gottesfeld, F. A. Uribe, and S. P. Armes, *J. Electrochem. Soc.* 139, L14 (1992).
593. M. Saurin and S. P. Armes, *J. Appl. Polym. Sci.* 56, 41 (1995).
594. J. D. Madden, R. A. Cush, T. S. Kanigan, C. J. Brennan, and I. W. Hunter, *Synth. Met.* 105, 61 (1999).
595. J. M. Sansinena, V. Olzabal, T. F. Otero, C. N. P. Dafonseca, and M. A. De Paoli, *Chem. Commun.* 1997, 2217 (1997).
596. A. Dellasanta, D. Derossi, and A. Mazzoldi, *Synth. Met.* 90, 93 (1997).
597. M. R. Gandhi, P. Murray, G. M. Spinks, and G. G. Wallace, *Synth. Met.* 73, 247 (1995).
598. R. H. Baughman, *Synth. Met.* 78, 339 (1996).
599. A. F. Diaz, J. Crowley, J. Bargon, G. Gardini, and J. B. Torrance, *J. Electroanal. Chem.* 121, 355 (1981).
600. J. M. Toussaint, B. Themans, J. M. Andre, and J. L. Bredas, *Synth. Met.* 28, C205 (1989).
601. J. M. Toussaint and J. L. Bredas, *Synth. Met.* 61, 103 (1993).
602. G. Pagani, A. Berlin, A. Canavesi, G. Schiavon, S. Zecchin, and G. Zotti, *Adv. Mater.* 8, 819 (1996).
603. G. Brocks, P. J. Kelly, and R. Car, *Synth. Met.* 57, 4243 (1993).
604. V. Brandl and R. Holze, *Ber. Bunsen. Ges. Phys. Chem.* 102, 1032 (1998).
605. R. Holze and V. Brandl, in "GDCh Monographie" (I. Russow, G. Sandstede, and R. Staab, Eds.), Vol. 14, p. 230. GDCh, Frankfurt, 1999.
606. K. P. Vidanapathirana, M. A. Careem, S. Skaarup, and K. West, *Solid State Ionics* 123, 287 (1999); T. Hagiwara, M. Hirasaka, K. Sato, and M. Yamaura, *Synth. Met.* 36, 241 (1990).
607. T. F. Otero and I. Cantero, *J. Electrochem. Soc.* 146, 4118 (1999).
608. K. West, T. Jacobsen, B. Zachau-Christiansen, M. A. Careem, and S. Skaarup, *Synth. Met.* 55, 1412 (1993).
609. T. F. Otero, J. Rodriguez, E. Angulo, and C. Santamaria, *Synth. Met.* 43, 2831 (1991).
610. S. M. Chung, W. K. Paik, and I. H. Yeo, *Synth. Met.* 84, 155 (1997).
611. B. R. Scharifker, E. Garcia-Pastoriza, and W. Marino, *J. Electroanal. Chem.* 300, 85 (1991).
612. I. Rodriguez, M. L. Marcos, and J. Gonzalez-Velasco, *Electrochim. Acta* 32, 1181 (1987).
613. E. M. Genies, G. Bidan, and A. F. Diaz, *J. Electroanal. Chem.* 149, 101 (1983).
614. D. J. Fermin and B. R. Scharifker, *J. Electroanal. Chem.* 357, 273 (1993).
615. B. S. Kim, W. H. Kim, S. N. Hoier, and S. M. Park, *Synth. Met.* 69, 455 (1995).
616. D. E. Raymond and D. J. Harrison, *J. Electroanal. Chem.* 361, 65 (1993).
617. D. E. Raymond and D. J. Harrison, *J. Electroanal. Chem.* 355, 115 (1993).
618. A. Hamnett, S. J. Higgins, W. J. Albery, and P. R. Fisk, *J. Electroanal. Chem.* 270, 479 (1989).
619. P. A. Christensen and A. Hamnett, *Electrochim. Acta* 36, 1263 (1991).
620. Y. T. Kim, D. L. Allara, R. W. Collins, and K. Vedam, *Thin Solid Films* 193, 350 (1990).
621. D. Stroud and A. Kazaryan, *Phys. Rev. B: Condens. Matter* 53, 7076 (1996).
622. L. M. Abrantes and J. P. Correia, *Electrochim. Acta* 44, 1901 (1999).
623. J. Bacskaï, G. Inzelt, A. Bartl, L. Dunsch, and G. Paasch, *Synth. Met.* 67, 227 (1994).
624. M. Yurtsever and E. Yurtsever, *Synth. Met.* 98, 221 (1999).
625. E. Yurtsever and M. Yurtsever, *Synth. Met.* 101, 335 (1999).
626. E. Kriván and C. Visy, "Proceedings of the 50th ISE Meeting," Pavia, Italy, 1999, Abstract 3b-399.
627. J. L. Brédas, D. S. Boudreaux, R. R. Chance, and R. Silbey, *J. Am. Chem. Soc.* 105, 6555 (1983).
628. J. T. Lei, W. B. Liang, and C. R. Martin, *Synth. Met.* 48, 301 (1992).
629. J. Hlavaty, V. Papez, L. Kavan, and P. Krtil, *Synth. Met.* 66, 165 (1994).

630. V. Brandl and R. Holze, *Ber. Bunsen. Ges. Phys. Chem.* 102, 1032 (1998).
631. R. Holze and V. Brandl, in "GDCh Monographie" (J. Russow, G. Sandstede, and R. Staab, Eds.), Vol. 14, p. 230. GDCh, Frankfurt, 1999.
632. R. Stankovic, O. Pavlovic, M. Vojnovic, and S. Jovanovic, *Eur. Polym. J.* 30, 385 (1994).
633. C. S. C. Bose, S. Basak, and K. Rajeshwar, *J. Phys. Chem.* 96, 9899 (1992).
634. T. Amemiya, K. Hashimoto, and A. Fujishima, *Denki Kagaku* 60, 1075 (1992).
635. T. Amemiya, K. Hashimoto, and A. Fujishima, *J. Phys. Chem.* 97, 4187 (1993).
636. T. Amemiya, K. Hashimoto, and A. Fujishima, *J. Phys. Chem.* 97, 9736 (1993).
637. T. Amemiya, K. Hashimoto, and A. Fujishima, *J. Electroanal. Chem.* 377, 143 (1994).
638. Y. Tezuka and K. Aoki, *J. Electroanal. Chem.* 273, 161 (1989).
639. Y. Tezuka, K. Aoki, H. Yajima, and T. Ishii, *J. Electroanal. Chem.* 425, 167 (1997).
640. Y. F. Li, *Electrochim. Acta* 42, 203 (1997).
641. Y. J. Qiu and J. R. Reynolds, *Polym. Eng. Sci.* 31, 417 (1991).
642. V. M. Schmidt and J. Heitbaum, *Electrochim. Acta* 38, 349 (1993).
643. J. H. Kaufman, K. K. Kanazawa, and G. B. Street, *Phys. Rev. Lett.* 53, 2461 (1984).
644. Q. J. Xie, S. Kuwabata, and H. Yoneyama, *J. Electroanal. Chem.* 420, 219 (1997).
645. D. Ofer, R. M. Crooks, and M. S. Wrighton, *J. Am. Chem. Soc.* 112, 7869 (1990).
646. D. R. Kim, W. Cha, and W. K. Paik, *Synth. Met.* 84, 759 (1997).
647. S. J. Higgins and A. Hamnett, *Electrochim. Acta* 36, 2123 (1991).
648. M. T. Giacomini, L. M. M. Desouza, and E. A. Ticianelli, *Surf. Sci.* 409, 465 (1998).
649. Q. B. Pei and O. Inganäs, *J. Phys. Chem.* 96, 10,507 (1992).
650. Q. B. Pei and O. Inganäs, *J. Phys. Chem.* 97, 6034 (1993).
651. Q. B. Pei and O. Inganäs, *Solid State Ionics* 60, 161 (1993).
652. C. M. Lee, J. Y. Kwak, and A. J. Bard, *J. Electrochem. Soc.* 136, 3720 (1989).
653. C. Lopez, M. F. M. Viegas, G. Bidan, and E. Vieil, *Synth. Met.* 63, 73 (1994).
654. Y. Son and K. Rajeshwar, *J. Chem. Soc., Faraday Trans.* 88, 605 (1992).
655. Y. Son and K. Rajeshwar, *J. Chem. Soc., Faraday Trans.* 88, 605 (1992).
656. A. El Hourch, A. Rakotondrainibe, B. Beden, P. Crouigneau, J. M. Leger, C. Lamy, A. A. Tanaka, and E. R. Gonzalez, *Electrochim. Acta* 39, 889 (1994).
657. D. Y. Kim, J. Y. Lee, D. K. Moon, and C. Y. Kim, *Synth. Met.* 69, 471 (1995).
658. Y. Son and K. Rajeshwar, *J. Chem. Soc., Faraday Trans.* 88, 605 (1992).
659. J. A. E. H. van Haare, L. Groenendaal, E. E. Havinga, R. A. J. Jansen, and E. W. Meijer, *Angew. Chem.* 108, 696 (1996).
660. D. J. Fermin, H. Teruel, and B. R. Scharifker, *J. Electroanal. Chem.* 401, 207 (1996).
661. J. A. E. H. van Haare, L. Groenendaal, E. E. Havinga, R. A. J. Jansen, and E. W. Meijer, *Angew. Chem.* 108, 696 (1996).
662. J. M. Kim, S. M. Chang, H. W. Lee, Y. S. Kwon, and Y. H. Oh, *Synth. Met.* 85, 1371 (1997).
663. S. Skaarup, K. West, B. Zachau-Christiansen, and T. Jacobsen, *Synth. Met.* 51, 267 (1992).
664. G. Zotti and G. Schiavon, *Synth. Met.* 30, 151 (1989).
665. M. Josowicz, K. Ashley, J. Janata, and S. Pons, *Anal. Chem.* 59, 253 (1987).
666. E. M. Genies, G. Bidan, and A. F. Diaz, *J. Electroanal. Chem.* 149, 101 (1983).
667. Y. Tezuka, K. Shinozaki, and K. Aoki, *Synth. Met.* 30, 369 (1989).
668. T. F. Otero and M. Bengoechea, *Langmuir* 15, 1323 (1999).
669. T. F. Otero, H. J. Grande, and J. Rodriguez, *J. Phys. Chem. B* 101, 3688 (1997).
670. E. Faulques, H. Kuzmany, and W. Wallnöfer, *J. Chem. Phys.* 90, 7585 (1989).
671. E. Faulques, W. Wallnöfer, and H. Kuzmany, in "Electronic Properties of Conjugated Polymers III" (H. Kuzmany, M. Mehring, and S. Roth, Eds.). Springer Series in Solid State Science, Vol. 91, p. 119. Springer-Verlag, Berlin, 1989.
672. B. Tian and G. Zerbi, in "Electronic Properties of Conjugated Polymers III" (H. Kuzmany, M. Mehring, and S. Roth, Eds.). Springer Series in Solid State Science, Vol. 91, p. 113. Springer-Verlag, Berlin, 1989.
673. R. Kostic, D. Rakovic, S. A. Stepanyan, I. E. Davidova, and L. A. Gribov, *J. Chem. Phys.* 102, 3104 (1995).
674. M. Kofranek, T. Kovar, A. Karpfen, and H. Lischka, *J. Chem. Phys.* 96, 4464 (1992).
675. J. Y. Jin, T. Ando, N. Teramae, and H. Haraguchi, *Bunseki Kagaku* 40, 799 (1991).
676. R. G. Davidson and T. G. Turner, *Synth. Met.* 72, 121 (1995).
677. G. Maia, E. A. Ticianelli, and F. C. Nart, *Z. Phys. Chem.* 186, 245 (1994).
678. L. Oddi, R. Capelletti, R. Fieschi, M. P. Fontana, and G. Ruani, *Mol. Cryst. Liq. Cryst.* 118, 179 (1985).
679. S. J. Hanh, W. J. Gadja, P. O. Vogelhut, and M. V. Zeller, *Synth. Met.* 14, 89 (1986).
680. Y. J. Qiu and J. R. Reynolds, *J. Polym. Sci., Part A: Polym. Chem.* 30, 1315 (1992).
681. D. A. Cheshier, P. A. Christensen, and A. Hamnett, *J. Chem. Soc., Faraday Trans.* 89, 303 (1993).
682. G. B. Street, T. C. Clarke, M. Krounbi, K. Kanazawa, V. Lee, P. Pfluger, J. C. Scott, and G. Weiser, *Mol. Cryst. Liq. Cryst.* 83, 253 (1982).
683. G. B. Street, S. E. Lindsey, A. I. Nazzal, and K. J. Wynne, *Mol. Cryst. Liq. Cryst.* 118, 137 (1985).
684. C. B. Pate and R. E. Nofle, *Synth. Met.* 38, 259 (1990).
685. J. H. Wang, *Surf. Interface Anal.* 15, 635 (1990).
686. P. A. Christensen and A. Hamnett, *Electrochim. Acta* 36, 1263 (1991).
687. H. Kato, O. Nishikawa, T. Matsui, S. Honma, and H. Kokado, *J. Phys. Chem.* 95, 6011 (1991).
688. J. T. Lei, W. B. Liang, and C. R. Martin, *Synth. Met.* 48, 301 (1992).
689. W. Liang, J. Lei, and C. R. Martin, *Synth. Met.* 52, 227 (1992).
690. J. Lei and C. R. Martin, *Synth. Met.* 48, 331 (1992).
691. H. Kato, O. Nishikawa, T. Matsui, S. Honma, and H. Kokado, *J. Phys. Chem.* 95, 6014 (1991).
692. A. G. Rangamani, P. T. McTigue, and B. Verity, *Synth. Met.* 64, 91 (1994).
693. I. Rodriguez, B. R. Scharifker, and J. Mostany, "Proceedings of the 50th ISE Meeting," Pavia, Italy, 1999, Abstract 3b-524.
694. Y. Furukawa, S. Tazawa, Y. Fujii, and I. Harada, *Synth. Met.* 24, 329 (1988).
695. T. Inoue, I. Hosoya, and T. Yamase, *Chem. Lett.* 1987, 563 (1987).
696. K. M. Cheung, B. J. E. Smith, D. N. Batchelder, and D. Bloor, *Synth. Met.* 21, 249 (1987).
697. J. Bukowska and K. Jackowska, *Synth. Met.* 35, 143 (1990).
698. J. Bukowska and K. Jackowska, *Electrochim. Acta* 35, 315 (1990).
699. C. K. Chong, C. B. Shen, Y. Fong, J. X. Zhu, F. X. Yan, S. Brush, C. K. Mann, and T. J. Vickers, *Vib. Spectrosc.* 3, 35 (1992).
700. G. Zerbi, M. Veronelli, S. Martina, A. D. Schlüter, and G. Wegner, *J. Chem. Phys.* 100, 978 (1994).
701. H. R. Virdee and R. E. Hester, *Croatia Chem. Acta* 61, 357 (1988).
702. C. M. Jenden, R. G. Davidson, and T. G. Turner, *Polymer* 34, 1649 (1993).
703. C. H. Olk, J. Heremans, and C. P. Beetz, *J. Mater. Res.* 3, 984 (1988).
704. C. Q. Jin, X. G. Kong, and X. J. Liu, *Synth. Met.* 55, 536 (1993).

705. G. Zerbi, M. Veronelli, S. Martina, A.-D. Schlüter, and G. Wegner, *Adv. Mater.* 6, 385 (1994).
706. G. Zerbi, M. Veronelli, S. Martina, A.-D. Schlüter, and G. Wegner, *Adv. Mater.* 6, 385 (1994).
707. G. Zotti, *Synth. Met.* 97, 267 (1998).
708. G. Zotti and G. Schiavon, *Chem. Mater.* 3, 62 (1991); *Synth. Met.* 41, 445 (1991).
709. C. J. Zhong, Z. Q. Tian, and Z. W. Tian, *J. Phys. Chem.* 94, 2171 (1990).
710. A. M. Waller and R. G. Compton, *J. Chem. Soc., Faraday Trans. I* 85, 977 (1989).
711. N. Nechtschein, F. Devreux, F. Genoud, E. Vieil, J. M. Pernaut, and E. Genies, *Synth. Met.* 15, 59 (1986).
712. J. L. Brédas, B. Thémans, J. G. Fripiat, J. M. André, and R. R. Chance, *Phys. Rev. B* 29, 6761 (1984).
713. J. L. Brédas, J. C. Scott, G. B. Street, and K. Yakushi, *Phys. Rev. B: Condens. Matter* 30, 1023 (1984).
714. J. H. Kaufman, N. Colaneri, J. C. Scott, and G. B. Street, *Phys. Rev. Lett.* 53, 1005 (1984).
715. F. Genoud, M. Gulielmi, M. Nechtschein, E. Genies, and M. Salmon, *Phys. Rev. Lett.* 55, 118 (1985).
716. R. Singh and A. K. Narula, *J. Appl. Phys.* 82, 4362 (1997).
717. A. Chaibi, N. Ferrer-Anglada, J. A. Gorri, L. Fajari, and M. C. Anglada, *Appl. Magn. Reson.* 12, 575 (1997).
718. T. Amemiya, K. Hashimoto, A. Fujishima, and K. Itoh, *J. Electrochem. Soc.* 138, 2845 (1991).
719. J. Oudard, R. D. Allendoerfer, and R. A. Osteryoung, *J. Electrochem. Soc.* 134, C141 (1987).
720. J. F. Oudard, R. D. Allendoerfer, and R. A. Osteryoung, *J. Electroanal. Chem.* 241, 231 (1988).
721. J. Rùhe, C. Kröhnke, T. Ezquerra, and G. Wegner, in "Electronic Properties of Conjugated Polymers III" (H. Kuzmany, M. Mehring, and S. Roth, Eds.). Springer Series in Solid State Science, Vol. 76, p. 298. Springer-Verlag, Berlin, 1987.
722. D. Schmeisser and W. Göpel, *Ber. Bunsen. Ges. Phys. Chem.* 97, 372 (1993).
723. D. Schmeisser, H. Naarmann, and W. Göpel, *Synth. Met.* 59, 211 (1993).
724. J. L. Bredas, D. S. Boudreaux, R. R. Chance, and R. Silbey, *J. Am. Chem. Soc.* 105, 6555 (1983).
725. G. B. Street, T. C. Clarke, M. Krounbi, K. Kanazawa, V. Lee, P. Pfluger, J. C. Scott, and G. Weiser, *Mol. Cryst. Liq. Cryst.* 83, 253 (1982).
726. E. N. Korol, *Synth. Met.* 63, 245 (1994).
727. T. C. Clarke, J. C. Scott, and G. B. Street, *IBM J. Res. Dev.* 27, 313 (1983).
728. G. B. Street, T. C. Clarke, M. Krounbi, K. Kanazawa, V. Lee, P. Pfluger, J. C. Scott, and G. Weiser, *Mol. Cryst. Liq. Cryst.* 83, 253 (1982).
729. E. M. Peters and J. D. van Dyke, *J. Polym. Sci., Part A: Polym. Chem.* 30, 1891 (1992).
730. C. M. Elliott, A. B. Kopelove, W. J. Albery, and Z. Chen, *J. Phys. Chem.* 95, 1743 (1991).
731. T. F. Otero and M. Bengoechea, *Electrochim. Acta* 41, 1871 (1996).
732. T. Ohtsuka, T. Wakabayashi, and H. Einaga, *Synth. Met.* 79, 235 (1996).
733. M. Sacak, U. Akbulut, and D. N. Batchelder, *Polymer* 39, 4735 (1998).
734. Y. F. Nicolau, S. Davied, F. Genoud, M. Nechtschein, and J. P. Travers, *Synth. Met.* 42, 1491 (1991).
735. P. Novák, T. Iwasita, P. A. Christensen, and W. Vielstich, *J. Electroanal. Chem.* 263, 37 (1989).
736. P. Novak and W. Vielstich, *J. Electrochem. Soc.* 137, 1681 (1990).
737. D. S. Park, Y. B. Shim, and S. M. Park, *J. Electrochem. Soc.* 140, 609 (1993).
738. D.-S. Park, Y.-B. Shim, and S.-M. Park, *J. Electrochem. Soc.* 140, 2749 (1993).
739. T. W. Lewis, G. G. Wallace, C. Y. Kim, and D. Y. Kim, *Synth. Met.* 84, 403 (1997).
740. F. Beck, U. Barsch, and R. Michaelis, *J. Electroanal. Chem.* 351, 169 (1993).
741. S. Ghosh, G. A. Bowmaker, R. P. Cooney, and J. M. Seakins, *Synth. Met.* 95, 63 (1998).
742. P. Novak, B. Rasch, and W. Vielstich, *J. Electrochem. Soc.* 138, 3300 (1991).
743. P. A. Christensen and A. Hamnett, *Electrochim. Acta* 36, 1263 (1991).
744. H. Xie, M. M. Yan, and Z. Y. Jiang, *Electrochim. Acta* 42, 2361 (1997).
745. C. C. Chen and K. Rajeshwar, *J. Electrochem. Soc.* 141, 2942 (1994).
746. T. F. Otero and J. Rodriguez, *J. Electroanal. Chem.* 310, 219 (1991).
747. E. A. Bzzaoui, S. Aeiyaach, and P. C. Lacaze, *J. Electroanal. Chem.* 364, 63 (1994).
748. E. A. Bzzaoui, S. Aeiyaach, J. Aubard, N. Felidj, G. Levi, N. Sakmeche, and P. C. Lacaze, *J. Chim. Phys. Phys.-Chim. Biol.* 95, 1526 (1998).
749. X. B. Wan, Y. Lu, X. R. Liu, L. Zhou, S. Jin, and G. Xue, *Chinese J. Polym. Sci.* 17, 99 (1999).
750. X. Wang, G. Shi, and Y. Liang, *Electrochem. Commun.* 1, 536 (1999).
751. G. Tourillon, in "Handbook of Conducting Polymers" (T. A. Skotheim, Ed.), Vol. 1, p. 294. Dekker, New York, 1986.
752. G. Tourillon and F. Garnier, *J. Electrochem. Soc.* 130, 2042 (1983).
753. R. L. Elenbaumer, K.-Y. Jen, G. G. Miler, H. Eckhardt, L. W. Shacklette, and R. Jow, in "Electronic Properties of Conjugated Polymers" (H. Kuzmany, M. Mehring, and S. Roth, Eds.). Springer Series in Solid State Science, Vol. 76, p. 400. Springer-Verlag, Berlin, 1987.
754. G. K. Chandler and D. Pletcher, in "Electrochemistry," Vol. 10, p. 117. Royal Chemistry Society, London, 1985.
755. A. F. Diaz and J. Bargon, in "Handbook of Conducting Polymers" (T. A. Skotheim, Ed.), p. 81. Dekker, New York, 1986.
756. G. Tourillon, in "Handbook of Conducting Polymers" (T. A. Skotheim, Ed.), Vol. 1, p. 293. Dekker, New York, 1986.
757. K. Kaneto, Y. Inuishi, and K. Yoshino, *Jpn. J. Appl. Phys.* 22, L567 (1983).
758. H. S. O. Chan and S. C. Ng, *Prog. Polym. Sci.* 23, 1167 (1998).
759. T. Hanawa, S. Kuwabata, H. Hashimoto, and H. Yoneyama, *Synth. Met.* 30, 173 (1989).
760. M. S. A. Abdou, F. P. Orfino, Z. W. Xie, M. J. Deen, and S. Holdcroft, *Adv. Mater.* 6, 838 (1994).
761. M. S. A. Abdou, F. P. Orfino, Y. Son, and S. Holdcroft, *J. Am. Chem. Soc.* 119, 4518 (1997).
762. Z. Q. Gao, D. Yap, and K. M. Zhang, *Anal. Sci.* 14, 1059 (1998).
763. C. Budrowski and J. Przulski, *Synth. Met.* 41, 597 (1991).
764. P. Schottland, M. Bouguettaya, and C. Chevrot, *Synth. Met.* 102, 1325 (1999).
765. T. Tatsuma, K. Ariyama, and N. Oyama, *Anal. Chim. Acta* 318, 297 (1996).
766. M. Hiller, C. Kranz, J. Huber, P. Bäuerle, and W. Schuhmann, *Adv. Mater.* 8, 219 (1996).
767. Z. Wang, H. S. Zhang, H. B. Mark, and J. F. Rubinson, *Anal. Lett.* 30, 1 (1997).
768. L. Torsi, M. Pezzuto, P. Siciliano, R. Rella, L. Sabbatini, L. Valli, and P. G. Zambonin, *Sens. Actuators, B* 48, 362 (1998).
769. B. L. Wheeler, A. Henderson, S. Vogel, S. Grey, J. Francis, G. Caple, and K. Cantrell, *J. Electrochem. Soc.* 136, 2769 (1989).
770. T. Hanawa, S. Kuwabata, H. Hashimoto, and H. Yoneyama, *Synth. Met.* 30, 173 (1989).
771. H. Yamato, M. Ohwa, and W. Wernet, *J. Electroanal. Chem.* 397, 163 (1995).
772. H. S. O. Chan, L. M. Gan, H. Chi, and C. S. Toh, *J. Electroanal. Chem.* 379, 293 (1994).
773. W. Zhang and S. Dong, *J. Electroanal. Chem.* 284, 517 (1990).

774. A. Laforgue, P. Simon, C. Sarrazin, and J. F. Fauvarque, *J. Power Sources* 80, 142 (1999).
775. C. Arbizzani, M. Catellani, M. Mastragostino, and C. Mingazzini, *Electrochim. Acta* 40, 1871 (1995).
776. C. Arbizzani, M. Mastragostino, and L. Meneghello, *Electrochim. Acta* 40, 2223 (1995).
777. M. Mastragostino, C. Arbozzani, M. C. Borghini, M. G. Cerroni, and R. Paraventi, "Proceedings of the Electrochemical Society Fall Meeting," San Antonio, 1996, Abstract 834.
778. M. Mastragostino, C. Arbozzani, M. C. Borghini, M. G. Cerroni, and R. Paraventi, "Proceedings of the Electrochemical Society Fall Meeting," San Antonio, 1996, Abstract 834.
779. J. C. Carlberg and O. Inganäs, *J. Electrochem. Soc.* 144, L61 (1997).
780. F. Fusalba, N. El Mehdi, L. Breau, and D. Bélanger, *Chem. Mater.* 11, 2743 (1999).
781. A. Rudge, I. Raistrick, S. Gottesfeld, and J. P. Ferraris, *Electrochim. Acta* 39, 273 (1994).
782. A. Rudge, J. Davey, I. Raistrick, S. Gottesfeld, and J. P. Ferraris, *J. Power Sources* 47, 89 (1994).
783. O. Haas, D. Häring, R. Kötz, P. Novák, B. Piro, and M.-C. Pham, "Proceedings of the 50th ISE Meeting," Pavia, Italy, 1999, Abstract 3b-328.
784. S. Glenis, F. Garnier, G. Horowitz, and G. Tourillon, *Thin Solid Films* 111, 93 (1984).
785. L. Sicot, C. Fiorini, A. Lorin, J. M. Nunzi, P. Raimond, and C. Senten, *Synth. Met.* 102, 991 (1999).
786. G. Horowitz and F. Garnier, *Sol. Energ. Mater.* 13, 47 (1986).
787. K. Kaneto, Y. Inuishi, and K. Yoshino, *Jpn. J. Appl. Phys.* 22, L567 (1983).
788. C. Arbizzani and M. Mastragostino, *Electrochim. Acta* 35, 251 (1990).
789. T. F. Otero, I. Cantero, and B. Azcano, *Int. J. Hydrogen Energy* 25, 221 (1999).
790. O. Inganäs, M. Sundberg, G. Gustafsson, J. O. Nilsson, S. Stafström, and B. Sjögren, in "Electronic Properties of Conjugated Polymers III" (H. Kuzmany, M. Mehring, and S. Roth, Eds.). Springer Series in Solid State Science, Vol. 91, p. 336. Springer-Verlag, Berlin, 1989.
791. M. Leclerc, M. Frechette, J. Y. Bergeron, M. Ranger, I. Levesque, and K. Faid, *Macromol. Chem. Phys.* 197, 2077 (1996).
792. K. Iwasaki, H. Fujimoto, and S. Matsuzaki, *Synth. Met.* 63, 101 (1994).
793. G. Kossmehl and M. Niemitz, *Synth. Met.* 41-43, 1065 (1991).
794. J. Roncali, *Chem. Rev.* 97, 173 (1997).
795. M. Pomerantz, "Handbook of Conducting Polymers," 2nd ed., p. 277. Dekker, New York, 1988.
796. J. C. Gustafsson, O. Inganäs, and A. M. Andersson, *Synth. Met.* 62, 17 (1994).
797. K. Kaneto, Y. Inuishi, and K. Yoshino, *Jpn. J. Appl. Phys.* 22, L412 (1983).
798. W. A. Gazotti, M. A. Depaoli, G. Casalbore-Miceli, A. Geri, and G. Zotti, *J. Appl. Electrochem.* 29, 753 (1999).
799. M. A. De Paoli, G. Casalbore-Miceli, E. M. Giroto, and W. A. Gazotti, *Electrochim. Acta* 44, 2983 (1999).
800. K. Kaneto, H. Agawa, and K. Yoshino, *J. Appl. Phys.* 61, 1197 (1987).
801. S. D. Jung, T. Zyung, W. H. Kim, C. J. Lee, and S. K. Tripathy, *Synth. Met.* 100, 223 (1999).
802. M. Theander, M. R. Anderson, and O. Inganäs, *Synth. Met.* 101, 331 (1999).
803. A. Bolognesi, C. Botta, and L. Cecchinato, *Synth. Met.* 102, 918 (1999).
804. M. R. Andersson, O. Thomas, W. Mammo, M. Svensson, M. Theander, and O. Inganäs, *J. Mater. Chem.* 9, 1933 (1999).
805. G. M. Tsivgoulis and J. M. Lehn, *Adv. Mater.* 9, 39 (1997).
806. M. R. Andersson, M. Berggren, G. Gustafsson, T. Hjetberg, O. Inganäs, and O. Wennerström, *Synth. Met.* 71, 2183 (1995).
807. P. Dyreklev, M. Berggren, O. Inganäs, M. R. Andersson, O. Wennerström, and T. Hjetberg, *Adv. Mater.* 7, 43 (1995).
808. M. Berggren, O. Inganäs, T. Granlund, S. Guo, G. Gustafsson, and M. R. Andersson, *Synth. Met.* 76, 121 (1996).
809. M. Granström, M. Berggren, O. Inganäs, M. R. Andersson, T. Hjetberg, and O. Wennerström, *Synth. Met.* 85, 1193 (1997).
810. M. R. Andersson, M. Berggren, T. Olinga, T. Hjetberg, O. Inganäs, and O. Wennerström, *Synth. Met.* 85, 1383 (1997).
811. J. C. Scott, S. A. Carter, S. Karg, and M. Angelopoulos, *Synth. Met.* 85, 1197 (1997).
812. M. R. Andersson, M. Berggren, O. Inganäs, G. Gustafsson, J. C. Gustafsson-Carlberg, D. Selse, T. Hjetberg, and O. Wennerström, *Macromolecules* 28, 7525 (1995).
813. Y. Kaminorz, E. Smela, O. Inganäs, and L. Brehmer, *Adv. Mater.* 10, 765 (1998).
814. Y. Cao, G. Yu, C. Zhang, R. Menon, and A. J. Heeger, *Synth. Met.* 87, 171 (1997).
815. F. Garten, J. Vrijmoeth, A. R. Schlatmann, R. E. Gill, T. M. Klapwijk, and G. Hadzi-Ioannou, *Synth. Met.* 76, 85 (1996).
816. M. Granström, *Polym. Adv. Technol.* 8, 424 (1997).
817. T. Granlund, M. Theander, M. Berggren, M. Andersson, A. Ruzeckas, V. Sundström, G. Björk, M. Granström, and O. Inganäs, *Chem. Phys. Lett.* 288, 879 (1988).
818. T. Granlund, M. Theander, M. Berggren, M. Andersson, A. Ruzeckas, V. Sundström, G. Björk, M. Granström, and O. Inganäs, *Synth. Met.* 102, 1038 (1999).
819. P. Barta, J. Sanetra, and M. Zagorska, *Synth. Met.* 94, 119 (1998).
820. J. Cornil, D. Beljonne, D. A. Dossantos, Z. Shuai, and J. L. Bredas, *Synth. Met.* 78, 209 (1996).
821. D. Braun, G. Gustafsson, D. McBranch, and A. J. Heeger, *J. Appl. Phys.* 72, 564 (1992).
822. M. Mazeca, K. G. Cittibabu, J. Kim, J. Kumar, A. Jain, W. Kim, and S. K. Tripathy, *Synth. Met.* 98, 45 (1998).
823. A. Tsumura, T. Ando, and H. Koezuka, *Appl. Phys. Lett.* 49, 1210 (1986).
824. A. Tsumura, T. Ando, and H. Koezuka, *Appl. Phys. Lett.* 49, 1210 (1986).
825. H. Koezuka, T. Ando, and A. Tsumura, *Synth. Met.* 18, 699 (1987).
826. A. Tsumura, T. Ando, and H. Koezuka, *Synth. Met.* 25, 11 (1988).
827. H. Koezuka, A. Tsumura, H. Fuchigami, and K. Kuramoto, *Appl. Phys. Lett.* 62, 1794 (1993).
828. P. Barta, J. Sanetra, P. Grybos, S. Niziol, and M. Trznadel, *Synth. Met.* 94, 115 (1998).
829. A. Assadi, M. Willander, C. Svensson, and J. Hellberg, *Synth. Met.* 58, 187 (1993).
830. P. Dyreklev, G. Gustafsson, O. Inganäs, and H. Stubb, *Synth. Met.* 57, 4093 (1993).
831. G. Horowitz, F. Garnier, A. Yassar, R. Hajlaoui, and F. Kouki, *Adv. Mater.* 8, 52 (1996).
832. H. E. Katz, *J. Mater. Chem.* 7, 369 (1997).
833. A. J. Lovinger and L. J. Rothberg, *J. Mater. Res.* 11, 1581 (1996).
834. Z. Bao and A. J. Lovinger, *Chem. Mater.* 11, 2607 (1999).
835. C. J. Neef, I. D. Brotherton, and J. P. Ferraris, *Chem. Mater.* 11, 1957 (1999).
836. J. C. Gustafsson-Carlberg, O. Inganäs, M. R. Andersson, C. Booth, A. Azen, and C. G. Granqvist, *Electrochim. Acta* 40, 2233 (1995).
837. P. Otto, *Int. J. Quantum Chem.* 52, 353 (1994); P. Otto and J. Ladik, *Synth. Met.* 36, 327 (1990).
838. T.-A. Chen and R. D. Rieke, *Synth. Met.* 60, 175 (1993).
839. P. Hapiot, F. Demanze, A. Yassar, and F. Garnier, *J. Phys. Chem.* 100, 8397 (1996).
840. L. S. Roman, M. R. Andersson, T. Yohannes, and O. Inganäs, *Adv. Mater.* 9, 1164 (1997).
841. L. S. Roman, W. Mammo, L. A. A. Pettersson, M. R. Andersson, and O. Inganäs, *Adv. Mater.* 10, 774 (1998).
842. L. S. Roman, L. C. Chen, L. A. A. Pettersson, W. Mammo, M. R. Andersson, M. Johansson, and O. Inganäs, *Synth. Met.* 102, 977 (1999).
843. E. Villa, E. Agosti, C. Castiglioni, M. C. Gallazzi, and G. Zerbi, *J. Chem. Phys.* 105, 9461 (1996).

844. J. W. Thackeray, H. S. White, and M. S. Wrighton, *J. Phys. Chem.* 89, 5133 (1985).
845. K. Faid, R. Cloutier, and M. Leclerc, *Synth. Met.* 55, 1272 (1993).
846. K. Faid, R. Cloutier, and M. Leclerc, *Macromolecules* 26, 2501 (1993).
847. B. Zinger, Y. Greenwald, and I. Rubinstein, *Synth. Met.* 41, 583 (1991).
848. A. Pron, J. E. Osterholm, P. Smith, A. J. Heeger, J. Laska, and M. Zagórska, *Synth. Met.* 57, 3520 (1993).
849. M. Leclerc and G. Daoust, *Synth. Met.* 41, 529 (1991).
850. Q. Pei, O. Ingasan, G. Gustafsson, M. Granstrom, A. Andersson, T. Hjertberg, O. Wennerstrom, J. E. Osterholm, and J. Laakso, *Synth. Met.* 55, 1221 (1993).
851. M. Sato, K. Kaeriyama, and S. Tanaka, *J. Chem. Soc.-Chem. Commun.* 1986, 873 (1986).
852. R. Hanna and M. Leclerc, *Chem. Mater.* 8, 1512 (1996).
853. S. D. D. V. Rughooputh, M. Nowak, S. Hotta, A. J. Heeger, and F. Wudl, *Synth. Met.* 21, 41 (1987).
854. B. Krische and M. Zagórska, *Synth. Met.* 28, C257 (1989).
855. B. Krische and M. Zagórska, *Synth. Met.* 33, 257 (1989).
856. B. Krische and M. Zagórska, *Synth. Met.* 28, C263 (1989).
857. G. Zotti and G. Schiavon, *Synth. Met.* 39, 183 (1990).
858. T. Yamamoto, M. Zama, M. Hishinuma, and A. Yamamoto, *J. Appl. Electrochem.* 17, 607 (1987).
859. B. Hortling, J. J. Lindberg, and M. Soder, *Angew. Makromol. Chem.* 107, 163 (1982).
860. S. Aeiyaich, E. A. Bazzouai, and P. C. Lacaze, *J. Electroanal. Chem.* 434, 153 (1997).
861. M. Gratzl, D. F. Hsu, A. M. Riley, and J. Janata, *J. Phys. Chem.* 94, 5973 (1990).
862. B. Krische and M. Zagórska, *Synth. Met.* 28, C263 (1989).
863. M. Zhou, M. Persin, and J. Sarrazin, *J. Appl. Electrochem.* 26, 711 (1996).
864. E. Ruckenstein and J. S. Park, *Synth. Met.* 44, 293 (1991).
865. E. Sable, H. Handel, and M. Lher, *Electrochim. Acta* 36, 15 (1991).
866. K. G. Jung, J. W. Schultze, M. Thönissen, and H. Münder, *Thin Solid Films* 255, 317 (1995).
867. B. Pépin-Donat, A. Viallat, E. Rebourt, M. Nechtschein, and B. Sixou, *Synth. Met.* 84, 217 (1997).
868. L. L. Miller, Y. Yu, E. Gunic, and R. Duan, *Adv. Mater.* 7, 547 (1995).
869. R. D. McCullough, *Adv. Mater.* 10, 93 (1998).
870. G. A. Pagani, *Heterocycles* 37, 2069 (1994).
871. J. Roncali, *Chem. Rev.* 92, 711 (1992).
872. K. M. Baumgärtner, M. Volmer-Uebing, J. Taborski, P. Bäuerle, and E. Embach, *Ber. Busen. Ges. Phys. Chem.* 95, 1488 (1991).
873. J. Bukowska and K. Jackowska, *Synth. Met.* 35, 135 (1990).
874. W. Fujita, N. Teramae, and H. Haraguchi, *Chem. Lett.* 1994, 511 (1994).
875. M. Olbrich-Stock, J. Posdorfer, and R. N. Schindler, *J. Electroanal. Chem.* 368, 173 (1994).
876. A. R. Hillman and E. F. Mallen, *J. Electroanal. Chem.* 243, 403 (1988).
877. S. N. Hoier and S.-M. Park, *J. Electrochem. Soc.* 140, 2454 (1993).
878. B. Rasch, P. Novak, and W. Vielstich, *Synth. Met.* 43, 2963 (1991).
879. P. A. Christensen, A. Hamnett, and A. R. Hillman, *J. Electroanal. Chem.* 242, 47 (1988).
880. F. Chao, M. Costa, E. Museux, and E. Levart, *Elektrokhimya* 29, 57 (1993).
881. C. Tian, G. Jin, F. Chao, and M. Costa, *Thin Solid Films* 233, 91 (1993).
882. A. Hamnett and A. R. Hillman, *J. Electrochem. Soc.* 135, 2517 (1988).
883. L. M. Abrantes and J. P. Correia, *Electrochim. Acta* 44, 1901 (1999).
884. J. Lukkari, M. Alanko, V. Pitkanen, K. Kleemola, and J. Kankare, *J. Phys. Chem.* 98, 8525 (1994).
885. J. Lukkari, L. Heikkila, M. Alanko, and J. Kankare, *Synth. Met.* 55, 1311 (1993).
886. J. Lukkari, R. Tuomala, S. Ristimäki, and J. Kankare, *Synth. Met.* 47, 217 (1992).
887. J. Lukkari, J. Kankare, and C. Visy, *Synth. Met.* 48, 181 (1992).
888. C. Visy, J. Lukkari, and J. Kankare, *Synth. Met.* 87, 81 (1997).
889. A. Smie, A. Synowczyk, J. Heinze, R. Alle, P. Tschuncky, G. Götz, and P. Bäuerle, *J. Electroanal. Chem.* 452, 87 (1998).
890. G. Tourillon, D. Guay, A. Fomtaine, R. Garrett, and G. P. Williams, *Faraday Discuss. Chem. Soc.* 89, 275 (1990).
891. A. Berlin, G. Zotti, G. Schiavon, and S. Zecchin, *J. Am. Chem. Soc.* 120, 13,453 (1998).
892. J. R. Diers, M. K. Dearmond, J. Guay, A. Diaz, R. L. Wu, J. S. Schumm, and J. M. Tour, *Chem. Mater.* 6, 327 (1994).
893. P. Tschuncky and J. Heinze, *Synth. Met.* 55, 1603 (1993).
894. M. Pagels, D. G. Weis, V. Rang, and J. Heinze, "Vortragstagung der GDCh-Fachgruppe Angewandte Elektrochemie," Freiberg, 1999, Abstract A-13.
895. T. F. Otero, J. Rodriguez, E. Angulo, and C. Santamaria, *Synth. Met.* 43, 2831 (1991).
896. G. B. Kilic, L. Toppare, and E. Yurtsever, *Synth. Met.* 78, 19 (1996).
897. M. Takakubo, *J. Electroanal. Chem.* 258, 303 (1989).
898. E. Yurtsever and M. Yurtsever, *Synth. Met.* 101, 335 (1999).
899. D. Jones, M. Guerra, L. Favaretto, A. Modelli, M. Fabrizio, and G. Distefano, *J. Phys. Chem.* 94, 5761 (1990).
900. J. A. E. H. van Haare, L. Groenendaal, H. W. I. Peerlings, E. E. Havinga, J. A. J. M. Vekemans, R. A. J. Janssen, and E. W. Meijer, *Chem. Mater.* 7, 1984 (1995).
901. J. A. E. H. van Haare, L. Groenendaal, E. E. Havinga, R. A. J. Janssen, and E. W. Meijer, *Angew. Chem.* 108, 696 (1996).
902. Z. G. Xu, G. Horowitz, and F. Garnier, *J. Electroanal. Chem.* 246, 467 (1988).
903. Y. Chen, H. Huang, and Z. Tian, *Chem. J. Chinese Univ.* 7, 917 (1986).
904. S. J. Dong and W. B. Zhang, *Synth. Met.* 30, 359 (1989).
905. M. Lapkowski, M. Zagórska, I. Kulszewicz-Bajer, and A. Pron, *Synth. Met.* 55, 1570 (1993).
906. M. Lapkowski, M. Zagórska, I. Kulszewicz-Bajer, and A. Pron, *J. Electroanal. Chem.* 341, 151 (1992).
907. Z. G. Xu and G. Horowitz, *J. Electroanal. Chem.* 335, 123 (1992).
908. C. Visy and J. Kankare, "Proceedings of the 50th ISE Meeting," Pavia, Italy, 1999, Abstract 3b-359.
909. C. Visy, M. Lakatos, A. Szucs, and M. Novak, *Electrochim. Acta* 42, 651 (1997).
910. U. Barsh, F. Beck, G. Hambitzer, R. Holze, J. Lippe, and I. Stassen, *J. Electroanal. Chem.* 369, 97 (1994).
911. F. Chao and M. Costa, *Synth. Met.* 39, 97 (1990).
912. K. Faid and M. Leclerc, *Chem. Mater.* 6, 107 (1994).
913. W. J. Plieth, J. Zerbino, C. Lahmann, and G. Kossmehl, *J. Electroanal. Chem.* 274, 213 (1989).
914. J. Zerbino, W. J. Plieth, and G. Kossmehl, *J. Electroanal. Chem.* 260, 361 (1989).
915. G. A. Pagani, *Heterocycles* 37, 2069 (1994).
916. J. L. Brédas, D. S. Boudreaux, R. R. Chance, and R. Silbey, *J. Am. Chem. Soc.* 105, 6555 (1983).
917. A. F. Diaz, J. Crowley, J. Bargon, G. Gardini, and J. B. Torrance, *J. Electroanal. Chem.* 121, 355 (1981).
918. C. Alemán and L. Julià, *J. Phys. Chem.* 100, 14,661 (1996).
919. J. Casado, V. Hernandez, S. Hotta, and J. T. L. Navarrete, *J. Chem. Phys.* 109, 10,419 (1998).
920. J. W. van der Horst, P. A. Bobbert, M. A. J. Michels, G. Brocks, and P. J. Kelly, *Synth. Met.* 101, 333 (1999).
921. H. Subramanian and J. B. Lagowski, *Int. J. Quantum Chem.* 66, 229 (1998).
922. C. Visy, J. Lukkari, and J. Kankare, *Synth. Met.* 55, 1620 (1993).
923. F. Moraes, D. Davidov, M. Kobayashi, T. C. Chung, J. Chen, A. J. Heeger, and F. Wudl, *Synth. Met.* 10, 169 (1985).

924. M. Onoda, T. Iwasa, T. Kawai, and K. Yoshino, *J. Phys. D: Appl. Phys.* 24, 2076 (1991).
925. K. Kaneto, F. Uesugi, and K. Yoshino, *J. Phys. Soc. Jpn.* 56, 3703 (1987).
926. D. Fichou, G. Horowitz, B. Xu, and F. Garnier, *Synth. Met.* 39, 243 (1990).
927. H. J. Ahonen, J. Kankare, J. Lukkari, and P. Pasanen, *Synth. Met.* 84, 215 (1997).
928. Q. B. Pei, G. Zuccarello, M. Ahlskog, and O. Inganäs, *Polymer* 35, 1347 (1994).
929. T. F. Otero and E. Angulo, *Synth. Met.* 55, 1430 (1993).
930. R. Holze, *Synth. Met.* 40, 379 (1991).
931. C. Yong and Q. Renyuan, *Solid State Commun.* 54, 211 (1985).
932. M. Akimoto, Y. Furukawa, H. Takeuchi, I. Harada, Y. Soma, and M. Soma, *Synth. Met.* 15, 353 (1986).
933. Y. Furukawa, M. Akimoto, and I. Harada, *Synth. Met.* 18, 151 (1987).
934. Z. Vardeny, E. Ehrenfreund, O. Brafman, A. J. Heeger, and F. Wudl, *Synth. Met.* 18, 183 (1987).
935. J. P. Lere-Porte, J. L. Sauvajol, S. Hasson, D. Chenouni, M. Galtier, and J. Petrisans, *Mol. Cryst. Liq. Cryst., Sect. A* 161, 223 (1988).
936. H. Neugebauer, A. Neckel, G. Nauer, N. Brinda-Konopik, F. Garnier, and G. Tourillon, *J. Phys. (Paris)* C10 44, 517 (1983).
937. H. Neugebauer, G. Nauer, A. Neckel, G. Tourillon, F. Garnier, and P. Lang, *J. Phys. Chem.* 88, 652 (1984).
938. H. Neugebauer, A. Neckel, and N. Brinda-Konopik, in "Electronic Properties of Polymers and Related Compounds" (H. Kuzmany, M. Mehring, and S. Roth, Eds.). Springer Series in Solid State Science, Vol. 63, p. 227. Springer-Verlag, Berlin, 1985.
939. J. Bukowska and K. Jackowska, *Synth. Met.* 35, 135 (1990).
940. J. Bukowska and K. Jackowska, *Synth. Met.* 35, 143 (1990).
941. E. Faulques, H. Kuzmany, and W. Wallnöfer, *J. Chem. Phys.* 90, 7585 (1989).
942. M. Kofranek, T. Kovar, H. Lischka, and A. Karpfen, *Theochem.* 91, 181 (1992).
943. S. Sunde, G. Hagen, and R. Ødegard, "Proceedings of ICSM 90," Tübingen, 1990, Abstract ECH 1.29.
944. A. Hidalgo, *J. Phys. Radium* 16, 366 (1955).
945. M. Rico, J. M. Orza, and J. Morcillo, *Spectrochim. Acta* 21, 689 (1965).
946. F. R. Dollish, W. G. Fateley, and F. F. Bentley, "Characteristic Raman Frequencies of Organic Compounds," p. 220. Wiley, New York, 1974.
947. D. W. Scott, *J. Mol. Spectrosc.* 31, 451 (1969).
948. J. Bukowska and K. Jackowska, *Synth. Met.* 35, 143 (1990).
949. F. Beck, P. Braun, and M. Oberst, *Ber. Bunsen. Ges. Phys. Chem.* 91, 967 (1987).
950. J. Geisselbrecht, J. Kürti, and H. Kuzmany, *Synth. Met.* 57, 4266 (1993).
951. E. A. Bazzaoui, J. P. Marsault, S. Aeiyaich, and P. C. Lacaze, *Synth. Met.* 66, 217 (1994).
952. T. Danno, J. Kastner, and H. Kuzmany, *Synth. Met.* 58, 257 (1993).
953. J. L. Sauvajol, D. Chenouni, J. P. Lereporte, C. Chorro, B. Moukala, and J. Petrisans, *Synth. Met.* 38, 1 (1990).
954. J. L. Sauvajol, G. Poussigie, C. Benoit, J. P. Lere-Porte, and C. Chorro, *Synth. Met.* 41, 1237 (1991).
955. G. Poussigie, C. Benoit, J. L. Savajol, J. P. Lereporte, and C. Chorro, *J. Chim. Phys. Phys.-Chim. Biol.* 89, 1091 (1992).
956. E. A. Bazzaoui, G. Levi, S. Aeiyaich, J. Aubard, J. P. Marsault, and P. C. Lacaze, *J. Phys. Chem.* 99, 6628 (1995).
957. G. Louarn, J. Y. Mevellec, J. P. Buisson, and S. Lefrant, *J. Chim. Phys. Phys.-Chim. Biol.* 89, 987 (1992).
958. G. Tourillon, D. Guay, A. Fontaine, R. Gerrett, and G. P. Williams, *Faraday Discuss. Chem. Soc.* 89, 275 (1990).
959. M. Boman, H. Agren, and S. Stafstrom, *J. Phys. Chem.* 99, 16,597 (1995).
960. E. A. Bazzaoui, S. Aeiyaich, J. Aubard, N. Felidj, P. C. Lacaze, N. Sakmeche, and G. Levi, *J. Raman Spectrosc.* 29, 177 (1998).
961. E. A. Bazzaoui, S. Aeiyaich, J. Aubard, N. Felidj, G. Levi, N. Sakmeche, and P. C. Lacaze, *J. Chim. Phys. Phys.-Chim. Biol.* 95, 1526 (1998).
962. J. L. Sauvajol, G. Poussigie, C. Benoit, J. P. Lereporte, and C. Chorro, *Synth. Met.* 41, 1237 (1991).
963. W. Wallnöfer, H. Kuzmany, and E. Faulques, in "Electronic Properties of Conjugated Polymers III" (H. Kuzmany, M. Mehring, and S. Roth, Eds.). Springer Series in Solid State Science, Vol. 91, p. 354. Springer-Verlag, Berlin, 1989.
964. M. Trznadel, M. Zagorska, M. Lapkowski, G. Louarn, S. Lefrant, and A. Pron, *J. Chem. Soc., Faraday Trans.* 92, 1387 (1996).
965. R. D. McCulloch and R. D. Lowe, *J. Chem. Soc., Chem. Commun.* 1992, 70 (1992).
966. R. K. Yuan, D. S. Ginley, D. Peramunage, and M. Tomkiewicz, *J. Electrochem. Soc.* 134, 886 (1987).
967. A. Ivaska, M. Koponen, P. Passiniemi, and J. E. Osterholm, *Mikrochim. Acta* 1, 259 (1988).
968. G. Louarn, J. Kruszka, S. Lefrant, M. Zagorska, I. Kulszewicz-Bajer, and A. Pron, *Synth. Met.* 61, 233 (1993).
969. E. Agosti, M. Rivola, V. Hernandez, M. Delzoppo, and G. Zerbi, *Synth. Met.* 100, 101 (1999).
970. L. Torsi, *Synth. Met.* 41, 575 (1991).
971. G. Tourillon, D. Gourier, P. Garnier, and D. Vivien, *J. Phys. Chem.* 88, 1049 (1984).
972. J. Chen, A. J. Heeger, and F. Wudl, *Solid State Commun.* 58, 251 (1986).
973. G. Zotti and G. Schiavon, *Synth. Met.* 31, 347 (1989).
974. G. Zotti and S. Zecchin, *Synth. Met.* 87, 115 (1997).
975. Y. Furukawa, *J. Phys. Chem.* 100, 15,644 (1996).
976. Y. Furukawa, *Synth. Met.* 69, 629 (1995).
977. F. Genoud, J. Kruszka, M. Nechtschein, M. Zagorska, I. Kulszewicz-Bajer, and A. Pron, *J. Chim. Phys.* 87, 57 (1990).
978. I. Kulszewicz-Bajer, M. Zagorska, F. Genoud, J. Kruszka, K. Stocka, A. Pron, and M. Nechtschein, *Synth. Met.* 35, 129 (1990).
979. M. Springborg, *Synth. Met.* 43, 3541 (1991).
980. G. Horowitz, A. Yassar, and H. J. von Bardeleben, *Synth. Met.* 62, 245 (1994).
981. B. Nessakh, G. Horowitz, F. Garnier, F. Deloffre, P. Srivastava, and A. Yassar, *J. Electroanal. Chem.* 399, 97 (1995).
982. M. G. Hill, J. F. Penneau, B. Zinger, K. R. Mann, and L. L. Miller, *Chem. Mater.* 4, 1106 (1992).
983. J. Fink, N. Nücker, B. Scheerer, and H. Neugebauer, *Synth. Met.* 18, 163 (1987).
984. J. A. Reedijk, H. C. F. Martens, S. M. C. van Bohemen, O. Hilt, H. B. Brom, and M. A. J. Michels, *Synth. Met.* 101, 475 (1999).
985. C. Aleman, *Macromol. Theory Simul.* 6, 237 (1997).
986. G. Zotti, *Synth. Met.* 97, 267 (1998).
987. K. Yoshino, D. H. Park, B. K. Park, M. Fujii, and R. Sugimoto, *Jpn. J. Appl. Phys.* 27, L1410 (1988).
988. Y. Harima, T. Eguchi, and K. Yamashita, *Synth. Met.* 95, 69 (1998).
989. M. Kabasakalogu, T. Kiyak, H. Toprak, and M. L. Aksu, *Appl. Surf. Sci.* 152, 115 (1999).
990. J. Kankare, E.-L. Kupila, F. Dini, F. Andreani, E. Salatelli, and M. Lanzi, "Proceedings of the 192nd ECS Meeting," Paris, 1998, Abstract 1282.
991. M. C. Morvant and J. R. Reynolds, *Synth. Met.* 92, 57 (1998).
992. E. Lankinen, G. Sundholm, P. Talonen, T. Laitinen, and T. Saario, *J. Electroanal. Chem.* 447, 135 (1998).
993. E. Lankinen, P. Talonen, G. Sundholm, T. Laitinen, and T. Saario, "Proceedings of the 192nd ECS Meeting," Paris, 1998, Abstract 1494.
994. E. Lankinen, M. Pohjakallio, G. Sundholm, P. Talonen, T. Laitinen, and T. Saario, *J. Electroanal. Chem.* 437, 167 (1997).

995. M. Pohjakallio, G. Sundholm, P. Talonen, C. Lopez, and E. Vieil, *J. Electroanal. Chem.* 396, 339 (1995); M. Pohjakallio, G. Sundholm, and P. Talonen, *J. Electroanal. Chem.* 406, 165 (1996).
996. E. Lankinen, M. Pohjakallio, G. Sundholm, O. R. Konestabo, and E. J. Samuelsen, *Acta Chem. Scand.* 50, 749 (1996).
997. L. M. Abrantes, J. P. Correia, and E. Vieil, "Proceedings of the 50th ISE Meeting," Pavia, Italy, 1999, Abstract 3b-926.
998. O. A. Semenikhin, E. V. Ovsyannikova, N. M. Alpatova, Z. A. Rotenberg, and V. E. Kazarinov, *Russ. J. Electrochem.* 30, 666 (1994).
999. O. A. Semenikhin, M. R. Ehrenburg, E. V. Ovsyannikov, and N. M. Alpatova, "Proceedings of the 50th ISE Meeting," Pavia, Italy, 1999, Abstract 3b-562.
1000. L. M. Abrantes and J. P. Correia, *Electrochim. Acta* 41, 1747 (1996).
1001. O. A. El-Rashiedy and S. Holdcroft, *J. Phys. Chem.* 100, 5481 (1996).
1002. F. Moraes, A. J. Heeger, M. Kobayashi, H. Schaffer, and F. Wudl, *Phys. Rev. B: Condens. Matter* 30, 2948 (1984).
1003. D. F. Hsu, M. Gratzl, A. M. Riley, and J. Janata, *J. Phys. Chem.* 94, 5982 (1990).
1004. K.-M. Mangold and K. Jüttner, in "GDCh Momographie," (J. Russov, G. Sandstede, and R. Staab, Eds.), Vol. 14, p. 47. GDCh, Frankfurt, 1999.
1005. K. Aoki, *J. Electroanal. Chem.* 373, 67 (1994).
1006. T. F. Otero, H. J. Grande, and J. Rodriguez, *J. Phys. Chem. B: At. Mol. Opt. Phys.* 101, 3688 (1997).
1007. A. Smie and J. Heinze, *Angew. Chem.* 109, 375 (1997).
1008. A. Fikus, U. Rammelt, and W. Plieth, *Electrochim. Acta* 44, 2025 (1999).
1009. K. Kaneto, Y. Kohno, and K. Yoshino, *Solid State Commun.* 51, 267 (1984).
1010. T. Hattori, W. Hayes, K. Kaneto, K. Wong, and K. Yoshino, *J. Phys. C: Solid State Phys.* 17, L803 (1984).
1011. N. Hosaka, H. Tachibana, N. Shiga, M. Matsumoto, and Y. Tokura, *Phys. Rev. Lett.* 82, 1672 (1999).
1012. Y. Tezuka, K. Aoki, and A. Ishii, *Electrochim. Acta* 44, 1871 (1999).
1013. G. Tourillon and F. Garnier, *J. Electroanal. Chem.* 161, 407 (1984).
1014. J. Guay, A. F. Diaz, J. Y. Bergeron, and M. Leclerc, *J. Electroanal. Chem.* 361, 85 (1993).
1015. J. P. Aimé, F. Bargain, M. Schott, H. Eckhardt, R. L. Elsenbaumer, G. G. Miller, M. E. McDonnell, and K. Zero, *Synth. Met.* 28, C407 (1989).
1016. G. W. Heffner and D. S. Pearson, *Macromolecules* 24, 6295 (1991).
1017. M. J. Winokur, P. Wamsley, P. Moulton, P. Smith, and A. J. Heeger, *Macromolecules* 24, 3812 (1991).
1018. S. D. D. V. Rughooputh, M. Nowak, S. Hotta, A. J. Heeger, and F. Wudl, *Synth. Met.* 21, 41 (1987).
1019. J. Li and K. Aoki, *J. Electroanal. Chem.* 453, 107 (1998).
1020. P. A. Christensen, A. Hamnett, and D. C. Read, *Electrochim. Acta* 39, 187 (1994).
1021. S. Servagent and E. Vieil, *J. Electroanal. Chem.* 280, 227 (1990).
1022. M. Onoda, T. Iwasa, T. Kawai, J. Nakayama, H. Nakahara, and K. Yoshino, *J. Electrochem. Soc.* 140, 397 (1993).
1023. M. Onoda, T. Iwasa, T. Kawai, K. Yoshino, J. Nakayama, and H. Nakahara, *Synth. Met.* 55, 1532 (1993).
1024. M. Zagórska and B. Krische, in "Electronic Properties of Conjugated Polymers III" (H. Kuzmany, M. Mehring, and S. Roth, Eds.), Springer Series in Solid State Science, Vol. 91, p. 343. Springer-Verlag, Berlin, 1989.
1025. R. Rühle, A. Berlin, and G. Wegner, in "Electronic Properties of Conjugated Polymers III" (H. Kuzmany, M. Mehring, and S. Roth, Eds.), Springer Series in Solid State Science, Vol. 91, p. 348. Springer-Verlag, Berlin, 1989.
1026. M. Leclerc and G. Daoust, *Synth. Met.* 41, 529 (1991).
1027. G. Daoust and M. Leclerc, *Macromolecules* 24, 455 (1991).
1028. C. Aléman and L. Julia, *J. Phys. Chem.* 100, 1524 (1996).
1029. G. Zotti, M. C. Gallazzi, G. Zerbi, and S. V. Meille, *Synth. Met.* 73, 217 (1995).
1030. J. Roncali, P. Marque, R. Garreau, F. Garnier, and M. Lemaire, *Macromolecules* 23, 1347 (1990).
1031. J. Roncali, L. H. Shi, and F. Garnier, *J. Phys. Chem.* 95, 8983 (1991).
1032. J. Roncali, A. Gorgues, and M. Jubault, *Chem. Mater.* 5, 1456 (1993).
1033. J. P. Ferraris and M. D. Newton, *Polymer* 33, 391 (1992).
1034. H. Shirakawa, S. Fukumoto, H. Tanaka, Y. Ugawa, K. Akagi, K. Kaeriyama, and H. Masuda, *J. Macromol. Sci., Chem. A* 28, 1245 (1991).
1035. H. Ishikawa, K. Amano, A. Kobayashi, M. Satoh, and E. Hasegawa, *Synth. Met.* 64, 49 (1994).
1036. P. Dyreklev and O. Inganäs, *J. Appl. Phys.* 76, 7915 (1994).
1037. P. Dyreklev and O. Inganäs, *Synth. Met.* 69, 387 (1995).
1038. F. Demanze, A. Yassar, and F. Garnier, *Adv. Mater.* 7, 907 (1995).
1039. F. Demanze, A. Yassar, and F. Garnier, *Macromolecules* 29, 4267 (1996).
1040. F. Demanze, A. Yassar, and F. Garnier, *Synth. Met.* 76, 269 (1996).
1041. J. Roncali, P. Marque, R. Garreau, F. Garnier, and M. Lemaire, *Macromolecules* 23, 1347 (1990).
1042. M. J. Nowak, S. D. D. V. Rughooputh, S. Hotta, and A. J. Heeger, *Macromolecules* 20, 965 (1987).
1043. F. Demanze, A. Yassar, and F. Garnier, *Synth. Met.* 78, 143 (1996).
1044. A. Pron, G. Louarn, M. Lapkowski, M. Zagórska, J. Glowczyk-Zubek, and S. Lefrant, *Macromolecules* 28, 4644 (1995).
1045. T. Hagiwara, M. Yamaura, K. Sato, M. Hirasaka, and K. Iwata, *Synth. Met.* 32, 367 (1989).
1046. E. E. Havinga, C. M. J. Mutsaers, and L. W. Jenneskens, *Chem. Mater.* 8, 769 (1996).
1047. M. E. Randazzo, L. Toppare, and J. E. Fernandez, *Macromolecules* 27, 5102 (1994).
1048. W. Wallnöfer, H. Kuzmany, and E. Faulques, in "Electronic Properties of Conjugated Polymers III" (H. Kuzmany, M. Mehring, and S. Roth, Eds.), Springer Series in Solid State Science, Vol. 91, p. 354. Springer-Verlag, Berlin, 1989.
1049. W. Wallnöfer, E. Faulques, H. Kuzmany, and K. Eichinger, *Synth. Met.* 28, C533 (1989).
1050. J. L. Brédas, *J. Chem. Phys.* 82, 3808 (1985).
1051. F. Wudl, M. Kobayashi, and A. J. Heeger, *J. Org. Chem.* 36, 3382 (1984).
1052. M. Kobayashi, N. Colaneri, M. Boysel, F. Wudl, and A. J. Heeger, *J. Chem. Phys.* 82, 5717 (1985).
1053. N. Colaneri, M. Kobayashi, A. J. Heeger, and F. Wudl, *Synth. Met.* 14, 45 (1986).
1054. Y. S. Lee and M. Kertesz, *Int. J. Quantum Chem. Symp.* 21, 163 (1987).
1055. W. Wallnöfer, E. Faulques, H. Kuzmany, and K. Eichinger, *Synth. Met.* 28, C533 (1989).
1056. E. Faulques, H. Kuzmany, and W. Wallnöfer, *J. Chem. Phys.* 90, 7585 (1989).
1057. G. Zerbi, M. C. Magnoni, I. Hoogmartens, R. Kiebooms, R. Carleer, D. Vanderzande, and J. Gelan, *Adv. Mater.* 7, 1027 (1995).
1058. L. Huchet, S. Akoudad, and J. Roncali, *Adv. Mater.* 10, 541 (1998).
1059. F. B. Kaufman, A. H. Shroeder, E. M. Engles, S. R. Kramer, and J. Q. Chambers, *J. Am. Chem. Soc.* 102, 483 (1980).
1060. M. R. Bryce, A. D. Chissel, J. Gopal, P. Kathirgamanathan, and D. Parker, *Synth. Met.* 39, 397 (1991).
1061. L. Huchet, S. Akoudad, E. Levillain, J. Roncali, A. Emge, and P. Bäuerle, *J. Phys. Chem. B* 102, 7776 (1998).
1062. B. Krische and M. Zagórska, *Synth. Met.* 28, C257 (1989).
1063. L. Zhou, X. R. Liu, and G. Xue, *Spectrosc. Lett.* 31, 1529 (1998).
1064. Y. Takenaka, T. Koike, T. Oka, and M. Tanahashi, *Synth. Met.* 18, 207 (1987).
1065. S. L. Wang, K. Tanaka, and T. Yamabe, *Synth. Met.* 32, 141 (1989).
1066. J. Nakayama, T. Konishi, S. Murabayashi, and M. Hoshino, *Heterocycles* 26, 1793 (1987).
1067. J. Fink, N. Nücker, B. Scheerer, and H. Neugebauer, *Synth. Met.* 18, 163 (1987).

1068. S. Aeiyaich, A. Kone, M. Dieng, J. J. Aaron, and P. C. Lacaze, *J. Chem. Soc., Chem. Commun.* 1991, 822 (1991).
1069. U. Barsch and F. Beck, *Synth. Met.* 55, 1638 (1993).
1070. S. Ren and D. Barkey, *J. Electrochem. Soc.* 139, 1021 (1992).
1071. J. Ochmanska and P. G. Pickup, *J. Electroanal. Chem.* 297, 211 (1991).
1072. P. G. Pickup, W. Kutner, C. R. Leidner, and R. W. Murray, *J. Am. Chem. Soc.* 106, 1991 (1984).
1073. D. Ofer, R. M. Crooks, and M. S. Wrighton, *J. Am. Chem. Soc.* 112, 7869 (1990).
1074. E. A. Bazzouai, J. Aubard, A. Elidrissi, A. Ramdani, and G. Levi, *J. Raman Spectrosc.* 29, 799 (1998).
1075. K. Uehara, T. Ichikawa, T. Serikawa, S. Yoshikawa, S. Ehara, and M. Tsunooka, *Thin Solid Films* 322, 198 (1998).
1076. X. Hong, J. C. Tyson, J. S. Middlecoff, and D. M. Collard, *Macromolecules* 32, 4232 (1999).
1077. M. Zagórska, I. Kulszewicz-Bajer, A. Prón, J. Sukiennik, P. Raimond, F. Kajzar, A.-J. Attias, and M. Lapkowski, *Macromolecules* 31, 9146 (1998).
1078. G. T. Li, G. Kossmeihl, H. P. Welzel, G. Engelman, W. D. Hunnius, W. Pleth, and H. S. Zhu, *Macromol. Chem. Phys.* 199, 2255 (1998).
1079. H. P. Welzel, G. Kossmeihl, G. Engelman, W. D. Hunnius, and W. Plieth, *Electrochim. Acta* 44, 1827 (1999).
1080. G. T. Li, G. Kossmeihl, H. P. Welzel, W. Plieth, and H. S. Zhu, *Macromol. Chem. Phys.* 199, 2737 (1998).
1081. J. Q. Li and K. Aoki, *J. Electroanal. Chem.* 458, 155 (1998).
1082. P. N. Bartlett and D. H. Dawson, *J. Mater. Chem.* 4, 1805 (1994).
1083. R.-M. Latonen, C. Kvarnström, and A. Ivaska, "Proceedings of the 50th ISE Meeting," Pavia, Italy, 1999, Abstract 3b-1026.
1084. B. Mirzyska, R. Borkowska, and J. Plochanski, *Polish J. Chem.* 68, 1863 (1994).
1085. D. S. K. Mudigonda, D. C. Loveday, and J. P. Ferraris, *Synth. Met.* 84, 349 (1997).
1086. A. Emge and P. Bäuerle, *Synth. Met.* 102, 1370 (1999).
1087. C. Taliani, R. Danieli, R. Zamboni, G. Giro, and F. Sannicò, in "Electronic Properties of Conjugated Polymers" (H. Kuzmany, M. Mehring, and S. Roth, Eds.). Springer Series in Solid State Science, Vol. 76, p. 326. Springer-Verlag, Berlin, 1987.
1088. P. Marrec, B. Fabre, and J. Simonet, *J. Electroanal. Chem.* 437, 245 (1997).
1089. J. Roncali, R. Garreau, and M. Lemaire, *J. Electroanal. Chem.* 278, 373 (1990).
1090. J. Roncali, R. Garreau, D. Delabouglise, F. Garnier, and M. Lemaire, *Synth. Met.* 28, C341 (1989).
1091. D. C. Loveday, M. Hmyene, and J. P. Ferraris, *Synth. Met.* 84, 245 (1997).
1092. D. Dini, F. Decker, and G. Zotti, "Proceedings of the 50th ISE Meeting," Pavia, Italy, 1999, Abstract 3b-329.
1093. J. Roncali, R. Garreau, and M. Lemaire, *J. Electroanal. Chem.* 278, 373 (1990).
1094. B. Fabre and J. Simonet, *Coord. Chem. Rev.* 180, 1211 (1998).
1095. L. M. Goldenberg, I. Levesque, M. Leclerc, and M. C. Petty, *J. Electroanal. Chem.* 447, 1 (1998).
1096. L. Lancellotti, R. Tubino, S. Luzzati, E. Licandro, S. Maiorana, and A. Papagni, *Synth. Met.* 93, 27 (1998).
1097. U. Rammlet, M. Wolter, N. Hebestreit, W. Plieth, D. Ferse, and H.-J. Adler, "Proceedings of the 50th ISE Meeting," Pavia, Italy, 1999, Abstract 3b-436.
1098. H. Yamato, K. Kai, M. Ohwa, W. Wernet, and M. Matsumura, *Electrochim. Acta* 42, 2517 (1997).
1099. J. M. Ortega, "Proceedings of the 50th ISE Meeting," Pavia, Italy, 1999, Abstract 3b-350.
1100. M. C. Pham, M. Mostefai, M. Simon, and P. C. Lacaze, *Synth. Met.* 63, 7 (1994).
1101. M. Mostefai, M. C. Pham, J. P. Marsault, J. Aubard, and P. C. Lacaze, *J. Electrochem. Soc.* 143, 2116 (1996).
1102. A. K. Agrawal and S. A. Jenekhe, *Chem. Mater.* 8, 579 (1996).
1103. G. Froyer, Y. Pelous, and G. Olliver, in "Electronic Properties of Conjugated Polymers" (H. Kuzmany, M. Mehring, and S. Roth, Eds.). Springer Series in Solid State Science, Vol. 76, p. 302. Springer-Verlag, Berlin, 1987.
1104. E. W. Chang, R. J. Kuk, and R. B. Kaner, *Synth. Met.* 55, 930 (1993).
1105. P. C. Lacaze, S. Hara, P. Soubiran, and S. Aeiyaich, *Synth. Met.* 75, 111 (1995).
1106. S. T. Selvan, A. Mani, S. Pitchumani, and K. L. N. Phani, *J. Electroanal. Chem.* 384, 183 (1995).
1107. E. Y. Pisarevskaya, S. S. Sedova, A. L. Ignatov, and N. A. Tomilova, *Russ. J. Electrochem.* 30, 831 (1994).
1108. P. Damlin, C. Kvarnström, and A. Ivaska, *Analyst* 121, 1881 (1996).
1109. K. Miyashita and M. Kaneko, *J. Electroanal. Chem.* 403, 53 (1996).
1110. M. A. Vorotynev and J. Heinze, "Proceedings of the 50th ISE Meeting," Pavia, Italy, 1999, Abstract 3b-819.
1111. J. L. Brédas, B. Themans, J. G. Fripiat, J. M. Andrè, and R. R. Chance, *Phys. Rev. B* 29, 6761 (1984).
1112. Y. Furukawa, *J. Phys. Chem.* 100, 15,644 (1996).
1113. P. Damlin, C. Kvarnström, H. Neugebauer, and A. Ivaska, "Proceedings of the 50th ISE Meeting," Pavia, Italy, 1999, Abstract 3b-1027.
1114. M. Bilkiewicz, B. Palys, and K. Jackowska, "Proceedings of the 50th ISE Meeting," Pavia, Italy, 1999, Abstract 3b-273.

This Page Intentionally Left Blank

ELECTRONIC SPECTRA OF CONJUGATED POLYMERS AND OLIGOMERS

Yukio Furukawa

Department of Chemistry, School of Science and Engineering, Waseda University,
Shinjuku-ku, Tokyo 169-8555, Japan

Contents

1. Introduction	303
2. Charge Carriers in Conjugated Polymers	304
2.1. Ground-State Structures	304
2.2. Self-Localized Excitations	305
3. Electronic Spectra	305
3.1. Neutral and Charged Oligomers	305
3.2. Neutral and Doped Polymers	313
4. Concluding Remarks	317
Acknowledgments	317
References	318

1. INTRODUCTION

The science and technology of conjugated conducting polymers have advanced very rapidly since the first report of metallic conductivities in doped polyacetylene in 1977 [1]. Following the case of polyacetylene, other conducting polymers, such as polypyrrole, polythiophene, poly(*p*-phenylene), polyaniline, poly(*p*-phenylenevinylene), and poly(2,5-thienylenevinylene), have been reported. The chemical structures of conjugated polymers are shown in Figure 1. They have a variety of chemical moieties such as the vinylene group, benzene rings, and heterocycles. A large number of studies published during the past 23 years have opened a new field in materials science that encompasses solid-state and theoretical physics, synthetic chemistry, and device engineering [2, 3]. Although conjugated polymers have been developed as organic conductors, they can be used for semiconductor devices instead of inorganic materials. Semiconductor devices fabricated with conjugated polymers, such as transistors [4, 5], photodiodes [6], and light-emitting diodes [7], have been proposed. Conjugated polymers with various substituents such as long alkyl chains are soluble in organic solvents. Since soluble and high-purity polymers became available, polymer semiconductor devices have been developed extensively [8–10]. Conjugated oligomers have been investigated as models of conjugated polymers, whereas they themselves have potential applications in electronic devices. Novel properties of con-

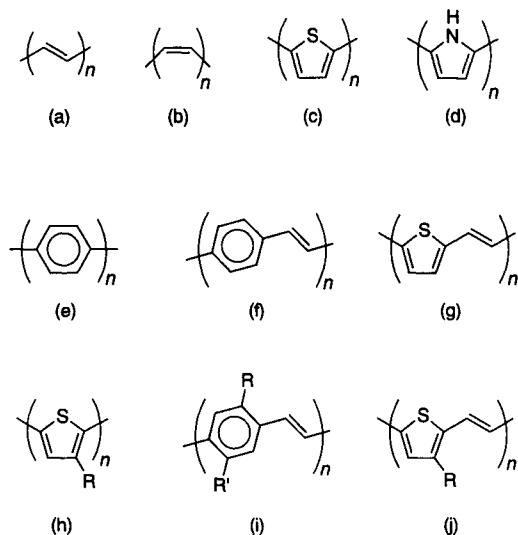


Fig. 1. Chemical structures of conjugated polymers: (a) *trans*-polyacetylene; (b) *cis*-polyacetylene; (c) polythiophene; (d) polypyrrole; (e) poly(*p*-phenylene); (f) poly(*p*-phenylenevinylene); (g) poly(2,5-thienylenevinylene); (h) substituted polythiophenes (R: H, C₆H₁₃, C₈H₁₇, C₁₀H₂₁, C₁₂H₂₅, etc.); (i) substituted poly(*p*-phenylenevinylene)s (R, R': H, OCH₃, OC₆H₁₃, OC₈H₁₇, etc.); (j) substituted poly(2,5-thienylenevinylene)s (R: H, C₄H₉, etc.).

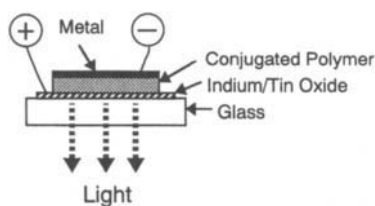


Fig. 2. Schematic structure of a light-emitting diode fabricated with a conjugated polymer.

jugated systems originate from π -electrons that respond easily to external electric and magnetic fields.

Most of the undoped conjugated polymers are organic semiconductors. Optical bandgaps of conjugated polymers are in the range from 1 to 3 eV [11]. When a conjugated polymer is irradiated by light across its bandgap, charge separation occurs. The charge separation can result in the formation of charge carriers and the polymer shows photoconductivity. Upon the addition of an electron acceptor such as C_{60} , photoconductivity is enhanced dramatically [12]. Thus, conjugated polymer- C_{60} composites are good active layers for photovoltaic devices such as photodetectors or solar cells. Electroluminescence, the generation of light by electrical excitation, is observed for organic materials. Conjugated polymers can be used for active layers in electroluminescent devices (light-emitting diodes). The schematic structure of a one-layer light-emitting diode fabricated with a conjugated polymer is shown in Figure 2. Spreitzer et al. [13] recently reported that light-emitting diodes fabricated with a copolymer of poly(*p*-phenylenevinylene) derivatives show very high power efficiency (16 lm/W); this value is comparable to that of light-emitting diodes fabricated with inorganic semiconductors or organic molecules. The process response for electroluminescence requires injection of electrons from one electrode and holes from the other, the capture of oppositely charged carriers (so-called recombination), and the radiative decay of the excited electron-hole state (exciton) produced by this recombination process.

Chemical doping is performed by exposing a polymer film in various ways to an electron acceptor (iodine, AsF_5 , H_2SO_4 , etc.) or an electron donor (alkali metals, etc.). The main process of doping is a redox reaction between polymer chains and acceptors or donors. Upon acceptor doping (p-type doping), an ionic complex that consists of positively charged polymer chains and counteranions (I_3^- , AsF_6^- , etc.) is formed. Counteranions are generated by reduction of acceptors. In the case of donor doping (n-type doping), an ionic complex that consists of negatively charged polymer chains and counterocations (Na^+ , K^+ , etc.) is formed. Counterocations are generated by oxidation of donors. Electrical conductivity can be controlled by the dopant content. Charge carriers are formed by chemical doping.

A deep understanding of creation, transport, and decay processes of charge carriers is important for understanding the electronic properties of conjugated polymers at both intact and doped states. The carrier in a conjugated polymer is not an electron or a hole, but a quasiparticle with structural changes of the polymer backbone, because of the strong electron-lattice interaction of the polymer. Solitons [14], polarons [15–17], and bipolarons [16–18] have been proposed as charge carriers. They are collectively called elementary excitations or self-localized excitations. They can, in principle, move along a polymer chain with geometrical changes and hop a polymer chain to a neighboring chain.

Actual samples of conjugated polymers have more or less disordered structures and a distribution of conjugation lengths. Thus, spectroscopic studies of well-defined model compounds including radical ions, divalent ions, and electronically excited states, are useful for a better understanding of the optical properties of conducting polymers. An introduction to the carriers in conjugated polymers is given in Section 2. In Section 3, we describe the electronic absorption spectra of neutral and doped polymers.

2. CHARGE CARRIERS IN CONJUGATED POLYMERS

2.1. Ground-State Structures

The question of whether the C–C bonds in an infinite polyene chain are equal or alternate in length has been discussed by quantum chemists since the 1950s [19, 20]. Bond alternation is closely related to the electronic properties of the polymer. A structure that has bond alternation is expected to be a semiconductor, because of the existence of bandgap. On the other hand, a structure that has no bond alternation is expected to be a metal, because of the nonexistence of bandgap. Various experimental results on oligoenes have shown the existence of alternating single and double bonds. The bond alternation in *trans*-polyacetylene has been confirmed by X-ray [21] and nutation nuclear magnetic resonance (NMR) [22] studies. According to the nutation NMR study [22], the lengths of the C–C and C=C bonds in *trans*-polyacetylene are 1.44 and 1.36 Å, respectively. However, it is difficult to determine exact structure parameters for conducting polymers from X-ray diffraction studies, because single crystals of the polymers are unavailable. It is then useful to examine the structures of the polymers and model oligomers by molecular orbital (MO) methods, especially at *ab initio* Hartree–Fock levels or in higher approximations, and density functional methods.

The ground states of conjugated polymers can be divided into two types: degenerate and nondegenerate. The total energy curve of a degenerate system in the ground state is schematically shown as a function of a structural deformation coordinate, R , in Figure 3; that for a nondegenerate system is shown in Figure 4. The prototype of degenerate polymers is *trans*-polyacetylene, which has alternating C–C and C=C bonds. There are two stable structures (A and B in Fig. 3) with alternating C–C and C=C bonds, whereas the structure with equal C–C bond lengths (C in Fig. 3) is unstable. The two stable structures are identical with each other and have the same total energy; in other words, they are degenerate. The C–C and C=C bond lengths are calculated to be 1.373 and 1.423, respectively, by extrapolation from bond lengths of *trans*-oligoenes calculated at the MP2/6-31G* level [23]. On the other hand, a nondegenerate polymer has no two identical structures in the ground state, namely, the benzenoid and quinoid structures as shown in Figure 4. Most conjugated polymers belong to this class. Let us consider polythiophene as an example of nondegenerate polymers. An *ab initio* MO calculation at the Hartree–Fock level with the 6-31G* basis set for α -terthiophene has shown that the C–C, C=C, and C–S bond lengths of the central ring are 1.430, 1.351, and 1.739 Å, respectively, and the interring C–C bond length is 1.464 Å [24]. Thus, polythiophene has a benzenoid structure and has bond alternation. Suppose a structural change from a benzenoid to quinoid structures. The energy of the quinoid structure is higher than that of the benzenoid. Degeneracy is lifted in this geometry.

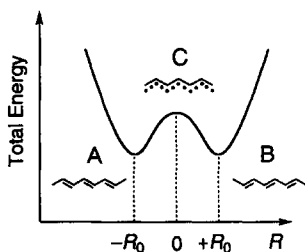


Fig. 3. Total energy as a function of a structural deformation coordinate R for *trans*-polyacetylene.

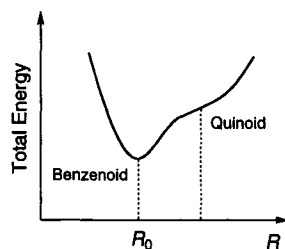


Fig. 4. Total energy as a function of a structural deformation coordinate R for a nondegenerate polymer.

2.2. Self-Localized Excitations

Types of self-localized excitations depend on the degeneracy of ground states. Consider polythiophene (Fig. 1c) as a typical nondegenerate polymer. The main process of chemical doping is the multistage oxidation (or reduction) reaction of conjugated polymer chains. In the case of acceptor doping, many electrons are removed from a polymer chain. The maximum charge transfer is typically about 7 mol% per carbon atom. When an electron is removed from an infinite polymer chain, charge $+e$ and spin $1/2$ are localized over several repeating units with structural changes (Fig. 5a). This is a self-localized excitation called a positive polaron. These structural changes associated with charge transfer are due to an electron–lattice (electron–phonon) interaction. For an oligomer, it is well known that the equilibrium geometry of a charged state is different from that of the neutral state. When another electron is removed from the positive polaron, charge $+2e$ is localized over several rings (Fig. 5b). This species is called a positive bipolaron. A positive bipolaron has charge $+2e$ and no spin. If a bipolaron is unstable, two polarons are formed as schematically shown in Figure 5c. Although the charge and spin are depicted as being localized on one carbon atom in Figure 5a–c, it has to be borne in mind that they extend over several rings with geometrical changes in real polymers. In the case of donor doping, a negative polaron and a negative bipolaron can be formed. Solitons are expected only for degenerate polymers such as *trans*-polyacetylene. Solitons can be formed between the A and B phases (Fig. 3). Solitons are classified into neutral, positive, and negative types according to their charges. A neutral soliton has no charge and spin $1/2$. A positive (or negative) soliton has charge $+e$ (or $-e$) and no spin. Solitons are nothing but bond-alternation defects or misfits in polyenes that were studied by the Hückel method in the early 1960s [19]. Self-localized excitations expected for conjugated polymers are listed in Table I. The self-localized excitations of conjugated polymers can be separately detected by electronic absorption, vibrational spectroscopy and electron-spin-resonance spectroscopy. In particular,

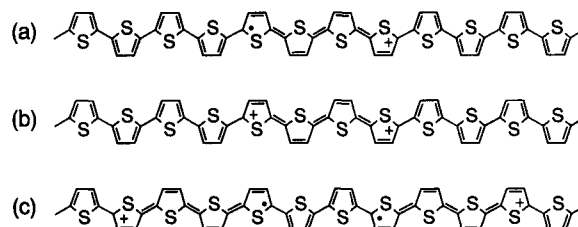


Fig. 5. Schematic structures of self-localized excitations in polythiophene: (a) a positive polaron, (b) a positive bipolaron, and (c) two positive polarons.

Table I. Self-localized Excitations and Chemical Terminologies

Self-localized excitation	Chemical term	Charge	Spin
Positive polaron	Radical cation	$+e$	$1/2$
Negative polaron	Radical anion	$-e$	$1/2$
Positive bipolaron	Closed-shell dication	$+2e$	0
Negative bipolaron	Closed-shell dianion	$-2e$	0
Neutral soliton	Neutral radical	0	$1/2$
Positive soliton	Cation	$+e$	0
Negative soliton	Anion	$-e$	0
Singlet exciton	S_1	0	0
Triplet exciton	T_1	0	1

electronic absorption spectroscopy gives us useful information on the electronic excitations in conjugated polymers.

3. ELECTRONIC SPECTRA

3.1. Neutral and Charged Oligomers

3.1.1. Oligothiophenes

The electronic absorption spectra of unsubstituted and substituted α -oligothiophenes have been reported [25–37]. Whereas the solubilities of unsubstituted oligothiophenes are low, various types of substituted oligothiophenes (Fig. 6) have been synthesized. As far as I know, the longest oligothiophene synthesized is a heptacosamer, which has 27 thiophene rings and shows absorption at 461 nm (2.69 eV) [34]. Neutral oligomers show an intense broad absorption band in the visible region. In most cases, vibrational progressions are not observed. The absorption band is assigned to the π - π^* transition. The absorption maxima and molar absorption coefficients are listed in Table II. The absorption maxima are plotted as closed triangles against the number of thiophene rings in Figure 7.

The radical cation and the divalent cation of each oligothiophene are model compounds of charge carriers in polythiophene. Thus, electronic absorption spectra of the radical cations and dications of oligothiophenes have been studied [26, 28–31, 33, 35, 38–46]. Oligothiophenes can be oxidized chemically by using oxidants such as FeCl_3 [38] and $\text{THI}^+(\text{ClO}_4^-)$ [35] (THI, thianthrene). For short-chain oligomers, a neutral oligomer is stepwise oxidized to its radical cation and dication. In the FeCl_3 oxidation processes, the reactions

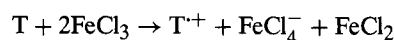


Table II. Absorption Maximum (λ_{\max}) and Molar Absorption Coefficient (ϵ) for Oligothiophenes

Oligomer ^a	λ_{\max} (nm) (eV ⁻¹)	ϵ (mol ⁻¹ dm ³ cm ⁻¹)	Solvent	Ref.
2T	302 (4.11)	12,500	Chloroform	[25]
3T	355 (3.49)	25,000	Chloroform	[25]
4T	390 (3.18)	45,500	Chloroform	[25]
5T	416 (2.98)	55,200	Chloroform	[25]
6T	432 (2.87)	60,000	Chloroform	[25]
2Dod-6T	425(2.92)	—	Dichloromethane	[35]
2Bu-7T	441 (2.81)	50,500	Dioxane	[37]
6Hex-9T	440 (2.82)	—	Chloroform	[32]
3Dod-9T	451 (2.75)	—	Dichloromethane	[35]
4Dec-12T	465 (2.67)	110,000	Chloroform	[29]
8Oct-13T	453 (2.74)	93,700	Tetrahydrofuran	[34]
10Hex-15T	456 (2.72)	—	Chloroform	[32]
12Oct-20T	461 (2.69)	151,700	Tetrahydrofuran	[34]
16Oct-27T	461 (2.69)	211,400	Tetrahydrofuran	[34]

^a $mRnT$, α -oligothiophenes with n thiophene rings; m , the number of substituents; R , substituent; Dod, dodecyl; Bu, butyl; Hex, hexyl; Dec, decyl; Oct, octyl.

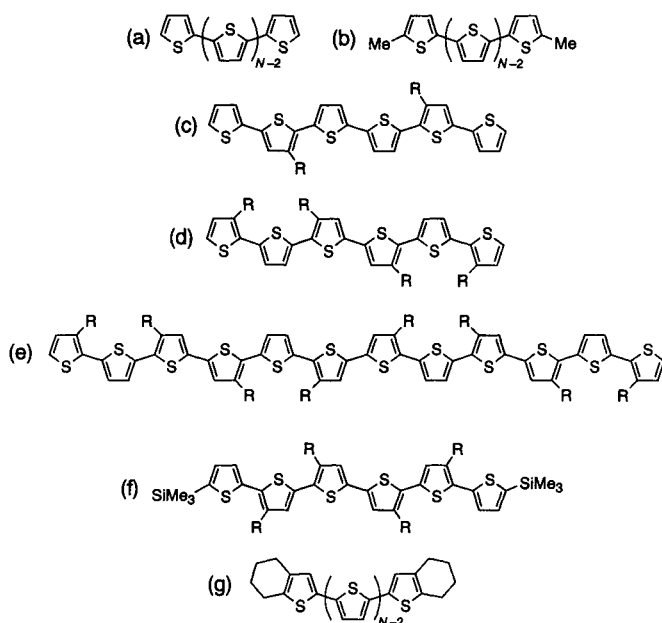
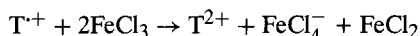
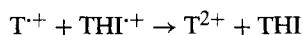
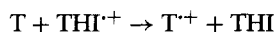


Fig. 6. Chemical structures of α -oligothiophenes: (a) unsubstituted oligothiophenes; (b) dimethyloligothiophenes (Me: CH₃); (c) and (d) partly β -substituted sexithiophenes (R: C₁₀H₂₁, C₁₂H₂₅); (e) partly β -substituted dodecamer (R: C₁₀H₂₁, C₁₂H₂₅); (f) partly β -substituted disilysexithiophene (R: n -C₄H₉); (g) end-capped oligothiophenes.



occur, where T is an oligothiophene. In the oxidation with $THI^+(ClO_4^-)$, the reactions



occur. In this case, the extent of oxidation can be measured by absorbance of the band due to the reduced THI. The radical cation

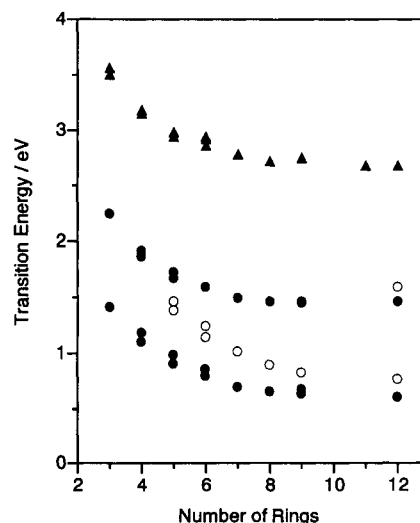


Fig. 7. Observed electronic transition energies of α -oligothiophenes in various states: ▲, neutral species; ●, radical cation; ○, dication.

gives rise to an electron-spin-resonance (ESR) signal, whereas the dication gives rise to no ESR signal.

The changes of the electronic absorption spectrum of a substituted sexithiophene (Fig. 6d; R = C₆H₁₃) upon the $THI^+(ClO_4^-)$ oxidation in a dichloromethane (CH₂Cl₂) solution are shown in Figure 8a [47]. The neutral oligomer gives rise to an absorption band at 3.00 eV. Two strong bands observed at 0.83 and 1.60 eV are attributed to the radical cation of the hexamer, whereas the intense band observed at 1.19 eV is attributed to the dication of the hexamer. Two peaks at 1.40 and 1.56 eV are attributable to vibrational transitions. The radical cation of each oligomer shows two intense bands.

A substituted dodecamer with 12 thiophene rings (Fig. 6e; R = C₆H₁₃) shows quite different spectral changes upon oxidation. The spectral changes of the dodecamer upon the $THI^+(ClO_4^-)$

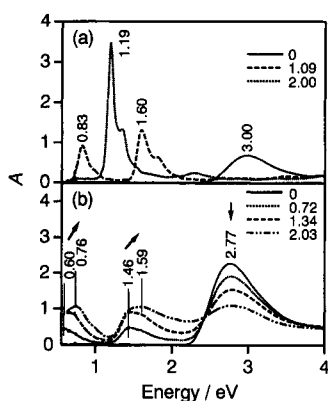


Fig. 8. Spectral changes of (a) β -substituted hexamer and (b) β -substituted dodecamer upon the $\text{THI}^+(\text{ClO}_4^-)$ oxidation in CH_2Cl_2 solution. The inset keys show the number of equivalents of $\text{THI}^+(\text{ClO}_4^-)$ added.

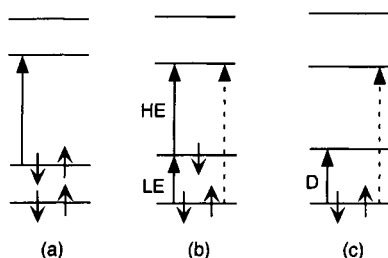
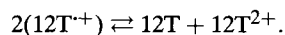


Fig. 9. Molecular orbital energy-level diagrams of (a) the neutral species, (b) the radical cation, and (c) the dication of an oligomer.

oxidation in dichloromethane are shown in Figure 8b. In these spectra, the stepwise oxidation reactions from neutral species to the radical cation and the dication are not observed, in contrast to the case of the hexamer. At low oxidation levels, two bands appear at 0.60 and 1.46 eV. Upon further oxidation, two bands at 0.76 and 1.59 eV become strong, whereas the 2.77-eV band attributed to neutral species is still observed. These spectral changes originate from the disproportionation reaction of the radical cation of the dodecamer [35]:



The 0.60- and 1.46-eV bands are attributed to the radical cation of the dodecamer, whereas 0.76- and 1.59-eV bands are ascribed to the dication of the dodecamer. Similar spectral changes were reported by van Haare et al. [35] for a dodecamer with different alkyl substituents. They also clarified that the divalent cation is singlet by using ESR spectroscopy.

The observed transition energies of radical cations versus the number of thiophene rings are plotted in Figure 7 as solid circles. Each radical cation gives rise to two bands in the near-infrared region [low energy (LE) band] and in the visible region [high energy (HE) band]. As the number of thiophene rings increases, the transition energy associated with the LE or HE band converges to a finite value. The molecular orbital diagram of the radical cation of an oligothiophene is shown in Figure 9b; the neutral state and the dication of the oligomer are shown in Figure 9a and c, respectively. The LE and HE bands of the radical cation of each oligothiophene are indicated by arrows in Figure 8b [31, 44, 48–50]. These transitions are dipole allowed and polarized along the chain

Table III. Optical Transition Energies (in eV) of Radical Cation Monomers and Dimers of Oligothiophenes

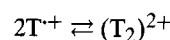
Oligomer ^a	Monomer		Dimer				Ref.
	LE	HE	D ₁	D ₂	D ₀	ΔH (kJ mol ⁻¹)	
2Me-3T	1.41	2.17	1.75	2.66	1.43	-42	[41]
EC-3T	1.32	2.00	1.63	2.57	1.25	—	[31]
EC-4T	1.05	1.79	1.37	2.25	1.09	-58	[31]
EC-5T	0.99	1.71	1.19	2.10	0.93	-65	[31]
EC-6T	0.84	1.59	0.98	1.81	—	—	[30]
2Dod-6T	0.87	1.60	1.12	1.81	—	-88	[30]
3Dod-9T	0.67	1.46	0.95	1.94	—	-61	[35]

^a2Me-3T, dimethylterthiophene (see Fig. 6b); EC-*n*T, end-capped oligothiophenes (see Fig. 6g); other abbreviations, see the footnote to Table II.

axis [44, 48]. For the charged oligomers with C_{2h} symmetry, the transition shown as a dotted arrow is dipole forbidden [44, 49, 50]. For the charged oligomers with C_{2v} symmetry, this transition is extremely weak, because the transition is polarized in the direction perpendicular to the chain axis [44, 48].

There are three possible states for the dication of an oligothiophene: closed-shell (bipolaronic structure), singlet biradical (two-polaron structure), and triplet biradical (two-polaron structure) [35, 51, 52]. The observed transition energies of dications versus the number of thiophene rings are plotted in Figure 7 as open circles. The dications of oligothiophenes up to nonamer give rise to one strong band (D band) and have closed-shell structures. The molecular orbital diagram of the closed-shell dication is shown in Figure 9c. The D band of the dication of each oligothiophene is indicated by an arrow in Figure 9c [46, 49]. This transition is dipole allowed and polarized along the molecular chain axis [31, 44, 48–50]. For the charged oligomers with C_{2h} symmetry, the transitions indicated by dotted arrows are dipole forbidden [44, 49, 50]. For the charged oligomers with C_{2v} symmetry, this transition is extremely weak, because the transition is polarized in the direction perpendicular to the molecular chain axis [44, 48]. The transition energy associated with the D band due to the dications decreases more rapidly than the energy associated with the LE and HE bands (see Fig. 7). It is surprising that the dication of dodecamer gives rise to two band, whereas the dications of oligothiophenes up to nonamer give rise to one intense band. This result probably indicates that the bipolaronic charged domain on a dication continues to expand with increasing number of rings. Then, the dication of duodecithiophene takes the singlet biradical state (two-polaron structure).

Hill et al. [40, 41] and Bäuerle et al. [30, 31] reported the singlet π -dimer formation of the radical cations of oligothiophenes. Upon lowering the temperature of a solution of a radical cation, the LE and HE bands of the radical cation show blue shifts, and an ESR signal that originates from the radical cation disappears. Consequently, the new absorption bands have been ascribed to the singlet π -dimer of the radical cations. These absorption bands due to the dimer are called D₁ and D₂ herein. A band that appears in the near-infrared range upon dimer formation is called D₀. The observed positions of the D₀, D₁, and D₂ bands are listed in Table III. There exists a monomer–dimer equilibrium,



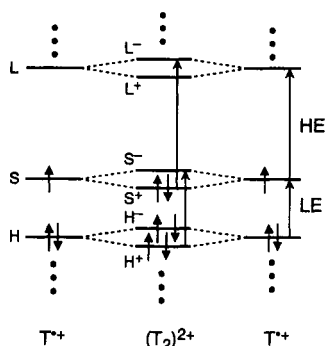


Fig. 10. Molecular orbital energy-level diagram for a singlet dimer of the radical cation of an oligothiophene.

where T is an oligothiophene. The enthalpies of dimer formation were obtained by van't Hoff plots for electronic absorption or ESR measurements, and they are listed in Table III. Bäuerle et al. [31] proposed the tentative assignments of the D_0 , D_1 , and D_2 bands within the framework of the Hückel theory. They also proposed the energy-level diagram of a radical-cation dimer (Fig. 10). A molecular orbital of the dimer is constructed by the linear combination of the orbitals of the monomers; each monomer level (such as L, S, and H in Fig. 10) is thus split into energetically lower (such as L^+ , S^+ , and H^+) and higher levels (such as L^- , S^- , and H^-). As a result, the levels of the dimer are fully occupied or unoccupied. This is in agreement with the experimental result that the ESR signal of the radical-cation monomer disappears upon dimer formation. Let us assume that the dimer has inversion symmetry. The D_1 band has been attributed to the transition between the H^+ and S^- levels, and the D_2 band is attributed to the transition between the S^+ and L^- levels [31]. In the case of unsubstituted and partly β -substituted hexamers, radical-cation dimers are present at room temperature [30]. On the other hand, no bands due to radical-cation dimers have been observed at room temperature for partly β -substituted disilyl oligothiophenes [28].

The photoexcitations of oligothiophenes were reviewed by Janssen [53]. Fluorescence is observed for oligothiophenes. The observed fluorescence band has been assigned to the dipole-allowed transition from the S_1 state that is derived from the ground state by the promotion of one electron from the highest occupied molecular level (HOMO) to the lowest unoccupied molecular level (LUMO) [54–57]. The maximum wavelengths and quantum efficiencies of oligothiophenes [37] are listed in Table IV. The electronic absorption spectra of the S_1 states were measured in the range from 1.3 to 2.9 eV by the Kerr ellipsometry method [58] and pump-probe time-resolved spectroscopy [59, 60]. One strong photoinduced band was obtained for each oligothiophene; this band was attributed to the $S_n \leftarrow S_1$ transition. Electronic absorption spectra attributed to the $T_n \leftarrow T_1$ transition of oligothiophenes have been reported [60–62]. The transition energy of each oligothiophene shows a downshift in going from a solution to a solid film; for example, the T_1 state of an undecamer gives rise to the band at 1.54 eV in a CH_2Cl_2 solution and at 1.26 eV in a solid film [62]. With increasing number of thiophene rings, the $T_n \leftarrow T_1$ and $S_n \leftarrow S_1$ transition energies decrease. The position of the $T_n \leftarrow T_1$ transition is higher than that of the $S_n \leftarrow S_1$ transition for each oligothiophene. The molecular and electronic structures of oligothiophenes have been calculated by using semiempirical molecular orbital methods [63–65].

Table IV. Maximum Wavelength (λ_F) and Quantum Efficiency (ϕ_F) of Fluorescence at Room Temperature for Oligothiophenes

Oligomer ^a	λ_F (nm) (eV^{-1})	ϕ_F	Solvent/matrix	Ref.
2T	362 (3.42)	0.017	Dioxane	[37]
3T	407 (3.05)	0.066	Dioxane	[37]
4T	437 (2.84)	0.18	Dioxane	[37]
5T	482 (2.57)	0.36	Dioxane	[37]
6T	502 (2.47)	0.41	Dioxane	[37]
2Bu-7T	522 (2.38)	0.34	Dioxane	[37]
8Oct-13T	554 (2.24)	—	Tetrahydrofuran	[34]
12Oct-20T	559 (2.22)	—	Tetrahydrofuran	[34]
16Oct-27T	560 (2.21)	—	Tetrahydrofuran	[34]

^aAbbreviations as cited in the footnote to Table II.

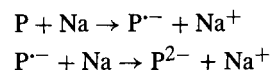
Table V. Absorption Maximum (λ_{max}) and Molar Absorption Coefficient (ϵ) for *p*-Oligophenyls in Chloroform^a

Number of rings	λ_{max} (nm) (eV^{-1})	ϵ ($\text{mol}^{-1} \text{dm}^3 \text{cm}^{-1}$)
2	251.5 (4.93)	18,300
3	280 (4.43)	25,000
4	300 (4.13)	39,000
5	310 (4.00)	62,500
6	317.5 (3.90)	>56,000

^aData from [66].

3.1.2. Oligophenyls

The electronic absorption spectra of unsubstituted and substituted *p*-oligophenyls have been reported [66–68]. Each oligomer shows an intense absorption in the ultraviolet region. The band is assigned to the π - π^* transition. The absorption maxima of biphenyl, *p*-terphenyl, *p*-quaterphenyl, *p*-quinquephenyl, and *p*-sexiphenyl are listed in Table V. The electronic absorption spectra of *p*-oligophenyls in the radical-anion and dianion states have been studied [68–75]. Furukawa et al. [73] showed that neutral terphenyl is stepwise reduced to its radical anion and dianion in tetrahydrofuran by using sodium (Na). In these reduction processes, the reactions



occur, where P is an oligophenyl. The reported transition energies [72–74] of the radical anions and the dianions in solutions are listed in Table VI. Each radical anion gives rise to two strong absorption bands: the LE and HE. On the other hand, each dianion gives rise to one strong band; this band is called D. The transition energies associated with the LE, HE, and D bands decrease with increasing number of rings. The transition energies due to the dianions (D band) decrease more rapidly than those due to the radical anions (LE and HE bands). This is also observed for the dications of oligothiophenes described previously. Buschow et al. [69] reported that the positions of the absorption bands due to the radical anions depend on the nature of solvents and counterions.

Table VI. Absorption Maxima of the Radical Anions and the Dianions of *p*-Oligophenylys in Solutions

Number of rings	Radical anion		Ref.	Dianion	Ref.
	LE (nm) (eV ⁻¹)	HE (nm) (eV ⁻¹)			
2	637 (1.95)	405 (3.06)	[69]	—	—
3	916 (1.35)	481 (2.58)	[73]	650 (1.91)	[73]
4	1205 (1.03)	518 (2.39)	[73]	775 (1.60)	[73]
5	1390 (0.89)	544 (2.28)	[73]	997 (1.24)	[73]
6	1560 (0.79)	558 (2.22)	[73]	1170 (1.06)	[73]

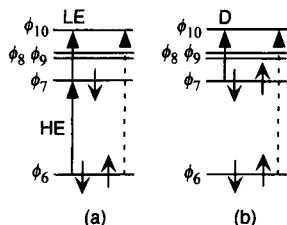


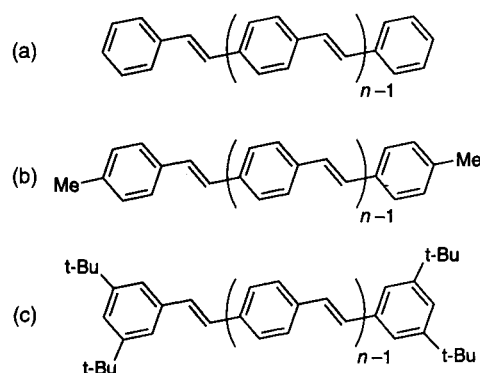
Fig. 11. Molecular orbital energy-level diagrams of (a) the radical anion and (b) the dianion of biphenyl.

ons; they discussed these observations in light of free ions and ion pairs.

Zahradník and Cársky [75] studied the electronic absorption spectrum of the radical anion of biphenyl using the Pariser–Parr–Pople method combined with a limited configuration interaction (CI). The molecular orbital energy-level diagram of the radical anion is similar to that shown in Figure 11. The ϕ_8 and ϕ_9 orbitals are associated with the transitions that have dipole moments perpendicular to the molecular long axis and very weak intensity. The LE and HE bands primarily originate from the transitions shown in Figure 11. Rubio et al. [76] calculated the electronic transition energies associated with the radical anion and radical cation of biphenyl using an *ab initio* multiconfigurational second-order perturbation theory (CASPT2). They interpreted the transition energies quantitatively and demonstrated the configurational nature of the transitions. It is reasonable to consider that the LE and HE bands of the radical anions of oligophenylys have natures similar to those of the LE and HE bands of the radical anion of biphenyl, respectively [73]. Note that the transitions indicated by dotted arrows are dipole forbidden under the planar structure with D_{2h} symmetry [73].

3.1.3. Oligophenylenevinylenes

Electronic absorption spectra of unsubstituted and substituted oligo-*p*-phenylenevinylenes (Fig. 12) in the neutral, radical-anion, dianion, and radical-cation states have been reported [77–87]. Neutral oligomers show an intense visible absorption band attributed to the π - π^* transition. The absorption wavelengths and molar absorption coefficients are tabulated in Table VII. Because the charged species are easily decomposed in the presence of a small amount of oxygen or water, contradictory experimental results were reported for the charged species of these oligomers. The data that seem to be most reliable have been selected from the reported articles. The transition energies of the radical anions and dianions are listed in Table VIII [88]; those of the radical

Fig. 12. Chemical structures of oligo-*p*-phenylenevinylenes. Me, CH₃; t-Bu, C(CH₃)₃.

cations are listed in Table IX. Each radical anion gives rise to two strong absorption bands (called LE and HE), and so does each radical cation. Each dianion gives rise to one strong absorption band (called D). The transition energy due to the D band of the dianions decreases more rapidly than those due to the LE and HE bands of the radical anions. Note that the formation of dianions has not been reported for long oligomers (the number of vinylene groups $N = 5$ and 6). The observed transition energies of the LE and HE bands are quite similar to those of the radical cation for each oligomer.

Karabunarliev et al. [89] studied the electronic absorptions associated with the radical anions of oligophenylenevinylenes using the Pariser–Parr–Pople/CI method on the basis of the structures obtained from the AM1 method. Cornil et al. [90] studied the radical anions and dianions of oligophenylenevinylenes by means of the intermediate neglect of differential overlap (INDO) CI method on the basis of the structures obtained from the AM1 method. According to their calculations, the LE and HE bands of each radical anion are assigned to the transitions indicated by arrows in Figure 13b, because the CI expansion coefficients of the corresponding configurations are predominant. On the other hand, the D band of each dianion is attributed to the transition indicated by an arrow in Figure 13c [90].

The radical-cation dimer of the oligophenylenevinylene ($n = 2$) is formed at low temperatures [91]. The radical cation gives rise to two bands at 1.03 and 1.95 eV, whereas the dimer gives rise to two bands at 1.26 and 2.36 eV. The observed blue shifts are 0.23 and 0.41 eV for the LE and HE bands, respectively. The enthalpy of dimer formation is 53 kJ mol⁻¹. These blue shifts and the enthalpy of formation are similar to those reported for the radical-cation dimers of oligothiophenes (see Table III).

Strong fluorescence is observed for oligophenylenevinylenes [77, 86]. The observed wavelengths are tabulated in Table X. The T_1 state of *trans*-stilbene was observed by means of flash photolysis [92]. The electronic absorption spectra associated with the triplet states of oligophenylenevinylenes ($n = 2$ –6) in KBr pellets were measured in the range from 1.3 to 2.3 eV [86]. Each oligomer gives rise to one strong absorption band attributed to the $T_n \leftarrow T_1$ transition [93–95]. For examples, 4Bu-PV2 gives rise to the band at 2.12 eV and 4Bu-PV6 gives rise to the band at 1.61 eV. Among oligophenylenevinylenes, the $S_n \leftarrow S_1$ absorption band of *trans*-stilbene was observed at 2.12 eV in a hexane solution [96]. The chain-length dependence of the $S_n \leftarrow S_1$ transitions has not been clarified yet.

Table VII. Absorption Maxima (λ_{\max}) and Molar Absorption Coefficients (ϵ) of Oligo-*p*-phenylenevinylenes

Oligomer ^a	λ_{\max} (nm) (eV ⁻¹)	ϵ (mol ⁻¹ dm ³ cm ⁻¹)	Solvent	Ref.
PV1	295 (4.20)	—	Hexane	[77]
2Me-PV1	317 (3.91)	—	Tetrahydrofuran	[85]
PV2	350 (3.55)	—	Hexane	[77]
2Me-PV2	360 (3.44)	—	Tetrahydrofuran	[85]
4Bu-PV2	359.8 (3.45)	56,200	Chloroform	[82]
PV3	385 (3.22)	—	Chloroform	[77]
2Me-PV3	386 (3.21)	—	Tetrahydrofuran	[85]
4Bu-PV3	386.9 (3.20)	87,100	Chloroform	[82]
PV4	385 (3.22)	—	Dioxane	[77]
4Bu-PV4	402.7 (3.08)	112,000	Chloroform	[82]
PV5	388 (3.20)	—	Dioxane	[77]
4Bu-PV5	412 (3.01)	112,000	Chloroform	[82]
PV6	388 (3.20)	—	Dioxane	[77]
4Bu-PV6	417.9 (2.97)	135,000	Chloroform	[82]
4Bu-PV7	415 (2.99)	—	Chloroform	[82]

^a*mR-PVn*: *m*, the number of substituents; *R*, substituents; Me, methyl; Bu, butyl; *n*, the number of vinylene groups. *PVn*, see Fig. 12a; 2Me-*PVn*, see Fig. 12b; 4Bu-*PVn*, see Fig. 12c.

Table VIII. Absorption Maxima of the Radical Anions and the Dianions of Oligo-*p*-phenylenevinylenes in Solutions

Oligomers ^a	Radical anion		Ref.	Dianion	Ref.
	LE (nm) (eV ⁻¹)	HE (nm) (eV ⁻¹)			
2Me-PV1	694 (1.79)	488 (2.54)	[85, 88]	520 (2.38)	[85]
4Bu-PV1	699 (1.77)	492 (2.52)	[81]	504 (2.46)	[81]
2Me-PV2	1136 (1.09)	631 (1.96)	[85, 88]	794 (1.56)	[85]
4Bu-PV2	1085 (1.14)	612 (2.03)	[81]	805 (1.54)	[81]
2Me-PV3	1449 (0.86)	711 (1.74)	[85, 88]	965 (1.28)	[85]
4Bu-PV3	1453 (0.85)	712 (1.74)	[81]	979 (1.27)	[81]
4Bu-PV4	1720 (0.72)	759 (1.63)	[81]	1176 (1.05)	[81]
4Bu-PV5	1923 (0.64)	786 (1.58)	[81]	—	—
4Bu-PV6	1976 (0.63)	794 (1.56)	[81]	—	—

^aAbbreviations as cited in the footnote to Table VII.

Table IX. Absorption Maxima of the Radical Cations and the Dication of Oligo-*p*-phenylenevinylenes in Solutions^a

Oligomer ^b	Radical cation		Dication
	LE (nm) (eV ⁻¹)	HE (nm) (eV ⁻¹)	
2Me-PV1	804 (1.54)	507 (2.45)	—
2Me-PV2	1200 (1.03)	636 (1.95)	990 (1.25)
2Me-PV3	1550 (0.80)	713 (1.74)	—

^aData from [87].

^bSee Figure 12b.

3.1.4. Oligoenes

The electronic spectra of oligoenes (which are also called polyenes) have been reviewed elsewhere [20, 97–99]. Whereas unsubsti-

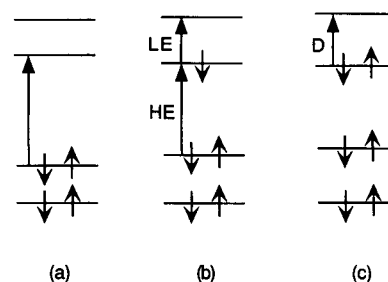
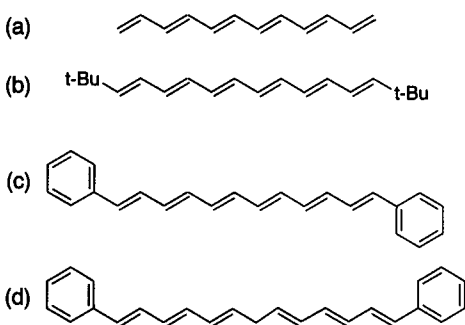


Fig. 13. Molecular orbital energy-level diagrams of (a) the neutral species, (b) the radical anion, and (c) the dianion of an oligomer.

tuted oligoenes are not stable, various types of substituted oligoenes have been studied. The absorption bands or peaks of all-trans conformers of unsubstituted oligoenes (Fig. 14a) [100–102], α , ω -dimethyloligoenes [101, 103, 104], α , ω -di-*tert*-butyloligoenes

Table X. Fluorescence Maximum Wavelengths of Oligo-*p*-phenylenevinylenes in KBr^a

Oligomer ^b	λ_F (nm) (eV ⁻¹)
PV1	362 (3.42)
PV2	444 (2.79)
PV3	493 (2.52)
PV4	521 (2.38)
PV5	521 (2.38)

^aData from [77].^bSee Figure 12a.Fig. 14. Schematic chemical structures of *trans*-oligoenes at neutral and charged states: (a) unsubstituted oligoenes; (b) α,ω -dibutyloligoene; (c) α,ω -diphenyloligoene ($N_C = 12$); (d) α,ω -diphenyloligoene anion ($N_C = 13$).Table XI. Absorption Maximum (λ_{\max}) of All-*trans*- α,ω -di-*tert*-butylpolyenes in *n*-Pentane^a

$N_{C=C}$	λ_{\max} (nm) (eV ⁻¹)
2	237.2 (5.23)
3	275.6 (4.50)
4	311.4 (3.98)
5	343.0 (3.61)
6	371.2 (3.34)
7	396.2 (3.13)
8	418.8 (2.96)
9	438.8 (2.83)
10	456.4 (2.72)
11	468.8 (2.64)
13	494 (2.51)

^aData from [105].

(Fig. 14b) [105], α,ω -diphenyloligoenes (Fig. 14c) [106, 107], and α,ω -dithienyloligoenes [108] have been reported. Each oligoene gives rise to an intense absorption with several peaks attributed to vibrational transitions in the ultraviolet or visible region. Note that the positions of electronic absorption bands strongly depend on solvents [20, 98]. This absorption band is dipole allowed, because the molar absorption coefficient is very large. Although the observed absorption peaks are due to vibrational transitions, a

Table XII. Absorption Maximum (λ_{\max}) of All-*trans*- α,ω -diphenylpolyenes in Benzene^a

$N_{C=C}$	λ_{\max} (nm) (eV ⁻¹)
1	319 (3.89)
2	352 (3.52)
3	377 (3.29)
4	404 (3.07)
5	424 (2.92)
6	445 (2.79)
7	465 (2.67)

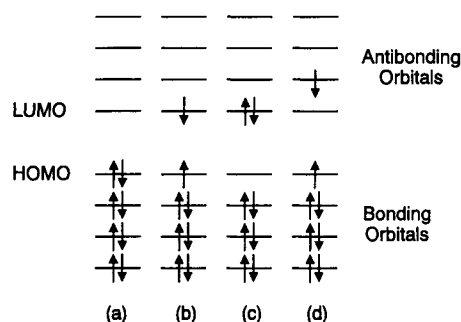
^aData from [107].

Fig. 15. Some configurations that describe the low energy singlet states of an oligoene.

precise vibrational analysis cannot be made because of the broad bandwidths. The position of the longest maximum in absorption spectra for α,ω -di-*tert*-butylpolyenes and α,ω -diphenylpolyenes are listed in Tables XI and XII, respectively. Although these absorption maxima (λ_{\max}) depend on the kind of substituents, they increase with increasing number of C=C bonds ($N_{C=C}$).

Let us consider an unsubstituted linear oligoene with N C=C double bonds, that is, $2N$ π -electrons. The number of molecular orbitals equals the number of π -electrons. These molecular orbitals can be classified into two types: N bonding and N antibonding. The three low-lying singlet states of linear oligoenes are described [20, 98] in terms of the configurations shown in Figure 15. The ground state S_0 is well described by the single configuration in which the N bonding orbitals are doubly occupied (Fig. 15a). The second excited state S_2 is described by the single configuration that is derived from the ground state by promoting one electron from the HOMO to the LUMO, as shown in Figure 15b. On the other hand, the S_1 state is a correlated state that cannot be written in terms of a single configuration because of electron correlation, but is approximately described by a linear combination of the doubly excited configuration in which two electrons are promoted from the HOMO to the LUMO (Fig. 15c) and the double jump configuration in which one electron is promoted from the HOMO to the LUMO+1 (Fig. 15d). Electron correlation is essential for a correct description of the electronic state ordering for linear oligoenes. (In most conjugated oligomers except for linear oligoenes, the ordering of S_1 and S_2 is reversed.) In the all-*trans* planar structure (C_{2h} symmetry), S_0 and S_1 have A_g symmetry and are called 1^1A_g and 2^1A_g , respectively; S_2 has B_u symmetry and is called 1^1B_u . As a result, the transition between S_0 and S_1 is dipole forbidden,

whereas the transition between S_0 and S_2 is dipole allowed. The intense absorptions described in the foregoing text are attributed to the $1^1B_u \leftarrow 1^1A_g$ transitions ($\pi\text{-}\pi^*$ transitions). This is a general property of linear oligoenes of all chain lengths independent of local symmetry and/or the presence of cis bonds. This is why the labels 1^1A_g for S_0 , 2^1A_g for S_1 , and 1^1B_u for S_2 are used in the literature on oligoenes even in cases where C_{2h} symmetry is not realized. Ordering that locates the 2^1A_g excited state below the 1^1B_u excited state is peculiar to linear oligoenes. The ordering of the A_g and B_u excited states is associated with fluorescence for conjugated oligomers.

The observed $1^1B_u \leftarrow 1^1A_g$ (0-0) transition energy, E_n , has been expressed as a function of the number of C=C double bonds ($N_{C=C}$) fitted by the equation [105]

$$E_n(\text{eV}) = E_\infty + \frac{k}{N_{C=C}} \quad (1)$$

where E_∞ and k are constants. From observed transition energies of α,ω -dibutyloligoenes, E_∞ and k are determined to be about 1.56 and 9.5 eV, respectively, in carbon disulfide and about 1.79 and 9.4 eV in pentane [105]. The differences between these estimated values come from the fact that the observed transition energies are sensitive to solvents. Equation (1) suggests that the 1^1B_u transition energy goes to a finite limit (E_∞) at infinite chain length.

The position of the observed weak fluorescence for each oligoene shows a considerable red shift in comparison with the position of its absorption band. In other words, a large Stokes shift is observed. This emission band is due to the transition from the 2^1A_g excited state to the 1^1A_g ground state. The absorption band associated with the $2^1A_g \leftarrow 1^1A_g$ transition is not observed, because it is expected to be extremely weak. The transition energy for the 2^1A_g excited state is always lower than that for the 1^1B_u state for each polyene.

α,ω -Diphenyloligoenyl anions are model compounds of a negative soliton in *trans*-polyacetylene. The chemical structure of a diphenyloligoenyl anion is schematically shown in Figure 14d. These compounds with odd numbers of carbon atoms at the oligoene parts have a negative charge, but no spin. The radical anions of α,ω -diphenyloligoenes are model compounds of a negative polaron in *trans*-polyacetylene. These compounds with even numbers of carbon atoms at the oligoene parts have a negative charge and spin 1/2. The observed electronic transition energies [109–111] of these charged compounds are plotted versus the numbers of oligoene carbon atoms (N_C) in Figure 16. The radical anion of each diphenyloligoene gives rise to two absorption bands [109]. The transition energies associated with the radical anions are shown as solid circles in Figure 16. The LE band is weak in intensity and the HE band is strong [109]; these spectral features are quite different from those reported for the radical ions of the oligothio-phenes, oligophenyls, and oligophenylenevinyls. The LE and HE bands are attributed to the transitions indicated by arrows in Figure 12b, which are from the calculations performed by means of the Pariser–Parr–Pople and Longuet–Higgins and Pople methods, including all singly excited configuration interactions [112]. On the other hand, each diphenyloligoenyl anion gives rise to one strong absorption band [100, 101], which is called band S. The transition energies of the S band are shown as open circles in Figure 16. The S band is ascribed to the transition from the nonbonding orbital to the LUMO shown in Figure 17 [112, 113]. Figure 16 shows that

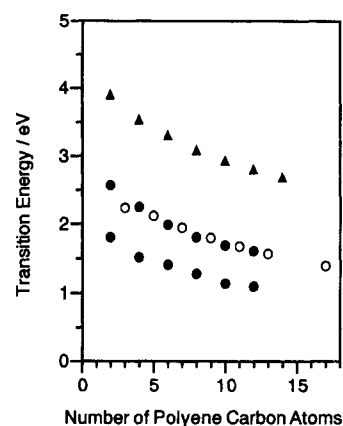


Fig. 16. Observed electronic transition energies of *trans*-oligoenes in various states. (a), \blacktriangle , neutral α,ω -diphenyloligoene; \bullet , radical anion of α,ω -diphenyloligoene; \circ , α,ω -diphenyloligoenyl anion.

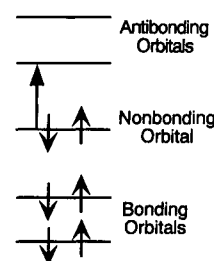


Fig. 17. Molecular orbital energy-level diagram of the anion of an odd oligoene.

Table XIII. Absorption Maxima of the Radical Cations of α,ω -Di-*tert*-butylpolyenes in Freon Matrix^a

$N_{C=C}$	LE (nm) (eV ⁻¹)	HE (nm) (eV ⁻¹)
3	626 (1.98)	430 (2.88)
4	738 (1.68)	498 (2.49)
5	861 (1.44)	571 (2.17)
6	1000 (1.24)	653 (1.90)
7	1180 (1.05)	734 (1.69)
8	1270 (0.98)	800 (1.55)
9	1440 (0.86)	879 (1.41)
11	1720 (0.72)	1010 (1.23)
13	1970 (0.63)	1110 (1.12)

^aData from [114].

the transition energies associated with the HE band are coincident with those associated with the S band. Parkes and Young [110] reported that the positions of the S band in diphenyloligoenyl anions strongly depend on the nature of solvents; these properties have been explained by the presence of loose ion pairs and tight ion pairs [110].

The radical cations of polyenes are models of a positive polaron in *trans*-polyacetylene. The electronic absorption spectra of the radical cations of α,ω -dibutyloligoenes have been reported [114]. The observed absorption maxima of the radical cations [114] of dibutyloligoenes are listed in Table XIII. Each radical cation gives

rise to two absorption bands: the LE band is weak in intensity and the HE band is strong. These spectral features are similar to those of the radical anions of diphenyloligoenes. According to studies performed by molecular orbital methods [114, 115], the intensities of the LE and HE bands have been explained by the configuration interactions.

The T_1 states of oligoenes including carotenoids have been studied by means of flash photolysis [116, 117]. Each oligoene gives rise to one strong absorption band attributed to the $T_n \leftarrow T_1$ transition. Note that spectra in the range below 1.88 eV have not been reported. The observed energies decrease with increasing $N_{C=C}$.

3.2. Neutral and Doped Polymers

The absorption of conjugated polymers appears in the region from ultraviolet to near-infrared. The optical absorption spectra of conjugated polymers have been studied from the experimental and theoretical standpoints [2]. The excitonic effect is essential and significant in conjugated polymers, although the band picture is very useful for a rough understanding of the electronic properties of conjugated polymers. The discussions about exciton and band pictures have been reviewed previously [118]. The peak and band shape of absorption depend on the molecular weight, substituents, state, and defect content of the polymer. The observed maxima of absorption in some typical polymers are listed in Table XIV [119–125]. The band edges are usually 0.3–0.5 eV lower than these maxima. Thus, optical bandgaps of conjugated polymers are in the range from 1 to 3.5 eV.

The charge carriers in conjugated polymers are polarons, bipolarons, and charged solitons. The importance of spinless charge carriers, charged solitons, and bipolarons has been pointed out [119, 122, 126]. The charge carriers in conjugated polymers can be generated by chemical doping, electrochemical doping, or photoirradiation. The maxima of the subgap absorption due to charged excitations generated by chemical doping and photoirradiation are compiled in Table XV [88, 119, 122, 124, 127–133]. Table XV shows that there are one or two subgap absorption bands. The two-band features observed for nondegenerate polymers, such as polythiophene, poly(*p*-phenylene), polypyrrole, poly(*p*-phenylenevinylene), and poly(2,5-thienylenevinylene), were discussed previously with regard to spinless bipolarons. However, recent studies on charged model compounds have revealed that the two-band features can be attributed to polarons and the one-band feature to bipolarons [50, 134–138]. Excitons as well as carriers play an important role in optical properties of conjugated polymers. The photoexcitation dynamics associated with excitons and carriers have been studied on a time scale from femtosecond to millisecond [139, 140]. The major species on the micro- to millisecond time scale are carriers that are charged self-localized excitations and triplet excitons that are neutral excitations.

3.2.1. Subgap Absorptions

Theoretical consideration provided the basis for the assignments of doping- and photoinduced electronic absorptions in conjugated polymers. Energy-level diagrams of electronic excitations in conjugated polymers are shown in Figure 18, according to a continuum electron–phonon-coupled model proposed by Fesser, Bishop, and Campbell [141]. Note that the Fesser–Bishop–Campbell model is a continuum version of the Su–Schrieffer–Heeger model, which

Table XIV. Maximum of Absorption in Conjugated Polymer Films

Polymer	Maximum (eV)	State/solvent	Ref.
<i>trans</i> -Polyacetylene	1.9	Film	[122]
Polythiophene	2.6	Film	[122]
Poly(<i>p</i> -phenylene)	3.4	Film	[120]
Polypyrrole	3.2	Film	[119]
Poly(isothianaphthene)	1.4	Film	[122]
Poly(<i>p</i> -phenylenevinylene)	2.85	Film	[125]
Poly(2,5-thienylenevinylene)	2.3	Film	[121]
Polyaniline			
Leucoemeraldine base	3.8	Film	[123]
Emeraldine base	2.0, 3.8	<i>N</i> -methylpyrrolidinone	[124]
Pernigraniline base	2.3, 3.8	<i>N</i> -methylpyrrolidinone	[124]

Table XV. Maximum of Subgap Absorptions Due to Charged Excitations in the Film State

Polymer	Method	Maximum (eV)	Ref.
<i>trans</i> -Polyacetylene	AsF ₆ [−] doping	0.7	[122]
	Na ⁺ doping	0.7	[122]
	Photodoping	0.48	[127]
Polythiophene	ClO ₄ [−] doping	0.65, 1.5	[122]
	N(<i>n</i> -Bu) ₄ ⁺ doping	0.65, 1.65	[128]
	Photodoping	0.4, 1.3	[129]
Poly(<i>p</i> -phenylene)	AsF ₆ [−] doping	0.9, 2.1	[130]
	N(<i>n</i> -Bu) ₄ ⁺ doping	0.7, 2.4	[130]
Polypyrrole	ClO ₄ [−] doping	1.0, 2.7	[119]
Poly(<i>p</i> -phenylenevinylene)	ClO ₄ [−] doping	0.9, 2.3	[131]
	Na ⁺ doping	1.55	[88]
	Photodoping	0.6, 1.6	[132]
Poly(2,5-thienylenevinylene)	Photodoping	0.44, 1	[133]
Polyaniline			
Emeraldine salt	HCl treatment	1.4, 3.0	[124]

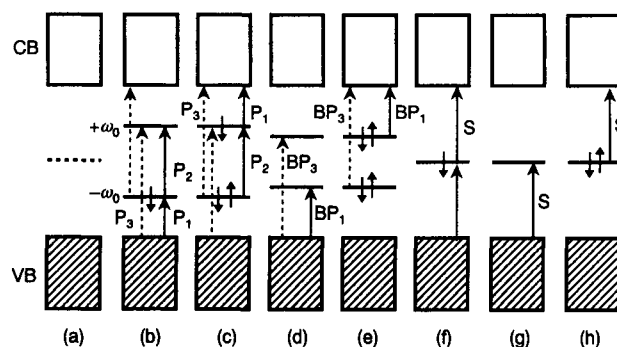


Fig. 18. Schematic electronic structures: (a) neutral polymer; (b) positive polaron; (c) negative polaron; (d) positive bipolaron; (e) negative bipolaron; (f) neutral soliton; (g) positive soliton; (h) negative soliton. CB, conduction band; VB, valence band. The full and dashed arrows represent allowed and forbidden optical transitions, respectively.

is a solid-state-physics version of the Hückel theory. The electronic transitions due to the electronic excitations can be correlated to those of the charged and electronically excited states of oligomers. In an infinite polymer chain, the interaction between repeating units leads to the formation of the valence band and the conduction band as shown in Figure 18a. The bandgap between the valence and conduction bands is expressed as $2\Delta_0$. For a polaron or a bipolaron, two localized electronic levels—bonding and antibonding—are formed symmetrically with respect to the gap center at $-\omega_0$ and $+\omega_0$, respectively (Fig. 18b–e), because of electron–hole symmetry. The positions of the localized electronic levels (i.e., $\pm\omega_0$) depend on the extent of the structural changes associated with the polarons and bipolarons. On the other hand, for solitons, one localized electronic level, which is nonbonding, is formed at the gap center (Fig. 18f and g).

3.2.1.1. Polarons

When a positive polaron is formed, one electron is removed from the $-\omega_0$ level (Fig. 18b). Thus, a positive polaron is expected to have the following intragap transitions:

- P₁ transition: $-\omega_0$ level \leftarrow valence band
- P₂ transition: $+\omega_0$ level $\leftarrow -\omega_0$ level
- P₃ transition: $+\omega_0$ level \leftarrow valence band, and conduction band $\leftarrow -\omega_0$ level

When a negative polaron is formed, one electron is added to the $+\omega_0$ level (Fig. 18c). In this case, three transitions are also expected. Within the Fesser–Bishop–Campbell model, the subgap absorptions due to the P₁ and P₂ transitions are much stronger than that due to the P₃ transition, because the P₃ transition is symmetry forbidden. Quantitatively, the intensities of these subgap absorptions are given as a function of the ratio ω_0/Δ_0 .

The radical cations of oligothiophenes and oligophenylenevinylenes, and the radical anions of oligophenyls and oligophenylenevinylenes give rise to two strong absorption bands, as described in the previous sections. These observations indicate that two subgap absorptions are expected for a polaron in a nondegenerate polymer. The radical anions and radical cations of oligoynes give rise to one strong absorption band and one weak band, as described previously. These observations indicate that one strong subgap absorption and one weak subgap absorption are expected for a polaron in *trans*-polyacetylene. This is probably because electron–electron interactions, which are not taken into account in the Fesser–Bishop–Campbell model, have a strong effect on the optical absorptions of a polaron in *trans*-polyacetylene.

3.2.1.2. Bipolarons

When a positive bipolaron is formed, two electrons are removed from the $-\omega_0$ level (Fig. 18d). Thus, a positive bipolaron is expected to have the following intragap transitions:

- BP₁ transition: $-\omega_0$ level \leftarrow valence band
- BP₃ transition: $+\omega_0$ level \leftarrow valence band

The transition from the $-\omega_0$ level to the $+\omega_0$ level is missing, because the $-\omega_0$ level is unoccupied. When a negative bipolaron is formed, two electrons are added to the $+\omega_0$ level and thus two transitions are again expected (Fig. 18e). Within the Fesser–Bishop–Campbell model, the subgap absorption due to the BP₁ transition is much stronger than that due to the BP₃ transition,

because the BP₃ transition is symmetry forbidden. Quantitatively, the intensities of these subgap absorptions are given as a function of the ratio ω_0/Δ_0 .

The dications of oligothiophenes up to nonamer and oligophenylenevinylenes, and the dianions of oligophenyls and oligophenylenevinylenes give rise to one strong absorption band. These observations indicate that one subgap absorption is expected for a bipolaron in a nondegenerate polymer.

3.2.1.3. Solitons

Soliton excitations are possible only in degenerate polymers such as *trans*-polyacetylene. For a neutral soliton, a nonbonding electronic level is occupied by one electron. Thus, a neutral soliton is expected to have a single intragap transition (Fig. 18f):

- S transition: soliton nonbonding level \leftarrow valence band, and conduction band \leftarrow soliton nonbonding level

When a positive soliton is formed, one electron is removed from the soliton nonbonding level. In this case, one transition is also expected (Fig. 18g). When a negative soliton is formed, one electron is added to the soliton nonbonding orbital; thus, one transition is again expected (Fig. 18h). Each of α,ω -diphenyloligoenyl anions that are model compounds of a negative soliton gives rise to one absorption band, as described in the previous section. Thus, a single subgap absorption is expected for solitons.

Shimoi, Abe, and Harigaya [135] and Shimoi and Abe [136] calculated the optical absorption spectra associated with a polaron and a bipolaron by using a Peierls–Hubbard Hamiltonian with electron–phonon coupling and electron–electron interaction terms. According to their calculations, a polaron gives rise to two subgap absorption bands and a bipolaron gives rise to a single subgap absorption band. Essentially, their results are consistent with those obtained by the Fesser–Bishop–Campbell model.

3.2.2. Polythiophenes

As a typical example of nondegenerate polymers, the optical absorption spectrum of neutral polythiophene [137] is shown in Figure 19. The bandgap of polythiophene is estimated to be 1.94 eV from the onset of the observed absorption. The maximum absorption in substituted polythiophenes depends on the kind of substituents. Regioregular poly(3-alkylthiophene)s have been synthesized by head-to-tail coupling of 3-alkylthiophene [142, 143]. The absorption spectra of regioregular poly(3-alkylthiophene)s show distinct vibrational progressions, although those of regiorandom polymers show no progressions [142, 143]. These observations indicate that the structures of these polymers are homogeneous. Fluorescence is observed for polythiophenes. The light-emitting diodes fabricated with various types of substituted polythiophenes show colors ranging from blue to near-infrared [144].

The doping- and photoinduced absorption spectra of polythiophene, substituted polythiophenes, and their composites have been reported [145–166]. Let us discuss the subgap absorptions due to charged excitations in unsubstituted polythiophene. The optical absorption spectrum of BF₄[−]-doped polythiophene [42, 46] and the photoinduced absorption spectrum of polythiophene [145] are shown in Figure 20. In the spectrum of BF₄[−]-doped polythiophene (Fig. 20a), doping-induced bands are observed at 0.73 and 1.68 eV, which are located below the gap edge, 1.94 eV. The 0.73-

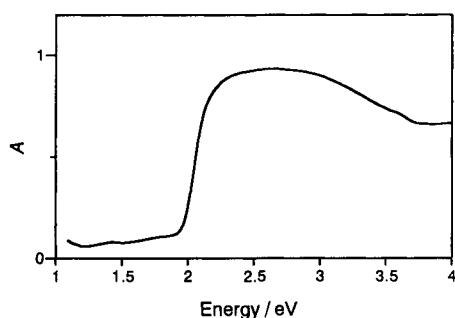


Fig. 19. Optical absorption spectrum of a polythiophene film.

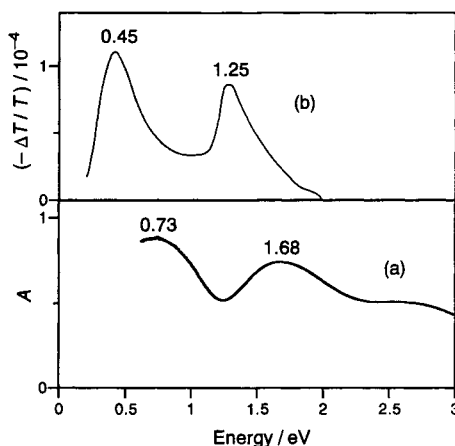


Fig. 20. (a) Optical absorption spectrum of a BF_4^- -doped polythiophene film (room temperature) and (b) photoinduced absorption spectrum of a polythiophene film (20 K).

and 1.68-eV absorption bands are assigned to the P_1 and P_2 transitions expected for a positive polaron. Thus, it can be concluded that positive polarons are formed on BF_4^- -doping (p-type doping). The electronic absorption spectra of ClO_4^- -doped polythiophene at various dopant content have been reported by Chung et al. [146] and Kaneto et al. [147]. The band positions depend slightly on the dopant content. At the maximum doping level, the two-band feature disappears and absorption extending to the infrared region is observed. This result is reminiscent of free carrier absorption. The optical absorption spectra of photogenerated carriers in conjugated polymers can be measured by the steady-state method, because the lifetimes of the photogenerated carriers are in the range from micro- to milliseconds. In the photoinduced difference absorption spectrum of polythiophene, two broad bands are observed at 0.45 and 1.25 eV as shown in Figure 20b [145]. The observed photon energy of each photoinduced absorption band is lower than that of the doping-induced band, as clearly shown in Figure 20. The 0.45- and 1.25-eV bands are assigned to the P_1 and P_2 transitions of polarons [129]. Thus, the charge separation induced by photoirradiation can result in the formation of a positive polaron and a negative polaron. Lane et al. [129] reported that the photoinduced absorption spectrum of a polythiophene film annealed at 573 K for 30 min is dominated by a single band at 0.9 eV (Table XV). This absorption band is assigned to the BP_1 transition of bipolarons [129].

The assignments of the doping- and photoinduced absorption bands of polythiophene, substituted polythiophenes, and their

composites are listed in Table XVI. Note that the two-band feature attributed previously to bipolarons has been newly ascribed to polarons. In addition to the previously described subgap absorption bands of polythiophene, additional bands have been observed in the range between 1.8 and 1.96 eV by modulation and time-resolved measurements [145, 148, 149, 166]. These bands have been ascribed to a triplet exciton [145, 148]. The observed positions, 1.96 eV, are higher than the position 1.54 eV [62] of the $T_n \leftarrow T_1$ absorption of undecamer in a CH_2Cl_2 solution. The positions of the bands attributed to triplet excitons in substituted polythiophenes are sensitive to the substituents and solvents, as shown in Table XVI. The photoinduced band observed at 1.8 eV is assigned to a polaron pair [149, 166]. In the composite of a conjugated polymer and buckminsterfullerene C_{60} , C_{60} acts as a strong electron acceptor upon photoirradiation [12, 161, 165]. Photoluminescence and electroluminescence are quenched upon doping by a small amount of C_{60} , whereas photoconductivity is enhanced [12, 161, 165]. In a polythiophene- C_{60} composite, charge separation occurs efficiently. Thus the intensities of the subgap absorptions due to polarons become strong. Friend and co-workers [167–169] reported *in situ* voltage-induced electronic absorption spectra of field-effect transistors fabricated with poly(3-hexylthiophene). They observed the absorption bands due to injected carriers in the electronic devices.

3.2.3. Polyarylenevinylenes

Poly(*p*-phenylenevinylene) derivatives are promising candidates for the active layer of polymer light-emitting diodes. Thus, various types of substituted poly(*p*-phenylenevinylene)s have been synthesized. Whereas these derivatives are soluble in organic solvents, a high-quality thin film of these polymers can be formed. The optical properties of these polymers have been reviewed previously [8, 169]. The electroluminescence spectrum of the device fabricated with a conjugated polymer is almost the same as that of the photoluminescence spectrum of the thin film of the polymer. The peaks in photoluminescence spectra are compiled in Table XVII [170, 171].

Doping- and photoinduced electronic absorptions in poly(*p*-phenylenevinylene), substituted poly(*p*-phenylenevinylene)s, and their composites, have been reported [88, 131, 132, 160, 164–166, 172–181]. In the optical absorption spectrum of ClO_4^- -doped poly(*p*-phenylenevinylene), doping-induced subgap absorption bands are observed at 0.9 and 2.3 eV (Table XV). These two bands are assigned to the P_1 and P_3 transitions of a polaron. Thus, positive polarons are formed upon ClO_4^- doping (p-type doping). On the other hand, a single band is observed at 1.55 eV in the absorption spectrum of Na-doped poly(*p*-phenylenevinylene) (Table XV). According to a Raman study [88] of Na-doped poly(*p*-phenylenevinylene), both negative polarons and negative bipolarons are generated upon Na doping. The observed 1.55-eV bands are overlapped by the absorptions of negative polarons and negative bipolarons [88]. The photoinduced bands observed at 0.6 and 1.6 eV (Table XV) are also assigned to the P_1 and P_3 transitions of polarons. Thus the charge separation induced by photoirradiation can result in the formation of a positive polaron and a negative polaron, as is the case in polythiophene.

The assignments of doping- and photoinduced absorption bands of polyarylenevinylenes and their composites are listed in Table XVIII. Note again that the two-band feature is assigned to polarons in this review, in contrast to the previous assignments that

Table XVI. Assignments of the Doping-Induced and Photoinduced Absorption Bands of Polythiophenes and Their Composites

Polymer ^a	Method ^b	Band (eV)	State/solvent	Species	Ref.
PT	PI	1.95	Film	Triplet exciton	[145]
		1.96	Film	Triplet exciton	[148]
		1.8	Film	Polaron pair	[166]
PMT	DI	0.65, 1.6	Film	Polaron	[154]
PET	DI	0.7, 1.6	Film	Polaron	[151]
PHT	DI	0.45, 1.65	Film	Polaron	[155]
	PI	0.35, 1.3	Film	Polaron	[155]
	VI	0.3–0.35, 1.35, 1.75	Device	Polaron	[169]
POT	DI	0.6, 1.6	Film	Polaron	[160]
	PI	<0.2, 1.25	Film	Polaron	[160, 162]
	PI	1.05	Film	Triplet exciton	[160]
PDT	PI	<0.35, 1.25	Film	Polaron	[158]
	PI	1.75	Film	—	[158]
	PI	0.55, 1.55	Chloroform	Polaron	[158]
	PI	2.1	Chloroform	—	[158]
PDDT	PI	1	Film	Triplet exciton	[156]
PMBET	PI	1.1	Film	Triplet exciton	[164]
	PI	1.24	Film	Polaron	[164]
	PI	<0.64, 1.47	1,2-Dichlorobenzene	Polaron	[163]
	PI	1.47	1,2-Dichlorobenzene	Triplet exciton	[163]
	PI	1.5	<i>p</i> -Xylene	Triplet exciton	[163]
POT-C ₆₀	PI	1.45	Film	Polaron	[160]
PMBET-C ₆₀	PI	<0.7, 1.26	Film	Polaron	[164]
	PI	<0.64, 1.47	1,2-Dichlorobenzene	Polaron	[163]
PMBET-A	PI	<0.7, 1.26	Film	Polaron	[164]

^aPT, polythiophene; PMT, poly(3-methylthiophene); PHT, poly(3-hexylthiophene); POT, poly(3-octylthiophene); PDT, poly(3-decylthiophene); PDDT, poly(3-dodecylthiophene); PMBET, poly(3-(2-(3-methylbutoxy)ethyl)thiophene); A, tetracyano-*p*-quinodimethane and its derivatives.

^bDI, doping induced; PI, photoinduced; VI, voltage induced.

Table XVII. Maximum Wavelength of Photoluminescence in Poly(*p*-phenylenevinylene) Derivatives

Polymer ^a	Wavelength (nm)	State/solvent	Ref.
PPV	550	Film	[170]
BuEH-PPV	560	Film	[8]
DOO-PPV	582	Film	[171]
MEH-PPV	555	Toluene	[170]
	630	Film	[170]
CN-PPV	555	Toluene	[170]
	690	Film	[170]

^aPPV, poly(1,4-phenylenevinylene); BuEH-PPV, poly(2-butyl-5-(2'-ethylhexyl)-1,4-phenylenevinylene); DOO-PPV, poly(2,5-dioctoxy-1,4-phenylenevinylene); MEH-PPV, poly(2-methoxy-5-(2'-ethylhexyloxy)-1,4-phenylenevinylene).

the two-band feature is due to bipolarons. In addition to these photoinduced absorption bands, additional bands have been observed

at 1.45 and 1.36 eV [132, 176]. These bands have been ascribed to triplet excitons [132, 176], because a single absorption attributed to the $T_n \leftarrow T_1$ transition is observed between 1.61 and 2.12 eV for each oligomer [86]; 4Bu-PV6 gives rise to the absorption due to the $T_n \leftarrow T_1$ transition at 1.61 eV. Brown et al. [180] reported the *in situ* voltage-induced absorption spectra of electroluminescent devices (polymer light-emitting diodes) fabricated with poly(*p*-phenylenevinylene). These *in situ* absorption measurements are useful in studying the mechanism of electroluminescence in the devices, because injected carriers cannot be detected by fluorescence spectroscopy, but by absorption spectroscopy.

3.2.4. Polyacetylene

In the optical absorption spectrum of AsF₆⁻-doped *trans*-polyacetylene, a single band is observed at 0.7 eV [122] (Table XV). This is half the bandgap (1.4 eV) [122] of *trans*-polyacetylene. This subgap absorption band is assigned to the S transition of a positive soliton generated by p-type doping, because the energy of the S transition is half the bandgap (Fig. 17g). The subgap absorption at 0.7 eV in Na-doped *trans*-polyacetylene is also attributed to the S transition of a negative soliton. Photoinduced electronic absorptions in

Table XVIII. Assignments of the Doping-Induced and Photoinduced Bands of Poly(arylenevinylene)s and Their Composites

Polymer ^a	Method ^b	Band (eV)	State/solvent	Species	Ref.
PPV	PI	1.45	Film	Triplet exciton	[132]
	PI	1.36	Film	Triplet exciton	[176]
	VI	0.65, 1.55	Device	Polaron	[180]
	VI	1.37	Device	Triplet exciton	[180]
DMO-PPV	DI	0.68, 1.76	Film	Polaron	[173]
	PI	0.45, 1.35	Film	Polaron	[173]
	PI	0.68, 1.80	Film	Polaron	[175]
	PI	1.35	Film	Triplet exciton	[175]
DOO-PPV	DI	0.60, 1.55	Film	Polaron	[173]
	PI	0.37, 1.36	Film	Polaron	[173]
	PI	0.35, 1.3	Film	Polaron	[174]
	PI	1.36	Film	Triplet exciton	[174]
MEH-PPV	DI	0.57, 1.59	Film	Polaron	[173]
	PI	0.43, 1.36	Film	Polaron	[173]
	PI	1.34	Film	Triplet exciton	[164]
BCHA-PPV	PI	1.47	Film	Triplet exciton	[178]
	PI	1.5	<i>p</i> -xylene	Triplet exciton	[178]
MEH-PPV/C ₆₀	PI	<0.7, 1.5–2.0	Film	Polaron	[164]
	PI	1.34	Film	Triplet exciton	[164]
DOO-PPV/C ₆₀	PI	0.45, 1.4	Film	Polaron	[166]
	PI	0.4, 1.8	Film	Polaron pair	[166]
BCHA-PPV/C ₆₀	PI	0.43, 1.47	Film	Polaron	[178]
PBTV	PI	0.55, 1.1	Chloroform	Polaron	[159]

^aPPV, poly(1,4-phenylenevinylene); DMO-PPV, poly(2,5-dimethoxy-1,4-phenylenevinylene); DHO, poly(2,5-dihexoxy-1,4-phenylenevinylene); DOO-PPV, poly(2,5-dioctoxy-1,4-phenylenevinylene); MEH-PPV, poly(2-methoxy-5-(2'-ethylhexyloxy)-1,4-phenylenevinylene); BCHA-PPV, poly(bis-2,5-*epi*-cholestanoxo-1,4-phenylenevinylene); PBTV, poly(3-butyl-2,5-thienylenevinylene).

^bAbbreviations as cited in footnote b of Table XVI.

trans-polyacetylene have been reported [181–185]. Photoinduced bands are observed at 0.5 and 1.35 eV. The band at 0.5 eV has been ascribed to charged solitons [182, 183], because the position at 0.5 eV is similar to that of the 0.7-eV band attributed to a positive soliton in acceptor-doped *trans*-polyacetylene. Orenstein and Baker [181] showed that the band at 1.35 eV can be correlated with the $T_n \leftarrow T_1$ transitions of oligoenes. A triplet exciton is viewed as a neutral soliton pair. Levey et al. [186] ascribed the 1.35-eV band to a neutral soliton on the basis of the results of light-induced ESR measurements. Wei et al. [174] confirmed this assignment by absorption detected magnetic resonance measurements. Burroughes et al. [187] reported the voltage-induced electronic absorption spectra of field-effect transistors fabricated with Durham polyacetylene; they observed a voltage-induced absorption band at 0.55 eV, which is assigned to injected charged solitons.

4. CONCLUDING REMARKS

The optical absorption and emission spectra of conjugated polymers and oligomers have been reviewed. The optical bandgaps of the conjugated polymers that are organic semiconductors range from 1 to 3.5 eV. The photoluminescence spectra of conjugated

polymers and oligomers are useful in designing electroluminescent devices (light-emitting diodes) fabricated with conjugated polymers. The subgap absorptions induced by chemical doping or photoirradiation are associated with self-localized excitations (solitons, polarons, bipolarons, and excitons) in conjugated polymers. Charged solitons, polarons, and bipolarons are charge carriers in conjugated polymers. Doping- and photoinduced absorptions have been studied on the basis of the absorption spectra of model compounds: the radical ions, the divalent ions, the anions, and the T_1 states of various oligomers. The two subgap absorptions are expected for a polaron and a single subgap absorption is expected for a bipolaron in nondegenerate polymers. In most nondegenerate polymers, such as polythiophenes, poly(*p*-phenylene)s, polypyrrole, poly(*p*-phenylenevinylene)s, and poly(2,5-thienylenevinylene)s, the doping- and photoinduced two-band features are observed and attributed to polarons. Thus polarons are the major carriers generated by chemical doping or photoirradiation.

Acknowledgments

The present work was supported in part by Toyota Physical and Chemical Research Institute, an International Joint Research

Grant from NEDO, and a grant-in-aid for scientific research on priority areas, "Molecular Physical Chemistry," from the Ministry of Education, Science, Sports, and Culture.

REFERENCES

- H. Shirakawa, E. J. Louis, A. G. MacDiarmid, C. K. Chiang, and A. J. Heeger, *J. Chem. Soc., Chem. Commun.* 1977, 578 (1977).
- H. Kiess, Ed., "Conjugated Conducting Polymers." Springer-Verlag, Berlin, 1992.
- H. S. Nalwa, Ed., "Organic Conductive Molecules and Polymers," Vols. 1-4. Wiley, New York, 1997.
- A. Tsumura, H. Koezuka, and T. Ando, *Appl. Phys. Lett.* 49, 1210 (1986).
- J. H. Burroughes, C. A. Jones, and R. H. Friend, *Nature* 335, 137 (1988).
- G. Yu, J. Gao, J. C. Hummelen, F. Wudl, and A. J. Heeger, *Science* 270, 1789 (1995).
- J. H. Burroughes, D. D. C. Bradley, A. R. Brown, R. N. Marks, K. Mackay, R. H. Friend, P. L. Burns, and A. B. Holmes, *Nature* 347, 539 (1990).
- F. Hide, M. A. Díaz-García, B. J. Schwartz, and A. J. Heeger, *Acc. Chem. Res.* 30, 430 (1997).
- S. Miyata and H. S. Nalwa, Eds., "Organic Electroluminescent Materials and Devices." Gordon and Breach, Amsterdam, 1997.
- R. H. Friend, R. W. Gymer, A. B. Holmes, J. H. Burroughes, R. N. Marks, C. Taliani, D. D. C. Bradley, D. A. Dos Santos, J. L. Brédas, M. Lögdlund, and W. R. Salaneck, *Nature* 397, 121 (1999).
- H. G. Kiess and G. Harbecke, in "Conjugated Conducting Polymers" (H. Kiess, Ed.), p. 184. Springer-Verlag, Berlin, 1992.
- N. S. Sariciftci, L. Smilowitz, A. J. Heeger, and F. Wudl, *Science* 258, 1474 (1992).
- H. Spreitzer, H. Becker, E. Kluge, W. Kreuder, H. Schenk, R. Demandt, and H. Schoo, *Adv. Mater.* 10, 1340 (1998).
- W. P. Su, J. R. Schrieffer, and A. J. Heeger, *Phys. Rev. Lett.* 42, 1698 (1979); *Phys. Rev. B* 22, 2099 (1980).
- W. P. Su and J. R. Schrieffer, *Proc. Natl. Acad. Sci. USA* 77, 5626 (1980).
- S. A. Brazovskii and N. N. Kirova, *Sov. Phys. JETP Lett.* 33, 4 (1981).
- A. R. Bishop, D. K. Campbell, and K. Fesser, *Mol. Cryst. Liq. Cryst.* 77, 253 (1981).
- J. L. Brédas, R. R. Chance, and R. Silbey, *Mol. Cryst. Liq. Cryst.* 77, 319 (1981).
- L. Salem, "The Molecular Orbital Theory of Conjugated Systems." Benjamin, New York, 1966.
- B. E. Kohler, in "Conjugated Polymers" (J. L. Brédas and R. Silbey, Eds.), pp. 405-434. Kluwer, Dordrecht, 1991.
- C. R. Fincher, Jr., C.-E. Chen, A. J. Heeger, A. G. MacDiarmid, and J. B. Hastings, *Phys. Rev. Lett.* 48, 100 (1982).
- C. S. Yannoni and T. C. Clarke, *Phys. Rev. Lett.* 51, 1191 (1983).
- S. Hirata, H. Torii, and M. Tasumi, *J. Chem. Phys.* 103, 8964 (1995).
- M. Ciofalo and G. L. Manna, *Chem. Phys. Lett.* 263, 73 (1996).
- F. Martinez, R. Voelkel, D. Naegle, and H. Naarmann, *Mol. Cryst. Liq. Cryst.* 167, 227 (1989).
- S. Hotta and K. Waragai, *J. Mater. Chem.* 1, 835 (1991).
- W. ten Hoeve, H. Wynberg, E. E. Havinga, and E. W. Meijer, *J. Am. Chem. Soc.* 113, 5887 (1991).
- J. Guay, P. Kasai, A. Diaz, R. Wu, J. M. Tour, and L. H. Dao, *Chem. Mater.* 4, 1097 (1992).
- A. Yassar, D. Delabouglise, M. Hmyene, B. Nessak, G. Horowitz, and F. Garnier, *Adv. Mater.* 4, 490 (1992).
- P. Bäuerle, U. Segelbacher, K.-U. Gaudl, D. Huttenlocher, and M. Mehring, *Angew. Chem. Int. Ed. Engl.* 32, 76 (1993).
- P. Bäuerle, U. Segelbacher, A. Maier, and M. Mehring, *J. Am. Chem. Soc.* 115, 10,217 (1993).
- M. Sato and M. Hiroi, *Chem. Lett.* 1994, 985 (1994).
- Y. Yu, E. Gunic, B. Zinger, and L. L. Miller, *J. Am. Chem. Soc.* 118, 1013 (1996).
- H. Nakanishi, N. Sumi, Y. Aso, and T. Otsubo, *J. Org. Chem.* 63, 8632 (1998).
- J. A. E. H. van Haare, E. E. Havinga, J. L. J. van Dongen, R. A. J. Janssen, J. Cornil, and J.-L. Brédas, *Chem. Eur. J.* 4, 1509 (1998).
- Y. Kanemitsu, K. Suzuki, Y. Masumoto, Y. Tomiuchi, Y. Shiraishi, and M. Kuroda, *Phys. Rev. B* 50, 2301 (1994).
- R. S. Becker, J. S. de Melo, A. L. Maçanita, and F. Elisei, *J. Phys. Chem.* 100, 18,683 (1996).
- D. Fichou, G. Horowitz, B. Xu, and F. Garnier, *Synth. Met.* 39, 243 (1990).
- J. V. Caspar, V. Ramamurthy, and D. R. Corbin, *J. Am. Chem. Soc.* 113, 600 (1991).
- M. G. Hill, K. R. Mann, L. L. Miller, and J.-F. Penneau, *J. Am. Chem. Soc.* 114, 2728 (1992).
- M. G. Hill, J.-F. Penneau, B. Zinger, K. R. Mann, and L. L. Miller, *Chem. Mater.* 4, 1106 (1992).
- Y. Furukawa, N. Yokonuma, M. Tasumi, M. Kuroda, and J. Nakayama, *Mol. Cryst. Liq. Cryst.* 256, 113 (1994).
- J. Poplawski, E. Ehrenfreund, J. Cornil, J. L. Brédas, R. Pugh, M. Ibrahim, and A. J. Frank, *Mol. Cryst. Liq. Cryst.* 256, 407 (1994).
- R. A. J. Janssen, D. Moses, and N. S. Sariciftci, *J. Chem. Phys.* 101, 9519 (1994).
- B. Nessakh, G. Horowitz, F. Garnier, F. Deloffre, P. Srivastava, and A. Yassar, *J. Electroanal. Chem.* 399, 97 (1995).
- N. Yokonuma, Y. Furukawa, M. Tasumi, M. Kuroda, and J. Nakayama, *Chem. Phys. Lett.* 255, 431 (1996).
- D. Okamura, Y. Furukawa, N. Katano, and J. Nakayama, unpublished data.
- J. Cornil, D. Beljonne, and J. L. Brédas, *J. Chem. Phys.* 103, 842 (1995).
- Y. Furukawa, *J. Phys. Chem.* 100, 15,644 (1996).
- Y. Furukawa, in "Primary Photoexcitations in Conjugated Polymers: Molecular Exciton versus Semiconductor Band Model" (N. S. Sariciftci, Ed.), pp. 496-523. World Scientific, Singapore, 1997.
- A. J. W. Tol, *Chem. Phys.* 208, 73 (1996).
- S. Irle and H. Lischka, *J. Chem. Phys.* 107, 3021 (1997).
- R. A. J. Janssen, in "Primary Photoexcitations in Conjugated Polymers: Molecular Exciton versus Semiconductor Band Model" (N. S. Sariciftci, Ed.), pp. 524-558. World Scientific, Singapore, 1997.
- D. Birnbaum and B. E. Kohler, *J. Chem. Phys.* 90, 3506 (1989).
- D. Birnbaum and B. E. Kohler, *J. Chem. Phys.* 95, 4783 (1991).
- D. Birnbaum, D. Fichou, and B. E. Kohler, *J. Chem. Phys.* 96, 165 (1992).
- N. Periasamy, R. Danieli, G. Ruani, R. Zamboni, and C. Taliani, *Phys. Rev. Lett.* 68, 919 (1992).
- F. Charra, D. Fichou, J.-M. Nunzi, and N. Pfeffer, *Chem. Phys. Lett.* 192, 566 (1992).
- D. V. Lap, D. Grebner, S. Rentsch, and H. Naarmann, *Chem. Phys. Lett.* 211, 135 (1993).
- D. Grebner, M. Helbig, and S. Rentsch, *J. Phys. Chem.* 99, 16,991 (1995).
- J. P. Reyftmann, J. Kagan, R. Santus, and P. Morliere, *Photochem. Photobiol.* 41, 1 (1985).
- R. A. J. Janssen, L. Smilowitz, N. S. Sariciftci, and D. Moses, *J. Chem. Phys.* 101, 1787 (1994).
- F. Negri and M. Z. Zgierski, *J. Chem. Phys.* 100, 2571 (1994).
- R. Colditz, D. Grebner, M. Helbig, and S. Rentsch, *Chem. Phys.* 201, 309 (1995).
- M. Belletête, N. D. Césaire, M. Leclerc, and G. Durocher, *Chem. Phys. Lett.* 250, 31 (1996).
- A. E. Gillam and D. H. Hey, *J. Chem. Soc.* 1170 (1939).
- J. Dale, *Acta Chem. Scand.* 11, 650 (1957).
- H. Gregorius, W. Heitz, and K. Müllen, *Adv. Mater.* 5, 279 (1993).

69. P. Balk, G. J. Hoijtink, and J. W. H. Schreurs, *Rec. Trav. Chim.* 76, 813 (1957).
70. K. H. J. Buschow, J. Dieleman, and G. J. Hoijtink, *J. Chem. Phys.* 42, 1993 (1965).
71. J. Sagiv, A. Yogev, and Y. Mazur, *J. Am. Chem. Soc.* 99, 6861 (1977).
72. H. Hiratsuka, Y. Hatano, Y. Tanizaki, and Y. Mori, *J. Chem. Soc. Faraday Trans. 2* 81, 1653 (1985).
73. Y. Furukawa, H. Ohtsuka, and M. Tasumi, *Synth. Met.* 55, 516 (1993).
74. R. K. Khanna, Y. M. Jiang, B. Srinivas, C. B. Smithhart, and D. L. Wertz, *Chem. Mater.* 5, 1792 (1993).
75. R. Zahradník and P. Cársky, *J. Phys. Chem.* 74, 1240 (1970).
76. M. Rubio, M. Merchán, E. Ortí, and B. O. Roos, *J. Phys. Chem.* 99, 14,980 (1995).
77. V. G. Drefahl, R. Kühmstedt, and H. Oswald, *Makromol. Chem.* 131, 89 (1970).
78. C. W. Spangler, T. J. Hall, L. S. Sapochak, and P.-K. Liu, *Polymer* 30, 1166 (1989).
79. C. W. Spangler and T. J. Hall, *Synth. Met.* 44, 85 (1991).
80. J. M. Oberski, A. Greiner, and H. Bässler, *Chem. Phys. Lett.* 184, 391 (1991).
81. R. Schenk, H. Gregorius, and K. Müllen, *Adv. Mater.* 3, 492 (1991).
82. R. Schenk, H. Gregorius, K. Meerholz, J. Heize, and K. Müllen, *J. Am. Chem. Soc.* 113, 2634 (1991).
83. A. Sakamoto, Y. Furukawa, and M. Tasumi, *J. Phys. Chem.* 96, 1490 (1992).
84. M. Deussen and H. Bässler, *Chem. Phys.* 164, 247 (1992).
85. A. Sakamoto, Y. Furukawa, and M. Tasumi, *J. Phys. Chem.* 96, 3870 (1992).
86. H. S. Woo, O. Lhost, S. C. Graham, D. D. C. Bradley, R. H. Friend, C. Quattrocchi, J. L. Brédas, R. Schenk, and K. Müllen, *Synth. Met.* 59, 13 (1993).
87. A. Sakamoto, Y. Furukawa, and M. Tasumi, *J. Phys. Chem.* 98, 4635 (1994).
88. Y. Furukawa, A. Sakamoto, and M. Tasumi, *Macromol. Symp.* 101, 95 (1996).
89. S. Karabunarliev, M. Baumgarten, N. Tsyutulkov, and K. Müllen, *J. Phys. Chem.* 98, 11,892 (1994).
90. J. Cornil, D. Beljonne, and J. L. Brédas, *J. Chem. Phys.* 103, 834 (1995).
91. A. Sakamoto, Y. Furukawa, and M. Tasumi, *J. Phys. Chem. B* 101, 1726 (1997).
92. W. G. Herkstroeter and D. S. McClure, *J. Am. Chem. Soc.* 90, 4522 (1968).
93. Z. G. Soos, S. Ramasesha, D. S. Galvão, and S. Etemad, *Phys. Rev. B* 47, 1742 (1993).
94. Z. Shuai, J. L. Brédas, and W. P. Su, *Chem. Phys. Lett.* 228, 301 (1994).
95. D. Beljonne, Z. Shuai, R. H. Friend, and J. L. Brédas, *J. Chem. Phys.* 102, 2042 (1995).
96. B. I. Greene, R. M. Hochstrasser, and R. B. Weisman, *Chem. Phys. Lett.* 62, 427 (1979).
97. L. Zechmeister, "Cis-Trans Isomeric Carotenoids, Vitamins A, and Arylpolyenes." Academic Press, New York, 1962.
98. B. S. Hudson, B. E. Kohler, and K. Schulten, *Excited States* 6, 1 (1982).
99. Y. Furukawa, in "The Chemistry of Dienes and Polyenes" (Z. Rapoport, Ed.), Vol. 1, pp. 149–172. Wiley, Chichester, 1997.
100. F. Sondheimer, D. A. Ben-Efram, and R. Wolovsky, *J. Am. Chem. Soc.* 83, 1675 (1961).
101. W. F. Forbes, R. Shilton, and A. Balasubramanian, *J. Org. Chem.* 29, 3527 (1964).
102. C. W. Spangler and D. A. Little, *J. Chem. Soc. Perkin Trans. 1* 1982, 2379 (1982).
103. P. Nayler and M. C. Whiting, *J. Chem. Soc.* 3037 (1955).
104. C. W. Spangler and R. A. Rathunde, *J. Chem. Soc., Chem. Commun.* 1989, 26 (1989).
105. K. Knoll and R. R. Schrock, *J. Am. Chem. Soc.* 111, 7989 (1989).
106. K. W. Hausser, R. Kuhn, A. Smakula, and K. H. Kreuchen, *Z. Phys. Chem.* B29, 363 (1935).
107. K. W. Hausser, R. Kuhn, and A. Smakula, *Z. Phys. Chem.* B29, 384 (1935).
108. C. W. Spangler, P.-K. Liu, A. A. Dembek, and K. O. Havelka, *J. Chem. Soc. Perkin Trans. 1* 1991, 799 (1991).
109. G. J. Hoijtink and P. H. van der Meij, *Z. Phys. Chem. Neue Folge* 20, 1 (1959).
110. H. M. Parkes and R. N. Young, *J. Chem. Phys. Perkin 2* 1980, 1137 (1980).
111. L. M. Tolbert and M. E. Ogle, *Synth. Met.* 41, 1389 (1991).
112. T. Yamabe, K. Akagi, T. Matsui, K. Fukui, and H. Shirakawa, *J. Phys. Chem.* 86, 2365 (1982).
113. Z. G. Soos and L. R. Ducasse, *J. Chem. Phys.* 78, 4092 (1983).
114. T. Bally, K. Roth, W. Tang, R. R. Schrock, K. Knoll, and L. Y. Park, *J. Am. Chem. Soc.* 114, 2440 (1992).
115. Y. Kawashima, K. Nakayama, H. Nakano, and K. Hirao, *Chem. Phys. Lett.* 267, 82 (1997).
116. P. Mathis and J. Kleo, *Photochem. Photobiol.* 18, 343 (1973).
117. F. W. Langkilde, R. Wilbrandt, and N.-H. Jensen, *Chem. Phys. Lett.* 111, 372 (1984).
118. N. S. Sariciftci, Ed., "Primary Photoexcitations in Conjugated Polymers: Molecular Exciton versus Semiconductor Band Model." World Scientific, Singapore, 1997.
119. J. L. Brédas and G. B. Street, *Acc. Chem. Res.* 18, 309 (1985).
120. M. Tabata, M. Satoh, K. Kaneto, and K. Yoshino, *J. Phys. Soc. Jpn.* 55, 1305 (1986).
121. S. Yamada, S. Tokito, T. Tsutsui, and S. Saito, *J. Chem. Soc., Chem. Commun.* 1987, 1448 (1987).
122. A. O. Patil, A. J. Heeger, and F. Wudl, *Chem. Rev.* 88, 183 (1988).
123. R. P. McCall, J. M. Ginder, J. M. Leng, H. J. Ye, S. K. Manohar, J. G. Masters, G. E. Asturias, A. G. MacDiarmid, and A. J. Epstein, *Phys. Rev. B* 41, 5202 (1990).
124. A. J. Epstein, R. P. McCall, J. M. Ginder, and A. G. MacDiarmid, in "Spectroscopy of Advanced Materials" (R. J. H. Clark and R. E. Hester, Eds.), pp. 355–396. Wiley, New York, 1991.
125. K. Pichler, D. A. Halliday, D. D. C. Bradley, P. L. Burn, R. H. Friend, and A. B. Holmes, *J. Phys. Condens. Matter* 5, 7155 (1993).
126. A. J. Heeger, S. Kivelson, J. R. Schrieffer, and W.-P. Su, *Rev. Mod. Phys.* 60, 781 (1988).
127. G. B. Blanchet, C. R. Fincher, T. C. Chung, and A. J. Heeger, *Phys. Rev. Lett.* 50, 1938 (1983).
128. K. Kaneto, S. Ura, K. Yoshino, and Y. Inuishi, *Jpn. J. Appl. Phys.* 23, L189 (1984).
129. P. A. Lane, X. Wei, and Z. V. Vardeny, *Phys. Rev. Lett.* 77, 1544 (1996).
130. M. Satoh, M. Tabata, F. Uesugi, K. Kaneto, and K. Yoshino, *Synth. Met.* 17, 595 (1987).
131. D. D. C. Bradley, G. P. Evans, and R. H. Friend, *Synth. Met.* 17, 651 (1987).
132. D. D. C. Bradley, N. F. Colaneri, and R. H. Friend, *Synth. Met.* 29, E121 (1989).
133. A. J. Brassett, N. F. Colaneri, D. D. C. Bradley, R. A. Lawrence, R. H. Friend, H. Murata, S. Tokito, T. Tsutsui, and S. Saito, *Phys. Rev. B* 41, 10,586 (1990).
134. Y. Furukawa, *Synth. Met.* 69, 629 (1995).
135. Y. Shimoi, S. Abe, and K. Harigaya, *Mol. Cryst. Liq. Cryst.* 267, 329 (1995).
136. Y. Shimoi and S. Abe, *Synth. Met.* 78, 219 (1996).
137. Y. Furukawa, *J. Phys. Chem.* 100, 15,644 (1996).
138. P. A. Lane and Z. V. Vardeny, in "Primary Photoexcitations in Conjugated Polymers: Molecular Exciton versus Semiconductor Band Model" (N. S. Sariciftci, Ed.), pp. 292–317. World Scientific, Singapore, 1997.
139. R. H. Friend, D. D. C. Bradley, and P. D. Townsend, *J. Phys. D: Appl. Phys.* 20, 1367 (1987).
140. T. Kobayashi, Ed., "Relaxation in Polymers." World Scientific, Singapore, 1993.

141. K. Fesser, A. R. Bishop, and D. K. Campbell, *Phys. Rev. B* 27, 4804 (1983).
142. R. D. McCullough, R. D. Lowe, M. Jayaraman, and D. L. Anderson, *J. Org. Chem.* 58, 904 (1993).
143. T.-A. Chen, X. Wu, and R. D. Rieke, *J. Am. Chem. Soc.* 117, 233 (1995).
144. M. Berggren, O. Inganäs, G. Gustafsson, J. Rasmussen, M. R. Anderson, T. Hjertberg, and O. Wennerström, *Nature* 372, 444 (1994).
145. Z. Vardeny, E. Ehrenfreund, O. Brafman, M. Nowak, H. Schaffer, A. J. Heeger, and F. Wudl, *Phys. Rev. Lett.* 56, 671 (1986).
146. T.-C. Chung, J. H. Kaufman, A. J. Heeger, and F. Wudl, *Phys. Rev. B* 30, 702 (1984).
147. K. Kaneto, S. Hayashi, S. Ura, and K. Yoshino, *J. Phys. Soc. Jpn.* 54, 1146 (1985).
148. K. Kaneto, Y. Kohno, and K. Yoshino, *Solid State Commun.* 51, 267 (1984).
149. G. S. Kanner, X. Wei, B. C. Hess, L. R. Chen, and Z. V. Vardeny, *Phys. Rev. Lett.* 69, 538 (1992).
150. G. Harbeke, E. Meier, W. Kobel, M. Egli, H. Kiess, and E. Tosatti, *Solid State Commun.* 55, 419 (1985).
151. M. Sato, S. Tanaka, and K. Kaeriyama, *Synth. Met.* 14, 279 (1986).
152. Y. H. Kim, S. Hotta, and A. J. Heeger, *Phys. Rev. B* 36, 7486 (1987).
153. K. Kaneto, F. Uesugi, and K. Yoshino, *Solid State Commun.* 1987, 64, 1195 (1987).
154. N. Colaneri, M. Nowak, D. Spiegel, S. Hotta, and A. J. Heeger, *Phys. Rev. B* 36, 7964 (1987).
155. Y. H. Kim, D. Spiegel, S. Hotta, and A. J. Heeger, *Phys. Rev. B* 38, 5490 (1988).
156. J. Rühe, N. F. Colaneri, D. D. C. Bradley, R. H. Friend, and G. Wegner, *J. Phys. Condens. Matter* 2, 5465 (1990).
157. Z. W. Sun and A. J. Frank, *J. Chem. Phys.* 94, 4600 (1991).
158. C. Botta, S. Luzzati, R. Tubino, and A. Borghesi, *Phys. Rev. B* 46, 13,008 (1992).
159. C. Botta, S. Luzzati, R. Tubino, D. D. C. Bradley, and R. H. Friend, *Phys. Rev. B* 48, 14,809 (1993).
160. L. Smilowitz, N. S. Sariciftci, R. Wu, C. Gettinger, A. J. Heeger, and F. Wudl, *Phys. Rev. B* 47, 13,835 (1993).
161. K. Yoshino, T. Akashi, K. Yoshimoto, M. Yoshida, S. Morita, and A. A. Zakhidov, *Mol. Cryst. Liq. Cryst.* 256, 343 (1994).
162. K. Lee, R. A. J. Janssen, N. S. Sariciftci, and A. J. Heeger, *Phys. Rev. B* 49, 5781 (1994).
163. R. A. J. Janssen, N. S. Sariciftci, and A. J. Heeger, *J. Chem. Phys.* 100, 8641 (1994).
164. R. A. Janssen, M. P. T. Christiaans, C. Hare, N. Martin, N. S. Sariciftci, A. J. Heeger, and F. Wudl, *J. Chem. Phys.* 103, 8840 (1995).
165. N. S. Sariciftci, *Prog. Quant. Electron.* 19, 131 (1995).
166. P. A. Lane, X. Wei, and Z. V. Vardeny, *Phys. Rev. B* 56, 4626 (1997).
167. K. E. Ziemelis, A. T. Hussain, D. D. C. Bradley, R. H. Friend, J. Rühe, and G. Wegner, *Phys. Rev. Lett.* 66, 2231 (1991).
168. P. J. Brown, H. Sirringhaus, and R. H. Friend, *Synth. Met.* 101, 557 (1999).
169. H. Sirringhaus, P. J. Brown, R. H. Friend, M. M. Nielsen, K. Bechgaard, B. M. W. Langeveld-Voss, A. J. H. Spiering, R. A. J. Janssen, E. W. Meijer, P. Herwig, and D. M. de Leeuw, *Nature* 401, 685 (1999).
170. I. D. W. Samuel, G. Rumbles, and R. H. Friend, in "Primary Photoexcitations in Conjugated Polymers: Molecular Exciton versus Semiconductor Band Model" (N. S. Sariciftci, Ed.), pp. 140–173. World Scientific, Singapore, 1997.
171. T. Ohnishi, S. Doi, Y. Ysuchida, and T. Noguchi, in "Photonic and Optoelectronic Polymers" (S. A. Jenkhe and K. J. Wynne, Eds.), pp. 345–357. American Chemical Society, Washington, DC, 1997.
172. N. F. Colaneri, D. D. C. Bradley, R. H. Friend, P. L. Burn, A. B. Holmes, and C. W. Spangler, *Phys. Rev. B* 42, 11,670 (1990).
173. K. F. Voss, C. M. Foster, L. Smilowitz, D. Mihailovic, S. Askari, G. Srdanov, Z. Ni, S. Shi, A. J. Heeger, and F. Wudl, *Phys. Rev. B* 43, 5109 (1991).
174. X. Wei, B. C. Hess, Z. V. Vardeny, and F. Wudl, *Phys. Rev. Lett.* 68, 666 (1992).
175. H. S. Woo, S. C. Graham, D. A. Halliday, D. D. C. Bradley, R. H. Friend, P. L. Burn, and A. B. Holmes, *Phys. Rev. B* 46, 7379 (1992).
176. K. Pichler, D. A. Halliday, D. D. C. Bradley, P. L. Burn, R. H. Friend, and A. B. Holmes, *J. Phys. Condens. Matter* 5, 7155 (1993).
177. J. M. Leng, S. Jeglinski, X. Wei, R. E. Benner, Z. V. Vardeny, F. Guo, and S. Mazumdar, *Phys. Rev. Lett.* 72, 156 (1994).
178. R. A. J. Janssen, J. C. Hummelen, K. Lee, K. Pakbaz, N. S. Sariciftci, A. J. Heeger, and F. Wudl, *J. Chem. Phys.* 103, 788 (1995).
179. S. V. Frolov, P. A. Lane, M. Ozaki, K. Yoshino, and Z. V. Vardeny, *Chem. Phys. Lett.* 286, 21 (1998).
180. A. R. Brown, K. Pichler, N. C. Greenham, D. D. C. Bradley, R. H. Friend, and A. B. Holmes, *Chem. Phys. Lett.* 210, 61 (1993).
181. J. Orenstein and G. L. Baker, *Phys. Rev. Lett.* 49, 1043 (1982).
182. Z. Vardeny, J. Orenstein, and G. L. Baker, *Phys. Rev. Lett.* 50, 2032 (1983).
183. G. B. Blanchet, C. R. Fincher, T. C. Chung, and A. J. Heeger, *Phys. Rev. Lett.* 50, 1938 (1983).
184. Z. Vardeny, H. T. Grahn, L. Chen, and G. Leising, *Synth. Met.* 28, D167 (1989).
185. P. D. Townsend and R. H. Friend, *Phys. Rev. B* 40, 3112 (1989).
186. C. G. Levey, D. V. Lang, S. Etemad, G. L. Baker, and J. Orenstein, *Synth. Met.* 17, 569 (1987).
187. J. H. Burroughes, C. A. Jones, and R. H. Friend, *Nature* 335, 137 (1988).

Chapter 8

STABILITY OF ELECTRICALLY CONDUCTING POLYMERS

F. Mohammad

Department of Applied Chemistry, Aligarh Muslim University, Aligarh-202002, India

Contents

1. Introduction	321
1.1. Electrically Conducting Polymers	321
1.2. Stability of Electrically Conducting Polymers	322
1.3. Stabilization	324
2. Stability of Individual Polymeric Systems	325
2.1. Polyacetylenes	325
2.2. Polyheterocyclics	326
2.3. Polyaromatics	334
2.4. Inorganic and Silicon Polymers	341
2.5. Phthalocyanines	342
2.6. Miscellaneous Systems	343
Acknowledgments	344
References	344

1. INTRODUCTION

1.1. Electrically Conducting Polymers

Polymers are generally insulators and they have been increasingly used as substitutes for structural materials, such as metals, wood, and ceramics, because they can be produced from cheap raw materials in addition to being light weight, low temperature processible, and corrosion resistant, and demonstrating high mechanical strength. However, until the last few decades, polymers have been unsuccessful in replacing metals and semiconductors in electrical and electronic applications owing to their insulating properties. The phenomenon of photoconduction in solid anthracene was observed at the very beginning of this century, as early as in 1906, by Pochettino [1]. Later, in 1941, Szent-Gyorgy [2] resuscitated the idea of electronic conduction by suggesting the movement of π -electrons from molecule to molecule in complex biological systems. The remarkable achievements in the field of inorganic semiconductors triggered research groups the world over to search for polymeric materials of practical potential in the electrical and electronics industry. An explosion of research and development work has been done to tailor polymers with desirable physical, chemical, electrical, and electronic properties during the last three decades, and the subject was widely reviewed during this period [3–10].

This review chapter deals with the class of intrinsically conducting polymers where chemical structure can produce, sustain, and assist the motion of charge carriers (electrons and holes) necessary for electrical conduction. For a polymer to be included in this class, it must possess a conjugated backbone, which provides a great degree of delocalization of π -electrons. The overlapping set of molecular orbitals gives a reasonable carrier mobility along the polymer chain. The charge carriers must be provided extrinsically by a charge-transfer process that is generally called doping, because pristine polymer contains no charge carriers. p-type and n-type doping of conjugated polymers is carried out by reaction with oxidants and reductants, respectively. Doping of conducting polymers involves the addition of a very high concentration of doping agent, in contrast to the substitution by a low concentration (parts per million level) of doping atoms in semiconductors such as in silicon and germanium [11–14]. In brief, to show electronic conduction a polymeric system must possess both an orbital system, which allows charge carriers to be mobile, and the charge carriers. A controlled variation of electrical conductivity over many orders of magnitude has, thus, become possible via such doping reactions (Fig. 1). In a conducting polymeric composite, an insulating polymer mixed with a critical amount of conducting material such as metal powder provides the electronic conduction, whereas the polymer matrix acts as a solid adhesive to keep the conducting

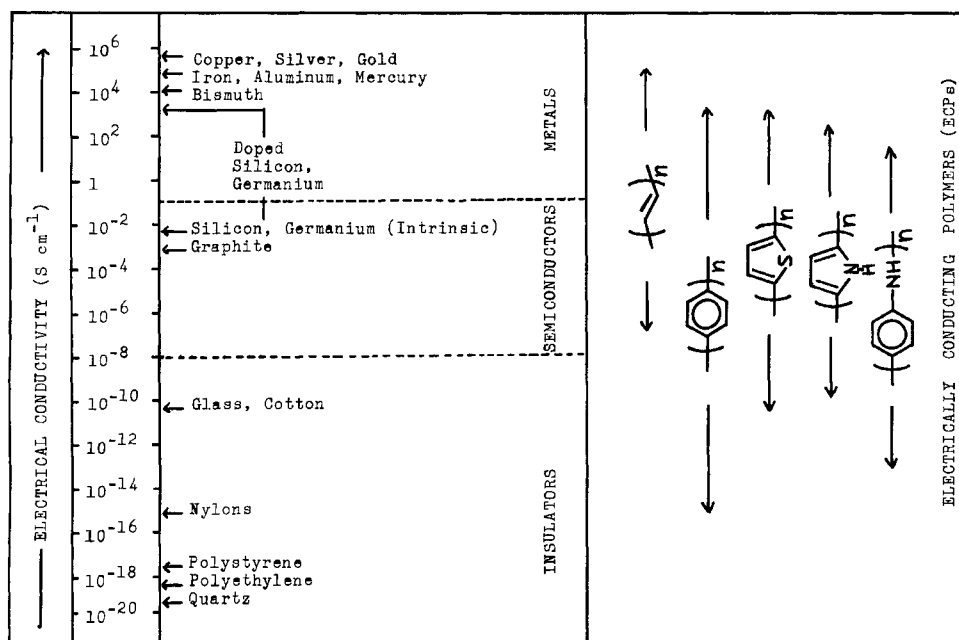


Fig. 1. Electrical properties of some important materials and electrically conducting polymers.

components together and render mechanical strength, but makes no contribution to electrical conduction. These conducting composites are enjoying a fairly good demand from industry due to their low cost, light weight, good mechanical strength, and reasonably high electrical conductivities; however, they are not the subject of this chapter [15].

There is a great variety of applications for electrical conducting polymers in electronic devices, electromagnetic shielding, interconnection technologies, renewable energy sources, semiconductor devices, thin film technology, sensors, electrochemomechanical devices, display devices, photovoltaics, smart windows, and so on [16–26]. Although knowledge of the environmental stability of a polymer (i.e., molecular, structural, and physical properties) is a prequalification for its use in a practical application, most conducting polymers were known to exist only in the form of intractable and nonprocessable powders until the last two decades. A trace amount of electrophilic reagent such as oxygen may cause serious damage to the long conjugated backbone of the polymer due to addition reactions of unsaturated bonds. This reactivity and instability of conjugated polymers has limited their use in most possible and promising applications. The emergence in the early 1970s of direct and precursor routes to high quality polyacetylene [27, 28] films and an electrochemical polymerization route to polyheterocyclics such as polythiophene [29] and polypyrrole [30, 31] further triggered investigations of these materials due to somewhat easier fabrication of experimental samples. In the forthcoming paragraphs, the various aspects of the stability of electrically conducting polymers (ECPs) are discussed.

1.2. Stability of Electrically Conducting Polymers

Polymers undergo chemical reactions just like any typical low molecular weight organic compound, leading to the deterioration of useful polymer properties. The ability of a polymer to retain its useful properties is defined as the stability. There are many external factors that a polymer has to withstand to retain its usefulness, such as heat, light, oxygen, ozone, moisture, mechanical stress, and

atmospheric pollutants, along with other operative mechanisms at the time of processing. The presence of superoxides, defects, and chemically reactive groups may also be taken as important causes of polymer instability [32–35]. Figure 2 details the various factors that may be important in the discussion of the stability of ECPs.

Electrically conducting polymers are long chain molecules that have a high degree of conjugation and few defects. This implies an electronic structure with an empty conduction band and a filled conduction band. For a perfect chain in a perfect lattice, there are no other sites between the two bands. The ionization potential of the polymer, that is, the energy required to remove the highest energy electron from the polymer, is an important property for ascertaining its stability toward chemical reactions that proceed via charge transfer, in general. Another property of interest is the bandgap, that is, the energy required to transfer an electron from the top the valence band to the bottom of the conduction band, which controls the electronic properties of the polymer. The bandgap also controls the electromotive force (emf) of batteries in which the polymer is used as an electrode [36–40].

1.2.1. Intrinsic Stability of ECPs

Pristine ECPs, on exposure to heat and light, undergo chain scission that leads to a lowering of molecular weight (i.e., conjugation length) as well as cross-linking that leads to an increase in molecular weight. These processes cause modification in the chemical structure of ECP chains, affecting their dopability and, therefore, their electroactivity. Pristine ECPs have been reported to contain spins, and inter- and intrachain reactions may alter the structure of these pure pristine polymers [41–44]. The action of heat on ECPs can cause bond scission at temperatures that correspond to the dissociation energies of the bonds present in the polymer. The higher is the dissociation energy of the bond, the higher is the temperature required to break the bond; hence, the weakest bond in the polymer chain determines its intrinsic stability. The presence of aromatic rings in the polymer backbone enhances the intrinsic sta-

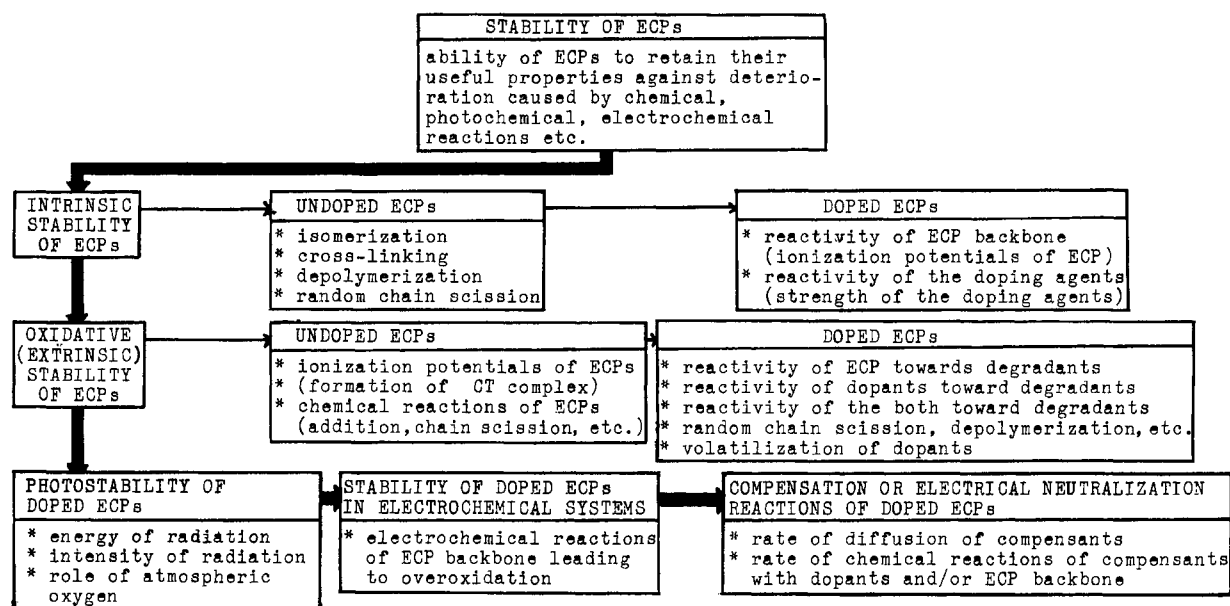


Fig. 2. Important factors in the study of stability and stabilization of electrically conducting polymers.

bility of ECPs due to the relative inertness of the phenylene rings. However, the stability may be affected further by the nature of the groups that link the phenylene rings in the polymer [45–47]. The intrinsic stability of doped ECPs is a function of the reactivity of the polymer backbone, that is, its ionization potential and the reactivity of the dopant (i.e., its oxidizing or reducing power). Due to its low ionization potential of 4.7 eV, polyacetylene is comparatively very reactive and, therefore, the stability of doped polyacetylene is decided by the strength of the doping agent [48]. The ionization potentials of polythiophene and polypyrrole are >5 and 4 eV, respectively; therefore, better stability of polythiophene, which is aromatic in nature [49], compared to polypyrrole and polyacetylene may be predicted for the undoped polymers [48]. The presence of aromatic rings in the polymer chain yields thermally stable polymers, which are further supported by the high ionization potentials of about 5.4 and 6.5 eV of poly(paraphenylene) and poly(*m*-phenylene), respectively [50].

1.2.2. Extrinsic or Oxidative Stability of ECPs

In the presence of atmospheric oxygen, the polymers that contain low dissociation energy bonds, such as O–O, C–N, C–Cl, and C–C, are the most susceptible to oxygen attack at elevated temperatures. In practice, the thermal stability of polymers is less than usually expected because of the accidental inclusion of weak linkages in the main chain. At the same time, polymers with C–F, phenyl, fused rings, and so forth are expected to show enhanced oxidative stability at higher temperatures [51, 52]. Polyacetylene may be taken as a linear analogue of benzene, because it also contains all vinylic hydrogens like those in benzene; hence, polyacetylene may be expected to show similar stability. The difference between the two is that polyacetylene has a very extended structure of π -electron overlap, resulting in a polymer of much lower ionization potential of 4.7 eV versus an ionization potential of 9.25 eV for benzene. The ionization potential of polyacetylene is low enough to allow electron transfer from the polyacetylene chain to oxygen, leading to the formation of a charge-transfer complex, which further lowers the activation energy for subsequent oxida-

tion. In the less ordered amorphous polyacetylene, there are states of lower energy within the bandgap that further ease the charge-transfer reaction of oxygen [53]. By analogy to polyacetylene, other undoped conjugated polymers would be expected to be unstable in oxygen if their ionization potentials are low enough to allow charge-transfer of oxygen. The ionization potentials of polypyrrole and polythiophene are 4 and >5 eV, respectively; hence, polypyrrole shows poor stability, whereas polythiophene shows comparatively better stability toward oxygen attack in the undoped state [54]. Polyphenylenes are reported to show high oxidative stability due to an aromatic backbone, and fairly high stability of polyaniline is also well documented [55, 56]. Unlike p-type doped polyacetylene, other p-type doped polymers are expected to be stable with respect to oxygen, but similarly vulnerable to the degradative reactions of their doping counterions as well as other chemicals that may cause chemical compensation of the doped polymers [57].

1.2.3. Photostability of ECPs

Electrically conducting polymers are finding a great relevance in photonic devices; hence, it is vital to understand their photostability. Sunlight contains infrared and visible radiation along with ultraviolet radiation in the range of 300–400 nm. The energy of radiation is related to wavelength by the equation

$$E \text{ (kJ/mol)} = \frac{1.19 \times 10^5}{\lambda \text{ (nm)}} \quad (1)$$

Therefore, 300-nm radiation, for example, is equivalent to about 397 kJ (about 95 kcal) of energy—enough to initiate many interesting reactions as evident from Table I, which gives the bond dissociation energies of various bonds generally present in polymers. When chemical bonds are broken by these radiations, free radicals are formed and the way in which they react decides the nature of the photochemical reaction. The bonds that absorb the radiation, the bonds that undergo cleavage, and the reactions of radicals all depend on the chemical behavior of the polymeric material. Especially where the primary radicals are mobile, as in conducting polymers, in polymer solutions, or in molten polymers, over-

Table I. Dissociation Energies of Bonds Typically Present in Polymers

Bond	Dissociation energy [kcal mol ⁻¹ (kJ mol ⁻¹)]
O—O	35 (146)
C—N	73 (305)
C—Cl	81 (339)
C—C	83 (347)
C—O	86 (360)
N—H	93 (389)
C—H	99 (414)
O—H	111 (464)
C=C	146 (611)
C≡N	213 (891)
C—F	103–123 (431–515)

Source: Adapted with permission from R. W. Dyson, Ed., "Specialty Polymers," 2nd ed., p. 13. Copyright © 1998, Blackie Academic & Professional, London.

all chemical reactions of free radicals so generated are very interesting. In the presence of oxygen, chemical reactions that involve oxygen radicals are possible and may lead to the extreme case of photoinitiated oxidation. Factors such as heat, oxygen, and other degrading agencies may further complicate the photostability of ECPs and their stabilization. As the number of conjugated bonds increases, the wavelength of maximum absorption encroaches on the visible region of the electromagnetic spectrum and may cause the formation of free radicals, homolytic bond fission, reaction with atmospheric oxygen, and so forth. However, the interaction of high energy radiation and ultrasonic radiation is less selective and very similar to mechanical degradation of polymers. A short exposure to high energy radiation leads to cross-linking, which causes a marked improvement in tensile strength, rigidity, resistance to flow, and chemical stability at elevated temperature. However, a longer exposure has a destructive effect that causes scission of bonds and effects electrical properties in both cases [58–61].

1.2.4. Stability of Doped ECPs in Electrochemical Systems

Electrically conducting polymers have been considered as potential candidates to replace traditional materials in primary and secondary battery electrode applications because of their high electrical conductivity, high selectivity to electrode reactions, low catalytic activity toward side reactions, sufficient mechanical strength, ease of fabrication, low cost, and so on. These materials are distinct from traditional inorganic materials, because they are neither dissolved nor redeposited during charging and discharging reactions and, hence, they may be expected to give long-life electrical storage systems. However, the electrode materials must possess high stability toward degradation reactions as well as moderate coefficients of diffusing ions during the charging–discharging process. The development of various types of systems may be expected because the number of electrically conducting polymers is growing day by day [62–64].

1.2.5. Compensation or Electrical Neutralization of Doped ECPs

A chemical compensation process is one in which, for example, a p-type doped polymer (i.e., oxidized polymer) reacts chemically

with reducing agents, such as NH₃, H₂O, Na, and K, and regains its insulating state. It may be considered as an n-type doping of a p-type doped polymer in which the polymer passes through an insulating stage and vice versa. The compensating reagents diffuse into the polymer matrix and neutralize the charge of the system by a charge-transfer reaction. The process of compensation may involve electronic interaction of the compensating reagent with carbonium ions, charge transfer, proton abstraction from polymer and/or compensating agent, or addition to C=C. Compensation leads to depletion of dopant concentration and a decrease in the conjugation length of the polymer that result in the loss of electroactivity. Under certain assumptions, the electrical conductivity may be considered to be a function of the conjugation length of the polymer and the amount of active dopant present in the polymer–dopant system, because the number of charge carriers depends on the dopant concentration. In a doped polymer, the rate and extent of electrical conductivity loss thus depends on the rate of diffusion of the compensating agent into the polymer matrix and the rate of chemical reaction between the polymer–dopant system and the compensating agent. The effect of chemical reactions that lead to depletion in the conjugation length due to the addition reaction of C=C bonds should also be given due importance discussing these processes [65–68].

1.3. Stabilization

The long conjugated backbone of electrically conducting polymers is sufficiently reactive due to the much lower ionization potential. Doping by oxidizing or reducing agents further enhances the reactivity, whereas doping agents themselves interact with the polymer and lead to the formation of permanent bonds. It is, therefore, extremely important to undertake some preventive measures to inhibit degradative reactions and impart stability to the polymer. These preventive measures collectively are known as polymer stabilization. There are several ways to stabilize polymers; some of them are given in the following list [69–72].

1. The stability of electrically conducting polymers may be improved by incorporating antioxidants, which are readily oxidized or form stable products after combining with the polymers. In general, antioxidants belong to the classes of phenols, aromatic amines, and compounds of amines and aminophenols with aldehydes, ketones, and thio compounds, as well as quinones. Radical traps such as azobisisobutyronitrile also may be used to improve the stability of these materials.
2. Predoped (by electron acceptors) electrically conducting polymers possess little tendency for electron transfer from the polymer to oxygen and, hence, show enhanced stability in the presence of oxygen.
3. Devices fabricated by using electrically conducting polymers may be encapsulated with some materials of reduced permeability to oxygen and moisture.
4. Blending of electrically conducting polymers with other more stable polymers may lead to better stability.
5. Electrically conducting polymers with better stability may be synthesized by applying newer concepts such as fluorine substitution, introduction of aromatic structures in the main chain, use of comparatively more stable doping agents, and fusion of aromatic structures with the main chain.

2. STABILITY OF INDIVIDUAL POLYMERIC SYSTEMS

2.1. Polyacetylenes

Polyacetylene is the simplest of all the conducting polymers. It can be prepared by direct polymerization of acetylene or by heating a precursor polymer under an inert atmosphere. With the development of newer methods of polymer stabilization, polyacetylene once again is attracting the attention of research groups due to its 1.5-eV bandgap, which is ideal for photovoltaic applications [73–75]. The stability and degradation of polyacetylene have been reviewed by Chien [76] and Pochan [77] in great detail. Polyacetylene was reported to be stable up to 300°C in an inert atmosphere by Ito et al. [78] and rapid weight loss was observed by thermogravimetry from 320°C under a helium atmosphere. Oxygen interaction with pristine polyacetylene leads to an increase in electrical conductivity due to the doping effect of oxygen. However, long-term exposure caused irreversible loss of electrical properties due to formation of carbonyl bonds, which interrupt the conjugation of the polymer backbone [79, 80]. Oxygen acts as a doping agent as well as a catalyst during isomerization of *cis*- to *trans*-polyacetylene, a comparatively more stable form of Shirakawa polymer [81, 82]. The interaction of triplet state oxygen with free radicals due to incomplete arrangement of electrons during isomerization was suggested by several workers to impart instability to the polymer [83–86]. Billingham et al. [87] reported the detailed study of Durham polyacetylene, which reacts rapidly with atmospheric oxygen as revealed by the change in resistivity (Fig. 3). Initially, electrical conductivity increased rapidly as oxygen formed the charge-transfer complex, but after a few hours, the electrical conductivity decreased due to irreversible oxidation and interruption in conjugation that prevented the charge flow. There was very little effect on the stability of antioxidant stabilized Durham polyacetylene; however, annealed polymer showed a five times slower rate of oxidation. Similar findings by Yang and Chien [88] claimed that most of the antioxidants were found to be ineffective in stabilizing Shirakawa polymer, including *N-t*-butyl-2-phenylnitron, a highly effective spin trapping additive for polyolefins. Durham polymer with 1–8 mol% of AsF_6^- counterion produced a conductive material that was stable for several weeks and remained resistant to oxidative degradation on exposure to dry air, whereas higher doping levels made the polymer unstable as manifested by the appearance of C–F bonds in the IR spectrum and decay in electrical conductivity [87]. According to Druy et al. [89], p-type doped polyacetylene is intrinsically unstable in terms of electrical conductivity in an argon atmosphere at ambient temperatures; however, the electrical conductivity of the doped polymer decreased at a faster rate in order $\text{I}_2 > \text{ClO}_4^- > \text{IrCl}_4^- > \text{FeCl}_3$ at 75 and 110°C. Doping the polymer with a strong oxidizing agent, ClO_4^- , gave high electrical conductivity, greater stability toward oxygen compared to undoped material, and high chemical reactivity that led to explosions as observed in TGA studies by several workers [77, 88, 89]. Ziegler–Natta polyacetylene was observed to be more stable, because the onset temperature of decomposition was 420°C [90] as compared to the polymer prepared by Aldissi [91] that had an onset temperature of 125°C in thermogravimetric experiments. Treatment of p-type doped polymer that contained differed counterions with HBF_4 produced a polymer with enhanced stability [92–94]. AsF_5 -doped Durham polyacetylene resulted in irreversible loss of electrical conductivity along with an increase in the optical absorption

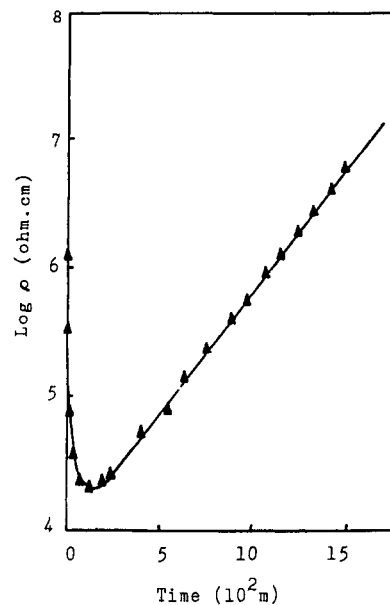


Fig. 3. Resistivity change on exposure of a 7- μm -thick film of polyacetylene to 600 torr of oxygen at 50. Reprinted with permission from N. C. Billingham et al., *Polym. Degrad. Stab.* 19, 323 (1987). Copyright © 1987, Elsevier Science Ltd., Oxford.

edge from 1.5 to 1.8 eV, indicating the formation of sp^3 carbon centers and leading to loss of conjugation length on exposure to 50 torr of dry ammonia. Addition to C=C, thus puncturing the conjugation, was further confirmed by the appearance of a new band at 1300 cm^{-1} due to C–N stretching in the IR spectrum of an exposed sample [95].

It has been observed that the stability of polymers increased with substitution on the backbone, but dopability was badly affected. Phenyl-substituted polyacetylene is fairly stable, but cannot be doped to produce a conducting material. The onset temperatures of thermal degradation of poly(phenylacetylene) and poly(methylacetylene) were reported to be 270 and 150°C, respectively, under nitrogen [96]. A number of disubstituted polyacetylenes were prepared by several workers [97–101] and their onset temperatures of initial weight loss ranged from 180 to 500°C as evident from Table II. Blending polyacetylene with polybutadiene had no impact on its stability, whereas blending with EPDM followed by cross-linking yielded slightly better air stability [102]. The stability of polypyrrole deposited on pristine as well as doped polyacetylene containing InCl_4^- , FeCl_4^- , ClO_4^- , and BF_4^- counterions was reported to be fairly stable in humid air (humidity 40%) and the polymer films could be handled in an ambient atmosphere without deterioration in electrical conductivity [103].

Blumstein and co-workers [104–106] synthesized nanocomposites of montmorillonite (Mont) and poly(2-ethylpyridine) (P2EPy) in which the polymer was intercalated between the layers of the clay. These types of materials are attracting the interest of many researchers due to their unique optical, electrical, mechanical, and thermal properties. Thermogravimetric studies on pure Ca^{2+} containing Mont revealed that it contains 3.2% sorption water released up to 110°C and 4.8% structural water released up to 600°C, whereas the total weight loss of CaMont–P2EPy composite in air includes adsorbed water, constitutional water, and the polymer to the extent of 25%. Polymer content in the composite, thus calculated to be 0.23-g polymer per gram of dehydrated clay,

Table II. Onset Temperature of Thermal Decomposition of Disubstituted Polyacetylenes in Air

Polymer	Onset temperature (°C)	Ref.
$\begin{array}{c} \text{---(C=C)}_n\text{---} \\ \\ \text{S} \\ \\ \text{Ph} \\ \\ n\text{-C}_{10}\text{H}_{21} \end{array}$	200	[97]
$\begin{array}{c} \text{---(C=C)}_n\text{---} \\ \\ \text{S} \\ \\ n\text{-Bu} \\ \\ \text{Ph} \end{array}$	180	[97]
$\begin{array}{c} \text{---(C=C)}_n\text{---} \\ \\ \text{Me} \\ \\ \text{Naphth} \end{array}$	340	[98]
$\begin{array}{c} \text{---(C=C)}_n\text{---} \\ \\ \text{Me} \\ \\ \text{Ph} \end{array}$	280	[98]
$\begin{array}{c} \text{---(C=C)}_n\text{---} \\ \\ \text{Ph} \\ \\ \text{Ph-SiMe}_3 \end{array}$	420	[99]
$\begin{array}{c} \text{---(C=C)}_n\text{---} \\ \\ \text{Ph} \\ \\ \text{Ph} \end{array}$	500	[99]
$\begin{array}{c} \text{---(C=C)}_n\text{---} \\ \\ \text{Ph} \\ \\ \text{Ph} \\ \\ t\text{-Bu} \end{array}$	380	[99]
$\begin{array}{c} \text{---(C=C)}_n\text{---} \\ \\ \text{Ph} \\ \\ \text{Ph-OPh} \end{array}$	420	[99]
$\begin{array}{c} \text{---(C=C)}_n\text{---} \\ \\ \text{Ph} \\ \\ \text{Ph} \\ \\ n\text{-Bu} \end{array}$	320	[99]

is in agreement with the results obtained from spectroscopic studies. Total weight loss of composite in nitrogen is 17.5% at 800°C; hence, 42% of the polymer remains in the composite at 800°C under nitrogen. Pure P2EPy polymer degrades completely by 570°C in air, but retains its weight to the extent of 24% by 800°C under nitrogen. The saturated polymer, poly(2-vinylpyridine) is known to degrade completely in air by 400°C under nitrogen. The enhanced stability of P2EPy may be attributed to the conjugated backbone of the polymer, which prefers to cross-link rather than to depolymerize [104]. When the polymer is intercalated in CaMont, it shows higher stability than the pure polymer. It has been suggested that this remarkable enhancement in the stability of the composite is due to steric factors that hinder the thermal motion of polymer segments sandwiched between the layers of clay, the hindered diffusion of volatile decomposition products, and the conjugated nature of the polymer backbone which leads to the formation of cross-linked structure on heating [106].

Shimizu and Yamamoto [107] reported the synthesis of a tetrathiafulvalene-substituted polyacetylene by Rh catalyzed polymerization. Tetrathiafulvalene (TTF) is a strongly electron donating molecule and forms highly conducting charge-transfer (CT) complexes with electron acceptors. The polymer, poly(2-ethynyl-tetrathiafulvalene) (I) was observed to be stable under nitrogen, but degraded gradually in the air. An IR spectrum of polymer ex-

posed to air for a month showed new absorption bands that correspond to the formation of $-\text{OH}$, $-\text{OOH}$, $-\text{O}-$, and epoxide due to oxidative degradation similar to that reported in the case of polyacetylene [108, 109]. However, no change in the color of the polymer was observed after 1 month. Pristine polymer showed an electrical conductivity of less than $1 \times 10^{-9} \text{ S cm}^{-1}$, which was enhanced to $2.1 \times 10^{-3} \text{ S cm}^{-1}$ (as measured on the compressed pellet of CT complex) when a CT complex with TCNQ was formed.

The work of Kim et al. [110] focused on polyacetylene fiber networks ranging in diameter from 60 to 80 nm. The dark red gel of low density foaml like polyacetylene doped with iodine showed a remarkably low temperature dependence of resistivity as compared to bulk polyacetylene film. Polyacetylene fiber networks were found to be more sensitive to air than the bulk polymer, because the resistance of the iodine-doped fiber network increased more rapidly than that of the bulk polyacetylene film on exposure to air.

2.2. Polyheterocyclics

Electrically conducting polymers based on polyheterocyclic monomers are of considerable interest due to their fascinating optical, electrical, and electrochemical properties. The electrical conductivity, processibility, and stability of these materials can be varied and controlled by manipulating the chemical structures using chemical modification techniques. These polymers are potential replacement materials for traditional inorganics in a wide range of applications such as batteries, field-effect transistors, light-emitting displays, electrochromic displays, and sensors. Polyheterocyclics based on polythiophene and polypyrrole are the most intensely studied. The stability studies of these polymers are covered in the subsequent subsections of this chapter and include homopolymers, copolymers, and substituted and ring fused materials.

2.2.1. Polythiophenes

Polythiophene and its derivatives show remarkable air stability in both oxidized and reduced form [111]. However, there are variable reports on their stability in different types of environments. The ionization potential of polythiophene is estimated to be above 5 eV, which is high enough to protect the polymer from forming a charge-transfer complex with oxygen to cause oxidative instability. Both electrochemically as-prepared polythiophene and polythiophene redoped after ammonia compensation showed much better air stability compared to polyacetylene [112, 113].

We performed a detailed stability study of the polymer containing various counterions and their ammonia compensated counterparts by thermogravimetry, UV-vis, IR, and electrical conductivity monitoring [114–117]. Polythiophene doped with BF_4^- counterions showed a weight loss of 18% in air as well as in nitrogen atmosphere, whereas a weight loss of 77% in air by 600°C and 7% in nitrogen by 700°C was observed in the thermogravimetric analysis. Perchlorate containing polythiophene showed a continuous weight loss with increasing temperature in both air and nitrogen, and was accompanied by explosions due to fast oxidation reaction with the polymer backbone.

Polythiophene containing BF_4^- counterions showed a loss of dopant on exposure to ambient and slightly higher temperatures without any loss of conjugation; however, at higher temperatures (around 175°C), it undergoes fast loss of dopant and then loss

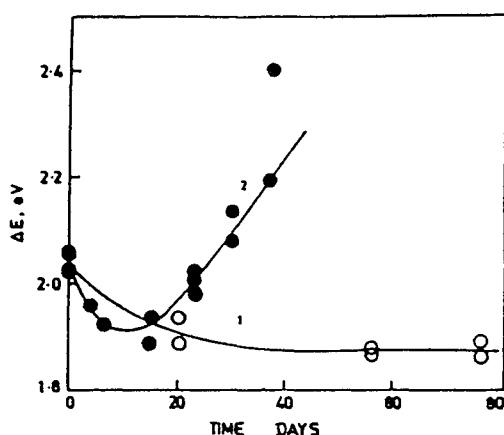


Fig. 4. Variations of band edge energy in UV-vis spectra of BF_4^- -doped polythiophene on ageing (1) at 80°C and (2) at 175°C . Reprinted with permission from F. Mohammad et al., *Bull. Electrochem.* 9(2/3), 109 (1993). Copyright © 1993, Central Electrochemical Research Institute, Tamil Nadu, India.

Table III. Changes in λ_{max} and Bandgap Estimated from UV-vis Spectra of Electrochemically Prepared Polythiophene that Contains BF_4^- Counterions During Thermal Degradation in Ambient Air^a

Time (days)	Sample 1		Sample 2	
	λ_{max} (nm)	BG (eV)	λ_{max} (nm)	BG (eV)
Degradation at 80°C				
00	476	2.06	478	2.02
13	505	1.87	505	1.88
20	509	1.89	509	1.94
56	502	1.87	503	1.89
76	501	1.87	503	1.90
Degradation at 175°C				
00	476	2.06	478	2.02
04	480	1.96	481	—
06	469	1.92	464	1.81
15	461	1.94	459	1.89
23	450	1.98	455	2.01
30	442	2.08	436	2.14
37	417	2.40	420	2.20

Source: Adapted with permission from F. Mohammad et al., *Bull. Electrochem.* 9(2/3), 109 (1993). Copyright © 1993, CECRI, India.

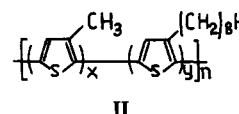
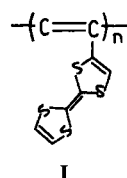
^aBG denotes bandgap. The method of estimation is given in [44]. Both samples are similar; their thickness may be slightly different.

of conjugation with an increase in bandgap energies. This observation contrasts to our previous findings, where no change in bandgap energies was observed in UV-vis studies as shown in Figure 4 and Table III. A faster decay in the intensity of the band associated with 2,5-linkages in the polymer at temperatures above 175°C in IR spectroscopic studies is indicative of random scission of the polymer backbone, which leads to the depletion of conjugation length and further supports the findings of the UV-vis studies. Polythiophene doped with AsF_6^- , BF_4^- , and ClO_4^- showed a vari-

Table IV. Apparent Rate Constants of Electrical Conductivity Loss for Polythiophene that Contains Various Counterions

Counterion	Initial electrical conductivity ($\Omega^{-1}\text{cm}^{-1}$)	T ($^\circ\text{C}$)	k'_2 (s^{-1})	
			In vacuum	Ambient air
BF_4^-	5.65	30	1.85×10^{-6}	4.74×10^{-5}
BF_4^-	0.97	30	3.91×10^{-6}	1.26×10^{-4}
BF_4^-	0.24	50	2.48×10^{-5}	8.25×10^{-5}
BF_4^-	7.58	50	3.90×10^{-5}	8.92×10^{-5}
BF_4^-	3.85	50	7.54×10^{-6}	6.82×10^{-5}
BF_4^-	0.27	60	2.14×10^{-4}	5.12×10^{-3}
BF_4^-	0.29	70	1.07×10^{-4}	5.44×10^{-4}
BF_4^-	7.30	70	2.59×10^{-5}	8.95×10^{-5}
BF_4^-	4.86	70	4.32×10^{-5}	7.03×10^{-4}
AsF_6^-	11.70	70	4.19×10^{-6}	2.67×10^{-6}
ClO_4^-	0.18	70	5.80×10^{-6}	1.53×10^{-5}

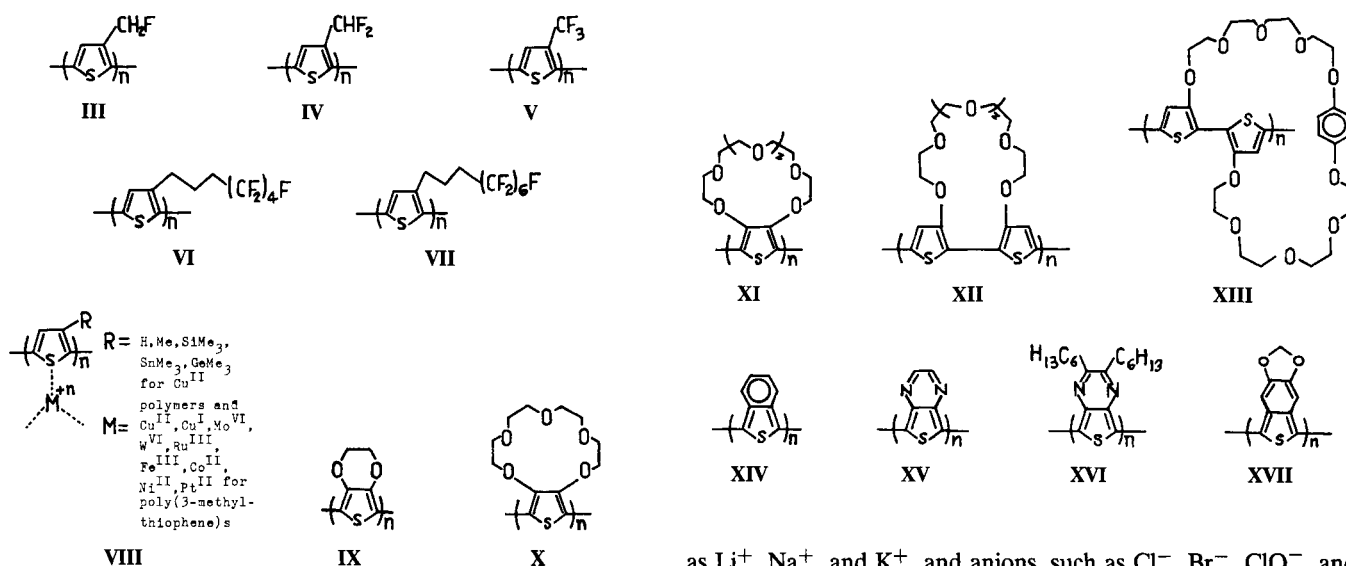
Source: Adapted with permission from F. Mohammad et al., *Bull. Electrochem.* 10(11/12), 508 (1994). Copyright © 1994, CECRI, India.



able loss of electrical conductivity under extremely dry conditions and in an ambient atmosphere, and data seem to fit with reciprocal decay kinetics as given in Table IV. However, Tourillon and Garnier [118] observed no instability in terms of electrical conductivity caused by the doping counterion (CF_3SO_3^-) in polythiophene on exposure to air for 8 months.

The synthesis and development of chemically stable and soluble poly(3-alkylthiophene) were reported by Elsenbaumer and co-workers [119, 120] and further development by a number of other groups [121, 122]. The thermal stability studies on poly(3-cyclohexylthiophene) and poly(3-hexylthiophene) revealed that the weight loss started at 45°C and the former polymer was slightly less stable than the latter [123], whereas when the solution of poly(3-hexylthiophene) was exposed to light, a reduction in the molecular weight of the polymer was seen at ambient temperatures [124].

The use of copolymers can simultaneously broaden and allow better control over electrical properties and stability. Pei and Inganas [125] synthesized a copolymer based on 3-*n*-octylthiophene and 3-methylthiophene that was processible and contained about 40% 3-*n*-octylthiophene molecules in the copolymer. This copolymer (II) yielded a material of fairly good conductivity ($5\text{--}10\text{ S cm}^{-1}$) on doping with FeCl_3 and displayed high stability in both the neutral and doped forms. The stability conferred by fluorine substitution, for example, is clearly associated with a relatively high value for the dissociation energy of C–F bonds combined with the effect of the high electronegativity of fluorine atom in shielding the carbon chain from attack. Ritter et al. [126] reported studies on polymers of fluorinated 3-methylthiophene derivatives



in which there is a gradual increase in the fluorine atoms in the methyl side chain. The redox potentials of these polymers are very high (in the range of 1.30–1.40 V) versus Ag and, therefore, are unstable and spontaneously dedope on exposure to air. I could find no report on the thermal stability of these polymer structures **III**, **IV**, and **V**. Buchner et al. [127] improved the redox potential of fluorine-substituted thiophene by adding $-\text{CH}_2$ spacers between the ring and the substituents by synthesizing polymers with structures **VI** and **VII**. Polymers thus prepared showed enhanced electroactivity, electrochemical stability, and elasticity.

Irreversible undoping that led to the loss of electrical properties in doped poly(alkylthiophene)s on thermal treatment was reported by Ingnas and co-workers. The rate of thermal undoping was observed to be faster in the case of longer chains substituted on the polythiophene when compared with unsubstituted polythiophene [128–131]. Random copolymers of methyl- and octyl-substituted polythiophene [132] and regular copolymers of dimer thiophene-*co*-octylphenylthiophene [133] demonstrated much better stability.

Polythiophene used as an electrode material showed much better stability as an anode in comparison to polyacetylene and polypyrrole in doping–undoping cycles. However, it still undergoes degradation that leads to the loss of electroactivity, electrical conductivity, electrochromic properties, mechanical strength, conjugation, and so forth as observed by several researchers [134–137]. The work of Tsai et al. [138] on electrochemical systems based on monosubstituted polythiophenes, revealed that polymethylthiophene was the most stable material for electrode applications whereas poly[3,4-bis-(ethylmercapto)thiophene] was the least stable. Somanathan and Wegner [139] observed that poly(3-hexylthiophene) retained its electroactivity even after 100 scans, whereas poly(3-cyclohexylthiophene) lost its electroactivity to a great extent after 20 scans in a cyclic voltammetry experiment. Czerwinski et al. [140] synthesized a variety of 3-substituted thiophene polymers incorporated with a number of metal ligands (**VIII**). When used as electrodes, all the materials that contained Cu^{II} exhibited remarkable stability without any observable change in cyclic voltammogram after being cycled for weeks in aqueous media. These experiments were performed in aqueous media in the pH range of 1–13 and the electrolytes contained cations, such

as Li⁺, Na⁺, and K⁺, and anions, such as Cl[−], Br[−], ClO₄[−], and NO₃[−], in the absence of oxygen.

Polymers produced from disubstituted polythiophene monomers at the 3 and 4 positions cause steric hindrance between the substituents on the adjacent thiophene rings that leads to loss of effective conjugation. Polymers based on 3,4-disubstituted thiophene monomers show much larger bandgap and much lower electrical conductivity compared to their monosubstituted counterparts [141]. To reduce steric hindrance, thiophene monomer was cycled between the 3 and 4 positions, grafted with flexible alkoxy groups, and electropolymerized by Dietrich et al. [142]. The small bandgap of this polymer (**IX**) is consistent with reduced steric hindrance and it showed remarkable stability in the doped state due to its low oxidation potential. Miyazaki and Yamamoto [143] synthesized a 3,4 crown ether-disubstituted polythiophene (**X**) with a low degree of polymerization. The resultant polymer showed excellent stability toward oxygen after n-type doping with sodium.

Swager et al. [144] used crown ether 3,4-disubstituted polythiophene to fabricate sensors for electron deficient organic compounds and alkali ions. The sensor device so fabricated showed high chemical reversibility and fast return to its original state in the absence of signal besides very good stability for longer exposure times for the electrode materials **XI**, **XII**, and **XIII**.

Poly(isothianaphthalene) (**XIV**), a very low bandgap polymer, has shown very good electroactivity and fairly good stability when undoped in a reverse scan of cyclic voltammetry between -1.4 and 0.1 V versus Ag/Ag⁺ [145]. Another polymer related to poly(isothianaphthalene) is polythieno(3,4-*b*)-pyrazine (**XV**), in which two CH groups have been replaced by sterically less demanding nitrogen atoms. A 2,3-dihexyl derivative of **XV** was prepared by Pomerantz et al. [146, 147] as shown in the structure **XVI**. This derivative showed an onset of decomposition at 230°C and 50% weight loss at 600°C under nitrogen in a thermogravimetric analysis experiment. However, this material was found to be unstable in air in the doped as well as in the undoped state. Whereas **XIV** was reported to be stable in air in the undoped state and unstable in air in the doped state, due to dedoping, Ikenoue et al. [148] reported the synthesis of a more stable derivative of **XIV** in which **XVII** could be cycled between doped and undoped states. This derivative showed thermal stability similar to that of the parent polymer.

Ohshita et al. [149] reported the synthesis and optical, electrochemical, and electron transporting properties if silicon-bridged

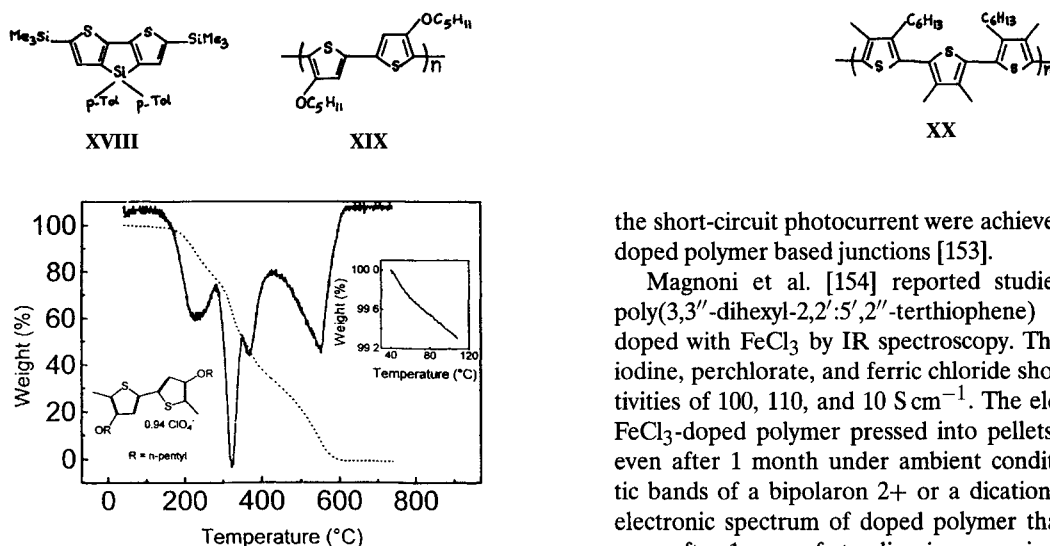


Fig. 5. Thermogravimetric curve (dotted line) of poly(4,4'-dipentoxy-2,2'-bithiophene) powder and its first derivative (full line), recorded in air. Sample weight, 1.289 mg; scan rate, $10^{\circ}\text{C min}^{-1}$. Insets: Expanded scale of the thermogravimetric curve and the formula of the polymer. Reprinted with permission from G. Casalbore-Miceli et al., *Synth. Met.* 94, 179 (1998). Copyright © 1998, Elsevier Science Ltd., Oxford.

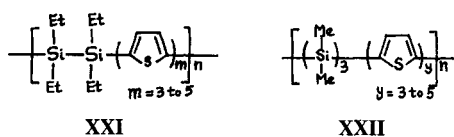
bithiophenes. The luminance of an electroluminescent device based on XVIII increased with operating voltage until a maximum value of ca. 8000 cd m^{-2} at 13 V of operating voltage. However, a rapid decrease in current density and luminescence was observed at higher voltage, probably due to the decomposition of the silicon-bridged bithiophene layer in the device. Polymers based on this monomer are expected to show luminance in combination with other polymer properties.

A detailed study of the photoelectrochemical, morphological, and stability properties of indium-tin oxide (ITO) polymer/Al junctions based on poly(4,4'-dipentoxy-2,2'-bithiophene) and poly(3-butylthiophene) has been reported [150–153]. The former polymer doped with BF_4^- was observed to be more stable under environmental conditions than its ClO_4^- -doped counterpart as evidenced by cyclic voltammetry studies [150]. Poly(4,4'-dipentoxy-2,2'-bithiophene) (XIX) doped with ClO_4^- showed a loss of 0.7% weight by 107°C due to removal of water as evident from the thermogravimetric curve shown in Figure 5. Another run of the same sample up to 107°C showed a further loss of 0.09% weight due to trapped water. When the same sample was stored in an ambient atmosphere for 2 h, it showed a loss in weight of 0.3%, suggesting the hygroscopic nature of the polymer. Polymer dedoping occurred between 128 and 280°C , which suggests 0.94 ClO_4^- ions per two thiophene rings with a weight loss of about 22%. A further weight loss of 43% was observed in two close steps in the temperature range of $280\text{--}430^{\circ}\text{C}$, suggesting the breakdown of the polymer backbone. On the basis of thermal data, a formula of $0.94\text{ClO}_4^- \cdot 0.2\text{H}_2\text{O}$ per bithiophene unit for composition of this polymer was suggested [151, 152]. The transport properties of ITO/polymer (XIX)/aluminum junctions were found to be strongly dependent on the extent of doping. A decrease of the reverse saturation current and of the quality factor, and a deterioration of the rectification properties of the junction were observed in the dark by increasing the doping level, whereas higher values of

the short-circuit photocurrent were achieved in the case of lightly doped polymer based junctions [153].

Magnoni et al. [154] reported studies on the stability of poly(3,3''-dihexyl-2,2':5',2''-terthiophene) (PDHTT) (XX) films doped with FeCl_3 by IR spectroscopy. The polymer doped with iodine, perchlorate, and ferric chloride showed electrical conductivities of 100, 110, and 10 S cm^{-1} . The electrical conductivity of FeCl_3 -doped polymer pressed into pellets remained unchanged even after 1 month under ambient conditions. The characteristic bands of a bipolaron $2+$ or a dication were observed in the electronic spectrum of doped polymer that remained unaltered even after 1 year of standing in open air and at room temperature. The polymer is reported to be very stable compared to other polythiophene-based polymers and it was suggested that this material is stable for several years at room temperature and fairly stable at higher temperatures. PDHTT doped with I_2 showed fast dedoping on heating at 100°C . The intensity of doping induced IR bands reduced to half in about 8 min and an IR spectrum of pristine polymer was recovered after 48 min. PDHTT doped with FeCl_3 showed much slower dedoping at higher temperatures of 140 and 170°C and the emergence of extra peaks at 1675 and 1717 cm^{-1} together with a broad band at $3100\text{--}3200\text{ cm}^{-1}$, indicative of carbonyl groups due to oxidative degradation of the polymer. Polymer heated at 130°C showed the onset of oxidation after 96 h, whereas the pristine polymer showed the onset of oxidation after 305 h on heating at 130°C in air as observed by IR spectroscopy. It was suggested that the temperature of 130°C represents a threshold temperature above which PDHTT starts to become unstable due to atmospheric agents and dopant counterions. It was also observed that highly doped polymer was more stable toward dedoping compared to lightly doped material when heated at 130°C . Whereas the electrical conductivity of a doped polymer very much depends on the extent of doping, hence the findings of Magnoni et al. [154] are very significant.

Kunugi et al. [155] chemically synthesized poly(tetraethylsilyl-arylene)oligo(2,5-thienylene) derivatives (DSmT ; $m = 3\text{--}5$) (XXI) that showed electrical conductivities of 5×10^{-3} , 0.6×10^{-3} , and $0.3 \times 10^{-3}\text{ S cm}^{-1}$ for DS5T, DS4T, and DS3T, respectively in their doped state. Reversible electrochemical doping and dedoping of the DS5T films were feasible by cycling the electrode potential between 0 and 1.2 V. At a potential more positive than 1.2 V, the overoxidation of an oligo(thienylene) unit and Si–Si bond cleavage took place, leading to decreased electrical conductivity of polymers. From their findings on molecular weight determination by gel permeation chromatography (GPC), Harima et al. [156] also suggested that the decomposed product contains one repeat unit of DS5T polymer. The Si–Si bond cleavage was supported by Fourier transform infrared (FTIR) spectroscopy in which the band that correspond to the Si–Si bond at 705 cm^{-1} disappeared, whereas the band that corresponds to Si–C (thienylene unit) at 1425 cm^{-1} remained; it was further supported by fluorescence measurements in which the decomposed products showed maxima that correspond to quaterthiophene and terthiophene in the voltammetric investigation of DS4T and DS3T polymers. Some-



what similar results on DS5T polymer were reported in another article by the same research group [157]. They observed the presence of a light yellowish green decomposition product in the solution from thicker films of the polymer during potential cycling at lower scan rates, suggesting the decomposition of polymer film yields soluble products in the MeCN:Et₄NBF₄ medium.

In a similar work on poly(hexamethyltrisilanylene)oligo(2,5-thienylene) (XXII), Zhu et al. [158] reported that voltammetric studies of the doping and dedoping process showed two pairs of redox peaks in MeCN that contained 0.1-M Et₄NBF₄. During potential cycling, the redox currents decreased considerably due to the decomposition of polymers. TSnT polymers were observed to produce species that had the basic structure of *n*T due to decomposition during cycling at higher positive potentials by GPC, FTIR, and fluorescence measurements. Cleavage of Si-Si bonds at the Si-Si-Si unit in the polymer main chains also took place. The product of decomposition further polymerized on the working electrode and played an important role in the oxidation behavior of TSnT polymers [158]. It is worth mentioning here that no anion doping occurs in the electrochemical oxidation of polysilanes as reported by Diaz and Miller [159] in their studies on poly(methylphenyl)silane.

2.2.2. Polypyrroles

Polypyrrole is also oxygen sensitive, because its ionization potential is 4.0 eV, which is comparatively lower than that of polyacetylene, (4.7 eV) and low enough to allow charge-transfer interaction with oxygen, whereas p-type doped polypyrrole is stable to oxygen, but similarly vulnerable to the attack of doping counterions. p-type doped polypyrrole is, thus, much more stable than polyacetylene, but reports vary about its stability [160]. An increase in electrical conductivity of undoped polypyrrole from 10⁻⁶ to 10⁻² Ω⁻¹ cm⁻¹ was observed after 1% (w/w) uptake of oxygen, but the reaction of oxygen occurred at the nitrogen atoms and oxidation was reversible electrochemically [161, 162]. The work of Samuelson and Druy [163] revealed that the doping counterion has a strong effect on retaining the electrical conductivity of this polymer and suggested a decrease of 1 order of magnitude for each year of exposure to ambient air at room temperature. A faster loss of electrical conductivity for perchlorate- and fluoroborate-doped polymers was reported and it was suggested that encapsulation of the polymer device can improve the environmental stability, because the instability of the polymer is due to atmospheric oxygen and/or water [163]. The synergic effect of water and oxygen on the electrical properties of fluoroborate-doped polypyrrole was observed by Erlandsson et al. [164]. The electrical conductivity of doped polymer remained unchanged after 200 days at 80°C under argon, but dropped rapidly in air at the same temperature [165], whereas Diaz et al. [166] claimed that the polymer is stable at 100–200°C, depending on the doping counterion. Electrochemically prepared polymers that contained BF₄⁻ and ClO₄⁻ counterions, observed by Kanazawa et al. [167] and Ogaswara et al. [168], respectively, were thermally stable up to 250 and 150°C, respectively.

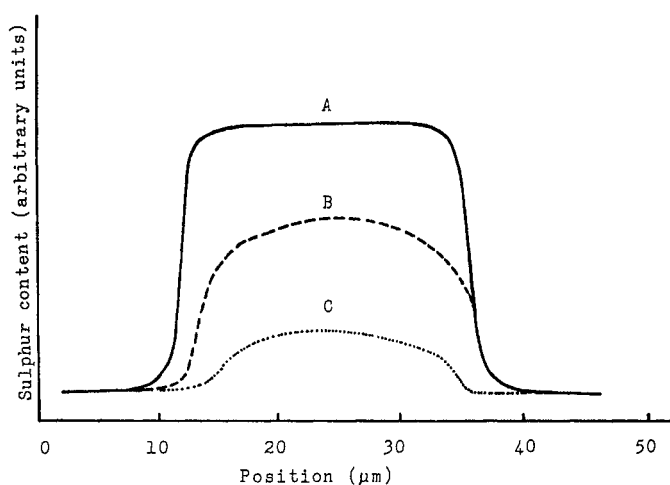


Fig. 6. Sulfur distribution within poly(pyrrolephenylsulfonate) films treated with a 2% aqueous NaOH solution for different amounts of time. The film thickness is around 30 μm. A, initial sample; B, treated for 120 min; C, treated for 240 min. Reprinted with permission from H. Munstedt, *Polymer* 27, 899 (1986). Copyright © 1986, Elsevier Science Ltd., Oxford.

In our thermogravimetric studies, polypyrrole that contained BF₄⁻ counterion showed weight loss in three steps, namely, 3% (45–125°C), 19.5% (125–285°C), and 22.5% (285–700°C) under nitrogen, leaving behind 55% of residue, whereas losses of 3% (45–125°C), 19.5% (125–285°C), and 48.5% (285–700°C) in air left behind a residue of 29% [169]. Salmon et al. [170] synthesized polypyrrole doped with a variety of counterions and observed that the polymer doped with CH₃C₆H₄SO₃⁻ was most thermally stable up to 280°C, but was less conductive in comparison to other materials.

Treatment of polyacetylene with acids or bases produced polymers with enhanced stability [171–173]; hence, studies were done to establish this effect on polypyrrole as well. Polypyrrole doped with phenylsulfonate and ClO₄⁻ counterions was electrochemically prepared and treated with different concentrations of sulfuric acid and sodium hydroxide. The polymer that contained phenylsulfonate counterions showed a depletion in sulfur content with increasing time of exposure (Fig. 6) and enhanced long-term stability of electrical properties at elevated temperature on base treatment (Fig. 7). The effect of acid treatment on the ageing stability of the polymer was somewhat similar. It was suggested that the base as well as the acid treatment of polypyrrole improved the stability of the polymer and that the process involved the replacement of counterions by other anions from the base or the acid, controlled by the diffusion behavior of counterions [174], as evident from Figure 8.

Loss of electroactivity, mechanical strength, and formation of carbonyl groups along with the formation of carbon dioxide were observed [175–181] when polypyrrole anode was cycled between charging and discharging in different electrolytic systems. However, in modified polypyrroles, the type of substituents at N, substituents on the pyrrole ring, and the conditions of synthesis also play an important role in deciding the stability of materials in electrochemical systems [175, 182–185].

The formation of carbonyl groups at the 3 position and of hydroxyl groups at the 4 position in overoxidized polypyrrole was reported by Beck et al. [180] when the polymer was studied electro-

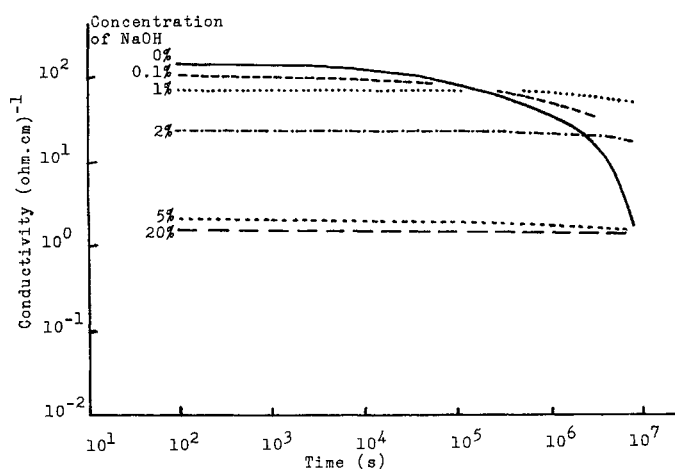


Fig. 7. Ageing behavior with regard to the electrical conductivity of poly(pyrrolephenylsulfonate) film exposed to NaOH solutions of different concentration. Film thickness, $90\ \mu\text{m}$; ageing temperature, 140°C ; time of exposure, 240 min. Reprinted with permission from H. Munstedt, *Polymer* 27, 899 (1986). Copyright © 1986, Elsevier Science Ltd., Oxford.

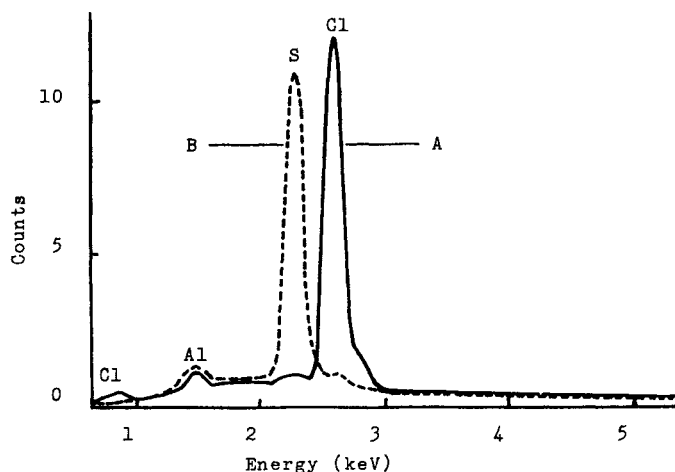


Fig. 8. Ion exchange in a $20\text{-}\mu\text{m}$ -thick poly(pyrrolephenylsulfonate) film after treatment with sulfuric acid as measured by EDX. A, initial sample; B, sample treated with 10% H_2SO_4 for 240 min. Reprinted with permission from H. Munstedt, *Polymer* 27, 899 (1986). Copyright © 1986, Elsevier Science Ltd., Oxford.

chemically in an aqueous medium in the presence of certain nucleophiles. Bromine substitution in the presence of Br^- and multi-methoxylation in presence of $0.5\ \text{M}\ \text{KF}$ in methanol, leading to the formation of sp^3 centers, also were observed [180]. Incorporation of sp^3 centers that led to a polymer of lowered electrical conductivity during electropolymerization of *N*-methylpyrrole in aqueous sodium sulfate solution also was observed [186, 187]. Chemically prepared polypyrrole showed good performance with respect to its mass capacity and stability during charging and discharging for more than 70 cycles in aqueous medium with no significant degradation [188]. A secondary battery based on lithium-polypyrrole [using poly(ethylene oxide) (PEO) and LiClO_4 solid electrolyte] showed fairly high coulombic efficiency of about 95% with an output voltage of 3.0 V. The battery did very well for 1400 cycles after an initial 100 scans required to reach the optimum value; however, the efficiency decreased to zero at the end of the charge-discharge

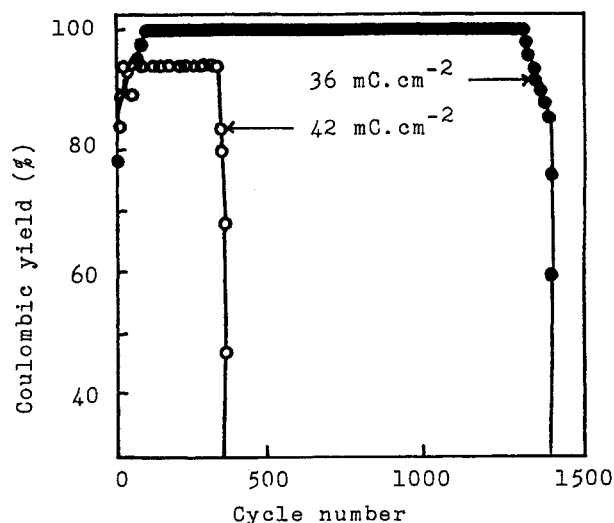


Fig. 9. Cyclability of Li-PEOLiClO₄-PPY batteries at 80°C charged at 36 and $42\ \text{mC}\cdot\text{cm}^{-2}$. Reprinted with permission from T. Osaka et al., *J. Electrochem. Soc.* 141(8), 1994 (1994). Copyright © 1994, Electrochemical Society, New York.

process due to sudden overoxidation of the polymer electrode as shown in Figure 9 [189].

Chen and Rjeshwar [190] observed polypyrrole film dissolution due to the formation of hypochlorite ions on the cathode by an electron transfer reaction between OH^- and Cl^- ions, leading to an unusual instability in the polymer electrode, whereas Momma et al. [191] reported a coulombic yield of 95% for 250 cycles, 90% for 300 cycles, and no discharging beyond 300 cycles for an electrochemical system with polypyrrole-poly(4-styrenesulfonate) composition cathode in LiClO_4 -DMSO (dimethylsulfoxide) electrolyte. No loss of electroactivity was observed in the cathode polymer of a LiClO_4 -PC (propylenecarbonate) electrolytic system. Quan et al. [192] found that electrochemical cycling caused irreversible oxidative degradation in the order $\text{HClO}_4 < \text{TsOH} < \text{H}_2\text{SO}_4 < \text{TsONa} < \text{Na}_2\text{SO}_4$ doped polypyrrole electrodes in aqueous media along with a decrease in the E_{pa} value from 1.14 to 0.96 V.

Two types of degradation processes were observed by Beck and Michaelis [193], namely, fast (electrochemical) followed by slow (chemical), in a polypyrrole- BF_4 anode corrosion experiment in aqueous media of pH ranging from 1 to 13. The fast corrosion of polypyrrole anode was due to anodic overoxidation as supported by the emergence of carbonyl and hydroxyl groups on the polymer backbone. However, the reversible cycling in an inert electrolyte such as acetonitrile led to a fairly improved stability in the polymer electrodes. The process of corrosion that leads to instability was proposed to involve three steps as shown in Figure 10. Work on the stability of polyhalopyrroles in electrochemical systems revealed that the degradation potential, E_d , depends on the nature of the substituents, which include those caused by steric hindrance and the inductive effect. In cyclic voltammetric studies, Audebert and Vidan [194] observed that poly(3,4-dichloropyrrole) showed the highest E_d in comparison to other poly(halopyrrole)s.

The thermal stability of chemically modified polypyrroles was studied by using a thermal analyzer and IR spectroscopy, and it was reported that the stability was enhanced in the order polypyrrole < polypyrrole-phthalic anhydride < polypyrrole-pyromellitic

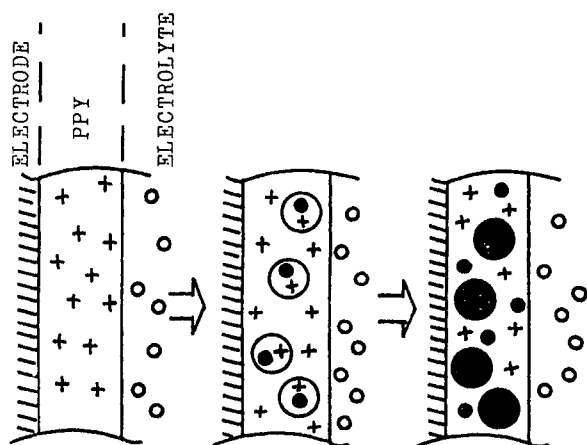


Fig. 10. Schematic representation of the chemical corrosion of polypyrrole in three steps. Left, initial state; middle, distribution equilibrium for nucleophiles; right, partial chemical conversion. +, radical cationic center; o, nucleophile in solution; ●, nucleophile in the solid; ●, reacted state. Reprinted with permission from F. Beck and R. Michaelis, *Werkstoffe und Korrosion* 42, 341 (1991). Copyright © 1991, Wiley-VCH, Weinheim.

Table V. Thermal Stabilities of Polypyrrole Anhydride-based Copolycondensates

Polymer system	Decomposition temperature (°C)				DSC peaks (°C)
	Initial	20%	50%	70%	
Polypyrrole	270	331	417	524	290–370 (broad & flat)
Polypyrrole-phthalicanhydride	290	351	438	554	370, 400 (small hump) 420
Polypyrrole-pyromellitic dianhydride	310	364	457	572	375, 420 (flat hump) 461 (small hump)

Source: Adapted with permission from M. Biswas and A. Roy, *J. Appl. Polym. Sci.* 54, 1483 (1994). Copyright © 1994, Wiley, New York.

dianhydride on substitution as evident from Table V [195, 196]. It was suggested that the substituent that causes more cross-linking produces more thermally stable material. This idea was further supported by other research [197–201], where polypyrrole condensed with other organics, such as polycarbazole, poly(*N*-vinylcarbazole) polystyrene, and polyacenequinone radical polymers, showed highly thermally stable matrices due to formation of additional C–C bonds, cyclic structures, and cross-linking. As detailed in Table VI, Biswas and Roy [202] observed an intermediate stability of poly(*N*-vinylcarbazole) in comparison to polypyrrole and poly(pyrrole-*N*-vinylcarbazole).

Kim and Elsenbaumer [203] reported the synthesis of *N*-substituted polypyrrole, where FeCl₃-doped poly(1-hexylpyrrole) and poly(1-dodecylpyrrole) (XXIII) showed electrical conductivities of 4.3×10^{-5} and 1.2×10^{-6} S cm⁻¹, respectively (four-in-line probe). Both polymers are stable in air for a long time. The air stability of electrochemically doped poly(1-alkylpyrrole)s [204] and polypyrrole [205] was already reported in previous literature. However, the poly(1-butyl-2,5-pyrrole) of this series is an

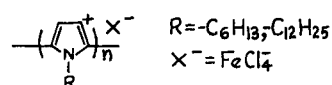
Table VI. Thermal Stabilities^a of Polypyrrole (PPY) Poly(*N*-vinylcarbazole) (PNVC), and Poly(pyrrole-*N*-vinylcarbazole) P(PY-NVC)

Polymer	Components (mol)			Decomposition temp. (°C)				<i>T_g</i> (°C)
	NVC	PY	FeCl ₃	<i>T_i</i>	20%	50%	70%	
PPY	—	0.029	0.0037	210	255	400	486	165
PNVC	0.029	—	0.0037	350	399	450	476	227
P(PY-NVC)	0.029	0.029	0.0037	352	317	425	497	200 ^b
P(PY-NVC)	0.029	0.029	0.0074	260	327	428	486	190 ^b
P(PY-NVC)	0.029	0.029	0.0148	262	350	466	527	180 ^b

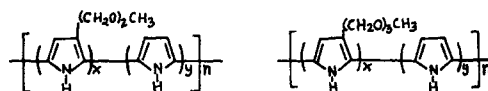
Source: Adapted with permission from M. Biswas and A. Roy, *J. Appl. Polym. Sci.* 54, 1483 (1994). Copyright © 1994, Wiley, New York.

^a *T_i* denotes the initial decomposition temperature; *T_g* denotes the glass transition temperature.

^b A 1:1 mixture of PNVC and PPY revealed two glass transition breaks that corresponded to 228 and 163°C, respectively.



XXIII



XXIV

XXV

exception and it degrades significantly in air after 3 days [204]. It also has been suggested that the lower electrical conductivities of these polymers are due to steric effects of long alkyl groups [204]. Kim and Elsenbaumer [206] also reported their studies on poly(1-hexylpyrrole vinylene), which exhibited an electrical conductivity of 6.18×10^{-7} S cm⁻¹ on exposure to air; on doping with FeCl₃ and AuCl₃, the electrical conductivity became 0.15 and 2.5 S cm⁻¹, respectively (four-in-line probe). Thermogravimetric analysis of neutral polymer showed an onset for weight loss at about 245°C, whereas melting transitions (*T_m*) were observed at about 140 and 150°C with differential scanning calorimetry (DSC) analysis [206].

Calvert et al. [207] synthesized copolymers of pyrrole with polyether-substituted pyrrole to examine the effect on the ion diffusion properties of the polymer, an essential requirement for battery applications. The charge storage capacity of both copolymers XXIV and XXV was found to be comparable with that of polypyrrole, although 50% of the copolymers contained the nonelectroactive polyether component. Copolymers could be charged to higher potentials and released more charge during discharges whereas polypyrrole showed signs of overcharging and irreversible reaction at a charging rate of 200 mA cm⁻² and collapsed more rapidly to 2.5 V versus lithium at a given discharge rate.

Takeoka et al. [208] investigated in great detail the effect of several antioxidants as well as the effect of various doping acids on the stability of electrical conductivity of electrochemically prepared polypyrrole. The electrical conductivity (EC) of polypyrrole already had been observed to increase initially and then, after a maximum value, decrease on heating. The increase in EC may be attributed either to annealing of the polymer or to the semicon-

Table VII. Stabilizing Effect of Various Antioxidants on the Electrical Conductivity of Electrochemically Prepared Polypyrrole

No.	Additive	σ_{BH} (S cm^{-1})	$\sigma_{\text{AH}}/\sigma_{\text{BH}}$
1	2,6-Dinitrophenol	9	0.20
2	2,4-Dinitrophenol	18	0.06
3	Pentachlorophenol	13	0.35
4	2-Methyl-4,6-dinitrophenol	10	0.20
5	2-Hydroxy-3-nitrobenzoic acid	16	0.30
6	<i>p</i> -Nitrophenol	29	0.45
7	<i>p</i> -Hydroxybenzoic acid	18	0.34
8	<i>p</i> -Bromophenol	23	0.24
9	<i>p</i> -Hydroxybenzaldehyde	38	0.29
10	3,5-Di- <i>t</i> -butyl-4-hydroxybenzaldehyde	31	0.24
11	<i>p</i> -Methoxyphenol	19	0.26
12	2,6-Di- <i>t</i> -butyl-phenol	15	0.18
13	2,6-Di- <i>t</i> -butyl-4-methylphenol	15	0.20
—	No addition	23	0.26

Source: Adapted with permission from S. Takeoka et al., *Bull. Chem. Soc. Jpn.* 71, 1471 (1998). Copyright © 1998, Chemical Society of Japan.

Table VIII. Stabilizing Effect of Doping Polypyrrole with Various Sulfonic Acid Derivatives

No.	Dopant	σ_{BH} (S cm^{-1})	$\sigma_8/\sigma_{\text{max}}^a$	σ_{AH} (S cm^{-1})
14	Sulfoethanoic acid	3	0.18	—
15	7,7-Dimethyl-2-oxobicyclo[2,2,1]-heptane-1-methanesulfonic acid	130	0.13	—
16	<i>p</i> -Methylbenzenesulfonic acid	120	0.33	25
17	<i>p</i> -Aminobenzenesulfonic acid	Not polymerized		
18	2-Naphthalenesulfonic acid	50	0.65	10
19	<i>m</i> -Benzenedisulfonic acid	50	0.88	35
20	1,5-Naphthalenedisulfonic acid	80	0.88	64
21	<i>p</i> -Hydroxybenzenesulfonic acid	30	0.90	20
22	2,5-Dihydroxybenzenesulfonic acid	Not polymerized		
23	<i>p</i> -Sulfobenzoic acid	20	0.85	12
24	<i>m</i> -Sulfobenzoic acid	50	0.94	50
25	4-Sulfo-1,2-benzenedicarboxylic acid	25	0.68	15
26	2-Sulfo-1,4-benzenedicarboxylic acid	7	0.86	6
27	2-Hydroxy-5-sulfobenzoic acid	75	0.95	70
28	<i>p</i> -Dodecylbenzenesulfonic acid	25	0.25	5

Source: Adapted from Ref. 208 with permission from S. Takeoka et al., *Bull. Chem. Soc. Jpn.* 71, 1471 (1998). Copyright © 1998, Chemical Society of Japan.

^a $\sigma_8 = \sigma$ at 150°C after 8-h heating; σ_{max} = maximum σ while heating at 150°C.

ducting property, whereas the decrease may be attributed to thermal degradation of the polymer [209, 210]. The thermal stability of the polypyrrole was evaluated in terms of $\sigma_t/\sigma_{\text{max}}$, σ_{BH} , and σ_{AH} , where σ_t is the EC at 150°C after heating the sample for t h, σ_{max} is the maximum EC at 150°C, σ_{BH} is the EC of the sample at room temperature before heating, and σ_{AH} is the EC of the sample at room temperature after heating. Long-term stability at 125°C was also measured, whereas the rate constant (k) was calculated from $t_{1/2}$, that is, the time after which the EC of the sample decreased to half. The studies also included the effect of heat treatment on the polymer sample as observed in the UV-vis or IR spectra. The effect of various antioxidants on the stability of polypyrrole in terms of the ratio $\sigma_{\text{AH}}/\sigma_{\text{BH}}$ are detailed in Table VII and the effect of various derivatives of sulfonic acid doping of polypyrrole on the stability of electrical properties are given in Table VIII. (The numbers in the left hand columns of Tables VII and VIII are used to identify the antioxidants or acids in the subsequent discussion.) Polypyrrole doped with *p*-methylbenzenesulfonic acid (16) showed similar behavior on heating at 150°C in air as well as under nitrogen up to σ_{max} as shown in Figure 11, after which a decrease of 33% of σ_{max} was observed in the sample at 150°C in air after 8 h due to loss of conjugation by oxidative degradation [208]. An increase in the intensity of bands that correspond to C=O and C—OH in FTIR and Raman spectra also were observed [211]. In contrast, the electrical conductivity of polypyrrole under nitrogen at 150°C was found to be stable for 8 h after an initial 11% decrease of σ_{max} . The thermal stability of the EC of polypyrrole became considerably poorer on incorporation of antioxidants as evident from Table VII. This decline is similar to that in polyacetylene [87]. However, doping with acids that have multiprotonating substituents showed maximum stabilization of the electrical properties of polypyrrole at 150°C in air. The effect of 2-hydroxy-5-sulfobenzoic acid (27), which was reported for the first time, was excellent, as evident from Table VIII and Figure 12.

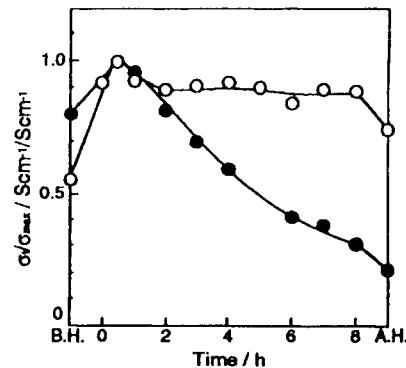


Fig. 11. Time courses of the electrical conductivity of polypyrrole under (○) nitrogen and (●) air. Reprinted with permission from S. Takeoka et al., *Bull. Chem. Soc. Jpn.* 71, 1471 (1998). Copyright © 1998, Chemical Society of Japan, Tokyo.

The electrical conductivity of polypyrrole doped with 16, 21, 24, and 27 and aged at 125°C for 1000 h was stabilized best by those dopants that had carboxy and or hydroxy substituents as shown in Figure 13. The half-lives of the EC of polypyrrole doped with 16, 21, 24, and 27 were observed to be 20.0, 33.9, 83.9, and 108.1 h, respectively. These observations infer that a dopant that contains a carboxy group has a higher stabilizing effect than a dopant that contains a hydroxy group, and that a dopant that contains two such acidic groups has a much higher effect on the stabilization of polypyrrole [208]. Whereas the bipolaron structure is mainly responsible for electronic conduction in polypyrrole, the band that corresponds to the bipolaron does not show any appreciable re-

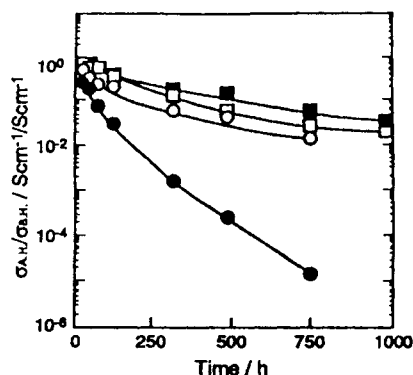


Fig. 12. Thermal stabilization of electrical conductivity of polypyrrole by dopant against heating at 150°C in air ○, 27, ●, 18, □, 16; ■, 16 + 6. Reprinted with permission from S. Takeoka et al., *Bull. Chem. Soc. Jpn.* 71, 1471 (1998). Copyright © 1998, Chemical Society of Japan, Tokyo.

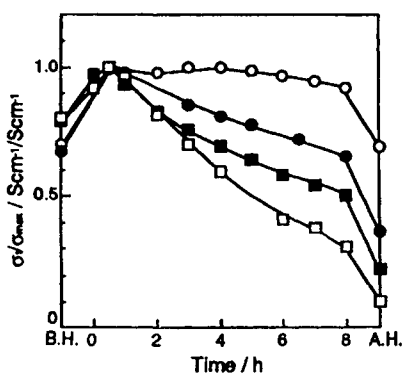


Fig. 13. Long-term stability of polypyrrole at 125°C in air: ●, 16, ○, 21, □, 24; ■, 27. Reprinted with permission from S. Takeoka et al., *Bull. Chem. Soc. Jpn.* 71, 1471 (1998). Copyright © 1998, Chemical Society of Japan, Tokyo.

duction in intensity in the case of polymer doped with 27. This observation from UV-vis studies further supports the inference that 27 is the most effective dopant. The materials from this study were suggested for use in devices where high chemical stability in air is a requirement for the conducting polymer.

One of the increasingly studied subjects with respect to electrically conductive polymers is their application in electrochemical sensors and detectors due to their versatility [212–215]. Synthesis of self-doped polypyrrole grafted with alkylsulfonate [216] and dodecylsulfonate [217] has been reported. A humidity sensor based on the latter polymer-dopant system showed a linear relationship between resistance and relative humidity (0–100%) with fairly good stability in air for about 6 months. Whereas a derivatized polypyrrole electrode (polypyrrole-*N*-carbodithionate) selectively detected the presence of Cu^{2+} ions in solution up to a lower limit of 1 ppm [218], the device showed a poor stability toward cycling in the case of Hg^{2+} ions in solution [219]. Detailed work on glucose amperometric biosensors based on glucose oxidase immobilized polypyrrole and poly(methylpyrrole) films has been reported [220–226]. Harsanyi [227] reviewed the subject of sensors based on polymer films extensively. Genies and Marchesiello [228] observed that glucose oxidase immobilized on the surface of the polypyrrole and poly(methylpyrrole) film-based amperometric biosensors was more sensitive and more stable over time than glucose oxidase immobilized during polymerization.

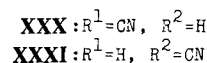
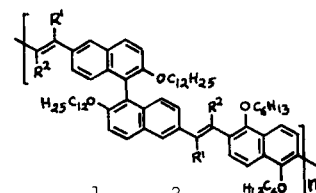
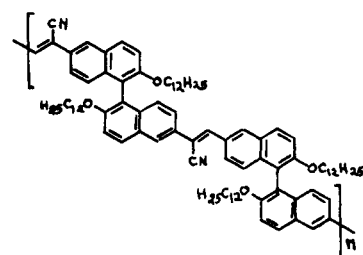
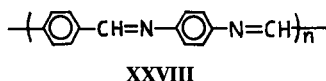
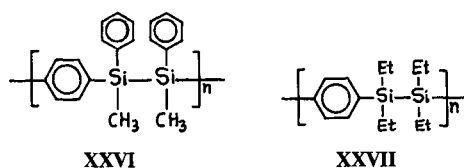
2.3. Polyaromatics

Excellent resistance to oxidation and thermal stability, in addition to their electroactivity are the most attractive features of polyaromatics, which are generally based on polyphenylene or its derivatives. The synthesis, characterization, and applications of polyaromatics have been widely covered in several reviews [229–232].

2.3.1. Polyphenylenes

Poly(*p*-phenylene) has fascinated many research groups due to its low cost, good mechanical strength, and high stability under thermal treatment as well as in electrochemical systems. Ried and Freitag [233] studied the thermal stability of polyphenyls and observed that the melting points depend mainly on the nature of the linkage between phenyl rings and less on the number of phenyl rings in the polymer. The highest melting points seen in *p*-polyphenyls improve little with halogenation; however, steric hindrance in the system caused the reverse effect. Several reports found that poly(*p*-phenylene) [234–237] is thermally stable up to 400°C in air and up to 550°C under nitrogen. Poly(*p*-phenylene) as well as poly(tetrafluoroethylene) have shown similar thermal stability and may be used safely up to similar temperature extremes [238]. When poly(*p*-phenylene) was thermally decomposed under vacuum, the production of biphenyl, *p*-terphenyl, 4-chlorobiphenyl, *p*-quaterphenyl, *p*-quinquephenyl, and higher *p*-oligophenyls was confirmed by IR, UV-vis and gas-liquid chromatography (GLC), and by comparing the melting points with standards [239]. Conductive block copolymers of polyphenylene and *p*-diethynylbenzene withstood heating for several hours at 400–450°C [240], whereas the azo derivative of this polymer showed no noticeable decomposition at 300°C [240]. Highly purified, only *p*-polymer of phenylene with degree of polymerization (DP) about 20 were reported to be stable up to 525°C with a weight loss of only 2.8% [241] and it was also observed that poly(*p*-phenylene) did not decompose even at 800°C and maintained 90% of its weight by 817°C, probably in the form of graphite [242].

Ohshita et al. [243] reported the electrochemical and optical properties of several poly[(disilanylene)oligophenylene] copolymers. When a film of **XXVI** was heated at 210°C for 20 h under vacuum and then cooled to room temperature, the λ_{max} of the film shifted from 254 nm to a higher energy of 269 nm and the oxidation peak in its cyclic voltammogram (CV) curves moved to higher potential of 1.38 V versus Ag/Ag^+ at 1.30 V. Dissolving the polymer film in tetrahydrofuran (THF) after heating at 210°C for 20 h yielded a reproduction of the original UV spectrum of the polymer in solution, indicating that no structural changes were involved in the process. Thermogravimetric analysis (TGA) of **XXVI** in a nitrogen atmosphere also suggested thermal stability of the polymer up to 210° [244]. Similar treatment of polymer film **XXVII** led to no changes in UV spectra and CV curves before and after annealing the polymer film at the same temperature [243]. Pisarevskaya and Levi [245] opined that the stability of poly(*p*-phenylene) as an anode during oxidation depends on the nucleophilic capacity of the medium in an electrochemical system. This opinion was further supported by the work of Beck and Pruss [246], who studied anodic oxidation and overoxidation of a carbon black composite of poly(*p*-phenylene) (3:40) on platinum mesh electrode in aqueous 8–18-M H_2SO_4 , 8–11.3-M HClO_4 , and 8-M HBF_4 and, hence, in solutions of different nucleophilicity. The cyclic voltammetric



XXX, XXXI

studies revealed two peaks: the first reversible peak was attributed to oxidation of poly(*p*-phenylene) and formation of some insertion compound, whereas the second irreversible peak, at a comparatively higher potential, was attributed to overoxidation of the polymer [246]. The polymer electrode was observed to become unstable below a concentration of 13 M of acid [245]. The molar ratio of Na⁺ doping ion in a poly(*p*-phenylene) cathode varied between 0.41 and zero when cycled between 0.05 and 0.75 V in an electrochemical cell with a sodium anode and Na⁺(BEt₄⁻)/THF electrolyte, suggesting that the total capacity of the polymer cathode can be utilized within a range of 0.7 V in a battery [247, 248].

Siu-Choon et al. [249] reported the synthesis of a copolymer that comprises alternating 1,4-phenylene and 3-butyl-2,5-thienylene repeat units that was used to fabricate a green light-emitting diode. Thermogravimetric studies of this polymer revealed that the material is stable up to 410°C in nitrogen and the maximum rate of degradation was observed around 500°C. The endothermic peaks at 45 and 100°C, seen in modulated differential scanning calorimetry, were attributed to melting of the side chains and the polymer backbone, respectively. The polymer was observed to be semicrystalline and a sharp glass transition temperature at 52°C was determined. Similar thermal transitions were reported by Ruiz et al. [250] for similar polyphenylene copolymers.

The redox interaction of electrically conducting polymers with certain gases has led to their use as active components in chemical sensors. They undergo doping and dedoping during cycling, with a change in their electrical conductivity to several orders of magnitude [227, 251, 252]. Chague et al. [253] reported the vapor phase synthesis of a copolymer based on 1,4-phenylene, poly(*p*-phenylene azomethine) (XXVIII), which showed good reversibility and sensitivity toward iodine vapor. Modification copolymer by introducing different functional groups, such as aromatic and nitro, showed a strong influence on the selectivity and sensitivity toward the exposure of several gases such as O₂, CO, CO₂, NO, SO₂, H₂, CH₄, and NH₃ [254]. Good reversibility and shorter response time to a few minutes was shown by 5–30-μm-thick copolymer layer arrangements on interdigitated electrode assemblies.

2.3.2. Poly(phenylenevinylene)s

Poly(*p*-phenylenevinylene) (PPV) and its derivatives are promising materials for polymer light-emitting diodes, because they possess fairly good mechanical properties, solution processibility, and several color generations [255–258]. The photoconductivity of PPV and its derivatives led to their use in photodiodes [259], electrophotography [260], optocouplers [261], and photovoltaic cells [262–264]. This photoconductivity can be further increased by many orders of magnitude by doping with C₆₀ compounds [265–267], for example. Poly(2-cyano-5-methoxy-1,4-phenylenevinylene) produced by thermal conversion showed an

electrooptic coefficient of 1.2 pm V⁻¹ that was stable during long annealing at 200°C [268]. These materials also have potential applications in charge storage devices. An energy density as high as 532 W h kg⁻¹ for Li-PPV cells has been reported [269]; this is comparatively much higher than polypyrrole or polyaniline. Diethoxy derivative of PPV was observed to show a low energy density of 240 W h kg⁻¹ and it showed no sign of degradation after up to 1000 charging-discharging cycles [270]. Gomez et al. [271] reported the synthesis of several derivatives of poly(arylenevinylene) block copolymer (XXIX, XXX, and XXXI). All three copolymers are oxidized at potentials above 1.2 V versus a saturated (SCE), which is comparatively higher than that of other conducting polymers, whereas all three are reduced at potentials around -1.5 V versus SCE in a cyclic voltammetric experiment with Bu₄NClO₄-CH₂Cl₂ and a glassy carbon working electrode. These copolymers showed intense photoluminescence and high electron affinity and, therefore, they are promising materials for light-emitting diodes.

Wang et al. [272] reported the thermal stability of a novel disilyl-substituted poly(*p*-phenylenevinylene) synthesized according to the scheme shown in Figure 14. Poly 2,5-bis(dimethyloctadecylsilyl)1,4-phenylenevinylene (ODS-PPV) (XXXII) showed the onset of decomposition at about 260°C and a weight loss of 10% was observed at 392°C in TGA studies. The degradation of the material involved two steps; the first step from 260 to 500°C with a maximum rate of decomposition at 460°C and a major weight loss, and the second step from 500 to 650°C with a maximum rate of decomposition at 588°C and a minor weight loss. A carbonaceous residue of about 11% remained above 650°C. This residue may also contain silicon dioxide. It is evident from TGA studies that ODS-PPV is stable enough for use in electroluminescent devices as shown in Figure 15.

Gao et al. [273] reported the fabrication of a bright-blue electroluminescent device based on an emissive dopant, a substituted ter-PV, 1,4-bis[4-(2-trimethylsilylvinyl)styryl]-2,5-dibutoxybenzene (BTSE) and an electron transporter, *N*-arylbenzimidazole (TPBI). The device doped with 10-wt% BTSE had a threshold voltage of about 3.8 V and a current efficiency of 3.2 cd A⁻¹ at a current density of 20 mA cm⁻². The device achieved a brightness of 11,000 cd m⁻² at a current density of 360 mA cm⁻², which is com-

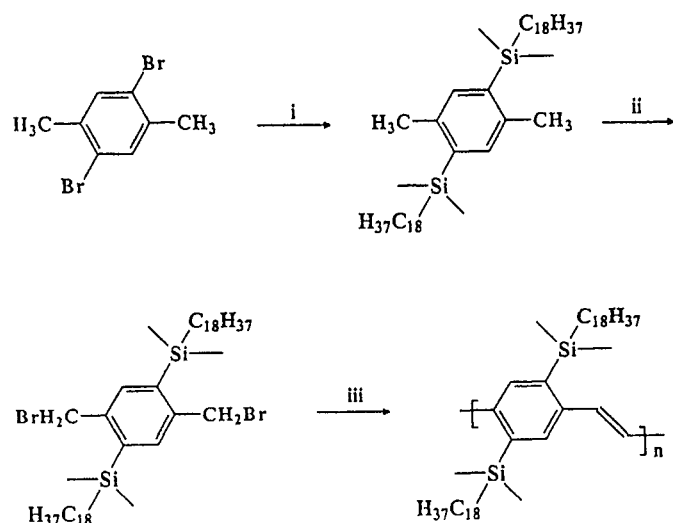


Fig. 14. The synthetic route for ODS-PPV. (i) $\text{Mg/THF, Me}_3\text{SiHC}_{18}\text{H}_{37}$, (ii) $\text{NBS/benzene/BPO}/h\nu$ and (iii) KOBU/THF . Reprinted with permission from L.-H. Wang et al., *Synth. Met.* 105, 85 (1999). Copyright © 1999, Elsevier Science Ltd., Oxford.

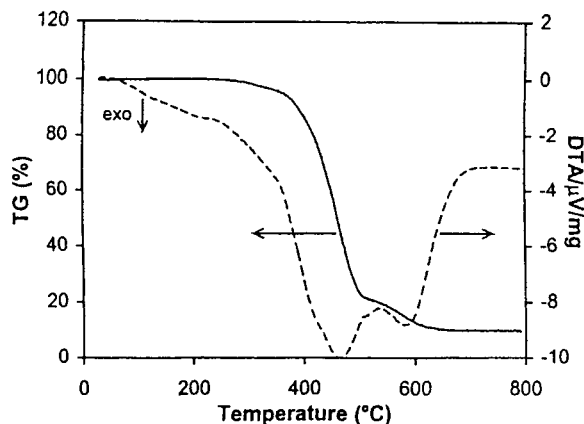
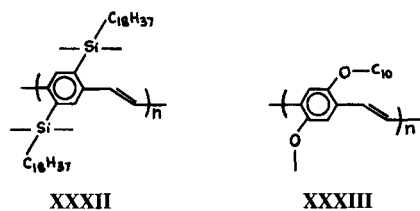


Fig. 15. Thermogravimetric analysis (TG solid line) and differential thermal analysis (DTA dotted line) of ODS-PPV in air. Reprinted with permission from L.-H. Wang et al., *Synth. Met.* 105, 85 (1999). Copyright © 1999, Elsevier Science Ltd., Oxford.



parable with the characteristics of most efficient devices reported to date [274]. The device was observed to be stable after storage for several months and showed very little degradation in performance after encapsulation in air.

Parker and co-workers [275, 276] fabricated a polymer light-emitting diode from a PPV derivative known as OC_1C_{10} (XXXIII). This diode operated for many thousands of hours at luminances in excess of 100 cd m^{-2} . The time dependence of the luminance in 3-cm^{-2} devices operating at a range of temperatures from 25 to 85°C with a current density of 8.3 mA cm^{-2} is given in Figure 16.

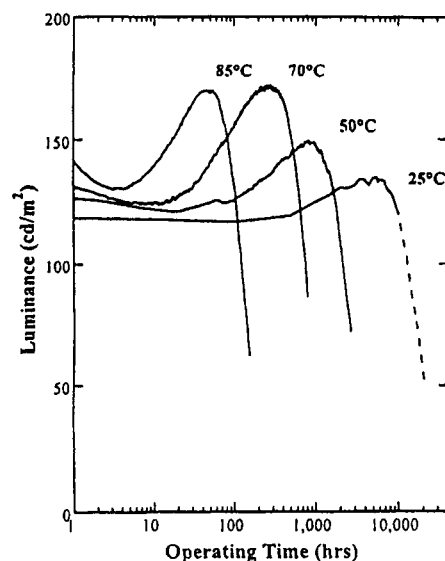


Fig. 16. Time dependence of luminance for 3-cm^2 device operated at a range of temperature. The current density is 8.3 mA/cm^2 . Reprinted with permission from I. D. Parker et al., *J. Appl. Phys.* 85(4), 2441 (1999). Copyright © 1999, American Institute of Physics, New York.

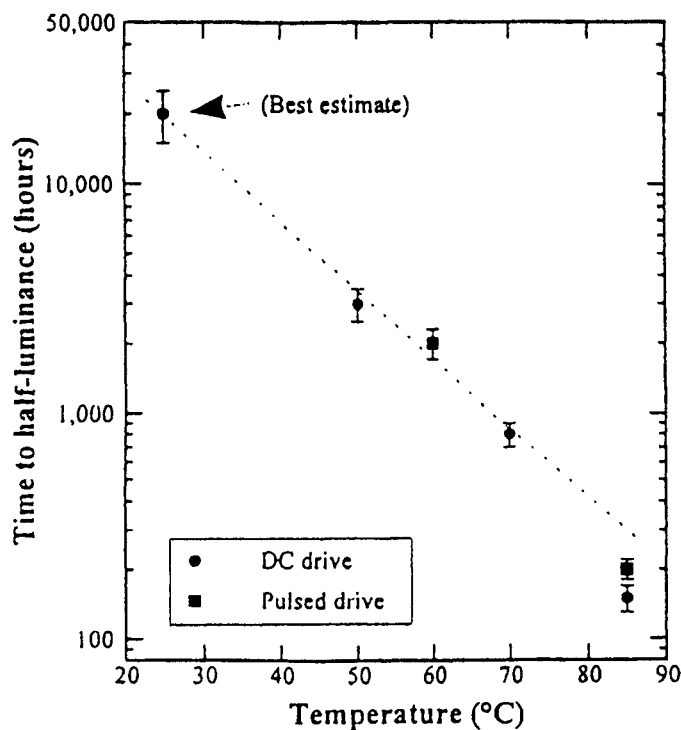


Fig. 17. Time for the device luminance to drop to half of its initial value plotted as a function of temperature. The circles indicate 3-cm^2 single pixel devices driven in dc; squares indicate data for pixelated displays driven in pulsed mode (1/16 duty cycle; 200 Hz; same average luminance as dc devices). The current density for the dc driven devices is 8.3 mA/cm^2 . Reprinted with permission from I. D. Parker et al., *J. Appl. Phys.* 85(4), 2441 (1999). Copyright © 1999, American Institute of Physics, New York.

The magnitude of change in luminance became more prominent with higher temperatures. Figure 17 shows the time for device luminance to drop to half of its original value, plotted as a function

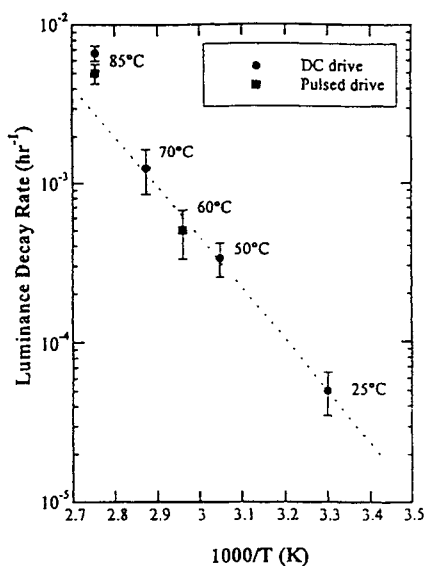
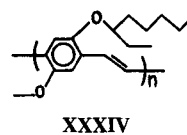


Fig. 18. Luminance decay rate [(time for the luminance to drop to half of its initial value)⁻¹] as a function of temperature. Data are plotted in Arrhenius form. The circles indicate 3-cm² single pixel devices driven in dc; squares indicate data for pixellated displays driven in pulsed mode (1/16 duty cycle; 200 Hz; same average luminance as dc devices). The current density for dc driven devices is 8.3 mA/cm². Reprinted with permission from I. D. Parker et al., *J. Appl. Phys.* 85(4), 2441 (1999). Copyright © 1999, American Institute of Physics, New York.



there is ample evidence in the obtained data for the formation of chain defects that behave like electron traps, leading to the decrease in electron mobility and increase in operating voltage [275]. Finally polymer OC₁C₁₀ was observed to possess a high redox stability, and each molecular unit on the polymer backbone is stable for more than 10¹⁰ redox cycles [275].

MacDiarmid and Huang [277] reported the fabrication of light-emitting diodes based on a novel conducting polymer, poly(2-methoxy-5-(2'-ethylhexyloxy)-1,4-phenylenevinylene) (MEH-PPV) (XXXIV), and described their characteristics in great detail. The Al-I₂-doped MEH-PPV-ITO device showed no significant degradation when operated at 14 V with a resting time of 5 min between each operation in ambient laboratory conditions. Similar device stability was found in Al-MEH-PPV-100% doped emeraldine base-ITO operated at 18 V with a resting time of 5 min between each operation in a laboratory atmosphere. A device with the configuration Al-MEH-PPV-1.76% HCl-doped emeraldine base-ITO, however, showed completely different results at an operation voltage of 28 V with 5 min resting time between each operation, but no degradation was apparent during the study [277].

of temperature, and Figure 18 shows the luminance decay rate, defined as (luminance half-life)⁻¹, plotted in Arrhenius form at a current density of 8.3 mA cm⁻² and at about 5°C above the ambient temperature. The linear trend up to 70°C in Figures 17 and 18 suggests that the same mechanism is involved in the degradation that leads to the decline in luminance below this temperature, with an activation energy of 0.67 ± 0.06 eV. However, the deviation of data from linearity at 85°C suggests an additional degradation mechanism, which may be related to the glass transition temperature of the polymer, which is around 80°C. Figures 17 and 18 also contain data for displays with an array of small pixels (0.25 mm²) operated in a pulsed, multiplexed mode of 1/16 duty cycle, 200 Hz, and an initial time-averaged luminance of 130 cd m⁻². The data suggest that the long-term luminance degradation is not specific to whether the driving scheme is dc or pulsed at high power with low duty cycle. An empirical expression of long-term luminance decrease of a device operated at a constant was also suggested on the basis of obtained data,

$$\frac{-\partial L}{\partial t} \propto Q \exp\left(\frac{-E_a}{kT}\right) \quad (2)$$

where $-\partial L/\partial t$ is the long-term luminance decay rate defined as (time to half the initial luminance)⁻¹, Q is the total charge passed through the device per unit area, E_a is the thermal activation energy (equal to 0.67 ± 0.06 eV), k is the Boltzmann constant, and T is the absolute temperature. On the basis of data, the presence of electrons that lead to degradation of the polymer layer is inferred. The gradual degradation of the polymer film, proportional to the number of electrons passed through the polymer, further suggests that the microscopic origin may be some form of redox instability in the polymer. The data obtained do not provide direct evidence of the microscopic processes responsible for the degradation, but

2.3.3. Polyanilines

Polyaniline has potential applications in areas such as organic semiconductors, corrosion inhibitors, color displays, energy storage devices, optoelectronic devices, and rechargeable polymer batteries. This polymer has been endowed with desirable electrical, electrochemical, and optical properties coupled with excellent environmental stability [278–287].

Chemically prepared polyaniline is stable up to as high as 650°C, but doped material reportedly undergoes HCl-H₂SO₄ removal that begins in the 230–300°C range and leads the polymer to the emeraldine base. This two-stage weight loss has been reported in several thermogravimetric studies [288–292], whereas some reports cite a third step that is due to water loss (as is the initial step). As studied by Palaniappan and Narayana [293], chemically prepared polyaniline in different acid media showed a three-step weight loss in thermogravimetric experiment after heat treatments at 150, 200, 275, and 375°C. The first step was attributed to the loss of water from doped polymer beginning at 110°C; the second minor step was due to removal of acid in the range of 110–275°C and the polymer underwent thermooxidative degradation beyond 275°C in the third step. The thermal stability of polyaniline doped with different acids was observed to be dependent on the doping counterion and no change in structure of the polymer was supported by IR and electronic spectra below 200°C [293]. Kahler et al. [294] observed that a HBr salt of chemically prepared polyaniline is the most thermally stable material among HF-, HCl-, HBr-, and HI-doped, highly conductive materials. Pereira da Silva et al. [295] reported the synthesis of polyaniline films doped with camphor sulfonic acid (HCSA) on platinum working electrodes with platinum counterelectrodes in a 0.5-M aniline + 1.0-M HCSA solution. Potential sweeps were between -0.2 and 0.75 V at a sweep rate of 0.05 V s⁻¹ versus SCE. The polymer stability was studied by Raman spectroscopy as a function of programmed temperature

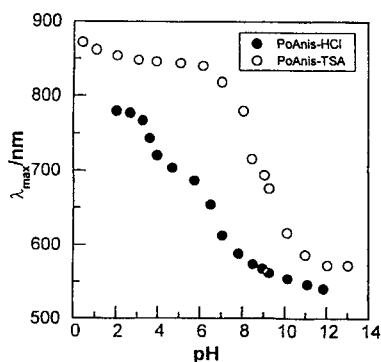


Fig. 19. Wavelengths that correspond to the maximum absorption as a function of pH for films of poly(*o*-methoxyaniline) doped with *p*-toluenesulfonic acid (○) and doped with HCl (●). Reprinted with permission from W. A. Gazotti, Jr., et al., *J. Electroanal. Chem.* 440, 193 (1997). Copyright © 1997, Elsevier Science Ltd., Oxford.

increase at a rate of $10^{\circ}\text{C min}^{-1}$ from room temperature to 150°C . Polyaniline doped with HCSA showed a great change in its Raman spectra on heating. The band located at 1380 cm^{-1} at room temperature, which is one of the most prominent bands in the spectrum, completely disappeared by 125°C . There was a continuous decrease in quinoid units with increasing temperature, because the intensity of the corresponding band decreased and shifted from the 1580-cm^{-1} band ($\nu\text{ C}=\text{C}$ quinoid ring) to higher frequencies (1592 cm^{-1} ; $\nu\text{ C}-\text{C}$ benzenoid units). These results are suggestive of a conformational change from a coil-like structure to an extended structure induced by temperature. A polymer power doped with HCSA and processed in *m*-cresol showed a negligible effect on the Raman spectrum as the temperature increased. These findings are further supported by the work of Li et al. [296], which showed that the emeraldine-like state is the most stable at high temperatures and that the $=\text{N}-/\text{-NH}-$ ratio (as determined by X-ray photoelectron spectroscopy of partially doped polyaniline) diminishes when heated to 200°C . Gazotti et al. [297] compared the stability of chemically prepared poly(*o*-methoxyaniline) doped with HCl and toluenesulfonic acid (TSA) by monitoring λ_{max} as a function of pH from 0 to 14 as shown in Figure 19. As is evident from the figure, the TSA-doped poly(*o*-methoxyaniline) is more stable compared to HCL doped, because deprotonation of the former is more difficult with the increase in pH. This is why the former showed good performance as an optical pH sensor [298].

Hugot-Le Goff and Cordova Torresi [299] studied the stability of polyaniline films under laser light by comparing *in situ* and *ex situ* spectra. The purple form of the polymer degraded at the impact laser point (i.e., 40-mW laser output) and considerable degradation was observed in *ex situ* experiments. Boucherit et al. [300] reported that a thin layer of water on the surface of the most unstable polymer sample was sufficient to protect it from degradation. Bernard et al. [301] reported *in situ* Raman spectroscopy studies on electrochromic polyaniline films that revealed the effect of pH and the influence of the sweep range on cycling lifetimes. The degradation mechanism was explained by the gradual formation of head-to-head coupling in a pH range of 0–3 in HCl+KCl solution when samples were cycled in various potential ranges.

Hand and Nelson [302] reported that *p*-benzoquinone is the main product of electrooxidation of polyaniline in acidic media and the dark green precipitate produced was quinone-hydroquinone. Arsov et al. [303] performed detailed work on the

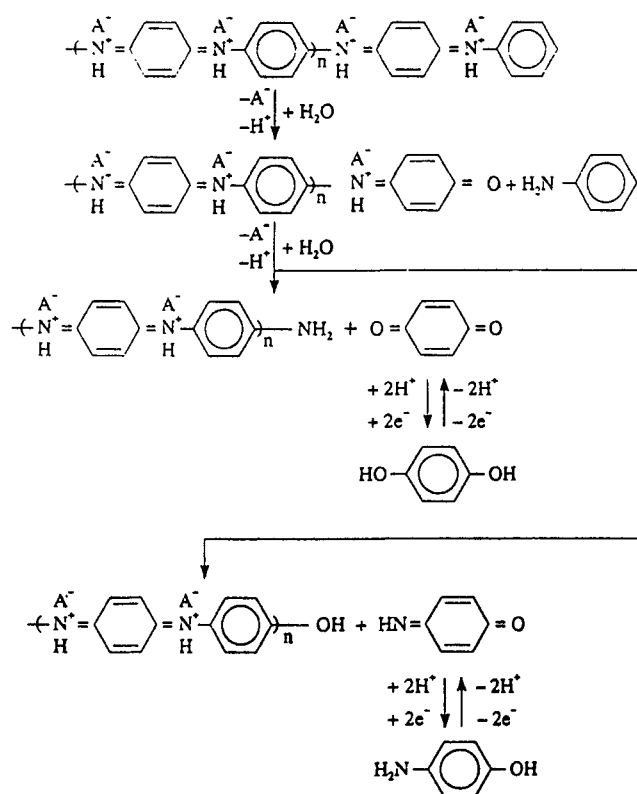


Fig. 20. Proposed mechanism of overoxidation of polyaniline. Reprinted with permission from L. D. Arsov et al., *J. Solid State Electrochem.* 2, 355 (1998). Copyright © 1998, Springer-Verlag, Berlin.

influence of the potential on the degradation of polyaniline by using electrochemical and Raman spectroscopic techniques. When cycled between the potential range of -0.65 to $+0.55\text{ V}$ in $1.0\text{-M H}_2\text{SO}_4 + 0.1\text{-M C}_6\text{H}_5\text{NH}_2$ at a rate of 20 mV s^{-1} , polyaniline-platinum electrode showed the emergence of redox peaks beyond $+0.2\text{ V}$ after the fifth cycle. The Raman spectrum showed a band at 1678 cm^{-1} and a shoulder at 1722 cm^{-1} , suggestive of the formation of $\text{C}=\text{O}$ bonds due to overoxidation and degradation. The products of degradation included *p*-benzoquinone, hydroquinone, *p*-aminophenol, quinoneimine, and oxidized polyaniline as proposed in the scheme given in Figure 20. Somewhat similar results were also reported for a polyaniline-coated titanium electrode immersed in $1\text{-M H}_2\text{SO}_4$ by Arsov [304].

Paul et al. [305] reported emulsion polymerization of aniline in the presence of 3-pentadecylphenylphosphoric acid (PDPPA) in a molar ratio of 1:1 as well as a polyaniline blend prepared by mechanical mixing of two components at room temperature. Intrinsically doped and blended polyaniline showed electrical conductivities of 6.1×10^{-1} and $2.4 \times 10^{-1}\text{ S cm}^{-1}$, respectively. Both polymers differed in their thermal stability quite a lot. When heated at a rate of $20^{\circ}\text{C min}^{-1}$ in a thermogravimetric experiment, the materials showed a small weight loss of 2–5% below 150°C due to loss of water and low molecular weight oligomers. In emulsion-polymerized PDPPA, the onset temperature of degradation was 280°C in a single step. However, the blend showed two-step decomposition starting at 240 and 350°C . Emulsion-polymerized polyaniline with PDPPA was observed to be more thermally stable than the polymer blend. These results were further supported by DSC studies.

Kim et al [306] reported the properties of an electrochromic window based on poly(aniline *N*-butylsulfonate)s (PANBUS) with and without a WO₃ layer. The best result was obtained from an EC window composed of PANBUS and WO₃ electrochromic layers with electrolyte films that contained 5% Nafion (SB5, SS5, and SBS5). In these systems, the transmittance changes were more than 95% at room temperature with applied step potentials of ± 1.5 V. The contrast between the colored and the bleached states upon cycling remained after 2300 cycles under 60-s cycle duration for ± 1.5 V. However, detachment of the electrolyte film from the PANBUS surface was observed by scanning electron microscopy (SEM) after 3000 cycles. Therefore, further improvements in the cyclability of the PANBUS EC window by using more adhering solid electrolyte was proposed. Kim et al. [307] studied PANBUS EC windows with a polycomponent electrolyte as well and they observed that the electrolyte SPEBMA5 and SPEST5 films sandwiched between two ITO glasses retained their transparency and adhesivity up to 3000 cycles in the range of ± 2.0 V at a rate of 60 s per cycle. Voids were formed and the adhesion of the film became poor after 3000 cycles. The color contrast of a PANBUS EC window was much improved with a more positive applied potential ($+2.5$ -V) limit, but the redox cyclability of more than 500 cycles could not be achieved, possibly due to oxidative degradation of the electrochromic polymer. The redox cyclability as high as 150,000 cycles for PANBUS has also been reported for other systems by the same group [308], who also observed that the liquid crystal alignment on the conductive PANBUS layer was stable for a long time [309]. Misra et al. [310] reported the synthesis of poly(2-ethylaniline) from a solution of 2-ethylaniline (0.1 M) and tetra-*n*-butylammoniumperchlorate (0.1 M) in 1,2-dichloroethane on a platinum electrode under nitrogen. The polymer deposited on the electrode surface was found to be quite stable and could be cycled repeatedly without any evidence of decomposition. Thermogravimetric analysis of the ClO₄⁻- and SbCl₆⁻-doped poly(2-ethylaniline) showed weight losses of 3.4 and 10% by 300 and 333°C, respectively, that may be due to dopant loss. ClO₄⁻-doped polymer lost 85% of its weight by 400°C, whereas SbCl₆⁻-doped polymer lost the same weight by 600°C; hence, the later material seems to be more thermally stable. Chemically prepared polyaniline and poly(dimethylaniline) examined by Toshima and Yan [311] showed three-step weight loss at around 100, 200, and 470°C under nitrogen that was attributed to the loss of water, loss of dopant, and thermal breakdown of the polymer backbone.

Electropolymerized poly(*o*-methylaniline) also showed a three-stage decomposition similar to the case of poly(dimethylaniline). Weight losses of about 12, 16, and 100% were observed in the temperature ranges of 40–120, 120–320, and 320–680°C, respectively. The first step was attributed to the loss of trapped water, the second, to the loss of chlorine or hydrogen chloride, and the third, to complete oxidative degradation of the polymer chain [312]. Gupta and Warhadpande [313] synthesized polymers from substituted anilines via a chemical method. Thermogravimetry showed that the *N*-substituted polymers were more stable than ring-substituted polymers as evident from the weight losses at 800°C for poly(*m*-toluidine) (62.2%), poly(*o*-toluidine) (61.6%), poly(*o*-anisidine) (100%), poly(acetanilide) (51.9%), poly(diphenylamine) (29.5%), and poly(*o*-naphthylamine) (69.7%). The polymers with strained chains possessed lower stability than polymers with flat chains.

Highly sulfonated polyaniline was synthesized by converting an emeraldine base into a leucoemeraldine base followed by sulfonation by fuming sulfuric acid [314–317]. This polymer had much bet-

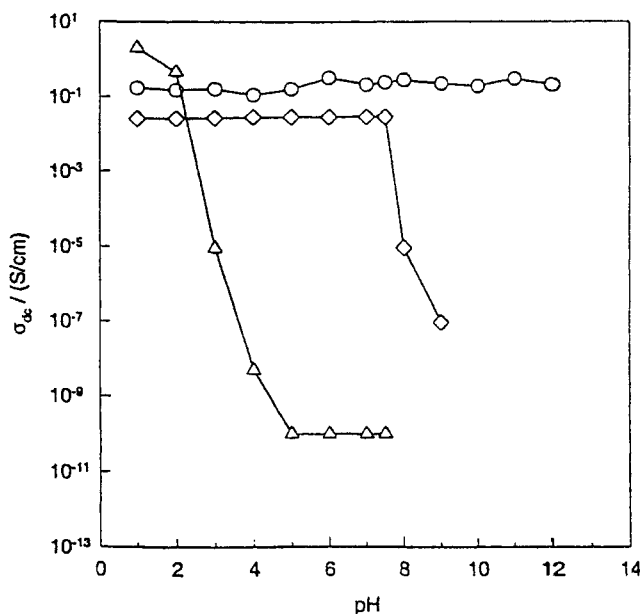


Fig. 21. pH dependence of dc conductivity at room temperature for leucoemeraldine base-sulfonated polyaniline (○), polyaniline-HCl (Δ), and emeraldine base-sulfonated polyaniline (◇). Reprinted with permission from X.-L. Wei et al., *J. Am. Chem. Soc.* 118, 2545 (1996). Copyright 1996, American Chemical Society, Washington, DC.

ter thermal stability than its parent polyaniline doped with HCl [318]. The dc conductivity of leucoemeraldine base sulfonated polyaniline was observed to be independent of pH in the available buffer range of pH 0–12 [319], whereas a decrease of 10 orders of magnitude in polyaniline:HCl (pH range 2–4) and of 5 orders of magnitude in emeraldine base sulfonated polyaniline (pH range of 7.5–9) was observed [320] as shown in Figure 21. This striking difference is due to a greater concentration of sulfonic acid groups in the polymer based on leucoemeraldine. This polymer film showed a stable voltammogram in 1.0-M HCl in the scan range of 0.0–0.6 V at a rate of 50 mV s⁻¹ after 5000 cycles; however, reversible degradation occurred as the potential was raised to 0.8 V [321, 322]. The sulfonated polyaniline is particularly durable for pH 4 and potential lower than 0.35 V versus Ag-AgCl (saturated). For example, the optical reflectance of a film on a platinum electrode changed less than 20% after 7 million cycles in 1-mol dm⁻³ HCl [323]. The sulfonated polyaniline showed a slow rate of weight loss upon heating to 220°C and a one-step weight loss beginning at 220°C, with smaller weight loss for 300–600°C. The slow rate of weight loss from 100 to 220°C, attributed to the loss of water, whereas the weight loss from 100 to 200°C is attributed to the elimination of some SO₃⁻ groups. The major weight loss above 220°C was associated with further removal of sulfonic groups from the polymer chain, and decomposition of the polymer backbone occurred at higher temperatures. However, the sodium salt of the polymer showed a very slow weight loss up to 220°C that may be due to the removal of water and lower oligomers. Weight loss starting at 350°C and extending to 600°C was the major operant and was most probably due to the dissociation of sulfonic groups from the polymer chain as seen by Yue et al. [324] in their thermogravimetric studies.

Aniline intercalated layered double hydroxides (LDHs) were synthesized and their thermal stability was studied by Challier and

Slade [325]. Terephthalate–Cu–Cr LDHs as well as hexacyanoferrate (II)–Cu–Al LDHs showed weight loss in two steps that were attributed to the removal of trapped water and the thermal breakdown of the intercalated system. The former LDHs showed comparatively better thermal stability than the latter.

Interest has been shown in double-strand (d-s) polyanilines by many researchers, because they offer fairly good stability under cycles of heat, water, or solvents [326–329] compared to traditional single-strand (s-s) polyanilines. These double-strand polyaniline complexes may be soluble in water or organic solvents, be suspendable as latex, or show strong adhesion with metals and polymers. The d-s polyanilines do not unwind or decompose in acids, bases, solvents, mild oxidant–reductants, or heat in contrast to s-s polyanilines, because s-s polyanilines lose dopant and become nonconductive under such conditions. DSC data confirm that this material is a molecular complex and not a simple blend of two components [326].

Variation of the electronic conductivity of conducting polymers with redox potential and pH of the environment is well established. On this basis, Hoa et al. [330] fabricated biosensors from polyaniline and a corresponding enzyme to estimate urea, glucose, hemoglobin, and neutral lipid. The relative change in conductance of the polyaniline film versus concentration followed a straight line for a reasonable range and reproducibility to within 10% was demonstrated, which suggests some instability during scanning. Dogan et al. [331] also fabricated sensors based on polyaniline and a composite of polyaniline with poly(bisphenol-A carbonate) using two-probe electrical conductivity measurements to estimate ammonia. The variation in resistance was found to be more reproducible in the case of the composite sensor than in that of the pure polymer. Concentration levels of 0.1, 0.05, and 0.025% produced relative resistance changes of 9.2, 4.7, and 3.1, respectively, for ammonia, with good repeatability on application of 60-s concentration pulses.

MacDiarmid et al. [332, 333] reported the synthesis of octaaniline, an oligomer of aniline, and its use in a device to detect organic vapors such as toluene. The reversibility of the octaaniline sensor toward toluene vapors was observed to be excellent (99.7%) with a satisfactory environmental stability after a few days.

2.3.4. Polyheteroaromatics

Polymers based on carbazole are well known for their fairly high thermal stability and good electrical properties on doping with electron acceptors, in addition to their excellent photoconductive efficiencies. Due to its fairly good toughness and fabricability, poly(*N*-vinylcarbazole) has been used as a photoconductor in electroreprographics in place of amorphous selenium [334–337]. The carbocomposite of poly(*N*-vinylcarbazole) showed the onset of decomposition at 200°C with a weight loss of 20–60% by 250–450°C and of 100% by 600°C. Composites with higher proportions of carbon black showed high electrical conductivity [338]. Biswas and Roy [339] reported that poly(*N*-vinylcarbazole) (PNVC) prepared with FeCl₃:NVC (molar ratio of 9:1) showed higher stability than preparation with a molar ratio of 6:1. Both polymers underwent 95% weight loss in TGA above 550°C. The higher stability of the former polymer was suggested to be due to higher molecular weight. However, the FeCl₃(ether)-initiated PNVC showed somewhat higher temperature (260°C) for the onset of decomposition than the aqueous suspension polymerized PNVC. The oxidative degradation that led to the breakdown of the polymer backbone

starts at 450°C as observed in DTA studies [339]. The synthesis of black shiny, nitrobenzene-soluble and iodine-doped poly(*N*-methyl-3,3'-carbazole) was reported by Wellinghoff et al. [340] who observed electrical conductivity in the range of 1–10 S cm⁻¹. The material showed long-term stability for many months in air at room temperature.

Highly stable polymers for electronic applications based on benzooxazole were reported by Mercer and McKenzie [341]. The polycondensates of 2,2'-bis[2-(4-aminophenoxy)benzoxazole-6-yl]hexafluoropropane with pyromellitic dianhydride, biphenyl, benzophenone, and so forth, after thermal imidization of the prepared polyamic acid films, showed the onset of degradation in the temperature range of 424–456°C. Crystalline poly(benzimidazole):H₃PO₄ complex showed good electrical conductivity and stability below 300°C, which makes it a potential material for fuel cell applications. The polymer in its doped state exhibits fairly good thermal stability at 250°C for 1000 h [342]. Phenyl-substituted polyquinazolines [343–347] were observed to be thermally stable up to 420°C in air, and polyimides also showed comparatively high thermal stability in air as well as in an inert environment. However, polypyrrrolinones were observed to be less thermally stable. Poly(1,2,4-triazine)s and polyphenylquinoxalines were found to be fairly thermostable, and the latter also showed good chemical stability. The least thermostable polyquinoline from di(4-acetylphenyl)ether did not show any degradation at 300°C, whereas the onset of weight loss in TGA was observed in the temperature range of 530–545°C and 530–570°C in air and nitrogen, respectively, in the case of poly(2,6-quinoline)s. Poly(*C*-phenylbenzimidazole)s showed better thermostability than poly(*N*-phenylbenzimidazole)s, whereas polyanthrazolines showed thermal degradation in the temperature ranges of 500–550 and 530–600°C in air and in an inert atmosphere, respectively [343–347]. The electrical conductivity of poly(*N*-vinylimidazole) doped with iodine and boron trifluoride decreased from 10⁻⁴ to 10⁻⁶ S cm⁻¹ after 2 months exposure to ambient atmosphere [348].

To improve the thermal stability of these polymers, Biswas and Mitra [349] prepared copolycondensates of carbazole (CBZ) with phthalic anhydride (PhAn), trimellitic anhydride (TMA), pyromellitic dianhydride (PMDA), 1,4,5,8-naphthalene tetracarboxylic dianhydride (NTDA), and benzophenone tetracarboxylic dianhydride (BTDA) along with similar copolycondensates of PNVC. The thermal stability of copolycondensates was observed to depend on anhydride moiety in the order NTDA > BTDA > PMDA > TMA > PhAn for both the types of materials as given in Table IX. Table X shows the isothermal degradation stability of pairs of polycondensates, and the data confirm the high thermal stability of NTDA over the other materials.

2.3.5. Miscellaneous Polyaromatics

Highly aromatic and photosensitive polymers such as polyimides are potential candidates in photonic applications. Wholly aromatic polyimides (XXXV) were observed to be white in color and soluble in polar aprotic solvents such as DMAc, DMF, HMPA, and NMP, whereas the polymers with *m*-phenylene units in backbone were also soluble in common organic solvents such as acetone, chloroform, and THF. All the materials showed excellent thermal stability up to 300°C in air without any weight loss, although initial weight losses of 5 and 10% were observed in the temperature ranges of 362–372°C and 376–384°C, respectively [350].

Table IX. Thermal Stabilities of the Carbazole Anhydride and Poly(*N*-vinylcarbazole)anhydride Copolycondensates

Polymer ^a	Temperature (°C)					DTA peak (endo.) at temp. (°C)
	T _i ^b	Polycondensate weight loss (%)				
		5	25	50	Complete	
CBZ-PhAn	300	325	405	465	585 (98%)	470
PNVC-PhAn	370	415	420	500	640 (98%)	490
CBZ-TMA	305	330	410	475	600 (97%)	460
PNVC-TMA	370	415	425	505	680 (98%)	495, 658
CBZ-PMDA	310	340	415	500	610 (98%)	475
PNVC-PMDA	375	420	470	540	700 (95%)	495, 656
CBZ-NTDA	330	430	515	545	620 (98%)	500
PNVC-NTDA	400	470	530	596	806 (97%)	518
CBZ-BTDA	315	420	480	535	620 (96%)	480
PNVC-BTDA	375	425	495	550	732 (97%)	495, 677
PNVC	375	420	430	440	520	—

Source: Adapted with permission from M. Biswas and P. Mitra, *J. Appl. Polym. Sci.* 42, 1989 (1991). Copyright © 1991, Wiley, Chichester.

^aAbbreviations: CBZ, carbazole; PNVC, poly(*N*-vinylcarbazole); PhAn, phthalic anhydride; TMA, trimellitic acid anhydride; PMDA, pyromellitic dianhydride; NTDA, naphthalene tetracarboxylic dianhydride; BTDA, benzophenone tetracarboxylic dianhydride.

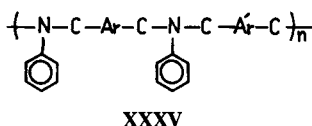
^bT_i denotes the initial decomposition temperature.

Table X. Isothermal Stability of Carbazole Anhydride and Poly(*N*-vinylcarbazole)anhydride Copolycondensates After Heating in Air

Polymer ^a	Total weight loss (%)							
	8 h		12 h		16 h		24 h	
	280°C	350°C	280°C	350°C	280°C	350°C	280°C	
CBZ-PMDA	4.92	20.96	12.66	21.61	15.22	23.59	19.33	
PNVC-PMDA	4.84	22.62	12.89	20.76	14.87	22.69	17.85	
CBZ-BTDA	4.66	19.08	11.12	23.48	14.12	26.73	18.36	
PNVC-BTDA	5.10	16.39	10.32	20.12	13.01	25.83	15.66	
CBZ-NTDA	3.46	6.48	8.01	12.97	12.69	18.00	17.84	
PNVC-NTDA	3.59	7.00	8.52	13.01	11.23	17.61	13.43	

Source: Adapted with permission from M. Biswas and P. Mitra, *J. Appl. Polym. Sci.* 42, 1989 (1991). Copyright © 1991, Wiley, Chichester.

^aAbbreviations are defined in Table IX.

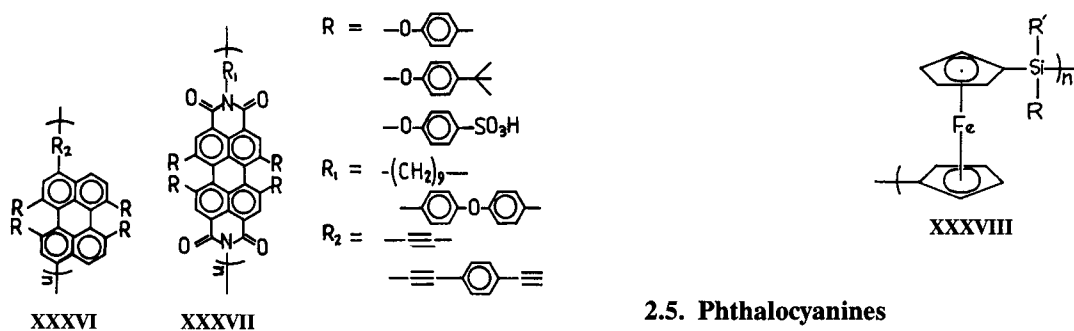


The thermal stability of electroactive polyacene quinone radical polymers was studied up to 1200°C under helium and the electrical conductivity was observed to pass through a minimum at about 500°C with a negative temperature dependence like in the case of degenerate semimetals; hence, these polymers show unique thermal properties [351]. The electrically conducting films of polyazulene were found to be stable in different environmental

conditions such as acids, bases, and common organic solvents. The films of polymer were stable up to 80°C, and a severe decrease in electrically conducting properties was the result of heat treatment [352]. Quante et al. [353] reported the synthesis of soluble and photostable polyperylene-based systems (XXXVI and XXXVII).

2.4. Inorganic and Silicon Polymers

Poly(sulfur nitride) [(SN)_x] was the first inorganic polymer with a backbone made up of nonmetallic elements to show an intrinsic electrical conductivity as high as 2.5 × 10³ S cm⁻¹ at room temperature [354]. Parathiocyanogen [(SCN)_x] is another similar inorganic polymer that was prepared electrochemically in the form

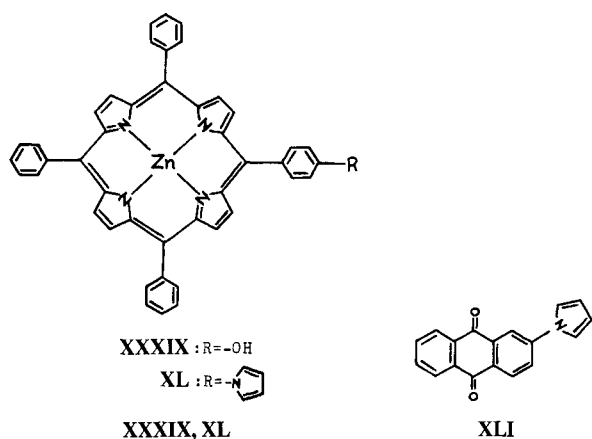


of yellow or orange-red powder and film by Bowmaker et al. [355]. This material was found to be stable even after several weeks of exposure to air as confirmed by Raman, IR, and X-ray photoelectron spectroscopy. The polymer may be described as a highly resistive semiconductor, because the electrical conductivity increased to $1.2 \times 10^{-4} \text{ S cm}^{-1}$ after doping with iodine for 7 days. The presence of conjugation in the polymer backbone is supported by a maximum at 440 nm in the UV-vis spectrum that may also be attributed to the delocalization of electrons along the polymer chain. In contrast to traditional conducting polymers such as polypyrrole, parathiocyanogen cannot be dedoped electrochemically, perhaps due to degradation of the polymer film during doping. However, paraselenocyanogen $[(\text{SeCN})_x]$ was observed to be unstable in air and, within a day, the orange color darkened to leave grey selenium on the electrode [356].

The unusual properties, such as photoconductivity, strong electronic absorption, and photosensitivity, shown by polysilanes are due to σ -electron delocalization along the Si-Si backbone. The σ -electrons are so loosely bound that the ionization energies become much lower for σ -electrons of polysilanes. The polymer is an insulator with an electrical conductivity of less than $10^{-12} \text{ S cm}^{-1}$ and it becomes electrically conductive on doping with oxidizing agents, as AsF_5 , SbF_5 , and H_2SO_4 . An electrical conductivity as high as 0.5 S cm^{-1} has been measured for polysilastyrene [357-359]. Polysilanes are inert toward oxygen at ordinary temperatures and stable up to 300°C ; however, they are prone to hydrolysis and undergo severe degradation on exposure to UV light. Poly(phenylsilane) showed much better photostability toward photodegradation than its alkyl counterparts [360-363]. Soluble block copolymers of dimethylsiloxane and different compositions of 4-vinylpyridine became electrically conductive on iodine doping and exhibited electrical conductivity as high as $3.8 \times 10^{-5} \text{ S cm}^{-1}$. The electrical conductivity reduced to $10^{-6} \text{ S cm}^{-1}$ in ambient atmosphere as well as on application of a vacuum. Incorporation of siloxane components in the polymer greatly improved the mechanical properties and the thermal stability without affecting the electrical properties of the 4-vinylpyridine component in the polymer [364]. Nagayama et al. [365] exploited the unique property of photodecomposition of polysilane by UV light in novel offset printing that requires no developing process. The polymers studied include poly(methylphenylsilane) and poly(methylphenylsilane-co-methyl-3,3,3-trifluoropropylsilane). Manners [366] reported the synthesis of poly(ferrocenylsilane)s, an alternate copolymer of ferrocene and organosilanes (XXXVIII). Poly(ferrocenylsilane)s possess interesting hole transport properties and partial oxidation leads to a great increase in electrical conductivity up to $10^{-3} \text{ S cm}^{-1}$ [367]. Further heating of this polymer to $500\text{--}1000^\circ\text{C}$ may yield magnetic ceramics [368].

2.5. Phthalocyanines

Phthalocyanine is a centrosymmetric planer molecule that has the general formula $\text{C}_{32}\text{H}_{18}\text{N}_8$, a tetrabenzo analog of naturally occurring tetraazaporphyrins [369-371]. Phthalocyanines absorb in the visible region in the range of 600-700 nm and form dark blue to metallic bronze to green materials that generally sublime on heating beyond 500°C . Their planer form is generally insoluble in common organic solvents and they have been used as dyes due to their good thermal stability [372, 373]. They have become attractive materials due to the ease of forming good quality films and their tailorable electrical and electronic properties, which makes them ideal for use in photoelectrochemical cells, photoconductors, rectifying devices, gas sensors, electrochromic devices, and optical data storage [374]. A central metal atom that controls the overall properties of the material is incorporated in place of two central hydrogen atoms of metal-free phthalocyanine to get a great variety of metallophthalocyanines (PcMs), many of which are very stable in the presence of oxygen [375]. The synthesis of mesogenic triphenylene-based porphyrazine complexes with a widely extended core system that leads to enhanced stability of the mesophase has been reported. These materials show liquid crystalline behavior over a wide range of temperatures from about 100 to 300°C [376]. Two dimensional planer poly(phthalocyanine) with Cu as the central atom showed electrical conductivity as high as $10^{-1} \text{ S cm}^{-1}$ that could be further increased to the extent of $10^2\text{--}10^3 \text{ S cm}^{-1}$ by doping. The polymers showed high thermal stability and can be used in devices that require temperature resistant components [377]. Doped with electron acceptors, cofacially linked poly(phthalocyaninato)metalloxanes $[\text{PcMO}]_n$ ($\text{M} = \text{Si}, \text{Ge}, \text{Sn}$) lead to electrically conductive materials that have oxidative stability up to 120°C [378-380]. In general, the fluorobridged $[(\text{PcMF})\text{I}_y]_n$ complexes ($\text{M} = \text{Al}, \text{Ga}, \text{Cr}$) showed lower thermal stability with regard to the loss of iodine compared to $[(\text{PcSiO})\text{I}_y]_n$ [381], whereas μ -ethynylphthalocyaninosilicon $[\text{PcSi}(\text{C}\equiv\text{C})]_n$ underwent decomposition on doping [382-386]. Doping of the bridged phthalocyaninato transition metal complexes $[\text{PcM}(\text{L})]_n$ ($\text{M} = \text{Fe}, \text{Ru}, \text{Os}, \text{Co}, \text{Rh}$; $\text{L} = \text{pyz}, \text{dib}$, etc.) produced electrically conductive materials ($\sigma_{\text{rt}} = 10^{-5}\text{--}10^{-1} \text{ S cm}^{-1}$) with thermal stability up to $120\text{--}130^\circ\text{C}$ [387-391]. Ottmar et al. [392] reported the fabrication of organic single- and double-layer electroluminescent devices based on substituted phthalocyanines such as tetra-*tert*-butylphthalocyanine, tetrakis(3-phenylneopentyl)phthalocyanine, and tetrakis(3-phenylneopentyl)phthalocyaninacopper(II). The device based on tetra-*tert*-butylphthalocyanine was found to be subject to swift severe degradation during operation, losing the blue color of the phthalocyanine layer, whereas the devices based on the other two materials showed stable electroluminescence with up to 60 V of driving current without any sign of short-term degradation. Balasubramaniam et al. [393] prepared electrochemically thin films of (i) homopolymers of zinc(II)porphyrins, ZnPOH and ZnPpyr



[where POH = 5-(4-hydroxy)phenyl-10,15,20-triphenylporphyrin (XXXIX) and Ppyr = 5-[4-(1-pyrrol-1-yl)phenyl]-10,15,20-triphenylporphyrin (XL)], (ii) sandwich porphyrin layers over anthraquinone films, and (iii) copolymers of zinc porphyrins with pyrrole-substituted anthraquinone, AQPyr (XLI). They reported the electrochemical behavior and spectrophotometric behavior of these films to evaluate the stability of the resulting polymers and their potential use as molecular materials in electrochemical and photochemical devices. The stability of the homopolymer and copolymer films in terms of the stability of the zinc porphyrin dications was observed to be influenced by the method of preparation as well as by the range of the scanning potential, similar to that in the case of poly(ZnPpyr) films [394]. The dication appeared to be unstable under the experimental conditions, leading to degradation of the film similar to the instability reported in the case of poly(vinyl-substituted zinc porphyrin) [395] and poly(pyrrole-substituted zinc porphyrin) [394, 395]. The stability of the films was observed to improve when they were scanned through selected potential range in which ZnP^{2+} dications were not formed. No change in degradation pattern was observed in the films scanned in the positive potential range only. The stability of the polymer films in terms of the stability of ZnP^{2+} was estimated by measuring the loss of electroactivity of the films, that is, the decrease in the ZnP^{+} - ZnP^{2+} voltammetric peak amplitude during repeated scanning in acetonitrile or dichloromethane solution that contained tetrabutylammonium tetrafluoroborate as shown in Figure 22. It is evident from Figure 22 that the stability of both pyrrole-substituted and hydroxy-substituted zinc porphyrin dications is improved significantly in sandwiched polymer films. The polymer films prepared from ZnPOH were observed to be more stable over a wide range of potential from -1.2 to $+1.8$ V in comparison to those prepared from ZnPpyr. Several other studies of these and similar materials have been reported as well [397-399]. Park et al. [400] reported fabrication of a NO_2 sensor by thermally depositing thin films of polycrystalline copper phthalocyanine on glass substrate. Significantly good selectivity was observed in terms of relative resistance with a sensitivity as low as 1 ppm and fairly good reproducibility as evident from Figure 23.

Mason et al. [401] studied multilayer electroluminescent ITO-(CuPc)-NPB-Alq-MgAg devices, where the optional copper phthalocyanine (CuPc) served as a buffer layer, *N,N'*-bis(1-naphthyl)-*N,N'*-diphenyl-1,1'-biphenyl-4,4'-diamine (NPB) served as a hole-transport layer, and tris(8-hydroxyquinoline)aluminum (Alq) served as an emissive as well as electron transport layer prepared

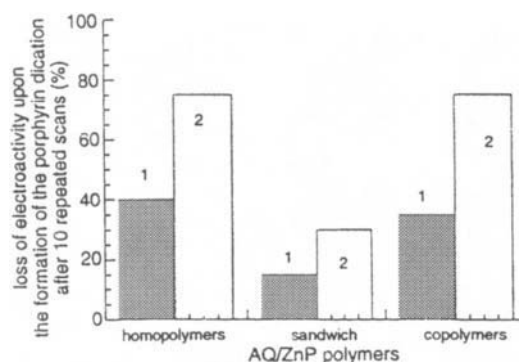


Fig. 22. Stability of the zinc porphyrin dication in homopolymer, sandwich, and copolymer films. Reprinted with permission from E. Balasubramanian et al., *J. Mater. Chem.* 5(4), 625 (1995). Copyright © 1995, Royal Society of Chemistry, London.

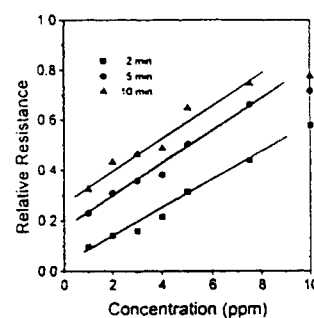
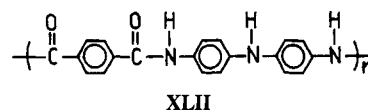


Fig. 23. Relative resistance of CuPc films vs NO_2 concentration measured 2-10 min after exposure to NO_2 . Reprinted with permission from C. Park et al., *Sens. Actuators, B* 30, 23 (1996). Copyright © 1996, Elsevier Science Ltd., Oxford.



by vapor deposition technique. The EL devices showed a relatively high drive voltage and had a mean time to half-brightness (or half-life) of only several hours when operated at 20 mA cm^{-2} , whereas the inclusion of CuPc or an oxidative treatment lowered the drive voltage significantly and increased the half-life to about 4000-5000 h.

2.6. Miscellaneous Systems

Gordon et al. [402] synthesized a copolymer of 4,4'-diaminodiphenylamine and terephthaloyl chloride by condensation polymerization. This copolymer (XLII) was successfully doped to fairly good electrical conductivity by exposing it to SO_3 . The doped polymer, however, was observed to be unstable in air, most likely due to the strong electron-withdrawing properties of the ketone functional groups in the polymer. The polymer composites of benzidine-iodine charge-transfer complexes in poly(vinylchloride), poly(vinylacetate), and polystyrene have been used as cathodes with zinc plates as anodes in the fabrication of solid-state galvanic cells by Srivastava and Singh [403]. Cell reaction during idle periods reduced the life of the cell, because the electrodes were in contact with each other. The cell life was enhanced from 100 h to several months by putting an insulating polymer film between the elec-

Table XI. Deposition Temperatures and Performance of Four Devices^a

Device	Deposition temperature (°C)			EL performance		
				Threshold voltage (V)	Voltage (V) at 10 mA cm ⁻²	Luminance (cd m ⁻²) at 20 mA cm ⁻²
	NPB	Alq	Mg:Ag			
A	RT	RT	RT	3.6	7.4	618
B	140	RT	RT	4.0	7.8	660
C	190	RT	RT	4.5	8.2	436
D	140	140	60	4.0	7.4	781

Source: Adapted with permission from Z. Q. Gao et al., *Appl. Phys. Lett.* 74, 3269 (1999). Copyright © 1999, American Institute of Physics, New York.

^aAbbreviations: RT, room temperature; NPB, *N,N'*-bis(1-naphthyl)-*N,N'*-diphenyl-1,1'-biphenyl-4,4'-diamine; Alq, tris(8-hydroxyquinoline)aluminum; Mg:Ag, magnesium–aluminum alloy.

trodes during idle periods. Such cells gave stable voltage output for about 100 h at a load of 10 kΩ.

By using high substrate temperature during vapor deposition, Gao et al. [404] fabricated organic electroluminescent devices with crystalline organic layers as given in Table XI in which NPB served as the hole-transport layer and Alq served as the electron-transporting and light-emitting layer sandwiched between an ITO anode and Mg:Ag cathode (full forms of abbreviations may be seen in Table XI). EL devices A, B, and D were stored in air (40% relative humidity) for 2 months. The EL devices B and D continued to possess electroluminescence at 9 V, whereas device A showed no emission at all after air exposure, suggesting that the storage stability at high humidity had been considerably enhanced for devices B and D as compared to device A. Judicious incorporation of a hole-transport layer of crystalline NPB during device fabrication was observed to improve the device performance instead of causing deterioration. With an eye toward use in solar energy conversion, Ambalagan and Natarajan [405] synthesized polymer coordinated chromium complexes (i) [Cr(bpy)₂(PAA)₂]⁺, (ii) [Cr(bpy)₂(PMA)₂]⁺, (iii) [Cr(phen)₂(PAA)₂]⁺, and (iv) [Cr(phen)₂(PMA)₂]⁺, where bpy denotes 2,2'-bipyridine, phen denotes 1,10-phenanthroline, PAA denotes poly(acrylic acid), and PMA denotes poly(methacrylic acid). Irradiation of the basic solutions of polymer–chromium complexes in the ligand field band at 436 nm showed a progressive decrease in the absorbance with a red shift. The spectral changes and the isosbestic points of the complexes were observed to be identical with those shown in the thermal reactions. The thermal reaction of these complexes showed aquation as found in other polypyridyl chromium(III) complexes. Ambalagan and Natarajan proposed a mechanism for the flash photolysis of these complexes based on their observations as shown in Figure 24. However, the complexes were found to be nonluminescent when the emission was monitored at several wavelengths in the range of 620–780 nm. The studies on the photoelectrochemical properties of thionine dye covalently bound to poly(acrylamidoglycolic acid) [406] as well as photochemical properties of ruthenium(II) polypyridyl complexes with macromolecular ligands, poly(methylolacrylamide-co-vinylpyridine), and poly(acrylamide-co-vinylpyridine) [407] also have been reported [408].

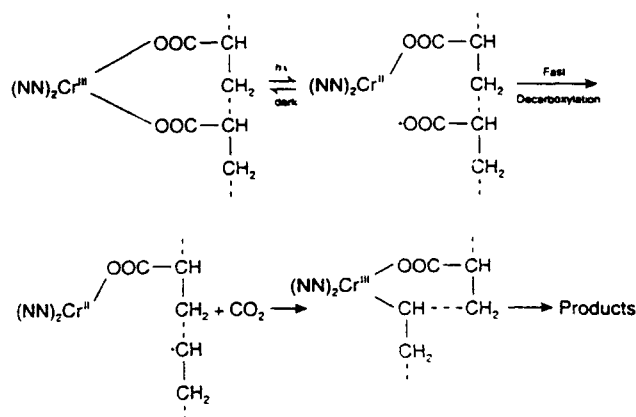


Fig. 24. Proposed mechanism for flash photolysis of polypyridyl complexes of chromium(III) bound to macromolecules. Reprinted with permission from K. Viswanathan and P. Natarajan, *J. Polym. Sci., Polym. Chem.* 29, 1734 (1991). Copyright © 1991, Wiley, Chichester.

Acknowledgments

The help rendered by all the authors who provided their reprints is very thankfully acknowledged. Constructive comments from H. S. Rathore and assistance from M. F. Ansari of the Department of Applied Chemistry are also gratefully acknowledged. Thanks also are extended to N. C. Billingham, University of Sussex, P. D. Calvert, University of Arizona, and P. J. S. Foot, Kingston University, UK. Thanks go out to Shahina, Tayyab, Fatima, Tahir, and Sadia for their day-to-day help and encouragement. Financial assistance from UGC project No.F.12-7/98(SR) for preparation of this work is appreciatively acknowledged.

REFERENCES

1. A. Pochettino, *Acad. Lincei. Rend.* 15, 355 (1906).
2. A. Szent-Gyorgyi, *Science* 93, 609 (1941); *Nature* 148, 157 (1941).
3. A. A. Berlin, *J. Polym. Sci.* 55, 621 (1961).
4. S. Maiti, *Indian J. Chem. Sect. A* 33, 524 (1994).
5. R. H. Baughman, J. L. Bredas, R. R. Chance, R. L. Elsenbaumer, and L. W. Shacklette, *Chem. Rev.* 82, 209 (1982).

6. J. R. Reynolds, *J. Mol. Electron.* 2, 1 (1986).
7. C. Lamy, J.-M. Leger, and F. Garnier, in "Handbook of Organic Conductive Molecules and Polymers" (H. S. Nalwa, Ed.), Vol. 3, p. 471. Wiley, Chichester, 1997.
8. B. Wessling, in "Handbook of Organic Conductive Molecules and Polymers" (H. S. Nalwa, Ed.), Vol. 3, p. 497. Wiley, Chichester, 1997.
9. J. Roncali, in "Handbook of Conducting Polymers" (T. A. Skotheim, R. L. Elsenbaumer, and J. R. Reynolds, Eds.), p. 331. Dekker, New York, 1998.
10. M. Pomerantz, "Handbook of Conducting Polymers" (T. A. Skotheim, R. L. Elsenbaumer, and J. R. Reynolds, Eds.), p. 277. Dekker, New York, 1998.
11. J. C. W. Chien, "Polyacetylene: Chemistry, Physics and Material Science." Academic Press, New York, 1984.
12. A. R. Blythe, "Electrical Properties of Polymers." Cambridge Univ. Press, Cambridge, 1979.
13. E. M. Genies and J. M. Pernaut, *Synth. Met.* 10, 117 (1984/85).
14. P. J. S. Foot and N. G. Shaker, *Mater. Res. Bull.* 18, 173 (1983).
15. D. C. Bott, in "Handbook of Conducting Polymers" (T. A. Skotheim, Ed.), Vol. 2, p. 1191. Dekker, New York, 1986.
16. J. L. Bredas, in "Handbook of Conducting Polymers" (T. A. Skotheim, Ed.), Vol. 2, p. 859. Dekker, New York, 1986.
17. J. R. Elis, in "Handbook of Conducting Polymers" (T. A. Skotheim, Ed.), Vol. 1, p. 487. Dekker, New York, 1986.
18. J. Kanicki, in "Handbook of Conducting Polymers" (T. A. Skotheim, Ed.), Vol. 1, p. 543. Dekker, New York, 1986.
19. M. Gazard, in "Handbook of Conducting Polymers" (T. A. Skotheim, Ed.), Vol. 1, p. 673. Dekker, New York, 1986.
20. A. G. MacDiarmid and R. B. Kaner, in "Handbook of Conducting Polymers" (T. A. Skotheim, Ed.), Vol. 1, p. 689. Dekker, New York, 1986.
21. S. M. Park, in "Handbook of Organic Conductive Molecules and Polymers" (H. S. Nalwa, Ed.), Vol. 3, p. 429. Wiley, Chichester, 1997.
22. C. Ziegler, in "Handbook of Organic Conductive Molecules and Polymers" (H. S. Nalwa, Ed.), Vol. 3, p. 677. Wiley, Chichester, 1997.
23. M. Angelopoulos, in "Handbook of Conducting Polymers" (T. A. Skotheim, R. L. Elsenbaumer, and J. R. Reynolds, Eds.), p. 921. Dekker, New York, 1998.
24. V. G. Kulkarni, in "Handbook of Conducting Polymers" (T. A. Skotheim, R. L. Elsenbaumer, and J. R. Reynolds, Eds.), p. 1059. Dekker, New York, 1998.
25. D. Naegle and R. Bittihn, "Proceedings of the Sixth International Conference on Solid State Ionics," Germisch partenkirchen, Sept. 1987.
26. L. W. Shacklette, T. R. Jow, M. Maxfield and R. Hatami, *Synth. Met.* 28, C655 (1989).
27. H. Shirakawa and S. Ikeda, *Polymer J.* 2, 231 (1971).
28. H. Shirakawa, E. J. Louis, A. G. MacDiarmid, C. K. Chiang, and A. J. Heeger, *J. Chem. Soc., Chem. Commun.* 1977, 382 (1977).
29. K. Kaneto, Y. Kohnno, K. Yoshino, and Y. Inuishi, *J. Chem. Soc., Chem. Commun.* 1983, 382 (1983).
30. A. Dall'olio, Y. Dascola, V. Varacca, and V. Vocchi, *Acad. Sci. Ser.* C267, 433 (1968).
31. A. F. Diaz, K. K. Kanazawa, and G. P. Gardini, *J. Chem. Soc., Chem. Commun.* 1979, 635 (1979).
32. F. Mohammad, in "Handbook of Organic Conductive Molecules and Polymers" (H. S. Nalwa, Ed.), Vol. 3, p. 795. Wiley, Chichester, 1997.
33. W. Schnabel, "Degradation and Stabilization of Polymers." Hanser Verlag, Munich, 1982.
34. Y. Kamiya and E. Nikki, in "Aspects of Degradation and Stabilization of Polymers" (H. H. G. Jellinek, Ed.), Chap. 3. Elsevier, Amsterdam, 1978.
35. A. A. Pud, *Synth. Met.* 66, 1 (1994).
36. N. C. Billingham, P. D. Calvert, P. J. S. Foot, and F. Mohammad, *Polym. Degrad. Stab.* 19, 323 (1987) and references therein.
37. G. B. Street, B. Themans, and J. M. Andre, *J. Chem. Phys.* 83, 1323 (1985).
38. J. C. W. Chien, "Polyacetylene, Chemistry, Physics and Material Science." Academic Press, New York, 1984.
39. J. M. Pochan, in "Handbook of Conducting Polymers" (T. A. Skotheim, Ed.), Vol. 2, p. 1383. Dekker, New York, 1986.
40. F. Mohammad, P. D. Calvert, and N. C. Billingham, "Proceedings of the 35th IUPAC International Symposium on Macromolecules," Univ. of Arkon, 1994, p. 724.
41. M. A. Druy, C. Tsang, N. Brown, A. J. Heeger, and A. MacDiarmid, *J. Polym. Sci., Polym. Phys. Ed.* 18, 429 (1980).
42. H. Kuzumani, E. Imhoff, D. Firchen, and A. Sarhangi, *Mol. Cryst. Liq. Cryst.* 77, 197 (1981).
43. G. Froyer, F. Maurice, P. Bernier, and P. McAndrew, *Polym. Commun.* 23, 1103 (1982) and references therein.
44. F. Mohammad, Ph. D. Thesis, University of Sussex, 1988.
45. J. M. G. Cowie, "Polymers: Chemistry and Physics of Modern Materials," 2nd ed. Blackie, Glasgow, 1991.
46. R. W. Dyson, Ed., "Speciality Polymers," 2nd ed., p. 13. Blackie, London, 1998.
47. A. H. Fawcett, Ed., "High Value Polymers." The Royal Society of Chemistry, Cambridge, 1991.
48. N. C. Billingham, P. D. Calvert, P. J. S. Foot, and F. Mohammad, *Polym. Degrad. Stab.* 19, 323 (1987) and references therein.
49. M. A. Druy, M. F. Rubner, and S. P. Walsh, *Synth. Met.* 13, 207 (1986) and references therein.
50. G. B. Street, B. Themans, and J. M. Andre, *J. Chem. Phys.* 83, 1323 (1985).
51. N. Grassie, in "Encyclopedia of Polymer Science and Technology" (H. F. Mark, N. G. Gaylord, and N. M. Bikales, Eds.), Vol. 4, p. 648. Interscience, New York, 1966.
52. F. Mohammad, P. D. Calvert, and N. C. Billingham, *Bull. Mater. Sci.* 18(3), 255 (1995).
53. D. J. Berets and D. S. Smiths, *Trans. Faraday Soc.* 64, 823 (1968).
54. P. Pfluger, M. Croumbi, G. B. Street, and G. Weiser, *J. Chem. Phys.* 78, 3212 (1983).
55. T. C. Tsai, D. A. Tree, and M. S. High, *Ind. Eng. Chem. Res.* 33, 2600 (1994).
56. W. Ried and D. Freitag, *Angew. Chem.* 80, 932 (1968).
57. F. Mohammad, P. D. Calvert, and N. C. Billingham, "Proceedings of the 2nd CECRI Research Conference on Polar Polymers," Karaikudi, India, 1989.
58. A. R. Blythe, "Electrical Properties of Polymers," Chap. 5, p. 90. Cambridge Univ. Press, Cambridge, 1979.
59. S. Merchant and P. J. S. Foot, *Mater. Sci. Eng., B* 9, 269 (1991).
60. R. C. Weast, Ed., "CRC Handbook of Chemistry and Physics," 64th ed. CRC Press, Boca Raton, FL, 1983.
61. D. H. Williams and I. Fleming, "Spectroscopic Methods in Chemistry," 3rd ed., p. 1. McGraw-Hill, Maidenhead, 1980.
62. J. Koryta, "Ions, Electrodes and Membranes." Wiley, Chichester, 1982.
63. F. Mohammad, P. D. Calvert, and N. C. Billingham, "Proceeding of the National Seminar on Economic Utilization of Renewable Energy Resources," Aligarh Muslim University, 1990.
64. V. Kubasov and S. Zaretsky, "Introduction to Electrochemistry." Mir, Moscow, 1987.
65. P. Foot, T. Ritchi, and F. Mohammad, *J. Chem. Soc., Chem. Commun.* 1536 (1988).
66. F. Mohammad, P. D. Calvert, and N. C. Billingham, *Bull. Electrochem.* 11(5), 231 (1995).
67. F. Mohammad, P. D. Calvert and N. C. Billingham, "Proceedings of the 35th IUPAC International Symposium on Macromolecules." University of Akron, 1994, p. 724.
68. F. Mohammad, *J. Phys. D: Appl. Phys.* 31, 951 (1998).
69. B. Wessling, in "Handbook of Organic Conductive Molecules and Polymers" (H. S. Nalwa, Ed.), Vol. 3, p. 497. Wiley, Chichester, 1997.
70. D. C. Bott, in "Handbook of Conductivity Polymers" (T. A. Skotheim, Ed.), Vol. 2, p. 1191. Dekker, New York, 1986.

71. M. Sato, K. Kaeriyama, and K. Someno, *Macromol. Chem.* 184, 2241 (1983).
72. H. H. Kuhn and A. D. Child, "Handbook of Conducting Polymers" (T. A. Skotheim, R. L. Elsenbaumer and J. R. Reynolds, Eds.), p. 993. Dekker, New York, 1998 and references therein.
73. J. W. Blatchford and A. J. Epstein, *Am. J. Phys.* 64, 120 (1996).
74. H. G. Kiess, Ed., "Conjugated Conducting Polymers." Springer-Verlag, Berlin, 1992.
75. S. Roth, *Indian J. Chem. Sect. A* 33, 453 (1994).
76. J. C. W. Chien, "Polyacetylene: Chemistry, Physics and Material Science." Academic, New York, 1984.
77. J. M. Pochan, "Handbook of Conducting Polymers" (T. A. Skotheim, Ed.), p. 1383. Dekker, New York, 1986.
78. T. Ito, H. Shirakawa, and S. Ikeda, *J. Polym. Sci. Chem.* 13, 1943 (1975).
79. D. J. Berets and D. S. Smith, *Trans. Faraday Soc.* 64, 823 (1968).
80. H. Shirakawa and S. Ikeda, *Polym. J.* 2, 231 (1971).
81. C. K. Chiang, Y. W. Park, A. J. Heeger, H. Shirakawa, E. J. Louis, and A. G. MacDiarmid, *J. Chem. Phys.* 69, 5098 (1978).
82. J. B. Goldberg, H. R. Crowe, P. R. Newman, A. J. Heeger, and A. G. MacDiarmid, *J. Chem. Phys.* 70, 1132 (1979).
83. A. Snow, P. Brant, D. Weber, and N. L. Yang, *J. Polym. Sci. Lett.* 17, 263 (1979).
84. G. Vansco and A. Rockenbauer, *Chem. Scr.* 17, 153 (1981).
85. J. C. W. Chien, F. E. Karasz, G. E. Wnek, A. G. MacDiarmid, and A. J. Heeger, *J. Polym. Sci. Lett.* 18, 45 (1980).
86. Y. Wada, "Physics and Chemistry of Materials with Low-Dimensional Structures" (H. Aoki, M. Tsukada, M. Schluter, and F. Levy, Eds.). Kluwer Academic, Dordrecht, 1992.
87. N. C. Billingham, P. D. Calvert, P. J. S. Foot, and F. Mohammad, *Polym. Degrad. Stab.* 19, 323 (1987).
88. X. Z. Yang and J. C. W. Chien, *J. Polym. Sci. Polym. Chem. Ed.* 23(3), 859 (1985).
89. M. A. Druy, M. F. Rubner, and S. P. Walsh, *Synth. Met.* 13, 207 (1986).
90. L. W. Shacklette, R. R. Chance, D. M. Ivory, G. G. Miller, and R. H. Baughman, *Synth. Met.* 1, 307 (1979).
91. M. Aldissi, *Polym. Prepr.* 26(2), 269 (1985).
92. A. G. MacDiarmid, R. J. Mammone, J. R. Krawczyk, and S. J. Porter, *Mol. Cryst. Liq. Cryst.* 105, 89 (1984).
93. R. J. Mammone and A. G. MacDiarmid, *Synth. Met.* 9, 143 (1984).
94. A. G. Alie and G. E. Wnek, *J. Chem. Soc., Chem. Commun.* 1983, 63 (1983).
95. P. Foot, T. Ritchi and F. Mohammad, *J. Chem. Soc., Chem. Commun.* 1988, 1536 (1988).
96. J. L. Fan and J. C. W. Chien, *J. Polym. Sci., Polym. Commun.* 21, 3453 (1983).
97. T. Watase, H. Tachimori, and T. Masuda, *Bull. Chem. Soc. Jpn.* 68(1), 393 (1995).
98. H. Kouzai, T. Masuda, and T. Higashimura, "Proceedings of the 35th IUPAC International Symposium on Macromolecules," University of Akron, 1994, p. 938.
99. T. Masuda, H. Tachimori, and T. Higashimura, "Proceedings of the 35th IUPAC International Symposium on Macromolecules," University of Akron, 1994, p. 106.
100. D. J. Liaw, K. R. Hu, and H. H. Chiang, "Proceedings of the 35th IUPAC International Symposium on Macromolecules," University of Akron, 1994, p. 109.
101. A. S. Luyt and H. C. M. Vosloo, "Proceedings of the 35th IUPAC International Symposium on Macromolecules," University of Akron, 1994, p. 938.
102. M. A. Druy, M. F. Rubner, and S. P. Walsh, *Synth. Met.* 13, 207 (1986).
103. G. Ahlgren and B. Krische, *J. Chem. Soc., Chem. Commun.* 1984, 946 (1984).
104. P. Zhou, L. Balogh, and A. Blumstein, *Polym. Mater. Sci. Eng.* 71, 127 (1994).
105. Y. S. Gal, H. N. Cho, S. K. Kwon, and S. K. Choi, *Polymer (Korea)* 12(1), 30 (1988).
106. A. Blumstein, H. Liu, and S. Tripathy, *ACS Polym. Prepr.* 39(2), 701 (1998).
107. T. Shimizu and T. Yamamoto, *J. Chem. Soc., Chem. Commun.* 1999, 515 (1999).
108. M. Hatano, S. Kanbara, and S. Okamoto, *J. Polym. Sci.* 51, 526 (1961).
109. H. W. Gibson and J. M. Pochan, *Macromolecules* 15, 242 (1982).
110. G. T. Kim, M. Burghard, D. S. Suh, K. Liu, J. G. Park, S. Roth, and Y. W. Park, *Synth. Met.* 105, 207 (1999).
111. B. D. Malhotra, N. Kumar, and S. Chandra, *Prog. Polym. Sci.* 12, 179 (1986).
112. Y. Cao, P. Wang, and R. Qian, *Makromol. Chem.* 186, 1093 (1985).
113. F. Mohammad, Ph. D. Thesis, University of Sussex, 1988.
114. F. Mohammad, P. D. Calvert, and N. C. Billingham, *Bull. Mater. Sci.* 18(3), 255 (1995).
115. F. Mohammad, P. D. Calvert, and N. C. Billingham, *Synth. Met.* 66, 33 (1994).
116. F. Mohammad, P. D. Calvert, and N. C. Billingham, *Bull. Electrochem.* 9(2/3), 109 (1993).
117. F. Mohammad, P. D. Calvert, and N. C. Billingham, *Bull. Electrochem.* 10(11/12), 508 (1994).
118. G. Tourillon and F. Garnier, *J. Electrochem. Soc.* 130, 2043 (1983).
119. R. L. Elsenbaumer, K. -Y. Jen, and R. Oboodi, *Synth. Met.* 15, 169 (1986).
120. G. G. Miller and R. L. Elsenbaumer, *J. Chem. Soc., Chem. Commun.* 1986, 1346 (1986).
121. M. Sato, S. Tanaka, and K. Kaeriyama, *J. Chem. Soc., Chem. Commun.* 1986, 873 (1986).
122. S. Hotta, S. D. D. V. Rughooputh, A. J. Heeger, and F. Wudl, *Macromolecules* 20, 212 (1987).
123. N. Somanathan and G. Wegner, *Indian J. Chem. Sect. A* 33, 572 (1994).
124. G. W. Heffner and D. S. Pearson, *Macromolecules* 24, 6295 (1991).
125. Q. Pei and O. Ingnas, *Synth. Met.* 46, 353 (1992).
126. S. K. Ritter, R. E. Nofle, and A. E. Ward, *Chem. Mater.* 5, 752 (1993).
127. W. Buchner, R. Garreau, M. Lemaire, and J. Roncali, *J. Electroanal. Chem.* 277, 355 (1990).
128. O. Ingnas, *Indian J. Chem. Sect. A* 33, 499 (1994).
129. G. Gustafsson, O. Ingnas, J. O. Nilsson, and B. Liedberg, *Synth. Met.* 26, 297 (1988).
130. G. Gustafsson, O. Ingnas, and J. O. Nilsson, *Synth. Met.* 28, 427 (1988).
131. G. Gustafsson, O. Ingnas, J. O. Nilsson, K. Uvdal, W. R. Salaneck, J. E. Osterholm, and J. Laakso, *Synth. Met.* 28, 445 (1988).
132. Q. Pei and O. Ingnas, *Synth. Met.* 46, 353 (1992).
133. M. Andersson, Q. Pei, T. Hjertberg, O. Ingnas, O. Wennerstorm, and J. E. Osterholm, *Synth. Met.* 55, 1227 (1993).
134. J. Bukowska and K. Jakowska, *Synth. Met.* 35, 143 (1990).
135. S. Wang, K. Tanaka, and T. Yamabe, *Synth. Met.* 32, 141 (1989).
136. H. Harada, T. Fuchigami and T. Nonaka, *J. Electroanal. Chem.* 303, 139 (1991).
137. B. Scrosati, S. Panero, P. Prospero, and M. Mastragostino, "Extend Abstracts of the 3rd International Meeting on Lithium Batteries," Kyoto, 1986, Sect. 1, p. 182.
138. E. W. Tsai, S. Basak, J. P. Ruiz, J. R. Reynolds, and K. Rajeshwar, *J. Electrochem. Soc.* 136, 3683 (1989).
139. N. Somanathan and G. Wegner, *Indian J. Chem., Sect. A* 33, 572 (1994).
140. A. Czerwinski, H. Zimmar, A. Amar, C. V. Pham, S. Pons, and H. B. Mark, *J. Chem. Soc., Chem. Commun.* 1985, 1158 (1985).
141. G. Tourillon and F. Garnier, *J. Electroanal. Chem.* 161, 51 (1984).
142. M. Dietrich, J. Heinze, G. Heywang, and F. Jonas, *J. Electroanal. Chem.* 369, 87 (1994).
143. T. Miyazaki and T. Yamamoto, *Chem. Lett.* 1994, 41 (1994).
144. T. M. Swager, M. J. Marsella, L. K. Bicknell, and Q. Zhou, "Proceedings of the 35th IUPAC International Symposium on Macromolecules," University of Akron, 1994.

145. M. Onada, H. Nakayama, S. Morita, and K. Yoshino, *J. Electrochem. Soc.* 141(2), 338 (1994).
146. M. Pomerantz, B. Chaloner-Gill, L. O. Harding, J. J. Tseng, and W. J. Pomerantz, *J. Chem. Soc., Chem. Commun.* 1992, 1672 (1992).
147. M. Pomerantz, B. Chaloner-Gill, L. O. Harding, J. J. Tseng, and W. J. Pomerantz, *Synth. Met.* 55, 960 (1993).
148. Y. Ikenoue, F. Wudl, and A. J. Heeger, *Synth. Met.* 40, 1 (1991).
149. J. Ohshita, M. Nodono, H. Kai, T. Watanabe, A. Kunai, K. Komaguchi, M. Shiotani, A. Adachi, K. Okita, Y. Harima, K. Yamashita, and M. Ishikawa, *Organometallics* 18(8), 1453 (1999).
150. N. Camaioni, G. Casalbore-Miceli, A. Geri, and S. Nicoletti, *Adv. Mater. Commun.* 11(6), 472 (1999).
151. G. Casalbore-Miceli, G. Beggiato, N. Camaioni, and A. M. Fichera, *Synth. Met.* 94, 179 (1998).
152. G. Casalbore-Miceli, N. Camaioni, M. Catellani, and M. C. Gallazi, *Synth. Met.* 95, 211 (1998).
153. N. Camaioni, G. Casalbore-Miceli, and G. Beggiato, *Synth. Met.* 104, 169 (1999).
154. W. C. Magnoni, M. C. Gallazi, and G. Zerbi, *Acta Polym.* 47, 228 (1996).
155. Y. Kunugi, Y. Harima, K. Yamashita, J. Ohshita, A. Kunai, and M. Ishikawa, *J. Electroanal. Chem.* 414, 135 (1996).
156. Y. Harima, L. Zhu, H. Tang, K. Yamashita, A. Takata, J. Ohshita, A. Kunai, and M. Ishikawa, *Synth. Met.* 98, 79 (1998).
157. H. Tang, L. Zhu, Y. Harima, K. Yamashita, J. Ohshita, A. Kunai, and M. Ishikawa, *Electrochim. Acta* 44, 2579 (1999).
158. L. Zhu, H. Tang, Y. Harima, K. Yamashita, A. Takata, J. Ohshita, and A. Kunai, *J. Electroanal. Chem.* 464, 158 (1999).
159. A. Diaz and R. D. Miller, *J. Electrochem. Soc.* 132, 834 (1985).
160. N. C. Billingham, P. D. Calvert, P. J. S. Foot, and F. Mohammad, *Polym. Degrad. Stab.* 19, 323 (1987).
161. P. Pfluger, M. Krounbi, G. B. Street, and G. Weiser, *J. Chem. Phys.* 78, 3212 (1983).
162. W. R. Salaneck, R. Erlandsson, J. Prejza, I. Lundstorm, and O. Inganäs, *Synth. Met.* 5, 125 (1985).
163. L. A. Samuelson and M. A. Druy, *Macromolecules* 19, 824 (1986).
164. R. Erlandsson, O. Inganäs, I. Lundstorm, and W. R. Salaneck, *Synth. Met.* 10, 303 (1985).
165. H. Munstedt, in "Electronic Properties of Polymers and Related Compounds" (H. Kuzumany, M. Mehring, and S. Roth, Eds.), p. 8. Springer-Verlag, Berlin, 1986.
166. A. F. Diaz, K. K. Kanazawa, and G. P. Gardini, *J. Chem. Soc., Chem. Commun.* 1979, 635 (1979).
167. K. K. Kanazawa, A. F. Diaz, R. H. Giess, W. D. Gill, F. Kwak, J. A. Logan, J. F. Rabolt, and G. B. Street, *J. Chem. Soc., Chem. Commun.* 1979, 854 (1979).
168. M. Ogaswara, K. Funahashi, T. Demura, T. Hagiwara, and K. Iwata, *Synth. Met.* 14, 61 (1986).
169. F. Mohammad, P. D. Calvert, and N. C. Billingham, *Bull. Mater. Sci.* 18(3), 255 (1995).
170. M. Salmon, A. F. Diaz, A. J. Logan, M. Krounbi, and J. Bargon, *Mol. Cryst. Liq. Cryst.* 83, 265 (1982).
171. A. G. MacDiarmid, R. J. Mammone, J. R. Krawczyk, and S. J. Porter, *Mol. Cryst. Liq. Cryst.* 105, 89 (1984).
172. J. Mammone and A. G. MacDiarmid, *Synth. Met.* 9, 143 (1984).
173. A. G. Elie and G. E. Wnek, *J. Chem. Soc., Chem. Commun.* 1983, 63 (1983).
174. H. Munstedt, *Polymer* 27, 899 (1986).
175. V. V. Kras'ko, A. A. Yakovleva, and Y. M. Kolotyrykin, *Elektrokhimiya* 2, 1432 (1986).
176. A. F. Diaz, J. J. Costillo, J. O. Logan, and W. J. Lee, *J. Electroanal. Chem.* 129, 115 (1981).
177. S. Cosnier, A. Deronzier, and A. Llobet, *J. Electroanal. Chem.* 280, 213 (1990).
178. J. Prejza, I. Lundstorm and T. Skotheim, *J. Electrochem. Soc.* 129, 1685 (1982).
179. F. Garnier, *Angew. Chem.* 101, 529 (1989).
180. F. Beck, P. Broun, and M. Oberst, *Ber. Bunsen Ges. Phys. Chem.* 91, 967 (1987).
181. A. F. Diaz, K. K. Kanazawa and G. P. Gardini, *J. Chem. Soc., Chem. Commun.* 1979, 535 (1979).
182. P. Novak and W. Vielstich, *Collect. Czech. Chem. Commun.* 57, 339 (1992).
183. G. Zotti, G. Schiavon, A. Berlin, and G. Pagani, *Synth. Met.* 28, 183 (1989).
184. G. Vidan and M. Gluglielmi, *Synth. Met.* 15, 45 (1986).
185. G. Zotti, G. Schiavon, A. Berlin, R. Ferraccioli, G. Pagani, and F. Sannicola, *Makromol. Chem.* 190, 405 (1989).
186. K. Hyodo and A. G. MacDiarmid, *Synth. Met.* 11, 167 (1985).
187. N. L. Weinberg and E. A. Brown, *J. Am. Chem. Soc.* 31, 4054 (1966).
188. N. Mermilliod and J. Tanguy, *J. Electrochem. Soc.* 133(6), 1073 (1986).
189. T. Osaka, T. Momma, K. Nishimura, S. Kakuda, and T. Ishii, *J. Electrochem. Soc.* 141(8), 1994 (1994).
190. C. C. Chen and K. Rajeshwar, *J. Electrochem. Soc.* 141(11), 2942 (1994).
191. T. Momma, K. Nishimura, T. Osaka, N. Kondo, and S. Nakamura, *J. Electrochem. Soc.* 141(9), 2326 (1994).
192. R. Quan, J. Qui, and B. Yan, *Synth. Met.* 14, 81 (1986).
193. F. Beck and R. Michaelis, *Werkstoffe und Korrosion* 42, 341 (1991).
194. P. Audebart and G. Vidan, *J. Electroanal. Chem.* 190, 129 (1985).
195. M. Biswas and A. Roy, *J. Appl. Polym. Sci.* 54, 1483 (1994).
196. M. Biswas and A. Roy, *J. Appl. Polym. Sci.* 54, 843 (1994).
197. M. Biswas and P. Mitra, *J. Appl. Polym. Sci.* 42, 1989 (1991).
198. M. Biswas and A. Majumdar, *J. Appl. Polym. Sci.* 42, 2489 (1991).
199. M. Biswas and S. Packirisamy, *J. Appl. Polym. Sci.* 2, 511 (1980).
200. M. Biswas and S. Chatterjee, *J. Appl. Polym. Sci.* 29, 829 (1984).
201. H. A. Pohl and D. A. Opp, *J. Phys. Chem.* 66, 2121 (1962).
202. M. Biswas and A. Roy, *J. Appl. Polym. Sci.* 49, 2189 (1993).
203. I. T. Kim and R. L. Elsenbaumer, *Synth. Met.* 84, 157 (1997).
204. A. F. Diaz, J. I. Castillo, K. K. Kanazawa, K. A. Logan, M. Salmon, and O. Fajardo, *J. Electroanal. Chem.* 133, 233 (1982).
205. K. K. Kanazawa, A. F. Diaz, R. H. Geiss, W. D. Gill, J. F. Kwak, J. A. Logan, J. F. Rabolt, and G. B. Street, *J. Chem. Soc., Chem. Commun.* 854 (1979).
206. I. T. Kim and R. L. Elsenbaumer, *Synth. Met.* 85, 1345 (1997).
207. P. Calvert, Z. Gardlund, T. Huntoon, H. K. Hall, and A. Padias, *Mater. Res. Soc. Symp. Proc.* 498, 485 (1998).
208. S. Takeoka, T. Hara, K. Fukushima, K. Yamamoto, and E. Tsuchida, *Bull. Chem. Soc. Jpn.* 71, 1471 (1998).
209. F. Mohammad, P. D. Calvert, and N. C. Billingham, *Bull. Electrochem.* 10(11-12), 508 (1994).
210. F. Mohammad, P. D. Calvert, and N. C. Billingham, *Bull. Mater. Sci.* 18(3), 255 (1995).
211. J. C. Thieblemont, A. Brun, J. Marty, M. F. Planche, and P. Calo, *Polymer* 36, 1605 (1995).
212. Q.-X. Zhou, L. Miller, and J. Valentine, *J. Electroanal. Chem.* 261, 147 (1989).
213. H. Shinohara, M. Aizawa, and H. Shirakawa, *J. Chem. Soc., Chem. Commun.* 1986, 87 (1986).
214. W. Zhang and S. Dong, *J. Electroanal. Chem.* 284, 517 (1990).
215. T. Hanawa, S. Kuwabata, and H. Yoneyama, *J. Chem. Soc., Faraday Trans.* 1(84), 1587 (1988).
216. G. Bidan, B. Ehui, and M. Lapokowski, *J. Phys. D: Appl. Phys.* 21, 1043 (1988).
217. L. Hwang, J. Ko, H. Rhee, and C. Kin, *Synth. Met.* 55-57, 3671 (1993).
218. D. O' Riordan and G. Wallace, *Anal. Chem.* 58, 128 (1986).
219. M. Imisides and G. Wallace, *J. Electroanal. Chem.* 246, 181 (1988).
220. M. Umana and J. Waller, *Anal. Chem.* 58, 2979 (1986).
221. P. Bartlett and R. Whitaker, *J. Electroanal. Chem.* 224, 27 (1987).
222. P. Bartlett and R. Whitaker, *J. Electroanal. Chem.* 224, 37 (1987).
223. N. Foulds and C. Lowe, *J. Chem. Soc., Faraday Trans.* 1(82), 1259 (1986).

224. T. Tatsuma, T. Watanabe, and T. Watanabe, *J. Electroanal. Chem.* 356, 245 (1993).
225. S. Porter, "Extended Abstracts of the ICSM'88," Santa Fe, 1988, p. 70.
226. D. Belanger, J. Nadreau, and G. Fortier, *J. Electroanal. Chem.* 274, 143 (1989).
227. G. Harsanyi, "Polymer Films in Sensor Applications: Technology, Materials, Devices and Their Characteristics." Technomic, Lancaster, 1994.
228. E. Genies and M. Marchesiello, *Synth. Met.* 55-57, 3677 (1993).
229. P. Kovacic and M. B. Jones, *Chem. Rev.* 87, 357 (1987).
230. J. G. Speight, P. Kovacic, and F. W. Koch, *J. Macromol. Sci. Rev., Macromol. Chem.* C5(2), 295 (1971).
231. N. Kirova, S. Brazovskii, and A. R. Bishop, *Synth. Met.* 100, 29 (1999).
232. S. Brasovskii, N. Kirova, A. R. Bishop, V. Klimov, D. McBranch, N. N. Barashkov, and J. P. Ferraris, *Opt. Mater.* 9, 472 (1998).
233. W. Ried and D. Freitag, *Angew. Chem.* 80, 932 (1968).
234. P. Kovacic and A. Kyriakis, *J. Am. Soc.* 85, 454 (1963).
235. P. Kovacic and R. M. Lange, *J. Org. Chem.* 28, 968 (1963).
236. K. N. Rao and S. K. Dayal, *Indian J. Appl. Chem.* 29, 45 (1966).
237. D. N. Vincent, *J. Macromol. Sci.* A3, 485 (1969).
238. P. Gresham, *Eng. Mater. Design* 1965, 821 (1965).
239. P. Kovacic and F. W. Koch, *J. Org. Chem.* 28, 1864 (1963).
240. A. A. Berlin, *J. Polym. Sci.* 55, 621 (1961).
241. W. Zerwinski, W. Bala, and L. Kreja, *Angew. Makromol. Chem.* 132, 123 (1985).
242. A. H. Fraser, "High Temperature Resistant Polymers." Interscience, New York, 1968.
243. J. Ohshita, K. Sugimoto, A. Kunai, Y. Harima, and K. Yamashita, *J. Organomet. Chem.* 580, 77 (1999).
244. J. Ohshita, K. Sugimoto, T. Watanabe, A. Kunai, M. Ishikawa, and S. Aoyama, *J. Organomet. Chem.* 564, 47 (1998).
245. E. Y. Pisarevskaya and M. D. Levi, *Electrokhimiya* 27, 496 (1991).
246. F. Beck and A. Pruss, *J. Electroanal. Chem.* 216, 157 (1987).
247. L. W. Shacklette, R. L. Elsenbaumer, and R. H. Baughman, *J. Phys. C: Solid State Phys.* 44, 559 (1983).
248. L. W. Shacklette, R. L. Elsenbaumer, R. R. Chance, J. M. Sowa, D. M. Ivory, G. G. Miller, and R. H. Baughman, *J. Chem. Soc., Chem. Commun.* 1982, 361 (1982).
249. N. Siu-Choon, J. Xu, H. S. O. Chan, A. Fujii, and K. Yoshino, *J. Mater. Chem.* 9, 381 (1999).
250. J. P. Ruiz, J. R. Dharia, J. R. Reynolds, and L. J. Buckley, *Macromolecules* 25, 849 (1992).
251. M. A. Nylander and I. Lundstrom, *Anal. Chem. Symp. Ser.* 17, 203 (1983).
252. P. Foot, T. Ritchi, and F. Mohammad, *J. Chem. Soc., Chem. Commun.* 1988, 1536 (1988).
253. J. Chague, C. Germain, C. Maleysson, and H. Robert, *Sens. Actuators* 7, 199 (1985).
254. G. Weddingen, "Extended Abstracts of the ICSM'88," Santa Fe, 1988, p. 271.
255. S. C. Moratti, "Handbook of Conducting Polymers" (T. A. Skotheim, R. L. Elsenbaumer, and J. R. Reynolds, Eds.), p. 343. Dekker, New York, 1998.
256. S. Scheinert, G. Paasch, S. Pohlmann, H. H. Horhold, and R. Stockmann, "Proceedings of ESSDERC'99," Lucerne, 1999.
257. J. Scherbel, P. H. Nguyen, G. Paasch, W. Brutting, and M. Schwoerer, *J. Appl. Phys.* 83, 5054 (1998).
258. S. Brazovskii, N. Kirova, and A. R. Bishop, *Opt. Mater.* 9, 465 (1998).
259. G. Yu, K. Pakbaz and A. J. Heeger, *Appl. Phys. Lett.* 64, 3422 (1994).
260. G. Drefahl, H. -H. Horhold, and J. Opfermann, German Democratic Republic Patent 75233, 1970.
261. G. Yu, C. Zhang, K. Pakbaz, and A. J. Heeger, *Synth. Met.* 71, 2241 (1995).
262. F. Wudl, P. M. Allemand, G. Srdanov, Z. Ni, and D. McBranch, "Materials for Nonlinear Optics: Chemical Perspectives" (S. R. Marder, J. E. Sohn, and G. D. Stucky, Eds.), American Chemical Society Washington, DC, 1991.
263. H. Antoniadis, B. R. Hsieh, M. A. Abkowitz, S. A. Jenekhe, and M. Stolka, *Synth. Met.* 62, 265 (1994).
264. S. Karg, W. Riess, M. Meier, and M. Schwoerer, *Synth. Met.* 55-57, 4186 (1993).
265. C. H. Lee, *Synth. Met.* 70, 1352 (1995).
266. K. Yoshino, *Jpn. J. Appl. Phys., Pt. 2A* 32, L357 (1993).
267. N. S. Sariciftci, L. Smilowitz, A. J. Heeger, and F. Wudl, *Science* 258, 1474 (1992).
268. J. J. Kim, S. -W. Kang, D. -H. Hwang, and H. -K. Shini, *Synth. Met.* 55-57, 4024 (1993).
269. S. Tanaka and J. R. Reynolds, *J. Macromol. Sci., Pure Appl. Chem.* A32, 1049 (1995).
270. T. Kawai, T. Iwasa, T. Kuwabara, M. Onada, and K. Yoshino, *Jpn. J. Appl. Phys.* 29, 1833 (1990).
271. R. Gomez, J. L. Segura, and N. Martin, *J. Chem. Soc., Chem. Commun.* 1999, 619 (1999).
272. L. -H. Wang, Z. -K. Chen, E. -T. Kang, H. Meng, and W. Huang, *Synth. Met.* 105, 85 (1999).
273. Z. Gao, C. S. Lee, I. Bello, S. T. Lee, R. -M. Chen, T. -Y. Luh, J. Shi, and C. W. Tang, *Appl. Phys. Lett.* 74(6), 865 (1999).
274. C. Hosokawa, H. Higashi, H. Nakamura, and T. Kusumoto, *Appl. Phys. Lett.* 67, 3853 (1995).
275. I. D. Parker, Y. Cao, and C. Y. Yang, *J. Appl. Phys.* 85(4), 2441 (1999).
276. I. D. Parker, E. Baggao, P. Bailey, Y. Cao, S. Draeger, A. J. Heeger, J. Kaminski, C. Knudson, T. Marx, B. Nilsson, J. Peltola, R. Pflanger, M. Raffetto, T. Ronnfeldt, B. Weber, and C. Zandonatti, unpublished work.
277. A. G. MacDiarmid and F. Huang, "Proceedings of the Fourth Franco-qui Colloquium," Brussels, 1998, p. 61.
278. A. F. Diaz and J. A. Logan, *J. Electroanal. Chem. Interfacial Electrochem.* 111, 111 (1980).
279. R. Nonfi and A. J. Nozik, *J. Electrochem. Soc.* 129, 2261 (1982).
280. D. W. DeBerry, *J. Electrochem. Soc.* 132, 1022 (1985).
281. J. A. Conklin, T. M. Su, S. -C. Huang and R. B. Kaner, in "Handbook of Conducting Polymers" (T. A. Skotheim, R. L. Elsenbaumer, and J. R. Reynolds, Eds.), p. 945. Dekker, New York, 1998.
282. A. J. Epstein and Y. Yang, *Mater. Res. Soc. Bull.* 1997, 13 (1977) and the references therein.
283. R. Tecklenburg, G. Paasch, and S. Scheinert, *Adv. Mater. Opt. Electron.* 8, 285 (1998).
284. P. A. Kilmartin and G. A. Wright, *Synth. Met.* 104, 145 (1999).
285. P. A. Kilmartin and G. A. Wright, *Synth. Met.* 88, 163 (1997).
286. P. A. Kilmartin and G. A. Wright, *Synth. Met.* 88, 153 (1997).
287. P. A. Kilmartin and G. A. Wright, *Electrochim. Acta* 41, 1677 (1996).
288. M. K. Troare, W. T. K. Stevenson, J. McKormic, R. C. Dorey, S. Wen, and D. Meyers, *Synth. Met.* 40, 137 (1991).
289. J. Yue, A. J. Epstein, Z. Zhong, P. K. Gallagher, and A. G. MacDiarmid, *Synth. Met.* 41-43, 765 (1991).
290. T. C. Tsai, D. A. Tree, and M. S. High, *Ind. Eng. Chem. Res.* 33, 2600 (1994).
291. H. L. Friedman, *J. Polym. Sci.* 6, 183 (1968).
292. A. A. Syed and M. K. Dinesan, in "Polymer Science: Contemporary Theme" (S. Sivaram, Ed.), p. 739. Tata McGraw-Hill, New Delhi, 1991.
293. S. Palaniappan and B. H. Narayana, *J. Polym. Sci., Polym. Chem.* 32, 2431 (1994).
294. M. Kahler, G. Negro, J. Naseer, and N. Ahmad, *Synth. React. Inorg. Met. Org. Chem.* 24, 147 (1994).
295. J. E. Pereira da Silva, S. I. Cordova de Torresi, D. L. A. de Fari, and M. L. A. Temperini, *Synth. Met.* in press.
296. Z. F. Li, E. T. Kang, K. G. Neoh, and K. L. Tan, *Synth. Met.* 87, 45 (1997).
297. W. A. Gazotti, Jr., M. J. D. M. Jannini, S. I. Cordoba de Torresi, and M. A. De Paoli, *J. Electroanal. Chem.* 440, 193 (1997).
298. M. P. T. Sotomayor, W. A. Gazotti, Jr., M. A. Paoli, and W. A. Oliveira, "Proceedings of the 18th Meeting of the Brazilian Chemical Society," Caxambu, Brazil, 1995, Abstract QA-140.

299. A. Hugot-Le Goff and S. I. Cordova Torresi, "Proceedings of the Electrochromic Materials Symposium," Electrochemical Society, 1990, Vol. 2, p. 157.
300. N. Boucherit, P. Delichere, S. Joiret, and A. Hugot-Le Goff, *Mater. Sci. Forum* 44-45, 51 (1989).
301. M. C. Bernard, S. I. Cordova-Torresi, and A. Hugot-Le Goff, *Sol. Energy Mater. Sol. Cells* 25, 225 (1992).
302. R. Hand and R. Nelson, *J. Am. Chem. Soc.* 6, 850 (1974).
303. L. D. Arsov, W. Plieth, and G. Kobmehl, *J. Solid State Electrochem.* 2, 355 (1998).
304. L. D. Arsov, *J. Solid State Electrochem.* 2, 266 (1998).
305. R. K. Paul, V. Vijayanathan, and C. K. S. Pillai, *Synth. Met.* 104, 189 (1999).
306. E. Kim, K.-Y. Lee, M.-H. Lee, J.-S. Shin, and S. B. Rhee, *Synth. Met.* 85, 1367 (1997).
307. E. Kim, K. Lee, and S. B. Rhee, *J. Electrochem. Soc.* 144(1), 227 (1997).
308. E. Kim, M.-H. Lee, B. S. Moon, C. Lee, and S. B. Rhee, *J. Electrochem. Soc.* 141(3), L26 (1994).
309. E. Kim, M.-H. Lee, and S. B. Rhee, *Mol. Cryst. Liq. Cryst.* 295, 79 (1997).
310. R. A. Misra, S. Dubey, B. M. Prasad, and D. Singh, *Indian J. Chem. Sect. A* 38, 141 (1999).
311. N. Toshima and H. Yan, *Bull. Chem. Soc. Jpn.* 68(3), 1056 (1995).
312. R. L. Clark and S. C. Yang, *Synth. Met.* 29, E337 (1989).
313. M. C. Gupta and S. V. Warhadpande, "Polymer Science: Contemporary Themes" (S. Sivaram, Ed.), p. 740. Tata McGraw-Hill, New Delhi, 1991.
314. J. Yue and A. J. Epstein, *J. Am. Chem. Soc.* 112, 2800 (1990).
315. X. Wei and A. J. Epstein, *Synth. Met.* 74, 123 (1995).
316. W. Lee, C. Du, S. M. Long, A. J. Epstein, S. Shimizu, T. Saitoh, and M. Uzawa, *Synth. Met.* 84, 807 (1997).
317. C.-H. Hsu, P. M. Peacock, R. B. Flippen, J. Yue, and A. J. Epstein, *Synth. Met.* 60, 223 (1993).
318. J. Yue, A. J. Epstein, Z. Zhong, P. K. Gallagher, and A. G. MacDiarmid, *Synth. Met.* 41, 765 (1991); T.-C. Tsai, D. A. Tree, and S. M. High, *Ind. Eng. Chem. Res.* 33, 2600 (1994).
319. X.-L. Wei, Y. Z. Wang, S. M. Long, C. Bobeczko, and A. J. Epstein, *J. Am. Chem. Soc.* 118, 2545 (1996).
320. J. Yue, G. Gordon, and A. J. Epstein, *Polymer* 33, 4409 (1992).
321. J. Yue, Z. H. Wang, K. R. Cromack, A. J. Epstein, and A. G. MacDiarmid, *J. Am. Chem. Soc.* 113, 2665 (1991).
322. A. Kobayashi, H. Yoneyama, and H. Tamura, *J. Electroanal. Chem.* 161, 419 (1984); 177, 293 (1984).
323. J. Yue and A. J. Epstein, *J. Chem. Soc., Chem. Commun.* 1992, 1540 (1992).
324. J. Yue, A. J. Epstein, Z. Zhong, P. K. Gallagher, and A. G. MacDiarmid, *Synth. Met.* 41-43, 765 (1991).
325. T. Challier and C. T. Slade, *J. Mater. Chem.* 4(3), 367 (1994).
326. L. Sun, H. Liu, R. Clark, and S. C. Yang, *Synth. Met.* 84, 67 (1997).
327. R. J. Racicot, R. L. Clark, H.-B. Liu, S. C. Yang, M. N. Alias, and R. Brown, *Proc. Mater. Res. Soc.* 413, 529 (1996).
328. G. P. Kota, L. Sun, H. Liu, and S. C. Yang, *Mater. Res. Soc. Symp. Proc.* 488, 359 (1998).
329. H. Liu, R. Clark and S. C. Yang, *Mater. Res. Soc. Symp. Proc.* 488, 747 (1998).
330. D. C. Hoa, T. N. Sureshkumar, N. S. Puneekar, R. S. Srinivasa, and A. Q. Contractor, *Anal. Chem.* 64, 2645 (1992).
331. S. Dogan, U. Akbulut, T. Yalcin, S. Suzer, and L. Toparre, *Synth. Met.* 60, 27 (1993).
332. A. G. MacDiarmid, W. J. Zhang, and J. Feng, "Proceedings of the APS Meeting," Los Angeles, 1998.
333. A. G. MacDiarmid, W. J. Zhang, J. Feng, F. Huang, and B. R. Hsieh, "Proceedings of ATEC'98," Atlanta, 1998, p. 1330.
334. M. Biswas and T. Uryu, *Rev. Macromol. Chem. Phys.* C26, 249 (1986).
335. R. C. Penwell, B. N. Ganguly, and T. W. Smith, *J. Polym. Sci. D.* 13, 63 (1978).
336. M. Biswas and S. K. Das, *Polymer* 23, 1723 (1982).
337. M. Biswas and S. Packirisamy, *Adv. Polym. Sci.* 70, 71 (1985) and references therein.
338. M. Biswas and A. Roy, *Polymer* 35(20), 4470 (1994).
339. M. Biswas and A. Roy, *Polymer* 34(13), 2903 (1993).
340. S. T. Wellinghoff, Z. Deng, T. J. Kedrovski, S. A. Dick, S. A. Jenekhe, and H. Ishida, *Mol. Cryst. Liq. Cryst.* 106, 289 (1984).
341. F. W. Mercer and M. T. McKenzie, *Polym. Prepr.* 34, 395 (1993).
342. M. H. Litt, H. Moaddel, C. E. Rogers, R. Savinell, and J. Wainwright, "Proceedings of the 35th IUPAC International Symposium on Macromolecules," University of Akron, 1994, p. 694.
343. V. V. Korshak and A. L. Rusanov, *Russ. Chem. Rev.* 52(6), 459 (1983).
344. B. Sillion and G. D. Guadamaris, *J. Polym. Sci.* C22, 827 (1969).
345. P. Schlack and G. Zuber, *Angew. Makromol. Chem.* 15(1), 25 (1971).
346. G. Lorenz, M. Gallus, W. Giessler, F. Bodesheim, H. Wieden, and G. E. Nischk, *Makromol. Chem.* 130, 65 (1969).
347. B. Sillion and G. D. Guadamaris, *C. R. Acad. Sci.* 165, 1234 (1967).
348. Z. Kucukyavuz and N. Abbasnejad, "Proceedings of the 35th IUPAC International Symposium on Macromolecules," University of Akron, 1994, p. 727.
349. M. Biswas and P. Mitra, *J. Appl. Polym. Sci.* 42, 1989 (1991).
350. Y. Saegusa, A. Inoo, and S. Nakamura, "Proceedings of the 35th IUPAC International Symposium on Macromolecules," University of Akron, 1994, p. 252.
351. H. A. Pohl and E. H. Engelhardt, *J. Phys. Chem.* 66, 2085 (1962).
352. R. J. Waltman, A. F. Diaz, and J. Bargon, *J. Electrochem. Soc.* 131, 1452 (1984).
353. H. Quante, P. Schlichting, and K. Mullen, "Proceedings of the 35th IUPAC International Symposium Macromolecules," University of Akron, 1994, p. 258.
354. M. M. Labes, P. Love and L. F. Nichols, *Chem. Rev.* 79, 1 (1979).
355. G. A. Bowmaker, P. A. Kilmartin, and G. A. Wright, *J. Solid State Electrochem.* 3, 163 (1999).
356. M. Bragadin, G. Scarponi, G. Capodaglio, P. Cescon, and F. Pucciarelli, *J. Electroanal. Chem.* 186, 113 (1985).
357. J. E. Mark, H. R. Allcock, and R. West, "Inorganic Polymers," Chap. 5. Prentice-Hall, Englewood Cliffs, NJ, 1992.
358. E. G. Rochow, "An Introduction to the Chemistry of the Silicone," 2nd ed. Wiley, New York, 1951.
359. R. West, L. D. David, P. I. Djurovich, K. I. Stearley, K. S. V. Srinivasan, and H. J. Yu, *J. Amer. Chem. Soc.* 103, 7352 (1981).
360. A. Watanabe, O. Ito, M. Matsuda, M. Suezawa, and K. Sumino, *Jpn. J. Appl. Phys., Part 1* 337A, 4133 (1994).
361. P. Trefonas, R. Miller, and R. West, *J. Am. Chem. Soc.* 107, 2737 (1985).
362. T. Karatsu, R. D. Miller, R. Sooriyakumaran, and J. Michl, *J. Am. Chem. Soc.* 111, 1140 (1989).
363. R. D. Miller, J. Rabolt, R. Sooriyakumaran, W. Fleming, G. N. Ficke, B. L. Farmer, and H. Kuzumany, in "Inorganic and Organometallic Polymers" (M. Zeldin, K. J. Wynne, and H. R. Allcock, Eds.). ACS Symposium Series, Vol. 360, p. 43. American Chemical Society, Washington, DC, 1988.
364. Z. Kucukyavuz, N. Nugay, and Z. Kucukyavuz, "Proceedings of the 35th IUPAC International Symposium on Macromolecules," University of Akron, 1994, p. 726.
365. N. Nagayama, Y. Tachibana, and M. Yokoyama, *Bull. Chem. Soc. Jpn.* 71, 2005 (1998).
366. I. Manners, *J. Chem. Soc. Chem. Commun.* 1999, 857 (1999).
367. R. Rulkens, R. Resendes, A. Verma, I. Manners, K. Murti, E. Fossum P. Miller, and K. Matyjaszewski, *Macromolecules* 30, 8165 (1997).
368. R. Paterson, D. A. Foucher, B.-Z. Tang, A. J. Lough, N. P. Raju, J. E. Greedan, and I. Manners, *Chem. Mater.* 7, 2045 (1995).
369. A. G. Dandridge, H. A. E. Drescher, and T. Thomas, British Patent 322169, 1929.
370. R. P. Linstead, *J. Chem. Soc.* 1934, 1016 (1934).
371. J. M. Robertson, "Organic Crystals and Molecules." Cornell Univ. Press, Ithaca, NY, 1953.

372. F. H. Moser and A. L. Thomas, "The Phthalocyanines," Vols. 1 and 2. CRC Press, Boca Raton, FL, 1983.
373. G. Lobbert, "Ullmann's Encyclopedia of Organic Compounds," Vol. A20. VCH, Weinheim, 1992.
374. M. Hanack and L. R. Subramanian, in "Handbook of Organic Conductive Molecules and Polymers" (H. S. Nalwa, Ed.), Wiley, Chichester, 1997.
375. R. Dieing, G. Schmid, E. Witke, C. Feucht, M. Dreben, J. Pohmer, and M. Hanack, *Chem. Ber.* 128, 589 (1995).
376. B. Mohr, G. Wegner, and K. Ohta, *J. Chem. Soc., Chem. Commun.* 1995, 995 (1995).
377. D. Wöhrle, in "Phthalocyanines: Properties and Applications" (C. C. Leznoff and A. J. P. Lever, Eds.), Vol. 1. VCH, Weinheim, 1989.
378. T. Inabe, M. K. Moguel, T. J. Marks, R. Burton, J. W. Lyding, and C. R. Kannewurf, *Mol. Cryst. Liq. Cryst.* 118, 349 (1985).
379. T. Inabe, M. K. Moguel, J. W. Lyding, R. L. Burton, and W. J. Carthy, *J. Am. Chem. Soc.* 108, 7595 (1986).
380. E. Orthmann, V. Enkelmann, and G. Wegner, *Makromol. Chem., Rapid Commun.* 4, 687 (1983).
381. P. Brant, R. S. Nohr, K. J. Wynne, and D. C. Weber, *Mol. Cryst. Liq. Cryst.* 81, 255 (1982).
382. M. Hanack, K. Mitulla, G. Pawlowski, and L. R. Subramanian, *Angew. Chem., Int. Ed. Engl.* 18, 322 (1979).
383. K. Mitulla and M. Hanack, *Z. Naturforsch. B: Chem. Sci.* 35, 1111 (1980).
384. M. Hanack, K. Mitulla, G. Pawlowski, and L. R. Subramanian, *J. Organomet. Chem.* 204, 315 (1981).
385. M. Hanack, W. Kowel, J. Metz, M. Mezger, G. Pawlowski, O. Schneider, H.-J. Schulze, and L. R. Subramanian, *Mater. Sci.* XX, 185 (1981).
386. M. Hanack, K. Mitulla and O. Schneider, *Chim. Scr.* 17 (1981).
387. M. Hanack and M. Lange, *Chemtracts Org. Chem.* 8, 131 (1995).
388. M. Hanack and M. Lange, *Adv. Mater.* 6, 819 (1994).
389. M. Hanack, A. Hirsch, A. Lange, M. Rein, G. Renz, and P. Vermeiren, *J. Mater. Res.* 6, 385 (1991).
390. M. Hanack, S. Deger, and A. Lange, *Coord. Chem. Rev.* 83, 115 (1988).
391. M. Hanack, A. Datz, R. Fay, K. Fischer, U. Keppeler, J. Koch, J. Metz, M. Metzger, O. Sphneider, and H.-J. Schulze, "Handbook of Conducting Polymers" (T. A. Skotheim, Ed.), Dekker, New York, 1986.
392. M. Ottmar, D. Hohnholz, A. Wedel, and M. Hanack, *Synth. Met.* 105, 145 (1999).
393. E. Balasubramaniam, G. Ramachandriah, P. Natarajan, G. Bied-Charreton, J. Devynck, and F. Bedioui, *J. Mater. Chem.* 5(4), 625 (1995).
394. G. Ramachandriah, F. Bedioui, J. Devynck, and C. Bied-Charreton, *J. Electroanal. Chem.* 319, 395 (1991).
395. J. Basu and K. K. Rohatgi-Mukerjee, *Soc. Energy Mater.* 21, 317 (1991).
396. A. Deronzier, R. Devaux, D. Limozin, and J. M. Latour, *J. Electroanal. Chem.* 324, 325 (1992).
397. V. Narayanan and P. Natarajan, *J. Polym. Sci., Polym. Chem.* 30, 2475 (1992).
398. K. Viswanathan and P. Natarajan, *Proc. Indian Natl. Sci. Acad.* 63A(2), 129 (1997).
399. E. Balasubramaniam and P. Natarajan, *J. Photochem. Photobiol., Chem.* 109, 39 (1997).
400. C. Park, D. H. Yun, S. Kim, and Y. W. Park, *Sens. Actuators, B* 30, 23 (1996).
401. M. G. Mason, L. S. Hung, C. W. Tang, S. T. Lee, K. W. Wong, and M. Wang, *J. Appl. Phys.* 86, 1688 (1999).
402. G. Gordon, J. Yue, and A. J. Epstein, unpublished work.
403. D. N. Srivastava and R. A. Singh, *Trans. SAEST* 33, 82 (1998).
404. Z. Q. Gao, W. Y. Lai, T. C. Wong, C. S. Lee, I. Bello, and S. T. Lee, *Appl. Phys. Lett.* 74, 3269 (1999).
405. K. Ambalagan and P. Natarajan, *J. Polym. Sci., Polym. Chem.* 29, 1739 (1991).
406. K. Viswanathan and P. Natarajan, *J. Photochem. Photobiol. Chem.* 95, 255 (1996).
407. R. Ramaraj and P. Natarajan, *J. Polym. Sci., Polym. Chem.* 29, 1339 (1991).
408. K. Ambalagan and P. Natarajan, *Proc. Indian Acad. Sci. (Chem. Sci.)* 103(6), 715 (1991).

Index

A

Acetate precursor route, 31
Acetylene polymerization
 catalytic, 6–7, 137–138
 noncatalytic, 7
 Shirakawa method, 132–133
Acyclic polyether-substituted ECP films, 114–115
Adsorption, 105
AES, *see* Auger electron microscopy
AFM, *see* Atomic force microscopy
Akagi technique, 136
Alkoxy precursor route, 30
2-Alkoxyanilines, 240
Alkyl-bridged poly(*p*-phenylene)s, 21
 α, ω -diphenylpolyenes, 311
 α, ω -diynes, 149–150
 α, ω -di-*tert*-butylpolyenes, 311
 α, ω -dimethyloligoenes, 310
Aluminum, interface and, 176–177
Amphiphiles
 hydrogen-bonding and, 193–194
 self-organized structures, 189–194
Analytes, molecular recognition, 111–112
Anilines, redox processes, 251–252
Anionic recognition, 122–124
Anodic electrochemical oxidation, 11, 14–15
ARA technique, 135–136
Aromatic structures
 bandgap and, 40–42
 combinations of, 44
 different rings, 23–25
 electrochemical synthesis, 11–18
 end groups, 44–45
 fused extended systems, 18–20
 ladder-type polymers, 20–21
 monomer unit, 42–44
 oxidation and, 11, 14–15
 polyaromatic synthesis and, 18–21
 quinoid structures and, 38–40
Atomic force microscopy (AFM), 215
ATR, *see* Attenuated total reflectance
Attenuated total reflectance (ATR), 213, 271
Auger electron spectroscopy (AES), 217

B

Bandgap
 aromaticity and, 40–42
 chemical structure and, 37–46
Benzene, oxidation of, 8–9
Benzoine condensation, 28
Benzothiazole condensation, 28
Benzvalene route, 141
Benzyllic halides, 28
Bi enzymatic systems, 109–111
Binary catalyst-oxidant systems, 8–9

Biosensors, 156
Bipolarons, 314
2,2'-Bithiophene, 265
Block copolymers
 amphiphiles and, 193–194
 polyacetylene and, 142–143
 self-organization in, 193–194
Bond-length alternation, 37–40
Bridged bithiophenes, 19–20

C

Calcium, interface and, 177
Calixarene-functionalized polymers, 119–120
Carrier mobility, 174
Catalyst aging, 134
Catalyst-oxidant systems, 8–9
Catalytic polymerization, 6–7
Cationic recognition, 114–122
CD, *see* Circular dichroism
Charge carriers
 in conjugated polymers, 304–305
 ground-state structures and, 304–305
 self-localized excitations and, 305
Charge-density-wave dynamics, 76–77
Charge transfer, photoinduced, 82–84
Chemical structure, electronic properties, 33–47
Chemical vapor deposition (CVD), 28–29, 172
Chromium, interface and, 177
Circular dichroism (CD), 213
Cis- versus *trans*-polyacetylene, 133
Colon method, 13
Compensation, stability and, 324
Composite electrolytes, polyaromatics and, 11
Conducting polymers, 321–322
 compensation and, 324
 doped, 324
 electrical neutralization, 324
 intrinsic, 33–35, 322–323
 metallic regime, 49–54, 66–71
 optical properties of, 65–78
 photostability of, 323–324
 polyacetylene and, 150–151
 polypyrrole, 75
 stability of, 321–345
 see also specific effects, types
Conjugated polymers, 304
 charge carriers in, 304–305
 electrical properties of, 1–86
 electronic spectra of, 303–318
 ground-state structures and, 304–305
 molecular and ionic recognition, 103–124
 optical properties of, 1–86
 photoinduced charge transfer, 82–84
 photophysics of, 82
 properties of, 1–86

- redox effects, 104–105
 - self-localized excitations and, 305
 - synthesis of, 1–86
 - see also* Copolymers; *specific effects, types*
 - Copolymers
 - graft copolymers, 144–145
 - of polyacetylene, 141–145
 - polyaromatics and, 21–23
 - pyrroles, 23, 265
 - of substituted phenylenes, 22–23
 - of substituted thiophenes, 23
 - Coupling reactions
 - benzyllic halides, 28
 - organometallics and, 9–10, 13–14
 - Covalent binding, 105
 - Critical states, 60–62
 - Cross-linking, 105
 - Crown ether-substituted ECP films, 117–119
 - Curtis method, 14
 - CVD, *see* Chemical vapor deposition
 - Cyclooctatetraene route, 140–141
 - Cytochromes, 105
- D**
- Degradation of polymers, 254–256, 265–266
 - DEMS, *see* Differential electrochemical mass spectrometry
 - 2,5-Dialkoxyanilines, 240
 - Dibutyloligoenes, 312
 - Dielectric function, 66, 74
 - Differential electrochemical mass spectrometry (DEMS), 215
 - Disordered systems, 64–65, 74–75
 - Dodecamer, 306
 - Doping
 - dedoping process, 226
 - electrical properties, 176
 - electrochemical, 154
 - electronic spectra, 313–317
 - neutralization and, 324
 - optical properties, 65–78
 - poly(*p*-phenylene vinylene) and, 176
 - primary/secondary, 225–226
 - stability and, 324
 - Drude model, 63–64, 71–73
 - Durham route, 139–140
- E**
- ECESR, *see* Electrochemical electron spin resonance spectroscopy
 - ECP, *see* Electrically conducting polymer films
 - EELS, *see* Electron energy loss spectroscopy
 - Effective number, of carriers, 67–69
 - Electrical properties
 - of conjugated polymers, 47–62
 - of poly(*p*-phenylene vinylene)s, 173–176
 - Electrically conducting polymer (ECP) films, 114–119, 323–324
 - Electrochemical doping, 154
 - Electrochemical electron spin resonance spectroscopy (ECESR), 215, 219, 222, 226, 235–242, 249, 262–264, 270, 274, 275, 278
 - Electrochemical oxidation, polyaromatics and, 11, 14–15
 - Electrochemical synthesis
 - polyanilines and, 33
 - polyaromatics and, 11–12, 14–15, 17–18
 - polypyrroles, 17–18
 - Electrochemically induced changes
 - polyaniline and, 227–251
 - polypyrrole and, 258–265
 - polythiophene and, 269–283
 - Electrochromic window, 339
 - Electrode material, 328
 - Electroluminescence, 81–82
 - Electrolytes, composite, 11
 - Electron acceptor, 304
 - Electron energy loss spectroscopy (EELS), 276
 - Electron mobility, 174
 - Electron spectroscopy for chemical analysis (ESCA), 217
 - Electron spin resonance (ESR) spectroscopy, 219, 232–241, 249, 252, 264, 274–275
 - Electronic spectra, 303–318
 - Electrooxidation, 218
 - Electropolymerization, 267
 - Electroreflectance spectroscopy (ERS), 213
 - Emeraldine base, 339
 - End groups, aromatics and, 44–45
 - Entrapment, in polymer film, 105
 - Environmental sensing technology, 155–156
 - Enzyme-containing polymers, 105–111
 - ERS, *see* Electroreflectance spectroscopy
 - ESCA, *see* Electron spectroscopy for chemical analysis
 - ESR, *see* Electron spin resonance spectroscopy
 - 3,4-Ethylenedioxythiophene-arylenes, 25
 - Excitons, 80–81
 - EXFAS, *see* X-ray absorption
 - Extended aromatic ring systems, 18–21
- F**
- Feast monomer, 140
 - Fermi glass, 75
 - Flavoproteins, 105
 - Fourier transform infrared (FTIR) spectrometers, 216, 283, 330
 - FTIR, *see* Fourier transform infrared spectrometers
 - Fullerene composites, 82–84
 - Furan-benzene, 25
- G**
- Gas-liquid separation membranes, 156–157
 - Gases, molecular recognition, 112–113
 - Gilch route, 30–31
 - Glucose oxidase, 106–109
 - Gold, interface and, 177
 - Graft copolymers, 144–145
 - Grignard method, 9
 - Ground-state structures, 304–305
 - Grubbs method, 11
- H**
- Hairy rods, 197–204
 - Hierarchical self-organization, 193–194
 - Horseradish peroxidase (HRP), 109
 - HRP, *see* Horseradish peroxidase
 - Hydrogen-bonding, supramolecular, 192–195
- I**
- ICP, *see* Intrinsically conducting polymers
 - Indium-doped tin oxide (ITO), 212
 - Inorganic polymers, stability of, 341–342
 - Inorganic solvents, polyaromatics and, 12
 - Insulating states, 60–62
 - Interphases, 211–212
 - Intrinsically conducting polymers (ICP), 10–11, 33–35, 209–212, 214, 284
 - Ionic conduction, self-organization and, 194–195
 - Ionic recognition, films and, 103–124
 - Isomerization, 154

- Isonaphthothiophene, 24
 Isothianaphthene, 24
 ITO, *see* Indium-doped tin oxide
- K**
- Kramers–Kronig analysis, 66
- L**
- Ladder-type polymers, aromatics and, 20–21
 Langmuir–Blodgett films, 186–187
 Lasers, 80, 180
 LEDs, *see* Light emitting diodes
 LEED, *see* Low-energy electron diffraction
 Leucoemeraldine base, 339
 Light emitting diodes (LED), 178–179, 257, 266, 336
 Light-emitting electrochemical cells, 180
 Linear chain model, 34
 Liquid crystal technique, 136–137
 Living systems, polyacetylene and, 145–148
 Localization-modified model, 71–73
 Louwet–Vanderzande route, 31–32
 Low-energy electron diffraction (LEED), 215
 Low-temperature reflectance, 76–77
 Luttinger catalysts, 7, 138
- M**
- Macroscopic properties, 212
 Magnesium, interface and, 177
 Magnetic susceptibility, 59–60
 Magnetoconductance, 54–58
 Marvel's precursor, 10
 McCullough method, 13–14
 McMurry reaction, 167
 Mechanical abuse detectors, 156
 Mechanical properties, 134
 MEHPPV, *see* Poly(2-methoxy-5-(2'-ethylhexyloxy)-1,4-phenylenevinylene)
 Melt salts, polyaromatics and, 12
 Metal-catalyzed coupling reactions, 9, 14
 Metal-insulator transition, in optical spectra, 73–75
 Metallic regime
 electrical properties and, 49–60
 nature of, 77–78
 optical spectra and, 66–71
 see also specific types, effects
 Metallophthalocyanines, 195–197
 Metalloporphyrins, 113
 Metathesis catalysts, 7, 28, 137–138
 Mirage effect, 215
 MNDO, *see* Modified neglect of differential overlap
 Modified neglect of differential overlap (MNDO), 239, 269
 Moisture detectors, 156
 Molecular recognition, 103–124
- N**
- N*-(3-sulfopropyl)aniline (NSPA), 221
N-methylaniline, 244–245, 246
 Naarmann technique, 135
 1,2-Naphthoquinone-4-sulfonate (NQS), 252
 Near edge X-ray absorption fine structure spectroscopy (NEXAFS), 268, 273
 Near infrared region (NIR), 212
 NEXAFS, *see* Near edge X-ray absorption fine structure spectroscopy
 Ni-catalyzed coupling reactions
 Colon method, 9–10, 13
 Curtis method, 14
 McCullough method, 13–14
 organometallic reactions and, 13–14
 Pd-catalyzed reactions, 14
 polyaromatics and, 13–14
 Rieke method, 14
 Stille method, 14
 Yamamoto method, 9–10, 13
 Nicotinamide adenine dinucleotide, 105
 NIR, *see* Near infrared region
 Noncatalytic methods, 7, 138
 Norbornene, 143
 NQS, *see* 1,2-naphthoquinone-4-sulfonate
 NSPA, *see* *N*-(3-sulfopropyl)aniline
 Nuclear magnetic resonance, 171
- O**
- Octaaniline, 340
 3-Octylthiophene, 282
 Oligoenes, 310–313
 Oligomers, spectra of, 303–318
 Oligophenylenevinylenes, 309–310
 Oligothiophenes, 305–308
 Optical properties
 conductivity, 66
 of conjugated polymers, 62–84
 doped conducting polymers and, 65–78
 low-temperature reflectance, 76
 metal-insulator transition, 74
 in metallic regime, 66–71
 PANI–CSA and, 66–67
 PEDOT–PF₆, 71
 PPy–PF₆ and, 68–69
 Shirakawa-type polyacetylene, 134
 see also specific types, effects
 Optically transparent electrodes (OTE), 212
 Optocouplers, 180
 Optoelectronic devices, 82–83
 Organometallic coupling reactions, 9–10, 13–14
 OTE, *see* Optically transparent electrodes
 Oxanorbornadiene route, 139
 Oxidative stability, 323–325
- P**
- PA, *see* Polyacetylene
 PANBUS, *see* Poly(aniline *N*-butylsulfonate)s
 PANI, *see* Polyaniline
 Paraphenylene, 282
 Pariser–Parr–Pople method, 309
 PAS, *see* Photoacoustic spectroscopy
 PASCA, *see* Positron annihilation spectroscopy
 PBD, *see* Probe beam deflection
 Pd-catalyzed reactions, 10, 14
 PDHT, *see* Poly(3-3,6-dioxyheptylthiophene)
 PDHTT, *see* Poly(3,3''-dihexyl-2,2':5',2''-terthiophene)
 PdT, *see* Polydithiophene
 PEDOT, *see* Poly(3,4-ethylenedioxythiophene)
 PEDOT–PF₆, 69–73
 Peierls instability, 34–35
 Pernigraniline sites, 233
 Phenyl vinyl sulfoxide route, 140
 Phenylvinylsulfoxide, 143
 Photoacoustic spectroscopy (PAS), 216
 Photochemical doping, 154
 Photoconductivity, 79–82
 Photodiodes, 179–180
 Photoexcitation spectroscopy, 78–79
 Photoinduced absorption spectroscopy, 78

- Photoinduced charge transfer, 82–84
 Photoluminescence spectroscopy, 79–80
 Photostability, 323–324
 Photothermal spectroscopy (PTS), 216
 Phthalocyanines, 342–343
 Pi-delocalization, 3, 45–46
 PiAT, *see* Poly(3-isoamylthiophene)
 PINT, *see* Polyisophthothiothiophene
 PITN, *see* Polyisothianaphthene
 PMT, *see* Poly(3-methylthiophene)
 PNT, *see* Poly(3-nonylthiophene)
 Polarons, 314
 bipolarons and, 237, 239–240
 primary photocarriers, 80–81
 Poly(1-alkylpyrrole), 332
 Poly(1-dodecylpyrrole), 332
 Poly(1-hexylpyrrole), 332
 Poly(2-methoxy-5-(2'-ethylhexyloxy)-1,4-phenylenevinylene) (MEHPPV), 337
 Poly(2-methoxy-*p*-phenylene vinylene), 173
 Poly(2-vinylpyridine), 326
 Poly(2,5-thienylenevinylene), 303
 Poly[3-(2,5,8-trioxanonyl)thiophene], 115
 Poly[3-(3,6-dioxahexyl)thiophene], 114–115
 Poly(3-3,6-dioxiheptylthiophene) (PDHT), 278–279
 Poly[3-(4-octylphenyl)-2,2'-bithiophene], 279
 Poly(3-alkylthiophene), 12–14, 327
 Poly(3-butylthiophene), 275
 Poly(3-cyclohexylthiophene), 327, 328
 Poly(3-hexylthiophene), 12, 327
 Poly(3-isoamylthiophene) (PiAT), 278–279
 Poly(3-methylthiophene) (PMT), 113, 268–269, 278–281
 Poly(3-nonylthiophene) (PNT), 278–279
 Poly[(3-octyloxy)-4-methylthiophene] (POMT), 277
 Poly(3-octylthiophene) (POT), 273, 279–280
 Poly(3-octylthiophene) (PT8), 277
 Poly[3-oligo(oxyethylene)-4-methylthiophene], 115
 Poly(3-tetradecylthiophene) (PT14), 277
 Poly(3,3'-dibutoxy-2,2'-bithiophene), 279
 Poly(3,3''-dihexyl-2,2':5',2''-terthiophene) (PDHTT), 329
 Poly[3,4-bis-(ethylmercapto)thiophene], 328
 Poly(3,4-dimethoxythiophene), 280
 Poly(3,4-ethylenedioxythiophene), 54
 Poly(3,4-ethylenedioxythiophene) (PEDOT), 70
 Poly(4,4'-dibutyl-2,2'-bithiophene), 275
 Poly(4,4'-dipentoxy-2,2'-bithiophene), 329
 Poly(4,4'-methylenedianiline), 239
 Polyacetylene (PA), 2, 132–145
 alkyne monomers and, 148–149
 applications for, 154–157
 copolymers of, 141–145
 discovery of, 132
 diynes and, 149–150
 electronic properties of, 150–154
 electronic spectra and, 315–316
 indirect routes to, 150
 living systems and, 145–148
 Peierls instability and, 34–35
 photochemical doping, 154
 polymer blends of, 145
 polymeric systems, 325–326
 precursor routes to, 138–141
 Shirakawa method, 132–133
 soluble, 8
 stereospecific polymerizations, 148
 substituted, 145–150, 145–150
 synthesis of, 6–8, 132–158
 Poly(alkoxythiophene), 12
 Poly(aniline *N*-butylsulfonate)s (PANBUS), 339
 Polyaniline (PANI), 113, 217
 degradation of polymers, 254–256
 disorder in, 75
 Drude model and, 71–72
 electrochemically induced changes, 227–251
 formation of, 218–227
 metal-insulator transition in optical spectra, 73
 redox processes and, 251–254
 spectroelectrochemistry of, 217–256
 synthesis of, 32–33
 Polyaromatics
 stability of, 334–341
 synthesis and, 8–26
 valence-bond theory, 36–37
 Poly(arylene methine)s, 25–26
 Polyarylenevinylenes, 315–316
 Polybenzo[*c*]thiophene, 18
 Polydithiophene (PdT), 239
 Polyelectrolyte/surfactant complexes, 190–192
 Polyether-functionalized polymers, 114–119
 Polyheteroacenes, 21
 Polyheteroaromatics, 340
 Polyheterocyclics, 326–334
 Polyisophthothiothiophene (PINT), 273, 280
 Polyisothianaphthene (PITN), 18, 273, 328
 Polymer-amphiphile complexes, 189–194
 Polymer LEDs, 81–82
 Poly(*N*-vinylcarbazole), 340
 Polynaphtho[2,3-*c*]thiophene, 18–19
 Poly(*o*-aminophenol), 283
 Poly(*o*-methoxyaniline), 338
 Poly(*p*-2,5-di-*n*-hexylphenylene), 10
 Poly(*p*-phenylene vinylene)s (PPV), 26–32, 163
 applications, 178–180
 doping and, 176
 electrical properties of, 173–176
 exitons and, 80–81
 interfaces with, 176–178
 oxides and, 177–178
 photocarriers in, 80–81
 physical properties of, 172–176
 polarons and, 80–81
 precursor routes, 28–32
 pristine form, 173
 stability of, 335–337
 structural properties of, 172–173
 synthesis of, 26–28, 163–181
 Poly(*p*-xylylene), 172
 Poly(perinaphthalene), 20–21
 Polyphenanthro[9,10-*c*]thiophene, 19
 Polyphenylenes, stability of, 334–335
 Polypyridine, 203
 Poly(pyrrole-*N*-vinylcarbazole), 332
 Polypyrrole-poly(4-styrenesulfonate), 331
 Polypyrrole (PPy), 105
 degradation of, 265–266
 electrochemically induced changes, 258–265
 formation of, 257–258
 low-temperature reflectance in, 76–77
 optical properties of, 75
 polyaromatic synthesis and, 16–18
 spectroelectrochemistry of, 256–266
 stability of, 330–334
 Polyrotaxanes, 120–121
 Polystyrenesulfonate, 110, 265

- Poly(sulfur nitride), 33–34, 341
Poly(*t*-butylacetylene), 148
Poly(tetrafluoroisothianaphthene), 45
Polythienothiophenes, 19
Polythiophenes (PT), 14, 15, 105, 239, 275, 305
 electrochemically induced changes, 269–283
 electronic spectra and, 266–283, 314–315
 formation of, 267–269
 polyaromatics and, 12–16
 stability of, 326–327
Polyvinylchloride (PVC) route, 138–139
Poly(vinylsulfonate), 110
POMT, *see* Poly[(3-octyloxy)-4-methylthiophene]
Positron annihilation spectroscopy (PASCA), 217
POT, *see* Poly(3-octylthiophene)
PPV, *see* Poly(*p*-phenylene vinylene)s
PPy, *see* Polypyrrole
Precursor routes, 7–8, 10–11, 28–32, 138–141, 165
Probe beam deflection (PBD), 215
Pseudopolyrotaxanes, 118
PT, *see* Polythiophene
PT14, *see* Poly(3-tetradecylthiophene)
PT8, *see* Poly(3-octylthiophene)
PTS, *see* Photothermal spectroscopy
PVC, *see* Polyvinylchloride
Pyrroles, 23–25, 265
- Q**
Quinoid structures, 38–40
- R**
Radiation detectors, 156
Random copolymers, 141–142
Rechargeable batteries, 155
Redox processes, 104–105, 251–252
Reductive electropolymerization, 12–16
Reflectance, 70–71, 73–74
Resonance Raman spectroscopy, 241
Resonance stability, 40–44
Rh catalysts, 7
Rieke method, 14
Ring-opening metathesis polymerization, 28, 140
Rod-coil block copolymers, 189
- S**
SAMs, *see* Self-assembled monolayers
Scanning tunnelling microscopy (STM), 215
Second harmonic frequency (SHG), 213
Secondary ion mass spectroscopy (SIMS), 217
Self-assembled monolayers (SAMs), 186–187
Self-localized excitations, 305
Self-organized supramolecular structures
 conductivity and, 185–206
 electrical switching and, 204–205
 hairy rods and, 197–204
 hydrogen-bonding, 194–195
 ionic conduction and, 194–195
 organic molecules, 195–197
SFG, *see* Sum frequency generation
SHG, *see* Second harmonic frequency
Shirakawa method, 132–137
Side chains, 44
Silicon polymers, 341–342
Silicon-substituted alkyne monomers, 148–149
SIMS, *see* Secondary ion mass spectroscopy
Solar cells, 155
Solitons, 150–151, 314
Soluble precursor routes, 165–167
Specific heat, 59–60
Spectroelectrochemistry, 209–286
SRS, *see* Surface Raman spectroscopy
Stability, 134, 321–345
Stacking, of organic molecules, 195–197
Stille method, 14
STM, *see* Scanning tunnelling microscopy
Subgap absorptions, 313
Sulfinyl precursor route, 31–32
Sulfonium precursor route, 29–30
Sum frequency generation (SFG), 213
Supramolecular structures, 185–206
Surface Raman spectroscopy (SRS), 216, 218, 220, 271
Suzuki coupling, 10
- T**
Temperature limit detectors, 156
Tetrathiafulvalene (TTF), 281
Thermopower, 58–59
THG, *see* Third harmonic frequency
Thin-film preparation, 171–172
Thiophenes, 12–13, 23–25
Third harmonic frequency (THG), 213
Time-of-flight technique (TOF), 174
TOF, *see* Time-of-flight technique
Toluidine, 241, 242
Trans-polyacetylene forms, 133
Triodes, 180
TTF, *see* Tetrathiafulvalene
- U**
Ullman reaction, 9
Ultraviolet photoelectron spectroscopy (UPS), 170–172
UPS, *see* Ultraviolet photoelectron spectroscopy (UPS)
UV-vis spectroscopy, 170–172, 275–283
- V**
Vibrational spectra, 169–170
VSO, *see* Phenylvinylsulfoxide
- W**
Wessling precursor route, 29–30
Wittig reaction, 164–165
- X**
X-ray absorption (EXFAS), 217
X-ray photoelectron spectroscopy (XPS), 172, 217
XANES, 217
Xanthate precursor route, 31
XPS, *see* X-ray photoelectron spectroscopy
- Y**
Yamamoto method, 9–10, 13
- Z**
Ziegler–Natta catalysts, 6–7, 132

This Page Intentionally Left Blank